OCS Study
BOEM 2019-057

Air Quality Modeling in the Gulf of Mexico Region

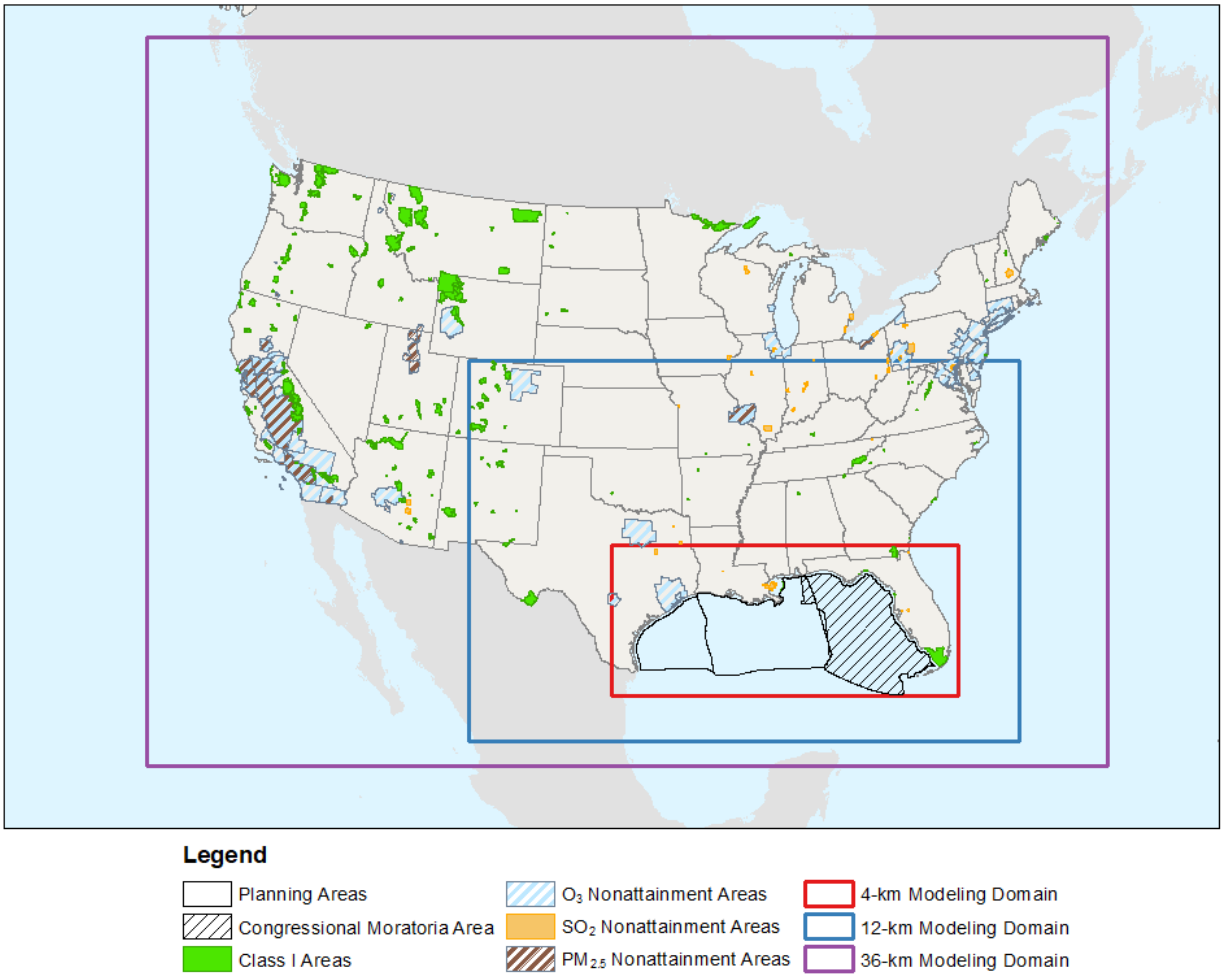

US Department of the Interior
Bureau of Ocean Energy Management
Gulf of Mexico OCS Region

BOEM
Bureau of Ocean Energy Management

OCS Study
BOEM 2019-057

Air Quality Modeling in the Gulf of Mexico Region

August / 2019

Authors:
Darcy Wilson, Till Stoeckenius, Bart Brashers, and Bebhinn Do

Prepared under Contract Number M14PC00007
By
Eastern Research Group, Inc.
1600 Perimeter Park Drive, Suite 200
Morrisville, NC 27560

Ramboll US Corporation
773 San Marin Drive, Suite 2115
Novato, CA 94998

Alpine Geophysics, LLC
7341 Poppy Way
Arvada, CO 80007

US Department of the Interior
Bureau of Ocean Energy Management
Gulf of Mexico OCS Region

BOEM
Bureau of Ocean Energy Management

DISCLAIMER

Study concept, oversight, and funding were provided by the U.S. Department of the Interior, Bureau of Ocean Energy Management (BOEM), Environmental Studies Program, Washington, DC, under Contract Number M14PC00007. This report has been technically reviewed by BOEM, and it has been approved for publication. The views and conclusions contained in this document are those of the authors and should not be interpreted as representing the opinions or policies of the U.S. Government, nor does mention of trade names or commercial products constitute endorsement or recommendation for use.

REPORT AVAILABILITY

To download a PDF file of this report, go to the U.S. Department of the Interior, Bureau of Ocean Energy Management Data and Information Systems webpage (http://www.boem.gov/Environmental-Studies-EnvData/), click on the link for the Environmental Studies Program Information System (ESPIS), and search on 2019-057. The report is also available at the National Technical Reports Library at https://ntrl.ntis.gov/NTRL/.

CITATION

Wilson, D., Stoeckenius, T., Brashers, B., Do, B. 2019. Air quality modeling in the Gulf of Mexico Region. New Orleans (LA): U.S. Department of the Interior, Bureau of Ocean Energy Management. Gulf of Mexico Region. OCS Study BOEM 2019-057. Prepared by the Eastern Research Group, Inc. 655 p.

ACKNOWLEDGMENTS

This report was made possible with the guidance and oversight of Ms. Holli Ensz (Contracting Officer's Representative), Mr. Martin Heinz, Ms. Cholena Ren, and Mr. Eric Wolvovsky from BOEM, as well as the following members of the *Air Quality Modeling in the Gulf of Mexico Region Study* Science Review Group: Ms. Theresa Pella, Dr. David Allen, and Dr. David Parrish.

Also, the authors would like to acknowledge the significant technical contributions that these individuals made to the study: Allison DenBleyker, Richard Billings, Roger Chang, Lindsay Dayton, Stacie Enoch, Steve Mendenhall, Regi Oommen, Heather Perez, Jennifer Sellers, Jody Tisano, and Marty Wolf from Eastern Research Group, Inc.; Jaegun Jung, Joe Knapik, Bonyoung Koo, JD McAlpine, Ralph Morris, Tejas Shah, Pradeepa Vennam, and Maria Zatko from Ramboll; and Dennis McNally, Gregory Stella, and Cynthia Loomis from Alpine Geophysics.

Contents

List of Figures

List of Tables

List of Abbreviations and Acronyms

AEO	Annual Energy Outlook
AERCOARE	meteorological preprocessor for AERMOD using the COARE overwater algorithm
AERMAP	AERMOD terrain preprocessor
AERMET	AERMOD meteorology preprocessor
AERMOD	American Meteorological Society/United States Environmental Protection Agency Regulatory Model
AERSCREEN	screening model based on AERMOD
AIS	automatic identification system
AMET	Atmospheric Model Evaluation Tool
AMSL	above mean sea level
Ap	accuracy of paired peak
APCA	Anthropogenic Precursor Culpability Assessment
AQRV	air quality related values
AQS	Air Quality System
ARW	Advanced Research WRF
BBL	barrel
BC	boundary condition
BELD3	Biogenic Emission Landuse Database version 3
BOEM	Bureau of Ocean Energy Management
BPIPPRM	Building Profile Input Program for PRIME
BSEE	Bureau of Safety and Environmental Enforcement
BTS	Bureau of Transportation Statistics
BY	base year
$\bar{c}$	average concentration value
CAA	Clean Air Act
CAAA	Clean Air Act Amendments
CAI	climatologically aided interpolation
CALMET	CALPUFF meteorological preprocessor
CALPOST	CALPUFF post-processor
CALPUFF	California Puff-Advection Model
CALWRF	CALPUFF WRF preprocessor
CAMD	Clean Air Markets Division
CAMx	Comprehensive Air Quality Model with Extensions
CAPE	convective available potential energy
CARET	Classification and Regression Training
CART	classification and regression tree
CASTNet	Clean Air Status and Trends Network
CB05	Carbon Bond Mechanism, version 5
CB6r2h	Carbon Bond Mechanism, version 6, mechanism 3
CB6r4	Carbon Bond Chemical Mechanism, version 6, revision 4
CEM	continuous emissions monitoring
CF	coarse-fine

CFL	Courant-Friedrichs-Lewy
CFSR	Climate Forecast System Reanalysis
CFSv2	Climate Forecast System model version 2
CMAQ	Community Multiscale Air Quality Modeling System
CMV	commercial marine vessel
c_n	the nth highest concentration
CO	carbon monoxide
c_o	observed concentration value
COARE	Coupled Ocean-Atmosphere Response Experiment
CONAPO	Consejo Nacional de Población
c_p	predicted concentration value
CSN	Chemical Speciation Network
DAT	deposit analysis threshold
DDM	Decoupled Direct Method
DMAX8	daily maximum 8-hour
DMS	dimethyl sulfide
DOCD	Development Operations Coordination Document
dv	deciview
DVB	base year design value
DVC	current design value
DVF	future year design value
EC	elemental carbon
ECA	Emission Control Area
ECH_4	excess methane
ECMWF	European Centre for Medium-range Weather Forecasting
EET	emission exemption threshold
EGU	electric generating unit
EIIP	Emission Inventory Improvement Program
EIS	Environmental Impact Statement
EP	Exploration Plan
ERA	European Centre for Medium-Range Weather Forecasting Reanalysis
ERG	Eastern Research Group, Inc.
ESP	Environmental Studies Program
ESPIS	Environmental Studies Program Information System
ESRL	Earth System Research Laboratory
f(RH)	RH adjustment factors
FAA	Federal Aviation Administration
FB	fractional bias
FDDA	four-dimensional data assimilation
FE	fractional gross error
FINN	Fire INventory from NCAR
FIPS	Federal Information Processing Standards
FLM	Federal Land Management
FNMOC	Fleet Numerical Meteorology and Oceanography Center
FPSO	floating production storage and offloading

FRM	Federal Reference Method
FSL	Forecast Systems Laboratory
ft	feet
FY	future year
g	gram(s)
gal	gallon(s)
GCM	global chemistry model
GDP	gross domestic product
GFP	Gulfport
GIRAS	Geographic Information Retrieval and Analysis System
GOADS	Gulfwide Offshore Activities Data System
GODAE	Global Ocean Data Assimilation Experiment
GOMESA	Gulf of Mexico Energy Security Act
GOM	Gulf of Mexico
GOMR	Gulf of Mexico Region
GPS	global positioning systems
GSE	ground support equipment
ha	hectare
HDDM	high order Decoupled Direct Method
HI	haze index
HONO	nitrous acid
hPa	hectopascal
HSAC	Helicopter Safety Advisory Conference
IC/BC	initial conditions/boundary conditions
ICAO	International Civil Aviation Organization
ICI	institutional/commercial/industrial
IHS	Information Handling Service
IMO	International Maritime Organization
IMPROVE	Interagency Monitoring of Protected Visual Environments
IOA	index of agreement
IPM	Integrated Planning Model
ISHO	integrated surface hourly observation
IVOC	intermediate volatility organic compounds
IWAQM	Interagency Workgroup on Air Quality Modeling
JAXA	Japan Aerospace Exploration Agency
K	kelvin
KBRO	meteorological call sign for Brownsville
KEYW	meteorological call sign for Key West
km	kilometer
KSIL	meteorological call sign for Slidell
KTPA	meteorological call sign for Tampa
Kv	vertical eddy diffusivities
kW	kilowatt(s)
kWh	kilowatt-hour
L	Monin-Obukhov length

LAI	leaf area index
lb	pound(s)
LCC	Lambert Conformal Conic
LNG	liquefied natural gas
LOOP	Louisiana Offshore Oil Port
LPG	liquefied petroleum gas
LSM	Land Surface Model
LTO	landing and takeoff
m	meter(s)
MADIS	Meteorological Assimilation Data Ingest System
MAG	Maricopa Association of Governments
MAGE	mean absolute gross error
MARAD	Maritime Administration
MATS	Modeled Attainment Test Software
MB	mean bias
MCIP	Meteorology-Chemistry Interface Processor
MEGAN	Model of Emissions of Gases and Aerosols from Nature
MERP	model emissions rates for precursors
METSTAT	Meteorological Statistical Program
µg	microgram(s)
mi	miles
Mm	megameters
MM5	Mesoscale Meteorological Model version 5
MMIF	mesoscale model interface
MNB	mean normalized bias
MNGE	mean normalized gross error
MODIS	Moderate Resolution Imaging Spectroradiometer
MOU	Memorandum of Understanding
MOVES	MOtor Vehicle Emission Simulator
MPE	model performance evaluation
MPTER	Multiple Point Gaussian Dispersion Algorithm with Optional Terrain Adjustment
MSW	Municipal solid waste
MTSA	Maritime Transportation Security Act
NAA	nonattainment areas
NAAQS	National Ambient Air Quality Standard
NADP	National Atmospheric Deposition Program
NAM	North American Model
NaN	not a number
NASA	National Aeronautics and Space Administration
NCAR	National Center for Atmospheric Research
NCDC	National Climatic Data Center
NCEP	National Centers for Environmental Prediction
NDBC	National Data Buoy Center
NEI	National Emissions Inventory
NEPA	National Environmental Policy Act

NH_3	ammonia
NH_4	ammonium
NMB	normalized mean bias
NME	normalized mean error
NMM	Nonhydrostatic Mesoscale Model
NO	nitric oxide
NO_2	nitrogen dioxide
NO_3	nitrate
NOAA	National Oceanographic Atmospheric Administration
NOMADS	National Operational Model Archive and Distribution System
NO_X	nitrogen oxides
NP	national park
NS	national seashore
NSR	New Source Review
NWR	national wildlife refuge
NWS	National Weather Service
OA	organic aerosol
OC	organic carbon
OCD	Offshore Coastal Dispersion Model
OCS	Outer Continental Shelf
OCSLA	OCS Lands Act
O&G	oil and gas
OGOR	Oil and Gas Operations Report
OLF	Outlying Landing Field
OLM	Ozone Limiting Method
OMI	Ozone Monitoring Instrument
OMSA	Offshore Marine Service Association
OSAT	Ozone Source Apportionment Technology
PAH	polycyclic aromatic hydrocarbon
PBL	Planetary Boundary Layer
PFP	Proposed Final Program
PGM	Photochemical Grid Modeling
PM_{10}	particulate matter with diameter less than or equal to 10 microns
$PM_{2.5}$	particulate matter with diameter less than or equal to 2.5 microns
PMC	PM coarse
PNO_3	particulate nitrate
ppb	parts per billion
ppm	parts per million
PR	precipitation radar
PRI	primary
PRISM	Parameter-elevation Regressions on Independent Slopes Model
PROD	production
PSAT	Particulate Source Apportionment Technology
PSD	prevention of significant deterioration
PSO	production storage and offloading

PSO_4	particulate sulfate
PVMRM	Plume Volume Molar Ratio Method
QA	quality assurance
QAPP	Quality Assurance Project Plan
QC	quality control
r_g	geometric correlation coefficient
RH	relative humidity
RHC	robust high concentration
RHR	Regional Haze Rule
RMSE	root mean squared error
RPD	rate-per-distance
RPH	rate-per-hour
RPO	Regional Planning Organization
RPP	rate-per-profile
RPV	rate-per-vehicle
RRF	relative response factor
RRTMG	Rapid Radiative Transfer Model for GCMs
SCC	Source Classification Code
SCICHEM	Second-Order Closure Integrated Puff Model with Chemistry
SCIPUFF	Second-order Closure Integrated Puff Model
SCREEN3	screening version of the Industrial Source Complex Model (ISC3)
SEARCH	SouthEastern Aerosol Research and Characterization network
SEMARNAT	Secretaría del Medio Ambiente y Recursos Naturales
SER	Significant Emission Rate
SF_6	sulfur hexafluoride
SIL	Significant Impact Level
SIP	State Implementation Plans
SMOKE	Sparse Matrix Operator Kernel Emissions model
SO_2	sulfur dioxide
SO_4	primary sulfate
SOA	secondary organic aerosol
SRG	Science Review Group
SSB	state seaward boundary
SST	sea surface temperature
SVOC	semi-volatile organic compounds
TAF	Terminal Area Forecast
TCEQ	Texas Commission on Environmental Quality
TIMS	Technical Information Management System
TOG	total organic gases
TOMS	Total Ozone Mapping Spectrometer
TOR	thermal optical reflectance
TPY	tons per year
TRI	Toxics Release Inventory
TRMM	Tropical Rainfall Measurements Mission
TSD	Technical Support Document

TSP	total suspended particulate
TUV	Tropospheric Ultraviolet and Visible
μ_g	geometric mean
UAA	unmonitored area analysis
UAM	Urban Airshed Model
USDOI	United States Department of Interior
USEPA	United States Environmental Protection Agency
USGS	United States Geological Survey
UTC	Universal Time Coordinate
UTM	Universal Transverse Mercator
VIRS	visible-infrared scanner
VMT	vehicle-miles of travel
VOC	volatile organic compound
VPOP	vehicle population
VR	visual range
WBD	windblown dust
WPS	WRF Preprocessing System
WRAP	Western Regional Air Partnership
WRF	Weather Research and Forecasting Mesoscale Model
WRFCAMx	Meteorological Input Preprocessor
wt%	weight percent
yr	year
YSU	Yonsei University

Executive Summary

Overview of Study

The U.S. Department of Interior (USDOI) Bureau of Ocean Energy Management (BOEM) has air quality jurisdiction westward of 87°30'W longitude on the Outer Continental Shelf (OCS) in the Gulf of Mexico Region (GOMR). Under the OCS Lands Act (OCSLA), BOEM is required to prescribe regulations for compliance with the National Ambient Air Quality Standards (NAAQS) to the extent that OCS oil and gas exploration, development, and production sources significantly affect the air quality of any state. The area of possible influence includes the states of Texas, Louisiana, Mississippi, Alabama, and Florida (Figure ES-1).

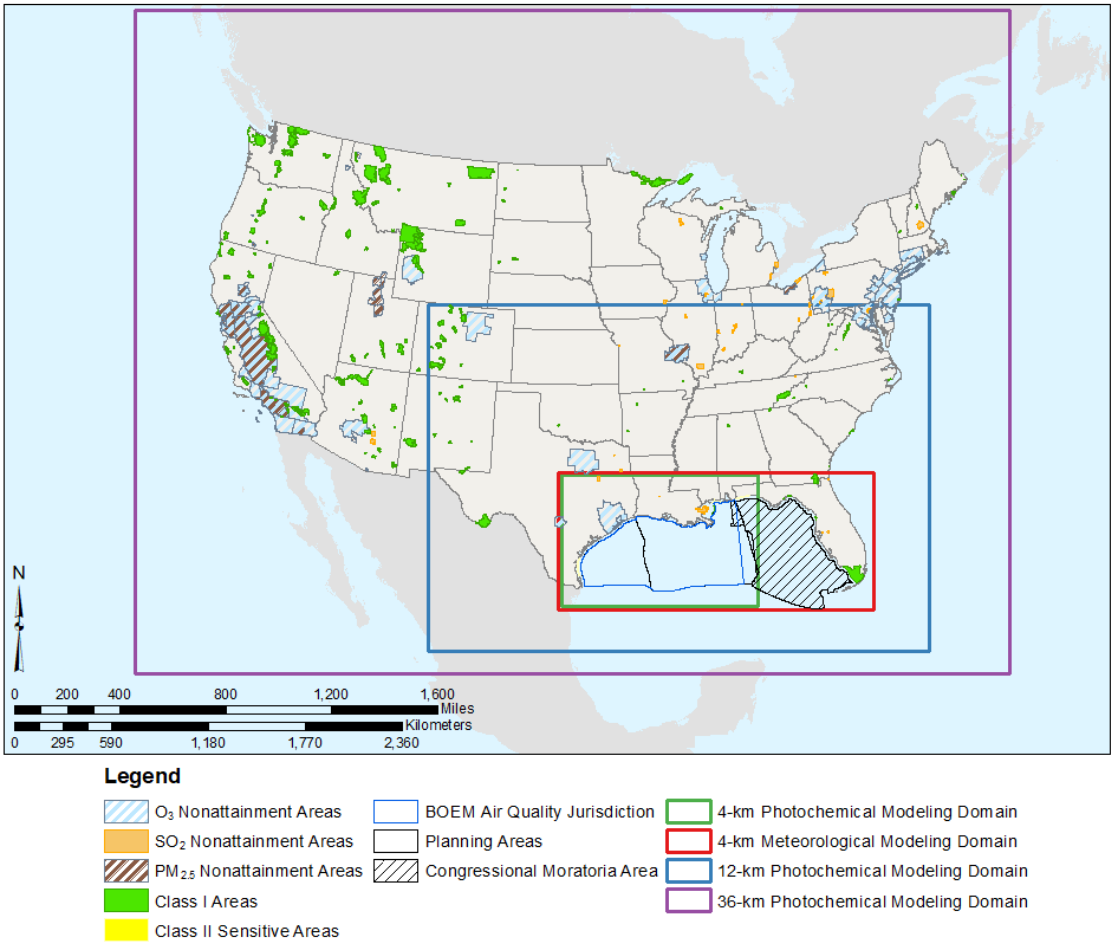

Figure ES-1. Location of *Air Quality Modeling in the GOMR Study* Modeling Domains with Class I Areas, Sensitive Class II Areas, and Nonattainment Areas

After promulgating a NAAQS, the U.S. Environmental Protection Agency (USEPA) designates areas that fail to achieve the NAAQS as nonattainment and requires states to submit emission control plans and demonstrate that the areas will achieve the NAAQS by a required date. Within the 4-km photochemical modeling domain, which is the focus of the cumulative air quality impacts assessment of this study, the Houston-Galveston-Brazoria, Texas, region and the San Antonio (Bexar County), Texas, area are designated nonattainment for the 2015 O_3 8-hour (70 ppb) standard; the Baton Rouge, Louisiana, area is an ozone (O_3) maintenance area for the 2008 O_3 8-hour (75 ppb) standard; and Saint Bernard and

Evangeline Parishes in Louisiana and Freestone and Anderson Counties in Texas are designated nonattainment for the 1-hour (75 ppb) SO_2 standard.

National Parks and wilderness areas designated as Class I areas under the Clean Air Act are given special protection for air quality based on more stringent Prevention of Significant Deterioration (PSD) increment levels that help restrict deterioration of air quality caused by new sources. These areas are also protected against excessive increases in visibility impairment, acid (sulfur and nitrogen species) deposition, and nitrogen eutrophication. Breton Wilderness is the only Class I area along the coastal western and central GOMR. Federal Land Managers also designate certain areas (Class II areas) under their jurisdiction as "sensitive" for tracking air quality impacts. The Breton National Wildlife Refuge, Padre Island National Seashore, and Gulf Islands National Seashore are sensitive Class II areas in the western and central GOMR.

In this *Air Quality Modeling on the GOMR Study*, air quality modeling was conducted to assess the existing pre- and potential post-lease impacts from OCS oil and gas development to the states, as required under OCSLA. BOEM will use this information in National Environmental Policy Act (NEPA) environmental impact statement (EIS) cumulative and visibility analyses. Past cumulative and visibility impacts studies used older, less sophisticated models and no longer support the current NAAQS.

BOEM will also use this information to assess post-lease impacts using emission exemption threshold (EET) formula screening methods to determine whether a proposed source will cause or contribute to a violation of the NAAQS. The NAAQS have undergone several revisions, including changes in indicators and averaging times, since the current EET formulas were developed. BOEM's EET screening approach is similar to the USEPA's PSD screening methods, which use Significant Emission Rates (SERs) and Significant Impact Levels (SILs) to determine the required level of detail in air quality analyses used to demonstrate that a new source will not cause or contribute to violation of a NAAQS or exceedance of a PSD increment.

BOEM contracted with a team consisting of Eastern Research Group, Inc. (ERG), Ramboll U.S. Corporation (Ramboll), and Alpine Geophysics, LLC (Alpine), to conduct meteorological modeling, develop emissions inventories, conduct photochemical modeling in support of the cumulative impact analyses, and conduct dispersion modeling and photochemical modeling in support of EET analyses. The following sections summarize the approach and results of these efforts.

Meteorological Modeling

Air quality modeling requires extensive data on meteorological parameters such as wind speed, wind direction, air temperature, and humidity to determine the rate that pollutants disperse and react in the atmosphere. Sources of meteorological information include datasets of measurements gathered at various locations within the GOMR domain. However, the onshore and, to a much larger extent, the offshore spatial coverage of these measurements is insufficient to describe the three-dimensional structure of the atmosphere away from measurement locations. Using measurement data as inputs, gridded meteorological models can estimate meteorological conditions in regions far from measurement sites. The results of these models are often used to establish conditions near remote pollutant sources or remote locations downwind of pollutant sources.

Ramboll performed five years (2010–2014) of meteorological modeling using the Weather Research and Forecasting (WRF) model to support the photochemical and dispersion air quality modeling conducted in this study. Section 2 of this report presents a model performance evaluation (MPE) of the 5-year WRF results. Appendix F of the *BOEM Gulf of Mexico Multisale Environmental Impact Statement for Proposed Gulf of Mexico OCS Oil and Gas Lease Sales 249, 250, 251, 252, 253, 254, 256, 257, 259, and*

261 (2017 Multisale EIS) assesses the WRF model performance specifically for calendar year 2012, which was used as the photochemical modeling base year.

The BOEM GOMR WRF meteorological model simulation for January 2010 through December 2014 reproduced the observed surface and upper-air meteorological variables very well. WRF performed exceptionally well at onshore locations based on the statistical (METSTAT) analysis for the 36-km and 12-km domains and reasonably well at onshore and offshore locations within the 4-km domain, with a small bias in spatially and temporally paired hourly wind directions at onshore towers and offshore buoys. Overall, the performance results show a very strong agreement between model predictions and surface observations.

Upper-air model performance in the 4-km domain at four locations in the GOMR where upper-air observations are available indicates accurate predictions of the vertical structure of the atmosphere, especially mixing layer heights and occurrences of surface-based temperature inversions. The daily and monthly five-year average precipitation analysis for the 4-km domain indicates there is a strong agreement between the modeled and observation-based precipitation estimates over land, including simulations of convergence zones and other enhanced rainfall areas. Comparisons with satellite-based precipitation accumulations do indicate an understatement of precipitation over water, most notably in the winter months. Although the cause of this is unknown, WRF precipitation predictions are historically biased high along the Gulf Coast states. Comparisons of predicted and observed wind roses at selected locations along the Gulf Coast show WRF was able to simulate offshore and onshore wind speeds and directions very well in the 4-km domain, thus indicating good fidelity reproduction of the land-sea breeze circulation.

Emission Inventory for the Cumulative Air Quality Impacts Analysis

To support the cumulative air quality impacts analyses, ERG developed comprehensive air emissions inventories within the GOMR for carbon monoxide (CO), lead (Pb), nitrogen oxides (NO_x), particulate matter with an aerodynamic diameter less than 2.5 micrometers ($PM_{2.5}$), particulate matter with an aerodynamic diameter less than 10 micrometers (PM_{10}), sulfur dioxide (SO_2), volatile organic compounds (VOCs), and ammonia (NH_3). Using data from BOEM and the USEPA, ERG compiled emissions data for the 4-, 12-, and 36-km modeling domains for anthropogenic (i.e., human-caused) sources including onshore and offshore stationary point and nonpoint area sources, onroad motor vehicles, nonroad equipment, locomotives, marine vessels, other offshore sources, and airports. ERG and Ramboll also compiled emissions data for non-anthropogenic sources. The 2012 base case emissions estimates were used in the photochemical MPE, whereby the predicted concentrations were evaluated against measured ambient concentrations. The results of the MPE indicated that the model generally performed within the range considered to be acceptable for USEPA regulatory applications.

To model the future year impacts associated with implementation of the Proposed Action for the 2017–2022 OCS Oil and Gas Leasing Program (2017–2022 Program), data were obtained from the BOEM 2014 Gulfwide Emissions Inventory and the USEPA for predicted 2017 emissions from all sources. For new emissions sources in the 2017–2022 Program, BOEM developed 10-sale and single-sale scenarios to represent hypothetical assumptions based on estimated amounts, timing, and general locations of OCS exploration, development, and production for offshore activities. The scenarios represent assumptions and estimates that are reasonably suitable for pre-sale impact analyses. Based on the predicted annual emissions estimates, 2036 was selected for use in modeling to represent a reasonable future emissions scenario that would potentially be associated with the Proposed Action's peak impact.

After extensive QA/QC, ERG provided the base case and future emissions estimates to Ramboll in the required photochemical modeling emissions preprocessing input formats. Appendix G of the 2017

Multisale EIS details the initial development of the base year and future year emissions inventories. BOEM then directed ERG to refine these inventories based on feedback received from BOEM, the USEPA, and the general public. Development of the refined emissions inventories is described in this report.

Cumulative Air Quality Impacts Analysis

In 2016, Ramboll conducted a photochemical modeling analysis using the initial base case and future year emissions inventories described in Appendix G of the 2017 Multisale EIS. Ramboll modeled air quality conditions for the base case and future year peak emissions scenario, assuming full development of all 10 lease sales associated with the Proposed Action. Results of the analysis were presented in Appendix H of the 2017 Multisale EIS. After completion of the initial modeling, BOEM directed Ramboll to prepare a revised modeling analysis using the revised future year emissions scenario described above. Based on lessons learned from the previous modeling work, Ramboll also incorporated a number of technical improvements in the revised modeling, including updates to reduce the overprediction of sea salt emissions.

Results of the revised photochemical modeling are presented in this report, including results for the 2012 base case and future year lease sale scenarios. These results present a comprehensive picture of projected future air quality conditions under development of one or all 10 lease sales as compared to 2012 base case conditions. In addition, source apportionment modeling results from the future year scenario provide estimates of the incremental air quality impact of new sources associated with development of the lease sales. Highlights of results of the air resource assessment presented in Section 4 are summarized below:

- Ozone design value concentrations are projected to decrease from 2012 levels at all air quality monitoring sites in the 4-km domain despite new emission sources associated with additional lease sales. The projected ozone reductions are due to reductions in emissions from other sources such as onroad vehicles and nonroad mobile sources, switching to cleaner fuels for marine vessels, and loss of production from older offshore oil and gas production platforms.
- Under the 10-sale scenario, the maximum contribution of the additional production platforms, support vessels, and helicopters to ozone design values at any monitoring site along the western or central Gulf Coast is calculated to be 1.2 ppb (1.7 percent of the NAAQS). The maximum contribution under the single lease sale scenario is calculated to be 0.3 ppb (0.4 percent of the NAAQS).
- A small area of O_3 increases off the Louisiana coast in the vicinity of the Louisiana Offshore Oil Port (LOOP) is anticipated, likely due to reductions in NO_x emissions at the LOOP that suppressed O_3 production in this area in the 2012 base case.
- The 24-hour and annual average $PM_{2.5}$ concentrations are projected to decrease from 2012 levels at all air quality monitoring sites in the 4-km domain despite the additional lease sales because of reductions in emissions from the other sources listed above. An exception is a small increase in annual $PM_{2.5}$ at Hidalgo Co., Texas which is unrelated to the 2017–2022 Program.
- The additional production platforms, support vessels, and helicopters associated with 10 lease sales are estimated to contribute no more than 0.1 $\mu g/m^3$ to the 24-hour or annual average $PM_{2.5}$ design values (0.3 and 0.8 percent of the 24-hour and annual NAAQS, respectively) at monitoring sites in the 4-km domain. Contributions over all model grid cells of new sources associated with the 10-sale scenario to modeled eighth highest 24-hour $PM_{2.5}$ are less than 0.8 $\mu g/m^3$ (2.3 percent of the NAAQS). The maximum contribution to the annual average $PM_{2.5}$ is 0.5 $\mu g/m^3$ (4 percent of the NAAQS). Maximum contributions over all model grid cells of new sources associated with

the single lease sale scenario to modeled 24-hour and annual $PM_{2.5}$ are nearly the same as under the 10-sale scenario.

- Incremental impacts on visibility in Class I and sensitive Class II areas associated with a single lease sale are calculated to be below the minimum significance threshold (0.5 deciview).
- Incremental impacts on visibility in Class I and sensitive Class II areas associated with the 10-sale scenario are calculated to exceed the upper significance threshold (1 deciview) on the eighth highest day by 1 percent at the Breton Island Wilderness Area, which is the only such area with a predicted incremental impact exceeding 1 deciview.
- Incremental nitrogen deposition from new sources associated with the single- or 10-sale scenario is calculated to exceed the data analysis thresholds established by Federal Land Managers at Class I and sensitive Class II areas along the western and central Gulf Coast. Incremental sulfur deposition is below the data analysis thresholds in all cases.

Emission Exemption Threshold Evaluation

The goal of the EET evaluation task was to test the efficacy of BOEM's existing EET formulas provided in 30 CFR 550.303(d). The EET formulas are used to determine whether a proposed source could cause or contribute to a violation of short-term or annual NAAQS. ERG and Alpine conducted dispersion and photochemical modeling to assess the efficacy of the EET formulas for direct release (primary) and secondary formation of pollutants. A common set of synthetic sources based on publicly available BOEM Air Quality Spreadsheets were used to ascertain the impacts from primary and secondary formation of chemically reactive pollutants such as PM and O_3. The emissions inventory used to evaluate the existing EETs differs from the emissions inventory used in the cumulative air quality impacts analysis task. ERG developed five synthetic source emission scenarios based on the calculation methods from the latest Air Quality Spreadsheets that must be submitted by operators/lessees for approval prior to initiation of drilling and production activities, then modeled them individually to assess their direct impacts. The modeled impacts from these synthetic sources were compared to the results of the existing EET formulas to determine how successfully the EETs screen *de minimis* sources (i.e., sources that will not impact the NAAQS).

As shown in the Table ES-1, the short-term NAAQS EET formula results were mixed, in that most pollutants saw false positive (i.e., the impact was under the SIL, but the formula determined that modeling was necessary) and false negative errors (i.e., the impact was over the SIL, but the formula determined that modeling not necessary). False negative errors were more common for the short-term standards (i.e., standards with averaging times ≤ 24 hours), were higher than the false positive rates, and ranged from 2 percent for the 1-hour NO_2 NAAQS to 36 percent for 24-hour $PM_{2.5}$ NAAQS.

Table ES-1. Short-Term NAAQS Results at the Shoreline[a]

Pollutant	Averaging Time	Evaluation Outcome (percentage of total)		
		Current EET Results Agree with Modeled Impacts	False Positive (Type I)	False Negative (Type II)
CO	1 hour	77%	0%	23%
	8 hours	84%	0%	16%
NO_2	1 hour	91%	7%	2%
$PM_{2.5}$	24 hours	64%	0%	36%
PM_{10}	24 hours	73%	0%	26%
SO_2	1 hour	73%	6%	21%
	3 hours	71%	8%	21%
	24 hours	72%	8%	20%

[a] Based on 3,300 modeling runs.

Table ES-2 shows that, for the annual NAAQS, the current EET formulas produce one very slight false negative error for $PM_{2.5}$ and false positive errors for all pollutants. That is, the EET formulas called for modeling when an impact larger than the SIL was not seen. These errors were especially common at distances greater than 50 miles to the shoreline.

Table ES-2. Long-Term NAAQS Results at the Shoreline[a]

Pollutant[b]	Evaluation Outcome (percentage of total)		
	Current EET Results Agree with Modeled Impacts	False Positive (Type I)	False Negative (Type II)
NO_2	59%	41%	0.0%
$PM_{2.5}$	96%	3%	1.2%
PM_{10}	93%	7%	0.0%
SO_2	73%	27%	0.0%

[a] Based on 3,300 modeling runs.
[b] There is no long-term NAAQS for CO.

Based on the synthetic sources tested, secondary formation of $PM_{2.5}$ and O_3 does not exceed the SILs. It does not appear that the EET formulas need to account for these emissions. However, BOEM may consider additional modeling of other platform emission scenarios, especially as new technologies and larger operations emerge.

BOEM has several options if the EET formulas are to be revised. Cubic and logistic function forms for regressions performed better than linear and quadratic forms. The ratio of false positive errors to false negative errors varied across the models. One alternative to using regressions explored in this study is the use of classification and regression tree (CART), which had good performance across all categories. Another alternative is to utilize the database of modeling results from this study to find a comparable operation to estimate impact. If this approach is used, BOEM will provide guidance on what constitutes a comparable facility.

Uncertainties and Recommendations

As discussed in Section 6 of this report, one of the key uncertainties associated with analyzing the air quality impacts from offshore oil and gas sources in the Gulf of Mexico is the magnitude of the modeled ozone and particulate matter concentrations over the Gulf waters; a BOEM research goal should be the collection of more offshore data that can be used in the meteorological and photochemical MPEs. This could be combined with a tracer study to characterize plume dispersion from point sources as plumes are blown across the coastal boundary. Top-down studies could also compare the results of this study's photochemical grid and dispersion modeling with ambient measurements made at or near the earth's surface, satellite remote sensing measurements of pollutant total column mass (and vertical profiles where available), and measurements made by aircraft overflights to validate emission inventories.

Recommendations for the EET evaluation task are that BOEM assess the results of the CART analyses performed in this study if the EET formulas are to be revised. BOEM can also continue to update the modeling database developed for this study as operators submit plans that include dispersion modeling. The results can be added to the database for use in a refresh of the analysis. Recent Air Quality Spreadsheets and future GOMR emissions estimates can also be used to assess whether the synthetic source emission estimates and emission release parameters are still representative and if additional modeling is needed.

1 Introduction

1.1 Study Overview

The U.S. Department of the Interior's (USDOI's) Bureau of Ocean Energy Management (BOEM) is required under the Outer Continental Shelf Lands Act (OCSLA) 1334(a)(8) to prescribe regulations for "compliance with the National Ambient Air Quality Standards (NAAQS) pursuant to the Clean Air Act to the extent that Outer Continental Shelf (OCS) oil and gas exploration, development, and production sources significantly affect the air quality of any state." BOEM's regulations are promulgated in 30 CFR 550 subparts B and C. BOEM's Gulf of Mexico Region (GOMR) manages responsible development of oil and gas and mineral resources on over 159 million acres of the OCS off Texas, Louisiana, Mississippi, Alabama, and Florida. The GOMR OCS comprises the Western, Central, and Eastern Gulf of Mexico (GOM) Planning Areas (shown in Figure 1-1). The Clean Air Act Amendments (CAAA) of 1990 designate air quality authorities in the GOMR, giving BOEM air quality jurisdiction westward of 87°30'W longitude and the U.S. Environmental Protection Agency (USEPA) air quality jurisdiction eastward of 87°30'W longitude. A portion of the Central Gulf of Mexico Planning Area and most of the Eastern Gulf of Mexico Planning Area is under restriction until 2022 as part of the Gulf of Mexico Energy Security Act (GOMESA) of 2006. The area restricted is the portion of the Eastern Planning Area within 125 miles of Florida, all areas in the Gulf of Mexico east of the Military Mission Line (86° 41'W longitude), and the area within the Central Planning Area that is within 100 miles of Florida. The GOMESA moratoria area is depicted on Figure 1-1. The figure also depicts the modeling domains covered by this study. The 36-kilometer (km) photochemical modeling domain shown in purple covers the continental U.S. and portions of Canada and Mexico. The more refined 12-km domain is shown in blue. The focus of this study is the 4-km meteorological domain and the smaller 4-km photochemical modeling domain.

The USEPA sets NAAQS for seven regulated pollutants: ozone (O_3), particulate matter with an aerodynamic diameter of 2.5 micrometers and smaller ($PM_{2.5}$), particulate matter with an aerodynamic diameter of 10 micrometers and smaller (PM_{10}), sulfur dioxide (SO_2), nitrogen dioxide (NO_2), carbon monoxide (CO), and lead (Pb), as shown in Table 1-1.

After promulgating a NAAQS, the USEPA designates areas that fail to achieve the NAAQS as nonattainment areas (NAAs) and requires states to submit State Implementation Plans (SIPs) that contain emission control plans and demonstrate that the NAA will achieve the NAAQS by the required date. After an area attains the NAAQS, it can be re-designated as a maintenance area and must continue to demonstrate compliance with the NAAQS. Figure 1-1 displays the locations of NAAs in the 36-km modeling domain.

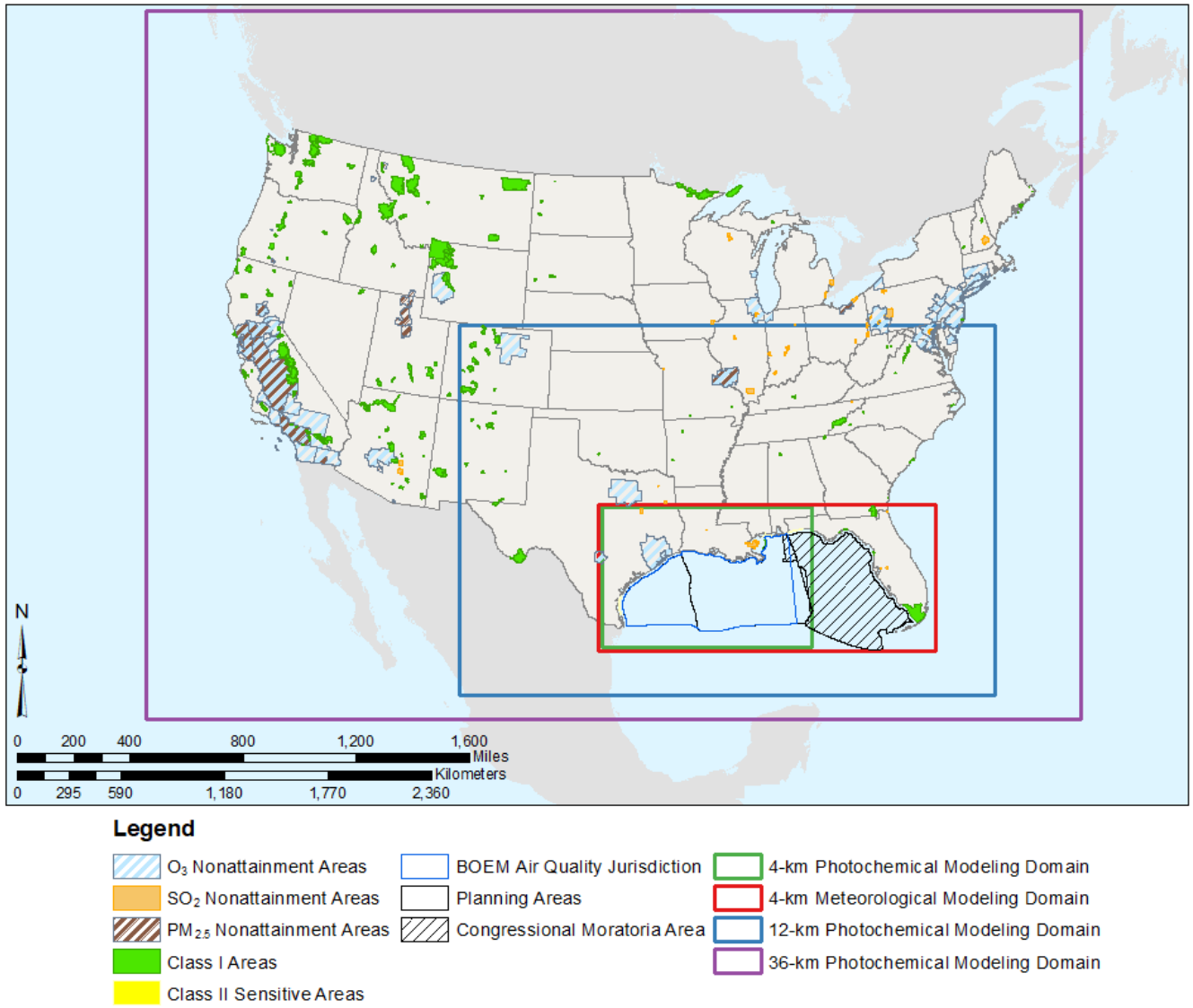

Figure 1-1. Location of *Air Quality Modeling in the GOMR Study* Modeling Domains with Class I Areas, Sensitive Class II Areas, and Nonattainment Areas

In addition, the Clean Air Act (CAA) designated 156 National Parks and wilderness areas as Class I areas that are offered special protection for air quality and air quality related values (AQRVs), and all other areas in the U.S. as Class II areas. Figure 1-1 displays the locations of the mandatory Class I areas (in green) in the GOMR. Federal Land Management (FLM) agencies have designated certain Class II areas as sensitive for tracking AQRV impacts. Sensitive Class II areas in the southeastern U.S. region are also shown in Figure 1-1 (in yellow).

Compared to Class II areas, Class I areas have lower Prevention of Significant Deterioration (PSD) increments that new sources may not exceed. They are also protected against excessive increases in several AQRVs, including visibility impairment, acid (sulfur and nitrogen) deposition, and nitrogen eutrophication. The Regional Haze Rule (RHR) specifies a goal of achieving "natural" visibility conditions by 2064 in Class I areas, and states must submit RHR SIPs that demonstrate progress toward that goal.

Table 1-1. NAAQS and PSD Increments[a]

Pollutant	Pollutant/Averaging Time	NAAQS	PSD Class I Increment	PSD Class II Increment
CO	1-hour[b]	**35 ppm** 40,000 µg/m^3	–	–
CO	8-hour[b]	**9 ppm** 10,000 µg/m^3	–	–
NO_2	1-hour[c]	**100 ppb** 188 µg/m^3	–	–
NO_2	Annual[d]	**53 ppb** 100 µg/m^3	2.5 µg/m^3	25 µg/m^3
O_3	8-hour[e]	**0.070 ppm** 137 µg/m^3	–	–
PM_{10}	24-hour[f]	**150 µg/m^3**	8 µg/m^3	30 µg/m^3
PM_{10}	Annual[g]	–	4 µg/m^3	17 µg/m^3
$PM_{2.5}$	24-hour[h]	**35 µg/m^3**	2 µg/m^3	9 µg/m^3
$PM_{2.5}$	Annual[i]	**12 µg/m^3**	1 µg/m^3	4 µg/m^3
SO_2	1-hour[j]	**75 ppb** 196 µg/m^3	–	–
SO_2	3-hour[k]	**0.5 ppm** 1,300 µg/m^3	25 µg/m^3	512 µg/m^3
SO_2	24-hour	–	5 µg/m^3	91 µg/m^3
SO_2	Annual[d]	–	2 µg/m^3	20 µg/m^3
Pb	3-Month[l]	0.15 µg/m^3	–	–

[a] ppb = parts per billion; ppm = parts per million; µg/m^3 = micrograms per cubic meter air
[b] No more than one exceedance per calendar year.
[c] 98th percentile, averaged over 3 years.
[d] Annual mean not to be exceeded.
[e] Fourth-highest daily maximum 8-hour ozone concentrations in a year, averaged over 3 years, NAAQS promulgated December 28, 2015.
[f] Not to be exceeded more than once per calendar year on average over 3 years.
[g] Three-year average of the arithmetic means over a calendar year.
[h] 98th percentile, averaged over 3 years.
[i] Annual mean, averaged over 3 years, NAAQS promulgated December 14, 2012.
[j] 99th percentile of daily maximum 1-hour concentrations in a year, averaged over 3 years.
[k] No more than one exceedance per calendar year (secondary NAAQS).
[l] In areas designated nonattainment for the Pb standards before the promulgation of the current (2008) standards, and for which implementation plans to attain or maintain the current (2008) standards have not been submitted and approved, the previous standards (1.5 µg/m^3 as a calendar quarter average) also remain in effect.

Table 1-2 summarizes the NAAs and maintenance areas in the southeastern U.S. SO_2 and Pb NAAs are focused around specific large industrial sources, whereas ozone NAAs are more regional, reflecting the formation of ozone as a secondary pollutant from emissions of nitrogen oxides (NO_x) and volatile organic compound (VOC) precursors from a wide range of sources.

Table 1-2. NAAs and Maintenance Areas in the Southeastern U.S. as of March 31, 2019[a]

Area	8-hr O_3 (1997)[b]	8-hr O_3 (2008)	8-hr O_3 (2015)	SO_2 (2010)	CO (1971)	Pb (2008)
Birmingham, AL	M	–	–	–	–	–
Troy, AL	–	–	–	–	–	M
Tampa, FL	–	–	–	–	–	M
Hillsborough-Polk Counties, FL	–	–	–	NAA	–	–
Nassau County, FL	–	–	–	NAA	–	–
Atlanta, GA	M	M	NAA	–	–	–
Charlotte-Rock Hill, NC-SC	M	M	–	–	–	–
Baton Rouge, LA	M	M	–	–	–	–
Evangeline Parish, LA	–	–	–	NAA	–	–
St. Bernard Parish, LA	–	–	–	NAA	–	–
Clarksville-Hopkinsville, TN-KY	M	–	–	–	–	–
Knoxville, TN	–	M	–	–	–	–
Sullivan County, TN	–	–	–	NAA	–	–
Memphis, TN-AR-MS	M	M	–	–	–	–
Beaumont-Port Arthur, TX	M	–	–	–	–	–
Houston-Galveston-Brazoria, TX	NAA	NAA	NAA	–	–	–
Dallas-Fort Worth, TX	NAA	NAA	NAA	–	–	–
Freestone-Anderson Counties, TX	–	–	–	NAA	–	–
Rusk-Panola Counties, TX	–	–	–	NAA	–	–
Titus County, TX	–	–	–	NAA	–	–
El Paso, TX	–	–	–	–	M	–
Frisco, TX	–	–	–	–	–	M
San Antonio (Bexar County), TX	–	–	NAA	–	–	–

[a] NAA=nonattainment area; M=maintenance area; blank cells indicate the area is in attainment of the NAAQS.
[b] Excluding former subpart 1 areas.

Figure 1-2 depicts the NAAs, Class I areas, and sensitive Class II areas within 4-km meteorological modeling domain in more detail.

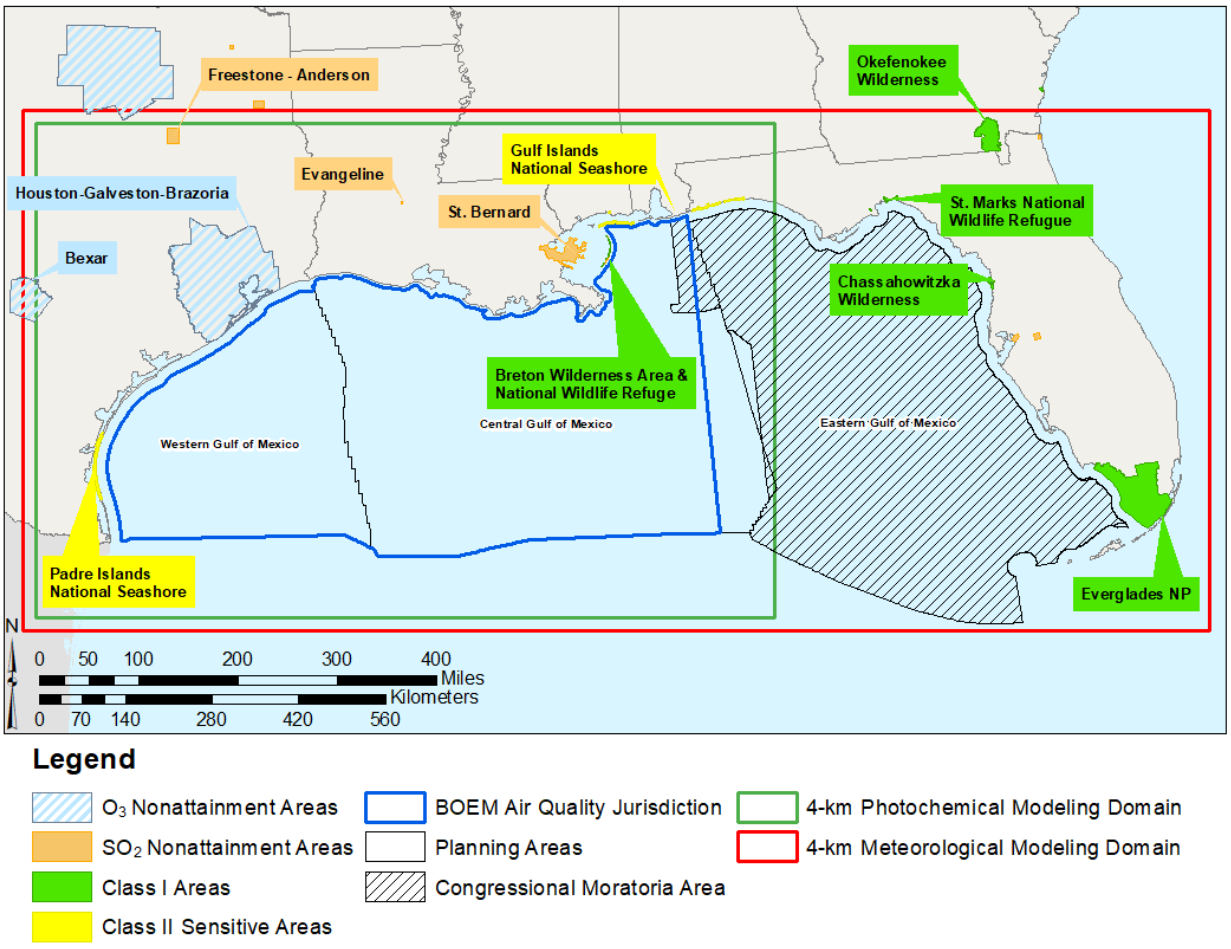

Figure 1-2. Nonattainment Areas, Class I Areas, and Sensitive Class II Areas Within 4-km Meteorological and Photochemical Modeling Domains

The U.S. Secretary of the Interior approved BOEM's Proposed Final Program (PFP) for the 2017–2022 Outer Continental Shelf Oil and Gas Leasing Program (2017–2022 Program) on January 17, 2017. The 2017–2022 PFP includes 10 proposed lease sales within the Western and Central/Eastern GOM Planning Areas (the combined GOM Program Area). The *Air Quality Modeling in the GOMR Study* cumulative air quality analysis examines the existing pre-lease and potential post-lease impacts of these lease sales with respect to the NAAQS and AQRVs, including visibility and acid deposition (sulfur and nitrogen), in nearby Class I and sensitive Class II areas, as well as incremental impacts of PSD pollutants (NO_2, PM_{10}, $PM_{2.5}$) with respect to PSD Class I and Class II increments.

BOEM contracted with a team consisting of Eastern Research Group, Inc. (ERG), Ramboll U.S. Corporation (Ramboll), and Alpine Geophysics, LLC (Alpine), to conduct photochemical and dispersion modeling for the GOMR to assess the OCS oil and gas development pre- and post-lease impacts to the states. BOEM uses this information pre-lease in National Environmental Policy Act (NEPA) environmental impact statement (EIS) cumulative analyses and post-lease in emission exemption threshold (EET) analyses to support compliance with OCSLA.

Air quality modeling requires several input datasets, including meteorology, emissions inventories, and pre-existing (ambient) pollutant concentrations. Figure 1-3 presents an overview of how these datasets fit together for the *Air Quality Modeling in the GOMR Study*.

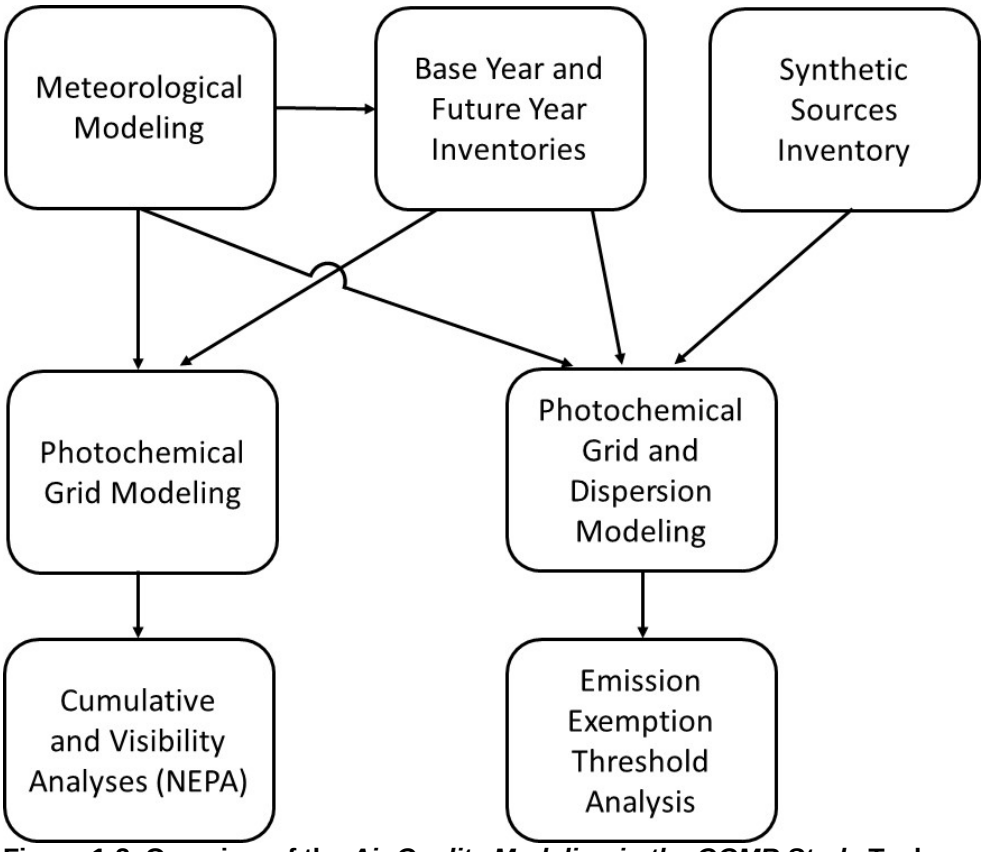

Figure 1-3. Overview of the *Air Quality Modeling in the GOMR Study* Tasks

Appendix F of the *BOEM Gulf of Mexico Multisale Environmental Impact Statement for Proposed Gulf of Mexico OCS Oil and Gas Lease Sales 249, 250, 251, 252, 253, 254, 256, 257, 259, and 261* (2017 Multisale EIS) (USDOI, BOEM, 2017) covers Ramboll's assessment of the Weather Research and Forecasting (WRF) model performance for just 2012, the photochemical modeling base year. Appendix G of the 2017 Multisale EIS details the initial development of the base year and future year emissions inventory. BOEM then directed ERG to refine these inventories based on feedback received from BOEM, the USEPA, and the general public.

Ramboll also conducted an initial photochemical modeling analysis of these lease sales, with the results presented in Appendix H of the 2017 Multisale EIS. Ramboll modeled air quality conditions for both a 2012 base case and for a future year representative of a peak emissions scenario expected to occur, assuming full development of the 10 lease sales. After completion of the initial modeling, BOEM directed Ramboll to prepare a revised modeling analysis. Using lessons learned from the previous modeling work, Ramboll incorporated a number of technical improvements in the revised modeling.

To assess the post-lease impacts, similar to the USEPA PSD program, BOEM requires that OCS oil and gas lessees and operators submit Exploration Plans (EPs) and Development Operations Coordination Documents (DOCDs) with calculations of potential emissions. BOEM uses screening methods to determine whether a proposed source will cause or contribute to a violation of the NAAQS. The EETs were established to determine whether a facility described in an EP or DOCD is exempt from further air quality review because the plan's potential emissions would have an insignificant impact on air quality. The current EET formulas were developed in the 1980s. Since then, the NAAQS have undergone several revisions, including changes in indicator and averaging times. This study evaluates the EET formulas to determine if they still apply to the current annual and short-term NAAQS.

This *Air Quality Modeling in the GOMR Study* report details the meteorological modeling conducted (Section 2); development of emissions inventories for use in photochemical grid modeling to support the cumulative air quality analyses (Section 3); photochemical grid modeling in support of the cumulative air quality analyses (Section 4); emission inventory development, dispersion modeling, and photochemical grid modeling in support of EET analyses (Section 5); and uncertainty and recommendations (Section 6).

1.2 References

USDOI, BOEM (U.S. Department of the Interior, Bureau of Ocean Energy Management). 2017. Gulf of Mexico OCS Oil and Gas Lease Sales: 2017-2022; Gulf of Mexico Lease Sales 249, 250, 251, 252, 253, 254, 256, 257, 259, and 261; Final Multisale Environmental Impact Statement. USDOI, BOEM, Gulf of Mexico OCS Region, New Orleans, LA. OCS EIS/EA BOEM 2017-009.

2 WRF Model Performance Evaluation

2.1 Introduction

Ramboll performed the meteorological modeling for this study, in support of photochemical grid modeling and dispersion modeling. This section details the meteorological model performance evaluation (MPE) of a WRF model run in the GOMR. The results evaluated represent five years (2010–2014) of WRF meteorological modeling.

Air quality modeling requires meteorological parameters such as wind speed, wind direction, air temperature, and humidity to determine the rate at which pollutants disperse and react in the atmosphere. Sources of meteorological information include datasets of measurements gathered at various locations within the GOMR domain. However, the spatial coverage of these measurements is insufficient to describe the three-dimensional structure of the atmosphere away from measurement locations. Using measurement data as inputs, gridded meteorological models can estimate meteorological conditions in regions far from measurement sites. The results of these models are often used to establish conditions near remote pollutant sources or remote locations downwind of pollutant sources. Within the GOMR domain, Ramboll identified the WRF meteorological model and used it to provide meteorological inputs for the air quality models.

Ramboll previously evaluated several existing meteorological datasets (USEPA continental U.S. [CONUS] WRF and Ramboll Training WRF datasets) and concluded that they had enough deficiencies and lacked the positive attributes necessary to select any of them for air quality modeling in the study area (Brashers et al., 2014, see Appendix B.1); therefore, new meteorological modeling was required. This WRF MPE documents the model performance for the full 2010–2014 five-year modeling period.

Brashers et al. (2014) showed a statistical analysis of the USEPA 12-km WRF, which can be compared to the statistical analysis presented in Section 2.3.1.2 of this report. The new WRF features noticeable improvements in wind speed and direction performance, with more modest improvements in temperature and humidity performance. In particular, the current 12-km WRF wind direction featured less spread in the bias between the years and lower gross error. The USEPA 12-km WRF featured year-to-year variations in wind speed bias and root-mean-square error (i.e., the points in the soccer plots for some years were distinctly shifted from the rest), while the current WRF wind speed soccer plots show the points for all months and all years very closely clustered—indicating consistent performance over time.

The statistical analysis of the Ramboll Training WRF dataset summarized in Brashers et al. (2014) for the 4-km domain can be compared to the figures presented in Section 2.3.1.2. The Training dataset simulated only one year but still featured notably worse performance for all parameters except temperature. The new WRF dataset features about half the maximum wind speed bias and root-mean-square error of the Training dataset and features much more consistent month-to-month wind direction performance.

2.2 WRF Modeling Methodology

Over the past decade, emergent requirements for numerical simulation of urban- and regional-scale air quality have led to intensified efforts to construct high-resolution emissions, meteorological, and air quality datasets. It is now possible, for example, to apply tailored, sophisticated mesoscale prognostic meteorological models and Eulerian and Lagrangian photochemical/aerosol models for multi-seasonal periods over near-continental scale domains to a specific air quality modeling project in a matter of weeks.

The WRF model is the current preferred model for atmospheric research and operational forecasting needs at mesoscale resolution (a few to several hundred km). It is a state-of-the-art atmospheric simulation system, commonly used to drive air quality dispersion models at the regional level.

The operational version of the model is the Nonhydrostatic Mesoscale Model (NMM) WRF core version 3, developed and maintained by the National Oceanic and Atmospheric Administration (NOAA) and the National Centers for Environmental Prediction (NCEP). The Advanced Research WRF (ARW) core, currently version WRF 3.7.1, is supported by the National Center for Atmospheric Research (NCAR) Mesoscale and Microscale Meteorology Division (NCAR, 2015). The modeling described in this report used WRF version 3.7.

The WRF model contains separate modules to compute different physical processes such as surface energy budgets, soil interactions, turbulence, cloud microphysics, and atmospheric radiation. Within WRF, the user has many options for selecting the different schemes for each type of physical process. A WRF Preprocessing System (WPS) generates the initial and boundary conditions used by WRF, based on topographic datasets, land use information, and larger-scale atmospheric and oceanic models. WRF version 3.7 contains approximately 558 model options or settings in its control file (called a namelist). Most have default values, and many others have *de-facto* default values that most WRF modelers use. The following section documents the specific model configurations and selections that have the strongest effect on WRF performance and were chosen for the new five-year dataset.

2.2.1 GOMR Air Quality Meteorological Modeling

Brashers et al. (2014) previously examined the USEPA continental U.S. (CONUS WRF) and Ramboll Training WRF datasets in detail and evaluated them using both quantitative and qualitative techniques. They determined that both datasets were inadequate for the study area, particularly in the offshore portions. The development of the new, high-resolution, five-year dataset was necessary to more accurately represent meteorological conditions in the overwater portions of the GOMR for use in air quality modeling.

2.2.2 Model Domain Configuration

The WRF domain configuration is composed of a system of simultaneous nested grids. Figure 2-1 shows the WRF modeling grids at 36, 12, and 4 km. All WRF grids are defined on a Lambert Conformal Conic (LCC) projection centered at 40°N, 97°W, with true latitudes at 33°N and 45°N (the “standard National Regional Planning Organization [RPO]” projection). The outermost domain with 36-km resolution includes the entire continental U.S. and parts of Canada and Mexico, and it captures synoptic-scale (storm-system-scale) structures in the atmosphere. The inner 12-km regional grid covers the southeastern U.S. and was used to ensure that large-scale meteorological patterns across the region are adequately represented and to provide boundary conditions for the 4-km domain.

The 4-km domain, shown in Figure 2-1, is centered on the coastal areas of the southeastern U.S. and overwater portions of the GOM. Table 2-1 provided the input configurations for this WRF domain. NX and NY are the number of east-west and north-south staggered grid points, respectively, in each domain. I-start and J-start indicate the western- and southern-nested grid starting indices with respect to the parent grid. Geographic resolution relates to the geographic datasets employed for each grid, in terms of minutes or seconds of degrees.

The 36-, 12-, and 4-km grids were run simultaneously with one-way nesting, meaning that meteorological information flows downscale via boundary conditions introduced from the respective coarser grid. The WRF modeling domain was defined to be slightly larger than the CAMx/CMAQ (Comprehensive Air Quality Model with Extensions/Community Multiscale Air Quality Modeling System) photochemical

grid modeling domains to eliminate boundary artifacts in the meteorological fields. Such boundary artifacts occur for both numerical reasons (the 3:1 grid spacing ratio) and because the imposed boundary conditions require some time/space to come into dynamic balance with WRF's atmospheric equations.

Table 2-1. BOEM GOMR WRF Domain Configuration

Grid Resolution	NX	NY	I-start	J-start	Geographic Resolution	Coverage
36 km	165	129	1	1	10-minute	CONUS
12 km	265	187	55	9	2-minute	SE CONUS
4 km	481	211	72	27	30-second	GOMR

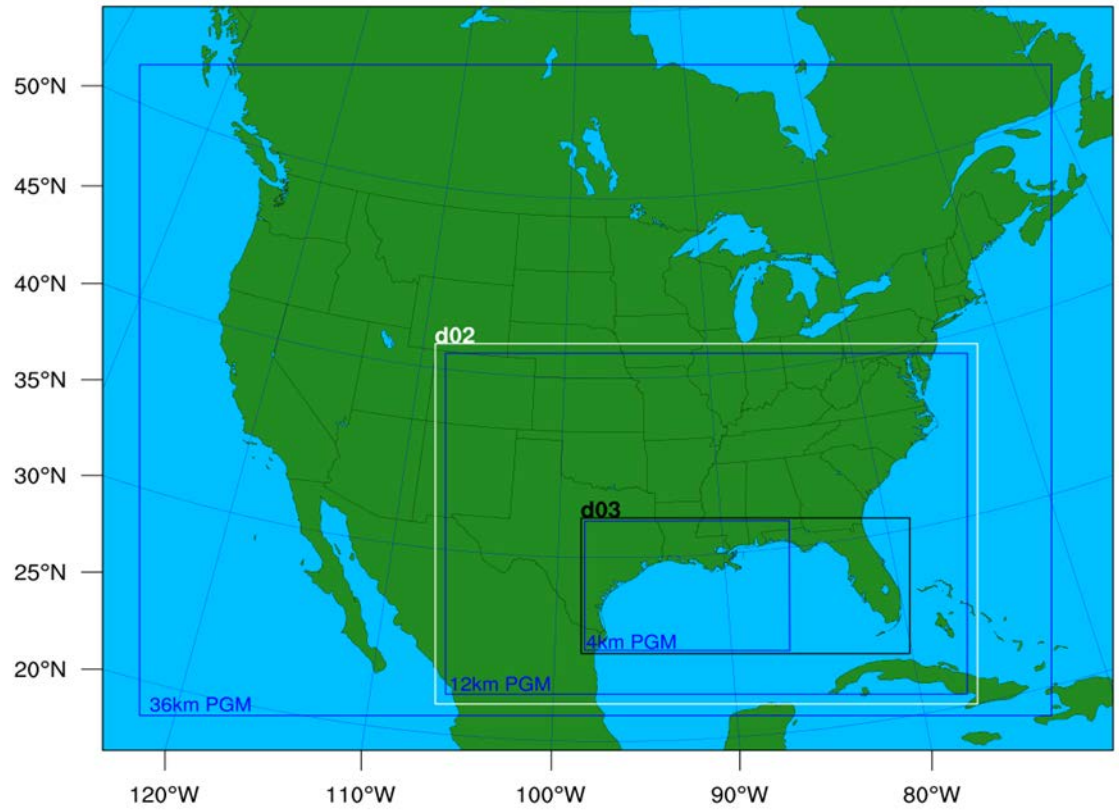

Figure 2-1. WRF 36-km CONUS (d01), 12-km SE Regional (d02), and 4-km GOMR (d03) Domains

2.2.3 Model Application

The GOMR meteorological modeling used the publicly available version of WRF, version 3.7. The WRF preprocessor programs GEOGRID, UNGRIB, METGRID, and OBSGRID were used to develop model inputs.

2.2.3.1 Model Vertical Resolution

The dataset was tested using both 33 and 37 vertical layers. Thirty-seven vertical layers allowed for higher vertical resolutions near the surface, which enabled the model to more accurately capture low-level inversions frequently present during winter. Additional layers in the mid-levels also allowed the model to more accurately recreate the convective updraft velocities seen in the summer months. The dataset model levels are shown in Table 2-2.

2.2.3.2 Topographic Inputs

Ramboll developed WRF's topographic information using the standard WRF terrain databases available from NCAR. The 36-km CONUS domain was based on the 10-minute (18 km) global data. The 12-km southeastern CONUS domain was based on the 2-minute (approximately 4 km) data. The 4-km GOMR domain was based on the 30-second (approximately 900 m) data.

2.2.3.3 Vegetation Type and Land Use Inputs

Ramboll developed vegetation type and land use information using the U.S. Geological Survey (USGS) land use database from the most recently released WRF databases with the WRF distribution. The number of land categories in the input data was the USGS default of 24. Ramboll used the standard WRF surface characteristics corresponding to each land use category.

2.2.3.4 Atmospheric Data Inputs

WRF relies on some other model or reanalysis output to provide initial and boundary conditions (IC/BC). Sensitivity tests were performed on several datasets to evaluate their effectiveness over the GOM. These datasets include the European Centre for Medium-Range Weather Forecasting Reanalysis (ERA)-Interim reanalysis product, available from the European Centre for Medium-Range Weather Forecasting (ECMWF) Data Portal website; Climate Forecast System Reanalysis (CFSR, ended in 2010) and Climate Forecast System model version 2 (CFSv2, after 2010) (Saha et al., 2014); and 12-km North American Model (NAM) archives available from the National Climatic Data Center (NCDC) NOAA National Operational Model Archive and Distribution System (NOMADS) server.

Ramboll chose the NAM dataset, because it had the lowest bias and error in model performance, and used it as first guess fields for WRF. Ramboll used the OBSGRID program to objectively reanalyze the dataset using traditional observation site data (meteorological towers) to the higher resolution of each WRF grid. These fields were then used to initialize the model and to conduct analysis nudging to guide the model to best match the observations.

Table 2-2. BOEM GOMR WRF Dataset Model Levels

Level	eta[a]	Pressure (mb)	Height (m)	Mid-Height (m)	Thickness (m)
0	1	1000	0.0		
1	0.9985	999	12.2	6.1	12.2
2	0.9970	997	24.5	18.4	12.2
3	0.9950	995	40.8	32.7	16.4
4	0.9930	993	57.2	49.0	16.4
5	0.9910	991	73.6	65.4	16.4
6	0.9880	989	98.3	85.9	24.7
7	0.9850	986	123.0	110.6	24.7
8	0.9800	981	164.3	143.6	41.3
9	0.9700	972	247.4	205.9	83.1
10	0.9600	962	331.2	289.3	83.8
11	0.9500	953	415.7	373.4	84.5
12	0.9400	943	500.8	458.2	85.1
13	0.9300	934	586.6	543.7	85.8
14	0.9100	915	760.5	673.5	173.8
15	0.8900	896	937.2	848.8	176.8
16	0.8700	877	1117.1	1027.1	179.8
17	0.8400	848	1392.8	1254.9	275.8
18	0.8000	810	1772.4	1582.6	379.6
19	0.7600	772	2166.7	1969.6	394.3
20	0.7200	734	2577.0	2371.9	410.3
21	0.6800	696	3005.0	2791.0	427.9
22	0.6400	658	3452.2	3228.6	447.3
23	0.6000	620	3921.0	3686.6	468.7
24	0.5500	573	4540.7	4230.8	619.8
25	0.5000	525	5203.7	4872.2	662.9
26	0.4500	478	5917.1	5560.4	713.4
27	0.4000	430	6690.5	6303.8	773.4
28	0.3500	383	7536.4	7113.5	846.0
29	0.3000	335	8472.3	8004.4	935.8
30	0.2500	288	9522.5	8997.4	1050.2
31	0.2000	240	10724.1	10123.3	1201.6
32	0.1500	193	12136.7	11430.4	1412.6
33	0.1000	145	13866.9	13001.8	1730.1
34	0.0600	107	15621.6	14744.2	1754.7
35	0.0270	76	17503.4	16562.5	1881.8
36	0.0000	50	19594.2	18548.8	2090.8

[a] WRF vertical coordinate

2.2.3.5 Time Integration

Adaptive time stepping was used to maximize the time step that the model can use while remaining numerically stable. The model time step was adjusted based on the domain-wide horizontal and vertical stability Courant-Friedrichs-Lewy (CFL) target value of 0.8.

2.2.3.6 Diffusion Options

There are three options in WRF for sixth-order diffusion: no diffusion, standard sixth-order diffusion, and Smagorinsky sixth-order diffusion. The standard sixth-order diffusion is not recommended by the developers of WRF. Therefore, Ramboll used a horizontal Smagorinsky first-order closure (km_opt = 4) with a sixth-order numerical diffusion and suppressed up-gradient diffusion (diff_6th_opt = 2).

2.2.3.7 Lateral Boundary Conditions

Lateral boundary conditions were specified from the initialization dataset on the 36-km domain with continuous updates nested from the 36-km domain to the 12-km domain, and from the 12-km domain to the 4-km domain using one-way nesting (feedback = 0).

2.2.3.8 Top and Bottom Boundary Conditions

The top boundary condition was an implicit Rayleigh dampening for the vertical velocity. Consistent with the model application for non-idealized cases, the bottom boundary condition was a physical, not free-slip.

2.2.3.9 Sea Surface Temperature Inputs

High-resolution sea surface temperature (SST) inputs help improve meteorological conditions for the overwater portions of the GOMR. The Fleet Numerical Meteorology and Oceanography Center (FNMOC) dataset, available from the Global Ocean Data Assimilation Experiment (GODAE) archives, was selected after extensive testing of several SST databases. The FNMOC high-resolution database is updated every six hours using satellite-derived (Advanced Very High Resolution Radiometer, or AVHRR) SST and in situ SST from ships and buoys with resolutions ranging from 12 km at the equator to 9 km at the mid-latitudes. The FNMOC SST database was chosen for the lowest SST bias and error in MPE tests, which used open-water observations from the National Data Buoy Center (NDBC) archives.

2.2.3.10 FDDA Data Assimilation

WRF was created as a forecast tool but can also be applied in “hindcast” mode. In forecast mode, the initial conditions for a run might be the most recent analysis (a gridded version of the current state of the atmosphere). In hindcast mode, we know the gridded state of the atmosphere and the SST at the beginning, during (every 6 hours), and at the end of the WRF run. These gridded datasets serve as the IC/BC. Using these BCs, an extra error term is introduced into the WRF equations, nudging the WRF atmosphere toward the real atmosphere. This is known as four-dimensional data assimilation (FDDA)—or analysis nudging—and is applied to every grid cell in the domain. It works best at larger grid spacing scales and for larger domains.

Observational nudging is the process of nudging just the single grid cell toward a single-point observation. The observation could be taken at a traditional meteorological tower, by a weather balloon, or by other non-traditional sources. Observation nudging works best at finer grid spacing scales and can be performed on higher-resolution domains using the Meteorological Assimilation Data Ingest System (MADIS) observation archive.

Ramboll ran the WRF model with analysis nudging and no observation nudging. For winds and temperature, analysis nudging coefficients of $5.0x10^{-4}$ and $3.0x10^{-4}$ were used on the 36- and 12-km domains, respectively. $3.0x10^{-4}$ is the default value, but Ramboll has had good success in the past using somewhat stronger nudging for winds. For water vapor mixing ratio, an analysis nudging coefficient of $1.0x10^{-5}$ was used for both the 36- and 12-km domains. Ramboll's previous experience WRF in the southeast U.S. has led to using a weaker nudging coefficient than the default to help avoid too much deep convection, which leads to an overprediction of precipitation. Ramboll applied analysis nudging of winds both near the surface and aloft, but did not perform nudging for temperature and mixing ratio in the lower atmosphere (i.e., within the boundary layer), a standard procedure for WRF modeling. Nudging within the boundary layer can interfere with the Planetary Boundary Layer (PBL) physics within WRF.

Ramboll used significant sensitivity testing to evaluate the impacts of observational nudging on the 4-km domain. The observational nudging coefficients for winds were tested at values set from 0 to $1.2x10^{-3}$ with a radius of influence at 50 km. Ramboll concluded that any observational nudging coefficient for winds above 0 caused excessive convection in the offshore portions of the GOM, resulting in an extreme overstatement of precipitation. Additionally, humidity nudging was tested at values ranging from 0 to $1.0x10^{-5}$. The lower nudging values also prevented excess moisture in the model, primarily through the summer months. Setting wind, temperature, and moisture coefficients all to 0 produced the most accurate precipitation results. These values are very similar to the nudging used in the USEPA 2011 CONUS WRF dataset (Gilliam and Pleim, 2010).

2.2.3.11 WRF Physics Options

The WRF model contains many different physics options. To achieve the best WRF performance in the dataset, Ramboll tested the model for the months of January and July 2012, evaluating various cumulus parameterizations, times between radiation physics calls, and land surface models. Table 2-3 lists the BOEM GOMR WRF physics options. These physics options were selected as the best performing options for the BOEM GOMR modeling based on our sensitivity tests.

Table 2-3. BOEM GOMR WRF Physics Options

Option	Scheme	Notes
Microphysics	Thompson	State-of-the-art microphysics model
Longwave Radiation	Rapid Radiative Transfer Model for General Circulation Models (RRTMG)	RRTMG includes random cloud overlap and improved efficiency over RRTM
Shortwave Radiation	RRTMG	Same as above, but for shortwave radiation
Land Surface Model (LSM)	Noah	Four-layer scheme with vegetation and sub-grid tiling
Planetary Boundary Layer (PBL) Scheme	Yonsei University (YSU)	YSU (Korea) Asymmetric Convective Model with non-local upward mixing and local downward mixing
Cumulus Parameterization	Kain-Fritsch in the 36-km and 12-km domains	Deep and shallow convection sub-grid scheme using a mass flux approach with downdrafts and convective available potential energy (CAPE) removal time scale

Option	Scheme	Notes
Analysis Nudging	Nudging applied to winds, temperature, and moisture in the 36-km and 12-km domains	Temperature and moisture nudged above PBL only
Observation Nudging	No nudging applied	Surface wind and moisture observational nudging can induce excessive convection, leading to increased rainfall
Surface Layer	Revised Mesoscale Meteorological Model version 5 (MM5) Monin-Obukhov scheme	In conjunction with YSU PBL scheme

2.2.3.12 WRF Application Methodology

Ramboll initialized the WRF model at 12Z every five days for calendar years 2010–2014. The model outputs results every 60 minutes, and the resulting output files were split at 12-hour intervals. Ramboll included 12 hours of spin-up in each five-day block before using the data in the subsequent evaluation.

2.3 WRF Model Performance Evaluation Results

Ramboll conducted a quantitative and qualitative evaluation of the BOEM GOMR WRF five-year simulation. The quantitative evaluation compared integrated surface hourly meteorological observations and offshore buoy observations with WRF predictions matched by time and location. The qualitative evaluation compared twice daily vertical profiles with upper-air data with WRF predictions matched by time and location and wind roses of coastal sites. Additionally, the evaluation compared monthly and daily total spatial precipitation fields based on observations and satellite with the WRF gridded monthly and daily total precipitation fields. The main features of the WRF simulation MPE are summarized below.

2.3.1 Quantitative Evaluation Using METSTAT

Ramboll performed a quantitative MPE of the BOEM GOMR WRF simulation using integrated hourly surface and onsite meteorological measurements and the publicly available Meteorological Statistical Program (METSTAT) software evaluation tool (Ramboll Environ US Corp. 2015). METSTAT calculates statistical performance metrics for bias, error, and correlation for surface winds, temperature, and mixing ratio (i.e., water vapor or humidity). To evaluate the performance of a meteorological model simulation for air quality model applications, a number of performance benchmarks for comparison are typically used. Table 2-4 lists the meteorological model performance benchmarks for simple (Emery et al., 2001) and complex (Kemball-Cook et al., 2005) situations. The simple benchmarks were developed by analyzing well-performing meteorological model evaluation results for simple, mostly flat terrain conditions and simple meteorological conditions (e.g., stationary high pressure). These evaluations were mostly conducted to support air quality modeling studies (e.g., ozone SIP modeling). The complex benchmarks were developed during the Western Regional Air Partnership's (WRAP's) regional haze modeling and are performance benchmarks for conditions such as the complex terrain of the Rocky Mountains and Alaska (Kemball-Cook et al., 2005). McNally (2009) analyzed multiple annual runs that included complex terrain conditions and suggested an alternative set of benchmarks for temperature under more complex conditions. The purpose of the benchmarks is to understand how good or poor the results are relative to other model applications run for the U.S.

In this section, Ramboll compared the WRF meteorological variables to the benchmarks as an indication of the BOEM GOMR WRF model performance. These benchmarks include bias and error in temperature, wind direction, and mixing ratio, as well as the wind speed bias and root mean squared error (RMSE) between the models and databases.

Table 2-4. Meteorological Model Performance Benchmarks for Simple and Complex Conditions

Parameter	Emery et al. (2001)	Kemball-Cook et al. (2005)	McNally (2009)
Conditions	Simple	Complex	Both
Temperature Bias	≤ ±0.5 K	≤ ±2.0 K	≤ ±1.0 K
Temperature Error	≤ 2.0 K	≤ 3.5 K	≤ 3.0 K
Temperature IOA[a]	≥ 0.8	(not addressed)	(not addressed)
Humidity Bias	≤ ±1.0 g/kg	≤ ±0.8 g/kg	≤ ±1.0 g/kg
Humidity Error	≤ 2.0 g/kg	≤ 2.0 g/kg	≤ 2.0 g/kg
Humidity IOA	≥ 0.6	(not addressed)	(not addressed)
Wind Speed Bias	≤ ±0.5 m/s	≤ ±1.5 m/s	(not addressed)
Wind Speed RMSE	≤ 2.0 m/s	≤ 2.5 m/s	(not addressed)
Wind Speed IOA	≥ 0.6	(not addressed)	(not addressed)
Wind Direction Bias	≤ ±10 degrees	(not addressed)	(not addressed)
Wind Direction Error	≤ 30 degrees	≤ 55 degrees	(not addressed)

[a] IOA = index of agreement

The output from the BOEM GOMR WRF simulation was compared against the NCDC's global-scale, quality-controlled DS3505 integrated surface hourly observational (ISHO) data (Smith et al., 2011) and the NDBC's buoy database (NDBC, 2018) as verification data. Global hourly and synoptic observations are compiled from numerous sources into a single common ASCII format and common data model. The DS3505 database contains records of most official surface meteorological stations from airports, military bases, reservoirs/dams, agricultural sites, and other sources dating from 1901 to the present, and quality control has corrected well over 99 percent of the errors present in the original data. The NDBC database contains records of moored buoys, coastal-marine automated network stations, and other sources dating from 1970 to the present.

2.3.1.1 Quantitative Statistics

Ramboll calculated several statistical measures as part of the meteorological model evaluation. Additional plots and graphs present these statistics on both hourly and daily timeframes. These measures were calculated for wind speed, wind direction, temperature, and humidity at the surface. The various statistical measures used for this evaluation are described below.

The statistics used to evaluate meteorological model performance are all given in absolute terms (e.g., wind speed error in meters per second [m/s]) rather than in relative terms (percent error), as is commonly shown for air quality assessments. The major reason for this is that a very different significance is associated with a given relative error for different meteorological parameters. For example, a 10 percent error for wind speed measured at 10 m/s is an absolute error of 1 m/s, a minor error. Yet a 10 percent error for temperature at 300 K is an absolute error of 30 K, an unacceptably large error. On the other hand, pollutant concentration errors of 10 percent at 1 part per billion (ppb) or 10 parts per million (ppm) carry practically the same significance.

Statistical Measures

Mean Observation (M_o): Calculated from all sites with valid data (i.e., data not removed during QA/QC procedures) within a given analysis region and for a given time period (hourly or daily):

$$M_o = \frac{1}{IJ}\sum_{j=1}^{J}\sum_{i=1}^{I} O_j^i$$

Where O_j^i is the individual observed quantity at site i and time j, and the summations are over all sites (I) and over time periods (J).

Mean Prediction (M_p): Calculated from simulation results that are interpolated to each observation to calculate the mean observation (hourly or daily):

$$M_p = \frac{1}{IJ}\sum_{j=1}^{J}\sum_{i=1}^{I} P_j^i$$

Where P^i_j is the individual predicted quantity at site *i* and time *j*. Note that mean observed and predicted winds are vector-averaged (for east-west component *u* and north-south component *v*) to derive mean wind speed and mean resultant direction.

Least Square Regression: Performed to fit the prediction set to a linear model that describes the observation set for all sites with valid data within a given analysis region and for a given time period (daily or episode). The y-intercept *a* and slope *b* of the resulting straight-line fit is calculated to describe the regressed prediction for each observation:

$$P_j^i = a + bO_j^i$$

The goal is for a 1:1 slope and a 0 y-intercept (no net bias over the entire range of observations), as well as a regression coefficient of 1 (a perfect regression). The slope and intercept facilitate the calculation of several error and skill statistics described below.

Bias (B): Calculated as the mean difference in prediction-observation pairings with valid data within a given analysis region and for a given time period (hourly or daily):

$$B = \frac{1}{IJ}\sum_{j=1}^{J}\sum_{i=1}^{I}\left(P_j^i - O_j^i\right)$$

Gross Error (E): Calculated as the mean *absolute* difference in prediction-observation pairings with valid data within a given analysis region and for a given time period (hourly or daily):

$$E = \frac{1}{IJ}\sum_{j=1}^{J}\sum_{i=1}^{I}\left|P_j^i - O_j^i\right|$$

Note that the bias and gross error for winds are calculated from the predicted-observed residuals in speed and direction (not from vector components *u* and *v*). The direction error for a given prediction-observation pairing is limited to range from 0 to ±180°.

RMSE: Calculated as the square root of the mean squared difference in prediction-observation pairings with valid data within a given analysis region and for a given time period (hourly or daily):

The RMSE, as with the gross error, is a good overall measure of model performance. However, large errors are weighted heavily (due to squaring) because:

$$RMSE = \left[\frac{1}{IJ}\sum_{j=1}^{J}\sum_{i=1}^{I}\left(P_j^i - O_j^i\right)^2\right]^{1/2}$$

Large errors in a small subregion may produce a large RMSE even though the errors may be small and quite acceptable elsewhere.

It is important to analyze RMSE. For example, if RMSE is only estimated (and it appears acceptable), it could consist largely of the systematic component. This error might be removed through improvements in the model inputs or use of more appropriate options, thereby reducing the error transferred to the photochemical model. On the other hand, if the RMSE consists largely of the unsystematic component, this indicates that further error reduction may require model refinement (new algorithms, higher resolution grids, etc.), or that the model cannot fully address the phenomena to be replicated. It also provides error bars that may be used with the inputs in subsequent sensitivity analyses.

2.3.1.2 METSTAT Evaluation Using Integrated Surface Hourly Observations

WRF performance can be evaluated by comparing WRF-predicted meteorology with actual observed data. Actual observed data was obtained from the NCDC's DS3505 dataset, known as the integrated surface hourly observations. DS3505 stations are the "gold standard" for meteorological towers, both in terms of data quality and tower siting. Generally located at airports, these stations follow auditing, data monitoring, and tower siting guidelines. Comparison of WRF-predicted meteorology with the DS3505 data is shown using soccer plots. Soccer plots use two performance metrics as X-axis and Y-axis values (e.g., wind direction bias as the X-axis and wind direction error as Y-axis) along with performance benchmarks. The closer the symbols are to the zero origin, the better the model performance. These plots help illustrate when two WRF performance metrics fall within the benchmark lines.

Soccer plots can also demonstrate the month-to-month consistency of a WRF dataset. If the points all cluster tightly (as in Figures 2-2 and 2-3) with no outliers, such that the individual values cannot be read from the axes, then the performance from month-to-month was very consistent. If there is a spread to the points (as in Figure 2-4) then the shape and color of the points can give added information—a modest cold bias during winter months, in this case. A very small year-to-year variation in the wind direction bias can be seen in Figure 2-2, with 2014 having the least bias. Little systematic variation in statistics can be seen in Figure 2-12, except for a tendency for the same month from different years to behave similarly.

Figure 2-2 through Figure 2-5 present soccer plots of WRF performance in the 36-km domain for all months, from 2010 through 2014, evaluated against all DS3505 observations within d01. WRF wind direction performed very well, with the majority of months falling within the simple conditions threshold. WRF wind speed also performed very well with a small positive bias, which is slightly higher in winter months and slightly lower in summer months. In Figure 2-4, WRF temperature performed well, with a small negative (cool) bias for several winter months. WRF humidity performance shows all months within the simple conditions benchmark and a slightly positive (wet) bias in summer months, as compared to winter months.

Figure 2-6 through Figure 2-9 present soccer plots of WRF performance in the 12-km domain for all months, from 2010 through 2014, evaluated against all DS3505 observations within d02. Wind direction, wind speed, temperature, and humidity all performed exceptionally well, with nearly every month falling within the simple conditions benchmark.

Figure 2-10 through Figure 2-13 present soccer plots of WRF performance in the 4-km domain for all months, from 2010 through 2014, evaluated against all DS3505 surface observations within the 4-km domain. Wind direction performed well, with over half of all months falling within the simple conditions threshold. There is a small positive wind direction bias, ranging from 0.1 to 7.0 degrees, with no single season displaying a higher or lower wind direction bias than another.

Figure 2-11 displays satisfactory wind speed performance in the 4-km domain. Most months fall within the complex conditions threshold with a positive wind speed bias, ranging from 0.3 to 1.3 m/s. Wind speed bias is higher in the winter months compared to a lower bias in the summer months. During sensitivity testing of nudging coefficients, Ramboll found that any value above 0 (no nudging) caused

excess convection and rainfall to be produced over the offshore portions of the Gulf. By reducing the nudging coefficients, wind speed performance decreased slightly with several of the winter months falling outside the complex conditions benchmark. This result illustrates the complexity of land-sea interactions within the GOM and the difficulty in increasing performance statistics on coastal winds.

WRF temperature performed well in the 4-km domain with the majority of months falling within the simple conditions benchmark, as shown in Figure 2-14. A slight positive (warm) bias exists in several months due to WRF over-forecasting temperatures through the winter. Humidity performance was exceptionally strong, with all months falling within the simple conditions benchmark. A slight positive humidity bias exists but is higher for summer months, suggesting that the model incorporated too much moisture into summertime Gulf weather regimes. Overall, the WRF model performed exceptionally well in the 36-km and 12-km domains and well in the 4-km GOMR domain for onshore surface wind direction, wind speed, humidity, and temperature observation comparisons.

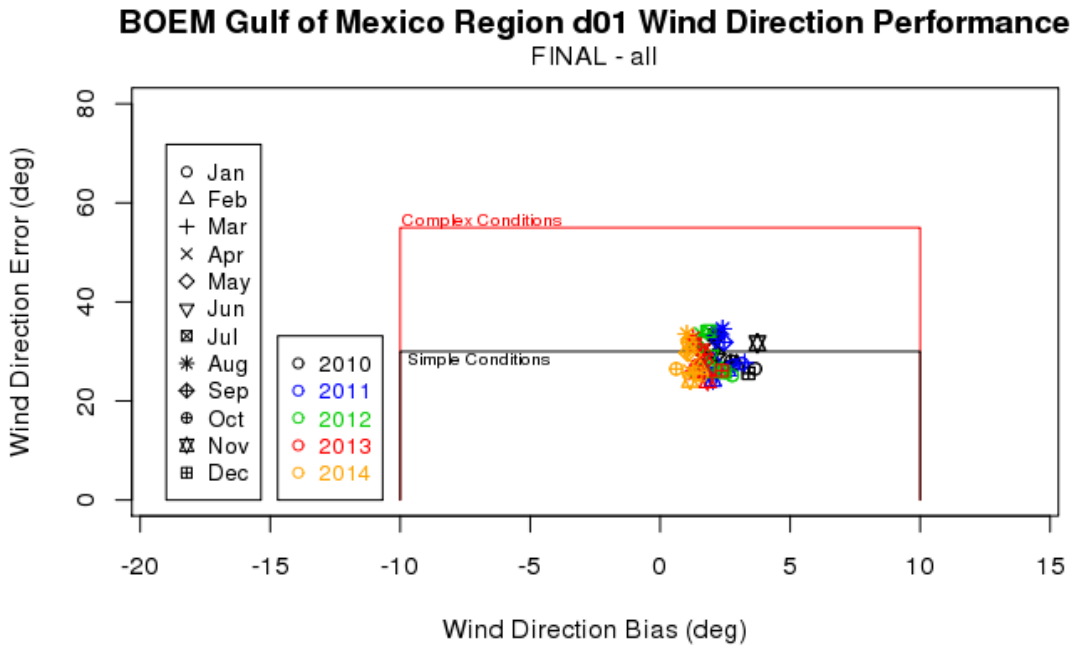

Figure 2-2. BOEM GOMR WRF 36-km METSTAT Wind Direction Performance
Note: Error shown is Gross Error (E)

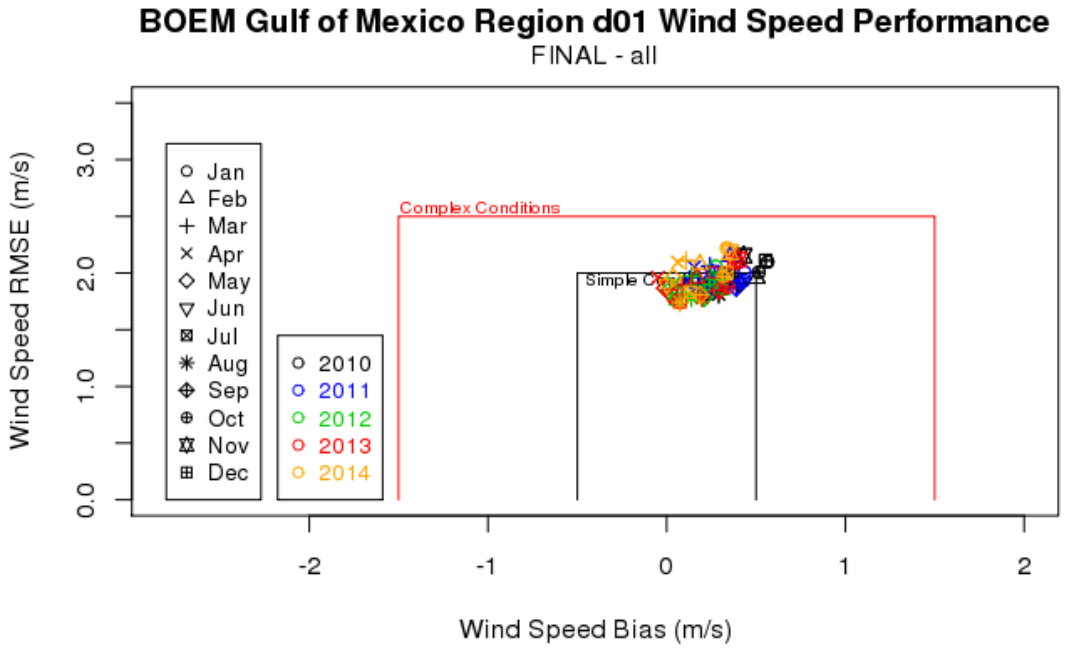

Figure 2-3. BOEM GOMR WRF 36-km METSTAT Grid Wind Speed Performance
Note: Error shown is Root Mean Squared Error (RMSE)

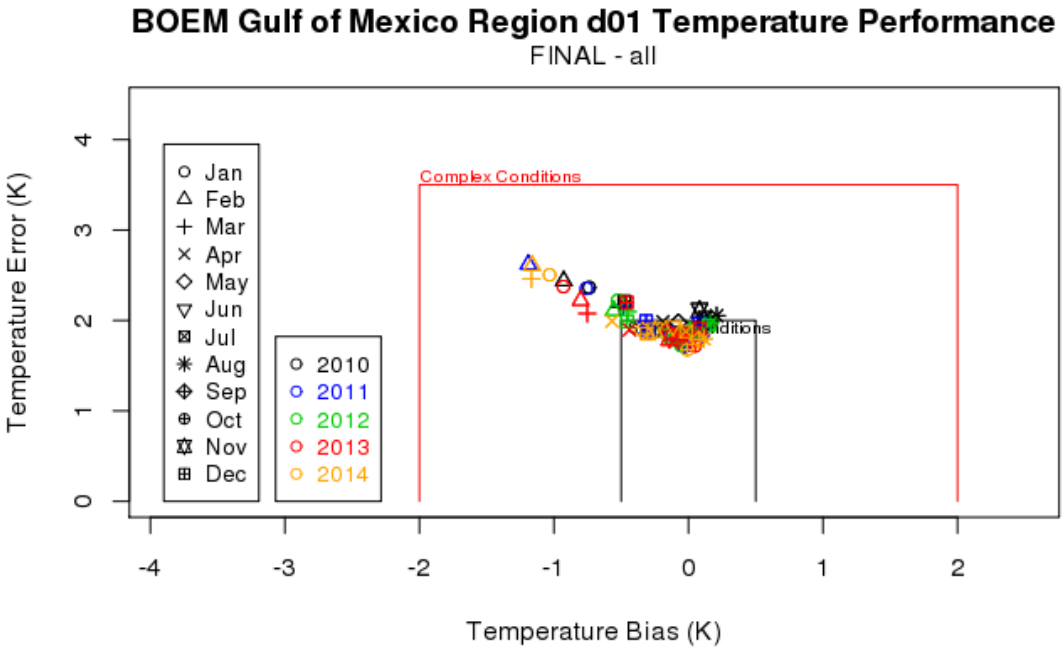

Figure 2-4. BOEM GOMR WRF 36-km METSTAT Temperature Performance
Note: Error shown is Gross Error (E)

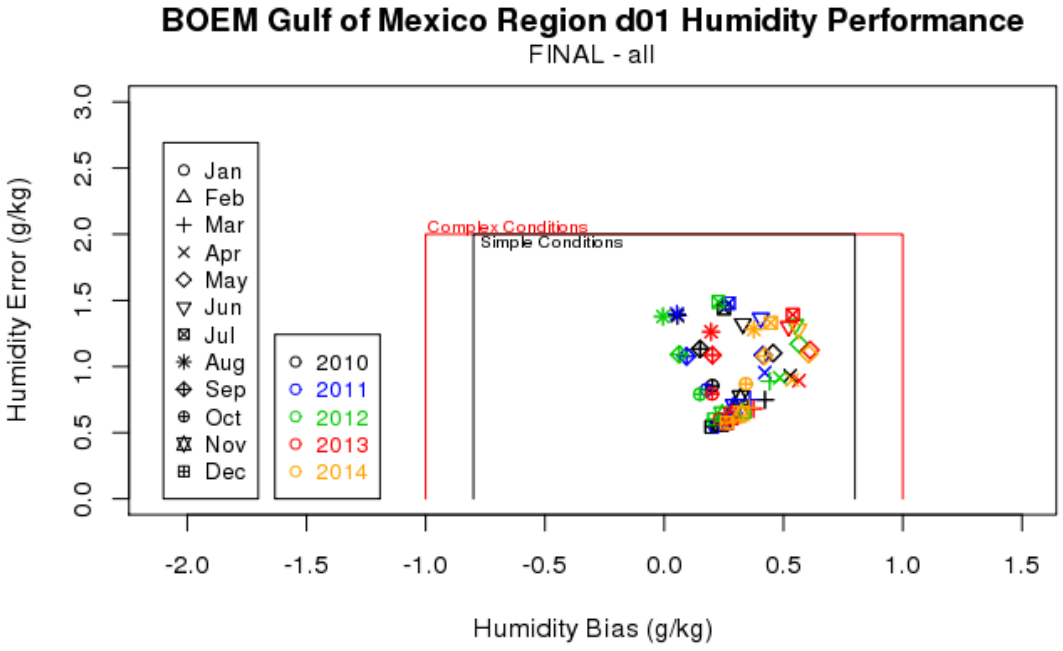

Figure 2-5. BOEM GOMR WRF 36-km METSTAT Humidity Performance
Note: Error shown is Gross Error (E)

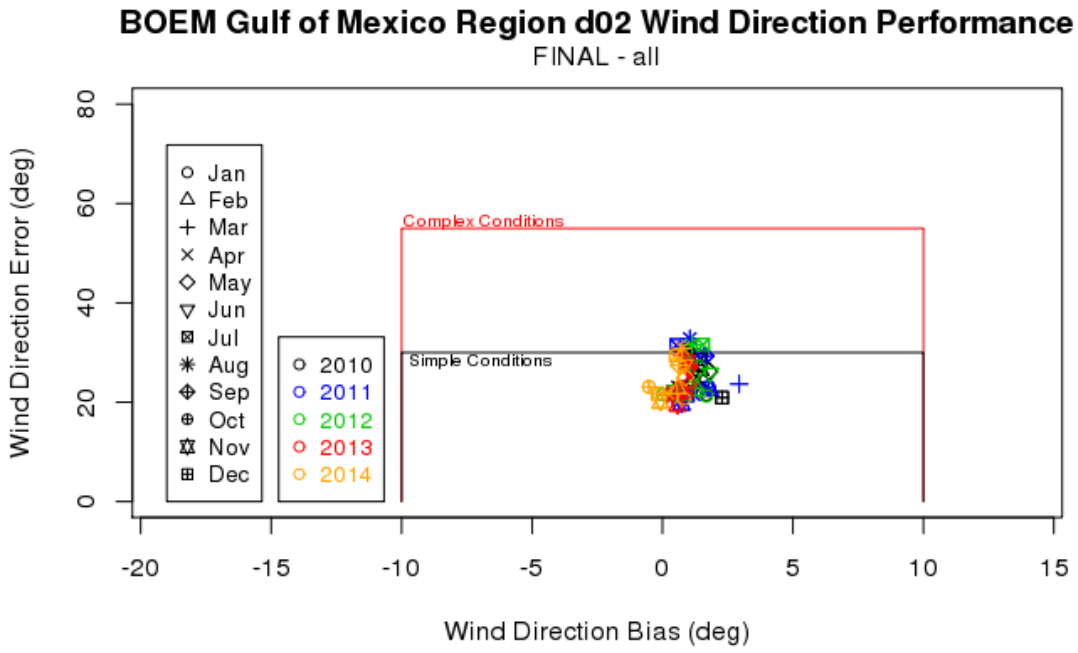

Figure 2-6. BOEM GOMR WRF 12-km METSTAT Wind Direction Performance
Note: Error shown is Gross Error (E)

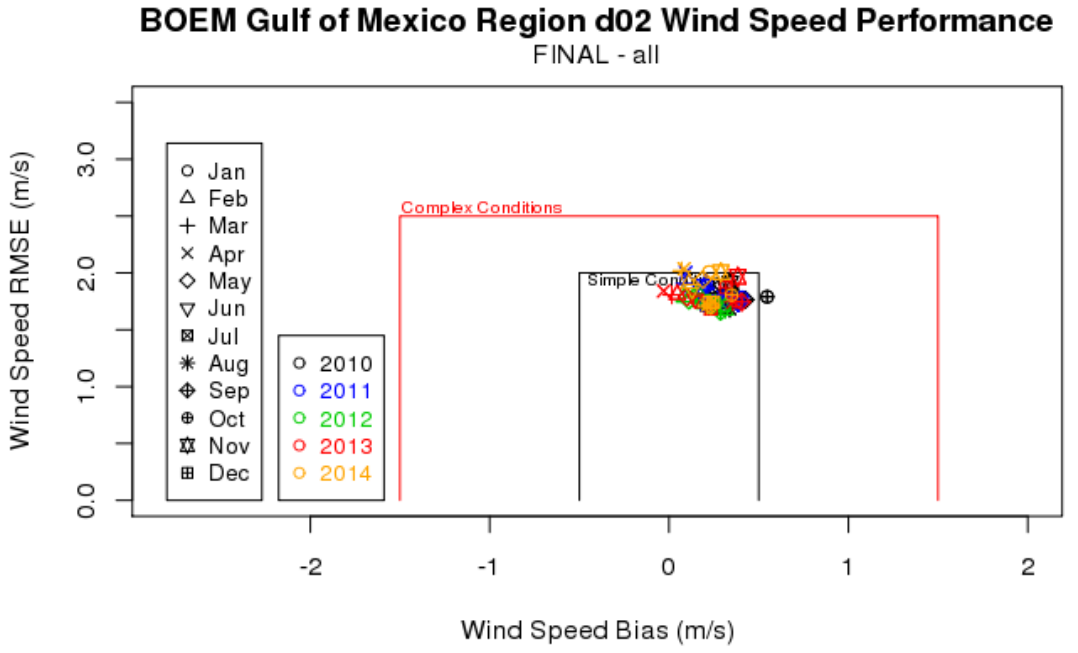

Figure 2-7. BOEM GOMR WRF 12-km METSTAT Wind Speed Performance
Note: Error shown is Root Mean Squared Error (RMSE)

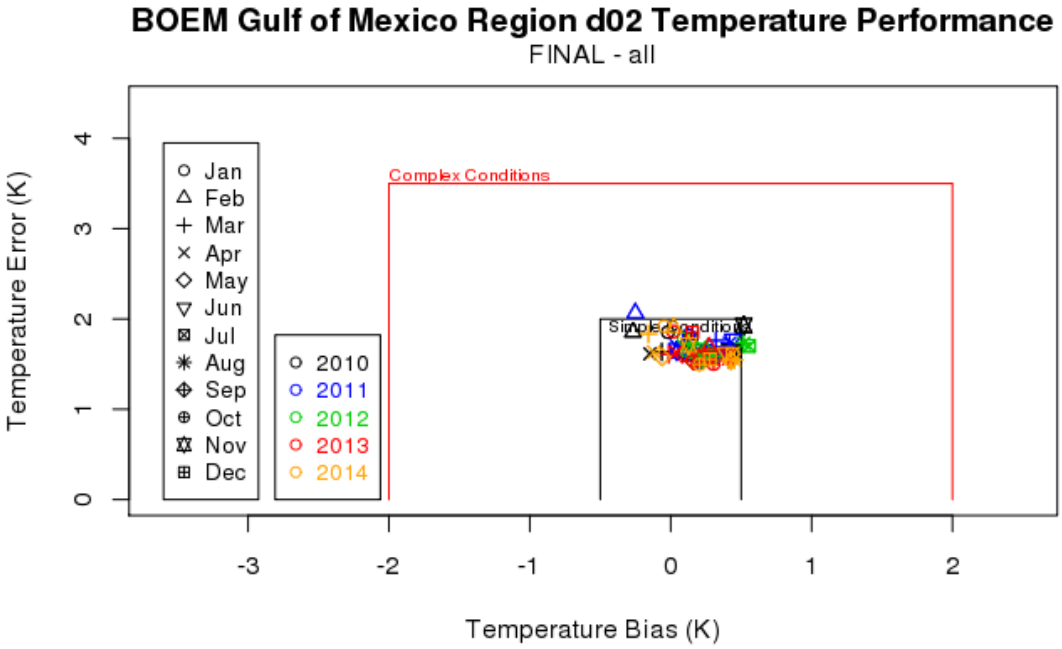

Figure 2-8. BOEM GOMR WRF 12-km METSTAT Temperature Performance
Note: Error shown is Gross Error (E)

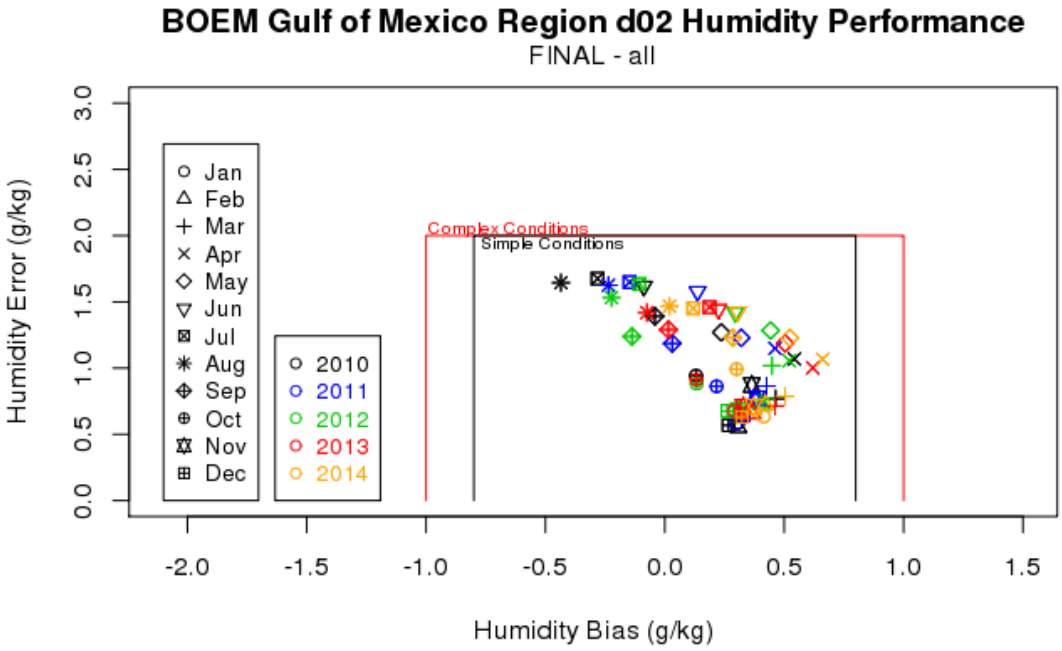

Figure 2-9. BOEM GOMR WRF 12-km METSTAT Humidity Performance
Note: Error shown is Gross Error (E)

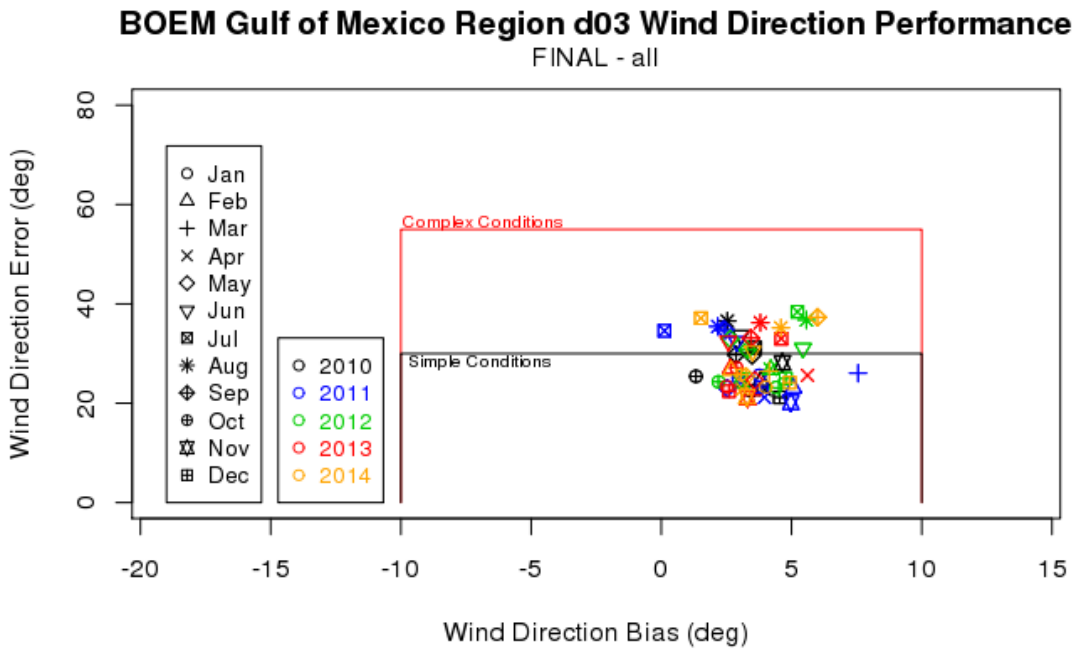

Figure 2-10. BOEM GOMR WRF 4-km METSTAT Wind Direction Performance
Note: Error shown is Gross Error (E)

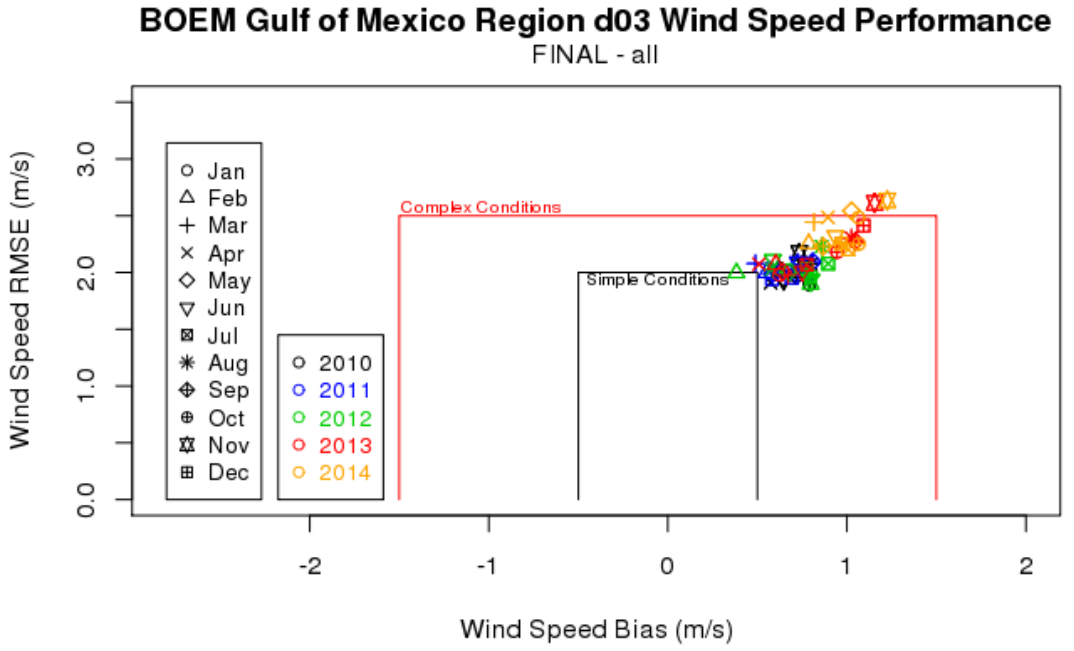

Figure 2-11. BOEM GOMR WRF 4-km METSTAT Wind Speed Performance
Note: Error shown is Root Mean Squared Error (RMSE)

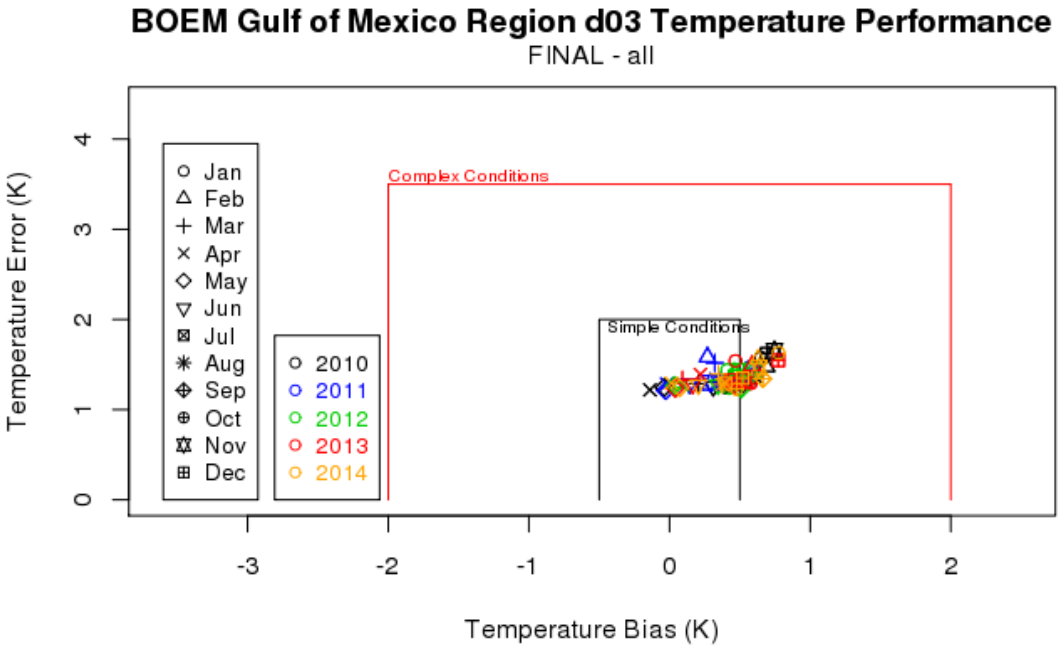

Figure 2-12. BOEM GOMR WRF 4-km METSTAT Temperature Performance
Note: Error shown is Gross Error (E)

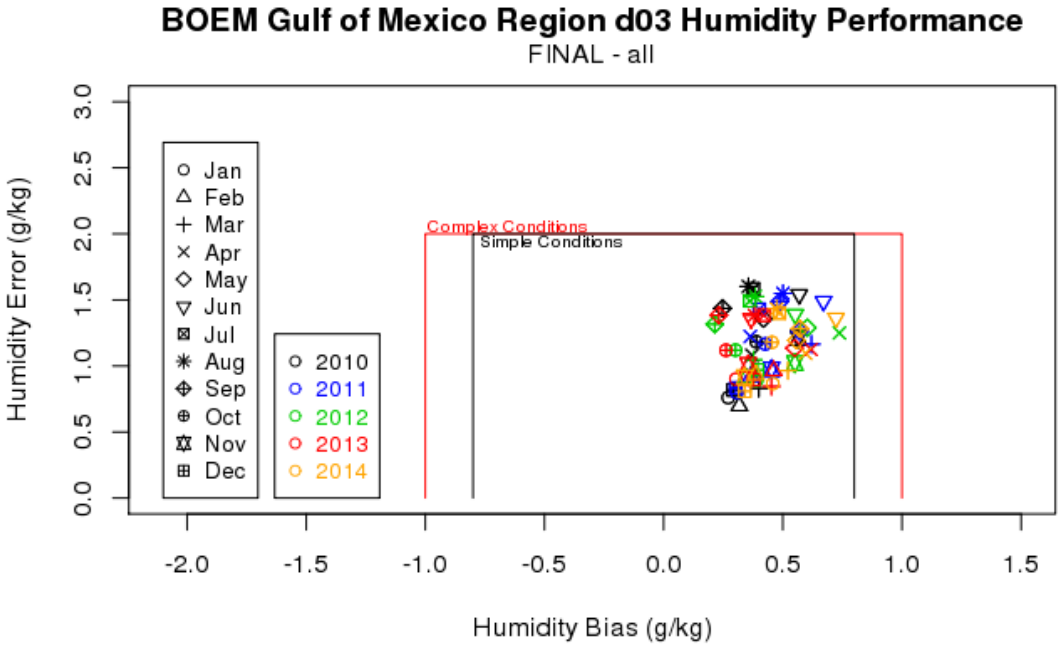

Figure 2-13. BOEM GOMR WRF 4-km METSTAT Humidity Performance
Note: Error shown is Gross Error (E)

2.3.1.3 METSTAT Evaluation Using Offshore Buoy Observations

Ramboll used METSTAT to evaluate WRF performance in the innermost 4-km domain using observations from meteorological buoys throughout the GOM, as shown in Figure 2-14. The hourly observations from 2010 through 2014 are stored in the NDBC archive and were downloaded and processed into a METSTAT readable format. Figure 2-15 through Figure 2-18 show the offshore METSTAT soccer plot results for BOEM GOMR.

WRF wind direction performed well, with over half of all months falling within the simple conditions benchmark. There is a slight positive wind direction bias, ranging from 0.1 to 6 degrees, which is very similar to the onshore METSTAT results in the 4-km domain. Wind speed performance was acceptable, with all months falling within the complex conditions benchmark. WRF displayed an increased (compared to onshore) positive wind speed bias of 0.4 to 1.2 m/s. The difficulties in measuring wind speeds and directions offshore, using buoys that bob and rotate and are not stationary like onshore meteorological towers, may lead to more variance in the measurements themselves. More variance in the measurements would lead to higher RMSE and gross errors when comparing WRF data to buoy observations. This might explain why the offshore wind direction and wind speed METSTAT results are not quite as good as those onshore. There are also fewer stations offshore to average for each month, leading to more outliers.

Some buoys also have lower anemometer heights (the height above the water where the wind measurements are taken) than the standard 10-m towers found onshore. Due to the difficulties in "correcting" a wind speed measurement to an equivalent 10-m high measurement, METSTAT compares the WRF wind speed at 10 m to the observed wind speed as if it were taken at 10 m. This can lead to an artificial increase in wind speed bias, which would depend on the actual anemometer height of each buoy.

Temperature performance is shown in Figure 2-20. Temperature bias and error are slightly higher (warmer) in the winter months compared to the summer months, suggesting that the model is over-forecasting surface temperatures or is influenced by the SST database input to WRF. WRF temperature predictions still performed well, even with the slightly higher biases.

Humidity performed well, with a majority of months falling within the simple conditions benchmark. A slightly higher positive (wet) bias exists in the summer months, compared to the winter months. Overall, the offshore METSTAT evaluation is very similar to the onshore evaluation, suggesting consistent performance over both the land and sea portions of the GOMR.

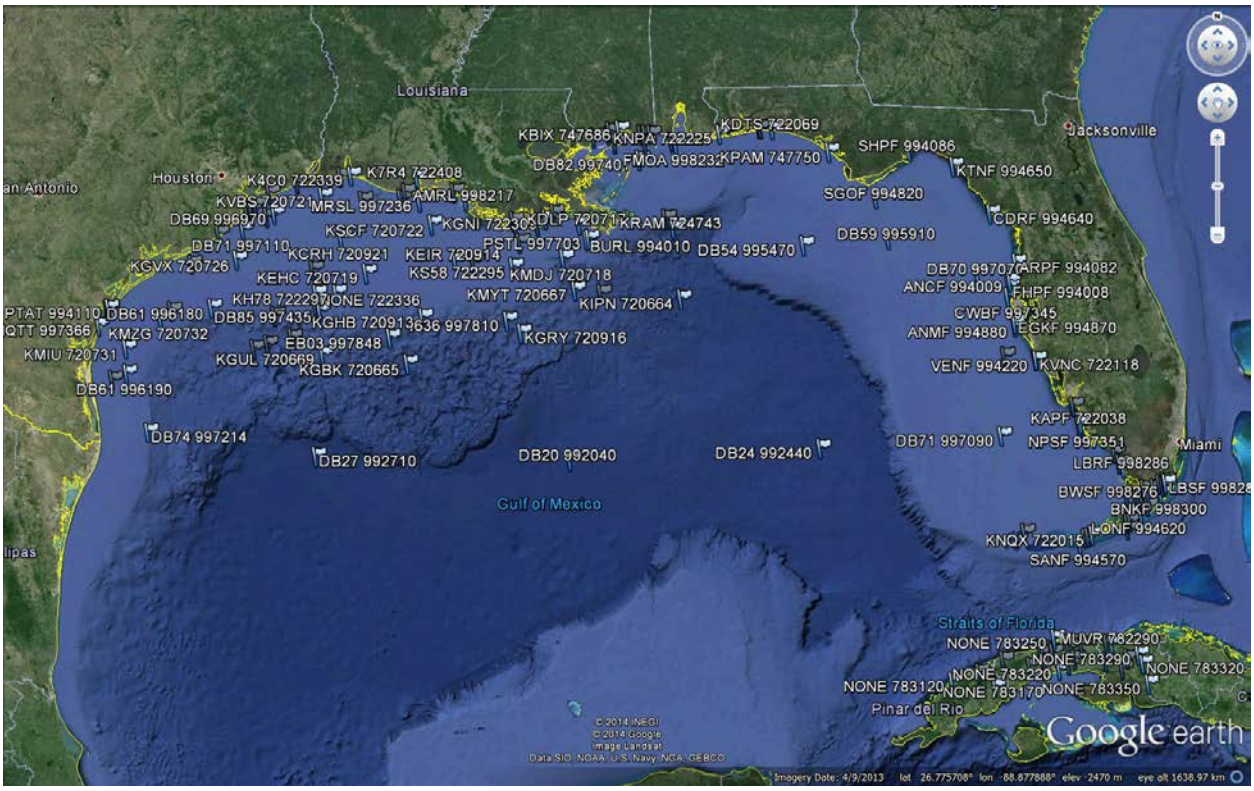

Figure 2-14. NDBC Meteorological Buoy Locations Used in Offshore METSTAT Analysis

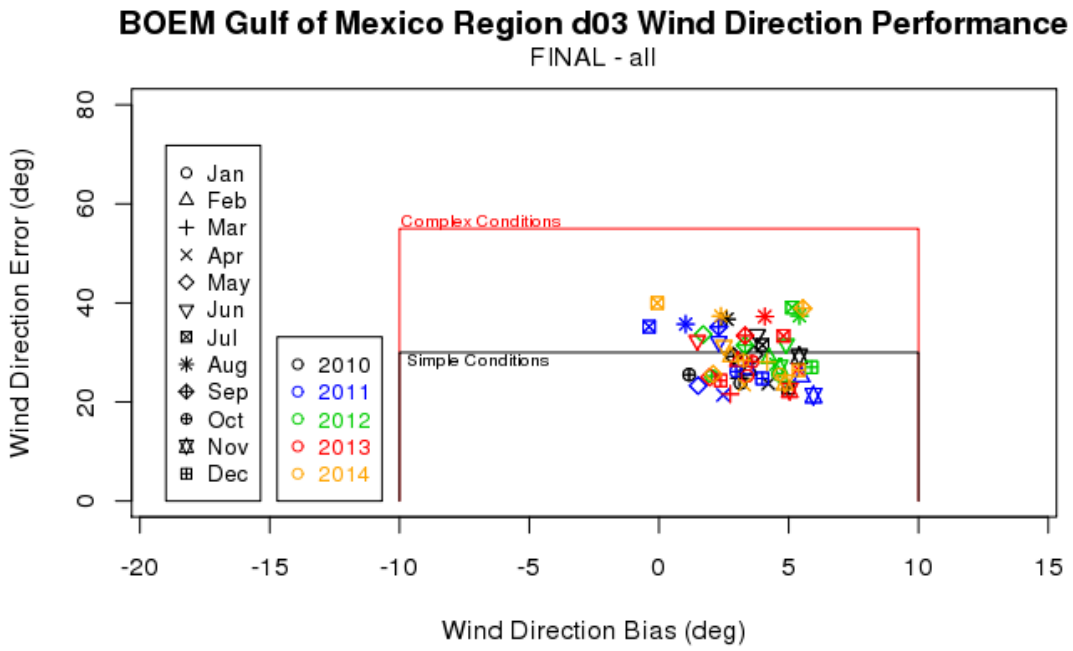

Figure 2-15. BOEM GOMR WRF Offshore 4-km METSTAT Wind Direction Performance
Note: Error shown is Gross Error (E)

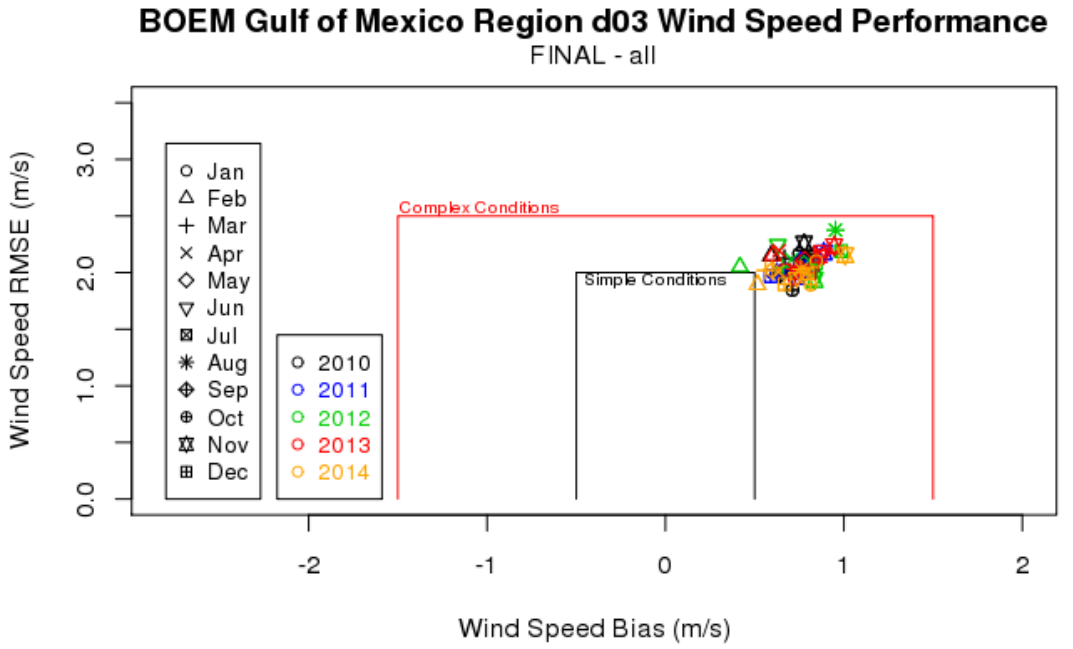

Figure 2-16. BOEM GOMR WRF Offshore 4-km METSTAT Wind Speed Performance
Note: Error shown is Root Mean Squared Error (RMSE)

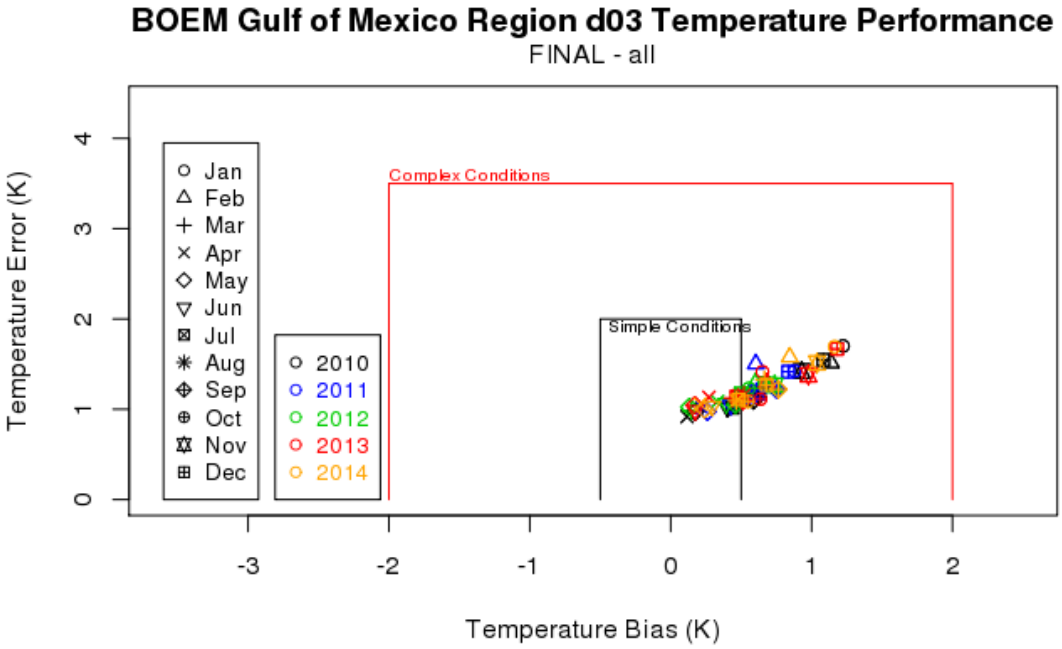

Figure 2-17. BOEM GOMR WRF Offshore 4-km METSTAT Temperature Performance
Note: Error shown is Gross Error (E)

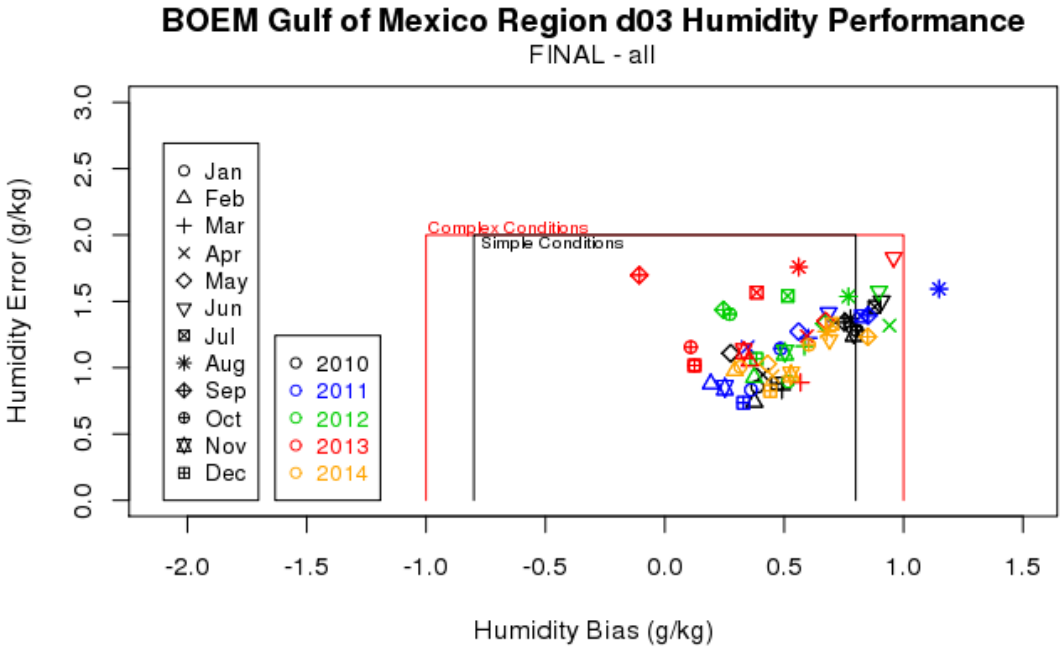

Figure 2-18. BOEM GOMR WRF Offshore 4-km METSTAT Humidity Performance
Note: Error shown is Gross Error (E)

2.3.2 Qualitative Evaluation Using Wind Roses

Ramboll chose 11 coastal sites surrounding the GOMR and seven ocean buoys to evaluate the frequency and intensity of onshore and offshore wind flow and WRF's performance at the land-sea interface. Figure 2-19 presents 2010–2014 average wind rose observations at each of these sites, which were obtained from the NCDC's quality-controlled D3505 meteorological dataset. Figure 2-20 shows wind roses displaying modeled surface wind speed and direction from the 2010–2014 4-km WRF domain dataset using the Mesoscale Model Interface (MMIF) program (Brashers and Emery, 2015). Overall, observed and modeled wind speeds and directions are in general agreement at most sites shown in Figures 2-19 and 2-20. Although model-measurement agreement is not perfect at any site, WRF is able to reproduce the most prevalent wind directions and wind speeds across much of the region.

At coastal sites, WRF performs satisfactorily at forecasting the frequency and intensity of onshore and offshore wind flow. In Texas and western Louisiana, onshore wind flow is dominant during this five-year period, which is well-predicted in WRF. Observed wind direction is more variable along the northern GOMR coast, with onshore and offshore flow more prevalent than east-west flow. WRF predicts more evenly distributed wind directions compared to observations at these sites, which may be related to challenges associated with simulating the complicated mix of land types (e.g., ocean, bay, delta, land) in the region. In western Florida, onshore and offshore winds are the most common wind directions in both observations and WRF. Similar to the northern GOMR, WRF predicts a more even distribution of wind directions compared to observations but still predicts that east-west flow is more common than north-south flow. The tendency for WRF to predict a more even wind direction distribution compared to observations may be related to how wind directions are observed and recorded. WRF can simulate winds from any direction with high resolution, whereas observations may be limited to set number of wind direction reporting bins, which are inherently coarser.

Overall, WRF does not clearly overestimate or underestimate onshore and offshore flow in the GOMR. Over the ocean, winds are generally from the east or southeast in the southern GOMR, which is well-predicted in WRF. WRF captures the overall tendency for lower wind speeds along the coast from central Louisiana to Florida, with higher wind speeds over the open ocean. However, WRF somewhat underpredicts the highest wind speeds over the open ocean. WRF also somewhat overpredicts the wind speeds along the Texas coast, especially near Corpus Christi, and predicts too much onshore flow along the southwest coast of Florida.

Figure 2-21 through Figure 2-26 provide a more direct comparison between observed and modeled wind speed and direction at each site between 2010 and 2014. Overall, WRF performs well at forecasting the frequency and intensity of onshore and offshore wind flow at the coastal sites.

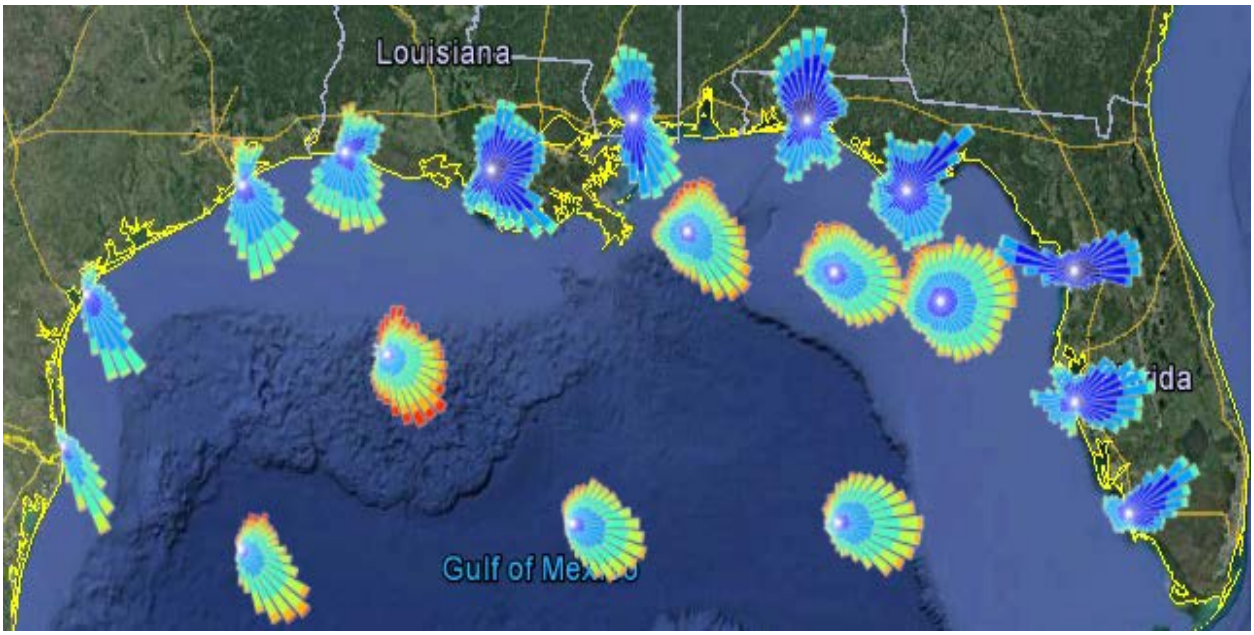

Figure 2-19. Wind Rose Observations in the GOM

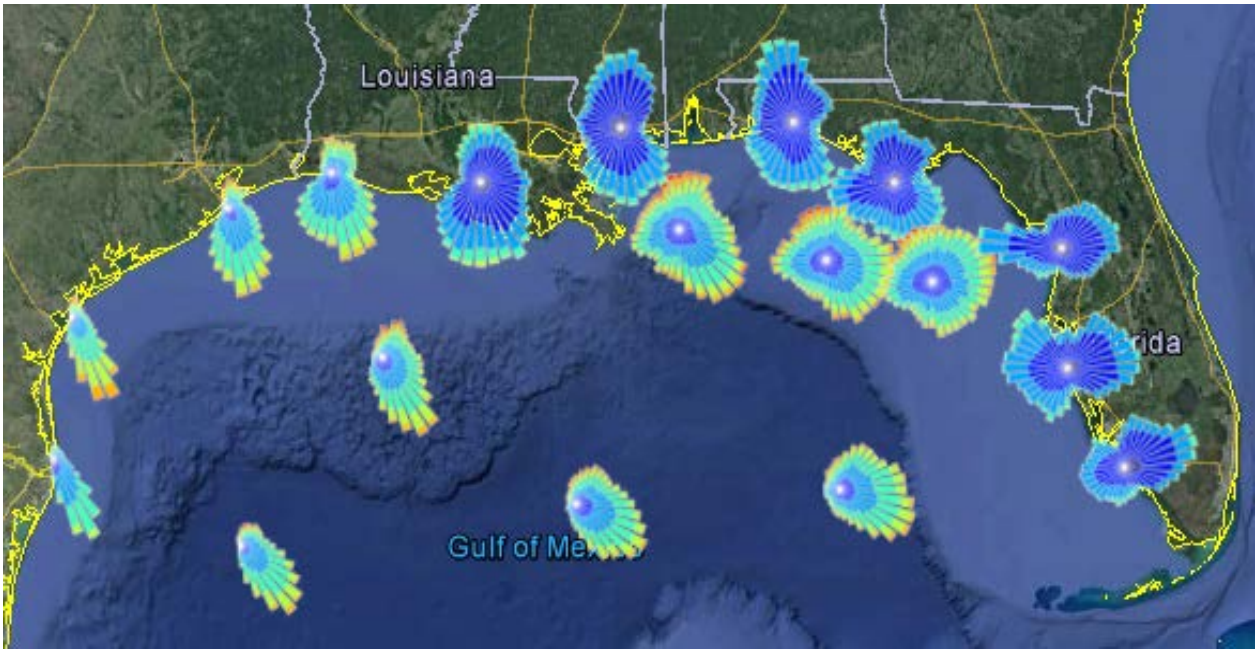

Figure 2-20. Wind Rose WRF Estimates in the GOM

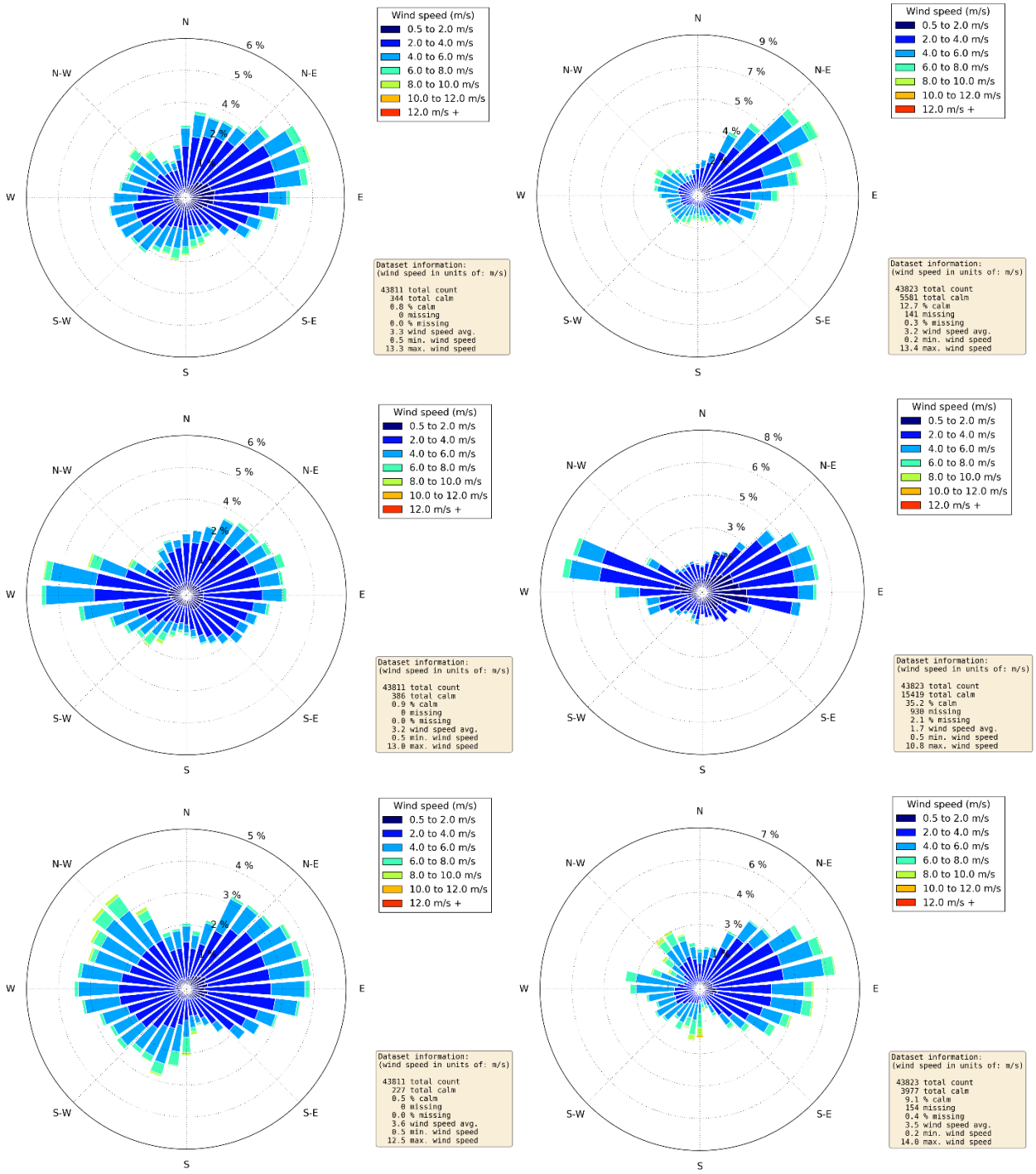

Figure 2-21. 2010–2014 Wind Roses of WRF Winds (left) Compared to Observed Winds (right) from Naples, FL (KAPF) (top); Crystal River, FL (KCGC) (middle); and Sarasota, FL (KSRQ) (bottom)

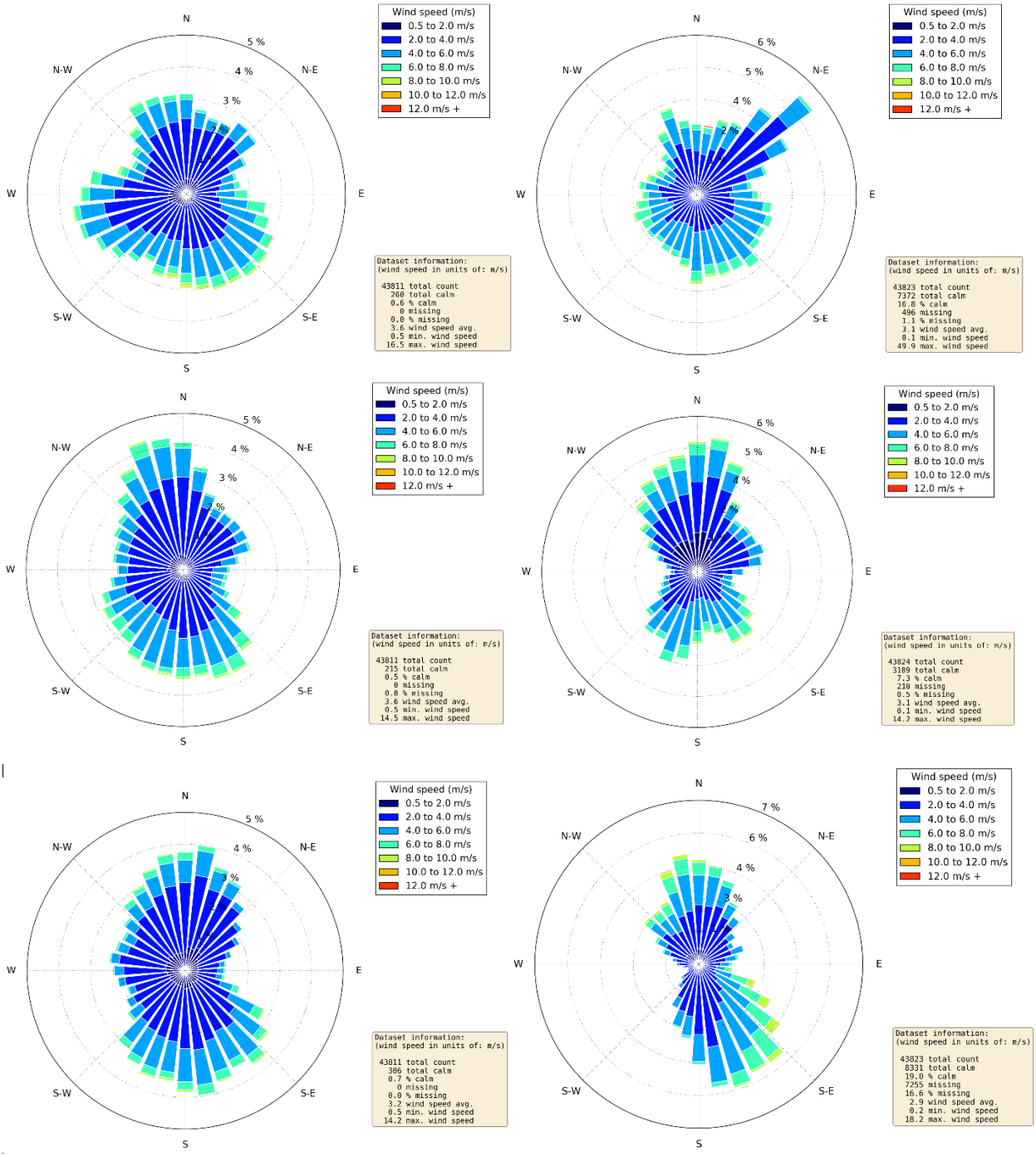

Figure 2-22. 2010–2014 Wind Roses of WRF Winds (left) Compared to Observed Winds (right) from Apalachicola, FL (KAAF) (top); Eglin Air Force Base, FL (KVPS) (middle); and Gulfport, MS (KGPT) (bottom)

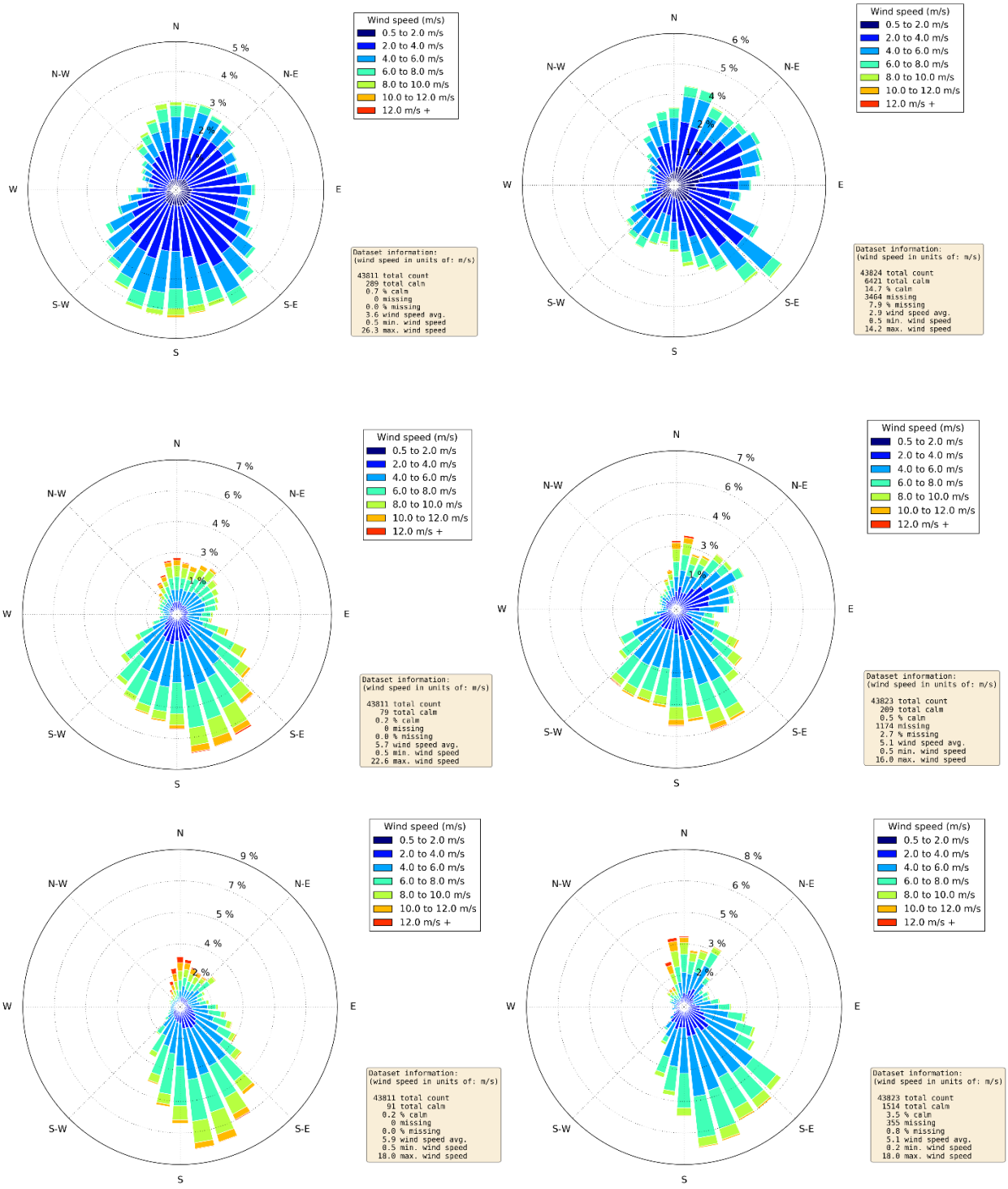

Figure 2-23. 2010–2014 Wind Roses of WRF Winds (left) Compared to Observed Winds (right) from Patterson, LA (KPTN) (top); Calcasieu, LA (CAPL) (middle); and Galveston, TX (KGLS) (bottom)

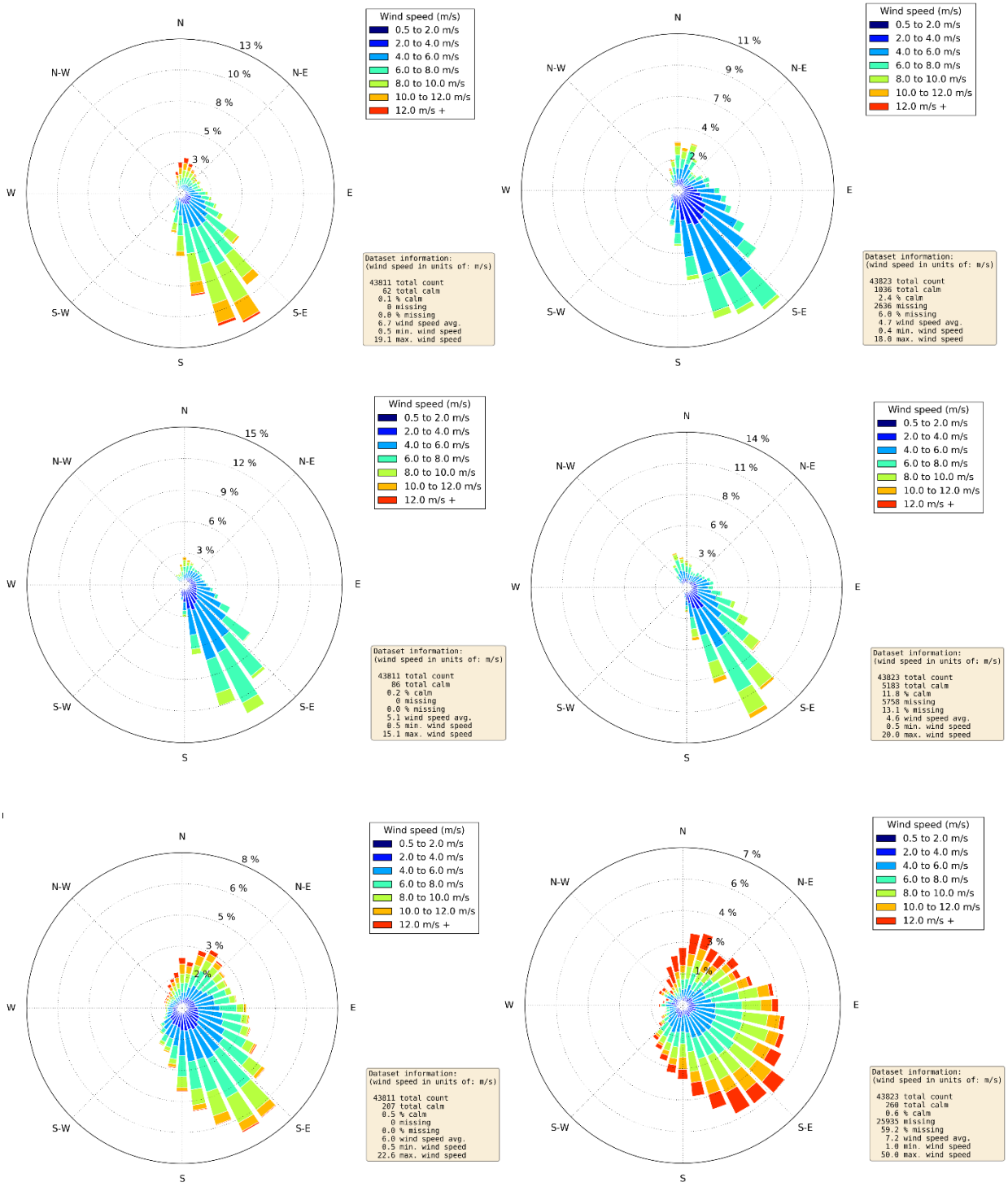

Figure 2-24. 2010–2014 Wind Roses of WRF Winds (left) Compared to Observed Winds (right) from Port Aransas, TX (KRAS) (top); Port Isabel, TX (PTIT) (middle); and Ocean Buoy EB03 (bottom)

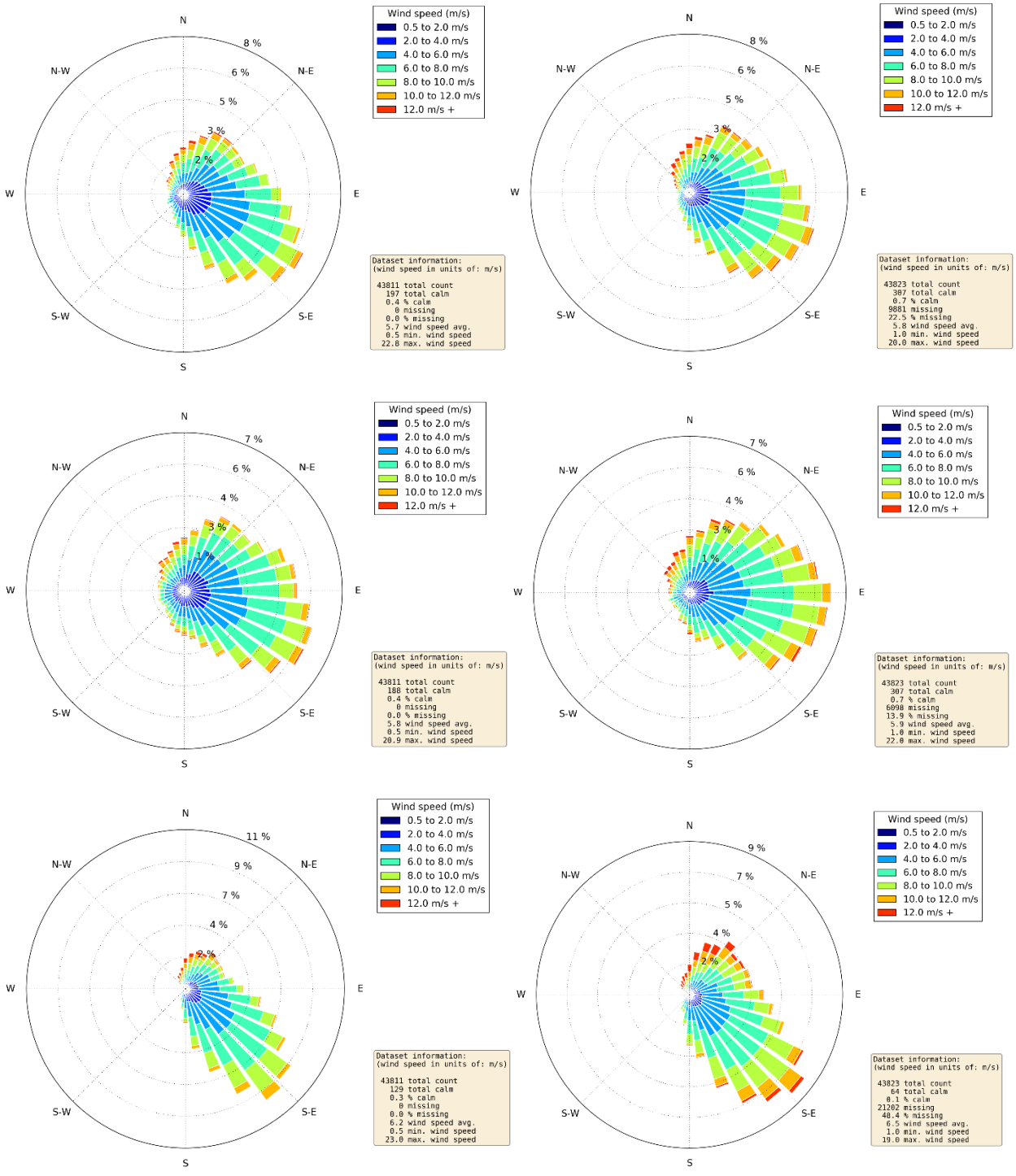

Figure 2-25. 2010–2014 Wind Roses of WRF Winds (left) Compared to Observed Winds (right) from Buoys DB20 (top), DB24 (middle), and DB27 (bottom)

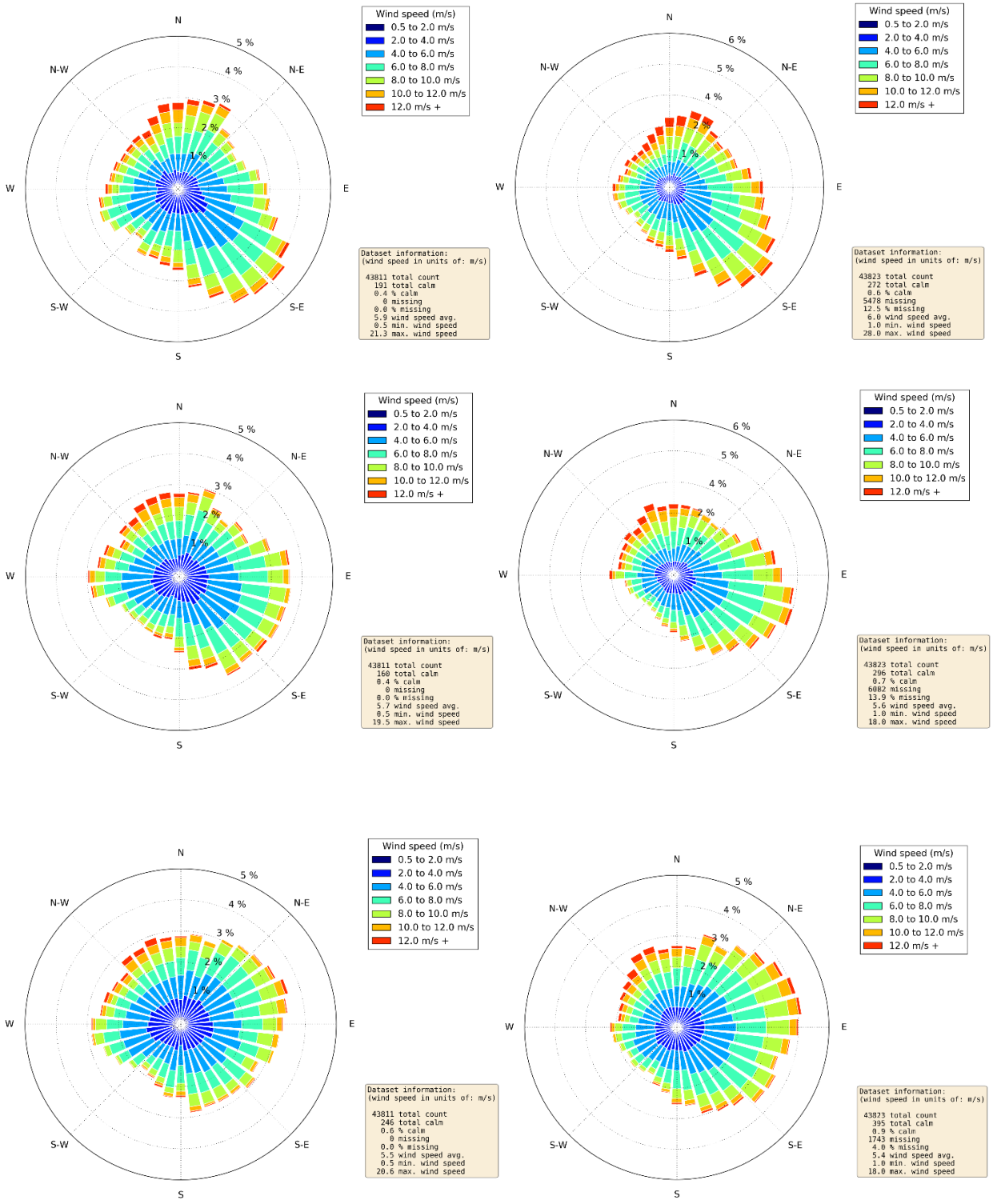

Figure 2-26. 2010–2014 Wind Roses of WRF Winds (left) Compared to Observed Winds (right) from Buoys DB50 (top), DB54 (middle), and DB59 (bottom)

2.3.3 Qualitative Evaluation Using Upper-Air Data

Ramboll created plots of the temperature, dew point, and wind speed sounding profiles for the vertical atmosphere for several observation sites—including Brownsville, Texas (KBRO); Slidell, Louisiana (KSIL); Tampa, Florida (KTPA); and Key West, Florida (KEYW)—and their corresponding WRF data points. A quasi-random selection of upper-air profiles was taken from the dataset to sample several different atmospheric situations. Dates of sounding analyses were chosen to span all typical states of the PBL throughout the modeling period. Preference was also given to days that included high 8-hour ozone events and complete or mostly complete sounding data Ramboll qualitatively compared these, paying particular attention to how well the WRF model reproduces the observed near-surface inversion layers.

It should be noted that these and other upper-air soundings were used in the WRF nudging. It is not surprising, therefore, that WRF mimics the profiles well. Given that fact, and the qualitative nature of the assessment, a more in-depth upper-air assessment is not warranted.

The National Weather Service (NWS) collects and maintains the KBRO, KSIL, KTPA, and KEYW radiosonde datasets. Radiosondes are launched from each location twice per day at approximately 00 and 12 UTC. Radiosondes provide high-resolution vertical profiles of temperature, humidity, wind speed, and wind direction throughout the troposphere. NOAA's Earth System Research Laboratory makes the data publicly available (NOAA-ESRL, 2015). Ramboll downloaded and stored the radiosonde data twice daily from 2010 to 2014 for each upper-air station in Forecast Systems Laboratory (FSL) format (a total of over 14,000 soundings) to compare the WRF model datasets.

For the qualitative analysis, Figure 2-27 to Figure 2-42 show a sampling of plots with the vertical profiles of temperature and humidity, as well as wind speed profiles, which Ramboll prepared using the observational and 4-km WRF dataset and the FSL sounding dataset. The analysis focuses on how well the WRF model reproduces the vertical atmosphere structure using upper-air observations from the selected sites within the 4-km domain that have timeframes that overlap with the WRF model. After viewing the plots created but not shown in this report (too many to include), some representative soundings were selected to demonstrate WRF performance during various typical boundary layer structures. In general, the model performed well, with model forecasts matching observed temperature and humidity profiles for the four locations, including observed inversions.

The left panel in Figure 2-27 shows a morning temperature sounding for Brownville, Texas. WRF forecasts the depth and height of the temperature inversion—which extends from the surface to 180 m—very well. The right panel indicates that WRF overpredicted wind speeds within the inversion layer. The left panel of Figure 2-28 displays a weak elevated subsidence inversion during a summer evening. The model forecasts the base of the inversion well at around 900 m. In the right panel, WRF forecasts winds very accurately within the PBL on this evening.

In Figure 2-29, WRF predicts the height and depth of the surface inversion well for Slidell, Louisiana, in the left panel. WRF again slightly overpredicts winds speeds in the inversion layer, as shown in the right panel. The left panel of Figure 2-30 shows a saturated sounding from the surface to 4,000 m. The model forecasts the high moisture content very well throughout the sounding profile. The right panel indicates that WRF forecasts wind speeds accurately this time, though some observations near the surface are missing.

The left panel in Figure 2-31 displays a very dry sounding for Tampa, Florida. WRF accurately reproduces the large dew point depression throughout the sounding profile. The left panel of Figure 2-32 displays a strong surface inversion on a late fall morning. The model forecasts the height and depth of the inversion well, from the surface to 100 m above ground level. Again, WRF overpredicts low-level

windspeeds in the inversion layer but models all wind speeds very well during the stable conditions. Upper-air winds represent the observations well on both days.

In Figure 2-33, WRF forecasts the elevated subsidence inversion well, with a mixing height top at around 1,000 m on the left panel. The dry air above the inversion is also represented well in this evening sounding at Key West, Florida. On the right panel, WRF represents wind speeds accurately throughout this subsidence inversion, but slightly underpredicts wind speeds above it. The magnitude of the underprediction is small compared to the magnitude of the local peak in wind speed, indicating good agreement despite the slight underprediction.

Figure 2-34 and Figure 2-35 show vertical profiles for the morning soundings at Key West and Tampa, respectively, on January 15, 2010. This day included surface-based temperature inversions at these sites. WRF represented the inversions reasonably well, and closely matched upper-air temperature profiles. WRF represented humidity profiles well too, except for a dry bias above the PBL near Slidell. Forecasted wind speed profiles were moderately accurate, but at both sites WRF overpredicted wind speeds within the inversion layer and underpredicted wind speeds above it. In the lower PBL where most of the pollutants would be transported, the magnitude of the overprediction is quite modest.

Figure 2-36 to Figure 2-38 show vertical profiles for evening soundings during May 4, 2010, a high ozone day in the Houston-Galveston-Brazoria region(TCEQ, 2011). Sounding data was available at the Brownsville, Key West, and Tampa sites during this event. WRF forecasts the stable temperature profiles very well at these three sites, with a slight underprediction of surface temperature in Brownsville. WRF forecasts drier upper-air conditions than observed above Brownsville and Tampa, but generally models dew point profiles accurately as well. Wind speed profiles correspond very closely, except for a small surface wind speed underprediction in Tampa.

Figure 2-39 to Figure 2-42 show vertical profiles for the evening soundings during September 25, 2013, another example high ozone day in the Houston-Galveston-Brazoria region. WRF temperature and humidity profiles represent the stable temperature profiles very closely above Brownsville, TX, and Key West, FL, on this day. WRF wind speeds also matched the observations well at Brownsville and Key West during this ozone event. Above Slidell, WRF forecasts the temperature profile relatively accurately but forms a slight surface-level inversion that is not seen in the observations, while failing to form the subsidence inversion layer quite as strongly as observed. WRF also underpredicts boundary layer moisture near Slidell. Meanwhile, WRF overpredicts wind speeds throughout the boundary layer at Slidell. At the Tampa site, WRF overpredicts surface temperature and misses a slight subsidence inversion but represents the upper-air temperature profile well. WRF slightly overpredicts wind speeds below the inversion and overpredicts upper-air wind speeds near Tampa.

In general, WRF performs about the same (no better or worse) in periods and regions of higher observed ozone for the few samples shown here. WRF's performance is acceptable-to-good for all soundings shown.

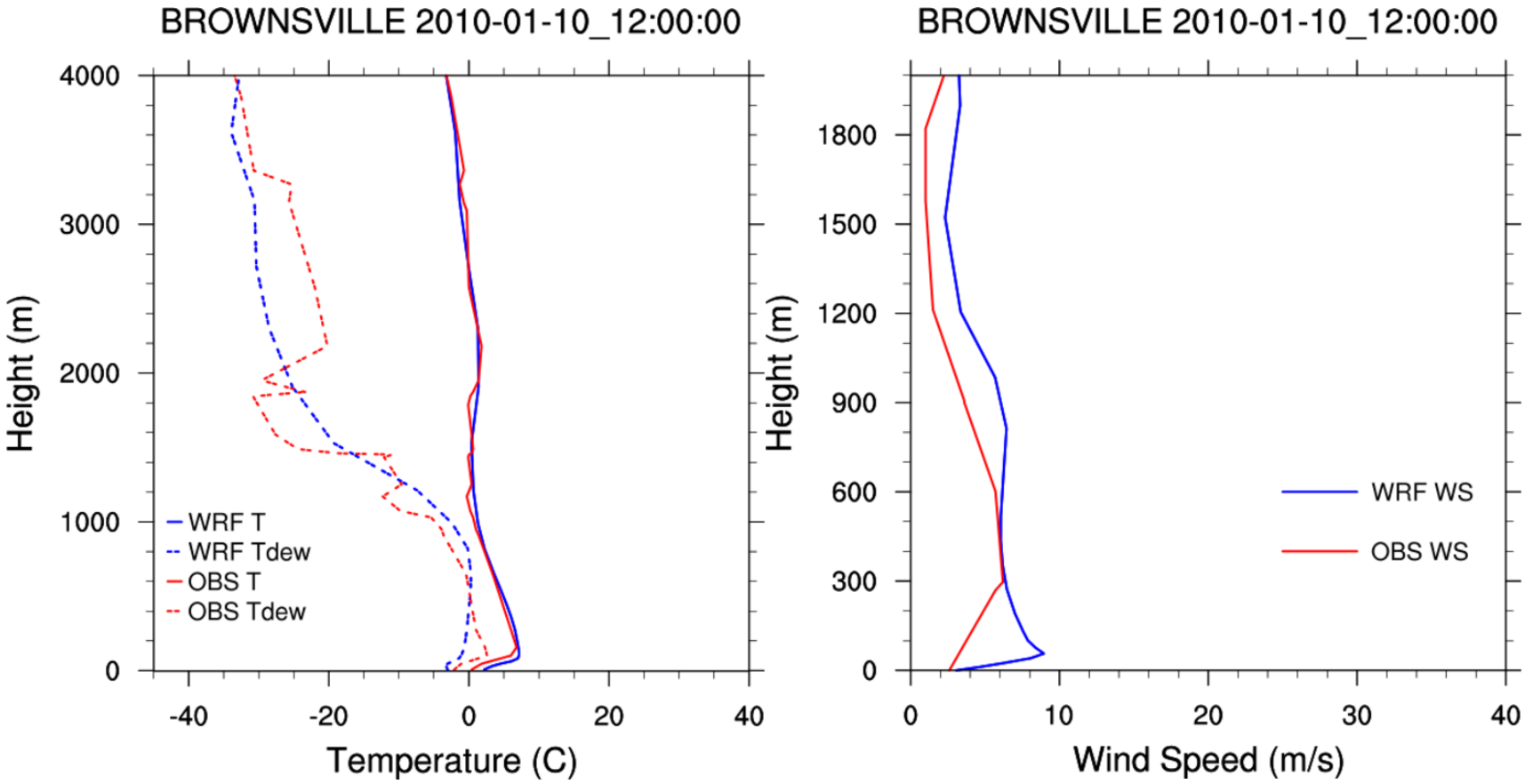

Figure 2-27. Vertical Profile Soundings Comparing the 4-km WRF (blue lines) to Upper-Air Observations Data (red lines) for Brownsville, TX, on January 10, 2010, at 12 UTC

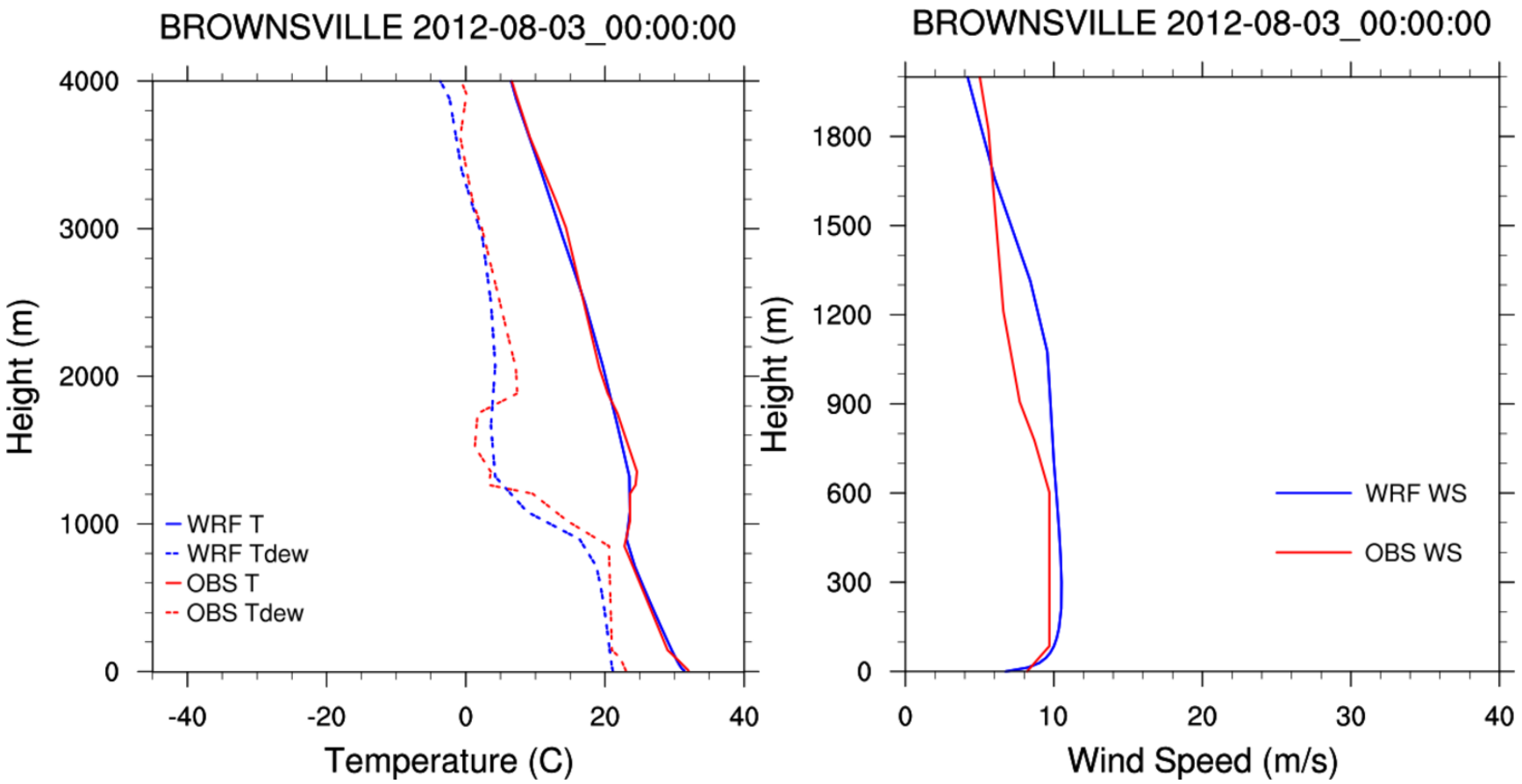

Figure 2-28. Vertical Profile Soundings Comparing the 4-km WRF (blue lines) to Upper-Air Observations Data (red lines) for Brownsville, TX, on August 3, 2012, at 00 UTC

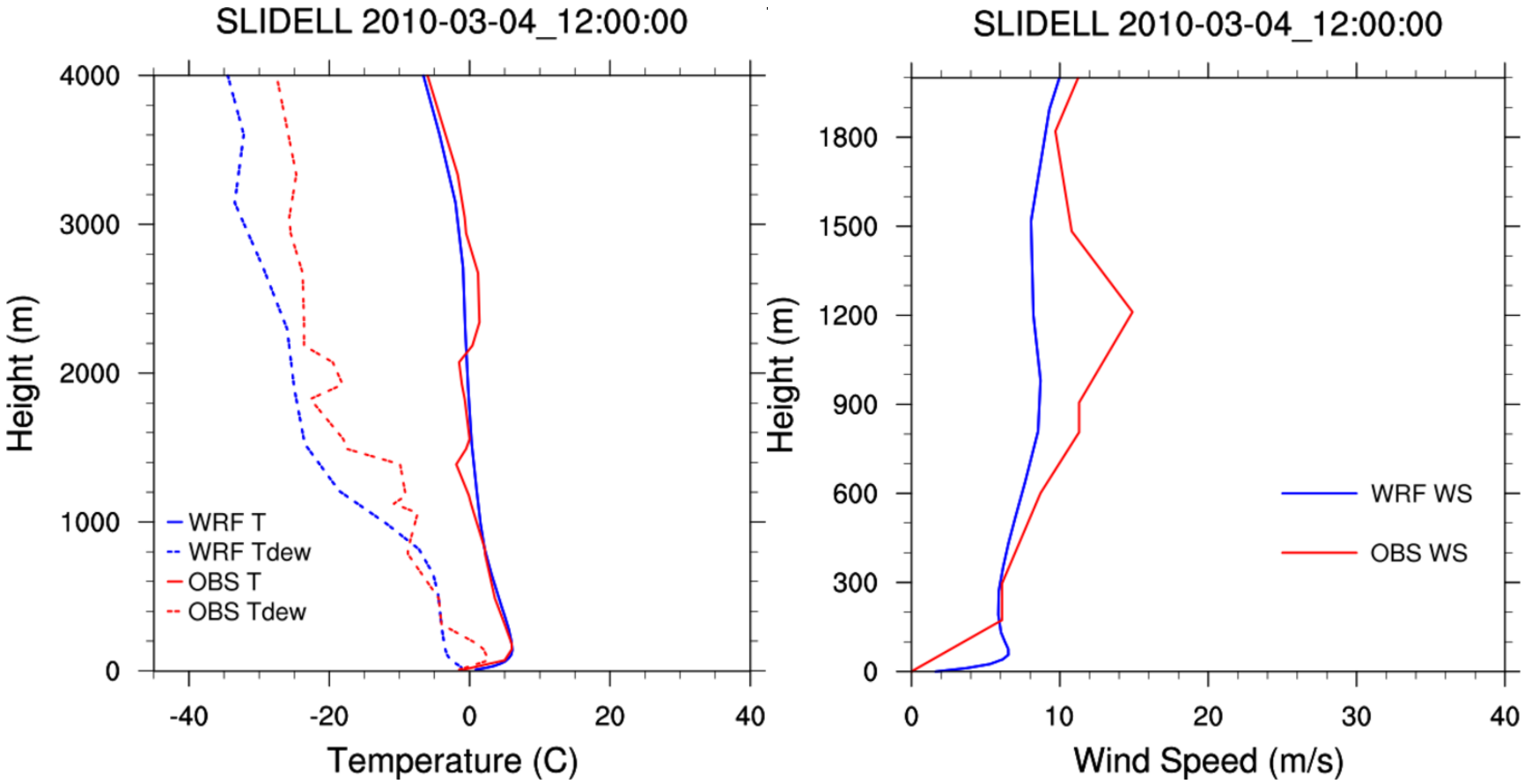

Figure 2-29. Vertical Profile Soundings Comparing the 4-km WRF (blue lines) to Upper-Air Observations Data (red lines) for Slidell, LA, on March 4, 2010, at 12 UTC

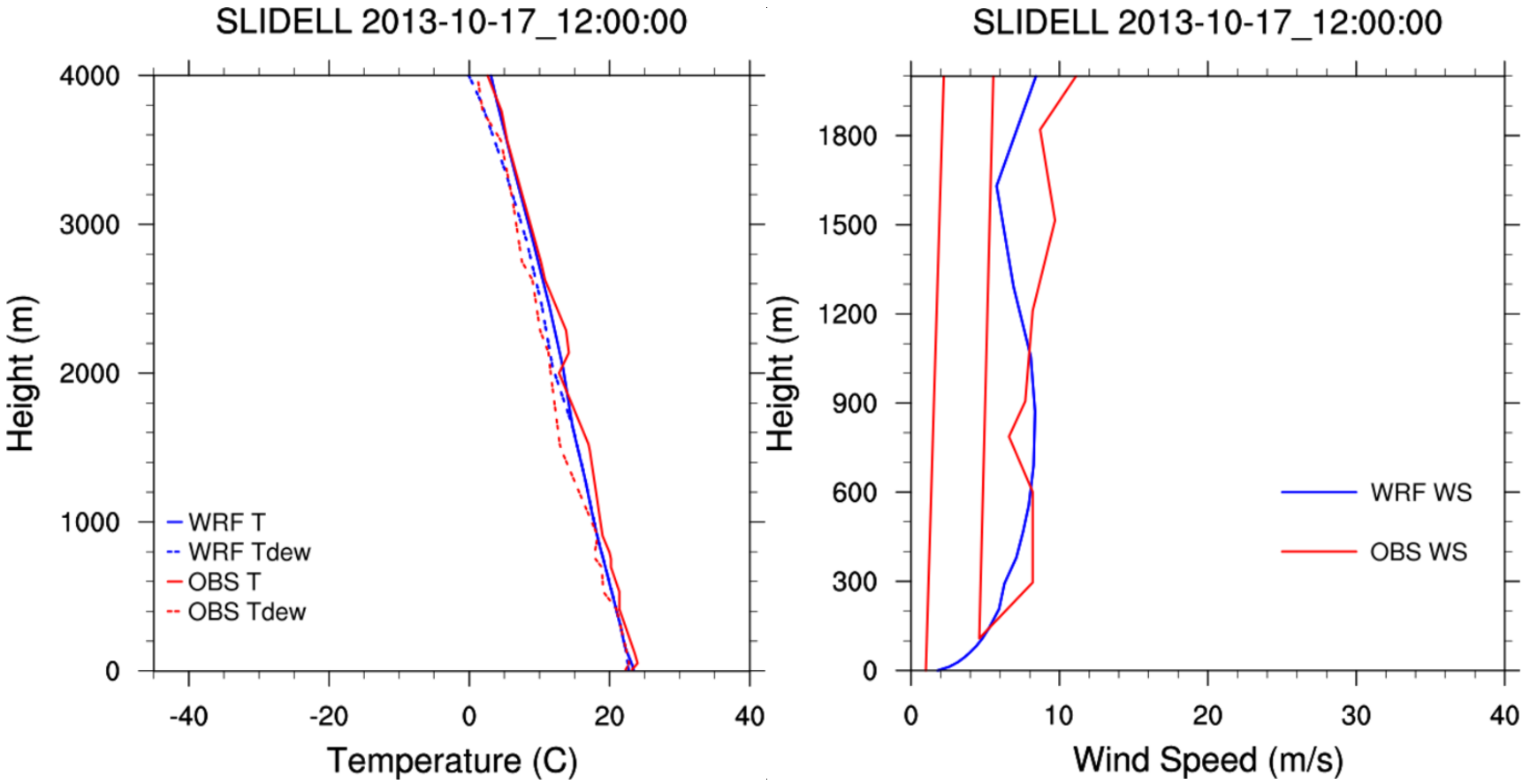

Figure 2-30. Vertical Profile Soundings Comparing the 4-km WRF (blue lines) to Upper-Air Observations Data (red lines) for Slidell, LA, on October 17, 2013, at 12 UTC

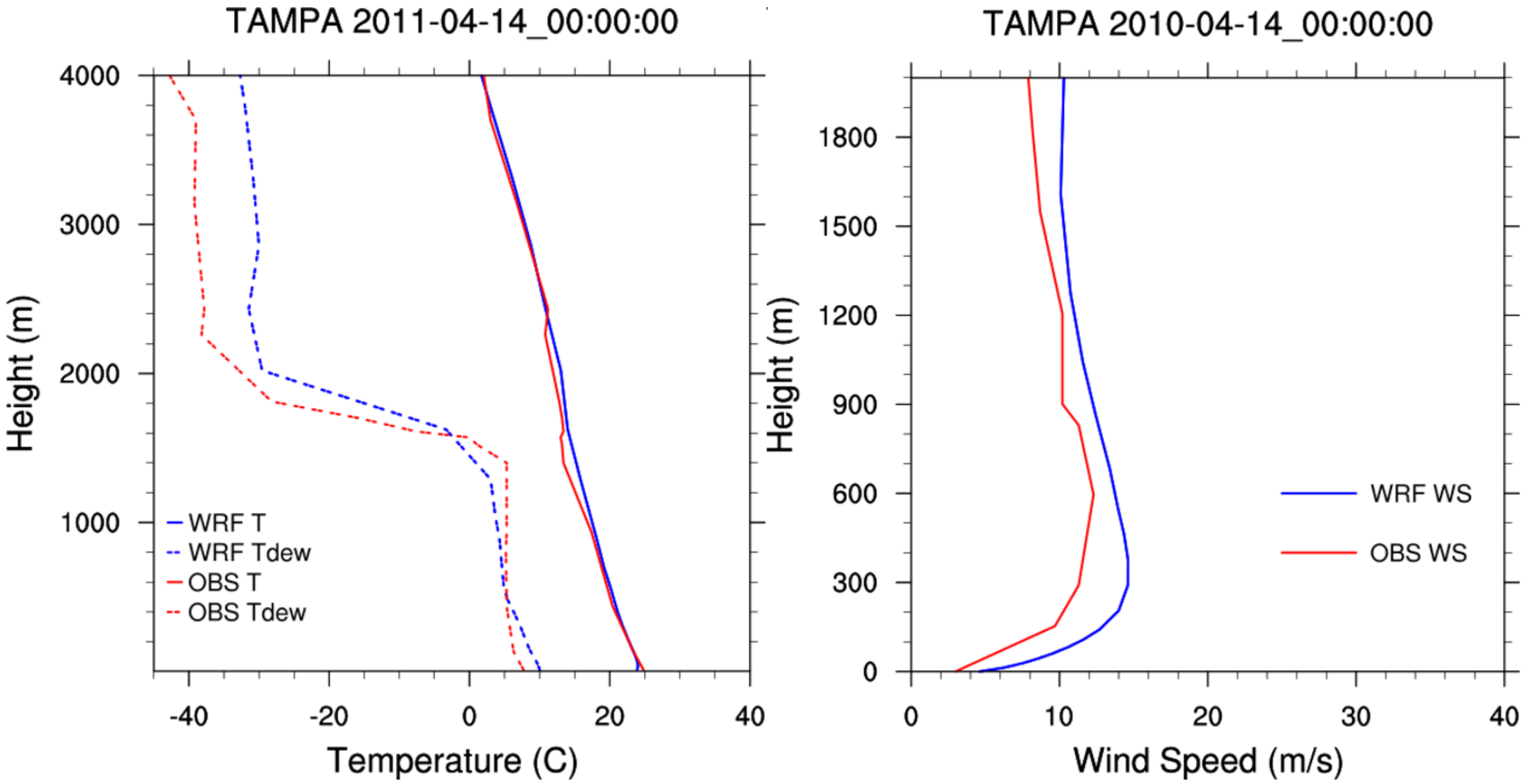

Figure 2-31. Vertical Profile Soundings Comparing the 4-km WRF (blue lines) to Upper-Air Observations Data (red lines) for Tampa, FL, on April 14, 2011, at 00 UTC

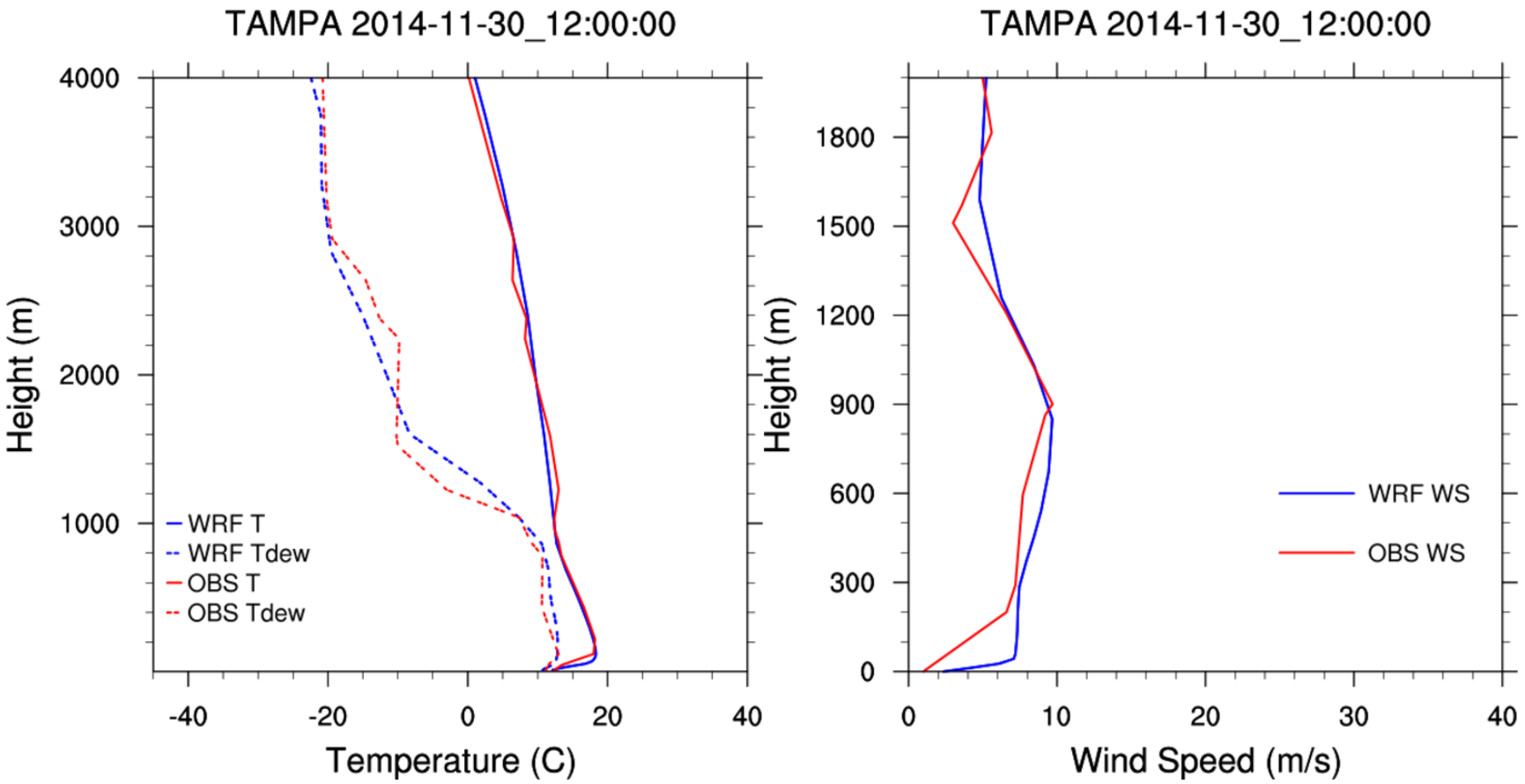

Figure 2-32. Vertical Profile Soundings Comparing the 4-km WRF (blue lines) to Upper-Air Observations Data (red lines) for Tampa, FL, on November 30, 2014, at 12 UTC

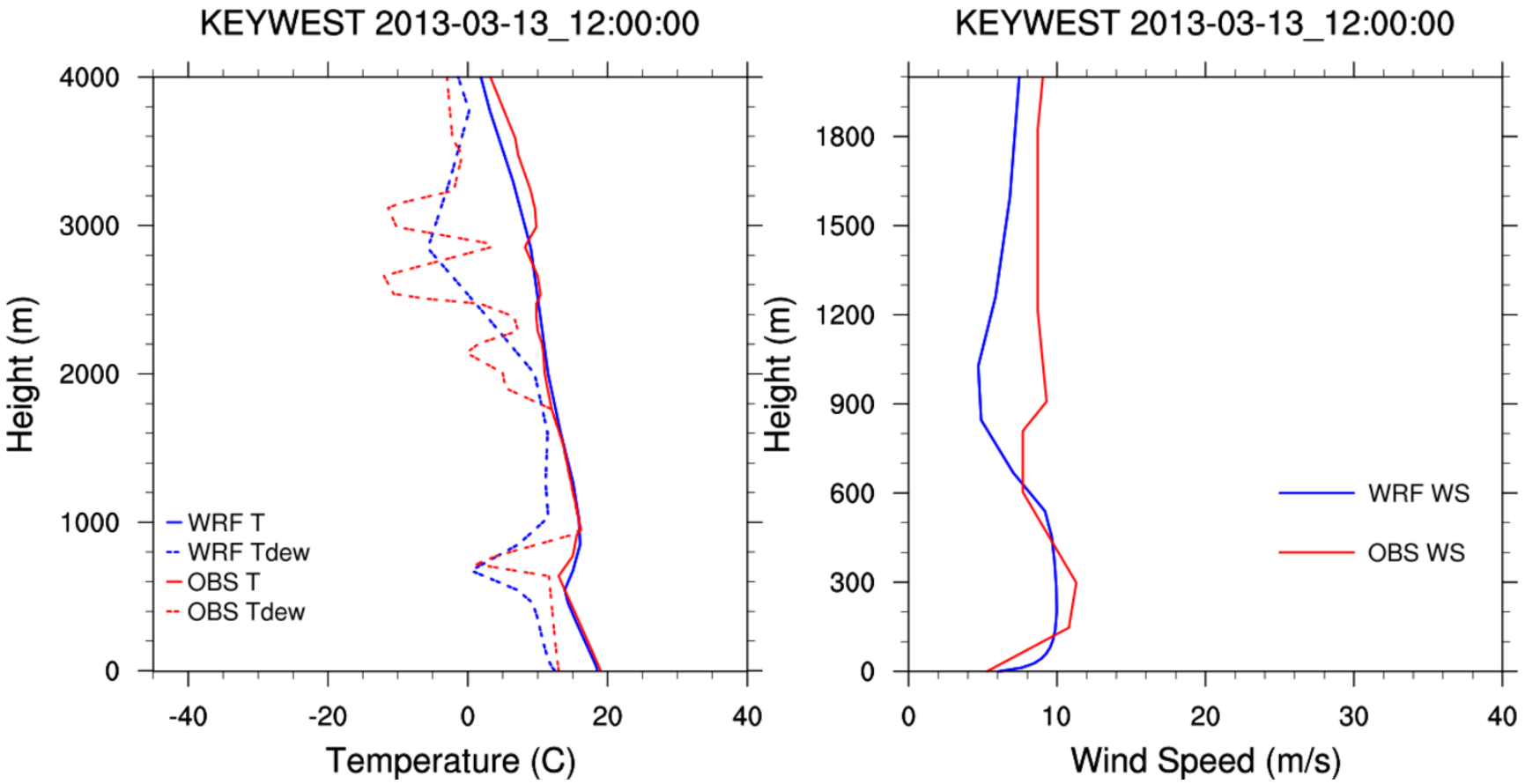

Figure 2-33. Vertical Profile Soundings Comparing the 4-km WRF (blue lines) to Upper-Air Observations Data (red lines) for Key West, FL, on March 13, 2013, at 12 UTC

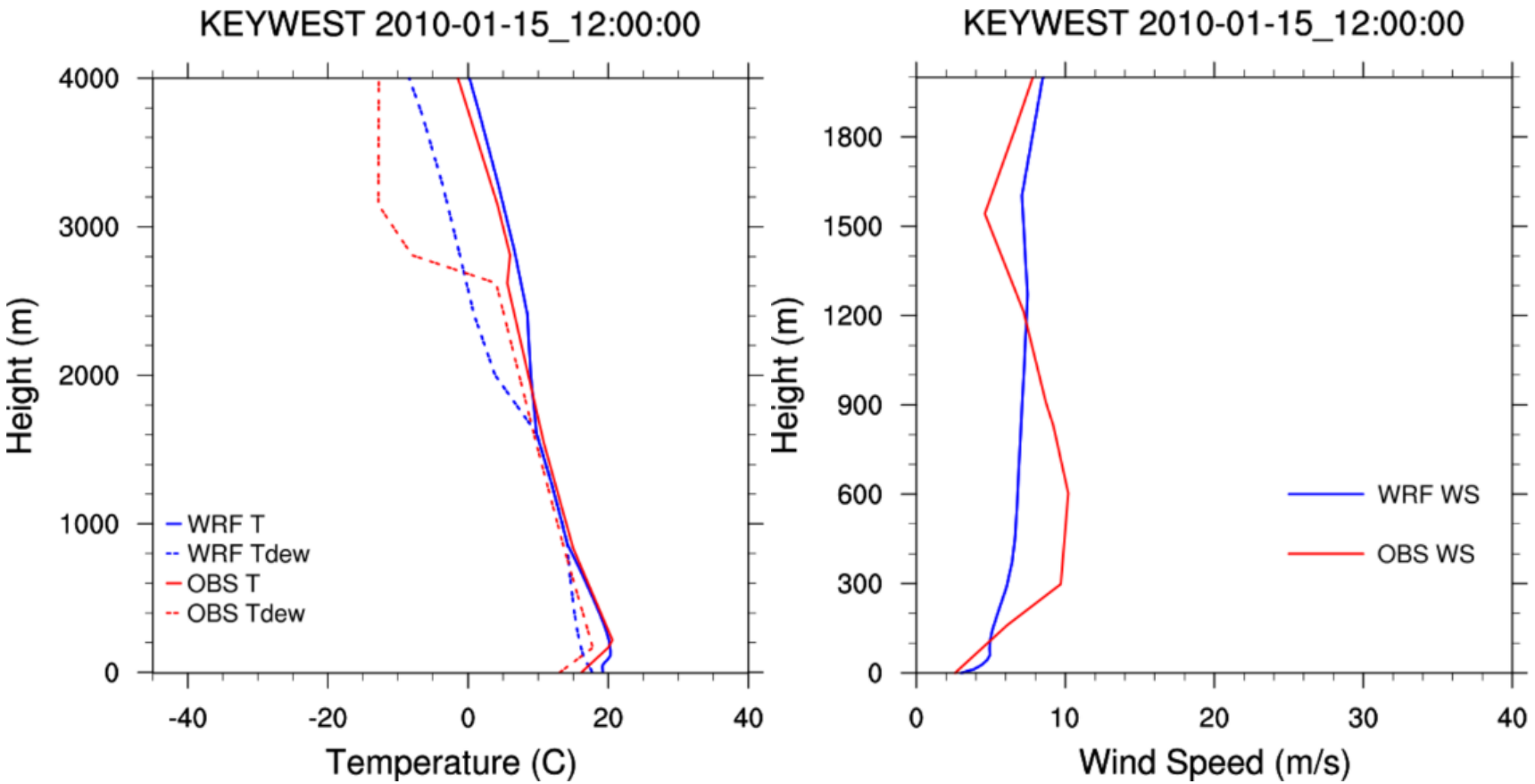

Figure 2-34. Vertical Profile Soundings Comparing the 4-km WRF (blue lines) to Upper-Air Observations Data (red lines) for Key West, FL, on January 15, 2010, at 12 UTC

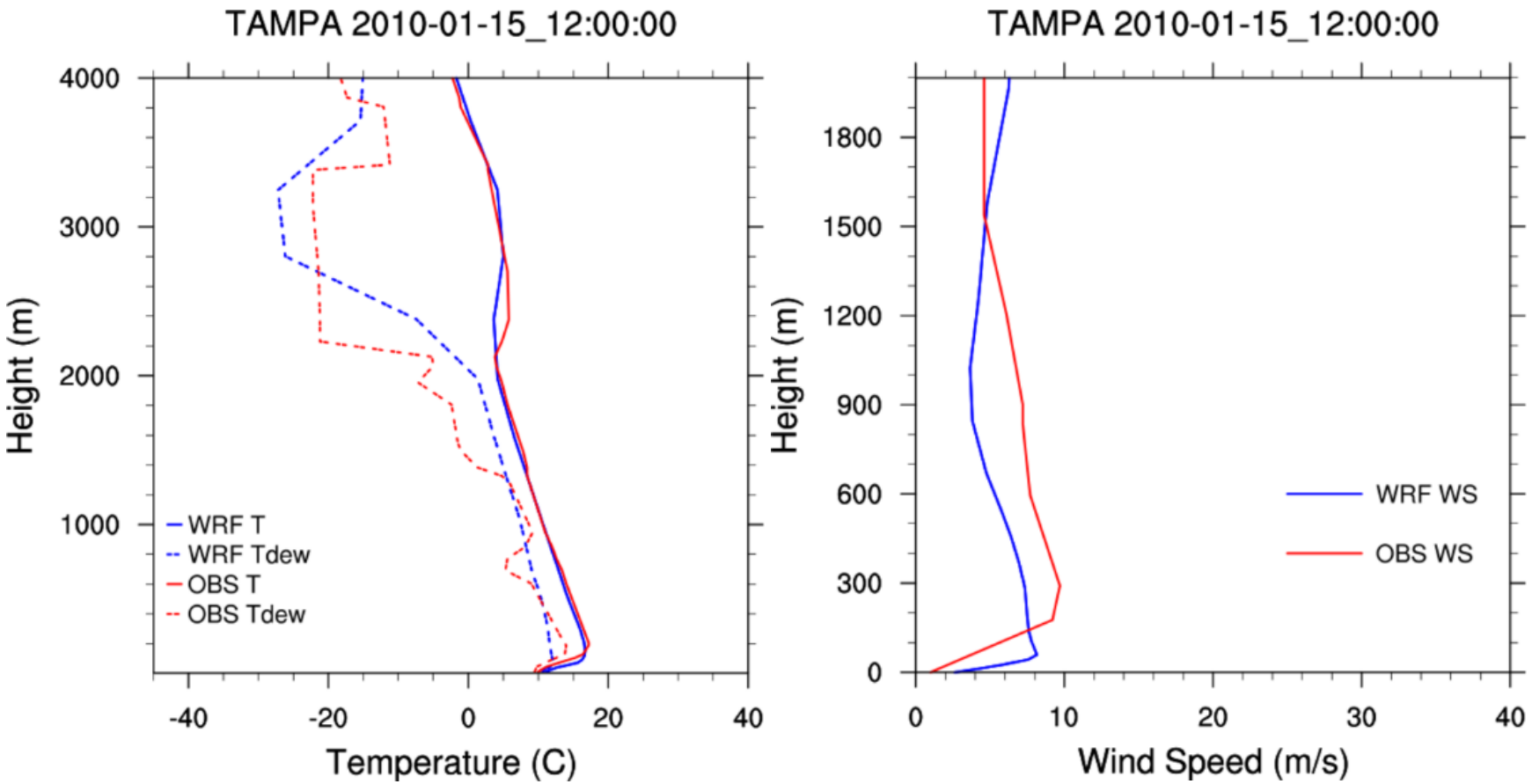

Figure 2-35. Vertical Profile Soundings Comparing the 4-km WRF (blue lines) to Upper-Air Observations Data (red lines) for Tampa, FL, on January 15, 2010, at 12 UTC

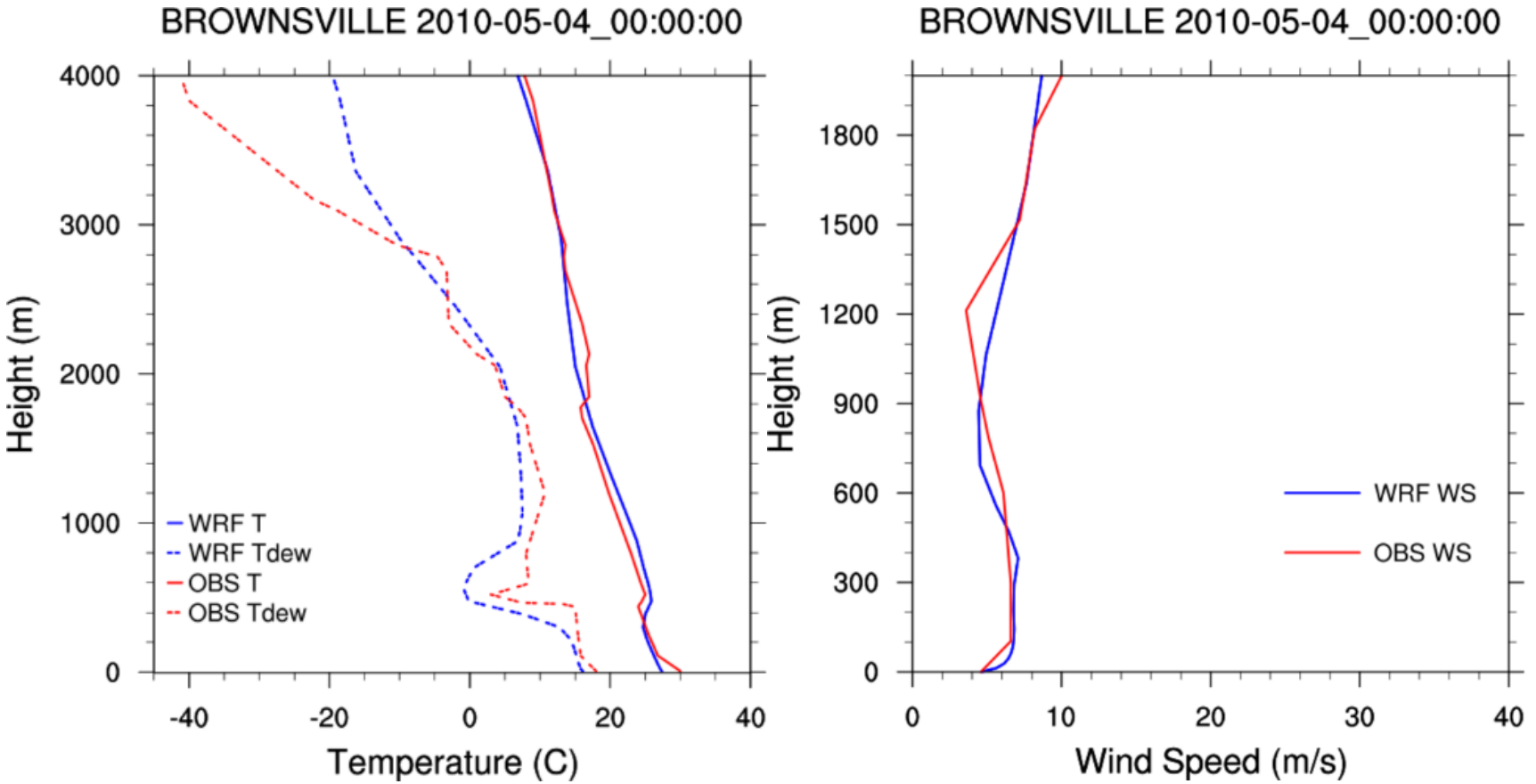

Figure 2-36. Vertical Profile Soundings Comparing the 4-km WRF (blue lines) to Upper-Air Observations Data (red lines) for Brownsville, TX, on May 4, 2010, at 00 UTC

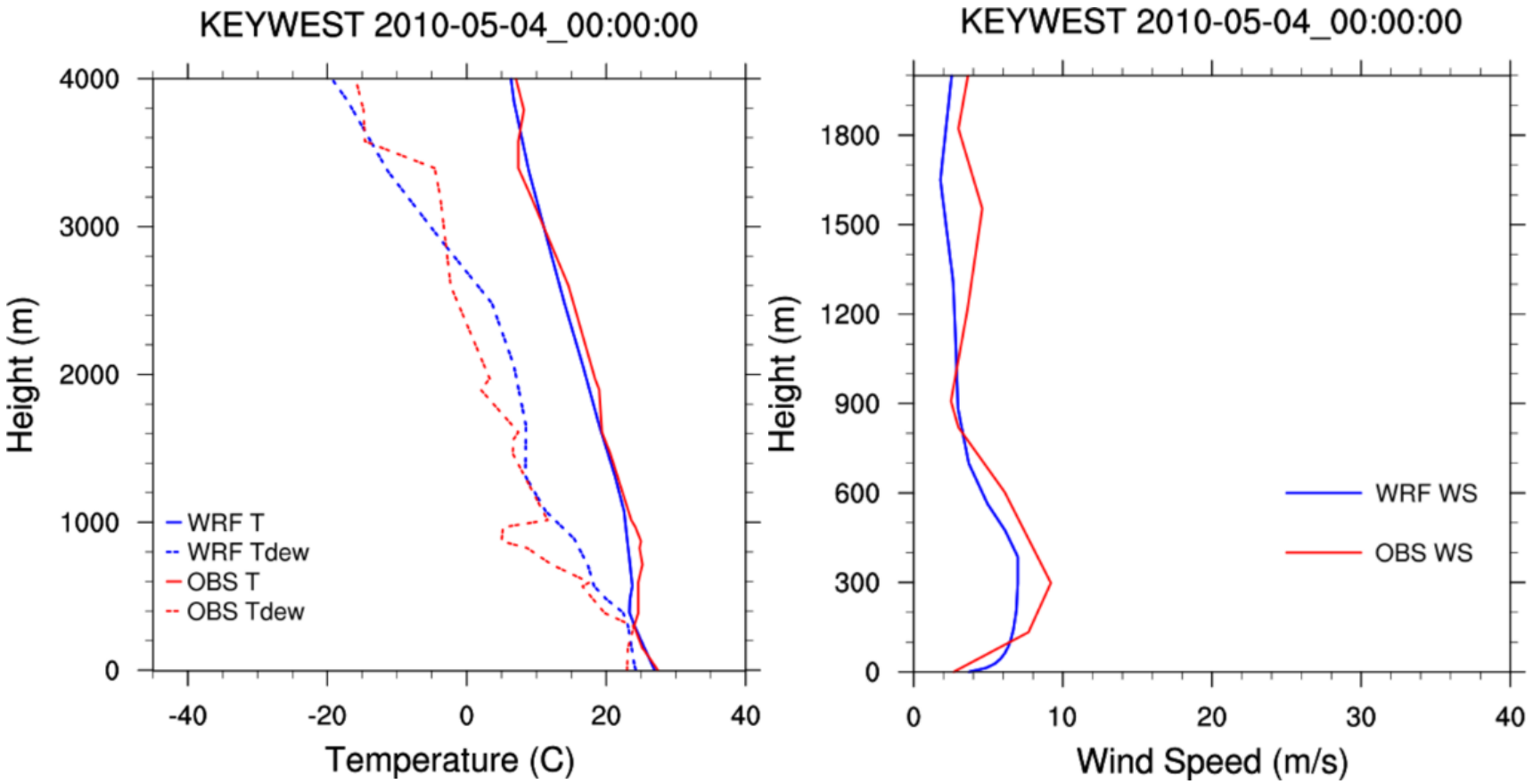

Figure 2-37. Vertical Profile Soundings Comparing the 4-km WRF (blue lines) to Upper-Air Observations Data (red lines) for Key West, FL, on May 4, 2010, at 00 UTC to Correspond With the May 3 High Ozone Event

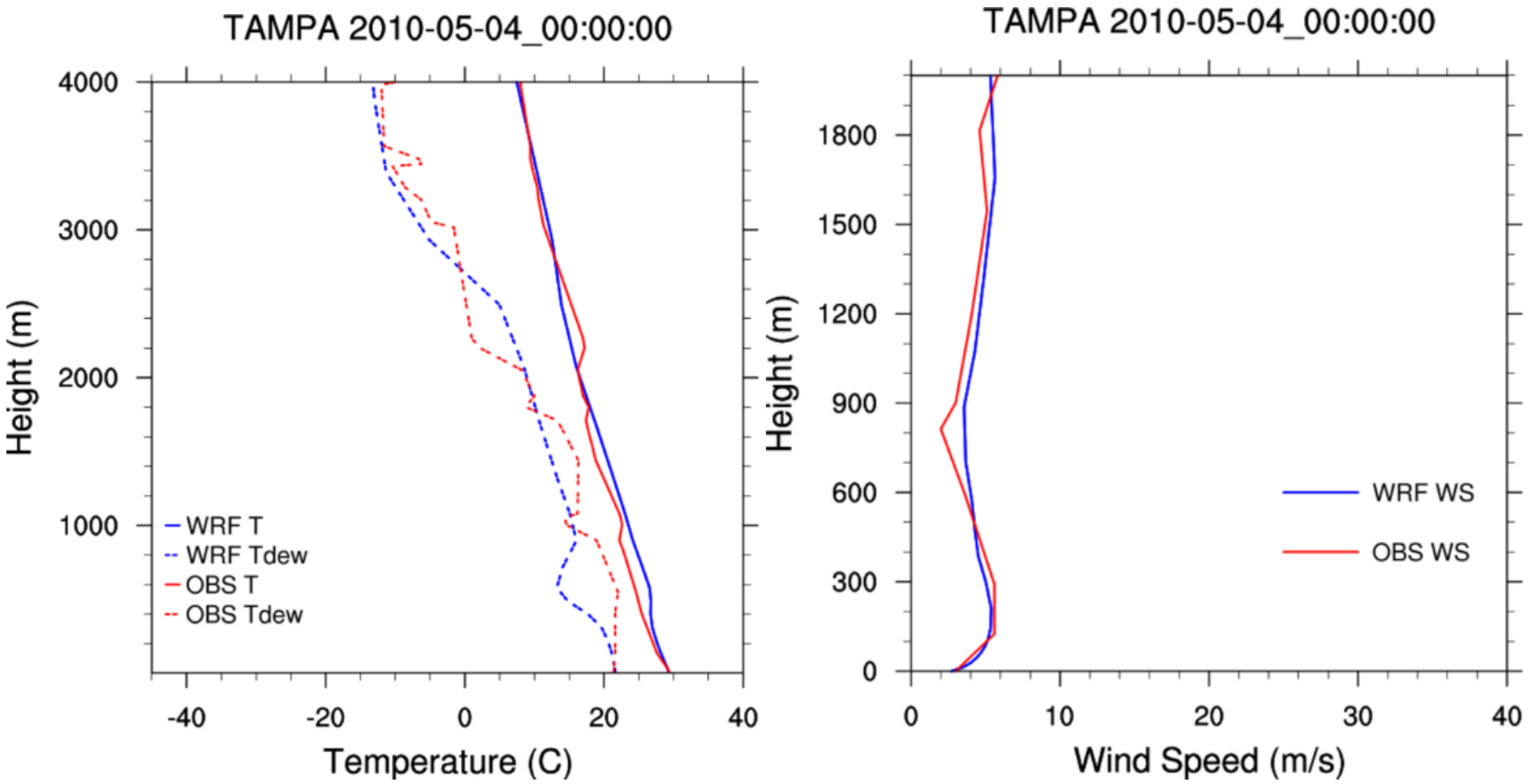

Figure 2-38. Vertical Profile Soundings Comparing the 4-km WRF (blue lines) to Upper-Air Observations Data (red lines) for Tampa, FL, on May 4, 2010, at 00 UTC to Correspond With the May 3 High Ozone Event

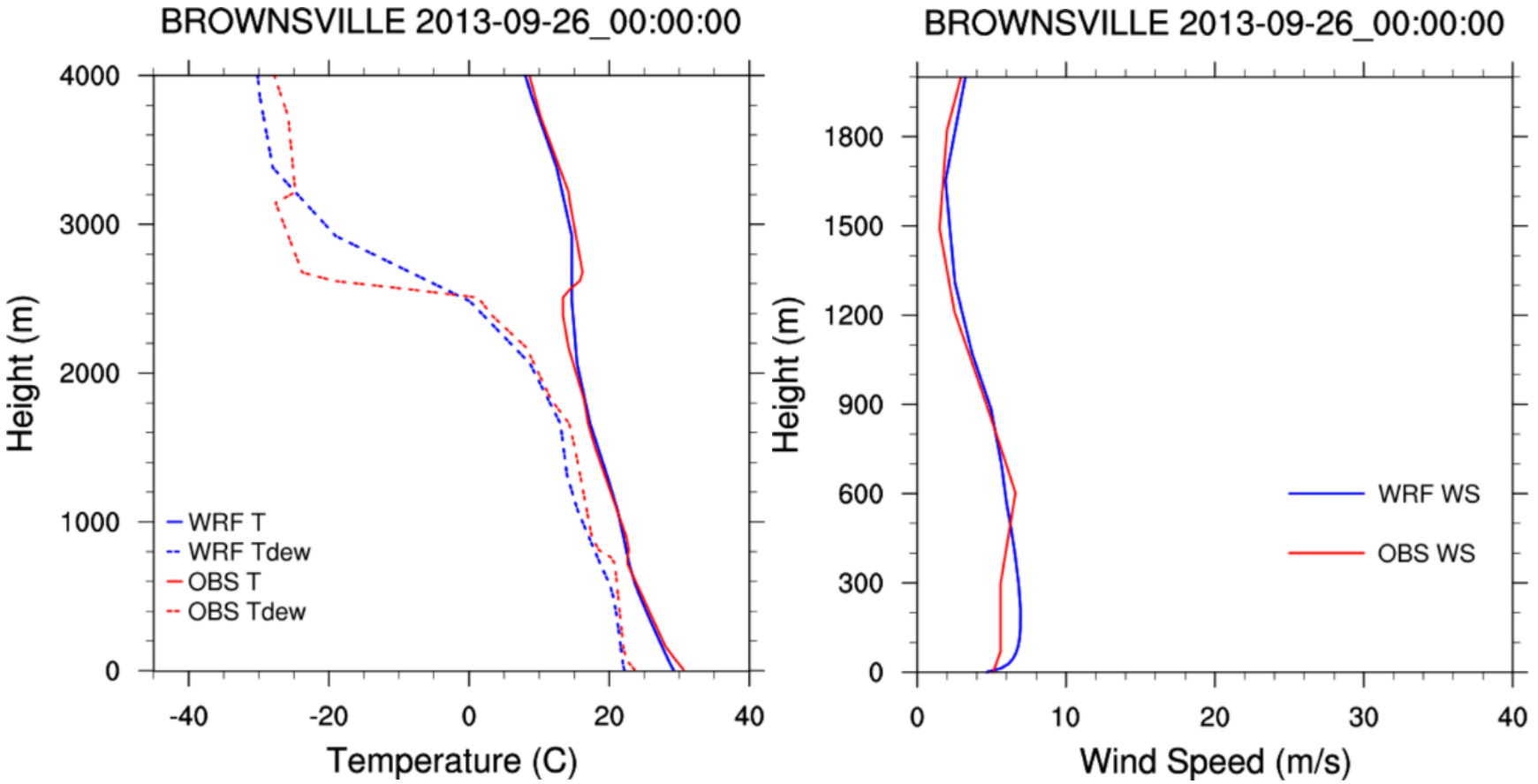

Figure 2-39. Vertical Profile Soundings Comparing the 4-km WRF (blue lines) to Upper-Air Observations Data (red lines) for Brownsville, TX, on September 26, 2013, at 00 UTC to Correspond With the September 25 High Ozone Event

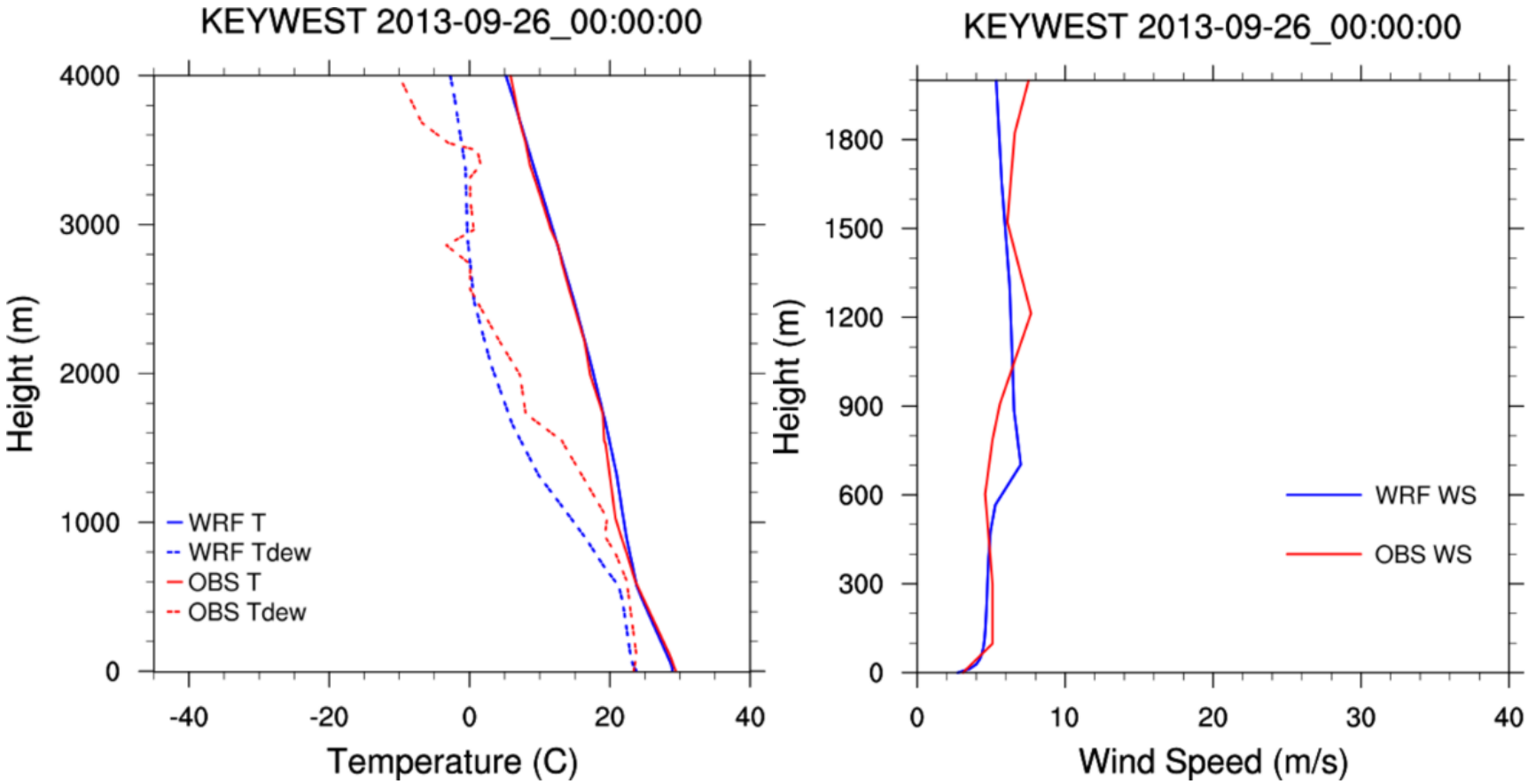

Figure 2-40. Vertical Profile Soundings Comparing the 4-km WRF (blue lines) to Upper-Air Observations Data (red lines) for Key West, FL, on September 26, 2013, at 00 UTC to Correspond With the September 25 High Ozone Event

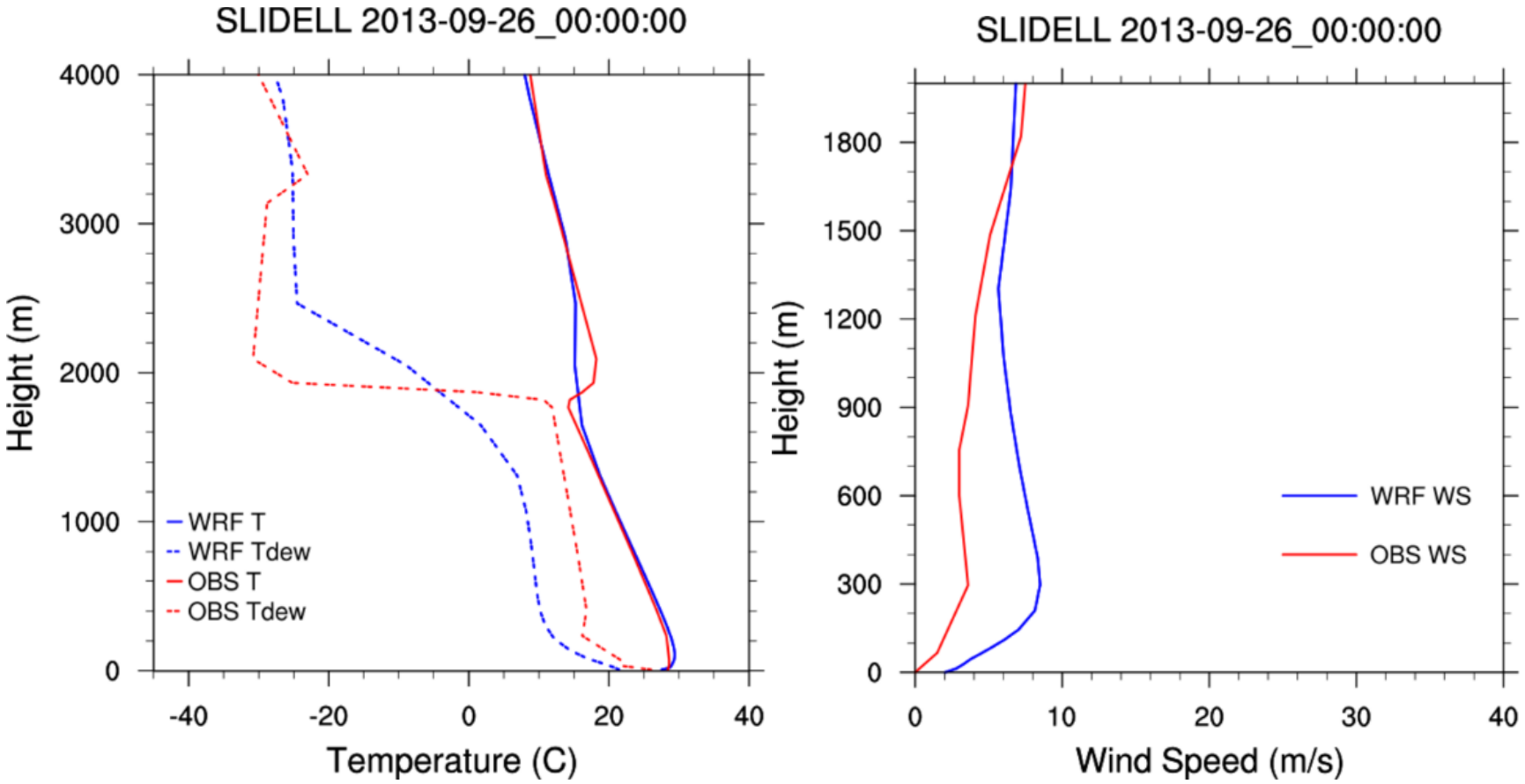

Figure 2-41. Vertical Profile Soundings Comparing the 4-km WRF (blue lines) to Upper-Air Observations Data (red lines) for Slidell, LA, on September 26, 2013, at 00 UTC to Correspond With the September 25 High Ozone Event

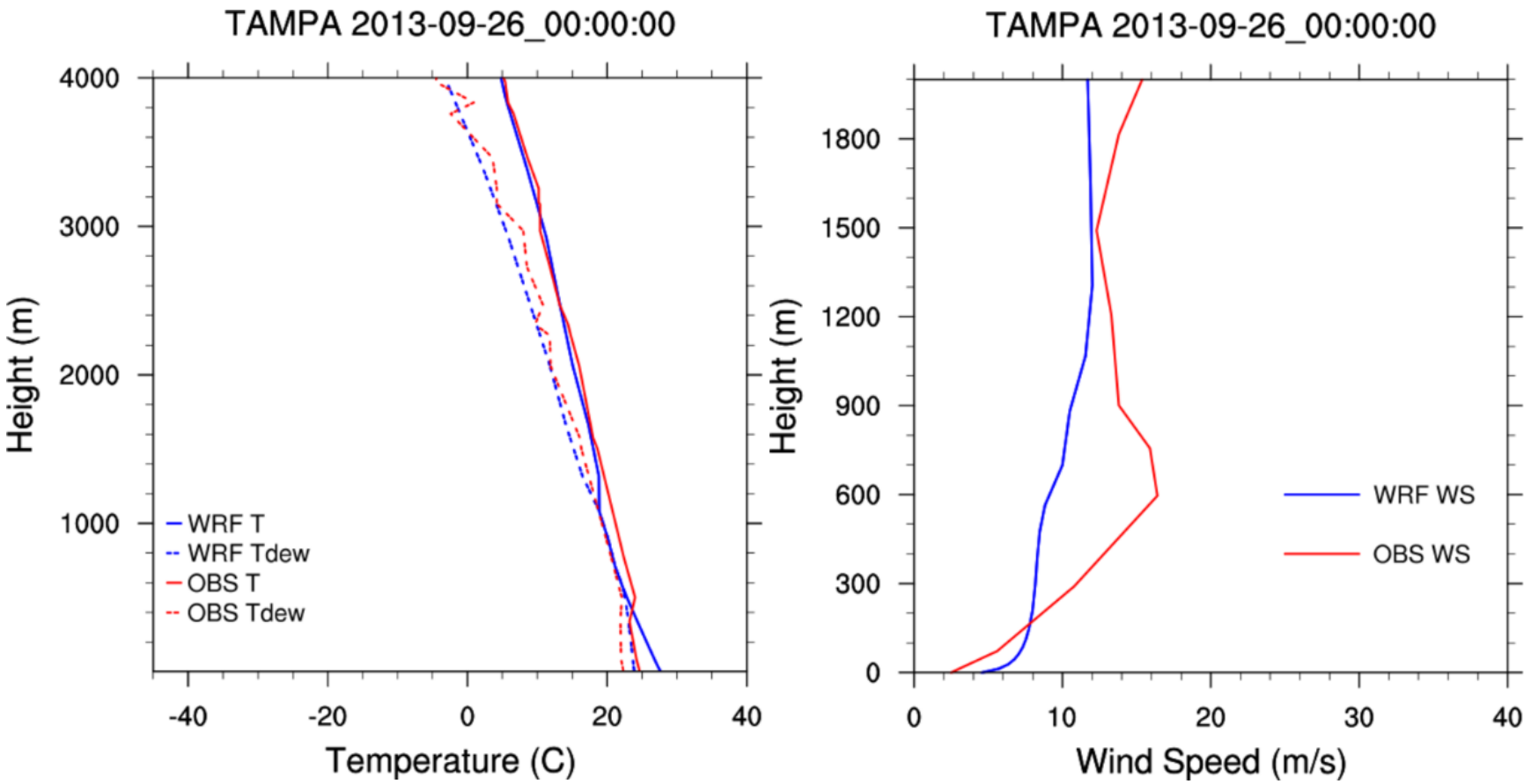

Figure 2-42. Vertical Profile Soundings Comparing the 4-km WRF (blue lines) to Upper-Air Observations Data (red lines) for Tampa, FL, on September 26, 2013, at 00 UTC to Correspond With the September 25 High Ozone Event

2.3.4 Qualitative Evaluation Using Precipitation

Precipitation removes chemicals and particulates from the air via wet deposition and thus is an important parameter for high-quality dispersion modeling. Precipitation can also be important in photochemical modeling of deposition. Several precipitation datasets were evaluated for use in model comparisons. Ramboll has used the Parameter-elevation Regressions on Independent Slopes Model (PRISM) dataset for rainfall extensively in the past, but it only covers the over-land portion of the modeling domain. Land-based radar retrievals of precipitation typically have larger uncertainty and are limited in geographic coverage to the area relatively near the coast; as a result, Ramboll only used PRISM data to evaluate model performance over land and did not use PRISM data for performance evaluation over water. Satellite-based retrievals are typically lower resolution and also feature larger uncertainty but cover the entire GOMR. Ramboll compared the BOEM GOMR WRF modeled precipitation output with the PRISM and Tropical Rainfall Measurements Mission (TRMM) satellite datasets.

The Oregon State University PRISM Climate Group gathers temperature and precipitation data from a range of monitoring networks, applies sophisticated quality control methods, and uses the data to produce spatial grids of climate parameters (Daly et al., 2008). The group models the time series datasets using climatologically aided interpolation (CAI), which uses the long-term average pattern to first guess the spatial pattern of climatic conditions. Both a daily product and a monthly product are available. The precipitation observations used in the daily PRISM product include radar measurements, which the monthly product does not take into account. This may cause dramatic local differences between the two datasets in monthly totals.

TRMM was a joint mission flown by the National Aeronautics and Space Administration (NASA, U.S.) and the Japan Aerospace Exploration Agency (JAXA, Japan) to improve our quantitative knowledge of the three-dimensional distribution of precipitation in the tropics. TRMM had a passive microwave radiometer (TRMM Microwave Imager, or TMI), the first active space-borne precipitation radar (PR), a visible-infrared scanner (VIRS), and other instruments. Coordinated observations are intended to result in a "flying raingauge" capability. The TRMM dataset is coarser than the PRISM data (0.5 degrees, or about 55 km, versus 4 km) but is available every three hours.

2.3.4.1 Evaluation over Land Using PRISM Precipitation

High-resolution (4-km) PRISM datasets cover the contiguous U.S. in both monthly and daily output versions (Daly et al., 2008). WRF precipitation output is compared to the PRISM over-land portions of the GOM for this study. Ramboll re-projected and aggregated the PRISM data to the WRF projection's grid cell locations, then plotted the resulting gridded data and saved the gridded fields. This allows for consistent visual qualitative comparison.

Figure 2-43 through Figure 2-54 show five-year average (2010–2014) monthly precipitation plots constructed from BOEM GOMR WRF output, masked to only display over-land measurements, and compared to PRISM five-year average (2010–2014) monthly plots for January through December in the 4-km domain d03. For the averaging months of January through March, WRF represents the spatial extent of the precipitation well, recreating the comparatively drier areas of central Texas and southern Florida. However, the model does underestimate the total amount of average monthly rainfall by roughly 1.5 inches across a small portion of southern Mississippi and south-central Louisiana during this period.

The model depicts both the spatial extent and amount of precipitation exceptionally well over land, compared to PRISM, for the averaging months of April through June. In July and August, WRF performs well in recreating the precipitation extent across the land portions of the domain, including the

convergence zones across the east and west coasts of Florida. The model does slightly overpredict the amount of rainfall accumulations in the southern Georgia and southern Alabama areas. This is likely due to the higher humidity rates in the model during the summertime period.

Figure 2-51 shows WRF and PRISM precipitation datasets for the five-year averaged month of September. WRF slightly underpredicts averaged precipitation rates over the land portion of the domain but over-forecasts the extent of rainfall over the northern Florida area. WRF performed exceptionally well from October through December, reproducing the extent and amount of rainfall very accurately, compared to PRISM totals. Overall, WRF performed very well in reproducing the spatial extent of precipitation for the over-land portions of GOMR through the averaged calendar months of 2010–2014.

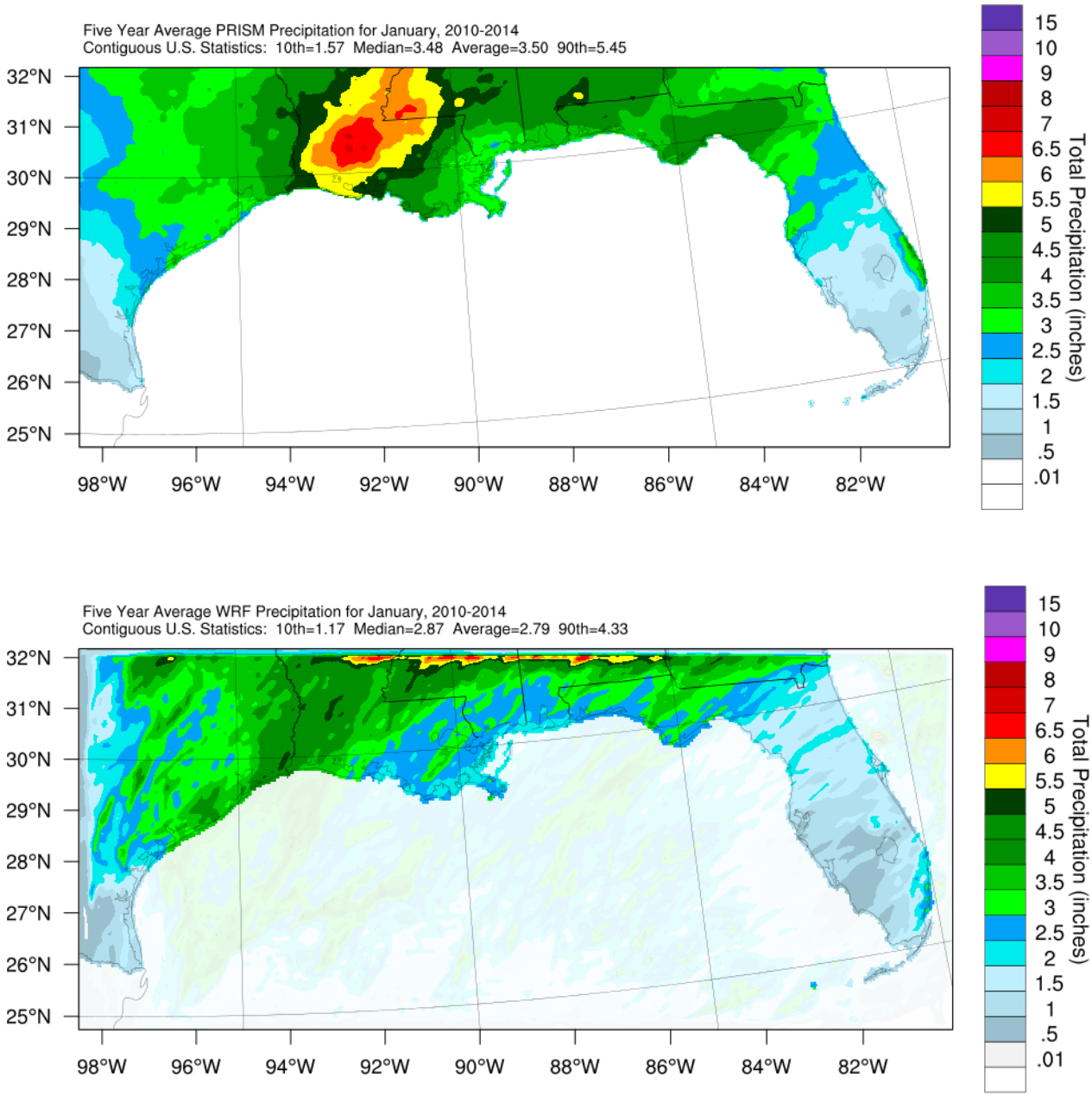

Figure 2-43. 5-Year Average (2010–2014) January PRISM Precipitation (top) and WRF Precipitation (bottom), 4-km Domain

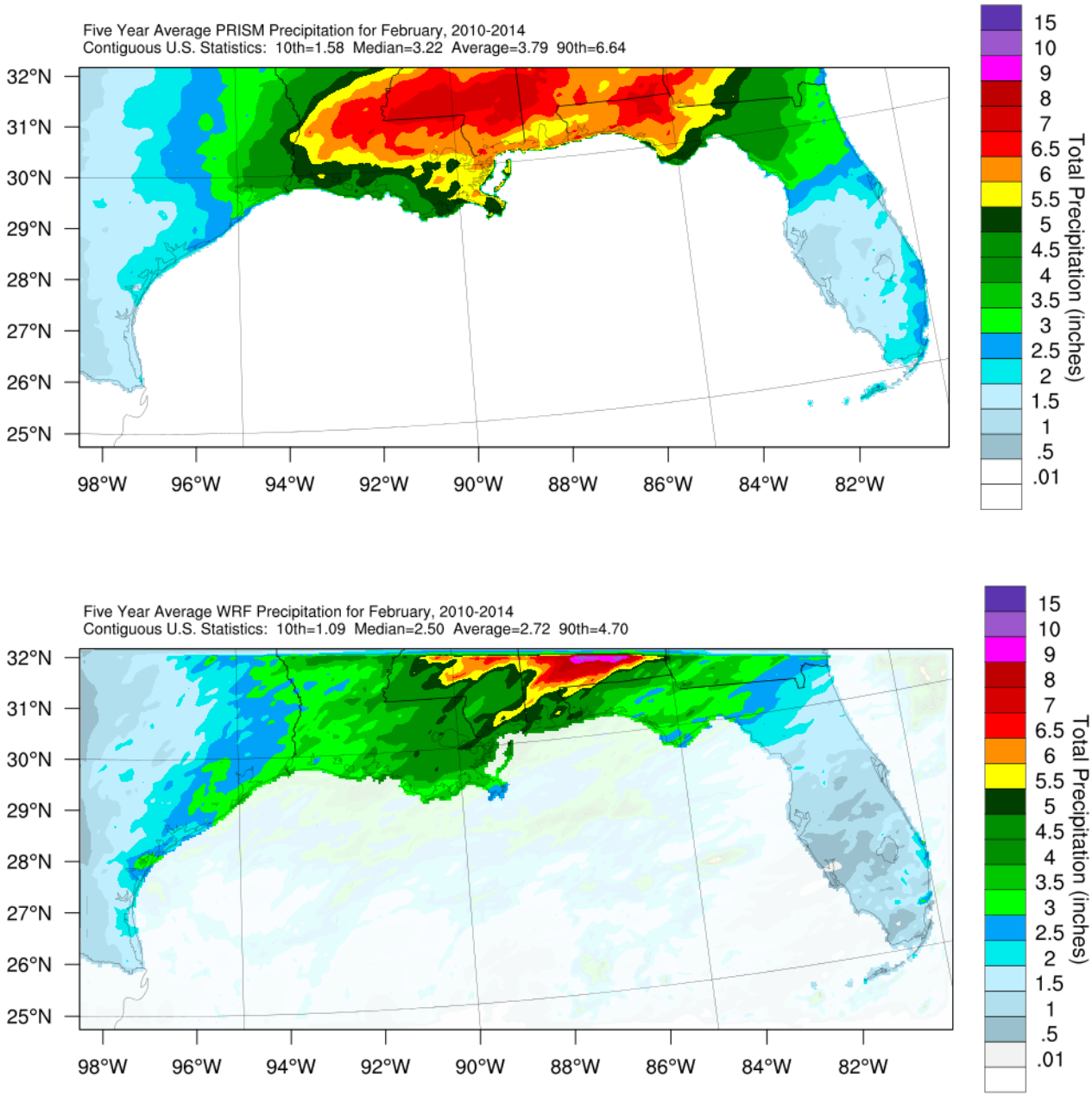

Figure 2-44. 5-Year Average (2010–2014) February PRISM Precipitation (top) and WRF Precipitation (bottom), 4-km Domain

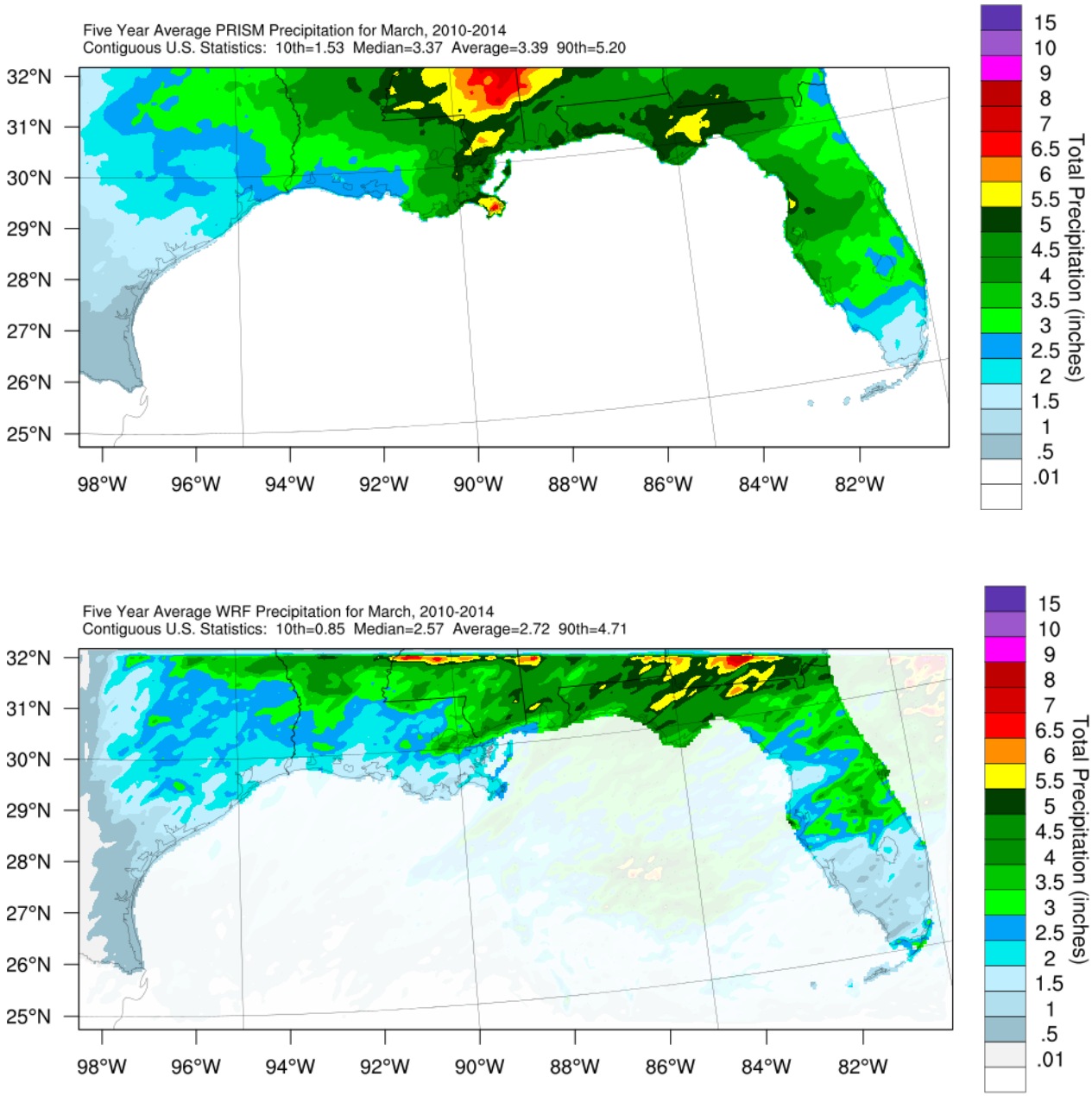

Figure 2-45. 5-Year Average (2010–2014) March PRISM Precipitation (top) and WRF Precipitation (bottom), 4-km Domain

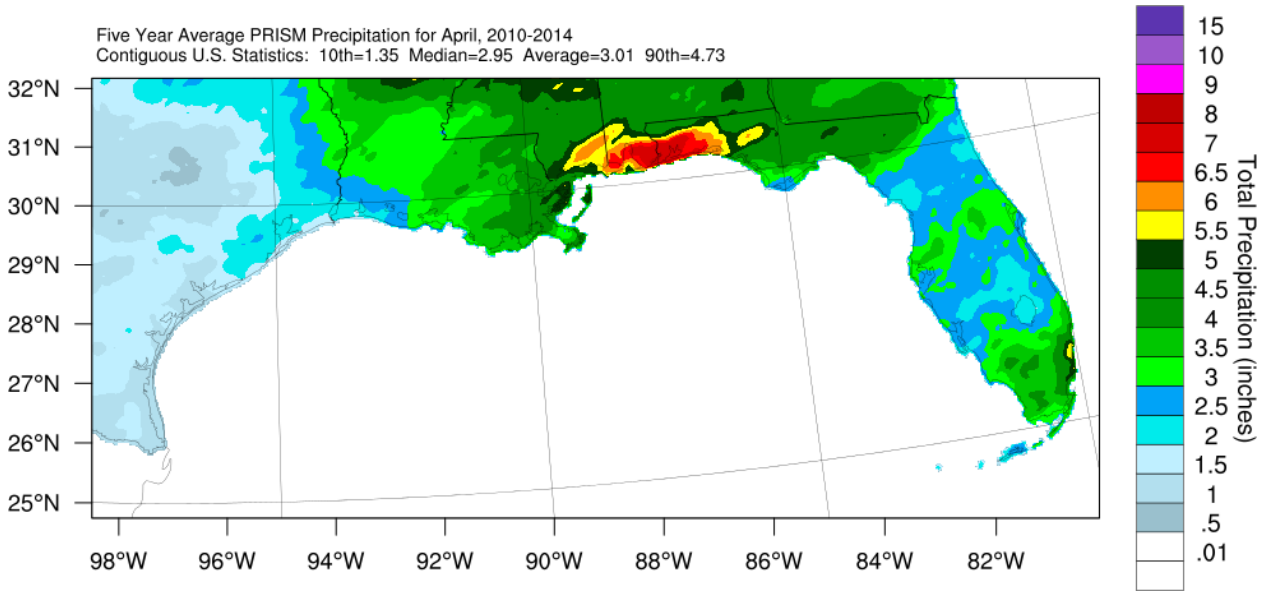

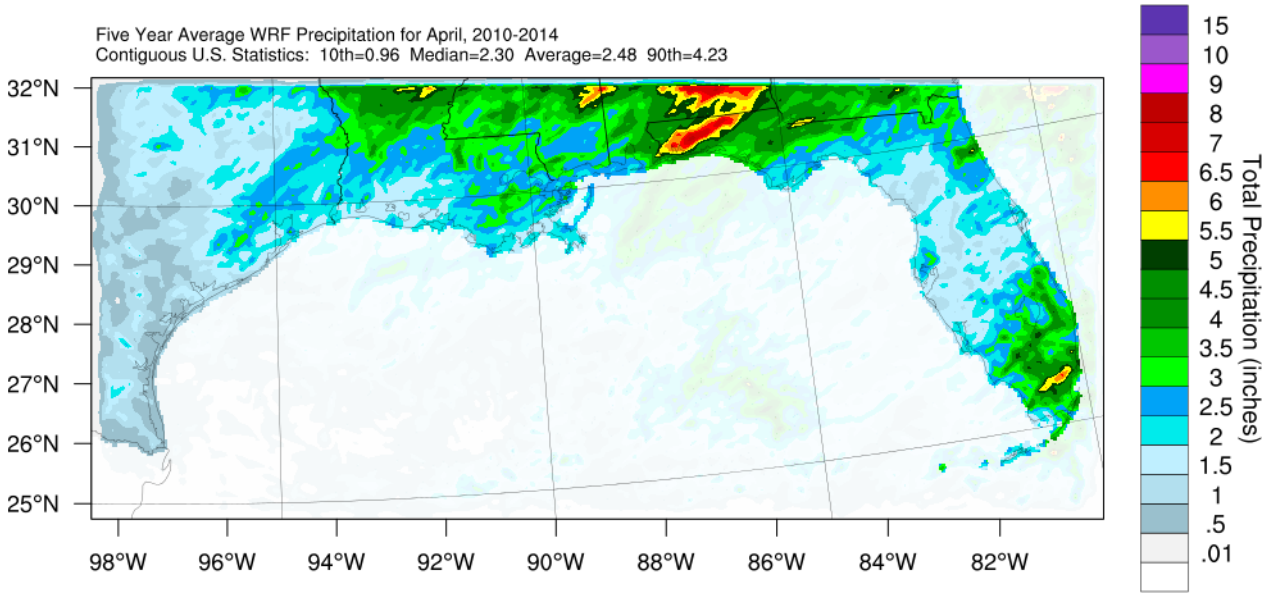

Figure 2-46. 5-Year Average (2010–2014) April PRISM Precipitation (top) and WRF Precipitation (bottom), 4-km Domain

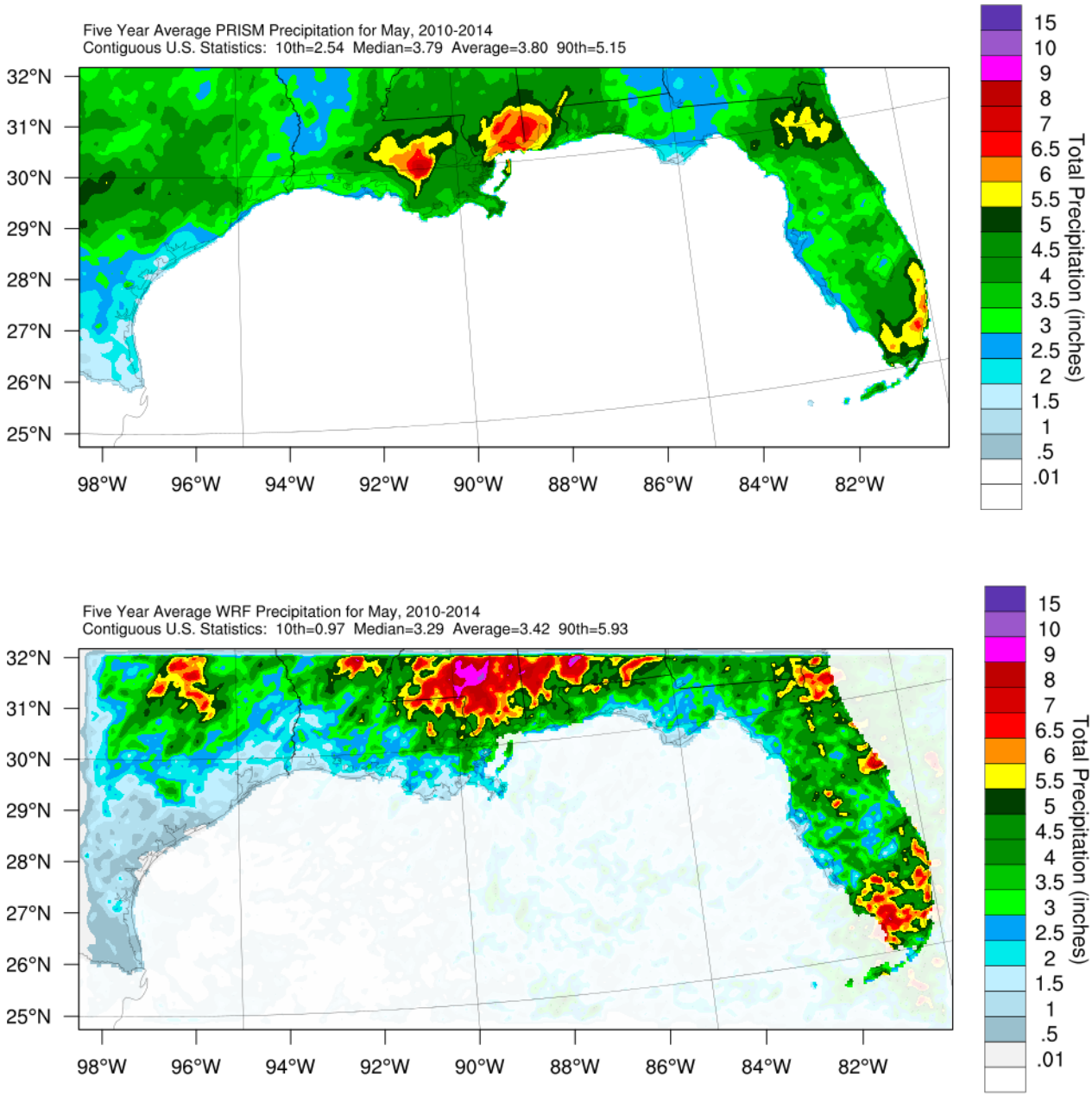

Figure 2-47. 5-Year Average (2010–2014) May PRISM Precipitation (top) and WRF Precipitation (bottom), 4-km Domain

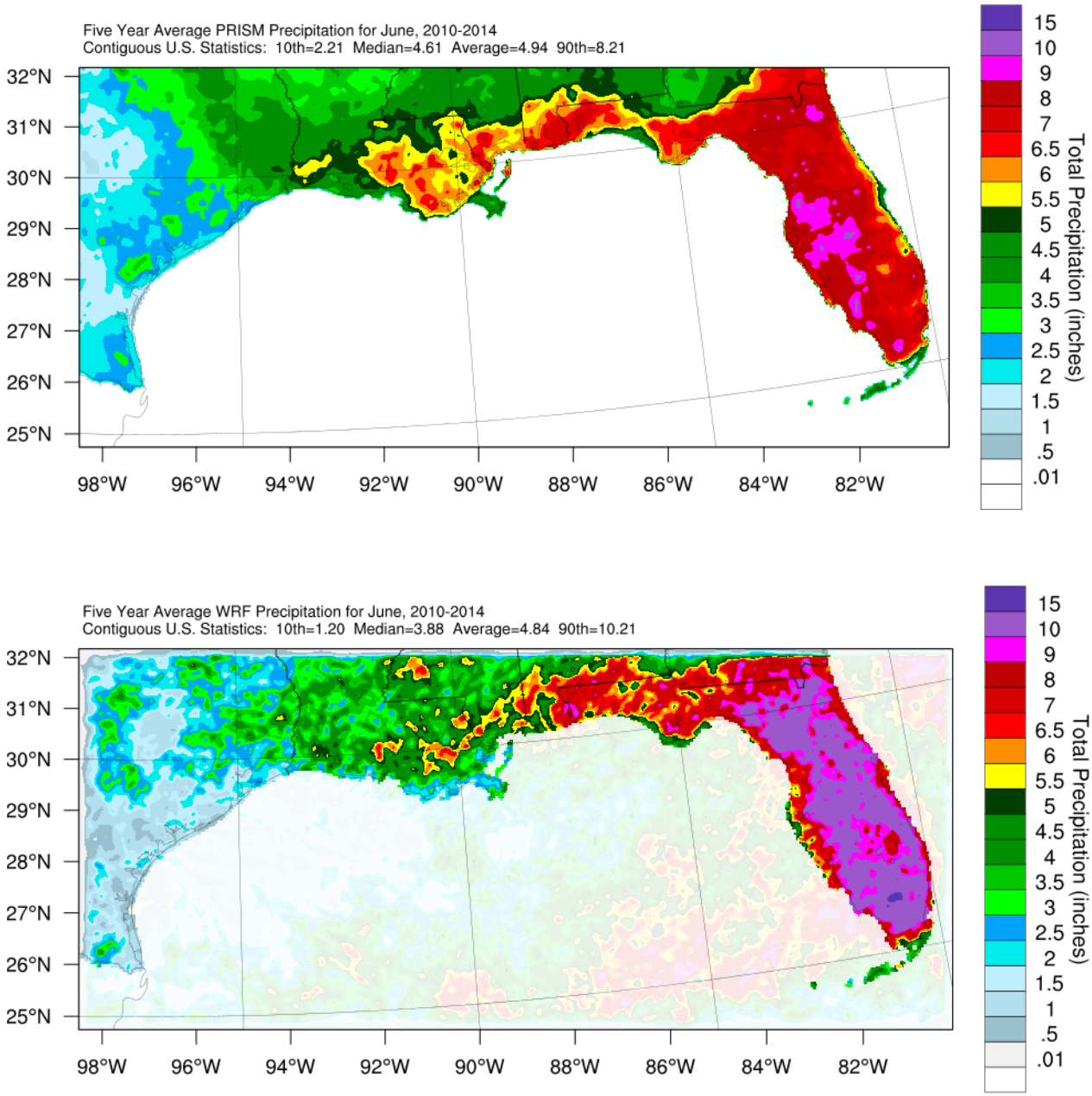

Figure 2-48. 5-Year Average (2010–2014) June PRISM Precipitation (top) and WRF Precipitation (bottom), 4-km Domain

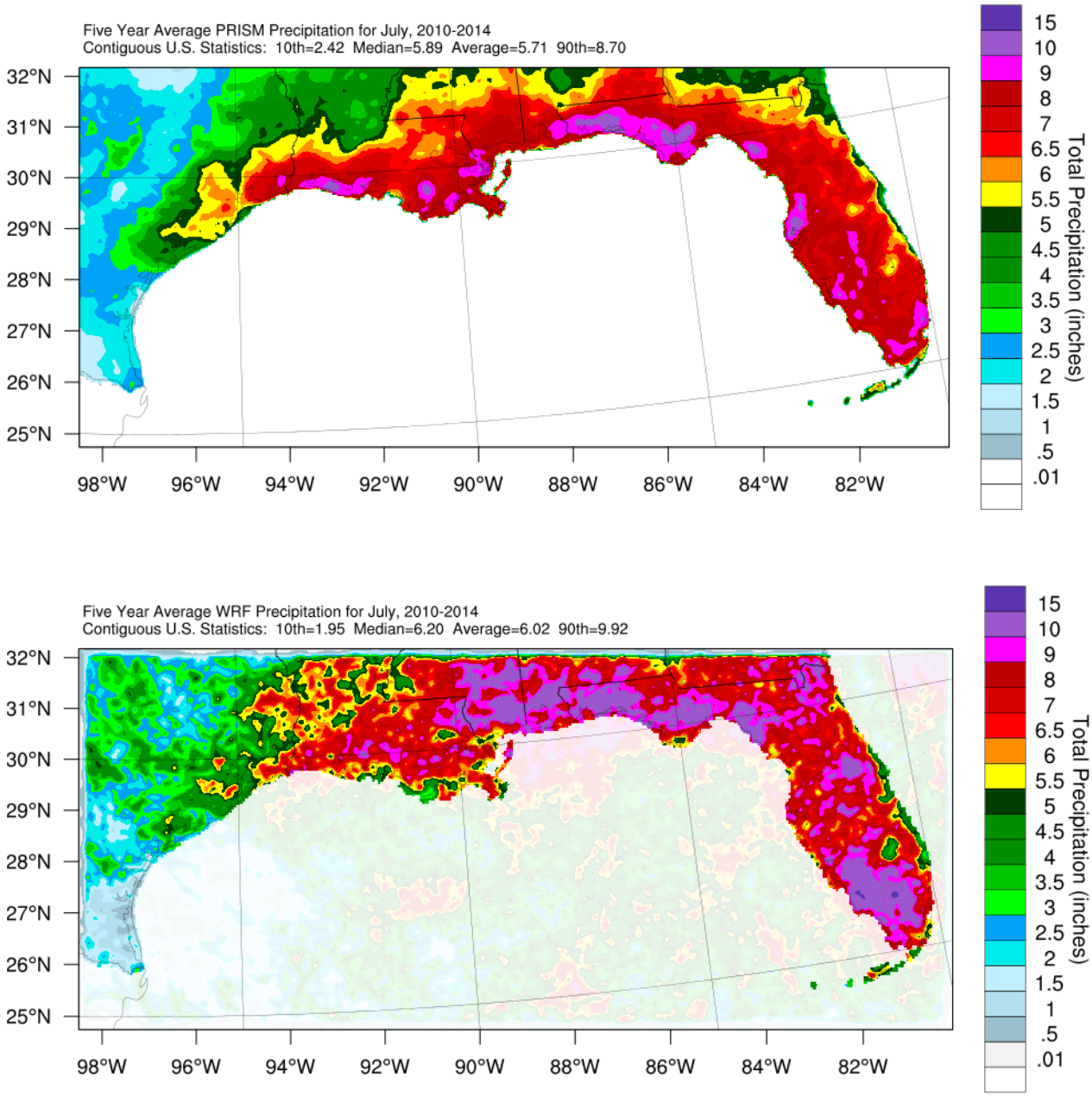

Figure 2-49. 5-Year Average (2010–2014) July PRISM Precipitation (top) and WRF Precipitation (bottom), 4-km Domain

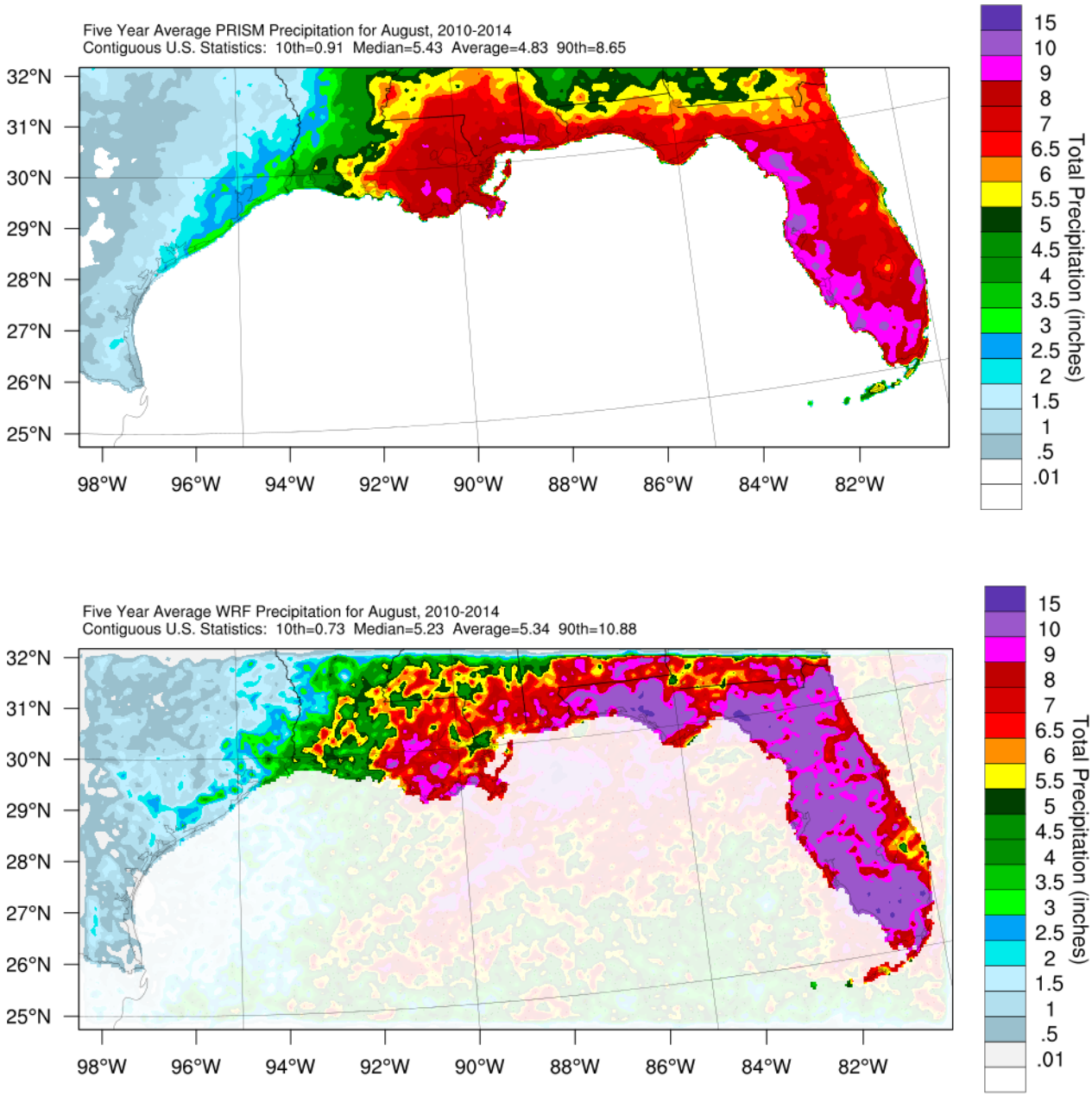

Figure 2-50. 5-Year Average (2010–2014) August PRISM Precipitation (top) and WRF Precipitation (bottom), 4-km Domain

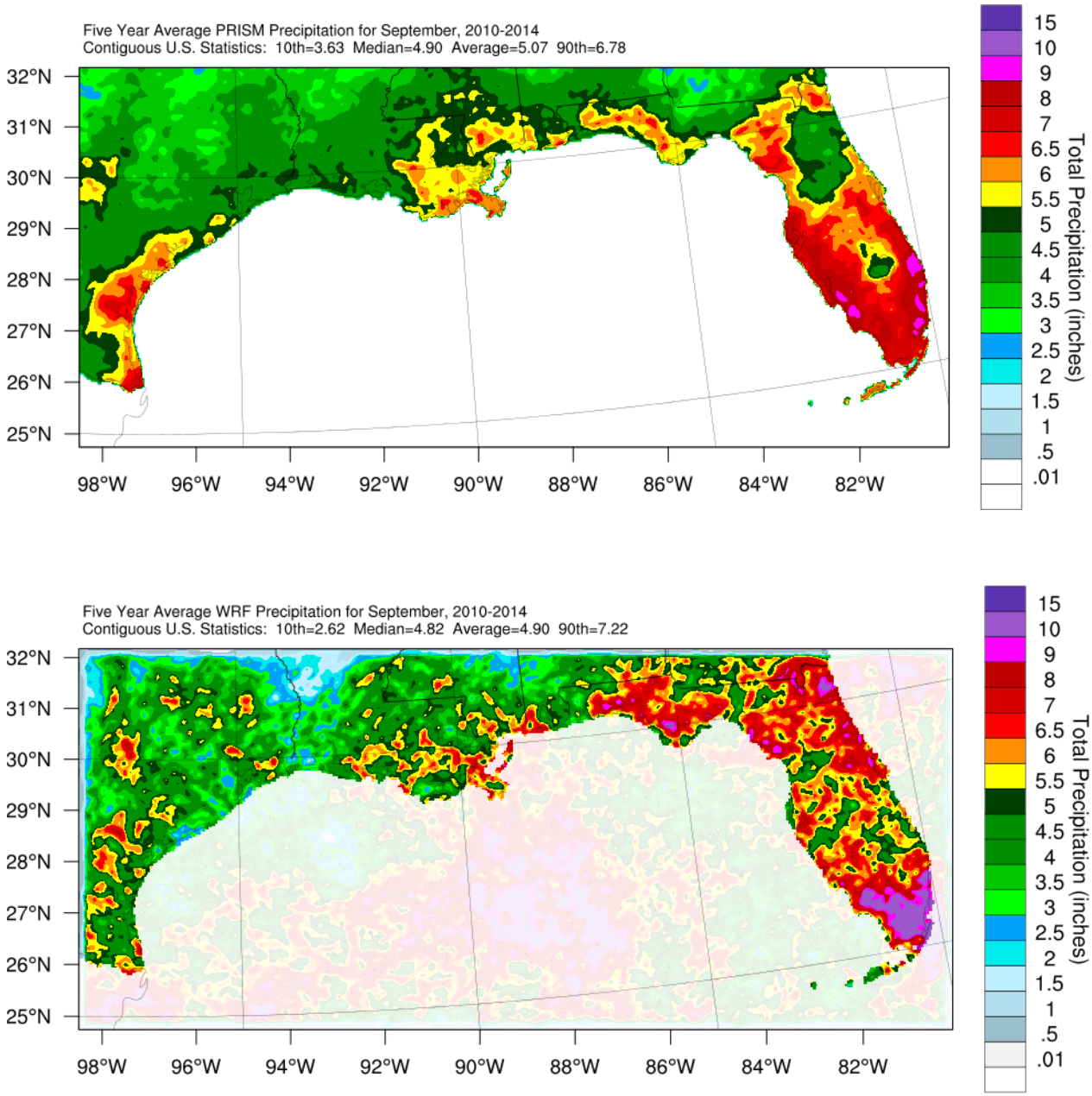

Figure 2-51. 5-Year Average (2010–2014) September PRISM Precipitation (top) and WRF Precipitation (bottom), 4-km Domain

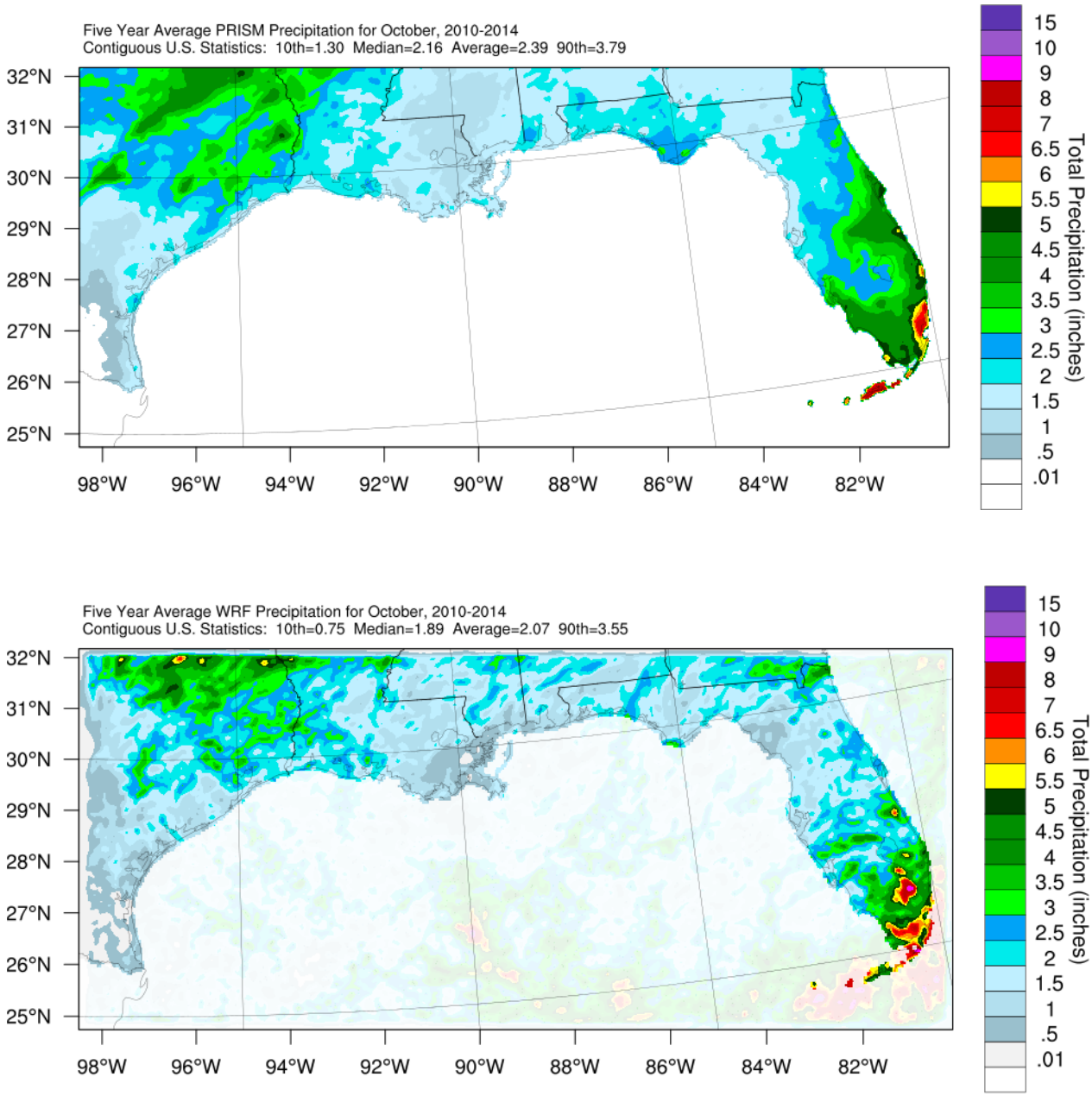

Figure 2-52. 5-Year Average (2010–2014) October PRISM Precipitation (top) and WRF Precipitation (bottom), 4-km Domain

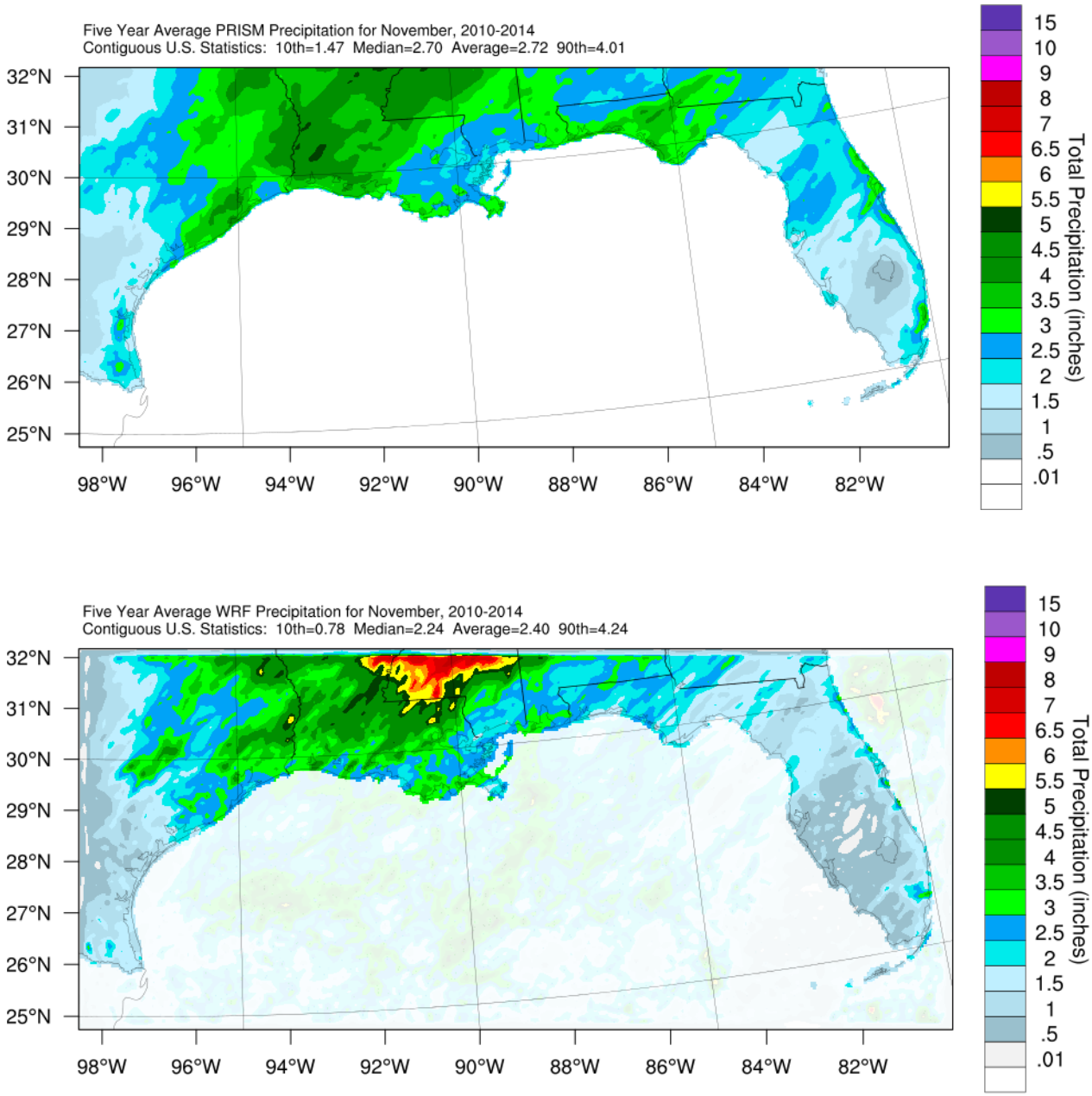

Figure 2-53. 5-Year Average (2010–2014) November PRISM Precipitation (top) and WRF Precipitation (bottom), 4-km Domain

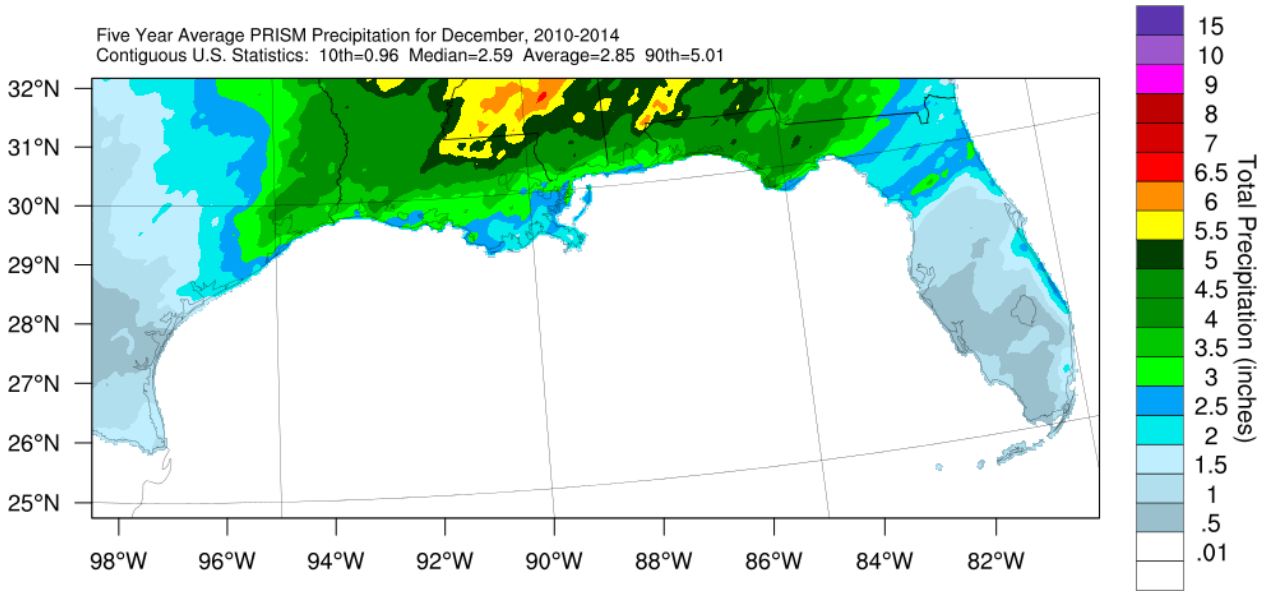

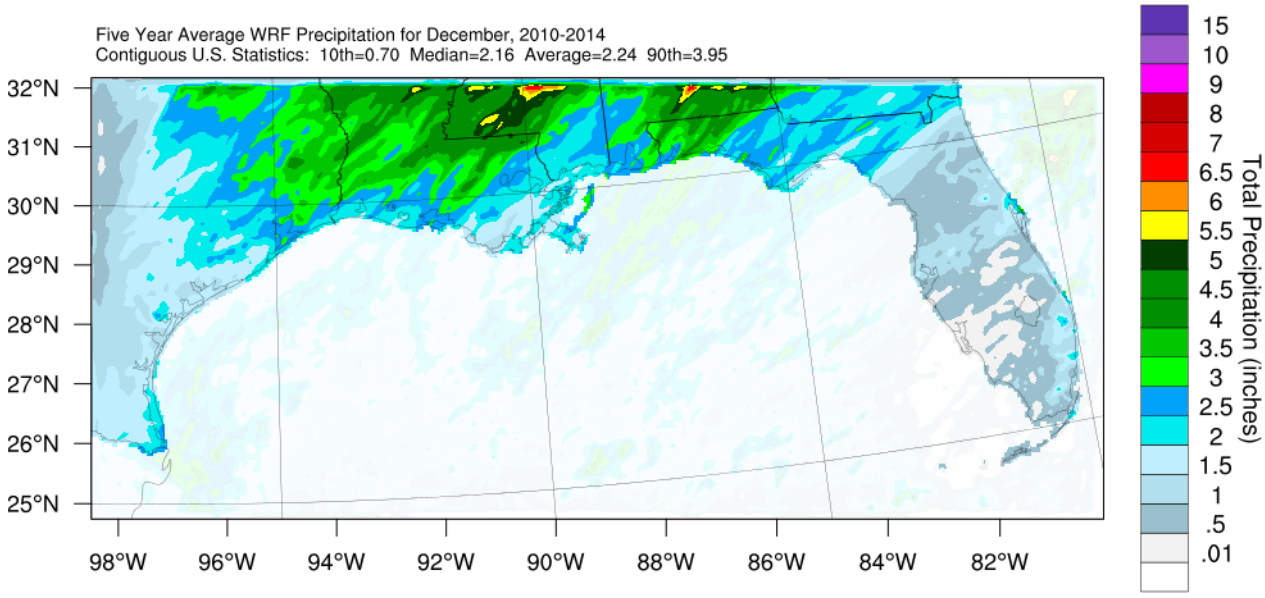

Figure 2-54. 5-Year Average (2010–2014) December PRISM Precipitation (top) and WRF Precipitation (bottom), 4-km Domain

2.3.4.2 Evaluation over Water Using Satellite Precipitation

Ramboll re-projected and aggregated the TRMM data to the WRF projection's grid cell locations, then plotted the resulting gridded data and saved the gridded fields. This allows for a consistent visual qualitative comparison. Figure 2-55 through Figure 2-66 show WRF precipitation averages compared to TRMM precipitation averages in the 12-km domain.

The 0.5-degree (approximately 55 km) TRMM dataset is at a lower resolution than the 4-km PRISM dataset; as a result, the satellite precipitation fields appear much coarser in the 4-km domain. Additionally, near the end of the WRF modeling period, the satellite hosting the TRMM sensor ran out of propellant. This caused its orbit to slowly decay, casting into doubt the validity of the derived rainfall quantities; thus, only a qualitative comparison is presented below. The following plots show TRMM data used to assess the accuracy of the WRF precipitation, and each month is presented as a 5-year average from the 2010–2014 modeling period.

In Figure 2-67 through Figure 2-71, WRF underpredicts precipitation over the offshore portions of the domain, compared to TRMM for the averaging months of January through May in the 4-km domain. January through May is not typically the season when high ozone values are observed. WRF performs well at predicting precipitation from June through October (Figure 2-72 through Figure 2-76) when high ozone values are typically observed in some onshore locations. The spatial extent of increased rainfall over the southeast Gulf states, stretching out over the coastlines, is well-represented through the summertime (ozone) months. In Figure 2-77 and Figure 2-78, WRF slightly underpredicts the amount of rainfall in the offshore portions of the Gulf, compared to the TRMM precipitation averages for November and December. Even with the coarse TRMM resolution, it appears the model has a slight dry bias in the overwater portions of the domain in the colder months.

Given the coarser resolution of the TRMM plots, WRF tends to under-forecast precipitation intensity overall in the offshore portions of the Gulf throughout the winter and spring months and does a satisfactory job at forecasting the amount of rainfall over water in the summer and fall months in the 4-km domain.

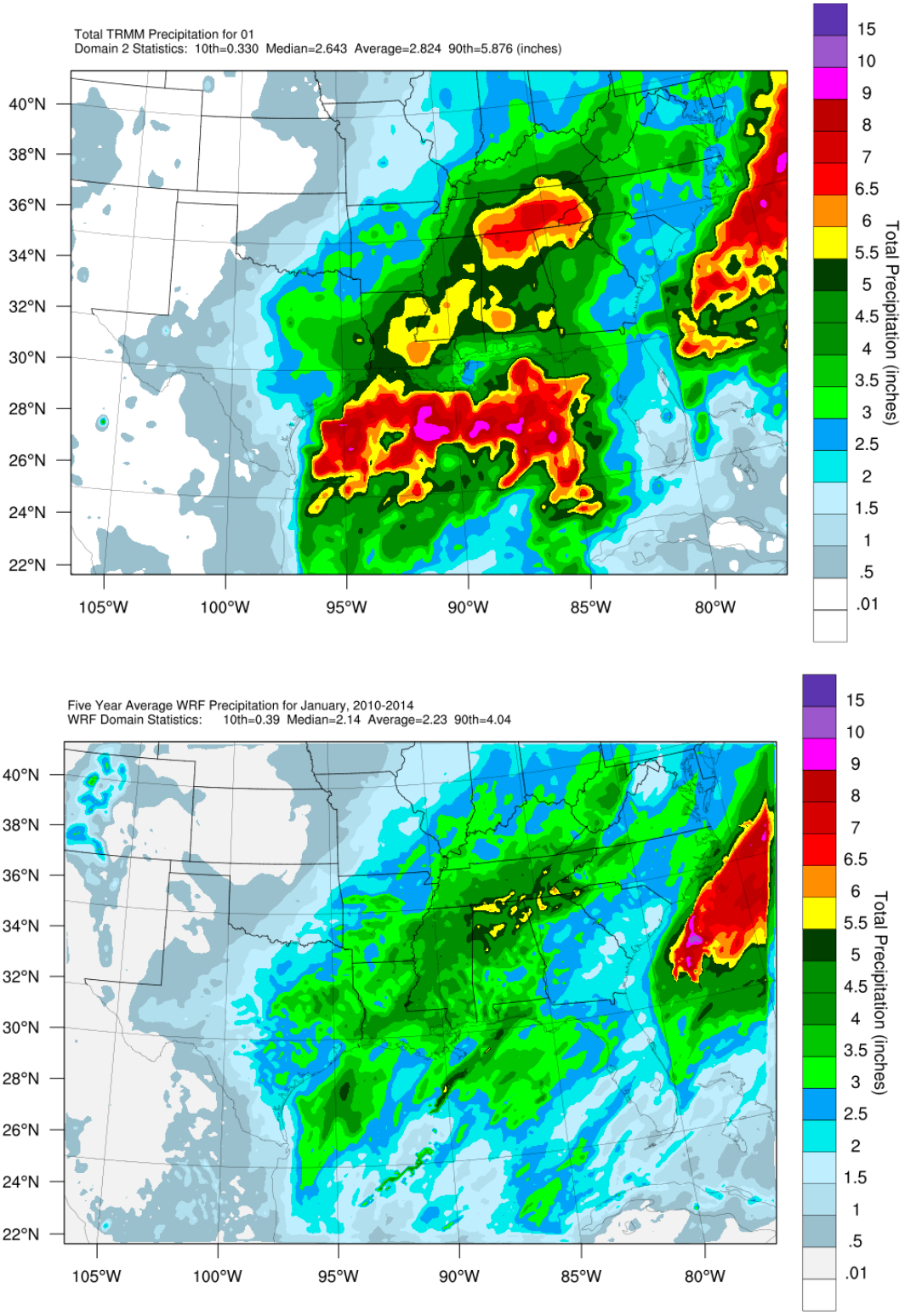

Figure 2-55. 5-Year (2010–2014) January TRMM Precipitation Average (top) and WRF Precipitation Average (bottom), 12-km Domain

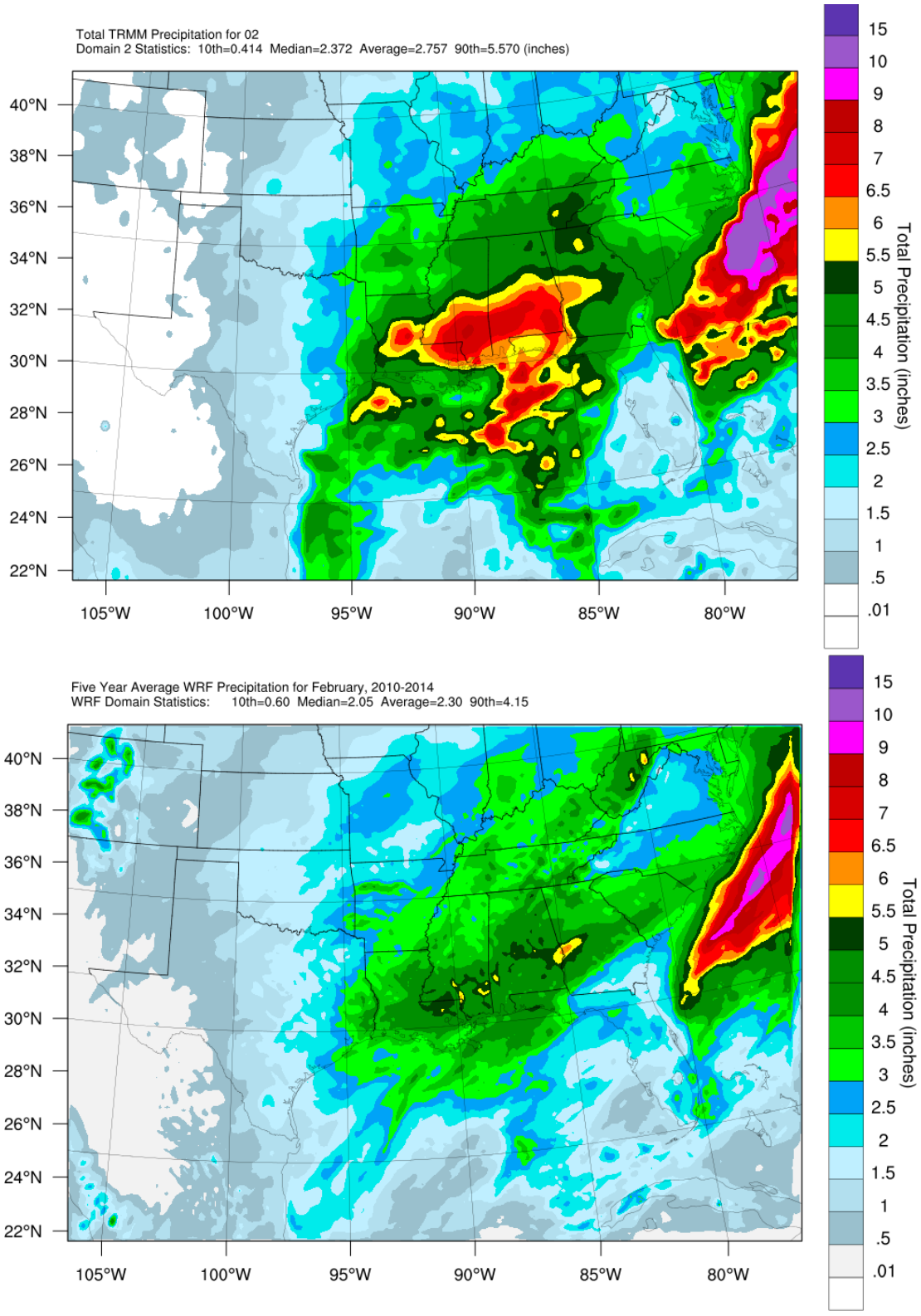

Figure 2-56. 5-Year (2010–2014) February TRMM Precipitation Average (top) and WRF Precipitation Average (bottom), 12-km Domain

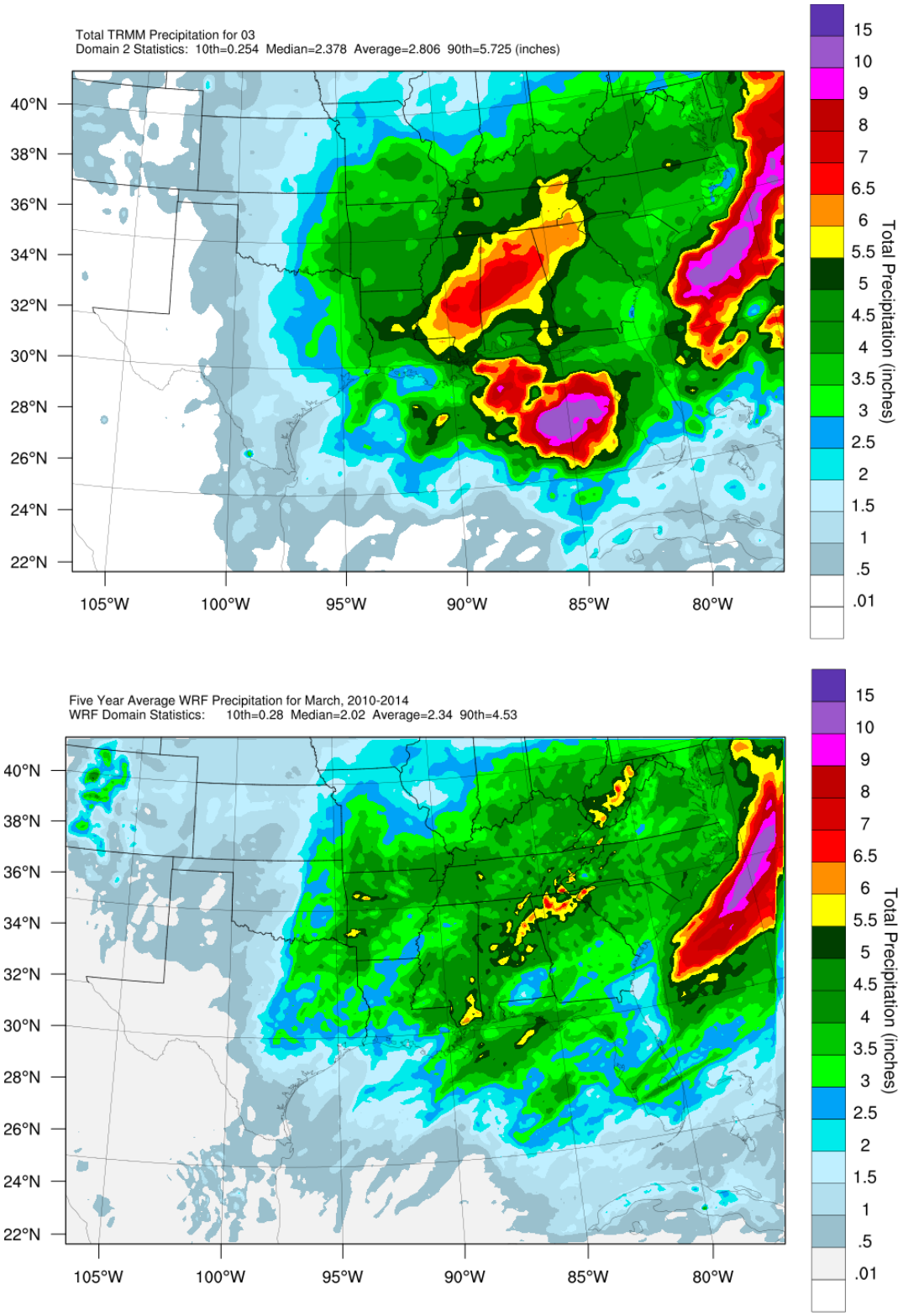

Figure 2-57. 5-Year (2010–2014) March TRMM Precipitation Average (top) and WRF Precipitation Average (bottom), 12-km Domain

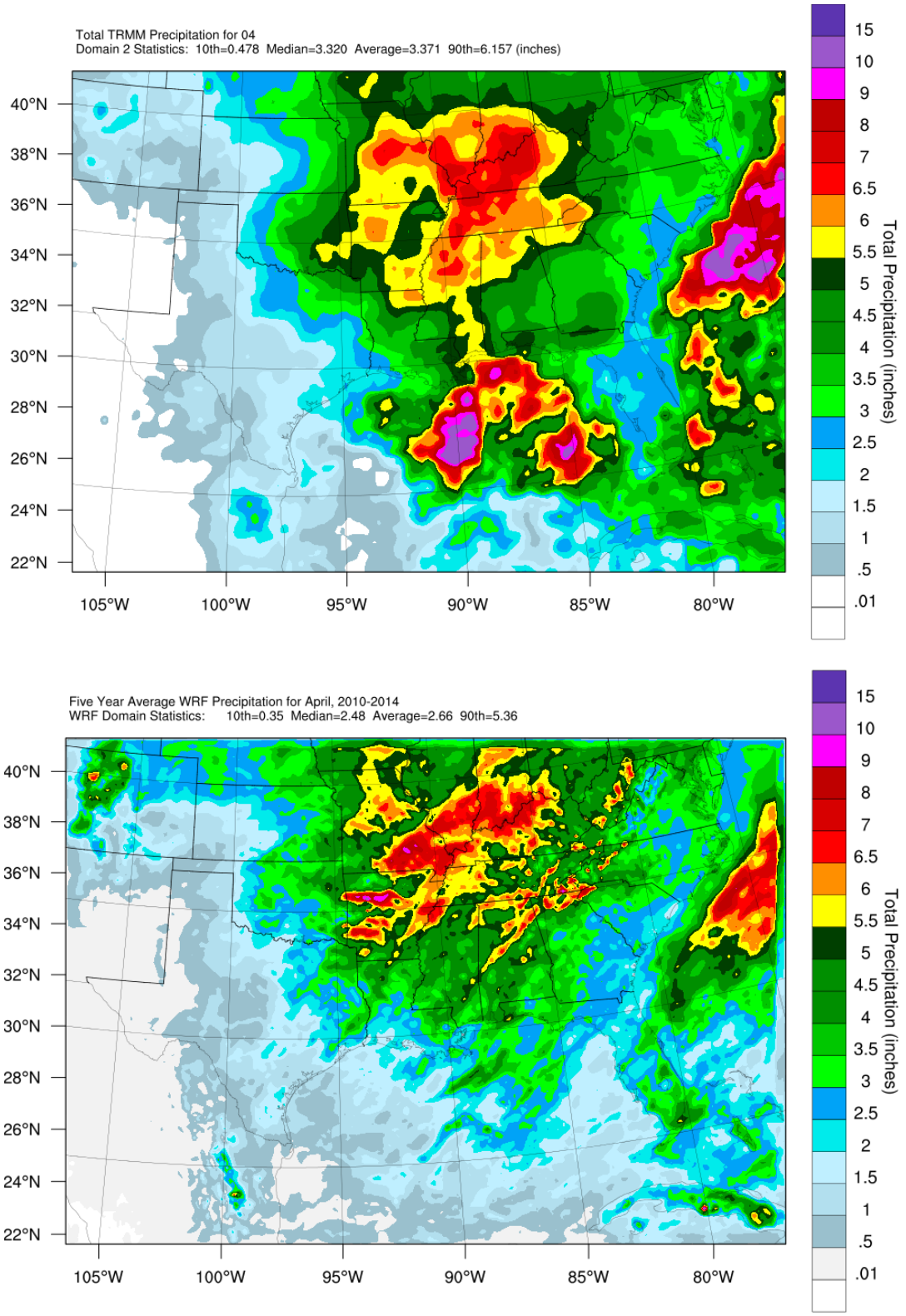

Figure 2-58. 5-Year (2010–2014) April TRMM Precipitation Average (top) and WRF Precipitation Average (bottom), 12-km Domain

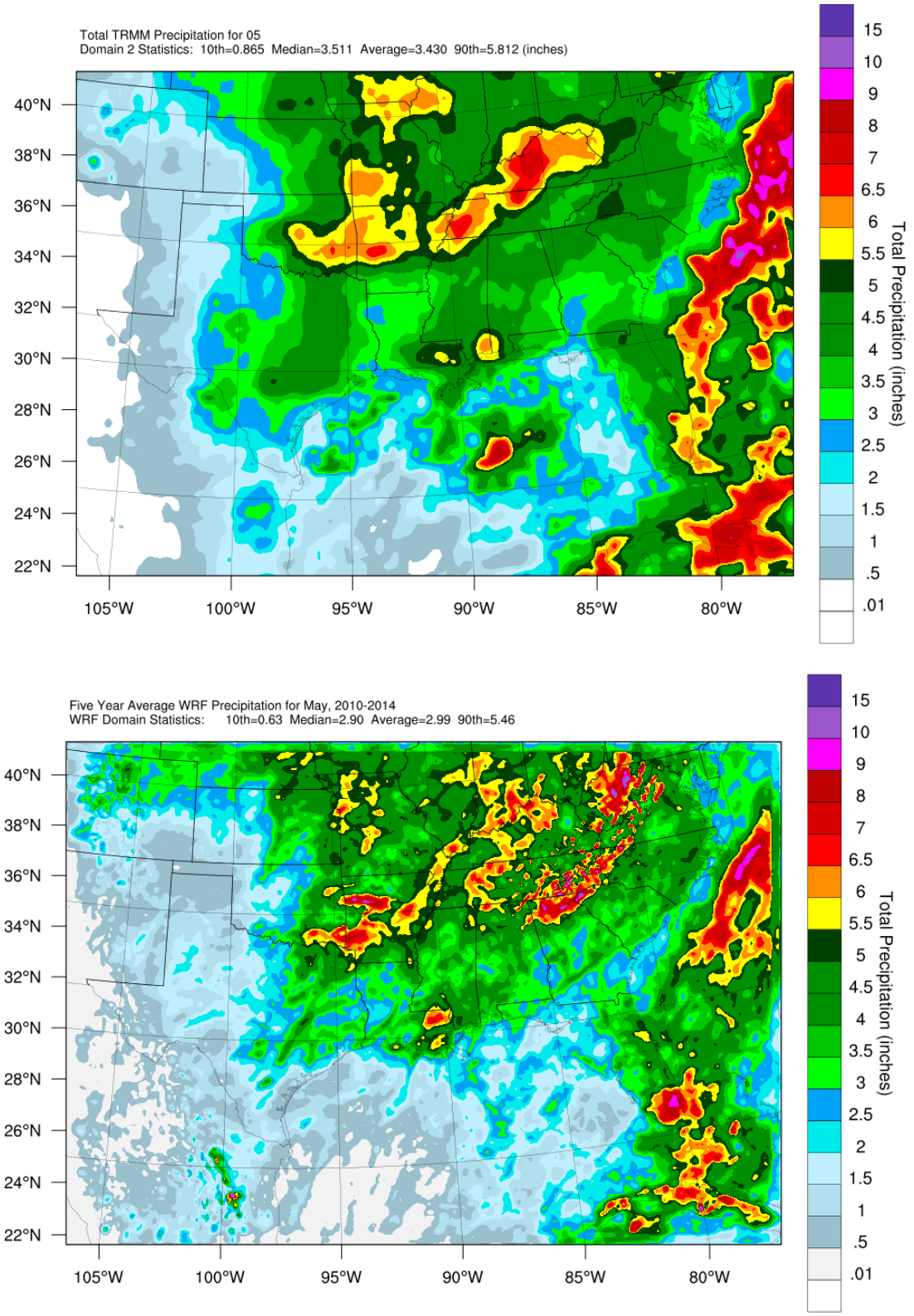

Figure 2-59. 5-Year (2010–2014) May TRMM Precipitation Average (top) and WRF Precipitation Average (bottom), 12-km Domain

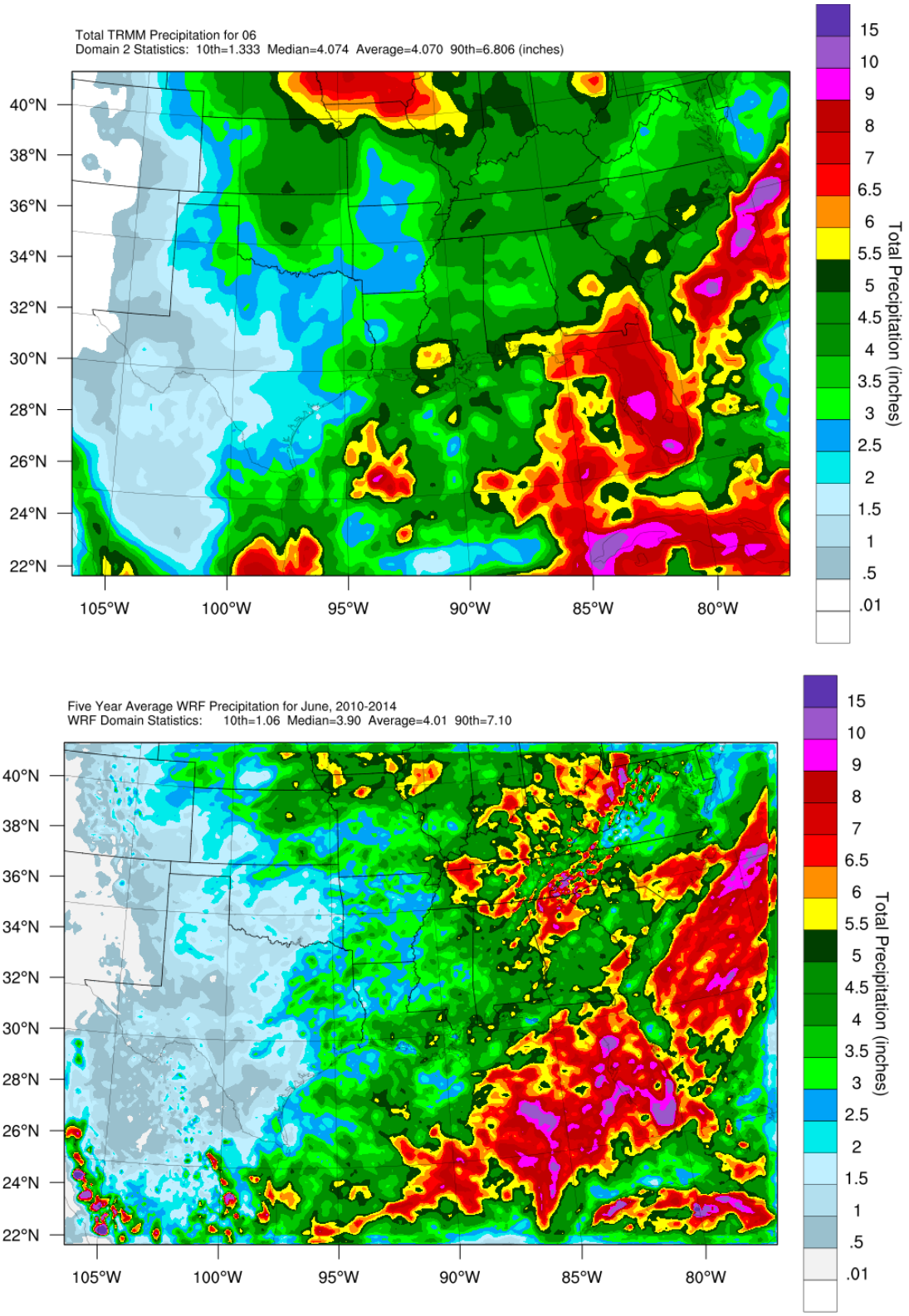

Figure 2-60. 5-Year (2010–2014) June TRMM Precipitation Average (top) and WRF Precipitation Average (bottom), 12-km Domain

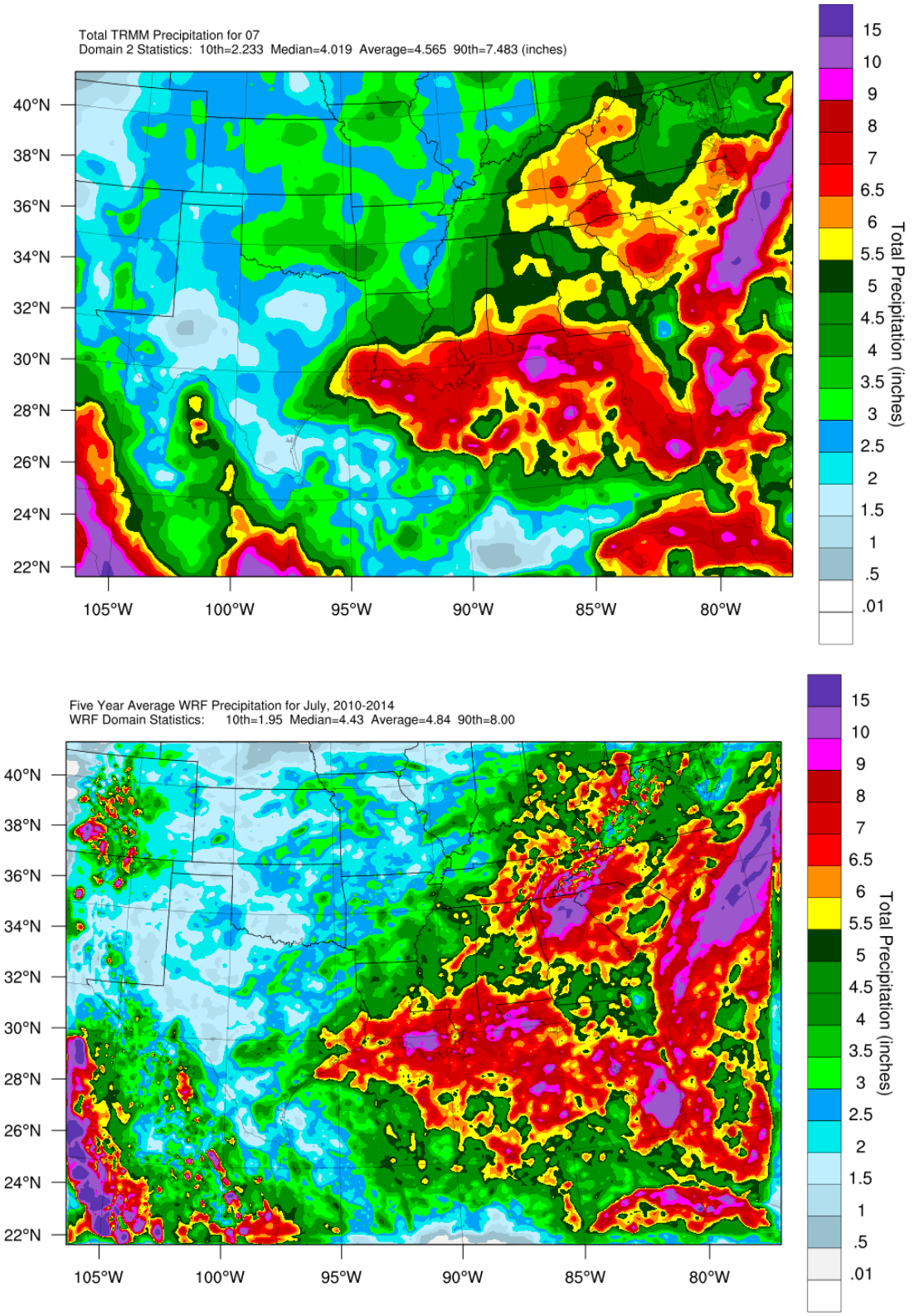

Figure 2-61. 5-Year (2010–2014) July TRMM Precipitation Average (top) and WRF Precipitation Average (bottom), 12-km Domain

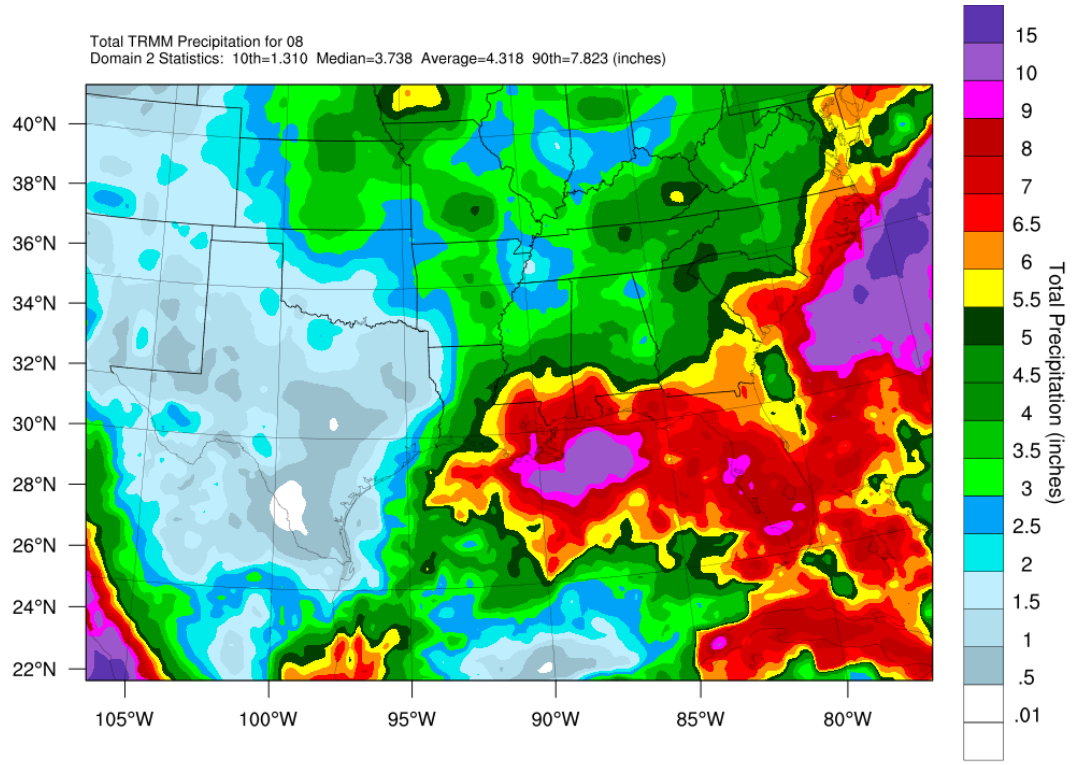

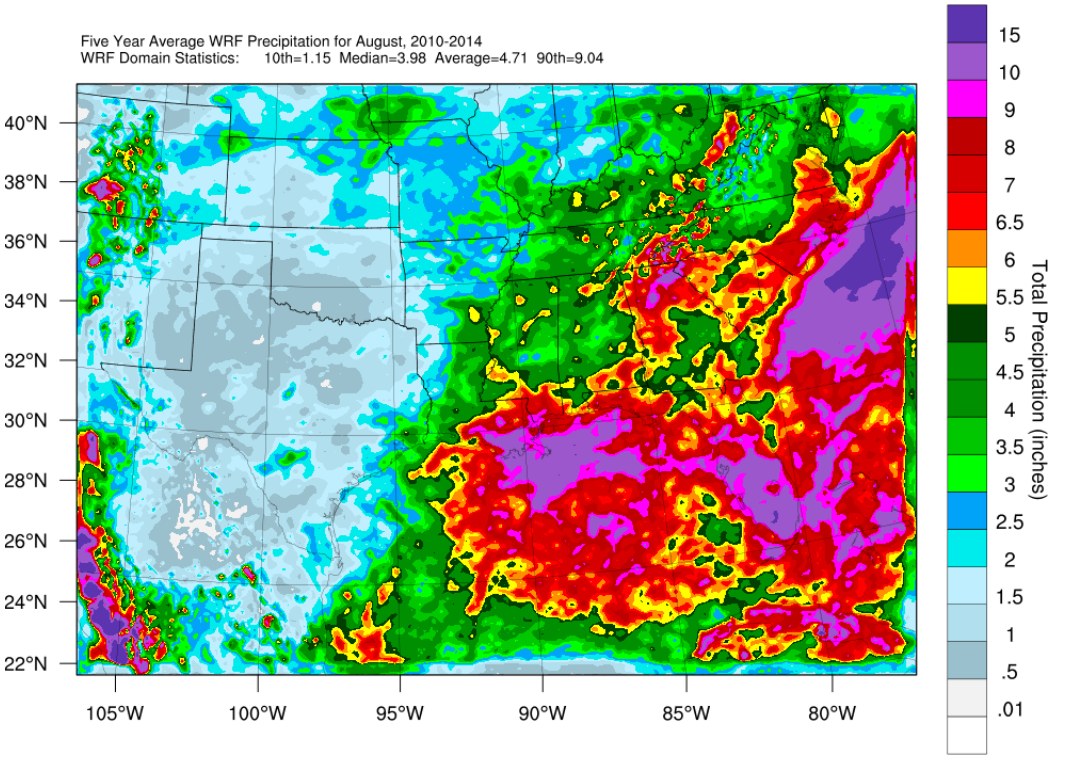

Figure 2-62. 5-Year (2010–2014) August TRMM Precipitation Average (top) and WRF Precipitation Average (bottom), 12-km Domain

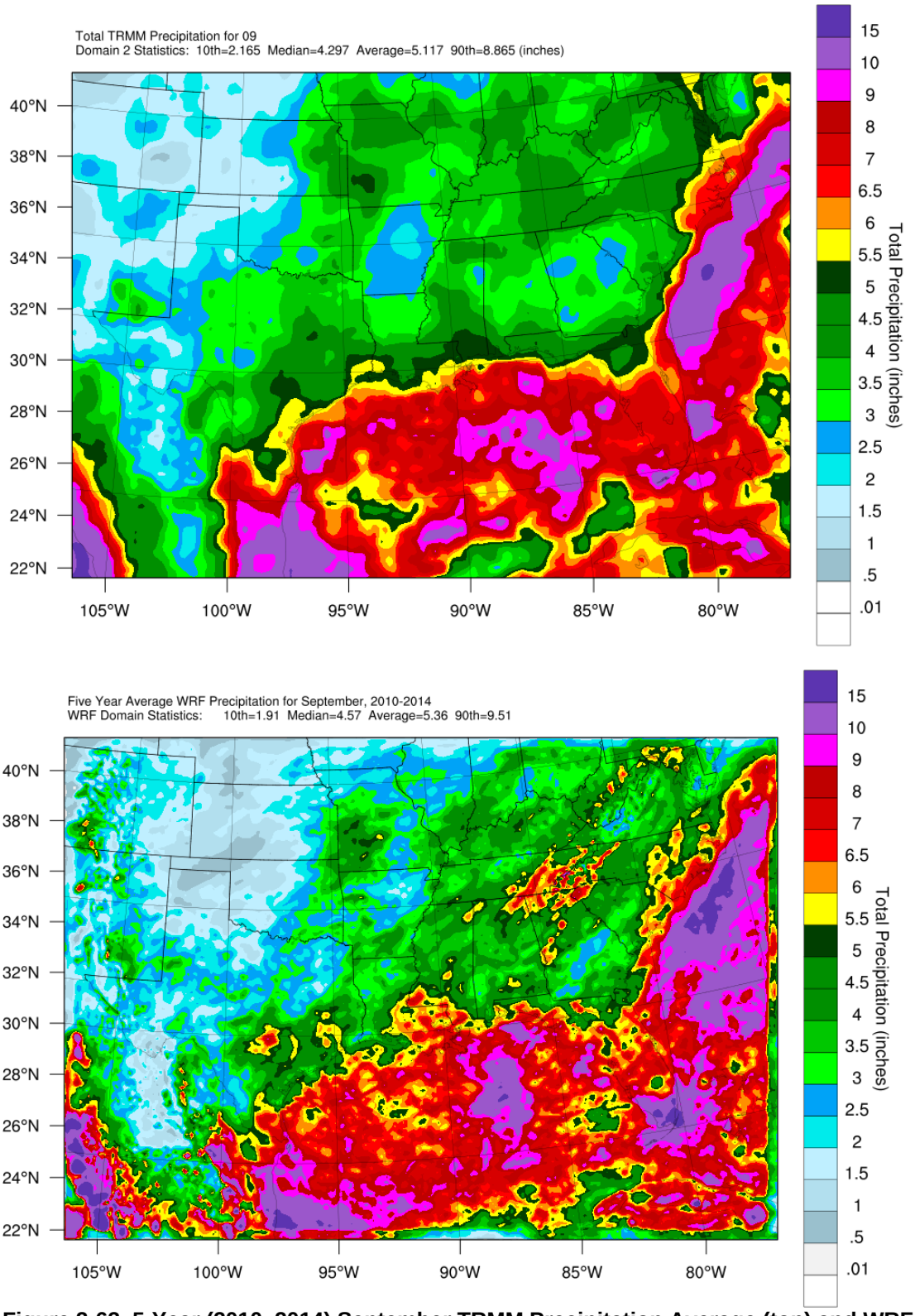

Figure 2-63. 5-Year (2010–2014) September TRMM Precipitation Average (top) and WRF Precipitation Average (bottom), 12-km Domain

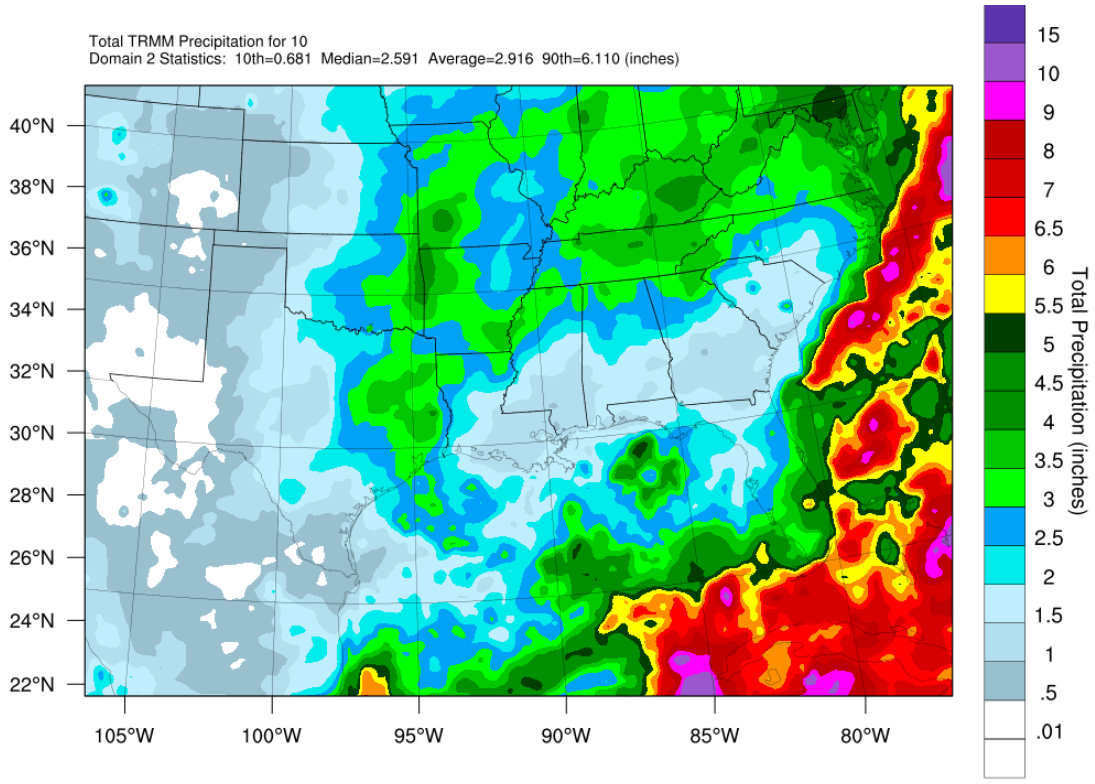

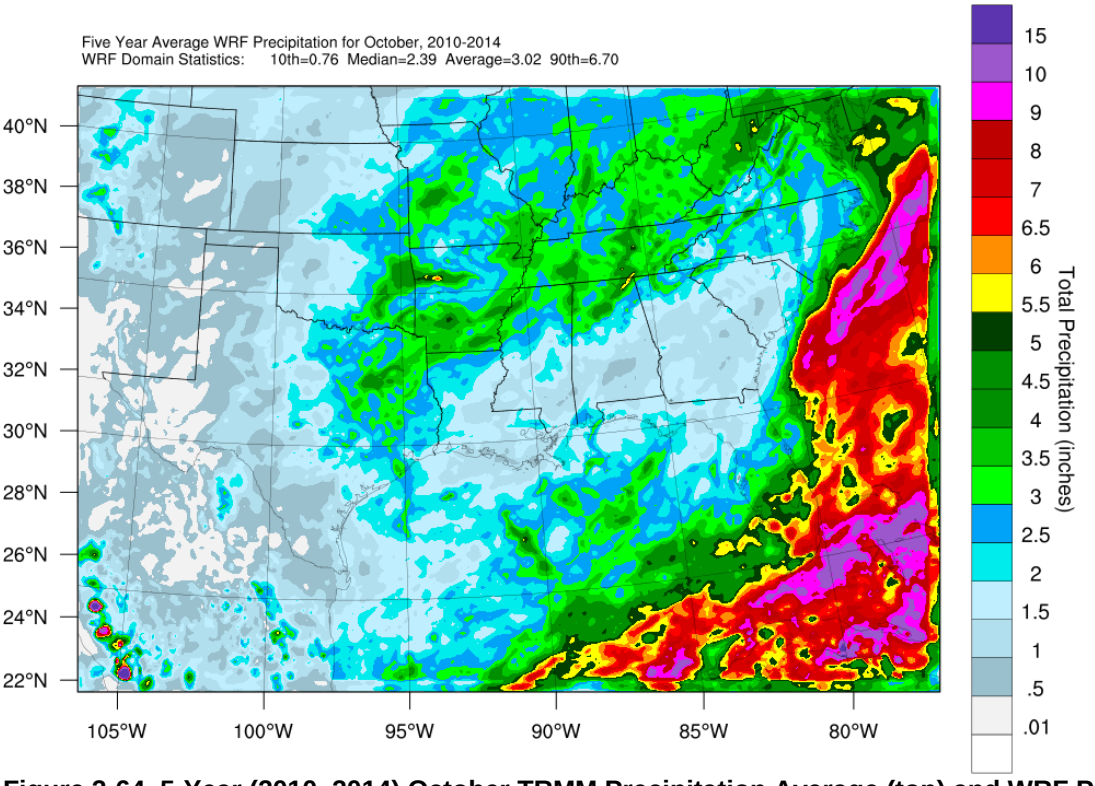

Figure 2-64. 5-Year (2010–2014) October TRMM Precipitation Average (top) and WRF Precipitation Average (bottom), 12-km Domain

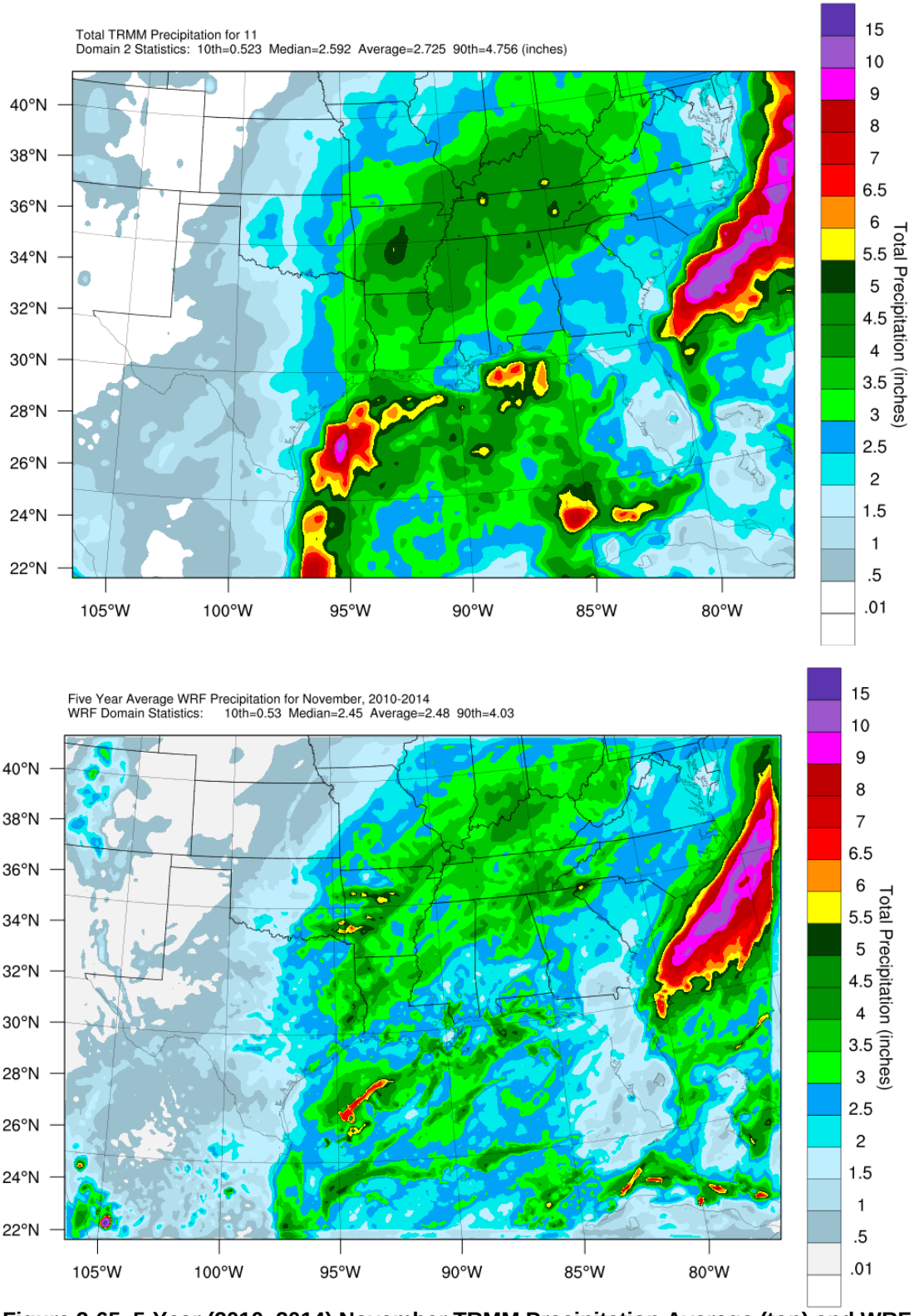

Figure 2-65. 5-Year (2010–2014) November TRMM Precipitation Average (top) and WRF Precipitation Average (bottom), 12-km Domain

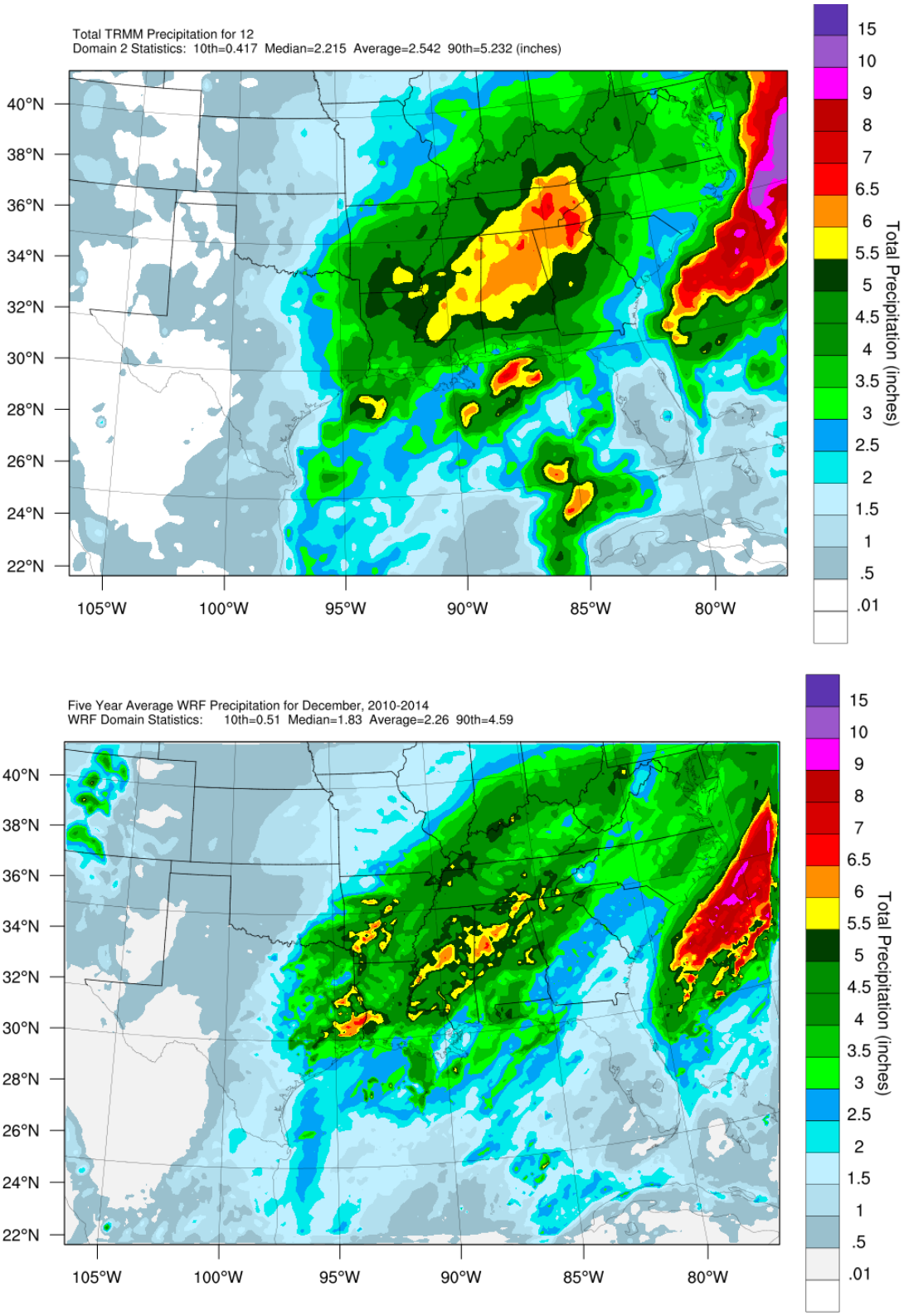

Figure 2-66. 5-Year (2010–2014) December TRMM Precipitation Average (top) and WRF Precipitation Average (bottom), 12-km Domain

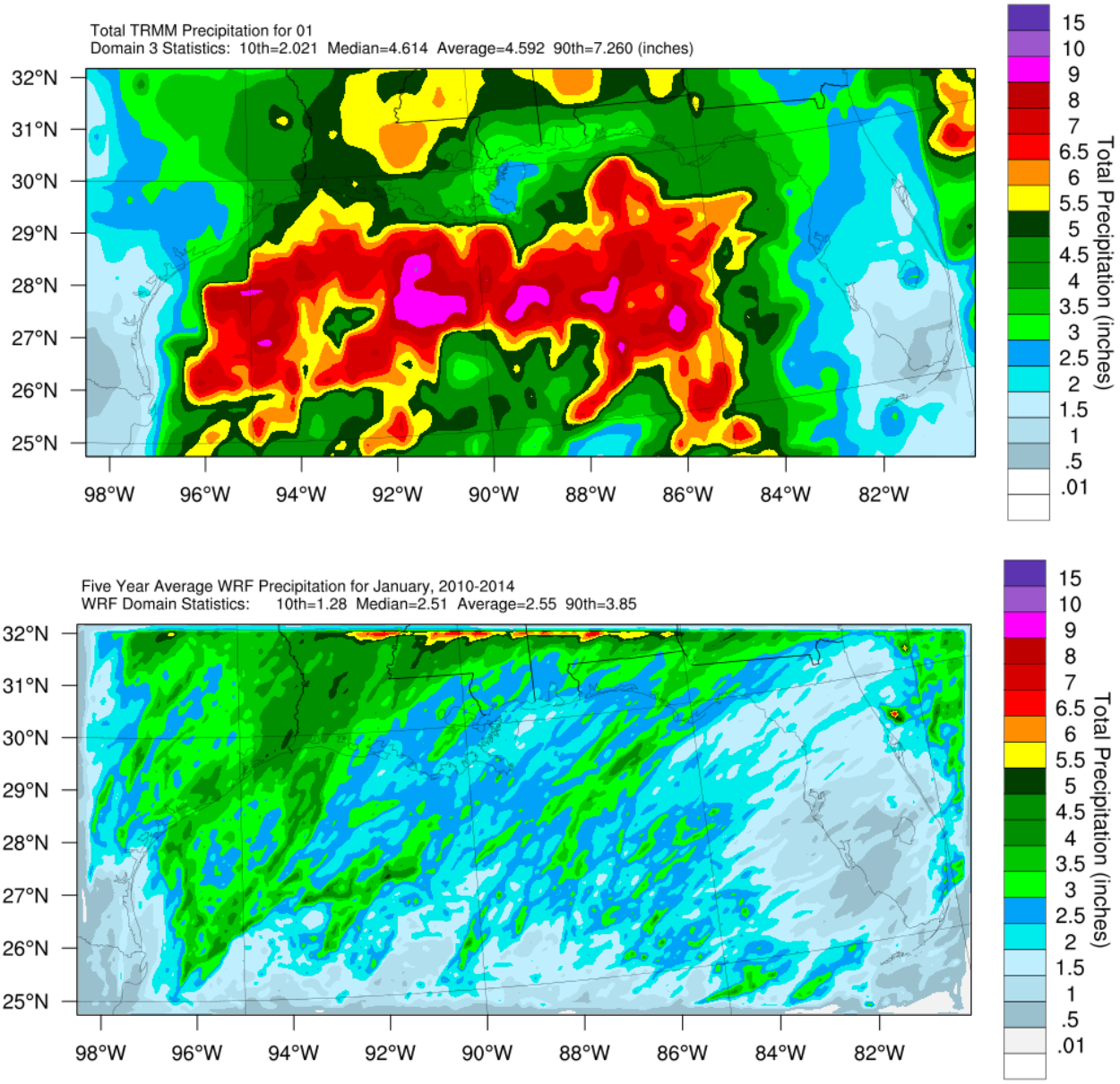

Figure 2-67. 5-Year Average (2010–2014) January TRMM Precipitation (top) and WRF Precipitation (bottom), 4-km Domain

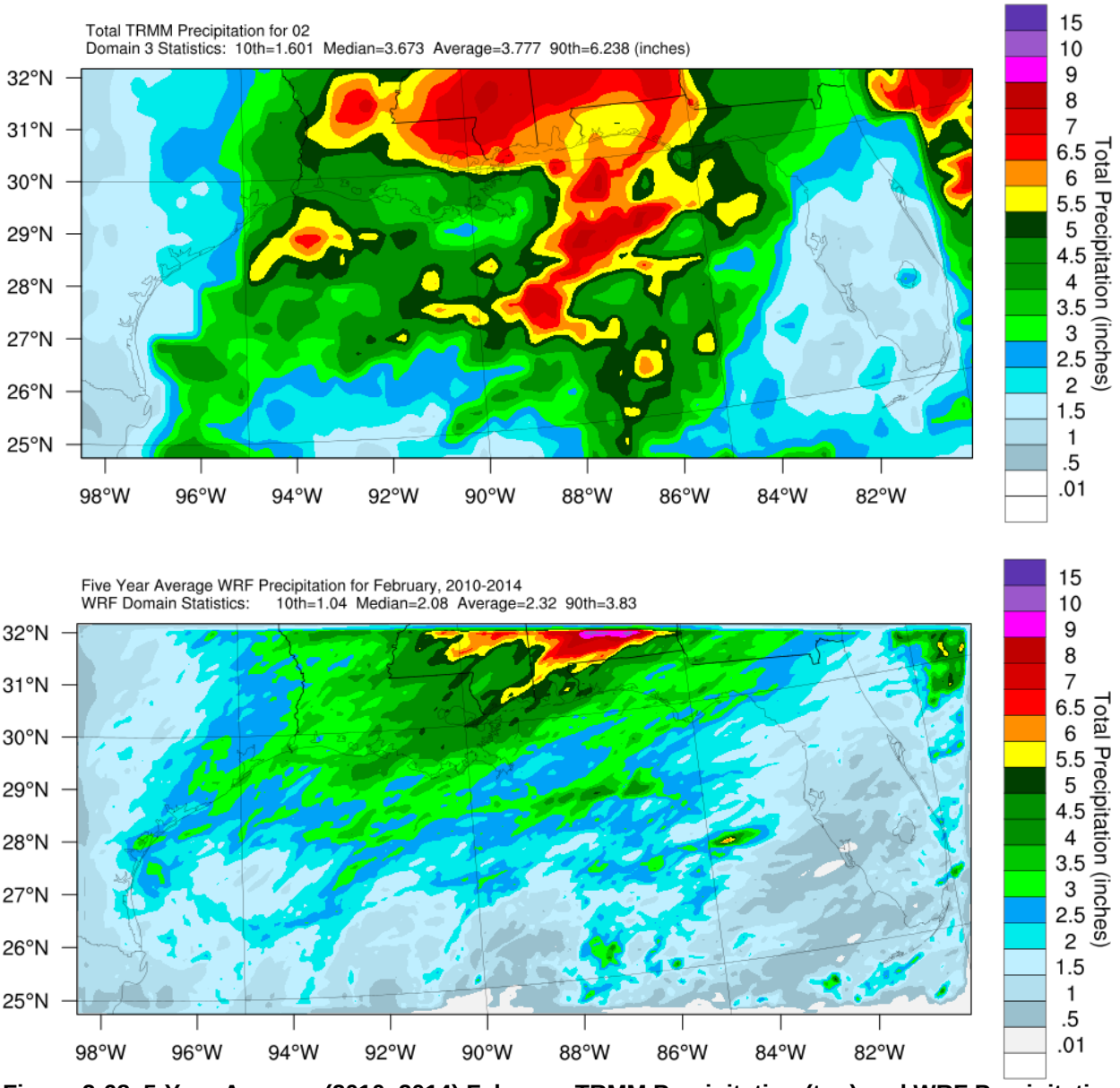

Figure 2-68. 5-Year Average (2010–2014) February TRMM Precipitation (top) and WRF Precipitation (bottom), 4-km Domain

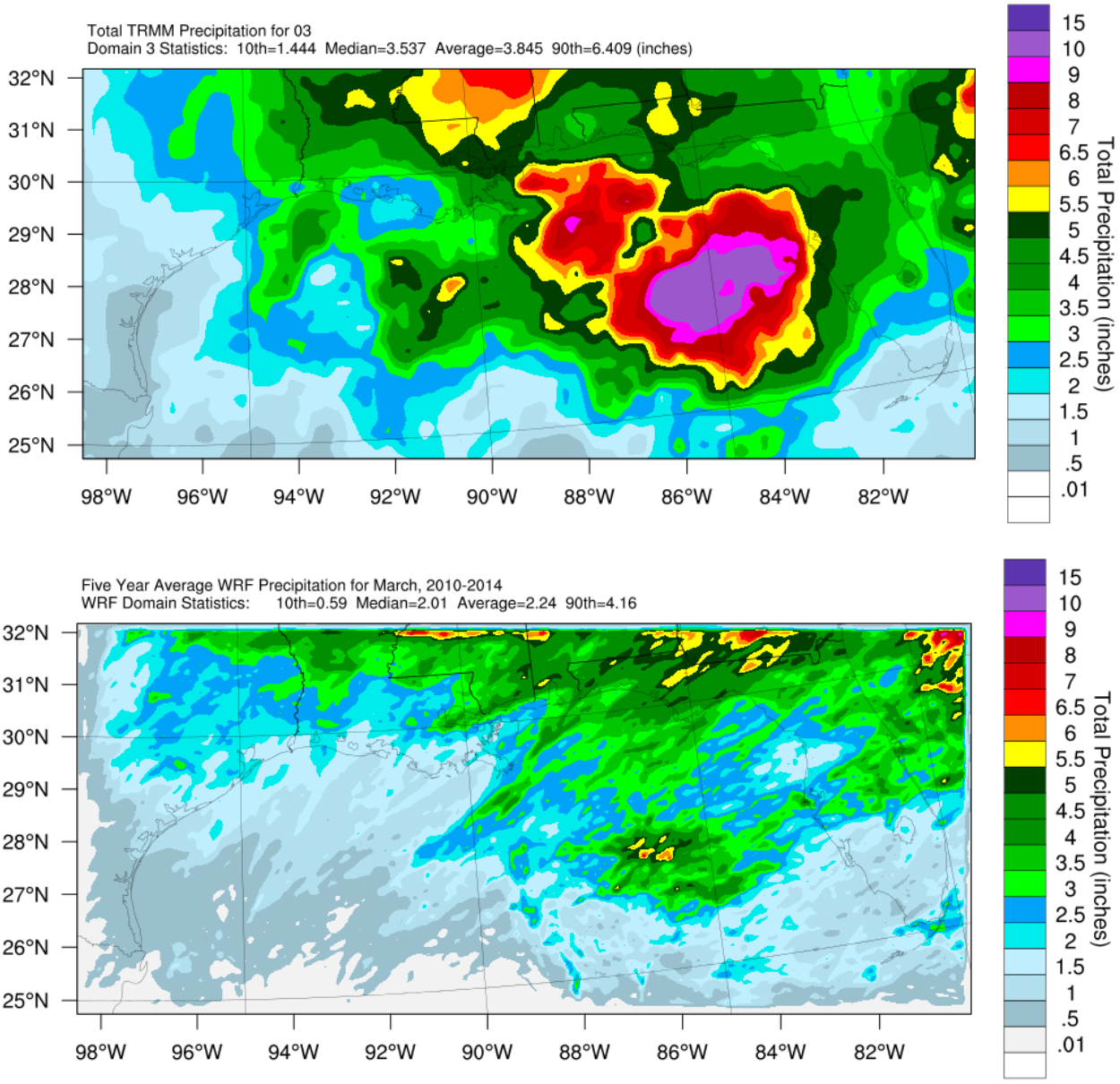

Figure 2-69. 5-Year Average (2010–2014) March TRMM Precipitation (top) and WRF Precipitation (bottom), 4-km Domain

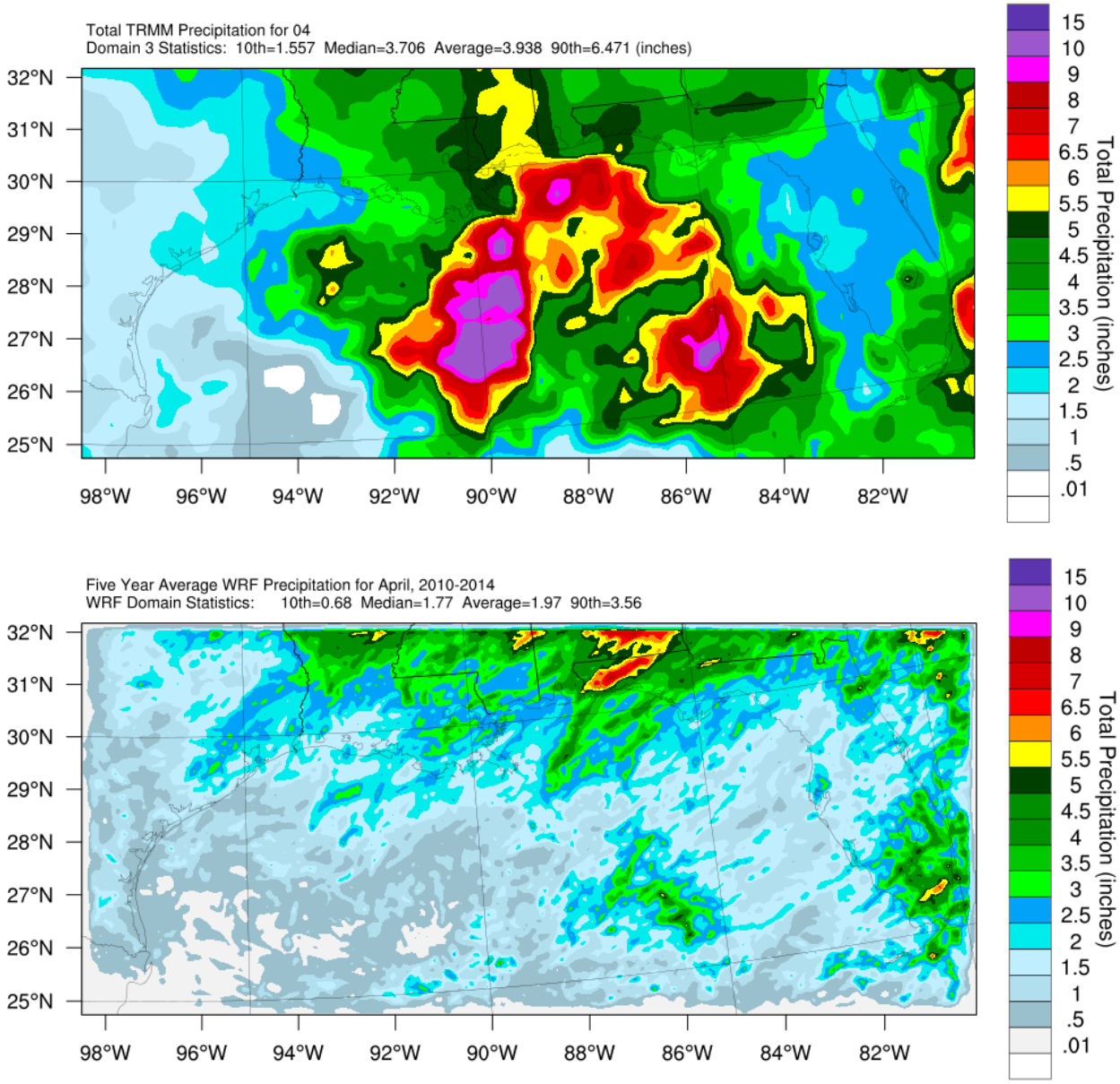

Figure 2-70. 5-Year Average (2010–2014) April TRMM Precipitation (top) and WRF Precipitation (bottom), 4-km Domain

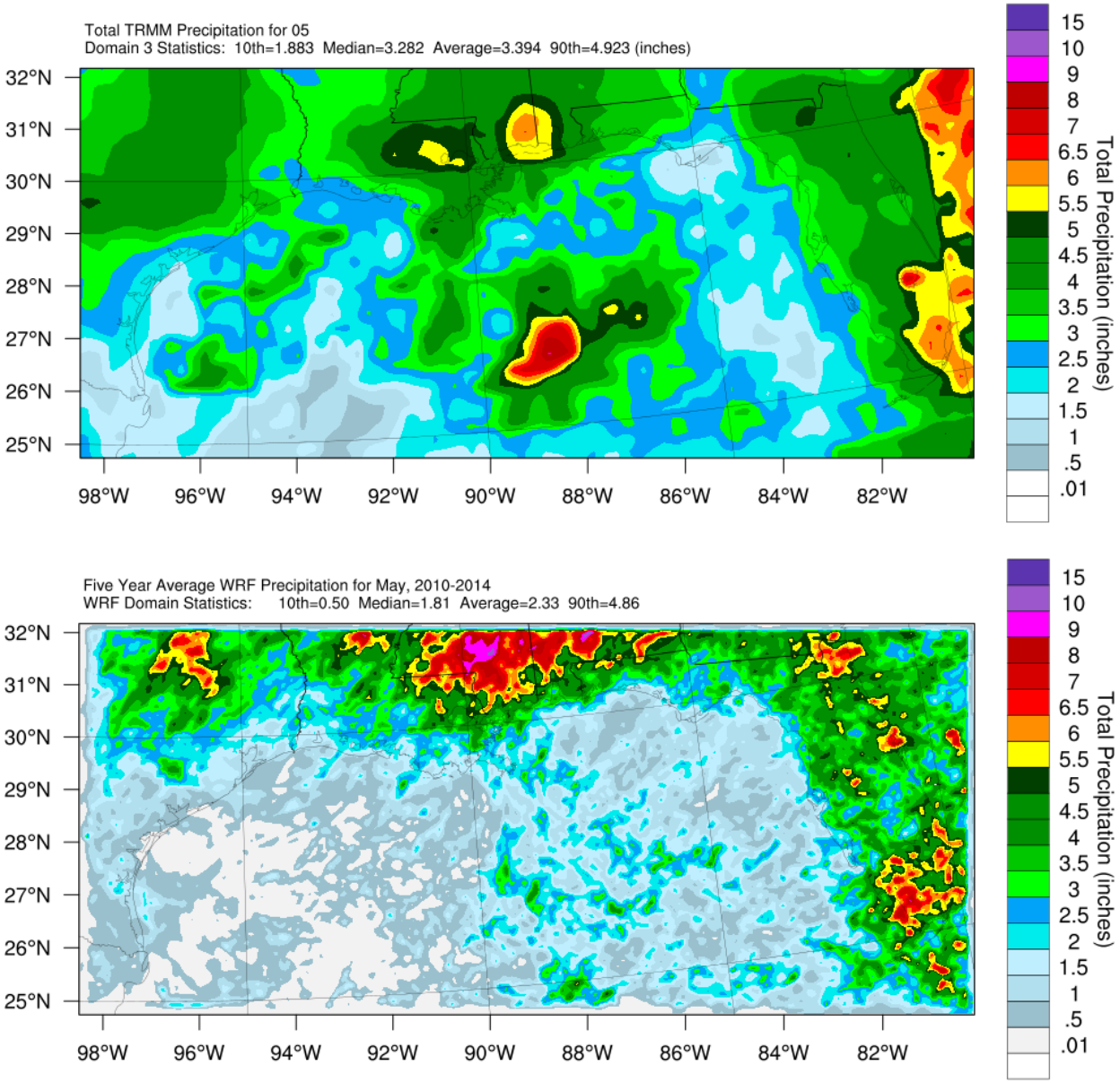

Figure 2-71. 5-Year Average (2010–2014) May TRMM Precipitation (top) and WRF Precipitation (bottom), 4-km Domain

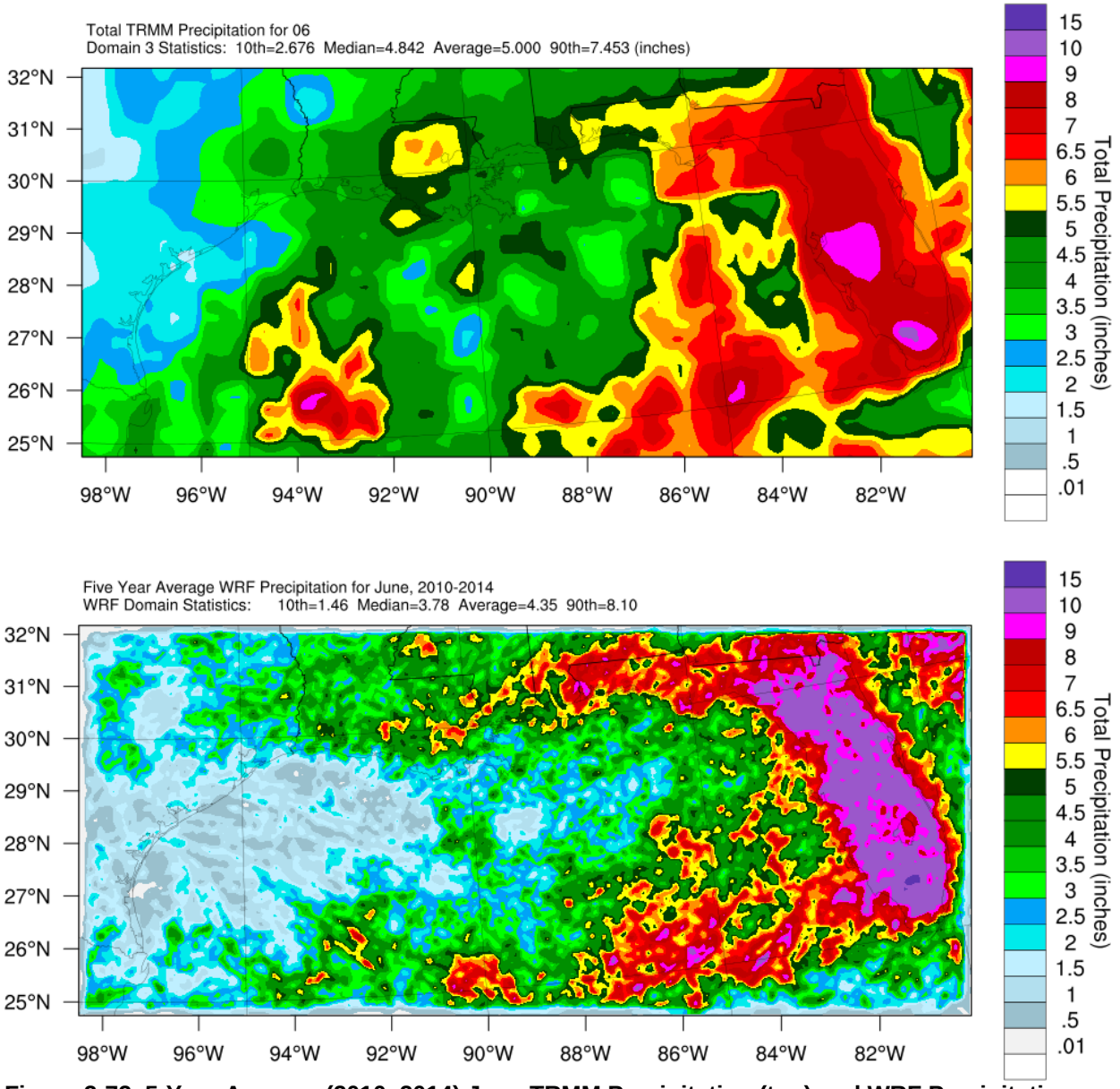

Figure 2-72. 5-Year Average (2010–2014) June TRMM Precipitation (top) and WRF Precipitation (bottom), 4-km Domain

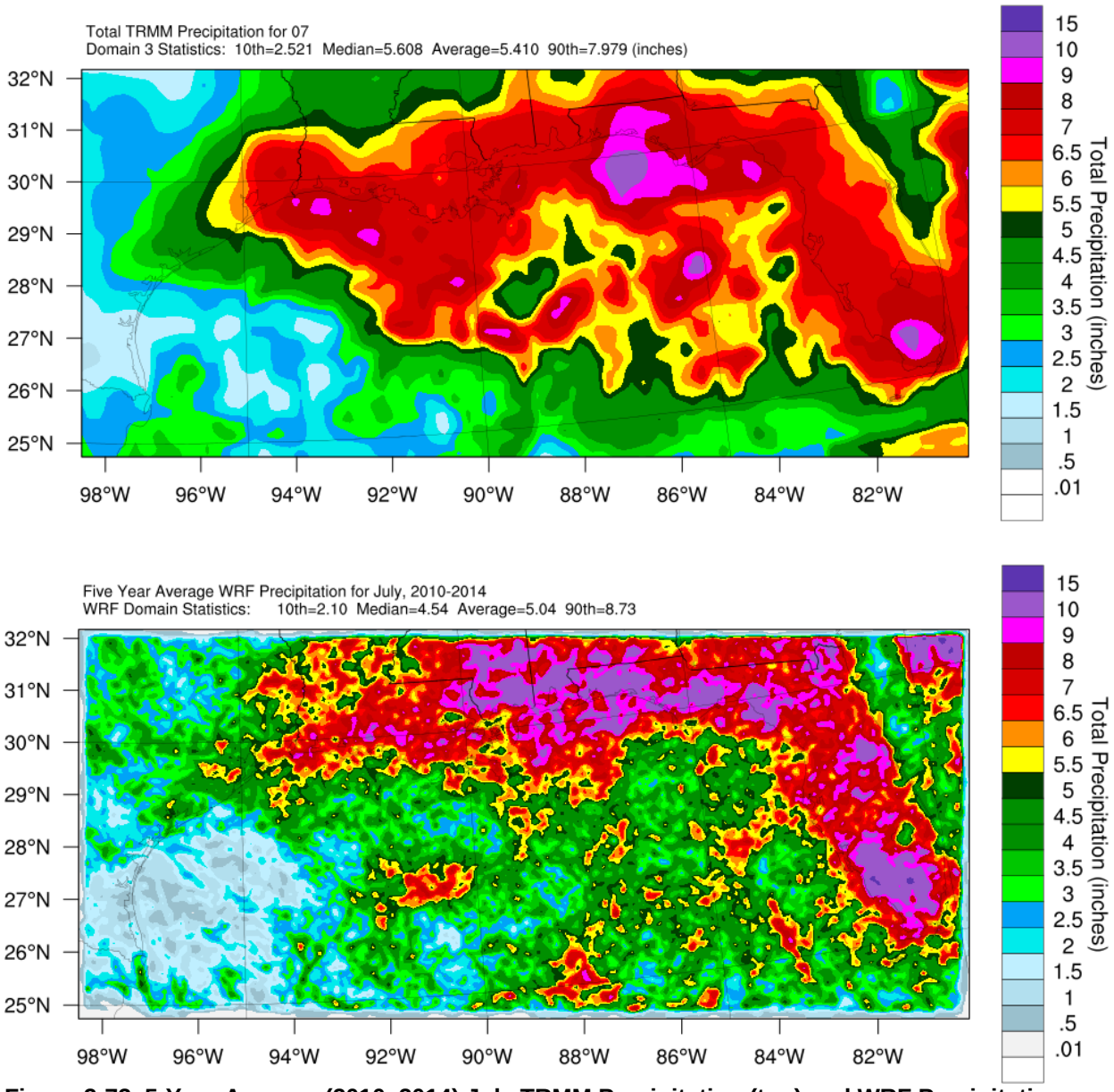

Figure 2-73. 5-Year Average (2010–2014) July TRMM Precipitation (top) and WRF Precipitation (bottom), 4-km Domain

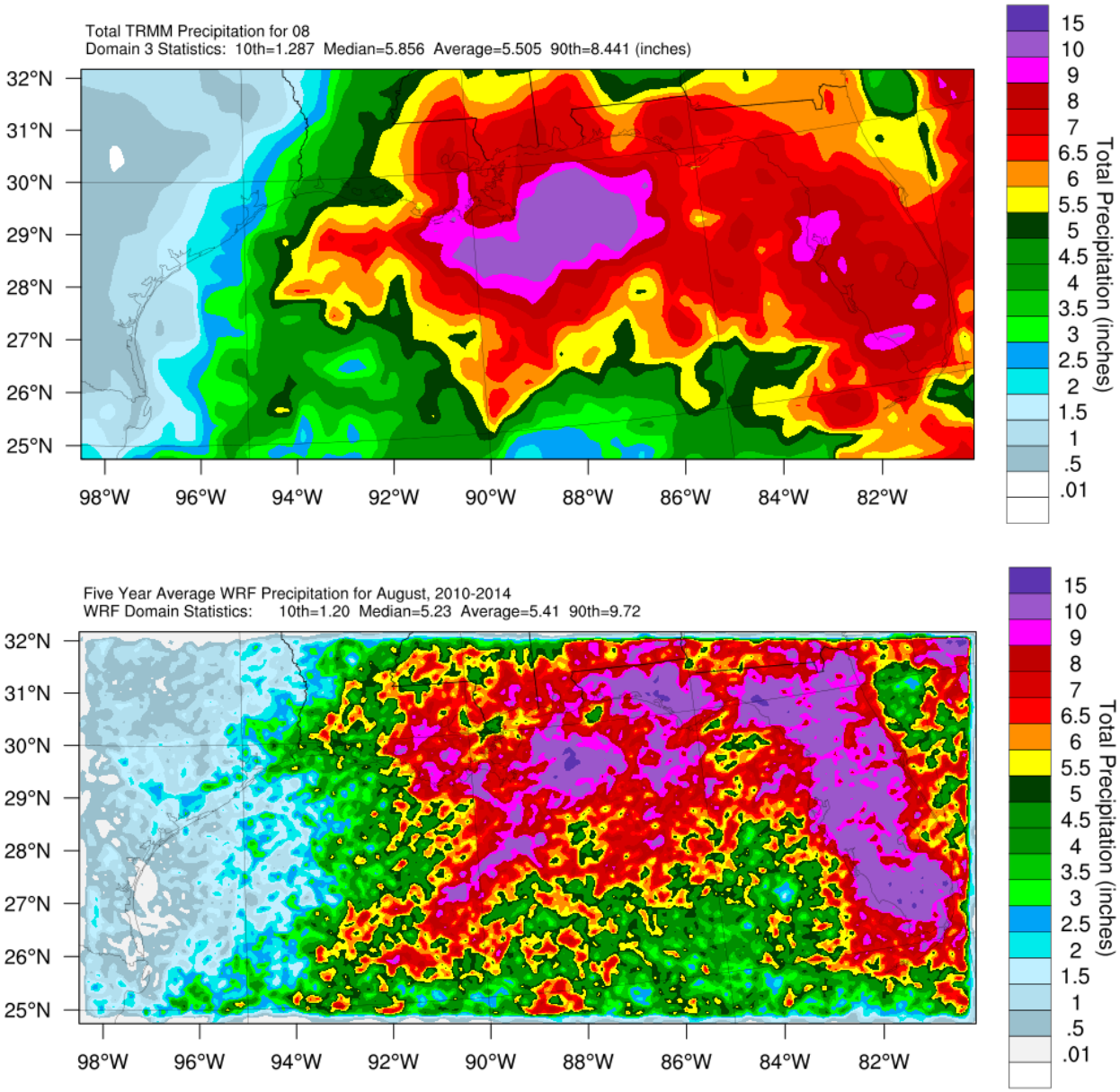

Figure 2-74. 5-Year Average (2010–2014) August TRMM Precipitation (top) and WRF Precipitation (bottom), 4-km Domain

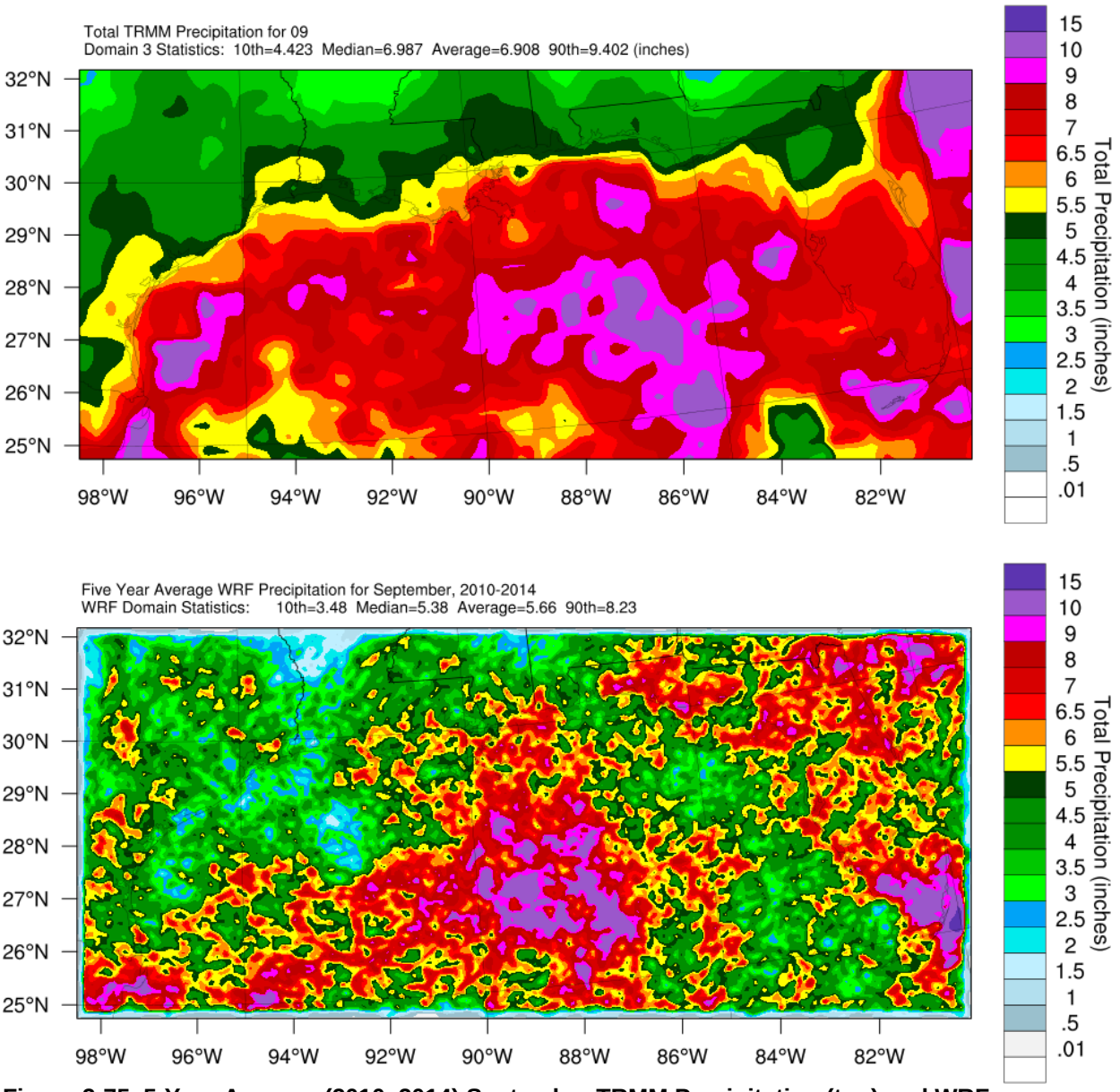

Figure 2-75. 5-Year Average (2010–2014) September TRMM Precipitation (top) and WRF Precipitation (bottom), 4-km Domain

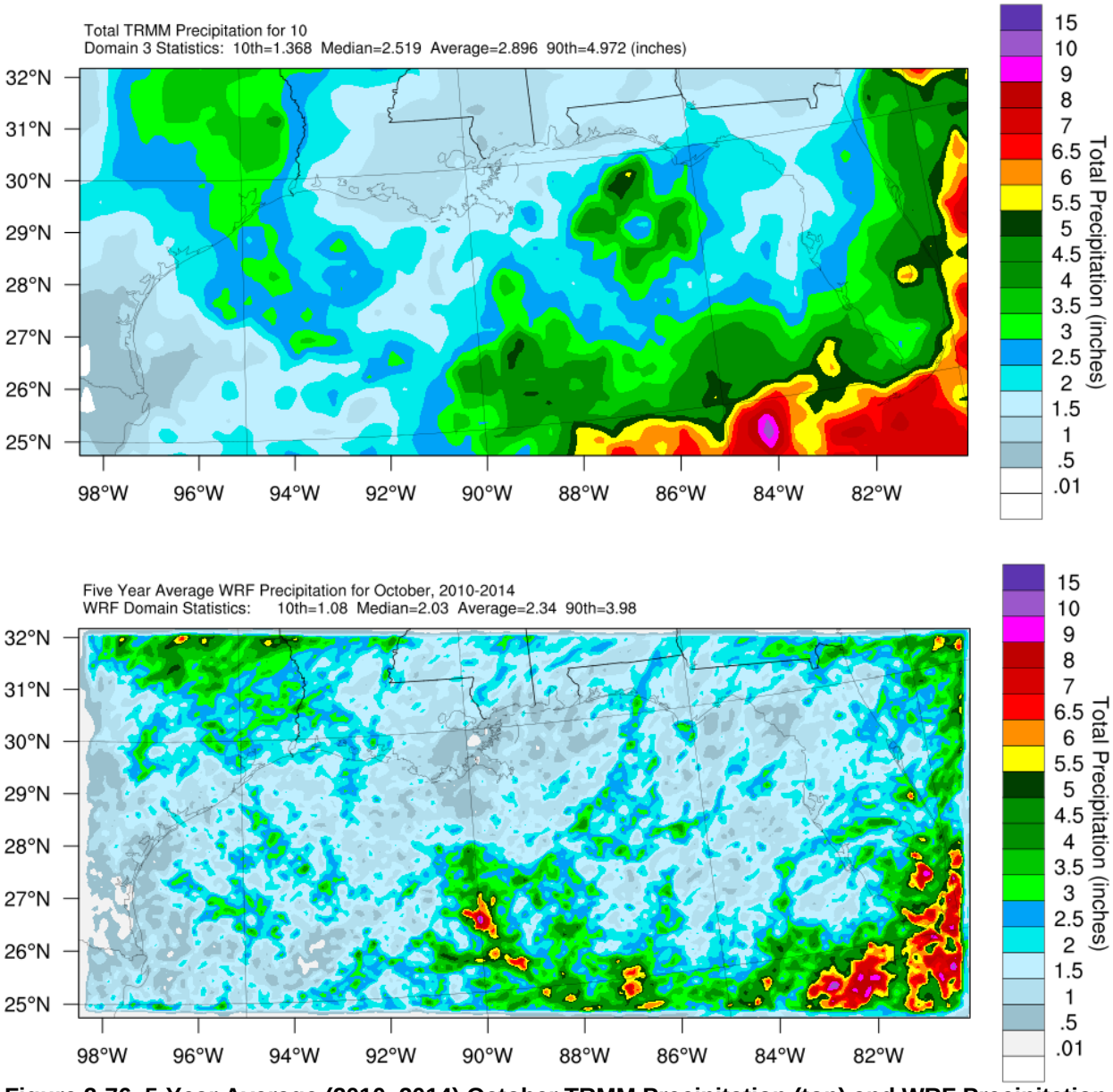

Figure 2-76. 5-Year Average (2010–2014) October TRMM Precipitation (top) and WRF Precipitation (bottom), 4-km Domain

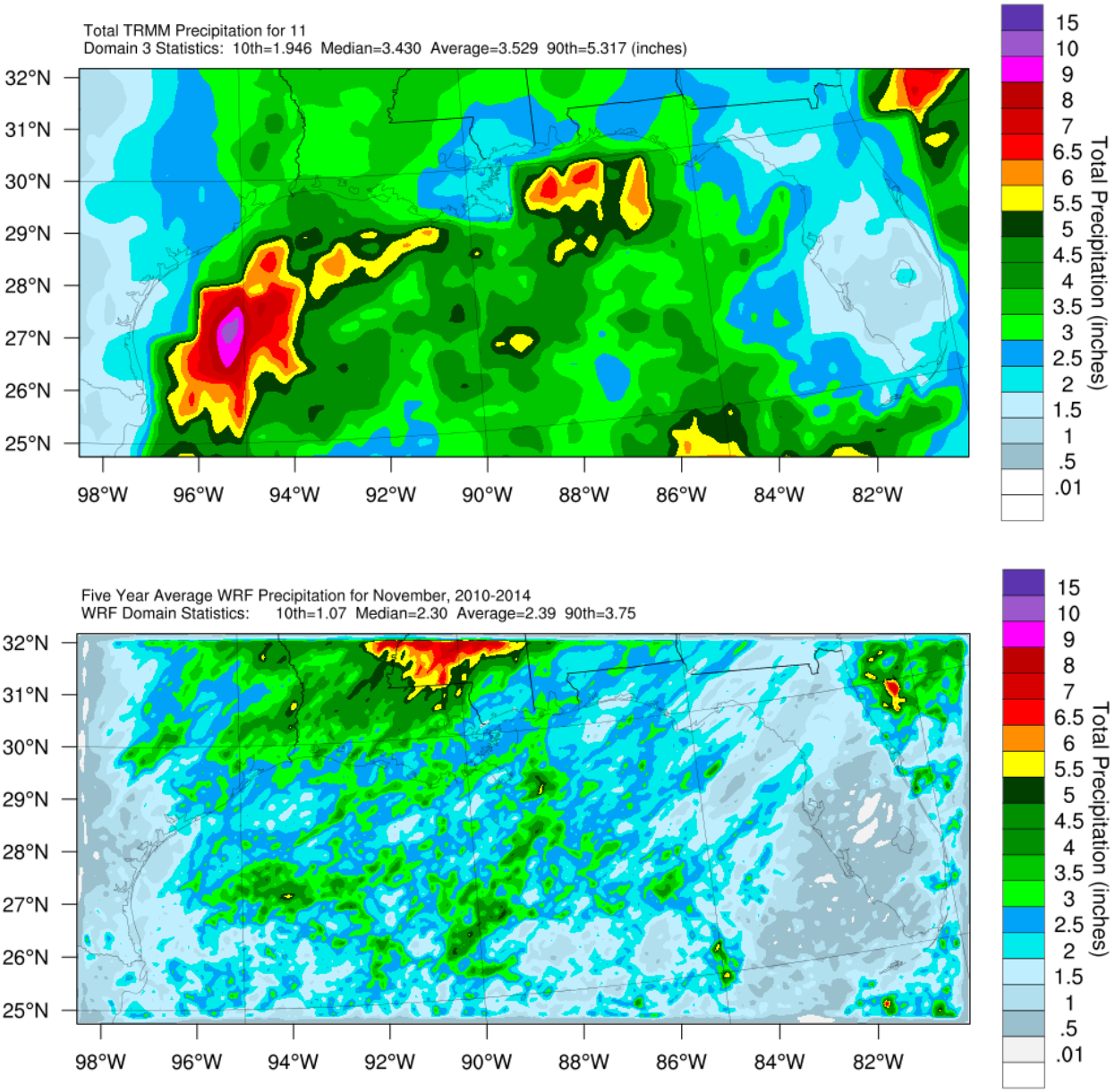

Figure 2-77. 5-Year Average (2010–2014) November TRMM Precipitation (top) and WRF Precipitation (bottom), 4-km Domain

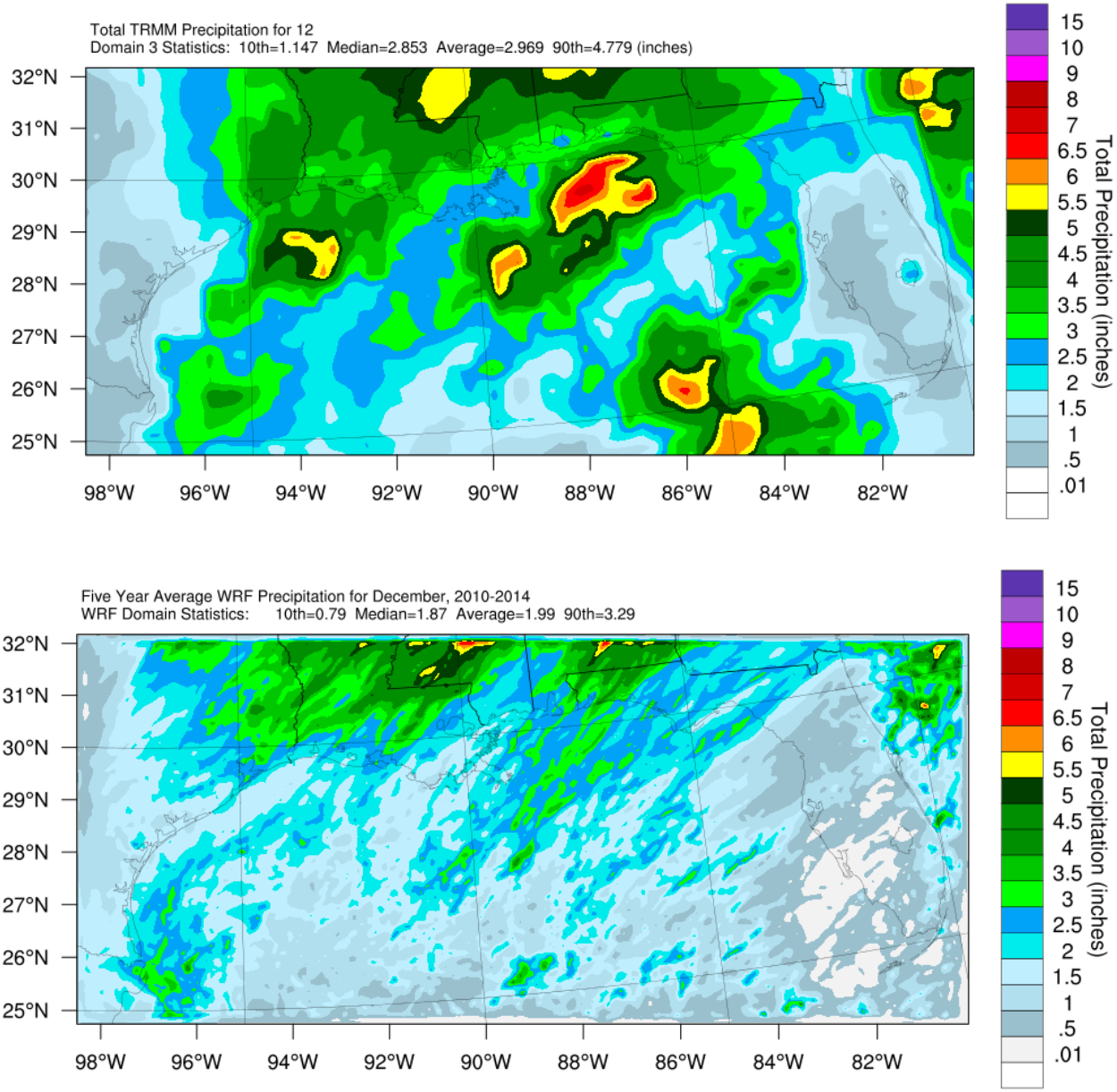

Figure 2-78. 5-Year Average (2010–2014) December TRMM Precipitation (top) and WRF Precipitation (bottom), 4-km Domain

2.3.4.3 Evaluation Using Tropical Cyclone Precipitation Events

To evaluate the accuracy of the WRF model for precipitation performance, Ramboll also analyzed short-term rainfall events for local- and regional-scale impacts. Daily precipitation plots were created for every 24-hour period from the 5-year WRF, PRISM, and TRMM databases. Tropical cyclone events were chosen as each storm system typically produces a wide area of enhanced rainfall for both onshore and offshore areas.

A tropical cyclone is a warm-core, non-frontal, synoptic-scale cyclone, originating over tropical or subtropical waters, with organized deep convection and a closed surface wind circulation about a well-defined center (NHC, 2015). A number of tropical cyclones impacted the Gulf Coast throughout the 2010–2014 modeling study. Increased rainfall events from two cyclones, Hurricane Isaac and Tropical Storm Debby, are presented in a qualitative comparison.

Hurricane Isaac made landfall along the coast of southern Louisiana on August 29, 2012, and moved northward, where it was downgraded to a tropical storm on August 30. Figure 2-79 shows daily precipitation plots from each dataset on August 30. WRF depicts the large cyclonic rotation and enhanced precipitation bands from Isaac over southeast Louisiana very well, compared to the PRISM dataset. Compared to TRMM, the model does appear to over-forecast the rainfall intensity for this 24-hour period.

Figure 2-80 shows daily precipitation plots as Tropical Storm Debby's outer rain bands began to impact Florida's west coast on June 25, 2012. WRF performed very well as compared to both PRISM and TRMM, forecasting the spatial extent of the large storm throughout the eastern GOM. The model did slightly underpredict the rainfall accumulations in this 24-hour period, compared to the observational and satellite databases.

Overall, WRF performed very well in recreating the daily precipitation events in these two scenarios. The 1,826 total daily precipitation plots from each WRF, PRISM, and TRMM dataset are available by request from BOEM.

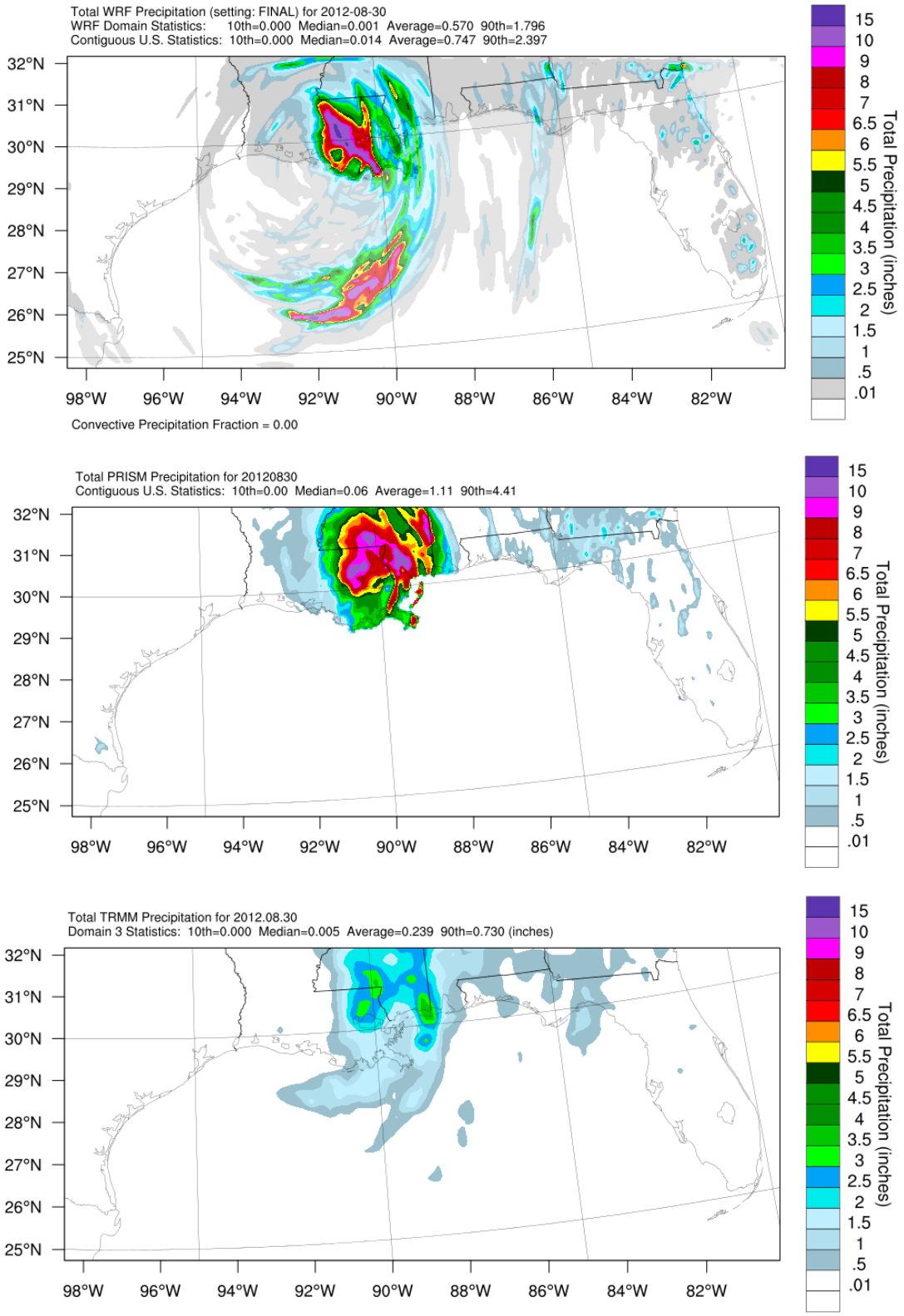

Figure 2-79. Daily Precipitation Plots from WRF (top), PRISM (middle), and TRMM (bottom) Databases on August 30, 2012

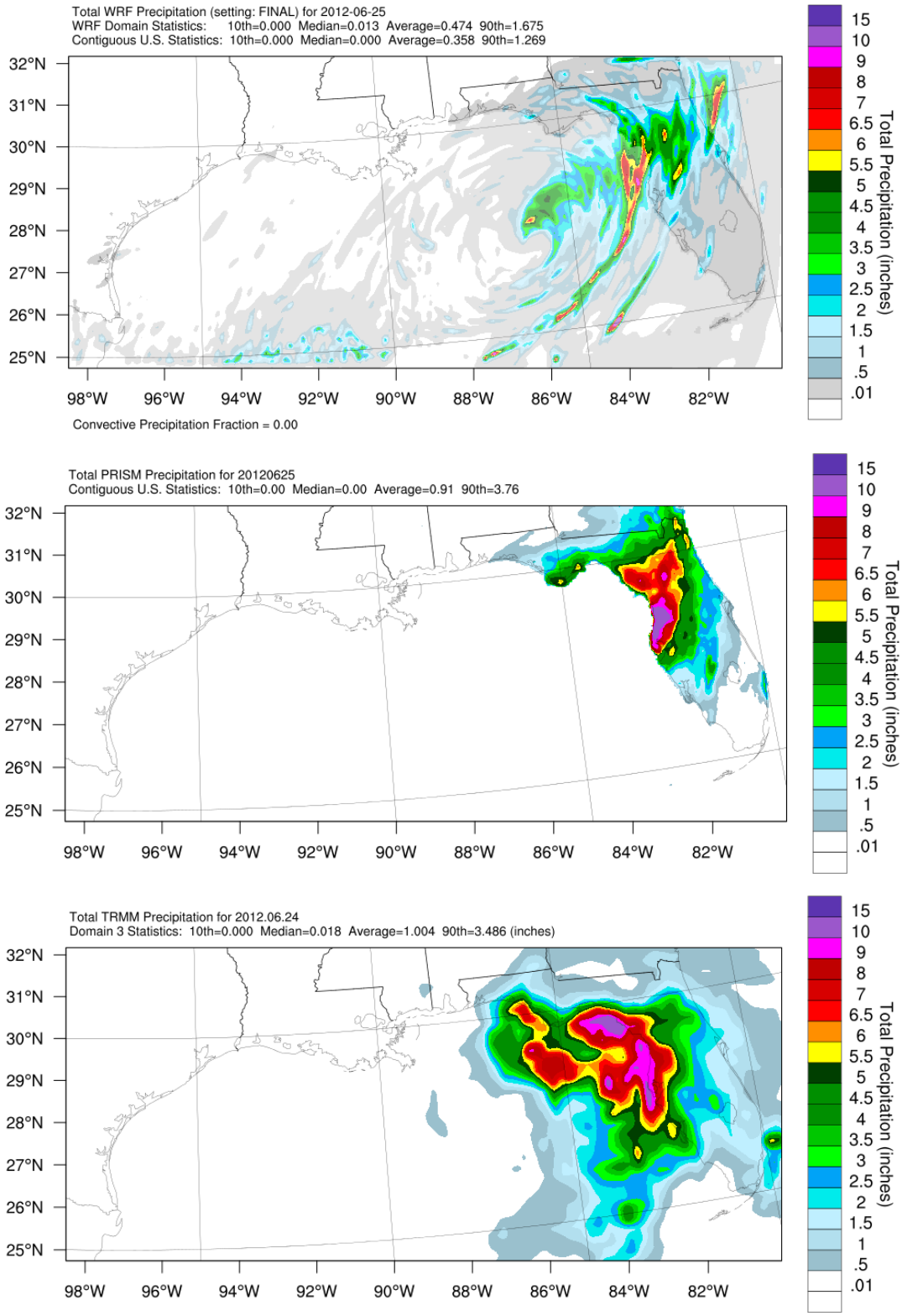

Figure 2-80. Daily Precipitation Plots from WRF (top), PRISM (middle), and TRMM (bottom) Databases on June 25, 2012

2.4 Summary and Conclusions

The BOEM GOMR WRF meteorological model simulation for January 2010–December 2014 reproduced the observed surface and upper-air meteorological variables very well. WRF performed exceptionally well in the onshore METSTAT analysis for the 36-km and 12-km domains and well in the onshore and offshore analysis for the 4-km domain, with a small bias in wind direction. This performance shows a very strong agreement overall between the model and surface observations.

Upper-air performance in the 4-km (d03) domain for the four selected locations throughout the GOM reflects accurate predictions of the vertical atmosphere, as shown in comparisons between WRF and radiosonde data, especially in mixing layer heights and cases of surface-based temperature inversions.

The daily and monthly 5-year average precipitation analysis for the 4-km (d03) domain indicates strong agreement between the model and observation-based precipitation measurements over land, including convergence zone and enhanced rainfall areas. The comparison with satellite-based precipitation accumulations does indicate an understatement of precipitation over water, most notably in the winter months.

Comparisons of selected wind roses in the region show WRF was able to forecast the offshore and onshore wind speed and wind direction very well in the 4-km domain. This suggests the model was able to accurately reproduce the land-sea breeze circulation, although this was not explicitly assessed.

The BOEM GOMR WRF modeling's superior performance provides a substantial basis for developing meteorological inputs for air quality modeling in the GOMR.

2.5 References

Brashers, B., C. Emery. 2015. The Mesoscale Model Interface Program (MMIF), Version 3.2, 2015-07-24, Draft User's Manual. Prepared for U.S. Environmental Protection Agency, Office of Air Quality Planning and Standards. Ramboll Environ US Corporation (Ramboll Environ). http://www.epa.gov/ttn/scram/models/relat/mmif/MMIFv3.2_Users_Manual.pdf (link verified 5/2/2019).

Brashers, B., J. Knapik, R. Morris. 2014. BOEM Contract No. M14PC00007, Task 2 WRF Meteorological Model Dataset Assessment for the Air Quality Modeling in the Gulf of Mexico Region. Technical Memorandum to Holli Ensz, Bureau of Ocean Energy Management, Gulf of Mexico Region. Prepared by ENVIRON International Corporation, Lynnwood, WA.

Daly, C., M. Halbleib, J.I. Smith, W.P. Gibson, M.K. Doggett, G.H. Taylor, J. Curtis, P.P. Pasteris. 2008. Physiographically sensitive mapping of climatological temperature and precipitation across the conterminous United States. Int. J. Climatol., http://prism.nacse.org/documents/Daly2008_PhysiographicMapping_IntJnlClim.pdf (link verified 5/2/2019).

Emery, C.A., E. Tai, G. Yarwood. 2001. Enhanced Meteorological Modeling and Performance Evaluation for Two Texas Ozone Episodes. Prepared for the Texas Natural Resource Conservation Commission (now TCEQ), by ENVIRON International Corp, Novato, CA. Available at: http://www.tceq.texas.gov/assets/public/implementation/air/am/contracts/reports/mm/EnhancedMetModelingAndPerformanceEvaluation.pdf (link verified 5/2/2019).

Gilliam, R.C., J.E. Pleim. 2010. Performance assessment of new land-surface and planetary boundary layer physics in the WRF-ARW. Journal of Applied Meteorology and Climatology 49, 760-774.

Kemball-Cook, S., Y. Jia, C. Emery, R. Morris. 2005. Alaska MM5 Modeling for the 2002 Annual Period to Support Visibility Modeling. Prepared for the Western Regional Air Partnership, by ENVIRON International Corp., Novato, CA. Available upon request from BOEM or Ramboll.

McNally, D.E. 2009. 12 km MM5 Performance Goals. Presentation to the Ad-Hoc Meteorology Group. June 25, 2009. Available at: http://www.epa.gov/scram001/adhoc/mcnally2009.pdf (link verified 5/2/2019).

National Center for Atmospheric Research (NCAR). 2015. WRF Source Codes and Graphics Software Downloads. Available at: http://www2.mmm.ucar.edu/wrf/users/download/get_source.html (link verified 5/2/2019).

NDBC (National Data Buoy Center). 2018. Programmatic Environmental Assessment for the National Oceanic and Atmospheric Administration National Data Buoy Center. Available at: https://www.ndbc.noaa.gov/pea/ndbc_final_pea_20180104.pdf (link verified 5/2/2019).

NHC (National Hurricane Center). 2015. National Hurricane Center 2015 Atlantic Hurricane Season. Available at: https://www.nhc.noaa.gov/data/tcr/index.php?season=2015&basin=atl (link verified 5/2/2019).

NOAA-ESRL (National Oceanic and Atmospheric Administration Earth System Research Laboratory). 2015. NOAA/ESRL Radiosonde Database. Available at: www.esrl.noaa.gov/raobs (link verified 5/2/2019).

NOAA-NCDC. 2014. NOAA NCDC Integrated Surface Database. Retrieved from: https://www.ncdc.noaa.gov/isd.

Ramboll Environ US Corp. 2015. METSTAT. Retrieved from http://www.camx.com/download/support-software.aspx (link verified 5/2/2019).

Saha, S., S. Moorthi, X. Wu, J. Wang, S. Nadiga, P. Tripp, D. Behringer, Y. Hou, H. Chuang, M. Iredell, M. Ek, et al. 2014. The NCEP Climate Forecast System Version 2 Journal of Climate J. Climate, 27, 2185–2208. doi: http://dx.doi.org/10.1175/JCLI-D-12-00823.1

Smith, A., N. Lott, R. Vose, 2011. The Integrated Surface Database: Recent Developments and Partnerships. Bulletin of the American Meteorological Society, 92, 704–708, doi:10.1175/2011BAMS3015.1

3 Emissions Inventory for the Cumulative Air Quality Impacts Assessment

3.1 Introduction

To complete the next step in the *Air Quality Modeling in the GOMR Study* and support subsequent air quality cumulative modeling analyses, ERG developed comprehensive air emissions inventories to depict emissions within the study area. This section defines the inventory scope and describes the data sources for each source type used to compile accurate and complete emissions estimates in a format suitable for use in the photochemical grid modeling discussed in Section 4 of this report. Emission estimates are needed for both a base case year and a future year as inputs to the photochemical grid modeling. The base case year is modeled in order to evaluate the predicted ozone, CO, NO, NO_2, NO_x, SO_2, total $PM_{2.5}$ mass, and speciated $PM_{2.5}$ concentrations against concurrent measured ambient concentrations in an MPE. More information on the use of a base case inventory in photochemical grid modeling can be found in the USEPA's Draft Modeling Guidance for Demonstrating Attainment of Air Quality Goals for Ozone, $PM_{2.5}$, and Regional Haze (USEPA, 2014a). Details on the results of the MPE are presented in Section 4.5 of this report. Future year emission estimates are required for additional modeling scenarios that will serve as a basis to predict future impacts from the implementation of the PFP for the 2017–2022 Program (i.e., the Proposed Action). Section 3.3 details the development of the base case emissions inventory, and Section 3.4 discusses the development of the future year emissions inventory.

3.2 Development of Emissions Inventories

The scope of this study's air pollutant emissions inventories for use in the cumulative air quality impacts assessment includes the following elements, which are described in detail below:

- **Pollutants:** specific air pollutants to include in the inventories
- **Base case year:** year selected for the base case inventory
- **Inventory sources:** range of source types (point, nonpoint area, mobile) and source categories
- **Geographical domain and spatial resolution:** geographic area within which emissions will be estimated, and the level of detail or specificity at which emissions will be estimated
- **Temporal resolution:** annual, monthly, daily, and hourly
- **Speciation:** speciation of PM and VOCs (see Section 4.3.4 of this report)
- **Future year:** year selected for modeling future scenario emission estimates

3.2.1 Pollutants

ERG estimated pollutant emissions based on BOEM's mandate under the OCSLA to assess the impacts of OCS oil and gas activities to the onshore NAAQS through air quality modeling. Pollutants consist of the following criteria air pollutants and criteria pollutant precursors as defined by CAA Title I:

- CO
- Pb
- NO_x stated as equivalent mass of NO_2

- $PM_{2.5}$ and PM_{10}
- SO_2
- VOCs, precursors to ozone formation
- Ammonia (NH_3), a precursor to PM formation

3.2.2 Base Case Year

In determining the calendar year to select for the base case emissions inventory, ERG initially considered 2011 based on data availability. Calendar year 2011 emissions data are readily available for most sources from the USEPA National Emissions Inventory (NEI) (USEPA, 2015a) and BOEM's *Year 2011 Gulfwide Emissions Inventory Study* (Wilson et al., 2014). However, 2011 was an unusually hot and dry year in the GOMR, particularly in Texas. The anomalous meteorological conditions during the 2011 warm season (April–October), which generally encompasses the period of maximum photochemical activity in the Gulf region, are illustrated by the surface air temperature and SST anomaly maps in Figure 3-1 (NOAA, 2015). The high temperatures impacted the Texas, Oklahoma, Arkansas, and Louisiana region in 2011, but much less so in 2012. Similarly, relatively strong SST incongruities were present in the GOMR during 2011 as compared to 2012. Figure 3-2 provides anomaly maps for January–April (NOAA, 2015). Anomalies for the first four months of 2012 were stronger in the Gulf region than in 2011 and appear to represent a hold-over from the 2011 warm season anomalies.

Focusing on the April–October time period, 2011 would appear to make this a poor choice for the base case analysis. Texas especially experienced record heat and dry conditions during summer 2011, whereas 2012 was well within the normal range, as shown in Figure 3-3 (Nielsen-Gammon, 2011), with the 2012 data point added using Southern Regional Climate Center data (SRCC, 2015). Texas and the surrounding region also experienced several large wildfires that contributed significant emissions and affected air quality in the GOMR: a total of 2.7 million acres burned in Texas in 2011 as compared to just 0.3 million acres in 2012 (NFIC, 2015). The acreage burned in 2012 is similar to the acreage burned in other years: 0.1 million acres in 2013, 0.2 million acres in 2014, and 0.3 million acres in 2015. Noting the significant fire impacts and highly anomalous weather conditions in 2011, the Texas Commission on Environmental Quality (TCEQ) also decided to use 2012 as the new base case year for modeling in support of ozone SIP development. Therefore, a 2012 base case year is more representative of "typical" conditions in the GOMR.

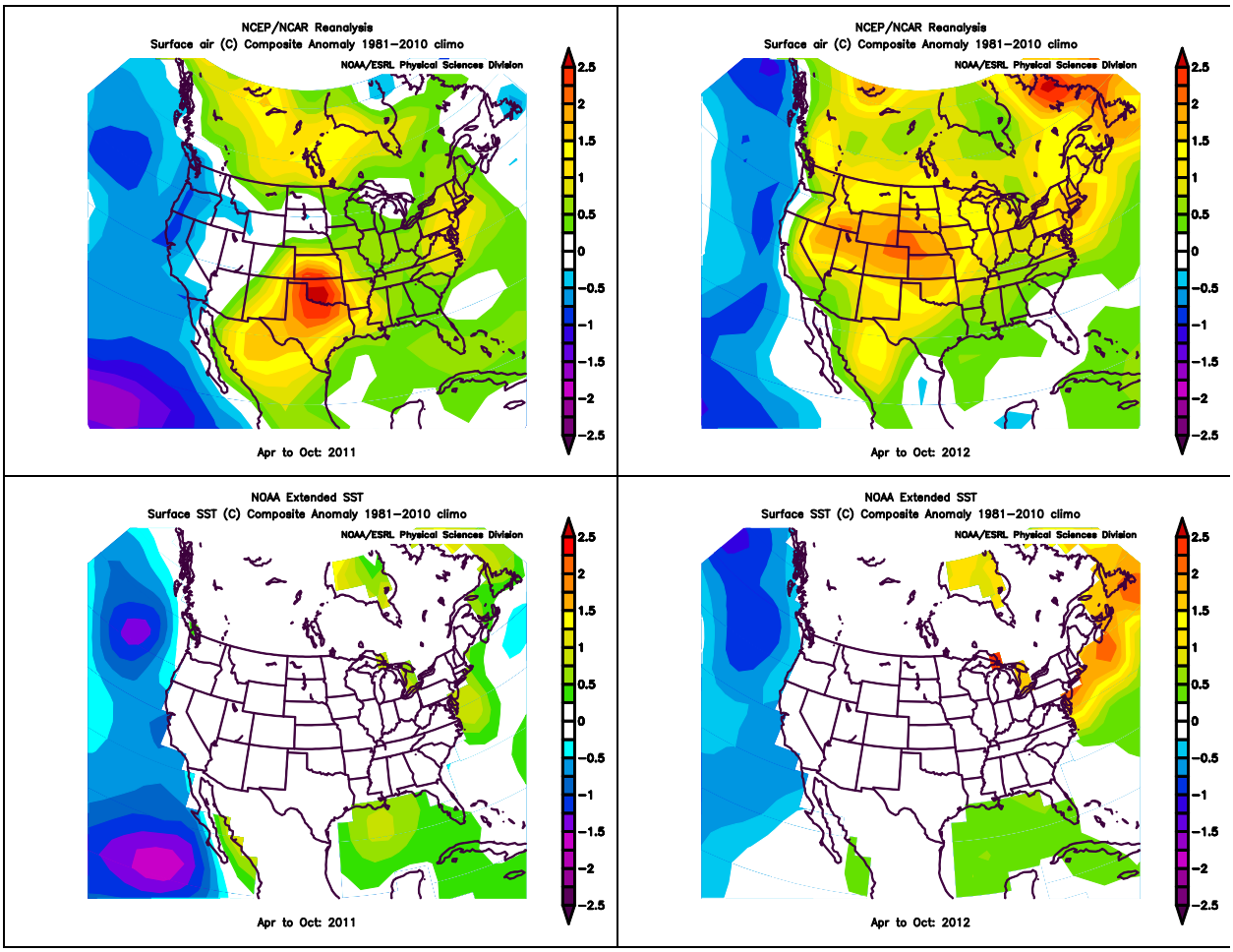

Figure 3-1. Surface Air Temperature (top) and SST (bottom) Anomalies for April–October 2011 (left) and 2012 (right) Relative to 1981–2010 Climate Means

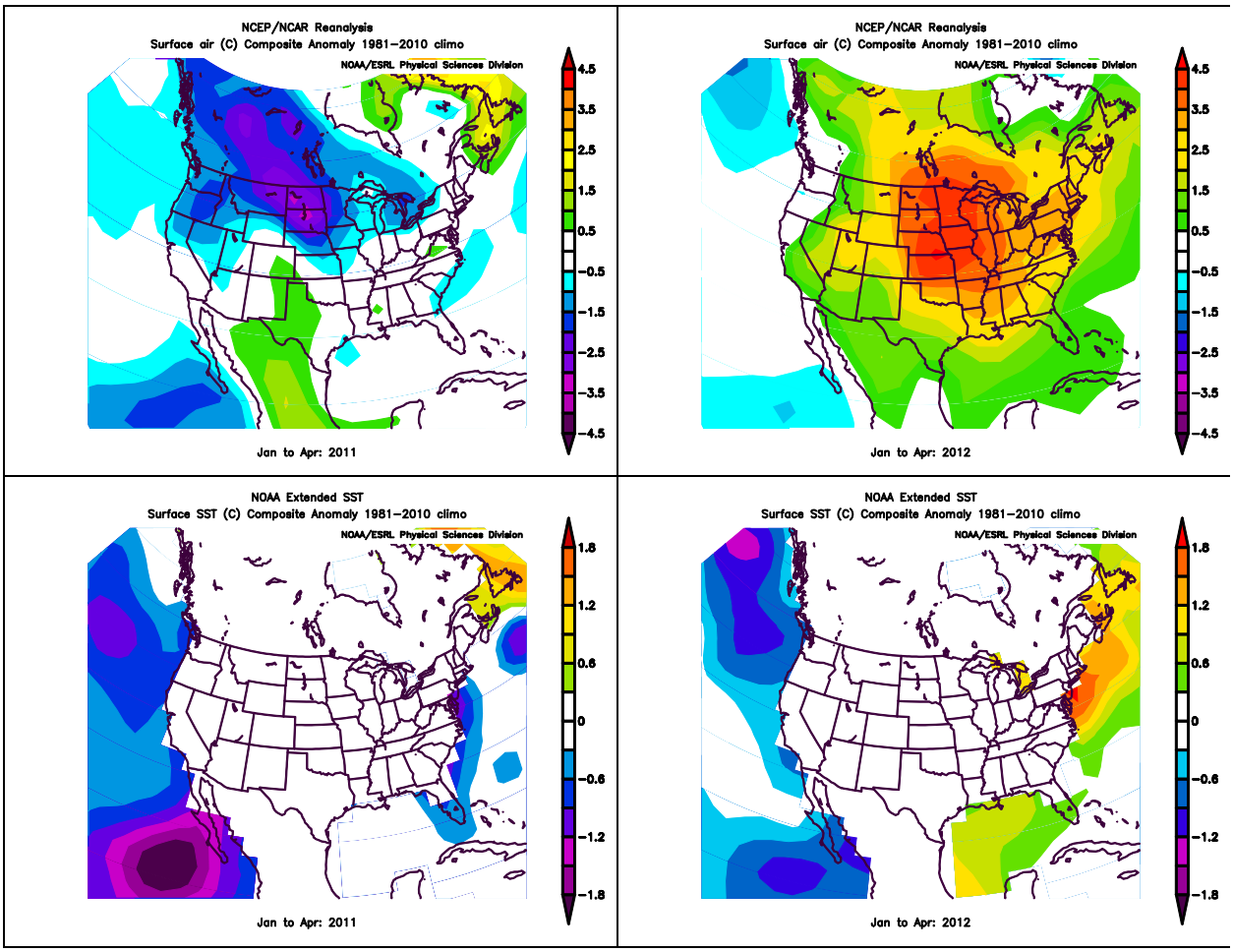

Figure 3-2. Surface Air Temperature (top) and SST (bottom) Anomalies for January–April 2011 (left) and 2012 (right) Relative to 1981–2010 Climate Means

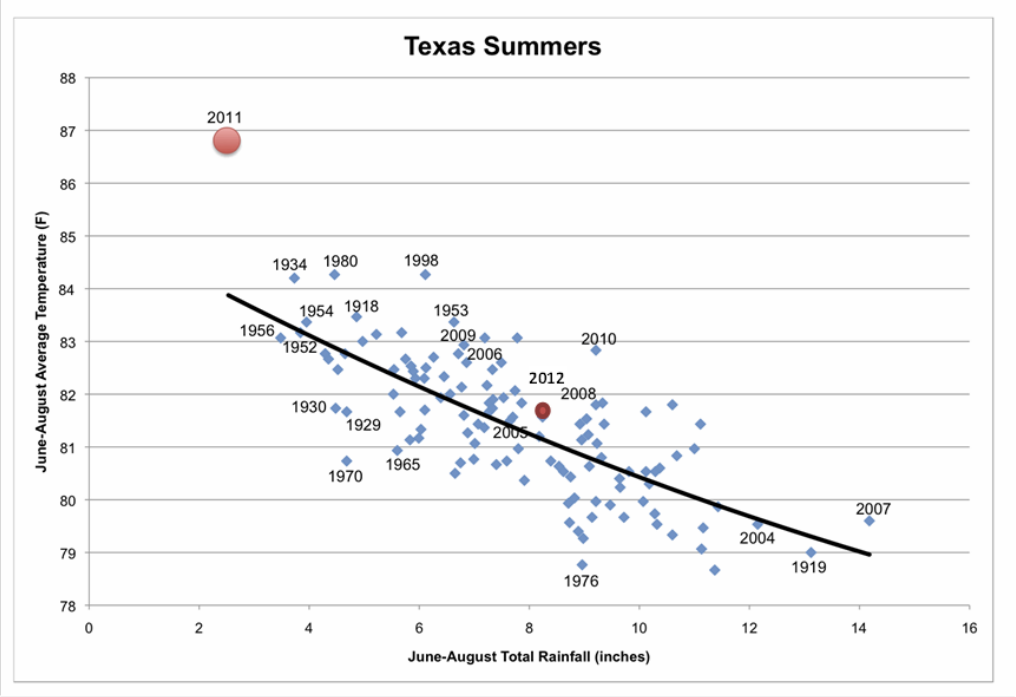

Figure 3-3. Summer (June–August) Average Daily Mean Temperature and Total Precipitation in Texas for Each Year From 1918–2012

3.2.3 Inventory Sources

ERG compiled emissions data from anthropogenic (i.e., human-caused) sources—including onshore and offshore stationary point and nonpoint area sources, onroad motor vehicles, nonroad equipment, locomotives, marine vessels, other offshore sources, and airports—for this study's emissions inventory. Table 3-1 lists the source groups and categories included in the emissions inventory, the pollutants applicable to each source, and the spatial and temporal resolution, described in detail below in the following sections. Note that emissions from non-anthropogenic sources (i.e., biogenic and geogenic sources) are discussed in Section 3.3.7.

3.2.4 Geographical Domain

The domain of this study's emissions inventory is the area depicted in Figures 1-1 and 2-1, particularly the 4-km domain encompassing the GOM OCS shown in Figure 1-2. This area is the focus of the emissions inventory efforts described in this section and includes parts of Alabama, Georgia, Louisiana, Mississippi, and Texas; all of Florida; the Western, Central, and Eastern GOM Planning Areas; and part of the Atlantic Ocean.

Emissions data were also required for the 36- and 12-km expanded domains depicted in Figures 1-1 and 2-1. ERG used 2011 NEI (version 2) and 2012 NEI data for the additional, expanded areas (USEPA, 2015a, 2015b). Any adjustments to the 2011 NEI reflecting a 2012 base case year (e.g., for airports and aircraft, locomotives) were made for the entire 36-km domain. As discussed in Section 3.3.8, ERG also compiled emissions inventory data for the domain within Mexico based on previously developed emissions inventories. As discussed in Section 3.3.9, emissions from the USEPA's most recent modeling platform were used for sources in Canada.

Table 3-1. GOMR Air Quality Modeling Study Source Categories for Cumulative Air Quality Impacts Analyses

Group and Source Category		CO	NO_x	SO_2	VOC	Pb	$PM_{2.5}$	PM_{10}	NH_3	Spatial Resolution[a]
NEI Onshore Sources	Point Sources	✓	✓	✓	✓	✓	✓	✓	✓	P
	Nonpoint Area Sources	✓	✓	✓	✓	✓	✓	✓	✓	A
	Onroad Mobile Sources	✓	✓	✓	✓	-	✓	✓	✓	A
	Commercial Marine Vessels	✓	✓	✓	✓	✓	✓	✓	✓	P, A[b]
	Locomotives	✓	✓	✓	✓	✓	✓	✓	✓	P, A[c]
	Aircraft and Airports	✓	✓	✓	✓	✓	✓	✓	✓	P
	Other Nonroad Mobile Sources	✓	✓	✓	✓	-	✓	✓	✓	A
Offshore Oil and Gas Production Sources	Platforms in State Waters	✓	✓	✓	✓	-	✓	✓		P
	Platforms in Western, Central, and Eastern GOM Planning Areas	✓	✓	✓	✓	✓	✓	✓	✓	P
	Drilling Rigs in Western, Central, and Eastern GOM Planning Areas	✓	✓	✓	✓	✓	✓	✓	✓	LB
	Pipelaying Vessels	✓	✓	✓	✓	✓	✓	✓	✓	LB
	Support Helicopters	✓	✓	✓	✓		✓	✓		LB
	Support Vessels	✓	✓	✓	✓	✓	✓	✓	✓	LB
	Survey Vessels	✓	✓	✓	✓	✓	✓	✓	✓	LB
Non-Oil and Gas Offshore Vessels and Activities	Commercial Fishing Vessels	✓	✓	✓	✓	✓	✓	✓	✓	LB
	Commercial Marine Vessels	✓	✓	✓	✓	✓	✓	✓	✓	LB
	Louisiana Offshore Oil Port	✓	✓	✓	✓	✓	✓	✓	✓	P
	Military Vessels	✓	✓	✓	✓	✓	✓	✓	✓	LB
	Recreational Vessels	✓	✓	✓	✓		✓	✓	✓	LB
	Vessel Lightering	✓	✓	✓	✓	✓	✓	✓	✓	P
Biogenic and Geogenic Sources	Subsurface Oil Seeps	-	-	-	✓	-	-	-	-	LB
	Mud Volcanoes	-	-	-	✓	-	-	-	-	LB
	Onshore Vegetation[d]	-	✓	-	✓	-	-	-	-	A
	Wildfires and Prescribed Burning[d]	✓	✓	✓	✓	-	✓	✓	✓	P
	Windblown Dust[d]	-	-	-	-	-	✓	✓	-	A
	Lightning[d]	-	✓	-	-	-	-	-	-	A
	Sea Salt Emissions[d]	-	-	-	-	-	✓	✓	-	A
Sources in Mexico and Canada	Point Sources[e]	✓	✓	✓	✓	✓	✓	✓	✓	P
	Nonpoint Area Sources	✓	✓	✓	✓	-	✓	✓	-	A
	Mobile Sources	✓	✓	✓	✓	-	✓	✓	-	A

[a] A = area source (modeling grid cell, spatial surrogate); P = point source (Universal Transverse Mercator [UTM] coordinates, stack parameters); LB = offshore lease block (modeling grid cell, spatial surrogate)
[b] Larger ports and shipping are represented as shape files; smaller ports as point sources.
[c] Rail yards are represented as point sources; railway segments as area sources.
[d] See Section 4.3.5 of this report for information on development of emissions estimates for these sources.
[e] Includes future offshore production sources.

3.3 Base Case Modeling Scenario Emission Estimates

Base case emission estimates are needed as inputs for air quality cumulative modeling analyses in the photochemical MPE (discussed in Section 4.5). The initial 2012 base case pollutant concentrations must be evaluated against concurrent measured ambient concentrations. The following sections discuss the compilation, development, and quality assurance/quality control (QA/QC) of the point source, nonpoint area source, onroad and nonroad mobile source, GOMR oil and gas production source, and biogenic and geogenic source base case emission estimates. Throughout this section, distinction is made between offshore OCS sources and offshore sources that fall within state waters. State waters in the GOMR lie within 9 nautical miles of the coasts of Florida and Texas, and within 3 nautical miles of the coasts of Alabama, Mississippi, and Louisiana. Emissions from sources located in state waters are associated with their respective states and are not represented as OCS sources.

3.3.1 Point Sources

As noted previously, calendar year 2011 emissions data are available for onshore point sources from the USEPA NEI (USEPA, 2015a). In a separate modeling effort, the USEPA prepared a criteria pollutant 2012 base year emissions inventory for some sectors, including onshore point sources (USEPA, 2015b). ERG obtained the USEPA 2012 point source emissions inventory, conducted QA/QC, and supplemented and revised the criteria pollutant estimates as needed. The USEPA prepared the point source emissions inventory, which included the following data:

1. 2012 data compiled by the USEPA from annual criteria pollutant reporting of Type A (large) sources that are submitted by responsible state, local, and tribal air agencies
2. 2012 electric generating unit (EGU) emissions (i.e., electric utilities) from the USEPA Clean Air Markets Division (CAMD) hourly emissions data
3. 2011 NEI data for other, smaller point sources that are not identified above
4. 2011 airport and aircraft emission estimates developed by the USEPA

Although the emissions data are likely complete for most point sources, ERG confirmed that offshore platforms within state boundaries are included in the NEI. Data from the USEPA's 2012 Toxics Release Inventory (TRI) were used to supplement missing Pb and NH_3 emission estimates (USEPA, 2015c).

The point source facilities in the counties/parishes in the 4-km modeling domain were identified based on the reported NEI coordinates (latitude/longitude).

The point source data obtained from the 2011 and 2012 NEI include:

- EIS facility site ID
- Facility name
- Facility location (address)
- County name and Federal Information Processing Standards (FIPS) code
- Emissions unit ID
- Emissions process ID
- Emissions release point ID
- Source classification code (SCC)
- Pollutant name and code
- Emissions (tons per year [TPY])

- Latitude/longitude coordinates
- Stack parameters

ERG conducted the following QA/QC activities specifically related to point sources: confirmed that emissions were not double counted, determined pollutant coverage by source category, checked locational coordinates and stack parameters, and verified consistency in data reporting. After QA/QC, ERG revised approximately 6 percent of coordinate pairs. ERG also populated missing stack parameters using calculational procedures where possible and used defaults from the USEPA where it was not possible to calculate missing stack parameters. The equation used to calculate missing parameters for stack flow, velocity, and diameter is:

$$\text{Stack Flow [cu ft/sec]} = (\pi\ [\text{Pi}] * (\text{Stack Diameter [ft]} / 2)^{2}) * \text{Stack Velocity [ft/sec]}$$

Additionally, ERG performed PM augmentation following the USEPA PM augmentation routine (USEPA, 2016a).

The airports and aircraft category includes emissions from aircraft during landings and takeoffs (LTOs) as well as airport ground support equipment (GSE) at airports within the study domain. The inventory focuses on commercial air carriers, air taxis, and general aviation, including helicopters based next to the GOM that provide support to offshore oil and gas production operations. With the exception of offshore helicopters that support OCS oil and gas production activities, all aircraft and airport emissions data were obtained from the USEPA's 2011 NEI. The 2011 emissions were adjusted to reflect 2012 activity based on the ratio of 2012 aircraft operations at each airport relative to 2011 operations by aircraft type, as reported in the Federal Aviation Administration's (FAA's) Terminal Area Forecast (TAF) data (FAA, 2015). If the TAF dataset did not include the airport, no adjustments were made.

3.3.2 Nonpoint Area Sources

The starting point for the 2012 nonpoint area source inventory was the data submitted by state and local agencies for the 2011 NEI. For completeness, if agencies do not provide estimates, the USEPA develops emission estimates for a number of nonpoint source categories (up to 165) for the NEI. The USEPA did not develop 2012 emission estimates for nonpoint area sources.

ERG prioritized key, top-emitting source categories of NO_x, PM, SO_2, and VOCs in Alabama, Florida, Georgia, Louisiana, Mississippi, and Texas and developed 2012 emission estimates using the USEPA nonpoint area source category tools (USEPA, 2014b). These categories include consumer products, architectural surface coatings, industrial maintenance coatings, open burning of municipal solid waste (MSW), residential and institutional/commercial/industrial (ICI) heating, upstream oil and gas, open burning of land clearing debris, paved and unpaved roads, and gasoline distribution Stage I.

Overall, the emission estimates for these sources were only marginally different from the 2011 estimates. However, this recalculation ensured a comparable emissions estimate for point source reconciliation. ERG conducted point source reconciliation for ICI, oil and gas, and gasoline distribution Stage I (bulk gasoline terminals) and verified that the USEPA's nonpoint file (now reported with onroad mobile sources) had no gasoline distribution Stage II (gas stations) records.

3.3.3 Onshore Mobile Sources

The onroad mobile source category includes exhaust and evaporative emissions from onroad motor vehicles (e.g., automobiles, light-duty trucks, heavy-duty trucks) and exhaust and evaporative emissions from nonroad mobile sources. These sources may include various types of construction equipment and industrial equipment. As discussed in Section 4.3.5 of this report, Ramboll used SMOKE-MOVES—

which integrates the Sparse Matrix Operator Kerner Emissions (SMOKE) Modeling System and the MOtor Vehicle Emission Simulator (MOVES)—with the MOVES2014 emission factor modeling for onroad mobile sources. The nonroad category includes nonroad engines, equipment, and vehicles. The USEPA ran MOVES for nonroad sources to develop the 2012 emission estimates for these categories.

ERG did not adjust locomotive emissions in the 2011 NEI to represent 2012 activities, because ERG confirmed that the 2011 and 2012 fuel usage data from the Surface Transportation Board R-1 Class 1 Railroad Annual Reporting Data (Surface Transportation Board, 2015) show only a slight (2 percent) reduction in 2012 levels from 2011 levels.

3.3.4 Offshore Helicopters

The GOMR has more helicopter traffic—primarily associated with offshore oil and gas support—than any other region of the U.S. ERG obtained offshore support helicopter emission estimates from the 2011 Gulfwide Emissions Inventory (Wilson et al., 2014), then supplemented these estimates with 2011 NEI helicopter data for onshore airports. The two datasets map out the full route between offshore platforms equipped with helipads and the closest onshore support facility; the NEI only addresses emissions at each airport for operations up to 3,000 ft of elevation (i.e., local mixing height). ERG ensured that the helicopter traffic data between the two datasets are comparable and do not double count emissions.

3.3.5 Offshore OCS Oil and Gas Production Platforms—Western and Central/Eastern GOM Planning Areas

The starting point for offshore OCS oil and gas production platforms in the Central and Western GOM Planning Areas was the 2011 Gulfwide Emissions Inventory (Wilson et al., 2014). ERG supplemented the 2011 inventory with NH_3 and Pb emission estimates for all applicable emission sources using factors from USEPA AP-42, *Compilation of Emission Factors* (USEPA, 2016b), and NH_3 emission factors from a 1994 USEPA report (Battye et al., 1994).

ERG conducted research to determine if the 2011 emissions values for platform sources should be adjusted to be more representative of 2012 emissions values. Offshore OCS oil and gas production values for 2011 and 2012 were obtained from the BOEM Oil and Gas Operations Reports, Part A (OGOR-A) (USDOI, BSEE, 2015). The OGOR-A data are presented at the lease level. Production of oil and gas (including deepwater production) decreased 8 percent in barrels of oil equivalent from 2011 to 2012. ERG did not apply a strict rule-of-thumb emissions threshold to determine when to adjust emissions, but the 2011 emission estimates were modeled without adjustment to be somewhat conservative.

3.3.6 Offshore Vessels

Offshore vessels can be grouped into 1) vessels that support the construction, operation, and decommissioning of oil and gas platforms (Section 3.3.6.1); and 2) vessels involved in other commercial, recreational, and military operations (Section 3.3.6.2). Offshore vessels in the GOMR operate in state waters and on the OCS. All marine vessels included in this study operate using diesel engines. These include very large propulsion engines as well as smaller auxiliary diesel engines that provide power for electricity generation, winches, pumps, and other onboard equipment. Smaller engines tend to use distillate grade diesel fuel, while large engines combust heavier residual blends.

40 CFR Section 1043.109(b) created the North American Emission Control Area (ECA), which includes the GOM (USEPA, 2010). This regulation limits marine fuel sulfur content to 1 percent after August 1, 2012, for any vessel with greater than 400 gross tonnage. Vessels below this threshold tend to use distillate fuels that are already at or below the 1 percent limit.

3.3.6.1 OCS Oil and Gas Production Support Vessels

3.3.6.1.1 Central/Eastern and Western GOMR Planning Areas

The offshore OCS oil and gas production sector consists of vessels operating on the OCS to support oil and gas production activities. Offshore OCS production requires a wide variety of vessels to support the exploration, development, and extraction of oil and gas. OCS oil and gas production support vessels include:

- Seismic survey vessels
- Drilling vessels
- Pipelaying vessels
- Crew boats
- Supply vessels

For the 2011 Gulfwide Emissions Inventory, automatic identification system (AIS) data from PortVision were used to map spatial aspects of vessel movements (PortVision, 2012). AIS is an automated tracking system that allows vessels to exchange location and contact data with other nearby ships, offshore platforms, satellites, and AIS base stations, enhancing navigation and reducing at-sea collisions.

On October 22, 2003, the U.S. harmonized the AIS mandates of the Safety of Life at Sea Convention with the Maritime Transportation Security Act of 2002 (MTSA), which requires the following vessels, including offshore support vessels, to participate in the AIS program:

- Passenger vessels of 150 gross tonnage or more
- Tankers, regardless of tonnage
- Vessels other than passenger vessels or tankers of 300 gross tonnage or more

Vessels that do not meet these thresholds, such as crew boats and smaller support vessels, can still voluntarily participate in AIS. The Offshore Marine Service Association (OMSA) encourages its members to equip their vessels with AIS transponders allowing for more efficient and safer ship movements in the highly congested central and western areas of the GOM. Because the AIS data were not deemed to be complete, ERG developed the marine vessel emission estimates based on other data sources such as BOEM drilling and pipelaying data and OMSA's vessel data, which include vessels below the AIS thresholds. Though not sufficiently complete to estimate emissions, the AIS data were considered representative of the traffic patterns in the GOM and were used to spatially allocate the calculated vessel emissions.

ERG used the spatially distributed support vessel emission estimates from BOEM's 2011 Gulfwide Emissions Inventory. Although the USEPA 2011 NEI also includes marine vessel emission estimates for the GOM, the emission estimates were derived from national vessel activity data. During QA/QC of the 2011 BOEM Gulfwide estimates, ERG also found and corrected an error in the vessel power rating for a number of smaller vessels.

As discussed above for offshore OCS oil and gas production platforms, the 2011 emission estimates for these vessels were not adjusted to reflect 2012 production levels. Sulfur oxides (SO_x) and PM (associated with sulfates) were not adjusted to account for the introduction of low-sulfur, ECA-compliant fuel in the last five months of 2012, because ERG determined that most support vessels are Category 1 or 2, which already use ECA-compliant fuels. In 2011, Category 1 and 2 vessels were required to use nonroad mobile source fuel with a sulfur content of 500 ppm, lower than the ECA-compliant fuel standard (1,000 ppm). Thus, this is the only fuel sold at marinas. Larger international vessels equipped with the Category 3 engines obtain their ECA-compliant fuel from bunker services. The USEPA emission factors differentiate

distillate nonroad-compliant fuels (500 ppm sulfur) from residual/distillate blend ECA-compliant fuels. ERG also developed emission estimates for NH_3 and Pb for vessels by speciating the PM emission estimates based on profiles included in the USEPA's NEI.

3.3.6.1.2 Eastern GOMR Planning Area

ERG obtained drilling vessel data from the USDOI Bureau of Safety and Environmental Enforcement (BSEE) to confirm that there was no drilling activity in the Eastern GOM Planning Area in 2012. ERG also reviewed the permits granted by the USEPA for offshore OCS platforms in the Eastern GOM Planning Area to confirm there were no active production platform activities in 2012. As discussed in Section 3.4.2, emission estimates were developed for drilling activity in the Eastern GOM Planning Area for the future scenario.

3.3.6.2 Non-Oil and Gas Production Offshore Vessels

Vessels not directly associated with the offshore OCS oil and gas production activities include:

- Commercial marine vessels (CMV)
- Louisiana Offshore Oil Port (LOOP)-associated vessels
- Commercial and recreational fishing vessels
- Ferries
- Research vessels
- Harbor craft
- Military vessels

CMVs include large ships that visit coastal ports and operate in deep waters, as well as smaller general cargo ships and tugs that move barges along waterways and rivers. For the Central and Western GOM Planning Areas, ERG used the CMV data from the 2011 Gulfwide Emissions Inventory. These estimates were based on U.S. Army Corps of Engineers entrance and clearance data for ports. It should be noted that the entrance and clearance data may include a limited number of passenger cruise ships; the data primarily only track vessels involved in international commerce.

Emission estimates for vessels operating in state waters, the Eastern GOM Planning Area, and the Atlantic Ocean were obtained from the USEPA's NEI. The NEI includes all vessels for all navigable U.S. waters. For this inventory the BOEM offshore vessel data replaced the NEI data for the Central/Eastern and Western GOM Planning Areas, as it was developed using more detailed data and covers the same vessel types.

The LOOP is a pumping port/platform for tankers to discharge crude oil to the mainland without having to maneuver through port traffic. Located 45 miles offshore, the LOOP has several emission sources. Similarly, there are four offshore lightering zones in the GOM (Southtex, Gulfmex No. 2, Offshore Pascagoula No. 2, and South Sabine Point) where smaller shuttle tankers can move product from very large crude carriers, bringing the oil to port while the large tankers remain off the coast. The LOOP and the lightering zones are not under BOEM jurisdiction; thus, they are not BOEM OCS oil and gas production sources. The 2011 Gulfwide Emissions Inventory identified tankers that visit the LOOP or the lightering zones with the shuttle tankers. The inventory also accounts for evaporative emissions from unloading and loading activities and emissions from the operation of generators and pumps at the LOOP. ERG adjusted the 2011 LOOP emission estimates to reflect the 18 percent decline in crude imports in 2012 based on the established inverse relationship between U.S. production levels and imported crude brought into the U.S. through the LOOP.

Emissions from commercial and recreational fishing vessels are also included in the 2011 inventory for Federal waters. ERG supplemented the BOEM data with the 2011 NEI data for these fishing vessels for operations in the Eastern GOM Planning Area, the Atlantic Ocean, and state waters.

For military vessels, ERG used the U.S. Navy and U.S. Coast Guard data from the 2011 inventory, as well as the NEI's Coast Guard data for state waters and Federal waters in the eastern part of the GOM and along the Atlantic coast.

ERG conducted research to determine that activity levels from 2011 to 2012 were similar for the other non-oil and gas vessels (e.g., tankers, container ships, bulk, and general cargo). Based on the most recent International Maritime Organization (IMO) data (IMO, 2015), fuel combustion was projected to remain constant from 2010 to 2015. Thus, ERG made no adjustments to approximate activities in 2012.

SO_2 and PM (associated with sulfates) were adjusted for Category 3 vessels to account for the introduction of low-sulfur, ECA-compliant fuel in the last five months of 2012.

3.3.7 Biogenic and Geogenic Sources

It is important to include non-anthropogenic emission sources in a photochemical modeling emissions inventory. ERG estimated emissions for subsurface oil seeps and mud volcanoes as part of the 2011 Gulfwide Emissions Inventory.

As discussed in Section 4.3.5 of this report, Ramboll estimated emissions for the following non-anthropogenic sources:

- Onshore vegetation (biogenic): Model of Emissions of Gases and Aerosols from Nature (MEGAN) (version 2.1) biogenic emissions model
- Wildfires, prescribed burns, and agricultural burning: USEPA's SMARTFIRE emissions inventory for the U.S.
- Windblown dust (WBD): WBD modeling using the WRF meteorological dataset.
- Lightning: WRF data (preprocessor)
- Sea salt emissions: WRF data (preprocessor)

Ramboll incorporated wildfire emission estimates from the Fire INventory from NCAR (FINN) for Mexico and Canada.

3.3.8 Sources in Mexico

The 4-, 12-, and 36-km modeling domains include portions of Mexico (Figure 3-4). As shown in Figure 3-5, the 4-km (d03) domain includes only the two northeastern border states of Mexico (i.e., Nuevo León and Tamaulipas) and consists of nine Mexican municipalities across these two states. One of the nine municipalities is in Nuevo León (i.e., China) with the rest being in Tamaulipas.

The 12-km (d02) domain includes municipalities in 13 Mexican states. Of these, four states (Coahuila, Durango, Nuevo León, and Tamaulipas) fall entirely within the 12-km domain. The remaining nine states are partially located within the domain. Table 3-2 presents a summary of states and the number of municipalities within each state that lie within the 12-km domain.

Figure 3-4 also indicates the major population centers within the two modeling domains. The population centers depicted have a population greater than 400,000. Among the population centers that lie within the 12-km domain, Monterrey and (Ciudad) Juárez are the largest, with populations greater than 1 million. The only major population centers in the 4-km domain are Matamoros and Reynosa.

Figure 3-4. Mexico Portion of the Modeling Domains

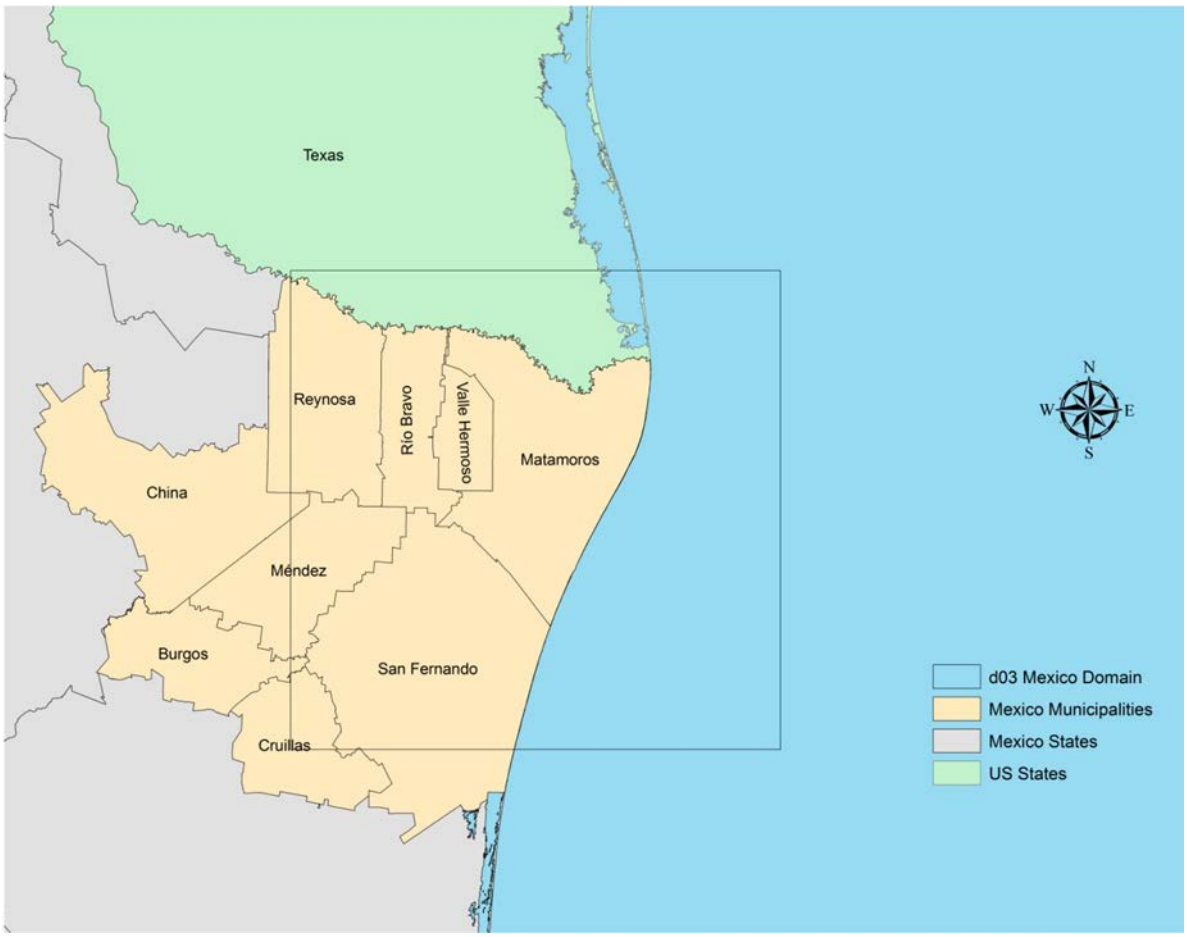

Figure 3-5. Mexico Portion of the 4-km Modeling Domain

Table 3-2. Mexican States and Municipalities in the 12-km Modeling Domain

State Code	State Name	Total Number of Municipalities	Number of Municipalities in the Modeling Domain
01	Aguascalientes	11	8
05	Coahuila	38	38
08	Chihuahua	67	62
10	Durango	39	39
14	Jalisco	125	8
18	Nayarit	20	10
19	Nuevo León	51	51
24	San Luis Potosí	58	34
25	Sinaloa	18	10
28	Tamaulipas	43	43
30	Veracruz	212	2
31	Yucatán	106	1
32	Zacatecas	58	42
	Total	**846**	**348**

The 36-km completely or partially includes an additional seven states (Table 3-3).

Table 3-3. Additional Mexican States and Municipalities in the 36-km Modeling Domain

State Code	State Name	Total Number of Municipalities	Number of Municipalities in the Modeling Domain
02	Baja California	5	5
03	Baja California Sur	5	5
11	Guanajuato	46	9
13	Hidalgo	84	1
22	Querétaro	18	3
23	Quintana Roo	10	3
26	Sonora	72	72
	Total	**240**	**98**

ERG developed the 2012 emissions inventories for the portions of Mexico within the 36-km modeling inventory domain using the municipality-level emission files from the 2008 Mexico National Emissions Inventory (MNEI) (SEMARNAT, 2014). ERG previously used these same municipality-level emission files to develop various similar modeling inventories, including:

- Year 2011 and 2015 projected inventories for the Maricopa Association of Government's (MAG's) 36-km modeling inventory domain, which is similar, but not identical, to BOEM's d01 modeling inventory domain (ERG, 2014a)
- Year 2018, 2025, and 2030 projected inventories for the entire country of Mexico for the USEPA (ERG, 2014b)
- Year 2011 and 2017 projected inventories for MAG's 36-km modeling domain (ERG, 2015)

To develop the 2012 Mexico emissions, ERG used methodologies from the previous inventory development efforts listed above. In addition, ERG conducted preparatory steps before projecting emissions forward to future years. Some of these additional preparatory steps were performed before developing the 2012 inventory for this study. Namely, ERG conducted additional QA/QC of the point source coordinates within the modeling inventory domain and conducted additional QA/QC of the area and nonroad source data.

In general, ERG projected the 2012 Mexico emissions by multiplying the base year 2008 emissions by a projection factor, as shown in the following equation:

$$E_{2012,s} = E_{2008,s} \times P_s$$

Where:

$E_{2012,s}$ = projected future year emissions for 2012 for source *s*
$E_{2008,s}$ = estimated base year emissions for 2008 for source *s*
P_s = projection factor for source *s*

A projection factor greater than 1.0 represented increasing emissions, while a projection factor less than 1.0 represented decreasing emissions. A projection factor of 1.0 represented a situation of no growth (i.e., projected emissions were equal to base year emissions). The projection factors were based on "surrogates" for all sources except onroad motor vehicles, as explained below.

3.3.8.1 Point Sources in Mexico

ERG used the following data sources as surrogates to develop point source projections for Mexico:

- Electricity generation sector:
  - Residual fuel oil usage (regional level) (SENER, 2014a)

    - Distillate fuel oil usage (regional level) (SENER, 2014a)
    - Natural gas usage (regional level) (SENER, 2014b)
    - Petroleum coke usage (national level) (SENER, 2014a)
    - Coal usage (national level) (SENER, 2014c)
- Oil and natural gas sector:
    - Crude oil production (national level) (SENER, 2014a)
    - Crude oil refining (regional level) (SENER, 2014a)
    - Natural gas demand (regional level) (SENER, 2014b)
- All other sectors:
    - Gross domestic product (GDP) (national level) (PCIF, 2014)

3.3.8.2 Nonpoint Area Sources in Mexico

ERG used the following data sources as surrogates to develop area source projections for Mexico:

- Population data:
    - Census data (municipality level) (INEGI, 2010)
    - Intracensal data (municipality level) (INEGI, 2005)
    - Population projections (municipality level) (CONAPO, 2012)
- Fuel usage:
    - Petroleum product usage (regional level) (SENER, 2014a)
    - Natural gas and liquefied petroleum gas usage (regional level) (SENER, 2014b)
    - Residential wood usage (national level) (SENER, 2014c)
- GDP estimates (national level) (PCIF, 2014)
- Agricultural acreage (SAGARPA, 2014a):
    - Total (state level)
    - Sugarcane (state level)
- Cattle head counts (state level) (SAGARPA, 2014b)

Future year population projections were available from the Consejo Nacional de Población (National Population Council) (CONAPO) for each of the 589 municipalities within the d01 inventory domain. However, to apply the 2012 population projections, ERG needed a 2008 population estimate for each municipality. ERG derived 2008 population estimates using linear interpolation between the 2005 intracensal populations (INEGI, 2005) and the 2010 census populations (INEGI, 2010). Agricultural acreage (both total and sugarcane) and livestock head count data were based on historical data for 2012 (SAGARPA, 2014a; SAGARPA, 2014b).

3.3.8.3 Mexican Onroad Mobile Sources

Instead of using projection methodologies, Mexican onroad motor vehicle emissions were generated using a version of the USEPA vehicle emissions model MOVES that was updated to reflect conditions in Mexico. MOVES2014 was the most recent version of the model available at the time of the analysis and reflects USEPA's latest estimate of vehicle emissions and default U.S. activity data (USEPA, 2014c).

To generate the onroad motor vehicles emissions, ERG had to determine the best approach for updating the model, culling data on vehicle fleet and activity data to replace U.S. defaults where possible, and reflecting significant differences in emission standards from the U.S. ERG updated MOVES databases for Mexico to estimate emissions in calendar year 2012. ERG then generated monthly inventories of Mexico's onroad emissions at the municipality level. Appendix C.1 provides a detailed discussion of the MOVES adaption for Mexico.

3.3.8.4 Mexican Nonroad Mobile Sources

Nonroad mobile sources in Mexico include CMVs, locomotives, aircraft, and nonroad equipment (i.e., airport GSE, construction and mining equipment, and agricultural equipment). ERG used diesel and jet fuel (*turbosina*) usage statistics (SENER, 2014a) and agricultural acreage statistics (SAGARPA, 2014a) as surrogates for projecting emissions from nonroad mobile sources in Mexico.

3.3.8.5 Mexican Offshore Platforms

ERG researched the offshore oil production activities off the coast of Mexico. Based on a report published by the Congressional Research Service, it was determined that there was no offshore production within the 36-km modeling domain in 2012 (Seelke et al., 2015).

3.3.9 Sources in Canada

ERG used emissions from the USEPA's most recent modeling platform (2010) for sources in Canada.

3.4 Future Year Modeling Scenario Emission Estimates

Emission estimates are required inputs for additional modeling scenarios that will serve as a basis to predict future impacts from the implementation of the PFP for the 2017–2022 Program (i.e., the Proposed Action). To model the future year impacts, a comprehensive emissions inventory was needed for the entire 36-km domain. This includes projected future emission estimates for onshore sources in the U.S., existing OCS oil and gas production sources in the GOMR, other sources in the GOMR not related to oil and gas production, and the portions of Canada and Mexico that lie within the 36-km modeling domain. These projected emissions were combined with the estimated emissions from the Proposed Action to estimate the cumulative air quality and AQRV impacts of the Proposed Action (see Section 4 of this report.).

ERG obtained projected emission estimates from the USEPA for onshore sources and mobile sources not within BOEM's jurisdiction and developed emission estimates for other non-BOEM sources, such as anticipated offshore deepwater oil and natural gas production off the coast of Mexico. Emission estimates from the *Year 2014 Gulfwide Emissions Inventory Study* (Wilson et al., 2017) were used for existing OCS oil and gas production sources as well as other emission sources in the GOMR.

For OCS oil and gas production sources associated with the Proposed Action for the 2017–2022 Program, ERG forecasted emissions based on detailed information provided by BOEM. BOEM provided information for the anticipated activities associated with Proposed Action's 10 proposed lease sales, as well as information on the anticipated activities associated with a single sale to facilitate the assessment of the cumulative and incremental air quality and AQRV impacts.

3.4.1 USEPA NEI Sources

In support of the proposed ozone NAAQS revisions, the USEPA released the 2011 air quality modeling platform (2011v6.1), with projections to 2018 and 2025 for point, nonpoint area, and mobile sources in the U.S. (USEPA, 2014d). In addition, the USEPA released the 2011 air quality modeling platform (2011v6.2), with projections to 2017, to support ozone transport modeling for the 2008 NAAQS and the 2015 ozone NAAQS (USEPA, 2015d). In early October 2015, the USEPA also released the 2011v6.2 base year 2025 projected inventory (USEPA, 2015d). ERG used the 2011v6.2 platform for calendar year 2017, primarily because the platform is based on the most recent version of the NEI (2011v.2). Calendar year 2017 was selected rather than 2025 because there is less uncertainty associated with the 2017 estimated emissions. For 2017, most of the controls that the USEPA factored in are already "on the

books" and not speculative. Using 2025 emission estimates would increase the use of speculative controls, some of which may not have been scrutinized by state agencies for reasonableness. These estimates could also change or may not come to fruition. The effect of these additional speculative controls is seen in the total emissions for each pollutant, as 2017 has higher estimates for all pollutants except NH_3 and PM_{10}. In this respect, 2017 proved to be a conservatively high estimate of emissions from these sources with less uncertainty.

The *Technical Support Document (TSD): Preparation of Emissions Inventories for the Version 6.2, 2011 Emissions Modeling Platform* (USEPA 2015d) provides details on the development of the 2011v6.2 future year modeling platforms. USEPA updates include the following:

- **EGUs:** updated unit-specific emissions estimates based on the USEPA's Integrated Planning Model (IPM) version 5.14 results
- **Point sources:** incorporated the impacts of current "on the books" federal and state regulations, facility closures, new facility construction, and other information provided by state and local agencies
- **Airports and aircraft:** updated based on airport-specific TAF data
- **Nonpoint area sources:** incorporated the impacts of federal and state regulations, information provided by state and local agencies, product and consumption indicators for upstream oil and natural gas activities, assumed growth/controls for residential wood combustion, and updated livestock NH_3 emission estimates based on livestock population projections
- **Onroad and nonroad mobile sources:** updated with the USEPA's MOVES2014 and NONROAD model runs using year-specific fuel mixture information, activity data, and control program information. (Although MOVES2014a was released in 2015 and incorporates some improvements in calculating onroad and nonroad equipment emissions, updated emission factors were not available for use in this study. The USEPA indicated that the improvements will not significantly affect the air quality modeling results based on these inventory data.)
- **Category 1 and 2 CMVs:** updated using projection factors from the U.S. Department of Energy's Annual Energy Outlook (AEO)
- **Category 3 CMVs:** updated for growth using IMO growth projections and compliance assumptions for the North American ECA regulatory program
- **Rail:** updated using projections from the AEO and USEPA fuel and exhaust regulatory control programs

For sources in Mexico, the USEPA air quality modeling platform 2011v6.2 includes projected 2018 emissions for onshore sources. Emissions for Mexico are based on the *Develop Mexico Future Year Emissions* report (ERG, 2014b).[1] The USEPA held emissions constant for biogenic sources and fires, as well as sources in Canada (at 2010 levels).

In addition, ERG considered the impacts on the Category 3 CMVs in the future scenario based on the lifting of the export ban on light condensate. On December 18, 2015, Congress ended the ban on such exports, and condensate exports began in early 2016 from Texas ports. It is unclear whether the ban on exporting actual crude oil will be lifted in the future, and to what extent this will affect tanker traffic patterns; most tankers leave U.S. ports empty. It is believed that returning tankers can accommodate the export of condensate; though this may change global tanker traffic patterns, it is currently uncertain to what extent U.S. domestic tanker traffic will be affected. Given these uncertainties, data are insufficient at this time to estimate the air quality impacts that this change will elicit.

[1] The projected emission estimates for the oil and gas sector (extraction, production, refining, and pipeline transportation of crude oil, natural gas, and refined petroleum products) in Mexico were developed based on a crude oil refining surrogate (SENER, 2014a, b).

3.4.2 Other Non-BOEM Sources

ERG confirmed that the 2017–2022 Program scenario spreadsheets (see Section 3.4.4) include offshore drilling in the Eastern GOM Planning Area under USEPA air quality jurisdiction. ERG also reviewed the USEPA OCS offshore oil and gas production permits to confirm that no production platforms were permitted to be constructed before or during 2017. Therefore, future offshore OCS drilling emissions are included, but future production platforms are not included in the Eastern GOM Planning Area.

ERG also developed projected emissions estimates for platforms off the coast of Mexico. ERG researched the impacts of restructuring the energy sector in Mexico, which is predicted to include deepwater production within the modeling domain. ERG used the production-based emission factors in Table 3-4 to estimate emissions based on projected deepwater production that falls just within the 12-km modeling domain (PEMEX, 2012). These emission factors were developed using the 2011 Gulfwide Emissions Inventory (Wilson et al., 2014) and an estimated deepwater production of 47 million barrels/year (PEMEX, 2012). The factors include the 2011 inventory estimates for major platforms (excluding caissons, living quarters, and wellhead protectors; including combustion, drilling, etc.), combined with production data from OGOR-A (USDOI, BSEE, 2015). Table 3-5 presents the resulting emission estimates.

As noted above, non-BOEM source activities in the GOMR are now based on the 2014 Gulfwide Emissions Inventory emission estimates. These sources include CMVs, commercial and recreational fishing, and military vessels. The 2014 inventory's SO_2 emission estimates were adjusted for non-BOEM marine vessels with Category 3 engines using residual diesel fuel to account for new fuel standards that would be in place before 2017. The North American ECA fuel standard limits the fuel sulfur content to 1 percent (1,000 ppm) for vessels with these engines, starting in 2015 (USEPA, 2010).

To avoid double counting with the USEPA NEI GOMR marine vessel emissions estimates, only the USEPA NEI GOMR marine vessel data for activities in state waters and east of the GOMESA were retained.

The LOOP and vessel lightering are also sources included in the 2014 Gulfwide Emissions Inventory. ERG also investigated the need to include a liquefied natural gas (LNG) port in federal waters, which was originally expected to be operational in 2019. On September 18, 2015, however, the Maritime Administration (MARAD) and the U.S. Coast Guard stopped the permit application process, as Delphin LNG, LLC, is amending the application. This potential source was not included in the future scenario given this uncertainty.

Table 3-4. Production-Based Emission Factors for Offshore Platforms in Mexican Waters

Pollutant	Emission Factor (lbs/BBL)[a]
CO	0.2919
NO_x	0.3492
PM_{10}-PRI[a]	3.48E-03
$PM_{2.5}$-PRI	3.47E-03
SO_2	1.33E-02
VOC	0.2271
Pb	9.07E-07
NH_3	1.66E-04

[a] BBL= barrel; PRI = primary
Source: Developed from the Year 2011 Gulfwide Emissions Inventory (Wilson et al., 2014).

Table 3-5. Emission Estimates for Offshore Platforms in Mexican Waters

Pollutant	Emissions (TPY)
CO	6,873.08
NO_x	8,220.48
PM_{10}-PRI	81.86
$PM_{2.5}$-PRI	81.63
SO_2	312.37
VOC	5,347.33
Lead	2.13
Ammonia	3.90

3.4.3 Central/Eastern and Western GOM Planning Area Existing Offshore OCS Oil and Gas Production Sources

The emissions inventory for existing oil and gas production sources is based on the 2014 Gulfwide Emissions Inventory (Wilson et al., 2017). ERG decided to use the 2014 inventory instead of the 2011 inventory for several reasons. First, the 2014 inventory is now publicly available; it was not available for consideration for use in this study in the initial round of photochemical modeling. Second, in the 2014 inventory, the methodology used to estimate emissions from marine vessels and spatially allocate the emissions in the GOMR is based on detailed AIS data, which uses global positioning systems (GPS) to track vessel movements. This yielded more detailed data, which ERG used to estimate marine vessel emissions. Last, although the 2014 emission estimates for these sources show a significant decrease in all pollutants from the 2011 estimates, the *Year 2014 Gulfwide Emissions Inventory Study* (Wilson et al., 2017) describes the detailed analysis that evaluated this trend, as well as trends with past BOEM Gulfwide inventories. Although no definitive conclusions can be drawn as to the cause of the decline in the emission estimates from 2011 to 2014, the improvements made in the vessel estimates, combined with increased deepwater production, well stimulation activities, installation of subsea production systems, and the decommissioning of less-productive platforms in shallow waters seems to indicate future production trends. Therefore, ERG believes the 2014 emissions inventory represents a better estimate of existing emission conditions to combine with future emission levels for impact estimation. Please refer to the *Year 2014 Gulfwide Emissions Inventory Study* for more details (Wilson et al., 2017).

3.4.4 Existing Offshore OCS Oil and Gas Production Platforms

The 2014 production platform emission estimates used to represent existing sources included all equipment types reported by operators to BOEM through the 2014 Gulfwide Offshore Activities Data System (GOADS-2014). This included any drilling emissions associated with drilling equipment attached to the platform. The non-platform estimates captured drilling emissions associated with vessels that are not attached to the platform.

To make the 2014 estimates more reflective of 2017, the diesel fuel sulfur content was revised, as only ultra-low-sulfur diesel fuel is expected to be available for use on offshore platforms (0.0015 wt% sulfur). In 2011, the assumed default value was 0.05 wt% sulfur. In developing the 2014 emissions inventory, BOEM used GOADS to request activity data from platform operators, including the diesel fuel sulfur content. ERG was therefore able to adjust any reported values that were above 0.0015 wt% sulfur to 0.0015 and recalculate the estimated emissions.

ERG also removed from the 2014 inventory 133 platforms that are now reported in BOEM's Technical Information Management System (TIMS) as decommissioned and evaluated the need to calculate emissions for additional platforms installed after 2014. According to TIMS, four structures were installed in 2015 and two in 2016. Only two of these six structures are located on a lease that has the production volume reported in OGOR-A. However, for both lease blocks, there is at least one other active platform that was installed in the 1960s. Because production data are only available at the lease block level in TIMS, ERG was unable to determine whether the reported production was associated with the new structure or existing structures. ERG did not, therefore, develop surrogate emission estimates for any newly installed structures.

Platforms are also routinely decommissioned as their productivity declines and new platforms are brought online. ERG compared the total number of platforms in the existing inventory and the Proposed Action scenario to the "cumulative scenario" provided by BOEM. Based on the Proposed Action's platform installation information compared to the decommissioning rate in the cumulative scenario, ERG developed a decommissioning rate of existing platforms that mirrors their installation rate to maintain a relative steady state of platforms within the inventory.

ERG selected structures to be decommissioned/removed from the inventory starting with the oldest platforms based on BOEM guidance on which geographic areas with water depths less than 200 m have the lowest production potential. For structures in depths greater than 200 m, decommissioning was based solely on the age of the structure. Older platforms were selected for decommissioning to mirror the typical 30- to 40-year lifespan of offshore platforms suggested by the BOEM data file. Where possible, structures for decommissioning mirrored additional sources' water depth categories and structure type (e.g., caisson, single well structure).

3.4.4.1 Existing Offshore OCS Oil and Gas Production Support Vessels and Helicopters

As with the non-BOEM vessel emissions, the future year emissions for vessels (i.e., non-platform sources) associated with the oil and gas production are based on the 2014 Gulfwide Emissions Inventory. As noted above, the 2014 inventory for marine vessels was based on detailed AIS data, which tracks vessel movements. The shift to the 2014 inventory allowed ERG to use the AIS data, which yielded much more detailed information needed to quantify emissions based on the vessel population, use, hours of operation, power ratings, engine classification, and vessel-specific propulsion operating loads. AIS identified approximately twice the number of oil and gas production support vessels in the 2014 inventory as compared to the 2011 inventory and quantified that the average propulsion engine power rating for these vessels was 50 percent of that assumed in the 2011 inventory. In addition, although the 2014

inventory included more vessels, the AIS data indicated that these vessels tend to idle at sea more than was assumed in the 2011 inventory, yielding significantly lower average engine operating loads.

ERG assumed that the AIS-based 2014 Gulfwide activity discussed above and activity levels for OCS oil and gas production vessels remained constant at 2014 levels. After careful consideration, ERG concluded that adjusting the AIS data to account for the future decommissioning of platforms would add another level of uncertainty to the inventory. As is, the estimate is conservatively high for 2017, though it is not as conservative as the 2011 data. The only emission level adjustment was made to the SO_2 estimates for marine vessels with Category 3 engines using residual diesel fuel, to account for new fuel standards that lowered sulfur content in the ECA. This mirrors the adjustment made to non-BOEM Category 3 marine vessels noted in Section 3.4.1.

3.4.5 Central/Eastern and Western GOM Planning Areas Proposed Action Offshore OCS Oil and Gas Production Source Activities

For offshore OCS oil and gas production sources predicted to begin operation in the 2017–2022 timeframe, BOEM provided information that formed the basis of the 2017–2022 Program. BOEM developed scenarios to represent hypothetical assumptions based on estimated amounts, timing, and general locations of OCS exploration, development, and production for offshore activities. BOEM developed the scenarios using historical information and trends in the OCS oil and gas industry.[2] The scenarios represent assumptions and estimates that are reasonably suitable for pre-sale impact analyses. BOEM developed forecasts of oil and gas exploration, discovery, development, and production. BOEM provided ERG with these projected levels of activity and locations (by planning area and water depth) with year-by-year estimates to depict offshore OCS oil and gas sources activity in the future scenario. ERG then used this information to develop emission estimates, such as number of wells drilled, number of platforms installed, and the additional activities listed below. The scenarios used to estimate emissions are based on mid-level oil prices (as opposed to low- or high-level prices). ERG used activity levels associated with mid-level fuel price forecast, as this fuel price has been predictive of actual conditions in previous BOEM EIS analyses.

ERG used the BOEM data to develop annual emission estimates for all categories and pollutants for each year of activity for OCS offshore oil and gas production sources associated with nine-sale source activities in the 2017–2022 Program, as described below. ERG also developed annual emission estimates for all categories and pollutants of OCS offshore oil and gas production sources associated with a single lease sale, again based on information provided by BOEM. The emission estimates cover the Western, Central, and Eastern GOM Planning Areas[3] under BOEM jurisdiction.

Annual emission estimates were developed for the following sources and activity levels over the five-year, 10-sale Proposed Action period:

- Exploration and delineation well drilling activities (1,671 wells drilled)
- Development and production well drilling activities (1,135 wells drilled)[4]
- Structure installation activities (535 platforms installed)
    - Caisson installation activities (478 caissons/single well platforms installed)
    - Multi-well structure installation activities (57 multi-well platforms installed)
- Floating production storage and offloading (FPSO) installation (1 FPSO installed)
- FPSO operation (1 FPSO in operation)

[2] For more information on historical OCS oil and gas production trends, please see the *Year 2014 Gulfwide Emissions Inventory Study* (Wilson et al., 2017).

[3] Excluding the GOMESA moratoria area.

[4] Including exploration wells re-entered and completed.

- FPSO removal (1 FPSO removed)
- Pipeline installation excluding state waters (7,251 km of pipeline installed)
- Platform oil and gas production (535 platforms in operation)
    - Caisson operations (478 caissons/single well platforms in operation)
    - Multi-well structure operations (57 multi-well platforms in operation)
- Platform removal (535 platforms removed)
- Support helicopters (1,235,000 round trips)
- Support helicopters (4,144,000 trips within a water depth)
- Support vessels (421,900 round trips)

Based on information provided in the BOEM forecasts, ERG also developed annual emission estimates for the following sources and single-sale activities:

- Exploration and delineation well drilling activities (464 wells drilled)
- Development and production well drilling activities (238 wells drilled)
- Structure installation activities (117 structures installed)
    - Caisson installation activities (100 caissons/single well platforms installed)
    - Multi-well structure installation activities (17 multi-well platforms installed)
- FPSO installation (0 FPSO installed)
- FPSO operation (0 FPSO in operation)
- FPSO removal (0 FPSO removed)
- Pipeline installation excluding state waters (1,638 km of pipeline installed)
- Platform oil and gas production (117 platforms in operation)
    - Caisson operation (100 caissons/single well platforms in operation)
    - Multi-well structure operations (17 multi-well platforms in operation)
- Platform removal (117 platforms removed)
- Support helicopters (371,000 round trips)
- Support helicopters (1,238,000 trips within a water depth)
- Support vessels (114,200 round trips)

The BOEM activity scenario spreadsheets provided information on each of these anticipated activities by year, as well as water depth (i.e., 0–60 m, 60–200 m, 200–800 m, 800–1,600 m, 1,600–2,400 m, and 2,400 m+). The anticipated water depths by planning area were used to spatially allocate the emissions.

BOEM provided activity levels by water depth for the Proposed Action for the Western, Central, and Eastern GOM Planning Areas' projected drilling activities (exploration and development), platform installation and removal activities, method of oil transportation, length of pipeline installed, number of service vessel trips, and number of helicopter trips. ERG used this information to estimate emissions for each source category based on methods used in past Gulfwide emissions inventory studies and other data compiled for BOEM to determine which estimates should be selected for photochemical modeling to support the cumulative air quality impacts analysis. In addition, BOEM provided information on a single lease sale within the 2017–2022 Program to support future BOEM NEPA EIS cumulative air quality analyses. ERG used this information to split the 10-sale activity information into a single-sale and nine-sale (i.e., the difference between the 10-sale and single sale) activity levels to develop emission estimates. ERG will use source apportionment to separately track emission estimates for the single sale and nine sales in the photochemical grid modeling. This will allow the modeling to estimate the impacts for a single sale within the 10-sale program and for the entire program at the same time.

The following sections discuss the emission estimation methods that ERG used for the BOEM oil and gas production sources in the future scenario.

3.4.5.1 Oil and Natural Gas Offshore OCS Production Platforms

To develop reasonable emission estimates for projected oil and natural gas production platforms, ERG first developed the emission factors in Table 3-6 based on the 2014 Gulfwide Emissions Inventory (Wilson et al., 2017). Based on input from the USEPA that offshore platform emissions can vary based on platform water depth, and the fact that the offshore oil and gas industry in the GOMR is trending toward more production in water depths greater than 300 m (i.e., deepwater production), the emission factors were developed based on the depth boundaries shown (60 m, 200 m, 800 m, 1,600 m, 2,400 m and greater than 2,400 m). These water depth-specific emission factors were assigned to each projected platform based on water depths defined in the BOEM scenario. The emission factors were developed after adjusting the diesel fuel sulfur content, as discussed in Section 3.4.4. ERG parsed the platforms in the 2014 inventory by water depth bin and developed the average emissions for each pollutant by platform. The averages for multi-well platforms excluded caissons, living quarters, and wellhead protectors and included all other equipment types reported in GOADS such as combustion equipment, fugitive sources, flares, and vents. Fugitive emissions are large sources of VOC emissions that stem from leaks from sealed surfaces associated with process equipment (Wilson et al., 2017).

Based on guidance from BOEM, emission factors for single well platforms in water depth less 200 m (caissons) were also developed. The caisson and multi-well platform emission factors are shown in Table 3-6.

Table 3-6. Future Scenario Production Platform Emission Factors (tons/platform/year)

	Caisson	Multi-Well by Water Depth					
	0–200 m	0–60 m	60–200 m	200–800 m	800–1,600 m	1,600–2,400 m	> 2,400 m
CO	0.35	29.46	58.25	131.71	144.34	121.14	40.29
NO_x	0.39	22.46	53.20	161.70	270.64	379.33	90.02
PM_{10}-PRI	5.6E-3	0.27	0.86	2.22	3.66	5.52	1.50
$PM_{2.5}$-PRI	5.6E-3	0.27	0.86	2.21	3.65	5.51	1.49
SO_2	6.4E-4	0.09	0.35	0.60	1.12	1.44	0.09
VOC	3.24	28.82	53.49	183.23	83.86	70.57	129.98
Pb	3.6E-8	5.3E-7	1.3E-6	1.8E-5	3.7E-5	4.7E-5	2.1E-4
NH_3	2.3E-4	3.4E-3	8.9E-3	4.8E-2	2.2E-1	2.1E-1	0.5E-1

Source: Developed from the Year 2014 Gulfwide Emissions Inventory (Wilson et al., 2017).

ERG developed emission estimates for platform sources based on platform installation and carried them forward until the projected platform removal dates (provided by planning area and water depth).

BOEM data noted all activities in the reasonably foreseeable future for actions initiated as part of the 2017–2022 Program. The data indicated the number of installations per year for these leases and provided an estimate of the decommissioning of these same platforms. In total, the activities of the 2017–2022 Program spanned 50 years (through calendar year 2071) to cover the estimated decommissioning year for the last platform installed under the action.

3.4.5.2 Offshore OCS Oil and Gas Production Support Helicopters

ERG obtained helicopter emission factors from the Switzerland Federal Office of Civil Aviation's (FOCA's) *Guidance on the Determination of Helicopter Emissions* (FOCA, 2009), as they are the most up-to-date emission factors available for helicopters. However, the LTO cycle used by FOCA was determined to be too short for typical trips taken in the GOM. ERG adjusted the time-in-mode values

based on the International Civil Aviation Organization (ICAO) test cycles, which are appropriate for offshore operations in the GOM. Table 3-7 presents the original FOCA time-in-mode values and the adjusted values.

Table 3-7. Helicopter Time-in-Mode Values

Source	Pre-Takeoff Idle (Min)	Takeoff Time (Min)	Approach Time (Min)	Post-Landing Idle (Min)	Total Idling (Min)	Total Flight (Min)
FOCA	4.0	3.0	5.5	1.0	5.0	8.5
Adjusted for this study	12.0	7.0	13.0	3.0	15.0	20.0

ERG recalculated the FOCA emission factors based on the adjusted time-in-mode values. The LTO-based emission factors for each helicopter type were also evaluated, and the maximum value was selected. To account for helicopter cruising emissions, ERG used the hourly emission rates in the FOCA data. It was assumed that one hour of transit time would be required per LTO cycle. Because the future fleet mix is unknown, ERG weighted the emission factors using fleet profile data from the Helicopter Safety Advisory Conference (HSAC, 2015). Table 3-8 lists the FOCA emission factors by helicopter and helicopter type and the weighted average emission factors. ERG developed the VOC emission factors by converting the hydrocarbon (HC) emission factors using data from the USEPA's *Procedures for Emission Inventory Preparation Volume IV: Mobile Sources* (USEPA, 1992). The aggregated general aviation conversion factor of 1.0631 for turbine engines was used because the GOMR's support helicopter fleet is primarily equipped with turbine engines. The $PM_{2.5}$ emission factors were speciated from PM_{10} factors using USEPA aircraft speciation data, and the SO_2 emission factors were developed based on a typical jet fuel sulfur concentration of 0.05 percent (UNEP, 2012). Emission factors were not available for NH_3 or Pb.

Table 3-8. FOCA Maximum Emission Factors by Helicopter Type (LTO)

Helicopter Type	Fuel/LTO (kg)	Emission Factors (lbs./LTO)						
		CO[a]	HC[a]	NO_x[a]	PM_{10}-PRI[a]	$PM_{2.5}$-PRI[b]	SO_2[c]	VOC[d]
Single	108.1245	3.53	2.70	2.08	0.06	0.06	0.23	2.87
Twin Light	109.7688	8.34	6.30	1.29	0.04	0.04	0.24	6.70
Twin Medium	242.3659	6.31	4.83	5.60	0.15	0.15	0.52	5.14
Twin Heavy	461.2306	3.96	3.20	13.31	0.33	0.32	0.99	3.40
Weighted Average	170.9537	4.68	3.59	3.83	0.10	0.10	0.37	3.82

[a] FOCA (2009)
[b] $PM_{2.5}$ = 97.6% of PM_{10}
[c] SO_2 (g/gal) = (fuel density) × (conversion factor) × (64 g SO_2/32 g S) × (S content of fuel)
[d] HC to VOC = * 1.0631

ERG also obtained the FOCA emission factors for one hour of flight. In the GOM, the assumed average travel distance is 70 miles, and the average speed of a helicopter is assumed to be 140 miles per hour, making the average flight per operation 0.5 hour. Table 3-9 presents the 0.5-hour cruising emission factors for helicopters.

Table 3-9. FOCA Maximum Emission Factors by Helicopter Type (Cruising)

Helicopter Type	Fuel (kg)	Emission Factors (lbs per 0.5 hour)						
		CO[a]	HC[a]	NO_x[a]	PM_{10}-PRI[a]	$PM_{2.5}$-PRI[b]	SO_2[c]	VOC[d]
Single	141.93	0.60	0.48	1.68	0.05	0.04	0.31	0.51
Twin Light	141.31	1.18	0.94	0.99	0.03	0.03	0.30	1.00
Twin Medium	367.54	0.91	0.74	5.30	0.14	0.13	0.79	0.79
Twin Heavy	666.13	0.75	0.64	11.00	0.26	0.26	1.44	0.68
Weighted Average	240.30	0.74	0.60	3.27	0.08	0.08	0.52	0.64

[a] FOCA (2009)
[b] $PM_{2.5}$ = 97.6% of PM_{10}
[c] SO_2 (g/gal) = (fuel density) × (conversion factor) × (64 g SO_2/32 g S) × (S content of fuel)
[d] HC to VOC = * 1.0631

3.4.5.3 Offshore OCS Oil and Gas Production Support Vessels

Four components are needed to estimate future offshore vessel emissions:

- Vessel characteristics (engine power and speed)
- Engine operating load (percent of maximum engine power)
- Hours of operation (typically determined by dividing the distance the vessel travels by its speed)
- Appropriate emission factors (grams per kilowatt-hour [kWh])

Because there is uncertainty about the location of future activities, ERG assumed a typical vessel trip based on the distance from the mid-point of each water depth bin (and planning area) to the closest port. ERG selected the nine closest ports based on the BOEM report, *Fact Book: Offshore Oil and Gas Industry Support Sectors* (Dismukes, 2010). The ports include the following:

- Ingleside, Texas
- Freeport, Texas
- Galveston, Texas
- Sabine Pass, Texas
- Cameron, Morgan City, Louisiana
- Intercoastal City, Louisiana
- Forchon, Louisiana
- Venice, Louisiana
- Pascagoula, Mississippi

3.4.5.3.1 Vessel Characteristics

In projecting future year activity, it is not always possible to identify specific vessel types and sizes that will be used. For this study, larger vessels that represent the upper bound of each vessel type will be assumed, such that actual future year emissions should be similar to or lower than emission estimates developed using this fleet profile.

For this analysis, ERG identified larger vessels based on data compiled from the Information Handling Service (IHS) Register of Ships (IHS, 2015). Vessels from the global fleet were used, because these larger ships move internationally based on local demand. It should also be noted that these larger vessels tend to be involved in deepwater activities, because they are designed for extended open-water operations. As trends to develop deeper-water locations in the GOM continue into the future, it is likely that these larger or similar vessels will support future year activities.

The selected vessels and their characteristics are presented in Table 3-10. The vessel engine category is required to correctly match the vessel to the appropriate emission factors. ERG estimated the USEPA vessel category by calculating the cylinder volume based on the stroke length and diameter of the cylinder. The USEPA categories are defined by the following cylinder volumes:

- Category 1: Cylinder displacement less than 5 liters
- Category 2: Cylinder displacement from 5 to 30 liters
- Category 3: Cylinder displacement greater than 30 liters

If a vessel's cylinder volume was unknown, ERG assumed that the vessel was powered by a Category 3 propulsion engine. It should also be noted that all of the selected vessels are foreign-flagged, but it is assumed that they refuel using U.S.-regulated marine fuels as they shift equipment and supplies from nearby U.S. ports.

Table 3-10. Summary of Vessel Characteristics

Vessel Type	Total Main Power (kW)	Vessel Name	Propulsion Engine Category	Speed (knots)
Drillship	48,666	Rowan Renaissance	3	12
Jackup	12,485	Bob Palmer	2 (auxiliary)	Not self-propelled
Platform Rig	8,100	Nabors Mods 087	2 (auxiliary)	Not self-propelled
Semi-Submersible	22,371	ENSCO 7500	2	3.5
Submersible	3,691	Hercules 78	2 (auxiliary)	Not self-propelled
FPSO	14,110[a]	Terra Nova FPSO	2	12.0
Floating Storage and Offloading Vessel	51,519	Africa	3	16.5
Stimulation Vessel	15,840	Norshore Atlantic	2	14
Oil Tanker	13,369	SPT Explorer	3	15
Anchor Handling Vessel	27,000	KL Sandefjord	3	17
Crew Boat	11,520	R. J. Coco Mccall	3	23
Supply Vessel	18,000	Aleksey Chirikov	3	15
Tug Boat	19,990	Yury Topchev	3	15
Pipelaying Vessel	67,200	Castorone	3	14

[a] Only includes distillate oil main engine kW (430 kW and 2 x 6,840 kW). Topside emissions are included in the deepwater production platform estimates.

Appendix C.2 provides detailed descriptions of the representative vessels selected for the future year fleet.

3.4.5.3.2 Operating Engine Load Factors

A vessel's engine power varies relative to the type of operation that is implemented. While cruising in open waters, the propulsion engine load is typically 84 percent of maximum load; during maneuvering, it can be 60 percent or lower, and when stationary it can be 10 percent or lower (USEPA, 2016c). Table 3-11 presents the aggregated load factors that this study used for propulsion and auxiliary engines.

Table 3-11. Load Factors to be Used in the Future Year Projections

Vessel Type	Load Factor
Propulsion Cruising	0.8–0.85
Propulsion Idle	0.1
Propulsion Crew/Supply Boat	0.45
Propulsion Drill Ship and Semi-Submersible	0.83
Propulsion Pipelaying Vessel	0.16
Propulsion Tug	0.68
Auxiliary Emergency Generator	0.75
Drilling Equipment	1

3.4.5.3.3 Marine Vessel Emission Factors

Based on the emission factors in the USEPA's 2014 NEI, ERG developed future year emission factors in terms of grams of pollutant emitted per load-adjusted engine kWh (Table 3-12). The factors presented below are applicable for foreign-flagged vessels that are not required to comply with USEPA exhaust standards, but that must comply with international ECA standards. These future year factors account for the reduction in fuel sulfur level associated with the ECA. Because Category 2 foreign-flagged offshore support vessels will refuel at U.S. ports, ERG anticipates that these vessels will use low-sulfur, compliant U.S. fuels. Also, ERG adjusted the NO_x emission factors to account for the 2016 ECA Tier III standard, which requires high-efficiency, after-treatment technology and is applicable for U.S. and foreign-flagged vessels. ERG did not adjust the Category 3 PM emission factors to account for reductions in PM as sulfate compounds, because the USEPA's adjustment equation provided a PM factor lower than the PM emission factor for Category 2 powered vessels.

Table 3-12. Marine Vessel Emission Factors (g/kWh)

Engine Category	NO_X	SO_2	PM_{10}	$PM_{2.5}$	VOC	CO	HC	NH_3	Pb
2	3.4	0.006	0.320	0.310	0.141	2.48	0.13	0.005	0.00003
3	3.4	0.362	0.450	0.437	0.632	1.40	0.60	0.003	0.00003

Source: USEPA, 2016b.

3.5 Results

3.5.1 Emission Estimates

ERG reviewed the emission estimates for the nine-sale and single-sale future BOEM oil and gas production sources (summed to represent the 2017–2022 Program Proposed Action 10-sale leasing program) to determine the best future year emissions to model. Figures 3-6 and 3-7 present graphical depictions of the nine-sale and single-sale emission estimates. Tables 3-13 and 3-14 present the resulting emission estimates associated with nine-sale and single-sale sources, with the highest year per pollutant bolded in the tables.

For the nine-sale portion of the Proposed Action (Figure 3-6), the emissions increase proportionally to the number of platforms added and operating as part of the action. The emissions peak in 2036 due to the combination of the peak in the number of structures, vessel round trips, and pipelaying activities. After 2036, platform decommissioning increases while installation decreases. This steady decline in structure

and vessel emissions drives the overall action emissions down. The secondary peak in 2041 corresponds to a peak in helicopter activity and emissions, which is an offset of the peak in vessel activity.

For the single sale, activity for the Proposed Action was "front-loaded"; that is, a large amount of the activity occurs in the first few years of the leasing action. The single sale exhibits an early peak in emissions in 2021, dips slightly, and maintains a slow increase until 2033, after which emissions drop off quickly through the remaining years of the action. These peaks correspond to dual peaks in vessel and helicopter activities. Vessel activity peaks in 2021, decreases until 2026, and then returns to a period maximum in 2033. Helicopters exhibit a similar dual peak behavior, with peaks in 2022/2023 and a slightly lower peak in 2033.

When combined to represent the total Proposed Action, emissions peak in 2036. As such, 2036 was selected as the emissions year to use in modeling to represent a reasonable maximum future emissions scenario that would potentially cause the Proposed Action's peak impact. This peak occurs far into the future because of the progressive nature of the activities associated with the Proposed Action as exploration and drilling activities taper off and production platforms are installed and put into production. ERG also examined the "cumulative" emission estimates—which consider existing BOEM production sources and the sources associated with the 2017–2022 Program—and found them to peak in 2036. Photochemical grid modeling for the cumulative air quality impacts analysis were conducted based on the emissions anticipated to have the greatest impact on the air quality of any state. This was determined based on the estimated annual emission trends. Although there is inherent uncertainty in the future scenario emissions estimates for onshore sources, existing offshore OCS oil and gas production sources, and emissions estimates associated with the Proposed Action, BOEM believes the future year emission estimates developed in this study can be used to effectively predict future air quality impacts from GOMR OCS activities.

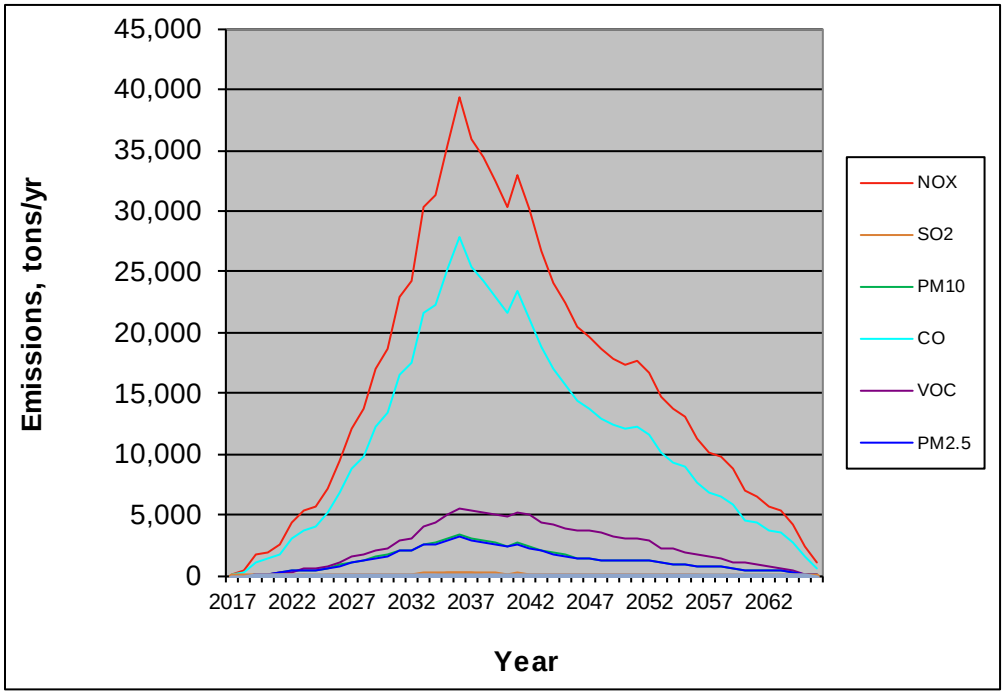

Figure 3-6. Nine-Sale Emission Estimates for All Planning Areas and Future Activities

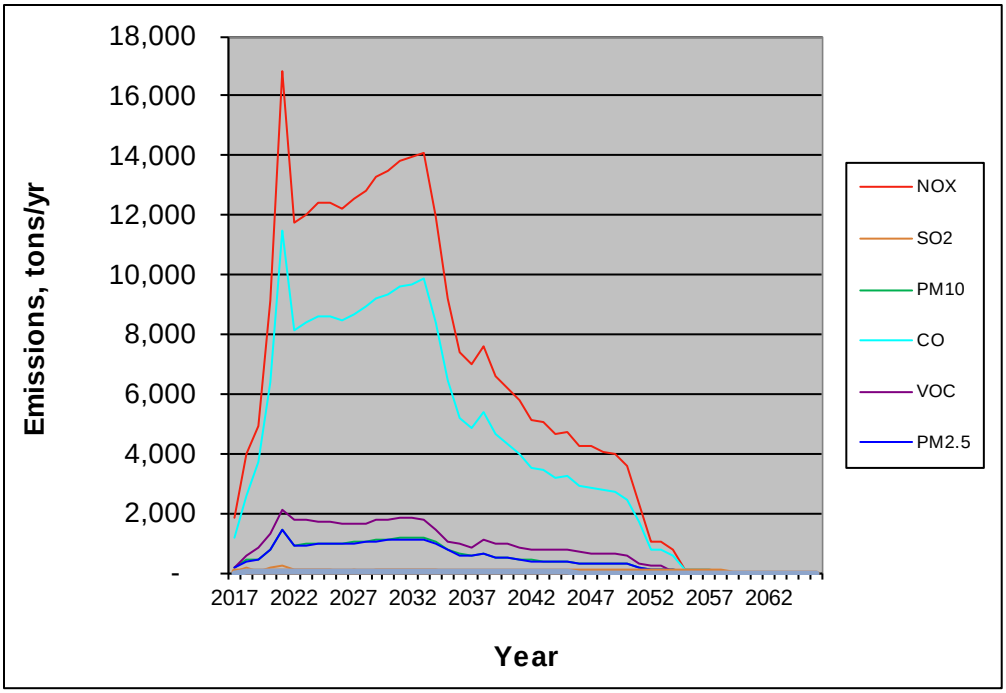

Figure 3-7. Highest Possible Emission Estimates for a Single Lease Sale for All Planning Areas and Future Activities

Table 3-13. Nine-Sale Emission Estimates for Western, Central, and Eastern GOM Planning Areas, All Depths, by Year and Pollutant

Year	NO_X (TPY)	SO_2 (TPY)	PM_{10} (TPY)	$PM_{2.5}$ (TPY)	VOC (TPY)	CO (TPY)	Pb (TPY)	NH_3 (TPY)
2017	160	0	15	15	7	116	0.00	0
2018	475	1	45	43	20	347	0.00	1
2019	1,743	48	180	175	147	1,135	0.02	2
2020	1,967	3	185	179	107	1,435	0.02	3
2021	2,553	21	239	232	236	1,843	0.02	4
2022	4,400	30	422	409	312	3,143	0.04	6
2023	5,435	93	531	515	562	3,760	0.05	7
2024	5,683	40	528	512	595	4,134	0.05	8
2025	7,254	69	678	657	802	5,232	0.06	10
2026	9,533	91	882	856	1,131	6,915	0.08	13
2027	12,178	134	1,126	1,092	1,541	8,770	0.10	16
2028	13,725	175	1,279	1,241	1,732	9,811	0.11	18
2029	16,995	175	1,557	1,510	2,019	12,192	0.14	23
2030	18,670	188	1,706	1,655	2,316	13,394	0.15	25
2031	22,908	199	2,080	2,018	2,865	16,481	0.19	32
2032	24,283	191	2,157	2,093	3,141	17,446	0.20	33
2033	30,267	235	2,654	2,575	4,036	21,660	0.24	41
2034	31,295	241	2,701	2,621	4,406	22,290	0.24	42
2035	35,429	267	3,047	2,957	5,061	25,221	0.28	48
2036	39,407	305	3,359	3,260	5,624	27,874	0.30	53
2037	35,866	251	3,009	2,920	5,402	25,433	0.27	48
2038	34,422	269	2,893	2,808	5,181	24,303	0.26	46
2039	32,443	245	2,696	2,617	5,055	22,940	0.24	43
2040	30,382	210	2,485	2,412	4,936	21,559	0.22	40
2041	32,985	219	2,699	2,621	5,202	23,380	0.24	44
2042	30,111	194	2,390	2,321	5,052	21,196	0.21	40
2043	26,686	161	2,104	2,043	4,429	18,829	0.19	35
2044	24,134	154	1,867	1,813	4,251	16,953	0.17	31
2045	22,422	135	1,713	1,664	3,947	15,749	0.15	29
2046	20,421	110	1,519	1,475	3,786	14,351	0.14	26
2047	19,622	106	1,449	1,408	3,669	13,748	0.13	25

Year	NO_X (TPY)	SO_2 (TPY)	PM_{10} (TPY)	$PM_{2.5}$ (TPY)	VOC (TPY)	CO (TPY)	Pb (TPY)	NH_3 (TPY)
2048	18,611	102	1,357	1,319	3,565	12,996	0.12	23
2049	17,823	94	1,306	1,268	3,238	12,373	0.12	22
2050	17,343	88	1,277	1,241	3,105	12,092	0.11	22
2051	17,692	85	1,315	1,277	3,088	12,268	0.12	23
2052	16,664	79	1,247	1,211	2,889	11,551	0.11	22
2053	14,667	65	1,117	1,085	2,256	10,084	0.10	20
2054	13,722	63	1,020	990	2,331	9,389	0.09	18
2055	13,174	59	990	961	1,985	9,000	0.09	17
2056	11,256	48	841	817	1,714	7,620	0.08	15
2057	10,184	46	740	719	1,666	6,838	0.07	13
2058	9,829	41	726	705	1,406	6,545	0.07	13
2059	8,766	35	657	638	1,142	5,846	0.06	11
2060	6,994	32	490	476	1,068	4,554	0.04	9
2061	6,500	29	474	461	986	4,348	0.04	8
2062	5,706	22	408	396	853	3,735	0.04	7
2063	5,397	20	393	382	656	3,496	0.04	7
2064	4,229	14	328	319	449	2,749	0.03	6
2065	2,493	7	204	198	165	1,663	0.02	3
2066	1,057	4	68	67	106	616	0.01	1

Table 3-14. Highest Possible Single-Sale Emission Estimates for Western, Central, and Eastern GOM Planning Areas, All Depths, by Year and Pollutant

Year	NO_X (TPY)	SO_2 (TPY)	PM_{10} (TPY)	$PM_{2.5}$ (TPY)	VOC (TPY)	CO (TPY)	Pb (TPY)	NH_3 (TPY)
2017	1,828	48	189	183	138	1,196	0.02	2
2018	4,004	155	411	399	535	2,552	0.03	5
2019	4,940	32	416	404	822	3,689	0.04	6
2020	9,140	136	798	775	1,295	6,374	0.07	12
2021	**16,854**	**205**	**1,461**	**1,418**	**2,091**	**11,505**	**0.13**	**23**
2022	11,717	76	928	901	1,757	8,149	0.08	16
2023	12,017	77	957	929	1,780	8,368	0.09	16
2024	12,393	70	1,000	970	1,724	8,621	0.09	17
2025	12,388	70	999	970	1,733	8,618	0.09	17
2026	12,245	64	993	964	1,645	8,493	0.09	17
2027	12,553	71	1,030	1,000	1,637	8,668	0.09	17
2028	12,834	60	1,053	1,022	1,643	8,908	0.10	18
2029	13,273	78	1,091	1,059	1,762	9,215	0.10	18
2030	13,452	78	1,108	1,075	1,779	9,346	0.10	19
2031	13,828	84	1,138	1,105	1,863	9,635	0.10	19
2032	13,931	80	1,152	1,118	1,836	9,696	0.10	19
2033	14,109	82	1,170	1,136	1,793	9,872	0.11	19
2034	11,912	71	1,010	980	1,439	8,409	0.09	16
2035	9,180	60	791	767	1,044	6,454	0.07	13
2036	7,368	46	616	598	950	5,167	0.06	10
2037	6,988	51	592	574	861	4,834	0.05	10
2038	7,606	38	623	604	1,078	5,382	0.06	10
2039	6,587	31	532	516	973	4,624	0.05	9
2040	6,194	41	499	484	950	4,302	0.05	8
2041	5,757	24	461	447	821	3,997	0.04	8
2042	5,129	23	402	390	789	3,538	0.04	7
2043	5,020	22	392	380	775	3,459	0.04	7
2044	4,639	22	356	346	746	3,181	0.03	6
2045	4,701	22	362	351	745	3,226	0.03	6
2046	4,262	16	325	316	671	2,891	0.03	6

Year	NO_X (TPY)	SO_2 (TPY)	PM_{10} (TPY)	$PM_{2.5}$ (TPY)	VOC (TPY)	CO (TPY)	Pb (TPY)	NH_3 (TPY)
2047	4,228	16	322	313	663	2,866	0.03	6
2048	4,061	16	306	298	653	2,744	0.03	6
2049	3,969	15	298	289	643	2,677	0.03	5
2050	3,569	13	283	274	547	2,438	0.03	5
2051	2,280	7	200	194	296	1,678	0.02	3
2052	1,070	5	86	84	246	795	0.01	1
2053	1,053	5	85	82	239	783	0.01	1
2054	787	1	74	72	39	574	0.01	1
2055	130	0	12	12	9	95	0.00	0
2056	106	0	10	10	8	77	0.00	0
2057	104	0	10	9	8	76	0.00	0
2058	23	0	2	2	1	17	0.00	0

3.5.2 Spatial Allocation

Similar to the base case modeling files, ERG spatially allocated the USEPA onshore (and offshore non-BOEM production vessels operating outside of the GOMR) emissions using the USEPA's spatial surrogates (and locational coordinates for point sources). All existing BOEM oil and gas production source emissions were allocated to locational coordinates for platforms and to the area-block level for vessels.

For source activities associated with the nine-sale and single-sale five-year program, ERG allocated the estimated emissions by planning area (Western versus Central/Eastern GOM) and by the six water depth categories (0–60 m, 60–200 m, 200–800 m, 800–1,600 m, 1,600–2,400 m, and > 2,400 m) as defined in BOEM's scenario. Figure 3-8 depicts the planning area boundaries and water depth contours. Note that the GOMESA moratoria area is not indicated in Figure 3-6. Emissions were not allocated to the GOMESA for this analysis.

BOEM provided guidance on which geographic areas with water depths less than 200 m have the "highest potential" for future structure placement throughout the GOMR based on resources. ERG placed structures in randomly selected lease blocks within these areas, planning areas, and water depths. Approximately 60 percent of the new platforms were placed in randomly selected blocks with the highest potential, and 40 percent in randomly selected blocks with the second-highest potential. Production platforms were located as point sources with discrete locational coordinates. Figure 3-9 shows all the selected locations. ERG randomly selected a subset of the Proposed Action locations for the single-sale structures (Figure 3-10).

ERG spatially allocated the emission estimates for exploratory drilling; development/production drilling; pipeline laying; and helicopter, support vessel, and shuttle tanker trips based on the anticipated future year activities by planning area and water depth, as provided by BOEM. For example, exploratory wells drilled in water depths of 0 to 60 m were allocated to locations in the 0- to 60-m water depth contour of each specified planning area in areas with high production potential. Drilling activities were assigned only to unleased blocks.

ERG assigned pipelaying vessel activities to leased and unleased blocks between existing or new platforms and existing pipeline locations. ERG's rationale was that the vessel support would occur where new pipelines would be installed between new platforms and existing pipelines, as well as along existing pipelines for maintenance purposes. Because support vessels and tankers transit multiple water depths while going to and from port, their emissions were allocated across multiple water depth contours based on assumed installed platform locations and closest port. That is, emissions were spatially assigned across the entire trip length from port to the point of interest.

Helicopter emissions are primarily associated with LTO activities, with transit emissions that occur above the boundary layer being a minor portion of total emissions. As such, ERG divided helicopter emissions between the platforms being serviced and the onshore heliport used as the helicopter's base of operations. Helicopter emissions were not assigned to locations with single well caissons.

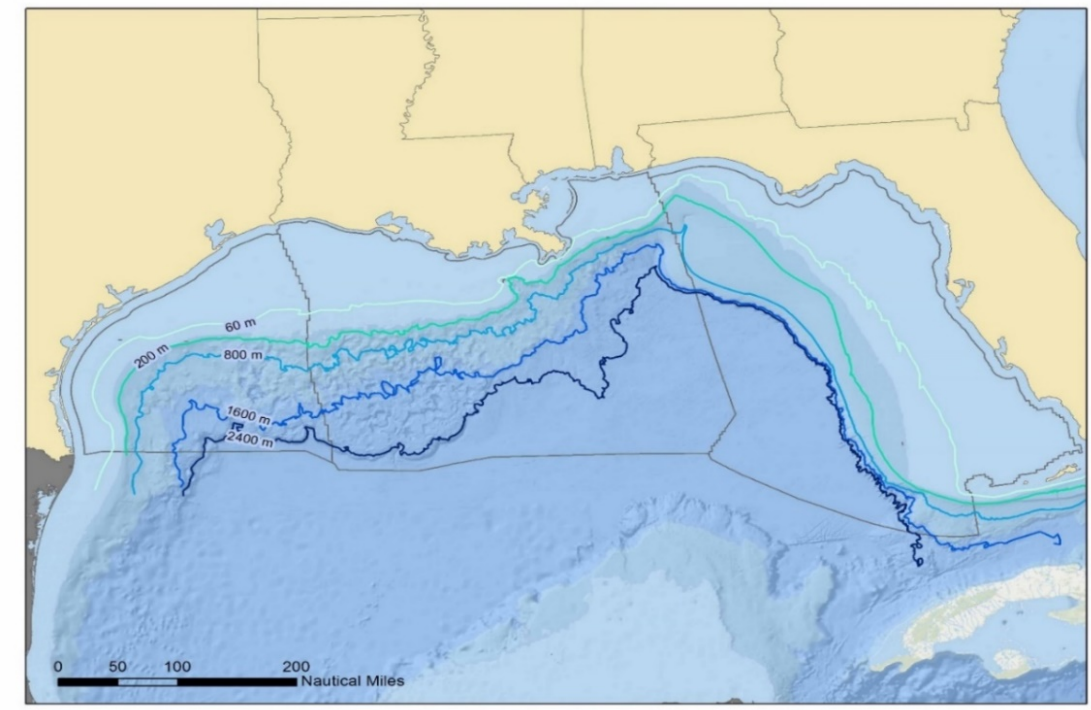

Figure 3-8. BOEM OCS Western, Central, and Eastern GOM Planning Areas (gray lines from left to right) and Contoured Water Depths

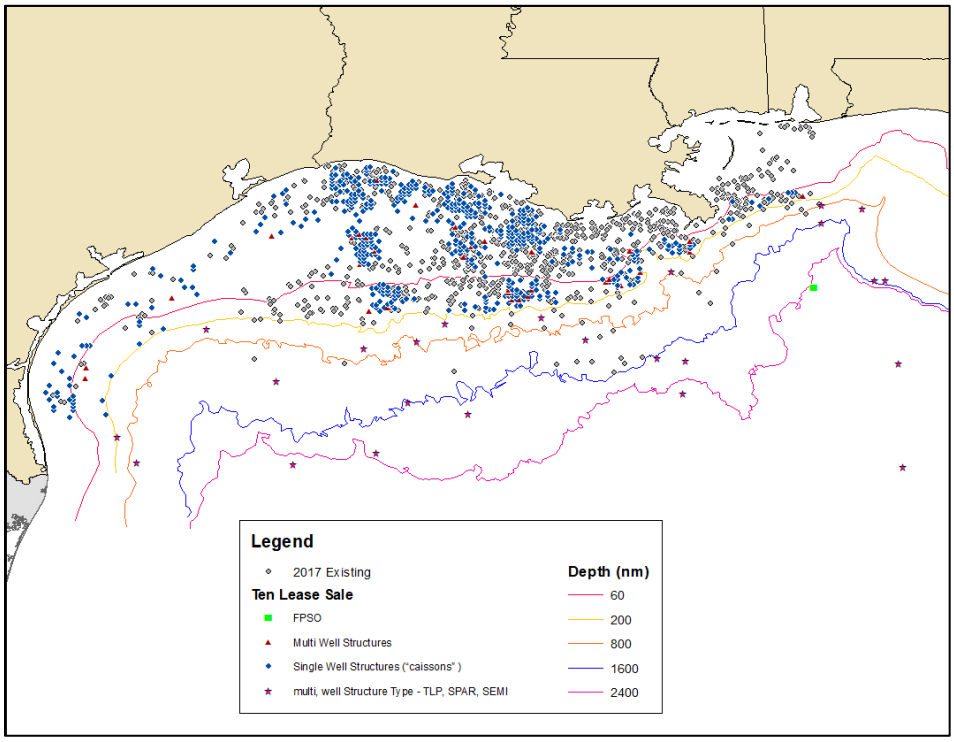

Figure 3-9. 10-Sale Placement of Anticipated Future Structures

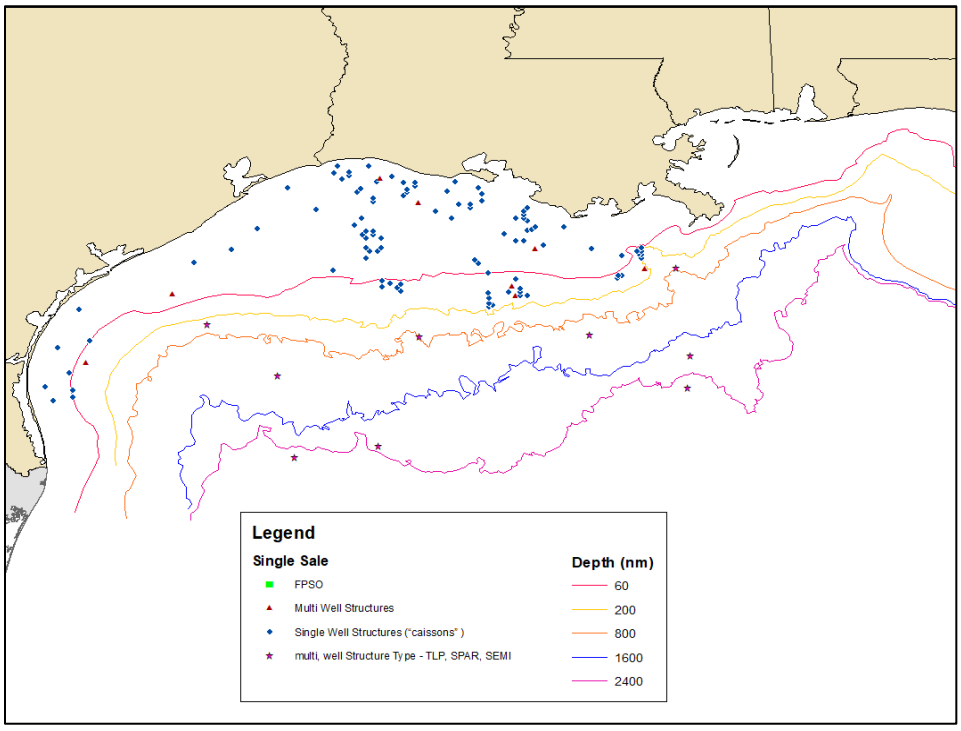

Figure 3-10. Single-Sale Placement of Anticipated Future Structures

3.6 Quality Assurance

ERG implemented quality assurance/quality control (QA/QC) activities on all data collected for the base case and future year emissions inventories. All collected information used to develop the inventories was checked and verified for reasonableness to the extent possible. For the primary data sources, ERG confirmed that all expected pollutants have emissions, geographical coordinates are within inventory domain (for point sources), all source categories are accounted for (nonpoint area sources), and emissions compare to prior versions (for state-provided updates). For the secondary data sources and calculations, the primary means to check the resulting emissions estimates were to replicate the values through independent sources. All calculations were checked by a second staff member who attempted to replicate the values by independently applying the input values and assumptions to verify that the same results could be produced. Data that were found to be questionable were examined in greater detail to determine what errors might be present and what adjustments might be needed. If data were revised or rejected, the procedures and assumptions used were thoroughly documented.

3.7 Uncertainty

Evaluating the uncertainty in emissions inventories has been an ongoing concern to the scientific community, because projecting emission estimates into the future is highly uncertain. The technical report *Emission Inventory Improvement Program* (EIIP) (EIIP, 1996) has a lengthy discussion on the uncertainty associated with projected emission estimates. Unfortunately, the sources of uncertainty mentioned in the EIIP report still apply. This section qualitatively summarizes some of the sources of uncertainty in the inventories developed for this study.

For the NEI components in the base and future year emissions inventory, the 2011 Technical Support Document (USEPA, 2015a) makes some mention of the uncertainty associated with the emission factors. Overall, all estimates are based on the best and most recent emission factors and/or emission models. The USEPA provides no uncertainty measures, as states, local agencies, tribes, and other entities submitting data to the USEPA are not required to quantify uncertainty in their estimates. Additional uncertainty is introduced when projecting inventories to a future year. Projections are based on the best possible projections of economic growth and activity levels based on key indicators (e.g., fuel cost) as well as economic models and predictors that come with their own uncertainty. Where possible, the USEPA corroborates specific controls to add to facilities and facility closures with state permits and other official memoranda. Additional closures and controls are integrated into future inventories based on state-indicated rulemakings and informal facility discussions.

ERG estimated emissions from non-NEI sources using the best data available and the most recent modeling platforms. This ensured the best science was used in the emissions estimate. Again, these estimates contain some level of uncertainty. For example, the future year platform emissions were estimated using emission factors based on average emissions of the existing platforms. These average emission factors took into account all emission sources reported in the 2014 Gulfwide Emissions Inventory, including fugitive emissions, discussed in Section 3.4.4.1, as potentially large sources of VOC emissions. Future platform actual emissions will vary from these estimates due to differences in platform configuration and equipment efficiency. In addition, as noted in Section 3.4.4, the Proposed Action scenario based on mid-level oil prices was deemed to represent reasonable activity level for use in the cumulative air quality impacts assessment modeling. It is possible, however, that the scenario and resulting emission estimates over- or underpredict actual activity levels for oil and gas production platforms, as well as associated support vessels and helicopters. Although it is not possible to compare many of the specific predicted activity levels, an evaluation of historical GOMR oil and natural gas production levels indicates that BOEM's predicted estimates of total oil and gas production levels in the

future scenario are at the mid-point of the 2005–2017 production levels. In addition, the number of non-caisson platforms anticipated to be installed is in range with historical non-caisson platform installations.

3.8 References

Battye, R., W. Battye, C. Overcash, S. Fudge. 1994. Development and Selection of Ammonia Emission Factors - Final Report. EC/R Incorporated, Durham, NC: Report prepared for USEPA Office of Research and Development.

CONAPO (Consejo Nacional de Población). 2012. Proyecciones de la Poblacion de Mexico 2010-2030. Internet address: https://www.gob.mx/cms/uploads/attachment/file/63977/Documento_Metodologico_Proyecciones_Mexico_2010_2050.pdf.

Dismukes, D.E. 2010. Fact Book: Offshore Oil and Gas Industry Support Sectors., New Orleans, LA, OCS Study BOEMRE 2010-042. 138 pp.: U.S. Dept. of the Interior, Bureau of Ocean Energy Management, Regulation and Enforcement, Gulf of Mexico OCS Region.

ERG (Eastern Research Group). 2014a. Technical Documentation for Year 2015 Ozone Precursor Emission Inventory for U.S., Mexico and Canada and Year 2011 Ozone Precursor Emission Inventory for Mexico., Sacramento, California. May 30: Prepared for Maricopa Association of Governments (MAG) by Eastern Research Group, Inc.

ERG. 2014b. Develop Mexico Future Year Emissions., Sacramento, California. Prepared for U.S. Environmental Protection Agency (USEPA) by Eastern Research Group, Inc. Internet address: ftp://ftp.epa.gov/EmisInventory/2011v6/v2platform/2011emissions/Mexico_Emissions_WA%204-09_final_report_121814.pdf

ERG. 2015. Technical Documentation for Year 2011 and Year 2017 Ozone Precursor Emission Inventories for Mexico and Canada., Sacramento, California. Prepared for Maricopa Association of Governments (MAG) by Eastern Research Group, Inc.

EIIP (Emission Inventory Improvement Program). 1996. VOLUME VI: Chapter 4 Evaluating the Uncertainty of Emission Estimates, Final Report, Research Triangle Park, North Carolina. Internet address: https://www.epa.gov/air-emissions-inventories/volume-6-quality-assurance-procedures-and-dars-software. Accessed November 1, 2017.

FAA (Federal Aviation Administration). 2015. U.S. Department of Transportation/Federal Aviation Administration, Terminal Area Forecast Online Dataset. Internet address: http://aspm.faa.gov/main/taf.asp

FOCA (Switzerland Federal Office of Civil Aviation). 2009. Guidance on Determination of Helicopter Emissions. Reference 0/3/33/33-05-20.

HSAC (Helicopter Safety Advisory Conference). 2015. 2014 Gulf of Mexico offshore helicopter operations and safety review., s.l.: Internet website: HSAC Helicopter Safety Advisory Committee. Internet address: http://www.hsac.org/library.

IHS (Information Handling Services). 2015. Register of Ships. 2014.

IMO (International Maritime Organization). 2015. Third IMO Greenhouse Gas Study 2014. Internet address: http://www.imo.org/en/OurWork/Environment/PollutionPrevention/AirPollution/Documents/Third%20Greenhouse%20Gas%20Study/GHG3%20Executive%20Summary%20and%20Report.pdf, s.l.: s.n.

INEGI (Insituto Nacional de Estadistica y Geografia). 2005. Conteo de Poblacion y Vivienda, 2005. Insituto Nacional de Estadistica y Geografia (National Institute of Statistics and Geography). Internet address: http://www.inegi.org.mx/programas/ccpv/2005/

INEGI. 2010. Censo de Poblacion y Vivienda 2010. Instituto Nacional de Estadistica y Geografia (National Institute of Statistics and Geography). Internet address: http://www.inegi.org.mx/programas/ccpv/2010/

NFIC (National Fire Information Center). 2015. Historical year-end fire statistics by state. Internet address: https://www.nifc.gov/fireInfo/fireInfo_statistics.html. Boise, ID: National Fire Information Center.

Neilsen-Gammon, J. 2011. Texas Drought: Spot the Outlier. Internet address: http://blog.chron.com/climateabyss/2011/08/texas-drought-spot-the-outlier.

NOAA (National Oceanic and Atmospheric Administration). 2015. GISS Surface Temperature Analysis. National Oceanic & Atmospheric Administration. Internet address: https://www.esrl.noaa.gov/psd/data/gridded/data.gistemp.html.

PCIF (Pardee Center for International Futures). 2014. International Futures Forecasting System. Pardee Center for International Futures, University of Denver, Denver, CO. Internet address: http://www.ifs.du.edu/ifs/frm_CountryProfile.aspx?Country=MX#Economy

PEMEX (Petroleos Mexicanos). 2012. Investor Presentation. April 2012. Internet address: https://www.pemex.com/ri/Publicaciones/Presentaciones%20Archivos/201205_p_inv_e_120508_LA.pdf

PortVision. 2012. AIS 2011 data provided to the U.S. Bureau of Ocean Energy Management associated with BOEM's Central and Western Areas' of the Gulf of Mexico

SAGARPA (Secretaria de Agricultura, Ganaderia, Desarrollo Rural, Pesda y Alimentacion). 2014a. Cierre de la Produccion Agricola por Cultivo. Secretaria de Agricultura, Ganaderia, Desarrollo Rural, Pesda y Alimentacion (Secretariat of Agriculture, Livestock, Rural Development, Fisheries and Food, Servicio de Information Agroalimentaria y Pesquera). Internet address: http://infosiap.siap.gob.mx:8080/agricola_siap_gobmx/ResumenDelegacion.do

SAGARPA. 2014b. Cierre de la Produccion Percuaria por Estado. Secretaria de Agricultura, Ganaderia, Desarrollo Rural,Resca y Alimentacion (Secretariat of Agriculture, Livestock, Rural Development, Fisheries and Food, Servicio de Infomacion Agroalimentaria y Pesquera). Internet address: http://infosiap.siap.gob.mx/repoAvance_siap_gb/pecAvanceEdo.jsp

Seelke, C.R., M. Ratner, M.A. Villarreal, P. Brown. 2015. Mexico's Oil and Gas Sector: Background, Reform Efforts, and Implications for the United States. Congressional Research Service. 7-5700. Internet address: https://www.fas.org/sgp/crs/row/R43313.pdf.

SEMARNAT (Secretaría del Medio Ambiente y Recursos Naturales). 2014. Inventario Nacional de Emisiones de México, 2008. Secretaría del Medio Ambiente y Recursos Naturales (Secretariat of the Environment and Natural Resources). Detailed municipality-level emission files provided by David Alejandro Parra Romero. January 31.

SENER (Secretaria de Energia). 2014a. Prospectiva de Petroleo Crudo y Petroliferos 2014-2028. Secretaria de Energia (Secretariat of Energy).

SENER. 2014b. Prospectiva de Gas Natural y Gas L.P. 2014-2028. Secretaria de Energia (Secretariat of Energy).

SENER. 2014c. Balance Nacional de Energia 2013. Secretaria de Engergia (Secretariat of Energy).

SRCC (Southern Regional Climate Center). 2015. Climate Information Data Portal. Internet address: https://climdata.srcc.lsu.edu.

Surface Transportation Board. 2015. R-1 Class 1 Railroad Annual Reporting Data. Internet address: http://www.stb.dot.gov/econdata.nsf/f039526076cc0f8e8525660b006870c9?OpenView

UNEP (United Nations Environment Programme). 2012. Aircraft Technology and Its Relation to Emissions, s.l.: Intergovernmental Panel on Climate Change, Chapter 7. Internet address: http://www.grida.no/climate/ipcc/aviation/088.htm

USDOI, BSEE (U.S. Department of the Interior, Bureau of Safety and Environmental Enforcement). 2015. Oil and Gas Operations Reports - Part A (OGOR-A) Well Production (1996-2015). Internet address: https://www.data.bsee.gov/Main/OGOR-A.aspx

USEPA (U.S. Environmental Protection Agency). 1992. Procedures for Emission Inventory Preparation, Volume IV: Mobile Sources. EPA 420-R-92-009.

USEPA. 2010. Designation of North American Emission Control Area to Reduce Emissions from Ships, Research Triangle Park, NC: U.S. Environmental Protection Agency, Office of Transportation and Air Quality, EPA-420-F-10-015. Internet address: https://nepis.epa.gov/Exe/ZyPDF.cgi/P100AU0I.PDF?Dockey=P100AU0I.PDF

USEPA. 2014a. Draft Modeling Guidance for Demonstrating Attainment of Air Quality Goals for Ozone, $PM_{2.5}$ and Regional Haze. U.S. Environmental Protection Agency, Research Triangle Park, NC. Internet address: http://www.epa.gov/ttn/scram/guidance/guide/Draft_O3-PM-RH_Modeling_Guidance-2014.pdf.

USEPA. 2014b. 2011 NEI Nonpoint Emission Estimation Tools and Methods, U.S. Environmental Protection Agency, Office of Air Quality Planning and Standards. Internet address: https://www.epa.gov/air-emissions-inventories/2011-national-emissions-inventory-nei-data

USEPA. 2014c. MOVES2014. Internet address: https://www.epa.gov/moves

USEPA. 2014d. Ozone NAAQS Emissions Modeling Platform (2011 v6.1). 2011, 2018 and 2025 Emissions Modeling Platform Technical Support Document, Research Triangle Park, NC. Internet address: https://www.epa.gov/air-emissions-modeling/2011-version-61-platform.

USEPA. 2015a. U.S. Environmental Protection Agency, Office of Air Quality Planning and Standards, Air Quality Assessment Division, Emission Inventory and Analysis Group, Research Triangle Park, NC. 2011 National Emissions Inventory (NEI), Version 2. Internet address: http://www.epa.gov/air-emissions-inventories/2011-national-emissions-inventory-nei-data

USEPA. 2015b. 2012 National Emissions Inventory (NEI), U.S. Environmental Protection Agency, Office of Air Quality Planning and Standards, Air Quality Assessment Division, Emission Inventory and Analysis Group. Internet address: http://www.epa.gov/ttn/chief/eiinformation.html

USEPA. 2015c. Toxic Release Inventory (TRI) Program. U.S. Environmental Protection Agency, Office of Environmental Information, Washington, DC. Internet address: http://www2.epa.gov/toxics-release-inventory-tri-program

USEPA. 2015d. 2011NEIv2-based Platform (2011 v6.2). 2011v6.2 Emissions Modeling Platform Technical Support Document for 2011, 2017, and 2025. Internet address: http://www.epa.gov/air-emissions-modeling/2011-version-62-platform, Research Triangle Park, NC: U.S. Environmental Protection Agency.

USEPA. 2016a. PM Augmentation Tool. Office of Air Quality Planning and Standards, Research Triangle Park, NC. Internet address: https://www3.epa.gov/ttnchie1/software

USEPA. 2016b. Compilation of air pollutant emission factors, volume 1: Stationary point and area sources. AP-42. U.S. Environmental Protection Agency, Office of Air Quality Planning and Standards, Research Triangle Park, NC. internet address: https://www.epa.gov/air-emissions-factors-and-quantification/ap-42-compilation-air-emissions-factors

USEPA. 2016c. 2014 National Emissions Inventory (NEI) Documentation. Research Triangle Park, NC: U.S. Environmental Protection Agency, Office of Air Quality Planning and Standards. Internet address: https://www.epa.gov/sites/production/files/2016-12/documents/nei2014v1_tsd.pdf

Wilson, D., R. Billings, R. Chang, H. Perez, J. Sellers. 2014. Year 2011 Gulfwide Emissions Inventory Study. OCS Study BOEM 2014-666., New Orleans, LA: U.S. Department of Interior, Bureau of Ocean Energy Management, Gulf of Mexico OCS Region.

Wilson, D., R. Billings, R. Chang, S. Enoch, B. Do, H. Perez, J. Sellers. 2017. Year 2014 Gulfwide Emissions Inventory Study: Final Report. OCS Study BOEM 2017-044, New Orleans, LA: U.S. Department of the Interior, BOEM, Gulf of Mexico OCS Region.

4 Cumulative Air Quality Impacts Analysis

4.1 Introduction

This analysis examines the potential air quality impacts of the single sale and 10 lease sales in the GOMR included in the Proposed Action for the 2017–2022 Program with respect to the:

- NAAQS for the criteria pollutants O_3, NO_2, SO_2, CO, $PM_{2.5}$, and PM_{10}
- AQRVs, including visibility and acid deposition (sulfur and nitrogen) in nearby Class I and sensitive Class II areas
- Incremental impacts of PSD pollutants (NO_2, PM_{10}, $PM_{2.5}$) with respect to PSD Class I and Class II increments

The PSD increments are provided here for information purposes only; this analysis does not constitute a regulatory PSD increment consumption analysis as would be required for major sources subject to the CAA's New Source Review (NSR) program requirements. In particular, incremental impacts are compared to the full allowable PSD increments; no attempt is made to identify existing PSD increment-consuming or increment-expanding sources.

Results of each impact analysis are compared with applicable "thresholds of concern," which have typically been used in air quality impact evaluations of other Federal actions, including onshore oil and gas leasing programs. The applicable comparison thresholds for criteria pollutant impacts are the corresponding NAAQS. For acid deposition impacts, thresholds are based on 1) incremental impacts considered sufficiently small as to have no consequential effect on the receiving ecosystems (i.e., deposition analysis thresholds), and 2) critical load levels above which cumulative ecosystem effects are likely to or have been observed. For visibility impacts, thresholds are based on incremental changes in light extinction below the level at which they would be noticeable to the average human observer. The remainder of this study provides additional information about these various thresholds.

Ramboll used the CAMx and CMAQ photochemical grid models (PGMs) to simulate the dispersion and chemical transformation of pollutants over the GOMR. Base case simulations were originally performed with both models (USDOI, BOEM, 2017), and Ramboll performed the updated and revised modeling described in this study entirely using CAMx, although outputs from the earlier CMAQ runs were used to develop gridded lightning NO_x and WBD emissions for input to CAMx, as described in Section 4.3.5.6.

Ramboll conducted photochemical modeling for two emission scenarios:

- **Base case scenario:** Using the 2012 base year emissions inventory described in Section 3, Ramboll evaluated model performance and defined current baseline air quality conditions.
- **Future year development scenario:** Using an emissions inventory that includes potential new sources associated with the lease sales and projections of emissions to 2017 for all other sources described in Section 3, Ramboll estimated the cumulative and incremental air quality and AQRV impacts of the lease sales.

Both scenarios used the same meteorological dataset and the same photochemical model configuration.

4.2 Meteorology

As discussed in Section 2 of this report, meteorological datasets are required to determine the rate that pollutants disperse and react in the atmosphere. These datasets include spatially and temporally varying parameters such as wind speed, wind direction, air temperature, and humidity, among others. Using measurement data as inputs, gridded meteorological models that simulate the fluid dynamics of the atmosphere can be used to estimate meteorological conditions over a complete modeling domain—including regions far from measurement sites—in a physically consistent fashion. Results of these meteorological models provide the inputs needed to exercise the photochemical grid air quality dispersion models used in this study. Figure 2-1 shows the WRF modeling grids at horizontal resolutions of 36, 12, and 4 km.

WRF ran the 36-, 12-, and 4-km grids simultaneously with one-way nesting, meaning that meteorological information flows downscale via BCs introduced from the respective coarser grid. The WRF modeling domain was defined to be slightly larger than the PGM domains to eliminate boundary artifacts in the meteorological fields. Such boundary artifacts occur for numerical reasons (the 3:1 grid spacing ratio) and because the imposed BCs require some time/space to come into dynamic balance with WRF's atmospheric equations. Section 2, WRF Model Performance Evaluation, discusses all meteorological modeling domains, techniques, inputs, vertical resolutions, parameters, nudging, physics options, and application strategies, along with quantitative and qualitative evaluation procedures and statistical benchmarks.

4.3 Emissions

To analyze the cumulative air quality impacts of the lease sales, ERG and Ramboll developed both a contemporary base year emissions inventory for the base case analysis and a projected future year inventory that includes emissions from all cumulative sources along with additional emissions anticipated to occur as a result of lease sales in which potential oil and gas exploration and production activities would occur. Both the base case and future year cumulative source inventories represent comprehensive compilations of pollutant emissions from all human activities as well as emissions from biogenic and geogenic sources.

4.3.1 Emissions Inventory Scope

As described in Section 3, the scope of the air pollutant emissions inventory for the *Air Quality Modeling in the GOMR Study* is defined in terms of pollutants, representative time periods for the base case and future year analysis, geographical domain, and sources to be included. Collection and compilation of emissions data are described in Section 3.

Specific pollutants were selected for inclusion in the inventories to support analysis of air quality impacts in terms of impacts on attainment of NAAQS and on AQRVs, including acid deposition and visibility. Inventoried pollutants are CO, NO_x (which includes nitric oxide [NO] and NO_2 and is stated in terms of equivalent mass of NO_2), $PM_{2.5}$, PM_{10}, SO_2, VOCs (which are precursors to formation of ozone and organic particulates), and NH_3 (a precursor to PM formation). Although Pb is also a criteria pollutant, oil and gas sources have negligible Pb emissions, and, as a result, Pb is typically not included in this type of study. Although the cumulative air quality impact analysis did not focus specifically on air toxics, compilation of VOC emissions by source type together with VOC speciation profiles by source type provides a mechanism for estimating emissions of individual air toxic species.

As discussed in Section 3 of this report, 2012 was selected as the base year as it was more representative of "typical" conditions in the GOMR. Emission estimates for calendar year 2017 were used as inputs for

additional modeling scenarios that serve as a basis to predict future impacts from the implementation of the 2017–2022 Program.

Figure 2-1 depicts modeling domains used for the *Air Quality Modeling in the GOMR Study* emissions inventory. Emissions were spatially allocated over the three PGM modeling domains: an outer 36-km horizontal grid resolution domain covering all of the U.S. and parts of Mexico and Canada, a regional 12-km resolution domain covering the southeastern U.S., and an inner 4-km domain encompassing the Central and Western GOM Planning Areas in the GOM OCS. Ramboll accounted for the influences of global emissions on the study area by using a global air quality model to specify domain BCs, as described in Section 4.4.

4.3.2 Spatial Resolution

The spatial resolution of the emissions inventory is source specific. For example, sources such as power plants are identified based on their geographic coordinates (latitude and longitude), while other sources, such as nonroad mobile sources (e.g., construction equipment) are spatially distributed using surrogates within their reporting county that are typically related to the category's (e.g., construction sites) activity distribution.

The resolution of the geographical area covered by the emissions inventory is based on the grid cell size needed for photochemical and dispersion modeling. Furthermore, the PGM resolution is dependent on the grid resolution of the WRF meteorological model output used. This is described further in Section 4.3.5.

4.3.3 Temporal Resolution

Ramboll estimated annual emissions (i.e., emissions generated during 2012) for all sources. However, hour-specific emissions were obtained for EGUs (i.e., electric utilities) from continuous emissions monitoring (CEM) data provided by the USEPA. Ramboll allocated emissions on an hourly, daily, and seasonal basis during the emissions modeling process (Section 4.3.5) using default temporal allocation factors from the SMOKE emissions model for some sources; other temporal allocations were source-specific, and profiles were developed and applied within the SMOKE model.

4.3.4 Speciation

When applying the PGM, PM emissions were allocated to individual PM species as part of the SMOKE emissions processing using PM speciation factors obtained from the USEPA's SPECIATE database for each source category (as defined by the SCC). The PM mass was thus broken into the mass associated with elemental carbon (EC), organic aerosol (OA), primary sulfate (SO_4), nitrate (NO_3), and other elements, as well as particle-bound VOCs such as polycyclic aromatic hydrocarbon (PAHs). Sea salt emissions are treated separately as described in Section 4.3.5.5.

Given current interest in the health effects and climate forcing potential of black carbon (which is represented as EC in the modeling inventory), Table 4-1 summarizes EC emissions within the 4-km modeling domain for source sectors under the future year scenario. Within this area, under the future year 10-sale scenario, platforms and support vessels would contribute 5% of total BC emissions, with an additional 5% accounted for by other sources (mostly vessels) operating within the GOM that are not associated with the lease sales.

Table 4-1. Annual PM and Black Carbon (EC) Emissions (tons) Within the 4-km Modeling Domain Under the Future Year Scenario

Source Sector	Total $PM_{2.5}$		Black Carbon	
	Tons	% of Total	Tons	% of Total
10-sale Support Vessels & Helicopters	3,684	1	2,841	5
10-sale Platforms	95	0	49	0
Other GOM	14,271	3	2,650	5
Other Anthropological Sources	161,755	32	20,204	38
Natural Sources	329,030	65	27,114	51
TOTAL:	508,834	100	52,857	100

SMOKE was also used to convert VOC emissions into the photochemical carbon bond mechanism-specific (e.g., CB05 or CB6r4) model species used in air quality models. The CB6r4 chemical mechanism used in CAMx also models excess methane (ECH_4) from local sources that is added to the global background methane value (1.75 ppm) in the chemical mechanism. The ECH_4 species is calculated as part of the speciation of the VOC emissions that are first adjusted to total organic gases (TOG) before calculating the CB6 chemical species. Thus, the ECH_4 species only includes methane emissions from local VOC sources and will not include methane emissions not associated with VOC sources.

4.3.5 Emissions Processing for Preparation of Model-Ready Emissions

4.3.5.1 SMOKE Processing

Ramboll used the anthropogenic emissions inventories discussed in Section 3 along with other data to prepare PGM-ready emission files using SMOKE version 3.6 and other methods, as described below. The inventories were processed through SMOKE to develop hourly, gridded, and speciated emissions required for input to the PGM at 36-, 12-, and 4-km grid resolutions. During emissions processing, Ramboll speciated annual emissions inventories to model species, temporally allocated them to hourly emissions, and spatially allocated them to grid cells.

Ramboll used the latest CB6r4 photochemical mechanism with active local methane emissions and halogen chemistry (Ramboll Environ, 2016) for the CAMx modeling and processed the emissions accordingly. The SMOKE emissions model was used to perform the following tasks:

- **Spatial allocation:** Ramboll used spatial surrogates in the USEPA 2011v6.2 modeling platform (USEPA, 2015a) to spatially distribute emissions to modeling grid cells. Spatial surrogates were generated by overlaying the PGM modeling grid on maps of geospatial indicators appropriate to each source category (e.g., housing units). The Surrogate Tool (Ran, 2014), a component of USEPA's Spatial Allocator system, was then used to calculate the fraction of geospatial indicator coverage in each model grid cell.

- **Temporal allocation:** Air quality modeling systems such as CAMx require hourly emissions input data. With the exception of a few source types (CEM data, biogenic emissions, and some fire inventories), most inventory data are estimated in the form of annual or average daily emissions. Ramboll used SMOKE to allocate annual emissions to months and across the diurnal cycle to account for seasonal, day-of-week, and hour-of-day effects. Temporal profiles and SCC cross-references from the USEPA 2011v6.2 modeling platform were used to incorporate seasonal and monthly variations into the development of the PGM-ready emissions.

- **Chemical speciation:** Emissions inventories for the *Air Quality Modeling in the GOMR Study*

included the following pollutants: CO, NO_x, VOCs, NH_3, SO_2, PM_{10}, and $PM_{2.5}$. Ramboll used SMOKE to convert inventoried VOC emissions into the CB6r4 photochemical mechanism model species. Chemical speciation profiles were assigned to inventory sources using cross-referencing data that matched the profiles and inventory sources based on country/state/county FIPS codes and SCCs. Ramboll used NO_x, VOC, and PM speciation profiles from the USEPA 2011v6.2 platform for SMOKE processing. In the USEPA 2011v6.2 platform, USEPA-generated emissions are for the older CB6r2 chemical mechanism previously used by CAMx. SMOKE also applied source-specific speciation profiles to convert inventoried NO_x emissions to NO, NO_2, and nitrous acid (HONO) components.[5] After SMOKE processing, Ramboll applied necessary species mapping to prepare CAMx-ready emissions in CB6r4/coarse-fine (CF) terms. CB6r4 chemistry also models local ECH_4 above the fixed background methane level. Ramboll also generated sea salt and halogen emissions from the GOM and other ocean portions of the modeling domain for use in CAMx, as described below.

4.3.5.2 Onroad Emissions

Ramboll generated onroad mobile emissions estimates using the SMOKE-MOVES emissions modeling framework (USEPA, 2015a), which leverages MOVES-generated outputs (https://www.epa.gov/moves) and hourly meteorological data. The SMOKE-MOVES processing allocates county-level vehicle-miles of travel (VMT), vehicle population, and speeds to grid cells using an appropriate spatial surrogate and then applies MOVES emission factors from a "lookup" table using hourly gridded meteorological data (temperature and humidity). SMOKE-MOVES requires MOVES-generated emission rate lookup tables, which differentiate emissions by process (e.g., running, start, vapor venting), vehicle type, road type, temperature, speed, hour of day, etc.

The USEPA's MOVES emission factors were used for the base case year (2012); emission factors for 2017 were used for the future year scenarios. The USEPA generated the MOVES lookup tables for a set of "representative counties" to which every other county is mapped. Ramboll processed the onroad emissions in the following four separate SMOKE processing streams, which were subsequently merged together into the onroad sector emissions file:

- **Rate-per-distance (RPD)** uses VMT as the activity indicator together with speed and speed profile information to compute on-network emissions from exhaust, evaporative, permeation, refueling, and brake and tire wear processes.
- **Rate-per-vehicle (RPV)** uses vehicle population (VPOP) counts to compute off-network emissions from exhaust, evaporative, permeation, and refueling processes.
- **Rate-per-profile (RPP)** uses VPOP activity data to compute off-network emissions from evaporative fuel vapor venting, including hot soak (immediately after a trip) and diurnal (vehicle parked for a long period) emissions.
- **Rate-per-hour (RPH)** uses hoteling hours activity data to compute off-network emissions for idling of long-haul trucks from extended idling and auxiliary power unit process.

Under this processing approach, onroad emissions are generated directly on the 36-, 12-, and 4-km model grids rather than county-level totals. Table 4-3 in Section 4.3.5.10 lists onroad emission totals within the 4-km modeling domain for the base and future year scenarios, along with totals from the other source categories. Emission reductions reflected in the future year scenario are generally a result of fleet turnover (i.e., the routine replacement of older vehicles with newer, cleaner vehicles). The sharp reduction (46

[5] Model results are affected by the selected source speciation profiles. In particular, the fraction of NO_x assumed to be emitted as NO_2 and as HONO can affect ozone production and the HONO fraction is not well known. Speciation profiles developed by the USEPA were used in this study.

percent) in SO_2 is partially due to a new gasoline sulfur standard that began on January 1, 2017. Under the Tier 3 fuel program, federal gasoline can contain no more than 10 ppm sulfur on an annual, average basis.

4.3.5.3 Biogenic Emissions

Ramboll generated biogenic emissions using NCAR's MEGAN version 2.1 biogenics model (Guenther et al., 2012; Sakulyanontvittaya et al., 2008). A new version of MEGAN (MEGAN3) has recently been developed (Guenther et al., 2017) but was not available in time for use in this study. Initial evaluations of MEGAN3 indicated lower estimates of isoprene emissions in better agreement with observations as compared to MEGAN2.1.

Biogenic emissions depend critically upon land use/landcover input data. Biogenic VOC and NO_x emissions vary considerably on spatial scales, ranging from a few meters to thousands of kilometers. The MEGAN model accounts for this variability with high-resolution estimates of vegetation type and quantity. The MEGAN landcover variables include total leaf area index (LAI), tree fraction, and plant species composition. These variables are determined based primarily on satellite observations, such as 2003 1-km^2 Moderate Resolution Imaging Spectroradiometer (MODIS) and 30-m resolution Landsat data (Guenther et al., 2006; Sakulyanontvittaya et al., 2008). MEGAN driving variables include weather data, LAI, plant functional type cover, and compound-specific emission factors that are based on plant species composition. All of these variables are available at various temporal scales and are provided in a geo-referenced gridded database in several formats (e.g., NetCDF, Esri Grid). The MEGAN database has global coverage at 30-sec (approximately 1-km) spatial resolution. The MEGAN model was applied using the specific daily meteorology (e.g., temperature and solar radiation) extracted from the 2012 WRF model outputs to generate day-specific biogenic emissions for the 2012 calendar year in the 36-, 12-, and 4-km PGM modeling domains.

4.3.5.4 Fire Emissions

Forest fire emissions are highly episodic and location specific. Using annual average fire emissions and temporally and spatially allocating these emissions using generic allocation schemes would result in significant inaccuracies. In this study, Ramboll used day-specific wild and prescribed fire (together called wildland fires) emission estimates developed by the USEPA for calendar year 2012 (USEPA, 2015b). The emission estimates are based on the SMARTFIRE2 framework and the BlueSky models.[6] The USEPA fire inventory was processed through SMOKE in a separate processing stream for CAMx. To prepare CAMx model-ready emissions using a plume rise algorithm in CMAQ, Ramboll calculated the plume rise in SMOKE. The model-ready emissions were written as three-dimensional NetCDF CMAQ-ready files that were converted into a CAMx "PTSOURCE" type file, where each grid cell centroid represents one virtual stack. The CMAQ2UAM program was used to convert three-dimensional fire emissions from SMOKE into CAMx format. Table 4-2 shows total annual criteria air pollutant emissions by fire type for all U.S. wildland fires within each of BOEM's PGM modeling domains.

[6] https://www.info.airfire.org

Table 4-2. 2012 Emissions Summary by Fire Type for the BOEM 36-, 12-, and 4-km Domains

Fire Type (SCC)	Domain	CO (TPY)	NO_x (TPY)	PM_{10} (TPY)	$PM_{2.5}$ (TPY)	SO_2 (TPY)	VOC (TPY)
Wildfires (2810001000)	36 km	59,794	613	5,901	5,001	387	14,050
	12 km	6,568	74	654	554	44	1,545
	4 km	1,087	6	103	87	6	254
Prescribed fires (2810015000)	36 km	27,331	391	2,796	2,370	211	6,453
	12 km	20,126	308	2,077	1,760	161	4,757
	4 km	7,020	58	680	577	41	1,646
Total	36 km	87,125	1,003	8,698	7,371	598	20,503
	12 km	26,694	382	2,731	2,314	206	6,302
	4 km	8,107	64	783	664	47	1,900

As noted above, the USEPA wildland fires inventory is restricted to fire sources within the lower 48 states and thus does not cover the portions of Canada and Mexico lying within the 36-, 12-, and 4-km PGM domains. To fill this gap, Ramboll used 2012 day-specific FINN estimates for Canada and Mexico. The FINN provides daily, 1-km resolution, global estimates of the trace gas and particle emissions from open burning of biomass, which includes wildfires, agricultural fires, and prescribed burning exclusive of biofuel combustion and trash burning. Each fire record was treated as a point source, and emissions were distributed vertically into multiple model layers to better represent each fire plume. Ramboll processed the day-specific FINN fire emissions in Canada and Mexico to develop elevated "point sources" of fire emissions, using plume rise estimates as a function of fire size based on WRAP's 2002 fire plume rise approach (Mavko and Morris, 2013). The chemical speciation profile for the MODIS fire emissions were derived from a study on biomass burning (Karl et al., 2007).

4.3.5.5 Sea Salt and Halogen Emissions

Ramboll estimated sea salt emissions for the initial round of CAMx simulations (USDOI, BOEM, 2017) using the existing CAMx sea salt emissions preprocessor, which employs a parameterization developed by Gong (2003) to calculate sea spray aerosol fluxes over the open ocean. The Gong parameterization consists of the whitecap fraction (the fraction of the ocean surface covered by whitecaps that are a function of wind speed, typically at 10 m above the water surface) and the size-dependent droplet production per unit whitecap area. The aerosol fluxes from breaking waves in the coastal surf zone used the same Gong parameterization but assumed 100 percent whitecap coverage, as suggested by Kelly et al. (2010).

Given evidence that the initial model runs overpredicted sea salt emissions—as described in Appendix H of USDOI, BOEM (2017)—Ramboll used an updated sea salt emissions preprocessor for the final round of simulations. The updated preprocessor implements a new parameterization proposed by Ovadnevaite et al. (2014) for open-ocean sea salt generation, which expresses the aerosol flux density function using a combination of multiple lognormally distributed modes for different droplet sizes. Each mode is formulated as a distinct function of the Reynolds number. Because the Reynolds number depends on viscosity of seawater as well as wind speed, and the seawater viscosity depends on SST and salinity, this parameterization inherently depends on the temperature and salinity. Also, the flux formula for each mode sets a threshold Reynolds number below which no wave breaking occurs (i.e., no sea salt emissions in areas of sufficiently low wind). The flux density function is given at a specific relative humidity (RH) (typically 80 percent). Previously, the sea salt emissions preprocessor did not take into account local RH conditions; the updated sea salt preprocessor now corrects the flux size distribution according to local RH using an empirical relationship between particle size and RH developed by Zhang et al. (2006). Although

no change was made to the surf zone sea salt generation algorithm, the assumed surf zone width has been reduced from 50 to 25 m, as suggested by Gantt et al. (2015).

The updated CAMx sea salt emissions processor was used with the 2012 WRF data to generate sea salt emissions for the 36-, 12-, and 4-km modeling domains. Sea salt composition is assumed to be 38.7 percent sodium, 53.8 percent chlorine, and 7.5 percent SO_4 (by weight) based on ionic composition from Lewis and Schwartz (2004). Ramboll adjusted the sodium fraction by adding non-sodium cations (magnesium, calcium, and potassium) to sodium, considering electroneutrality, and then re-normalized the mass ratios.

Halogen chemistry over the ocean depletes ozone concentrations near the surface, so it is especially important in the GOMR. Consistent with the CB6r4 halogen chemical mechanism, the CAMx in-line iodine emissions module generated inorganic iodine and hypoiodous acid emissions as a function of surface ozone concentration, wind speed, and SST (Emery et al., 2016a).

Oceanic emissions of dimethyl sulfide (DMS) are not explicitly modeled in CAMx. However, DMS emissions and DMS chemistry are included in the GEOS-Chem global model used to generate BCs for the CAMx modeling used in this study. DMS from GEOS-Chem is added to the CAMx CB6r4 SO2 BC, and methylsulfonic acid from GEOS-Chem is added to the CAMx CB6r4 PSO4 BC. Though DMS emissions within the CAMx domain are not modeled, their main effect would be to increase natural (background) sulfate, which is not likely to significantly affect predictions of impacts of new oil and gas exploration and development source emissions on PM species.

4.3.5.6 Lightning NO_x Emissions

NO_x is formed in lightning channels as the heat released by the electrical discharge converts the nitrogen (N_2) and oxygen (O_2) to NO. Modeling lightning and its emissions is an area of active research. For example, the mechanism for the buildup of electric potential within clouds is not well-understood, and modeling the production, transport, and fate of emissions from lightning is complicated by the fact that the cumulus towers associated with lightning may be at sub-grid scale depending on the model resolution. Given the importance of lightning NO_x in the tropospheric NO_x budget and in understanding its effect on upper tropospheric ozone and the hydroxyl radical, lightning NO_x is typically incorporated in global modeling (e.g., Tost et al., 2007; Sauvage et al., 2007; Emmons et al., 2010) and has also been integrated into many regional modeling studies (e.g., Allen et al., 2012; Koo et al., 2010).

For this study, Ramboll converted the in-line calculation of spatially and temporally resolved lightning NO_x emissions from the CMAQ simulations—described in Appendix H of USDOI, BOEM (2017)—into a format suitable for use in CAMx. CMAQ lightning NO_X emissions were derived from the convective precipitation rate provided in the Meteorology-Chemistry Interface Processor (MCIP) files.

4.3.5.7 Windblown Dust

For this study, Ramboll prepared the spatially and temporally resolved in-line calculation of windblown dust (WBD) emissions from the CMAQ simulations for input to CAMx. CMAQ in-line WBD emission calculations were based on wind speed and soil moisture parameters that the WRF model passed to CMAQ.

4.3.5.8 QA/QC of Processed Emissions

Emissions were processed by major source category in several different processing “streams” to simplify the emissions modeling process and facilitate the QA/QC of results. SMOKE includes QA and reporting features to keep track of the adjustments at each step of emissions processing and to ensure that data integrity is not compromised. Ramboll carefully reviewed the SMOKE log files for significant error

messages and ensured that it used appropriate source profiles. In addition, SMOKE output summary reports were reviewed and compared with input emission totals.

4.3.5.9 Development of Model-Ready Emissions

The CAMx requires two types of emission files for every episode day; both types are Urban Airshed Model (UAM)-based Fortran binary files:

- **Surface-level 2D emissions:** This file contains two-dimensional gridded fields of low-level (i.e., surface) emissions rates for all emitted species to be modeled. All pre-merged gridded emissions inputs were merged together to generate merged two-dimensional gridded anthropogenic low-level (layer 1) emission inputs.

- **Elevated point source emissions:** This file contains stack parameters and emissions rates for all elevated point sources and emitted species to be modeled.

The merged two-dimensional gridded anthropogenic emissions, which were originally output from SMOKE in CMAQ format, were converted into CAMx format using the CMAQ2CAMX program.[7] Ramboll then merged natural source categories (sea salt, biogenic, fires, lightning, and WBD) with the surface-level emissions using the MRGUAM processor to develop CAMx model-ready emissions. Ramboll first converted model species from CMAQ to be compatible with CAMx, then converted CMAQ two-dimensional and in-line point emission files to CAMx area/point source emission files using the CMAQ2CAMx interface program. The point source emissions files in UAM-based binary format were merged together to develop the final CAMx-ready point source emissions. The elevated point source file is independent of the modeling grid because it contains horizontal (X, Y) coordinates for each point source, and so one file includes all point sources in the 12- and 4-km BOEM modeling grids. In addition, CAMx requires separate emission inputs for source groups being tracked in the future year scenario's source apportionment modeling.

4.3.5.10 Summary of Processed Emissions

This section summarizes 2012 base case and future year scenario emissions for the BOEM 12- and 4-km domains organized by source category.

Emission categories used in these summaries are defined below:

Sector	Sector Description
Fugitive Dust	Anthropogenic fugitive dust from paved and unpaved roads, as well as agricultural, construction, and mining sources
Fires	Agricultural fires, wildfires, and prescribed burning
C1C2 CMV and Rail	Locomotive and smaller CMVs with Category 1 and 2 (C1C2) main engines
C3 CMV	CMVs with Category 3 (C3) main engine emissions in state waters; includes port and underway emissions
Biogenic	Vegetation and soils throughout modeling domain
Nonpoint	Stationary nonpoint sources

[7] http://www.camx.com/download/support-software.aspx

Sector	Sector Description
RWC	Residential wood combustion
Nonroad	Off-road equipment included in USEPA's NONROAD model
Area Oil and Gas (O&G)	Nonpoint oil and gas sector onshore sources
Onroad	Motorized vehicles that are normally operated on public roadways (passenger cars, motorcycles, minivans, sport-utility vehicles, light-duty trucks, heavy-duty trucks, and buses)
Non-U.S. Area	Stationary nonpoint sources and nonroad equipment outside the U.S.; includes C1C2 CMV emissions in the Eastern GOM Planning Area
Non-U.S. Onroad	Motorized vehicles that are normally operated on public roadways outside of the U.S.
BOEM Gulfwide	All marine vessel activity in the GOM, including BOEM OCS oil and gas support vessels and helicopters, under the "no-sale" scenario
Non-U.S. State Point (with GOM offshore platforms)	Stationary point sources not located in any U.S. state; includes BOEM and PEMEX offshore platforms in the GOM and point sources in Mexico
Point O&G	Point oil and gas sector onshore sources and oil and gas platforms in state waters
EGU Point	EGU point sources
Non-EGU Point	NEI point sources that are not in the EGU or Point O&G sectors
BOEM OCS Platform w/SingleLeaseSale	Additional BOEM OCS oil and gas production platforms associated with a single lease sale from the 2017–2022 GOM Multisale EIS scenario
BOEM OCS Sup. Vessel w/SingleLeaseSale in Federal Waters	Additional BOEM oil and gas production support vessels and helicopters associated with a single lease sale from the 2017–2022 GOM Multisale EIS scenario: C1C2C3 and helicopter emissions in Federal waters related to single-sale scenario
C1C2 Sup. Vessel w/SingleLeaseSale in State Waters	Additional BOEM oil and gas production support vessels and helicopters associated with a single lease sale from the 2017–2022 GOM Multisale EIS scenario: C1C2 emissions in state waters related to single-sale scenario
C3 Sup. Vessel w/SingleLeaseSale in State Waters	Additional BOEM oil and gas production support vessels and helicopters associated with single lease sales from the 2017–2022 GOM Multisale EIS scenario: C3 emissions in state waters related to single-sale scenario
Helicopter at U.S. Airports w/SingleLeaseSale	Helicopter emissions at U.S. airports related to single-sale scenario

Sector	Sector Description
BOEM OCS Platform w/NineLeaseSale	Additional BOEM OCS oil and gas production platforms associated with the remaining nine lease sales from the 2017–2022 GOM Multisale EIS scenario
BOEM OCS Sup. Vessel w/NineLeaseSale in Federal Waters	Additional BOEM oil and gas production support vessels and helicopters associated with the remaining nine lease sales from the 2017–2022 GOM Multisale EIS scenario: C1C2C3 and helicopter emissions in Federal waters related to nine-sale scenario
C1C2 Sup. Vessel w/NineLeaseSale in State Waters	Additional BOEM oil and gas production support vessels and helicopters associated with the remaining nine lease sales from the 2017–2022 GOM Multisale EIS scenario: C1C2 emissions in state waters related to nine-sale scenario
C3 Sup. Vessel w/NineLeaseSale in State Waters	Additional BOEM oil and gas production support vessels and helicopters associated with the remaining nine lease sales from the 2017–2022 GOM Multisale EIS scenario: C3 emissions in state waters related to nine-sale scenario
Helicopter at U.S. Airports w/NineLeaseSale	Helicopter emissions at U.S. airports related to nine-sale scenario

These summary data are based on the 4-km domain SMOKE processing of 2012 base case and future year inventories, as described above. With the exception of fugitive dust and biogenic sources, emissions are summarized from the SMKMRG program's SMOKE reports. Ramboll adjusted fugitive dust emissions after SMOKE processing to account for fugitive dust correction factors derived from the Biogenic Emission Landuse Database version 3 (BELD3). Application of these dust transport correction factors accounts for suppression of grid-scale dust emissions via deposition on proximate vegetation surfaces such as roadside trees and bushes. As noted above, biogenic emissions were generated using the MEGAN model outside of SMOKE; thus, they are generated directly on the 36-, 12-, and 4-km grids rather than by state/county.

Base case and future year emissions are compared graphically in Figure 4-1. Table 4-3 summarizes NO_x, VOC, SO_2, and $PM_{2.5}$ air pollutant emissions for the 2012 base case and future year scenarios by major source category within the 4-km domain in short TPY. Table 4-4 summarizes the changes in emissions between the base and future year scenarios.

Tables 4-3 and 4-4 and Figure 4-1 show that NO_x emissions in both the Western and Central GOM Planning Areas and in the rest of the 4-km domain (which includes the eastern GOM and onshore sources) are projected to decrease in the future year by 12 percent and 10 percent, respectively, despite emission increases from new sources under the 10-sale scenario. VOC emissions in the Western and Central GOM Planning Areas are projected to decrease by 6 percent but increase slightly (2 percent) in the remainder of the 4-km domain. $PM_{2.5}$ emissions are projected to remain nearly unchanged. A breakdown of sources in the Western and Central GOM Planning Areas as shown in the right-hand column of Figure 4-1 shows that reductions in existing sources due to projected declines in production more than offset the projected additional NO_x and VOC emissions from new sources associated with the 10-sale scenario. As shown in Tables 4-3 and 4-4, SO_2 emissions show the largest change between the current and future year and are projected to decrease by 61 percent in the Western and Central GOM Planning Areas and 38 percent in the remainder of the 4-km domain.

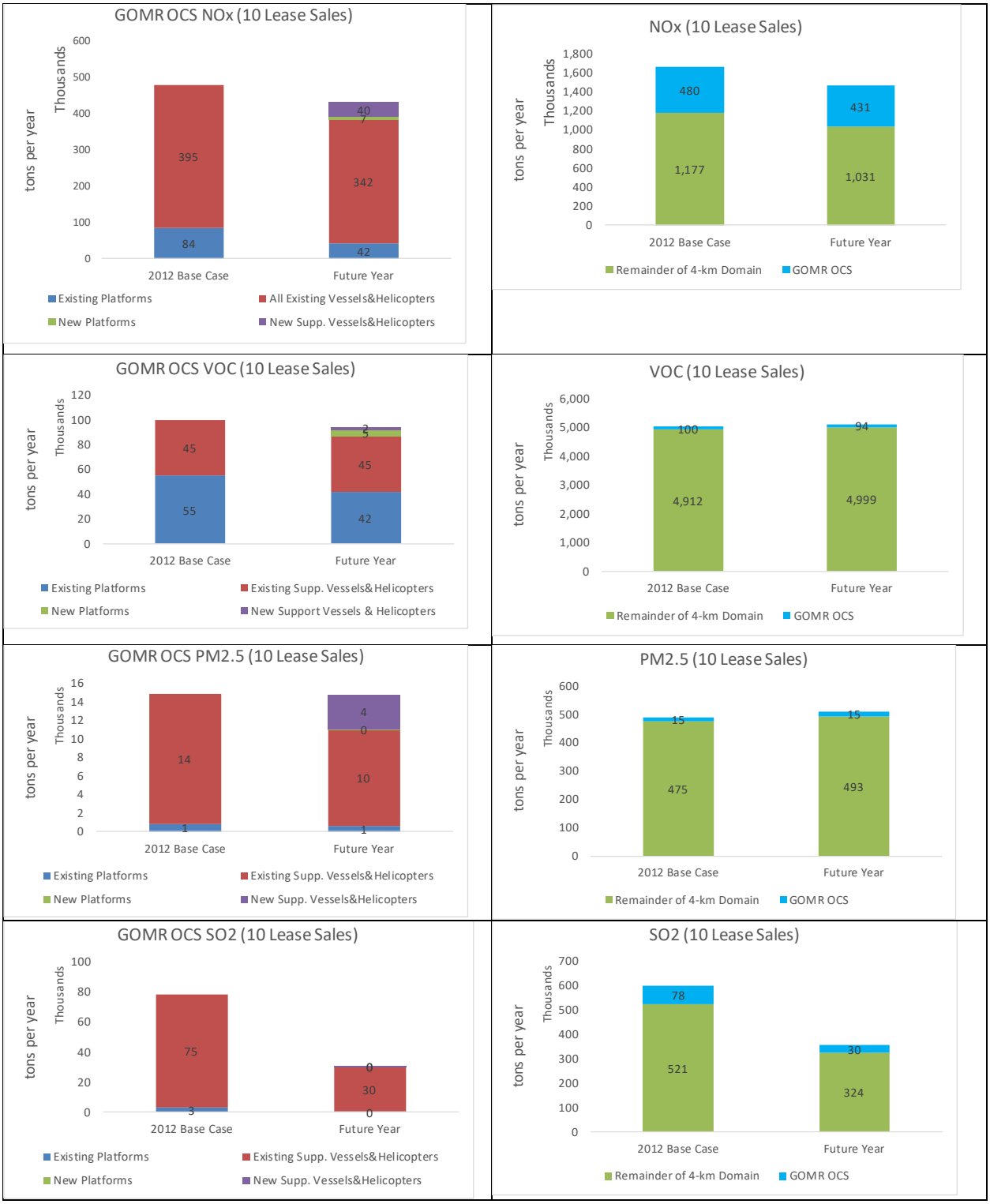

Figure 4-1. Base case and future year (10 lease sale) scenario NO_x, VOC, $PM_{2.5}$ and SO_2 emissions (thousands of TPY) from existing and new BOEM sources in the Western and Central Gulf (left) and as compared to sources in the remainder of the 4-km modeling domain (right)

Note: Minor amounts of new support vessel traffic emissions in state waters (1,854 tons NO_x, 88 tons VOC, 169 tons $PM_{2.5}$, 3 tons SO_2) are included in the future year GOMR OCS area source emissions totals shown here and emissions from vessels and platforms outside of the Western and Central GOM Planning Areas are included in the "Remainder of 4-km Domain" total.

Table 4-3. 2012 Base Case and Future Year Emissions Summary by Sector Within the 4-km Modeling Domain

Sectors	2012 Base Year (TPY)				Future Year Scenario (TPY)			
	NO_x	$PM_{2.5}$	SO_2	VOC	NO_x	$PM_{2.5}$	SO_2	VOC
Fugitive Dust	-	70,526	-	-	-	78,180		
Fires	27,335	250,850	17,852	559,643	27,335	250,850	17,852	559,643
C1C2 CMV and Rail	171,436	5,416	2,039	4,896	139,026	3,876	280	3,760
C3 CMV	37,978	2,189	18,867	1,440	35,953	387	860	1,709
Biogenic	19,015	-	-	3,140,424	19,015	-	-	3,140,424
Nonpoint	81,009	46,898	7,277	287,033	85,050	51,126	3,047	285,508
RWC[a]	227	1,916	28	2,309	241	1,953	30	2,305
Nonroad	76,345	6,994	153	112,683	52,636	4,826	79	78,780
Area O&G	69,331	1,991	530	506,972	74,065	2,768	1,067	641,692
Onroad	270,364	8,468	1,731	145,061	183,305	7,124	940	106,904
Non-U.S. Area	38,832	4,362	719	15,208	35,625	4,429	502	16,787
BOEM Gulfwide	395,483	14,806	74,698	45,216	342,262	11,521	29,843	44,747
Non-U.S. Onroad	13,894	438	73	6,217	9,097	447	27	4,041
Non-U.S. Point (with GOM offshore platforms)	106,344	2,668	7,795	57,361	74,119	2,750	4,847	53,198
Point O&G	50,765	2,294	25,431	19,596	47,526	2,480	23,543	21,442
EGU Point	137,932	18,099	306,031	3,545	117,518	21,925	136,784	4,371
Non-EGU Point	159,962	52,632	135,981	104,387	172,040	60,413	134,595	120,106
BOEM OCS Platform w/SingleLeaseSale	-	-	-	-	2,120	30	8	1,496
BOEM OCS Sup. Vessel w/SingleLeaseSale in Federal Waters	-	-	-	-	5,636	503	19	277
C1C2 Sup. Vessel w/SingleLeaseSale in State Waters	-	-	-	-	386	35	1	16
C3 Sup. Vessel w/SingleLeaseSale in State Waters	-	-	-	-	0	0	0	0
Helicopter at U.S. Airports w/SingleLeaseSale	-	-	-	-	80	2	10	50
BOEM OCS Platform w/NineLeaseSale	-	-	-	-	4,629	65	18	3,865
BOEM OCS Sup. Vessel w/NineLeaseSale in Federal Waters	-	-	-	-	32,660	3,002	244	1,790
C1C2 Sup. Vessel w/NineLeaseSale in State Waters	-	-	-	-	1,468	134	2	61
C3 Sup. Vessel w/NineLeaseSale in State Waters	-	-	-	-	1	0	0	11
Helicopter at U.S. Airports w/NineLeaseSale	-	-	-	-	275	7	34	171
TOTAL:	1,656,252	490,547	599,205	5,011,991	1,462,068	508,834	354,632	5,093,154

[a] Reductions in urban areas applied per Adelman et al. (2015).

Table 4-4. Changes in Emissions Between the 2012 Base Case and Future Year Emissions (short TPY) by Source Category Within the 4-km Modeling Domain

Sectors	Future Year–Base Year (TPY)				Future Year–Base Year (%)			
	NO_x	$PM_{2.5}$	SO_2	VOC	NO_x	$PM_{2.5}$	SO_2	VOC
Fugitive Dust	0	7,653	0	0	--	11%	--	--
Fires	0	0	0	0	0%	0%	0%	0%
C1C2 CMV and Rail	(32,410)	(1,540)	(1,759)	(1,136)	-19%	-28%	-86%	-23%
C3 CMV	(2,026)	(1,803)	(18,007)	269	-5%	-82%	-95%	19%
Biogenic	0	0	0	0	0%	--	--	0%
Nonpoint	4,040	4,229	(4,231)	(1,525)	5%	9%	-58%	-1%
RWC[a]	14	37	1	(3)	6%	2%	5%	0%
Nonroad	(23,709)	(2,168)	(73)	(33,904)	-31%	-31%	-48%	-30%
Area O&G	4,734	776	537	134,720	7%	39%	101%	27%
Onroad	(87,059)	(1,343)	(791)	(38,157)	-32%	-16%	-46%	-26%
Non-U.S. Area	(3,207)	68	(218)	1,579	-8%	2%	-30%	10%
BOEM Gulfwide	(53,221)	(3,539)	(44,854)	(469)	-13%	-25%	-60%	-1%
Non-U.S. Onroad	(4,797)	10	(46)	(2,176)	-35%	2%	-63%	-35%
Non-U.S. Point (with GOM offshore platforms)	(32,226)	81	(2,949)	(4,163)	-30%	3%	-38%	-7%
Point O&G	(3,239)	187	(1,888)	1,846	-6%	8%	-7%	9%
EGU Point	(20,413)	3,859	(169,247)	826	-15%	22%	-55%	23%
Non-EGU Point	12,078	7,781	(1,385)	15,719	8%	15%	-1%	15%
BOEM OCS Platform w/Single Lease Sale	2,120	30	8	1,496	--	--	--	--
BOEM OCS Sup. Vessel w /Single Lease Sale in Federal Waters	5,636	503	19	277	--	--	--	--
C1C2 Sup. Vessel w/ Single Lease Sale in State Waters	386	35	1	16	--	--	--	--
C3 Sup. Vessel w/ Single Lease Sale in State Waters	0	0	0	0	--	--	--	--
Helicopter at U.S. Airports w/ Single Lease Sale	80	2	10	50	--	--	--	--
BOEM OCS Platform w/ Nine Lease Sale	4,629	65	18	3,865	--	--	--	--
BOEM OCS Sup. Vessel w/ Nine Lease Sale in Federal Waters	32,660	3,002	244	1,790	--	--	--	--
C1C2 Sup. Vessel w/ Nine Lease Sale in State Waters	1,468	134	2	61	--	--	--	--
C3 Sup. Vessel w/ Nine Lease Sale in state waters	1	0	0	11	--	--	--	--
Helicopter at U.S. Airports w/ Nine Lease Sale	275	7	34	171	--	--	--	--
TOTAL:	**(194,186)**	**18,066**	**(244,574)**	**81,163**	**-12%**	**4%**	**-41%**	**2%**

[a] Reductions in urban areas applied per Adelman et al. (2015).

Figure 4-2 displays locations of NO_x emissions in short TPY within the 4-km domain from new BOEM OCS oil and gas production platforms under a single lease sale and remaining nine lease sales from the 2017–2022 GOM Multisale EIS scenario. As shown in this figure, deepwater platforms have higher annual emissions than shallow-water platforms and new platforms included in the single sale scenario are generally interspersed among new platforms included in the remaining nine lease sales.

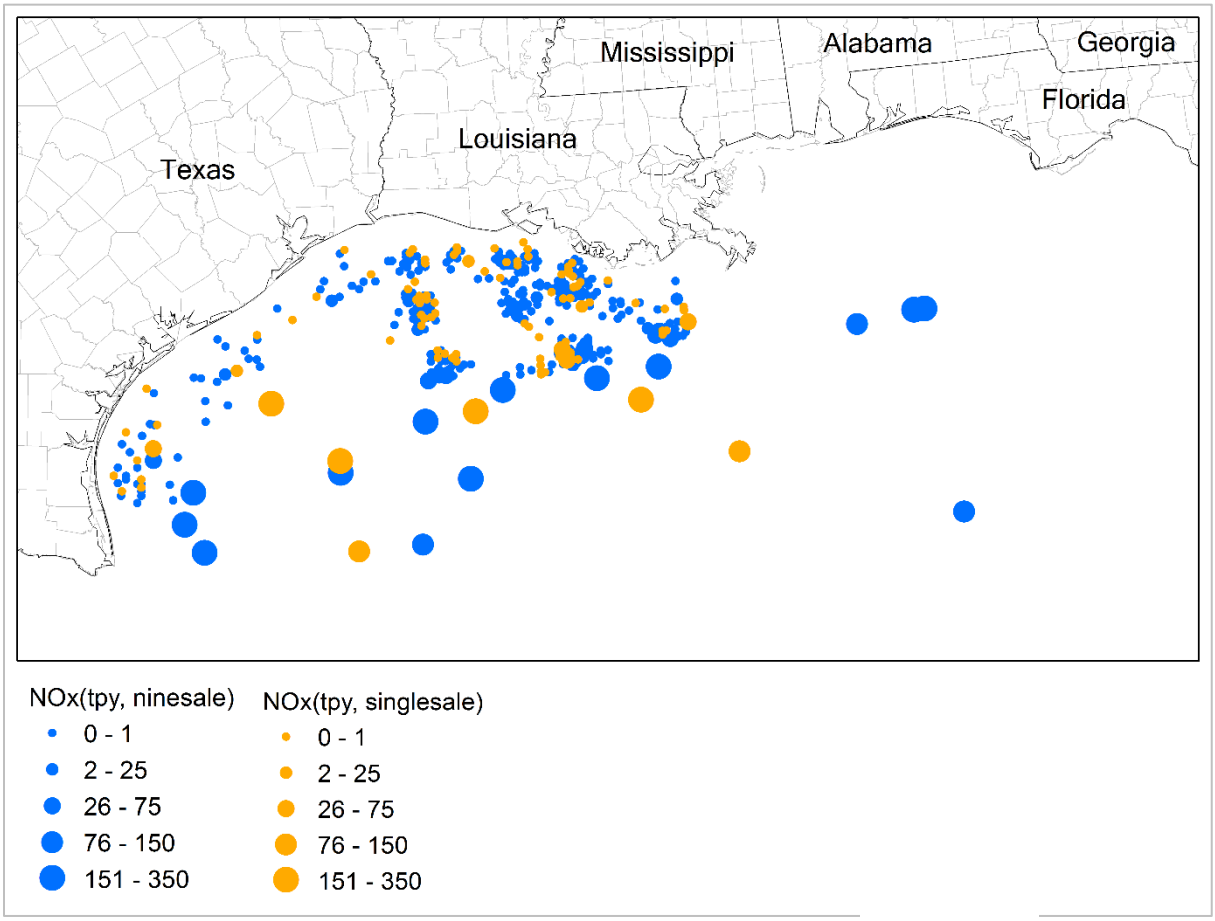

Figure 4-2. Spatial Distribution of NO_x Emissions (TPY) from New OCS Oil and Gas Production Platforms Under the Single Lease Sale and Remaining Nine Lease Sales from the 2017–2022 GOM Multisale EIS Scenario

Figure 4-3 presents 4-km spatial plots for the same pollutants for additional OCS oil and gas support vessels and helicopters under the future year, single-sale scenario. Figure 4-4 shows emissions for additional OCS oil and gas support vessels and helicopters under the future year, nine-sale scenario. Figure 4-5 shows emissions for OCS oil and gas platforms, and Figure 4-8 shows emissions from support vessels and helicopters, under the future year, no-sale alternative. The apparent disconnect between the support vessel (and helicopter) spatial emission patterns between Figure 4-8 for the no-sale scenario and Figures 4-5 and 4-6 for the future year scenarios is due to scaling differences, making the pattern of vessel emissions more apparent for the future year scenarios. The future year support vessel emission estimates were mapped between the future platform locations, drilling locations, pipelaying locations, and specific ports. Because the no-sale scenario is based on the 2014 Gulfwide Emissions Inventory (Wilson et al., 2017), which includes all marine vessels derived from actual vessel traffic patterns, it is harder to discern individual routes.

Figure 4-9 shows emissions for all other marine vessel activity in Federal waters of the GOM under the future year scenarios. Figure 4-10 shows emissions for all other anthropogenic U.S. sources under the future year scenarios.

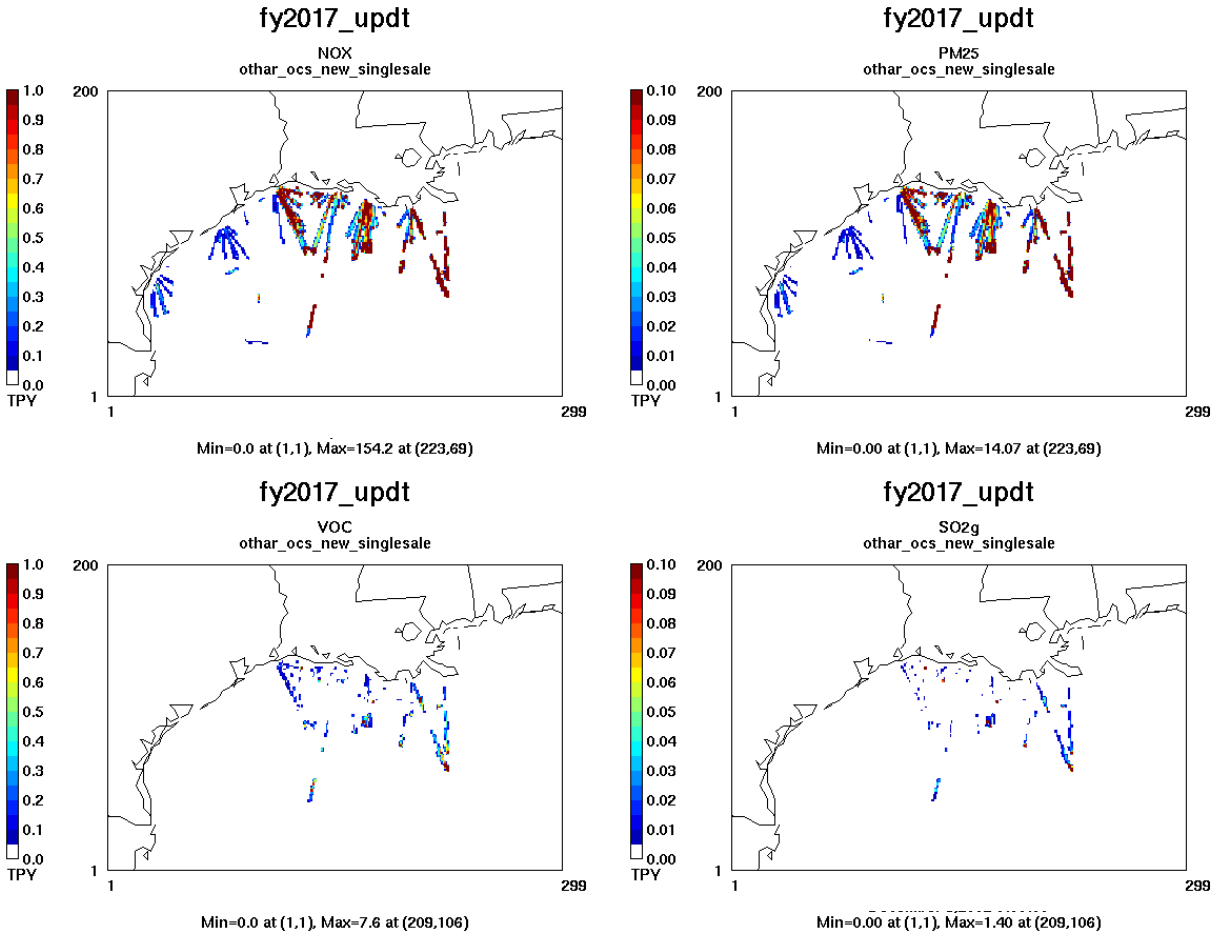

Figure 4-3. Spatial Distribution of NO_x, $PM_{2.5}$, SO_2, and VOC Emissions (TPY) from BOEM's OCS Additional Oil and Gas Support Vessels and Helicopters Under a Single Lease Sale from the 2017–2022 GOM Multisale EIS Scenario

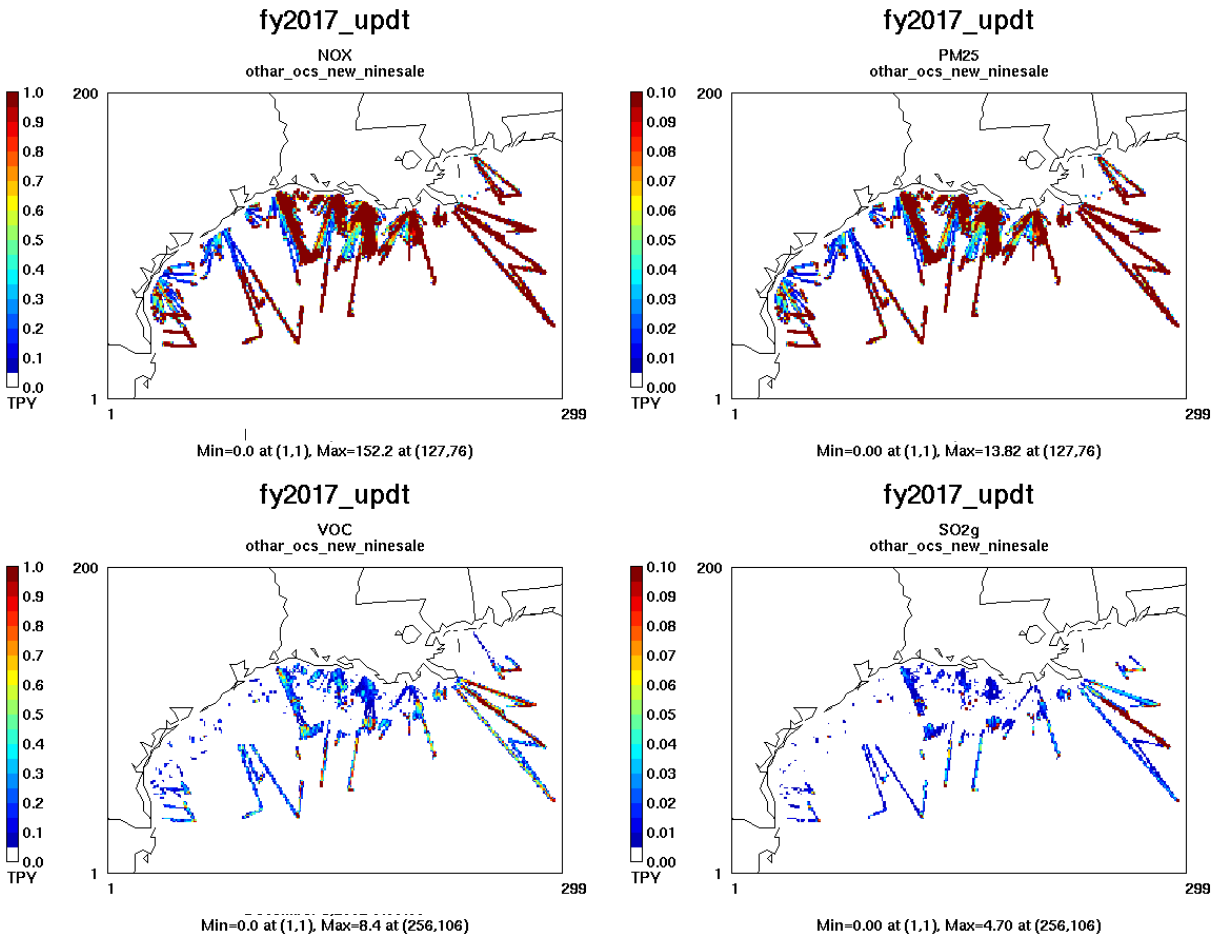

Figure 4-4. Spatial Distribution of NO_x, $PM_{2.5}$, SO_2, and VOC Emissions (TPY) from BOEM's OCS Additional Oil and Gas Support Vessels and Helicopters Under the Remaining Nine Lease Sales from the 2017–2022 GOM Multisale EIS Scenario

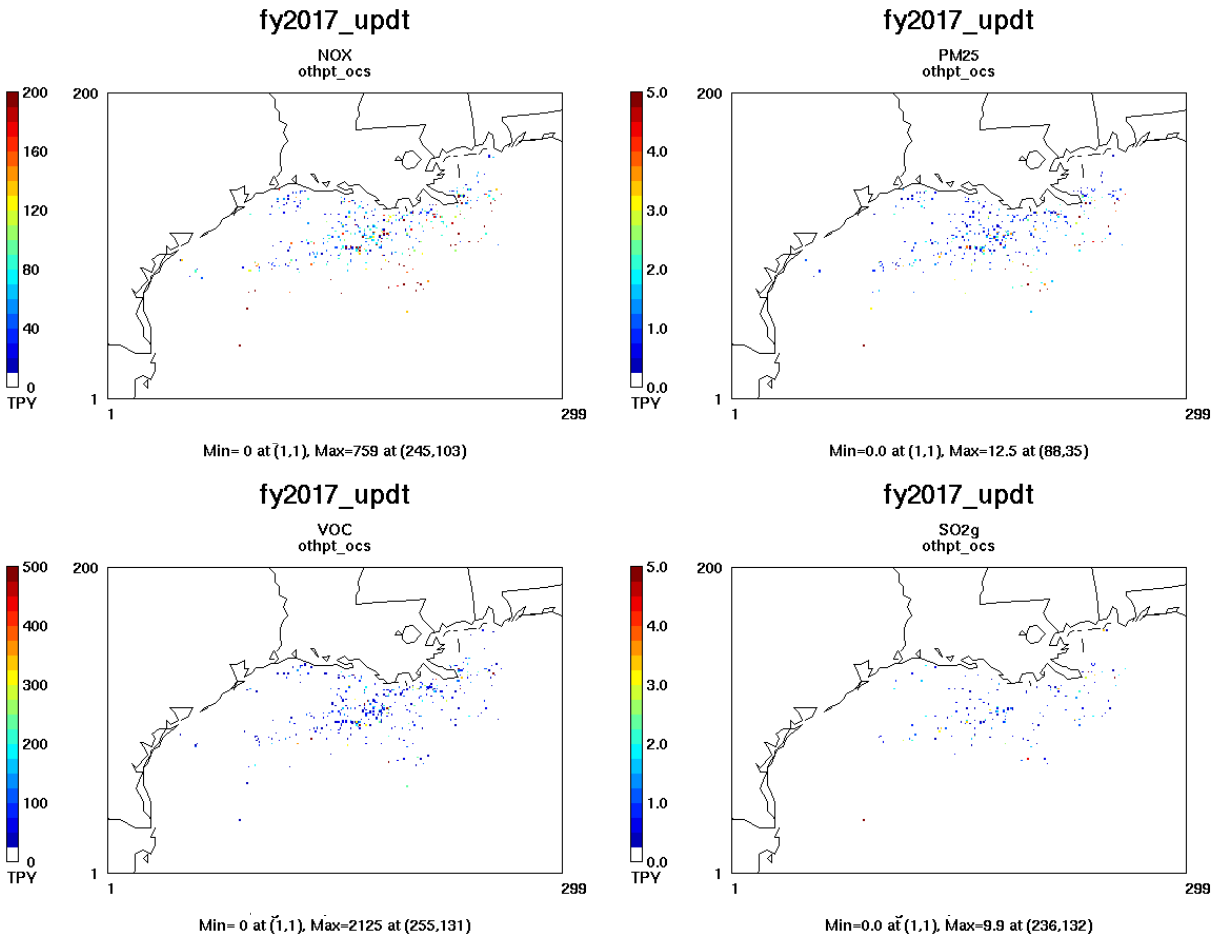

Figure 4-5. Spatial Distribution of NO_x, $PM_{2.5}$, SO_2, and VOC Emissions (TPY) from BOEM's OCS Oil and Gas Platforms Under the No-Sale Scenario in the 4-km Domain

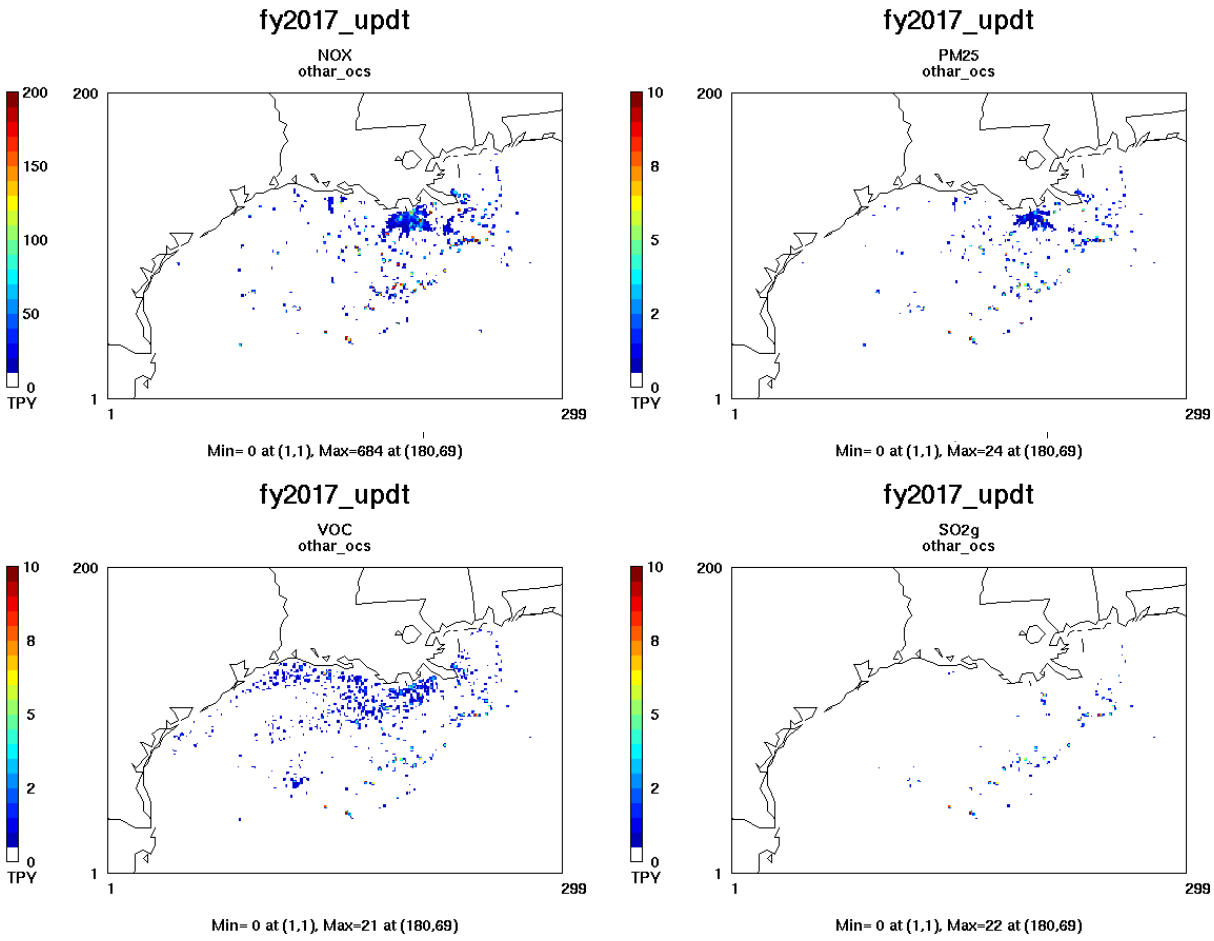

Figure 4-6. Spatial Distribution of NO_x, $PM_{2.5}$, SO_2, and VOC Emissions (TPY) from BOEM's OCS Oil and Gas Support Vessels and Helicopters Under the No-Sale Scenario in the 4-km Domain

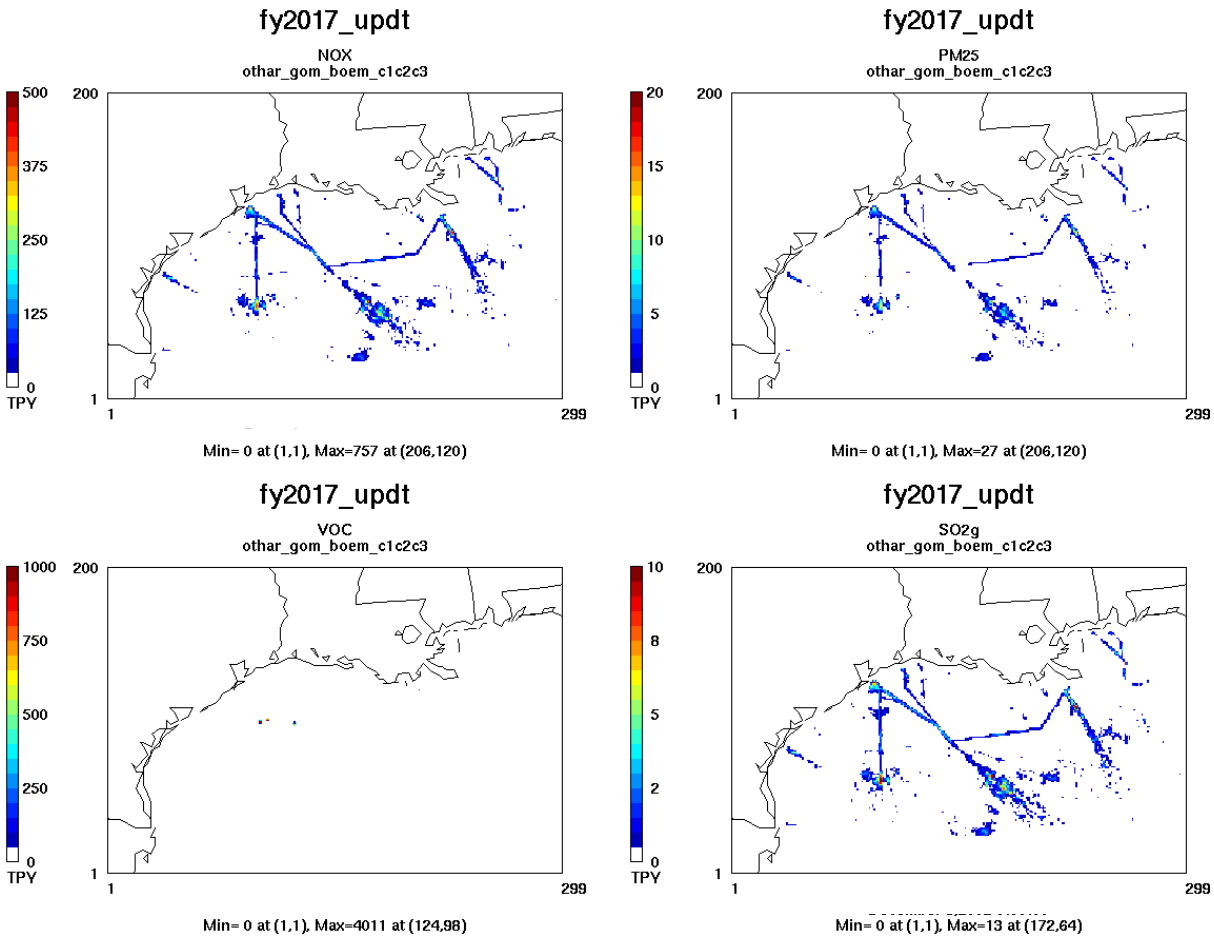

Figure 4-7. Spatial Distribution of NO_x, $PM_{2.5}$, SO_2, and VOC Emissions (TPY) from All Other Marine Vessel Activity in Federal Waters Within 4-km Domain Under the Future Year Scenarios

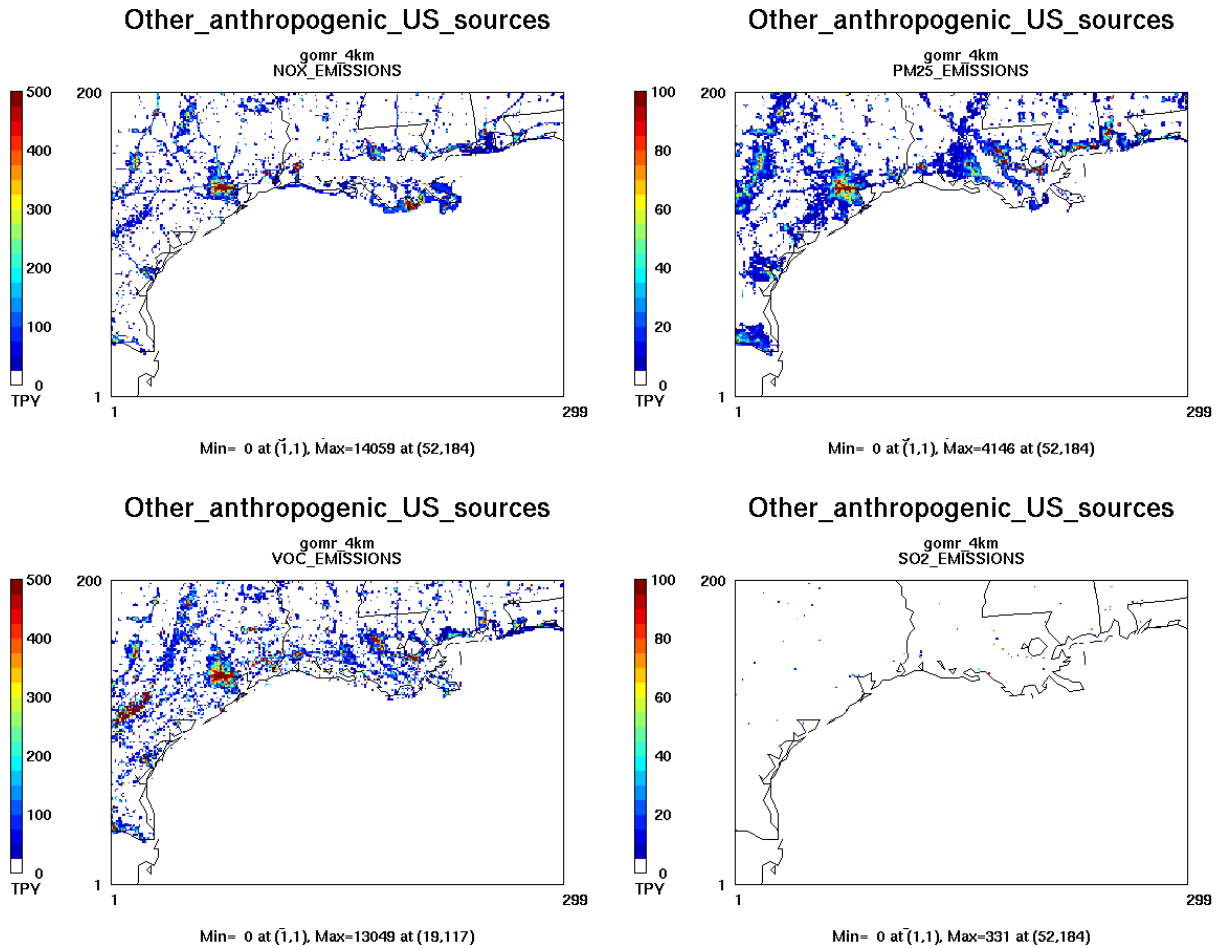

Figure 4-8. Spatial Distribution of NO_x, $PM_{2.5}$, SO_2, and VOC Emissions (TPY) from Other Anthropogenic U.S. Sources for the Future Year Scenarios Within BOEM's 4-km Domain

4.3.6 Source Apportionment Design

Source apportionment, as applied in CAMx, provides a means of assessing the contributions of specified sources or categories of sources to predicted ozone and PM concentrations under the air quality conditions being simulated. Source contributions can be calculated for ozone and PM using CAMx's ozone or PM source apportionment routines. Ramboll applied source apportionment analyses to the future year scenario to analyze the pre- and post-lease OCS oil and gas impacts to short-term and annual NAAQS, AQRVs, and PSD increments. BOEM selected the 13 source categories for source apportionment listed in Table 4-5.

Table 4-5. Source Categories for the Future Year Scenario Source Apportionment Analysis

Category ID	Sources
SC1	Fires (U.S., Canada, and Mexico)
SC2	Biogenic and other natural sources (e.g., lightning NO_x and sea salt)
SC3a	Additional BOEM OCS oil and gas production platforms associated with a single lease sale from the 2017–2022 GOM Multisale EIS scenario
SC3b	Additional BOEM OCS oil and gas production platforms associated with remaining nine lease sales from the 2017–2022 GOM Multisale EIS scenario
SC4a	Additional BOEM oil and gas production support vessels and helicopters associated with a single lease sale from the 2017–2022 GOM Multisale EIS scenario
SC4b	Additional BOEM oil and gas production support vessels and helicopters associated with remaining nine lease sales from the 2017–2022 GOM Multisale EIS scenario
SC5a	BOEM's OCS oil and gas production platforms under the no-sale scenario
SC5b	BOEM's OCS oil and gas production support vessels and helicopters under the no-sale scenario
SC6	All other marine vessel activity in the GOM, not associated with OCS oil and gas activities
SC7	Other anthropogenic U.S. sources[a]
SC8	Mexican and Canadian anthropogenic sources[b]
SC9	ICs
SC10	BCs

[a] Includes onshore oil and gas production sources and oil and gas production sources in state waters.
[b] Also includes oil and gas production sources.

These source categories aggregate similar sources based on jurisdiction (i.e., sources under BOEM's jurisdiction versus other Federal agencies) and sources beyond direct domestic regulatory control (e.g., natural emission sources and foreign sources). Additional OCS oil and gas production platforms and support vessel and helicopter trips associated with the lease sales are included as a separate source category, thus providing estimates of the impacts of these new sources, which are projected to occur under the future year scenario associated with the lease sales. Separate source categories are included for the single lease sale scenario (SC3a and SC4a) and for the remaining nine lease sales (SC3b and SC4b) that make up the 10-sale package. Platforms and support vessel and helicopter emissions projected for the future year scenario under the no-sale scenario are also included as separate source apportionment categories; these may be referred to as "existing" platforms and "existing" support vessels and helicopters, although they are not all the same as sources that are included in the 2012 base case inventory.

4.4 Base Case Photochemical Grid Modeling

4.4.1 Overview

Ramboll applied the CAMx PGM to a set of nested domains with horizontal resolutions of 36-, 12-, and 4-km centered on the GOMR (Figure 2-1). For the 2012 base case analysis, Ramboll ran CAMx with the 2012 base case emissions. Ramboll obtained CAMx-required meteorological fields from the WRF meteorological model results for 2012, which were developed as described in Section 2. Modeling procedures were based on the USEPA's current and revised draft modeling guidance procedures (USEPA, 2007, 2014a). Additional features of the modeling approach include the following:

- ERG developed anthropogenic and non-anthropogenic model-ready emissions for the 2012 base case, as described in Section 3.
- Photochemical grid modeling was based on CAMx version 6.40 with the CB6r4 photochemical mechanism, including active ECH4 emissions and halogen chemistry.
- Day-specific BCs for the lateral boundaries of the 36-km modeling domain were based on 2012 GEOS-Chem v10-01 global chemistry model (GCM) output.
- Ramboll conducted an MPE for the 2012 base case simulation using all available aerometric data within the modeling domain; Section 4.5 presents the results.

4.4.2 Model Grid Configuration

The PGM domain configuration is composed of a system of nested grids with 36-, 12-, and 4-km horizontal resolution, as shown in Figure 2-1. Table 4-6 provides the modeling grid definitions for the WRF and CAMx simulations. The 4-km PGM modeling domain excludes the GOMESA Congressional Moratoria Area in the eastern GOM to limit the grid dimension to a more manageable size for computational efficiency. However, results are presented for both areas within the 4-km grid and for sensitive areas within the 12-km grid outside of the 4-km grid in Section 4.7.

Table 4-6. Domain Grid Definitions for the WRF and CAMx Modeling

Modeling Grid	WRF		CAMx	
	Origin[a] coordinates (x, y) (km)	Grid dimension (column × row)	Origin[a] coordinates (x, y) (km)	Grid dimension (column × row)
36-km grid	(-2,592, -2,304)	(164 × 128)	(-2,736, -2,088)	(148 × 112)
12-km grid	(-1,008, -2,016)	(264 × 186)	(-948, -1,956)	(254 × 176)
4-km grid	(-156, -1,704)	(480 × 210)	(-136, -1,684)	(299 × 200)

[a] Southwest corner of each domain grid.

For CAMx, Ramboll extracted BCs for the 12-km domain from the 36-km simulation results and modeled the 12- and 4-km grids using two-way nesting (allowing interactions between the two grids in both directions). Specification of the CAMx vertical domain structure depends on the definition of the WRF vertical layers structure. Ramboll ran the WRF simulation with 36 vertical layer interfaces (which is equivalent to 35 vertical layers) from the surface up to 50 mbar (approximately 20 km above mean sea level [AMSL]). The WRF model employs a terrain-following coordinate system called eta (η) coordinate, which is defined by relative pressure differences between layers. As shown in Table 4-7, the WRF levels were more finely stratified near the surface in an attempt to improve simulation of the atmospheric boundary layer structure and processes. A layer collapsing scheme was adopted for the CAMx simulations, whereby multiple WRF layers were combined into a single CAMx layer to improve the PGM

computational efficiency. Table 4-7 also shows the layer collapsing from the 35 WRF layers to 28 PGM layers. The mixing heights over the study domain are typically below 2 km. Therefore, the WRF modeling layers up to the 20th layer (approximately 2.5 km) were directly mapped to the PGM layers (no layer collapsing) to better simulate the stable thermal stratification of the boundary layer and avoid errors potentially introduced by layer collapsing. Above the 20th WRF layer, two WRF layers were combined into a single PGM layer up to the 50 hPa region top.

Table 4-7. Vertical Layer Interface Definition for WRF Simulations (left most columns) and the Layer Collapsing Scheme for the CAMx Layers (right columns)

WRF					CAMx		
Layer Interface	Eta (η)	Pressure (mbar)	Height (m)	Thickness (m)	Layer	Layer Top Height (m)	Thickness (m)
36	0	50	19,383.7	2,068.3	28	19,383.7	3,929.9
35	0.027	76	17,315.3	1,861.6			
34	0.06	107	15,453.7	1,735.9	27	15,453.7	3,447.4
33	0.1	145	13,717.8	1,711.5			
32	0.15	193	12,006.3	1,397.4	26	12,006.3	2,586.1
31	0.2	240	10,608.9	1,188.7			
30	0.25	288	9,420.2	1,039.0	25	9,420.2	1,964.7
29	0.3	335	8,381.2	925.8			
28	0.35	383	7,455.5	836.9	24	7,455.5	1,602.0
27	0.4	430	6,618.6	765.1			
26	0.45	478	5,853.5	705.7	23	5,853.5	1,361.5
25	0.5	525	5,147.7	655.8			
24	0.55	573	4,491.9	613.1	22	4,491.9	1,076.8
23	0.6	620	3,878.8	463.7			
22	0.64	658	3,415.1	442.5	21	3,415.1	865.8
21	0.68	696	2,972.7	423.3			
20	0.72	734	2,549.4	405.9	20	2,549.4	405.9
19	0.76	772	2,143.4	390.1	19	2,143.4	390.1
18	0.8	810	1,753.4	375.5	18	1,753.4	375.5
17	0.84	848	1,377.8	272.8	17	1,377.8	272.8
16	0.87	877	1,105.0	177.9	16	1,105.0	177.9
15	0.89	896	927.2	174.9	15	927.2	174.9
14	0.91	915	752.3	171.9	14	752.3	171.9
13	0.93	934	580.3	84.9	13	580.3	84.9
12	0.94	943	495.4	84.2	12	495.4	84.2
11	0.95	953	411.2	83.5	11	411.2	83.5
10	0.96	962	327.6	82.9	10	327.6	82.9
9	0.97	972	244.8	82.2	9	244.8	82.2
8	0.98	981	162.5	40.9	8	162.5	40.9
7	0.985	986	121.7	24.4	7	121.7	24.4
6	0.988	989	97.2	24.4	6	97.2	24.4
5	0.991	991	72.8	16.2	5	72.8	16.2
4	0.993	993	56.6	16.2	4	56.6	16.2
3	0.995	995	40.4	16.2	3	40.4	16.2
2	0.997	997	24.2	12.1	2	24.2	12.1
1	0.9985	999	12.1	12.1	1	12.1	12.1
0	1	1,000	0.0	–	–	–	–

4.4.3 Meteorology

Given the objectives of the air quality analysis and the availability of full annual WRF simulations for 2009–2013, Ramboll exercised the CAMx model for a full calendar year. The decision to model for an entire calendar year rather than just a single season is consistent with the need to address ozone, $PM_{2.5}$, visibility, and annual deposition. Given the extremely hot, dry, and smoky conditions during 2011 (discussed in Section 3), Ramboll selected the 2012 calendar year for the base year, base case modeling.

Meteorological inputs for CAMx were generated by processing the WRF outputs using appropriate meteorological input preprocessors. WRFCAMx version 4.3 was used to translate WRF output meteorological fields to daily CAMx meteorological inputs. For a single day, 25 hours of meteorology must be present (midnight–midnight, inclusive), as these fields represent hourly instantaneous conditions, and CAMx internally time-interpolates these fields to each model time step. Precipitation fields are not time-interpolated, but rather time-accumulated, so cloud/precipitation files contain one less hour than other meteorological files (e.g., 24 hours of clouds/precipitation versus 25 hours for other meteorological fields).

Several methodologies are available in WRFCAMx to derive vertical eddy diffusivity (Kv) fields from WRF output. For this modeling, Ramboll used a method consistent with the Yonsei University (YSU) bulk boundary layer scheme (Hong and Noh, 2006)—the default option in WRF—to generate the Kv profile. The lower bound Kv value is set based on the land use type for each grid cell. Another issue is deep cumulus convection, which is difficult to simulate in a grid model because of the small horizontal spatial scale of the cumulus tower. Inadequate characterization of this convective mixing can cause ozone and precursor species to be overestimated in the boundary layer. To address this issue, a patch was developed that increases transport of air from the PBL into the free troposphere and up to the cloud top within cloudy grid cells (ENVIRON, 2012). This patch was shown to improve surface layer ozone in a recent modeling study in Texas (Kemball-Cook et al., 2015) and was thus also employed in this study.

WRFCAMx provides an option to process sub-grid cloud data from WRF fields. Selecting the “DIAG” sub-grid cloud method diagnoses sub-grid cloud fields from WRF gridded thermodynamic fields. The DIAG option is generally selected for the 36- and 12-km WRF output extraction, but not for grid spacing less than about 10 km. However, a recent modeling study showed that without sub-grid cloud, the 4-km grid produced too much ozone over the Houston area due to enhanced photochemistry (Nopmongcol et al., 2014). Therefore, the DIAG option was used for the 4-km grid as well as the 36- and 12-km grids.

4.4.4 Configuration of Model Input Parameters

Table 4-8 summarizes the configuration of the CAMx model. Additional key configuration selections include the following:

- **Chemical mechanism:** Gas-phase chemistry using the CB6r4 photochemical mechanism, including active local ECH_4 emissions and halogen chemistry. For particles, CAMx was configured to use the CF aerosol scheme, which models primary species using two static modes (coarse and fine), while all secondary species are modeled as fine particles only.
- **Photolysis rates:** CAMx requires a lookup table of photolysis rates as well as gridded albedo/haze/ozone/snow as input. Day-specific ozone column data are based on the Total Ozone Mapping Spectrometer (TOMS) data measured using the satellite-based Ozone Monitoring Instrument (OMI). Albedo is based on land use data, which includes enhanced albedo values when snow cover is present. For CAMx there is an ancillary snow cover input based on WRF output that overrides the land use-based albedo input, and uses an enhanced snow cover albedo value. Ramboll used the Tropospheric Ultraviolet and Visible (TUV) Radiation Model photolysis rate processor to prepare the lookup table of clear-sky photolysis rates. CAMx is configured to use the in-line TUV to adjust for cloud cover and account for the effects that aerosol loadings

have on photolysis rates; this latter effect on photolysis may be especially important in adjusting the photolysis rates due to the occurrence of PM concentrations associated with emissions from fires. The same photolysis rates were used in the 2012 base case and future year scenario model runs.

- **Land use:** Ramboll generated land use fields based on U.S. Geological Survey (USGS) Geographic Information Retrieval and Analysis System (GIRAS) data (Price et al., 2007). The WRF estimated snow cover data is used to override the USGS land cover categories when snow cover is present.
- **Meteorological inputs:** The WRF-derived meteorological fields were processed to generate CAMx meteorological inputs using the WRFCAMx processor.
- **Plume-in-grid:** Ramboll did not use the sub-grid-scale, plume-in-grid module to avoid unacceptably long model run times and because most sources in the OCS are far upwind of the receptor sites of interest. Nevertheless, consideration should be given to evaluating the sensitivity of model results to sub-grid-scale dispersion of plumes from offshore point sources in future studies given the limited turbulence and resulting long coherent plume lifetimes which can occur in the marine boundary layer.
- **BCs:** BCs for the 36-km domain were derived from a GEOS-Chem GCM run for 2012 as described above. BCs for the 12/4-km model runs were based on BCs extracted from the 36-km simulations. The lateral BCs for the 36-km grid were based on results from a GEOS-Chem v10-01 GCM simulation for year 2012 with halogen chemistry added by Ramboll and reduced lightning NO_x (as implemented in v11-01). Ramboll used the GEOS2CAMx processor to interpolate from the GEOS-Chem horizontal and vertical coordinate system to the CAMx coordinate system and to map the GEOS-Chem chemical species to the CAMx chemical mechanisms. Maximum ozone precursor BC concentrations were capped along the Gulf and southeast Atlantic boundaries as implemented by Johnson et al. (2015) to minimize overpredictions of ozone formation in the southeastern U.S.; no cap was applied to ozone BC concentrations.
- **Advection/diffusion methods:** The piecewise parabolic method advection solver was used for horizontal transport (Colella and Woodward, 1984) along with the spatially varying (Smagorinsky, 1963) horizontal diffusion approach. CAMx used K-theory for vertical diffusion with CMAQ-like vertical diffusivities from WRFCAMx.
- **ICs:** The 36-km simulation used default ICs that represent clean remote conditions. A 10-day spin-up period was then used to eliminate any significant influence of the ICs. ICs and BCs for the nested (12/4-km) grid simulations were extracted from the parent (36-km) grid simulation outputs with a shorter (three-day) spin-up period.

Table 4-8. CAMx Model Configuration

Science Options	Configuration	Notes
Model codes	CAMx V6.40	-
Horizontal grid	36/12/4 km	See Figure 2-1
36-km grid	148 x 112 cells	
12-km grid	254 x 176 cells	
4-km grid	299 x 200 cells	
Vertical grid	28 vertical layers (layer-collapsed from 36 WRF layers)	See Table 4-6
Grid interaction	36/12-km one-way nesting	-

Science Options	Configuration	Notes
	12/4-km two-way nesting	
ICs	Clean ICs	Use 10-day spin-up for the 36-km grid; three-day spin-up for the nested (12/4-km) grids
BCs	36 km from GCM simulation	2012 output data from GEOS-Chem v10-01 GCM run with added halogen chemistry and reduced lightning NO_x (from v11-01 update)
Land use data	Land use fields based on USGS GIRAS data	Added explicit distinction between ocean and fresh water for properly generating in-line inorganic reactive iodine emissions
Photolysis rate preprocessor	TUV V4.8	Clear-sky photolysis rates based on day-specific data
Chemistry		
Gas phase	CB6r4	Updated isoprene chemistry; heterogeneous hydrolysis of organic nitrates; active methane chemistry and ECH_4 tracer species (Hildebrandt Ruiz and Yarwood, 2013); I-16b halogen chemistry and in-line inorganic reactive iodine emissions (Yarwood et al., 2014; Emery et al., 2016a)
Aerosol phase	CF	Coarse and fine mode aerosols
Meteorological input preprocessor	WRFCAMx V4.3	Compatible with CAMx V6.40
Diffusion Scheme		
Horizontal grid	Explicit horizontal diffusion	Spatially varying horizontal diffusivities determined based on the methods of Smagorinsky (1963)
Vertical grid	K-theory 1st-order closure	WRFCAMx-derived vertical diffusivities based on the YSU PBL scheme (Hong and Noh, 2006); land use dependent minimum diffusivity (minimum Kv = 0.1 to 1.0 m^2/s) with cloud Kv patch to address deep convective mixing (ENVIRON, 2012)
Deposition Scheme		
Dry deposition	ZHANG03	Dry deposition scheme by Zhang et al. (2001; 2003)
Wet deposition	CAMx-specific formulation	Scavenging model for gases and aerosols (Seinfeld and Pandis, 1998); improved algorithm for gas and PM uptake to precipitation (Emery et al., 2016b)
Numerical Solvers		
Gas-phase chemistry	Euler Backward Iterative solver	Hertel et al., 1993
Horizontal advection	Piecewise parabolic method	Colella and Woodward, 1984
Vertical advection	Implicit scheme w/vertical velocity update	-

4.5 Model Performance Evaluation

Ramboll compared the results from the CAMx base case model runs with available air quality observations within the 12/4-km domain to evaluate the model's ability to accurately reproduce observed

conditions. The CAMx MPE focused on ozone and PM species, as these predictions play the primary role in the air quality impact analysis. Evaluation of the CAMx 2012 base case simulation followed USEPA's PGM guidance (USEPA, 2014a). The MPE used the Atmospheric Model Evaluation Tool (AMET),[8] which is discussed in USEPA's latest PGM guidance (USEPA, 2014a). AMET requires that a monitoring site have at least 75 percent valid data capture to be used in the MPE, which eliminated observed data from some sites.

4.5.1 Implications of WRF Model Performance on PGM Simulations

Section 2 presents the WRF MPE results. The meteorological model performance's effects on PGM modeled concentrations, visibility, and deposition are difficult to predict because of the multiple effects the meteorological model can have. As described in Section 2 of this report, overall WRF model performance was found to be good with no indications of any unusual significant impediments to PGM performance due to errors in meteorology.

4.5.2 Ambient Data Used in the MPE

Ozone model performance was evaluated using observed hourly and daily maximum 8-hour (DMAX8) ozone concentrations from the USEPA's Air Quality System (AQS)[9] and the Clean Air Status and Trends Network (CASTNet).[10] Figure 4-9 displays the locations of the AQS ozone sites in the 4-km domain used in the MPE. Also shown in Figure 4-9 are CASTNet ozone monitoring sites in the southeastern U.S. used in the MPE; only the ALC18 site is within the 4-km domain. Ozone date from the SouthEastern Aerosol Research and CHaracterization network (SEARCH) monitoring network (see Figure 4-10) were also used in the MPE; the Outlying Landing Field (OLF) and Gulfport (GFP) sites lie within the 4-km domain. Historically, CASTNet ozone monitoring sites operated by the National Park Service (NPS) were included as part of the AQS (i.e., ozone compliance monitors), while those operated by the USEPA were not. This changed several years ago, and now all CASTNet ozone data are also reported in the AQS. Apart from this overlap, most AQS monitoring sites tend to be more urban-oriented, while CASTNet sites tend to be more rural. Therefore, this study presents separate performance results for the AQS and CASTNet monitoring sites to gain insight into ozone performance at urban versus rural sites.

[8] https://www.cmascenter.org/help/documentation.cfm?MODEL=amet&VERSION=1.1

[9] https://www.epa.gov/aqs

[10] http://java.epa.gov/castnet/

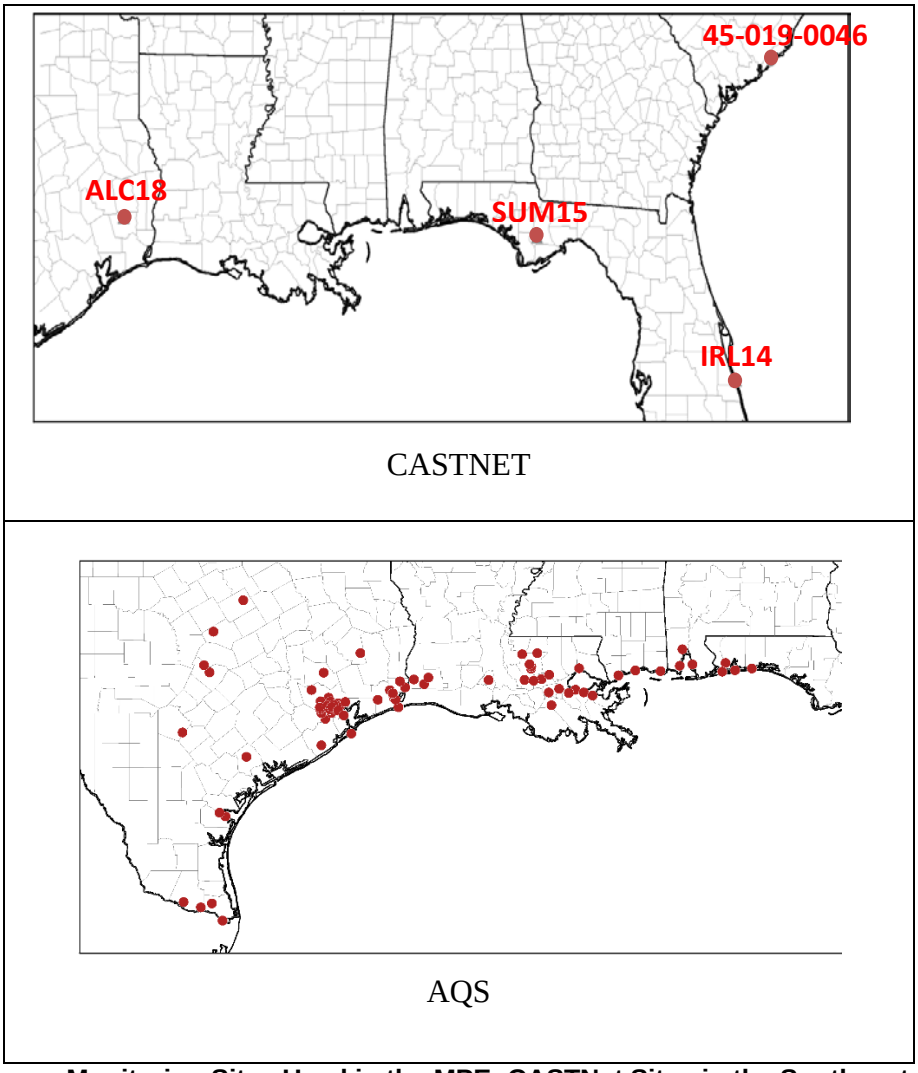

Figure 4-9. Ozone Monitoring Sites Used in the MPE: CASTNet Sites in the Southeastern U.S. (top) and AQS Sites Within the 4-km Modeling Domain (bottom)

Ramboll evaluated $PM_{2.5}$ model performance using observed speciated PM data from the Chemical Speciation Network (CSN), Interagency Monitoring of PRotected Visual Environments (IMPROVE),[11] and SEARCH monitoring sites in the southeastern U.S., as shown in Figure 4-10. Note that only six of the SEARCH sites (North Birmingham (BHM), Centreville (CTR), GFP, Jefferson Street (JST), OLF, and Yorkville (YRK)) collected data in 2012. These data were augmented by 24-hour integrated total $PM_{2.5}$ mass measurements using Federal Reference Method (FRM) or equivalent method monitoring sites reporting to the AQS. Most of these FRM sites collect samples once every three days, although some collect data every day. CSN data consist of 24-hour integrated particulate samples analyzed for SO_4, NO_3, NH_4, EC, organic carbon (OC), and elements using a one-in-three- or one-in-six-day sampling frequency. The IMPROVE network collects 24-hour average $PM_{2.5}$ and PM_{10} mass and speciated $PM_{2.5}$ concentrations (with the exception of ammonium [NH_4]) using a one-in-three-day sampling frequency. SEARCH network data consist of hourly and 24-hour $PM_{2.5}$ mass and speciated $PM_{2.5}$ data (including NH_4). The FRM and CSN monitoring sites tend to be more urban, whereas the IMPROVE sites are mostly located at National Parks and wilderness areas and are thus more rural.

[11] http://vista.cira.colostate.edu/IMPROVE/

Additional monitoring sites within the modeling domain collect hourly $PM_{2.5}$ and PM_{10} total mass. However, automated hourly PM measurements are in some cases subject to additional measurement artifacts and uncertainties relative to data collected on filters and do not include speciated PM measurements. Although MPE results were generated using hourly PM data, they are not shown here for the sake of brevity and to maintain consistency with the 24-hour PM NAAQS and the speciated PM results. Some hourly PM data, including speciated PM data, are available at SEARCH network sites. Comparison of MPE results for model bias and error did not show large overall differences between the hourly and daily SEARCH network comparisons.

Nitrate and sulfate wet deposition data from the National Acid Deposition Monitoring Network (NADP, 2016) were used for comparison with modeled deposition values. Three NADP sites are located within the 4-km modeling domain: site LA30 in Washington Parrish, Louisiana, north of New Orleans; site TX03 in Bee County, Texas, northwest of Corpus Christi; and site TX10 in Colorado County, Texas, west of Houston.

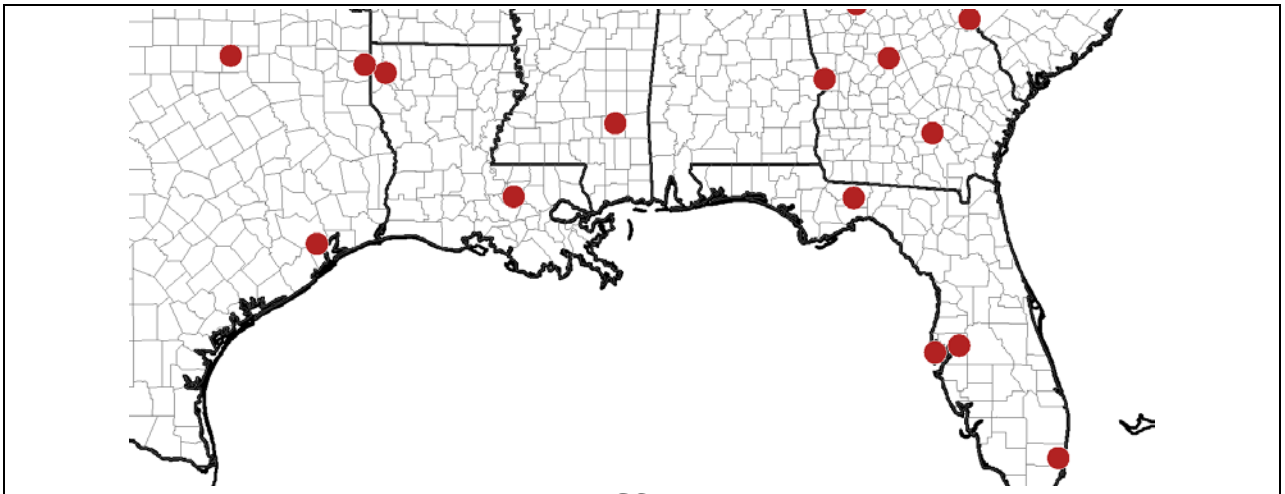

CSN

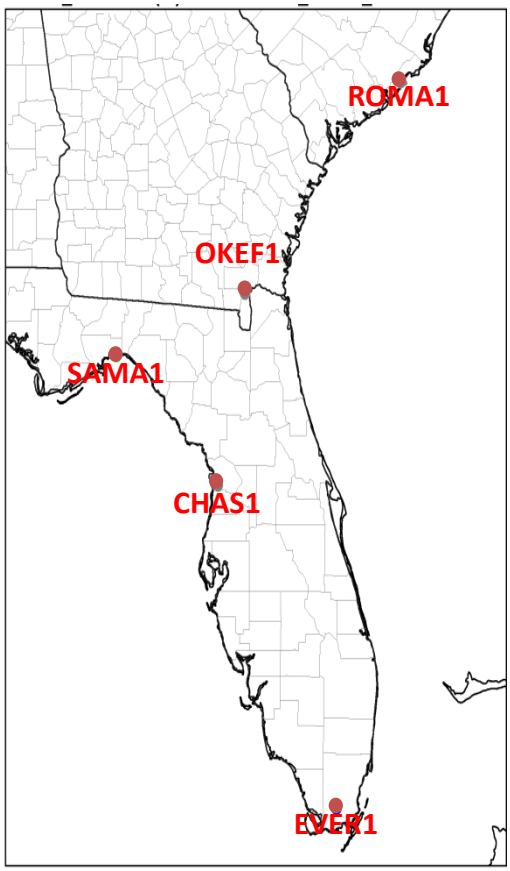

IMPROVE

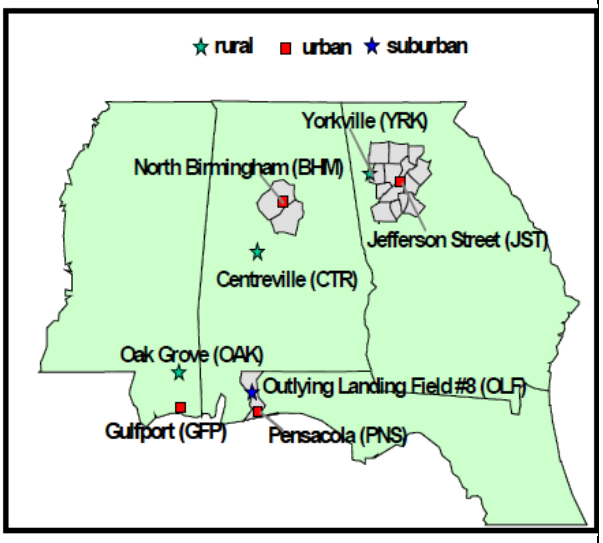

SEARCH (source: EPRI, 2011)

Figure 4-10. Speciated PM Monitoring Sites Used in the MPE: CSN Network (top), IMPROVE Network (bottom left), and SEARCH Network (bottom right)

4.5.3 Model Performance Statistics

Table 4-9 defines statistical performance measures applicable to the air quality MPE.

Table 4-9. Definitions of MPE Statistical Metrics

Statistical Measure	Mathematical Expression	Notes
Ap: Accuracy of paired peak	$\frac{P - O_{peak}}{O_{peak}}$	Comparison of the peak observed value (O_{peak}) with the predicted value at same time and location
NME: Normalized Mean Error	$\frac{\sum_{i=1}^{N}\lvert P_i - O_i\rvert}{\sum_{i=1}^{N} O_i}$	Reported as %
RMSE: Root Mean Squared Error	$\left[\frac{1}{N}\sum_{i=1}^{N}(P_i - O_i)^2\right]^{1/2}$	Reported as %
FE: Fractional Gross Error	$\frac{2}{N}\sum_{i=1}^{N}\left\lvert\frac{P_i - O_i}{P_i + O_i}\right\rvert$	Reported as % and bounded by 0% to 200%
MAGE: Mean Absolute Gross Error	$\frac{1}{N}\sum_{i=1}^{N}\lvert P_i - O_i\rvert$	Reported as concentration (e.g., µg/m^3)
MNGE: Mean Normalized Gross Error	$\frac{1}{N}\sum_{i=1}^{N}\frac{\lvert P_i - O_i\rvert}{O_i}$	Reported as %
MB: Mean Bias	$\frac{1}{N}\sum_{i=1}^{N}(P_i - O_i)$	Reported as concentration (e.g., µg/m^3)
MNB: Mean Normalized Bias	$\frac{1}{N}\sum_{i=1}^{N}\frac{(P_i - O_i)}{O_i}$	Reported as %
FB: Fractional Bias	$\frac{2}{N}\sum_{i=1}^{N}\left(\frac{P_i - O_i}{P_i + O_i}\right)$	Reported as %, bounded by -200% to +200%
NMB: Normalized Mean Bias	$\frac{\sum_{i=1}^{N}(P_i - O_i)}{\sum_{i=1}^{N} O_i}$	Reported as %

For over two decades, ozone model performance for bias and error has been compared against the USEPA's 1991 ozone modeling guidance model performance goals as follows (USEPA, 1991):

- MNB $\leq \pm 15\%$
- MNGE $\leq 35\%$

In the USEPA's 1991 ozone modeling guidance, these performance metrics were for hourly ozone concentrations that were consistent with the form of the ozone NAAQS in those days. The MNB performance statistic uses hourly predicted and observed ozone concentrations paired by time and

location and is defined as the difference between the predicted and the observed hourly ozone divided by the observed hourly ozone concentrations averaged over all predicted/observed pairs within a given region and for a given time period (e.g., by day, month, or modeling period). The MNGE is defined similarly, only it uses the absolute value of the difference between the predicted and observed hourly ozone concentrations and is thus an unsigned metric. Because the MNB and MNGE performance metrics divide by the observed ozone concentrations, they weigh performance for low ozone concentrations highly and can become unstable as the observed ozone approaches zero. Consequently, they are no longer recommended. Instead, the FB/FE and NMB/NME are the preferred bias and error statistical performance measures (USEPA, 2014a).

For PM species, a separate set of model performance statistics and performance goals and criteria have been developed as part of the regional haze modeling performed by several RPOs. The USEPA's modeling guidance notes that PM models might not be able to achieve the same level of model performance as ozone models. Indeed, $PM_{2.5}$ species definitions are defined by the measurement technology used to measure them, and different measurement technologies can produce very different $PM_{2.5}$ concentrations. Given this, several researchers have developed PM model performance goals and criteria that are less stringent than the ozone goals that are shown in Table 4-10 (Boylan, 2004; Boylan and Russell, 2006; Morris et al., 2009a, b). However, unlike the 1991 ozone model performance goals that use the MNB and MNGE performance metrics, the FB and FE are typically used for PM species with no observed concentration threshold screening. The FB/FE differs from the MNB/MNGE in that it divides the difference in the predicted and observed concentrations by the average of the predicted and observed values, rather than just the observed value as in the MNB/MNGE. This results in the FB being bounded by -200% to +200% and the FE being bounded by 0% to +200%. Additional statistical performance metrics evaluate correlation, scatter, and NMB/NME, as shown in Table 4-10.

Table 4-10. Ozone and PM Model Performance Goals and Criteria

Bias (FB/NMB)	Error (FE/NME)	Comment
≤±15%	≤35%	Ozone model performance goal that would be considered very good for PM species
≤±30%	≤50%	PM model performance goal; considered good PM performance
≤±60%	≤75%	PM model performance criteria; considered average PM performance

More recently, the USEPA compiled and interpreted the model performance from 69 PGM studies in the peer-reviewed literature between 2006 and March 2012 and developed recommendations on what should be reported in an MPE (Simon, Baker and Phillips, 2012). Although these recommendations are not official USEPA guidance, Ramboll integrated the following recommendations in this CAMx MPE:

- PGM MPE studies should at a minimum report the mean bias (MB) and mean error (ME) or alternatively, the root mean square error (RMSE), normalized mean bias (NMB) and normalized mean error (NME), and/or fractional bias (FB) and fractional error (FE).
- Use of the MNB and MNGE is not encouraged because they are skewed toward low observed concentrations and can be misinterpreted due to the lack of symmetry around zero.
- The model evaluation statistics should be calculated for the highest temporal resolution available (e.g., hourly ozone) and for important regulatory averaging times (e.g., DMAX8 ozone).
- It is important to report processing steps, how the predicted and observed data were paired, and whether data are spatially/temporally averaged before the statistics are calculated.

- Predicted values should be taken from the grid cell that contains the monitoring site, although bilinear interpolation to the monitoring site point can be used for higher-resolution modeling (< 12 km).

- $PM_{2.5}$ should also be evaluated separately for each major component species (e.g., SO_4, NO_3, NH_4, EC, OA, and remainder other $PM_{2.5}$ [$OPM_{2.5}$]).

- Evaluation should be performed for subsets of the data, including high observed concentrations (e.g., ozone > 60 ppb), by subregion and by season or month.

- Spatial displays should be used to evaluate model predictions away from the monitoring sites. Time series of predicted and observed concentrations at a monitoring site should also be used.

- It is necessary to understand measurement artifacts to meaningfully interpret the MPE.

4.5.4 Approach

The PGM evaluation focused on both hourly and daily maximum 8-hour (DMAX8) ozone concentrations; total $PM_{2.5}$ mass and speciated $PM_{2.5}$ concentrations; gaseous NO_2, SO_2, and CO concentrations; and visibility. Ramboll performed the evaluation across all monitoring sites within either the southeastern U.S., as shown in the top panel of Figure 4-10 (to capture the regional CSN and IMPROVE network sites), or the 4-km modeling domain (Figure 2-1). Ramboll also evaluated each individual site on an annual, seasonal (quarterly), and monthly basis. In addition to generating numerous statistical performance metrics (see Table 4-9), Ramboll depicted model performance using four main types of graphical displays:

- Soccer plots of monthly bias and error that are compared against the ozone performance goals and the PM performance goals and criteria (see Table 4-9). Monthly soccer plots allowed Ramboll to easily identify when performance goals/criteria were achieved and evaluate performance across seasons.

- Spatial statistical performance maps that display bias/error on a map at the monitoring site locations to better understand spatial attributes of model performance along with tabular summaries of statistical performance metrics.

- Time series plots that compare predicted and observed concentrations at a monitoring site as a function of days.

- Scatter plots of predicted and observed concentrations.

Ramboll produced all performance statistics and displays by matching the predicted and observed concentrations with time and location using the modeled prediction in the 12/4-km grid cell containing the monitoring site.

Ramboll evaluated CAMx model performance for PM by comparing total $PM_{2.5}$ mass and speciated $PM_{2.5}$ measurements against the PM performance goals and criteria in Table 4-10. The PM goals and criteria are not as stringent as those for ozone because the measurements and the PM emissions are much more uncertain; more processes are also involved in PM (e.g., dispersion, transformation and deposition of primary PM, and formation of secondary PM from gaseous precursors). Each PM measurement technique has its own artifacts; different measurement technologies could produce observed $PM_{2.5}$ values that differ by as much as 30 percent. The USEPA's latest PGM guidance includes a section on PM measurement artifacts for monitoring technologies used in routine U.S. networks (USEPA, 2014a). Thus, the PM model performance needs to account for these measurement uncertainties and artifacts when interpreting model performance, as even a "perfect" model may not achieve the PM performance goals and criteria.

PM_{10} consists of fine ($PM_{2.5}$) and coarse (PMC) modes. $PM_{2.5}$ is composed of the following component species:

- SO_4—typically in the form of ammonium sulfate
- NO_3—typically in the form of ammonium nitrate but may also occur to some extent as sodium nitrate in coastal areas impacted by sea salt aerosols
- NH_4—associated with SO_4 and NO_3
- EC—also called black carbon and light absorbing carbon
- OA—includes primary and secondary organic aerosol and is composed of OC and other atoms (e.g., oxygen) that adhere to the OC
- $OPM_{2.5}$—primarily crustal in nature (soil) but can also include other compounds as well as measurement artifacts, determined by subtracting the sum of individual measured species from the measured total $PM_{2.5}$

Ramboll calculated model performance statistics for total PM mass using observations from the FRM, CSN, SEARCH, and IMPROVE networks, and then evaluated PM_{10} and $PM_{2.5}$ component species using data from the CSN, SEARCH, and IMPROVE sites.

4.5.5 MPE Results

This section presents the results of the MPE for the 12/4-km grid run.

4.5.5.1 Ozone

The Figure 4-11 soccer plots summarize model performance results for ozone in terms of monthly NMB and NME for AQS and CASTNet network monitors within the 4-km and 12-km domains. Model performance for most months is within the ± 15 percent NMB and < 35 percent NME ozone performance goals listed in Table 4-10 (which corresponds to the innermost “goal” box shown in the figure), with the principal exceptions being performance during July, August, and September. Note that only one CASTNet site—ALC188, Alabama-Coushatta in Polk County, Texas—is located within the 4-km domain. This site recorded generally low (30 to 40 ppb) ozone concentrations during most of July, which CAMx overpredicted (see Figure 4-12).

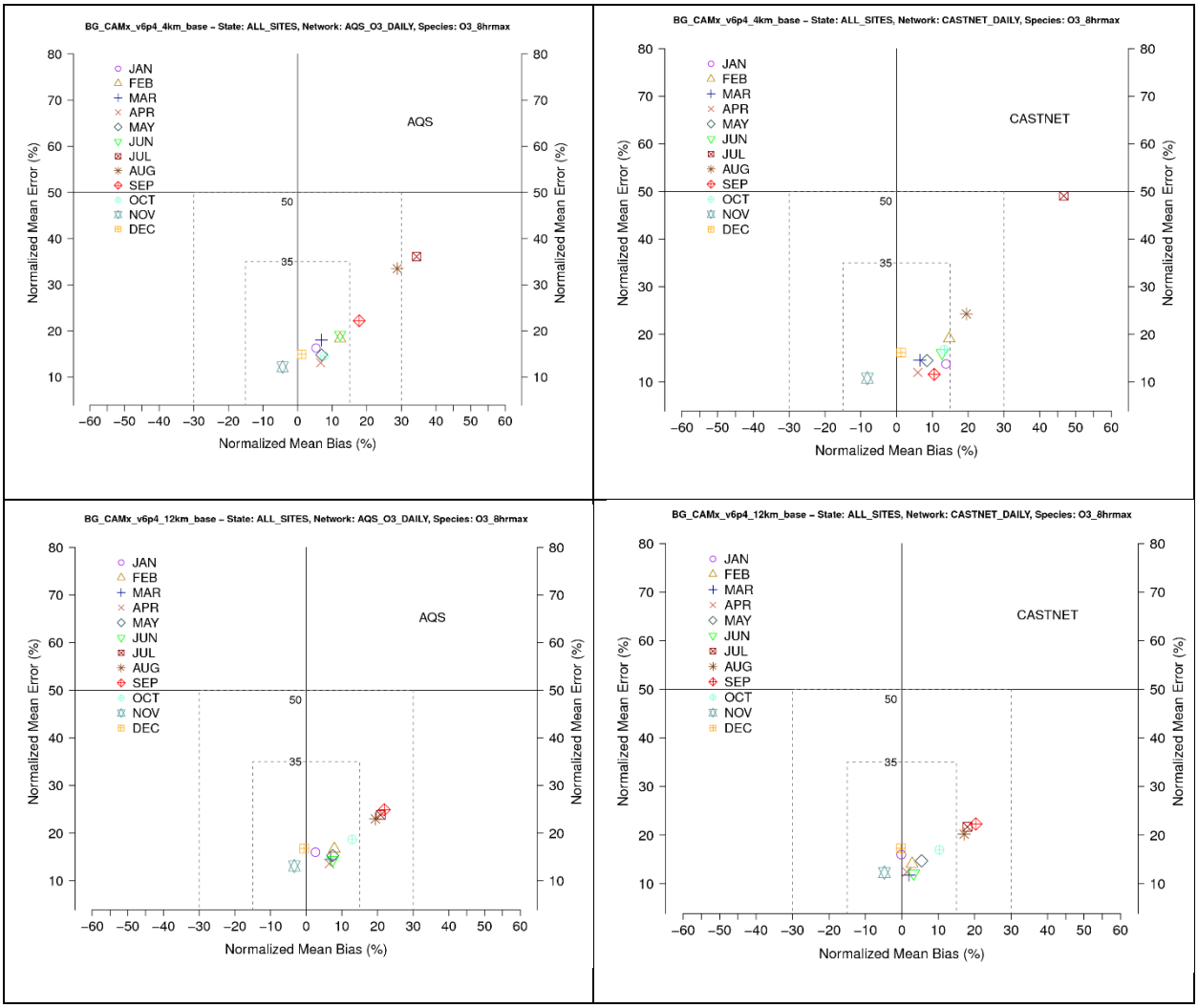

Figure 4-11. Monthly NMB and NME for DMAX8 Average Ozone at AQS (left) and CASTNet (right) Monitoring Sites Within the 4-km (top) and 12-km (bottom) Domains

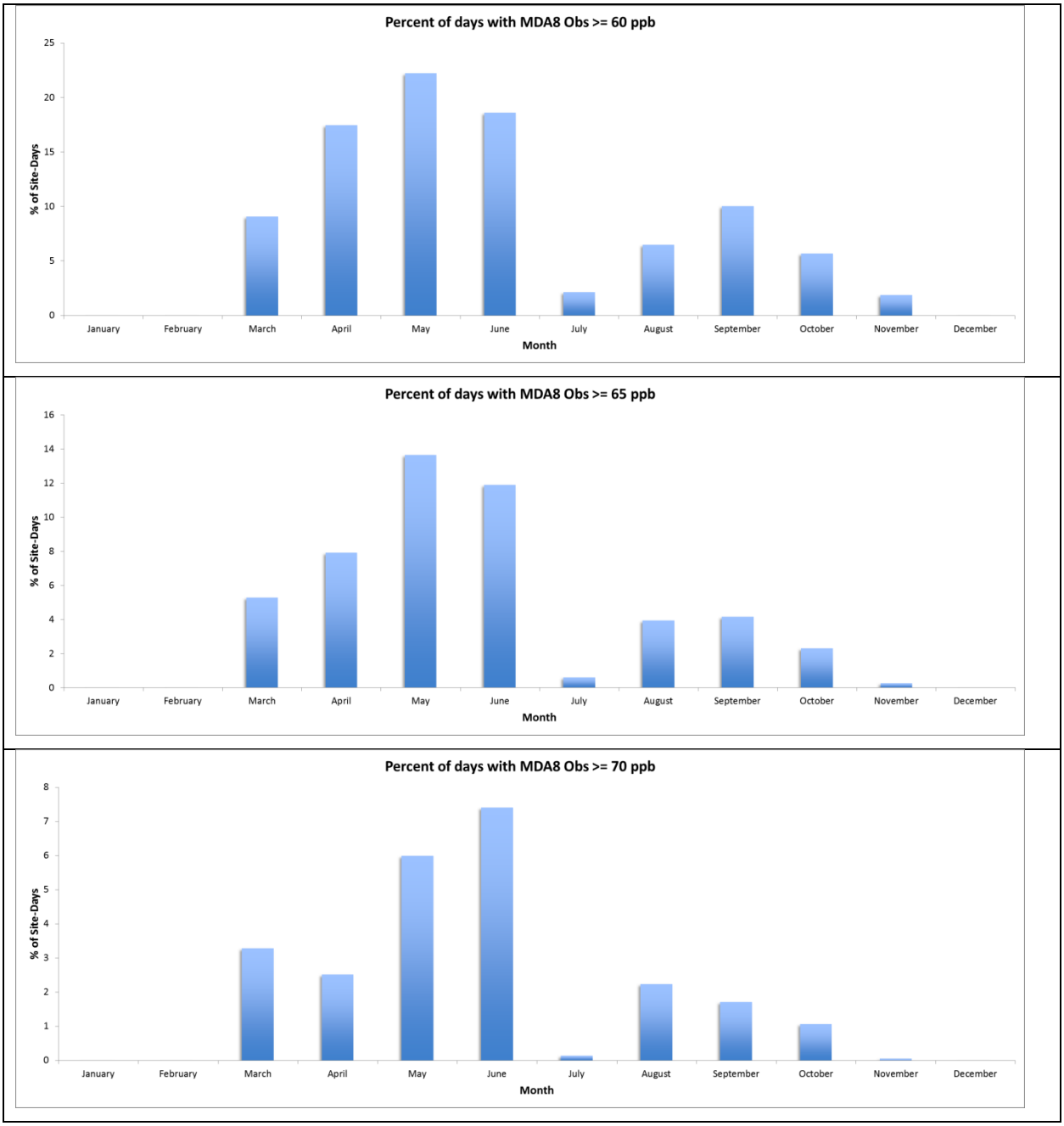

Figure 4-12. Fraction of Site-Days during Each Month of 2012 with Observed DMAX8 Ozone Exceeding 60 (top), 65 (middle), or 70 (bottom) ppb Over All Monitoring Sites in the 4-km Domain

As illustrated by the threshold exceedance counts in Figure 4-12, the ozone season in the southernmost U.S. generally follows a bimodal distribution with a pronounced ozone peak in spring and a secondary peak in late summer to early fall. There is a noticeable lack of high ozone events during July. This seasonal pattern is reproduced in the modeling results as shown in Figure 4-13. Ramboll summarized model performance statistics generated using the AMET tool by calendar quarter. Further analysis of ozone model performance results focuses on Q2 (April–June) and Q3 (July–September), as these roughly coincide with the seasonal ozone peaks.

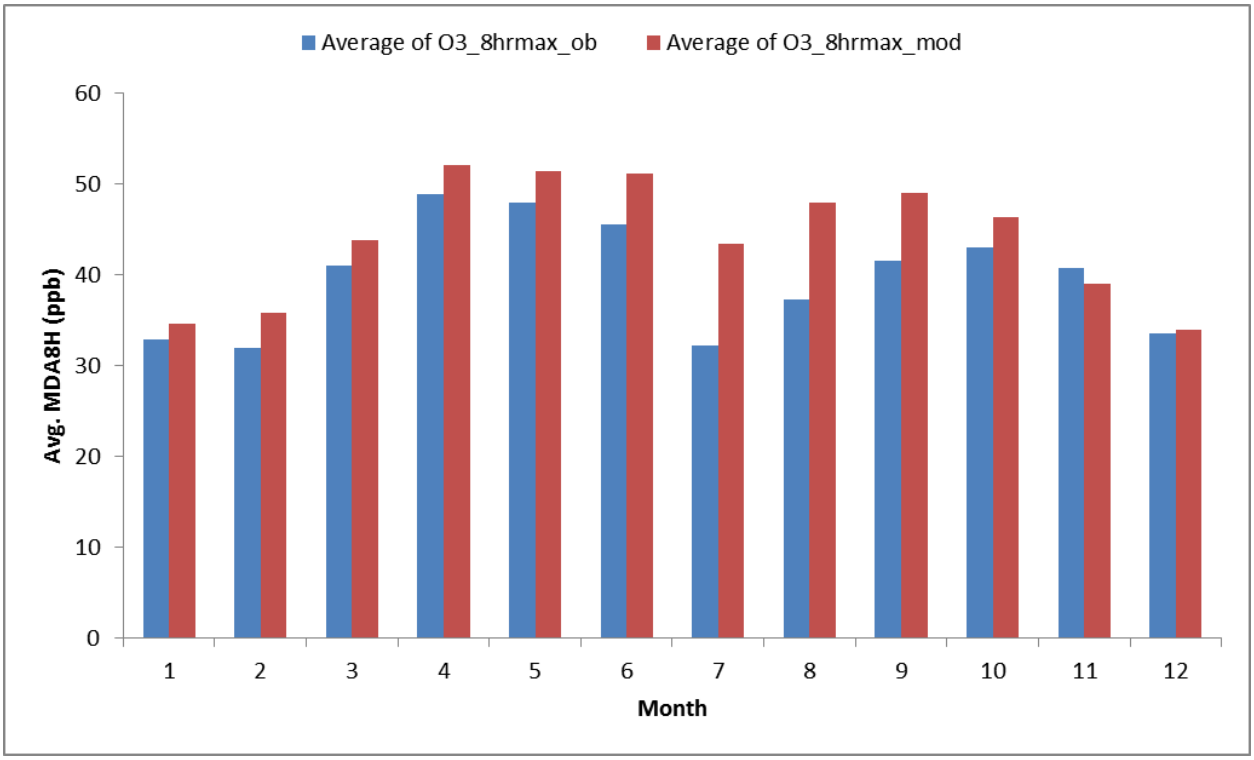

Figure 4-13. Observed (blue) and Predicted (red) Monthly Mean DMAX8 Average Ozone over All Sites in the 4-km Modeling Domain

The scatter plots in Figure 4-14 illustrate ozone model performance for Q2 (April–May) and Q3 (July–September) over sites in the 4-km domain. Standard scatter plots are shown in the left-hand column and corresponding scatter density plots are shown in the right-hand column. Colors in the scatter density plot indicate the normalized fraction of data in each 2-ppb bin, thus revealing the data density variations that are otherwise obscured in regions with numerous overlapping points in the standard scatter plots. Model performance in Q2 is better than in Q3, as evidenced by lower bias (NMB of 8.5 percent in Q2 versus 26.5 percent in Q3). The scatter density plots show that the Q3 bias is primarily associated with overprediction of mid- and low-range values with less bias for values exceeding 60 ppb. Summaries of ozone performance statistics with a 60-ppb observed ozone cut-off applied are further discussed below.

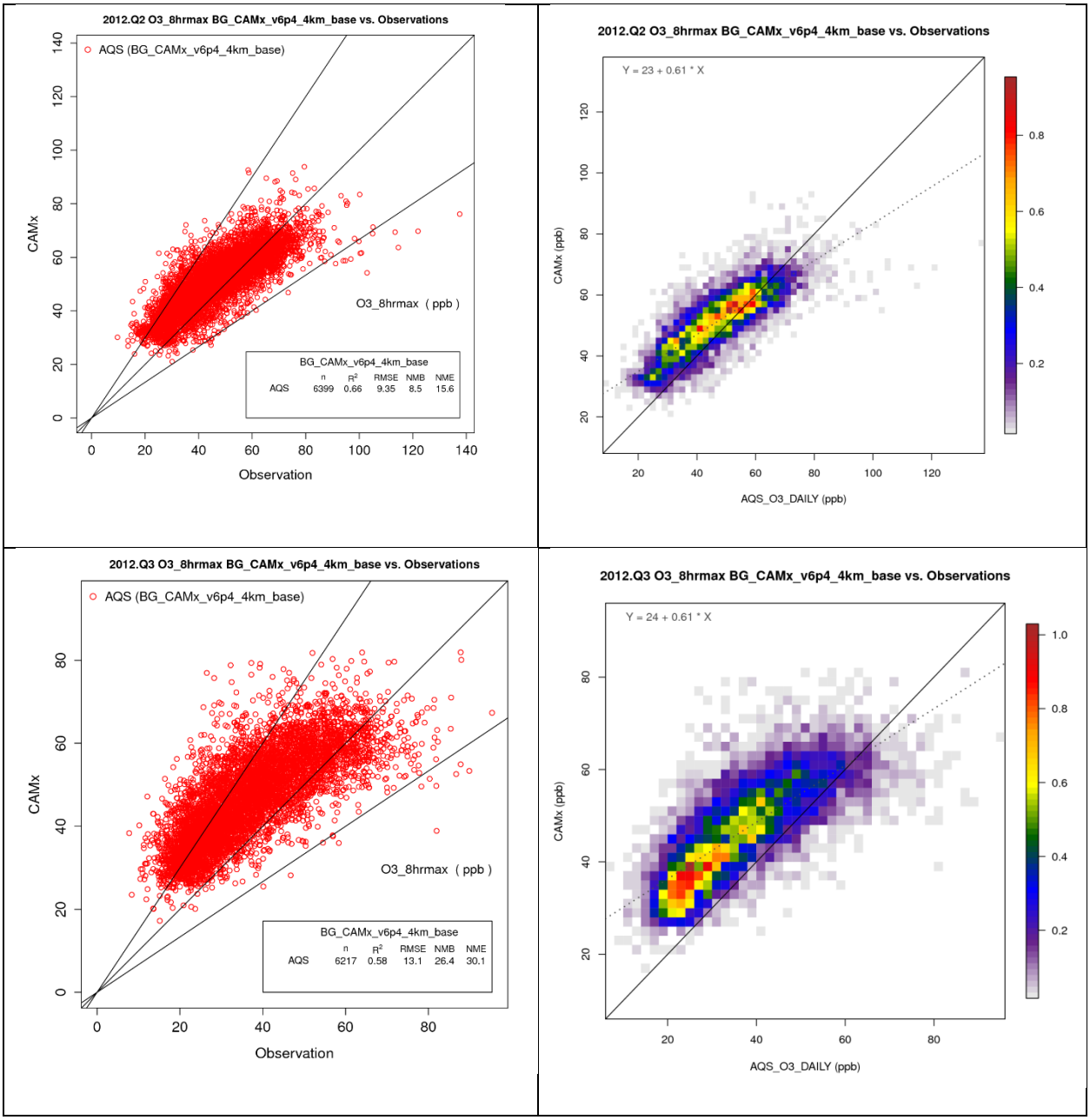

Figure 4-14. Scatter (left) and Scatter Density (right) Plots for Observed vs. Predicted DMAX8 Ozone in Q2 (top) and Q3 (bottom) for all AQS Monitoring Sites in the 4-km Modeling Domain
Note: Black lines in left panels indicate 1:1, i.e., perfect agreement, and ± 50% bounds; solid black line in right-hand panels indicate 1:1; dashed line is least squares regression fit as shown by regression equation in upper left.

Figure 4-15 shows the spatial distribution of NMB over the full 12-km domain. These results are based on the 12-km gridded model resolution for all sites shown. NMB is within ± 15 percent at most sites during Q2 but exceeds +15 percent at most sites along the Gulf Coast and throughout the southern tier and southeast Atlantic states in Q3.

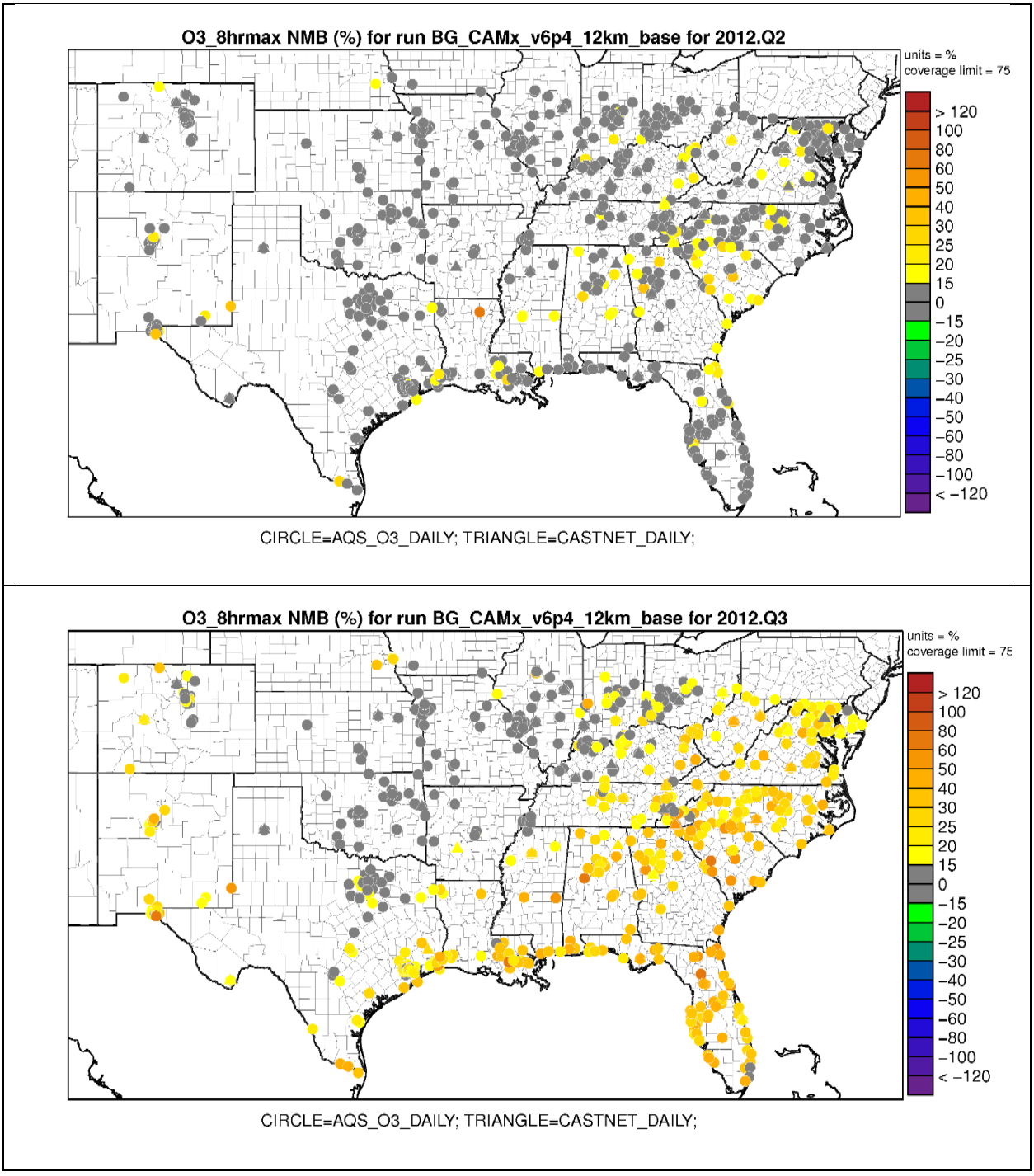

Figure 4-15. NMB for DMAX8 Ozone in Q2 (top) and Q3 (bottom) for the 12-km Domain

The USEPA recommends that ozone model performance statistics be calculated using a 60 ppb observed ozone concentration cut-off value (Simon, Baker and Philips, 2012; USEPA 2014). That is, the model performance statistics are calculated for all predicted and observed ozone pairs, matched by time and location, for which the observed value is 60 ppb or higher. Table 4-11 lists model performance summary statistics derived from the 4-km resolution model output for hourly and DMAX8 ozone with no concentration cut-off applied and with cut-offs of 40 or 60 ppb applied for Q2 and Q3. NMB and NME values that exceed the USEPA's performance goals are highlighted in Table 4-11. Biases trend from positive to slightly negative as the threshold concentration increases, but they are always within the

performance goal for Q2 (with the exception of hourly ozone NMB) and also under application of the 40 and 60 ppb thresholds in Q3. NME is always within the USEPA performance goal, except for hourly values in Q3 when no cut-off is applied.

Table 4-11. Model Performance Statistics at Different Observed Ozone Concentration Screening Thresholds Based on All Monitoring Sites in the 4-km Domain[a]

Monitor Site	Q2 (April–June)			Q3 (July–September)		
	N	NMB (%)	NME (%)	N	NMB (%)	NME (%)
USEPA Performance Goal	-	≤±15%	≤35%	-	≤±15%	≤35%
Ozone Cut-Off Concentrations	DMAX8 Ozone					
0	6,399	8.5	15.6	6,217	26.4	30.1
40	4,326	2.4	11.2	2,318	8.8	15.6
60	1,246	-6.8	10.0	375	-9.1	12.1
Ozone Cut-Off Concentrations	Hourly Ozone					
0	152,772	16.3	32.5	150,896	42.0	53.7
40	53,213	-3.3	16.1	22,751	2.4	19.0
60	11,229	-11.6	14.9	3,498	-13.7	17.4

[a] Red cells indicate values exceeding USEPA performance goals.

Time series of observed and predicted DMAX8 ozone are plotted[12] in Figure 4-16 for the monitoring site in each county in the Houston-Galveston-Brazoria ozone nonattainment area, with the highest ozone design values during the 2010–2014 design value periods (2010–2012, 2011–2013, 2012–2014): Northwest Harris County site (AQS ID 48-201-0029)[13]; Manvel Croix Park, Brazoria County (AQS ID 48-039-1004); and Galveston 99th St., Galveston County (AQS ID 48-167-1034).

Time series of observed and predicted DMAX8 ozone are plotted in Figure 4-17 for two monitoring sites in the former Baton Rouge ozone nonattainment area: Louisiana State University (LSU) (AQS ID 22-033-0003) and Carville (AQS ID 22-047-0012). These sites typically had the highest ozone design values in the Baton Rouge area during the 2010–2014 design value periods.

The time series for the ALC188 (Alabama-Coushatta, Texas) CASTNet site (the only CASTNet site in the 4-km domain) are shown in Figure 4-18.

Overall model performance as seen in these time series is good, especially in Q2 and in the Houston-Galveston area. The model tends to overpredict in Q3 at Galveston and more noticeably at the Baton Rouge sites and the CASTNet site, consistent with the results for all AQS sites presented above.

[12] Note occasional periods of missing data in the time series presented in this and other figures are identifiable as straight lines drawn between points two or more days apart.

[13] This site recorded either the maximum or was within 1 ppb of the maximum ozone design value of all sites in Harris County during this period.

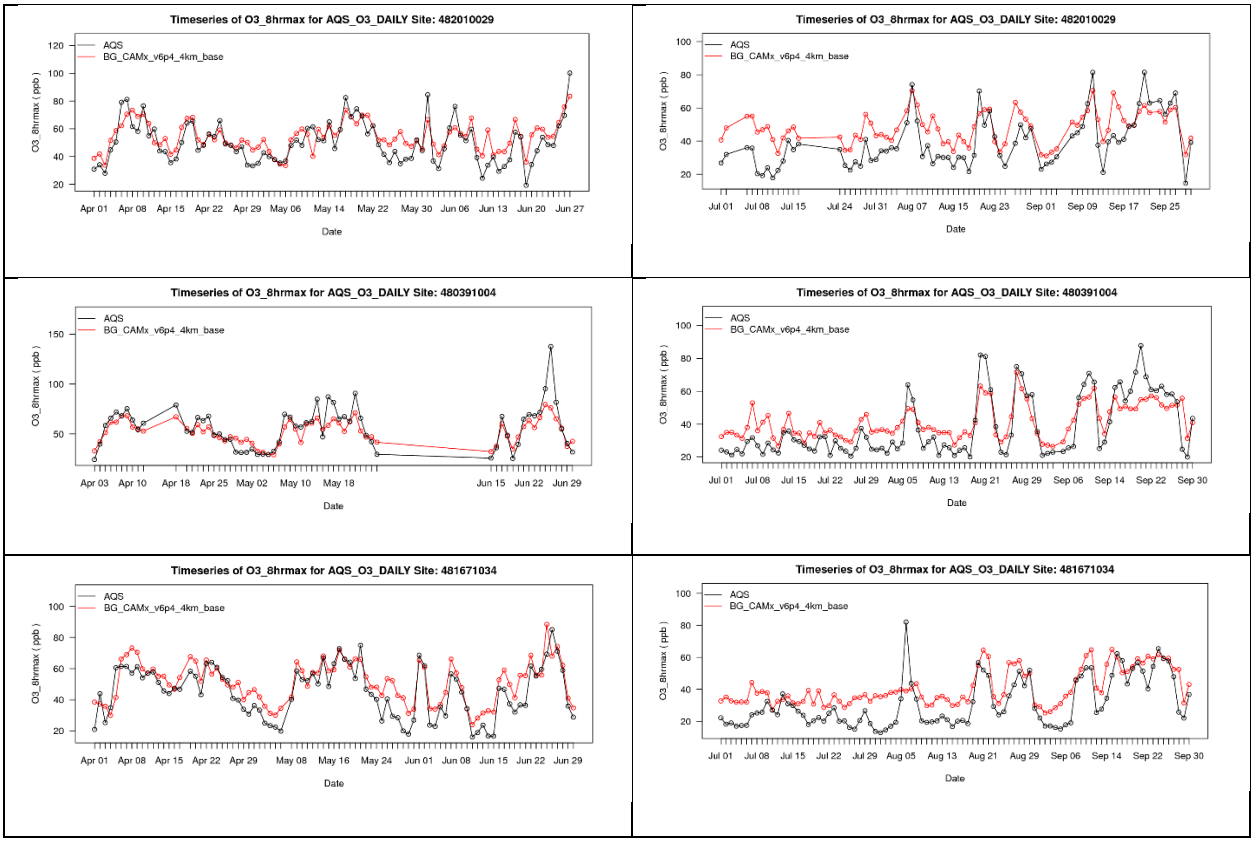

Figure 4-16. Time series of DMAX8 Ozone at Monitoring Sites with Highest Design Values in Harris (top), Brazoria (middle), and Galveston (bottom) Counties, Texas, for Q2 (left) and Q3 (right)

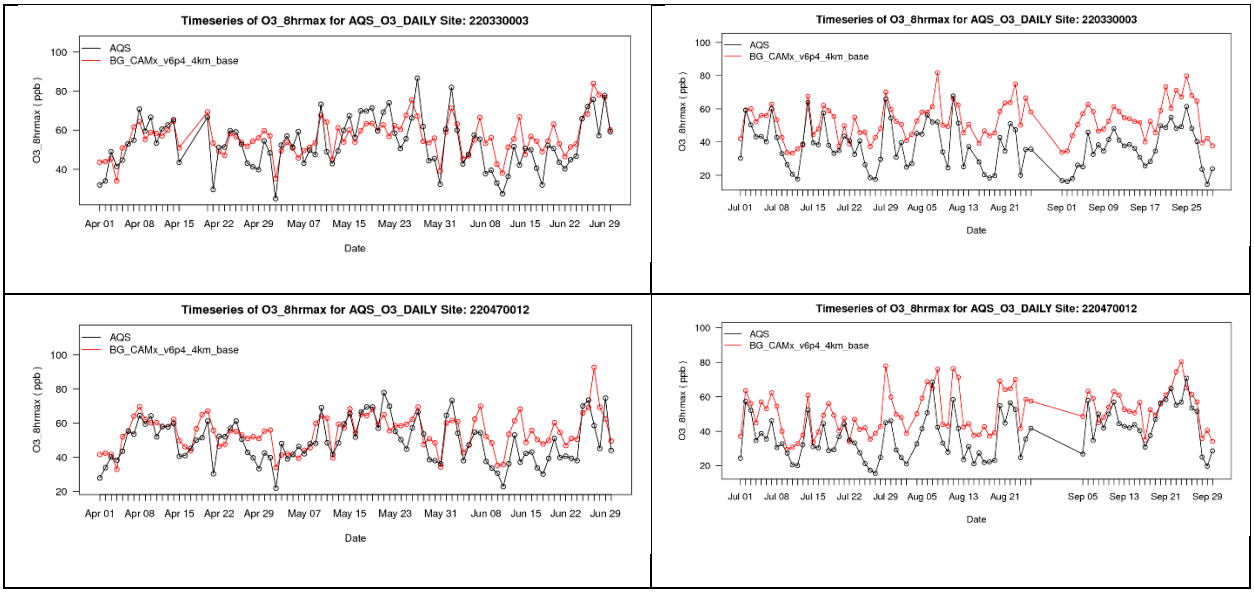

Figure 4-17. Time Series of DMAX8 Ozone at Monitoring Sites in the Former Baton Rouge Nonattainment Area: LSU (top) and Carville (bottom) for Q2 (left) and Q3 (right)

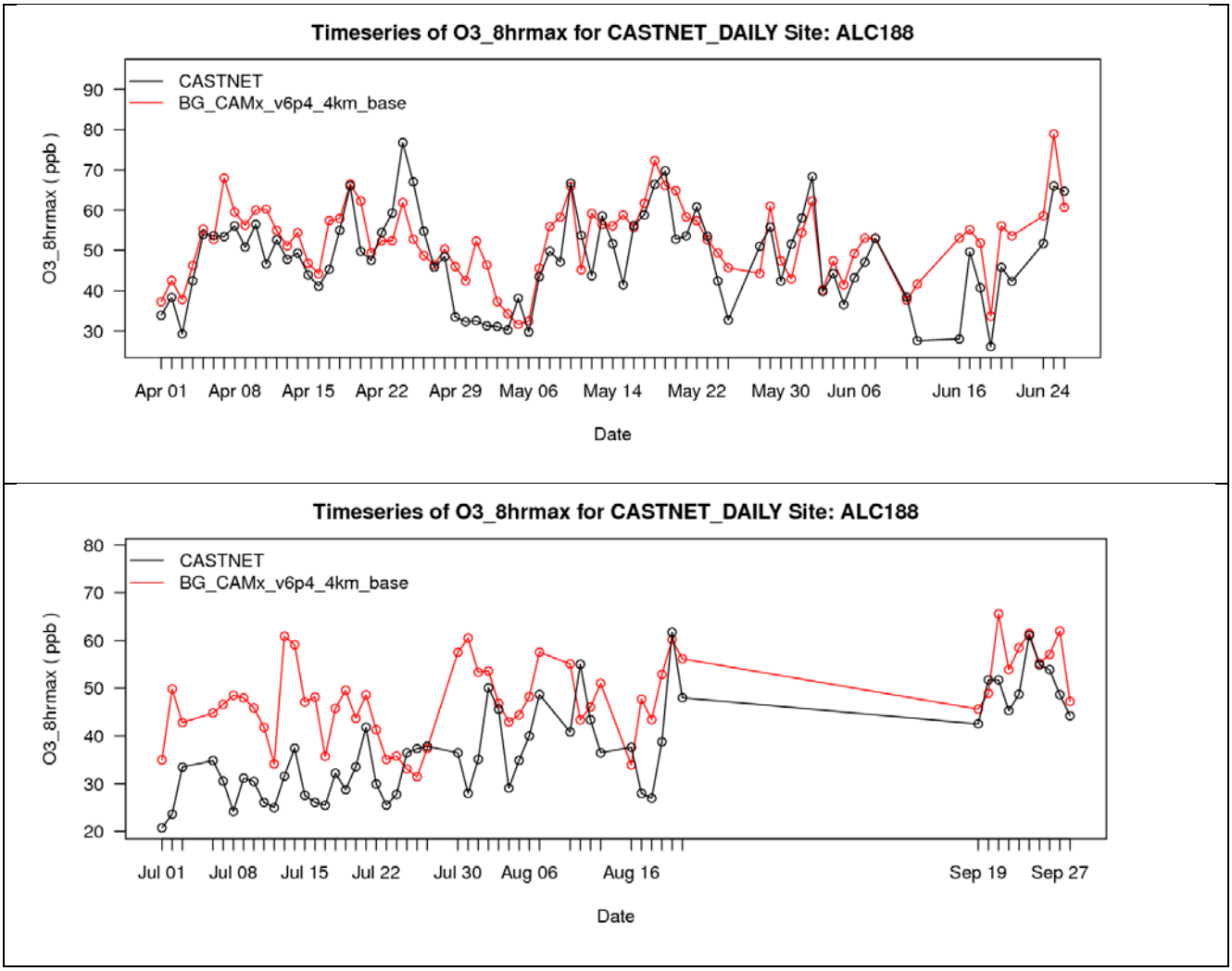

Figure 4-18. Time Series of DMAX8 Ozone at the ALC188 (Alabama-Coushatta, Texas) CASTNet Monitoring Site for Q2 (top) and Q3 (bottom)

4.5.5.2 Particulate Matter

Ramboll evaluated the CAMx model's PM performance for total $PM_{2.5}$ mass and speciated $PM_{2.5}$ measurements. Ramboll compared PM performance against the performance goals and criteria in Table 4-10. The PM goals and criteria are not as stringent as those for ozone because both PM measurements and PM emissions are subject to greater uncertainties, and PM formation and transformation processes are more complex and difficult to model. Each PM measurement technique has its own artifacts; different measurement technologies can produce different observed $PM_{2.5}$ values that differ by as much as 30 percent. The USEPA's latest PGM guidance includes a section on PM measurement artifacts for monitoring technologies used in routine U.S. networks (USEPA, 2014a). PM model performance results must be evaluated in light of these measurement uncertainties and artifacts, as even a "perfect" model may not achieve the PM performance goals and criteria relative to the imperfect measurements. As discussed above, PM_{10} consists of $PM_{2.5}$ and PMC modes.

Ramboll evaluated the CAMx 2012 base case simulation for total $PM_{2.5}$ mass using observations from the FRM, CSN, and IMPROVE monitoring networks and then evaluated for PM_{10} and $PM_{2.5}$ component species. Ramboll also used numerous hourly $PM_{2.5}$ and PM_{10} monitoring sites in the region in the MPE, but results for these are not presented here as they may suffer from additional measurement artifacts and uncertainties and are not directly comparable to the speciated PM data.

Daily total $PM_{2.5}$ mass was measured at FRM, IMPROVE, and CSN network monitors, and hourly $PM_{2.5}$ was measured at FRM equivalent and non-FRM monitoring sites. Because only three CSN sites and no IMPROVE network sites are located within the 4-km CAMx modeling domain, some performance statistics are presented here for all monitors within the southeastern U.S. domain shown in Figure 4-19.[14]

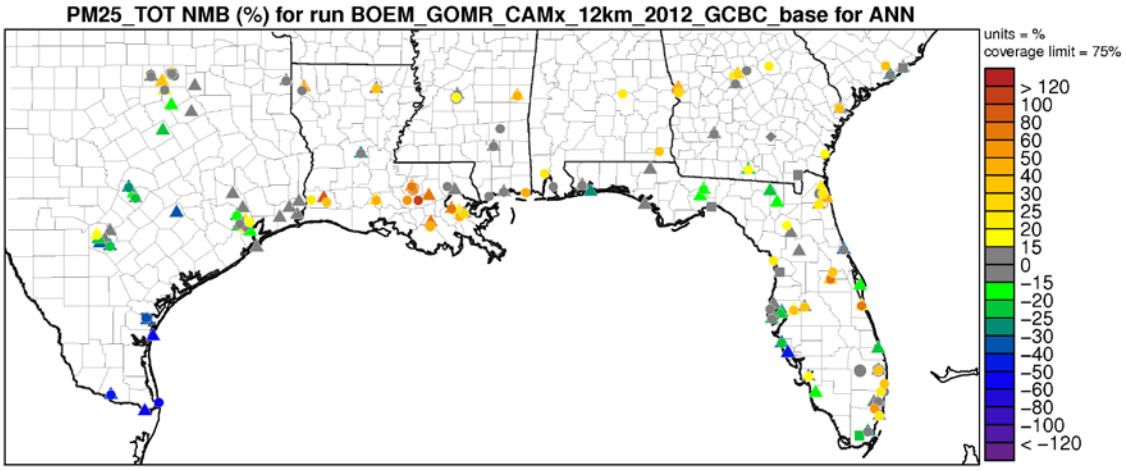

Figure 4-19. PM Monitoring Sites in the Southeastern U.S. Domain, Color-Coded to Indicate NMB of Annual Mean Values
Note: Triangles = AQS hourly, squares = IMPROVE, diamonds = CSN, circles = AQS FRM daily

Figure 4-20 displays soccer plots of total $PM_{2.5}$ mass model performance across the FRM (daily samples), CSN, and IMPROVE monitoring networks in the southeastern U.S. domain. These results are based on 12-km resolution CAMx output. The soccer plots include boxes that represent the performance goals for ozone (most inner), PM (middle), and the PM performance criteria (most outer) listed in Table 4-9. Performance for the late fall and winter months (October–January) is characterized by larger positive NMB and higher NME in each network. The sign of the bias is less consistent for December. This bias is somewhat more extreme in the FRM and CSN data. Performance results are within the PM performance criteria in all cases and within or nearly within the PM performance goals for most months except for January and October–December at FRM sites (positive bias) and May–August (and, to a lesser extent, April) at IMPROVE sites (negative bias).

[14] This area corresponds to the high-resolution domain used for the meteorological (WRF) modeling described in Section 2 and lies within the 12-km photochemical modeling domain.

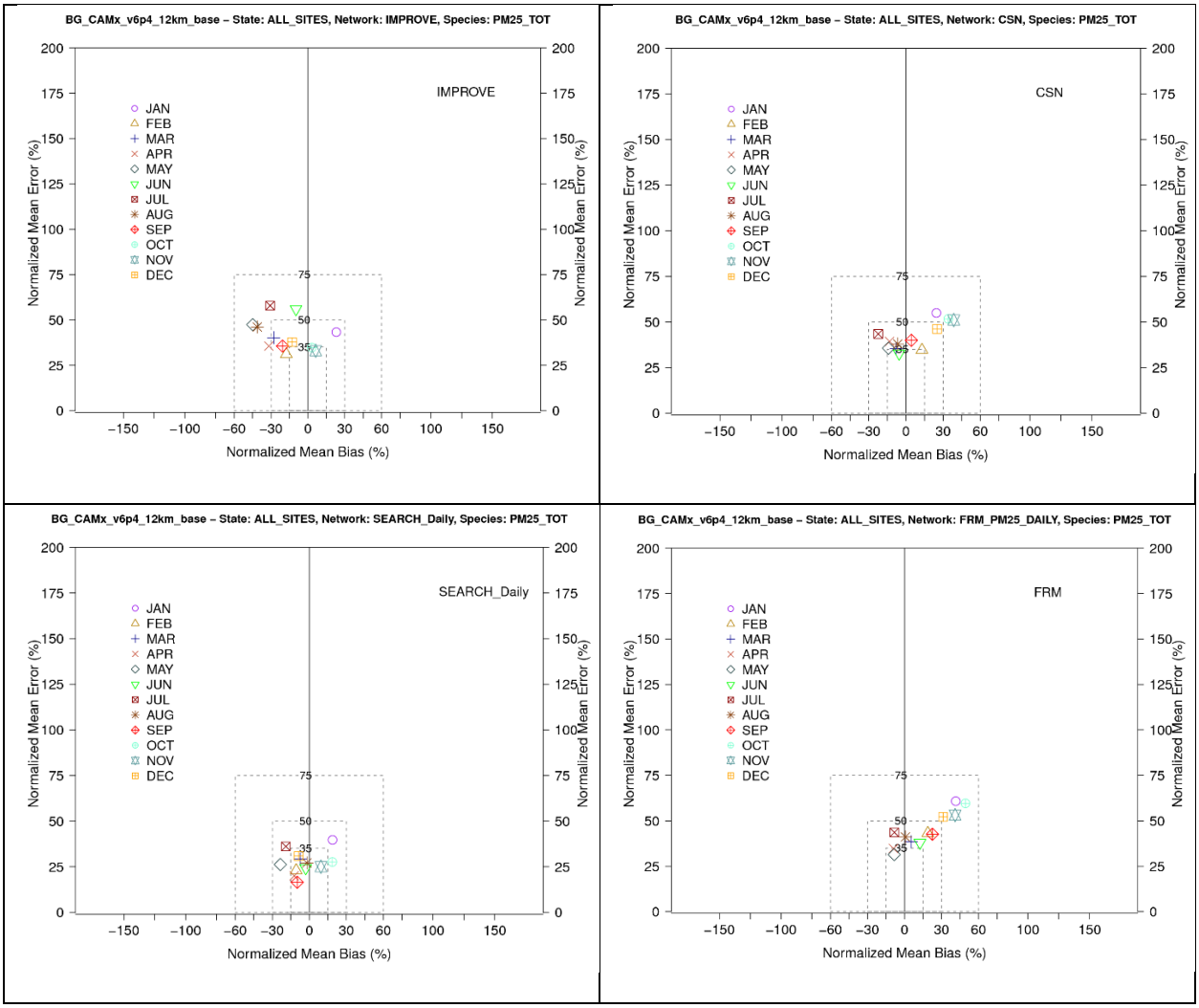

Figure 4-20. Soccer Plots of Total $PM_{2.5}$ Mass Model Performance Across the IMPROVE (top left), CSN (top right), SEARCH (bottom left), and FRM Daily (bottom right)
Note: Monitoring networks for sites in the southeastern U.S. domain shown in Figure 4-19.

As illustrated in Figure 4-21, overprediction in Q4 appears to be partially associated with $OPM_{2.5}$. Measured $OPM_{2.5}$ likely consists mostly of crustal material (dust) and sea salt. Modeled $OPM_{2.5}$ is defined as the sum of unspeciated PM, crustal material, and sea salt, with crustal material likely contributing the bulk of the mass at most locations. Although sodium predictions are biased high in Q4, the contribution to total mass is limited. $OPM_{2.5}$ is also overpredicted in Q4 at IMPROVE sites, with the bulk of the overprediction attributable to crustal material (not shown).

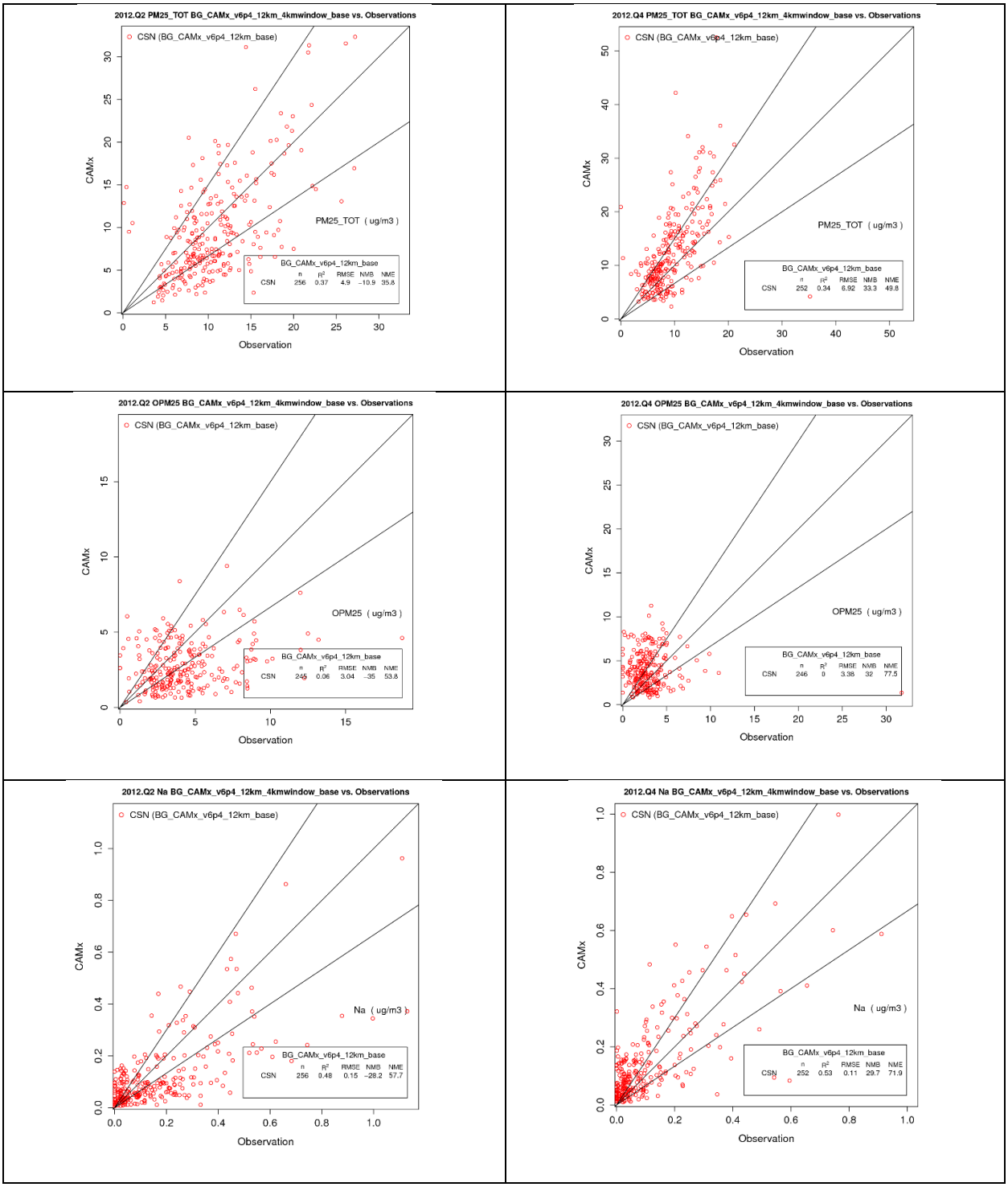

Figure 4-21. Comparisons of Predicted with Observed Daily Average PM at CSN during Q2 (left) and Q4 (right) for Total $PM_{2.5}$ (top), $OPM_{2.5}$ (middle), and Sodium (bottom)
Note: Black lines in each panel indicate 1:1, i.e., perfect agreement, and ± 50% bounds.

Figure 4-22 presents comparisons of particulate OC and EC performance statistics. NMB and NME are within the PM performance criteria with the exception of July and August EC predictions at CSN sites; the overprediction bias is smaller at SEARCH sites. EC NMB at IMPROVE sites is approximately

5 percent for July–September (not shown). The SEARCH, CSN, and IMPROVE networks all used the thermal optical reflectance (TOR) method to determine OC and EC in 2012.

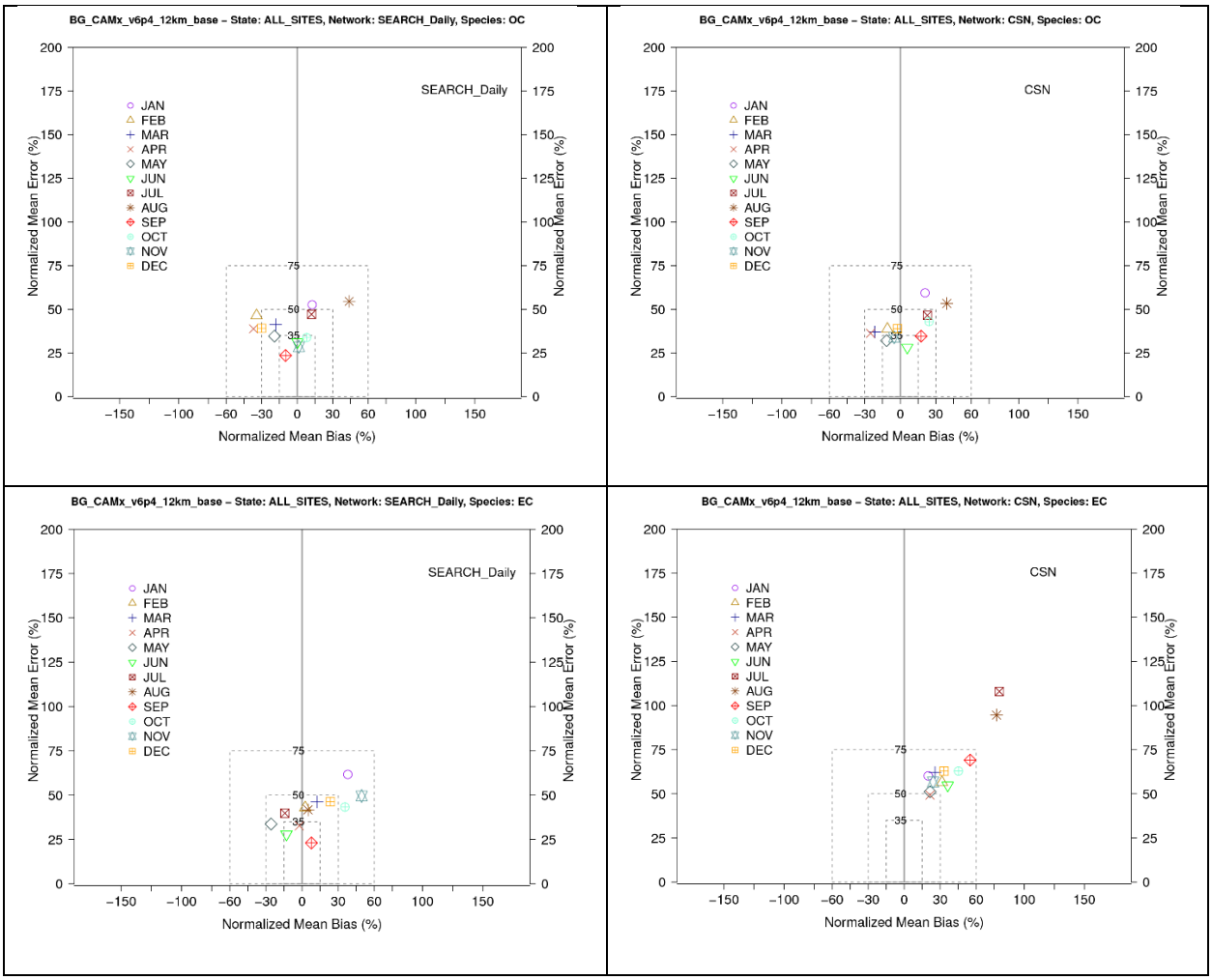

Figure 4-22. Comparisons of Observed vs. Predicted OC (top) and EC (bottom) at SEARCH (left) and CSN (right)

4.5.5.3 Nitrogen Species (NO_2, NO_y, and NO_3)

Figures 4-23 and 4-24 show soccer plot summaries of NMB and NME for nitrogen species for monitoring sites in the 4-km domain. NO_2 performance is dominated by a positive bias, which is most pronounced during June–September (based on the AQS data); NME values for the hourly NO_2 predictions exceed the 75 percent criteria in most months. Oxidized nitrogen (NO_y)—which is only measured at the SEARCH monitoring sites—is also overpredicted. Observed daily average NO_3 at SEARCH sites is generally less than 0.3 µg/m^3, whereas CAMx predicts many values above 1 µg/m^3 during Q1; NO_3 values are in better agreement for June–August. Overprediction of NO_x in the southeastern U.S. has been observed in other photochemical modeling studies and may be a result of overstated mobile source NO_x emissions in the NEI (Travis et al., 2016). This in turn may be at least partially responsible for the ozone overprediction bias noted in Section 4.5.5.1. However, additional inventory verification and modeling sensitivity analyses are needed to confirm this.

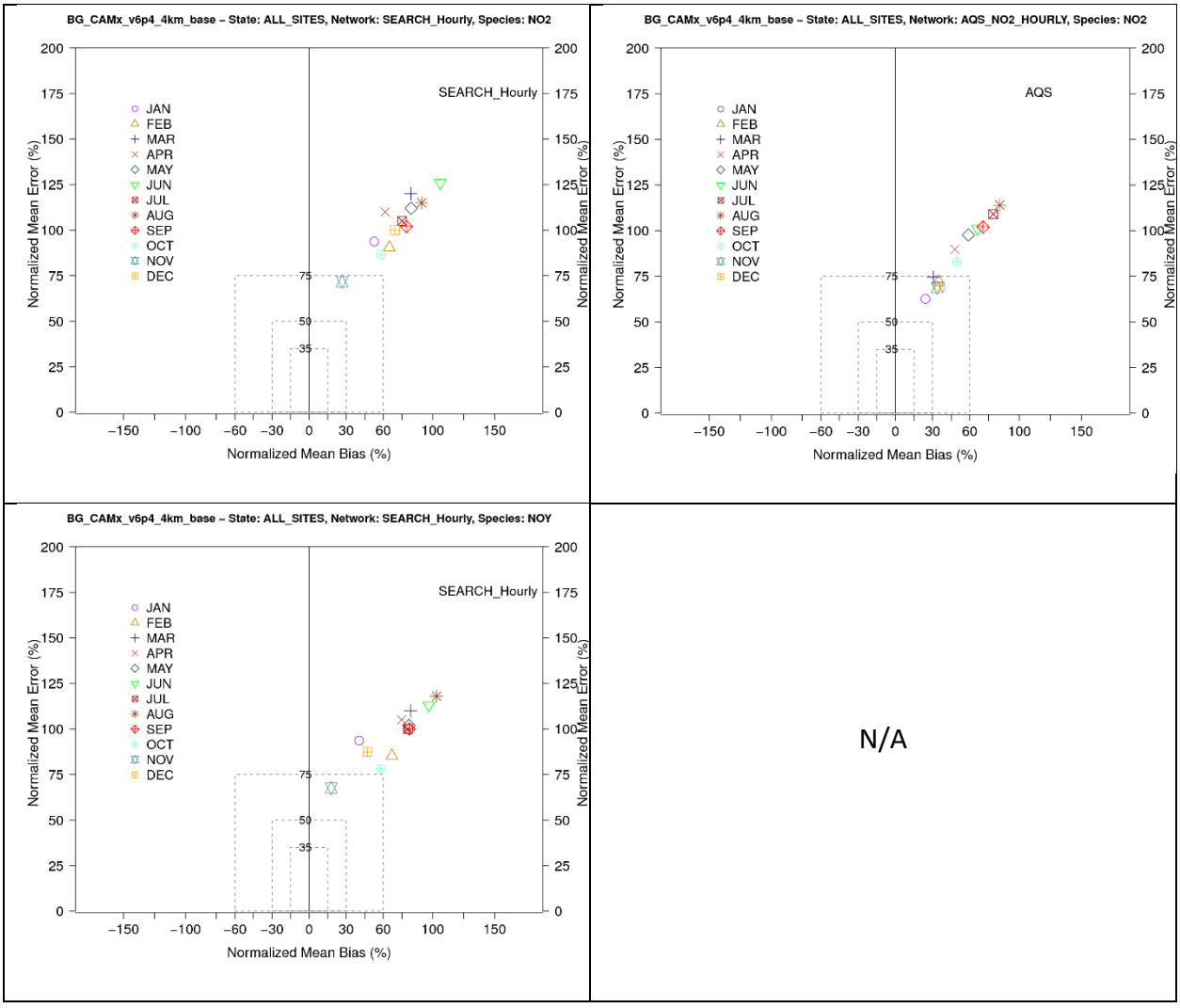

Figure 4-23. Monthly NMB and NME for Hourly NO_2 (top) and Daily NO_y (bottom) at SEARCH Network Sites (left) and AQS Sites (right) in the 4-km Domain

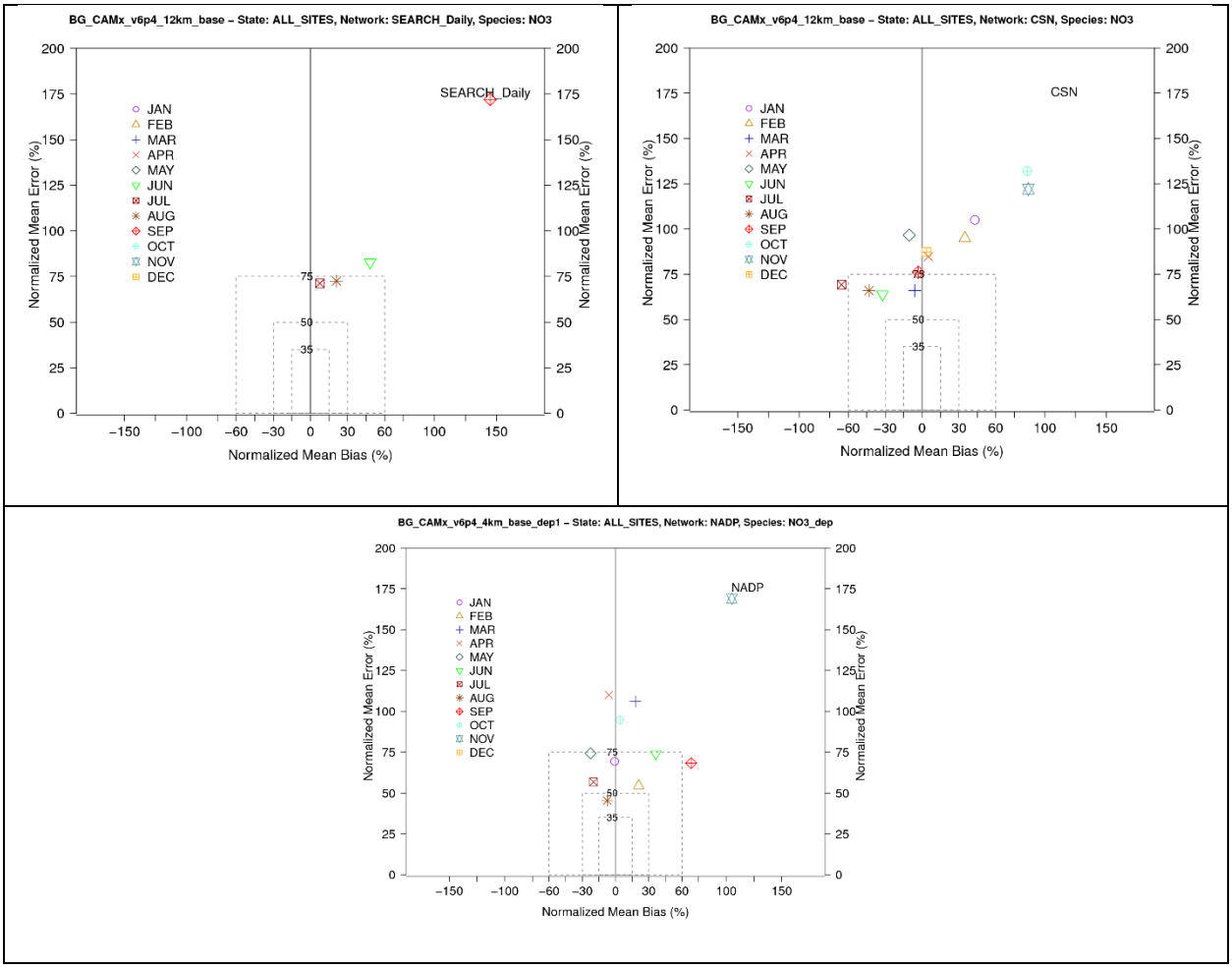

Figure 4-24. Monthly NMB and NME for NO_3 at SEARCH Network Monitoring Sites (top left) and CSN Sites (top right) in the Southeastern U.S. and NO_3 Deposition at National Atmospheric Deposition Program (NADP) Sites in the 4-km Domain (bottom)[15]

4.5.5.4 Sulfur Species (SO_2 and SO_4)

Figure 4-25 summarizes model performance for hourly SO_2 within the 4-km domain in terms of monthly NME and NMB. AQS network SO_2 monitors are typically located to represent the influence of major utility or industrial SO_2 sources and thus typically measure short-term peaks associated with plume impacts from a relatively isolated source. Some industrial facilities, such as oil refineries, may be subject to upset conditions resulting in temporary increases in SO_2 emissions, the timing and magnitude of which are not reflected in the model input emissions. In addition, monitors near large ports may be influenced by discrete plumes from passing marine vessels that could be sufficient enough to cause 1-hour peaks in the monitoring data. Because marine vessel emission inputs to the model are temporally averaged, the model cannot properly simulate these discrete events. As a result of these factors, the timing, location, and magnitudes of peak SO_2 concentrations are not expected to be well-represented in the gridded model results. Given these characteristics of the SO_2 monitoring data, we would expect large 1-hour SO_2 modeling biases and errors, as shown in Figure 4-25. Examination of NMB over all sites in the 12-km domain (Figure 4-26) shows wide variations in bias from site to site, including between sites in the 4-km domain, consistent with varying exposures of monitors to different SO_2 sources. The large overall SO_2

[15] Note: Additional months for SEARCH NO_3 are not shown, as the NMB and NME exceed the upper axis limits.

NMB in the 4-km domain (top row of Figure 4-25) is associated with zero or near-zero observed values at the monitoring site. These values are slightly overpredicted by the 4-km grid cell average model at some sites with very low correlations between observed and predicted hourly averages.

In contrast to problems with SO_2 predictions, the model performs well for SO_4 at SEARCH and CSN network sites (see the middle row of Figure 4-25). The much better model performance for SO_4—which is a secondary species less subject to the site-specific characteristics of SO_2 concentrations—supports the hypothesis that most SO_2 modeling errors are associated with the site-specific factors mentioned above. SO_4 deposition is underpredicted in most months.

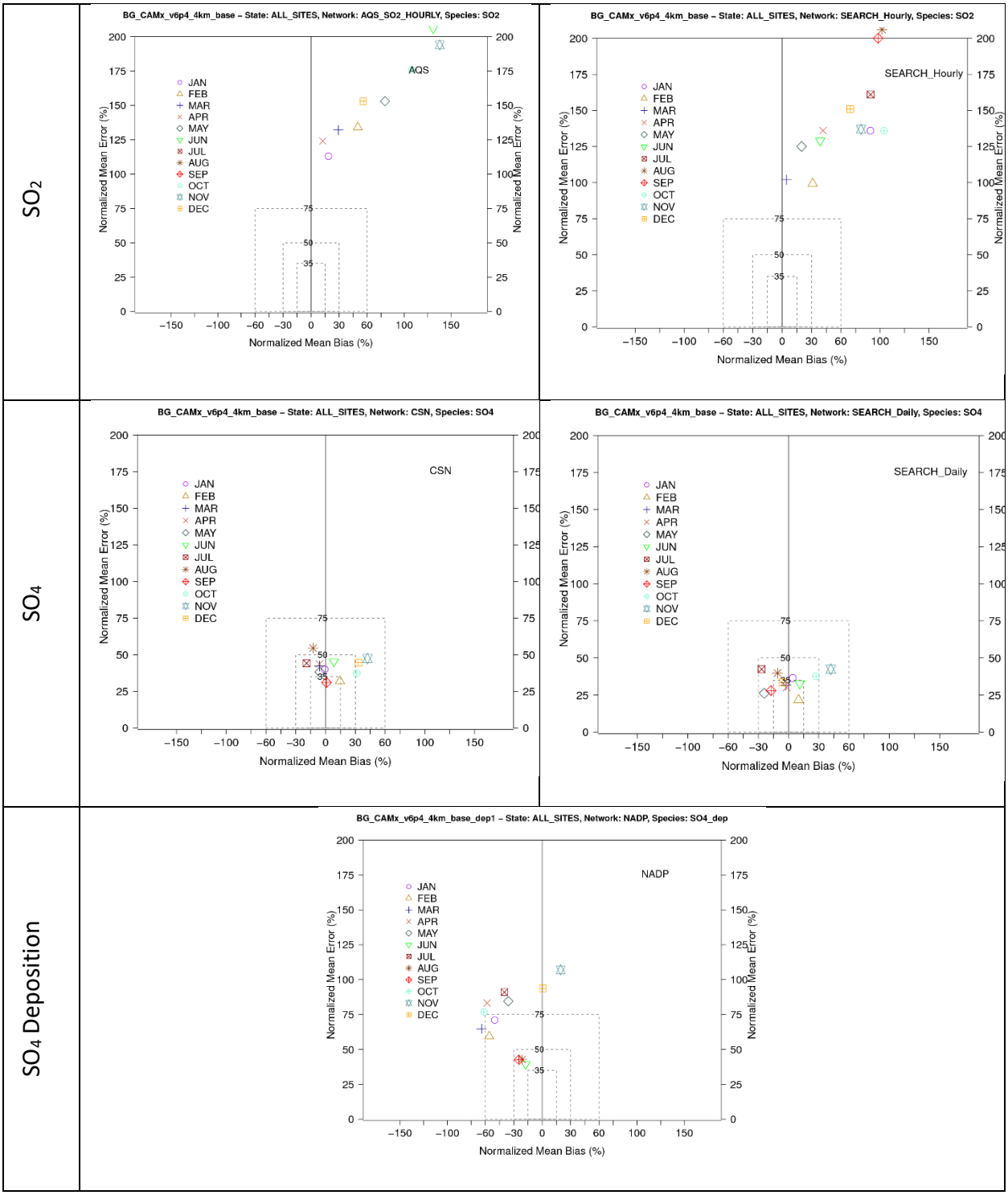

Figure 4-25. Monthly NMB and NME at Monitoring Sites in the 4-km Domain for SO_2 (top row, AQS sites left panel, SEARCH sites right panel), SO_4 (middle row, CSN sites left panel, SEARCH sites right panel), and SO_4 Deposition Measured at NADP Sites (bottom row)

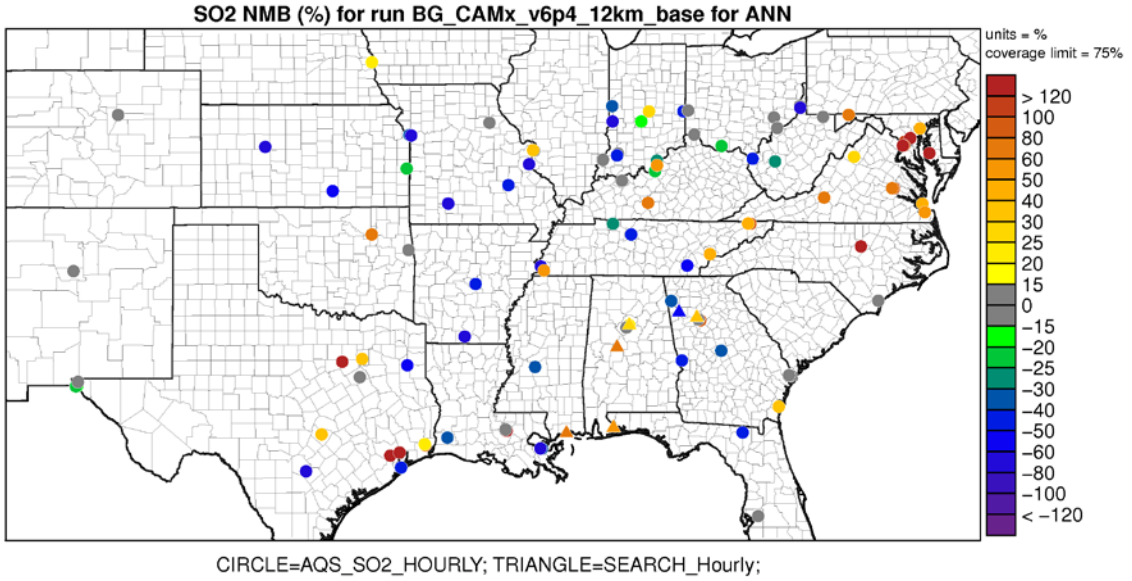

Figure 4-26. Annual NMB for Hourly SO_2 Based on 12-km Resolution CAMx Results

4.5.5.5 Ammonium (NH_4)

Figure 4-27 summarizes model performance for particulate NH_4 at monitors within the 4-km domain in terms of monthly NME and NMB. Performance at the two SEARCH network sites (OLF and GFP) falls within the PM criteria bounds (except in January), but positive biases and large errors are seen at the three CSN sites. Results based on all sites in the southeastern U.S. domain (at 12-km resolution) are very similar (not shown). The NH_4 overestimation bias at the CSN sites may be due in part to NO_3 overprediction (Figure 4-24), as SO_4 is showing biases closer to zero (Figure 4-25). Examination of individual CSN site results within the 4-km domain shows acceptable or nearly acceptable performance at the Houston, Texas, site (NMB = 30 percent; NME = 60 percent) and the Laurel, Mississippi, site (NMB = 48 percent; NME = 64 percent) but large positive biases and errors at the Baton Rouge, Louisiana, monitor. Prediction biases for NO_3 are small at Houston (NMB = 6 percent) and Laurel (NMB = 19%) but much larger at Baton Rouge (NMB = 62 percent); thus, the excess predicted NH_4 at Baton Rouge appears to be associated with excess predicted NO_3.

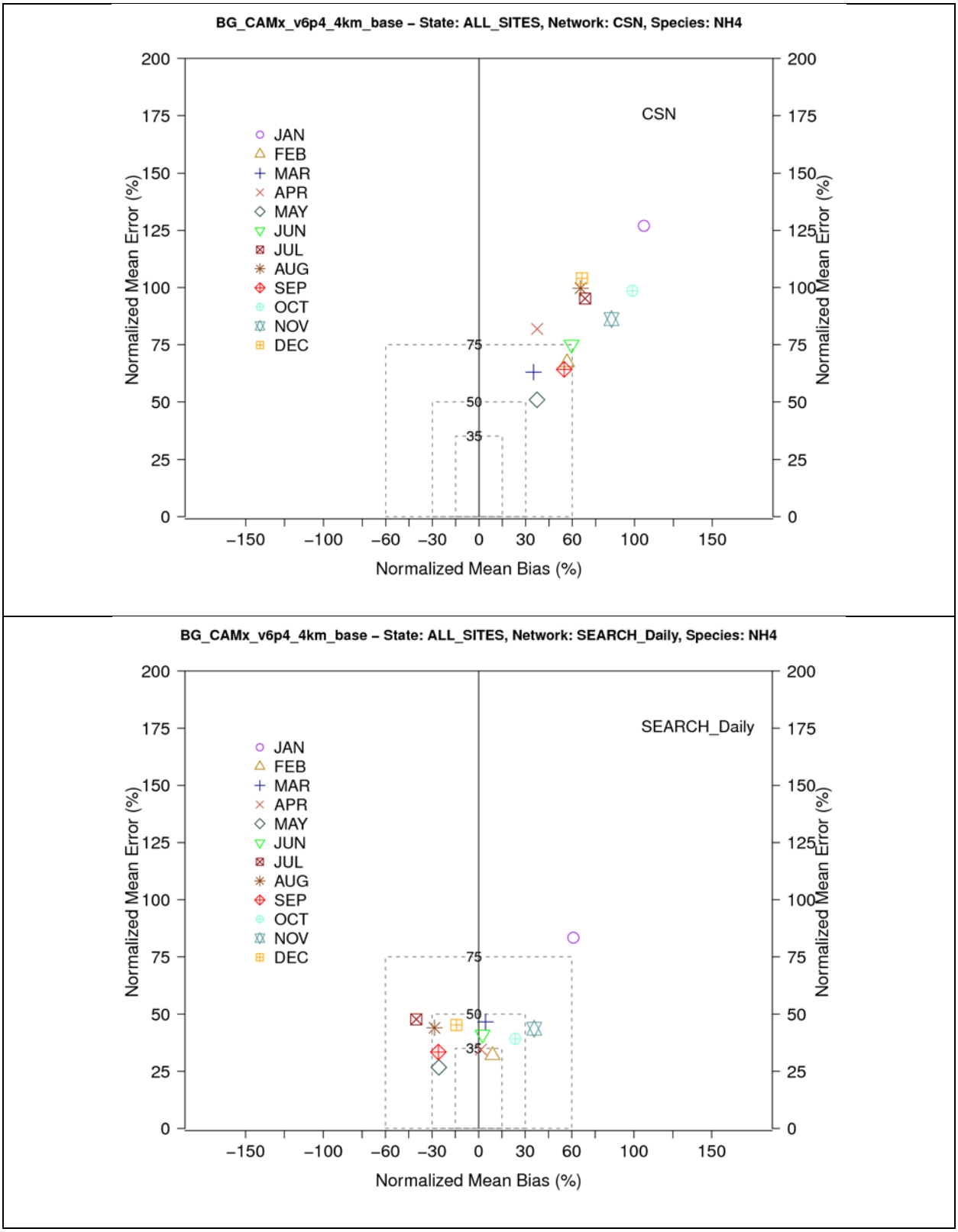

Figure 4-27. Monthly NMB and NME for Daily Average NH_4 at CSN (top) and SEARCH (bottom) Network Sites in the 4-km Modeling Domain

4.5.5.6 Carbon Monoxide (CO)

Model performance for hourly CO within the 4-km domain is summarized in terms of monthly NME and NMB in Figure 4-28. Hourly CO is underpredicted on average at AQS sites, where the model's 4-km grid resolution does not adequately resolve the influence of local mobile sources at sub-grid scales; model performance is better at the SEARCH sites.

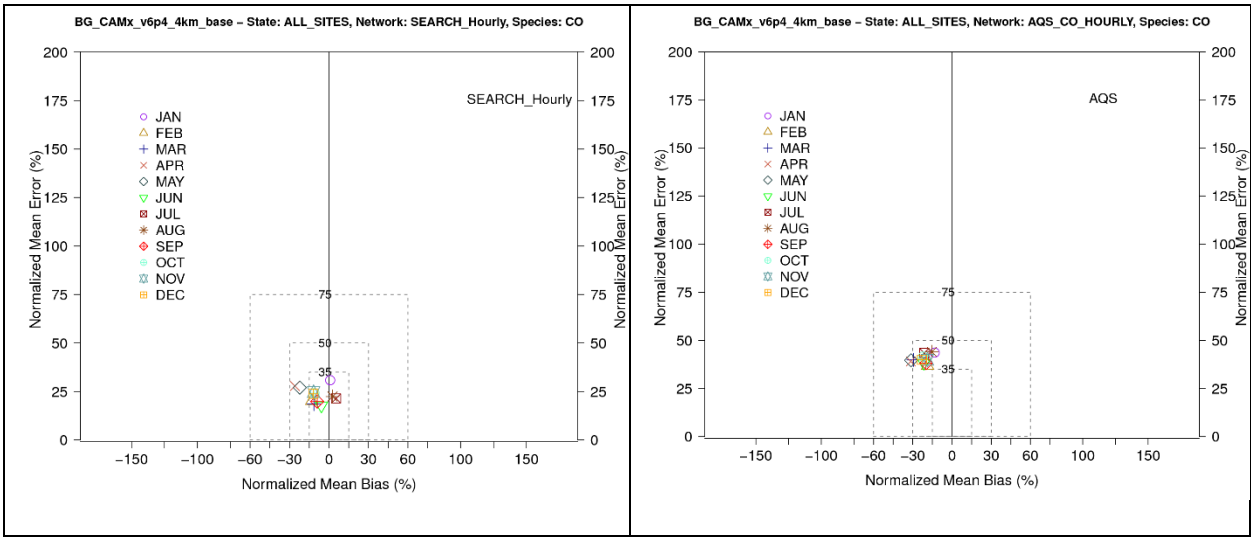

Figure 4-28. Monthly NMB and NME for Hourly CO at SEARCH Network Sites (left) and AQS Sites (right)

4.5.5.7 Summary

Results of the MPE described above indicate that the model is generally performing within the range considered to be acceptable for regulatory applications according to USEPA guidance for O_3 and $PM_{2.5}$. The results' overprediction of late summer ozone in the southeastern U.S. has been observed in other studies (e.g., Johnson et al., 2015) and is likely associated with a combination of factors that are the subject of ongoing research within the modeling community. A recent study suggests this bias may be at least partially related to overestimation of anthropogenic NO_x emissions (Travis et al., 2016), which would be consistent with overprediction of NO_2 noted in Figure 4-23. As is characteristic of most modeling results, the overprediction bias is reduced at higher concentrations, and performance is well within the USEPA Guideline values over monitoring sites within the 4-km domain when an hourly or DMAX8 average concentration cut-off of 40 ppb is applied.

Model performance in terms of NMB and NME for total $PM_{2.5}$ mass falls within the USEPA performance criteria in all cases and within or nearly within the more stringent USEPA performance goals for most months. A tendency toward overprediction in winter is associated with WBD, suggesting that dust emissions are overestimated. Dust emissions are difficult to estimate and typically have a high degree of uncertainty, but their impact on modeled estimates of combustion emission source contributions (which are the main focus of this study) to total $PM_{2.5}$ mass is expected to be minimal.

Particulate OC and EC performance is within or nearly within the USEPA goals for all months except for July and August, when CSN sites overpredicted EC; this was not seen at the SEARCH sites despite the fact that both networks use the TOR method for quantifying EC. NO_2 and NO_y are overpredicted, with NMB and NME exceeding USEPA criteria in most months. However, there is no systematic overprediction of particulate NO_3, although correlations are low and errors are large; the USEPA NME criteria are exceeded in most months. Model performance deficiencies for nitrogen species are a common

feature of photochemical modeling studies given the complexities of nitrogen chemistry. This situation is especially acute in coastal areas because of uncertainties in sea salt emission estimates. Another potential source of model performance deficits is the inaccuracy of speciated PM measurements, including errors related to volatilization of particle-bound NO_3 during sample collection and processing.

Given that model performance is within USEPA performance criteria for ozone and $PM_{2.5}$, and no unexpected performance issues were encountered for individual PM species, the 2012 base case model results described above are judged to be reasonably adequate to support use of the model for estimating the impacts of new offshore oil and gas production sources on regional air quality. Not unexpectedly, the most significant area of uncertainty relates to the impacts of NO_x emissions on PM, NO_3 deposition, and visibility.

4.6 Air Resource Assessment Approach

4.6.1 Future Year Modeling

Ramboll ran CAMx with the future year scenario emissions inventory, including emissions from sources associated with the proposed lease sales described in Section 3. Model results were post-processed for analysis of air quality impacts with respect to the NAAQS and AQRVs; PSD increments were also calculated for information purposes. Source apportionment technology was used to estimate source group impacts, including impacts of potential new sources associated with the lease sales. Details of the source apportionment and post-processing procedures are presented in this section.

4.6.1.1 Source Apportionment Design

Ramboll used the CAMx Ozone Source Apportionment Technology (OSAT) and Particulate Source Apportionment Technology (PSAT) tools to obtain the separate air quality, deposition, and visibility impacts associated with existing and proposed OCS exploration and development in the GOM, as well as from other emission sources in the GOM and several other source categories described in Section 3. The CAMx OSAT and PSAT tools use reactive tracers that operate in parallel to the host PGM to provide air quality and deposition contributions from a user-selected source category. CAMx determines the contributions of emissions from each source category to the total CAMx model concentrations and depositions during the simulation. A detailed description of the CAMx source apportionment tools is available in the CAMx user's guide (Ramboll Environ, 2016).

Ramboll used the Anthropogenic Precursor Culpability Assessment (APCA) version of the CAMx OSAT in the future year scenario modeling. APCA differs from OSAT in that it distinguishes between natural and anthropogenic emissions. For example, when ozone is formed due to the interaction of biogenic VOC and anthropogenic NO_x under VOC-limited conditions, OSAT would assign the ozone formed to the biogenic VOC, whereas APCA recognizes that biogenic VOC is uncontrollable and redirects the ozone formed to the anthropogenic NO_X. Thus, APCA only assigns the ozone formed to natural emissions when it is due to natural VOC interacting with natural NO_X emissions. APCA requires that the first source category specified in the model input file is always natural emissions. Previously, OSAT and APCA used four reactive tracers to track the ozone contributions of each source group: NO_X emissions (N_i), VOC emissions (V_i), and ozone formed under VOC-limited ($O3V_i$) and NO_X-limited ($O3N_i$) conditions. Since CAMx v6.30, the reactive tracers used for OSAT/APCA have been expanded to track odd oxygen and nitrogen through NO_y chemistry to account for NO_x recycling of ozone. OSAT/APCA now requires 10 reactive tracers for each source group: V_i, $O3V_i$, $O3N_i$, NIT_i (NO and HONO), RGN_i (NO_2, NO_3 radical, N_2O_5, and INO_3), TPN_i (peroxynitric acid, peroxyacetyl nitrate, and its analogues), NTR_i (organic nitrates), $HN3_i$ (HNO_3), OON_i (odd oxygen in NO_2 formed from $O3N_i$), and OOV_i (odd oxygen in NO_2 formed from $O3V_i$).

For PM, three families of PSAT source apportionment tracers were used to track contributions of SO_4, NO_3/NH_4, and primary PM that require two, eight, and six reactive tracers, respectively, for each family. Five of the eight nitrogen-containing tracers (NIT_i, RGN_i, TPN_i, NTR_i, and $HN3_i$) are shared with OSAT/APCA. Thus, combined APCA/PSAT source apportionment uses 21 reactive tracers to track the contribution of each source category. Ramboll did not use the secondary organic aerosol (SOA) family of PSAT tracers in the future year scenario source apportionment modeling because only a few specific kinds of VOC species form SOA (i.e., isoprene, terpenes, sesquiterpenes, and aromatics). These VOCs are mainly emitted by biogenic sources, although some aromatic species (e.g., toluene and xylene) are emitted by anthropogenic sources (e.g., gasoline combustion). Furthermore, oil and gas exploration and production emissions generally contain only minor amounts of aromatic VOC emissions, and the chemistry of SOA is quite complex, involving numerous gaseous, semi-volatile, and particulate species. PSAT thus requires 14 tracers to track the SOA contributions of each source group (Ramboll Environ, 2016). As a result, including SOA would greatly increase the number of reactive tracers and the computer time needed for the CAMx source apportionment run without a significant gain in useful output information.

4.6.1.2 Future Year Source Apportionment Simulation

Ramboll simulated the CAMx 2017 source apportionment for the January 1–December 31 calendar year over the 12/4-km southeastern U.S. modeling domain shown in Figure 2-1. Ramboll obtained the BCs defining inflow concentrations around the lateral boundaries of the 12-km domain from a future year CAMx simulation of the 36-km continental U.S. domain shown in Figure 2-1. Both the base and future year simulations are based on the same 2012 WRF meteorology and 36-km domain BCs obtained from the global GEOS-Chem model simulation, and they used the same model configuration as the base case simulation described in Section 4.4.

4.6.2 Post-Processing of Future Year Source Apportionment Modeling Results

4.6.2.1 Overview

Ramboll post-processed the CAMx future year scenario source apportionment modeling outputs to compare them against the NAAQS and PSD concentration increments in Table 4-12 and other thresholds of concern, as discussed below. To analyze NAAQS and AQRV impacts at Class I and sensitive Class II areas, Ramboll used thresholds of concern that were defined by the FLM agency that manages each Class I/II area, as prescribed in the June 23, 2011, Memorandum of Understanding for evaluating onshore oil and gas production air quality/AQRV impacts (USDOA, USDOI, USEPA, 2011).

CAMx source apportionment results for individual source categories were used to evaluate the incremental impacts of each set of hierarchical source groups defined in Table 4-13. Groups A1–A4 represent "existing" sources under the no-sale scenario (which is referred to as the no action alternative within the NEPA context). Source group B1 represents emissions from new oil and gas platforms, and source group B2 represents the new platforms and emissions from the additional support vessel and helicopter trips in the OCS region associated with the new platforms under the single-sale scenario. Similarly, source group C1 represents emissions from new oil and gas platforms, and source group C2 represents the new platforms and emissions from the additional support vessel and helicopter trips in the OCS region associated with the new platforms under the 10-sale scenario.

Table 4-12. NAAQS and PSD Increments

Pollutant	Pollutant/Averaging Time	NAAQS	PSD Class I Increment[a]	PSD Class II Increment[a]
CO	1-hour[b]	**35 ppm** 40,000 µg/m^3	–	–
CO	8-hour[b]	**9 ppm** 10,000 µg/m^3	–	–
NO_2	1-hour[c]	**100 ppb** 188 µg/m^3	–	–
NO_2	Annual[d]	**53 ppb** 100 µg/m^3	2.5 µg/m^3	25 µg/m^3
O_3	8-hour[e]	**0.070 ppm** 137 µg/m^3	–	–
PM_{10}	24-hour[f]	**150 µg/m^3**	8 µg/m^3	30 µg/m^3
PM_{10}	Annual[g]	–	4 µg/m^3	17 µg/m^3
$PM_{2.5}$	24-hourh[h]	**35 µg/m^3**	2 µg/m^3	9 µg/m^3
$PM_{2.5}$	Annual[i]	**12 µg/m^3**	1 µg/m^3	4 µg/m^3
SO_2	1-hour[j]	**75 ppb** 196 µg/m^3	–	–
SO_2	3-hour[k]	**0.5 ppm** 1,300 µg/m^3	25 µg/m^3	512 µg/m^3
SO_2	24-hour	–	5 µg/m^3	91 µg/m^3
SO_2	Annual[d]	–	2 µg/m^3	20 µg/m^3

[a] The PSD demonstrations serve information purposes only and do not constitute a regulatory PSD increment consumption analysis.
[b] No more than one exceedance per calendar year.
[c] 98th percentile, averaged over 3 years.
[d] Annual mean not to be exceeded.
[e] Fourth-highest DMAX8 ozone concentrations in a year, averaged over 3 years, NAAQS promulgated December 28, 2015.
[f] Not to be exceeded more than once per calendar year on average over 3 years.
[g] 3-year average of the arithmetic means over a calendar year.
[h] 98th percentile, averaged over 3 years.
[i] Annual mean, averaged over 3 years, NAAQS promulgated December 14, 2012.
[j] 99th percentile of daily maximum 1-hour concentrations in a year, averaged over 3 years.
[k] No more than one exceedance per calendar year (secondary NAAQS).

Table 4-13. Source Groups for Incremental Impacts Analysis

Group Name	Sources	Description	Source Categories (see Table 4-5)[a]
No-Sale Scenario[b]			
A1	OCS platforms	"Existing" platforms	**SC5a**
A2	Group A1 plus support vessels	All "existing" BOEM OCS oil and gas sources	SC5a **+SC5b**
A3	Group A2 plus other OCS vessels operating in the OCS and other U.S., Mexican, and Canadian anthropogenic emissions	All anthropogenic sources	SC5a+SC5b **+SC6+SC7+SC8**
A4	Group A3 plus natural sources (fires, bio- and geogenic sources) and BCs	All sources	SC5a+SC5b+SC6+SC7+SC8 **+SC1+SC2+SC10**
Single-Sale Scenario			
B1	New platforms	New platforms	**SC3a**
B2	Group B1 plus support vessels	All new sources	SC3a**+SC4a**
B3	Group B2 plus existing platforms and support vessels	All BOEM OCS oil and gas sources	SC3a+SC4a**+SC5a+SC5b**
B4	Group B3 plus other vessels operating in the OCS and other U.S., Mexican, and Canadian anthropogenic emissions	All anthropogenic sources	SC3a+SC4a+SC5a+SC5b**+SC6+SC7+SC8**
B5	Group B4 plus natural sources (fires, bio- and geogenic sources) and BCs	All sources	SC3a+SC4a+SC5a+SC5b+SC6+SC7+SC8**+SC1+SC2+SC10**
10-Sale Scenario			
C1	New platforms	New platforms	**SC3a+SC3b**
C2	Group C1 plus support vessels	All new sources	SC3a+SC3b**+SC4a+SC4b**
C3	Group C2 plus existing platforms and support vessels	All BOEM OCS oil and gas sources	SC3a+SC3b+SC4a+SC4b**+SC5a+SC5b**
C4	Group C3 plus other vessels operating in the OCS and other U.S., Mexican, and Canadian anthropogenic emissions	All anthropogenic sources	SC3a+SC3b+SC4a+SC4b+SC5a+SC5b**+SC6+SC7+SC8**
C5	Group C4 plus natural sources (fires, bio- and geogenic sources) and boundary conditions	All sources	SC3a+SC3b+SC4a+SC4b+SC5a+SC5b+SC6+SC7+SC8**+SC1+SC2+SC10**

[a] Bold indicates source categories added to previous groups.
[b] The "no-sale" scenario represents future year emissions without inclusion of new sources from the proposed lease sales.

4.6.2.2 Comparison Against NAAQS

Ramboll post-processed CAMx future year scenario predicted total concentrations from all emission sources and compared them with the applicable NAAQS in Table 4-12 in two different ways. First, the CAMx predictions were compared directly against each NAAQS. This is referred to as the "absolute" prediction comparison. These absolute prediction comparisons may be misleading in cases in which the model exhibits significant prediction bias. In recognition of this, USEPA modeling guidance (USEPA, 2007; 2014a) recommends using the model in a relative sense when projecting future year ozone, $PM_{2.5}$, and regional haze levels, and the USEPA has developed the Modeled Attainment Test Software (MATS) (Abt, 2014) for making such future year projections. This approach uses the ratio of future year to current

year modeling results to develop relative response factors (RRFs) that are applied to observed current year design values (abbreviated as either DVC or DVB) to make future year design value (DVF) projections (i.e., DVF = DVC x RRF). Ramboll applied MATS to the prediction of both ozone and $PM_{2.5}$ DVFs. MATS was also used to assess the cumulative visibility impacts at IMPROVE monitoring sites in the 12-km domain, as discussed in more detail below.

Although comparisons of model results are presented for all NAAQS, readers should note that modeled impacts of new sources relative to the short-term (i.e., 1-hour) NAAQS for NO_2, SO_2, and CO are subject to greater uncertainties than are modeled impacts relative to longer-term (e.g., 8-hour, 24-hour, and annual average) NAAQS. This is because the calculated maximum 1-hour design values associated with the new sources typically occur very close to each source. The model's 4-km grid resolution does not adequately resolve such fine-scale impacts. In addition, these local-scale impacts are sensitive to the exact physical characteristics of, and short-term temporal variations in emissions from, individual sources. However, such detailed information about the proposed new sources is not generally available at this point in the planning process.

4.6.2.3 Impacts at Class I and Sensitive Class II Areas

Ramboll calculated the incremental air quality/AQRV contributions associated with emissions from each source group in Table 4-13 at the Class I and sensitive Class II areas shown in Figure 4-29. The selected areas include all Class I and sensitive Class II areas within the 4-km modeling domain plus additional Class I areas within the 12-km modeling domain. Table 4-14 lists those areas that are located on the Gulf Coast or in nearby states and thus are of greatest interest to this analysis; see Section 4.7.3.1 for a complete list of all areas shown in Figure 4-30 along with results of the visibility analyses.

Receptors for each Class I and sensitive Class II area were defined based on the spatial extent of the Class I/II area shapefiles obtained from the applicable FLM agency. Ramboll used GIS to determine the set of grid cells overlapping each area by at least 5 percent. Model results for the identified grid cells were then used to represent predicted ambient concentrations and deposition in each area.

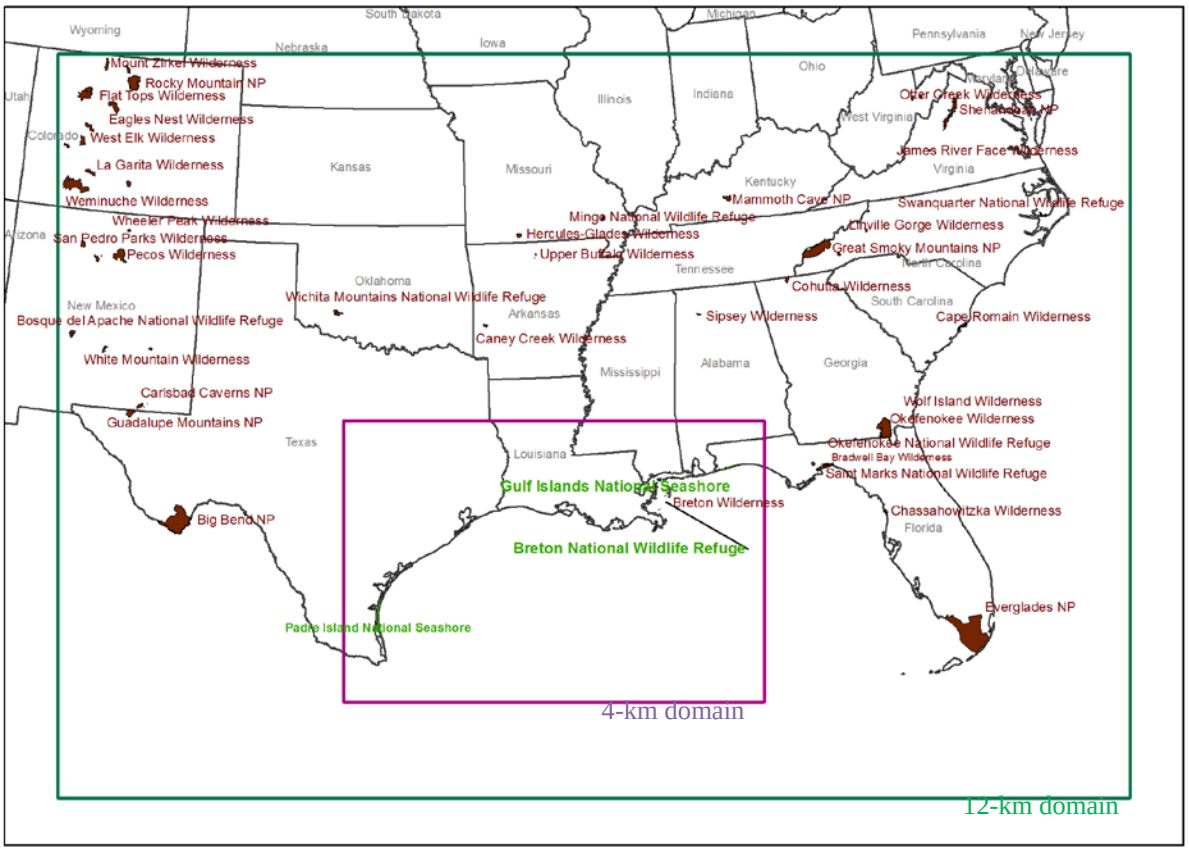

Figure 4-29. Class I (maroon) and Sensitive Class II (green) Areas Within the 4-km and 12-km Modeling Domains for Which Incremental Air Quality/AQRV Impacts Were Calculated

Table 4-14. Class I and Sensitive Class II Areas on Gulf Coast and in Nearby States[a]

Type	Name	Agency	State	Modeling Domain
Class I	Breton Wilderness	FWS	LA	4 km
Class II	Breton NWR	FWS	LA	4 km
Class II	Gulf Islands NS	NPS	MS, FL	4 km
Class II	Padre Island NS	NPS	TX	4 km
Class I	Bradwell Bay	USFS	FL	12 km
Class I	St. Marks	FWS	FL	12 km
Class I	Chassahowitzka	FWS	FL	12 km
Class I	Everglades NP	NPS	FL	12 km
Class I	Okefenokee	FWS	GA	12 km
Class I	Wolf Island	FWS	GA	12 km

Type	Name	Agency	State	Modeling Domain
Class I	Cohutta	USFS	GA	12 km
Class I	Sipsey	USFS	AL	12 km
Class I	Guadalupe Mts	NPS	TX	12 km
Class I	Big Bend	NPS	TX	12 km
Class I	Wichita Mts	FWS	OK	12 km
Class I	Caney Creek	USFS	AR	12 km
Class I	Upper Buffalo	USFS	AR	12 km

[a] FWS = U.S. Fish and Wildlife Service; NP = National Park; NS = National Seashore; NWR = National Wildlife Refuge; USFS = Forest Service

4.6.2.3.1 Incremental Visibility Impacts

Ramboll calculated visibility impacts for each source group using incremental concentrations as quantified by the CAMx PSAT tool. Changes in light extinction from CAMx model concentration increments due to emissions from each source group were calculated for each day at grid cells representing each Class I and sensitive Class II area. The procedures described by the Federal Land Managers' Air Quality Related Values Work Group (FLAG, 2010) were used in the incremental visibility assessment analysis.

The visibility evaluation metric used in this analysis is based on the haze index (HI), which is measured in deciview (dv) units and defined as follows:

$$HI = 10 \times \ln[b_{ext}/10]$$

Where b_{ext} is the atmospheric light extinction measured in inverse megameters (Mm^{-1}) and is calculated primarily from atmospheric concentrations of particulates. A more intuitive measure of haze is visual range (VR), which is defined as the distance at which a large black object just disappears from view and is measured in km. VR is related to b_{ext} by the formula VR = 3,912 / b_{ext}. The advantage of using the HI rather than VR is that a given change in HI is approximately associated with the same degree of perceived change in visibility regardless of the baseline conditions, whereas small changes in VR are much more noticeable under clean conditions as compared to hazy conditions.

Ramboll added the incremental concentrations due to each source group to natural background extinction in the extinction equation (b_{ext}) and calculated the difference between the HI with the source group concentrations included and the HI based solely on natural background concentrations. This quantity is the change in HI, which is referred to as "delta deciview" (Δdv):

$$\Delta dv = 10 \times \ln[b_{ext(SC+background)}/10] - 10 \times \ln[b_{ext(background)}/10]$$

$$\Delta dv = 10 \times \ln[b_{ext(SC+background)}/b_{ext(background)}]$$

Here, $b_{ext(SCi+background)}$ refers to atmospheric light extinction due to impacts from the source category plus background concentrations, and $b_{ext(background)}$ refers to atmospheric light extinction due to natural background concentrations only.

For each source group, the estimated visibility degradation at the Class I areas and sensitive Class II areas due to the source group are presented in terms of the number of days that exceed a threshold change in deciview (Δdv) relative to background conditions. The number of days with a Δdv greater than 0.5 and 1.0 are reported.

IMPROVE Reconstructed Mass Extinction Equations

The FLAG (2010) procedures for evaluating visibility impacts at Class I areas use the revised IMPROVE reconstructed mass extinction equation to convert PM species in $\mu g/m^3$ to light extinction (b_{ext}) in inverse megameters (Mm^{-1}) as follows:

$$b_{ext} = b_{SO4} + b_{NO3} + b_{EC} + b_{OCM} + b_{Soil} + b_{PMC} + b_{SeaSalt} + b_{Rayleigh} + b_{NO2}$$

Where:

$$b_{SO4} = 2.2 \times f_S(RH) \times [\text{Small Sulfate}] + 4.8 \times f_L(RH) \times [\text{Large Sulfate}]$$

$$b_{NO3} = 2.4 \times f_S(RH) \times [\text{Small Nitrate}] + 5.1 \times f_L(RH) \times [\text{Large Nitrate}]$$

$$b_{OCM} = 2.8 \times [\text{Small Organic Mass}] + 6.1 \times [\text{Large Organic Mass}]$$

$$b_{EC} = 10 \times [\text{Elemental Carbon}]$$

$$b_{Soil} = 1 \times [\text{Fine Soil}]$$

$$b_{CM} = 0.6 \times [\text{Coarse Mass}]$$

$$b_{SeaSalt} = 1.7 \times f_{SS}(RH) \times [\text{Sea Salt}]$$

$b_{Rayleigh}$ = Rayleigh Scattering (Site-specific)

$b_{NO2} = 0.33 \times [NO_2 \text{ (ppb)}]$ {or as: $0.1755 \times [NO_2 (\mu g/m^3)]$}

f(RH) are RH adjustment factors that account for the fact that sulfate, nitrate, and sea salt aerosols are hygroscopic and are more effective at scattering solar radiation at higher RH. FLAG (2010) recommends using monthly average f(RH) values rather than the hourly averages recommended in the previous FLAG (2000) guidance document to moderate the effects of extreme weather events on the visibility results.

The revised IMPROVE equation treats “large sulfate” and “small sulfate” separately because large and small aerosols affect an incoming beam of light differently. However, the IMPROVE measurements do not separately measure large and small sulfate; they measure only the total $PM_{2.5}$ sulfate. Similarly, CAMx writes out a single concentration of particulate sulfate for each grid cell. The new IMPROVE equation includes a procedure for calculating the large and small sulfate contributions based on the magnitude of the model output sulfate concentrations; the procedure is documented in FLAG (2010). The sulfate concentration magnitude is used as a surrogate for distinguishing between large and small sulfate concentrations. For a given grid cell, the large and small sulfate contributions are calculated from the model output sulfate (which is the “Total Sulfate” referred to in the FLAG [2010] guidance) as:

For Total Sulfate $< 20\ \mu g/m^3$:

[Large Sulfate] = ([Total Sulfate] / $20\ \mu g/m^3$) × [Total Sulfate]

For Total Sulfate $\geq 20\ \mu g/m^3$:

[Large Sulfate] = [Total Sulfate]

For all values of Total Sulfate:

[Small Sulfate] = [Total Sulfate] – [Large Sulfate]

The procedure is identical for nitrate and organic mass.

The PSAT source apportionment algorithm does not separately track NO_2 concentrations but instead tracks a group of reactive nitrogen compounds with odd oxygen (RGN) that consists of NO_2, NO_3 radical, N_2O_5, and INO_3. Thus, for each hour and each grid cell representing a Class I/II area, a source group's incremental PSAT RGN contribution is converted to NO_2 by multiplying by the total (all emissions) CAMx model NO_2/RGN concentration ratio. This same procedure is also used for contributions to NO_2 concentrations.

Although sodium and particulate chloride are treated in the CAMx core model, these species are not carried in the CAMx PSAT tool. This does not affect the calculations of visibility impacts from individual source groups other than impacts from the natural source category (SC2).

Ramboll processed the predicted daily average modeled concentrations due to each source group for receptor grid cells containing Class I and sensitive Class II areas. Ramboll used the revised IMPROVE reconstructed mass extinction equation FLAG (2010) to obtain changes in b_{ext} at each sensitive receptor area that are converted to deciview and reported.

Annual average natural conditions for each Class I area were obtained from Table 6 in FLAG (2010) and monthly RH factors for each Class I area from Table 7-9 in FLAG (2010). The Δdv was calculated for each grid cell that overlaps a Class I or sensitive Class II area by 5 percent or more for each day of the annual CAMx run. The highest Δdv across all grid cells overlapping a Class I or sensitive Class II area by at least 5 percent was selected to represent the daily value at that Class I/II area. Visibility impacts due to emissions from each source group that exceed the 0.5 and 1.0 Δdv thresholds are noted.

4.6.2.3.2 Cumulative Visibility Impacts

Ramboll assessed the cumulative visibility impacts of the lease sales following U.S. Fish and Wildlife Service (FWS) and NPS recommendations (FWS and NPS, 2012). This approach is based on an abbreviated RHR method that estimates the future year visibility at Class I and sensitive Class II areas for the average of the worst 20 percent (W20%) and best 20 percent (B20%) visibility days with and without the effects of the source group emissions on visibility impairment. The cumulative visibility impacts used CAMx model output from the 2012 base year and 2017 future year emission scenarios in conjunction with monitoring data to produce cumulative visibility impacts at each Class I and sensitive Class II area. Ramboll used the USEPA's MATS (USEPA, 2014b) to make the 2017 visibility projections for the W20% and B20% days. The basic steps in the recommended cumulative visibility method are as follows (FWS and NPS, 2012):

1. Calculate the observed average 2012 current year cumulative visibility impact using the HI (in deciviews) at each Class I area, and use representative IMPROVE measurement data to determine the W20% and B20% visibility days. MATS is designed to use five years of monitoring data centered on the base case year, which for 2012 would include 2010–2014. However, MATS only includes IMPROVE monitoring data through 2012, so Ramboll used the 2008–2012 five-year period to define the visibility baseline conditions in the MATS visibility projections.

2. Estimate the RRFs for each component of $PM_{2.5}$ and for coarse mass corresponding to the new IMPROVE visibility algorithm using the CAMx 2012 and 2017 model output. The RRFs are based on the average concentrations across a 3x3 array of 4-km grid cells centered on the IMPROVE monitoring site location.

3. Use the RRFs and ambient data to calculate 2017 future year daily concentration data for the B20% and W20% days. Use the CAMx 2012 base case and 2017 standard model concentration estimates and PSAT source apportionment modeling results two ways:

a. 2017 total emissions: Use total 2017 CAMx concentration results due to all emissions.

b. 2017 no cumulative emissions: Use PSAT results to eliminate contributions of PM concentrations associated with each source group.

4. Use the information in step 3 to calculate the average future year visibility for the B20% and W20% visibility days and the future year emissions.

5. Assess the average differences in cumulative visibility impacts for each source group and also compare the future and current observed baseline visibility conditions.

Because IMPROVE observations were necessary, Ramboll used monitoring data from nearby Class I areas to represent areas without any IMPROVE monitors.

4.6.2.3.3 Sulfur and Nitrogen Deposition

Ramboll processed CAMx-predicted wet and dry fluxes of sulfur- and nitrogen-containing species to estimate total annual sulfur and nitrogen deposition values at each Class I and sensitive Class II area. The maximum annual sulfur and nitrogen deposition values from any grid cell that intersects a Class I receptor area were used to represent deposition for that area, in addition to the average annual deposition values of all grid cells that represent a Class I receptor area. Although the convention in the past has been to report just the maximum deposition in any Class I/II area receptor, the average metric may be considered a more relevant parameter for evaluating potential environmental effects because deposition relates to the total amount deposited across an entire watershed. Maximum and average predicted sulfur and nitrogen deposition impacts are reported separately for each source group.

Ramboll calculated nitrogen deposition impacts by summing the nitrogen contained in the fluxes of all nitrogen species modeled by the CAMx PSAT. CAMx species used in the nitrogen deposition flux calculation include reactive gaseous nitrogen compounds (NO, NO_2, NO_3 radical, HONO, N_2O_5, and INO_3), peroxyacetyl nitrate and its analogues (PAN, PANX, PNA, OPAN, and INTR), organic nitrates (NTR1, NTR2, and CRON), particulate nitrate formed from primary emissions plus secondarily formed particulate nitrate (PNO_3), gaseous nitric acid (HNO_3), gaseous ammonia (NH_3), and particulate ammonium (PNH_4). CAMx species used in the sulfur deposition calculation primarily include SO_2 emissions and particulate sulfate ion from primary emissions plus secondarily formed sulfate (PSO_4).

FLAG (2010) recommends that applicable sources assess impacts of nitrogen and sulfur deposition at Class I areas. This guidance recognizes the importance of establishing critical deposition loading values ("critical loads") for each specific Class I area, as these critical loads completely depend on local atmospheric, aquatic, and terrestrial conditions and chemistry. Critical load thresholds are essentially a level of atmospheric pollutant deposition below which negative ecosystem effects are not likely to occur. FLAG (2010) does not include any critical load levels for specific Class I areas and refers to site-specific critical load information on FLM websites for each area of concern. This guidance does, however, recommend using NPS and FWS deposition analysis thresholds (DATs; NPS, 2011). The DATs represent screening level values for nitrogen and sulfur deposition for individual projects with deposition impacts below the DATs considered negligible. A DAT of 0.005 kilograms per hectare per year (kg/ha-yr) has been established for both nitrogen and sulfur deposition and in western Class I areas. A DAT of 0.01 kg/ha/yr has been established for both nitrogen and sulfur deposition for areas in the eastern U.S. As a screening analysis, results for source group B (new platforms and associated support vessels and aircraft associated with the lease sales) were compared to the DATs. Comparison of deposition impacts from cumulative sources to the DAT is not appropriate.

For the 2012 base case and the 2017 future year scenario, Ramboll compared annual total nitrogen and sulfur deposition against critical load values established by FLM agencies. Published nitrogen critical

load values for NPS-managed areas include minimum critical loads of 3 kg/ha-yr at Gulf Islands National Seashore, the Guadalupe Mountains, and Big Bend National Park, as well as 5 kg/ha-yr at Padre Island National Seashore and Everglades National Park (NPS, 2016). These values represent the minimum critical loads for each biological community type (forests, herbaceous plants, lichen, mycorrhizal fungi, nitrate leaching). Because the NPS areas have no separate critical load values for sulfur, Ramboll set the sulfur critical loads equal to the nitrogen values for this analysis. Nitrogen and sulfur critical load values for areas managed by the U.S. Forest Service (USFS) include 5 kg/ha-yr at Bradwell Bay, Cohutta, Sipsey, Caney Creek, and Upper Buffalo. The 5 kg/ha-yr critical load value for these areas applies separately to nitrogen and to sulfur deposition. No published critical load values were found for FWS-managed areas; critical loads for these areas were set by reference to NPS and USFS critical loads based on proximity and similarity of ecoregion types. Using this approach, Ramboll set both nitrogen and sulfur critical loads for Breton Wilderness, Breton National Wildlife Refuge, St. Marks, Chassahowitzka, Okefenoke, and Wolf Island at 3 kg/ha-yr based on the Gulf Islands National Seashore value for eastern temperate forests. The value for Wichita Mountains was set at 5 kg/ha-yr based on the NPS Chickasaw National Recreation Area Great Plains ecoregion value.

4.6.2.4 PSD Increments

The maximum contribution of new oil and gas exploration and development emissions in the GOMR due to the lease sales were reported for each Class I and sensitive Class II area and compared against the PSD increments in Table 4-12. Under the CAA, a PSD increment consumption analysis requires major stationary sources subject to PSD review to demonstrate that emission increases from the proposed source in conjunction with all other emissions increases or reductions in the impacted area (typically within 50 km) will not cause or contribute to concentrations of air pollutants that exceed PSD increments. PSD increments have been established for NO_X, SO_2, and PM in Class I and Class II areas. BOEM-authorized actions due to the lease sales do not typically constitute major stationary sources and do not typically trigger PSD permits or review. However, this analysis includes a comparison of ambient concentrations from an accumulation of new oil and gas exploration and development sources within the entire study area to PSD increments at specific Class I and Class II areas for information purposes. This information will help state agencies track potential minor source increment consumption and aid FLM managers or tribal governments responsible for protecting air resources in Class I areas.

4.7 Air Resource Assessment Results

4.7.1 NAAQS Impacts

Ramboll used the future year CAMx modeling results to examine future air quality relative to the NAAQS and the individual contributions of each source group relative to the NAAQS. For the ozone and $PM_{2.5}$ NAAQS, comparisons are presented both in terms of the "absolute" CAMx results and in terms of using the base case and future year CAMx results to scale the DVC or DVB to obtain the projected DVF, as recommended by the USEPA's modeling guidelines (USEPA, 2007; 2014) and described in Section 4.6.2.2.

4.7.1.1 Ozone NAAQS Analysis Using Relative Model Results

Ramboll used the USEPA's MATS v2.6.1 to project future year ozone DVF, using the CAMx 2012 base case and future year scenario modeling results as described in Section 4.6.2.2. Ramboll used the MATS unmonitored area analysis (UAA) procedures to project the DVF at ambient air monitoring site locations and throughout the 4-km modeling domain.

4.7.1.1.1 Monitored Ozone Design Value Projections Using MATS

Tables 4-15 and 4-16 list MATS results for the DVFs at individual ambient air monitoring sites in the 4-km domain. Updated MATS data files containing ozone design values based on 2010–2014 ozone observations were obtained from the USEPA (2016). To make future year projections, MATS starts with a DVC that is based on an average of three ozone design values from the five-year period centered on the base case modeling year, which was 2012 for this analysis. Thus, MATS DVCs are based on ozone design values from the 2010–2012, 2011–2013, and 2012–2014 periods. MATS projects ozone DVFs using the changes in DMAX8 ozone concentrations near (3 x 3 array of 4-km grid cells) a monitor based on the ratio of future year to current year modeling results to scale the observed DVCs. These model-derived scaling factors are RRFs (DVF = DVC x RRF). The RRFs are based on the 10 highest modeled ozone days above a threshold ozone concentration. MATS used a lower bound observed ozone threshold value of 50 ppb.

Of the 74 monitors with valid DVCs as calculated by MATS, 39 have DVCs exceeding the NAAQS (defined as a value of at least 71 ppb). A total of 17 sites have predicted DVFs exceeding the NAAQS. DVFs are less than DVCs at all 74 sites, reflecting the overall reduction in ozone precursor emissions in the future year scenario noted in Section 4.3.5.10.

Ramboll determined each source group's contributions to the DVFs as the difference between the DVF calculated from the CAMx results with all sources included and a revised DVF calculated after first subtracting out the individual hourly contributions of each source group in the future year model run. These source group contributions are tabulated in Table 4-16. The maximum contribution from source group C2 (new platforms and support vessels and helicopters associated with the 10-sale action) is 1.2 ppb at a site in Jefferson County (Beaumont-Port Arthur), Texas. The maximum contribution from source group B2 (new platforms and support vessels and helicopters associated with the single-sale action) is 0.3 ppb and occurs at the same site. Table 4-16 also shows combined contributions of new and existing BOEM OCS platforms and support traffic under the 10-sale and single-sale scenarios (source groups C3 and B3, respectively). The maximum contribution under the 10-sale scenario is 4.4 ppb at Santa Rosa County, Florida, and the maximum under the single-sale scenario is 3.7 ppb at the same location. Table 4-16 also shows contributions from just existing BOEM OCS platforms and support traffic (source group A2), the maximum value of which is also 3.7 ppb at the same location.

Ramboll identified one site in Texas (Clinton Drive in Harris County) where the contribution of the new platforms and associated support vessels and aircraft under the 10-sale action (source group C2) to the DVF was enough to push it from just below the 70 ppb NAAQS (with source group C2 contributions removed) to just above the NAAQS when all sources were included. This did not occur at any other monitoring site within the 4-km domain. The contribution from source group C2 at the Clinton Drive monitoring site was 0.4 ppb and the DVF was 71.3 ppb (comparisons to the 70 ppb NAAQS were made after truncating design values to the nearest ppb). The DVC at this site was also greater than 70 ppb, as noted above. The contribution of just the new platforms associated with the 10-sale action at this monitor was 0.1 ppb (not shown), which was not large enough by itself to push the DVF above 70 ppb. Similarly, the contribution of new platforms and support vessels under the single-sale scenario (source group B2) was not large enough to push the DVF above 70 ppb.

Table 4-15. DVC and DVF Ozone Design Values (ppb) at Ambient Air Monitoring Sites Within the 4-km Modeling Domain from MATS[a]

Site ID	Site Name	State	DVC	DVF
10030010	Fairhope High School, Fairhope, Alabama	AL	68.0	62.8
10970003	Chickasaw, Mobile Co., Alabama	AL	67.3	62.7
10972005	Bay Rd., Mobile Al.	AL	72.0	66.6
120330004	Ellyson Industrial Park-Copter Road	FL	67.7	63.4
120330018	NAS Pensacola	FL	70.7	65.8
120910002	720 Lovejoy Rd	FL	65.0	60.8
121130015	1500 Woodlawn Way	FL	69.3	64.9
220050004	11153 Kling Road	LA	71.3	67.9
220190002	Highway 27 And Highway 108	LA	70.7	65.5
220190008	2646 John Stine Road	LA	66.7	62.5
220190009	2284 Paul Bellow Road	LA	70.0	65.0
220330003	East End of Aster Lane	LA	75.3	70.6
220330009	1061-A Leesville Ave	LA	72.3	67.7
220330013	11245 Port Hudson-Pride Rd. Zachary, La	LA	69.0	63.2
220470009	65180 Belleview Road	LA	70.3	64.5
220470012	Highway 171, Carville	LA	73.3	68.5
220511001	West Temple Pl	LA	71.3	67.3
220550007	646 Cajundome	LA	69.7	65.7
220570004	Nicholls University Farm Highway 1	LA	71.0	65.2
220630002	Highway 16, French Settlement	LA	72.3	67.8
220710012	Corner of Florida Ave & Orleans Ave	LA	68.3	65.3
220770001	Ted Davis Residence. Highway 415	LA	74.0	68.3
220870004	4101 Mistrot Dr. Meraux, LA 70075	LA	68.0	62.6
220890003	1 River Park Drive	LA	67.7	64.5
220930002	St. James Courthouse, Hwy 44 @ Canapella	LA	66.3	62.2
220950002	Anthony F. Monica Street	LA	72.0	68.4
221030002	1421 Hwy 22 W, Madison Ville, LA 70447	LA	72.3	67.7
221210001	1005 Northwest Drive, Port Allen	LA	68.0	63.2
280450003	400 Baltic St	MS	66.3	62.1
280470008	47 Maple Street	MS	70.3	65.1
280590006	Hospital Road at Co. Health Dept.	MS	71.3	66.6
480271047	1605 Stone Tree Drive	TX	73.7	71.0
480290052	F Range, 1000yd Marker Off Wilderness Tr	TX	80.3	78.2
480290059	14620 Laguna Rd.	TX	68.7	66.6
480391004	4503 Croix Pkwy	TX	85.0	81.4
480391016	109 B Brazoria Hwy 332 West	TX	69.3	65.2
480610006	344 Porter Drive	TX	60.7	58.5
481391044	900 FM 667 Ellis County	TX	69.3	66.6
481671034	9511 Avenue V 1/2	TX	75.3	70.0

Site ID	Site Name	State	DVC	DVF
482010024	4510 1/2 Aldine Mail Rd.	TX	76.7	73.7
482010026	1405 Sheldon Road	TX	73.0	69.8
482010029	16822 Kitzman	TX	80.0	75.7
482010046	7330 1/2 North Wayside	TX	73.7	70.5
482010047	4401 1/2 Lang Rd.	TX	77.0	74.1
482010051	13826 1/2 Croquet	TX	78.7	76.3
482010055	6400 Bissonnet Street	TX	78.7	76.8
482010062	9726 1/2 Monroe	TX	76.7	73.5
482010066	3333 1/2 Hwy 6 South	TX	77.7	74.8
482010070	5425 Polk Ave., Suite H	TX	75.0	72.2
482010416	7421 Park Place Blvd	TX	77.3	73.9
482011015	1001 B Lynchburg Road	TX	71.0	67.6
482011034	1262 1/2 Mae Drive	TX	78.0	74.9
482011035	9525 Clinton Dr	TX	74.7	71.3
482011039	4514 1/2 Durant St.	TX	78.3	74.5
482011050	4522 Park Rd.	TX	76.3	71.9
482150043	2300 North Glasscock	TX	59.3	57.8
482151048	325 Golf Course Road	TX	60.0	57.9
482450009	1086 Vermont Avenue	TX	71.7	67.5
482450011	800 El Vista Road & 53rd Street	TX	74.0	67.8
482450022	12552 Second St.	TX	70.3	65.8
482450101	6019 Mechanic	TX	75.0	68.7
482450102	SETRPC 43 Jefferson Co Airport C64	TX	67.0	62.5
482450628	SETRPC Port ArthurC628	TX	69.3	63.6
482451035	Seattle Street	TX	69.3	64.9
483091037	4472 Mazanec Rd	TX	71.7	69.1
483390078	9472 A Hwy 1484	TX	78.0	74.7
483491051	Corsicana Airport	TX	70.0	68.0
483550025	Corpus Christi State School, Airport Rd	TX	69.3	66.1
483550026	9860 La Branch	TX	68.3	65.2
483611001	2700 Austin Ave	TX	69.3	64.3
483611100	Intersection of Tx Hwys 62 and 12	TX	68.0	63.3
484530014	3724 North Hills Dr, Austin, TX 78758	TX	71.3	67.9
484530020	12200 Lime Creek Rd.	TX	71.7	67.9
484690003	106 Mockingbird Lane	TX	66.3	63.6

[a] Values exceeding the 70 ppb, 8-hour NAAQS after truncation to nearest ppb are shown in red.

Table 4-16. DVC and DVF Ozone Design Values (in ppb) and Reduction in DVF with Contributions from Individual Source Groups Removed[a]

Site ID	State	County	DVC	DVF	Reduction in DVF with Source Group Removed				
					10-Sale		Single-Sale		No-Sale
					C2	C3[b]	B2	B3[c]	A2
10030010	AL	Baldwin County	68.0	62.8	0.5	2.3	0.1	2.0	2.0
10970003	AL	Mobile County	67.3	62.7	0.3	1.3	0.0	1.0	1.0
10972005	AL	Mobile County	72.0	66.6	0.2	0.8	0.0	0.6	0.6
120330004	FL	Escambia County	67.7	63.4	0.4	2.4	0.0	2.1	2.0
120330018	FL	Escambia County	70.7	65.8	0.6	3.4	0.1	3.0	2.9
120910002	FL	Okaloosa County	65.0	60.8	0.9	4.0	0.1	3.5	3.4
121130015	FL	Santa Rosa County	69.3	64.9	0.8	4.4	0.2	3.9	3.7
220050004	LA	Ascension Parish	71.3	67.9	0.3	1.3	0.1	1.1	1.1
220190002	LA	Calcasieu Parish	70.7	65.5	0.6	1.8	0.1	1.3	1.2
220190008	LA	Calcasieu Parish	66.7	62.5	0.6	1.7	0.1	1.2	1.1
220190009	LA	Calcasieu Parish	70.0	65.0	0.5	1.7	0.1	1.3	1.2
220330003	LA	East Baton Rouge Parish	75.3	70.6	0.3	1.4	0.0	1.2	1.1
220330009	LA	East Baton Rouge Parish	72.3	67.7	0.3	1.3	0.0	1.1	1.0
220330013	LA	East Baton Rouge Parish	69.0	63.2	0.4	1.6	0.1	1.2	1.2
220470009	LA	Iberville Parish	70.3	64.5	0.2	0.5	0.1	0.4	0.3
220470012	LA	Iberville Parish	73.3	68.5	0.1	0.7	0.0	0.6	0.6
220511001	LA	Jefferson Parish	71.3	67.3	0.5	2.8	0.1	2.4	2.3
220550007	LA	Lafayette Parish	69.7	65.7	0.4	1.3	0.1	1.0	0.9
220570004	LA	Lafourche Parish	71.0	65.2	0.2	0.7	0.0	0.5	0.5
220630002	LA	Livingston Parish	72.3	67.8	0.5	2.3	0.1	1.9	1.8
220710012	LA	Orleans Parish	68.3	65.3	0.5	2.9	0.2	2.5	2.4
220770001	LA	Pointe Coupee Parish	74.0	68.3	0.3	1.2	0.1	0.9	0.9
220870004	LA	St. Bernard Parish	68.0	62.6	0.5	2.8	0.1	2.4	2.3
220890003	LA	St. Charles Parish	67.7	64.5	0.3	1.2	0.1	1.0	0.9
220930002	LA	St. James Parish	66.3	62.2	0.2	0.6	0.0	0.4	0.4
220950002	LA	St. John the Baptist Parish	72.0	68.4	0.3	1.2	0.1	1.0	1
221030002	LA	St. Tammany Parish	72.3	67.7	0.7	3.3	0.2	2.8	2.6
221210001	LA	West Baton Rouge Parish	68.0	63.2	0.3	1.1	0.1	0.9	0.8
280450003	MS	Hancock County	66.3	62.1	0.5	2.4	0.2	2.1	2
280470008	MS	Harrison County	70.3	65.1	0.3	1.7	0.0	1.5	1.4
280590006	MS	Jackson County	71.3	66.6	0.4	2	0.1	1.8	1.7
480271047	TX	Bell County	73.7	71.0	0.1	0.3	0.0	0.3	0.3
480290052	TX	Bexar County	80.3	78.2	0.1	0.4	0.0	0.3	0.3

Site ID	State	County	DVC	DVF	Reduction in DVF with Source Group Removed				
					10-Sale		Single-Sale		No-Sale
					C2	C3[b]	B2	B3[c]	A2
480290059	TX	Bexar County	68.7	66.6	0.1	0.2	0.0	0.1	0.1
480391004	TX	Brazoria County	85.0	81.4	0.3	1.1	0.0	0.8	0.8
480391016	TX	Brazoria County	69.3	65.2	0.4	1.9	0.0	1.5	1.4
480610006	TX	Cameron County	60.7	58.5	0.2	0.6	0.0	0.4	0.4
481391044	TX	Ellis County	69.3	66.6	0.1	0.1	0.0	0.1	0.1
481671034	TX	Galveston County	75.3	70.0	0.8	3.3	0.1	2.7	2.5
482010024	TX	Harris County	76.7	73.7	0.5	1.7	0.1	1.3	1.2
482010026	TX	Harris County	73.0	69.8	0.4	1.6	0.1	1.2	1.1
482010029	TX	Harris County	80.0	75.7	0.5	1.4	0.1	1.1	1
482010046	TX	Harris County	73.7	70.5	0.4	1.5	0.1	1.2	1.1
482010047	TX	Harris County	77.0	74.1	0.4	1.2	0.1	0.9	0.8
482010051	TX	Harris County	78.7	76.3	0.3	1.1	0.1	0.9	0.8
482010055	TX	Harris County	78.7	76.8	0.3	1.1	0.1	0.9	0.8
482010062	TX	Harris County	76.7	73.5	0.4	1.3	0.1	1.0	1
482010066	TX	Harris County	77.7	74.8	0.3	1	0.1	0.8	0.8
482010070	TX	Harris County	75.0	72.2	0.3	1.1	0.0	0.8	0.8
482010416	TX	Harris County	77.3	73.9	0.3	1	0.0	0.8	0.8
482011015	TX	Harris County	71.0	67.6	0.4	1.5	0.1	1.2	1.1
482011034	TX	Harris County	78.0	74.9	0.4	1.5	0.1	1.2	1.1
482011035	TX	Harris County	74.7	71.3	0.4	1.2	0.1	0.9	0.9
482011039	TX	Harris County	78.3	74.5	0.3	1.4	0.1	1.1	1
482011050	TX	Harris County	76.3	71.9	0.6	2.4	0.1	1.8	1.7
482150043	TX	Hidalgo County	59.3	57.8	0.2	0.5	0.1	0.3	0.3
482151048	TX	Hidalgo County	60.0	57.9	0.1	0.4	0.0	0.3	0.2
482450009	TX	Jefferson County	71.7	67.5	0.2	0.7	0.0	0.5	0.5
482450011	TX	Jefferson County	74.0	67.8	0.5	1.9	0.1	1.4	1.3
482450022	TX	Jefferson County	70.3	65.8	0.3	0.8	0.1	0.6	0.6
482450101	TX	Jefferson County	75.0	68.7	1.2	3.5	0.3	2.6	2.4
482450102	TX	Jefferson County	67.0	62.5	0.4	1.2	0.1	0.9	0.9
482450628	TX	Jefferson County	69.3	63.6	0.6	2.1	0.1	1.6	1.5
482451035	TX	Jefferson County	69.3	64.9	0.4	1.6	0.1	1.2	1.2
483091037	TX	McLennan County	71.7	69.1	0.1	0.2	0.0	0.1	0.1
483390078	TX	Montgomery County	78.0	74.7	0.4	1.2	0.1	0.9	0.9
483491051	TX	Navarro County	70.0	68.0	0	0.1	0.0	0.1	0.1
483550025	TX	Nueces County	69.3	66.1	0.5	1.8	0.1	1.4	1.3
483550026	TX	Nueces County	68.3	65.2	0.5	1.7	0.0	1.3	1.2
483611001	TX	Orange County	69.3	64.3	0.5	2	0.1	1.6	1.5
483611100	TX	Orange County	68.0	63.3	0.4	1.6	0.1	1.3	1.2

Site ID	State	County	DVC	DVF	Reduction in DVF with Source Group Removed				
					10-Sale		Single-Sale		No-Sale
					C2	C3[b]	B2	B3[c]	A2
484530014	TX	Travis County	71.3	67.9	0.1	0.5	0.0	0.4	0.4
484530020	TX	Travis County	71.7	67.9	0.1	0.5	0.0	0.4	0.3
484690003	TX	Victoria County	66.3	63.6	0.4	1.2	0.1	0.9	0.9

[a] Values exceeding the 70 ppb, 8-hour NAAQS after truncation to nearest ppb are shown in red.
[b] The sum of C2 and A2 contributions in this table does not always exactly equal the C3 contribution due to rounding.
[c] The sum of B2 and A2 contributions in this table does not always exactly equal the B3 contribution due to rounding.

4.7.1.1.2 Ozone MATS Unmonitored Area Analysis

Figure 4-30 displays the MATS UAA results, which were generated using the observed ozone data in MATS and the base year and future year scenario CAMx results. The MATS UAA spatially interpolates the DVCs obtained from observations across the modeling domain using modeled spatial gradients as described in EPA's modeling guidance (USEPA, 2014a) and then calculates the DVF for each model grid cell by multiplying the interpolated DVC by the RRF value (the ratio of the modeled future year to base year design values) in each grid cell. Although results of the MATS UAA are presented here over the full 4-km modeling domain, it should be noted that results of the spatial interpolation over the GOM (which covers more than half of the domain) are subject to significant uncertainty as they are not well constrained by observations due to the lack of monitoring sites over the Gulf (see Section 4.7.1.2 for a discussion of the high predicted ozone values over the Gulf waters).

DVFs calculated using the MATS UAA procedure are lower than DVCs throughout most of the 4-km modeling domain, with the exception of small, localized increases near new platform sources and just offshore of Lafourche Parrish, Louisiana, in the vicinity of the LOOP. The calculated increase near the LOOP is likely due to reductions in NO_x emissions, which are calculated to have suppressed ozone production in this area in the 2012 base case.

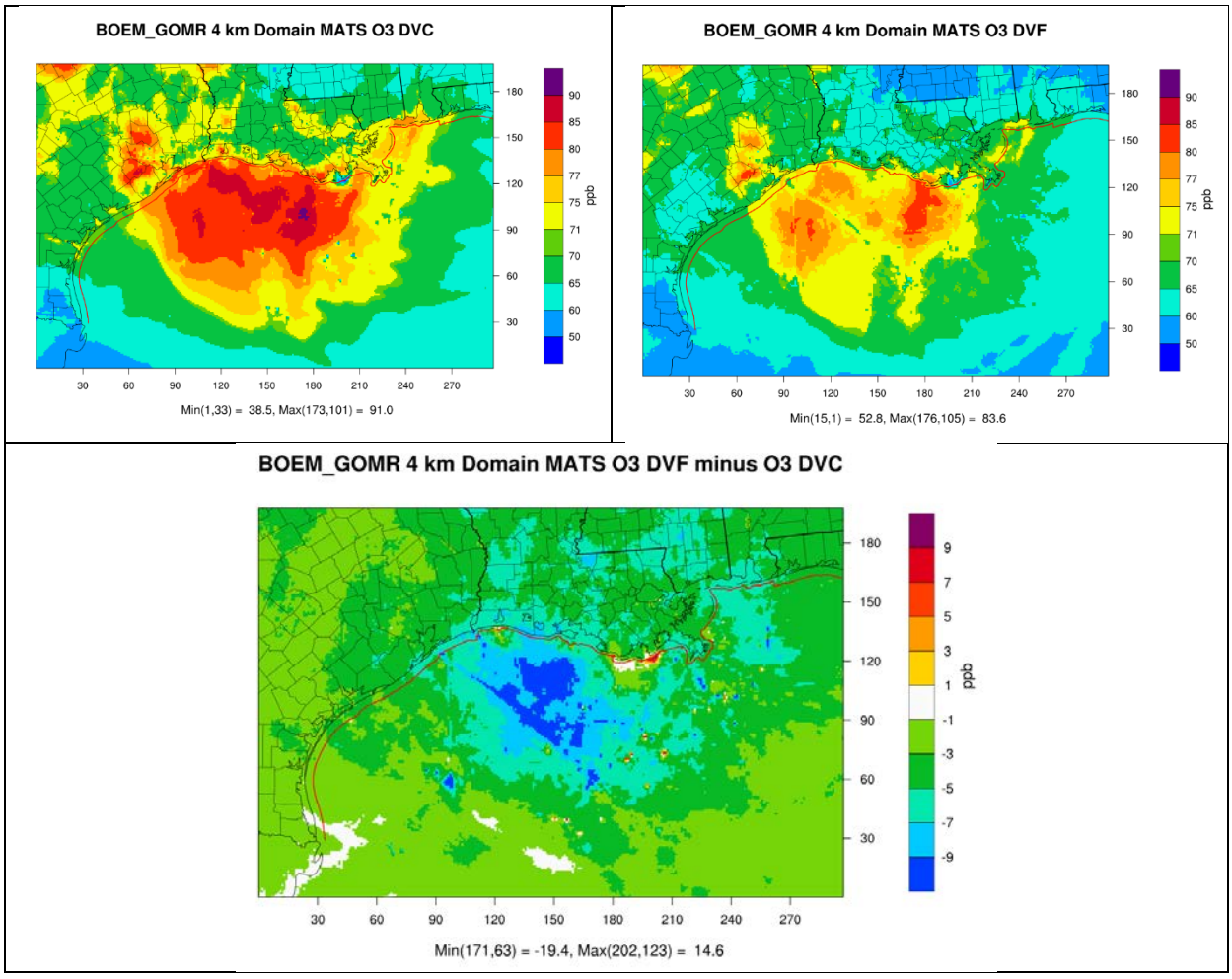

Figure 4-30. DVC (top left), DVF (top right), and Their Differences (DVF–DVC; bottom)
Note: Calculated using the MATS UAA tool; red line parallel to coast represents the state seaward boundary.

The left column of Figure 4-31a and Figure 4-31b shows the MATS UAA DVF values calculated after first removing the hourly contributions from source groups B2 (new platforms and associated support vessels and aircraft under the single-sale scenario), B3 (B2 plus existing platforms and support traffic), C2 (new platforms and associated support vessels and aircraft under the 10-sale scenario), C3 (C2 plus existing platforms and support traffic), and A2 (just existing platforms and support traffic). Contributions of source groups B2, B3, C2, C3, and A2 calculated as the difference between these DVF values and the DVF values from all sources (as shown in the upper right-hand corner of Figure 4-31a) are shown in the right column of Figure 4-32. Source group B2 and C2 contributions are centered in the Gulf offshore of Louisiana with a peak impact of 1.9 ppb for source group B2, 13.8 ppb for B3, 4.9 ppb for C2, and 16.0 ppb for C3. Maximum impacts from the state seaward boundaries inland are below approximately 0.6 ppb for source group B2, less than approximately 2.4 ppb for C2, less than approximately 8 ppb for B3, and less than approximately 10 ppb for C3. Source group A2 impacts are centered in approximately the same location in the Gulf as C2, with a maximum contribution of 13.8 ppb; source group A2 impacts from the state seaward boundaries inland are below approximately 8 ppb.

Source Group[a]	DVF with Source Group Contribution Removed	Source Group Contribution[b]
B2	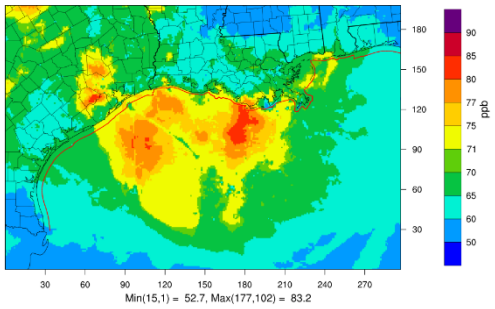	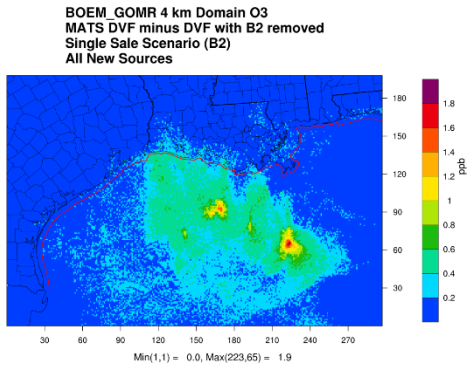
B3	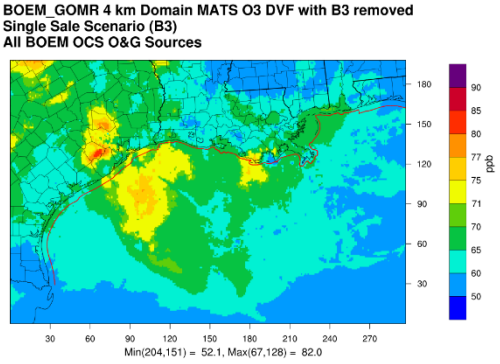	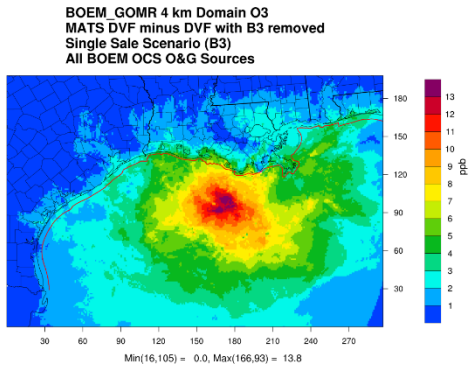

Figure 4-31a. MATS UAA DFVs Calculated After Removing the Hourly Contributions from a Source Group (left column) and the Corresponding Contributions of the Source Group to the DVFs (right column)

Note: Red line parallel to coast represents the state seaward boundary.

[a] As defined in Table 4-13.

[b] Source group contributions are determined by subtracting the DVF values calculated after removing the hourly source group contributions from the DVF values calculated when all sources are included.

Source Group[a]	DVF with Source Group Contribution Removed	Source Group Contribution[b]
C2	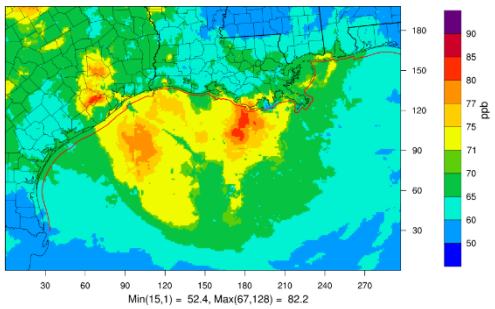	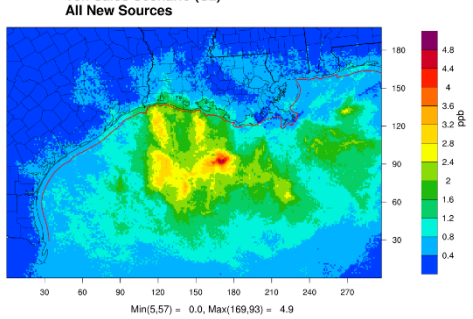
C3	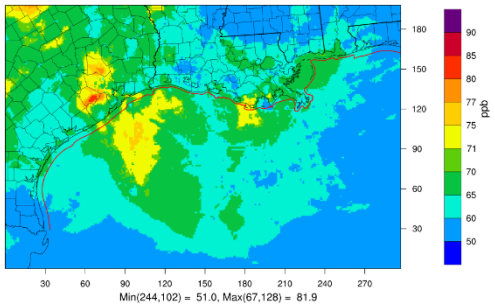	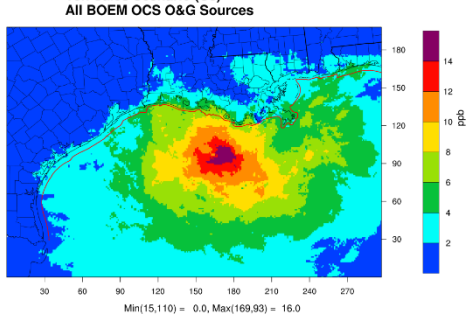
A2	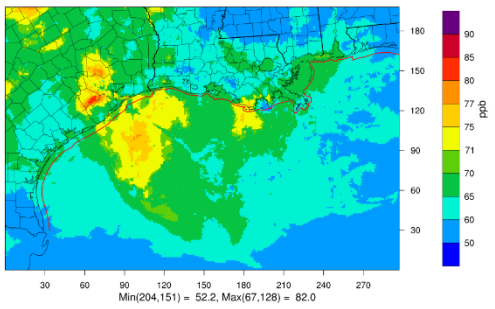	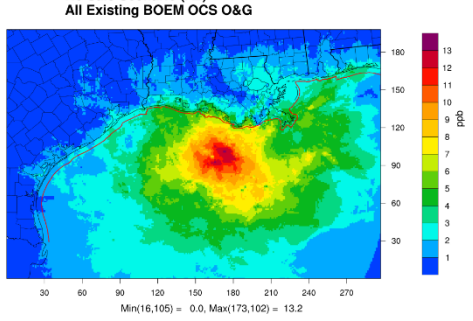

Figure 4-31b. MATS UAA DFVs Calculated After Removing the Hourly Contributions from a Source Group (left column) and the Corresponding Contributions of the Source Group to the DVFs (right column)

Note: Red line parallel to coast represents the state seaward boundary.

[a] As defined in Table 4-13.

[b] Source group contributions are determined by subtracting the DVF values calculated after removing the hourly source group contributions from the DVF values calculated when all sources are included.

4.7.1.2 Ozone NAAQS Analysis Using Absolute Modeling Results

This section analyzes and compares the CAMx source apportionment absolute modeling results from the future year scenario with the ozone NAAQS. The ozone NAAQS is defined as the three-year average of the fourth-highest maximum daily average 8-hour (MDA8) ozone concentration. Because only one calendar year of modeling results are available for the base year and future year scenarios, the future year fourth-highest MDA8 ozone concentration is used as a pseudo-NAAQS comparison metric.

Figure 4-32 shows the modeled fourth-highest MDA8 values in each model grid cell for the base and future year scenarios and their corresponding differences. Similar to the MATS results in Figure 4-30, the fourth-highest MDA8 is lower under the future year scenario throughout most of the 4-km domain with isolated areas of NO_x emission increases located downwind of new platforms offshore or reductions from some sources that had been contributing to local ozone losses in the base year through titration of O_3 by NO.

Results in Figure 4-32 show a broad area of elevated fourth-highest MDA8 values over the GOM, which in some cases exceed the values predicted in urban areas such as the Houston ozone nonattainment area. Predictions of elevated ozone levels over large bodies of water are a common feature of photochemical model results (Reidmiller et al., 2009) but are difficult to verify given the lack of measurements in these areas. A review of movies of hourly ozone predictions in the surface grid cell layer over the 4-km domain suggests that episodes of high ozone over the Gulf are commonly associated with or closely preceded by offshore flow carrying ozone (and presumably ozone precursors) out over the Gulf where, in contrast to ozone over land, the elevated concentrations persist, often into the next day. Additional offshore ozone formation was also observed, both during the initial offshore flow period and on subsequent day(s). We speculate that reduced vertical mixing and a lack of ozone destruction mechanisms result in an environment that can lead to higher ozone concentrations over the Gulf than over land. Elevated ozone over the Gulf was not observed during sustained periods of onshore flow, indicating that interaction with a continental airmass is necessary for development of high ozone over the Gulf.

Source apportionment results (Figure 4-33) indicate that all BOEM oil and gas sources (future year 10-sale scenario) are predicted to locally contribute as much as 29 ppb to the elevated offshore MDA8 values. Comparison with Figure 4-32 shows that this maximum contribution coincides with a predicted impact from all sources of 82 ppb, thus representing 35percent of the total modeled ozone at that location.

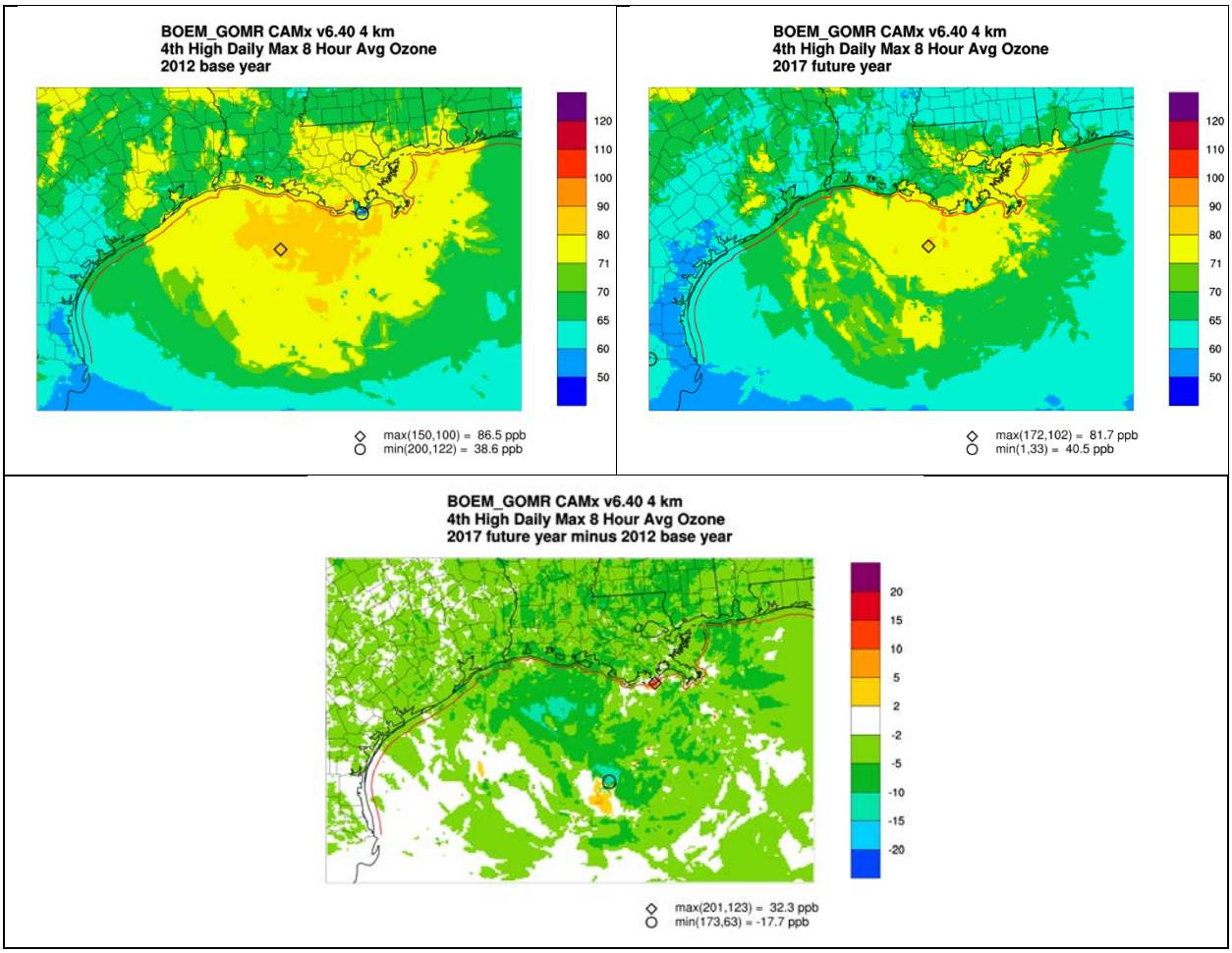

Figure 4-32. Modeled Fourth-Highest MDA8 Ozone for the Base Year (upper left) and Future Year (upper right) Scenarios and Their Differences (bottom center)
Note: Red line parallel to coast represents the state seaward boundary.

Figure 4-33 shows contributions of selected source groups to the future year fourth-highest MDA8 values for all sources (note the different color scale in the top row of the figure). These contributions are matched in time to the fourth-highest MDA8 values for all sources; contributions may be different during other periods with elevated MDA8 values. As shown in Figure 4-33, new platforms and associated support vessels and helicopters under the single-sale scenario (source group B2) are estimated to contribute as much as 4.2 ppb to design values over the Gulf. Within the states out to the state seaward boundary, the contributions range from near zero in nearly all locations to approximately 1.6 ppb in an isolated area along the coast of southwestern Louisiana. Under the 10-sale scenario, contributions from new platforms and support vessels and helicopters (source group C2) along and inland of the state seaward boundaries are mostly less than 2 ppb with the peak impact off the southwestern Louisiana coast in the 5 to 6 ppb range. When contributions from all other OCS platforms and support vessels and helicopters are included along with the new sources under either the single-sale scenario (source group B3), the 10-sale scenario (source group C3), or the no-sale scenario (source group A2), contributions to the fourth-highest MDA8 values along and inland of the state overwater boundaries are greater in most locations with maximum values in the 8 to 14 ppb range. Comparing these values with the predicted future year scenario's fourth-highest MDA8 value in the top right panel of Figure 4-32 indicates that the bulk of the ozone predicted over the Gulf is attributable to sources of emissions other than BOEM OCS platforms and support vessels and helicopters. These sources include other ship traffic in the Gulf, land-based anthropogenic sources, non-anthropogenic emissions, and boundary conditions.

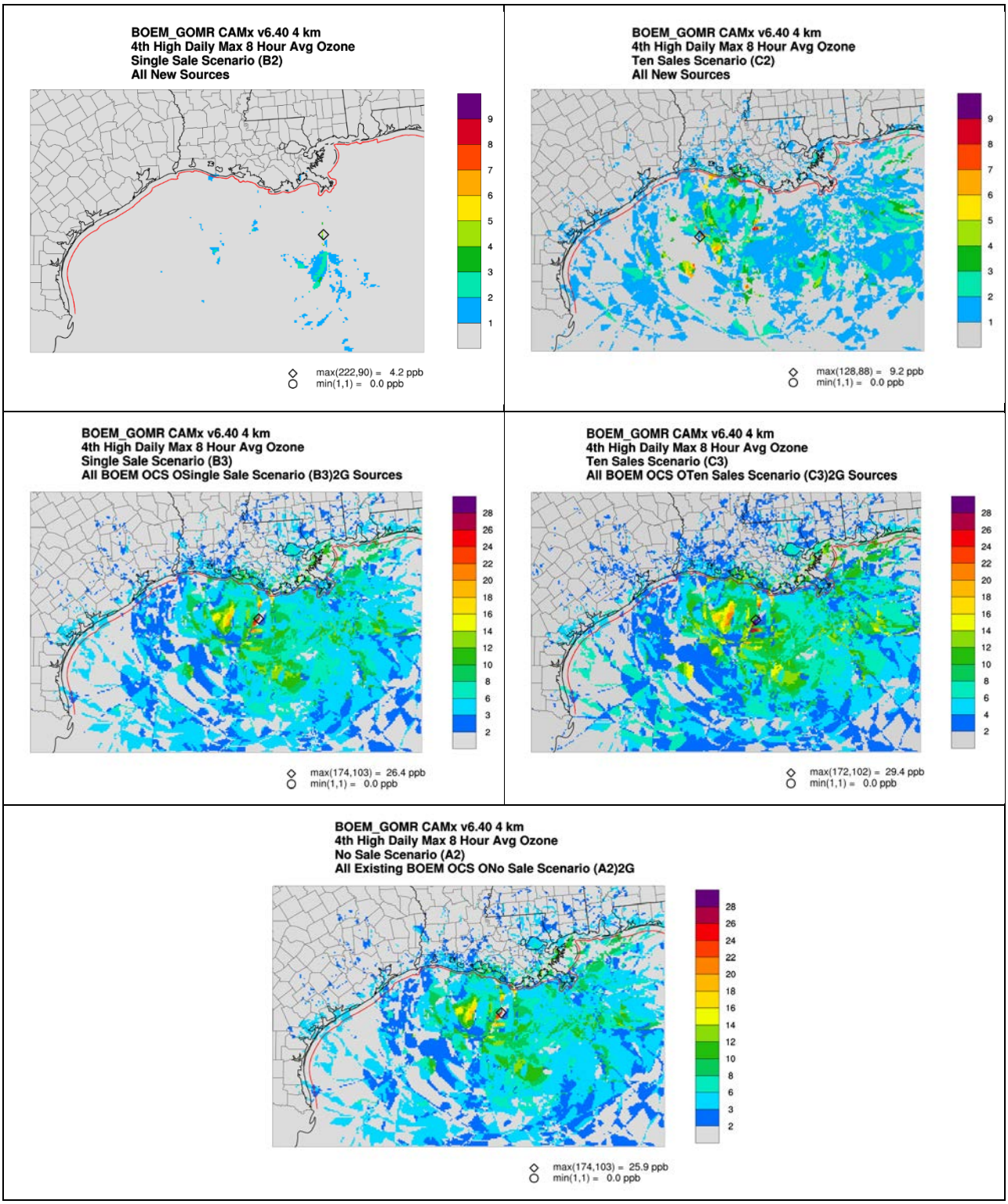

Figure 4-33. Contributions of New Platforms and Support Vessels and Helicopters Under the Single-Sale Scenario (top left) and 10-Sale Scenario (top right), All OCS Platforms and Support Vessels Under the Single-Sale (middle left) and 10-Sale (middle right) Scenarios, and All OCS Platforms and Support Vessels under the No-Sale Scenario (bottom) to the Future Year Scenario's Fourth-Highest MDA8 Values for All Sources

Note: Red line parallel to coast represents the state seaward boundary.

4.7.1.3 $PM_{2.5}$ NAAQS Analysis Using Relative Model Results

There are two $PM_{2.5}$ NAAQS: one for 24-hour averaging time that is expressed as a three-year average of the annual 98th percentile in a year with a threshold of 35 µg/m^3 and an annual average over three years with a threshold of 12 µg/m^3. With one year of complete everyday modeling, the annual 98th percentile will correspond to the eighth-highest 24-hour $PM_{2.5}$ concentration in a year.

Ramboll predicted future year 24-hour and annual average $PM_{2.5}$ design values using model results in a relative sense, as it did for ozone design values in Section 4.7.1.1. The MATS software was used to generate predicted DVFs from DVBs or DVCs. MATS was configured to use ambient measurements of total $PM_{2.5}$ for the period 2008–2012 to generate DVCs based on an average of three overlapping three-year average DVs—as recommended in the USEPA's guidance (USEPA, 2014a)—and speciated $PM_{2.5}$ monitoring data for the period 2010–2012 to generate the projected DVFs based on model-predicted species RRFs.

4.7.1.3.1 24-Hour $PM_{2.5}$

As described for the ozone NAAQS analysis, Ramboll used MATS to calculate DVFs for the 24-hour and annual $PM_{2.5}$ NAAQS. The USEPA (2016) provided observational data for MATS to calculate the DVCs. For total $PM_{2.5}$, observational data covered the period 2008–2012; for the speciated $PM_{2.5}$ calculations, observational data covered the period 2010–2012.

Table 4-17 shows the results of the MATS analysis. All DVCs and DVFs are below the 35 µg/m^3 NAAQS, and the DVFs are projected to be lower than the DVCs at all sites. Table 4-18 shows the reductions in the projected DVFs calculated after removing source contributions from source groups C2 (all new platforms and support vessels and helicopters under the 10-sale scenario), C3 (C2 plus "existing" platforms and support traffic), B2 (all new platforms and support vessels and helicopters under the single-sale scenario), B3 (B2 plus "existing" platforms and support traffic), and A2 ("existing" platforms and support vessels and helicopters under the no-sale scenario). All source group contributions calculated in this manner are less than or equal to 0.1 µg/m^3.

Table 4-17. DVC and DVF 24-Hour $PM_{2.5}$ Design Values ($\mu g/m^3$) for Monitoring Sites in the 4-km Modeling Domain from MATS

Site ID	Site Name	State	County	DVC	DVF
10030010	Fairhope High School, Fairhope, Alabama	AL	Baldwin County	19.5	17.5
10970003	Chickasaw, Mobile Co., Alabama	AL	Mobile County	19.1	17.1
10972005	Bay Rd. Mobile, AL	AL	Mobile County	20.0	17.7
120330004	Ellyson Industrial Park-Copter Road	FL	Escambia County	19.2	17.6
220190009	2284 Paul Bellow Road	LA	Calcasieu Parish	18.6	16.7
220190010	Common and East McNeese	LA	Calcasieu Parish	20.5	18.3
220330009	1061-A Leesville Ave	LA	East Baton Rouge Parish	21.0	19.0
220331001	Highway 964	LA	East Baton Rouge Parish	16.7	13.9
220470005	St Gabriel Agricultural Exp. Station	LA	Iberville Parish	21.0	19.7
220470009	65180 Belleview Road	LA	Iberville Parish	18.6	17.3
220511001	West Temple Pl	LA	Jefferson Parish	18.7	17.0
220512001	Patriot St. and Allo St.	LA	Jefferson Parish	18.5	16.4
220550006	121 East Point Des Mouton	LA	Lafayette Parish	18.8	16.7
220550007	646 Cajundome	LA	Lafayette Parish	20.2	17.8
220790002	8105 Tom Bowman Drive	LA	Rapides Parish	19.6	17.4
220870007	24 E. Chalmette Circle	LA	St. Bernard Parish	20.2	17.4
221050001	21549 Old Hammond Hwy, Hammond, LA 70403	LA	Tangipahoa Parish	18.8	16.9
221090001	4047 Highway 24 North Gray	LA	Terrebonne Parish	17.6	16.0
221210001	1005 Northwest Drive, Port Allen	LA	West Baton Rouge Parish	21.7	20.0
280010004	Natchez Municipal Water Works Brenham St	MS	Adams County	20.3	17.5
280350004	205 Bay Street	MS	Forrest County	22.4	20.9
280450003	400 Baltic St	MS	Hancock County	20.0	17.3
280470008	47 Maple Street	MS	Harrison County	18.3	15.7
280590006	Hospital Road at Co. Health Dept.	MS	Jackson County	20.8	18.7
280670002	26 Mason St.	MS	Jones County	23.0	21.6
480290059	14620 Laguna Rd.	TX	Bexar County	21.4	20.9

Site ID	Site Name	State	County	DVC	DVF
480612004	Lot B 69 1/2	TX	Cameron County	22.7	21.0
482010058	7210 1/2 Bayway Drive	TX	Harris County	20.8	19.8
482011035	9525 Clinton Dr	TX	Harris County	24.0	22.6
483550032	3810 Huisache Street	TX	Nueces County	24.3	23.0
484530020	12200 Lime Creek Rd.	TX	Travis County	20.7	18.8
484530021	2600 B Webberville Rd.	TX	Travis County	21.8	20.3

Table 4-18. DVC and DVF 24-Hour $PM_{2.5}$ Design Values and Reduction in DVF with Contributions from Individual Source Groups Removed ($\mu g/m^3$)

Site ID	State	County	DVC	DVF	Change in DVF with Source Group Removed				
					10-Sale		Single-Sale		No-Sale
					C2	C3[a]	B2	B3[b]	A2
10030010	AL	Baldwin County	19.5	17.5	0.0	0.0	0.0	0.0	0.0
10970003	AL	Mobile County	19.1	17.1	0.0	0.0	0.0	0.0	0.0
10972005	AL	Mobile County	20.0	17.7	0.0	0.0	0.0	0.0	0.0
120330004	FL	Escambia County	19.2	17.6	0.1	0.1	0.1	0.1	0.1
220190009	LA	Calcasieu Parish	18.6	16.7	0.0	0.0	0.0	0.0	0.0
220190010	LA	Calcasieu Parish	20.5	18.3	0.0	0.0	0.0	0.0	0.0
220330009	LA	East Baton Rouge Parish	21.0	19.0	0.0	0.0	0.0	0.0	0.0
220331001	LA	East Baton Rouge Parish	16.7	13.9	0.0	0.0	0.0	0.0	0.0
220470005	LA	Iberville Parish	21.0	19.7	0.0	0.0	0.0	0.0	0.0
220470009	LA	Iberville Parish	18.6	17.3	0.0	0.0	0.0	0.0	0.0
220511001	LA	Jefferson Parish	18.7	17.0	0.0	0.0	0.0	0.0	0.0
220512001	LA	Jefferson Parish	18.5	16.4	0.1	0.1	0.0	0.1	0.1
220550006	LA	Lafayette Parish	18.8	16.7	0.1	0.1	0.0	0.1	0.1
220550007	LA	Lafayette Parish	20.2	17.8	0.0	0.0	0.0	0.0	0.0
220790002	LA	Rapides Parish	19.6	17.4	0.0	0.0	0.0	0.0	0.0
220870007	LA	St. Bernard Parish	20.2	17.4	0.0	0.0	0.0	0.0	0.0
221050001	LA	Tangipahoa Parish	18.8	16.9	0.0	0.1	0.0	0.1	0.0

Site ID	State	County	DVC	DVF	Change in DVF with Source Group Removed				
					10-Sale		Single-Sale		No-Sale
					C2	C3[a]	B2	B3[b]	A2
221090001	LA	Terrebonne Parish	17.6	16.0	0.0	0.0	0.0	0.0	0.0
221210001	LA	West Baton Rouge Parish	21.7	20.0	0.0	0.0	0.0	0.0	0.0
280010004	MS	Adams County	20.3	17.5	0.0	0.0	0.0	0.0	0.0
280350004	MS	Forrest County	22.4	20.9	0.0	0.0	0.0	0.0	0.0
280450003	MS	Hancock County	20.0	17.3	0.0	0.0	0.0	0.0	0.0
280470008	MS	Harrison County	18.3	15.7	0.0	0.0	0.0	0.0	0.0
280590006	MS	Jackson County	20.8	18.7	0.0	0.0	0.0	0.0	0.0
280670002	MS	Jones County	23.0	21.6	0.0	0.0	0.0	0.0	0.0
480290059	TX	Bexar County	21.4	20.9	0.0	0.0	0.0	0.0	0.0
480612004	TX	Cameron County	22.7	21.0	0.0	0.0	0.0	0.0	0.0
482010058	TX	Harris County	20.8	19.8	0.0	0.0	0.0	0.0	0.0
482011035	TX	Harris County	24.0	22.6	0.0	0.0	0.0	0.0	0.0
483550032	TX	Nueces County	24.3	23.0	0.0	0.0	0.0	0.0	0.0
484530020	TX	Travis County	20.7	18.8	0.0	0.0	0.0	0.0	0.0
484530021	TX	Travis County	21.8	20.3	0.0	0.0	0.0	0.0	0.0

[a] The sum of C2 and A2 contributions in this table does not always exactly equal the C3 contribution due to rounding.
[b] The sum of B2 and A2 contributions in this table does not always exactly equal the B3 contribution due to rounding.

4.7.1.3.2 Annual Average $PM_{2.5}$

Table 4-19 shows MATS projections of DVF for the annual average $PM_{2.5}$ design values. The only design value exceeding the 12 µg/m^3 annual average NAAQS is the DVC at the Clinton Drive monitor in Houston, Texas. The projected DVF value at this location is below the NAAQS. DVFs are projected to be less than the DVCs at all monitoring sites except for a 0.2 µg/m^3 increase at the Hidalgo County monitoring site just west of Brownsville, Texas.

Table 4-20 shows reductions in the projected annual average DVFs calculated after removing source contributions from source groups C2, C3, B2, B3, and A2 (i.e., DVF from Table 4-19 minus DVF calculated with hourly source group contributions removed). The largest of the source group C2, C3, B2, B3, or A2 contributions calculated in this manner are 0.1 µg/m^3; contributions at most monitoring sites are less than 0.05 µg/m^3.

Table 4-19. DVC and DVF Annual Average $PM_{2.5}$ Design Values for Monitoring Sites in the 4-km Modeling Domain[a]

Site ID	Site Name	State	DVC	DVF
10030010	Fairhope High School, Fairhope, Alabama	AL	9.8	8.8
10970003	Chickasaw, Mobile Co., Alabama	AL	9.7	8.8
10972005	Bay Rd. Mobile, AL	AL	9.2	8.2
120330004	Ellyson Industrial Park-Copter Road	FL	8.9	8.2
220190009	2284 Paul Bellow Road	LA	8.6	7.6
220190010	Common and East McNeese	LA	9.1	8.2
220330009	1061-A Leesville Ave	LA	10.3	9.4
220331001	Highway 964	LA	9.3	8.2
220470005	St Gabriel Agricultural Exp. Station	LA	10.2	9.4
220470009	65180 Belleview Road	LA	8.9	7.9
220511001	West Temple Pl	LA	9.0	8.0
220512001	Patriot St. and Allo St.	LA	9.2	8.2
220550006	121 East Point Des Mouton	LA	8.9	8.0
220550007	646 Cajundome	LA	9.1	8.1
220790002	8105 Tom Bowman Drive	LA	8.8	7.8
220870007	24 E. Chalmette Circle	LA	10.5	9.5
221050001	21549 Old Hammond Hwy, Hammond, LA 70403	LA	9.0	7.9
221090001	4047 Highway 24 North Gray	LA	8.5	7.5
221210001	1005 Northwest Drive, Port Allen	LA	10.8	10.0
280010004	Natchez Municipal Water Works Brenham St	MS	10.2	9.2
280350004	205 Bay Street	MS	11.7	10.8
280450003	400 Baltic St	MS	9.9	8.8
280470008	47 Maple Street	MS	9.6	8.4
280590006	Hospital Road at Co. Health Dept.	MS	9.5	8.8
280670002	26 Mason St.	MS	11.8	11.2
480290059	14620 Laguna Rd.	TX	9.0	8.8
480612004	LOT B 69 1/2	TX	11.0	10.6
482010058	7210 1/2 Bayway Drive	TX	11.1	10.8
482011035	9525 Clinton Dr	TX	12.4	11.6

Site ID	Site Name	State	DVC	DVF
482150043	2300 North Glasscock	TX	10.4	10.6
483550032	3810 Huisache Street	TX	10.3	9.9
484530020	12200 Lime Creek Rd.	TX	8.4	7.9
484530021	2600 B Webberville Rd.	TX	10.2	9.8

[a] Red values exceed the 12 µg/m^3 NAAQS.

Table 4-20. Annual Average $PM_{2.5}$ Future Year Design Values (DVF) and Change in DVF ($\mu g/m^3$) with Contributions from Individual Source Groups Removed

Site ID	State	County	DVC	DVF	Change in DVF with Source Group Removed				
					10-Sale		Single-Sale		No-Sale
					C2	C3	B2	B3	A2
10030010	AL	Baldwin County	9.8	8.8	0.0	0.0	0.0	0.0	0.0
10970003	AL	Mobile County	9.7	8.8	0.0	0.0	0.0	0.0	0.0
10972005	AL	Mobile County	9.2	8.2	0.0	0.0	0.0	0.0	0.0
120330004	FL	Escambia County	8.9	8.2	0.0	0.0	0.0	0.0	0.0
220190009	LA	Calcasieu Parish	8.6	7.6	0.0	0.0	0.0	0.0	0.0
220190010	LA	Calcasieu Parish	9.1	8.2	0.0	0.0	0.0	0.0	0.0
220330009	LA	East Baton Rouge Parish	10.3	9.4	0.0	0.0	0.0	0.0	0.0
220331001	LA	East Baton Rouge Parish	9.3	8.2	0.0	0.0	0.0	0.0	0.0
220470005	LA	Iberville Parish	10.2	9.4	0.0	0.0	0.0	0.0	0.0
220470009	LA	Iberville Parish	8.9	7.9	0.0	0.0	0.0	0.0	0.0
220511001	LA	Jefferson Parish	9.0	8.0	0.0	0.0	0.0	0.0	0.0
220512001	LA	Jefferson Parish	9.2	8.2	0.1	0.1	0.0	0.1	0.1
220550006	LA	Lafayette Parish	8.9	8.0	0.0	0.1	0.0	0.1	0.0
220550007	LA	Lafayette Parish	9.1	8.1	0.0	0.0	0.0	0.0	0.0
220790002	LA	Rapides Parish	8.8	7.8	0.0	0.0	0.0	0.0	0.0
220870007	LA	St. Bernard Parish	10.5	9.5	0.0	0.0	0.0	0.0	0.0
221050001	LA	Tangipahoa Parish	9.0	7.9	0.0	0.0	0.0	0.0	0.0
221090001	LA	Terrebonne Parish	8.5	7.5	0.0	0.0	0.0	0.0	0.0
221210001	LA	West Baton Rouge Parish	10.8	10.0	0.0	0.0	0.0	0.0	0.0
280010004	MS	Adams County	10.2	9.2	0.0	0.0	0.0	0.0	0.0
280350004	MS	Forrest County	11.7	10.8	0.0	0.0	0.0	0.0	0.0
280450003	MS	Hancock County	9.9	8.8	0.0	0.0	0.0	0.0	0.0
280470008	MS	Harrison County	9.6	8.4	0.0	0.0	0.0	0.0	0.0
280590006	MS	Jackson County	9.5	8.8	0.1	0.1	0.0	0.1	0.1
280670002	MS	Jones County	11.8	11.2	0.0	0.0	0.0	0.0	0.0
480290059	TX	Bexar County	9.0	8.8	0.0	0.0	0.0	0.0	0.0
480612004	TX	Cameron County	11.0	10.6	0.0	0.0	0.0	0.0	0.0
482010058	TX	Harris County	11.1	10.8	0.1	0.1	0.0	0.1	0.1
482011035	TX	Harris County	12.4	11.6	0.1	0.1	0.1	0.1	0.1
482150043	TX	Hidalgo County	10.4	10.6	0.0	0.0	0.0	0.0	0.0
483550032	TX	Nueces County	10.3	9.9	0.0	0.0	0.0	0.0	0.0
484530020	TX	Travis County	8.4	7.9	0.0	0.0	0.0	0.0	0.0
484530021	TX	Travis County	10.2	9.8	0.0	0.0	0.0	0.0	0.0

[a] Red values exceed the 12 $\mu g/m^3$ NAAQS.

Figure 4-34 displays the MATS UAA results for the annual average $PM_{2.5}$ DVC, DVF, and the difference (DVF-DVC).[16] Reductions in annual average $PM_{2.5}$ design values associated with emission reductions from all sources combined are projected throughout nearly the entire domain with the exception of increases of up to approximately 5 µg/m^3 in a few isolated locations. Figure 4-35 shows source group contributions determined by subtracting the DVF with the contribution of a source group removed from the DVF calculated with all sources included. Contributions from source group C2 are generally less than 0.5 µg/m^3; contributions from source group B2 are less than 0.4 µg/m^3. Adding contributions from source group A2 (existing platforms and support traffic) under either the 10-sale scenario (C3) or the single-sale scenario (B3) or by itself increases the maximum contribution to 0.7 µg/m^3. As in the case of the ozone UAA described above, it should be noted that results of the spatial interpolation over the GOM (which covers more than half of the domain) are subject to significant uncertainty as they are not well constrained by observations due to the lack of monitoring sites over the Gulf.

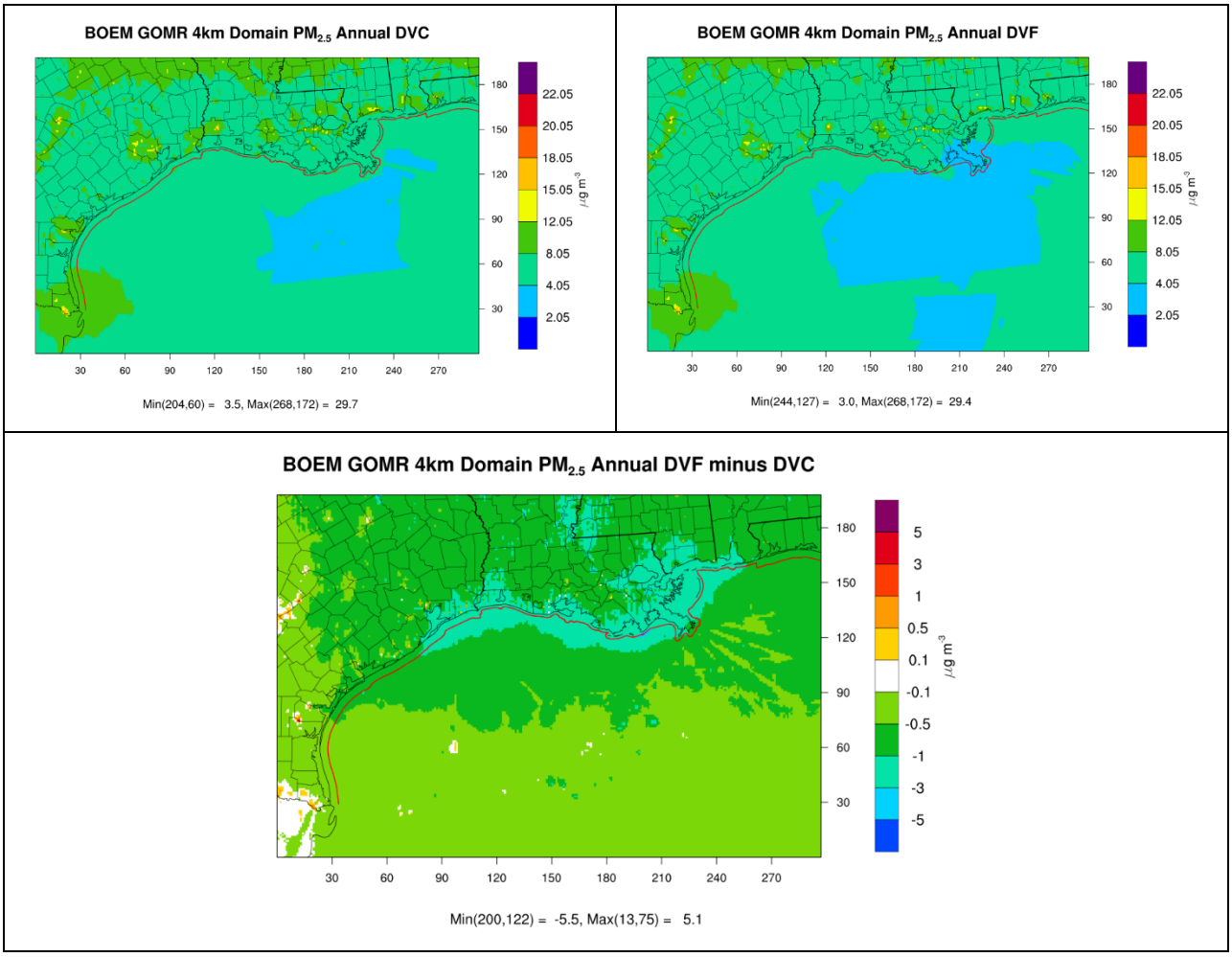

Figure 4-34. DVC and DVF Annual Average $PM_{2.5}$ Design Values from the MATS UAA (top left and top right, respectively) and the Difference (DVF-DVC; bottom)
Note: Red line parallel to coast represents the state seaward boundary.

[16] The UAA analysis was only performed for the annual average $PM_{2.5}$ NAAQS because the MATS software cannot calculate UAA results for the 24-hour average $PM_{2.5}$ NAAQS.

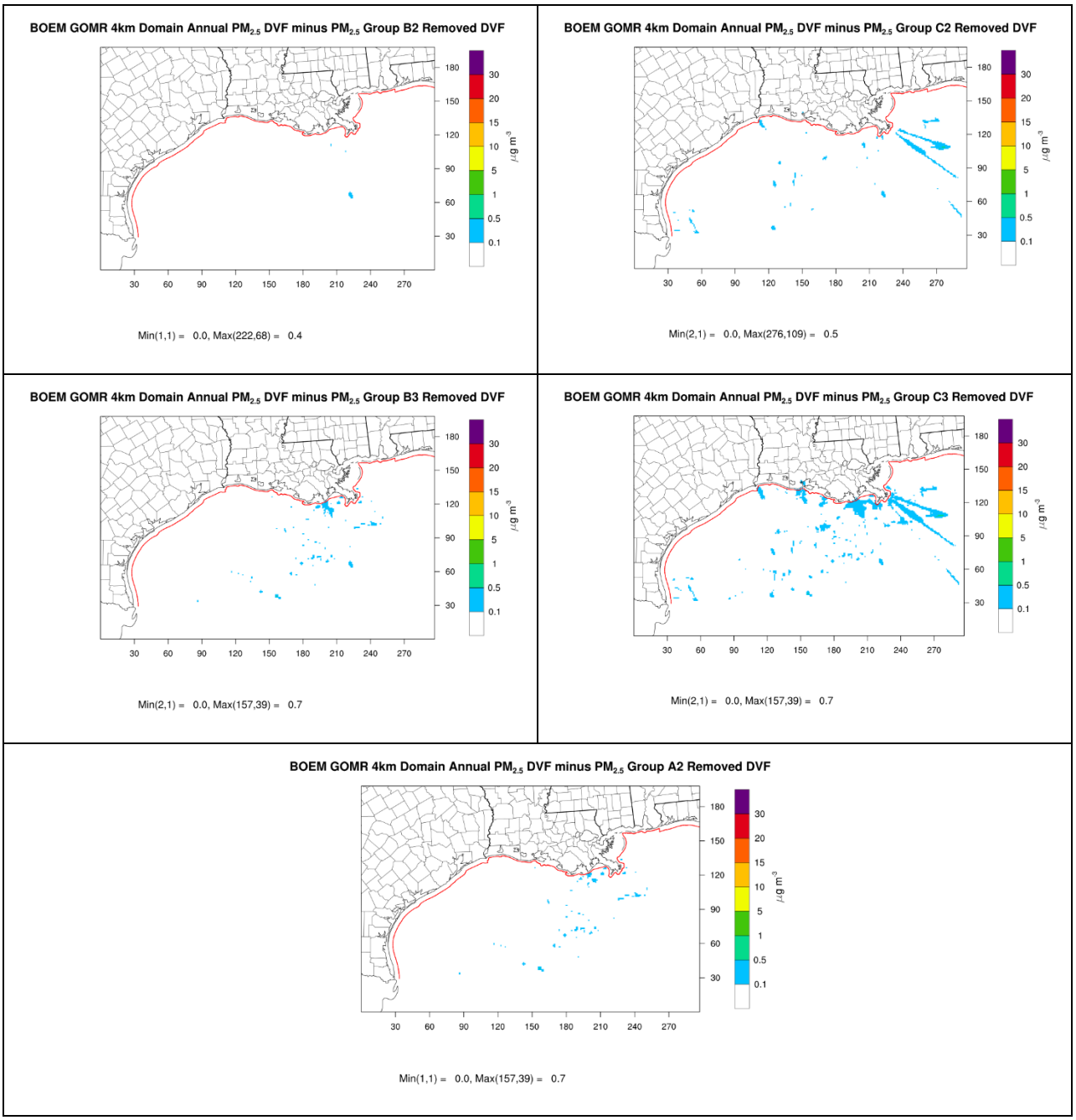

Figure 4-35. Contributions of Source Groups B2 under the Single-Sale Scenario (top left); C2 Under the 10-Sale Scenario (top right); and B3 (middle left), C3 (middle right), and A2 Under the No-Sale Scenario (bottom) to the Future Year Annual Average $PM_{2.5}$ Concentration for All Sources Based on the MATS UAA

Note: Red line parallel to coast represents the state seaward boundary.

4.7.1.4 $PM_{2.5}$ NAAQS Analysis Using Absolute Model Predictions

This section analyzes and compares the CAMx source apportionment absolute modeling results from the future year scenario with the $PM_{2.5}$ 24-hour and annual NAAQS.

4.7.1.4.1 24-Hour $PM_{2.5}$

The 24-hour $PM_{2.5}$ NAAQS is defined as the three-year average of the annual 98th percentile daily average, which corresponds to the eighth-highest daily average in each year assuming complete data. Because only one calendar year of modeling results are available for the base year and future year scenarios, Ramboll selected the future year eighth-highest daily average $PM_{2.5}$ concentration for comparison with the NAAQS.

Figure 4-36 shows the modeled eighth-highest daily $PM_{2.5}$ concentrations in each model grid cell for the base and future year scenarios and their corresponding differences. Areas of high predicted $PM_{2.5}$ occur at a few locations along the Louisiana and east Texas Gulf coasts and along the Mississippi River in Louisiana in both the base and future year scenarios. Although predicted eighth-highest daily $PM_{2.5}$ concentrations in these areas exceed the 35 µg/m^3 NAAQS, both monitored DVCs and projected DVFs are below the NAAQS at monitoring sites in these areas, as noted above. The difference plot at the bottom of Figure 4-36 shows $PM_{2.5}$ reductions in the majority of the domain with only isolated areas of increases in $PM_{2.5}$. Where $PM_{2.5}$ increases are predicted, they are limited to less than 15 µg/m^3 for nearly all grid cells, although the maximum increase in any grid cell is 44.6 µg/m^3, which occurs in Vermilion County, LA. Reductions in $PM_{2.5}$ over coastal waters is at least partially related to tightening of the large vessel (Category 3 marine engine) fuel sulfur content requirements within the North American ECA from 10,000 ppm to 1,000 ppm in 2015.

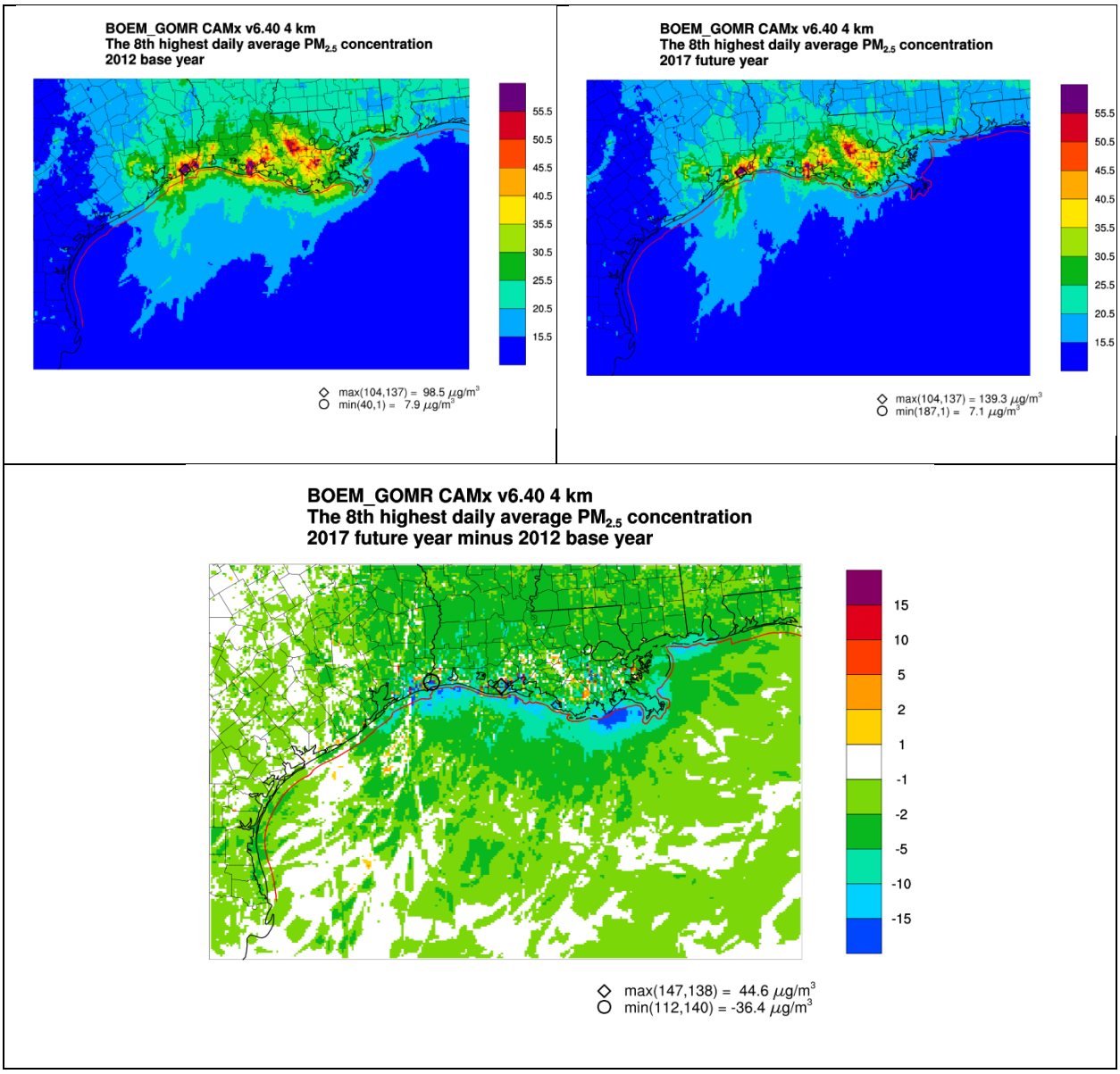

Figure 4-36. Modeled Eighth-Highest Daily Average $PM_{2.5}$ Concentrations for the Base Year (top left), Future Year (top right), and the Future–Base Difference (bottom)
Note: Red line parallel to coast represents the state seaward boundary.

Figure 4-37 shows source group contributions to the annual eighth-highest daily average $PM_{2.5}$ concentrations under the future year scenario. These contributions are matched in time to the eighth-highest daily average $PM_{2.5}$ concentrations for all sources; contributions may be different during other periods with elevated daily average $PM_{2.5}$ values. Contributions of the new sources associated with the single lease sale (source group B2) are less than 0.15 µg/m^3 except for an isolated location in the Gulf where the maximum contribution is 0.7 µg/m^3. Contributions from all (new and existing) OCS platforms and support vessels and helicopters under the single-sale scenario (source group B3) are less than 2.1 µg/m^3. Contributions of new sources associated with the 10 lease sales (source group C2) are less than 0.8 µg/m^3; contributions from all OCS platforms and support vessels and helicopters under the 10-sale scenario (source group C3) are less than 2.6 µg/m^3. Contributions from all OCS platforms and support vessels and helicopters under the no-sale scenario (source group A2) are less than 1.9 µg/m^3.

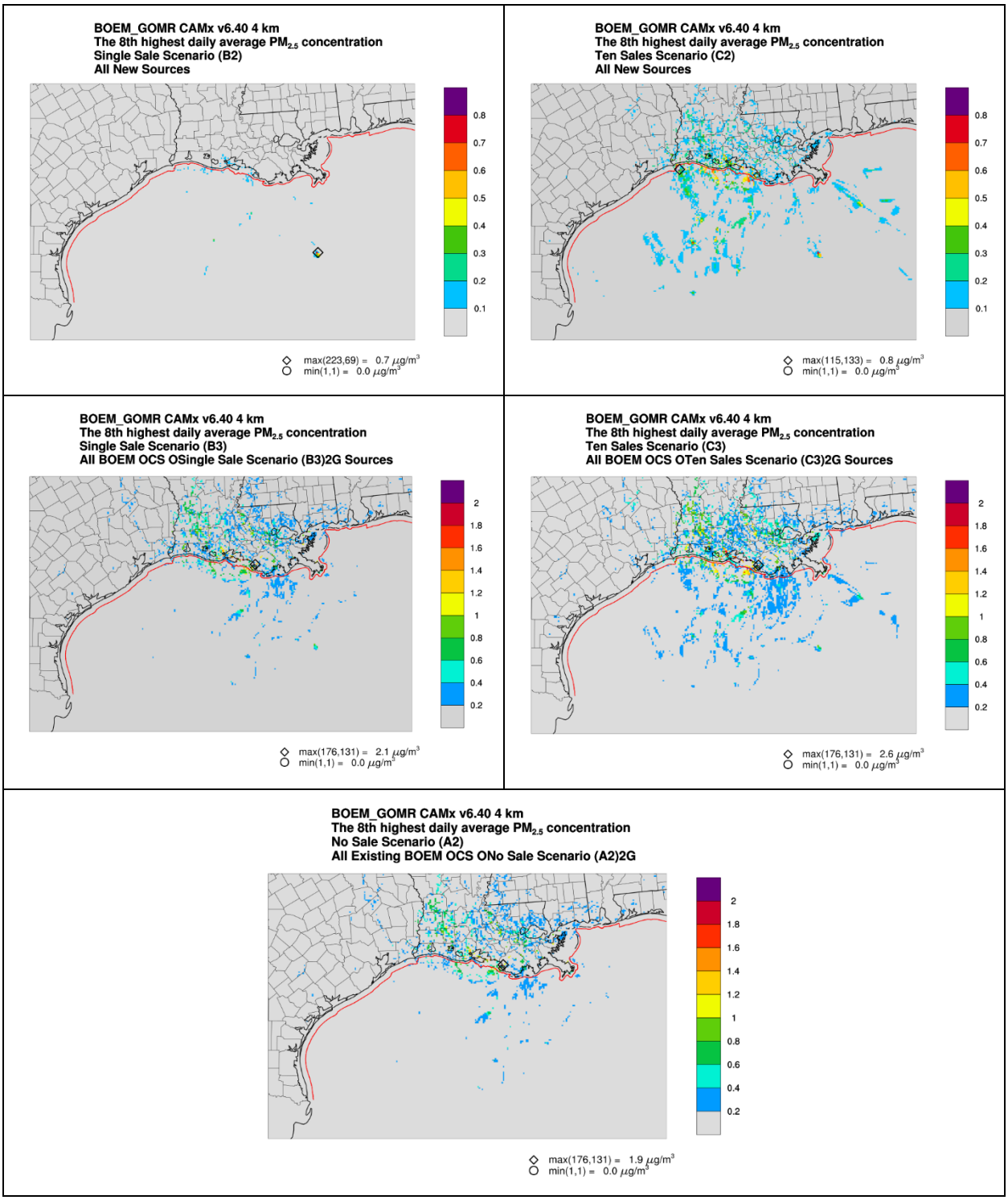

Figure 4-37. Contributions of New Platforms and Support Vessels and Helicopters Under the Single-Sale (top left) and 10-Sale (top right) Scenarios, All Sources Under the Single-Sale (middle left) and 10-Sale (middle right) Scenarios, and All sources under the No Action Alternative (bottom) to the Future Year Eighth-Highest Daily Average $PM_{2.5}$ for All Sources

Note: Red line parallel to coast represents the state seaward boundary.

4.7.1.4.2 Annual Average $PM_{2.5}$

Figure 4-38 shows the modeled annual average $PM_{2.5}$ for the base year, future year, and the future–base differences. Average $PM_{2.5}$ concentrations decrease throughout the domain, with increases in some isolated grid cells associated with emission increases at some stationary sources. Reductions along the immediate Louisiana state coastal boundary are as large as 9.2 µg/m^3.

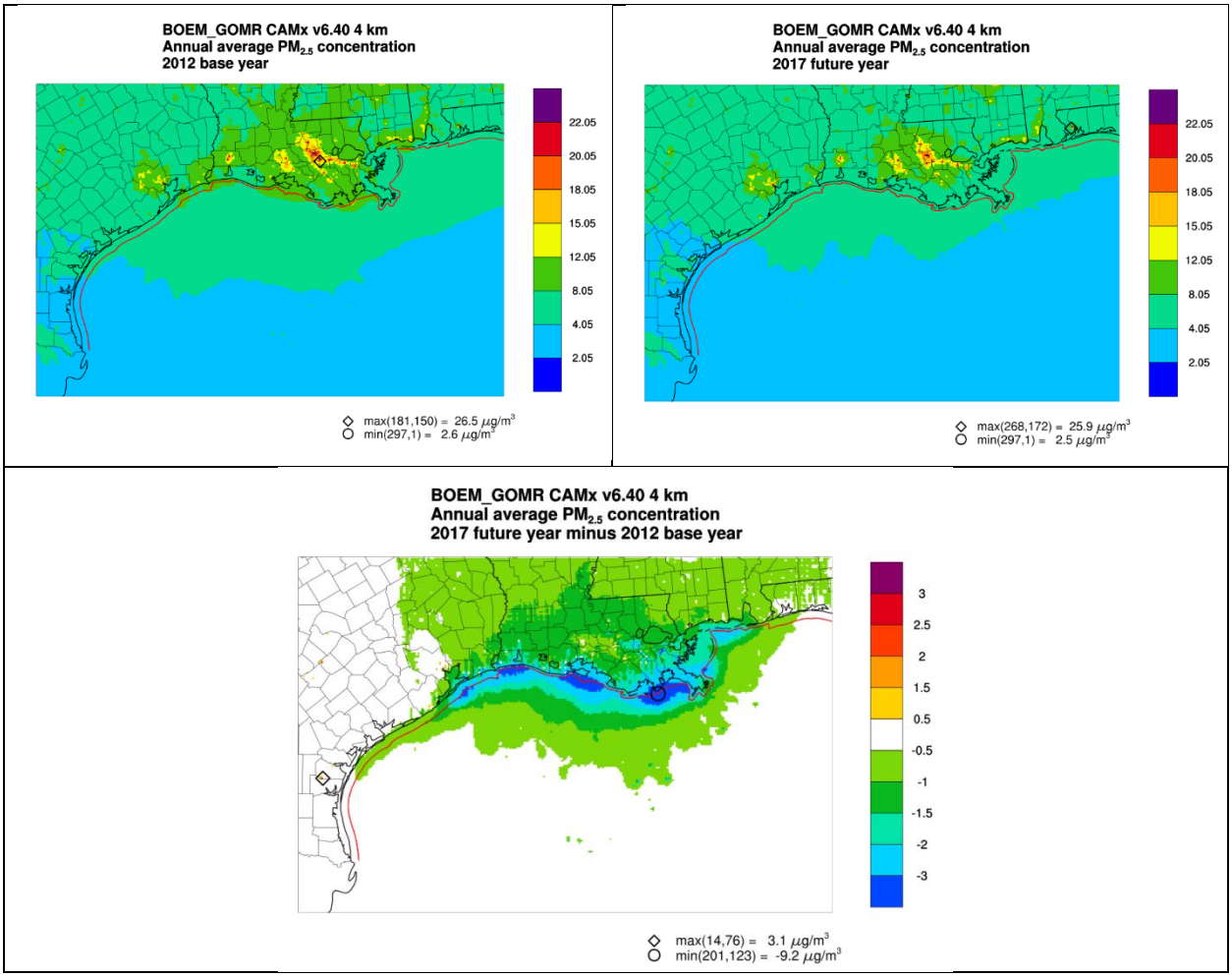

Figure 4-38. Modeled Annual Average $PM_{2.5}$ Concentrations for the Base Year (top left), Future Year (top right), and the Future–Base Difference (bottom)
Note: Red line parallel to coast represents the state seaward boundary.

Figure 4-39 shows source group contributions to the annual average $PM_{2.5}$ concentrations under the future year scenario. Impacts of the new sources associated with the single-sale scenario (source group B2) are largely focused offshore with a maximum value of 0.5 µg/m^3. Impacts from all (new and existing) OCS platforms and support traffic under the single-sale scenario (source group B3) are more widespread but still centered offshore, where impacts approach approximately 0.3 µg/m^3 along the Louisiana state seaward boundary. Impacts from new sources under the 10-sale scenario (source group C2) and all OCS sources and support traffic under the 10-sale scenario (source group C3) are similar but more widespread, with little to no change in the maximum impacts. Impacts from all OCS sources and support traffic under the no-sale scenario (source group A2) are similar.

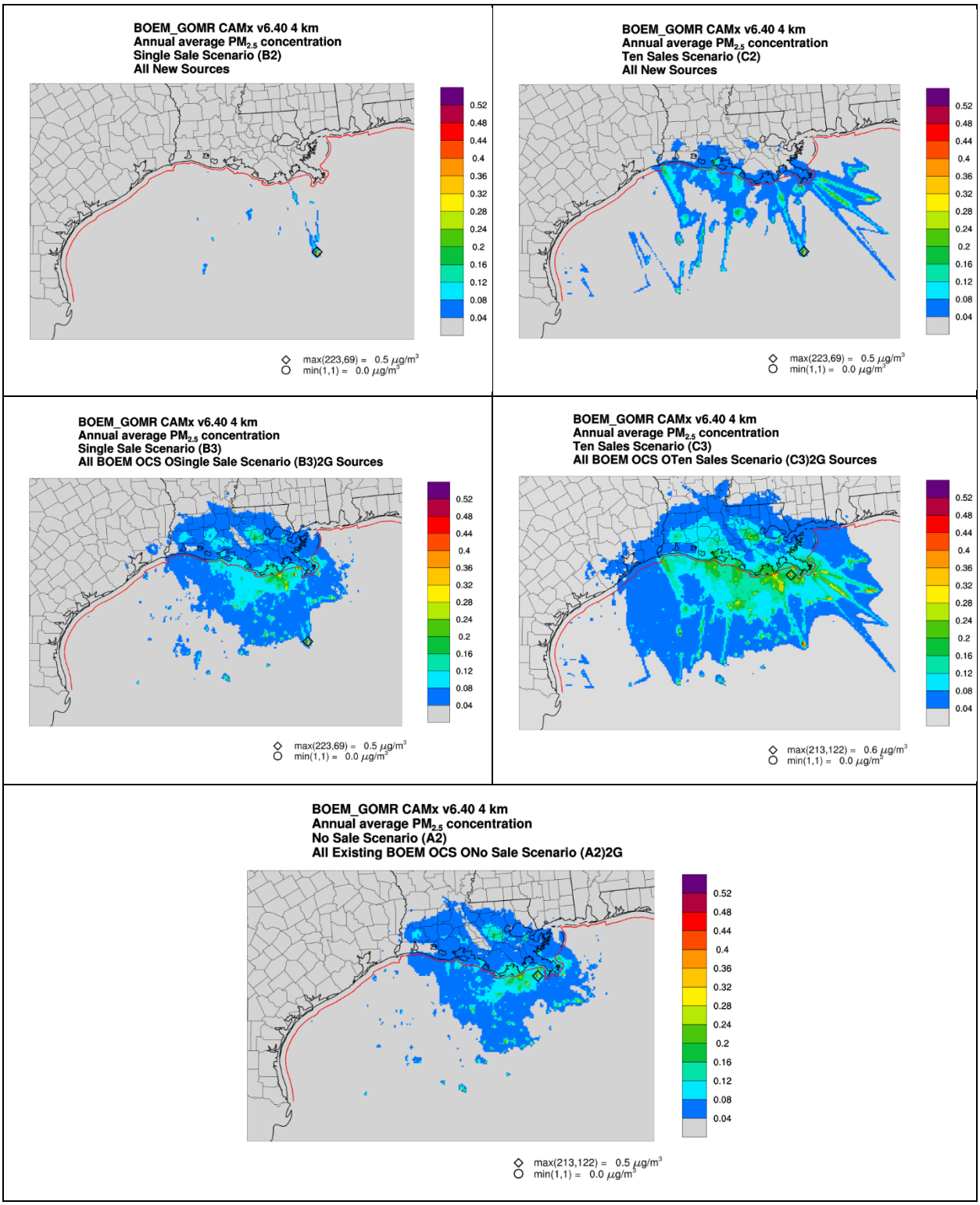

Figure 4-39. Contributions of Source Groups B2 Under the Single-Sale Scenario (top left), C2 Under the 10-Sale Scenario (top right), B3 under the Single-Sale Scenario (middle left), C3 Under the 10-Sale Scenario (middle right), and A2 Under the No-Sale Scenario (bottom) to the Future Year Annual Average $PM_{2.5}$ for All Sources

Note: Red line parallel to coast represents the state seaward boundary.

4.7.1.5 NAAQS Analysis for Other Criteria Air Pollutants

4.7.1.5.1 PM_{10}

Figure 4-40 displays modeled second-highest daily average PM_{10} concentrations, which can be compared with the 24-hour average PM_{10} NAAQS (150 µg/m^3) for the base and future scenarios and the base–future differences. Areas of elevated PM_{10} are evident in urban and port areas; other hotspots are likely associated with fires along the Gulf coasts of Texas and Louisiana. Ramboll modeled PM_{10} decreases associated with vessel emission reductions (see Section 4.7.1.4.1) just offshore of the Louisiana and southeast Texas Coast. Linear patterns of increases and decreases farther out over the Gulf are associated with shifts in ship traffic routes.

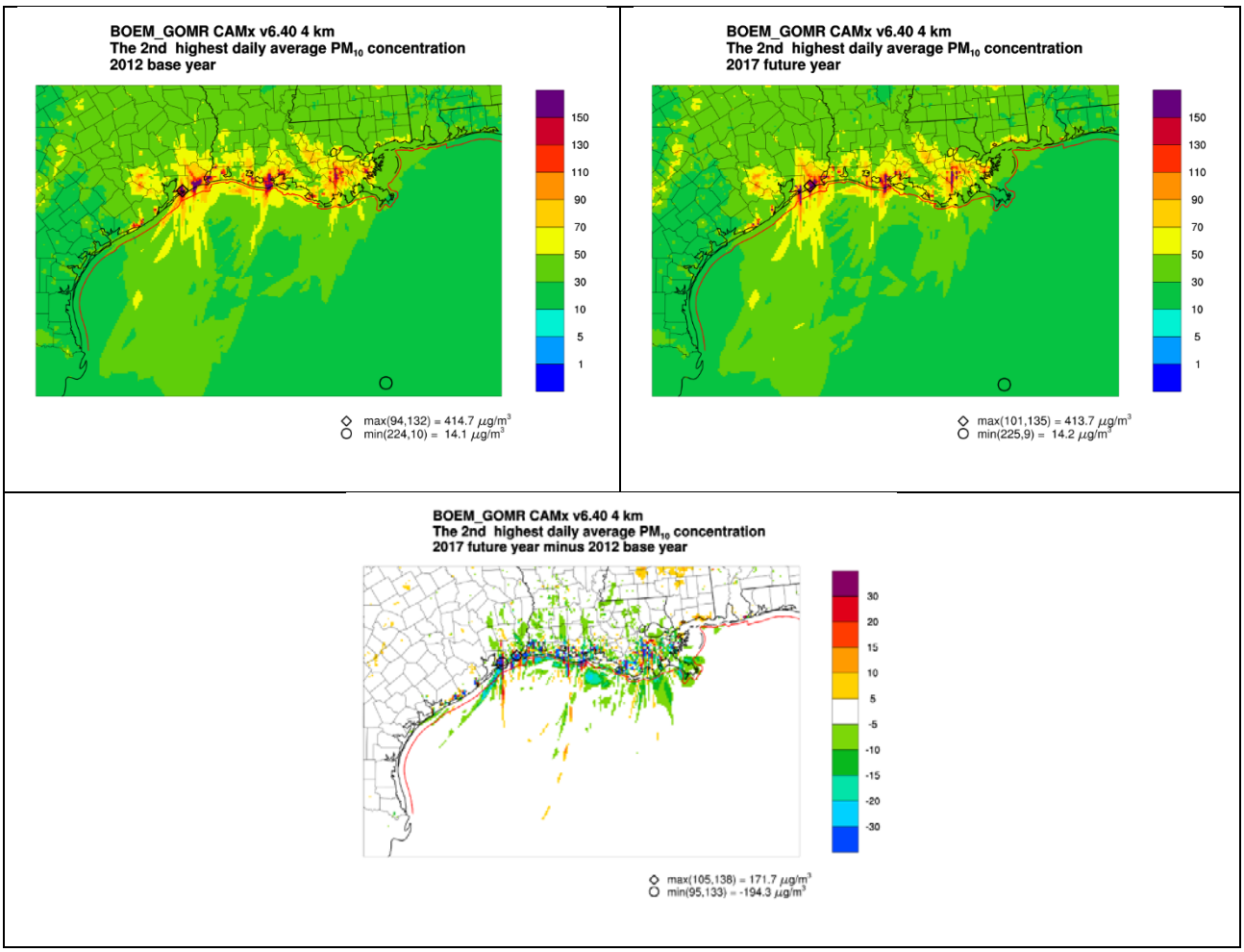

Figure 4-40. Modeled Second-Highest 24-Hour Average PM_{10} Concentrations for the Base Year (top left), Future Year (top right), and the Future–Base Difference (bottom)
Note: Red line parallel to coast represents the state seaward boundary.

Figure 4-41 shows source group contributions to the second-highest daily average PM_{10} concentrations. Contributions of new platforms and associated support vessels and aircraft under the single-sale scenario (source group B2) are predicted to be less than 0.5 µg/m^3, while contributions of these sources under the 10-sale scenario (source group C2) are predicted to be less than 1 µg/m^3 or less than 0.7 percent of the 150 µg/m^3 NAAQS. The maximum contribution of all OCS oil and gas platforms and support vessels and helicopters under the 10-sale scenario (source group C3) is 3.8 µg/m^3 (2.5 percent of the NAAQS), as

compared to 3.0 µg/m^3 under the single-sale scenario (source group B3) and 2.8 µg/m^3 under the no-sale scenario (source group A2).

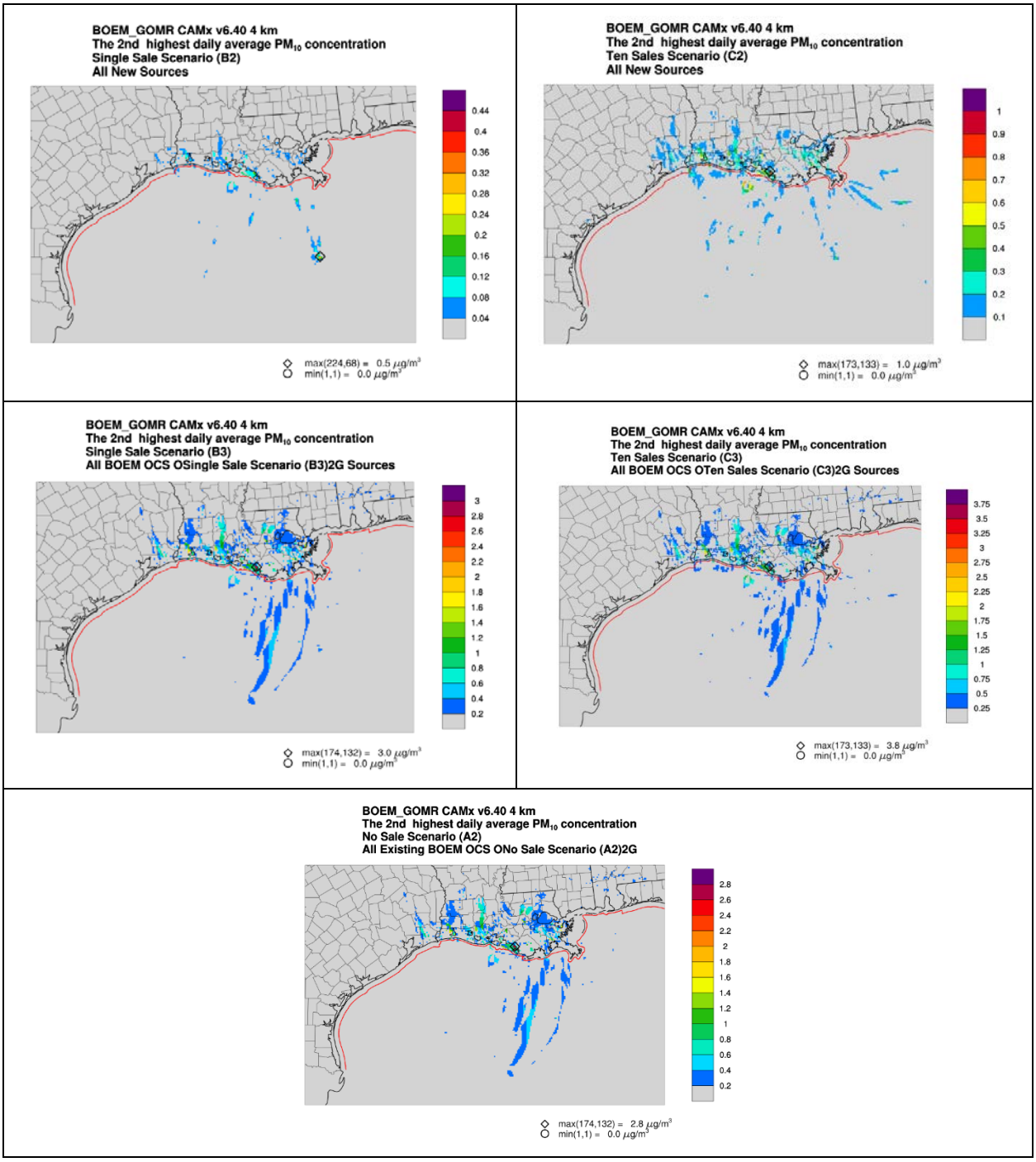

Figure 4-41. Contributions of Source Groups B2 Under the Single-Sale Scenario (top left), C2 Under the 10-Sale Scenario (top right), B3 Under the Single-Sale Scenario (middle left), C3 under the 10-Sale Scenario (middle right), and A2 Under the No-Sale Scenario (bottom) to the Future Year Second-Highest Daily Average PM_{10} Concentration for All Sources
Note: Red line parallel to coast represents the state seaward boundary.

4.7.1.5.2 NO_2

Results are presented here for both the 1-hour average NO_2 NAAQS (100 ppb) and the annual average NO_2 NAAQS (53 ppb). Figures 4-42 and 4-43 display modeled 1-hour average NO_2 design values (based on the eighth-highest daily average) for the base and future year scenarios along with source group contributions to the future year design values. All modeled 1-hour NO_2 concentrations are below the NAAQS (100 ppb); concentrations in the immediate vicinity of the LOOP peak at 99.9 ppb for the base year. Concentrations decrease between the base and future year scenarios at most locations except for increases offshore that are associated with new sources under the 10-sale future year scenario. These increases range up to 52 ppb. Increases of up to approximately 20 ppb are also evident at entrances to major ports. Decreases are projected over the coastal waters of Louisiana and Mississippi; these are associated with reductions in domestic vessel fuel use between 2012 and 2017.

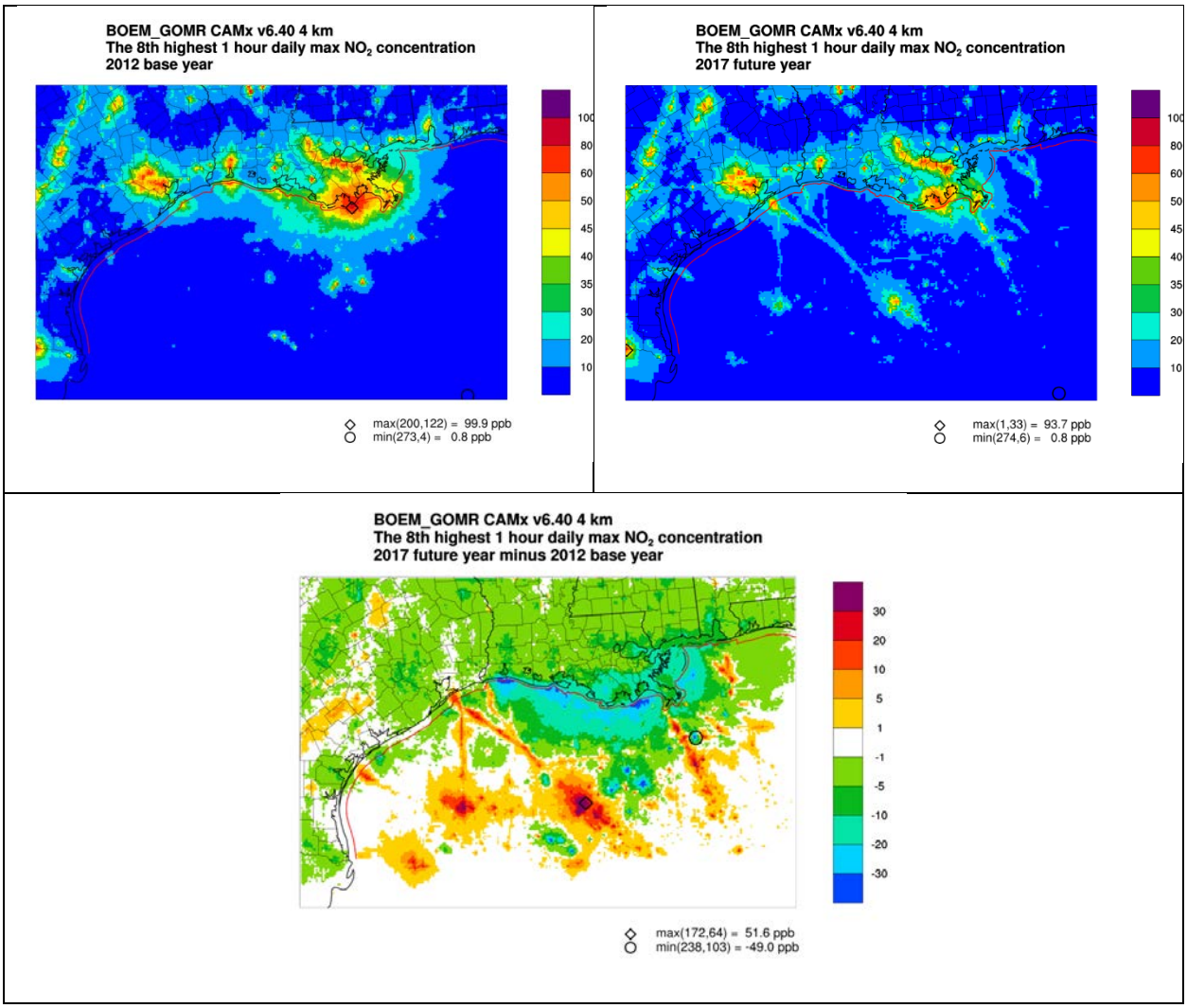

Figure 4-42. Modeled Eighth-Highest 1-hour NO_2 Concentrations for the Base Year (top left), Future Year (top right), and the Future–Base Difference (bottom)
Note: Red line parallel to coast represents the state seaward boundary.

Figure 4-43 shows source group contributions to the eighth-highest daily average NO_2 concentrations. Contributions from new platforms and support vessels and helicopters associated with the single-sale (source group B2) and 10-sale (source group C2) scenarios are less than 5 ppb inside the state seaward

boundaries. Contributions from all OCS platforms and support traffic are less than approximately 20 ppb inside the state seaward boundaries under the 10-sale, single-sale, and no-sale scenarios.

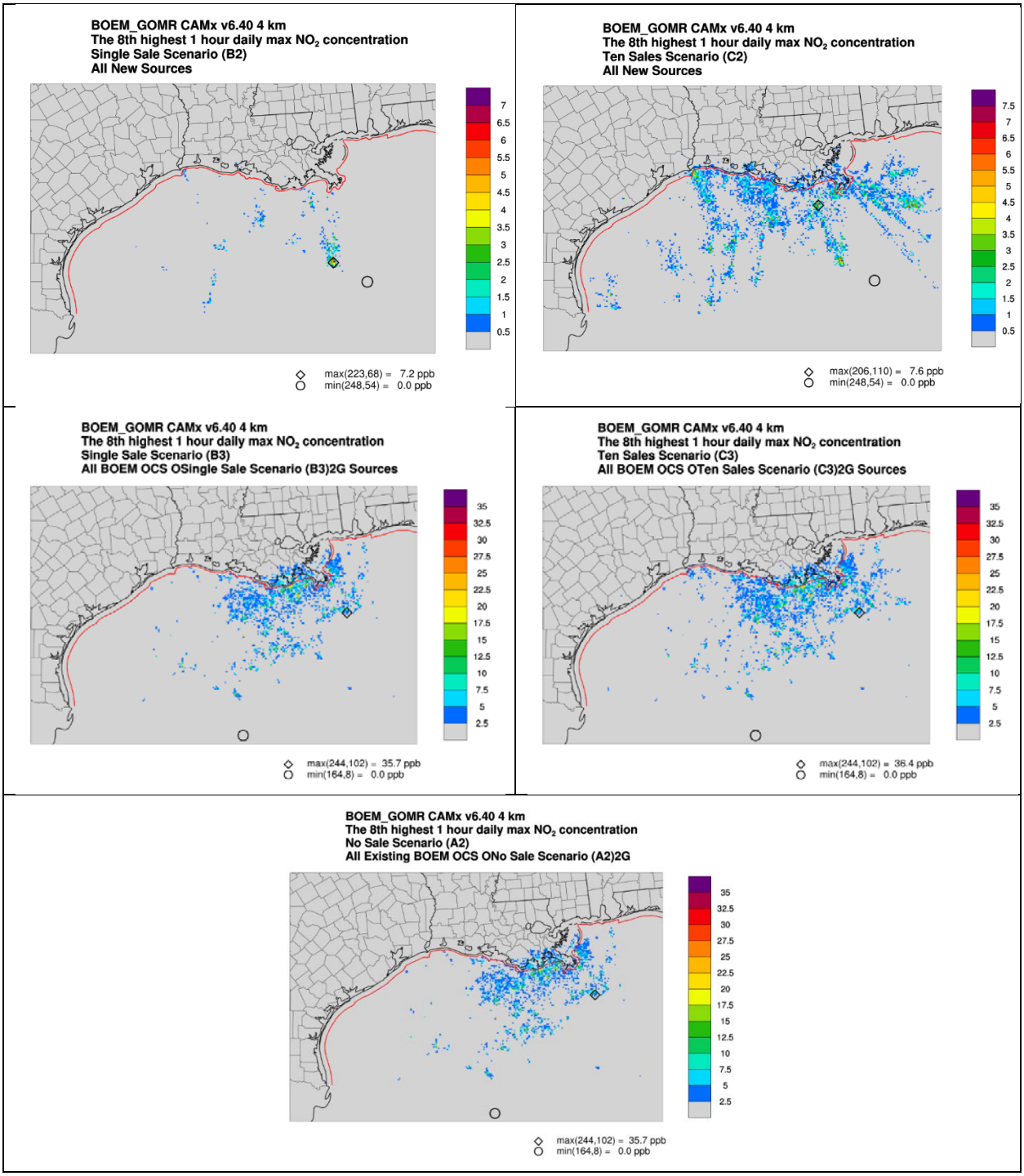

Figure 4-43. Contributions of Source Groups B2 Under the Single-Sale Scenario (top left), C2 Under the 10-Sale Scenario (top right), B3 Under the Single-Sale Scenario (middle left), C3 Under the 10-Sale Scenario (middle right), and A2 Under the No-Sale Scenario (bottom) to the Future Year Eighth-Highest Daily Average NO_2 Concentrations for All Sources
Note: Red line parallel to coast represents the state seaward boundary.

Figures 4-44 and 4-45 display modeled annual average NO_2 concentrations for the base and future year scenarios along with source group contributions to the future year annual averages. All modeled concentrations are below the 53 ppb NAAQS. Increases between the base and future year scenarios of as much as 8 ppb are modeled to occur over the Gulf. Concentration reductions are predicted to occur primarily along the Louisiana Coast.

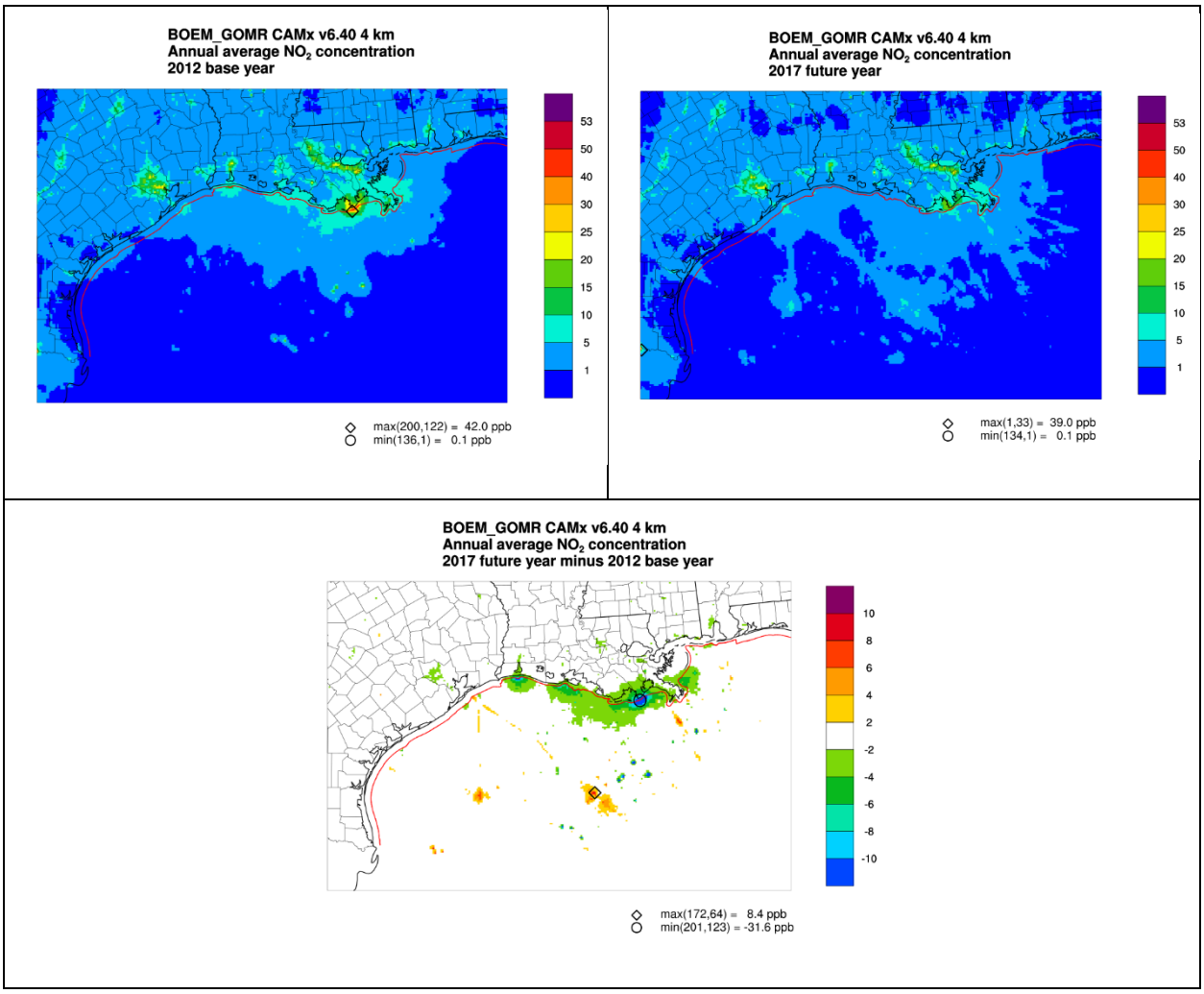

Figure 4-44. Modeled Annual Average NO_2 Concentrations for the Base Year (top left), Future Year (top right), and the Future–Base Difference (bottom)
Note: Red line parallel to coast represents the state seaward boundary.

Figure 4-45 shows source group contributions to the annual average NO_2 concentrations. These results are similar to those for 1-hour NO_2 shown above but with maximum contributions of about 2.4 ppb from new sources associated with either the single or 10 lease sale and maximum impacts from all OCS platforms and support traffic of 8.3 ppb (16 percent of the NAAQS).

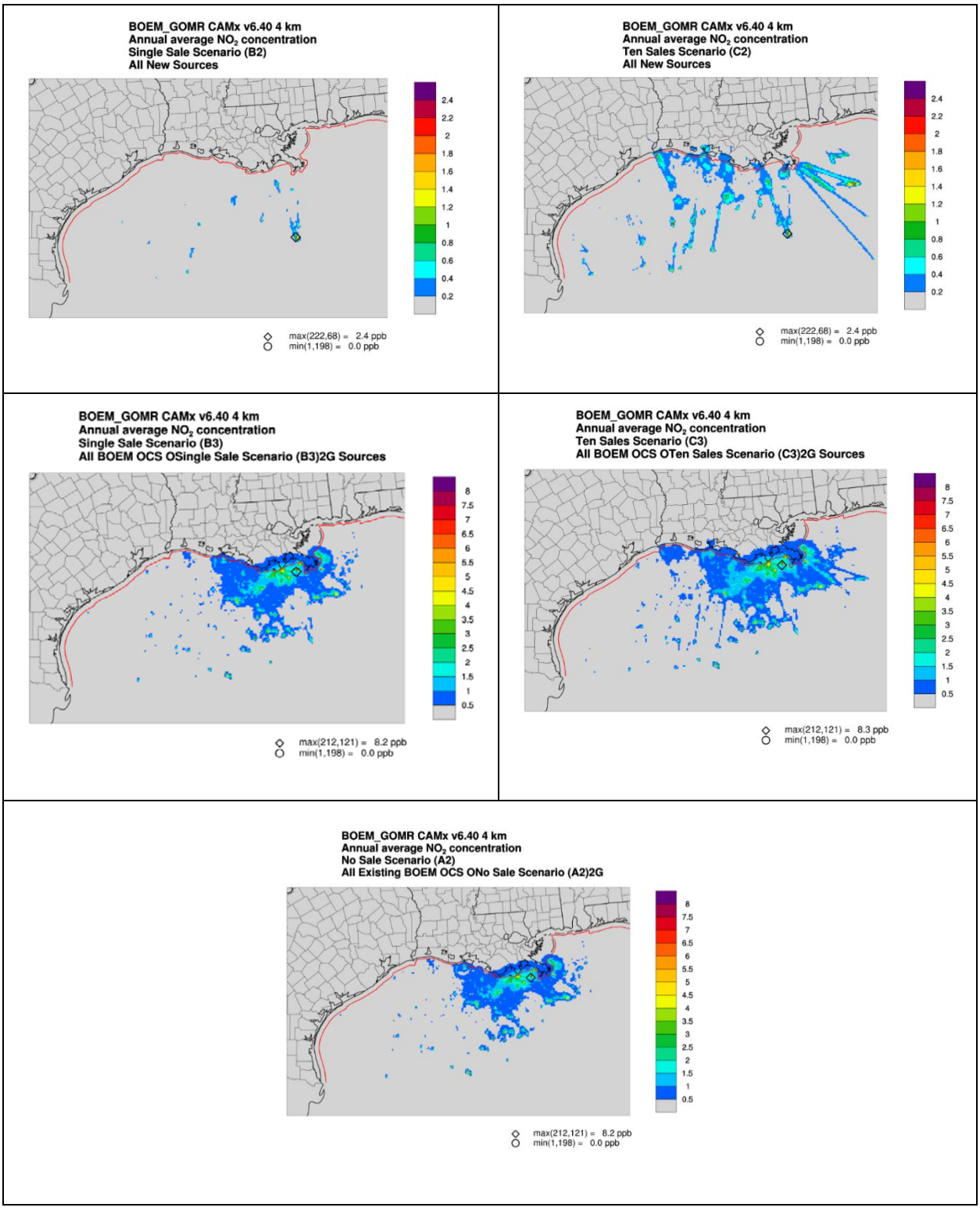

Figure 4-45. Contributions of Source Groups B2 Under the Single-Sale Scenario (top left), C2 Under the 10-Sale Scenario (top right), B3 Under the Single-Sale Scenario (middle left), C3 Under the 10-Sale Scenario (middle right), and A2 Under the No-Sale Scenario (bottom) to the Future Year Annual Average NO_2 Concentrations for All Sources

Note: Red line parallel to coast represents the state seaward boundary.

4.7.1.5.3 SO_2

Results are presented here for both the 1-hour average primary SO_2 NAAQS (75 ppb) and the 3-hour average secondary SO_2 NAAQS (0.5 ppm).

Figure 4-46 displays modeled 1-hour SO_2 design values (based on the fourth-highest daily maximum 1-hour average SO_2 concentration) for the base, future, and future minus base scenarios. Modeled values for the base year are generally below the 75 ppb NAAQS except in the immediate vicinity of some major point sources. Sources in areas with deepwater platforms are evident in the base case scenario with maximum impacts up to 40 ppb. Concentrations decrease in most locations in the future year scenario as sources are retired or apply control equipment with projected maximum impacts all below the NAAQS.

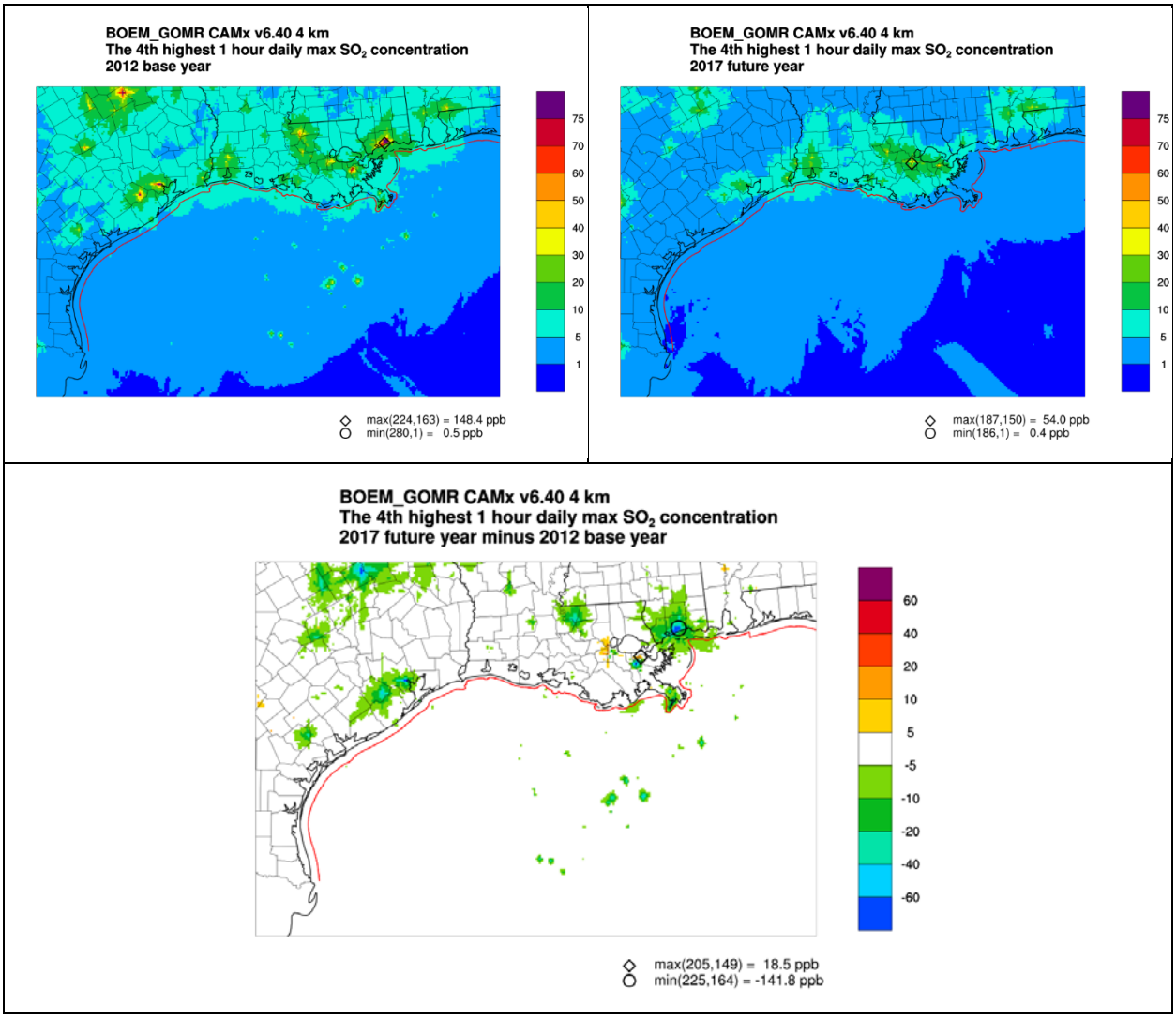

Figure 4-46. Modeled Fourth-Highest Daily Maximum 1-hour SO_2 Concentrations for the Base Year (top left), Future Year (top right), and the Future–Base Difference (bottom)
Note: Red line parallel to coast represents the state seaward boundary.

Figure 4-47 shows source group contributions to the modeled 1-hour SO_2 concentrations. New sources associated with the lease sales are modeled to contribute less than 0.3 ppb. All OCS platforms and vessel traffic are modeled to contribute less than 1.5 ppb to the 75 ppb NAAQS.

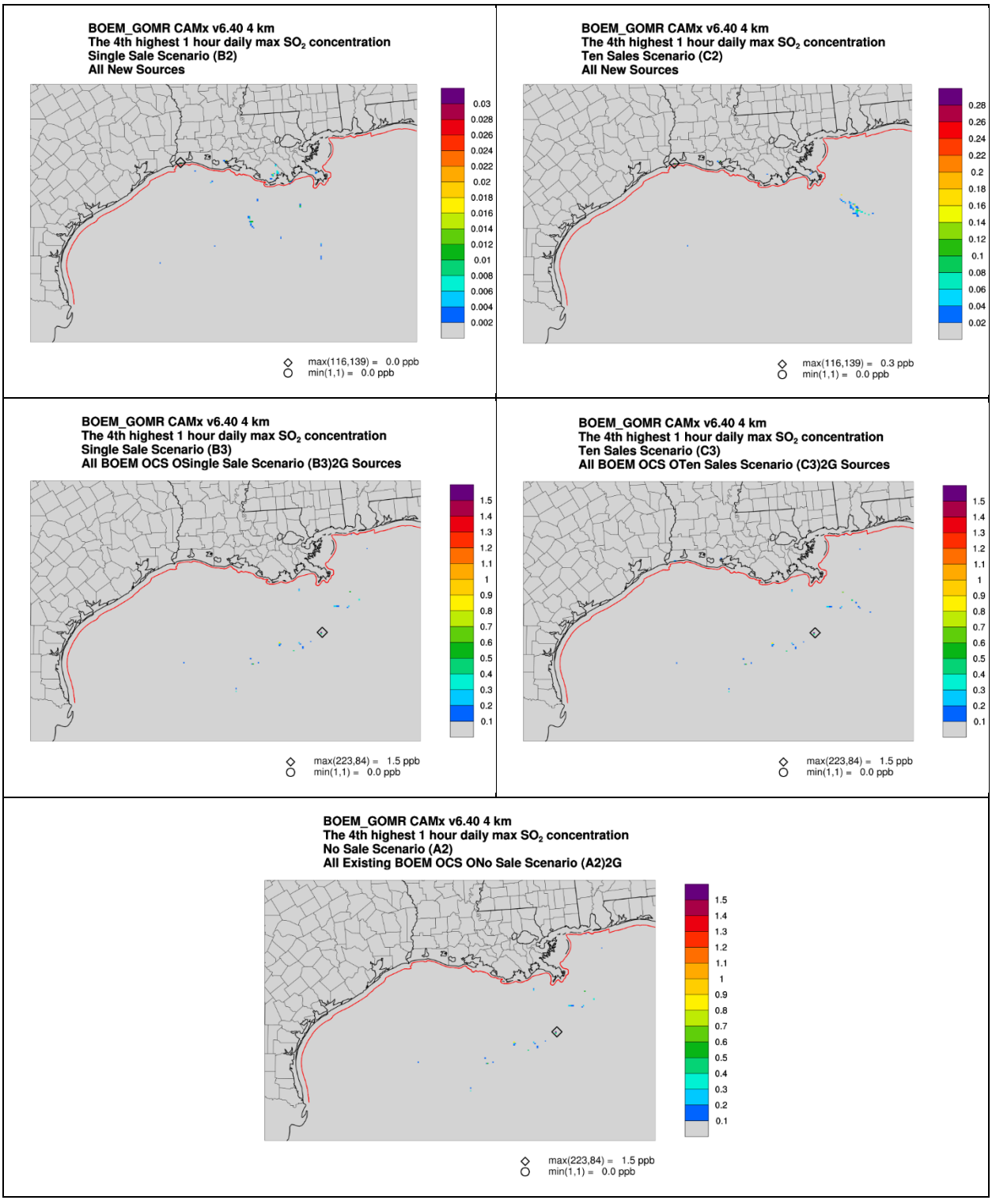

Figure 4-47. Contributions of Source Groups B2 Under the Single-Sale Scenario (top left), C2 Under the 10-Sale Scenario (top right), B3 Under the Single-Sale Scenario (middle left), C3 Under the 10-Sale Scenario (middle right), and A2 Under the No-Sale Scenario (bottom) to the Future Year Fourth-Highest Daily Maximum 1-hour SO_2 Concentration for All Sources

Note: Red line parallel to coast represents the state seaward boundary.

Figure 4-48 displays modeled 3-hour SO_2 design values (based on the annual second-highest block 3-hour average SO_2 concentration) for the base, future, and future minus base scenarios. All modeled values are below the NAAQS (500 ppb). The overall pattern of these results is similar to those for 1-hour SO_2 described for Figure 4-46 above.

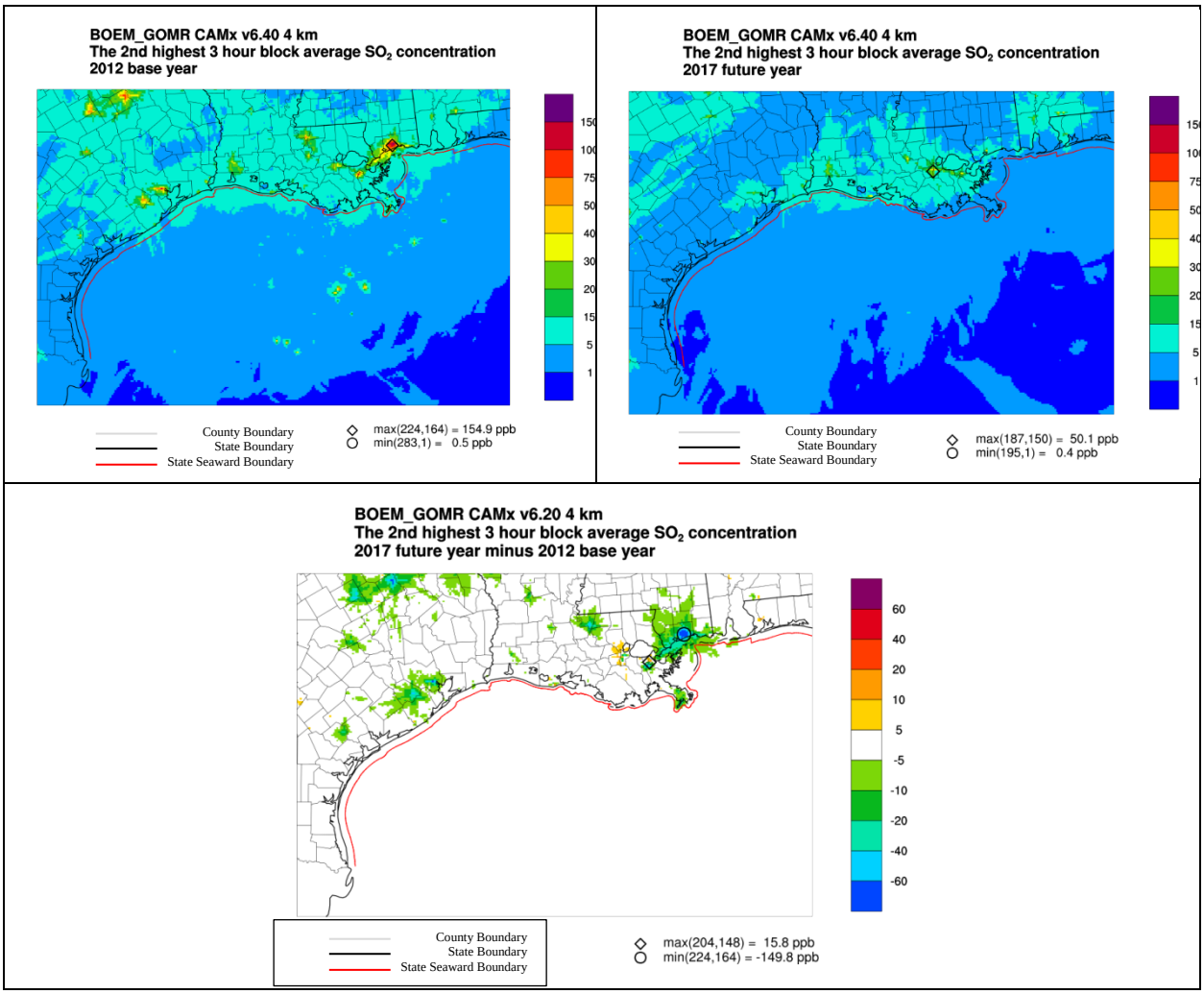

Figure 4-48. Modeled Annual Second-Highest Block 3-Hour SO_2 Concentrations for the Base Year (top left), Future Year (top right), and the Future–Base Difference (bottom)
Note: Red line parallel to coast represents the state seaward boundary.

Figure 4-49 shows source group contributions to the modeled 3-hour SO_2 concentrations. Results are similar to those for the 1-hour SO_2 concentrations described for Figure 4-47 above.

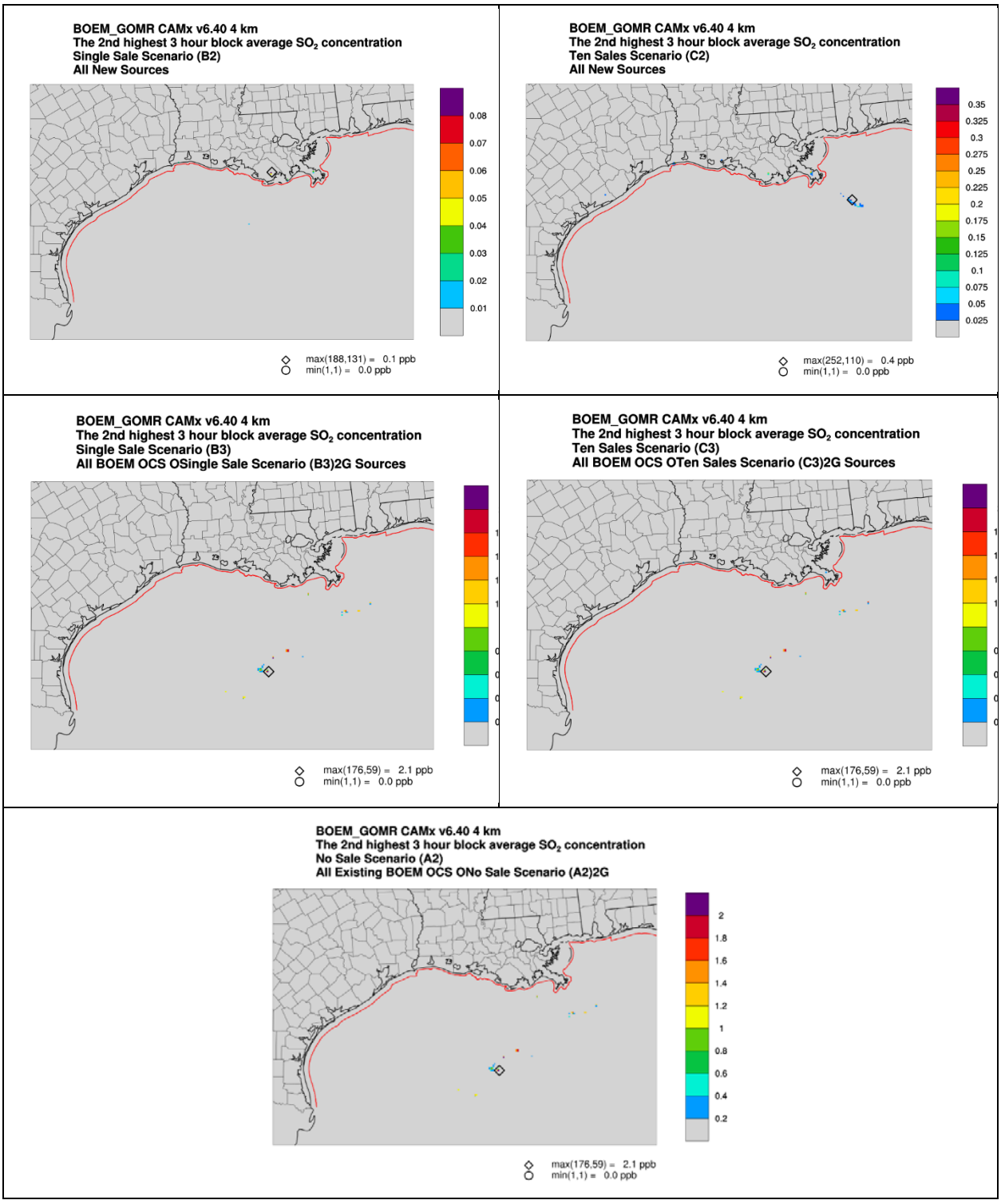

Figure 4-49. Contributions of Source Groups B2 Under the Single-Sale Scenario (top left), C2 Under the 10-Sale Scenario (top right), B3 under the Single-Sale Scenario (middle left), C3 Under the 10-Sale Scenario (middle right), and A2 Under the No-Sale Scenario (bottom) to the Future Year Second-Highest 3-hour Block Average SO_2 Concentration for All Sources

Note: Red line parallel to coast represents the state seaward boundary.

4.7.1.5.4 CO

Results are presented here for the 8-hour average (9 ppm) and 1-hour average (35 ppm) CO NAAQS. Figure 4-50 displays modeled 8-hour CO design values (based on the annual 2nd highest non-overlapping running 8-hour average) for the base, future, and future – base scenarios. Similarly, Figure 4-51 displays modeled 1-hour CO design values (based on the annual 2nd highest daily maximum 1-hour average) for the base, future, and future – base scenarios. All values are below their respective NAAQS levels. The differences between the base and future year scenarios are less than 5 ppm.

Individual source group contributions to CO design values were not calculated as the CAMx source apportionment methods do not include tracers for CO.

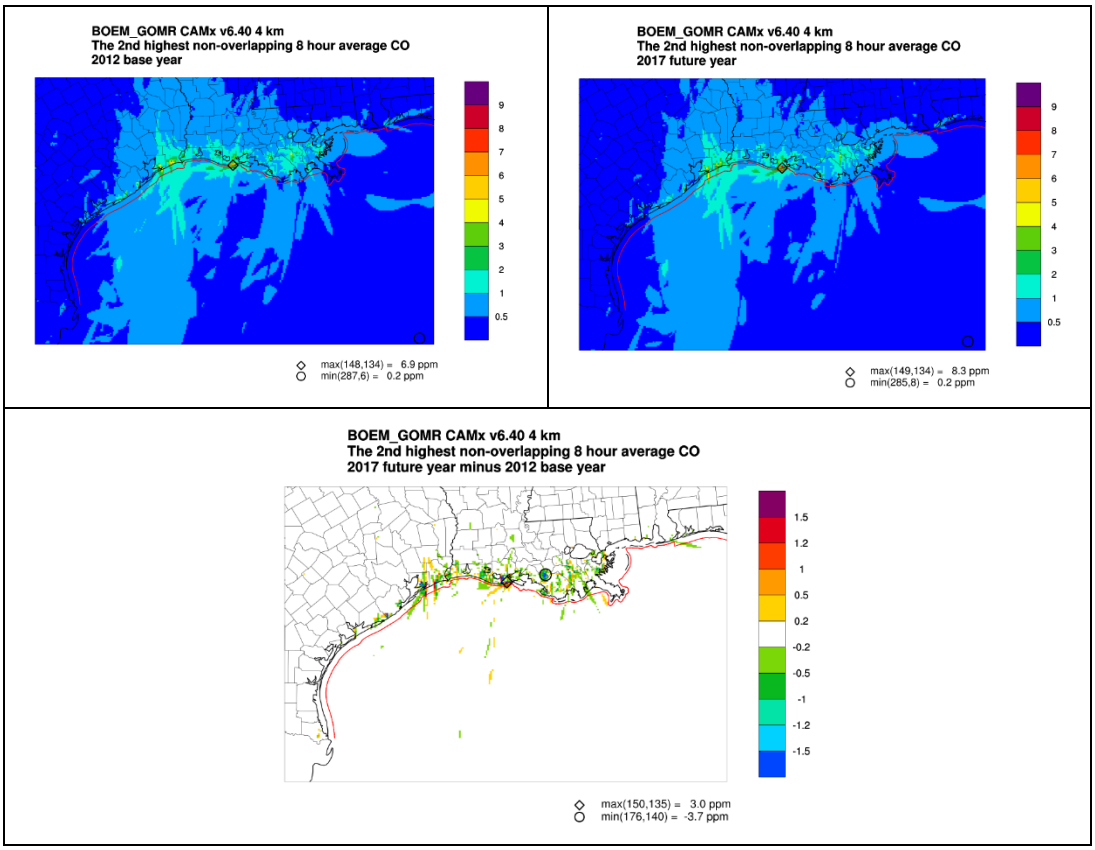

Figure 4-50. Modeled Annual 2nd Highest Non-overlapping Running 8-hour Average CO Concentrations for the Base Year (top left), Future Year (top right), and the Future–Base Difference (bottom)
Note: Red line parallel to coast represents the state seaward boundary.

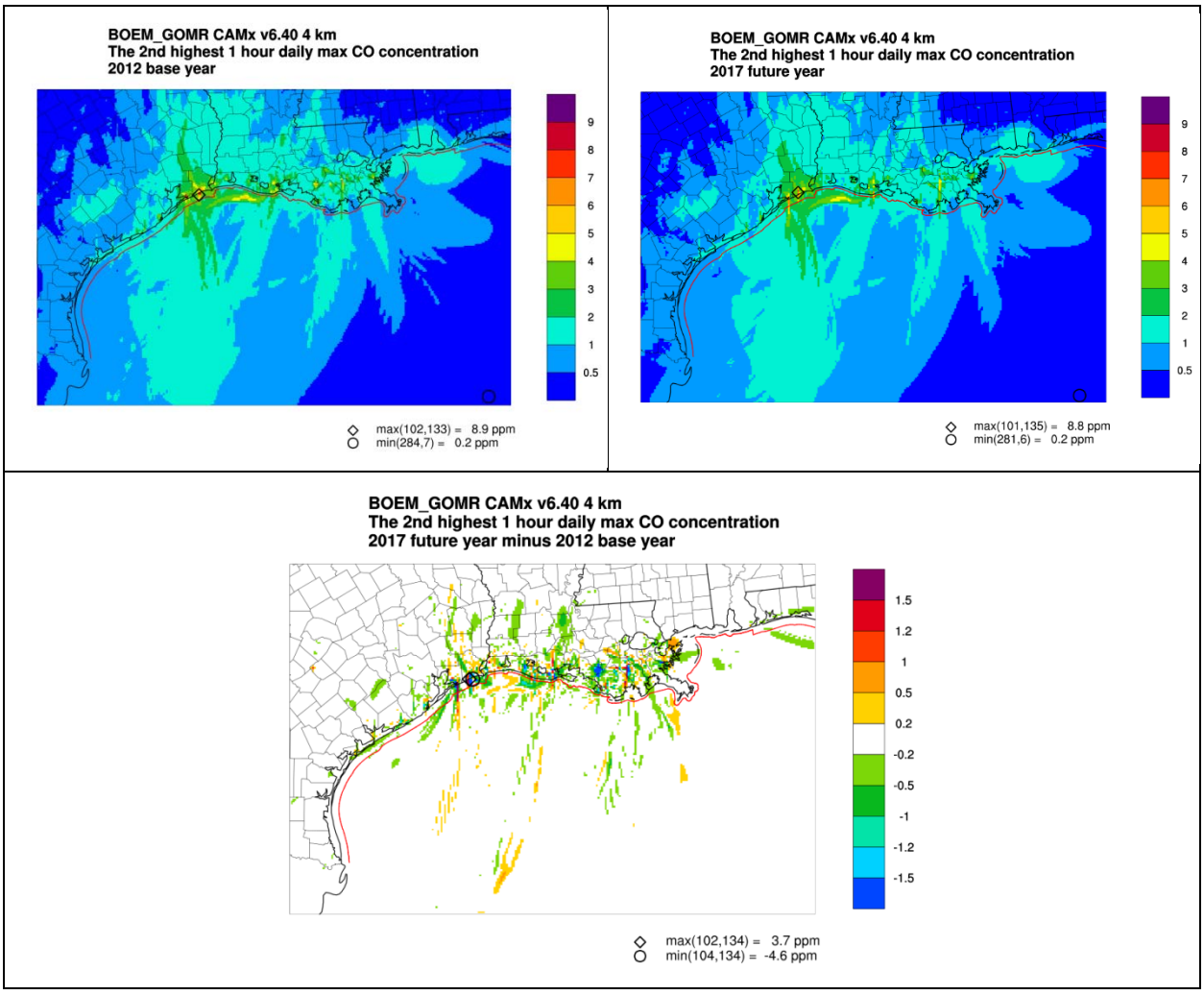

Figure 4-51. Modeled Annual 2nd Highest 1-hour Average CO Concentrations for the Base Year (top left), Future Year (top right), and the Future–Base Difference (bottom)
Note: Red line parallel to coast represents the state seaward boundary.

4.7.2 PSD Increments

Incremental impacts of each source group at Class I and sensitive Class II areas were calculated for all pollutants for which PSD increments have been set (NO_2, SO_2, PM_{10}, $PM_{2.5}$). Increment consumption is based on the source group contribution calculated from the CAMx source contribution results. Increment consumption for 24-hour averages and the 3-hour average SO_2 are based on the annual second-highest values. Comparisons of impacts from the lease sales with maximum allowed PSD increments are presented here as an evaluation of a "threshold of concern" for potentially significant adverse impacts, but do not represent a regulatory PSD increment consumption analysis as would be required for major sources subject to the NSR program requirements of the CAA. Incremental impacts are compared here to the full allowable PSD increments; no attempt is made to identify existing PSD increment-consuming or increment-expanding sources.

Results of the PSD increments analysis are summarized in Table 4-21 in terms of the maximum increment consumption over all Class I/II areas within the 4-km modeling domain. Maximum impacts occur at the Breton Wilderness Class I area for all PSD pollutants and averaging times. Concentration increments from source groups B2 (new sources under the single-sale scenario) and C2 (new sources under the 10-sale scenario) as well as from source groups B3 and C3 (all OCS oil and gas sources under the single and 10-sale scenarios, respectively) are all less than the maximum allowed PSD increments for all pollutants and averaging times. A summary of impacts from source groups B2, B3, C2 and C3 for all Class I/II areas is provided in Table 4-22.

Table 4-21. Maximum Source Group Contributions for PSD Pollutants at Class I and Sensitive Class II Areas in the 4-km Modeling Domain

Group	Max @ any Class I area	Percent of PSD Class I Increment	Class I Area where Max occurred	Max @ any Class II area	Percent of PSD Class II Increment	Class II Area where Max occurred
PM_{10} Annual (Class I, II Increment = 4 µg/m^3, 17 µg/m^3)						
B2	0.005	0.1%	Breton Wild.	0.003	0.0%	Breton NWR
B3	0.078	1.9%	Breton Wild.	0.065	0.4%	Breton NWR
C2	0.052	1.3%	Breton Wild.	0.032	0.2%	Padre Is.
C3	0.125	3.1%	Breton Wild.	0.093	0.5%	Breton NWR
PM_{10} 24-Hour (Class I, II Increment = 8 µg/m^3, 30 µg/m^3)						
B2	0.056	0.7%	Breton Wild.	0.034	0.1%	Breton NWR
B3	0.752	9.4%	Breton Wild.	0.526	1.8%	Breton NWR
C2	0.273	3.4%	Breton Wild.	0.183	0.6%	Padre Is.
C3	1.027	12.8%	Breton Wild.	0.651	2.2%	Breton NWR
$PM_{2.5}$ Annual (Class I, II Increment = 1 µg/m^3, 4 µg/m^3)						
B2	0.004	0.4%	Breton Wild.	0.003	0.1%	Breton NWR
B3	0.077	7.7%	Breton Wild.	0.064	1.6%	Breton NWR
C2	0.051	5.1%	Breton Wild.	0.031	0.8%	Padre Is.
C3	0.123	12.3%	Breton Wild.	0.093	2.3%	Breton NWR
$PM_{2.5}$ 24-Hour (Class I, II Increment = 2 µg/m^3, 9 µg/m^3)						
B2	0.055	2.8%	Breton Wild.	0.033	0.4%	Breton NWR
B3	0.750	37.5%	Breton Wild.	0.525	5.8%	Breton NWR
C2	0.272	13.6%	Breton Wild.	0.181	2.0%	Padre Is.
C3	1.024	51.2%	Breton Wild.	0.649	7.2%	Breton NWR
NO_2 Annual (Class I, II Increment = 2.5 µg/m^3, 25 µg/m^3)						
B2	0.010	0.4%	Breton Wild.	0.005	0.0%	Breton NWR
B3	0.704	28.2%	Breton Wild.	0.466	1.9%	Breton NWR
C2	0.142	5.7%	Breton Wild.	0.062	0.2%	Padre Is.
C3	0.819	32.8%	Breton Wild.	0.521	2.1%	Gulf Is.
SO_2 Annual (Class I, II Increment = 2 µg/m^3, 20 µg/m^3)						
B2	0.000	0.0%	Breton Wild.	0.000	0.0%	Breton NWR
B3	0.002	0.1%	Breton Wild.	0.002	0.0%	Breton NWR
C2	0.001	0.0%	Breton Wild.	0.000	0.0%	Padre Is.
C3	0.002	0.1%	Breton Wild.	0.002	0.0%	Breton NWR

Group	Max @ any Class I area	Percent of PSD Class I Increment	Class I Area where Max occurred	Max @ any Class II area	Percent of PSD Class II Increment	Class II Area where Max occurred
SO_2 24-Hour (Class I, II Increment = 5 µg/m^3, 91 µg/m^3)						
B2	0.001	0.0%	Breton Wild.	0.000	0.0%	Breton NWR
B3	0.010	0.2%	Breton Wild.	0.034	0.0%	Breton NWR
C2	0.005	0.1%	Breton Wild.	0.003	0.0%	Padre Is.
C3	0.014	0.3%	Breton Wild.	0.034	0.0%	Breton NWR
SO_2 3-Hour (Class I, II Increment = 25 µg/m^3, 512 µg/m^3)						
B2	0.002	0.0%	Breton Wild.	0.001	0.0%	Breton NWR
B3	0.026	0.1%	Breton Wild.	0.109	0.0%	Breton NWR
C2	0.012	0.0%	Breton Wild.	0.007	0.0%	Padre Is.
C3	0.033	0.1%	Breton Wild.	0.110	0.0%	Breton NWR

Table 4-22. Source Group Contributions for PSD Pollutants at all Class I and Sensitive Class II Areas in the 4-km Modeling Domain

Source Group B2									
Pollutant			NO_2 (µg/m^3)	PM_{10} (µg/m^3)		PM_{25} (µg/m^3)		SO_2 (µg/m^3)	
Averaging Time			Annual	24-hour	Annual	24-hour	Annual	3-hour	24-hour	Annual
Class I	State	Owner	PSD Class I Increment[1]							
			2.5	8	4	2	1	25	5	2
Breton Wilderness	LA	FWS	0.010	0.056	0.005	0.055	0.004	0.002	0.001	0.000
Class II	State	Owner	PSD Class II Increment							
			25	30	17	9	4	512	91	20
Breton NWR	LA	FWS	0.005	0.034	0.003	0.033	0.003	0.001	0.000	0.000
Gulf Islands	FL, MS	NPS	0.003	0.032	0.003	0.032	0.003	0.000	0.000	0.000
Padre Island	TX	NPS	0.005	0.012	0.002	0.012	0.002	0.000	0.000	0.000
Source Group B3									
Pollutant			NO_2 (µg/m^3)	PM_{10} (µg/m^3)		PM_{25} (µg/m^3)		SO_2 (µg/m^3)	
Averaging Time			Annual	24-hour	Annual	24-hour	Annual	3-hour	24-hour	Annual
Class I	State	Owner	PSD Class I Increment							
			2.5	8	4	2	1	25	5	2
Breton Wilderness	LA	FWS	0.704	0.752	0.078	0.750	0.077	0.026	0.010	0.002
Class II	State	Owner	PSD Class II Increment							
			25	30	17	9	4	512	91	20
Breton NWR	LA	FWS	0.466	0.526	0.065	0.525	0.064	0.030	0.012	0.002
Gulf Islands	FL, MS	NPS	0.136	0.392	0.048	0.391	0.048	0.109	0.034	0.001
Padre Island	TX	NPS	0.010	0.096	0.008	0.096	0.008	0.001	0.001	0.000

Source Group C2										
Pollutant			NO_2 ($\mu g/m^3$)	PM_{10} ($\mu g/m^3$)		PM_{25} ($\mu g/m^3$)		SO_2 ($\mu g/m^3$)		
Averaging Time			Annual[3]	24-hour[2]	Annual[3]	24-hour[4]	Annual[3]	3-hour[2]	24-hour[2]	Annual[3]
Class I	**State**	**Owner**	**PSD Class I Increment**							
			2.5	8	4	2	1	25	5	2
Breton Wilderness	LA	FWS	0.142	0.273	0.052	0.272	0.051	0.012	0.005	0.001
Class II	**State**	**Owner**	**PSD Class II Increment**							
			25	30	17	9	4	512	91	20
Breton NWR	LA	FWS	0.060	0.183	0.032	0.181	0.031	0.007	0.003	0.000
Gulf Islands	FL, MS	NPS	0.062	0.154	0.026	0.153	0.026	0.005	0.002	0.000
Padre Island	TX	NPS	0.040	0.117	0.020	0.117	0.020	0.001	0.000	0.000
Source Group C3										
Pollutant			NO_2 ($\mu g/m^3$)	PM_{10} ($\mu g/m^3$)		PM_{25} ($\mu g/m^3$)		SO_2 ($\mu g/m^3$)		
Averaging Time			Annual	24-hour	Annual	24-hour	Annual	3-hour	24-hour	Annual
Class I	**State**	**Owner**	**PSD Class I Increment**							
			2.5	8	4	2	1	25	5	2
Breton Wilderness	LA	FWS	0.819	1.027	0.125	1.024	0.123	0.033	0.014	0.002
Class II	**State**	**Owner**	**PSD Class II Increment**							
			25	30	17	9	4	512	91	20
Breton NWR	LA	FWS	0.521	0.651	0.093	0.649	0.093	0.034	0.015	0.002
Gulf Islands	FL, MS	NPS	0.190	0.509	0.070	0.507	0.070	0.110	0.034	0.002
Padre Island	TX	NPS	0.045	0.160	0.026	0.160	0.026	0.001	0.001	0.000

4.7.3 AQRV Impacts

4.7.3.1 Visibility

4.7.3.1.1 Incremental Visibility Impacts

Incremental visibility impacts were calculated for new sources associated with the single-sale and 10-sale scenarios (source groups B2 and C2, respectively). Cumulative visibility impacts (i.e., impacts from all sources, including both new sources and "existing" platforms and support traffic) are described in Section 4.7.3.1.2. Incremental visibility impacts are calculated from incremental concentrations as quantified by the CAMx PSAT source apportionment tool simulation of for each source group. Changes in light extinction from CAMx model concentration increments due to emissions from each source group were calculated for each day at grid cells that intersect Class I and sensitive Class II areas within the 12-km modeling domain.

Calculation of incremental visibility impacts followed procedures recommended by the FLM (FLAG, 2010) as described in Section 4.6.2.3.1.

For each source group, the estimated visibility degradation at each Class I and sensitive Class II area in the 12-km modeling domain due to emissions from the source group are presented in terms of the number of days that exceed a threshold change in deciview (Δdv) relative to background conditions. The number of days with a Δdv greater than 0.5 and 1.0 are reported.

Results of the FLAG (2010) incremental visibility impact assessment for source groups B2 (new platforms and support vessels and helicopters under the single-sale scenario) and C2 (new platforms and support vessels and helicopters under the 10-sale scenario) are presented in Tables 4-23 and 4-24. For source group B2, the annual maximum Δdv do not exceed the 0.5 threshold at any Class I or Class II area; the maximum incremental impact from source group B2 is 0.31 at Breton Wilderness. Incremental impacts for source group C2 are larger. The maximum 8th highest Δdv is 1.01 at Breton Wilderness, and all three of the Class II areas have days with Δdv exceeding 0.5 (but not 1.0); the maximum 8th highest Δdv in the Class II areas is 0.11 at Gulf Islands National Seashore.

Table 4-23. Incremental Visibility Impacts Relative to Natural Background Conditions from Source Group B2

Area	Max Δdv	8th High Δdv	No. Days	
			>1.0	>0.5
Class I Areas				
Bandelier NM	0.00032	0.00006	0	0
Black Canyon of the Gunnison NM	0.00002	0.00000	0	0
Bosque del Apache National Wildlife Refuge	0.00054	0.00007	0	0
Bosque del Apache (Chupadera Unit) Wilderness	0.00040	0.00005	0	0
Bosque del Apache (Indian Well Unit) Wilderness	0.00040	0.00005	0	0
Bosque del Apache (Little San Pascual Unit) Wilderness	0.00076	0.00011	0	0
Big Bend NP	0.00296	0.00154	0	0
Bradwell Bay Wilderness	0.02518	0.01331	0	0
Breton Wilderness	0.30789	0.14637	0	0
Caney Creek Wilderness	0.06314	0.02472	0	0
Cape Romain Wilderness	0.01855	0.00573	0	0
Carlsbad Caverns NP	0.00174	0.00068	0	0
Chassahowitzka Wilderness	0.06130	0.01979	0	0
Cohutta Wilderness	0.02119	0.00568	0	0
Dolly Sods Wilderness	0.00427	0.00160	0	0
Eagles Nest Wilderness	0.00007	0.00001	0	0
Everglades NP	0.03904	0.00942	0	0
Flat Tops Wilderness	0.00001	0.00000	0	0
Great Sand Dunes NM	0.00018	0.00002	0	0
Great Smoky Mountains NP	0.00825	0.00371	0	0
Guadalupe Mountains NP	0.00175	0.00048	0	0
Hercules-Glades Wilderness	0.02249	0.00969	0	0
James River Face Wilderness	0.00330	0.00175	0	0
Joyce-Kilmer-Slickrock Wilderness	0.00901	0.00382	0	0
La Garita Wilderness	0.00014	0.00001	0	0
Linville Gorge Wilderness	0.00604	0.00187	0	0
Mammoth Cave NP	0.01621	0.00709	0	0
Maroon Bells-Snowmass Wilderness	0.00006	0.00000	0	0
Mingo National Wildlife Refuge	0.03104	0.01717	0	0
Mount_Zirkel Wilderness	0.00001	0.00000	0	0
Okefenokee National Wildlife Refuge	0.02264	0.01589	0	0
Otter Creek Wilderness	0.00433	0.00156	0	0
Pecos Wilderness	0.00054	0.00012	0	0
Rawah Wilderness	0.00004	0.00000	0	0
Rocky Mountain NP	0.00009	0.00001	0	0
Saint Marks National Wildlife Refuge	0.05014	0.02862	0	0
Salt Creek Wilderness	0.00148	0.00073	0	0

Area	Max Δdv	8th High Δdv	No. Days	
			>1.0	>0.5
San Pedro Parks Wilderness	0.00027	0.00006	0	0
Shenandoah NP	0.00875	0.00316	0	0
Shining Rock Wilderness	0.00671	0.00321	0	0
Sipsey Wilderness	0.02952	0.01063	0	0
Swanquarter National Wildlife Refuge	0.00580	0.00251	0	0
Upper Buffalo Wilderness	0.02073	0.00903	0	0
Weminuche Wilderness	0.00015	0.00001	0	0
West Elk Wilderness	0.00006	0.00000	0	0
Wheeler Peak Wilderness	0.00024	0.00006	0	0
White Mountain Wilderness	0.00076	0.00018	0	0
Wichita Mountains National Wildlife Refuge	0.01124	0.00495	0	0
Wichita Mountains (Charons Garden Unit) Wilderness	0.01109	0.00412	0	0
Wichita Mountains (North Mountain Unit) Wilderness	0.01125	0.00427	0	0
Wolf Island Wilderness	0.02364	0.00809	0	0
Class II Areas				
Breton National Wildlife Refuge	0.17373	0.10943	0	0
Gulf Islands National Seashore	0.16074	0.11171	0	0
Padre Island National Seashore	0.08668	0.03798	0	0

Table 4-24. Incremental Visibility Impacts Relative to Natural Background Conditions from Source Group C2

Area	Max Δdv	8th High Δdv	No. Days	
			>1.0	>0.5
Class I Areas				
Bandelier NM	0.00208	0.00057	0	0
Black Canyon of the Gunnison NM	0.00010	0.00001	0	0
Bosque del Apache National Wildlife Refuge	0.00351	0.00064	0	0
Bosque del Apache (Chupadera Unit) Wilderness	0.00255	0.00044	0	0
Bosque del Apache (Indian Well Unit) Wilderness	0.00260	0.00044	0	0
Bosque del Apache (Little San Pascual Unit) Wilderness	0.00491	0.00079	0	0
Big Bend NP	0.01903	0.01173	0	0
Bradwell Bay Wilderness	0.15421	0.11238	0	0
Breton Wilderness	1.33373	1.00904	8	57
Caney Creek Wilderness	0.32959	0.13869	0	0
Cape Romain Wilderness	0.09622	0.03609	0	0
Carlsbad Caverns NP	0.01103	0.00520	0	0
Chassahowitzka Wilderness	0.47247	0.16208	0	0
Cohutta Wilderness	0.12354	0.04583	0	0
Dolly Sods Wilderness	0.02615	0.01161	0	0
Eagles Nest Wilderness	0.00049	0.00005	0	0
Everglades NP	0.21866	0.05669	0	0
Flat Tops Wilderness	0.00008	0.00001	0	0
Great Sand Dunes NM	0.00118	0.00021	0	0
Great Smoky Mountains NP	0.05203	0.02748	0	0
Guadalupe Mountains NP	0.01097	0.00390	0	0
Hercules-Glades Wilderness	0.12032	0.05789	0	0
James River Face Wilderness	0.01970	0.01047	0	0
Joyce-Kilmer-Slickrock Wilderness	0.04776	0.02390	0	0
La Garita Wilderness	0.00094	0.00003	0	0
Linville Gorge Wilderness	0.04052	0.01327	0	0
Mammoth Cave NP	0.08048	0.04583	0	0
Maroon Bells-Snowmass Wilderness	0.00040	0.00002	0	0
Mingo National Wildlife Refuge	0.13583	0.08554	0	0
Mount_Zirkel Wilderness	0.00007	0.00001	0	0
Okefenokee National Wildlife Refuge	0.18702	0.08975	0	0
Otter Creek Wilderness	0.02674	0.01085	0	0
Pecos Wilderness	0.00348	0.00098	0	0
Rawah Wilderness	0.00026	0.00003	0	0
Rocky Mountain NP	0.00052	0.00007	0	0
Saint Marks National Wildlife Refuge	0.44600	0.25497	0	0
Salt Creek Wilderness	0.00999	0.00532	0	0

Area	Max Δdv	8th High Δdv	No. Days	
			>1.0	>0.5
San Pedro Parks Wilderness	0.00181	0.00043	0	0
Shenandoah NP	0.05145	0.02071	0	0
Shining Rock Wilderness	0.04367	0.02489	0	0
Sipsey Wilderness	0.16360	0.06866	0	0
Swanquarter National Wildlife Refuge	0.05423	0.02031	0	0
Upper Buffalo Wilderness	0.10673	0.05673	0	0
Weminuche Wilderness	0.00099	0.00011	0	0
West Elk Wilderness	0.00038	0.00002	0	0
Wheeler Peak Wilderness	0.00157	0.00042	0	0
White Mountain Wilderness	0.00501	0.00150	0	0
Wichita Mountains National Wildlife Refuge	0.06555	0.02897	0	0
Wichita Mountains (Charons Garden Unit) Wilderness	0.06434	0.02520	0	0
Wichita Mountains (North Mountain Unit) Wilderness	0.06554	0.02666	0	0
Wolf Island Wilderness	0.13364	0.04651	0	0
Class II Areas				
Breton National Wildlife Refuge	0.92174	0.73072	0	30
Gulf Islands National Seashore	0.77863	0.59667	0	18
Padre Island National Seashore	0.63020	0.33822	0	3

4.7.3.1.2 Cumulative Visibility Analysis

For the cumulative visibility impacts analysis, the MATS software was applied with observed PM species concentrations and monthly average RH from IMPROVE monitoring sites for 2010–2014 to calculate daily visibility impairment at Class I areas from which the W20% and B20% visibility days metrics are determined as described in Section 4.6.2.3.2. IMPROVE observations from monitoring sites in nearby Class I areas were used to represent conditions in Class I areas that do not have a co-located monitoring site. Table 4-25 shows the Class I area of interest in the first column, and the IMPROVE site used to represent observed visibility at the Class I area is shown in the third column. For example, the IMPROVE data from Dolly Sods Wilderness was used to represent observed visibility for both Dolly Sods and the Otter Creek wildernesses. MATS includes mappings of IMPROVE site to Class I areas. However, MATS does not include a mapping for the Bradwell Bay Class I area, and therefore cumulative visibility results for this area is not included in this analysis.

Tables 4-25 and 4-26 present results for the W20% visibility days and Tables 4-27 and 4-28 present results for the B20% visibility days. Visibility improvement between the base and future year scenarios (i.e., positive BY minus FY results in Tables 4-26 and 4-28) are seen at most Class I areas, with eight areas experiencing reductions in visibility on the W20% days. All of these areas are in New Mexico or Colorado. Contributions from new platforms and support traffic under the single (B2) or 10-lease (C2) sale scenarios to these eight areas are all less than 0.005 dv. The maximum contribution from new and existing platforms and support vessels and helicopters associated with the single-sale scenario (Source Group B3) to any area on the W20% days is 0.09 dv at Breton Island, LA. The maximum contribution from new and existing platforms and support vessels and helicopters associated with the 10-sale scenario (Source Group C3) is 0.11 dv, also at Breton Island, LA.

For the B20% visibility days, 14 areas experience reductions in visibility; all but two of these areas are located in New Mexico and Colorado. The two exceptions are Big Bend NP and Guadalupe Mountains NP in Texas. Contributions from new platforms and support traffic under the single (B2) or 10-lease (C2) sale scenarios to these 11 areas are all less than 0.005 dv. The maximum contribution from new and existing platforms and support vessels and helicopters associated with the single-sale scenario (Source Group B3) is 0.06 dv at Breton Island, LA. The maximum contribution from new and existing platforms and support vessels and helicopters associated with the 10-sale scenario (Source Group C3) is 0.08 dv, also at Breton Island, LA.

Table 4-25. Cumulative Visibility Results for 20% Worst Visibility Days (W20%) at Class I Areas for Base (2012) Year (BY) and Future Year (FY) Scenarios with all Sources Included and with Contributions from Each Source Group Removed

Class I Name	State	IMPROVE Site[a]	BY DV	FY DV	FY DV without Source Group				
					Single-Sale		10-Sale		No-Sale
					B2	B3	C2	C3	A2
Bandelier NM	NM	BAND1	11.83	12.24	12.24	12.24	12.24	12.24	12.24
Big Bend NP	TX	BIBE1	16.53	16.34	16.34	16.34	16.34	16.34	16.34
Black Canyon of the Gunnison NM	CO	WEMI1	9.64	9.62	9.62	9.62	9.62	9.62	9.62
Bosque del Apache	NM	BOAP1	14.55	14.90	14.90	14.90	14.90	14.90	14.90
Breton Wilderness	LA	BRIS1	23.39	20.48	20.47	20.39	20.45	20.37	20.40
Caney Creek Wilderness	AR	CACR1	21.83	19.98	19.98	19.96	19.97	19.96	19.96

Class I Name	State	IMPROVE Site[a]	BY DV	FY DV	FY DV without Source Group				
					Single-Sale		10-Sale		No-Sale
					B2	B3	C2	C3	A2
Carlsbad Caverns NP	TX	GUMO1	15.57	15.53	15.53	15.53	15.53	15.53	15.53
Chassahowitzka	FL	CHAS1	21.15	19.90	19.90	19.89	19.89	19.88	19.89
Cohutta Wilderness	GA	COHU1	22.30	19.88	19.88	19.88	19.88	19.88	19.88
Dolly Sods Wilderness	WV	DOSO1	22.02	18.65	18.65	18.65	18.65	18.65	18.65
Eagles Nest Wilderness	CO	WHRI1	8.28	8.24	8.24	8.24	8.24	8.24	8.24
Everglades NP	FL	EVER1	17.88	17.26	17.26	17.26	17.26	17.26	17.26
Flat Tops Wilderness	CO	WHRI1	8.28	8.24	8.24	8.24	8.24	8.24	8.24
Great Sand Dunes NM	CO	GRSA1	11.67	11.87	11.87	11.87	11.87	11.87	11.87
Great Smoky Mountains NP	TN	GRSM1	21.86	18.84	18.84	18.84	18.84	18.84	18.84
Guadalupe Mountains NP	TX	GUMO1	15.57	15.53	15.53	15.53	15.53	15.53	15.53
Hercules-Glades Wilderness	MO	HEGL1	22.49	20.68	20.68	20.67	20.68	20.67	20.67
James River Face Wilderness	VA	JARI1	22.05	19.57	19.57	19.57	19.57	19.57	19.57
Joyce-Kilmer-Slickrock Wilderness	TN	GRSM1	21.86	18.84	18.84	18.84	18.84	18.84	18.84
La Garita Wilderness	CO	WEMI1	9.64	9.62	9.62	9.62	9.62	9.62	9.62
Linville Gorge Wilderness	NC	LIGO1	20.86	18.06	18.06	18.06	18.06	18.06	18.06
Maroon Bells-Snowmass Wilderness	CO	WHRI1	8.28	8.24	8.24	8.24	8.24	8.24	8.24
Mammoth Cave NP	KY	MACA1	24.48	21.49	21.49	21.49	21.49	21.49	21.49
Mingo	MO	MING1	24.06	22.34	22.34	22.34	22.34	22.33	22.34
Mount Zirkel Wilderness	CO	MOZI1	8.90	8.85	8.85	8.85	8.85	8.85	8.85
Okefenokee	GA	OKEF1	22.44	21.32	21.32	21.31	21.31	21.31	21.31
Otter Creek Wilderness	WV	DOSO1	22.02	18.65	18.65	18.65	18.65	18.65	18.65
Pecos Wilderness	NM	WHPE1	9.75	10.01	10.01	10.01	10.01	10.01	10.01
Rawah Wilderness	CO	MOZI1	8.90	8.85	8.85	8.85	8.85	8.85	8.85
Cape Romain	SC	ROMA1	22.49	21.05	21.05	21.04	21.05	21.04	21.04
Rocky Mountain NP	CO	ROMO1	11.85	11.72	11.72	11.72	11.72	11.72	11.72
Salt Creek	NM	SACR1	18.11	18.89	18.89	18.89	18.89	18.89	18.89
St. Marks	FL	SAMA1	21.63	19.87	19.87	19.86	19.86	19.85	19.86

Class I Name	State	IMPROVE Site[a]	BY DV	FY DV	FY DV without Source Group				
					Single-Sale		10-Sale		No-Sale
					B2	B3	C2	C3	A2
San Pedro Parks Wilderness	NM	SAPE1	10.35	10.60	10.60	10.60	10.60	10.60	10.60
Shenandoah NP	VA	SHEN1	21.39	18.24	18.24	18.24	18.24	18.24	18.24
Shining Rock Wilderness	NC	SHRO1	18.87	16.52	16.52	16.52	16.52	16.52	16.52
Sipsey Wilderness	AL	SIPS1	22.60	20.38	20.38	20.38	20.38	20.38	20.38
Swanquarter	NC	SWAN1	21.41	19.73	19.73	19.73	19.73	19.73	19.73
Upper Buffalo Wilderness	AR	UPBU1	21.63	19.82	19.82	19.80	19.81	19.79	19.80
West Elk Wilderness	CO	WHRI1	8.28	8.24	8.24	8.24	8.24	8.24	8.24
Weminuche Wilderness	CO	WEMI1	9.64	9.62	9.62	9.62	9.62	9.62	9.62
White Mountain Wilderness	NM	WHIT1	14.56	15.12	15.12	15.12	15.12	15.12	15.12
Wheeler Peak Wilderness	NM	WHPE1	9.75	10.01	10.01	10.01	10.01	10.01	10.01
Wichita Mountains	OK	WIMO1	21.27	20.23	20.23	20.23	20.23	20.23	20.23
Wolf Island	GA	OKEF1	22.44	21.32	21.32	21.31	21.31	21.31	21.31

[a] Indicates state in which assigned IMPROVE monitor is located

Table 4-26. Differences in Cumulative Visibility Results for 20% Worst Visibility Days (W20%) at Class I Areas Between the Future Year (FY) and Base Year (BY) Scenarios and Contributions of Each Source Group to the Future Year Scenario Visibility

Class I Name	State[a]	IMPROVE Site	BY - FY DV	Difference in FY DV without Source Group				
				Single-Sale		10-Sale		No-Sale
				B2	B3	C2	C3	A2
Bandelier NM	NM	BAND1	-0.41	0.00	0.00	0.00	0.00	0.00
Big Bend NP	TX	BIBE1	0.19	0.00	0.00	0.00	0.00	0.00
Black Canyon of the Gunnison NM	CO	WEMI1	0.02	0.00	0.00	0.00	0.00	0.00
Bosque del Apache	NM	BOAP1	-0.35	0.00	0.00	0.00	0.00	0.00
Breton-2	LA	BRIS1	2.91	0.01	0.09	0.03	0.11	0.08
Caney Creek Wilderness	AR	CACR1	1.85	0.00	0.02	0.01	0.02	0.02
Carlsbad Caverns NP	TX	GUMO1	0.04	0.00	0.00	0.00	0.00	0.00
Chassahowitzka	FL	CHAS1	1.25	0.00	0.01	0.01	0.02	0.01
Cohutta Wilderness	GA	COHU1	2.42	0.00	0.00	0.00	0.00	0.00
Dolly Sods Wilderness	WV	DOSO1	3.37	0.00	0.00	0.00	0.00	0.00
Eagles Nest Wilderness	CO	WHRI1	0.04	0.00	0.00	0.00	0.00	0.00
Everglades NP	FL	EVER1	0.62	0.00	0.00	0.00	0.00	0.00

Class I Name	State[a]	IMPROVE Site	BY - FY DV	Difference in FY DV without Source Group				
				Single-Sale		10-Sale		No-Sale
				B2	B3	C2	C3	A2
Flat Tops Wilderness	CO	WHRI1	0.04	0.00	0.00	0.00	0.00	0.00
Great Sand Dunes NM	CO	GRSA1	-0.20	0.00	0.00	0.00	0.00	0.00
Great Smoky Mountains NP	TN	GRSM1	3.02	0.00	0.00	0.00	0.00	0.00
Guadalupe Mountains NP	TX	GUMO1	0.04	0.00	0.00	0.00	0.00	0.00
Hercules-Glades Wilderness	MO	HEGL1	1.81	0.00	0.01	0.00	0.01	0.01
James River Face Wilderness	VA	JARI1	2.48	0.00	0.00	0.00	0.00	0.00
Joyce-Kilmer-Slickrock Wilderness	TN	GRSM1	3.02	0.00	0.00	0.00	0.00	0.00
La Garita Wilderness	CO	WEMI1	0.02	0.00	0.00	0.00	0.00	0.00
Linville Gorge Wilderness	NC	LIGO1	2.80	0.00	0.00	0.00	0.00	0.00
Maroon Bells-Snowmass Wilderness	CO	WHRI1	0.04	0.00	0.00	0.00	0.00	0.00
Mammoth Cave NP	KY	MACA1	2.99	0.00	0.00	0.00	0.00	0.00
Mingo	MO	MING1	1.72	0.00	0.00	0.00	0.01	0.00
Mount Zirkel Wilderness	CO	MOZI1	0.05	0.00	0.00	0.00	0.00	0.00
Okefenokee	GA	OKEF1	1.12	0.00	0.01	0.01	0.01	0.01
Otter Creek Wilderness	WV	DOSO1	3.37	0.00	0.00	0.00	0.00	0.00
Pecos Wilderness	NM	WHPE1	-0.26	0.00	0.00	0.00	0.00	0.00
Rawah Wilderness	CO	MOZI1	0.05	0.00	0.00	0.00	0.00	0.00
Cape Romain	SC	ROMA1	1.44	0.00	0.01	0.00	0.01	0.01
Rocky Mountain NP	CO	ROMO1	0.13	0.00	0.00	0.00	0.00	0.00
Salt Creek	NM	SACR1	-0.78	0.00	0.00	0.00	0.00	0.00
St. Marks	FL	SAMA1	1.76	0.00	0.01	0.01	0.02	0.01
San Pedro Parks Wilderness	NM	SAPE1	-0.25	0.00	0.00	0.00	0.00	0.00
Shenandoah NP	VA	SHEN1	3.15	0.00	0.00	0.00	0.00	0.00
Shining Rock Wilderness	NC	SHRO1	2.35	0.00	0.00	0.00	0.00	0.00
Sipsey Wilderness	AL	SIPS1	2.22	0.00	0.00	0.00	0.00	0.00
Swanquarter	NC	SWAN1	1.68	0.00	0.00	0.00	0.00	0.00
Upper Buffalo Wilderness	AR	UPBU1	1.81	0.00	0.02	0.01	0.03	0.02
West Elk Wilderness	CO	WHRI1	0.04	0.00	0.00	0.00	0.00	0.00
Weminuche Wilderness	CO	WEMI1	0.02	0.00	0.00	0.00	0.00	0.00

Class I Name	State[a]	IMPROVE Site	BY - FY DV	Difference in FY DV without Source Group				
				Single-Sale		10-Sale		No-Sale
				B2	B3	C2	C3	A2
White Mountain Wilderness	NM	WHIT1	-0.56	0.00	0.00	0.00	0.00	0.00
Wheeler Peak Wilderness	NM	WHPE1	-0.26	0.00	0.00	0.00	0.00	0.00
Wichita Mountains	OK	WIMO1	1.04	0.00	0.00	0.00	0.00	0.00
Wolf Island	GA	OKEF1	1.12	0.00	0.01	0.01	0.01	0.01

[a] Indicates state in which assigned IMPROVE monitor is located

Table 4-27. Cumulative Visibility Results for 20% Best Visibility Days (B20%) at Class I Areas for Base (2012) Year (BY) and Future Year (FY) Scenarios with all Sources Included and With Contributions from Each Source Group Removed

Class I Name	State[a]	IMPROVE Site	BY DV	FY DV	FY DV without Source Group				
					Single-Sale		10-Sale		No-Sale
					B2	B3	C2	C3	A2
Bandelier NM	NM	BAND1	3.90	4.20	4.20	4.20	4.20	4.20	4.20
Big Bend NP	TX	BIBE1	5.74	5.77	5.77	5.77	5.77	5.77	5.77
Black Canyon of the Gunnison NM	CO	WEMI1	2.02	2.18	2.18	2.18	2.18	2.18	2.18
Bosque del Apache	NM	BOAP1	5.77	5.90	5.90	5.90	5.90	5.90	5.90
Breton-2	LA	BRIS1	13.64	12.15	12.15	12.09	12.12	12.07	12.09
Caney Creek Wilderness	AR	CACR1	9.83	9.31	9.31	9.31	9.31	9.31	9.31
Carlsbad Caverns NP	TX	GUMO1	5.37	5.48	5.48	5.48	5.48	5.48	5.48
Chassahowitzka	FL	CHAS1	13.56	13.29	13.29	13.29	13.29	13.29	13.29
Cohutta Wilderness	GA	COHU1	11.03	10.30	10.30	10.30	10.30	10.30	10.30
Dolly Sods Wilderness	WV	DOSO1	9.04	8.41	8.41	8.41	8.41	8.41	8.41
Eagles Nest Wilderness	CO	WHRI1	0.43	0.38	0.38	0.38	0.38	0.38	0.38
Everglades NP	FL	EVER1	11.08	10.90	10.90	10.90	10.90	10.90	10.90
Flat Tops Wilderness	CO	WHRI1	0.43	0.38	0.38	0.38	0.38	0.38	0.38
Great Sand Dunes NM	CO	GRSA1	3.73	3.76	3.76	3.76	3.76	3.76	3.76
Great Smoky Mountains NP	TN	GRSM1	10.70	9.59	9.59	9.59	9.59	9.59	9.59
Guadalupe Mountains NP	TX	GUMO1	5.37	5.48	5.48	5.48	5.48	5.48	5.48
Hercules-Glades Wilderness	MO	HEGL1	10.73	10.42	10.42	10.42	10.42	10.42	10.42
James River Face Wilderness	VA	JARI1	11.64	10.63	10.63	10.63	10.63	10.63	10.63
Joyce-Kilmer-Slickrock Wilderness	TN	GRSM1	10.70	9.59	9.59	9.59	9.59	9.59	9.59
La Garita Wilderness	CO	WEMI1	2.02	2.18	2.18	2.18	2.18	2.18	2.18
Linville Gorge Wilderness	NC	LIGO1	9.49	8.87	8.87	8.87	8.87	8.87	8.87
Maroon Bells-Snowmass Wilderness	CO	WHRI1	0.43	0.38	0.38	0.38	0.38	0.38	0.38
Mammoth Cave NP	KY	MACA1	13.48	12.49	12.49	12.48	12.49	12.48	12.49

Class I Name	State[a]	IMPROVE Site	BY DV	FY DV	FY DV without Source Group				
					Single-Sale		10-Sale		No-Sale
					B2	B3	C2	C3	A2
Mingo	MO	MING1	12.44	11.97	11.96	11.96	11.96	11.96	11.96
Mount Zirkel Wilderness	CO	MOZI1	0.85	0.82	0.82	0.82	0.82	0.82	0.82
Okefenokee	GA	OKEF1	13.07	12.61	12.61	12.61	12.61	12.61	12.61
Otter Creek Wilderness	WV	DOSO1	9.04	8.41	8.41	8.41	8.41	8.41	8.41
Pecos Wilderness	NM	WHPE1	1.02	1.26	1.26	1.26	1.26	1.26	1.26
Rawah Wilderness	CO	MOZI1	0.85	0.82	0.82	0.82	0.82	0.82	0.82
Cape Romain	SC	ROMA1	13.39	12.73	12.73	12.73	12.73	12.73	12.73
Rocky Mountain NP	CO	ROMO1	1.52	1.50	1.50	1.50	1.50	1.50	1.50
Salt Creek	NM	SACR1	7.54	8.11	8.11	8.11	8.11	8.11	8.11
St. Marks	FL	SAMA1	12.88	12.20	12.20	12.19	12.19	12.18	12.19
San Pedro Parks Wilderness	NM	SAPE1	1.20	1.36	1.36	1.36	1.36	1.36	1.36
Shenandoah NP	VA	SHEN1	8.60	7.70	7.70	7.70	7.70	7.70	7.70
Shining Rock Wilderness	NC	SHRO1	5.24	4.70	4.70	4.70	4.70	4.70	4.70
Sipsey Wilderness	AL	SIPS1	12.68	11.98	11.98	11.98	11.98	11.97	11.98
Swanquarter	NC	SWAN1	11.57	10.89	10.89	10.89	10.89	10.89	10.89
Upper Buffalo Wilderness	AR	UPBU1	9.62	9.16	9.16	9.15	9.16	9.15	9.15
West Elk Wilderness	CO	WHRI1	0.43	0.38	0.38	0.38	0.38	0.38	0.38
Weminuche Wilderness	CO	WEMI1	2.02	2.18	2.18	2.18	2.18	2.18	2.18
White Mountain Wilderness	NM	WHIT1	3.25	3.51	3.51	3.51	3.51	3.51	3.51
Wheeler Peak Wilderness	NM	WHPE1	1.02	1.26	1.26	1.26	1.26	1.26	1.26
Wichita Mountains	OK	WIMO1	9.21	9.03	9.03	9.03	9.03	9.03	9.03
Wolf Island	GA	OKEF1	13.07	12.61	12.61	12.61	12.61	12.61	12.61

[a] Indicates state in which assigned IMPROVE monitor is located

Table 4-28. Differences in Cumulative Visibility Results for B20% Visibility Days at Class I Areas Between the Future Year (FY) and Base Year (BY) Scenarios and Each Source Group's Contributions to the Future Year Scenario Visibility

Class I Name	State[a]	IMPROVE Site	BY - FY DV	Source Group Contribution to FY DV				
				Single-Sale		10-Sale		No-Sale
				B2	B3	C2	C3	A2
Bandelier NM	NM	BAND1	-0.30	0.00	0.00	0.00	0.00	0.00
Big Bend NP	TX	BIBE1	-0.03	0.00	0.00	0.00	0.00	0.00
Black Canyon of the Gunnison NM	CO	WEMI1	-0.16	0.00	0.00	0.00	0.00	0.00
Bosque del Apache	NM	BOAP1	-0.13	0.00	0.00	0.00	0.00	0.00
Breton-2	LA	BRIS1	1.49	0.00	0.06	0.03	0.08	0.06
Caney Creek Wilderness	AR	CACR1	0.52	0.00	0.00	0.00	0.00	0.00
Carlsbad Caverns NP	TX	GUMO1	-0.11	0.00	0.00	0.00	0.00	0.00
Chassahowitzka	FL	CHAS1	0.27	0.00	0.00	0.00	0.00	0.00
Cohutta Wilderness	GA	COHU1	0.73	0.00	0.00	0.00	0.00	0.00
Dolly Sods Wilderness	WV	DOSO1	0.63	0.00	0.00	0.00	0.00	0.00
Eagles Nest Wilderness	CO	WHRI1	0.05	0.00	0.00	0.00	0.00	0.00
Everglades NP	FL	EVER1	0.18	0.00	0.00	0.00	0.00	0.00
Flat Tops Wilderness	CO	WHRI1	0.05	0.00	0.00	0.00	0.00	0.00
Great Sand Dunes NM	CO	GRSA1	-0.03	0.00	0.00	0.00	0.00	0.00
Great Smoky Mountains NP	TN	GRSM1	1.11	0.00	0.00	0.00	0.00	0.00
Guadalupe Mountains NP	TX	GUMO1	-0.11	0.00	0.00	0.00	0.00	0.00
Hercules-Glades Wilderness	MO	HEGL1	0.31	0.00	0.00	0.00	0.00	0.00
James River Face Wilderness	VA	JARI1	1.01	0.00	0.00	0.00	0.00	0.00
Joyce-Kilmer-Slickrock Wilderness	TN	GRSM1	1.11	0.00	0.00	0.00	0.00	0.00
La Garita Wilderness	CO	WEMI1	-0.16	0.00	0.00	0.00	0.00	0.00
Linville Gorge Wilderness	NC	LIGO1	0.62	0.00	0.00	0.00	0.00	0.00
Maroon Bells-Snowmass Wilderness	CO	WHRI1	0.05	0.00	0.00	0.00	0.00	0.00
Mammoth Cave NP	KY	MACA1	0.99	0.00	0.01	0.00	0.01	0.00
Mingo	MO	MING1	0.47	0.01	0.01	0.01	0.01	0.01
Mount Zirkel Wilderness	CO	MOZI1	0.03	0.00	0.00	0.00	0.00	0.00
Okefenokee	GA	OKEF1	0.46	0.00	0.00	0.00	0.00	0.00

Class I Name	State[a]	IMPROVE Site	BY - FY DV	Source Group Contribution to FY DV				
				Single-Sale		10-Sale		No-Sale
				B2	B3	C2	C3	A2
Otter Creek Wilderness	WV	DOSO1	0.63	0.00	0.00	0.00	0.00	0.00
Pecos Wilderness	NM	WHPE1	-0.24	0.00	0.00	0.00	0.00	0.00
Rawah Wilderness	CO	MOZI1	0.03	0.00	0.00	0.00	0.00	0.00
Cape Romain	SC	ROMA1	0.66	0.00	0.00	0.00	0.00	0.00
Rocky Mountain NP	CO	ROMO1	0.02	0.00	0.00	0.00	0.00	0.00
Salt Creek	NM	SACR1	-0.57	0.00	0.00	0.00	0.00	0.00
St. Marks	FL	SAMA1	0.68	0.00	0.01	0.01	0.02	0.01
San Pedro Parks Wilderness	NM	SAPE1	-0.16	0.00	0.00	0.00	0.00	0.00
Shenandoah NP	VA	SHEN1	0.90	0.00	0.00	0.00	0.00	0.00
Shining Rock Wilderness	NC	SHRO1	0.54	0.00	0.00	0.00	0.00	0.00
Sipsey Wilderness	AL	SIPS1	0.70	0.00	0.00	0.00	0.01	0.00
Swanquarter	NC	SWAN1	0.68	0.00	0.00	0.00	0.00	0.00
Upper Buffalo Wilderness	AR	UPBU1	0.46	0.00	0.01	0.00	0.01	0.01
West Elk Wilderness	CO	WHRI1	0.05	0.00	0.00	0.00	0.00	0.00
Weminuche Wilderness	CO	WEMI1	-0.16	0.00	0.00	0.00	0.00	0.00
White Mountain Wilderness	NM	WHIT1	-0.26	0.00	0.00	0.00	0.00	0.00
Wheeler Peak Wilderness	NM	WHPE1	-0.24	0.00	0.00	0.00	0.00	0.00
Wichita Mountains	OK	WIMO1	0.18	0.00	0.00	0.00	0.00	0.00
Wolf Island	GA	OKEF1	0.46	0.00	0.00	0.00	0.00	0.00

[a] Indicates state in which assigned IMPROVE monitor is located

4.7.3.2 Acid Deposition

CAMx-predicted wet and dry fluxes of sulfur- and nitrogen-containing species were processed to estimate total annual sulfur (S) and nitrogen (N) deposition values at each Class I and sensitive Class II area in the 12/4-km modeling domain. The maximum annual S and N deposition values from any grid cell that intersects a Class I or sensitive Class II area receptor was used to represent deposition for that area, in addition to the average annual deposition values of all grid cells that intersect a Class I or sensitive Class II area receptor. Maximum and average predicted S and N deposition impacts were estimated separately for each source group and together across all source groups.

As a screening analysis, incremental deposition values in Class I/II areas for source groups B2 (new sources associated with a single lease sale) and C2 (new sources associated with the 10-sale scenario), were compared to the eastern and western U.S. DATs listed in Table 4-29. These DATs are specified in the FLAG (2010) guidance. Results of the incremental deposition analysis are summarized in Table 4-30 for Class I/II areas in the 4-km modeling domain. Deposition results were also obtained for all other sensitive areas throughout the 12-km modeling domain but the highest deposition values all occurred within the 4-km domain. The dividing line between the eastern and western DATs specified in the FLAG guidance is the Mississippi River, which makes sense for most locations in the U.S., but it is not necessarily clear which DAT would be most appropriate for GOM coastal locations so results are compared here against both DATs. Comparisons of deposition impacts from cumulative sources as represented by the other source groups listed in Table 4-13 to the DAT are not appropriate. Incremental nitrogen deposition exceeds the western and eastern DATs at all four locations although the average deposition at Padre Islands NS (0.0037 kg/ha/yr) is below both DATs. Incremental sulfur deposition is below the DATs in all cases.

Table 4-29. Deposition Analysis Threshold Values (kg/ha/yr) as Defined in the FLM Guidance

	Nitrogen	Sulfur
East	0.010	0.010
West	0.005	0.005

Table 4-30. Incremental Deposition Impacts (kg/ha/yr) from Source Groups B2 and C2 at Class I and Sensitive Class II Areas in the 4-km Domain

Area		Source Group B2				Source Group C2			
		Nitrogen		Sulfur		Nitrogen		Sulfur	
		Max	Avg	Max	Avg	Max	Avg	Max	Avg
Breton Wilderness	Annual Deposition	0.0180	0.0150	0.0002	0.0002	0.0966	0.0837	0.0020	0.0013
	Exceeds Eastern DAT?	Yes	Yes	No	No	Yes	Yes	No	No
	Exceeds Western DAT?	Yes	Yes	No	No	Yes	Yes	No	No
Breton NWR	Annual Deposition	0.0168	0.0157	0.0002	0.0002	0.0894	0.0860	0.0014	0.0013
	Exceeds Eastern DAT?	Yes	Yes	No	No	Yes	Yes	No	No
	Exceeds Western DAT?	Yes	Yes	No	No	Yes	Yes	No	No
Gulf Islands NS	Annual Deposition	0.0265	0.0103	0.0002	0.0001	0.1608	0.0689	0.0014	0.0010
	Exceeds Eastern DAT?	Yes	Yes	No	No	Yes	Yes	No	No
	Exceeds Western DAT?	Yes	Yes	No	No	Yes	Yes	No	No
Padre Islands NS	Annual Deposition	0.0105	0.0037	0.0000	0.0000	0.1039	0.0338	0.0003	0.0002
	Exceeds Eastern DAT?	Yes	No	No	No	Yes	Yes	No	No
	Exceeds Western DAT?	Yes	No	No	No	Yes	Yes	No	No

Cumulative deposition from all sources combined for the base case and future year scenarios were compared against applicable critical load levels in each Class I/II area for which critical loads were identified as described in Section 4.6.2.3.3. Results are summarized in Table 4-31. Cumulative nitrogen deposition is projected to decrease in all areas between the 2012 base case and the 2017 future year, consistent with an overall reduction in NO_x emissions. Nevertheless, maximum nitrogen deposition is modeled to continue exceeding the critical load thresholds under the Future Year scenario for all areas except Padre Island. Sulfur deposition values are lower, and larger sulfur emission reductions help to reduce sulfur deposition from above the critical load to below the critical load at Breton Wilderness, Breton NWR and Cohutta Wilderness (based on maximum grid cell values). The maximum grid cell sulfur deposition in the future year scenario is calculated to be below the critical load at all locations except Gulf Islands.

Table 4-31. Cumulative Nitrogen (N) and Sulfur (S) Deposition Impacts (kg/ha/yr) Under the Base and Future Year Scenarios (red indicates values exceeding the critical load threshold)

Class I/II Area	Critical Load Threshold	2012 Base Case				2017 Future Year			
		N-Max	N-Avg	S-Max	S-Avg	N-Max	N-Avg	S-Max	S-Avg
Big Bend NP	3	4.6	2.8	2.4	1.2	4.6	2.9	2.3	1.1
Breton Wilderness	3	8.0	7.3	4.1	3.6	5.8	5.5	2.5	2.1
Breton National Wildlife Refuge	3	7.8	7.3	3.8	3.6	5.9	5.6	2.3	2.1
Gulf Islands National Seashore	3	14.2	7.3	5.5	4.4	11.1	5.8	3.4	2.7
Padre Island National Seashore	5	4.8	2.2	1.6	1.2	4.6	2.1	1.1	0.9
Bradwell Bay Wilderness	5	7.8	7.4	2.8	2.5	7.1	6.7	2.0	1.8
Saint Marks National Wildlife Refuge	3	7.9	5.9	2.7	2.1	7.2	5.3	2.0	1.5
Saint Marks Wilderness	3	6.5	5.3	2.0	1.9	5.9	4.8	1.4	1.4
Chassahowitzka Wilderness	3	8.3	7.5	2.7	2.6	7.3	6.7	2.0	2.0
Everglades NP	5	9.8	6.7	4.2	2.4	9.3	6.4	2.7	1.9
Okefenokee National Wildlife Refuge	3	7.1	6.6	2.5	2.2	6.6	6.1	2.0	1.8
Okefenokee Wilderness	3	7.7	6.4	2.7	2.2	7.1	5.9	2.3	1.8
Wolf Island Wilderness	3	4.0	3.7	2.2	2.1	3.6	3.4	1.6	1.5
Cohutta Wilderness	5	13.3	11.5	5.5	4.5	12.1	10.5	3.8	3.1
Sipsey Wilderness	5	10.4	10.0	3.5	3.4	9.8	9.4	2.3	2.3
Guadalupe Mountains NP	3	3.9	2.8	1.2	0.7	3.8	2.7	1.1	0.6
Wichita Mountains (Charons Garden Unit) Wilderness	5	5.9	5.9	1.8	1.8	5.7	5.7	1.6	1.6
Wichita Mountains (North Mountain Unit) Wilderness	5	6.7	6.7	1.9	1.9	6.4	6.4	1.6	1.6
Wichita Mountains National Wildlife Refuge	5	6.9	6.4	1.9	1.8	6.6	6.1	1.6	1.5
Caney Creek Wilderness	5	10.3	10.1	4.0	3.8	9.9	9.8	2.6	2.5
Upper Buffalo Wilderness	5	8.0	8.0	2.6	2.6	7.5	7.5	1.7	1.7

4.7.4 Summary of Air Resource Impacts

A condensed summary of air resource impact estimates is presented here for the reader's convenience. Methods used to calculate these impacts are described in Section 4.6.

4.7.4.1 NAAQS Impacts

Maximum impacts of the proposed lease sales with respect to the NAAQS are summarized in Tables 4-32 and 4-33. In Table 4-32, maximum contributions from new platforms and support vessels and helicopters associated with the single-sale scenario (Source Group B2) and 10-sale scenario (Source Group C2) as well as from "existing" sources under the no-sale scenario (Source Group A2) are listed separately for offshore and onshore portions of the 4-km modeling domain for each NAAQS. For purposes of this analysis, "offshore" was defined based on BOEM's northern GOM shoreline boundary (USDOI BSEE, 2018) as the union of all gray shaded 4-km model grid cells shown in Figure 4-52. While this area includes some inland bays and inlets, maximum offshore impacts listed in Table 4-31 typically occur out over the Gulf (see Figures 4-31, 4-33, 4-35, 4-37, 4-39, 4-41, 4-43, 4-45, 4-47, and 4-49). For ozone and annual average $PM_{2.5}$, impacts calculated via both the RRF UAA method and the "absolute" method as described in Sections 4.7.1.1.2 and 4.7.1.3.2 are shown. As expected, impacts from platforms and support vessels in the Gulf are higher offshore than onshore, and impacts from the single sale sources (B2) are less than from the 10-sale sources (C2). In addition, impacts from "existing" sources (A2) are greater than those from the new sources. Ozone impacts calculated using RRFs are lower than those based on the "absolute" model results. This is a result of the tendency toward overprediction of ozone by the model throughout much of the 4-km domain noted in Section 4.5.5.1.

Maximum ozone impacts from single sale (B2), 10 sale (C2), and "existing" (A2) sources in the Houston-Galveston-Brazoria and San Antonio (Bexar County) ozone nonattainment areas of Texas are shown in Table 4-33. The Houston nonattainment area is entirely within the 4-km modeling domain, while the San Antonio (Brexar County) nonattainment area straddles the western border of the 4-km domain with part of the county lying within the 12-km domain. Model output from the 12- and 4-km domains were combined to obtain the results listed for San Antonio. For comparison purposes, we also list the maximum source contributions calculated using the monitor RRF method over all monitors in the 4-km domain.[17] Impacts from sources in the GOMR are higher in Houston than in San Antonio, which lies further inland. As noted above, impacts from potential new platforms and support vessels and helicopters (B2 and C2) are less than those from "existing" platforms and vessels (A2). Impacts from new sources under the 10-sale scenario calculated via the RRF method are less than 0.8 ppb. Impacts calculated using the "absolute" method are higher due to the model's tendency toward ozone overprediction.

[17] Two of the three ozone monitoring sites in the Bexar County (San Antonio) ozone nonattainment area (Camp Bullis and Calaveras Lake) are within the 4-km domain but the San Antonio Northwest ozone monitoring site is just outside of the 4-km domain).

Table 4-32. Maximum Impacts Relative to NAAQS Over Offshore and Onshore Portions of the 4-km Modeling Domain

NAAQS		Analysis Method	Single Sale (B2)		10 Sale (C2)		Existing (A2)	
Pollutant Avg. Time	Level		Offshore	Onshore	Offshore	Onshore	Offshore	Onshore
Ozone 8-Hr	70 ppb	RRF[a]	1.9	0.5	4.9	2.1	13.2	7.6
		Absolute[b]	4.2	1.3	9.2	5.4	25.9	14.1
$PM_{2.5}$ Annual	12 $\mu g/m^3$	RRF[a]	0.4	0.1	0.5	0.1	0.7	0.1
		Absolute[b]	0.5	0.04	0.5	0.2	0.5	0.2
$PM_{2.5}$ 24-Hr	35 $\mu g/m^3$	Absolute[b]	0.7	0.2	0.8	0.7	1.6	1.9
PM_{10} 24-Hr	150 $\mu g/m^3$	Absolute[b]	0.5	0.2	0.8	1.0	2.4	2.8
NO_2 1-Hour	100 ppb	Absolute[b]	7.2	0.8	7.6	3.4	35.7	11.1
NO_2 Annual	53 ppb	Absolute[b]	2.4	0.4	2.4	1.2	8.2	1.9
SO_2 1-Hr	75 ppb	Absolute[b]	0.01	0.03	0.2	0.3	1.5	0.02
SO_2 3-Hr	500 ppb	Absolute[b]	0.01	0.1	0.4	0.2	2.1	0.01

[a] Results from Relative Response Factor (RRF) unmonitored area analysis (UAA) approach (see Section 4.6.2.2; UAA only available for 8-hr ozone and annual average $PM_{2.5}$)

[b] Results represent maximum source group contributions to the corresponding modeled NAAQS design value within all offshore or onshore grid cells within the 4-km modeling domain (see Section 4.6.2.2).

Table 4-33. Maximum Impacts Relative to NAAQS in Houston and San Antonio Ozone Nonattainment Areas

NAAQS			Single Sale (B2)			10 Sale (C2)			Existing (A2)		
Pollutant Avg. Time	Level	Analysis Method	Houston	San Antonio	All Monitored Areas[c]	Houston	San Antonio	All Monitored Areas	Houston	San Antonio	All Monitored Areas
Ozone 8-Hr	70 ppb	RRF[a]	0.1	0.0	0.3	0.8	0.1	1.2	2.5	0.3	3.7
		Absolute[b]	0.3	0.1	-	1.7	0.6	-	7.2	1.8	-

[a] Results from Relative Response Factor (RRF) approach at monitoring sites (see Section 4.6.2.2).

[b] Results represent maximum source group contributions to the corresponding modeled NAAQS design value over all grid cells covering all or a portion of the nonattainment area (see Section 4.6.2.2).

[c] Maximum RRF result over all monitoring sites within the 4-km modeling domain; absolute model results were not extracted for individual monitoring sites.

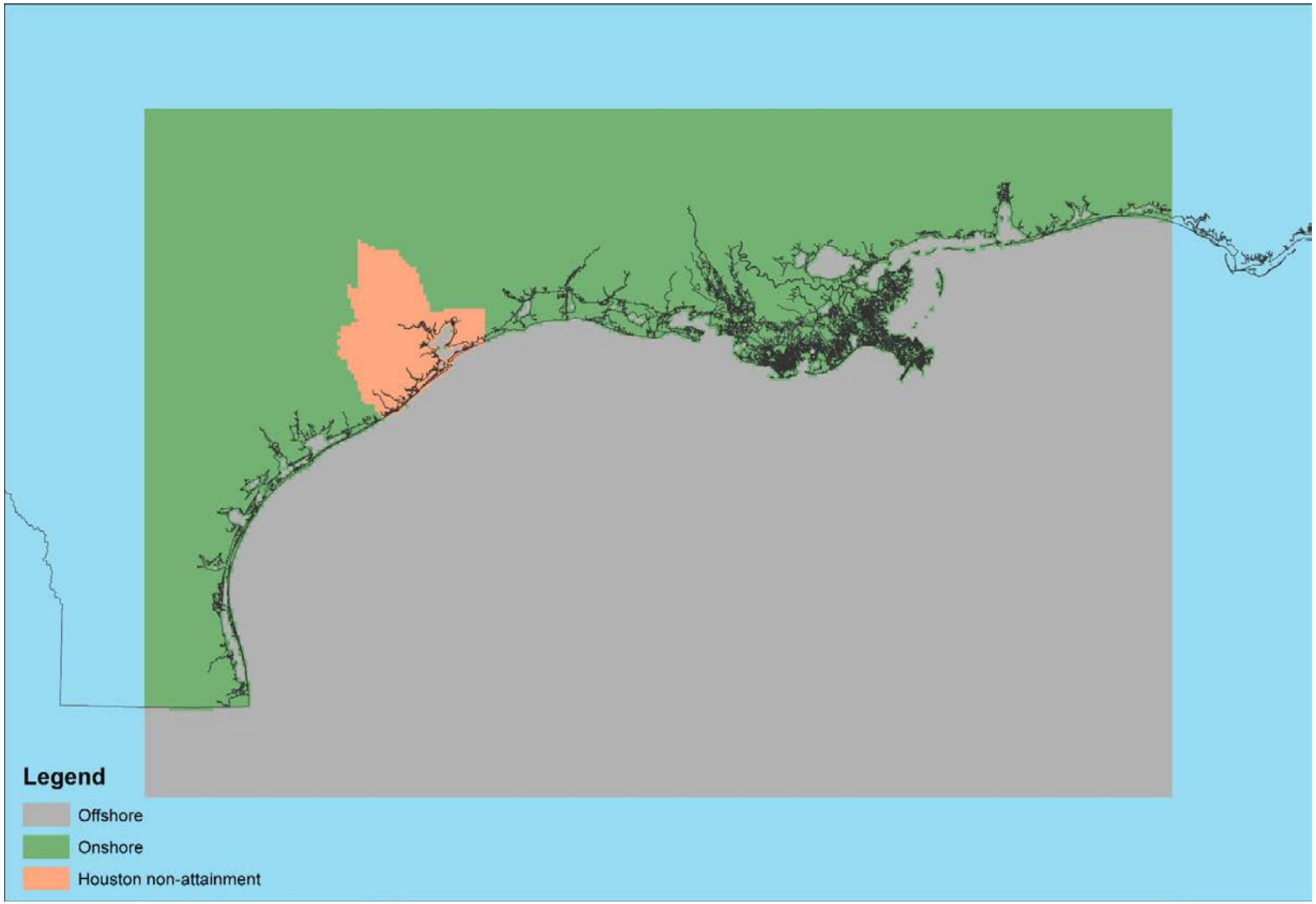

Figure 4-52. Division of Offshore and Onshore Areas and Houston-Galveston-Brazoria Ozone Nonattainment Area Used to Generate Results in Tables 4-32 and 4-33.

4.7.4.2 PSD and AQRV Impacts

As noted in Sections 4.7.2 and 4.7.3, nearly all maximum impacts from potential new single- and 10-sale sources within Class I and Sensitive Class II areas occur at Breton Island, as this is the area closest to these sources (see Figure 4-30). We therefore summarize the PSD and AQRV impacts (visibility and deposition) for Breton Island in this section; results for other Class I and sensitive Class II areas are presented in Sections 4.7.2 and 4.7.3.

PSD results for the Breton Island Class I area are summarized in Table 4-34. Concentration increments from new (B2 and C2) and existing (A2) sources are all below the Class I PSD increments. As noted in Section 4.7.2, comparisons of impacts from the lease sales with maximum allowed PSD increments are presented here as an evaluation of a "threshold of concern" for potentially significant adverse impacts, but do not represent a regulatory PSD increment consumption analysis as would be required for major sources subject to the NSR program requirements of the CAA. Incremental impacts are compared here to the full allowable PSD increments; no attempt is made to identify existing PSD increment-consuming or increment-expanding sources.

Table 4-34. Maximum PSD Impacts in the Breton Island Class I Area

Pollutant/Avg. Time	PSD Class I Area Increment	Single Sale (B2)	10 Sale (C2)	Existing (A2)
$PM_{2.5}$ 24-Hr[a]	2 µg/m^3	0.055	0.272	0.750
$PM_{2.5}$ Annual[b]	1 µg/m^3	0.004	0.051	0.073
PM_{10} 24-Hr[a]	8 µg/m^3	0.056	0.273	0.751
PM_{10} Annual[b]	4 µg/m^3	0.005	0.052	0.073
NO_2 Annual[b]	2.5 µg/m^3	0.010	0.142	0.694
SO_2 3-Hr[c]	25 µg/m^3	0.002	0.012	0.026[d]
SO_2 24-Hr[a]	5 µg/m^3	0.00	0.005	0.010[d]
SO_2 Annual[b]	2 µg/m^3	< 0.0005	0.001	0.002

[a] Impacts based on 2nd max 24-hr average contribution, max grid cell

[b] Impacts based on annual average contribution, max grid cell

[c] Impacts based on second-highest 3-hour block average, max grid cell

[d] Higher values (0.109 for 3-hr avg., 0.034 for 24-hr avg.) are calculated at Gulf Islands sensitive Class II area

Incremental visibility impacts at Breton Island from new (B2 and C2) and existing (A2) sources are summarized in Table 4-35. The 8th highest Δdv calculated for new platforms and associated support vessels and helicopters under the 10-sale scenario (C2) just exceeds the 1-dv threshold contained in the FLAG (2010); in a total of 8 days during the year are calculated to exceed the 1-dv threshold. Visibility impacts from single sale scenario sources (B2) do not exceed the lower 0.5-dv threshold. However, as noted in Section 4.7.3.1.2, the cumulative contributions of the 10-sale sources (C2) together with "existing" platforms and support vessels (A2) on days with the 20% worst visibility at Breton Island is calculated to be 0.11 dv; the impact on the 20% best visibility days is calculated to be 0.08 dv.

Table 4-35. Maximum Incremental Visibility Impacts in the Breton Island Class I Area[a]

Source Group	Max Δdv	8th High Δdv	No. Days	
			> 1.0 dv	> 0.5 dv
Single Sale (B2)	0.31	0.15	0	0
10 Sale (C2)	1.33	1.01	8	57
Existing (A2)	4.03	2.45	63	120

Annual nitrogen and sulfur deposition impacts at Breton Island are summarized in Table 4-36. Nitrogen deposition is calculated to exceed the DATs specified in FLAG (2010) even just for new platforms and support vessels and helicopters under the sing sale scenario (B2). Sulfur deposition from new sources (B2, C2) is also below the DATs except for "existing" platforms and support vessels and helicopters (A2), which just exceed the more stringent western DAT.

Table 4-36. Total Annual Maximum Nitrogen and Sulfur Deposition (kg/ha/yr) at Breton Island Class I Area[a]

	Deposition Analysis Threshold		Single Sale (B2)	10 Sale (C2)	Existing (A2)
	East	West			
Nitrogen	0.01	0.005	0.0180	0.0966	0.4303
Sulfur	0.01	0.005	0.0002	0.0020	0.0061

[a] The calculated maximum nitrogen deposition contributions for B2, C2, and A2 are higher at Gulf Islands National Seashore (0.0265, 0.1608, and 0.5337 kg/ha/yr, respectively), although the average values are higher at Breton Island.

4.8 Uncertainties

4.8.1 Uncertainties Related to Model Performance

CAMx model performance within the 4-km domain was generally within performance criteria described in USEPA guidance (USEPA, 2014a). Similar to other modeling studies, ozone overprediction was observed in the southeastern U.S. As noted previously, a recent study suggests this may be at least partially related to over estimation of anthropogenic NO_x emissions (Travis et al., 2016).

As is typical with regional photochemical modeling applications, model performance is better for ozone than for total PM mass (PM_{10} and $PM_{2.5}$) and some PM species. Of particular interest is overprediction bias of fine ($PM_{2.5}$) particulate nitrate, which may skew estimates of source contributions to visibility and nitrate deposition. This is discussed in more detail below. In addition to errors in emissions and inaccuracies in meteorological and photochemical grid model formulations, comparisons of model predictions with observations are affected by shortcomings in the available air quality monitoring data, which are particularly significant for PM as described in Section 4.5.5.2.

4.8.2 Other Sources of Uncertainties

Numerous factors contribute to uncertainties in model predictions. Uncertainties in meteorological inputs to the photochemical model are significant, especially with respect to factors, such as moist convection, influencing the degree of vertical mixing. Uncertainties in the magnitudes of biogenic and geogenic emission sources as well as anthropogenic emissions are additional important contributors to modeling uncertainties. A key source of uncertainties in coastal areas is related to the estimated magnitude and size distribution of sea salt emissions. A revised sea salt emissions preprocessor was used in this study as described in Section 4.3.5. Lower sea salt emission fluxes estimated using the revised preprocessor resulted in significantly less overprediction of sodium and particulate nitrate as compared to results

initially obtained using the old preprocessor. Nevertheless, some overprediction of particulate nitrate is still present as noted above.

Another source of uncertainty related to nitrate is the extent to which particulate nitrate is predicted to occur in the coarse as compared to the fine mode. CAMx simulations performed for the GOMR modeling study employed the CF scheme which represents secondary (chemically formed) PM species using a single fine mode ($PM_{2.5}$) size bin, while primary inert PM species (e.g., dust particles) are allocated into both the fine and coarse mode size bins. This is a good approximation under many atmospheric conditions where fine particles usually provide much larger particle surface area for gas-particle partitioning of secondary PM species than coarse particles. In coastal environments, however, abundant coarse sea salt aerosols may play an important role in secondary PM formation. Therefore, ignoring coarse secondary PM species may introduce errors in the model results. For example, if a significant fraction of nitrate is portioned into coarse mode particles which settle out of the atmosphere faster than fine particles, the impacts of NO_x sources may be overstated. However, the potential significance of such errors is not obvious. Given its importance in evaluation of NO_x source impacts in coastal environments, a simple sensitivity analysis was performed to further examine this particular issue. This sensitivity analysis is described in Appendix D.1. Results of the sensitivity analysis suggest that accounting for coarse mode nitrate may slightly reduce overprediction of particulate nitrate.

4.9 References

Abt. 2014. Modeled Attainment Software, User's Manual. Abt Associates Inc., Bethesda, MD. April. Internet address: https://www3.epa.gov/ttn/scram/guidance/guide/MATS_2-6-1_manual.pdf.

Adelman, Z., U. Shanker, D. Yang, R. Morris. 2015. Three-State Air Quality Modeling Study CAMx Photochemical Grid Model Draft Model Performance Evaluation Simulation Year 2011. University of North Carolina at Chapel Hill and ENVIRON International Corporation, Novato, CA. June. Internet address: http://views.cira.colostate.edu/wiki/Attachments/Modeling/3SAQS_Base11a_MPE_Final_18Jun2015.pdf.

Allen, D.J., K.E. Pickering, R.W. Pinder, B.H. Henderson, K.W. Appel, A. Prados. 2012. Impact of lightning-NO on eastern United States photochemistry during the summer of 2006 as determined using the CMAQ model. Atmos. Chem. Phys., 10, 107–119.

Boylan, J.W. 2004. "Calculating Statistics: Concentration Related Performance Goals", paper presented at the USEPA PM Model Performance Workshop, Chapel Hill, NC. 11 February.

Boylan, J.W., A.G. Russell. 2006. PM and Light Extinction Model Performance Metrics, Goals, and Criteria for Three-Dimensional Air Quality Models. Atmospheric Environment 40 (2006) 4946-4959.

Colella, P., P.R. Woodward. 1984. The Piecewise Parabolic Method (PPM) for Gas-dynamical Simulations. J. Comp. Phys., 54, 174-201.

Emery, C., Z. Liu, B. Koo, G. Yarwood. 2016a. Improved Halogen Chemistry for CAMx Modeling. Prepared for Jim Smith, Texas Commission on Environmental Quality. Ramboll Environ, Novato, CA. Internet address: https://www.tceq.texas.gov/assets/public/implementation/air/am/contracts/reports/pm/5821661842FY1613-20160526-environ-CAMx_Halogens.pdf.

Emery, C., B. Koo, P. Karamchandani, W.C. Hsieh, A. Wentland, G. Wilson, G. Yarwood. 2016b. Updates to CAMx: Secondary Organic Aerosol Chemistry, Heterogeneous Aerosol Chemistry, and Wet Deposition. Prepared for the U.S. Environmental Protection Agency, Research Triangle Park, NC (September 2016).

Emmons, L.K., S. Walters, P.G. Hess, J.-F. Lamarque, G.G. Pfister, D. Fillmore, C. Granier, A. Guenther, D. Kinnison, T. Laepple, J. Orlando, X. Tie, G. Tyndall, C. Wiedinmyer, S.L. Baughcum, S. Kloster. 2010. Description and evaluation of the Model for Ozone and Related Tracers, version 4 (MOZART-4), Geosci. Model Dev., 3, 43–67.

ENVIRON. 2012. Dallas-Fort Worth Modeling Support: Improving Vertical Mixing, Plume-in-Grid, and Photolysis Rates in CAMx, Prepared for: Texas Commission on Environmental Quality by ENVIRON International Corporation. Internet address: https://www.tceq.texas.gov/assets/public/implementation/air/am/contracts/reports/pm/5821110365FY1206-20120820-environ_dfw_modeling_support.pdf

EPRI (Electric Power Research Institute). 2011. The Southeast Aerosol Research and Characterization Network: SEARCH. Electric Power Research Institute, Palo Alto CA. Internet address: https://yosemite.epa.gov/sab/sabproduct.nsf/B99E5E7B1FC13632852575B50069AAC2/$File/EPRI-SEARCH+for+EPA+SAB+INC+May+14-15+2009+Meeting.pdf.

FLAG, 2000. Federal Land Managers' Air Quality Related Values Workgroup (FLAG) Phase I Report. December. Internet Address: https://irma.nps.gov/DataStore/Reference/Profile/2257845.

FLAG (Federal Land Managers' Air Quality Related Values Work Group). 2010. FLAG: Phase I Report – Revised (2010). Natural Resource Report NPS/NRPC/NRR – 2012/232. Internet address: https://irma.nps.gov/DataStore/Reference/Profile/2125044.

FWS and NPS (Fish and Wildlife Service and National Park Service). 2012. Letter on Cumulative Visibility Metric Approach from Sandra V. Silva, Chief, Branch of Air Quality, U.S. Fish and Wildlife Service and Carol McCoy, Chief, Air Resource Division, National Park Service to Kelly Bott, Wyoming Department of Environment. February 10.

Gantt, B., Kelley, J.T., and J.O. Bash, 2015. Updating sea spray aerosol emissions in the Community Multiscale Air Quality (CMAQ) model version 5.0.2. Geosci. Model Dev., 8, 3733–3746, 2015; doi:10.5194/gmd-8-3733-2015.

Gong, S.L. 2003. A parameterization of sea-salt aerosol source function for sub- and super-micron particles. Global Biogeochem. Cycles, 17(4), 1097.

Guenther, A.B., T. Karl, P. Hartley, C. Weidinmyer, P. Palmer, C. Geron. 2006. Estimates of global terrestrial isoprene emissions using MEGAN (Model of Emissions of Gases and Aerosols in Nature). Atmos. Chem. Phys. 6, 3181-3210.

Guenther, A.B., X. Jiang, C.L. Heald, T. Sakulyanontvittaya, T. Duhl, L.K. Emmons, X. Wang. 2012. The Model of Emissions of Gases and Aerosols from Nature version 2.1 (MEGAN2.1): an extended and updated framework for modeling biogenic emissions, Geosci. Model Dev., 5, 1471-1492, doi: 10.5194/gmd-5-1471-2012.

Guenther, A., T. Shah, L. Huang, A. Wentland, J. Jung, R. Beardsley, J. Johnson, W.C. Hsieh, S. Kemball-Cook, G. Yarwood. 2017. A Next Generation Modeling System for Estimating Texas

Biogenic VOC Emissions. Prepared for Elena McDonald-Buller, Texas Commission on Environmental Quality (TCEQ) and Doug Boyer, TCEQ Project Liaison. August. Internet address: http://aqrp.ceer.utexas.edu/projectinfoFY16_17/16-011/16-011%20Final%20Report.pdf

Hertel O., R. Berkowics, J. Christensen, O. Hov. 1993. Test of two numerical schemes for use in atmospheric transport-chemistry models. Atmos. Environ., 27, 2591-2611.

Hildebrandt Ruiz, L., G. Yarwood. 2013. Interactions between organic aerosol and NOy: Influence on oxidant production. Final Report prepared for the Texas AQRP (Project 12-012) by the University of Texas at Austin and ENVIRON International Corporation, Novato, CA. Internet address: http://aqrp.ceer.utexas.edu/projectinfoFY12_13/12-012/12-012%20Final%20Report.pdf.

Hong, S.-Y., Y. Noh. 2006. A New Vertical Diffusion Package with an Explicit Treatment of Entrainment Processes. Monthly Weather Review, 134, 2318-2341.

Johnson, J., K. Bonyoung, S. Kemball-Cook, A. Wentland, J. Jung, W. Hsieh, G. Yarwood, 2015. Photochemical Modeling of June 2012 for Northeast Texas. Ramboll Environ, December.

Karl, T.G., T.J. Christian, R.J. Yokelson, P. Artaxo, W.M. Hao, A. Guenther, 2007. The Tropical Forest and Fire Emissions Experiment: method evaluation of volatile organic compound emissions measured by PTR-MS, FTIR, and GC from tropical biomass burning, Atmos. Chem. Phys., 7, 5883–5897.

Kelly, J.T., P.V. Bhave, C.G. Nolte, U. Shankar, K.M. Foley. 2010. Simulating emission and chemical evolution of coarse seasalt particles in the Community Multiscale Air Quality (CMAQ) model, Geosci. Model Dev., 3, 257-273, doi:10.5194/gmd-3-257-2010.

Kemball-Cook, S., G. Yarwood, J. Johnson, B. Dornblaser, M. Estes. 2015. Evaluating NOx Emission Inventories for Regulatory Air Quality Modeling Using Satellite and Air Quality Model Data. Atmos. Env. (submitted).

Koo, B., C.-J. Chien, G. Tonnesen, R. Morris, J. Johnson, T. Sakulyanontvittaya, P. Piyachaturawat, G. Yarwood. 2010. Natural emissions for regional modeling of background ozone and particulate matter and impacts on emissions control strategies. Atmos. Environ., 44, 2372-2382.

Lewis, E., S. Schwartz. 2004. Sea Salt Aerosol Production: Mechanisms, Methods, Measurements and Models-A Critical Review. Geophysical Monograph Series, Volume 152, American Geophyscial Union.

Mavko, M., R. Morris. 2013. DEASCO3 Project Updates to the Fire Plume Rise Methodology to Model Smoke Dispersion. Technical Memo prepared as part of Join Science Form (JSP) project Deterministic and Empirical Assessment of Smoke's Contribution to Ozone. December 3. Internet address: https://wraptools.org/pdf/DEASCO3_Plume_Rise_Memo_20131210.pdf.

Morris, R.E., B. Koo, B. Wang, G. Stella, D. McNally, C. Loomis. 2009a. Technical Support Document for VISTAS Emissions and Air Quality Modeling to Support Regional Haze State Implementation Plans. ENVIRON International Corporation, Novato, CA and Alpine Geophysics, LLC, Arvada, CO. Available upon request from BOEM/Ramboll.

Morris, R.E., B. Koo, T. Sakulyanontvittaya, G. Stella, D. McNally, C. Loomis, T.W. Tesche. 2009b. Technical Support Document for the Association for Southeastern Integrated Planning (ASIP)

Emissions and Air Quality Modeling to Support $PM_{2.5}$ and 8-Hour Ozone State Implementation Plans. ENVIRON International Corporation, Novato, CA and Alpine Geophysics, LLC, Arvada, CO. Available upon request from BOEM/Ramboll.

NADP (National Atmospheric Deposition Program). 2016. National Trends Network (NTN) data. Internet address: http://nadp.slh.wisc.edu/.

NPS. 2011. Federal Land Managers' Interagency Guidance for Nitrogen and Sulfur Deposition Analyses. Natural Resources Report NPS/NRSS/ARD/NRR—2011/465. Internet address: https://irma.nps.gov/DataStore/Reference/Profile/2180652.

NPS. 2016. Critical loads for resource protection. National Park Service. Internet address: https://www.nps.gov/subjects/air/critical-loads.htm.

Nopmongcol, O., B. Koo, L. Parker, J. Jung, G. Yarwood. 2014. Comprehensive Air Quality Model with extensions (CAMx) inputs to Community Model for Air Quality (CMAQ) Inputs Converter. Final Report prepared for Jim Smith, TCEQ. August.

Ovadnevaite, J., A. Manders, G. de Leeuw, D. Ceburnis, C. Monahan, A.-I. Partanen, H. Korhonen, C.D. O'Dowd. 2014. A sea spray aerosol flux parameterization encapsulating wave state, Atmos. Chem. Phys., 14, 1837-1852, doi:10.5194/acp-14-1837-2014.

Price, P.V., N. Nakagaki, K.J. hit, and R.M. Clawges. 2007. Enhanced historical land-use and land-cover data sets of the U.S. Geological Survey. Internet address: http://pubs.usgs.gov/ds/2006/240/.

Ramboll Environ. 2016. CAMx User's Guide: Comprehensive Air Quality Model with Extensions, Version 6.40. Ramboll Environ, Novato, CA. Internet address: www.camx.com.

Reidmiller, D.R., A.M. Fiore, D.A. Jaffe, D. Bergmann, C. Cuvelier, F.J. Dentener, B.N. Duncan, G. Folberth, M. Gauss, S. Gong, P. Hess, J. E. Jonson, T. Keating, A. Lupu, E. Marmer, R. Park, M.G. Schultz, D.T. Shindell, S. Szopa, M.G. Vivanco, O. Wild, A. Zuber. 2009. The influence of foreign vs. North American emissions on surface ozone in the U.S. Atmos. Chem. Phys., 9, 5027-5042.

Sakulyanontvittaya, T., T. Duhl, C. Wiedinmyer, D. Helmig, S. Matsunaga, M. Potosnak, J. Milford, A. Guenther, 2008. Monoterpene and sesquiterpene emission estimates for the United States. Environ. Sci. Techno. 42, 1623–1629.

Sauvage, B., R.V. Martin, A. van Donkelaar, X. Liu, K. Chance, L. Jaeglé, P I. Palmer, S. Wu, T.M. Fu. 2007. Remote sensed and in situ constraints on processes affecting tropical tropospheric ozone, Atmos. Chem. Phys., 7, 815–838.

Seinfeld, J.H., S.N. Pandis. 1998. Atmospheric Chemistry and Physics: From Air Pollution to Climate Change. John Wiley and Sons, Inc., NY.

Simon, H., K.R. Baker, S. Phillips. 2012. Compilation and interpretation of photochemical model performance statistics published between 2006 and 2012. Atmospheric Environment 61, 124-139.

Smagorinsky, J. 1963. General Circulation Experiments with the Primitive Equations: I. The Basic Experiment. Mon. Wea. Rev., 91, 99-164.

Tost, H., P.J. Joeckel, J. Lelieveld. 2007. Lightning and convection parameterisations - uncertainties in global modeling, Atmos. Chem Phys., 7(17), 4553–4568.

Travis, K.R., D.J. Jacob, J.A. Fisher, P.S. Kim, E.A. Marais, L. Zhu, K. Yu, C.C. Miller, R.M. Yantosca, M.P. Sulprizio, et al. 2016. Why do models overestimate surface ozone in the southeast United States? Amos. Chem. Phys., 16, 13561–13577.

USDOA, USDOI, USEPA (U.S. Department of Agriculture, U.S. Department of the Interior, and U.S. Environmental Protection Agency). 2011. Memorandum of understanding among the U.S. Department of Agriculture, U.S. Department of the Interior, and U.S. Environmental Protection Agency for Federal oil and gas decisions through the National Environmental Policy Act Process. June 23 2011. Internet address: https://www.epa.gov/sites/production/files/2014-08/documents/air-quality-analyses-mou-2011.pdf.

USDOI, BOEM (U.S. Department of the Interior, Bureau of Ocean Energy Management). 2017. Gulf of Mexico OCS Oil and Gas Lease Sales: 2017-2022; Gulf of Mexico Lease Sales 249, 250, 251, 252, 253, 254, 256, 257, 259, and 261; Final Multisale Environmental Impact Statement. USDOI, BOEM, Gulf of Mexico OCS Region, New Orleans, LA. OCS EIS/EA BOEM 2017-009.

USDOI, BSEE (USDOI, Bureau of Safety and Environmental Enforcement). 2018. File SDETABS.COAST70_SDE (NAD 1927) available from https://pubs.usgs.gov/of/2004/1089/gis-data.html (personal communication, S. Gonzales, BSEE, U.S. Department of the Interior, 2 August).

USEPA (U.S. Environmental Protection Agency). 1991. Guidance for Regulatory Application of the Urban Airshed Model (UAM), Office of Air Quality Planning and Standards, U.S. Environmental Protection Agency, Research Triangle Park, N.C. Internet address: http://www.epa.gov/ttn/scram/guidance/guide/uamreg.pdf.

USEPA. 2007. Guidance on the Use of Models and Other Analyses for Demonstrating Attainment of Air Quality Goals for Ozone, $PM_{2.5}$, and Regional Haze. EPA-454/B-07-002, U.S. Environmental Protection Agency, Research Triangle Park, NC, April.

USEPA. 2014a. Draft Modeling Guidance for Demonstrating Attainment of Air Quality Goals for Ozone, $PM_{2.5}$ and Regional Haze. U.S. Environmental Protection Agency, Research Triangle Park, NC. Internet address: http://www.epa.gov/ttn/scram/guidance/guide/Draft_O3-PM-RH_Modeling_Guidance-2014.pdf.

USEPA. 2014b. Modeled Attainment Test Software (MATS). Internet address: https://www.epa.gov/scram/photochemical-modeling-tools.

USEPA. 2015a. 2011 National Emissions Inventory, version 2: Technical Support Document. U.S. Environmental Protection Agency, Research Triangle Park, NC. Internet address: https://www.epa.gov/sites/production/files/2015-10/documents/nei2011v2_tsd_14aug2015.pdf. Accessed July 2018.

USEPA. 2015b. Fire emissions data. Internet address: ftp://ftp.epa.gov/EmisInventory/fires/. October.

USEPA. 2016. Personal communication, Brian Timin, Office of Air Quality Planning and Standards. May 13.

Wilson, D., R. Billings, R. Chang, H. Perez, J. Sellers. 2014. Year 2011 Gulfwide Emissions Inventory Study. U.S. Dept. of the Interior, Bureau of Ocean Energy Management, Gulf of Mexico OCS Region, New Orleans, LA. OCS Study BOEM 2014-666.

Wilson, D., R. Billings, R. Chang, S. Enoch, B. Do, H. Perez, J. Sellers. 2017. Year 2014 Gulfwide Emissions Inventory Study. U.S. Dept. of the Interior, Bureau of Ocean Energy Management, Gulf of Mexico OCS Region, New Orleans, LA. OCS Study BOEM 2017-044.

Yarwood, G., T. Sakulyanontvittaya, O. Nopmongcol, B. Koo. 2014. Ozone Depletion by Bromine and Iodine over the Gulf of Mexico. Final Report prepared for Jocelyn Mellberg, TCEQ. November.

Zhang, L., S. Gong, J. Padro, L Barrie. 2001. A size-segregated particle dry deposition scheme for an atmospheric aerosol module. Atmos. Environ., 35, 549-560.

Zhang, L., J.R. Brook, R. Vet. 2003. A revised parameterization for gaseous dry deposition in air-quality models. Atmos. Chem. Phys., 3, 2067-2082.

Zhang, K.M., M.E. Knipping, A.S. Wexler, P.V. Bhave, S.G. Tonnesen. 2006. Reply to comment on “Size distribution of sea-salt emissions as a function of relative humidity”, Atmos. Environ., 40, 591-592, doi:10.1016/j.atmosenv.2005.08.044.

5 Emission Exemption Threshold Evaluation

The goal of EET evaluation modeling is to thoroughly test the efficacy of the existing exemption formulas in 30 CFR 550.303 (Section 5.1.2). BOEM recognizes that OCS oil and gas sources and associated activities have the potential to impact air quality on both a local (near field within approximately 50 km of the source) and regional scale (far field greater than 50 km from the source). ERG and Alpine used dispersion modeling (Sections 5.6 and 5.7) and photochemical modeling (Section 5.8) to assess the efficacy of the EET formulas for both primary and secondary formation of pollutants. A common set of synthetic sources was used for both the dispersion and PGM modeling to ascertain the impacts from direct release (primary) and secondary formation of chemically reactive pollutants such as PM and O_3. These sources are described in Section 5.4.2.1.

ERG and Alpine modeled impacts from these synthetic sources and compared them to the results of the existing EET formulas to determine how successfully the EETs screen *de minimis* sources; Section 5.10 discusses EET improvement options.

5.1 Introduction

To better understand the goals of this task, one needs to understand the USEPA and BOEM permitting processes. The following sections outline the current air quality standards and USEPA process followed by a discussion of the BOEM plan submittal process and current EET formulas.

5.1.1 NAAQS

As previously noted, the USEPA established NAAQS for O_3, SO_2, NO_2, CO, Pb, and PM. The PM NAAQS are set with respect to either the concentration of PM_{10} or $PM_{2.5}$ instead of total suspended particulate (TSP). Section 4, Table 4-12 of this report summarizes the current NAAQS levels.

Any proposed new source or existing source making modifications and seeking permits in a maintenance, attainment, or unclassifiable area must show PSD; additional analysis must show that emissions from any new or modified facility do not increase pollutant concentrations from the baseline concentration over the maximum allowable amount. This maximum allowable amount, or PSD increment, varies for each criteria pollutant.

The USEPA allows PSD programs to use screening methods to streamline the permitting process where the proposed construction is not anticipated to have a significant impact on air quality. These screening levels include use of Significant Emission Rates (SERs) and Significant Impact Levels (SILs) to determine the level of air quality analysis needed to demonstrate that source emissions will not cause or contribute to a violation of a NAAQS or PSD increment. SERs act as an initial screening to determine if a source must provide additional analysis of the ambient air quality impacts (i.e., modeling). The USEPA regulations only require sources emitting at a level greater than or equal to the SER to conduct additional analysis. The next step is to compare the estimated impacts from source modeling to the appropriate SIL. Generally, if the impacts of the individual source are greater than the level of an SIL, then a cumulative impact analysis is required (i.e., modeling that considers the combined impact of the proposed source and other sources in the affected area) to demonstrate that the proposed source will not cause or significantly contribute to a violation of the NAAQS or PSD increment. Table 5-1 summarizes the PSD SILs for Class I and II areas.

USEPA permitting guidance (USEPA, 2014b) allows sources to compare the concentration that results from combining the background concentration and the highest impact from the source to the NAAQS. If

this total is less than the NAAQS, then the source is not considered to have a significant impact on air quality.

Table 5-1. Current SILs for Each NAAQS

Pollutant		NAAQS Averaging Time	SIL			
			Class I Area		Class II Area	
			µg/m³	ppb	µg/m³	ppb
CO [a]		1-hour	–	–	2,000	2,000
		8-hour	–	–	500	400
Pb		Rolling 3-month avg	–	–	–	–
NO_2 [a,b]		1-hour	–	–	7.5	4
		Annual	0.1	0.05	1	0.5
O_3 [c]		8-hour	–	–	2.0	1.0
PM [a,c,d]	$PM_{2.5}$	24-hour	–	–	1.2	–
		Annual	–	–	0.2	–
	PM_{10}	24-hour	–	–	5	–
		Annual	–	–	1	–
SO_2 [e]		1-hour	–	–	7.9	3
		3-hour	1	0.4	25	10
		24-hour	0.2	0.1	5	2
		Annual	0.1	0.04	1	0.4

[a] The Class II SILs for CO (1-hr and 8-hr) PM_{10} (annual, 24-hr), NO_2 (annual), and SO_2 (annual, 24-hr and 3-hr) are found in 40 CFR 51.165(b)(2).

[b] The 1-hr NO_2 Class II SIL is based on USEPA's "General Guidance for Implementation of the 1-hour NO_2 NAAQS in PSD Permits, Including an Interim 1-hour NO_2 Significant Impact Level, June 28, 2010" (USEPA, 2010a).

[c] The O_3 and $PM_{2.5}$ SILs are based on USEPA's "Guidance on Significant Impact levels for Ozone and Fine Particulates in the Prevention of Significant Deterioration Permitting Program, April 17, 2018." (USEPA, 2018)

[d] The $PM_{2.5}$ Class I SILs are based on USEPA's "Guidance for $PM_{2.5}$ Permit Modeling, May 20, 2014" (USEPA, 2014b).

[e] The 1-hr SO2 Class II SIL is based on USEPA's "Guidance Concerning the Implementation of the 1-hour SO_2 NAAQS for the Prevention of Significant Deterioration Program, August 23, 2010" (USEPA, 2010b).

5.1.2 BOEM EET Formulas

As previously noted, BOEM must comply with the NAAQS by ensuring that OCS offshore oil and gas exploration, development, and production sources do not significantly impact the air quality of any state. To assess the impact of OCS development, BOEM requires operators/lessees to submit EPs and DOCDs for offshore oil and gas activities. The two documents pertain to the two major phases of offshore development. An EP describes all exploration activities planned for a specific lease or group of leases, and a DOCD describes development and production activities proposed for a lease or group of leases. Both documents include the timing of the proposed activities, information concerning drilling vessels, the distance to shore for each proposed well or production platform or other structure, a description of all equipment, and potential emissions of the proposed activities.

Like the USEPA PSD program, BOEM developed screening methods to determine whether a proposed source will cause or contribute to a violation of the NAAQS. The EETs were established to determine whether a facility described in an EP or DOCD is exempt from further air quality review because the plan's potential emissions would have an insignificant impact on the air quality of any state.

In the current exemption formulas in 30 CFR 550.303, referred to as the EET formulas in this study, the lessees compare the highest annual emissions from the proposed activities for each air pollutant calculated

in their EP or DOCD to the emission exemption amount "E" for each air pollutant calculated using the following formulas:

For CO:

$$E = 3400 \times (D)^{(2/3)}$$

For TSP, SO_2, NO_x, and VOCs:

$$E = 33.3 \times D$$

Where:

E = emission exemption amount expressed in TPY

D = distance of the proposed activity from the closest onshore area of a state expressed in statute miles

If the amount of these projected emissions is less than or equal to the emission exemption amount E for the air pollutant, the facility is considered to not significantly impact the NAAQS of onshore areas and is exempt from further air quality review. The current EET formulas do not currently address Pb or O_3 directly, address TSP rather than PM_{10} and $PM_{2.5}$, and they do not address any short-term NAAQS.

The current EET formulas were developed in the 1980s and were based on Offshore Coastal Dispersion (OCD) modeling results compared to the NAAQS established at that time. Since then, the NAAQS have undergone several revisions, including changes in indicator and averaging times. For example, the EET formula originally used TSP—not PM_{10} or $PM_{2.5}$—as the indicator for the PM standard. This task evaluated the EET formulas to determine if they still apply to the current annual and short-term NAAQS and to extend the thresholds for secondarily formed pollutants (ozone and secondary $PM_{2.5}$).

Modeled impacts along the shoreline and state seaward boundary are compared to the current level of the SILs, or interim SILs, listed in Table 5-1.

5.2 Air Quality Model Selection

Model selection for this task started with a review of the USEPA's recently revised Guideline on Air Quality Models (40 CFR Part 51, Appendix W, March 2017, hereafter referred to as "USEPA Guideline"). The USEPA Guideline recommends and suggests the most appropriate model, or suites of models, for various scenarios. The following sections outline the decision-making process behind the model selection for the near-field and far-field modeling conducted under this task.

5.2.1 Near-Field Modeling

The USEPA-preferred near-field model for modeling sources over land is the American Meteorological Society/United States Environmental Protection Agency Regulatory Model (AERMOD). The AERMOD modeling system consists of three basic components:

- AERMAP: processes terrain data and develops elevations for the receptor grid/sources (USEPA, 2004a).
- AERMET: processes overland meteorological data (USEPA, 2004b)
- AERMOD dispersion model: estimates ambient concentrations (USEPA, 2004c)

These modules also have several additional components to process data or develop necessary parameters. However, the sources modeled in this analysis are oil and gas exploration, development and production platforms to be developed on the OCS, not over land.

The USEPA Guideline and BOEM guidance (30 CFR 550.218 and 30 CFR 550.249) recommend the OCD model (Chang and Hahn, 1997; DiCristofaro and Hanna, 1989) for offshore/overwater sources. The OCD model is specially formulated to incorporate overwater plume transport and dispersion, as well as changes that occur as the plume crosses the shoreline. However, the OCD model is no longer maintained and was last revised in January 2000. Not only does this mean that the model science has not kept up with the latest advances (e.g., plume meander for low wind conditions, calculations for the 98^{th} and 99^{th} percentile concentrations necessary for comparisons with the recent 1-hour NO_2 and SO_2 NAAQS revisions), but the model also has not been updated to run on modern operating systems.

To address the shortcomings in the OCD model, the USEPA adapted AERMOD for the overwater environment by developing the AERMOD Coupled Ocean-Atmosphere Response Experiment (COARE) model preprocessor. AERMOD-COARE has been suggested as an alternative to the OCD model, and USEPA Region 10 office approved it as an alternative to OCD in an ice-free Arctic environment (USEPA, 2011a). The approach received concurrence from the USEPA Model Clearinghouse in May 2011 (USEPA, 2011b). In 2012, the USEPA supported the development of a unified computer code that implements the AERMOD-COARE methodology, called AERCOARE. The AERCOARE preprocessor (Richmond and Morris, 2012) is analogous to AERMET—the overland meteorological preprocessor—for the overwater environment. AERCOARE applies an air-sea flux algorithm to overwater meteorological measurements or predicted hourly meteorological data from MMIF (Brashers and Emery, 2014) to estimate surface energy fluxes. It then assembles these estimates and other measurements for subsequent dispersion model simulations with AERMOD. AERCOARE also provides support for missing data, adds options for treating overwater mixing heights, and can consider many different input data formats.

Figure 5-1 shows the possible near-field modeling system configurations for both onshore (using AERMET) and offshore (using AERCOARE) locations. The solid green path, observational data (OBS) → AERMET → AERMOD, is the USEPA-approved overland modeling platform. The solid blue path, OBS → OCD, is the approved overwater modeling platform under the current USEPA Guideline. The solid red path, OBS → AERCOARE → AERMOD, is the alternate modeling platform approved by USEPA Region 10 and the USEPA Model Clearinghouse for use over water in the Arctic during open-water conditions.

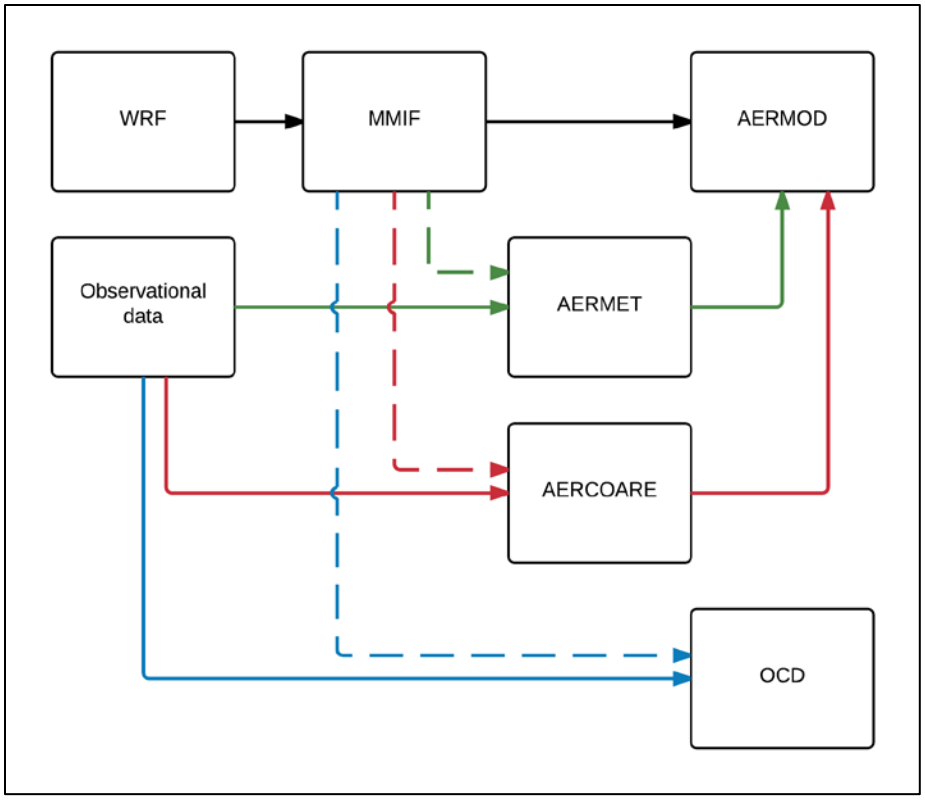

Figure 5-1. Potential Near-Field Dispersion Modeling Platforms

Changes to the USEPA Guideline (80 FR 45340) allow data from a meteorological (prognostic) model, such as WRF, to be used in dispersion modeling when collecting site data is time- or cost-prohibitive and a representative NWS site is not available. For this portion of the study, all modeled sources are over water. This presents an observational challenge, because buoys are the best source of data but do not measure all the parameters needed in dispersion modeling. Establishing meteorological monitoring for this study was cost-prohibitive. Therefore, it is advantageous to use modeled meteorological data for this project. Figure 5-1 includes the additional modeling platform options available using the modeled meteorological data (dashed paths).

The recent changes to the USEPA Guideline specify that the AERMET preprocessor must be used with the AERMOD model when using either observed or prognostic data. To use AERMOD—the most scientifically advanced model—over water with modeled meteorological data, additional model justification must be provided. USEPA Guideline Section 3.2.2 on alternative model equivalency outlines various measures that justify the use of an alternative modeling platform as comparable to the USEPA-recommended modeling platform. As part of this study, Ramboll provided additional justification (outlined below) similar to the USEPA Guideline procedures. The full model justification document is provided in Appendix E.1. This study does not support a permitting action under USEPA jurisdiction, but instead supports BOEM's GOMR EP and DOCD program; however, BOEM still sought the USEPA's comment and agreement on the modeling approach.

Ramboll performed the model justification by comparing various combinations of models against the following five tracer dispersion field studies:

- Cameron, Louisiana: July 1981 and February 1982 (Dabberdt et al., 1982)
- Carpinteria, California: September 1985 (Johnson and Spangler, 1986)

- Øresund (between Denmark and Sweden): May/June 1984 (Gryning, 1985)
- Pismo Beach, California: December 1981 and June 1982 (Schacher et al., 1982)
- Ventura, California: September 1980 and January 1981 (Schacher et al., 1982)

The model justification tested the equivalence of the approved overwater model, OBS → OCD, with the following model combinations:

- WRF → MMIF → AERMOD (solid black path in Figure 5-1)
- WRF → MMIF → AERCOARE → AERMOD (dashed red path in Figure 5-1)
- WRF →MMIF → OCD (dashed blue path in Figure 5-1)
- WRF → MMIF → CALPUFF

The analysis shows that the WRF → MMIF → AERMOD method performs just as well as the regulatory default model OCD and the WRF → MMIF → AERCOARE → AERMOD approach for offshore emission sources less than 50 km from the point of impact. Details of the model justification were presented to BOEM and the USEPA for comment and approval. The model justification technical support document is included in Appendix E.1 of this report. Section 5.3 below discusses the meteorological data used to run the modeling platform, along with the approach for processing the meteorological data, in more detail.

5.2.2 Regional (Far-Field) Modeling

The USEPA Guideline and BOEM guidance also identified three models for far-field analysis:

- CMAQ/CAMx
- Second-order Closure Integrated Puff Model (SCIPUFF)
- California Puff-Advection Model (CALPUFF)

CMAQ (Byun and Ching, 1999) and CAMx (ENVIRON, 2014) are photochemical models that are typically used on a regional scale but can be used up to global scale. Both models are publicly available and have adopted the "one-atmosphere" concept under which ozone, $PM_{2.5}$, air toxics, visibility and other air quality issues are evaluated within a single modeling platform. Recognizing the importance of capturing the chemical transformations in the one-atmosphere approach, Alpine conducted photochemical modeling for secondarily formed pollutants (ozone and secondary $PM_{2.5}$). ERG used the results from the photochemical modeling to evaluate the existing EET formulas, as discussed in Section 5.9.

SCIPUFF (Sykes et al., 1998) models primary pollutants in both short-range and long-range settings. The model incorporates linear chemical transformations and deposition. The USEPA Guideline identifies SCIPUFF as an "alternative model," and a memorandum of understanding between the U.S. Department of Agriculture, USDOI, and USEPA also notes this status and its potential use on a case-by-case basis (USDA, 2011).

The CALPUFF modeling system (Scire et al., 2000) was once the USEPA-preferred model for long-range transport (50 km to several hundred km). Recent changes to the USEPA Guideline removed CALPUFF as the preferred model. The removal does not mean that CALPUFF cannot be used, but that it is not preferred over other potential models. This study used the CALPUFF model because no other widely used air quality model is technically superior for long-range transport.

The CALPUFF modeling system is similar to AERMOD in that it uses a system of preprocessors in addition to the main model. The three main components of the CALPUFF modeling system for this study are MMIF (processes meteorological data), CALPUFF (transport and dispersion model), and CALPOST (processes output files).

This study used CALPUFF for the regional/far-field dispersion modeling for directly emitted pollutants and the photochemical models for secondarily formed pollutants. Section 5.3 discusses the meteorological data used to run CALPUFF, along with the approach for processing the meteorological data, in more detail.

Based on the availability of advanced source apportionment treatments, the CAMx model was used to assess ozone and secondary $PM_{2.5}$ exemption threshold formulas. CMAQ was also considered for the secondary modeling as part of the cumulative air quality impacts analysis modeling discussed in Section 4 of this report. An initial comparison the performance of CAMx and CMAQ was conducted, and it was concluded that CAMx performed better in the GOMR and base year modeling proceeded with CAMx as the PGM of choice.

The CAMx modeling platform (e.g., grid definition, science options) that Alpine used to assess ozone and secondary $PM_{2.5}$ EET formulas is the same as the platform Ramboll used in PGM modeling to examine cumulative air quality impacts. As part of the cumulative impact and visibility modeling, the modeling platform underwent extensive QA and multi-species MPE. The use of a consistent modeling platform provides consistency between the cumulative impacts and exemption-level threshold modeling. Section 5.8 presents details of the CAMx application approach.

5.3 Meteorological Data and Preprocessing

Air quality models require hourly surface meteorological data as inputs. The USEPA Guideline specifies that a minimum of one year of site-specific data, or five years of representative NWS data should be used. The guideline also states that additional years (up to five) should be used when available to account for year-to-year variations in meteorological conditions when modeling with site-specific data.

Recent changes to the USEPA Guideline allow the use of modeled, or prognostic, meteorological data where there is no representative NWS station and it is prohibitive or not feasible to collect adequately representative site-specific data. The only source of offshore meteorological data are buoys, which do not collect all the wind data needed for dispersion modeling. The harsh conditions at sea also make it difficult to meet the data completeness criteria for meteorological data. Given the limited availability of data and difficulty in collecting data over water, the GOMR meets the USEPA Guideline criteria for using modeled meteorological data with dispersion models.

Section 2 of this report describes the development of the meteorological dataset used in this task. The results were five years of 4-km grid resolution WRF simulations, representing 2010–2014; data for the dispersion modeling inputs were extracted from these outputs. These hindcast WRF runs provided a complete dataset for each year, including upper-air values. The preprocessing steps necessary for the dispersion and photochemical modeling are discussed in Sections 5.3.1 and 5.3.2, respectively.

5.3.1 Dispersion Modeling Preprocessing

To process the WRF modeling outputs into a format for AERMOD and CALPUFF modeling systems, Alpine used the MMIF (Brashers and Emery, 2014) program. The USEPA developed MMIF to convert WRF meteorological model output fields to the parameters and formats required for direct input into dispersion models, including SCICHEM, AERMOD, and CALPUFF. The USEPA Guideline changes allow for the use of MMIF-extracted meteorological data in regulatory modeling.

For this study, MMIF version 3.2 was used to extract and convert the needed meteorological data for dispersion modeling from the WRF modeling output. For CALPUFF modeling runs, MMIF was used in place of the CALPUFF meteorological preprocessor (CALMET). All available observational data were

ingested into WRF, so using the CALPUFF WRF preprocessor (CALWRF) and CALMET would not have added any benefit or accuracy to the final fields.

For AERMOD, Alpine used MMIF to extract the data from the WRF modeling outputs for a one-half-degree-spaced grid out to 100 km from the shoreline. The closest extraction point to the modeling location was used in AERMOD modeling. The extracted source locations are shown in Figure 5-2. Along the vertical (ordinate), the extractions include all WRF levels up to 5 km above ground level.

BOEM now has the full WRF files if operators should wish to extract site-specific meteorological data for their modeling efforts to support future EPs and DOCDs. BOEM also has AERMOD extractions that can be used to support future near-field modeling efforts by operators in the GOMR. To support future far-field modeling efforts by the operators, Alpine generated three overlapping "tiles" of WRF study area input data that preserve the 4-km grid spacing. The tiles were selected to separately cover the Western, Central, and Eastern GOM Planning Areas with a 100-km overlap between each tile. The tile definitions are presented in Section 5.7.1.1. ERG delivered these default meteorology files for future projects to BOEM along with all other modeling files described in Sections 5.6 and 5.7.

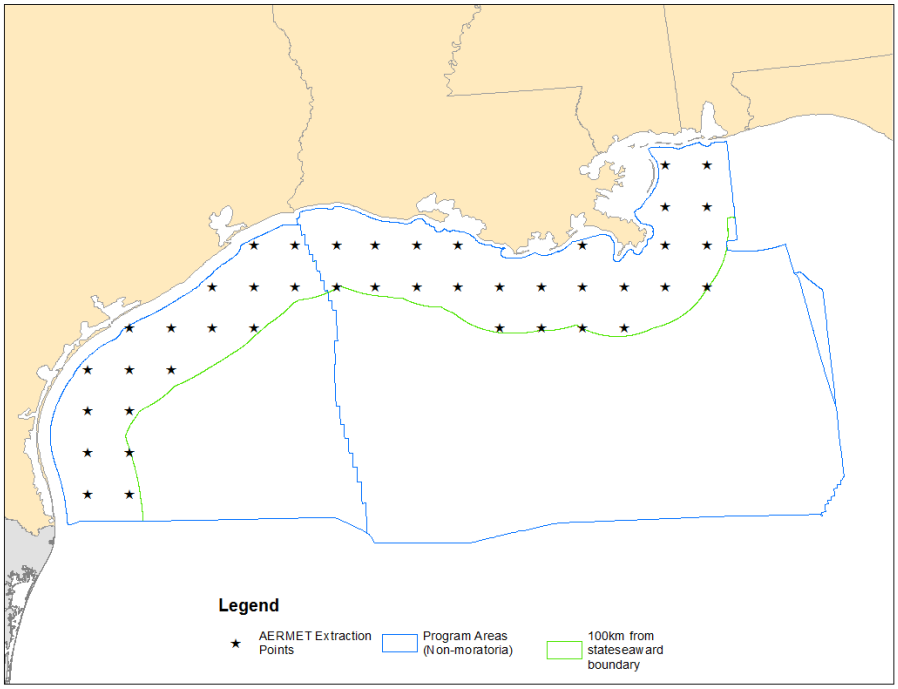

Figure 5-2. Location of Meteorological Input Data File Extractions for AERMOD

5.3.2 PGM Preprocessing

WRFCAMx version 4.3 was used to translate WRF output meteorological fields to daily CAMx meteorological inputs. To model a single day, 25 hours of meteorology must be present (midnight–midnight, inclusive), as these fields represent hourly instantaneous conditions. CAMx internally time-interpolates these fields to each model time step. Precipitation fields are not time-interpolated, but rather time-accumulated, so cloud/precipitation files contain one less hour than other meteorological files (e.g., 24 hours of clouds/precipitation versus 25 hours for other meteorological fields). Several methodologies are available in WRFCAMx to derive Kv fields from WRF output. For this modeling, a method consistent with the YSU bulk boundary layer scheme (Hong and Noh, 2006; the default option in WRF) was used to generate the Kv profile. The lower bound Kv value is set based on the land use type for each grid cell.

Another issue is deep cumulus convection, which is difficult to simulate in a grid model because of the small horizontal spatial scale of the cumulus tower. Inadequate characterization of this convective mixing can cause ozone and precursor species to be overestimated in the boundary layer. To address this issue, ENVIRON (2012) developed a code patch that increases transport of air from the PBL into the free troposphere and up to the cloud top within cloudy grid cells. This patch was shown to improve surface layer ozone in a recent modeling study in Texas (Kemball-Cook et al., 2015) and was thus used in this modeling study.

Another WRFCAMx option allows the processing of sub-grid cloud data from WRF fields. Selecting the "DIAG" sub-grid cloud method diagnoses sub-grid cloud fields from WRF gridded thermodynamic fields. The DIAG option is generally selected for the 36- and 12-km WRF output extraction, but not for grid spacing less than about 10 km. However, a recent modeling study showed that without a sub-grid cloud, the 4-km grid produced too much ozone over the Houston area due to enhanced photochemistry (Nopmongcol et al., 2014). Therefore, this study used the DIAG option for the 4-km grid as well as the 36 and 12-km grids.

5.4 Modeling Emissions Inventory

PGM modeling requires emissions for all sources in the region, in addition to the sources whose impacts are being evaluated. Section 5.4.1 describes the emissions inventory used in photochemical modeling. Section 5.4.2 presents sources to be assessed for the exemption thresholds.

5.4.1 PGM EET Baseline Emissions Inventory

The emissions inventory for the PGM EET modeling was the same as the base year inventory used in the cumulative impact analysis modeling. Section 3 of this study details the emissions inventory development. The additional sources needed to round out the inventory for PGM modeling are discussed below.

5.4.2 EET Inventory

The emissions inventory used to evaluate the existing EETs differs from the emissions inventory used in the cumulative air quality impacts analysis task. ERG derived a series of "synthetic" sources based on existing and foreseeable platforms in the GOMR and modeled them individually to assess their direct impacts. For the photochemical modeling, ERG added a subset of the "synthetic" sources to the base year emissions developed for the study's cumulative air quality impacts analysis task. This ensured consistency in the reactivity of the atmosphere between the cumulative impact and EET modeling. That is, results from the two modeling exercises were comparable, and the differences in impacts were solely due to the synthetic sources.

As noted in Section 5.1, one of the study objectives was to evaluate the existing formulas used to exempt oil and gas sources—including exploratory drilling and production platforms—from modeling requirements. As currently written, these formulas provide an emissions threshold based on the drilling operation or platform distance to shore that these platforms must fall below to be exempt from further modeling. The reason for using synthetic, representative sources is twofold. First, using synthetic sources avoids the perception that BOEM is questioning previous exemption analyses for existing sources. This study does not intend to review previous plans and question the validity of the analyses for current exploration or production operations. Second, the developed synthetic sources allow the flexibility to pair various emission levels with various distances to shore to ensure the formula is tested with the full range of possible values, regardless of whether the combinations currently exist in the GOMR. By capturing the full range of possibilities, including combinations that do and do not currently exist, the existing

exemption threshold formulas can be thoroughly tested for any limitations, including combinations of emissions and distance to shore for platform sources that are not currently leased.

The following sections outline the emission levels, source characteristics, and locations that define the synthetic sources used for the study.

5.4.2.1 Synthetic Source Emissions

Testing the EETs using a wide range of emission values ensures that this study's conclusions will still apply in the future if regulation and controls reduce emissions from offshore sources, or when technology shifts to larger operations or configurations that could have emissions higher than currently seen. If new EET formulas need to be developed, the range of synthetic source emissions defines the valid emissions used in the formulas.

ERG developed emission rates for the following emission scenarios:

1. Drilling EP with support vessels and well testing
2. Production and drilling plan DOCD with support vessels
3. Production and drilling plan DOCD with support vessels, pipeline emissions, and facility installation and well testing
4. Production-only DOCD with support vessels
5. FPSO vessel

All five scenarios were developed for small-, medium-, and large-scale operations using the calculation methods from the latest EP and DOCD spreadsheets.

ERG randomly selected and reviewed EPs and DOCDs, which were submitted to BOEM for approval and publicly available on its website, for typical platform configurations and initial emission levels across the GOMR. The review was limited to the last five years to ensure that the platform configurations represent modern operational setups and emission levels. A spreadsheet was developed that tracked the emission levels and activities from the randomly selected EPs and DOCDs. Each operation was classified into one of the five scenarios or "other" based on the activities reported. The operation scale (i.e., small medium, or large) was then based on the estimated NO_x emission levels seen across all the scenarios. ERG defined small-scale operations as emitting less than 300 TPY of NO_x, medium-scale operations as emitting 300 to 3,000 TPY, and large-scale as emitting greater than 3,000 TPY. The emission estimates focused on NO_x because it is the pollutant with the largest emissions range, based on BOEM's Gulfwide emissions inventories, that would need to be covered by the EET formulas.

ERG then randomly selected operations representative of each size class and emission scenario to represent each scenario-size combination. ERG acknowledges the emission estimates from the EP and DOCD spreadsheets can be an overestimation of the emissions at platforms. However, actual operations throughout the GOMR likely fall within range of emissions provided by these equipment scenarios. These specific scenarios were further adjusted, as outlined below, to provide additional variation and represent a "typical" operation in the GOMR.

The equipment configuration (e.g., equipment types and horsepower ratings) from these operations was then entered into the latest version of the EP and DOCD emission reporting spreadsheets for refined emission estimates. The selected configurations were adjusted to account for a full suite of emission sources. For example, all production operations (scenarios 2, 3, and 4) were adjusted to include at least one vent or flare (whose volume includes upsets). This ensured all equipment types were portrayed in an emission scenario. Table 5-2 summarizes the scenarios and indicates any equipment required under each scenario. Appendix E.2 includes a summary of the equipment used in each scenario.

Table 5-2. Summary of Mandatory Equipment Under Each Scenario

Scenario	Description	Includes (At Least One)
1	Drilling (DRI) EP with support vessels, well testing	Drillship/prime mover, crew, supply, and tug support vessel
2	Production (PROD) & DRI DOCD with support vessels	Prime mover, support vessel, diesel engine, flare or vent, and fugitives (default of 11,420 components with light oil stream type)
3	PROD & DRI DOCD with support vessels, pipeline emissions, facility installation, and well testing	Prime mover, support vessel, diesel engine, flare or vent, and fugitives (default of 11,420 components with light oil stream type); drillship/prime mover, crew, supply and tug support vessel; well testing; pipeline installation vessel and facility installation vessel
4	PROD-only DOCD with support vessels	Support vessel, diesel engine, flare or vent, and fugitives (default of 11,420 components with light oil stream type)
5	FPSO	Support vessel, diesel engine, flare or vent, and fugitives (default of 11,420 components with light oil stream type), as well as one floating production storage and offloading (FSPO) vessel/prime mover

After adding all the representative equipment for each scenario, ERG made additional modifications to operational hours and activity levels to ensure an adequate variation in the annual and hourly emission levels to be modeled. The goal was to represent both high and low production scenarios during testing. Hourly emission rates were consistent with the maximum hourly emission rate calculations (i.e., the total hourly emission rate if all equipment was operated at the same time) in the EPs and DOCDs. The annual emission values were then rounded to the nearest hundred to reinforce that the modeled emissions are synthetic sources (e.g., 15,897 rounded to 15,900). Table 5-3 presents the annual emission levels, and Table 5-4 presents the hourly emission levels to be used in short-term NAAQS (i.e., standards with an averaging time of 24 hours or less) modeling. These rates are then converted to grams per second, as that is the emission rate accepted by the dispersion modeling. This emissions rate is then used for every hour of modeling to identify the highest possible impact from the source.

The emission levels presented in Table 5-3 were compared to the 2011 Gulfwide inventory (Wilson et al., 2014) and available USEPA Eastern GOM Planning Area permits to ensure total platform emission values were consistent with actual emissions currently seen in the GOMR. The Eastern GOM Planning Area comparisons included the USEPA-permitted emission levels both with and without permit restrictions to ensure the synthetic sources are representative of both USEPA mitigated and unmitigated emission levels. The unmitigated emission estimate is based on all equipment listed in the permit operating 24 hours a day for the project duration. When multiple emission scenarios were included in a USEPA Eastern GOM Planning Area permit, each emission level was calculated and included in the comparison.

Table 5-5 compares the 2011 Gulfwide inventory and Eastern GOM Planning Area permits to the synthetic source emission levels. The maximum emission levels for the synthetic emission scenarios are well above the levels seen in the 2011 Gulfwide inventory and GOM Eastern Planning Area permits. This suggests the levels more than capture typical operation emission levels.

Table 5-3. Modeled Emissions Levels for Synthetic Sources

Scenario	Description	Size	Emissions (TPY)							
			PM_{10}	$PM_{2.5}$	SO_2	NO_x	NH_3	VOC	CO	Pb
1	DRI EP with support vessels, well testing	L	200	200	1,800	8,100	1	300	2,200	0.013
		M	50	50	500	2,100	0	90	600	0.005
		S	5	5	1	200	0	4	40	0.001
2	PROD & DRI DOCD with support vessels	L	500	500	3,800	25,300	2	1,900	6,300	0.09
		M	20	20	70	1,900	1	500	400	0.001
		S	7	7	7	500	0	400	80	0.002
3	PROD & DRI DOCD with support vessels, pipeline emissions, facility installation, and well testing	L	500	500	500	16,700	0	800	4,000	0.013
		M	20	20	80	800	0	200	300	0.006
		S	7	7	60	300	0	80	80	0.004
4	PROD-only DOCD with support vessels	L	30	30	6	2,800	0	500	1,000	0.001
		M	8	8	20	1,200	0	500	700	0.0003
		S	5	5	4	100	0	500	30	0
5	FPSO	L	100	100	900	4,600	1	600	1,200	0.008
		M	70	70	500	3,000	1	600	800	0.002
		S	30	30	300	1,300	0	200	300	0.002

Table 5-4. Modeled Emission Levels for Synthetic Sources in Pounds per Hour

Scenario	Description	Size	Maximum Hourly Emissions (pounds/hour)							
			PM_{10}	$PM_{2.5}$	SO_2	NO_x	NH_3	VOC	CO	Pb
1	DRI EP with support vessels, well testing	L	117	114	1,041	4,622	0.56	194	1,250	0.003
		M	43	42	381	1,691	0.2	71	457	0.001
		S	20	20	71	720	0.04	24	178	0.0002
2	PROD & DRI DOCD with support vessels	L	364	359	1,412	37,873	0.75	648	5,549	0.021
		M	152	151	58	25,058	0.35	166	3,038	0.0002
		S	88	87	124	12,866	0.06	150	1,606	0.0004
3	PROD & DRI DOCD with support vessels, pipeline emissions, facility installation, and well testing	L	203	199	1,008	7,590	0.54	390	1,920	0.003
		M	61	59	453	2,369	0.28	191	676	0.0013
		S	32	32	284	1,293	0.15	239	348	0.001
4	PROD-only DOCD with support vessels	L	25	25	90	1,342	0.09	2673	416	0.0003
		M	6	6	25	415	0.06	110	193	0.0001
		S	1	1	1	29	0	113	7	0
5	FPSO	L	68	66	600	2,777	0.49	210	747	0.002
		M	33	33	165	2,197	0.16	150	396	0.001
		S	21	21	182	871	0.26	132	232	0.001

Table 5-5. Comparison of Emission Ranges from the GOM Inventories

Pollutant	Emission Range (TPY)		
	Synthetic Sources	2011 Gulfwide Inventory	Eastern GOMR Permits[a]
CO	30–6,300	<0.01–1,729	252–4,302
NO_x	100–25,300	<0.01–3,404	860–14,638
PM_{10}	5–500	<0.01–30	27–172
$PM_{2.5}$	5–500	<0.01–30	10–168
SO_2	1–3,800	<0.01–349	2–28
VOC	4–2,500	<0.01–2,473	8–137

[a] Emissions based on OCS-EPA-R4006 (USEPA, 2011c), OCS-EPA-R4007 (USEPA, 2011d), OCS-EPA-R4008-M1 (USEPA, 2013), OCS-EPA-R4009 (USEPA, 2012).

5.4.2.2 Synthetic Source Stack Parameters

Dispersion modeling also requires that the emission source have defined stack characteristics (release height, exit temperature, exit velocity, and stack diameter). Temperature, exit velocity, and diameter are required for plume rise calculations within the model (USEPA, 2004d). The rise of the plume impacts the dispersion and ultimate concentration of the plume at the receptor sites, as the initial plume rise affects whether the plume splits across the boundary layer. To determine the sensitivity of synthetic source dispersion to the stack parameters, ERG ran the SCREEN3 (USEPA, 1995) model to determine the plume rise for various stack configurations. SCREEN3 was used instead of AERSCREEN because of its fast setup and run time, and because it natively prints out the initial plume rise using the same formulas as AERMOD. ERG reviewed BOEM's 2011 Gulfwide inventory and identified 38 different combinations of typical stack parameters for testing, which include configurations with maximum stack parameter values. Of these combinations, only six showed an initial plume rise above 200 m. The WRF modeling files for the study were then reviewed to determine the lowest PBL heights for the study period. Although the PBL height can drop as low as 200 m after frontal passage for coastal locations during the winter, the PBL typically maintains a height of at least 500 m over the ocean. None of the stack parameter combinations tested exceed a 500-meter plume rise. Therefore, ERG used the average stack parameters for the synthetic sources because no stack combination known to occur is expected to cause plumes to rise above the PBL over the ocean.

ERG determined equipment-specific stack parameters for the theoretical sources using average stack parameters from the 2011 Gulfwide inventory. Separate averages were calculated for equipment on shallow-water (defined here as water depth less than 200 m) and deepwater (defined here as water depth greater than or equal to 200 m) platforms to account for the different equipment configurations for these depths. Table 5-6 lists the equipment-specific stack parameters used in the modeling. Not all equipment types are present under each scenario.

The USEPA's *Screening Procedures for Estimating the Air Quality Impact of Stationary Sources, Revised* (EPA-454/R-92-019) allows sources that emit the same pollutant from several stacks with similar parameters that are within about 100 m to be treated as if all of the emissions were coming from a single representative stack. Thus, based on the results of the stack parameter analysis, ERG combined equipment with similar stack parameters on the platform to simplify the modeling setup.

To be consistent with the current formulation and application of the emission exemption formulas, ERG placed vessel emissions adjacent to the platform for this modeling and evaluation. The vessels characterized as volumes were placed adjacent to the center of the platform to mimic the vessels anchored or idling next to the platform to provide support. To define the volume dimensions, ERG obtained dimensions of vessels known to operate in the GOM from the PortVision AIS database to develop

average dimensions for each type of vessel. The dimensions used for the volume sources are presented in Table 5-7.

Table 5-6. Average Platform Equipment Stack Parameters by Water Depth

Equipment Type	Water Depth	Stack Parameter			
		Height (ft)	Diameter (ft)	Temperature (F)	Velocity (ft/sec)
Boiler/heater/burner (BOI)	Deep	95.85	1.90	471.03	51.53
	Shallow	82.93	1.19	406.93	31.48
Diesel or gasoline engine (DIE)	Deep	101.08	0.86	824.48	153.93
	Shallow	73.81	0.61	836.01	118.15
Drilling rig (DRI)	Deep	10.00	0.50	70.00	20.00
	Shallow				
Combustion flare (FLA)	Deep	220.40	1.17	1,744.18	34.00
	Shallow	192.76	1.02	1,743.58	57.97
Fugitives (FUG)	Deep	87.47	0.003	72.00	0.0003
	Shallow	62.88			
Glycol dehydrator unit (GLY)	Deep	61.60	0.37	188.10	7.27
	Shallow	77.35	0.51	202.19	8.94
Natural gas engine (NGE)	Deep	94.31	1.44	1,037.83	140.02
	Shallow	71.49	0.84	1,017.44	99.26
Natural gas, diesel, and dual-fuel turbine (NGT)	Deep	119.30	3.32	880.01	271.94
	Shallow	74.71	1.98	945.21	183.28
Storage tank (STO)	Deep	65.60	0.45	76.40	40.55
	Shallow	67.30	0.49	81.86	11.21
Cold vent (VEN)	Deep	154.58	0.80	77.46	21.25
	Shallow	84.88	0.71	73.06	8.68
Amine gas sweeting unit (AMI)	Deep	10.00	0.50	– [a]	20
	Shallow	10.00	0.50	– [a]	20
Loading operations (LOA)	Deep	61.61	0	– [a]	0.0003
	Shallow	64.44	0	– [a]	0.0003
Mud degassing (MUD)	Deep	10.00	0.50	– [a]	20
	Shallow	10.00	0.50	– [a]	20
Pneumatic pumps (PNE)	Deep	66.29	0.15	– [a]	25.8
	Shallow	58.88	0.09	– [a]	59.6
Pressure level controllers (PRE)	Deep	64.44	0	– [a]	0.0003
	Shallow	61.61	0	– [a]	0.0003

[a] Modeled at ambient temperature based on meteorological inputs

Table 5-7. Vessel Parameters for Characterization as Volumes

Vessel Type	Ship Height (m)	Ship Width (m)	Ship Length (m)	Release Height (ft)	Sigma Y (ft)	Sigma Z (ft)
Crew	6.53	21.61	110.49	3.27	25.70	1.52
Drillship	11.75	38.52	229.71	5.87	53.42	2.73
FPSO	11.26	35.50	201.64	5.63	46.89	2.62
Pipelaying	8.47	31.91	175.87	4.23	40.90	1.97
Shuttle	6.53	21.61	110.49	3.27	25.70	1.52
Supply	4.19	13.72	62.60	2.10	14.56	0.98
Support	6.53	21.61	110.49	3.27	25.70	1.52
Tug	4.63	10.69	35.18	2.31	8.18	1.08
Workboat	6.53	21.61	110.49	3.27	25.70	1.52

Initially, support vessels were going to be modeled as area sources to replicate the emissions release over the area the vessel was most likely to operate in; however, preliminary modeling showed characterizing vessels as area sources produced startlingly high impacts. After further review, including the additional sensitivity modeling and comparison presented in Appendix E.3, "Vessel Characterization Testing Summary," ERG shifted to characterizing vessels as volumes with plume rise. The sensitivity modeling demonstrated that characterizing vessels as volumes produced higher impacts than characterizing the sources as points, but lower impacts than characterizing vessels as areas. As such, characterizing a vessel as volume sources provided a conservatively high estimate without being as extreme as using an area source. In addition, the model justification report in Appendix E.1 notes that the OCD's treatment of area sources is more akin to volume sources in AERMOD and CALPUFF.

5.4.2.3 Synthetic Source Locations

ERG paired the emissions with distances to shore that are representative of the 2011 Gulfwide inventory platform locations and active lease blocks. ERG then placed sources along these distances from shore throughout the GOMR. Performing the modeling for the same synthetic sources at different locations in the GOMR (i.e., in both the Western and Central/Eastern GOM Planning Areas) helped show if meteorology in different GOMR areas creates different impacts.

ERG generated the distances to shore for platforms reported in the 2011 Gulfwide inventory and all the active lease blocks. The active lease blocks were determined using the "Active Lease Polygons" shapefile on BOEM's "Geographic Mapping Data in Digital Format" website (USDOI, BOEM, 2015), with distances to shore calculated using ArcGIS. The distances from the 2011 Gulfwide inventory approximate the distances for all existing platforms. They represent the distance to shore for the lease block's centroid and include active lease blocks in the Eastern GOM Planning Area. By using the two datasets, ERG ensured that the distances to shore reflect both the current platform population and other areas being explored for production. Table 5-8 summarizes the preliminary distance to shore information of the platforms reported in the 2011 Gulfwide inventory.

Table 5-8. Summary Statistics for Distance to Shore

Emission Value	Distance to Shore (statute mile)	
	2011 Study	Active Lease Blocks
Minimum Value	2	2
25th Percentile	10	54
Average	32	103
Median (50th Percentile)	22	103
75th Percentile	43	151
Maximum	190	243

The overall lease block minimum distance to shore of 2 mi occasionally falls outside the BOEM planning area boundary. ERG adjusted the distances in Table 5-8 to distance from the state seaward boundary instead of the shoreline. This ensures all locations selected were placed just outside state waters. The adjustment reduced the distances in Table 5-8 by 9 mi (the largest width of state waters). Figure 5-3 shows the adjusted distance contours, which served as the initial distances for synthetic sources.

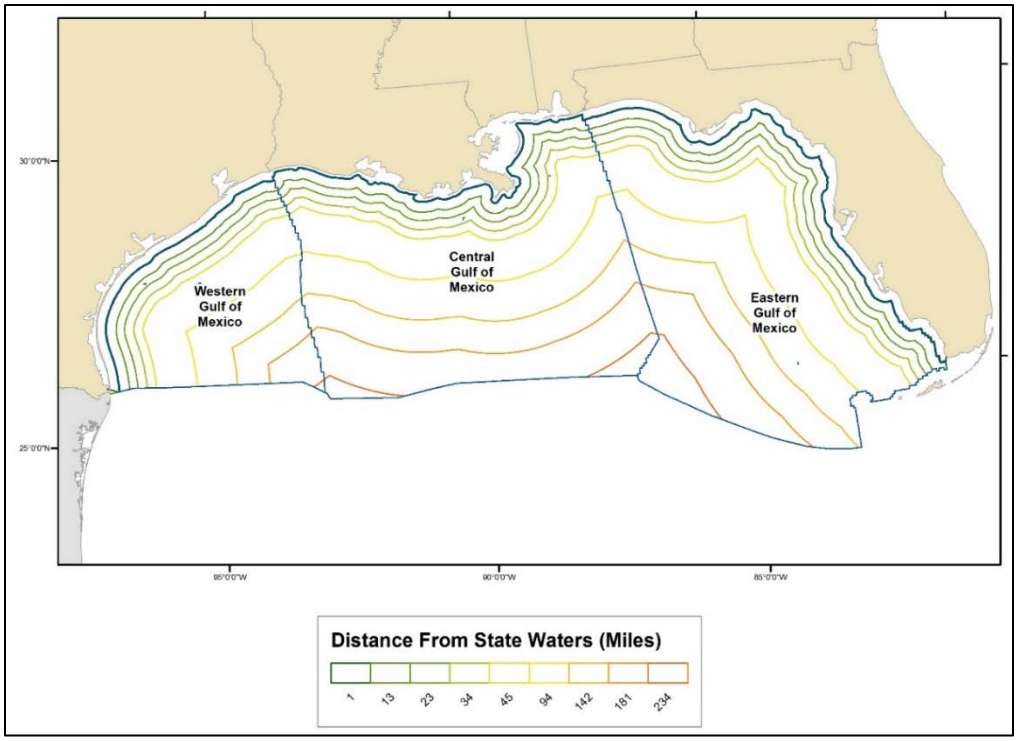

Figure 5-3. Summary of Distances from the State Seaward Boundary

ERG then selected grid cells from the PGM domain that fell along each contour. The final location on all distance contours (denoted by a D and a three-digit distance from the seaward boundary) are the centroids of 4-km PGM modeling grid cells that touch the distance contours. This provides further variability in distance to shore, as noted by the ranges in Table 5-9. The starting point along each contour was shifted for each contour to produce staggered locations throughout the BOEM planning areas. The synthetic sources have an approximate spacing of 40 km. Figure 5-4 shows the synthetic source locations in the study area. The locations include those near the Class I, sensitive Class II, and nonattainment areas in the region to focus the EET formula evaluation on the most sensitive areas. The synthetic source was placed at the center of the cell, and the shortest distance to shore was calculated for EET formula evaluation.

ERG modeled the synthetic sources in CAMx using the source apportionment technique to track the ozone and secondary $PM_{2.5}$ contributions of individual species. To minimize the interaction of the synthetic sources, the PGM modeling was divided into a number of simulations, with nearby synthetic sources split into different CAMx simulations.

Table 5-9. Summary of Modeled Location Distances

Distance Contour	Distance to State Seaward Boundary (statute miles)		Distance to Shoreline (statute miles)	
	Average	Range	Average	Range
D001	2	1–3	11	4–28
D013	13	12–14	21	17–38
D023	23	22–25	31	25–35
D034	34	33–35	41	36–48
D045	45	43–47	52	48–57
D094	94	93–95	101	96–106
D142	142	140–144	148	144–154
D181	180	179–182	186	183–193
D243	233	233–234	238	236–242

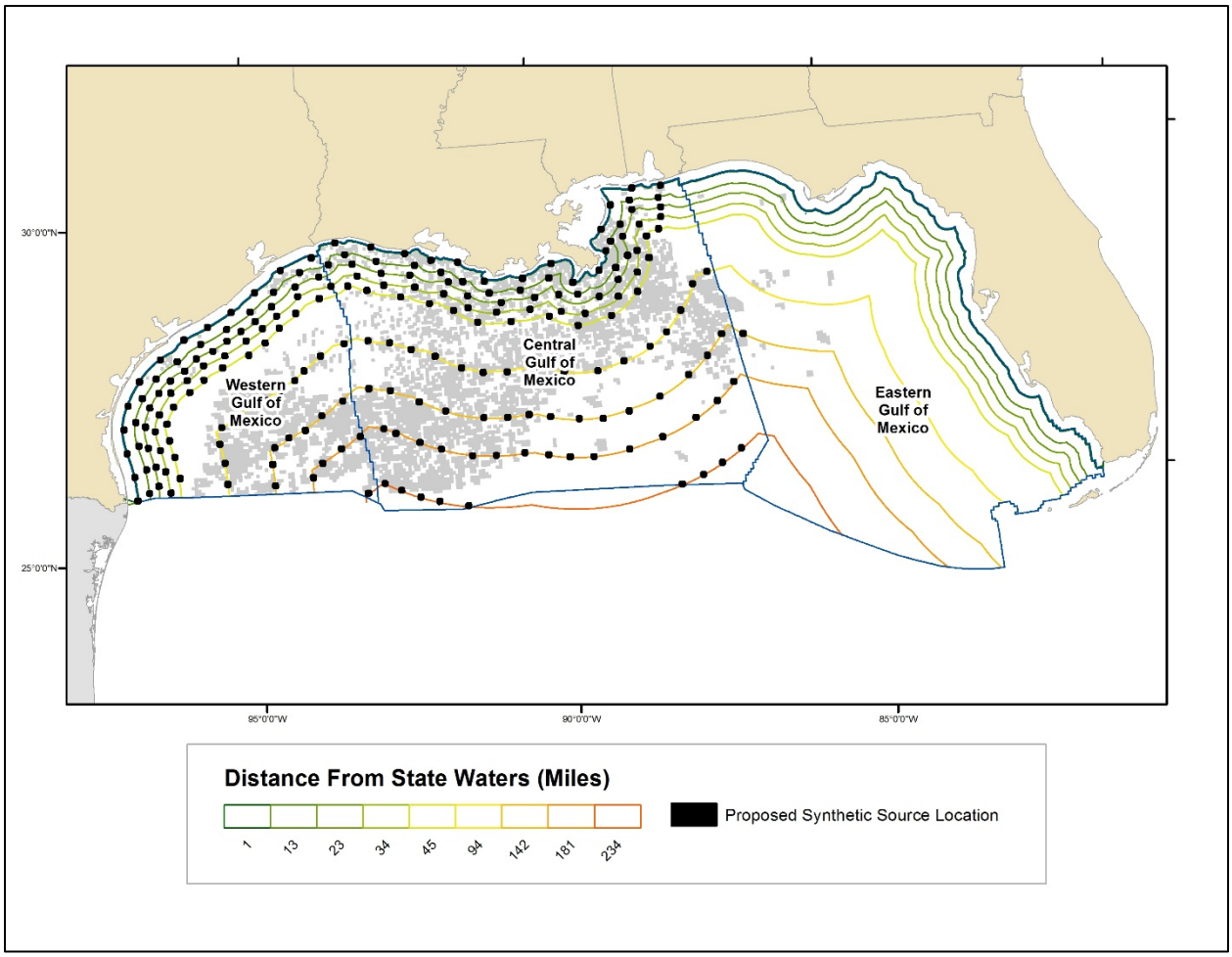

Figure 5-4. Synthetic Source Placement

5.5 Modeling Receptors

As part of this study, ERG conducted a modeling sensitivity analysis to determine the optimal receptor spacing for the EET modeling and as a common set of receptors for modeling submitted to BOEM by operators. This would ensure consistency across modeling submitted in support of EPs and DOCDs. Receptor spacing has the potential to affect modeling results, as a receptor must be positioned within the center of the plume to capture peak concentrations. Finer receptor spacing (smaller distance between receptors) will typically have a receptor hit the center of the plume and will report a higher impact. Coarser receptor spacing will not have a point within the peak contour of the plume and could miss peak impact concentrations. The goal of the receptor sensitivity analysis was to see if there is a receptor spacing that maximizes the impact captured and minimizes the number of receptors used in modeling. Conclusions of the analysis were that distance from shore and type of source modeled (i.e., point versus volume) affect the ability of the coarser resolutions to capture peak plume concentration. Appendix E.4 summarizes the results of the receptor sensitivity analysis.

ERG placed receptors both along the shoreline and along the state seaward boundary at 500-m intervals. For nearshore sources, receptors were placed at narrower intervals (i.e., 100 m) where the plume was anticipated to have the highest impact, based on predominant wind directions. Modeling results were reviewed to ensure the peak plume concentration is being captured by the receptor grids. Where

necessary, adjustments were made to the receptor placement and spacing when the initial receptor placement was lacking.

The shoreline receptors follow a generalized coastline (1:20,000,000 resolution) (U.S. Census Bureau, 2014a), rather a strict shoreline definition that would follow every coastal feature (1:500,000 resolution) (U.S. Census Bureau, 2014b). This simplifies the receptor placement by not strictly following large coastal features such as bays, lagoons, and mouths of rivers. Figure 5-5 provides an example of this generalization along the Louisiana shoreline. The receptors, shown with 100-m spacing, cut across the mouth of a bay at the center of the figure and take a straight-line path instead of strictly following the coast at the top of the image.

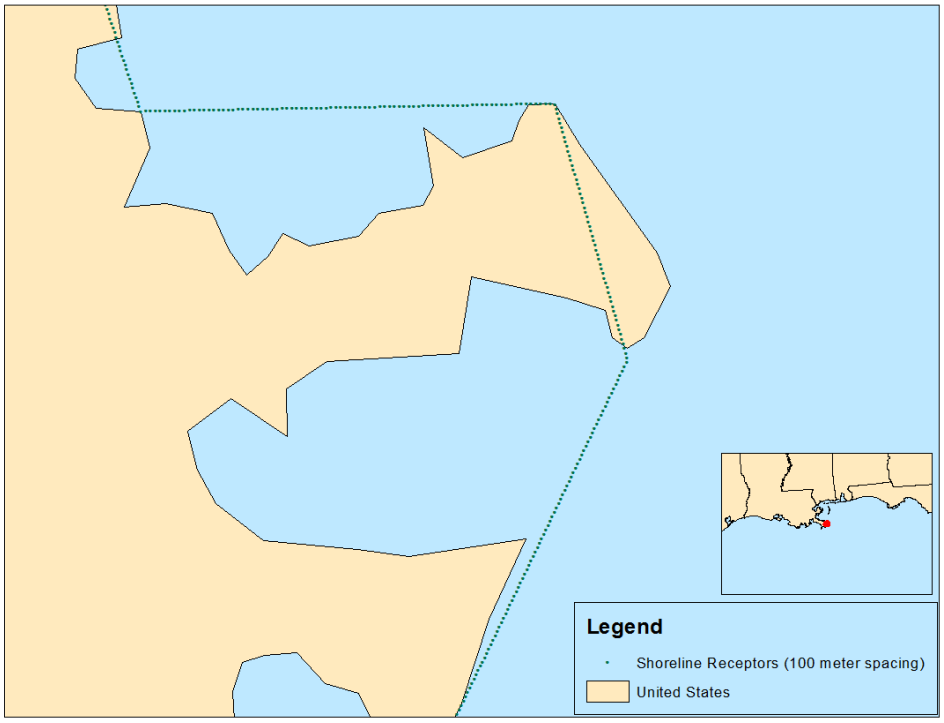

Figure 5-5. Example of Generalized Shoreline Receptors

As this placement method also excludes barrier islands, ERG placed a separate set of receptors on Breton Island, a Class I area. The Class I receptors were placed consistent with receptor locations established by the Federal Land Managers for onshore PSD permits.

For the CAMx modeling for secondary impacts, impacts were evaluated for all grid cells along the shoreline.

5.6 AERMOD Modeling Configuration

AERMOD has several options that can be used to optimize the modeling run for the source and its surrounding area. The study utilized AERMOD version 16216r, as it was the latest version of AERMOD at the time of model executions. The model was run with the regulatory default options as specified by USEPA Guideline.

5.6.1 Background Concentrations

The USEPA Guideline recommends that the ambient background concentration be added to the modeling analysis to assess the impact of sources on ambient air quality. The background concentration represents emissions from natural and anthropogenic sources that are not included in the modeling analysis. Accounting for background concentrations can be done by monitoring data in isolated areas, or explicitly modeling nearby sources in multi-source areas.

However, ERG only modeled the contribution of the synthetic emission sources to each receptor. Similar to multi-tier permit modeling methods for onshore sources, this contribution was then compared to the SIL to determine if there is a significant impact that warrants a more robust modeling analysis of the source. This approach is in line with the intent of the EET formulas to screen for significant impacts. This approach also removes the actual level of the NAAQS and background levels from the equation when developing new EET formulas.

The impact anticipated from a source depends only on its emission level, distance to shore, and the prevailing meteorology. By basing any new EET formulas on an estimated impact level when the NAAQS levels are revised, the equations are still applicable because they do not depend on those values. The EET formulas will have to be re-evaluated only when the averaging times for the NAAQS are changed or the SILs are adjusted.

The use of additional ozone data to estimate of the conversion of NO_x to NO and NO_2 is discussed in Section 5.6.4.1. Background ozone values were integrated into the CALPUFF results to enable the NO_x chemistry options. Section 5.7.2 discusses this and other CALPUFF options.

5.6.2 Urban/Rural Classification

Several parameters are used to describe the character of the modeled domain, including surface roughness length, albedo, and Bowen ratio. These parameters are incorporated into AERMOD's surface meteorological dataset.

AERMOD has an option to classify areas as urban and will modify the run to also calculate the effects of increased surface heating from urban areas. The USEPA Guideline specifies two methods for determining if an area is predominately urban or rural: by the dominance of a specific land use or by population data in the study area.

In general, all overwater areas are considered rural. For those sources tested within 3 km of land, ERG used the Auer method to verify the land use classification. The Auer land use analysis examines a 3-km radius surrounding the facility. If more than 50 percent of the land in this circle is considered urban, the analysis uses urban dispersion coefficients. This method is consistent with the permit guidance issued by the study states.

5.6.3 Building Downwash

Building downwash is the effect buildings have on plume dispersion. When a plume flows over a structure, eddies are formed on the downwind side of the building. These eddies, or building wakes, can pull the plume to the ground much sooner than if the building was not present and result in an increased concentration in the immediate downwind area. Building downwash can be a particular issue when receptors are placed near the emission source.

ERG used the Building Profile Input Program for PRIME (BPIPPRM) algorithm in AERMOD to evaluate the need to account for the platform sources' downwash and the difference in impact. Overall,

the difference in impacts between runs with and without BPIPPRM were minimal. To streamline the synthetic source modeling, ERG ran all sources without BPIPPRM.

5.6.4 Modeling Approach

5.6.4.1 Approach for NO_2

The NO_x emissions from combustion sources are partly NO and partly NO_2. After the combustion gas exits the stack, additional NO_2 can be created due to atmospheric reactions. The NAAQS and increments were developed for NO_2. Therefore, a method to estimate how much of the released NO is converted to NO_2 was needed to compare a modeled concentration to an NO_2 standard or increment.

The USEPA Guideline discusses a tiered approach to modeling the annual average NO_2 impacts:

- Tier 1: Assume total conversion of NO to NO_2
- Tier 2: Multiply Tier 1 results by an empirically derived NO_2/NO_x ratio (e.g., national default ratio of 0.8 [one hour] and 0.75 [annual])
- Tier 3: Conduct a detailed analysis on a case-by-case basis

The Tier 3 analysis is a refined screening assessment using either the ozone limiting method (OLM) or the plume volume molar ratio method (PVMRM and PVMRM2). The OLM and PVMRM methods are accepted regulatory options within AERMOD. The OLM method (Cole and Summerhays, 1979) limits the conversion of NO to NO_2 on an hourly basis based upon the amount of O_3 in the lower atmosphere. Guidance on the revised NO_2 NAAQS (USEPA, 2010a) notes that the OLM is a detailed screening technique for point sources, particularly for scenarios with multiple sources where plume overlap is likely to occur (USEPA, 2014a). PVMRM determines the conversion rate for NO_x to NO_2 by calculating the NO_x moles emitted into the plume and the amount of O_3 moles contained within the plume volume between the source and receptor (Hanrahan, 1999). Both methods require representative hourly ozone data.

Because of its modeling approach (i.e., use of single synthetic sources) and desire for a conservative estimate of NO_2 levels to be protective of public health, ERG decided to use the Tier 1 approach to the NO_2 modeling.

5.6.4.2 Approach for Other Pollutants

ERG modeled all other pollutants separately on an hourly basis to ensure compliance with the USEPA averaging rules for each NAAQS.

5.6.4.3 Approach for Secondary Formation

The concentrations for secondarily formed pollutants, $PM_{2.5}$ and O_3, were estimated using the PGM modeling discussed in Section 5.8.4. The procedures used to estimate concentrations and evaluate the EET formulas are discussed in Section 5.9.

5.7 CALPUFF Modeling Configuration

The USEPA Guideline recently removed CALPUFF from being the preferred long-range transport model. This removal does not mean that CALPUFF cannot be used; rather, it means that CALPUFF is not preferred over other potential models. This study used the CALPUFF model because no other widely used air quality model is technically superior to it for long-range transport.

In this study, the current regulatory release versions of the CALPUFF programs were used. Their version numbers are presented in Table 5-10.

Table 5-10. CALPUFF Modeling System Components

Program	Version	Level
MMIF	3.2	140801
CALPUFF	5.8.4	130731
CALPOST	6.221	080724
POSTUTIL	1.56	070627

5.7.1 Modeling Domain

The 4-km WRF domain is quite large (472 x 211grid cells), and a CALPUFF domain that encompasses the majority of the region was necessary. If a single CALPUFF meteorological input file was generated for the entire domain, the file sizes would be so large that the model would be very time-consuming to run, and distribution of the files would be difficult. Therefore, to reduce the file sizes and make the model run faster, Alpine split the region into three different overlapping "tiles," while preserving the 4-km grid spacing. The tiles were selected to separately cover the Western, Central, and Eastern GOM Planning Areas with a 100-km overlap between each tile. The tile definitions are presented in Table 5-11 and Figure 5-6. As noted in Section 5.3.1, ERG provided these data files to BOEM for operator use in future modeling demonstrations.

For the CALPUFF modeling, Alpine used the same LCC projection parameters as the WRF modeling (40°N, 97°W, with true latitudes at 33°N and 45°N, and the NWS-84 datum—the standard RPO projection).

Table 5-11. CALPUFF Modeling Domain Definitions

Region	X Origin (km)	Y Origin (km)	Number of X Grid Cells	Number of Y Grid Cells
West	-136	-1684	190	201
Central	-700	-1684	240	201
East	744	-1684	240	201

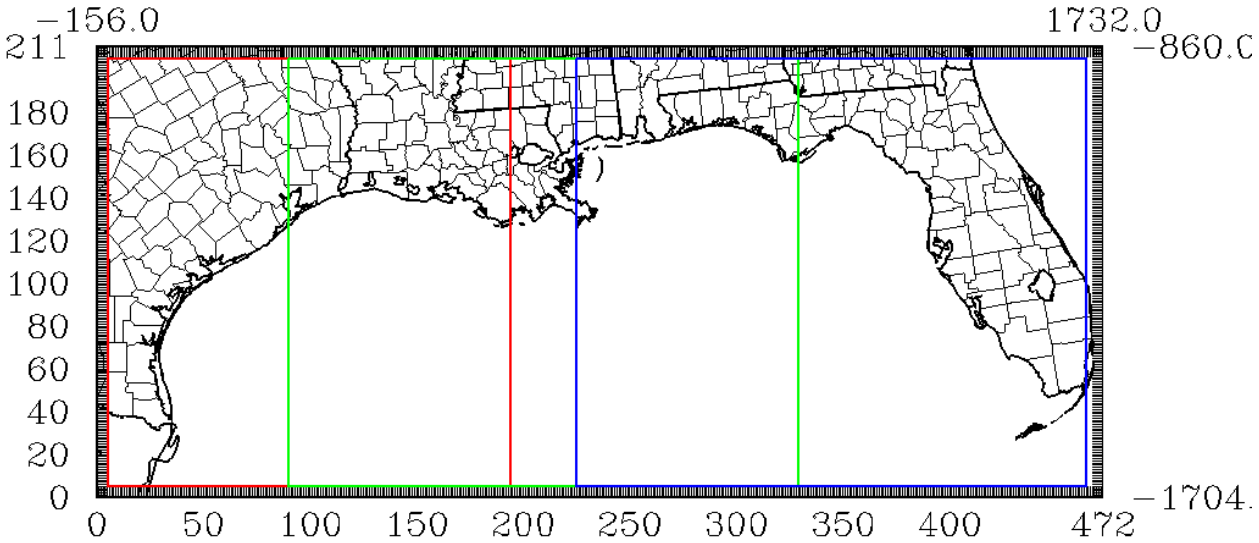

Figure 5-6. CALPUFF Modeling Domains

5.7.1.1 MMIF

As noted in Section 5.3.1, MMIF was used to generate the meteorology data for the CALPUFF runs. The default technical options were chosen to avoid recalculating PBL depth and to use Golder stability (Golder, 1972).

5.7.2 CALPUFF Additional Inputs and Model Options

Similar to AERMOD, CALPUFF needs information in addition to meteorological condition inputs and has several options that can improve model performance under various conditions. This section briefly outlines CALPUFF's additional inputs and technical options.

Additional Background Ozone Values: In order to enable the options to implement the chemistry options in the CALPUFF, Alpine took background ozone values from the PGM modeling, then processed the gridded, hourly photochemical model results onto a regular grid in the OZONE.DAT format to form monthly averaged diurnal varying values.

Technical Options: For the CALPUFF technical options, Alpine followed the USEPA Guideline and the Interagency Workshop on Air Quality Modeling (IWAQM) Phase 2 guidance (USEPA, 1998).

The modeling used RIVAD/ARM3 (Morris et al., 1988) chemistry, which is a regulatory default in CALPUFF and has been accepted for use by operators in the GOMR. Using a chemistry scheme is important because NO_x and SO_2 emissions are chemically transformed as pollutants are transported across the GOMR. The RIVAD/ARM3 scheme treats the NO and NO_2 conversion process in addition to the NO_2 to total NO_3 and SO_2 to SO_4 conversions. Because the RIVAD/ARMS2 chemistry explicitly treats NO and NO_2, the NO_x emissions were speciated using the standard 90 percent NO, 10 percent NO_2 split. The use of chemistry is consistent with current BOEM practices for far-field modeling to support EPs and DOCDs in the GOMR.

5.8 CAMx Modeling Configuration

Alpine used conducted PGM modeling using CAMx to assess cumulative air quality impacts for two types of emission scenarios:

1. Base case modeling used to evaluate model performance and define current baseline air quality conditions.
2. Future development scenario modeling based on a future year emissions projection, used to estimate the air quality and AQRV impacts of each modeled future year scenario relative to base case conditions.

For the EET PGM modeling, the base case 2012 emissions inventory was used to eliminate the uncertainty in the future year emissions inventory projection. As part of the cumulative air quality impacts assessment modeling, the PGM modeling platforms were evaluated against available observations. This MPE also applies to the EET modeling platform. This use of a consistent modeling platform provided consistency between the cumulative air quality impacts assessment and EET modeling.

5.8.1 Model Domain Configuration

The PGM domain for the EET modeling is consistent with the domain cumulative air quality impacts assessment presented in Section 4 of this report. In short, Figure 5-7 shows the PGM grids at 36, 12, and 4 km along with the corresponding WRF modeling grids. All grids are defined on an LCC projection centered at 40°N, 97°W, with true latitudes at 33°N and 45°N (the standard RPO projection).

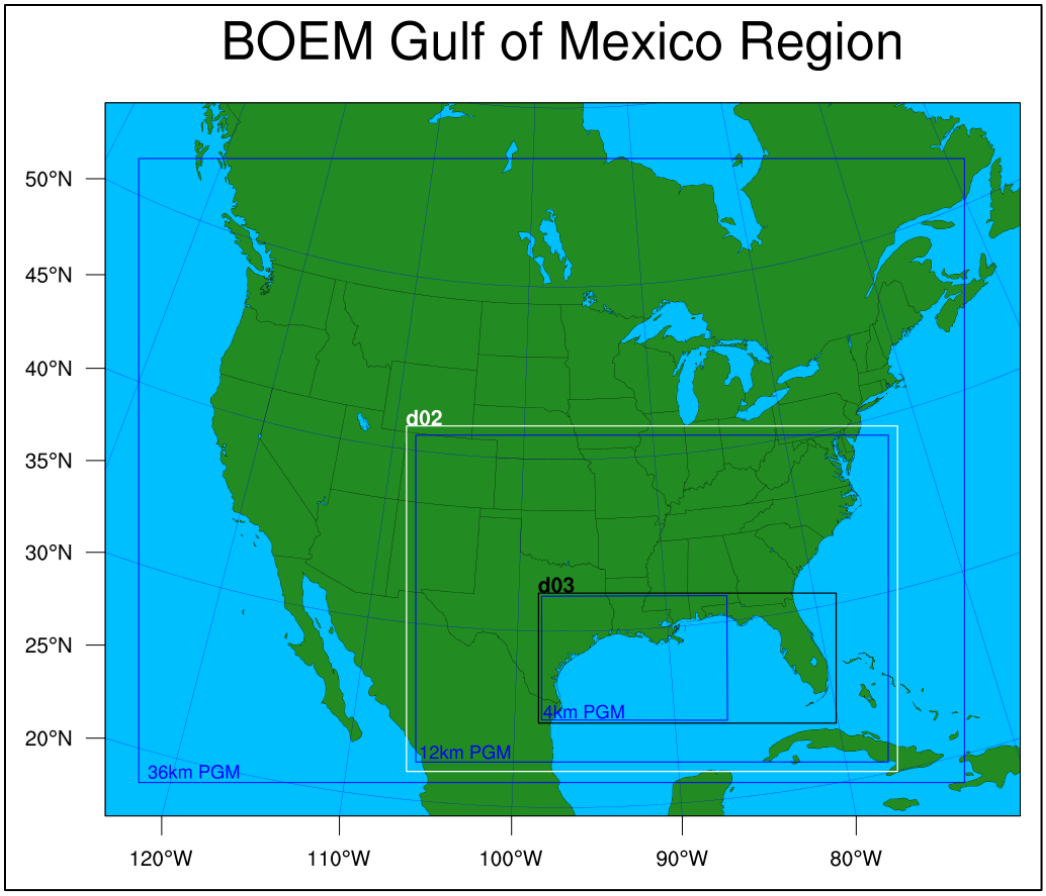

Figure 5-7. Horizontal Modeling Grids for the WRF and PGM Simulations
The WRF 12- and 4-km grids are denoted by "d02" and "d03," respectively; the WRF 36-km grid is represented by the outer boundary of the map.

For CAMx, the 36-km simulation results provide BCs for the 12-km modeling grid, and the 12- and 4-km grids were modeled using two-way nesting (allowing interactions between the two grids in both directions).

5.8.2 Episode Selection

Given the extremely hot, dry, and smoky conditions in the southeastern U.S., particularly Texas during 2011, the ERG team selected 2012 for the base year base case modeling. This selection matches the base year selection from the cumulative air quality impacts assessment presented in Section 4 of this study. The modeling covers the entire calendar year.

5.8.3 Base Model Configuration

Alpine conducted PGM modeling using CAMx version 6.40 (released in December 2016) and used the Carbon Bond Chemical Mechanism, version 6, revision 4 (CB6r4), which includes the latest chemical kinetic rates and halogen chemistry.

The models were configured to predict both ozone and PM species, so that they can be used to evaluate ozone and PM concentrations and associated precursor EET formulas as well as AQRVs (visibility and deposition). CAMx used the CF aerosol scheme in which primary species are modeled using two static modes (coarse and fine), while all secondary species are modeled as fine particles only. Table 5-12 summarizes the CAMx science configurations and options used for this study. Specification of model

configurations is guided by the principle that the main benefit of applying two different models is obtaining two alternative air quality impact estimates using the best available, state-of-the-art modeling techniques associated with each model.

Table 5-12. CAMx Model Configurations for the GOMR Modeling

Science Options	Configuration	Notes
Model codes	CAMx V6.40	Released December 2016
Horizontal grid	36/12/4 km	The 4-km grid may be revised based on computational cost.
36-km grid	148 x 112 cells	
12-km grid	254 x 176 cells	
4-km grid	299 x 200 cells	
Vertical grid	24 vertical layers (layer-collapsed from 32 WRF layers)	See Section 4 of this report; layer 1 thickness ~20 m; model top at ~20-km AMSL (50 hPa)
Grid interaction	36/12-km one-way nesting 12/4-km two-way nesting	–
ICs	Clean ICs	10-day spin-up for the 36-km grid; three-day spin-up for the nested (12/4-km) grids
BCs	36 km from GCM simulation	Initially used GEOS-Chem GCM 2012 output data; investigate use of MOZART GCM output for BCs as a sensitivity test as well as BC adjustments based on recent Texas modeling study
Land use data	Land use fields based on USGS GIRAS data	–
Photolysis rate preprocessor	TUV V4.8	Clear-sky photolysis rates based on day-specific TOMS data
Chemistry		
Gas phase	CB6r2h	Updated isoprene chemistry; heterogeneous hydrolysis of organic nitrates; active methane chemistry and ECH_4 tracer species (Hildebrandt Ruiz and Yarwood, 2013); halogen chemistry (Yarwood et al., 2014)
Aerosol phase	CF	Coarse and fine mode aerosols
Meteorological input preprocessor	WRFCAMx V4.3	Compatible with CAMx V6.20
Diffusion Scheme		
Horizontal grid	Explicit horizontal diffusion	Spatially varying horizontal diffusivities determined based on the methods of Smagorinsky (1963)
Vertical grid	K-theory 1^{st}-order closure	WRFCAMx-derived vertical diffusivities based on the YSU PBL scheme (Hong and Noh, 2006); land use dependent minimum diffusivity (minimum Kv = 0.1 to 1.0 m^2/s) with a cloud Kv patch recently developed to address deep convective mixing (ENVIRON, 2012)
Deposition Scheme		
Dry deposition	ZHANG03	Dry deposition scheme by Zhang et al. (2001; 2003)
Wet deposition	CAMx-specific formulation	Scavenging model for gases and aerosols (Seinfeld and Pandis, 1998)
Numerical Solvers		
Gas-phase chemistry	Euler backward iterative solver	Hertel et al. (1993)
Horizontal advection	Piecewise parabolic method	Colella and Woodward (1984)
Vertical advection	Implicit scheme with vertical velocity update	–

5.8.4 EET Source Configuration

The CAMx model contains advanced tools that are very useful for assessing source attribution for ozone and $PM_{2.5}$. The following section describes how these options were used in the study.

5.8.4.1 Ozone EET Configuration

The CAMx OSAT uses reactive tracers that operate in parallel to the host model. Four tracers correspond to each source group's VOC and NO_x concentrations (Vi and Ni), and ozone is attributable to the source group's VOC concentrations (O3Vi) or NO_x concentrations (O3Ni). In the CAMx OSAT (Ramboll Environ, 2016) approach, when ozone is formed in a grid cell, it is attributable to a source group based on the relative contributions of the source group's VOC or NO_x concentration to the total VOC or NO_x concentration in that grid cell. This attribution is further based on a determination of whether the ozone was formed under VOC-limited or NO_x-limited conditions. Thus, in OSAT, the O3Vi and O3Ni reactive tracers indicate how much of the ozone is formed under VOC-limited versus NO_x-limited conditions.

CAMx contains an optional source apportionment technique called the APCA. This option attributes ozone to biogenic (uncontrollable) sources when it is formed due to the interaction of biogenic VOC with biogenic NO_x. When ozone is formed under VOC-limited conditions due to the interaction of biogenic VOC with anthropogenic NO_x, APCA redirects the assignment to the anthropogenic NO_x (O3N) source group. Alternately, OSAT would assign the interaction to the biogenic VOC (O3V) source group. Thus, with APCA, the O3V and O3N tracers for anthropogenic sources no longer represent ozone formed from those sources, but also include the biogenic VOC contributions. The APCA technique better enables CAMx source apportionment to be used to develop anthropogenic emission control strategies. For this BOEM application, ERG used CAMx to evaluate potential new sources, which, if modeled, would be wholesale additions of new sources to the model. The OSAT technique most closely approximates the addition of new sources. Furthermore, the selection of OSAT ensures all the ozone formation due to the additional of these OCS source would be attributed back to the platform and not to biogenic sources.

The standard OSAT ozone source apportionment treatment was used for the ozone EET assessment. To minimize the interaction of the synthetic sources and lower the CAMx model's memory and processing requirements, the photochemical modeling was split into a number of different simulations, with nearby synthetic sources split into different CAMx simulations.

Alpine and ERG extracted the ozone concentrations from the gridded model output files for all receptors and used them to develop ozone-specific exemption-level formulas. This allowed the ozone impacts to be related back to either the VOC or the NO_x precursor emissions. Depending on the chemical regimes, it is possible that the ozone concentrations may not be sensitive to changes in one of the precursors.

Because ozone is primarily highest in the warmer months, Alpine only ran the ozone analysis from April to October, the period of highest ozone concentrations on the Gulf Coast and based any ozone EET formulas on a single meteorological year.

Decoupled Direct Method (DDM) and higher order Decoupled Direct Method (HDDM) were briefly considered. However, HDDM and DDM are formulated to examine the sensitivity of air concentrations to changes in source emissions, rather than the total impact of a set of sources. HDDM and DDM are more appropriate to show the response to an emission control strategy or emissions perturbation. CAMx source apportionment more closely approximates the air quality impact of adding a new source to the model, which is what an operator would do should the project not pass the EET screening. For this study, we were interested in this total contribution to the ambient concertation for the calculation of the model emission rates for precursors (MERPs).

5.8.4.2 Secondary $PM_{2.5}$ EET Configuration

The CAMx PSAT works similarly to the OSAT treatment. PSAT is designed to source apportion the following PM species modeled in CAMx:

- Particulate sulfate (PSO_4)
- Particulate nitrate (PNO_3)
- NH_4
- Particulate mercury
- SOA
- Six categories for primary PM

The particulate sulfate and nitrate were traced in CAMx, with each of the synthetic sources described in Section 4.2 simulated as a separate source group. The oil and gas production sources in the Gulf have negligible emissions of the types of VOC species that are precursors to SOA (isoprene, terpenes, sesquiterpenes, and aromatics), so the analysis did not include SOA. Intermediate volatile organic compounds (IVOCs) and semi-volatile organic compounds (SVOCs) can contribute to OA formation. However, the data necessary to include these organic species in the inventory are limited. Therefore, IVOCs and SVOCs are not included in this analysis, which is consistent with the cumulative air quality impacts assessment modeling.

The sulfate and particulate nitrate concentrations were extracted from the gridded model output files for all receptors. The USEPA's *Guidance for $PM_{2.5}$ Permit Modeling* (USEPA, 2015c) specifies that the sulfate and particulate nitrate concentrations are to be added to the primary $PM_{2.5}$ concentrations predicted by the dispersion models. A complication is that although the primary $PM_{2.5}$ impacts were run for five years, the secondary component is only available for a single year. Part of this EET evaluation included combining the peak secondary $PM_{2.5}$ from the 2012 modeling with the peak primary $PM_{2.5}$ for each year.

5.9 Methodology Used to Assess Current EETs

Under current policy, if a facility's calculated highest annual total emissions for each pollutant (CO, VOC, NO_x, SO_2, $PM_{2.5}$, and PM_{10}) are below the threshold values, the facility is exempt from further review. As the NAAQS become more stringent, these thresholds must be re-examined to ensure that OCS oil and gas production sources are subject to the appropriate level of modeling analysis to determine onshore impacts. ERG examined the results of the modeling described in the previous sections to determine if the current EET formulas have adequately identified sources with minimal impact on pollutant concentrations to any state for all NAAQS averaging times and forms.

ERG applied the current EET formulas to each of the modeled synthetic sources to determine the level of impact at the receptors compared to the established SILs for each NAAQS. ERG compared the results of the exemption formulas (i.e., whether the scenario was above or below the threshold) to the comparison of the modeled impact to the SIL, which noted whether a significant impact was seen from the emission scenario. This produced three outcomes with respect to the EET analysis:

- **Pass:** A correct evaluation. Emissions from the scenario were above the EET, which indicated modeling was needed and the modeling impacts were above the SIL, or emissions from the scenario were below the EET, which indicated modeling was not needed and the modeled impacts were below the SIL.
- **False positive (Type I error):** Emissions from the scenario were above the EET, which indicated modeling was needed; however, the modeled impact was below the SIL.

- **False negative (Type II error):** Emissions from the scenario were below the EET, which indicated modeling was not necessary; however, the modeled impact was above the SIL.

From an operational standpoint, when the EET formulas are a false positive, the operator's modeling efforts were not necessary. Conversely, a false negative means that the project impact could exceed the SIL, but the operator did not have to confirm this with modeling and did not disclose the possibility of an exceedance.

The maximum hourly rate was used to develop emissions in grams per second (g/s) for the short-term standards. This value is used to model all hours in order to catch the maximum impact possible from the source. In reality, this level of operation is unlikely for all 8,760 hours in a year. As demonstrated by the estimated annual emission rates of the scenarios originally presented in Table 5-4, and presented in Table 5-13 below for NO_2, the "actual" emissions rate can vary dramatically from the "maximum" annual rate. To account for this difference in emissions, short-term standard analyses used the "maximum" annual rate as it was more reflective of the emissions level modeled that the "actual" emissions.

Section 5.10 summarizes the AERMOD and CALPUFF modeling results at the shoreline for all distances. For brevity, only the NO_2 modeling results are discussed. Additional figures for other pollutants are in Appendix E.5. Dispersion modeling results at the state seaward boundary were also analyzed and are presented in Appendix E.6. An analysis of secondary formation at the shoreline is discussed in Section 5.10.3; an analysis of secondary formation was not conducted at the seaward boundary.

Table 5-13. NO_2 Maximum Emission Rates Modeled

Scenario	Emissions Rate (tpy)	Emission Rate (g/s)	Maximum Annual Emission Rate (tpy)
1L	8,100	582.34	20,243.59
1M	2,100	213.11	7,408.24
1S	200	90.68	3,152.26
2L	25,300	4,771.92	165,883.87
2M	1,900	3,157.30	109,755.64
2S	500	1,621.04	56,351.40
3L	16,700	956.32	33,244.07
3M	800	298.48	10,375.91
3S	300	162.92	5,663.51
4L	2,800	169.05	5,876.60
4M	1,200	52.35	1,819.82
4S	100	3.68	127.93
5L	4,600	349.84	12,161.31
5M	3,000	276.88	9,625.04
5S	1,300	109.70	3,813.45

5.10 Results

Results are presented with respect to the parameters used in the current EET formulas. That is, total emission in TPY and distance to shore (or state seaward boundary) in statute miles. This helps put the impacts in the context of the current formulas, which can show if certain ranges of these input parameters consistently lead to error is the EET results.

5.10.1 Short-Term NAAQS

For the short-term standards (NAAQS with averaging times of less than or equal to 24 hours), the highest impacts occur at the modeling points closest to shore (i.e., D001) and the higher emission scenarios. This can be seen in Figure 5-8 for the NO_2 1-hour NAAQS, as the D001 contour is at the top of the columns for each emission level. ERG intentionally placed the very high emission sources in the D001 contour closest to shore seen in Figure 5-8 in order to fully evaluate the existing EETs. It was important to test a full range of emission values at all locations to limit the potential for extrapolation in any updated EET method. The plumes from the sources closest to shore have less time to disperse, so higher values were anticipated at these locations. Also, higher impacts were expected for the higher emission scenarios. The 2S and 2M scenarios proved to be exceptions to higher impacts with the high emissions. After closer investigation, it was determined that the large maximum annual emissions rate for these sources was driven by flare upsets included in the scenarios. It is possible that the heat associated with these emission sources created a very buoyant plume, which resulted in the plume either entirely or partially penetrating the boundary layer. This could reduce the impact at the receptors set at the shoreline, as the plume might not re-enter the surface layer at the shoreline. Scenarios 2L, 3L, 3M, 5L, 5M, and 5S also include flares with upsets; however, they are not as large as the 2S and 2M scenario flare upset emissions and do not make up a large portion of the total annual emissions. Dips in impacts for these scenarios can been seen in Figure 5-8, but not to the extent of the 2S and 2M. This finding emphasizes the need to model various platform configurations in order to catalog the difference in impacts of varying equipment types.

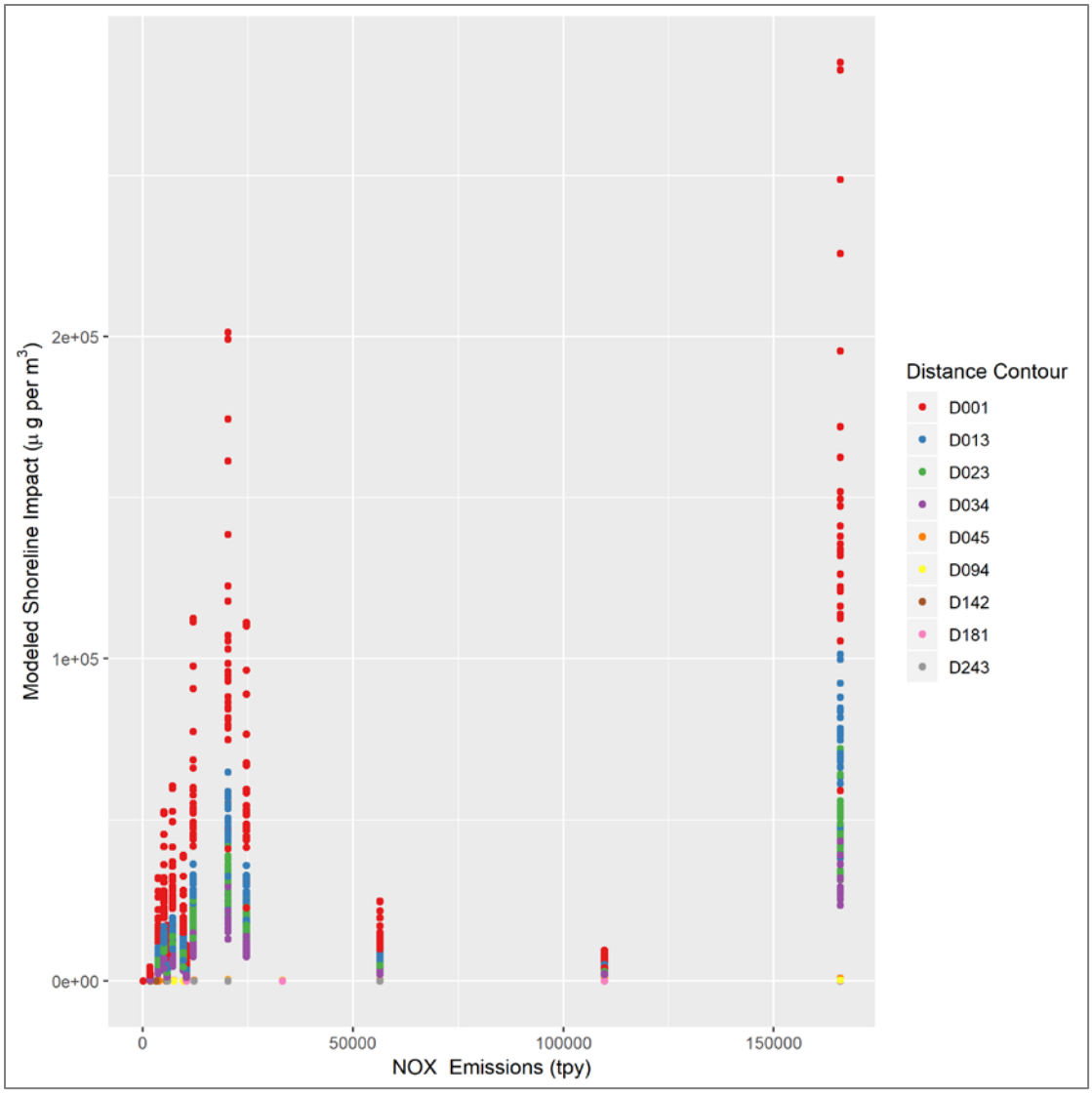

Figure 5-8. Scatter Plot of NO_2 1-hour Modeling Results

When impacts were compared to the current EET formulas, there was a high level of agreement between the modeling and EET-estimated significance (Figure 5-9 and Table 5-14). False negative rates (when the impact was above the SIL, but the formula determined that modeling was not necessary) ranged from 2 percent for the NO_2 1-hour NAAQS to 36 percent for the $PM_{2.5}$ 1-hour NAAQS.

Table 5-14. Short-Term NAAQS Outcomes at the Shoreline[a]

Pollutant	Averaging Time	Evaluation Outcome (percentage of total)		
		Pass	False Positive (Type I)	False Negative (Type II)
CO	1 hour	77%	0%	23%
	8 hours	84%	0%	16%
NO_2	1 hour	91%	7%	2%
$PM_{2.5}$	24 hours	64%	0%	36%
PM_{10}	24 hours	73%	0%	26%
SO_2	1 hour	73%	6%	21%
	3 hour	71%	8%	21%
	24 hours	72%	8%	20%

[a] Based on 3,300 modeling runs.

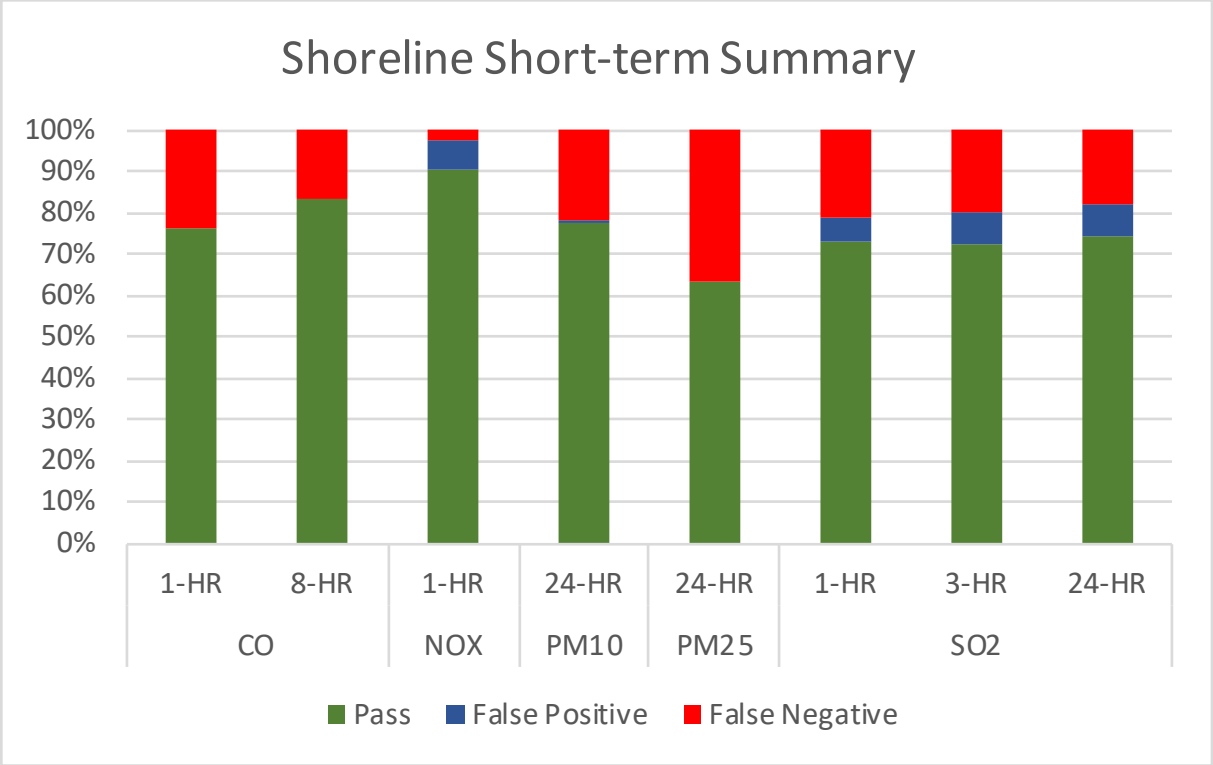

Figure 5-9. Shoreline Short-Term Standard Results

Overall, the EET formulas generally have a moderate false negative rate for the combinations of emissions and distances tested. That is, the current EETs occasionally do not recommend modeling for some facilities that cause an impact larger than the SIL at the shoreline. Figure 5-10 shows where these errors occur with respect to the distance to shore and emission rate modeled. Figure 5-10 is a scatter plot of all distance and emission combinations modeled. These points are color-coded based on error type, with the black line indicating the current EET formula (33.3*D). The figure can be interpreted as follows:

- Non-red points under the line were below the current EET, indicating that modeling was not necessary.
- Green points under the line with “Pass” errors indicate that the modeling showed an impact below the SIL.

- Red points under the line with errors (false negative) depict runs where the EET indicated that the project was below the *de minimis* threshold and did not need further analysis; however, modeling showed that the project did have a shoreline impact greater than the SIL. Most of these Type II errors occur close to shore, as the nearshore location would not have a lot of time to disperse and could have higher impacts.
- All points above the line indicate runs where the EET indicated a project above the *de minimis* threshold that required additional modeling.
- Green points above the line with "Pass" errors showed an impact above the SIL at the shoreline.
- Blue points indicate "False Positive" Type I errors above the EET threshold and would have required modeling under the current process but did not have a modeled impact above the SIL. Most of the false positive errors occur at further distances to shore, with lower emission rates.

Appendix E.5 includes plots like Figure 5-10 for other pollutants and averaging times. Appendix E.6 presents the results at the state seaward boundary, and Appendix E.7 presents the results for Pb.

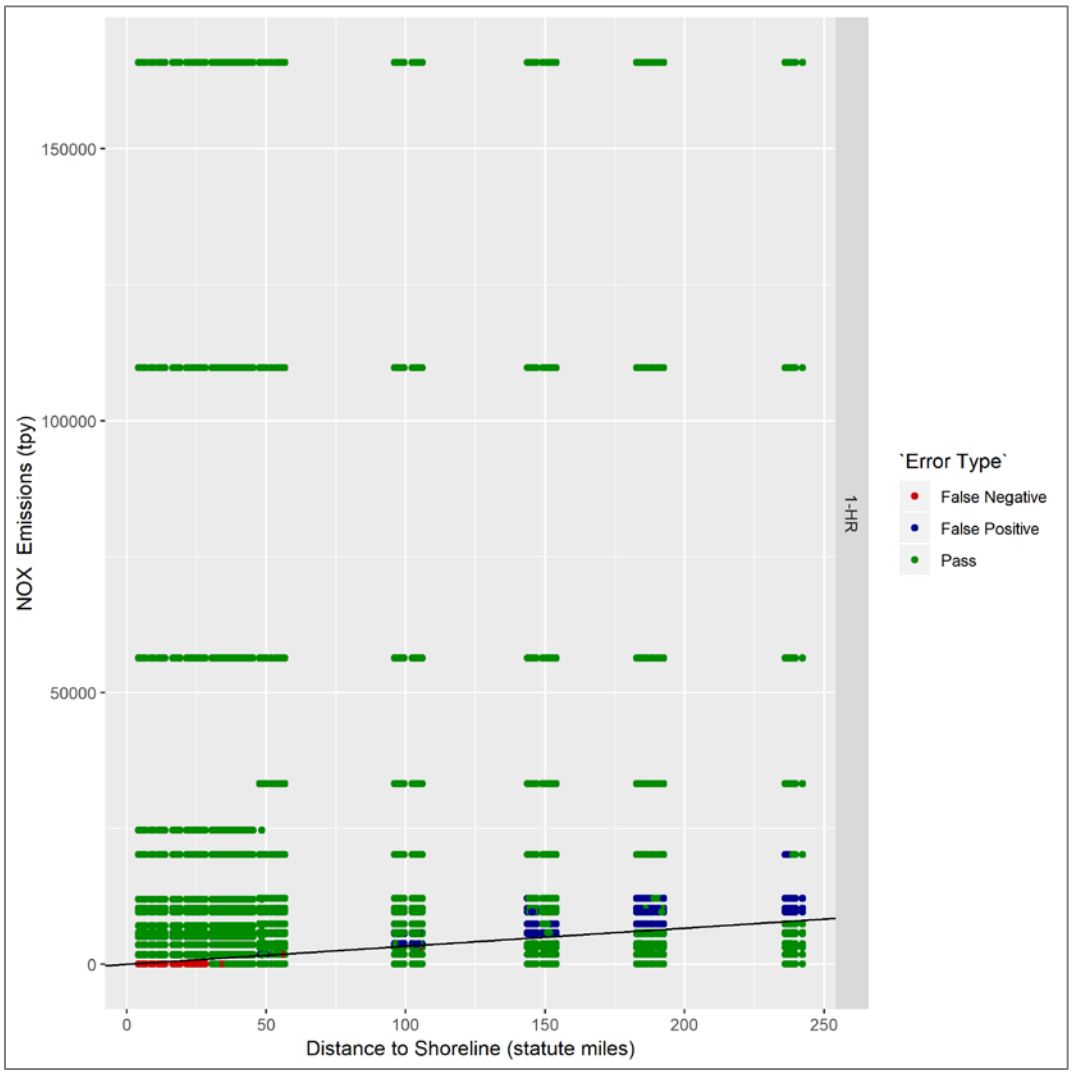

Figure 5-10. Scatter Plot of NO_2 1-hour Modeling Results at the Shoreline
Black line indicates the current EET formulation.

5.10.2 Long-Term NAAQS

For the long-term standards (NAAQS with annual averaging times), the highest impact occurs at the closest distance and highest emissions rate (Figure 5-11). This pattern of highest impact closest to the shoreline for the highest emission rate holds for all pollutants.

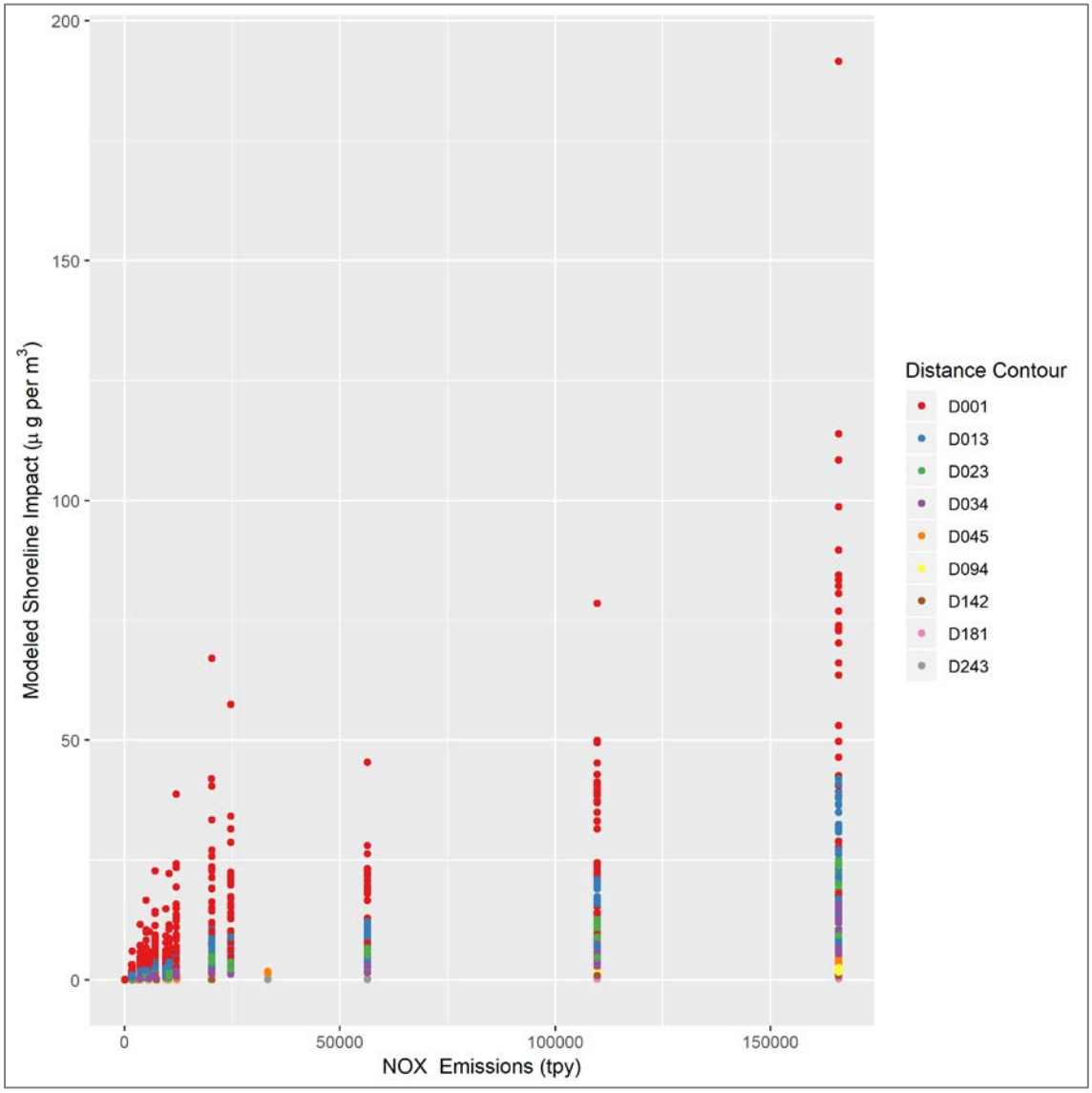

Figure 5-11. Scatter Plot of NO_2 Annual Results at the Shoreline

For the annual NAAQS, the current EET formulas saw more false positive errors. That is, the current EET formulas called for modeling when the impact was not larger than the SIL (Table 5-15 and Figure 5-12). Type I errors were especially common at distance greater than 50 mi to the shoreline (Figure 5-13).

A conservatively high emission rate was modeled using the calculated *maximum* hourly emission rate for all averaging times, consistent with USEPA regulatory modeling. Modeling an *annualized* hourly emission rate (total annual emission divided by operating hours) would produce a lower emission rate and therefore result in a lower impact in the modeling. Modeling at the *maximum* hourly emission rate suggests the current EET formulas for the annual NAAQS are especially conservative, thus requiring

more modeling than potentially necessary. This outcome, however, is less of a concern than a high false negative rate.

Table 5-15. Long-Term NAAQS Outcomes at the Shoreline[a]

Pollutant[b]	Evaluation Outcome (percentage of total)		
	Pass	False Positive (Type I)	False Negative (Type II)
NO_2	59%	41%	0.0%
$PM_{2.5}$	96%	3%	1.2%
PM_{10}	93%	7%	0.0%
SO_2	73%	27%	0.0%

[a] Based on 3,300 modeling runs.
[b] There is no long-term NAAQS for CO.

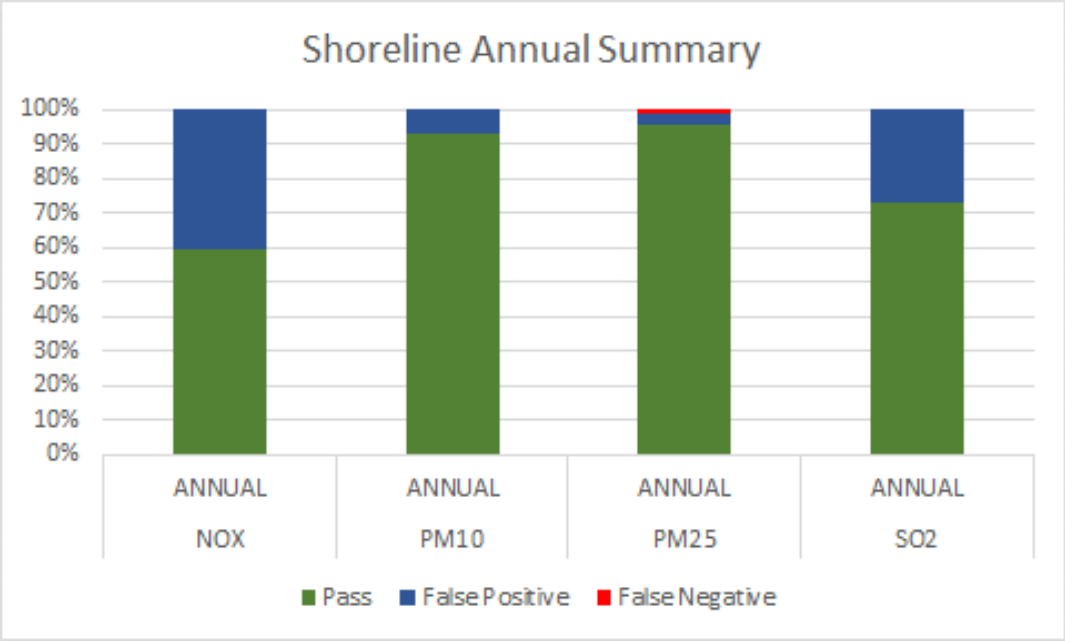

Figure 5-12. Shoreline Annual Standard Results Summary

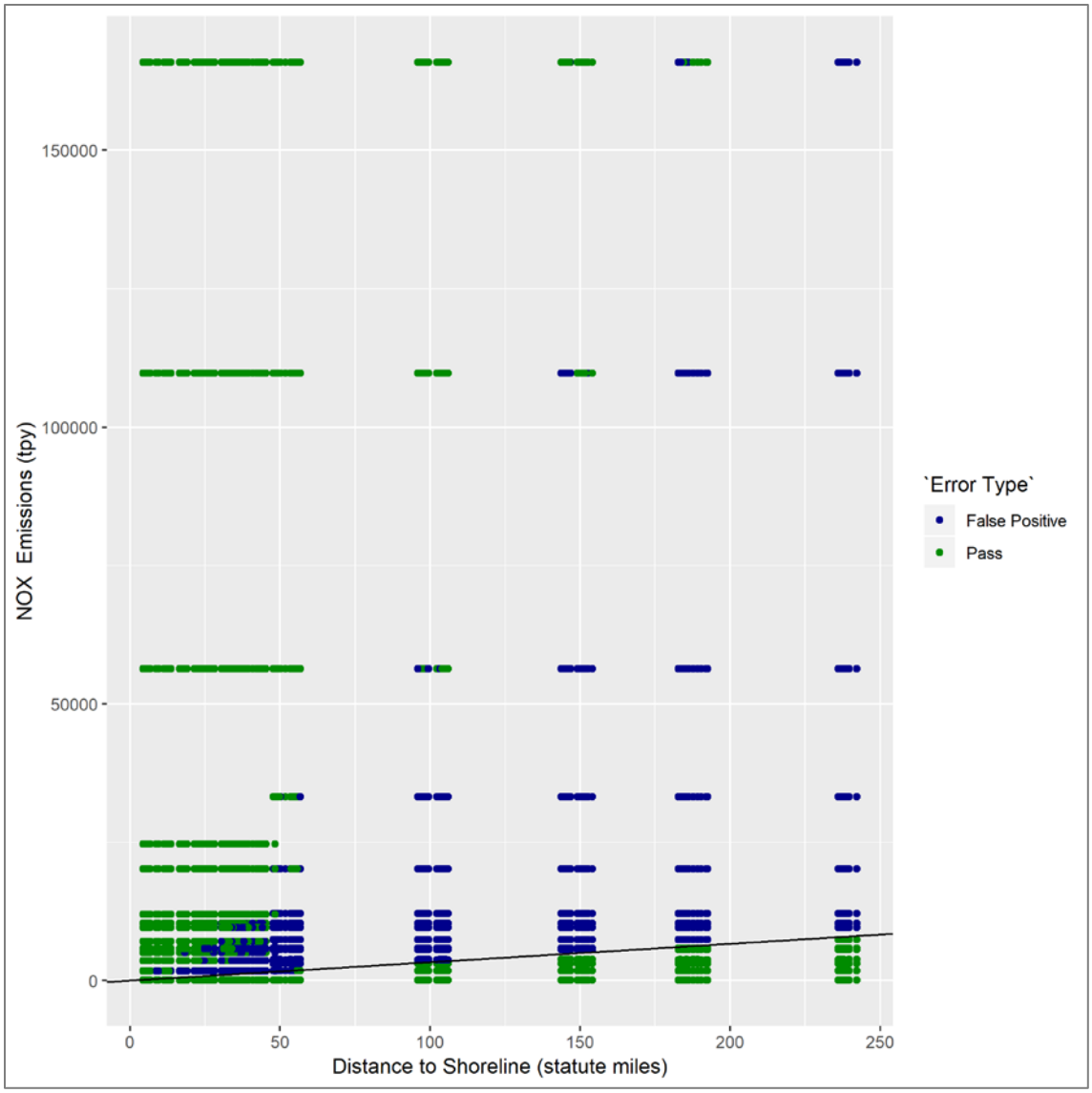

Figure 5-13. Scatter Plot of NO_2 Annual Results at the Shoreline
Black line indicates the current EET formulation.

5.10.3 Secondary Formation

Modeling of single-source impacts on secondarily formed pollutants, $PM_{2.5}$ and O_3, is an evolving area for air quality modeling. The recent USEPA Guideline updates include new memoranda (USEPA 2015a, b, c) and expanded guidance (USEPA 2016a, b, c) on secondary formation that represent a slight shift in the modeling approach described in the USEPA's *Guidance for $PM_{2.5}$ Modeling* (USEPA, 2014b).

The latest USEPA guidance documents (from 2015 and 2016) include a two-tiered demonstration approach for secondary formation. The first tier uses pre-established, technically credible relationships between precursor emissions and a source's impacts to assess secondary formation. The second tier applies more sophisticated, case-specific PGMs conducted consistently with new USEPA single-source modeling guidance (USEPA, 2015c).

As part of the first tier, USEPA permit applicants can use a new demonstration tool for ozone and $PM_{2.5}$ precursors referred to as MERPs. MERPs offer a screening method that would represent a level of

precursor emissions that is not expected to contribute significantly to concentrations of secondarily formed $PM_{2.5}$ or O_3.

To derive a MERP value, the model-predicted relationship between precursor emissions from hypothetical sources and their downwind maximum impacts can be combined with a critical air quality threshold using the following equation:

$$MERP = SIL * \left(\frac{Modeled\ emission\ rate\ from\ hypothetical\ source}{Modeled\ air\ quality\ impact\ from\ hypothetical\ source}\right)$$

Where the SIL, or other critical air quality thresholds, is expressed as a concentration of $PM_{2.5}$ ($\mu g/m^3$) or O_3 (ppb or ppm); modeled emission rate is expressed in TPY; and modeled air quality impact is expressed in units of $\mu g/m^3$ (ppb) for $PM_{2.5}$ and O_3.

The modeled impacts would reflect the maximum downwind impacts for $PM_{2.5}$ and O_3. The final MERP is expressed as an annual emission rate in TPY. Thus, the calculated MERPs act similar to an EET in that a project with emissions less than the MERP is anticipated to cause no significant, or *de minimis*, impacts on the air quality from secondary formation.

As part of its 2016 guidance on MERPs (USEPA 2016b), the USEPA used source apportionment modeling to calculate MERP values for each $PM_{2.5}$ and ozone precursor for several hypothetical sources around the country. The hypothetical sources modeled had emissions rates of 500, 1,000, or 3,000 TPY. These modeling results were used to develop a "most conservative" MERP value for each region, which is summarized in Table 5-16. The conservative MERPs are only for regions in the continental U.S., because the initial analysis did not include offshore areas.

Table 5-16. Regional Most Conservative MERPs (TPY)

Precursor	U.S. Area	8-hr O_3	Daily $PM_{2.5}$	Annual $PM_{2.5}$
NO_x	Central	126	1,820	7,427
NO_x	Eastern	107	2,467	10,037
NO_x	Western	184	1,155	3,184
SO_2	Central	–	256	1,795
SO_2	Eastern	–	675	4,013
SO_2	Western	–	225	2,289
VOC	Central	948	–	–
VOC	Eastern	814	–	–
VOC	Western	1,049	–	–

As noted in Section 5.8, ERG performed CAMx source apportionment modeling to assess the potential impacts from the secondary formation of $PM_{2.5}$ and ozone. The 2L and 4L synthetic source scenarios were chosen (Table 5-17) because they had relatively large $PM_{2.5}$, SO_2, NO_x, and VOC emissions, which suggested the CAMx modeling would show a response. The two scenarios also provided very different ratios of NO_x to VOC, which could impact the formation of ozone.

A subset of locations from the dispersion modeling were selected for the source apportionment modeling. ERG selected locations that minimized plume overlap and were found throughout both planning areas at varying distances to shore. Figure 5-14 indicates the selected synthetic source locations used in the modeling, and Table 5-18 summarizes their distances to shore. The modeling was conducted in two separate runs, with each run using a different emission scenario for all locations.

Table 5-17. Emission Scenarios for Source Apportionment Modeling

Scenario	Description	Size	Emissions (TPY)					
			PM_{10}	$PM_{2.5}$	SO_2	NO_x	NH_3	VOC
2	PROD & DRI DOCD with support vessels	L	1,594	1,571	6,185	165,884	3	2,837
4	PROD-only DOCD with support vessels	L	110	108	396	5,877	0.4	11,707

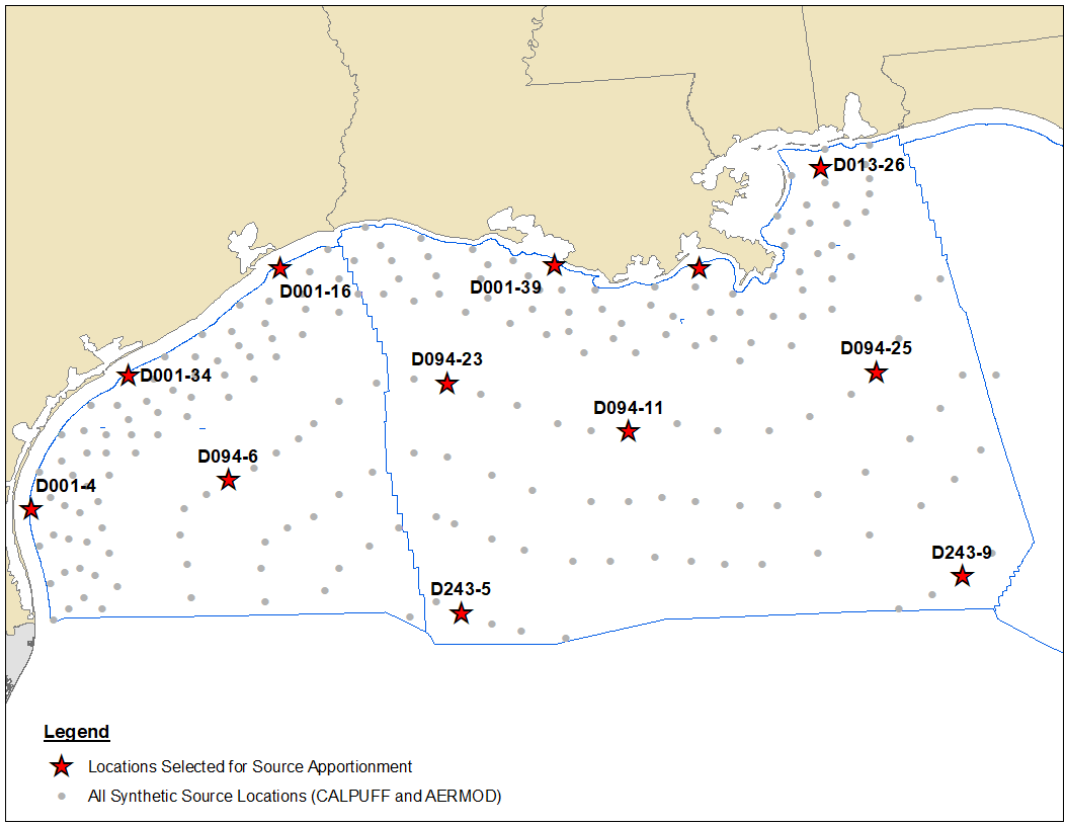

Figure 5-14. Locations Selected for Source Apportionment
Red stars indicate the locations selected, while black dots represent all synthetic source locations.

Table 5-18. Selected Locations and Distances to Shore

Location	Distance to Shore (statute miles)
D001-4	12.3
D001-34	12.1
D001-16	11.9
D001-39	6.4
D001-38	11.4
D013-26	23.2
D094-6	103.4
D094-23	96.2
D094-11	98.8
D094-25	97.0
D243-5	238.8
D243-9	236.2

The secondary formation of PM from either emission scenario was minimal, as noted in Table 5-19. For reference, the SIL for the $PM_{2.5}$ 24-hour standard is 1.2 µg/m^3 (0.07 in Class I areas) and for the annual

standard is 0.2 µg/m^3 (0.06 in Class I areas). The results of the source apportionment modeling show secondary formation contributions were well below the SILs for both the Class I and Class II areas.

Table 5-19. PM Source Apportionment Modeling Result Ranges

Species	Shoreline Impacts (µg/m^3)			
	2L		4L	
	24-HR	Annual	24-HR	Annual
Particulate Nitrate (PN3)	[< 0.001–0.066]	[0.000–0.002]	[0.000–0.003]	[< 0.001]
Particulate Sulfate (PS4)	[0.000–0.016]	[< 0.001]	[0.000–0.001]	[< 0.001]
Sum of PN3 and PS4 matched in time and space (PN3PS4)	[< 0.001–0.068]	[0.000–0.002]	[0.000–0.003]	[< 0.001]

The formation of ozone from either emission scenario was also minimal, as noted in Table 5-20. For reference, the SIL for the O_3 8-hour standard is 1 ppb. The results of the source apportionment modeling show secondary formation contributions were below the SIL. Location D001-04 had the highest response, which was approximately 80 percent of the SIL. Two nearshore locations (D001-16 and D001-34) approached half the SIL with the 2L emission scenario.

Table 5-20. 8-Hour Ozone Source Apportionment Modeling Result Ranges

Species	Shoreline Impacts (ppb)	
	2L	4L
Sum of O3N and O3V matched in time and space (O3)	[< 0.001–0.827]	[< 0.001–0.057]
Ozone formed from NO_x emissions (O3N)	[< 0.001–0.821]	[< 0.001–0.056]
Ozone formed from VOC emissions (O3V)	[< 0.001–0.014]	[< 0.001–0.002]

The minimal impacts seen here may seem contradictory to results presented in the Cumulative Air Quality Impacts Analysis section (Section 4), where the OCS and future year emission increases resulted in increases in onshore impacts, particularly in the case of ozone. However, the impact reported in Tables 5-17 and 5-18 show the range of impacts from individual platform, and not collectively for all the modeled sources. The scenario emissions are also considerably lower than the combination of emission sources that contributed to the impact seen in the cumulative impact modeling presented in Section 4. As noted in Section 5.4.2.1, the scenario emissions include activity at the platform (platform equipment and vessels servicing the platform) and do not take into account any other increase in emissions that may result for the added platform or other emission sources (e.g., vessel transit across the GOM, LOOP emissions). Within this context, the small impact attributable to a single platform source does make sense compared to the impacts from all the OCS sources (i.e., the 543 future platforms added plus supporting sources) presented in Section 4. ERG used the source apportionment modeling to develop MERP values for OCS sources. Calculations were based on the MERP equation shown above and used the modeled emission rates presented in Table 5-17, the maximum impacts seen in the domain (summaries in Tables 5-19 and 5-20), and the SILs presented in Table 5-1. The calculations using these values are summarized in Tables 5-21 and 5-22. Given the minimal modeled response, MERPs were calculated based on the maximum impacts seen in the source apportionment modeling (Tables 5-21 and 5-22). Even then, the modeled response for the tested synthetic sources were very low, especially compared to the USEPA conservative MERPs presented in Table 5-16, which led to very large MERPs. This means it would take an almost exceptional emission level to approach a response higher than the SILs, based on the tested configurations. For future efforts, it would be worth exploring different platform configurations (i.e., stack parameters and emission combinations) to determine if other combinations would yield MERPs in typical platform emission ranges.

Table 5-21. $PM_{2.5}$ MERPs Based on Source Apportionment Modeling

NAAQS	Emission Scenario	Precursor	SIL (µg/m³)	Emission Rate (tpy)	Estimated Impact (µg/m³)	MERP (TPY)
Daily $PM_{2.5}$	2L	NO_x	1.2	165,884	0.066	3,018,680
		SO_2		6,185	0.016	454,028
	4L	NO_x		5,877	0.003	2,431,191
		SO_2		396	0.001	455,959
Annual $PM_{2.5}$	2L	NO_x	0.2	165,884	0.00161	20,595,195
		SO_2		6,185	0.00049	2,536,707
	4L	NO_x		5,877	0.00008	14,360,591
		SO_2		396	0.00003	2,584,519

Table 5-22. Ozone MERPs Based on Source Apportionment Modeling

NAAQS	Emission Scenario	Precursor	SIL (µg/m³)	Emission Rate (TPY)	Estimated Impact (µg/m³)	MERP (TPY)
8-hour O_3	2L	NO_x	1.0	165,884	0.821	202,132
		VOC		6,185	0.014	209,682
	4L	NO_x		5,877	0.056	104,662
		VOC		396	0.002	5,711,846

5.10.4 EET Reformulations

Developing a revised EET requires statistical classification—i.e., determining which set of categories a new "observation" belongs in. For this project, the category is either above or below the SIL, and the "observation" is the result of the synthetic source modeling with a known emission level (E) and distance to shore (D). More simply put, statistical classification is defining the boundary that separates the red from the blue circles in Figure 5-15.

Several different methods, or classification algorithms, can be implemented to achieve a final function that defines the boundary between the categories. ERG used several different classification algorithms to develop options for revised EETs. The following sections discuss these using the $PM_{2.5}$ 24-hour results as an example. These example reformulations use the same predictive parameters as the existing EET formulas (distance to shore [statute miles] and annual emissions [TPY]). These are parameters operators actively know about their operations and already provided to BOEM in their plans and therefore do not represent an additional burden for the operators. For the short-term NAAQS, it may prove beneficial for BOEM to move to using the maximum hourly rate, as opposed to the total annual emissions, as the modeled rate for these standards is based off the maximum hourly rate.

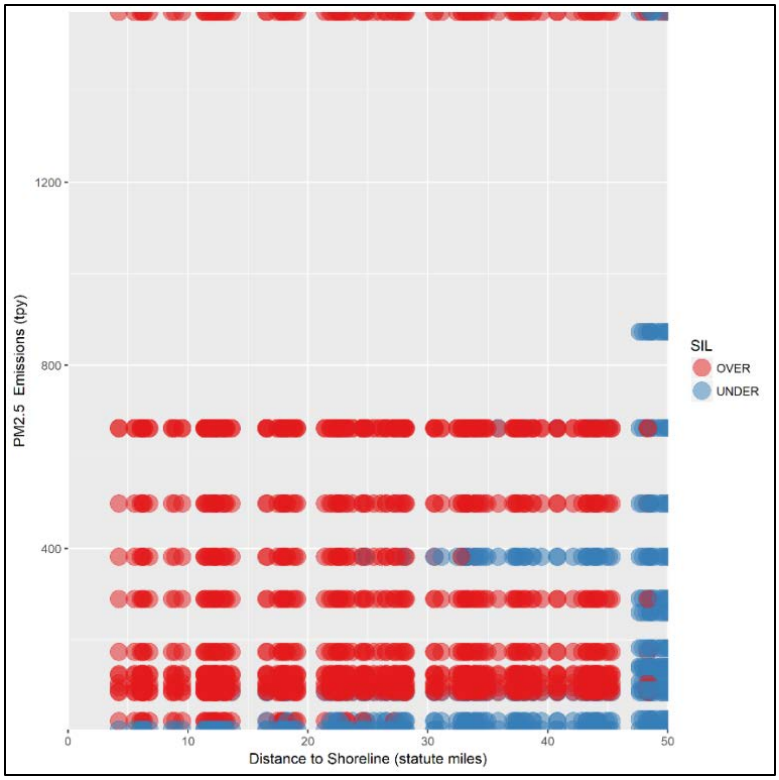

Figure 5-15. $PM_{2.5}$ 24-Hour Modeling Results, Zoomed to First 50 km
Red circles indicate combination modeling runs that estimated impacts above the SIL, while blue circles represent estimates below the SIL.

5.10.4.1 Supplemental Modeling Data

To facilitate the development of a revised EET, ERG modeled additional sources to supplement the evaluation dataset. These new runs were conducted for single sources at lower emission rates to better define the transition between categories in the nearshore environment. The additional sources include single-source runs at a unit emission rate (1 g/s). The single sources included a cold stack (1C), a hot stack (1P), a vessel modeled as a point source (1X), and a single vessel as a volume source (1V). The 1C source parameters for a short vent, which is based on select permits with low-level cold release vents. The 1P source parameters matches the natural gas engine parameters used in study's modeling inventory. The 1X source uses stack parameters based on those used in the USEPA modeling studies (Mason et al., 2008), which were based on several inventory sources. Table 5-23 summarizes the stack parameters for the point sources.

For the 1V source parameters, vessel dimensions needed to define volume sources were obtained from the PortVision AIS database (developed in BOEM's Year 2014 Gulfwide Emissions Inventory Study) based on vessels known to operate in the GOMR. These dimensions were used to determine the average dimension for each vessel type. These average vessels were then merged to produce an average vessel for modeling. Table 5-24 lists the volume source parameterization.

Runs were conducted at all the synthetic source locations along in the near shore environment (i.e., first 5 contours of Figure 5-4). Figure 5-16 shows the original evaluation runs with the supplemental runs. Compared to Figure 5-15, there are fewer gaps in the nearshore and low- and mid-emission ranges.

Table 5-23. Single-Source Scenario Point Source Parameters

Scenario	Stack parameter			
	Height (ft)	Diameter (ft)	Temperature (F)	Velocity (ft/sec)
Cold stack (1C)	39.3	2.4	– [a]	34.4
Hot stack (1P)	94.3	1.4	1,037.8	140.2
Vessel as points (1X)	65.5	2.6	539.6	82.0

[a] Modeled at ambient temperature based on meteorological inputs.

Table 5-24. Single-Source Scenario Volume Source Parameters

Scenario	Stack parameter		
	Height (ft)	Sigma Y(ft)	Sigma Z (ft)
Single volume source (1V)	16.4	328.1	16.4

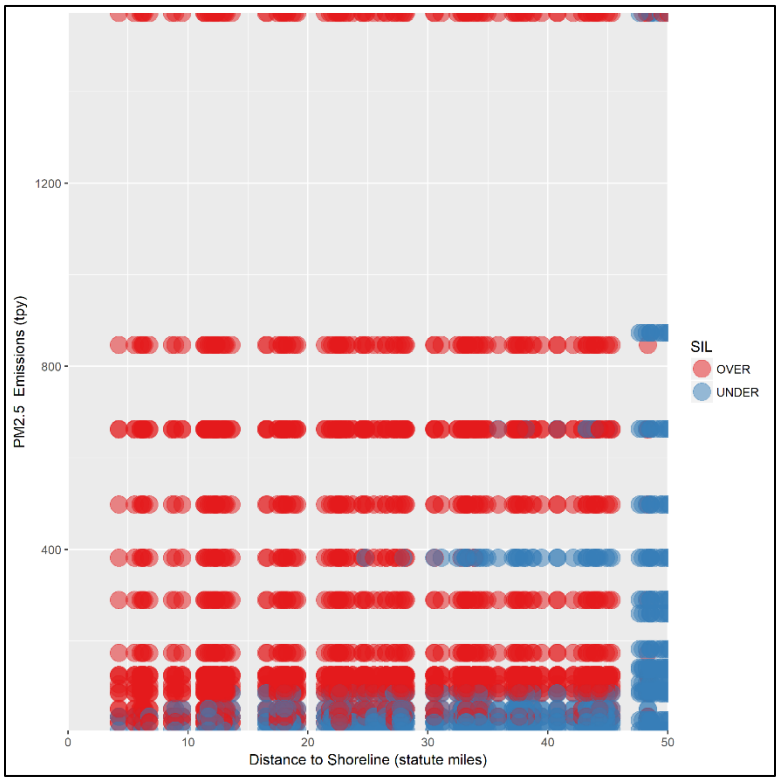

Figure 5-16. $PM_{2.5}$ 24-Hour Modeling Results, with Supplemental Data
Red circles indicate combination modeling runs that estimated impacts above the SIL, while blue circles represent estimates below the SIL.

5.10.4.2 Revised Classification Methods

ERG used the *R* statistical software to classify various modeling functions. The code primarily uses the standard regression functions and the *caret* package (**C**lassification **A**nd **RE**gression **T**raining).[18] For each method tested, both the distance to shore and total annual emissions in TPY were used as predictors of whether the source would model above the SIL.

[18] The *caret* package is available at: https://CRAN.R-project.org/package=caret.

ERG ran each method with a five-fold cross-validation process. In this process, the dataset is evenly divided into five subsets. The code estimates the statistical model with four of the five subsets, and then tests the model with the withheld subset to quantify model accuracy. This is repeated for each of the subsets, so each of the five subsets is used only once in validation to ensure any developed exemption threshold models appropriately screen the different platform scenarios.

5.10.4.2.1 Linear Regression Analysis

ERG initially attempted to develop a linear boundary to discern the over/under SIL decision. ERG used *R*'s generalized linear model (glm) function to generate a multivariate linear model using both distance to shore and total emissions to predict the impact concentration:

$$Impact\ Concentration = a(D) + b(E)$$

Where D is distance to shore in statute miles, E is total annual emission in TPY, and a and b are derived coefficients. The function solves for the best values of the equation's coefficients. The equation was then rearranged to solve for D, substituting in the level of the SIL:

$$D = \frac{b(E)}{-a} + \frac{(-SIL)}{-a}$$

Figure 5-17 shows the results of the linear regression analysis for the $PM_{2.5}$ 24-hour NAAQS, based on a final formula of:

$$E = 1.87D + 52.17$$

The figure shows the original EET formula (black line) and the linear revision (orange line). Points below the line would have been exempted from modeling, while those above would have been required to model. For the revised linear formula, more of the location modeled above the SIL (red circle) does fall above the line. This is reflected in the higher pass rate in Table 5-25. However, there is an increase in the false positive errors, particularly for sources farther out to sea, as seen in a number of blue circles above the orange line to the right side of the graph.

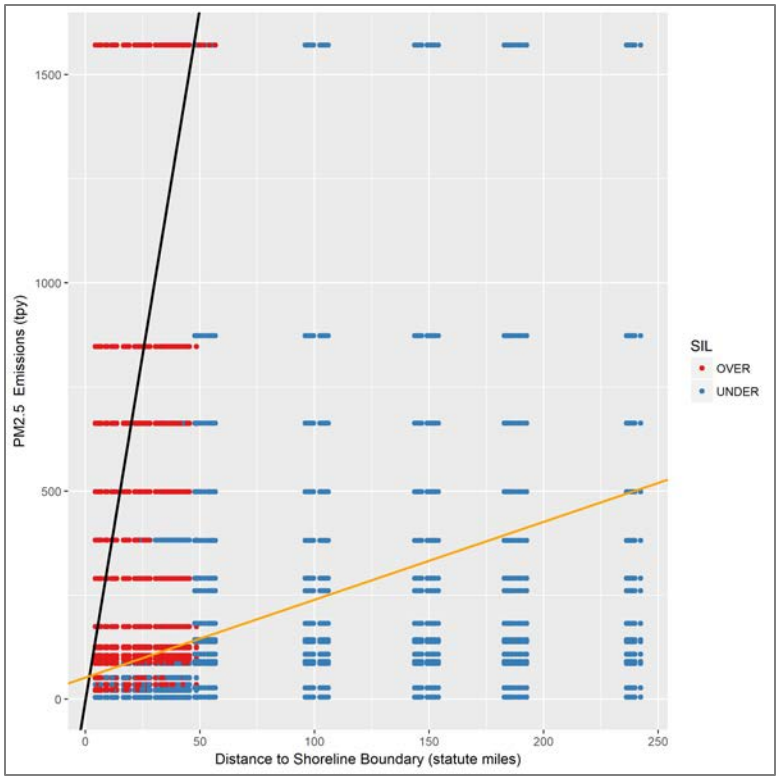

Figure 5-17. Linear Regression Analysis for the $PM_{2.5}$ 24-Hour Modeling Results
Red circles indicate combination modeling runs that estimated impacts above the SIL, while blue circles represent estimates below the SIL. The black line indicates the original EET formula (33.3*D), while the orange line shows the equations tested.

Table 5-25. Comparison of Linear Model Outcomes to the Original EET

Formula ID (Color)	False Positive	False Negative	Pass	Formula
Original (black)	0.00%	38.01%	61.99%	33.3*D
EQL1 (orange)	16.44%	13.51%	70.05%	1.87*D+52.17

5.10.4.2.2 Nonlinear Regression Analysis

Visual inspection of the data suggests a quadratic or cubic function might better represent the decision boundary. These functions asymptotically approach zero but have a sharper upward turn, which could improve the false positive rate from the linear models.

ERG fit an initial cubic function to the data using the nonlinear least squares (nls) function in *R*. the nls functions determine the nonlinear (weighted) least squares estimates of the parameters of an initial nonlinear model. The nls analysis started with the initial form of

$$Impact\ Concentration = (aD)^2$$

The nls results were then plotted and manually tweaked to better capture the decision boundary. Figure 5-18 shows the equation overlaid with the data, and Table 5-26 summarizes the revised outcomes. The formula is a better fit than the linear models for replicating passes, including capturing passes for low emission rates in the nearshore environment.

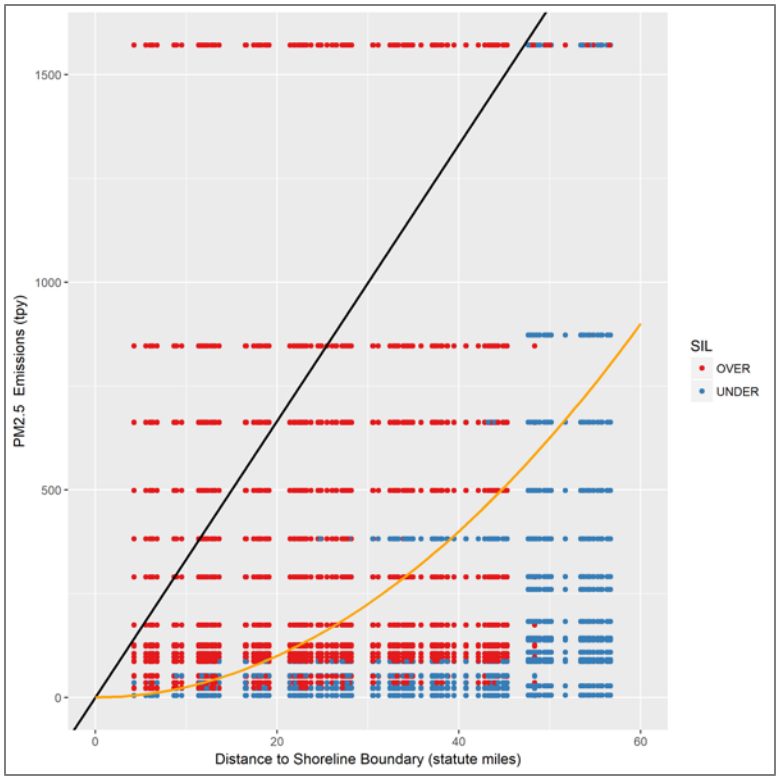

Figure 5-18. Quadratic Regression Analysis for the $PM_{2.5}$ 24-Hour Modeling Results
Red circles indicate combination modeling runs that estimated impacts above the SIL, while blue circles represent estimates below the SIL. The black line indicates the original EET formula (33.3*D), while the orange line shows the equations tested.

Table 5-26. Comparison of Quadratic Model Outcomes to the Original EET

Formula ID (plot color)	False Positive	False Negative	Pass	Formula
Original (black)	0.00%	38.01%	61.99%	33.3*D
EQ_Q1 (orange)	3.04%	18.39%	78.57%	$(0.5*D)^2$

Based on the results shown in Figure 5-18, ERG pursued a function form that could more slowly increase from zero, but then produce a rapid upward turn as it approached 45 miles from the shoreline. A series of cubic functions were tested to see if the outcome would improve. ERG fit an initial cubic function to the data using the nls function in *R*, using the following form:

$$Impact\ Concentration = (aD)^3$$

Like the quadratic fit, this was plotted and then manually tuned to improve the fit to the decision boundary. Figure 5-19 shows three versions attempted, with the outcomes summarized in Table 5-27. Like the quadratic equation, the percentage of pass and false positive results increased, while the miss rate decreased. The three models are also extreme in their response, in that any outcome that is not a pass largely falls into either the false negative or false positive error type as opposed to being distributed across both.

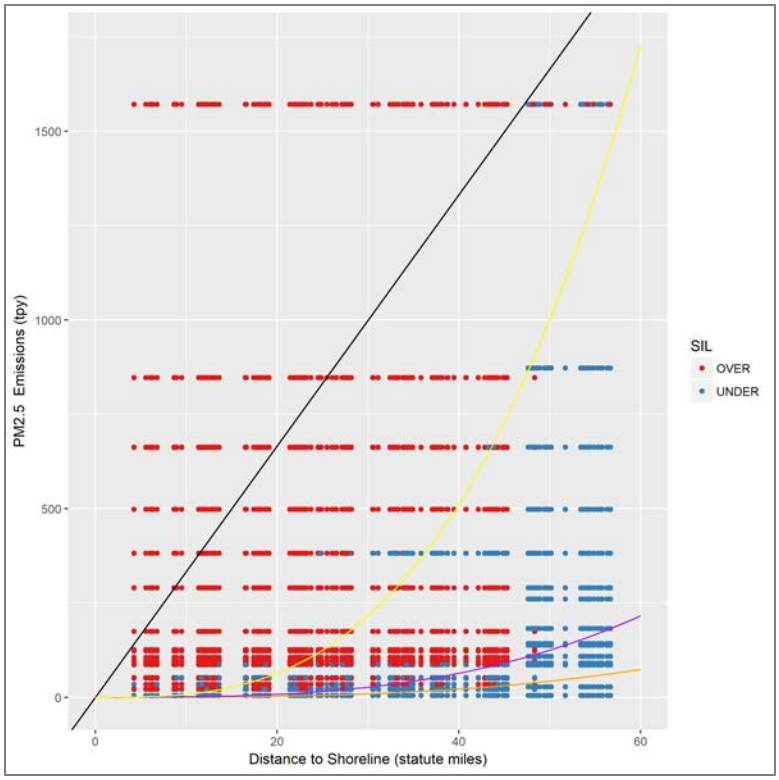

Figure 5-19. Cubic Regression Functions of the $PM_{2.5}$ 24-Hour Modeling Results
Red circles indicate combination modeling runs that estimated impacts above the SIL, while blue circles represent estimates below the SIL. The black line indicates the original EET formula (33.3*D), while the colored lines show other equations tested.

Table 5-27. Comparison of Cubic Model Outcomes to the Original EET

Equation ID	False Positive	False Negative	Pass	Formula
EQ_Q3 (purple)	15.53%	1.31%	83.16%	$(.1*D)^3$
EQ_Q2 (yellow)	2.76%	16.27%	80.97%	$(.2*D)^3$
EQ_Q10 (orange)	26.55%	0.02%	73.43%	$(.07*D)^3$
Original EET (black)	0.00%	38.01%	61.99%	33.3*D

As before, ERG used the nls function to fit an initial logistic curve, with the nls function estimating values for the three theta coefficients:

$$Impact\ Concentration = \frac{theta1}{(1 + e^{(-(theta2+theta3*D))})}$$

ERG then adjusted the initial model to fit the decision boundary and provide additional options. Figure 5-20 shows the equations plotted against the modeled data, with Table 5-28 summarizing the revised outcomes. The pass rate is consistent with other functional forms; however, the remaining data are more evenly distributed between false positive and false negative outcomes.

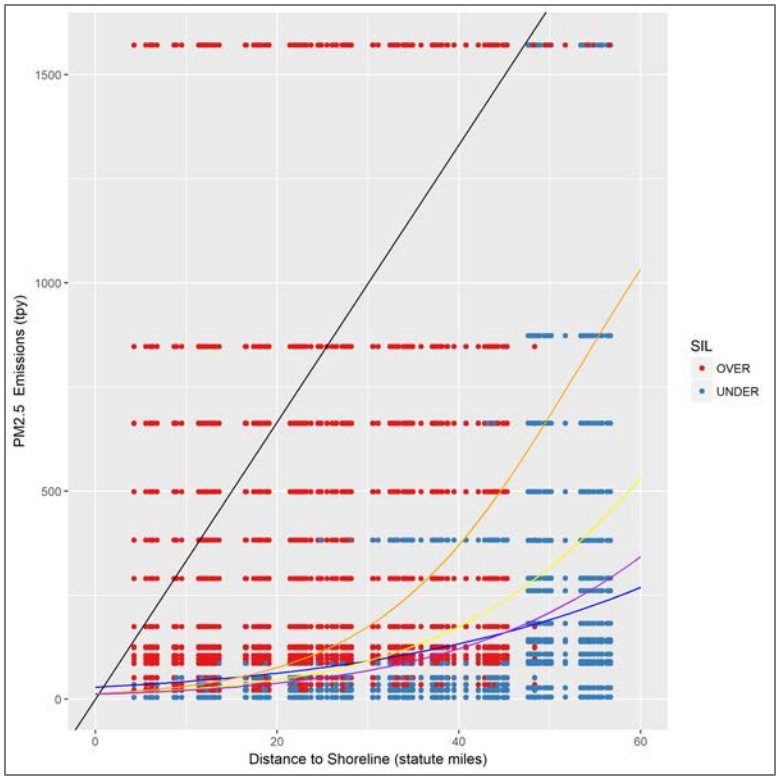

Figure 5-20. Logistic Regression Functions of the $PM_{2.5}$ 24-Hour Modeling Results
Red circles indicate combination modeling runs that estimated impacts above the SIL, while blue circles represent estimates below the SIL. The black line indicates the original EET formula (33.3*D), while the colored lines show other equations tested.

Table 5-28. Comparison of Logistic Model Outcomes to the Original EET

Row Labels	False Positive	False Negative	Pass	Formula
EQ_Q7 (purple)	8.33%	8.35%	83.33%	(1600/(1 + exp(-(-4.9 + 0.06*D))))
EQ_Q6 (yellow)	6.68%	10.56%	82.75%	(1600/(1 + exp(-(-4.9 + 0.07*D))))
EQ_Q5 (orange)	2.93%	17.01%	80.07%	(1600/(1 + exp(-(-4.8 + 0.09*D))))
EQ_Q4 (blue)	9.02%	11.13%	79.85%	(1600/(1 + exp(-(-4.0 + 0.04*D))))
Original EET (black)	0.00%	38.01%	61.99%	33.3*D

5.10.4.2.3 Classification and Regression Tree Analysis

ERG also conducted classification and regression tree (CART) analyses to develop classification decision trees for each NAAQS. A classification decision tree predicts whether a new source will produce a significant impact during air quality modeling and is composed of if-then conditions that lead to a classification prediction. The conditions are determined via a recursive portioning method, based on specified predictor variables.

For the EET analysis, ERG developed decision trees based on the distance to shore and total annual emissions. Figure 5-21 shows the decision region and boundary for the $PM_{2.5}$ 24-hour NAAQS decision tree. The CART analysis captured the low emission source near shore as under the SIL, unlike the other

options. The decision tree (Figure 5-22) has four if-then decisions that resulted in the four final bins at the bottom of the figure. These if-then decisions can be easily coded in the EP and DOCD worksheets using "if statements" to arrive at each bin. Table 5-29 compares the outcomes from the CART analysis to the original EET. The CART analysis performed very well, with a higher pass rate (92 percent) that the regression models. Appendix E.8 presents the results of the EET CART analyses conducted for all NAAQS.

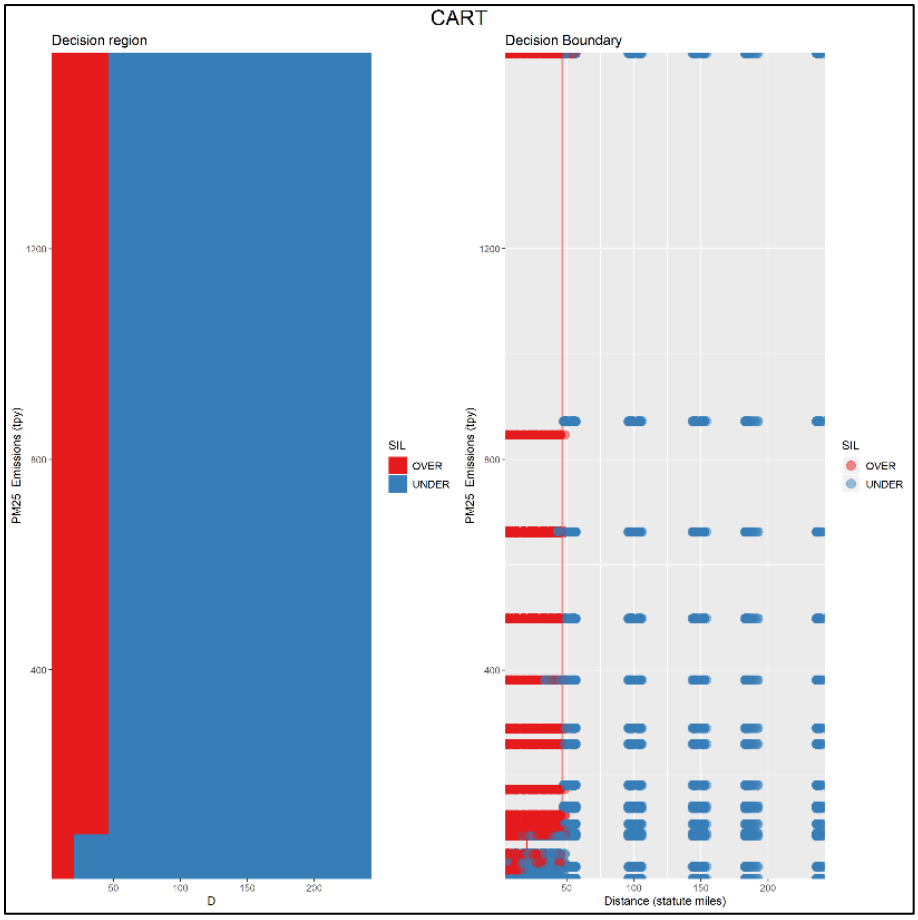

Figure 5-21. CART Analysis for the $PM_{2.5}$ 24-Hour Modeling Results
The plot on the left shows the determine-decision regions, with red shading indicating results above the SIL, and blue shading below. The plot on the right shows the decision boundary (red line) overlaid on the original data.

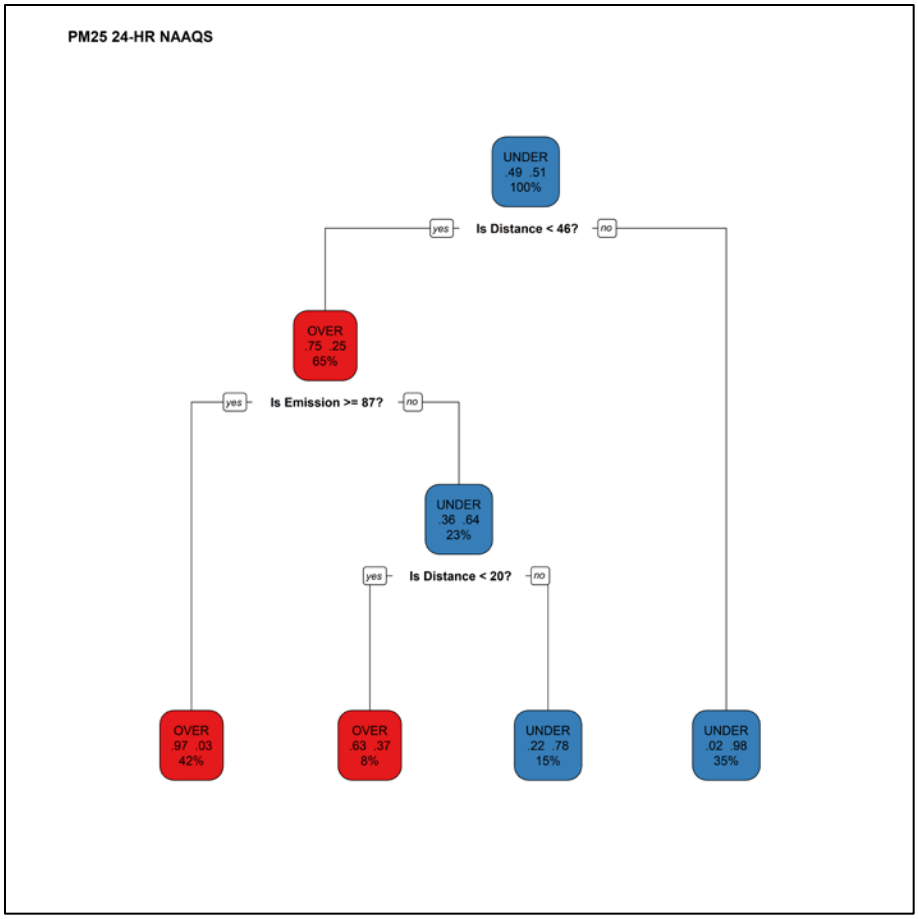

Figure 5-22. CART Decision Tree for the $PM_{2.5}$ 24-Hour Modeling Results
At each decision point, the branch to the right indicates a response of "no." The boxes at each decision point indicate the probability that the source is over (middle row, left) or under (middle row, right) the SIL, and the percentage of the total values in the bin (bottom).

Table 5-29. Comparison of CART Outcomes to the Original EET for the $PM_{2.5}$ 24-Hour NAAQS

Formula ID	False Positive	False Negative	Pass	Formula
Original	0.00%	36.27%	63.73%	33.3*D
CART	4.27%	3.93%	91.80%	– [a]

[a] The CART tool is a decision tree coded as a series of nested "if statements" to calculate false positive, false negative, and pass rates.

5.10.5 Other Revision Options

An alternative approach to the EET formulas would be to use the modeling information from this task to estimate impacts based on comparable modeled sources. For example, an operator could identify a hypothetical source modeling run at a comparable emission rate and distance to shore as the proposed source to evaluate the likelihood of a significant impact. If the comparable hypothetical source impacts are below SIL values, the proposed source should be as well. Because ERG did not model all possible iterations of emission levels and distances to shore, there would have to be concessions in matching to ensure a protective estimate (i.e., conservatively high estimate of impact). For example, a comparable source should select a hypothetical source with higher emission rates in the absence of an exact match.

The results from any modeling submitted to BOEM could also be added to the database to provide additional sources for comparison. Additionally, the database does include unit emission rate source (i.e., 1 gs^{-1}) impact runs for three source types: 1) elevated hot stack, 2) short cold stack, and 3) vessel characterized as a volume (used in this study for sensitivity purposes). These results could be scaled and combined to estimate a more comparable emissions rate.

5.11 Summary

In this task, dispersion and photochemical modeling results were used to evaluate the efficacy of the existing EET formulas that are currently used by BOEM as a screening tool to determine whether modeling is necessary for submitted plans. Several locations throughout the GOMR were selected to conduct modeling at varying emission levels that are representative of the emission ranges seen in OCS sources. The dispersion modeling was designed to mimic the modeling that would be required by BOEM, with the results then compared to the results of the EET formulas to determine whether the EET formulas accurately predicted the need for modeling. The short-term NAAQS EET formula results were a mixed bag of results in that most pollutants saw both false positive and false negative errors. The false negative error rates (i.e., the impact was over the SIL, but the formula determined that modeling not necessary) were higher than the false positive rates and ranged from 2% for the NO_2 1-hour NAAQS to 34% for $PM_{2.5}$ 1-hour NAAQS.

For the annual NAAQS, the current EET formulas produce no false negatives and only false positive errors for all pollutants. That is, the EET formulas called for modeling when an impact larger than the SIL was not seen. The false positive errors were especially common at distance greater than 50 mi to the shoreline.

Results that considered the state seaward boundary were similar, with the caveat that the CALPUFF far-field modeling was performed with vessels characterized as point sources as opposed to volume sources.

As outlined in Section 5.10.5, BOEM has several options they can consider for moving forward for reformulation of the existing EET formulas, including a CART tool. BOEM should also consider moving away from the annual total emissions for the pollutants with a short-term NAAQS and consider using the maximum hourly emission rate as the modeled emission rate would be derived from this value. The analysis shows that additional OCS emissions scenarios should be modeled to further quantify the variability in impacts from different OCS equipment mixes. Any future modeling efforts could focus on more emission scenarios at fewer locations in the GOMR.

Photochemical modeling was used to evaluate the impact of single sources on secondary ozone and particulate matter formation. The modeling showed limited secondary formation of either pollutant based on the emission levels tested.

5.12 References

Brashers, B., C. Emery. 2014. Draft User's Manual. The Mesoscale Model Interface Program (MMIF) Version 3.1, 2014-06-06. Prepared for OAQPS, Research Triangle Park, NC 27711, USEPA Contract No. EP-D-07-102, Work Assignments 2-06, 4-06, 5-08, and 10-1. August 2014. Internet address: http://www.epa.gov/ttn/scram/models/relat/mmif/MMIFv3.1_Users_Manual.pdf

Byun, D.W., J.K.S. Ching, eds. 1999. Science algorithms of the EPA Models-3 community multiscale air quality (CMAQ) modeling system. EPA/600/R-99/030, March 1999. Internet address: http://www.epa.gov/AMD/CMAQ/CMAQdocumentation.html

Chang, J.C., K.J. Hahn. 1997. User's Guide for the Offshore and Coastal Dispersion (OCD) Model Version 5. MMS Contract No. 1435-96-PO-51307, November, 1997. Internet address: http://www.epa.gov/ttn/scram/dispersion_prefrec.htm#ocd

Cole, H.S., J.E. Summerhays. 1979. A Review of Techniques Available for Estimation of Short-Term NO_2 Concentrations. Journal of the Air Pollution Control Association, 29(8): 812–817.

Colella, P., P.R. Woodward. 1984. The Piecewise Parabolic Method (PPM) for Gas-dynamical Simulations. J. Comp. Phys., 54, 174-201.

Dabberdt, W.F., R. Brodzinsky, B.C. Cantrell, R.M. Trudeau. 1982. Atmospheric Dispersion Over Water and In The Shoreline Transition Zone, Final Report Volume II: Data. Prepared for American Petroleum Institute by SRI International, Menlo Park, California, 94025.

DiCristofaro, D.C., S.R. Hanna. 1989. OCD The Offshore and Coastal Dispersion Model, Version 4, Volume I: User's Guide. MMS Contract No. 14-12-001-30396.

ENVIRON. 2012. Dallas-Fort Worth Modeling Support: Improving Vertical Mixing, Plume-in Grid, and Photolysis Rates in CAMx, Prepared for: Texas Commission on Environmental Quality. August. Internet address: https://www.tceq.texas.gov/assets/public/implementation/air/am/contracts/reports/pm/5821110365FY1206-20120820-environ_dfw_modeling_support.pdf

ENVIRON. 2014. User's Guide – Comprehensive Air Quality Model with Extensions – Version 6.10. ENVIRON International Corporation, Novato, California. Internet address: http://www.camx.com.

Golder, D. 1972. Relations among Stability Parameters in the Surface Layer. Boundary Layer Meteor., 3, 47-58.

Gryning, S-E. 1985. The Øresund Experiment—A Nordic Mesoscale Dispersion Experiment Over a Land-Water-Land Area. Bull. Amer. Meteor. Soc., 66, 1403–1407. Internet address: http://dx.doi.org/10.1175/1520-0477(1985)066<1403:TENMDE>2.0.CO;2

Hanrahan, P.L. 1999. The Plume Volume Molar Ratio Method for Determining NO_2 / NO_X Ratios in Modeling—Part I: Methodology. J. Air & Waste Manage. Assoc., 49: 1324–1331.

Hertel O., R. Berkowics, J. Christensen, O. Hov. 1993. Test of two numerical schemes for use in atmospheric transport-chemistry models. Atmos. Environ., 27, 2591-2611.

Hildebrandt Ruiz, L., G. Yarwood. 2013. Interactions between organic aerosol and NOy: Influence on oxidant production. Final Report prepared for the Texas AQRP (Project 12-012) by the University of Texas at Austin and ENVIRON International Corporation, Novato, CA. Internet address: http://aqrp.ceer.utexas.edu/projectinfoFY12_13/12-012/12-012%20Final%20Report.pdf.

Hong, S.Y., Y. Noh. 2006. A New Vertical Diffusion Package with an Explicit Treatment of Entrainment Processes. Monthly Weather Review, 134, 2318-2341.

Johnson, V.C., T.C. Spangler. 1986. Tracer Study Conducted to Acquire Data for Evaluation of Air Quality Dispersion Models, prepared by WESTEC Services, Inc., San Diego, CA for API, Washington.

Kemball-Cook, S., G. Yarwood, J. Johnson, B. Dornblaser, M. Estes. 2015. Evaluating NO_x Emission Inventories for Regulatory Air Quality Modeling Using Satellite and Air Quality Model Data. Atmospheric Environment, 117: 1-8, doi: 10.1016/j.atmosenv.2015.07.002.

Mason, R., P. Dolwick, P. Carey, E. Kinnee, M. Wilson. 2008. Emissions processing and sensitivity air quality modeling of category 3 commercial marine vessel emissions. In: Proceedings from 17th Annual International Emission Inventory Conference, Portland, OR.

Morris, R.E., R.C. Kessler, S.G. Douglas, K.R. Styles, G.E. Moore. 1988. Rocky Mountain Acid Deposition Model Assessment: Acid Rain Mountain Mesoscale Model (ARM3). U.S. Environmental Protection Agency, Atmospheric Sciences Research Laboratory, Research Triangle Park, NC.

Nopmongcol, O., B. Koo, L. Parker, J. Jung, G. Yarwood. 2014. Comprehensive Air Quality Model with extensions (CAMx) inputs to Community Model for Air Quality (CMAQ) Inputs Converter. Final Report prepared for Jim Smith, TCEQ. August.

Ramboll Environ. 2016. CAMx User's Guide: Comprehensive Air Quality Model with Extensions, Version 6.40. Ramboll Environ, Novato, CA. Internet address: www.camx.com.

Richmond, K., R. Morris. 2012. Draft User's Manual: AERCOARE Version 1.0. Prepared for USEPA Region 10, 1200 Sixth Avenue, Seattle, WA 98101, EPA Contract EP-D-08-102, Work Assignment 5-17, EPA 910-R-12-007, October 2012. Internet address: http://www.epa.gov/ttn/scram/models/relat/aercoare/AERCOAREv1_0_Users_Manual.pdf

Schacher, G.E., K.L. Davidson, C.W. Fairall. 1982. Atmospheric Marine Boundary Layer Convective Mixing Velocities in the California Coastal Region. Atmos. Environ., 16, 1183-1192.

Scire, J.S., D.G. Strimaitis, R.J. Yamartino. 2000. A User's Guide for the CALPUFF Dispersion Model (Version 5). Earth Tech, Inc., Concord, Massachusetts.

Seinfeld, J.H., S.N. Pandis. 1998. Atmospheric Chemistry and Physics: From Air Pollution to Climate Change. John Wiley and Sons, Inc., NY.

Smagorinsky, J. 1963. General Circulation Experiments with the Primitive Equations: I. The Basic Experiment. Mon. Wea. Rev., 91, 99-164.

Sykes, R.I., S.F. Parker, D.S. Henn, C.P. Cerasoli, L.P. Santos. 1998. PC-SCIPUFF Version 1.2PD Technical Documentation. ARAP Report No. 718. Titan Corporation, Titan Research & Technology Division, ARAP Group, P.O. Box 2229, Princeton, NJ.

U.S. Census Bureau. 2014a. Cartographic Boundary Shapefiles [cb_2014_us_state_500k]. Washington, D.C.: Bureau of the Census, 2014. Internet address: https://www.census.gov/geo/maps-data/data/cbf/cbf_state.html

U.S. Census Bureau. 2014b. Cartographic Boundary Shapefiles [cb_2014_us_state_20m]. Washington, D.C.: Bureau of the Census, 2014. Internet address: https://www.census.gov/geo/maps-data/data/cbf/cbf_state.html

USDA (U.S. Department of Agriculture). 2011. Memorandum of Understanding among the U.S. Department of Agriculture, U.S. Department of The Interior, and U.S. Environmental Protection

Agency, Regarding Air Quality Analyses and Mitigation for Federal Oil And Gas Decisions Through the National Environmental Policy Act Process.

USDOI, BOEM (U.S. Department of the Interior, Bureau of Ocean Energy Management). 2015. Active Lease Polygons [shapefile]. Geographic Mapping Data in Digital Format. Internet address: https://www.data.boem.gov/Main/Mapping.aspx (accessed June 02, 2015).

U.S. Environmental Protection Agency (USEPA). 1995. SCREEN3 Model User's Guide. September 1995., Publication No. EPA-454/B-95-004. Office of Air Quality Planning and Standards, Research Triangle Park, NC. Internet address: https://www3.epa.gov/ttn/scram/userg/screen/screen3d.pdf

USEPA. 1998. Interagency Workgroup on Air Quality Modeling (IWAQM) Phase 2 Summary Report and Recommendations for Modeling Long Range Transport Impacts, EPA-454/R-98-019, December 1998. Internet address: http://www.epa.gov/scram001/7thconf/calpuff/phase2.pdf

USEPA. 2004a. User's Guide for the AERMOD Terrain Preprocessor (AERMAP). Publication No. EPA-454/B-03-003. OAQPS, Research Triangle Park, NC, September 2004.

USEPA. 2004b. User's Guide for the AERMOD Meteorological Preprocessor (AERMET). Publication No. EPA-454/B-03-002. OAQPS, Research Triangle Park, NC, November 2004.

USEPA. 2004c. User's Guide for the AMS/EPA Regulatory Model – AERMOD. Publication No. EPA-454/B-03-001. OAQPS, Research Triangle Park, NC, September 2004.

USEPA. 2004d. AERMOD: Description of Model Formulation. EPA-454/R-03-004. U.S. Environmental Protection Agency, Research Triangle Park, North Carolina 27711.

USEPA. 2010a. "Applicability of Appendix W Modeling Guidance for the 1-hour NO_2 National Ambient Air Quality Standard." June 28, 2010 memorandum from Tyler Fox to Regional Air Division Directors.

USEPA. 2010b. "Guidance Concerning the Implementation of the 1-hour SO_2 NAAQS for the Prevention of Significant Deterioration Program." August 23, 2010 memorandum from Steven Page to Regional Air Division Directors. https://www.epa.gov/sites/production/files/2015-07/documents/appwso2.pdf

USEPA. 2011a. Memorandum: COARE Bulk Flux Algorithm to Generate Hourly Meteorological Data for Use with the AERMOD Dispersion Program; Section 3.2.2.e Alternative Refined Model Demonstration. From Herman Wong, USEPA Regional Office Modeling Contact to Tyler Fox, Lead Air Quality Modeling Group, Office of Air Quality Planning and Standards. April 1, 2011.

USEPA. 2011b. Memorandum: Model Clearinghouse Review of AERMOD-COARE as an Alternative Model for Application in an Arctic Marine Ice Free Environment. From George Bridgers, USEPA Model Clearinghouse Director, to Herman Wong, USEPA Regional Atmospheric Scientist, Office of Environmental Assessment, OEA-095, USEPA Region 10, May 6, 2011.

USEPA. 2014a. Clarification on the Use of AERMOD Dispersion Modeling for Demonstrating Compliance with the NO_2 National Ambient Air Quality Standard. September 30, 2011 memorandum from R. Chris Owen and Roger Brode to Regional Dispersion Modeling Contacts.

USEPA. 2014b. Guidance for $PM_{2.5}$ Modeling. May 20, 2014, Publication No. EPA-454/B-14-001. Office of Air Quality Planning and Standards, Research Triangle Park, NC. Internet address: http://www.epa.gov/ttn/scram/guidance/guide/Guidance_for_PM25_Permit_Modeling.pdf.

USEPA. 2011c. Permit No. OCS-EPA-R4006. Permit to Construct and Operate Under the Outer Contental Shelf Air Regulations. USEPA Region 4, Atlanta, GA. Internet address: https://www.epa.gov/sites/production/files/2015-08/documents/shell-final_permit_112811_clean.pdf.

USEPA. 2011d. Permit No. OCS-EPA-R4007. Permit to Construct and Operate Under the Outer Contental Shelf Air Regulations. USEPA Region 4, Atlanta, GA. Internet address: https://www.epa.gov/sites/production/files/2015-08/documents/eni_final_permit-10.27.2011.pdf.

USEPA. 2012. Permit No. OCS-EPA-R4009. Permit to Construct and Operate Under the Outer Contental Shelf Air Regulations. USEPA Region 4, Atlanta, GA. Internet address: https://www.epa.gov/sites/production/files/2015-08/documents/murphy_final_permit-051112-clean_0.pdf.

USEPA. 2013. Permit No. OCS-EPA-R4008-M1. Permit to Construct and Operate Under the Outer Contental Shelf Air Regulations. USEPA Region 4, Atlanta, GA. Internet address: https://www.epa.gov/sites/production/files/2015-08/documents/bhpbminormodification_r4008-m1_webversion.pdf.

USEPA. 2015a. Proposed Approach for Demonstrating $PM_{2.5}$ PSD Compliance. Memorandum from Tyler J Fox, USEPA/OAQPS to Docket No. EPA-HQ-OAR-2015-0310. (June 30).

USEPA. 2015b. Proposed Approach for Demonstrating Ozone PSD Compliance, Memorandum from Tyler J Fox, USEPA/OAQPS to Docket No. EPA-HQ-OAR-2015-0310. (June 30).

USEPA. 2015c. Guidance on the Use of Models for Assessing the Impacts from Single Sources on Secondarily Formed Pollutants Ozone and $PM_{2.5}$. Office of Air Quality Planning and Standards. EPA 454/P-15-001.

USEPA. 2016a. Guidance on Significant Impact Levels for Ozone and Fine Particles in the Prevention of Significant Deterioration Permitting Program, Memorandum from Tyler J Fox, EPA/OAQPS to Regional Air Division Directors. (August 1)

USEPA. 2016b. Draft $PM_{2.5}$ Precursor Demonstration Guidance. Office of Air Quality Planning and Standards. EPA-454/P-16-001.

USEPA. 2016c. Guidance on the Development of Modeled Emission Rates for Precursors (MERPs) as a Tier l Demonstration Tool for Ozone and $PM_{2.5}$ under the PSD Permitting Program. Office of Air Quality Planning and Standards. EPA-454/R-16-006.

USEPA. 2018. “Guidance on Significant Impact levels for Ozone and Fine Particulates in the Prevention of Significant Deterioration Permitting Program.” April 17, 2018 memorandum from Peter Tsirigotis to Regional Air Division Directors. https://www.epa.gov/sites/production/files/2018-04/documents/sils_policy_guidance_document_final_signed_4-17-18.pdf

Wilson, D., R. Billings, R. Chang, H. Perez, J. Sellers. 2014. Year 2011 Gulfwide Emissions Inventory Study. U.S. Dept. of the Interior, Bureau of Ocean Energy Management, Gulf of Mexico OCS Region, New Orleans, LA. OCS Study BOEM 2014-666.

Yarwood, G., T. Sakulyanontvittaya, U. Nopmongcol, B. Koo. 2014. Ozone Depletion by Bromine and Iodine over the Gulf of Mexico. Final Report prepared for the Texas Commission on Environmental Quality, Austin, Texas (November 2014).

Zhang, L., S. Gong, J. Padro, L. Barrie. 2001. A size-segregated particle dry deposition scheme for an atmospheric aerosol module. Atmos. Environ., 35, 549-560.

Zhang, L., J.R. Brook, R. Vet. 2003. A revised parameterization for gaseous dry deposition in air-quality models. Atmos. Chem. Phys., 3, 2067-2082.

6 Uncertainty and Recommendations

The results presented in this report are based on numerical simulations of complex atmospheric processes. Such simulations can only be feasibly performed by making numerous assumptions and approximations, which collectively contribute to uncertainties in the results. Uncertainties arise from limitations in both model inputs and model formulations. For example, emission inputs to chemical transport models such as those used in this study represent only rough approximations to the actual spatial and temporal emissions, and the gas and particulate phase chemical mechanisms contained in these models do not reliably simulate the vast complexity of atmospheric chemical processes under all conditions. Although widely used and generally accepted state-of-the-art models and modeling procedures were used in this study, it must be recognized that the results are subject to significant levels of uncertainty. However, given the extremely large number of model inputs and parameters and their nonlinear interactions, it is not feasible to conduct a rigorous and comprehensive uncertainty analysis. We instead focus here on areas of uncertainties that are of particular significance to simulations of air quality impacts from offshore oil and gas sources in the GOM. Recommendations specific to activities that BOEM could undertake primarily focus on the magnitude of the modeled ozone concentrations (as well as uncertainties in the modeled PM concentrations) in the GOMR; a long-term research goal should be the collection of more offshore data that can be used in the meteorological and photochemical MPEs.

BOEM is currently working with several other Federal agencies to conduct air quality research in the GOMR. BOEM and the USEPA formed the Overwater Team IWAQM to coordinate overwater modeling research. BOEM has also entered into an interagency agreement with the NASA Atmospheric Chemistry and Dynamics Lab to study the potential for using satellite data to monitor offshore air quality.

6.1 Meteorological Modeling

Past studies in the GOMR found that difficulties in the meteorological modeling had negative impacts on the performance of the photochemical modeling (McKeen et al., 2009; Djalalova et al., 2010; Lee et al., 2011). There are limitations in the ability of meteorological modeling to reproduce the depth of the marine boundary layer, estimate the extent of penetration of the sea breeze into the land environment, and estimate the extent of penetration of the land breeze into the marine environment.

To more fully test the meteorological data, it would be useful to investigate the ability to reproduce repetitive daily cycles. In particular, the ability to reproduce the land-sea breeze circulation with appropriate timing of onsets of direction changes may be useful, as this circulation is important for transportation of onshore emissions into the marine environment (and vice versa). Transport and dispersion, in the vertical as well as the horizontal dimension, of pollutant emissions are certainly very important.

The complex boundary layer structure in the land-sea interface depends critically on the vertical dimension; comparisons based on available radiosonde and profiler data sets may be useful in judging the meteorological modeling results. Much more extensive comparisons could be done with even a limited measurement program within the marine environment of the GOMR. In addition, though there are currently limited opportunities for comparisons between existing observational data sets and modeling results within the marine environment, limited comparisons could be done based upon observed and modeled meteorological relationships that are expected to be at least approximately constant over multiple years.

BOEM may pursue a tracer study in the GOMR. A tracer study involves the release of a nonreactive, traceable gas (usually sulfur hexafluoride [SF_6] or perfluorocarbons) from a source. Atmospheric concentrations are then monitored to characterize plume dispersion in and around the source. For BOEM,

attention could be paid to the area in and around an elevated platform to quantify the effects of building downwash and unique flow characteristics of an offshore platform (i.e., elevated solid building on a lattice or legged understructure, as opposed to a typical building that is solid down to the surface). This would provide an up-to-date data set for model performance comparisons for OCS sources. A tracer study could also be used to further the USEPA's investigation of downwash at platforms, which could lead to further improvements of AERMOD in the overwater environments. BOEM should consider including meteorological observations as part of a tracer study to 1) validate meteorological model performance over water and 2) provide a comparison dataset to model meteorology to verify that WRF meteorology accurately reproduces observed meteorological data in the overwater environment. An alternative to the tracer study would be a series of wind tunnel experiments that simulate the various wind flow scenarios around unique building characteristics of OCS sources. These results could be used validate and improve algorithms in air quality dispersion models.

6.2 Photochemical Grid Modeling

Modeling the offshore environment is also problematic due to the lack of air quality and meteorological data over the GOMR, limiting the ability to validate the photochemical model results over much of the inner (4-km grid resolution) modeling domain. Comparisons of model predictions with data from onshore measurement stations suggest that, with a few exceptions, model performance is mostly within limits generally accepted as representing acceptable performance for regulatory applications of regional air quality models. This does not, however, rule out the possibility of more significant model errors over water or along portions of the shoreline where monitoring data are scarce. Any unrecognized model deficiencies in these areas could lead to misinterpretation of model results in other portions of the domain.

Similar to past studies (see Travis et al., 2016, and references therein), models used in this study exhibited a tendency to overpredict ozone on average in the southeastern U.S. during July–September. Sources of this common model bias are not entirely clear; Travis et al. (2016) argue it may be related to overestimates of mobile source NO_x emissions, which would be consistent with the large NO_x overprediction bias observed in this study. Peak ozone levels over portions of the Gulf predicted in this study are higher than predicted and observed values on land, including within the Houston nonattainment area and other major urban areas as shown in Figure 4-32 of this report. In the absence of more data, it is not possible to directly verify the accuracy of these overwater ozone predictions. Although Berlin et al. (2013) and other researchers have found that background ozone concentrations transported into the Houston area are substantially lower when winds are from the GOM, this does not entirely remove the possibility of occasional high ozone events over portions of the Gulf. As noted in Section 4.7.1.2, sustained periods of onshore flow in the Western Gulf are associated with low ozone in the model; the predicted peak overwater ozone events are associated with preceding offshore advection of heavily polluted air followed by additional ozone production. Additional data are needed to resolve this issue. Future work might consider using back-trajectory models such as HYSPLIT to assess the origins of air parcels with high ozone.

As noted in Section 4.8, a significant source of uncertainty in modeling coastal environments is specification of the mass flux and size distribution of sea salt emissions. Comparisons of predicted and observed fine mode sodium concentrations within the 4-km domain indicate no large systematic bias but normalized mean errors are typically ~ 50% or more, suggesting that the current sea salt emissions model requires further improvement. This is of particular significance for evaluating impacts of proposed new sources of NO_x, as sodium nitrate may be an important contributor to visibility impairment and a significant proportion of nitrate may occur in the coarse (PM_{10}–$PM_{2.5}$) rather than the fine ($PM_{2.5}$) mode. Although the results of a sensitivity analysis (Appendix D.1) suggest that predicted fine particulate nitrate is not significantly lower when coarse mode nitrate formation is simulated using a simple PM modeling scheme, additional analysis is needed to confirm this conclusion.

Although the results of regional-scale modeling of ozone and PM at the 4-km horizontal grid resolution used in this study are unlikely to be overly sensitive to the treatment of sub-grid-scale plume dispersion from point sources (at least beyond the immediate vicinity of large point sources, which is not the focus of this study), less is known about plumes from overwater sources, which may frequently be subject to much lower levels of turbulent diffusion than is the case for sources on land. Due to the large number of overwater sources, computational constraints precluded our ability to explicitly resolve point source emissions using available plume-in-grid modeling algorithms in this study. However, sensitivity tests could be conducted to further explore this issue.

6.3 Development of Emissions Estimates

Developing emissions inventories and evaluating the uncertainty associated with inventories is an ongoing process in the air quality field. Overall, developing emissions estimates by combining emission factors with estimated activity levels does not accurately predict actual emissions when compared to direct source measurements. In the future, BOEM may consider expanding on past studies noted above and focus on directly measuring emissions associated with key oil and gas exploration and production NO_x sources in the GOMR. BOEM should continue to work collaboratively with the USEPA and other Federal agencies, state and local air quality agencies, and industry stakeholders to stay abreast of ongoing research in the emissions inventory activities in the GOMR.

Sensitivity analyses and top-down tests could be conducted to help identify and evaluate the relative importance of different sources of uncertainties. Top-down tests in particular are needed to ensure accurate modeling in the GOMR. A top-down test could compare the results of this study's photochemical grid and dispersion modeling with ambient measurements, satellite measurements of total column masses of pollutants, and measurements made by aircraft overflights. This type of assessment could determine whether the inventory correctly predicts that specific areas are experiencing increases or decreases in emissions. BOEM's interagency agreement with NASA will consist of top-down tests. The study goals include estimating criteria pollutant (and precursor) background concentrations, identifying pollutant concentrations in areas surrounding the largest emission sources in the GOMR, and validating photochemical modeling results at multiple vertical atmospheric heights. The results of this study will likely guide future BOEM air quality modeling studies.

There are also uncertainties in the magnitude of biogenic and geogenic emissions estimates, as well as the emission estimates developed for sources in Mexico. BOEM should keep abreast of ongoing studies in this area, notably studies conducted by TCEQ, the USEPA, and the Secretaría del Medio Ambiente y Recursos Naturales, (SEMARNAT), and incorporate updated emission estimates into future modeling studies.

6.4 EET Evaluation

The largest source of uncertainty in the EET modeling is in the representation of the universe of possible platform configurations and resulting emission levels possible from OCS sources. Factors such as emission release height and temperature can impact on how well a plume disperses. Although the scenarios used in the EET evaluation mimicked known equipment configurations, it is impossible to test all configurations. To mitigate such uncertainty, BOEM can treat the modeling database developed for this study as a living database. That is, as operators submit plans that include dispersion modeling, the results are added to the database for use in a refresh of the analysis. A simple refresh of the analysis can occur when the database grows by a significant number (e.g., when 100 new data points are added). With the updated database BOEM can again check to see if the pass/false and positive/false negative ratios for all pollutants are still acceptable. Additionally, BOEM can conduct a review of the triennial Gulfwide

emission inventories to determine if the synthetic source emission release parameters used are still representative, and if total platform emission levels are comparable to the modeled scenarios. In instances where the Gulfwide inventory is significantly different from the scenarios used in this study, BOEM should consider conducting additional modeling to ensure the EET formulas are performing in a satisfactory manner. BOEM should also consider revisiting the EET evaluation in the event of major shifts in the NAAQS. Specifically, if a NAAQS revision introduces an averaging time not represented in the modeling (e.g., 2-hour), additional modeling and analysis would be needed to verify that the EET formulas are still effective.

6.5 References

Berlin, S.R., A.O. Langford, M. Estes, M. Dong, D.D. Parrish. 2013. Magnitude, decadal changes and impact of regional background ozone transported into the greater Houston, Texas area, Environmental Science & Technology, 47(24), 13985-13992, doi:10.1021/es4037644.

Djalalova, I., J.M. Wilczak, S.A. McKeen, G.A. Grell, S.E. Peckham, M. Pagowski, L. DelleMonache, J. McQueen, Y. Tang, P. Lee. 2010. Ensemble and bias-correction techniques for air quality model forecasts of surface O_3 and $PM_{2.5}$ during the TEXAQS-II experiment of 2006, Atmospheric Environment, 44(4), 455-467, doi:10.1016/j.atmosenv.2009.11.007.

Lee, S.-H., S.-W. Kim, W.M. Angevine, L. Bianco, S.A. McKeen, C.J. Senff, M. Trainer, S.C. Tucker, R.J. Zamora. 2011. Evaluation of urban surface parameterizations in the WRF model using measurements during the Texas Air Quality Study 2006 field campaign, Atmospheric Chemistry and Physics, 11(5), 2127-2143, doi:10.5194/acp-11-2127-2011.

McKeen, S., G. Grell, S. Peckham, J. Wilczak, I. Djalalova, E.-Y. Hsie, G. Frost, J. Peischl, J. Schwarz, R. Spackman, J. Holloway, J. de Gouw, C. Warneke, W. Gong, V. Bouchet, S. Gadreault, J. Racine, J. McHenry, J. McQueen, P. Lee, Y. Tang, G. R. Carmichael, R. Mathur. 2009. An evaluation of real-time air quality forecasts and their urban emissions over eastern Texas during the summer of 2006 Second Texas Air Quality Study field study, Journal of Geophysical Research, 114(D00F11), doi:10.1029/2008JD011697.

Travis, K.R., D.J. Jacob, J.A. Fisher, P.S. Kim, E.A. Marais, L. Zhu, K. Yu, C.C. Miller, R.M. Yantosca, M.P. Sulprizio, A.M. Thompson, P.O. Wennberg, J.D. Crounse, J.M. St. Clair, R.C. Cohen, J.L. Laughner, J.E. Dibb, S.R. Hall, K. Ullmann, G.M. Wolfe, I.B. Pollack, J. Peischl, J.A. Neuman, X. Zhou. 2016. Why do models overestimate surface ozone in the Southeast United States? Atmos. Chem. Phys., 16, 13561-13577, doi: 10.5194/acp-16-13561-2016.

Appendix B.1

WRF Meteorological Model Dataset Assessment for the Air Quality Modeling in the Gulf of Mexico Region

December 23, 2014

MEMORANDUM

To: Holli Ensz, Bureau of Ocean Energy Management, Gulf of Mexico Region

From: Bart Brashers, Joe Knapik and Ralph Morris; ENVIRON International Corp.

Subject: BOEM Contract No. M14PC00007, Task 2 WRF Meteorological Model Dataset Assessment for the Air Quality Modeling in the Gulf of Mexico Region

---

ENVIRON objectively evaluated the three existing meteorological datasets for sufficient quality for use in air quality modeling of the greater Gulf of Mexico Region (GOMR). This memorandum discusses the configurations of the two most suitable WRF[1] datasets, compares them against meteorological observations and makes recommendations concerning their use for air quality modeling of the greater GOMR. This memorandum consists of the following sections:

- Introduction
- Summary of Existing Datasets
    - ICF/Earth Tech CALMET/OCD Dataset
    - EPA CONUS 12-km WRF Dataset
    - ENVIRON Training WRF Dataset
- Performance Analysis of Two Existing WRF Datasets
    - Surface Temperature, Wind and Humidity Performance
    - Vertical Profile Performance
- Conclusions and Recommendations
- References

[1] See http://www.mmm.ucar.edu/wrf/users/wrfv3.6/updates-3.6.1.html

INTRODUCTION

BOEM is required under the Outer Continental Shelf Lands Act (OCSLA) 1334(a)(8) to comply with the National Ambient Air Quality Standards (NAAQS) to the extent that Outer Continental Shelf (OCS) offshore oil and gas exploration, development, and production sources do not significantly affect the onshore air quality of any state. The GOMR OCS area of possible influence includes the states of Texas, Louisiana, Mississippi, Alabama, and Florida.

On August 26, 2014, BOEM awarded a contract to a team led by Eastern Research Group, Inc. (ERG, with team members ENVIRON and Alpine Geophysics) to perform an Air Quality Modeling Study in the GOMR (Contract #M14PC00007). Under the Study, photochemical and dispersion air quality modeling will be conducted in the GOMR to assess the OCS oil and gas development pre and post-lease impacts to the states, if any, as required under OCSLA. This information will be used by BOEM pre-lease for National Environmental Policy Act (NEPA) Environmental Impact Statement (EIS) cumulative analysis, and post-lease in the exemption level threshold analysis and to support compliance with OCSLA. The study will assess results of photochemical modeling to estimate the potential cumulative impacts, if any, of offshore OCS air emissions to the air quality of any state. This study will also use the results of that photochemical modeling and additional dispersion modeling to assess if BOEM's exemption level thresholds (as defined in 30 CFR 550.303) need to be revised based on newer NAAQS, and will propose new exemption level thresholds, if necessary.

Air quality modeling requires various input datasets, including emissions sources, meteorology, and pre-existing pollutant concentrations. ENVIRON will perform the meteorological assessment and modeling for the Study. The first task is an assessment of existing meteorological datasets.

ENVIRON was able to identify three existing datasets with the geographic coverage necessary for this Study. All three datasets are described below. After an initial review, two "finalists" were identified and were further evaluated using both quantitative and qualitative techniques. These included paired-in-time statistics (bias, error, etc.) using the METSTAT programs and examination of vertical profiles. The results of this detailed evaluation are provided in this memorandum, along with ENVIRON's recommendations.

SUMMARY OF EXISTING DATASETS

ICF/EARTH TECH CALMET/OCD DATASET

In the OCS Study MMS 2008-029, ICF International and Earth Tech, Inc. used 40-km (before April 2002) and 20-km (after April 2002) rapid update cycle (RUC) analyses to develop a 5-year (2000–2004) meteorological dataset for use with CALPUFF and OCD. This dataset has a few drawbacks, most notably it does not support CAMx or CMAQ directly. The 40-/20-km horizontal resolution may also be insufficient to resolve the sea breeze or thermal internal boundary layer (TIBL), similar to the 12-km WRF datasets (discussed below). Additionally, the dataset has low vertical resolution near the surface, limiting the ability to account for near-surface inversions, land-sea coastal interactions and other features that may strongly affect pollutant dispersion. Finally, this dataset would have to be re-processed for use with AERCOARE.

Because of these limitations, this dataset is rejected as unable to fulfill the needs of the Study.

USEPA CONUS 12-KM WRF DATASET

The U.S. Environmental Protection Agency (USEPA) Office of Research and Development (ORD) Atmospheric Modeling and Analysis Division in Research Triangle Park, NC, has produced a number of annual WRF runs that cover the conterminous United States (CONUS) using 12-km grid resolution. The EPA modeling domain extends south to the middle of Cuba, covering the GOMR, as shown in Figure 1. These WRF runs were optimized for use with the community multi-scale air quality model (CMAQ), and use the Pleim-Xu surface layer and planetary boundary layer schemes. These schemes were in turn developed to best represent the interaction between the atmosphere and a plant-covered ground surface, and have not been tested extensively for overwater situations.

These data are at 12-km horizontal resolution. The model results will need to be evaluated to determine if the resolution is sufficiently fine to resolve the sea breeze phenomenon or TIBL at the land-sea boundary. Because there are limited to no observations to make such an evaluation, the TIBL evaluation will likely be more qualitative based on our knowledge of coastal meteorology rather than based on hard data. ENVIRON has previously obtained these WRF outputs for the years of 2006–2008 and 2011, from the Lake Michigan Air Directors Consortium (LADCO). USEPA has also produced WRF runs for the years of 2009–2010 and 2011–2013.[2] The model setup and selected parameterization schemes are summarized in Table 1.

ENVIRON TRAINING WRF DATASET

To our knowledge, there has been only one WRF dataset developed specifically for the GOMR: the one-year (2011) WRF run developed by ENVIRON to be used over water with the recent WRF/MMIF/AERCOARE 40-hour training course[3]. This WRF dataset has not previously been extensively studied or vetted.

The WRF domain configuration is comprised of a system of simultaneous nested grids. Figure 2 shows the WRF modeling grids at 36/12/4 km. All WRF grids are defined on a Lambert Conformal Conic (LCC) projection centered at 40°N, 97°W with true latitudes at 33°N and 45°N (the "standard RPO projection"). The outermost domain with 36-km resolution includes the entire conterminous United States and parts of Canada and Mexico. The inner 12-km regional grid covers the Southeast United States region and is used to ensure that large-scale meteorological patterns across the region are adequately represented and improve projection/grid consistency and time resolution between the 12-km fields and the 4-km boundary conditions. The 4-km domain is centered over the Western Gulf of Mexico. Geographic resolution was developed using the standard WRF topographic information databases.

[2] Rob Gilliam (EPA/ORD/AMAD), personal communication, November 17, 2014

[3] 24-28 March 2014, held at BOEM New Orleans, led by ENVIRON's Bart Brashers and Ken Richmond; BOEM Contract No. TR-14-0089.

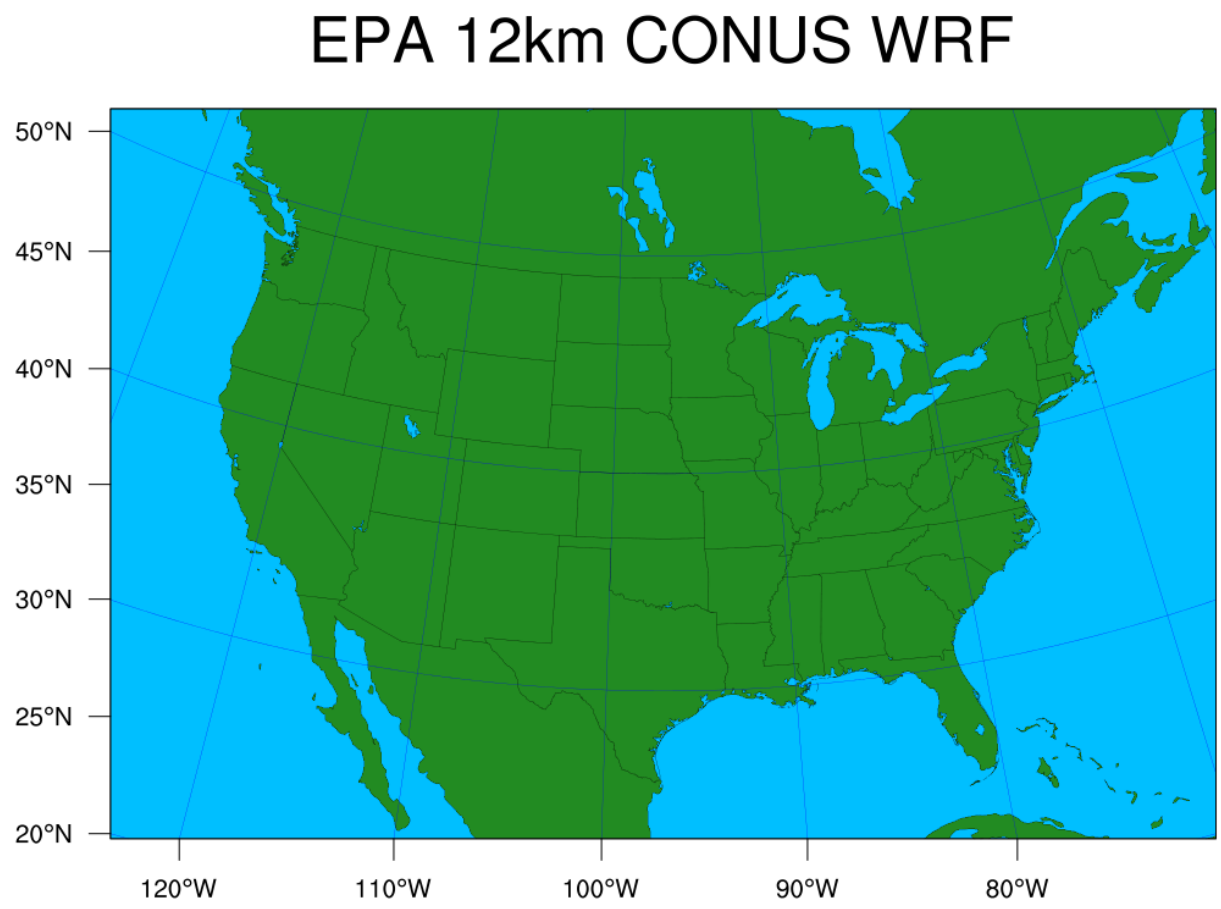

Figure 1. USEPA 12-km CONUS WRF Domain

The initial WRF model MPE showed significant problems with the 4-km domain for most of the year, including persistent unrealistic convection during the summer months. Subsequent testing found two ways to eliminate this feature: (1) use more than 24 vertical layers, or (2) turn off observational nudging. The Training dataset was produced quickly in order to meet a demanding schedule, so a reduced set of layers was used. ENVIRON has also noted a reduction of summertime convection in the Midwest and Desert Southwest in other WRF simulations, when observational nudging is reduced or eliminated.

Additionally, due to missing data in the 12-km NAM inputs, some 5-day intervals were run using 40-km NAM inputs. These intervals showed large biases in temperature and humidity. Several optimizations were attempted after the initial setup, including to the WRF Preprocessing System, and the 36-km and 12-km domains appeared to verify well. The final configuration to the database is summarized in Table 1.

Table 1. Setup and Configuration Overview of Existing WRF Datasets

Setup / Schemes	EPA CONUS WRF	ENVIRON Training WRF
Horizontal Resolution	12 km only	36/12/4 km
Vertical Resolution	34 levels, 1st layer 40m thick	37 levels, 1st layer 12 m thick
Microphysics	Morrison	Thompson
Longwave Radiation	RRTMG	RRTMG
Shortwave Radiation	RRTMG	RRTMG
Land Surface Model (LSM)	Pleim-Xiu	NOAH
Planetary Boundary Layer (PBL) scheme	ACM2	YSU
Cumulus parameterization	Kain-Fritsch 2	Kain-Fritsch 2 in the 36-km and 12-km domains. None in the 4 km domain.
Analysis nudging	3-D Nudging applied to winds, temperature, and moisture. No analysis nudging in the PBL. 2-D Nudging applied to winds, temperature, and moisture.	Nudging applied to winds, temperature, and moisture in the 36-km and 12-km domains. Temp. and moisture nudged above PBL only. Nudging every 3 hours.
Observation Nudging	No OBS nudging	Nudging of the surface wind, temperature and moisture in the 4-km domain
Initialization Dataset	12-km NAM	12-km NAM, some 40-km NAM for missing periods
Domain feedback	No nested grids	“One-way” nesting – no feedback between grids

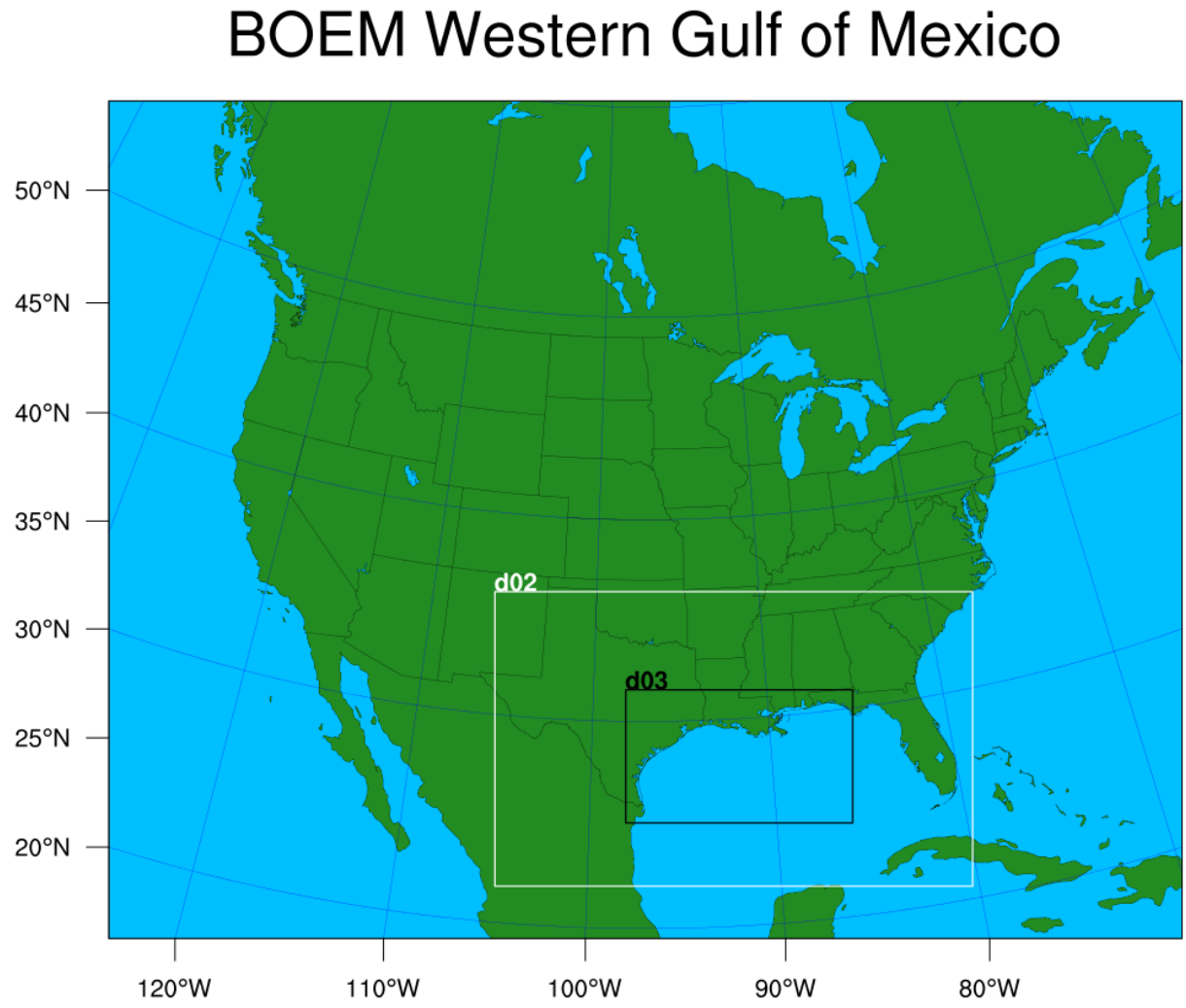

Figure 2. ENVIRON Training WRF 36-km CONUS (d01, entire map), 12-km SE Regional (d02), and 4-km GOMR (d03) Domains

PERFORMANCE ANALYSIS OF TWO EXISTING WRF DATASETS

As described by Tesche (1994), a rigorous meteorological model evaluation consists of two components: an *operational evaluation* and a *scientific evaluation*. The operational evaluation entails an assessment of the model's ability to correctly estimate surface and boundary layer wind, temperature, and mixing ratios largely independent of whether the actual process descriptions in the model are accurate. It essentially tests whether the predicted meteorological fields are reasonable, consistent, and agree adequately with available observations in time and space. In most cases, the operational evaluation focuses on the model's ability to reproduce hourly wind speed, wind direction, temperature, and moisture observations across the modeling domain. It provides only limited information about whether the results are correct from a scientific perspective or whether they are the fortuitous product of compensating errors; thus a

"successful" operational evaluation is a necessary but insufficient condition for achieving a sound, reliable performance testing exercise. An additional, scientific evaluation is also needed.

The scientific evaluation addresses the accuracy of the meteorological processes simulated by the model through testing the model as an entire system as well as its component parts. The scientific evaluation seeks to determine whether the model's behavior, in the aggregate and in its component modules, is consistent with prevailing theory, knowledge of physical processes, and observations. The main objective is to reveal the presence of bias and internal (compensating) errors in the model that, unless discovered and rectified, or at least quantified, may lead to erroneous or fundamentally incorrect technical or policy decisions.

Examples of similar recent analyses of WRF performance can be found in reports ENVIRON has prepared for the Louisiana Department of Environmental Quality (ENVIRON, 2013a) and the Western Regional Air Partnership (WRAP) West-wide Jump-start Air Quality Modeling Study (WestJumpAQMS; ENVIRON, 2013b).

SURFACE TEMPERATURE, WIND AND HUMIDITY PERFORMANCE

Statistical comparisons provide a quantitative assessment of model performance. The problem with evaluating statistics is that the more data pairings that are summarized in a given metric, the better the statistics generally look, and so calculating a single set of statistics for a very large area would not yield significant insight into performance. Therefore, the statistical analysis is refined to sub-regions within the modeling domain. Results from the sub-regional evaluations give clues regarding any necessary modifications to be made in the model configuration.

The quantitative model performance evaluation of WRF used the global-scale quality-controlled National Climatic Data Center dataset "Integrated Surface Hourlies" (DS3505). WRF predictions were compared to meteorological measurements using the publicly available METSTAT[4] evaluation tool. METSTAT calculates statistical performance metrics for bias, error and correlation for surface winds, temperature, and mixing ratio (i.e., water vapor concentration or humidity) and can produce time series of predicted and observed meteorological variables and performance statistics.

In 2001, the Texas Commission on Environmental Quality (TCEQ, formerly the Texas Natural Resource Conservation Commission) sponsored an MM5 modeling project in which ENVIRON derived and proposed a set of daily performance "benchmarks" for typical meteorological model performance (Emery et al., 2001). These standards were based upon the evaluation of a variety of about 30 MM5 and RAMS air quality applications conducted up to that point, as reported by Tesche et al. (2001).

The purpose of these benchmarks was not necessarily to give a passing or failing grade to any one particular meteorological model application, but rather to put its results into the proper context. For example, expectations for modeling of complex terrain might not be as high as flat homogeneous terrain. The key to the benchmarks is to understand how poor or good the results are relative to the universe of other model applications run throughout various areas of the United States. Often lost in the statistical evaluation is the need to critically evaluate all aspects

[4] See http://www.camx.com/download/support-software.aspx, scroll down to METSTAT

of the model via diagnostic and process-oriented approaches. The same must be stressed for the meteorological performance evaluation.

Emery et al. (2001) carefully considered the appropriateness and adequacy of the proposed benchmarks based upon the results of MM5 simulations performed and reported in that study. More recently these benchmarks have been considered in annual meteorological modeling studies that include areas with complex terrain and more complicated meteorological conditions. As part of the WRAP meteorological modeling of the western United States, including the Rocky Mountain Region and the complex conditions in Alaska, Kemball-Cook et al., (2005) proposed model performance benchmarks for complex conditions. McNally (2009) analyzed multiple annual WRF runs that included complex terrain conditions and suggested refined set of benchmarks for temperature and humidity.

Table 2 lists the meteorological model performance benchmarks for simple conditions (Emery et al., 2001) and complex conditions (Kemball-Cook et al., 2005 and McNally, 2009).

Table 2. WRF/MM5 Performance Benchmarks

Parameter	Emery et al. (2001)	Kemball-Cook et al. (2005)	McNally (2009)
Conditions	Simple	Complex	Complex
Temperature Bias	≤ ±0.5 K	≤ ±2.0 K	≤ ±1.0 K
Temperature Error	≤ 2.0 K	≤ 3.5 K	≤ 3.0 K
Humidity Bias	≤ ±1.0 g/kg	≤ ±0.8 g/kg	≤ ±1.0 g/kg
Humidity Error	≤ 2.0 g/kg	≤ 2.0 g/kg	≤ 2.0 g/kg
Wind Speed Bias	≤ ±0.5 m/s	≤ ±1.5 m/s	(not addressed)
Wind Speed RMSE	≤ 2.0 m/s	≤ 2.5 m/s	(not addressed)
Wind Dir. Bias	≤ ±10 degrees	(not addressed)	(not addressed)
Wind Dir. Error	≤ 30 degrees	≤ 55 degrees	(not addressed)

The METSTAT program also allows the monthly results from multiple meteorological model runs to be plotted together to ease the inter-comparison of performance, using “soccer plots.” These plots use a measure of bias on the x-axis, and a measure of error on the y-axis. Because bias may be positive or negative but error is expressed as a positive number (e.g., RMSE), the benchmarks discussed in the next section form lines that resemble a soccer goal, when added to the plot. By plotting each monthly average statistic as a separate point, the seasonal and/or year-to-year model performance variations can easily be seen as “outlier” points.

When run over a large area, positive and negative biases tend to cancel out, potentially obscuring poorer model performance. A typical method used in METSTAT analyses in the past is to run the statistics for a series of sub-domains, or “boxes” within the larger domain. The boxes are chosen strategically to delineate and encompass areas where one thinks the statistics might change.

ENVIRON applied METSTAT to the USEPA 12-km CONUS WRF output using only observations from buoys in the Gulf of Mexico and stations within 2 km of the shoreline. The location of the buoys and stations in the GOMR are shown in Figure 3. The METSTAT results are shown in Figure 4. The soccer plots show monthly-averaged bias on the x-axis, and monthly-averaged error on the y-axis. As can be seen in the soccer plots, WRF’s wind speed performance

during 2006 was somewhat biased, with increased error compared to other years. The wind direction performance was reasonable, with only a few months exceeding the “simple conditions” envelope. The temperature performance was slightly worse for 2008, but mostly within the typical performance envelope, and the humidity performance was acceptable.

Figure 5 presents soccer plots of WRF model performance in the 12-km domain for each month of 2011 in the ENVIRON Training WRF dataset, evaluated against the GOMR observations shown in Figure 3. WRF’s wind direction performed well for the year, with only two months making it into the “complex conditions” envelope. The wind speed performance was acceptable, with three months contained within the simple conditions criteria. Humidity performed poorly, with bias ranging from 0.5–2.0 g/kg and seven months exceeding both simple and complex conditions benchmarks. Temperatures displayed a slight positive bias and error values ranged from 1.0–2.0 K, with all but three months falling within the simple conditions envelope. The temperature error was due to substituting NAM40 for periods of missing NAM12 initialization data—the NAM40 produced a serious and consistent negative temperature bias.

Soccer plots of WRF performance in the ENVIRON Training 4-km dataset for each month in 2011 are presented in Figure 6. Wind direction biases ranged from -5.0 to 7.0 degrees with two months not meeting the complex conditions benchmark. Wind speed also performed poorly, with errors ranging from 2.0 to 5.0 m/s and the largest biases in July, August, and September. A larger area of both increased winds and convective precipitation also developed over the Western GOMR during this same time frame. Primarily comprised of persistent cumuliform cloud development in a spiral arrangement, this area of spurious convection was indicative of a tropical cyclone. However, further investigation did not yield verification of any known tropical storms in the region. Additionally, humidity performance was positively biased in this domain as mixing ratio bias and error were noticeably higher in the summer months and slightly lower in the winter months. This is likely from WRF slightly overpredicting mixing ratios due to the increased precipitation throughout the region during the summer months compared to the cooler, drier air masses in the winter months. Temperatures were the exception in this case, performing well in the 4-km domain. The model and observations show a reasonably strong agreement for temperatures throughout the year.

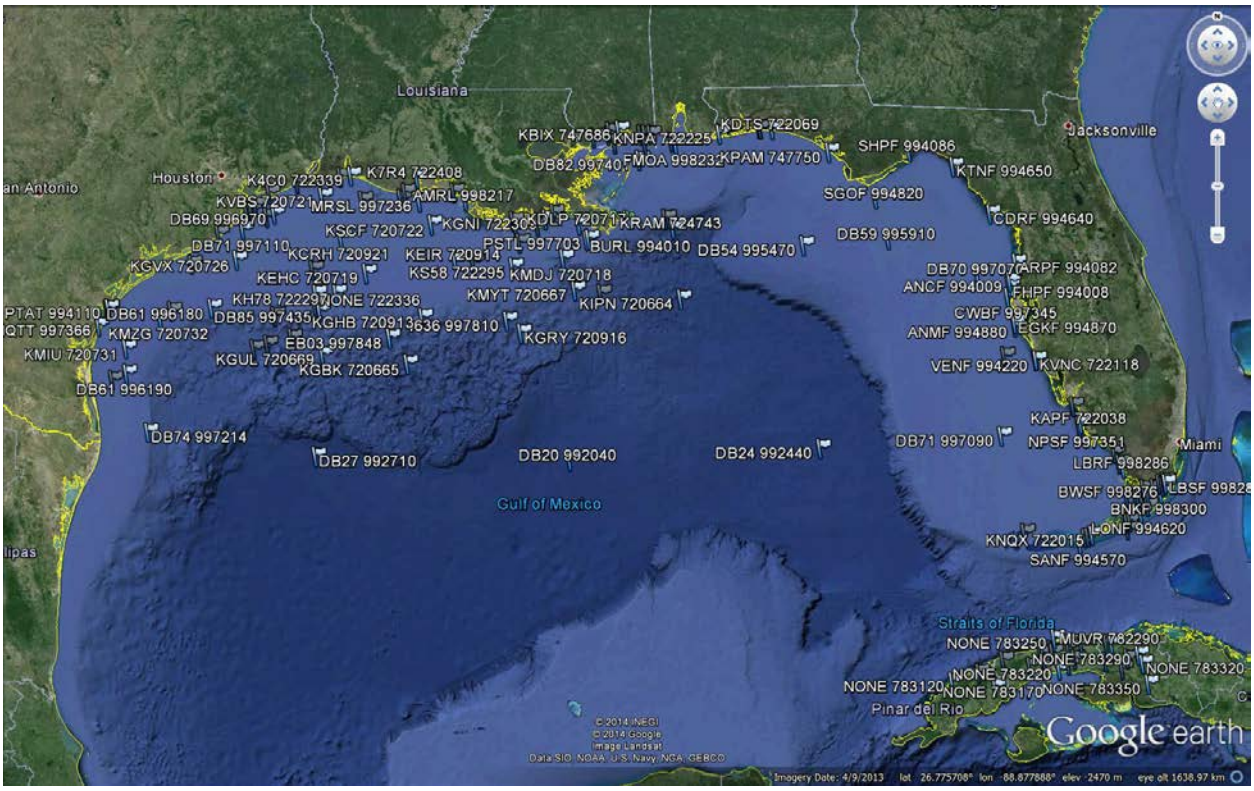

Figure 3. Location of Buoys and Surface Observing Stations Within 2 km of the Shoreline in the GOMR

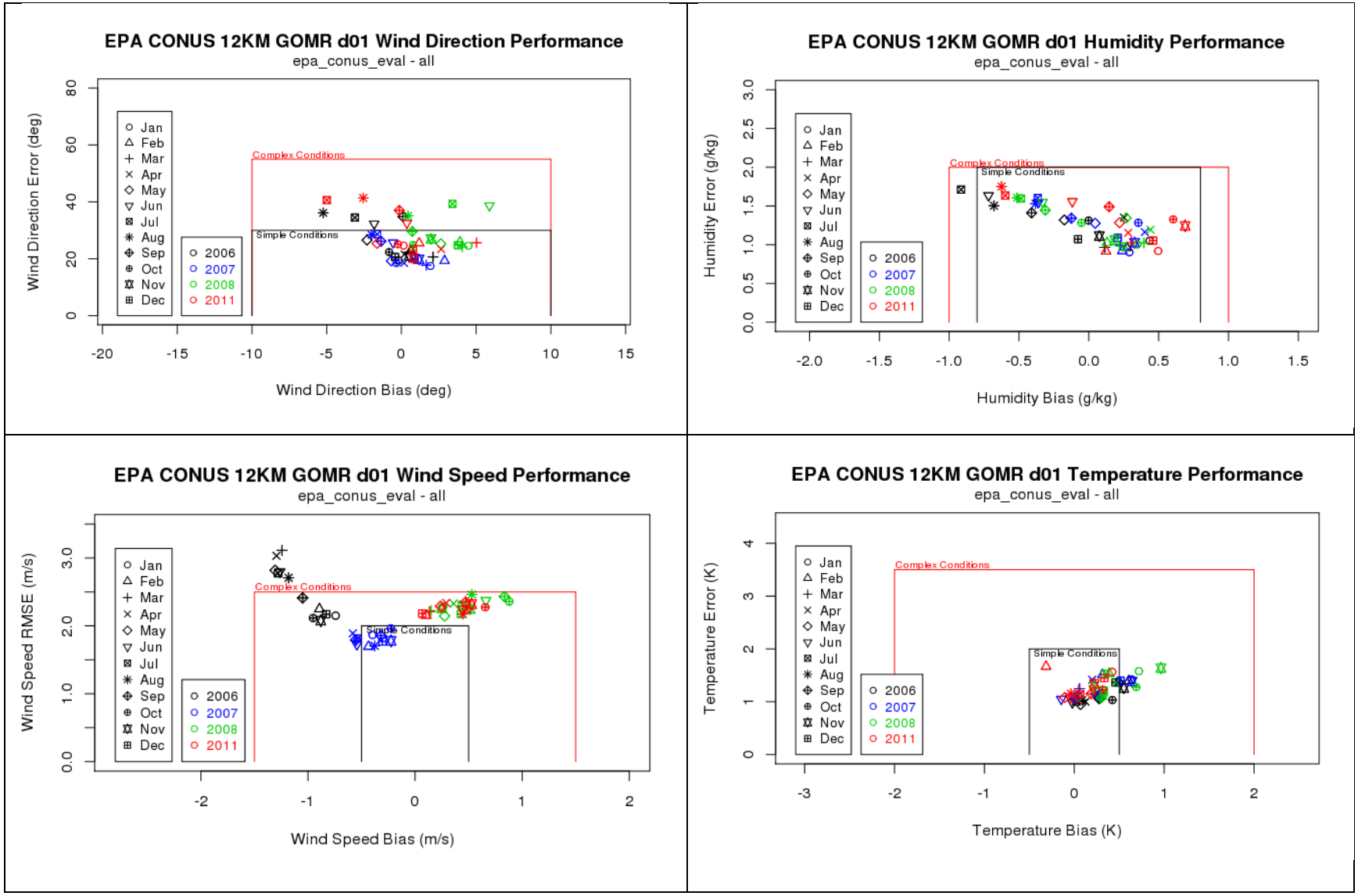

Figure 4. Monthly Wind Direction (top left), Humidity (top right), Wind Speed (bottom left), and Temperature (bottom right) Soccer Plots of Gulf of Mexico Stations in the USEPA CONUS 12-km WRF Domain

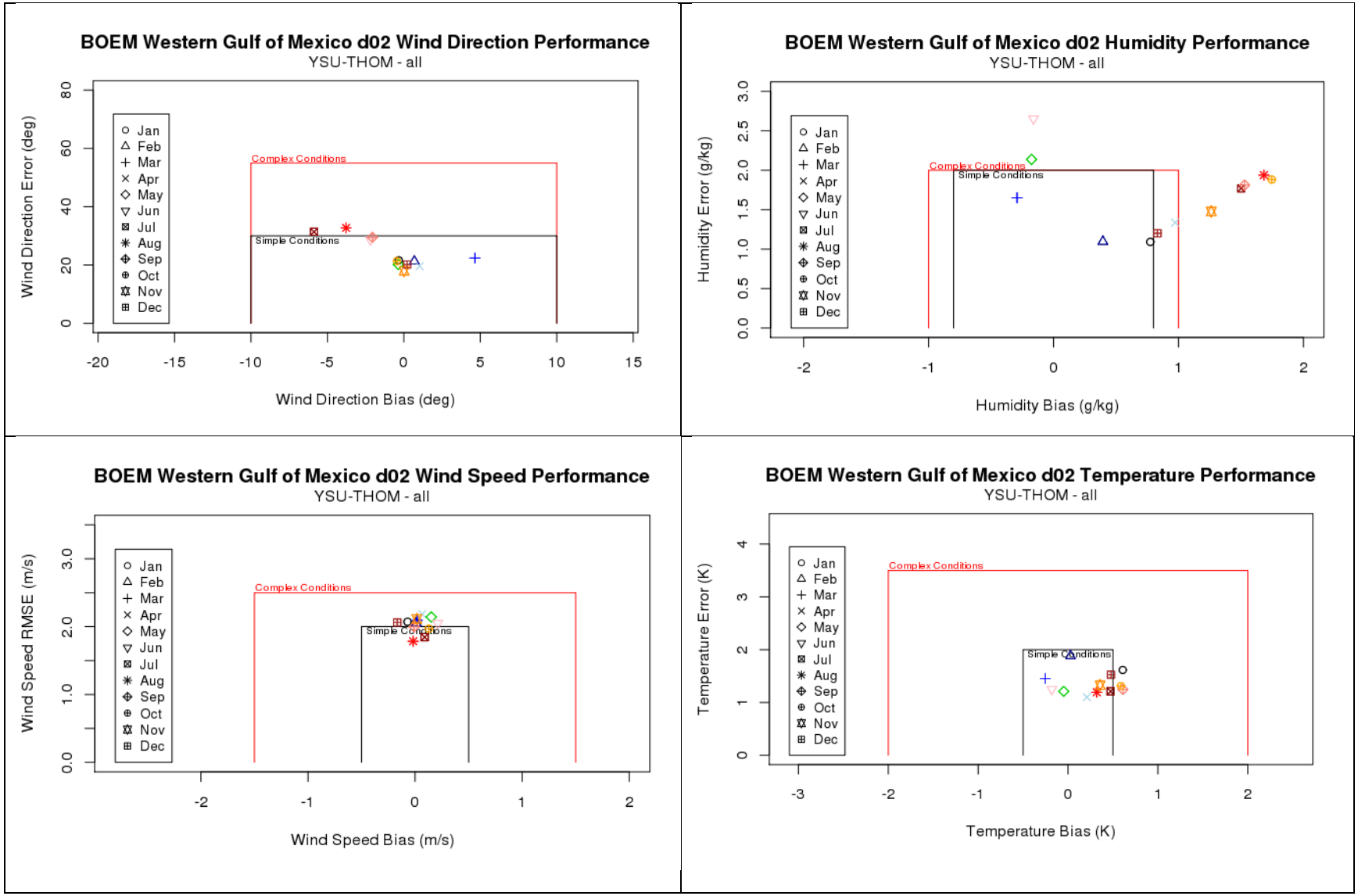

Figure 5. Monthly Wind Direction (top left), Humidity (top right), Wind Speed (bottom left), and Temperature (bottom right) Soccer Plots of Gulf of Mexico Stations in the 12-km ENVIRON Training WRF Domain

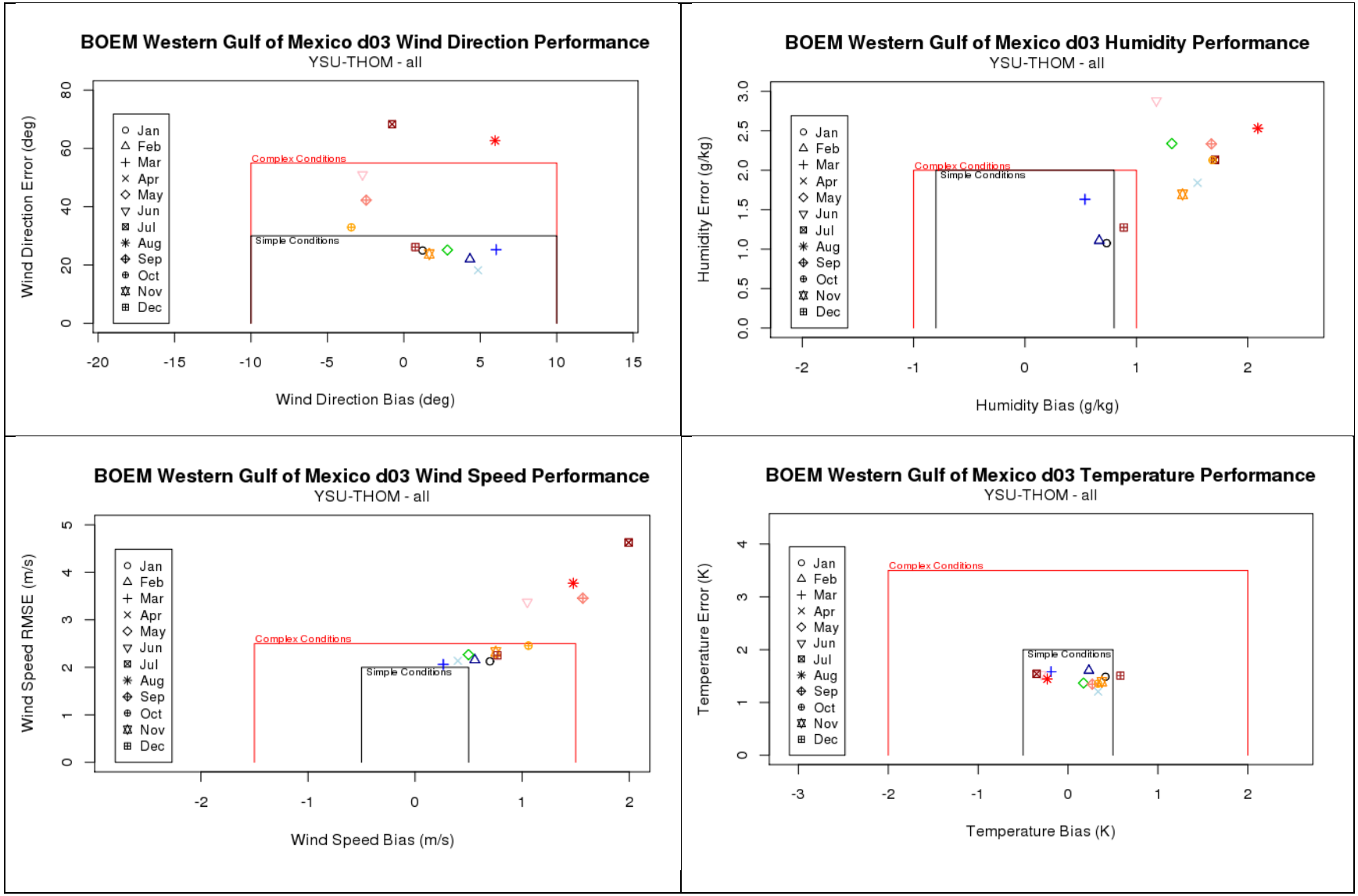

Figure 6. Monthly Wind Direction (top left), Humidity (top right), Wind Speed (bottom left), and Temperature (bottom right) Soccer Plots of All ds3505 Stations in the 4-km ENVIRON Training WRF Domain

VERTICAL PROFILE PERFORMANCE

Vertical profile plots showing WRF modeled data and observed upper-air soundings were created to evaluate the performance of the vertical atmospheric structure. The upper-air observation locations from Brownsville, TX, and Slidell, LA, were selected from the GOMR. The following figures display vertical profile comparisons of WRF temperatures and dew points (blue lines) against actual upper-air temperatures and dew point (red lines) from each location using both WRF datasets in both the winter and summer scenarios.

Figure 7 displays vertical soundings for the USEPA 12-km CONUS dataset on two semi-randomly chosen dates, January 10, 2011 (a winter morning), and July 24, 2011 (a summer morning). These soundings were chosen because they both featured low-level stable layers, which are important to dispersion models. WRF depicts the temperature profiles reasonably well for both locations, with accurate low-level moisture and temperature inversions reflected near the surface in winter, but it missing the weaker inversion during the summer.

WRF did not handle temperature well overall in the 4-km ENVIRON Training datasets, primarily in the boundary layer. As shown in Figure 8, temperatures were over-estimated by 4.0 °C at Slidell, LA, on January 10, 2011, at 00 UTC and by 5.0 °C on July 24 at 12 UTC, indicating the model bias again in the cool season. There is also a drier bias near the surface in both locations as low-level moisture is generally under-predicted. Additionally, the weaker low-level temperature inversions at both locations on July 24, 2011, at 12 UTC are not reflected in the WRF dataset. The mid-level moisture over Slidell on January 10 was the exception; the 4-km WRF profile handled the dew point spread well.

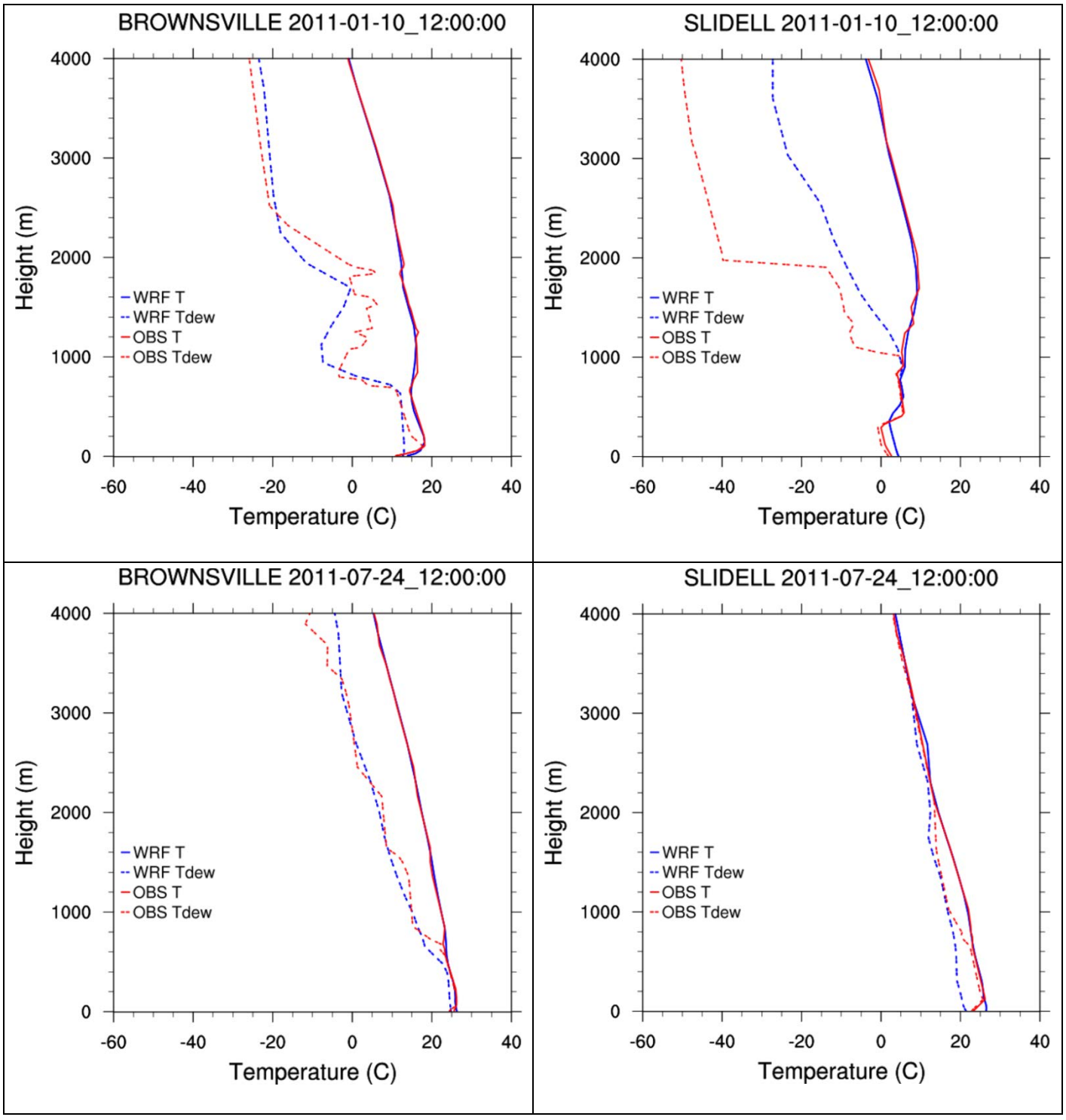

Figure 7. Vertical Profiles Comparing EPA CONUS 12km WRF Data (blue lines) to Actual Upper-Air Data (red lines) Brownsville, TX, and Slidell, LA

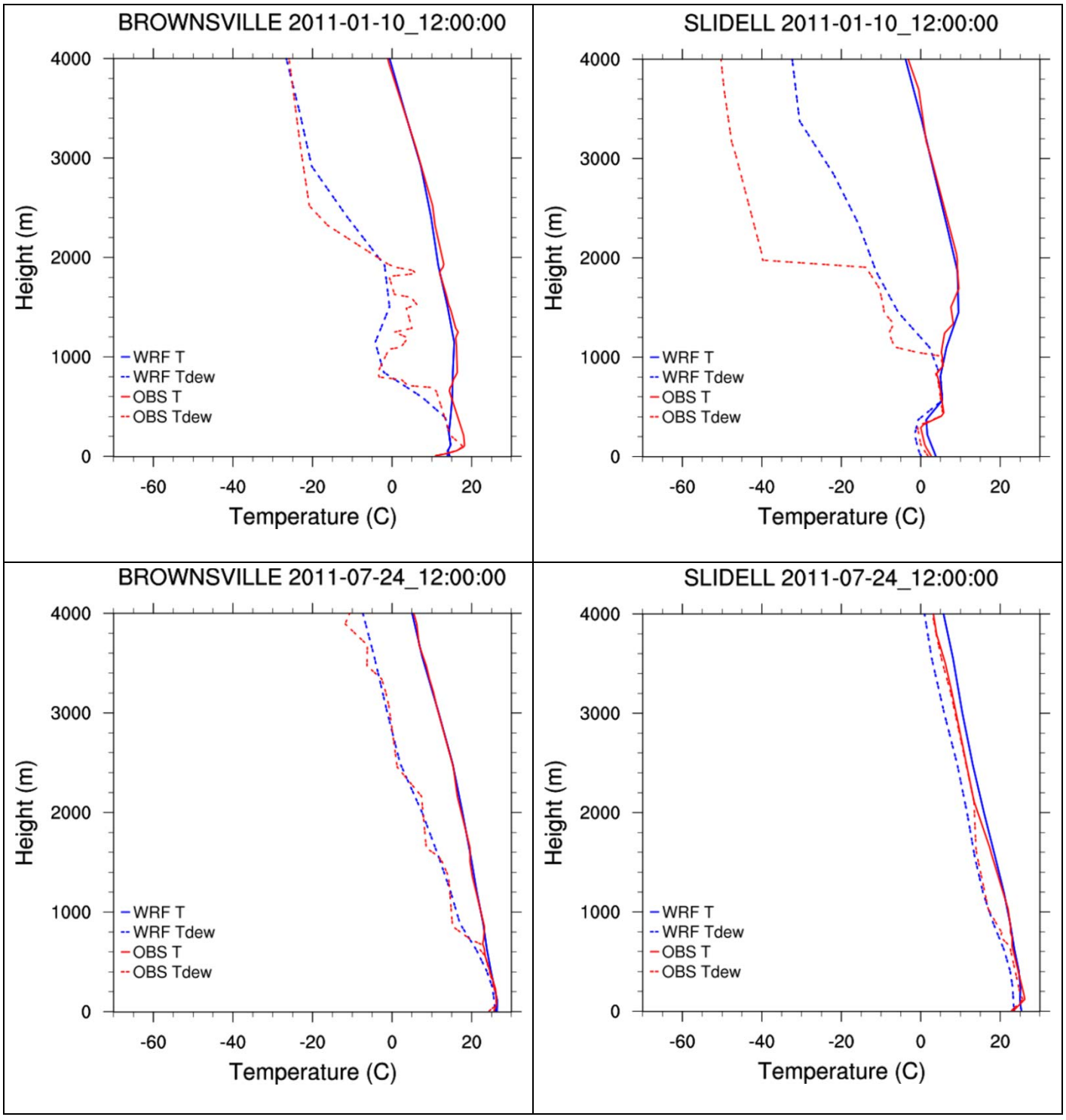

Figure 8. Vertical Profiles Comparing ENVIRON Training 4-km WRF Data (blue lines) to Actual Upper-Air Data (red lines) on for Brownsville, TX, and Slidell, LA

CONCLUSION AND RECOMMENDATIONS

Currently, neither the USEPA CONUS 12-km nor the ENVIRON Training WRF dataset is adequate for air quality modeling of the GOMR. Deficiencies exist in both datasets and there are not enough positive attributes to select either WRF application. The USEPA CONUS 12-km WRF dataset, originally developed for overland simulations, is not suited for the Study area. Its lower horizontal and vertical resolutions likely do not resolve finer-scale coastal interactions well, though we lack the observational data to properly assess this phenomenon. Additionally, WRF model performance varies somewhat from year to year. In the ENVIRON Training WRF dataset, surface temperature, wind, and humidity parameters were acceptable in the 12-km domain, but did not perform well against DS3505 integrated surface hourly data in the 4-km domain. Warm season convective precipitation, primarily in the Southeastern United States, is also not well simulated in this dataset. Vertical profiles revealed inversions, which were not present, and significant surface temperature biases.

ENVIRON recommends development of a new WRF dataset specifically designed for the GOMR in order to more accurately represent meteorological conditions in overwater portions of the Study area. Optimizing WRF performance for the GOMR will be based on various WRF modeling techniques. Some aspects of the model configuration can be recommended based on recognition of the state-of-the-art procedures of WRF modeling. This includes aspects concerning the numerical solver settings and selected physical models. The RRTMG radiation models, Thompson microphysics model, and NOAH LSM represent the state-of-the-art model set up for general WRF modeling in the mid-latitudes.

REFERENCES

Emery, C.A., E. Tai, G. Yarwood. 2001. *Enhanced Meteorological Modeling and Performance Evaluation for Two Texas Ozone Episodes*. Prepared for the Texas Natural Resource Conservation Commission (now TCEQ), by ENVIRON International Corp, Novato, CA. Available at: http://www.tceq.texas.gov/assets/public/implementation/air/am/contracts/reports/mm/EnhancedMetModelingAndPerformanceEvaluation.pdf

ENVIRON. 2013a. *Photochemical Modeling for the Louisiana 8-hour Ozone State Implementation Plan, Technical support document.* Prepared for the Louisiana Department of Environmental Quality, by ENVIRON International Corp., Novato, CA. Available at: https://deq.louisiana.gov/assets/docs/Air/8-HourOzoneNAAQSModelingProject_2008/LDEQ_TSD_4Oct13.pdf

ENVIRON. 2013b. *Western Regional Air Partnership (WRAP) West-wide Jump-start Air Quality Modeling Study (WestJumpAQMS) Final Report*. Prepared for the Western Regional Air Partnership, by ENVIRON International Corp., Novato, CA. Available at: http://www.wrapair2.org/pdf/WestJumpAQMS_FinRpt_Finalv2.pdf

Kemball-Cook, S., Y. Jia, C. Emery, R. Morris. 2005. *Alaska MM5 Modeling for the 2002 Annual Period to Support Visibility Modeling*. Prepared for the Western Regional Air Partnership, by ENVIRON International Corp., Novato, CA. Available upon request from BOEM/Ramboll.

McNally, D.E. 2009. *12 km MM5 Performance Goals*. Presentation to the Ad-Hoc Meteorology Group. June 25, 2009. Available at: http://www.epa.gov/scram001/adhoc/mcnally2009.pdf

Tesche, T.W. 1994. *Evaluation Procedures for Regional Emissions, Meteorological, and Photochemical Models*. Presented at the 86th Annual Meeting of the Air and Waste Management Association, 14-18 June, Denver, CO.

Tesche, T.W., D.E. McNally, C.A. Emery, E. Tai. 2001. *Evaluation of the MM5 Model Over the Midwestern U.S. for Three 8-hour Oxidant Episodes*. Prepared for the Kansas City Ozone Technical Workgroup, by Alpine Geophyisics, LLC, Ft. Wright, KY, and ENVIRON International Corp., Novato, CA.

Appendix C.1

Development of the 2012 Onroad Mexican Emission Estimates

C.1 DEVELOPMENT OF THE 2012 ONROAD MEXICAN EMISSION ESTIMATES

C.1.1 General MOVES Model Approach

The first step in applying MOtor Vehicle Emission Simulator (MOVES) to Mexico was to determine the appropriate MOVES run strategy. There are multiple ways to customize MOVES to local conditions. For U.S. use, MOVES provides a default database, which enables estimation of onroad emissions to significant detail (i.e., by vehicle class, fuel type, road type, and model year) for all 3,222 counties in the U.S. and for all calendar years including 1990 and 1999 through 2050. To accomplish this requires a massive underlying database with model inputs for vehicle activity, population, meteorology, fuel properties, road characteristics, projection factors, and emission rates. Default results are generated when the National Scale is selected in MOVES and rely heavily on a "top-down" allocation approach, where national totals of vehicle population and activity are allocated to individual U.S. counties based on available county-level surrogates. As an alternative to the default National Scale approach, MOVES also provides the County Scale feature to allow users to improve estimates in a "bottom-up" fashion, allowing customization of many of these elements through data importers. When County Scale is selected, MOVES supplies a template for users to provide data directly at the county level (the County Data Manager). This feature is relied on for development of the U.S. Environmental Protection Agency's (USEPA's) National Emissions Inventory (NEI) and modeling uses required under the Clean Air Act, such as State Implementation Plan (SIP) inventories and transportation conformity analyses.

Customizing MOVES to Mexico could therefore be done following either the National or County Scale approaches. The main consideration was the level of detailed data available for adapting to Mexico. The MOVES County Scale requires information (such as vehicle population, vehicle miles traveled, etc.) to be provided at the level of geographic detail being modeled. This approach was developed focused on local inventories, where detailed data is more likely to be available. The USEPA does, in fact, use County Scale for the National Emissions Inventory (NEI), but even for this application, local data are not available for many U.S. counties, requiring use of national defaults for around half of the counties in the U.S.

An assessment of potential data sources in Mexico found that detailed information necessary to calculate emission inventories at the County Scale, as done for the U.S., are not available. Several data sources were identified at more aggregate levels of detail, however. Eastern Research Group, Inc. (ERG) decided that developing a national default database for Mexico would therefore be preferable, because a) the National Scale is more amenable to the available data in Mexico; and b) once developed, a national default database provides means to estimate emissions in each Mexican municipality (or state) for multiple years.

In general, to develop a national default database for Mexico required:

- Domain-wide totals of vehicle fleet and activity inputs such as populations, kilometers traveled, age distribution, and speeds;
- Factors to allocate vehicle population and activity to the Mexican municipality levels;
- Localized data on meteorology, fuels, and vehicle inspection/maintenance; and

- Updated emission rate database to reflect significant differences between U.S. and Mexican vehicle standards.

Section C.2 discusses how ERG developed each input for Mexico.

C.1.2 Development of Inventories for Mexico

ERG worked with consultant Verónica Garibay-Bravo to obtain data for developing Mexico-specific inputs. Ms. Garibay-Bravo worked closely with representatives from the National Institute of Ecology and Climate Change (INECC) to obtain underlying data used in Mexico's most recent NEI and provided the data to ERG for use in MOVES. The specific data and sources are discussed in Section C.1.2.1. Section C.1.2.2 then discusses the specific MOVES tables updated to reflect the Mexico data and any analysis required of the source data to prepare it for MOVES. In some cases, sufficient data for Mexico were not available, so U.S. defaults were used. Note, vehicle miles traveled (VMT) and vehicle kilometers traveled (VKT) are used interchangeably in this section, though MOVES requires VMT as input.

C.1.2.1 Data Sources

Onroad motor vehicle activity data sources in Mexico are scarce compared to the U.S. Although several data sources are available pertaining to vehicle emissions, vehicle population, and VKT, they are frequently inconsistent or based on outdated information. Also, most fuel quality and sales data are not publicly available. Recently, however, several studies have been carried out mostly by the INECC, the National Institute of Geography and Statistics (INEGI), the National Population Council, and the state-owned fuels company (PEMEX) to overcome these limitations. Although most of the information generated in these studies has not yet been published, ERG was able to access internal reports and spreadsheets through direct communication with INECC staff, who shared the databases used in their most recent mobile source emission estimates for 2013. Hence, unless otherwise noted, the following information was provided directly by INECC (2015).

C.1.2.1.1 Vehicle Population and Age Distribution

In Mexico, vehicle registration is carried out by state authorities, requiring different formats and level of detail tailored to their particular needs. Usually, local authorities add new vehicles to the registry every year but rarely remove vehicles that are no longer in use. According to Mexican emission inventory experts, this has historically led to an overestimation of the vehicle fleet in emissions inventories. To avoid this, we used INECC estimates of vehicle population and age distribution instead of vehicle registration. These are considered more realistic because INECC derived retirement rates from several field studies carried out between 2007 and 2012 by INECC and the Mexican Petroleum Institute (IMP). INECC applied these retirement rates to historical state-level vehicle sales provided by the automotive industry, resulting in adjusted vehicle population at the state level. Imported used vehicle registries from the Mexican Treasury and Customs Authority (*Secretaría de Hacienda y Crédito Público* [SHCP]) were also used to add these vehicles and obtain total population by age and vehicle type. These estimates were used for a recent 2013 emissions estimate developed by INECC.

C.1.2.1.2 Vehicle Kilometers Traveled (VKT)

Inventories in Mexico had traditionally used one average VKT number for the whole country based on a limited number of surveys performed in Mexico City or on a travel demand modeling (TDM) exercise carried out for seven representative cities for the 1999 Mexico NEI. For this Study, ERG used data from surveys conducted by INECC between 2007 and 2011 in 20 cities, from which average national-level VKT by vehicle age and vehicle type (light, medium, and heavy duty) were derived.

C.1.2.1.3 Road Network

Road type distribution was taken from the INEGI website (INEGI, 2015). GIS-based downloadable files include detailed, city-level data of the road network to 2011. ERG used these files and a technical report to harmonize INEGI's road types to those used in MOVES. Significant analysis and data processing were done to produce road type distributions by municipality, as described in Section C.2.2.

C.1.2.1.4 Fuels

In Mexico, fuels are distributed and sold by a single, state-owned company (PEMEX). Gasoline and diesel sales are publicly available from PEMEX website but only at the state level. However, through INECC, we obtained fuel sales at the municipality level provided by PEMEX for 2013. Because fuel quality certificates are not publicly available, ERG used the specifications in the current fuel quality standard as a reference. Actual sulfur concentrations in fuels, however, differ from the standard. ERG relied on expert opinion from INECC as to which municipalities have access to low-sulfur fuels.

C.1.2.1.5 Inspection/Maintenance Programs

Inspection/maintenance (I/M) programs in Mexico are managed by state or local environmental authorities; however, these are enforced only in a limited number of cities. For example, the I/M program in Mexico City has tighter controls and more stringent conditions than those in other cities, but some cities adjacent to the Mexico City Metropolitan Area have adopted these conditions to avoid transit restrictions. The Federal environmental authority (SEMARNAT) compiles compliance data from all states in Mexico periodically. We used the latest internal status report (2012) provided by INECC, with information gathered by SEMARNAT, focused on this work for I/M areas within the BOEM 36-km modeling domain.

C.1.2.1.6 Mexico Emission Standards

INECC provided information on Mexico vehicle standards relative to U.S. standards for light vehicles and heavy-duty trucks, summarized in Table C.1-1. Overall, Mexican vehicle emission standards are outdated compared to U.S. standards. For light-duty vehicles, current Mexican specifications (known as NOM42) were partially adapted from a combination of Tier 1 and Tier 2 Bins 5 through 9 USEPA limit values, with a 50,000-mile durability. European Euro 4 certificates are also accepted. Emissions from medium duty vehicles are not currently regulated in Mexico. Heavy-duty gas and diesel vehicles are regulated based on NOM 76 and NOM 44, respectively; a primary difference being that Mexico has yet to implement the low NO_x and PM diesel standards implanted in the U.S. beginning in 2007.

According to the International Council on Clean Transportation (ICCT), based on analysis of 2012 model year data, a significant proportion of new cars and light trucks in Mexico comply with more stringent U.S. emission standards (ICCT and INECC, 2015). This suggests that light-duty vehicle emissions may be lower than required. However, data on potential overcompliance were not available for enough years to account for this effect over time. As discussed in Section C.1.2.3., for this work we used the "on-the-book" NOM regulations in Mexico to develop Mexico-specific emission rates, without accounting for overcompliance. This is considered a conservative first step in developing Mexico-specific emission rates.

C.1.2.1.7 Human Population

Current population was taken from 2010 census counts at the municipality level performed by INEGI and available on their website, projected population data were downloaded from the National Population Council (CONAPO) website (CONAPO, 2015).

Table C.1-1. Mexico Vehicle Standard Information Provided by INECC

Cars & Light Trucks (NOM 42)	Heavy-Duty Trucks & Buses (NOM 44 & 76)
MY 1990 and older: No aftertreatment, no fuel injection to carburetor. **MY 1991–1992:** 2- and 3-way catalytic converters. **MY 1993-2005:** U.S. Tier 0 Emission limits at 0 km (no durability requirements). **MY 1999–2005:** U.S. Tier 0 Emission limits at 0 km, no OBD required. **MY 2007–2009:** Emission limits at 80,000 km and OBD requirements. Phase-in – 2007, 25%; 2008, 50%; 2009, 75%. **MY 2007–2009:** U.S. Tier 1 emission limits for PM; U.S. Tier 2 Bin 10 limits for NO_x (Euro 3 accepted). Phase-in – 2007, 25%; 2008, 50%; 2009, 75%; 2010, 75%; 2011, 50%; 2012, 30%. **MY 2010 onwards:** U.S. Tier 1 emission limits for PM and U.S. Tier 2 Bin 7 limits for NO_x. Euro 4 also accepted. Phase-in – 2010, 25%; 2011, 50%; 2012, 70%; 2013, 100%. Although the regulation does not consider full Tier 2 standards (mainly due to fuel quality), it is reasonable to suppose that Tier 2 vehicles are currently being sold in Mexico, due to the high integration between Mexican manufacturers in the U.S. market.	**Diesel (NOM 44)** **MY 1993 and older:** No control **MY 1994–1997:** same as U.S. **MY 1998–2008:** U.S. 1998 (or similar Euro) **MY 2009 onwards:** U.S. 2004 (or similar Euro) **Timeline of Mexico and USEPA/Euro standards:** USEPA 1991: Required in Mexico 1993 USEPA 1994: Required in Mexico 1994 USEPA 1998: Required in Mexico 1998 USEPA 2004: Required in Mexico 2008 USEPA 2007: Not considered in Mexican regulations USEPA 2010: Proposed phase-in starting 2018 EURO I 1992: Not sold in Mexico EURO II 1996: Not sold in Mexico EURO III 2000: Required in Mexico 2006 EURO IV 2005: Required in Mexico 2008 EURO V: Not considered in current Mexican regulations EURO V 2013: Proposed phase-in starting 2018 **Gas (NOM 76)** **MY 1997 and older:** No Control **MY 1998 onwards:** NOM 076 "A" (Comparable to U.S. Tier 1 HD Gas Standards) Emissions from medium duty vehicles are not currently regulated in Mexico. However, since manufacturers have to comply with U.S. and European regulations for these vehicles, it is reasonable to assume that they comply in a similar way as the light-duty vehicles.

C.1.2.1.8 Meteorology

Temperature data for a base year were loaded into the MOVES database to be used for any calendar year model run. State-average maximum and minimum temperatures by year and month are published by the Comisión Nacional Del Agua (CONAGUA) Servicio Meteorológico Nacional (SMN) (CONAGUA, 2015). Hourly temperatures and/or humidity data were not available at this level of coverage; temperature and humidity information is available for

individual weather stations across Mexico, but due to concern with coverage and the level of effort necessary to convert these to municipality-specific meteorology, these were not pursued. Instead, as discussed in Section C.1.2.2, an approach developed by the USEPA to convert min/max temperatures to hourly diurnal profiles was used to generate hour temperatures by state, which were then applied to each municipality in a state. Monthly diurnal profiles of relative humidity were assigned to Mexico using MOVES data from the U.S. border states.

C.1.2.2 Updates to MOVES Database Tables

The data sources outlined in Section C.1.2.1 were processed, in some cases with additional analysis, into the format needed by MOVES. The MOVES database is a relational database with dozens of underlying, linked tables providing the model with information on the geography, vehicle fleet, activity, fuels, meteorology, and emissions required to produce emission inventories specified in the run specification file, along with necessary information files. Only a subset of 22 tables were updated for Mexico, based on a) Mexico fleet, activity, meteorology, and fuel data discussed in Section C.1.2.1; b) informational tables needed to update U.S. counties and states to Mexico municipalities and states; and c) the need to adapt MOVES emission rates to Mexico emission standards. Table C.1-2 provides a list of MOVES tables updated for Mexico. All other MOVES tables were left as in the U.S. default database.

Table C.1-2. MOVES Database Tables Updated for Mexico Runs

MOVES-Mexico Database Table Name	Purpose/Description
County	List of municipalities in Mexico
State	List of states in Mexico
CountyYear	Stage II refueling program efficiency
FuelUsageFraction	E85 usage for flex-fuel vehicles
IMCoverage	Inspection and maintenance program description and coverage
Link	Enables county-specific emissions output in an inventory run
RegionCounty	Assignment of each county to a fuel region
Zone	Allocation of the off-network activity from nationwide to municipality
ZoneMonthHour	Diurnal temperature and relative humidity profiles for each month of year
ZoneRoadType	Allocation of the on-network activity from nationwide to municipality. On-network activity includes source hours operating, which is how VMT gets allocated to each municipality
HPMSVTypeYear	Nationwide VMT, annual total, by HPMS vehicle classification
SourceTypeYear	Nationwide vehicle population by source use type classification
SourceTypeAgeDistribution	Average fleet age distributions, MAG-domain average Also two external table versions (1) border and (2) non-border
Alternative Vehicle & Fuel Technology (AVFT)	Gasoline/diesel relative fractions for each source use type and vehicle model year
RoadTypeDistribution	Distribution of VMT to road types
FuelSupply	Assigns specific fuels to each fuel region by month and calendar year
FuelFormulation	Parameters for every fuel (e.g., sulfur level and vapor pressure)
MonthVMTFraction	Allocates annual VMT to the 12 months of year
EmissionRateByAge	Base emission rates by age, model year group, regulatory class, fuel type, pollutant, emission process, and operating mode
CumTVVCoeffs	Coefficients used by MOVES to calculate tank vapor venting

The following sections include a description of how each of these tables were updated.

C.1.2.2.1 County

The County table was updated to list all municipalities in Mexico by 4- or 5-digit county code. Although the emission inventories in this Study are limited to municipalities fully or partially in the inventory modeling domain, the database was populated with all municipalities so that the top-down allocation approach used by MOVES national scale worked correctly. The table also contains a binary altitude description of low or high (L or H), barometric pressure, and geographic phase-in area (GPA) fractions (GPA does not apply in Mexico). Altitude was set to low (L) everywhere in Mexico, and barometric pressure was set to the mean value of the low altitude counties in U.S.

C.1.2.2.2 State

The State table was updated to include all states in Mexico, by 1- or 2-digit integer code. This Study is limited to states covered in the modeling inventory domain, listed in Table C.1-3 below.

Table C.1-3. Mexico States in BOEM Domain

stateID	stateName	stateAbbr
1	Aguascalientes	AG
2	Baja California	BC
3	Baja California Sur	BS
5	Coahuila	CO
8	Chihuahua	CH
10	Durango	DG
11	Guanajuato	GT
13	Hidalgo	HG
14	Jalisco	JA
18	Nayarit	NA
19	Nuevo León	NL
22	Querétaro	QT
23	Quintana Roo	QR
24	San Luis Potosí	SL
25	Sinaloa	SI
26	Sonora	SO
28	Tamaulipas	TM
30	Veracruz	VE
31	Yucatán	YU
32	Zacatecas	ZA

C.1.2.2.3 County Year

The County Year table contains fractions representing the efficiency of Stage II refueling control programs for each county and year. Stage II refueling emissions are hydrocarbon emissions during gasoline refueling at service stations from either the pump dispenser itself (spillage losses) or the vehicle tank (vapor displacement losses). Control programs reduce these hydrocarbon emissions. However, refueling in this inventory came from area source emission inventory and did not come out of MOVES. This table was a structural update only to include all Mexican municipality codes that exist in Mexico.

C.1.2.2.4 Fuel Usage Fraction

The Fuel Usage Fraction table allows the user to specify relative fractions of gasoline versus E85 use in flex-fuel vehicles by county and calendar year. All E85 was turned off for Mexico. This table was also updated to include all Mexican municipality codes.

C.2.2.5 IM Coverage

The IM Coverage table defines specifics of vehicle inspection/maintenance (I/M) programs by municipality. I/M programs in Mexico are mostly idle tests, although some dynamometer testing is done in the state of Baja California. To reflect idle testing, we selected the Two-Speed Idle (TSI) test to represent the IM tests labeled as "static" and the Accelerated Simulation Mode (ASM) to represent those labeled as "dynamometer" in the raw data. The remainder of fields were populated using the local I/M program data discussed in Section C.1.2.1.

Additional analysis was performed to calculate compliance factors for Mexico's I/M programs. In MOVES, the compliance factor determines the portion of the passenger cars and light truck fleet that actually receive the emissions benefit of a particular I/M test. The compliance factors were calculated as the ratio of the number of vehicles tested to the total light-duty gasoline population. For areas that had I/M, the average compliance was 45%. The minimum compliance factor was only 3% (in Mérida, Yucatán) because only official vehicles are subject to I/M in that city. Note that due to the scope of the original onroad inventory work for MAG, the I/M program data were only populated in MOVES for whole states with at least one municipality coinciding with the MAG modeling domain. Because the MAG domain does not completely cover the 36-km domain, some municipalities in the inventory have emissions from light-duty vehicles that do not reflect I/M benefits, despite having an I/M program. The impacted area in the inventory is relatively small and located along the southern edge of the 36-km domain. The specific areas are 14 municipalities located in 3 central states, including: Guanajuato (9 municipalities), Hidalgo (1 municipality), and Querétaro (4 municipalities).

There was no Mexico data available on grace period or other exempted model years, so ERG adopted those particular parameters from the U.S. database.

C.1.2.2.6 Link

The Link table is informational to define county and road type pairs, and it was only updated for the purpose of this work to include all the Mexican municipality codes.

C.1.2.2.7 Region County

The Region County table assigns each municipality to a fuel region. Source data on fuel formulations discussed in Section C.1.3.1 specified differences in sulfur, Reid Vapor Pressure (RVP), and oxygenate use by municipality depending on whether it was located (1) inside or outside a metropolitan area, (2) in a border or non-border state, and (3) within RVP regions. This unique combination of metropolitan area, border state, and RVP region resulted in six fuel regions in Mexico, shown in Table C.1-4.

Table C.1-4. Fuel Regions Defined for Mexico

Fuel Region	Metropolitan Area	Border State	Volatility Group
1	No	No	2
2	Yes	Yes	2
3	No	Yes	1
4	No	No	3
5	No	No	1
6	Yes	Yes	1

Diesel sulfur content is 15 ppm in border states and metropolitan areas and is 500 ppm elsewhere. Gasoline sulfur content is 30 ppm in metropolitan areas and a mix of 30 ppm and 300 ppm sulfur fuel elsewhere. However, due to complication attempting to adjust sulfur effects in MOVES, ERG ran the entire domain at 30 ppm sulfur. This was considered a better alternative than applying very high U.S.-specific gasoline sulfur correction factors for advanced technology vehicles to the majority of older technology gasoline vehicles in Mexico that did not merit the adjustment.

Volatility group refers to RVP of gasoline. RVP requirements vary by month and region in Mexico. From Table E-3 above:

- Volatility Group 1 – least stringent RVP restriction
  - 69 kPa (10 psi) March to October
  - 79 kPa (11.5 psi) January–February and November–December
  - Covers the Monterrey metropolitan area and the states of Nuevo León, Chihuahua, Durango, Coahuila, Tamaulipas, San Luis Potosí
- Volatility Group 2 – moderately stringent RVP restriction
  - 62 kPa (9 psi) June–August
  - 69 kPa (10 psi) Mar–May and Sep–Oct
  - 79 kPa (11.5 psi) Jan–Feb and Nov–Dec
  - Covers the states Aguascalientes, Jalisco, Guanajuato, Michoacán, Zacatecas, Morelos, Tlaxcala, México, Distrito Federal, Hidalgo, Querétaro, Veracruz, Campeche, Puebla, Tabasco, Yucatán, Quintana Roo, Baja California, Baja California Sur, Sonora, Sinaloa, Nayarit, Colima, Guerrero, Oaxaca, and Chiapas.
- Volatility Group 3 – most stringent RVP restriction
  - 54 kPa (7.8 psi) year-round
  - Mexico City and Guadalajara metropolitan areas

C.1.2.2.8 Zone

The Zone table allocates off-network activity (related to the emission processes of start, evaporative, and extended idle emissions) from national level to municipality level. The activity allocated for off-network activity includes number of vehicle starts, source hours parked (SHP), and source hours idling (SHI). However, we did not include extended idling emissions in this inventory because this activity was deemed significantly smaller in Mexico than in the U.S.

The starts allocation was created using surrogates, as follows:

1. National to State based on relative state-level vehicle population data
2. State to County based on relative county-level human population within each state

The SHP allocations were created by calculating SHP at the state level outside of MOVES to force the resulting MOVES-allocated vehicle population to match state totals in the source data discussed in Section C.1.2.1. The equation for this calculation was Target_Population – SHO = SHP. The SHP was then normalized at the state level to create fractions that summed to one (1) over state, which were then subsequently further subdivided into municipalities using relative human population by municipality within each state. Start and Park allocations are shown below in Table C.1-5, along with running allocations discussion in the Zone Road Type table.

Table C.1-5. Allocation Factors by Mexican State

State	Running (SHO)	Start	Park (SHP)
Aguascalientes	0.013	0.013	0.012
Baja California	0.047	0.047	0.042
Baja California Sur	0.012	0.012	0.011
Campeche	0.007	0.007	0.005
Coahuila	0.027	0.027	0.026
Colima	0.008	0.008	0.007
Chiapas	0.016	0.016	0.013
Chihuahua	0.048	0.048	0.045
Distrito Federal	0.133	0.133	0.132
Durango	0.015	0.015	0.014
Guanajuato	0.041	0.041	0.043
Guerrero	0.021	0.021	0.022
Hidalgo	0.024	0.024	0.025
Jalisco	0.088	0.088	0.092
México	0.076	0.076	0.078
Michoacán	0.047	0.047	0.049
Morelos	0.014	0.014	0.015
Nayarit	0.010	0.010	0.010
Nuevo León	0.059	0.059	0.061
Oaxaca	0.019	0.013	0.014
Puebla	0.030	0.036	0.037
Querétaro	0.013	0.013	0.013
Quintana Roo	0.010	0.010	0.010
San Luis Potosí	0.024	0.024	0.024
Sinaloa	0.029	0.029	0.030
Sonora	0.029	0.029	0.030
Tabasco	0.013	0.013	0.013
Tamaulipas	0.041	0.041	0.042
Tlaxcala	0.006	0.006	0.006
Veracruz	0.045	0.045	0.046
Yucatán	0.015	0.015	0.015
Zacatecas	0.018	0.018	0.019

C.1.2.2.9 Zone Month Hour

The Zone Month Hour tables contains temperature and humidity data for each municipality by month and hour of the day. For the BOEM runs, state-level averages where applied to each municipality in the state. 2011 min/max temperatures for each state and month from CONAGUA were run through the USEPA's temperature profile generator to estimate hourly temperatures. Because no average humidity data were available for Mexico, 30-year average data contained in the U.S. MOVES default database (calculated average RH hourly profile over the four U.S. border states of Arizona, New Mexico, Texas, and California) were applied to all of Mexico.

C.1.2.2.10 Zone Road Type

The Zone Road Type table contains allocations that distribute national total VMT to municipalities, separately by road type. The allocation from nation to state reflect relative VKT at the state level based on 2013 state-level vehicle populations and VKT data discussed in Section C.1.2.1. However, there was no VKT information available at the municipality or state levels, so ERG used a surrogate of roadway distance from a GIS dataset where the roadway network included distinction by roadway type. The primary data used were state-level GIS shapefiles of lane-meters of roadway by a Mexico road type classification from INEGI, discussed in Section C.1.2.2. The detail of Mexico road type allowed us to determine the mix of Unrestricted Access vs. Restricted.

Using the GIS roadway data, we performed a GIS intersection analysis to determine which links were located in each municipality and totaled their lane-meters (total roadway capacity) accordingly. Road types from the GIS dataset were mapped to either "Restricted Access" or "Unrestricted Access" MOVES definitions, as shown in Table C.1-6, based on road definitions from INEGI (2007, 2011).

Table C.1-6. Road Type Mapping

GIS Roadtype	MOVES
ANDADOR	---
AVENIDA	UNRESTRICTED
BOULEVARD	RESTRICTED
CALZADA	UNRESTRICTED
CALLE	UNRESTRICTED
AMPLIACION	UNRESTRICTED
CALLEJON*	UNRESTRICTED
CERRADA*	UNRESTRICTED
CIRCUITO	RESTRICTED
CIRCUNVALACION	UNRESTRICTED
CONTINUACION	UNRESTRICTED
CORREDOR	UNRESTRICTED
DIAGONAL	UNRESTRICTED
EJE VIAL	UNRESTRICTED
PASAJE (PEDESTRIAN)	---
PEATONAL	---
PERIFERICO	RESTRICTED
PRIVADA*	UNRESTRICTED
PROLONGACION	UNRESTRICTED
RETORNO	UNRESTRICTED
VIADUCTO	RESTRICTED
CARRETERA	RESTRICTED

* These are very narrow roads or backstreets, with less, very slow traffic. Mostly destined for limited access to houses.

The INEGI road network did not provide any information on rural vs. urban split. ERG therefore conducted an analysis to develop a relationship between urban/rural split and population density, based on MOVES default road distribution by county and U.S. county population density data from the U.S. Census. For this analysis, ERG obtained U.S. county population and land area data from the U.S. Census Bureau, respectively (U.S. Census Bureau, 2014). ERG determined the fraction of roads that are urban using data from the default MOVES 2014 database. ERG obtained population densities and fractions of unrestricted and restricted lane miles for the municipalities (INEGI, 2010).

Generation of the primary categories in the *roadTypeDistribution* table (i.e., fractions of urban restricted, urban unrestricted, rural restricted, and rural unrestricted road types) required an estimate of both the fraction of roads classified as urban and the number of restricted and unrestricted lane miles. Direct information on urban fraction in the Mexican municipalities was unavailable, so we used data from U.S. counties to derive a relationship between population density and urban fraction. Population and land area data were obtained from the U.S. Census Bureau, as described in Data Sources above; from these, population density can be calculated. The urban fractions for U.S. counties were calculated using the *zoneRoadType* and

roadTypeDistribution tables from MOVES 2014. The relationship between urban fraction and population density was satisfactorily captured by a logistic function. Using this best-fit line, we estimated urban fractions for the municipalities based on their population densities. To determine the fraction of restricted and unrestricted lane miles, we extracted total urban and restricted lane miles from the INEGI GIS dat. Using the product of the urban (rural) fraction and the unrestricted (restricted) lane miles, normalized by total lane miles, we then calculated the *roadTypeVMTFraction* for each road type and applied this to all *sourceTypeIDs*.

After assigning urban road fractions to each municipality, the lane-meters by municipality from the GIS analysis were multiplied by urban fractions and (rural fractions, as 1 – urban) to result in the surrogate of total roadway distance by the four MOVES road types for each municipality. The total roadway distances were normalized by MOVES road type to fit the format of the Zone Road Type table. The state-level VKT determined part of the allocations from national to state, but the GIS and population density analysis drive the allocation from state to municipality. Shown in Table C.1-4 are the aggregated state-level allocations for roadways (SHO) along with allocations for starts and park discussed in C.1.2.2.8.

C.1.2.2.11 Highway Performance Monitoring System (HPMS) Vehicle Type Year

This table contains annual, nationwide total VMT by calendar year and HPMS vehicle groups. Source data included (1) 2013 state-level vehicle population discussed in Section C.1.2.1, (2) 2013 national VKT per vehicle per year, and (3) fuel projections. National vehicle populations were calculated by using per-vehicle VMT from Section C.1.2.1, converting Mexico vehicle classes to MOVES source use types using methods described for the Source Type Year table, then finally aggregating over source types to arrive at HPMS groups. The 2013 VMT was then back-casted to 2011 and projected to 2017 using domestic fuel sales projections. Totals for the BOEM domain only are shown in Table C.1-7.

Table C.1-7. Annual Mexico BOEM Domain VMT Estimates by Source Type in 2012

Source Type	BOEM Domain 2012 VMT
Motorcycles	25,332,138
Passenger Cars	150,623,217
Passenger Trucks	2,932,120
Light Commercial Trucks	112,389,342
Transit Buses	6,089,536
Single Unit Short Haul	12,727,958
Single Unit Long Haul	753,088
Combination Short Haul	5,564,744
Combination Long Haul	12,884,771

C.1.2.2.12 Source Type Year

This table contains national total vehicle population by source use type by calendar year. The source data was 2013 state-level vehicle population by Mexico vehicle type. Data provided were in a different set of Mexico-specific vehicle classes, which needed to be mapped to MOVES source use types to represent the Mexico fleet. The mapping used is shown in Table C.1-8 below.

INECC informed ERG that "Public light transport trucks" include SUVs and vans but not pickups, and "Pickup Trucks" are for transferring a product (both passenger and commercial). Population in the class "Trucks with GVW > 3 ton" was mapped to Single Unit Trucks, and the "Trailer trucks" were mapped to Combination Unit Trucks.

Table C.1-8. Vehicle Classes in Mexico Data Mapped to MOVES Source Types

#	Mexico Vehicle Type	MOVES Source Type	
1	Motorcycles	11	Motorcycle
2	Passenger cars	21	Passenger car
3	Taxi		
4	Public transport light truck	31	Passenger Truck
5	Pickup trucks	32	Light Commercial Truck
6	Trucks with GVW < 3 ton		
7	Buses	42	Transit Bus
8	Microbus/Midibus		
9	Trucks with GVW > 3 ton	52	X% Single Unit Short-haul Truck
		53	100–X% Single Unit Long-haul Truck
10	Trailer trucks	61	Y% Combination Short-haul Truck
		62	100–Y% Combination Long-haul Truck

Because we do not have use type data to distinguish long-haul vs. short-haul activity, U.S. default splits were used. The 2013 population was back-casted to 2012 using human population growth trends at the national level.

Population estimates within the Study domain for 2012 by source type (as mapped from Mexico vehicle classes from Table C.1-8 above) are shown in Table C.1-9.

Table C.1-9. Mexico Domain Vehicle Population Estimates by Source Type in 2012

Source Type	2012 Population
Motorcycles	516,053
Passenger Cars	5,465,187
Passenger Trucks	104,523
Light Commercial Trucks	3,908,579
Transit Buses	76,567
Single Unit Short Haul	267,364
Single Unit Long Haul	11,140
Combination Short Haul	49,300
Combination Long Haul	51,724

C.1.2.2.13 Source Type Age Distribution

Source data were the 2013 state-level vehicle populations data discussed in Section C.2.1, which was provided by individual model year. The Mexico classes were mapped to MOVES source use types, and distributions normalized over the 30 years available so that distributions sum to one (1). Because MOVES uses 31 years (age 0 to 30, inclusive), we divided the age 30 population by two to cover both age bins, 30- and 31-year-old vehicles. The core database was populated using only data from states where at least one municipality coincided with the 36-km domain, which covers most, but not all of the 36-km domain. Because of this difference in alignment, three central Mexican states located along the southern edge of the 36-km domain were not included in the domain-wide age distribution in MOVES-Mexico: Guanajuato, Hidalgo, and Querétaro. In addition to the domain-wide data, two external database tables were created using data specific to the border states and non-border states, separated to account for unique distributions of cars and light trucks in border area, which have a high number of aged vehicles (~ 10 years old) coming over from the U.S. The same age distributions in MOVES-Mexico are applied to all years, including 2012 for the BOEM modeling. Although MOVES has capability to project age distribution dynamically using vehicle growth and scrappage curves, the underlying data do not apply in Mexico so this feature of MOVES was not used for this Study.

C.1.2.2.14 Alternative Vehicle & Fuel Technology (AVFT)

The AVFT table determines the distribution of fuel types by source type and vehicle model year. The source data were the 2013 state-level vehicle population data discussed in Section C.1.2.1, which included a split of population by gas and diesel. ERG mapped the Mexico vehicle classes to MOVES source use types using the methods described for the Source Type Year table, preserving the details of vehicle model year and fuel type. ERG then normalized the populations so that for each model year the gas and diesel fractions summed to one (1).

C.1.2.2.15 Road Type Distribution

The Road Type Distribution table contains national fractions of VMT that occur on the four MOVES road types by source type. This table leveraged off the roadway network analysis described for the Zone Road Type table. At the stage where total lane-meters are stored by the four MOVES road types, ERG summed over the nation, and normalized. The national road type distribution is shown in Table C.1-10 below. The distribution is the same for each source type, because no information was available to allow them to vary by source type, and the U.S. defaults were not considered applicable in this case.

Table C.1-10. Mexico Road Type Fraction by Source Type

Source Type	Rural Restricted	Rural Unrestricted	Urban Restricted	Urban Unrestricted
All Source Types	0.232	0.284	0.107	0.376

C.1.2.2.16 Fuel Supply & Fuel Formulation

These tables provide the market share and properties of individual fuel formulations, broken down for each fuel region and month for the year 2012. Details of these fuels are described in detail in the discussion under Region County table.

C.1.2.2.17 Month VMT Fraction

This table allocates annual total VMT from HPMS vehicle type Year to months. Month VMT Fractions were updated using domestic PEMEX total fuel sales (gasoline + diesel together) relative in each month of the year. The assumption is that VMT will track with fuel sales.

C.1.2.3 Emission Rate Updates

C.1.2.3.1 Overview of Approach

Emission rates in MOVES were updated to reflect significant differences in vehicle emission controls between Mexico and the U.S. For this project, ERG combined two different methods to estimate emissions rates for the Mexico fleet: one for 2007 and newer light-duty vehicles, based on an adaptation of work ERG previously performed for the USEPA in developing the beta MOVES International model, and another method for both heavy-duty and older light-duty vehicles, based on fleet technology penetration. These two methods are described below.

C.2.3.2 Mapping U.S. Rates to Mexico

For Mexico, the approach taken was to adapt the U.S.-based emission rates to Mexico based on differences between the two countries in the level of emission standard and implementation years, summarized earlier in Table C.1-1. For all heavy-duty vehicles, and light-duty prior to 2006 model year, this adaptation took the form of simply re-mapping the U.S. emission rates

other model years in correspondence with Mexico standards. This approach was taken because for these vehicle classes and model years, there is a direct correspondence between Mexico vehicle standard levels and previous year U.S. standards. Mexico emission rates for 2006 and later cars and light trucks (regulatory class 20 and 30) were generated using the method (and a modified version of a script) that USEPA used to generate U.S. based rates in MOVES, as detailed in the next section.

To facilitate the development of Mexico rates, a mapping between Mexico and U.S. vehicle standards was required. This was developed based on the information provided by INECC from Table C.1-1. Tables C.1-11 through C.1-13 show the mapping of Mexico standards to U.S. standards, and how model years were correlated to enact this mapping.

Table C.1-11. Car and Light-Duty Truck (Regulatory Class 20 and 30) Exhaust Model Year Mappings

Mexico Model Year Range	Correlated U.S. Technology/Standard	U.S. Model Year or Bins Applied
1980–1990	Pre-Catalyst	1970
1991–1992	Catalyst	1980
1993–2006	Tier 0	1990
2007–2009	Tier 2 Bin 10 Phase-In	25/50/75%
2010–2012	Tier 2 Bin 7 Phase-In	25/50/70%
2013 and later	Tier 2 Bin 7	100%

Table C.1-12. Heavy-Duty Diesel Truck (Regulatory Class 40-48) Model Year Mappings

Mexico Model Year Range	Correlated U.S. Technology/Standard	U.S. Model Year or Bins Applied
1980–1992	Pre-Control	1980
1993	1991	1992
1994–1997	1994	1996
1998–2008	1998 (Electronic Control)	2000
2009 and later	2004 (EGR)	2004

Table C.1-13. Heavy-Duty Gas Truck (Regulatory Class 40-48) Model Year Mappings

Mexico Model Year Range	Correlated U.S. Technology/Standard	U.S. Model Year or Bins Applied
1980–1997	Pre-Control	1980
1998 and later	Tier 1	1998

C.1.2.3.3 Adjustment Scripts

In the case of fleet technology penetration, ERG created a spreadsheet tool that allows users to select technology penetration by both type and calendar year and use that information to reweight the existing Federal Test Procedure (FTP) phase-in fractions developed by the USEPA. Technology penetration fractions sum to 1.0, and vary from pre-Tier 1 technologies all the way through Low Emission Vehicle Phase 2 (LEV2; with Euro technologies integrated. Technology fractions can be provided for each model year to be analyzed, and users may alter or delay introduction of certain technologies as appropriate for their fleet. These inputs produced reweighted technology fractions by model year and technology type, which were also subsequently converted to comma-separated values (CSV) format and input to the modified SAS program.

For heavy-duty vehicles and older light-duty vehicles (2006 and older), the approach presented above did not apply. Instead, ERG developed a series of MySQL scripts to shift the default emission rates by model year in the MOVES Emission Rate by Age table (ERBAT) consistent with mappings shown in the tables above. These rates were then combined with the 2006 and later LD rates described above to arrive at a single ERBAT that could be used for all MOVES runs performed in Mexico.

C.1.2.3.4 Evaporative Emissions

According to INECC, evaporative emissions are not explicitly regulated in Mexico. However, for the purpose of this work, it was assumed that the level of evaporative control that corresponds with exhaust control in the U.S. would be in place in Mexico. An updated Cumulative Tank Vapor Venting Coefficient (CumTVVCoeff) table was prepared based on the mappings shown in Tables C-14 and C-15 for cars/light trucks and heavy gas trucks.

Table C.1-14. Car and Light-Duty Truck Evaporative Model Year Mappings

Mexico Model Year Range	Correlated U.S. Technology/Standard	U.S. Model Year or Bins Applied
1980–1992	Uncontrolled	1971–1977
1993–2007	Pre-Enhanced Control	1978–1995
2008–2050	Tier 2 Enhanced	2008–2016

Table C.1-15. Heavy-Duty Gas Truck Evaporative Model Year Mappings

Mexico Model Year Range	Correlated U.S. Technology/Standard	U.S. Model Year or Bins Applied
1980–1997	Pre-Enhanced Control	1978–1995
1998 and later	Enhanced Control	1998

C.1.2.4 Inventory Runs

Multiple runs of MOVES were needed to produce the emissions output needed for the onroad portion of the inventory. In order to efficiently generate the MOVES run input files (runspecs) for the 2012 MOVES runs, ERG developed a Perl preprocessing script to build the input files based on a template input file and arrays containing the required parameters of municipalities, months, years, fuel types, and emission processes that needed to be included in each unique run.

Such a large number of MOVES runs would have been a large computational burden for a standalone desktop machine. After initial runtime tests, ERG decided to setup the MOVES runs to execute in an Amazon cloud computing environment using methods adapted from ERG's support of USEPA's Office of Air Quality Planning and Standards (OAQPS) and Office of Transportation and Air Quality (OTAQ) for the NEI.

The cloud MOVES runs were grouped in units of three runs together (to separate fuels and emission processes for efficiency). There were 1,767 instances of this set of three runs. Each instance corresponds to two Amazon central processing unit (CPUs) with 4 GB of RAM, and ERG was permitted the use of 500 instances at a time. Therefore, the 1,767 instances were run in four batches. The total runtime was approximately 1,000 hours of processing time, which is about 1.3 months. The expense of using Amazon computing was a minimal cost to the project, roughly equivalent to two staff hours. ERG developed a Perl post-processing script that converts the raw MOVES output of emissions and VMT activity contained in the 1,767 MOVES output databases into a single onroad emissions by municipality, SCC, pollutant, and source type. The post-processing script executes a number of MySQL queries that (1) add labels to the database results and (2) perform basic addition and division calculations. The addition of labels was necessary to differentiate fuel processed from the MOVES outputs, as well as to make the results more easily understandable and readable.

National Scale runs covering the 589 municipalities in the Study domain were executed for each month of 2012. Output was provided by Weekday and Weekend (Post-Processed to Average Day outside MOVES). Three run specification files were developed for each municipality/year: 1) exhaust volatile organic compound (VOC), carbon monoxide (CO), and nitrogen oxides (NO_x) in a runspec run with Day pre-aggregation, 2) evaporative VOC in a runspec with Hour pre-aggregation (required, but slows runtime) outputs by Day, and 3) particulate matter with diameter less than or equal to 10 microns (PM_{10}), PM with diameter less than or equal to 2.5 microns ($PM_{2.5}$), sulfur dioxide (SO_2), and ammonia (NH_3) in a runspec with Day pre-aggregation and geographically varying gasoline sulfur values. As previously mentioned in Section E.2.2.7 of this appendix, gasoline sulfur was set to 30 ppm to prevent MOVES from over-adjusting emissions from older technology vehicles in Mexico based on U.S. model year technology and sulfur effects. However, for the particulate matter sulfate (SO_4) and SO_2, it is important to reflect sulfur content in the fuel because MOVES uses a mass balance to calculate these pollutants, and there is no conflict for these pollutants between vehicle technology and accuracy in the results. Therefore, for runspec types (1) and (2), the 30 ppm sulfur gasoline was used, but in runspec type (3), the correct geographically varying mix of 30 ppm and 300 ppm sulfur gasoline was used. Municipalities in states along the U.S. border called an external database with the border age distribution data. Likewise, other municipalities not in these states

received the non-border age distribution. Runspecs that contained PM, SO_2, and NH_3 called an external database containing the distribution of 30 ppm and 300 ppm gasoline sulfur that varied by municipality. Vehicles operating in metropolitan areas use 100 percent 30 ppm sulfur gasoline; other areas use a mix of 15 percent 30 ppm sulfur gasoline and 85 percent 300 ppm sulfur gasoline.

All runs reference the external databases EmissionRateByAge and CumTVVCoeffs, and all runs produced outputs by SCC, municipality, year, month, and day type. This resulted in 1,767 MOVES runs in total (589 counties × 3 runspecs = 1,767) running in parallel on Amazon Cloud, with an elapsed runtime of about one hour.

C.1.2.5 References

CONAGUA (Comisión Nacional Del Agua). Servicio Meteorológico Nacional (SMN). 2015. Internet address: https://smn.conagua.gob.mx/es/.

CONAPO (National Population Council). 2015. Población total con estimación en 2010 según tamaño localidad 2 tam - total. Sistema de consulta. Sistema Estatal y Municipal de Base de Datos. Internet address: http://sc.inegi.org.mx/cobdem/resultados.jsp?w=13&Backidhecho=198&Backconstem=197&constembd=199&tm=%27Backidhecho:3,Backconstem:3,constembd:3. Accessed May 26, 2015.

ICCT and INECC (International Council on Clean Transportation and National Institute of Geography and Statistics). 2015. "Market Analysis of New Light-Duty Vehicles Sales in Mexico and Comparison to U.S. Market." Presentation April 2015.

INECC (National Institute of Ecology and Climate Change). 2015. Personal communication with José Andrés Aguilar-Gómez, Deputy Director for Emission Inventories and Air Quality Modeling, INECC, and Scott Fincher, Eastern Research Group (ERG), June 12, 2015.

INEGI (National Institute of Geography and Statistics). 2007. Diccionario de datos de localidades urbanas. Internet address: https://www.inegi.org.mx/default.html. Downloaded: 06/12/2015.

INEGI. 2010. Censo Nacional de Población y Vivienda, Sistema Estatal y Municipal de Datos (SIMBAD). Population from National Census, by Municipality. Internet address: http://sc.inegi.org.mx/cobdem/. Downloaded: 5/26/2015.

INEGI, 2011. Documento técnico descriptivo – Conjunto de datos vectoriales de carreteras y vialidades. Edición 1.0. Internet address: https://www.inegi.org.mx/default.html. Downloaded: 06/12/2015.

INEGI. 2015a. Conjunto de Datos Vectoriales de Carreteras y Vialidades Urbanas Edición 1.0 (Distribución por Entidad Federativa). Sistema de consulta. Internet address: https://www.inegi.org.mx/default.html. Accessed June 12, 2015.

INEGI. 2015b. Diccionaro de datos de localidades urbanas.pdf, INEGI. Internet address: https://www.inegi.org.mx/default.html. Accessed May 26, 2015.

U.S. Census Bureau. 2014. Washington, D.C. Internet address: https://www.census.gov/programs-surveys/geography.html. Accessed May 26, 2015

Appendix C.2

Example Vessels Selected for Future Year Analysis

C.2. EXAMPLE VESSELS SELECTED FOR FUTURE YEAR ANALYSIS

C.2.1 Drilling Rigs

Drilling vessels are used for exploratory drilling to supplement the geologic information provided by survey vessels. The drilling rig drills into the ocean floor by rotating a drill bit attached to lengths of tubular pipe. Several different types of drill rigs operate in the Gulf of Mexico, including drillships, jackups, platform drilling rigs (not associated with a production platform), semisubmersibles, and submersibles. Application of the appropriate drilling rig varies relative to the water depth where they operate. For example, jackups are able to work in water up to 375 feet deep, semisubmersibles and submersibles operate in water with depths of 300 to 2,000 feet, and drillships operate in waters with depths greater than 2,000 feet.

C.2.1.1 Drillship

The drillship identified as an example vessel representing the larger drill ships is the Rowan Renaissance (IMO 9630066). According to Rowan Companies, the Rowan Renaissance is a Marshall Island flagged ultra-deep water drillship with a rated water depth of 12,000 feet and a drilling depth of 40,000 feet. This vessel was delivered in 2014 from the Hyundai Heavy Industry Shipyard in South Korea. The drillship is 752 feet in length and 118.1 feet wide, accommodating up to 210 workers. This vessel is powered by six Himsen engines with a total kilowatt rating of 48,666 kW. It is equipped with dynamic positioning using retractable thrusters. Topside equipment includes five mud pumps, three 100 ton boom cranes, and one 165 ton crane for deployment of subsea equipment.

Reference/image source: Rowan.com

C.2.1.2 Jackup Drilling Rig

The jackup rig that represents the largest vessel of this type is the Bob Palmer (IMO 8765436). According to Rowan Companies, the Bob Palmer is a super gorilla XL class jackup, delivered in 2003 by Le Tourneau at the Marathon Vicksburg Mississippi shipyard and updated in 2007. This vessel has a rated water depth of 490 feet and has 170 foot derrick with maximum drilling depth of 35,000 feet. RigZone lists the Bob Palmer as a Marshall Islands-flagged vessel, with a vessel power rating of 12,658 kW, including six 1,600 kW engines associated with the prime mover and an emergency generator of the same size. Other diesel power is used by mud pumps.

Reference/image source: Rigzone.com, Rowan.com, drillingcontractor.com

C.2.1.3 Platform Drilling Rig

Deep water spar production platforms occasionally need drilling rigs that can be assembled on the production platform and removed when they are no longer needed. The selected platform exploratory drilling rig for this upper bound category is the Modular Offshore Dynamic Series (MODS) 087. According to RigZone, the MODS 087 is a platform rig owned by Nabors Offshore with a vessel power rating of 8,100 kW, including 3,000 kW for drawworks and three 1,700 kW engines for mud pumps. The Nabors' MODS rigs are lightweight and have a small footprint, but are able to withstand strong wind and wave action typical of deep water locations. The MODS 087 rig was built in 1980 and has a drilling depth of 25,000 feet.

Reference/image source: rigzone.com, offshore-mag.com

C.2.1.4 Semisubmersible Drilling Rig

The drilling rig identified as a representative for larger semisubmersible is the ENSCO 7500 (IMO 8765008). According to RigZone, the ENSCO 7500 is Liberia flagged, built in 2000 by TDI Halter Marine in Orange, Texas. This rig is a fifth generation ultra-deep water semisubmersible drilling rig with a rated water depth of 8,000 feet and is equipped with a 170-foot derrick that allows for a drilling depth of 35,000 feet. This vessel has a power rating of 22,371 kW, including six EMD 3,700 kW engines. The rig can accommodate 140 personnel.

Reference/image source: ENSCOplc.com, rigzone.com, shipspotting.com

C.2.1.5 Submersible Drilling Rig

The Hercules 78 (IMO 8750390) was identified as a typical large submersible drilling unit. This submersible was built in 1983 by Chicago Bridge and Iron in Pascagoula, Mississippi. This vessel, owned by TODCO, is a drilling rig with a water depth rating of 85 feet and a drilling depth of 30,000 feet. According to RigZone, this vessel has a power rating of 3,691 kW.

Reference/image source: subsea.org

C.2.2 FPSO

Increasingly, vessels are used as production platforms that store processed crude in the hull, which is eventually transferred to shuttle tankers that carry the crude to shore side facilities for storage or further processing. The floating storage and production vessel (FPSO) identified with the highest power rating is the Terra Nova FPSO (IMO 9183532). This vessel is a Canadian-flagged FPSO, owned by Suncor Energy, and constructed in 2000 by the Daewoo Shipyard in South Korea. This FPSO is 292.2 meters in length and 45.5 meters wide. It has a storage capacity of 960,000 barrels of oil and can accommodate up to 120 workers. The vessel's total power rating for this vessel is of 115,432 kW (IHS, 2015). Only 14,110 kW are associated with the main propulsion engines.

Reference/image source: Suncor.com, marinetraffic.com

C.2.3 FSO

In some cases extracted crude can be pumped directly into a storage vessel and transferred to a shuttle tanker that delivers the crude to nearby refineries. The AFRICA (IMO 9224764) was identified as one of the larger floating storage vessels (FSO). The FSO AFRICA is a Marshall Islands-flagged vessel converted in 2002 from the tanker TI Africa. This vessel is 378.4 meters long, 98.05 meters wide, and can accommodate up to 84 personnel with a storage capacity of 3 million barrels. This vessel has a power rating of 51,519 kW (IHS, 2015). The dynamic positioning system has a power rating of 1,000–2,000 kW.

Reference/image source: Marinetraffic.com, sofec.com

C.2.4 Shuttle Oil Tanker

For stationary production platforms, FPSOs, and FSOs that are not connected to a subsea pipeline, shuttle tankers are used to move the extracted crude to shore. The tanker identified as represent a larger shuttle tanker is the SPT Explorer (IMO 9313486). The Skaugen Petrotrans (SPT) Company is one of the major lightering companies that account for the majority of ship-to-shore transfers of crude oil and LNG. According to SPT, the SPT Explorer is a Bahamas-flagged tanker with a cubic capacity of 719,636 barrels. This vessel is 240.5 meters in length and 42 meters in width. Constructed in 2008 by Tsuneishi Tadotsu in Tadotsu, Japan, the power rating on this vessel is 13,369 kW (IHS, 2015).

Reference/image source: Skaugen Petrotrans

C.2.5 Stimulation Vessel

The Norshore Atlantic (IMO 9545675) was identified as the stimulation vessel with the largest power rating. This vessel, registered in Norway and owned by Norshore, was delivered in 2014 from the Otto Marine yard in Batam, Indonesia. According to Norshore, the Atlantic is a multi-purpose drilling vessel that is 115.4 meters in length and 28 meters wide. The vessel's main engines include four MAK 9M25 engines and two MAK 6M25 engines, with a total propulsion power rating of 15,840 kW (IHS, 2015). The vessel is also equipped with four AvK DSG 125 and two AvK DSG 114 generators providing 14,400 kW of power. There is also a 500 kW emergency generator. For propulsion, the vessel has two 3,000 kW Tolls Royce AZP 120s. It also has three thrusters: two 1500 kW Rolls Royce TT2400, and one 660 kW TT1800; it also has one UL 2001 for dynamic positioning.

In addition to identification of a representative vessel, additional information was compiled about typical vessel operations to ensure the kW-hours were correctly estimated. Based on a communication with Dennis McDaniel and Sofia Lamon at Anadarko Petroleum Corporation, there are six stimulation vessels currently operating in the Gulf of Mexico. These vessels are similar to other support vessels, except they are equipped with large heavy-duty pumps, have storage tanks for fluids used in stimulation events, and are equipped with reels to store high pressure hoses. Generally, operators of stimulation vessels are notified 48 to 72 hours prior to a job, and they travel from a previous job site or port to the new site. They first assess the site and review operation and safety activities with staff on the rig. Once the stimulation vessel is in position, dynamic position (DP) thrusters maintain the vessel's position; in typical conditions the DP system is operating 50% of the time the vessel is on site (approximately 12 to 24 hours per job). Rig set up is implemented where the high pressure hose is unwound from the reel and gradually dropped to the well head. Once the hose is connected to the well head, the line is tested for leaks. Fracturing fluids are pumped into the well at relative high pressure for a period from 4 to 12 hours (average 8 hours). After the stimulation episode is completed, the process is reversed; the hose is disconnected from the well head and wound back onto the reel. The vessel can repeat the process for adjacent well heads as required by the operator prior to moving offsite. Note that most stimulation vessels are able to support a wide variety of subsea system maintenance activities in addition to fracturing operations.

In general, the fleet of stimulation vessels in the Gulf of Mexico currently has a utilization rate of 70 to 75%. Each site visit has a duration of 2 to 5 days, including transit times, port visit for restocking, and regular maintenance activities. A typical vessel will make 35 site visits in a year. Fracturing activities can be implemented for all types of wells, including deep water sites.

To estimate typical levels of activity for stimulation vessels the following assumptions were made:

- A typical site visit is 5 days.
- DP is operating for approximately 60 hours.
- Pumps and mixers are operating approximately 8 hours per job, and during the 5-day period, it is assumed that three jobs are implemented, which would equate to 24 hours of operation for the high pressure pumps and mixers.
- During the 5-day site visit, smaller auxiliary engines are operating to provide electricity for normal electricity demand activities, such as cabin cooling and lighting, navigation systems, operation of cranes, winches, and safety devices.

BOEM's 2017–2022 National OCS Oil and Gas Leasing Program (2017–2022 Program) information did not include activity specifically for stimulation vessels, therefore annual emissions were developed and apportioned to each planning area. It was also assumed that activities for these vessels would remain constant over the study period.

Table C.2-1 below shows the estimated hours of operation for a simulation vessel per site and annually.

Table C.2-1. Stimulation Vessel Activity in Hours per Visit and Annual Hours of Operation

Operation	Hours Per Site Visit	Annual Hours Per Vessel
Transit	32	1,130
DP	12	420
Pumps and mixers	8	280
Auxiliary engines	24	840

The hours of operation provided in the above table are rough approximations; actual vessel-specific activity may be significantly greater than or lower than the values shown here. The estimated annual hours were applied to the power data for the Norshore Atlantic as a surrogate vessel, and load factor assumptions were applied to estimate kW-hours per stimulation vessel. The projected number of stimulation vessels was based on the observation that in 2015 there were six vessels in operation. The GOMR oil production rate in 2015 was 1.52 million barrels of oil per day. In the 2017–2022 Program information, the anticipated oil production rate was 0.045 million barrels of oil per day for the Western GOM Planning Area and 0.527 million barrels of oil per day for the Central/Eastern GOM Planning Area, providing an anticipated total production rate of 0.572 million barrels per day in 2036. Based on the observation that six stimulation vessels are associated with a production rate of 1.52 million barrels per day in 2015, it is estimated that 2.3 stimulation vessels would be associated with the additional production of 0.572 million barrels per day. This estimate of the stimulation vessels needed for the projected lease activity is applied to the total annual kW-hrs per vessel to get total annual stimulation vessel kW-hrs (Table C.2-2).

Table C.2-2. Stimulation Vessel Activity (kW-hrs)

Operation	Annual Hours Per Vessel	Power Rating kW	Load Factor	kW-hrs
Transit	1,130	6,000	0.85	5,763,000
DP	420	5,160	0.50	1,083,600
Pumps/mixers/compressors	280	14,400	0.65	2,620,800
Auxiliary engines	840	500	0.60	252,000
Total Annual kW-hrs				9,719,400
Projected vessel operations (2.3 vessel equivalents)				22,354,620

These kW-hrs were applied to the Category 2 vessel emission factors to estimate annual emissions (Table C.2-3). The total emissions were split by area based on the projected daily production rates noted above.

Table C.2-3. Stimulation Vessel Emissions by Planning Area (tons per year)[a]

	NO_x	SO_2	PM_{10}	$PM_{2.5}$	VOC	CO	HC	NH_3	Pb
CPA/EPA	71.4	0.1	6.7	6.5	3.0	52.1	2.7	0.10	0.00063
WPA	12.6	0.02	1.2	1.1	0.5	9.2	0.5	0.02	0.00001
Total	84.0	0.102	7.9	7.7	3.5	61.2	3.2	0.12	0.00074

[a] Totals may not sum due to rounding.

Reference: Norshore Atlantic specifications and photo: Norshore.com, marinetraffic.com, personal correspondence between Dennis McDaniel and Sofia Lamon, Anadarko Petroleum Corporation, and Richard Billings, Eastern Research Group, Inc. January 15, 2016.

C.2.6 Pipelaying Vessel

Saipem's Castorone (IMO 944194) is one of the larger pipelaying vessels, with a power rating of 67,200 kW (eight 8,400 kW main engines and a 1,200 kW emergency generator). The Castorone was constructed in 2012 at the Keppel Shipyard in Singapore and registered in the Bahamas. The vessel has worked in the Gulf of Mexico despite being an ice-class pipelaying vessel. This vessel is 330 meters in length and 39 meters in width and can house up to 702 people. This vessel has a maximum speed of 14 knots and has a pipelaying capacity of triple joint 12 meter pipe or double joint 18 meter pipe, with pipe size up to 48 inches.

Reference/image source: Saipem.com

C.2.7 Support Vessels

Historically, service vessels operating in the Gulf of Mexico include 1) anchor handling vessels, 2) crew boats that transport workers to and from work sites, 3) supply vessels, and 4) tug boats that transport heavy equipment and supplies.

C.2.7.1 Anchor Handling Vessel

The anchor handling vessel with the highest vessel power rating was identified as KL Sandefjord (IMO 9470466). This vessel is a Norwegian flagged tug/supply vessel built in 2011 at the Vard Langsten in Tomrefjord, Norway. The Sandefjord is 95 meters long and 24 meters wide and has a vessel power rating of 27,000 kW (IHS, 2015).

Reference/image source: marinetraffic.com, maritime-connector.com

C.2.7.2 Crew Boat

The crew boat with the largest vessel power rating was identified as R. J. Coco McCall (IMO: 9618109). The R. J. Coco McCall is a Marshall Island flagged passenger vessel that was built in 2011. This vessel is 57.93 meters in length and 10.36 meters wide and has a vessel power rating of 11,520 kW (IHS, 2015).

Reference/image source: marinetraffic.com, shipspotting.com

C.2.7.3 Supply Vessel

The Aleksey Chirikov (IMO 9613551) is representive of a larger supply vessel. This Russian-flagged offshore supply ship, built in 2013 by Arctech Helisinki Shipyard in Finland, which is currently owned and operated by Sovcomflot. This vessel is 99.9 meters in length and 21.26 meters wide and has a vessel power rating of 18,000 kW (IHS, 2015).

Reference/image source: marinetraffic.com

C.2.7.4 Tug Boat

The tug boat with the largest power rating was identified as Yury Topchev (IMO 9338230). The Yury Topchev is a Russian-flagged tug, built in 2006 at the Havyard Leirvik yard in Leirvik-Sogn yard in Norway and is currently owned and operated by Gazflot. This vessel is 99.3 meters in length and 19.04 meters wide and has a vessel power rating of 19,990 kW (IHS, 2015).

Reference/image source: marinetraffic.com

C.2.8 References

IHS (Information Handling Services). 2015. Register of Ships. 2014.

Appendix D.1

Coarse Nitrate Sensitivity Analyses

Introduction

The Comprehensive Air Quality Model with Extensions (CAMx) simulations for the Gulf of Mexico Region (GOMR) air quality study parameterize particle formation using the Coarse-Fine (CF) scheme (Ramboll Environ, 2016). The CF scheme represents particulate matter (PM) species formed in the atmosphere from gaseous precursors (secondary PM) using a single fine mode ($PM_{2.5}$) size bin, while primary inert PM species (e.g., dust particles) are allocated into both the fine and coarse mode ($PM_{10} - PM_{2.5}$) size bins. This is a good approximation under many atmospheric conditions where fine particles ($PM_{2.5}$) dominate particle surface area and consequently increases in particle mass due to chemistry occur mainly in the $PM_{2.5}$ size range. However, formation of coarse mode secondary aerosols can become important where abundant coarse mode particles (e.g., dust or sea salt) are available for binding with sulfate or nitrate ions, and for hygroscopic aerosols (e.g., sodium nitrate) that can grow into the coarse size range by water uptake. In coastal marine environments such as the GOMR, abundant coarse sea salt aerosols may play an important role in secondary PM formation. Therefore, neglecting coarse secondary PM species—particularly coarse mode nitrate (NO_3)—may bias the model results.

We conducted two sensitivity analyses to investigate the potential importance of coarse mode secondary PM formation. To accomplish this, we compare CAMx results using the CF scheme with CAMx results using an alternative particle scheme that accounts for potential coarse mode secondary PM formation. This alternative scheme—called the simplified CMU scheme—is described in the next section. We compared model results under the CF and CMU schemes for a 21-day episode characterized by high coastal NO_3 and sea salt concentrations taken from the CAMx 2012 base case GOMR modeling scenario. We also compared results using the CF and CMU schemes in model runs in which several hypothetical new offshore oil and gas platform nitrogen oxide (NO_X) sources were added to the simulation. These comparisons provide an indication of the potential effect of including coarse mode nitrate specifically on modeled impacts of new offshore sources such as might be associated with newly developed oil and gas leases.

Alternative Aerosol Modeling Scheme with Coarse Secondary PM

In addition to the CF scheme, CAMx provides an alternative aerosol modeling approach called the CMU scheme (Pandis et al., 1993), which represents the aerosol size distribution using several discrete size bins (typically 4 to 10 size bins are used) and allocates secondary PM formation to each bin—including coarse mode bins—according to the aerosol surface area present in the bin. Using multiple size bins provides a more realistic representation of the particle size distribution but requires many more PM model species (the number of PM components multiplied by the number of size bins) than the CF scheme, thus leading to a significant increase in model run time. To limit computational burden and quickly assess the effects of coarse secondary PM formation on model results for this study, we simplified the CMU scheme to model both primary and secondary PM species using just two size bins (one for fine and one for coarse mode particles). We disabled mass transfer between the size bins, which the CMU scheme normally includes, to avoid artificial and excessive mixing of fine and coarse particles due to the wide gap between the representative (geometric mean) diameters of the two size bins. The

simplified two-bin CMU scheme allows CAMx to form secondary aerosol in both the fine and coarse size ranges as illustrated in Figure D.1-1.

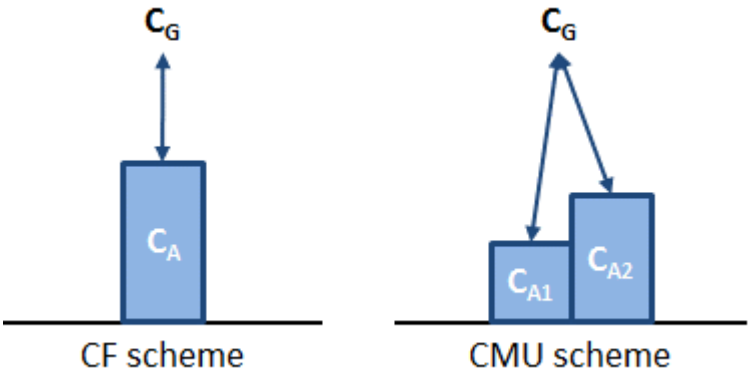

Figure D.1-1. Illustration of Gases (C_G) Condensing/Evaporating to Aerosol (C_A) With a Single Size Mode (fine) in the CF Scheme Versus Two Size Modes (fine and coarse) in the CMU Scheme

Base Case Sensitivity Test

Input Data

We used the 2012 full annual base case CAMx modeling database for testing the formation of secondary coarse mode particles within the simplified two-bin CMU scheme described above. We reviewed results from the annual 2012 base case simulation performed using the CF scheme to identify a suitable period for the sensitivity analysis characterized by relatively high sea salt and high nitrate impacts along portions of the Gulf Coast. We selected a 26-day period (November 8 to December 3) with the first 5 days used as a spin-up period to reduce the impact of initial conditions.

Fine-mode sea salt aerosol emissions of Na, Cl, and SO_4 for the 2012 base case CAMx simulation were generated by the CAMx sea salt preprocessor as described in Section 4.3.5.5. For the sensitivity test, the preprocessor was re-run to add coarse mode sea salt emissions. Similarly, the GEOS2CAMx processor was re-run to add coarse sea salt to the CAMx 36-km domain boundary concentrations (BCs) using the 2012 GEOS-Chem global simulation results of coarse sea salt particles (SALC).

As in the full annual simulation, CAMx was first run for the 36-km grid alone with the revised BCs that include coarse mode sea salt. Results from this simulation were then used as BCs for the (two-way nested) 12- and 4-km grid simulation (modeling domains are depicted in Figure 2-1). Except for changing the aerosol scheme from CF to simplified CMU, the CAMx configuration remained the same as in the full annual base case simulation.

Results and Discussion

Base Case Comparison

The CAMx modeling results with the CMU scheme were compared with results from the CF scheme. Figure D.1-2 shows average concentrations over the 12-km modeling domain of fine ($PM_{2.5}$) NO_3, NH_4, Cl, Na, and SO_4 predicted by the CF and CMU schemes and their differences. Because no transfer of particle mass between the fine and coarse size bins is allowed by the simplified CMU scheme, both schemes show almost identical $PM_{2.5}$ mass concentrations of non-volatile components, Na and SO_4. The schemes can differ for secondary $PM_{2.5}$ species that form by condensation of gaseous precursors. In most areas of the domain, the CMU scheme predicts less fine mode NO_3 than the CF scheme because a portion of the available nitric acid (HNO_3) is partitioned to coarse mode particles such as sodium nitrate ($NaNO_3$) by the CMU scheme. This leads to less HNO_3 being available to form fine mode $NaNO_3$ and NH_4NO_3. In some portions of the Gulf of Mexico and west Texas, the CMU scheme predicts higher $PM_{2.5}$ NH_4. This may be attributed to increased NH_4Cl formation from hydrogen chloride (HCl) released from the coarse mode sea salt particles when coarse $NaNO_3$ forms. Differences in $PM_{2.5}$ Cl between the two schemes are mostly small except near the eastern boundary of the domain, where the CMU scheme predicts slight increases in $PM_{2.5}$ Cl due to the influence of coarse mode chloride from the CAMx BCs that can migrate from coarse to fine mode by evaporation/condensation of HCl gas.

Base Case Model Performance

Predictions of $PM_{2.5}$ NO_3, NH_4 and Cl by the CF and CMU schemes were evaluated against ambient measurements at the IMPROVE, CSN, and SEARCH monitoring sites. Figure D.1-3 presents scatter plots of observed vs. modeled 24-hour average concentrations of these $PM_{2.5}$ components at monitoring sites within the full 12-km modeling domain and just within the 4-km domain. As shown in the full annual 2012 base case model performance evaluation presented in Section 4.5.5.3 of the main report, CAMx with the CF scheme generally overestimates $PM_{2.5}$ NO_3. Allowing formation of coarse nitrate the CMU scheme somewhat reduces this overestimation bias, though the improvement is not dramatic. Conversely, $PM_{2.5}$ Cl is underestimated by both aerosol schemes with the CMU scheme again showing slightly better performance. It should be noted that there is only one IMPROVE site (Breton Island, LA) within the 4-km modeling domain, and the model performance at this site may not adequately represent performance which can be expected over the entire 4-km grid.

These results demonstrate that accounting for coarse mode nitrate formation may lead to a slightly better agreement with observed PM measurements. Overall, however, the CMU scheme did not significantly improve model performance, indicating that there are likely other factors contributing to the remaining performance issues.

Sensitivity to New Source Emissions

To better understand the effect of coarse mode secondary PM formation on new source impacts over the GOM region, we conducted sensitivity simulations using the 2012 base case modeling scenario that added three new hypothetical offshore point sources of nitric oxide (NO) emissions. As shown in Figure D.1-4, the hypothetical new sources are located in the Outer Continental

Shelf region as close to the shoreline as possible (right at the edge of the BOEM Planning Area) so that their emission plumes likely reach inland areas. As shown in Table D.1-1, each hypothetical source emits NO at the rate of 1,000 TPY into the fourth model layer, which extends from 40.4 to 56.6 m above the surface.

Table D.1-1. Locations and Emissions for Hypothetical Point Sources of Nitric Oxide (NO)

Source	Location		Effective Plume Height (m)	NO Emissions (TPY)
	Latitude	Longitude		
A	29.268	-94.571	50	1,000
B	29.025	-89.036	50	1,000
C	30.124	-88.386	50	1,000

Impacts of the new sources are calculated by subtracting predicted concentrations in the base case from the simulations with the new sources added. Both the CF and simplified two-bin CMU aerosol schemes were applied to assess the new source impacts on modeled $PM_{2.5}$ nitrate (PNO3). The sensitivity simulations were run for the same episodes used in the base case sensitivity analysis (November 8 to December 3, 2012) with simulation results for the first 5 days discarded to minimize the effect of initial conditions.

Figure D.1-5 (a) compares domain-wide maximum new source impacts on 24-h average PNO3 by the CF and CMU schemes over the 4-km modeling domain. Both schemes predict very similar maximum impacts (which may occur at different locations) except on the last day of the test period (December 3). The magnitudes of maximum and minimum (spatially paired) differences in new source impacts between the two schemes are less than 0.05 $\mu g/m^3$, except for the last day when the CF scheme predicted a 0.08 $\mu g/m^3$ higher PNO3 impact than the CMU scheme, as shown in Figure D.1-5 (b).

Figure D.1-6 shows spatial distributions of the new source impacts on PNO3 by the CF and CMU schemes and their differences in the 4-km modeling domain on one high impact day (November 23). On this day, both schemes predict similar domain maximum PNO3 impacts (0.23 $\mu g/m^3$ by CF and 0.24 $\mu g/m^3$ by CMU), both occurring within one grid cell of each other in Chambers County, Texas, downwind of hypothetical source A.[1] The maximum spatially paired difference in predictions under the two schemes occurs downwind of Source C just south of Mobile, AL, but an almost equal sized increase (0.03 $\mu g/m^3$) occurs nearby, indicating that the location of the PNO3 impact area from Source C is slightly shifted under the CMU scheme compared to the CF scheme, with little change in the maximum impact. On December 3 (Figure D.1-7), both schemes show maximum new source impacts near Biloxi, Mississippi (from the hypothetical source C) with the CMU scheme predicting a smaller peak impact of 0.12 $\mu g/m^3$ compared to 0.18 $\mu g/m^3$ under the CF scheme which is a difference of about 30%.

Results in Figures D.1-6 and D.1-7 show that maximum differences between the CF and CMU schemes in 24-hour average incremental contributions of PNO3 from offshore NO_X sources in

[1] Closer to the source, both aerosol schemes show negative impacts on PNO3 (i.e., the additional NO emissions decreased PNO3 concentrations). This is a result of the added NO from the new source suppressing oxidant concentrations, thus delaying formation of HNO3 and PNO3.

Federal waters just outside the state seaward boundary are negligible throughout the 4-km domain during the 21-day test period except for one day (3 December) during which there was a sizable difference at one location near Biloxi, MS, where the CMU prediction was ~ 30% less than the CF prediction.

Summary and Conclusions

Results from the sensitivity analyses described above indicate that reductions in PNO3 under the CMU scheme compared to the CF scheme are ~ 5% along the Louisiana Coast west to Galveston, where PNO3 impacts are highest. Thus, the simplified particle size mode treatment for secondary PM employed by the CF scheme introduces only a small positive bias in predicted fine mode PNO3. Consequently, comparisons of predictions under both particle schemes with fine mode NO_3 observations show that only a small fraction of the large PNO3 over prediction bias can be attributed to neglecting coarse mode NO_3 formation under the CF scheme.

Maximum differences between the CF and CMU schemes in 24-hour average incremental contributions of PNO3 from offshore NO_X sources in Federal waters just outside the state seaward boundary are negligible throughout the 4-km domain during the 21-day test period except for one day in which there was a sizable difference (the CMU prediction was ~ 30% less than the CF prediction) at one location. In other words, biases in modeled offshore NO_X source PNO3 impacts introduced by ignoring coarse mode NO_3 formation in the CF scheme are negligible under most circumstances, although there may be isolated instances of differences as large as ~30%.

Overall, results of this sensitivity analysis show that the assumption of negligible coarse mode secondary particle formation employed by the CF scheme is appropriate and does not introduce significant errors in estimates of particulate NO_3 impacts.

References

Pandis, S.N., A.S. Wexler, J.H. Seinfeld. 1993. Secondary organic aerosol formation and transport, II, Predicting the ambient secondary organic aerosol size distribution. Atmos. Environ., 27A, 2403-2416.

Ramboll Environ. 2016. CAMx User's Guide: Comprehensive Air Quality Model with Extensions, Version 6.40. Ramboll Environ, Novato, CA. Internet address: www.camx.com. Accessed August 7, 2018.

(a) $PM_{2.5}$ NO_3

CF

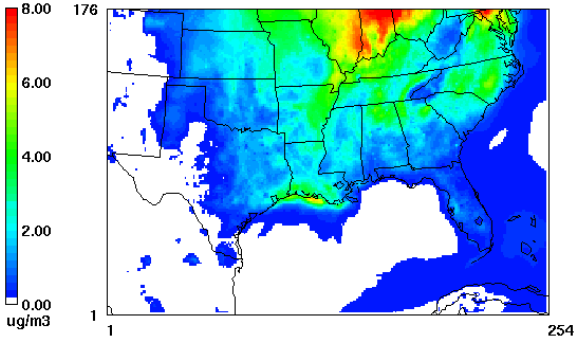

Min=0.00 at (1,1), Max=8.87 at (166,175)

CMU

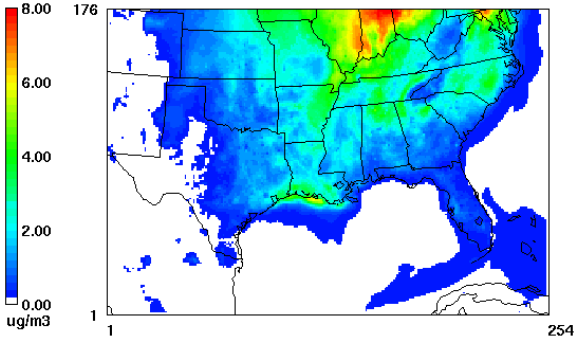

Min=0.00 at (1,1), Max=8.16 at (166,175)

CMU – CF

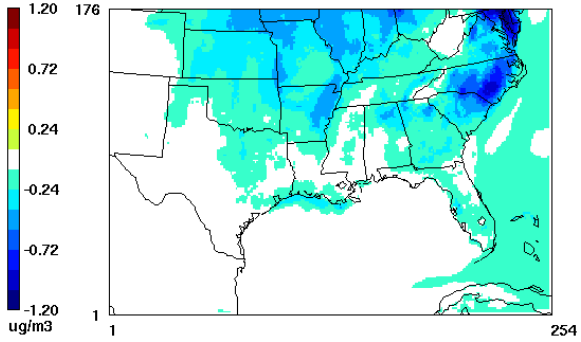

Min=-1.16 at (229,171), Max= 0.06 at (200,159)

(b) $PM_{2.5}$ NH_4

CF

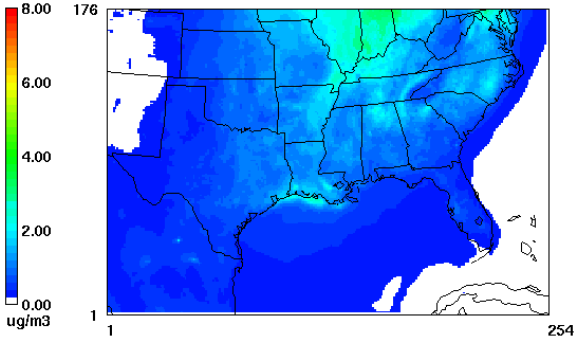

Min=0.00 at (1,1), Max=3.29 at (167,175)

CMU

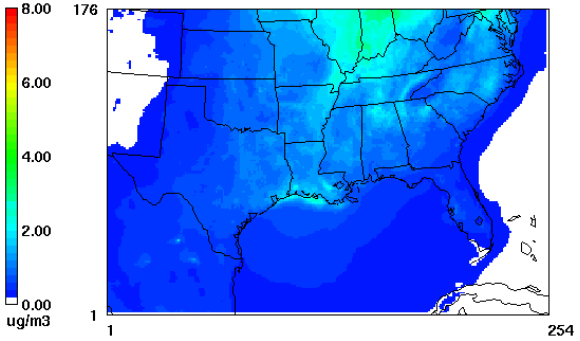

Min=0.00 at (1,1), Max=3.10 at (161,175)

CMU – CF

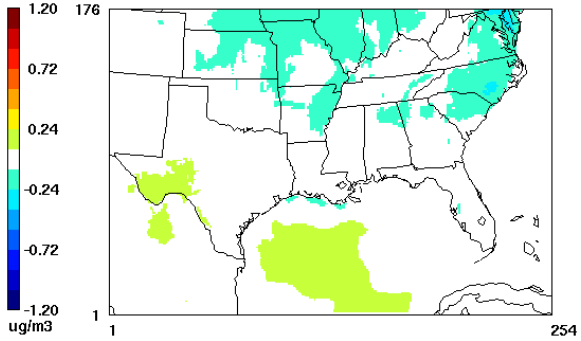

Min=-0.32 at (229,171), Max= 0.13 at (41,80)

(c) $PM_{2.5}$ Cl

CF

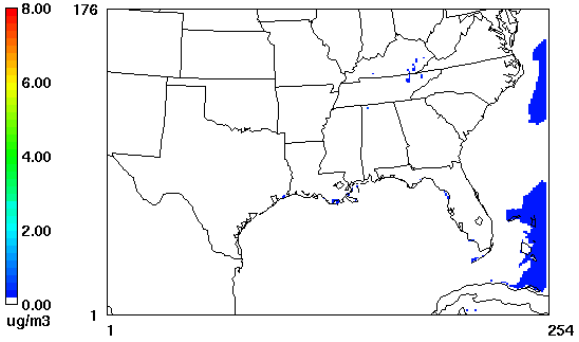

Min=0.00 at (1,1), Max=0.64 at (151,119)

CMU

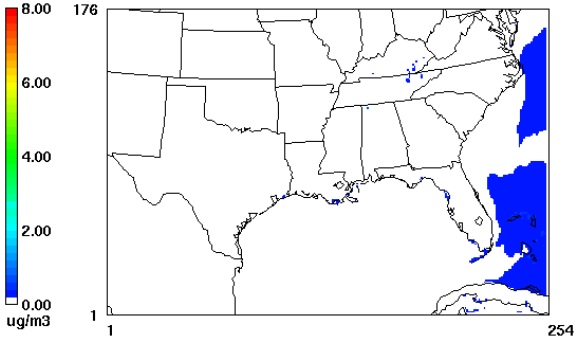

Min=0.00 at (1,1), Max=0.74 at (211,43)

CMU – CF

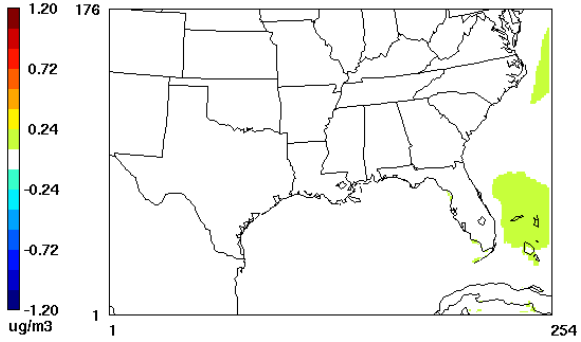

Min=-0.03 at (177,144), Max= 0.15 at (211,43)

(d) $PM_{2.5}$ Na

CF

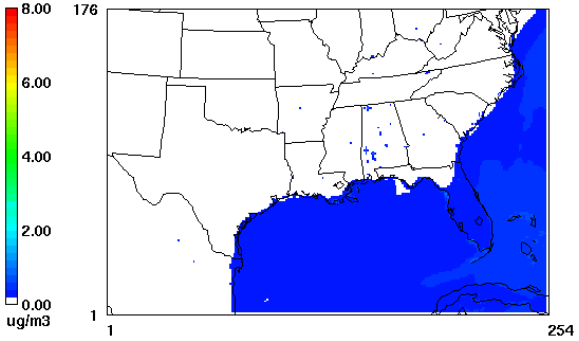

Min=0.00 at (1,1), Max=1.22 at (211,43)

CMU

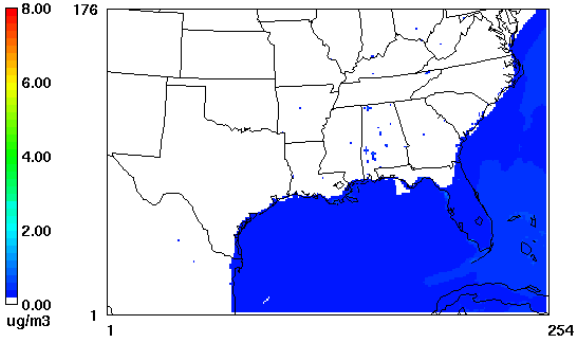

Min=0.00 at (1,1), Max=1.22 at (211,43)

CMU – CF

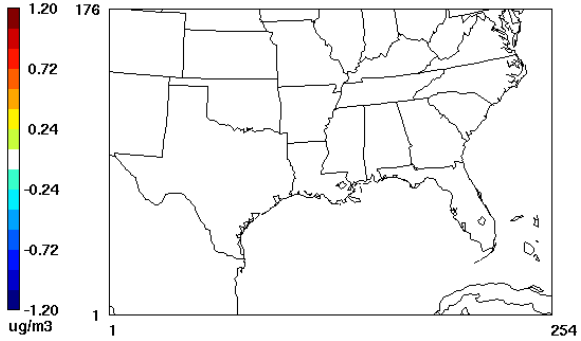

Min=-0.01 at (249,121), Max= 0.00 at (73,4)

(e) $PM_{2.5}$ SO_4

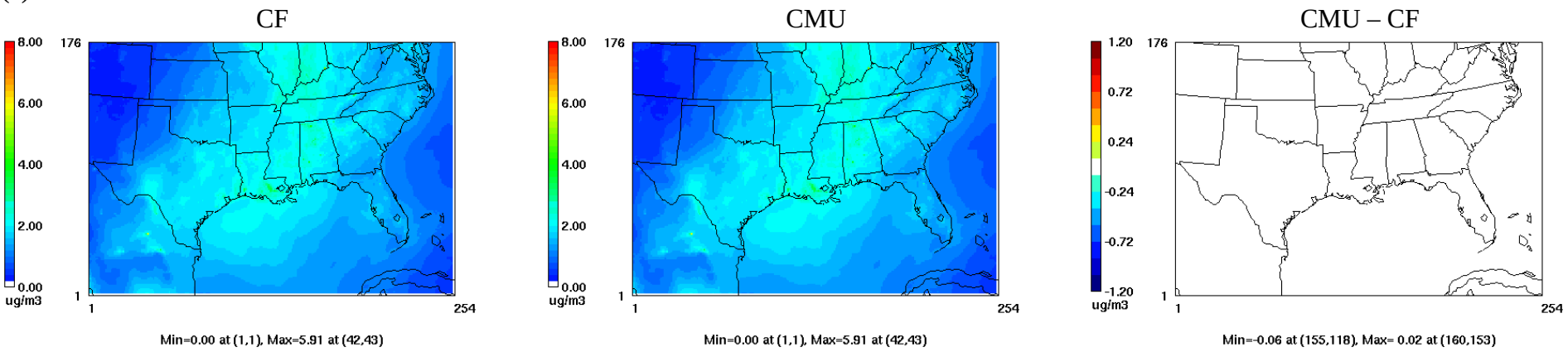

Figure D.1-2. Episode Average Concentrations ($\mu g/m^3$) of Inorganic $PM_{2.5}$ Constituents Predicted by the CF (left) and CMU (middle) Schemes and Differences Between the Two Schemes (right) for a) NO_3, b) NH_4, c) Cl, d) Na, and e) SO_4

(a) $PM_{2.5}$ NO_3 at IMPROVE sites

12-km grid

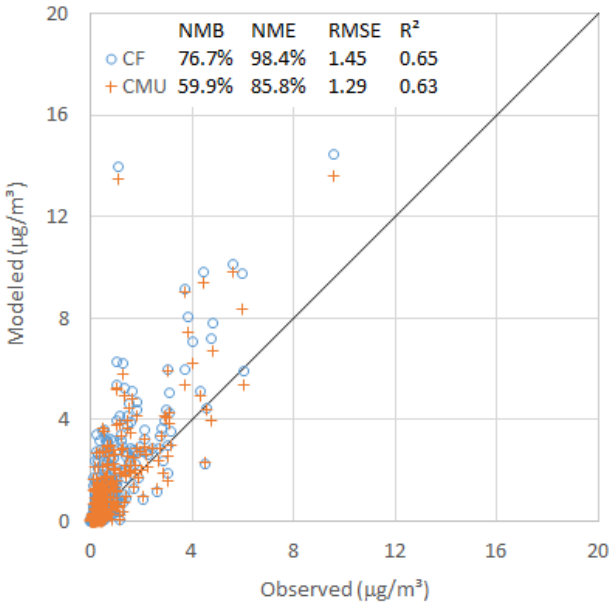

4-km grid

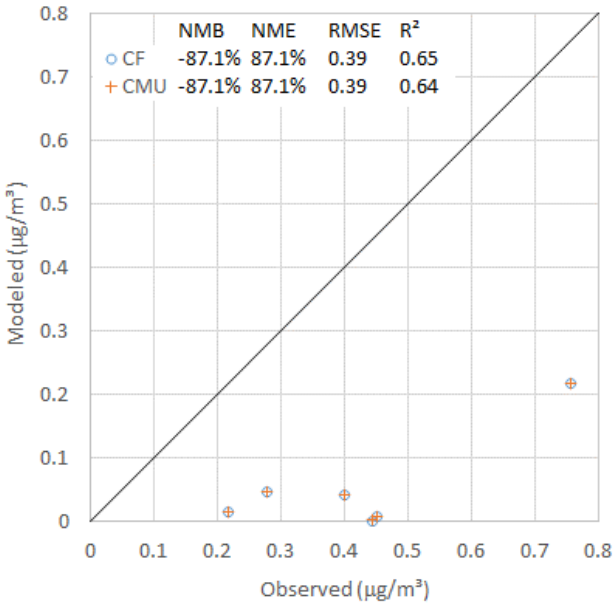

(b) $PM_{2.5}$ NH_4 at IMPROVE sites

12-km grid

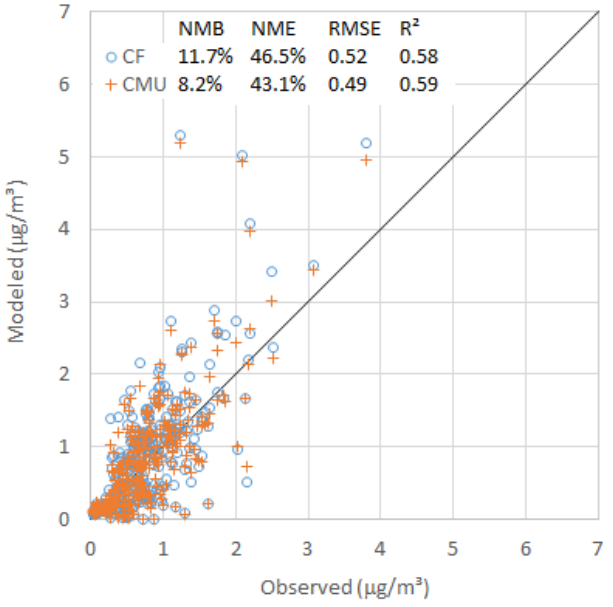

4-km grid

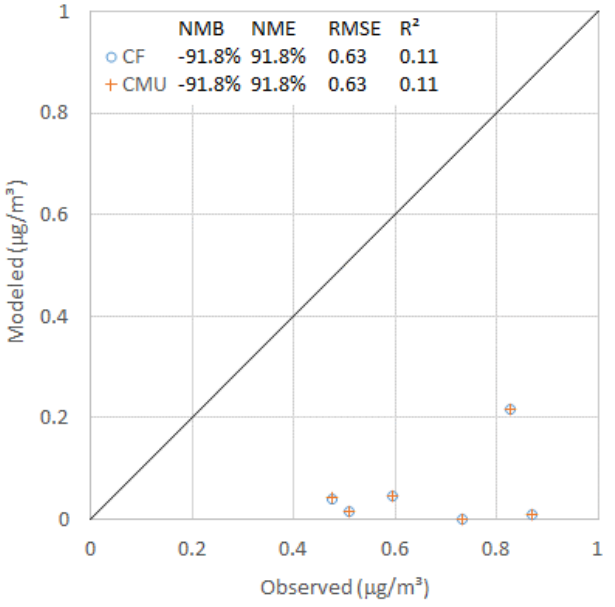

(c) $PM_{2.5}$ Cl at IMPROVE sites

12-km grid

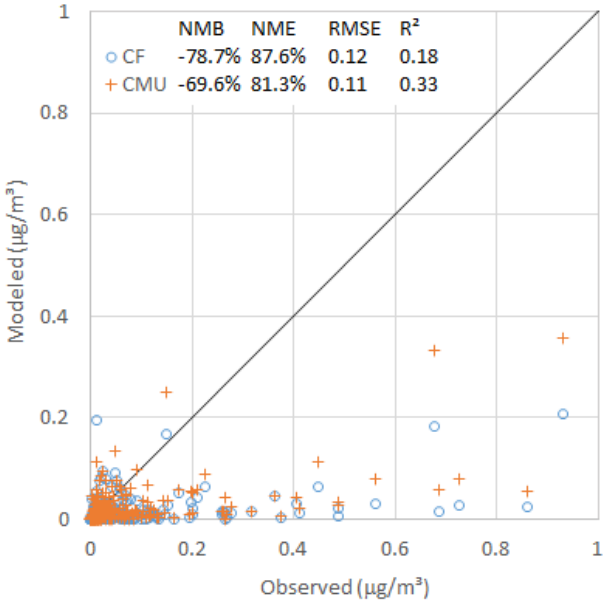

4-km grid

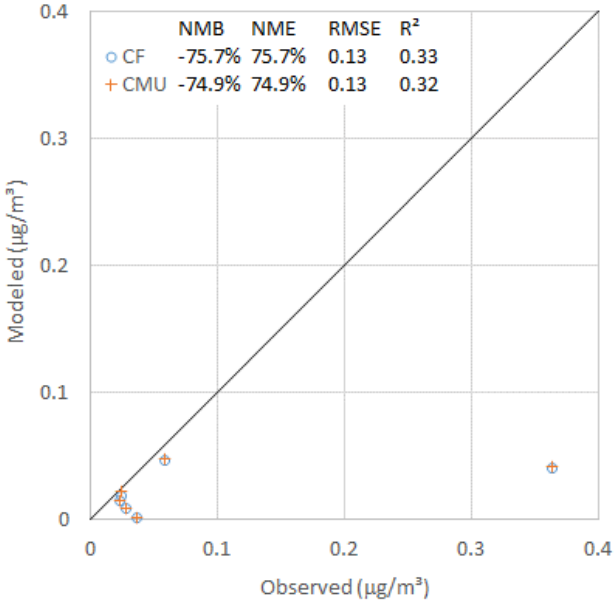

(d) $PM_{2.5}$ NO_3 at CSN sites

12-km grid

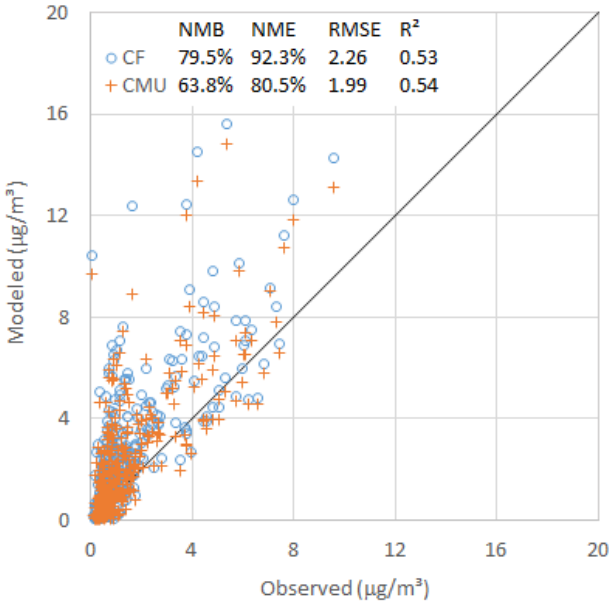

4-km grid

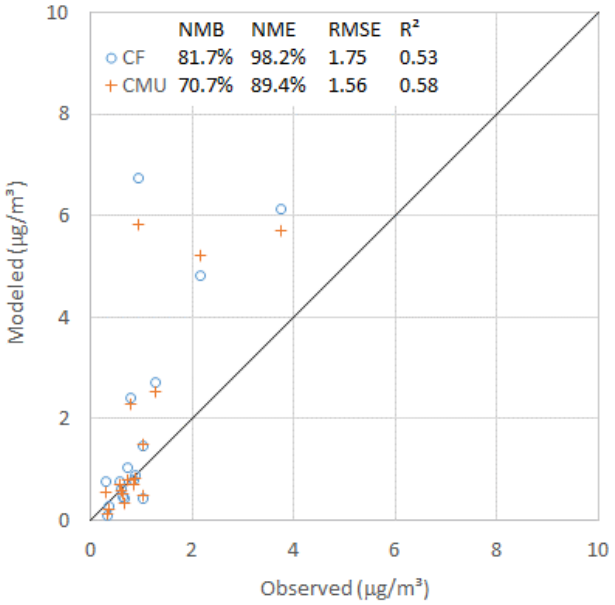

(e) $PM_{2.5}$ NH_4 at CSN sites

12-km grid

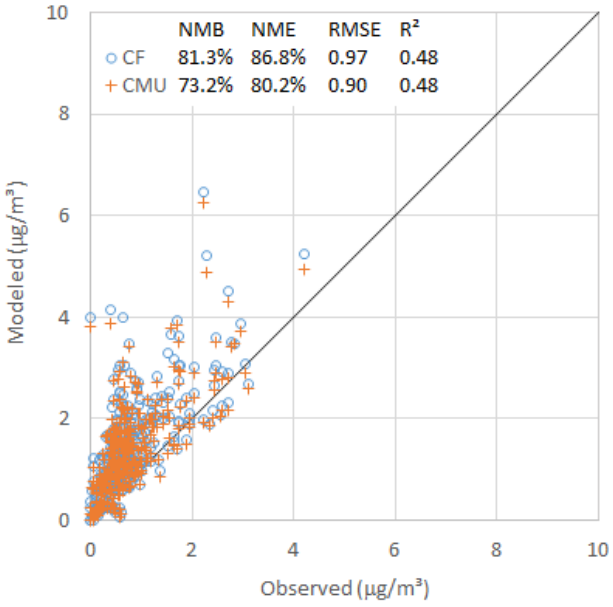

4-km grid

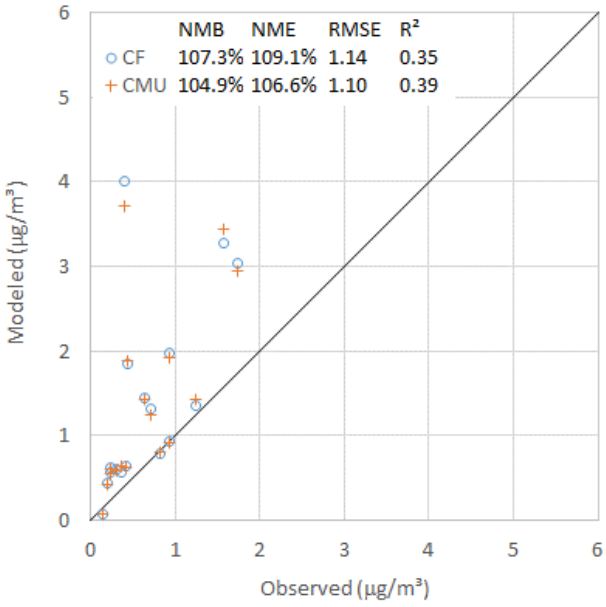

(f) $PM_{2.5}$ Cl at CSN sites

12-km grid

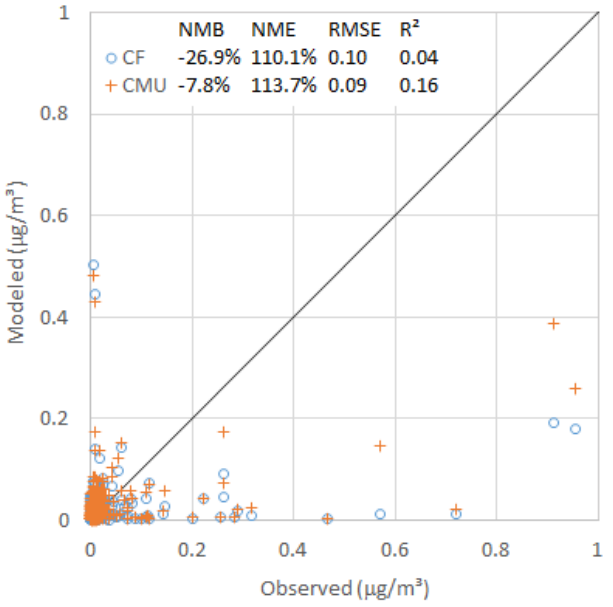

4-km grid

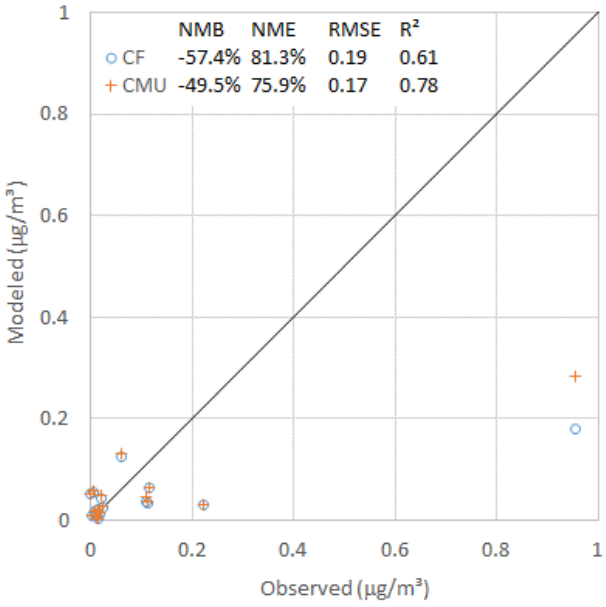

(g) $PM_{2.5}$ NO_3 at SEARCH sites

12-km grid

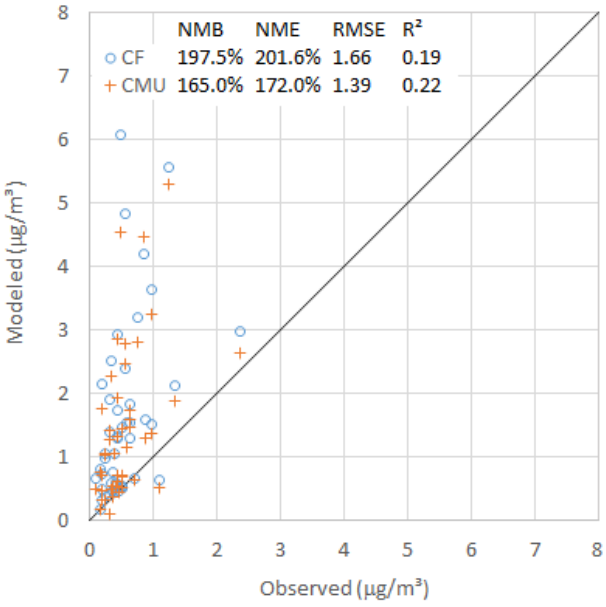

4-km grid

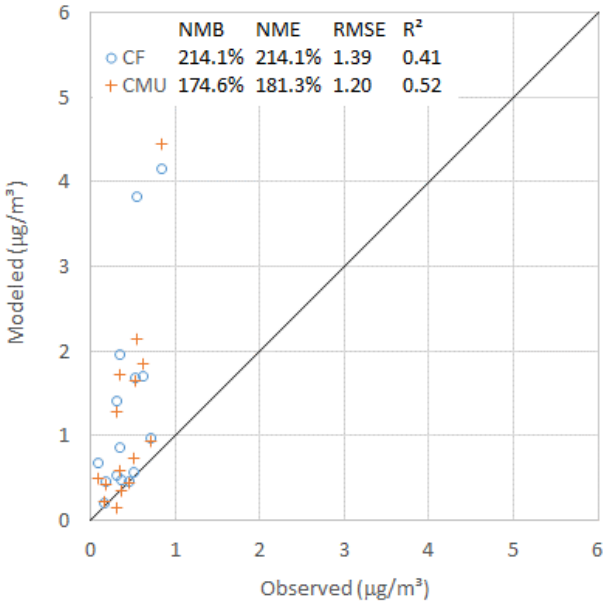

(h) $PM_{2.5}$ NH_4 at SEARCH sites

12-km grid

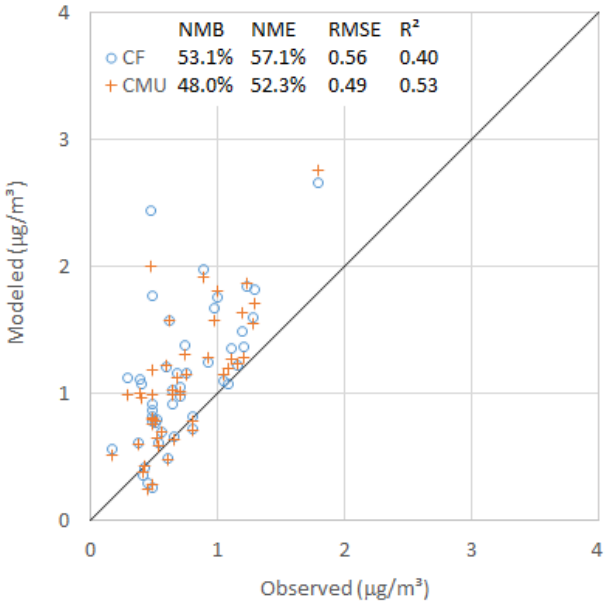

4-km grid

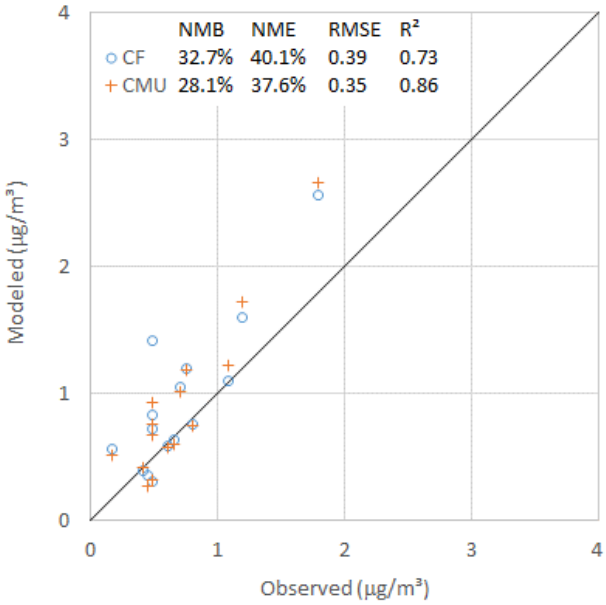

(i) $PM_{2.5}$ Cl at SEARCH sites

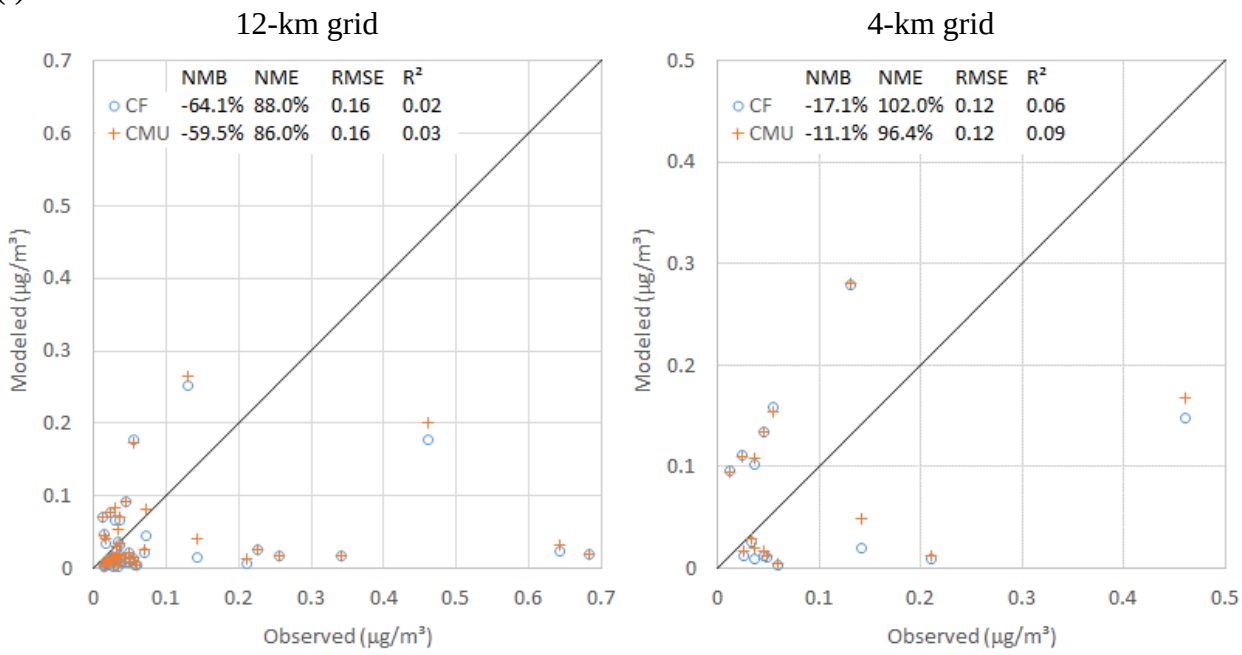

Figure D.1-3. Scatter Plots of Observed (at IMPROVE, CSN, and SEARCH monitoring networks) vs. Modeled (from CF and CMU schemes) 24-hour Average Concentrations of $PM_{2.5}$ Nitrate (NO_3), Ammonium (NH_4), and Chloride (Cl)

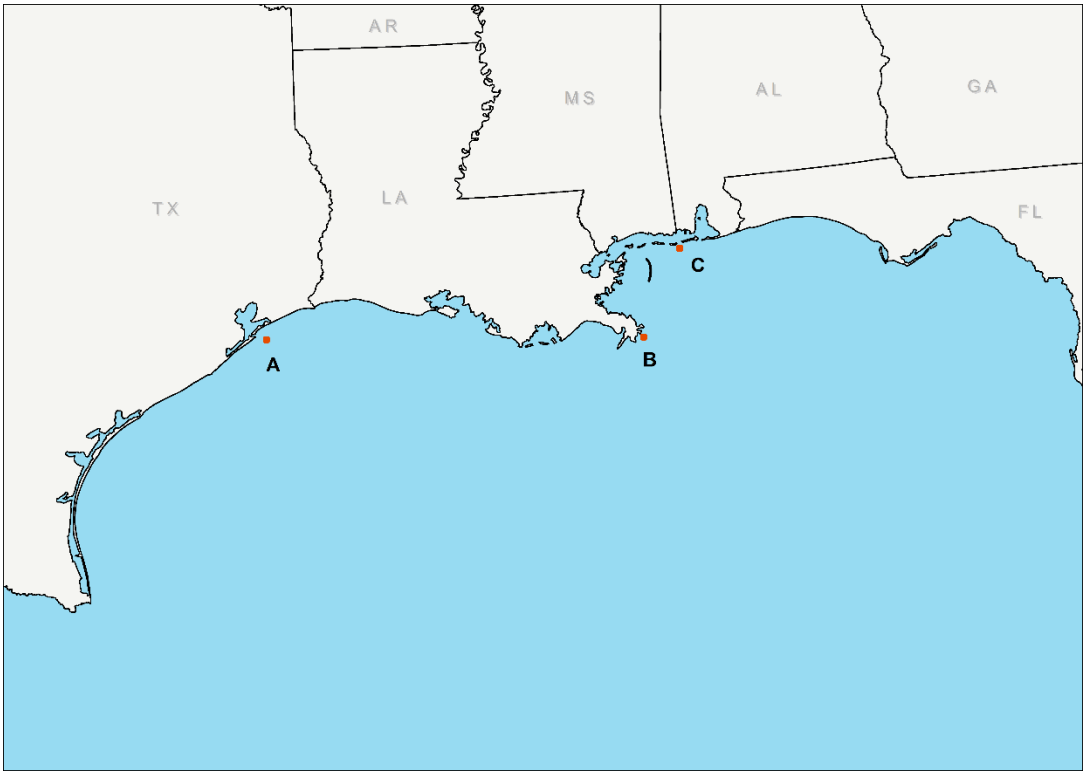

Figure D.1-4. Locations of the New Hypothetical Sources Added

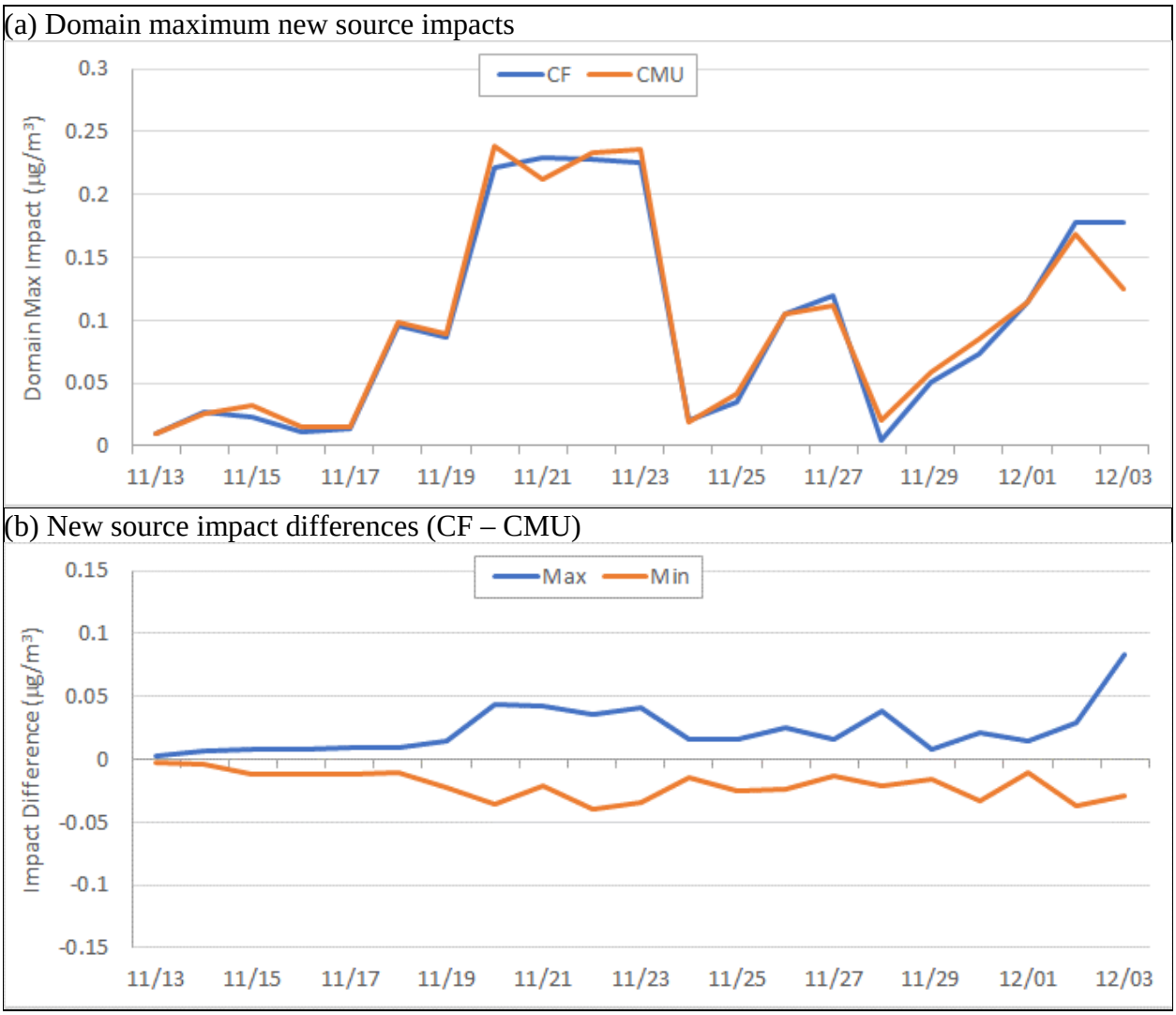

Figure D.1-5. (a) 4-km Domain Maximum New Source Impacts on 24-h Average $PM_{2.5}$ Nitrate by the CF and CMU Schemes; (b) Domain Maximum and Minimum Differences in the New Source Impacts (CF – CMU)

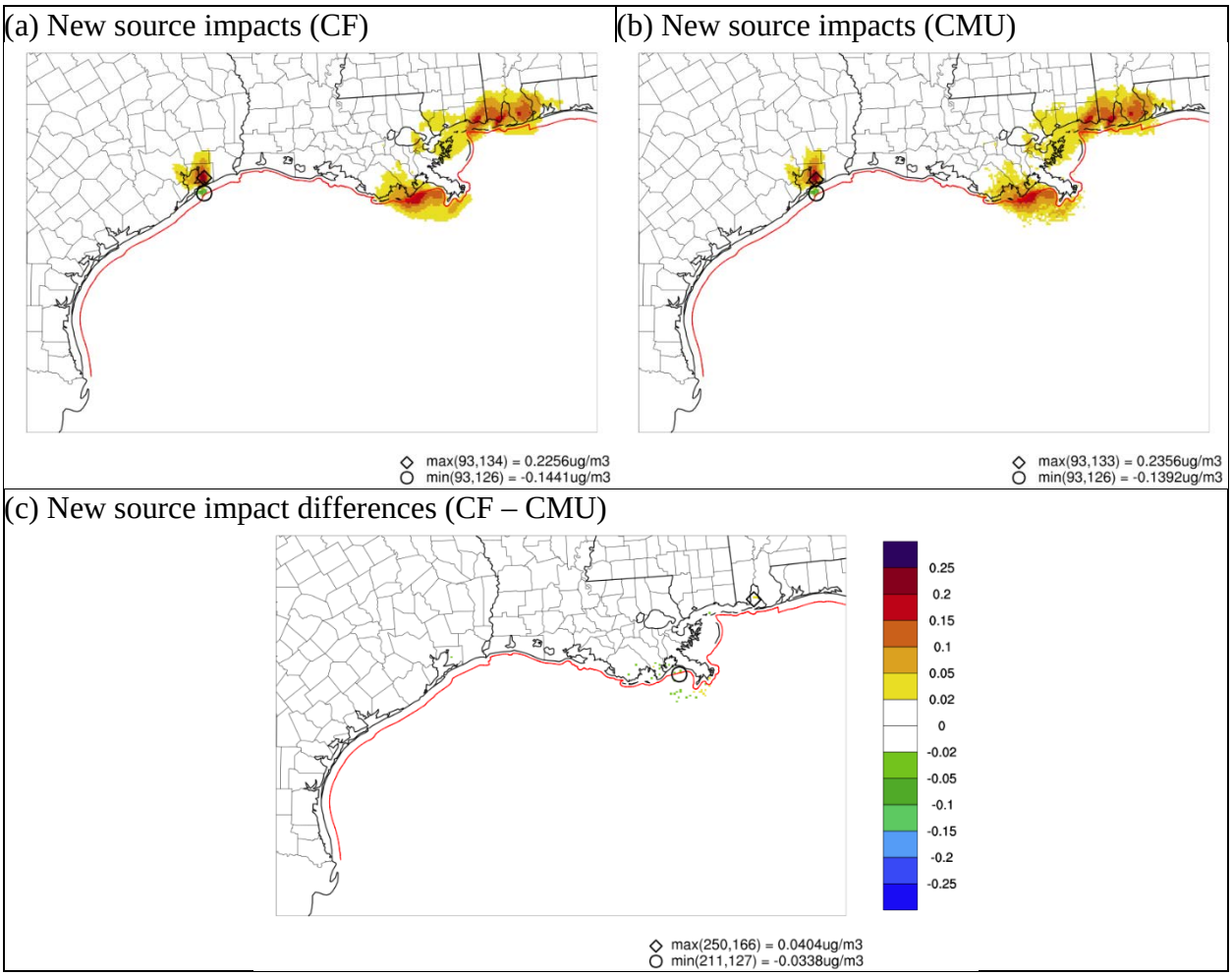

Figure D.1-6. New Source Impacts on 24-h Average $PM_{2.5}$ Nitrate by the CF and CMU Schemes and Their Differences in the 4-km Modeling Domain on November 23, 2012

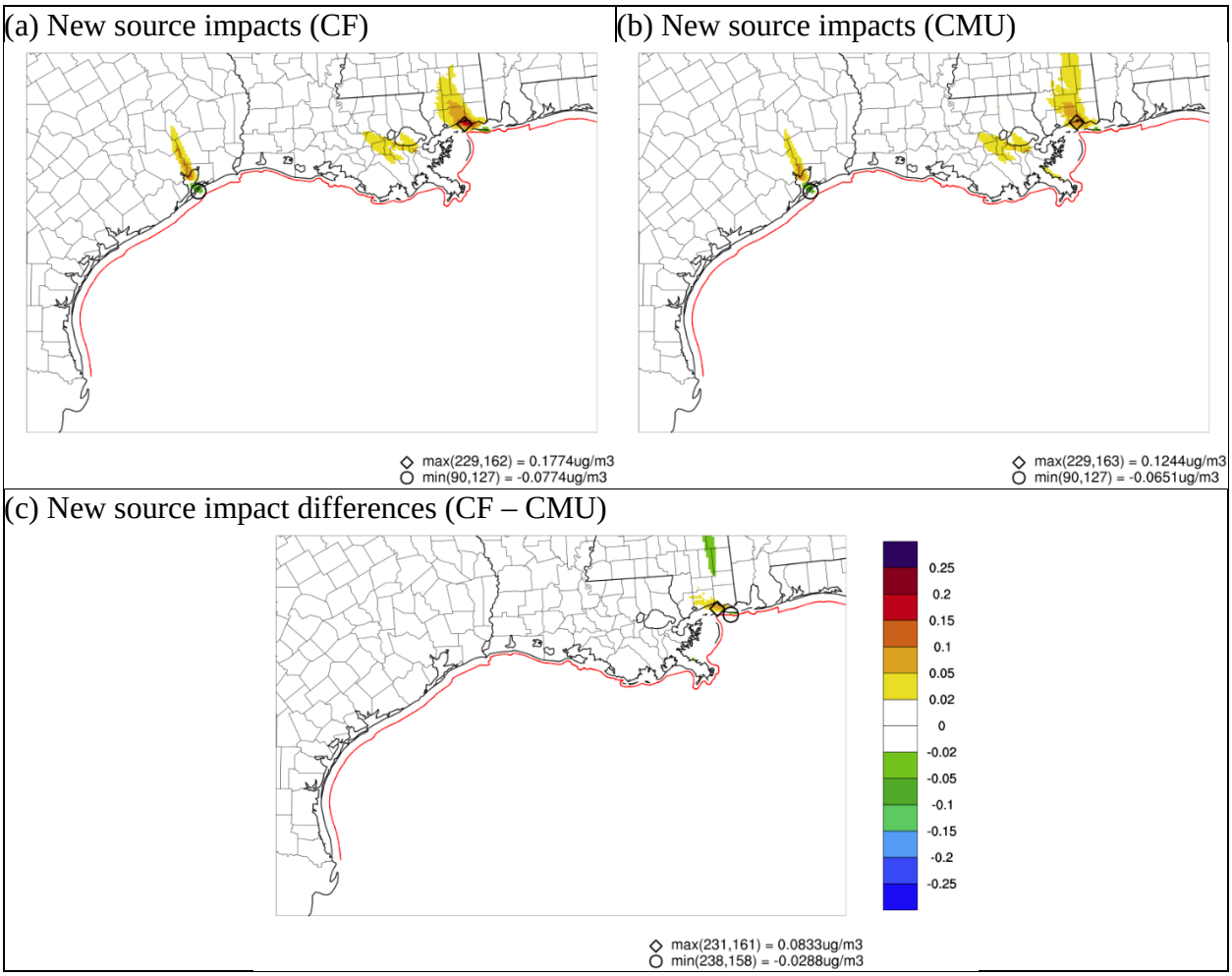

Figure D.1-7. New Source Impacts on 24-h Average $PM_{2.5}$ Nitrate by the CF and CMU Schemes and Their Differences in the 4-km Modeling Domain on December 3, 2012

Appendix E.1

Model Justification Demonstration to Support Outer Continental Shelf Dispersion Modeling in the Gulf of Mexico Region

Prepared for:

Bureau of Ocean Energy Management
Office of Environmental Programs
Environmental Sciences Division
45600 Woodland Road
Sterling, VA 20166

Contract Number M14PC00007

Prepared by:

Ramboll Environ US Corporation
19020 33rd Ave. W., Suite 310
Lynnwood, WA 98036-4754

February 3, 2017

TABLE OF CONTENTS

TABLES

FIGURES

ACRONYMS AND ABBREVIATIONS

AERCOARE	AERMOD-COARE
AERMAP	AERMOD terrain preprocessor
AERMET	AERMOD meteorology preprocessor
AERMOD	American Meteorological Society/Environmental Protection Agency Regulatory Model
AERSURFACE	AERMOD preprocessor for roughness
AFB	Absolute fractional bias
ARW	Advanced Research WRF
BOEM	Bureau of Ocean Energy Management
CALMET	CALPUFF meteorological and terrain preprocessor
CALPOST	CALPUFF post-processor
CALPUFF	California Puff-Advection Model
c_o	Observed concentration value
c_p	Predicted concentration value
$\bar{c}$	Average concentration value
c_n	The nth highest concentration
COARE	Coupled Ocean Atmospheric Response Experiment
CPM	Composite performance metric
CPA	Central GOM Planning Area
ECMWF	European Center for Medium-Range Weather Forecasting
ERA	ECMWF Reanalysis Project Interim Reanalysis
FF2	Fraction-factor-of-two
GOMR	Gulf of Mexico Region
IWAQM	Interagency Workgroup on Air Quality Modeling
L	Monin-Obukhov length
LCC	Lambert Conformal Conic
METSTAT	Meteorological Statistics program (ENVIRON Int. Corp. 2014) used for evaluating mesoscale model output performance against surface observations.
MIXHT	Mixing height
MM5	Fifth Generation Mesoscale Model
MMIF	Mesoscale Model Interface Program
MMM	Mesoscale meteorological model

MPTER ..... Multiple Point Gaussian Dispersion Algorithm with Optional Terrain Adjustment

NaN ..... Not a number

NCAR ..... National Center for Atmospheric Research

NO_2 ..... Nitrogen dioxide

NO_X ..... Nitrogen oxides

NWS ..... National Weather Service

OCD ..... Offshore Coastal Dispersion Model

OCS ..... Outer Continental Shelf

OCSLA ..... Outer Continental Shelf Lands Act

OLM ..... Ozone Limiting Method

PBL ..... Planetary boundary layer

PFL file ..... Upper-air profile file

PG ..... Pasquill-Gifford

$PM_{2.5}$ ..... Particulate matter with diameter less than or equal to 2.5 microns

PM_{10} ..... Particulate matter with diameter less than or equal to 10 microns

PSD ..... Prevention of significant deterioration

PVMRM ..... Plume Volume Molar Ratio Method

Q-Q ..... Quantile-Quantile (statistical plot)

RHC ..... Robust high concentration

r_g ..... Geometric correlation coefficient

RPO ..... National Regional Planning Organization

SCICHEM ..... Second-Order Closure Integrated Puff Model with Chemistry

SF6 ..... Sulfur hexafluoride

SFC file ..... Surface meteorological file

SO_2 ..... Sulfur dioxide

SSB ..... State Seaward Boundary

SST ..... Sea Surface Temperature

TIBL ..... Thermal internal boundary layer

USEPA ..... U.S. Environmental Protection Agency

USGS ..... U.S. Geological Survey

UTM ..... Universal Transverse Mercator

w* ..... Convective scaling velocity

WPA ..... Western GOM Planning Area

WRF.....Weather Research and Forecasting Mesoscale Model

μ_g.....Geometric mean

VG.....Geometric mean variance

YSU .....Yonsei University

1. INTRODUCTION

The Outer Continental Shelf Lands Act (OCSLA), 43 U.S.C. §§ 1331-1356(a), gives the Secretary of the Department of the Interior (Secretary) the authority to administer provisions relating to the leasing of the Outer Continental Shelf (OCS) for oil and gas exploration and production. In 1978, Congress amended OCSLA to allow the Secretary to promulgate regulations "for compliance with the national ambient air quality standards pursuant to the Clean Air Act (42 U.S.C. 7401 et seq.), to the extent that activities authorized under this Act significantly affect the air quality of any State." If oil and gas activities in the OCS significantly impact air quality of any state, the OCS facility is subject to regulations and emissions controls to ensure compliance with the National Ambient Air Quality Standards.

As stated in 30 CFR 550.218(e), air dispersion modeling of sources under the Bureau of Ocean Energy Management (BOEM) jurisdiction must be conducted using a model that is approved by the BOEM Director and in accordance with the guidelines in Appendix W of 40 CFR Part 51, often called the U.S. Environmental Protection Agency (USEPA) *Guideline on Air Quality Models* ("USEPA *Guideline*"). The USEPA *Guideline* was updated recently (USEPA, 2017[1]) and provides a number of preferred models in its Appendix A to Appendix W that do not require justification before use for recommended applications. The previous version of the USEPA *Guideline* was last updated in 2005.

The Offshore Coastal Dispersion Model (OCD) is the preferred dispersion model for overwater sources for short-range transport (source-to-receptor distances less than 50 km). The 2017 USEPA *Guideline* does not currently list a preferred dispersion model for long-range transport over water, but the previous (2005) version listed CALPUFF as the preferred model for long-range transport over land. AERMOD is the preferred dispersion model for overland short-range modeling.

The last substantial change to the OCD model was in 1997[2], almost two decades ago (though there was a small bug fix released in 2000[3]). AERMOD, unlike OCD, has undergone continuous updates to both its scientific algorithms and its input and output formats. OCD uses the older Pasquill-Gifford (PG) stability classifications, while AERMOD uses the more modern (and numerically continuous) Monin-Obukhov similarity theory. OCD cannot directly read modern meteorological datasets readily available on the Internet, as AERMOD can. OCD does not provide outputs that are directly comparable to the statistical forms of the more recent National Ambient Air Quality Standards. The graphical user interface that came with the 1997 release of OCD cannot be run on modern computers. For these and other reasons, BOEM wishes to use AERMOD for short-range modeling within its jurisdiction. BOEM has already approved the use of CALPUFF for long-range modeling within its jurisdiction.

---

1 On January 20, 2017, the White House declared that regulations that have been published in the Federal Register but have not yet reached their effective date are to be postponed for 60 days, making the new effective date March 17, 2017. See http://www.politico.com/f/?id=00000159-be8f-da97-a9dd-becf15ae0001.

2 See https://www3.epa.gov/ttn/scram/mcbs/ocdz2.txt

3 See https://www3.epa.gov/ttn/scram/mcbs/ocdz3.txt

Section 8.3 of the 2005 USEPA *Guideline* and Section 8.4 of the 2017 USEPA *Guideline* state that the meteorological data used in dispersion modeling should be representative of the climate in the vicinity of the emissions source. Section 8.3 of the 2005 USEPA *Guideline* discusses the use of mesoscale meteorological model (MMM) output data for long-range transport modeling. Although not strictly forbidden, the use of MMM data for short-range dispersion modeling was not encouraged in the 2005 USEPA *Guideline*. However, Section 8.4.5 of the 2017 USEPA *Guideline* allows for the use of prognostic meteorological model output data where there is no National Weather Service (NWS) station in close proximity to the emissions source, or where it is unfeasible or too expensive to measure site-specific meteorological data. In offshore situations, suitable meteorological datasets in close proximity to a desired emission source are often unavailable or prohibitively expensive to obtain.

In this model comparison study, we evaluate the preferred model for short-range transport of emissions from offshore sources, OCD, to two alternative models, AERMOD and CALPUFF, using prognostic MMM output.

1.1 Use of Dispersion Models for Offshore Emissions Sources

The AERMOD modeling system (USEPA, 2004a) is the preferred near-field (< 50 km) regulatory model used for the overland air quality assessment requirements associated with air emissions permitting[4]. AERMOD is a dispersion model that contains planetary boundary layer (PBL) parameterizations based on Monin-Obukhov similarity theory, which rely upon heat and momentum fluxes to simulate the structure and evolution of the PBL. AERMOD relies upon a complex set of meteorological input to characterize the PBL and uses turbulence parameters to estimate dispersion rates. See USEPA (2004a) for a complete description of AERMOD and its meteorological and terrain preprocessors, AERMET and AERMAP, respectively.

1.1.1 Scientific Deficiencies of AERMET Over Water

Although AERMOD is the preferred near-field model for regulatory purposes on land, it is not the recommended model for overwater regulatory applications. AERMOD's meteorological preprocessor, AERMET (USEPA, 2004b), was not designed to simulate meteorological conditions over the ocean and relies on several assumptions that are reasonable over land but not reasonable over water.

AERMET assumes that all daylight hours feature a convective boundary layer, and all night-time hours have a stable boundary layer. Over the world's oceans, energy fluxes are strongly dependent on air-sea temperature differences, which is turn is dependent on the angle of the wind compared to the sea surface temperature gradient, and relatively insensitive to patterns of diurnal heating and cooling. When conditions feature warm advection (blowing from warmer water to cooler water), then a stable boundary

[4] As promulgated under 40 CFR Part 51, Appendix W. The AERMOD modeling system is available to the public at the USEPA modeling website: http://www.epa.gov/scram001/dispersion_prefrec.htm

layer develops, regardless of the time of day. Similarly, when conditions indicate cold advection (blowing from cooler water to warmer water), then we find convective conditions, even at night.

About 90% of the net incoming solar radiation at the surface of the ocean is converted to latent heat flux (evaporation), leaving about 10% for sensible heat flux (Hartmann, 1994; p. 105). AERMET assumes that 90% of incoming solar radiation is converted to sensible heat flux, which is a poor assumption over water.

AERMET neglects the effect of latent heat flux in its calculation of the Monin-Obukhov surface layer parameters, which is equivalent to assuming latent heat is negligible compared to sensible heat flux. This assumption makes the problem tenable over land, where measurements of the soil water content are not routine, and there exists no simple method to estimate latent heat flux. Given a near-surface measurement of relative humidity (converted to mixing ratio) and a soil water mixing ratio, one could calculate the latent heat flux. While the former are routine measurements, the latter are not. This lack of availability of input data, combined with the reasonable assumption over land that latent heat flux is negligible, guided the development of AERMET. However, offshore measurements (buoys) routinely measure sea surface temperature. By assuming the air in contact with the water surface is at the saturation point for that temperature, the problem becomes solvable over water without having to neglect the latent heat flux.

Over land, the roughness length is relatively constant in time, and can be related to land-use types. The AERMOD modeling system has a preprocessor named AERSURFACE, which calculates the roughness length in various upwind sectors based on U.S. Geological Survey (USGS) land-use datasets. Land use is assumed to vary on scales of months to quarters, and the snow cover is included for all hours of a quarter (i.e., without hourly or daily snow cover measurements). However, over water, the roughness length is a function of wind speed—the faster the wind, the rougher the sea surface as wave heights grow due to increasing surface stress. It must therefore be allowed to vary hourly to be able to simulate dispersion over water correctly using AERMOD.

All of these parameters are related via Monin-Obokhov similarity theory:

- The sign of the Monin-Obukhov length (stable vs. convective)
- The value of the Monin-Obuhhov length
- The value of the roughness length
- The value of the sensible and latent heat fluxes

AERMET uses Monin-Obukhov similarity theory but incorporates various assumptions that make the equations solvable over land given typical measurements. Neither AERCOARE nor the Weather Research and Forecasting Mesoscale Model (WRF) make these simplifying assumptions. Therefore, this model justification study chooses to eliminate AERMET as a meteorological processing option and instead considers using mesoscale meteorological output from WRF, either directly or processed through AERCOARE. Because AERCOARE (Section 1.1.2) and WRF (Section 1.1.4) both implement Monin-

Obukhov surface layer theory in a similar way, AERCOARE is most useful when using observations, or a blend of observations and WRF output.

1.1.2 The Development of AERCOARE

The Coupled Ocean Atmosphere Response Experiment (COARE) air-sea flux algorithms are better suited to handle atmospheric conditions over water, and these algorithms have been used to develop AERMOD-COARE (AERCOARE)[5] model (USEPA, 2012), a potential replacement for AERMET. AERCOARE uses air-sea temperature differences and a number of other marine features to calculate the meteorological parameters needed for overwater and coastal dispersion modeling. AERCOARE-AERMOD (using the current beta version of AERCOARE) has been approved by the USEPA Model Clearinghouse as an acceptable alternative dispersion modeling approach on a case-by-case basis, where it must be shown that proper procedural protocol in line with the USEPA *Guideline* is followed (Bridgers, 2011; Wong, 2011). A recent study by the USEPA (Wong et al., 2016) evaluated the performance of AERCOARE-AERMOD against two air dispersion models and measurements from several tracer studies. Wong et al. (2016) found that AERCOARE-AERMOD is a viable alternative to the OCD model (DiCristofaro and Hanna, 1989), which is the USEPA-recommended model for offshore assessment of emission sources, as promulgated under Appendix A to Appendix W, 40 CFR Part 51. Note that Wong et al. (2016) used overwater measurements, not MMM (WRF) output, to drive OCD, AERMOD, and CALPUFF. USEPA (2015b) and USEPA (2015c) used MMM (WRF) output to drive AERMOD. One of the primary conclusions of the USEPA/BOEM study (USEPA 2015b, USEPA 2015c) was that model performance using WRF output in lieu of observations was very similar.

1.1.3 Deficiencies of the OCD model

OCD uses an AERCOARE-like algorithm to calculate overwater meteorological parameters and is a Gaussian plume dispersion model originally based on the Multiple Point Gaussian Dispersion Algorithm with Optional Terrain Adjustment (MPTER) model (USEPA, 1980), with updated overwater plume transport, plume dispersion, and treatment of plumes as they cross shorelines. However, OCD does not contain some of the more recent features included in other dispersion models, including the PRIME downwash algorithm (Schulman, et al., 2000), Plume Volume Molar Ratio Method (PVMRM) (Hanrahan, 1999), and Ozone Limiting Method (OLM) (Cole and Summerhays, 1979). Additionally, OCD is unable to calculate receptor averaged percentiles associated with sulfur dioxide (SO_2), nitrogen dioxide (NO_2), and particulate matter with diameter less than or equal to 2.5 microns ($PM_{2.5}$) concentrations required for compliance demonstration.

Section 6.2.3 of the USEPA *Guideline* recognizes that Gaussian plume models, such as OCD, are not useful for long-range transport, which is defined by the USEPA as distances greater than 50 km. The CALPUFF modeling framework is the currently[6] recommended model for long-range transport modeling

[5] AERCOARE is made publicly available by the USEPA at the website: http://www.epa.gov/ttn/scram/dispersion_related.htm

[6] The proposed revisions to Appendix W state that CALPUFF will no longer be the preferred regulatory model for long-range transport and will instead be used as a screening tool.

and has been authorized by the BOEM Director for use at source-receptor distances greater than 50 km[7]. Unlike AERMOD and OCD, CALPUFF is a non-steady state dispersion model that simulates and tracks chemicals in Gaussian puffs of air rather than Gaussian plumes. CALPUFF was developed by Sigma Research Corporation (now part of Exponent, Inc.) (Scire et al., 2000a, 2000b). CALMET is the meteorological preprocessor linked to CALPUFF, although other meteorological inputs can be used instead. CALPUFF simulates processes such as chemical removal, wet and dry deposition, complex terrain algorithms, building downwash, and plume fumigation.

1.1.4 WRF Monin-Obukhov Similarity Theory

WRF and other MMMs parameterize the surface in a way that is similar to AERMET over land and the COARE algorithm over water. It uses land-use based parameterizations for roughness length over land, and a Charnock-like parameterization over water. However, WRF calculates both latent and sensible heat flux everywhere, varying in time (e.g., variable wind speed over water, variable snow cover over land, variable ice cover over water).

1.2 Advantages of Using Prognostic Mesoscale Meteorological Model (MMM) Output in Dispersion Models

Currently accepted overwater dispersion modeling methods require observational datasets; however, recent changes to Appendix W allow MMM output to be a viable replacement (USEPA, 2017). Oceanic observational datasets are typically provided by meteorological buoys or instruments on platforms, and observational coverage over the ocean is sparse. It would be advantageous if MMMs, such as the WRF model (Skamarock, et al., 2008), could be used to provide meteorological data for dispersion models in areas where observational data are lacking.

The Mesoscale Model Interface Program (MMIF)[8] (Brashers and Emery, 2014) is a tool that converts prognostic MMM output fields into the format required for direct input into several dispersion models, including AERMOD, OCD, and CALPUFF. MMIF uses geophysical and meteorological data from the WRF model (Advanced Research WRF [ARW] core, versions 2 and 3) or the Fifth Generation Mesoscale Model (MM5, version 3). MMIF retains the same grid projection and resolution as supplied by WRF but can produce outputs for any sub-domains within the meteorological modeling grids. Vertically resolved WRF output can be aggregated or interpolated, which allows for user-defined vertical layering. MMIF can pass PBL heights from WRF directly into dispersion models or independently diagnose PBL heights based upon other meteorological variables from WRF. Because the MMIF output retains these additional parameters critical to characterizing the atmosphere overwater, this model comparison study will focus on the use of WRF meteorological output, as extracted by MMIF, to drive the dispersion models.

---

[7] In April of 2012, the BOEM Director approved the use of CALPUFF and OCD version 5 for use in the Gulf of Mexico OCS Region.

[8] MMIF is provided as a "related" alternative software for regulatory dispersion modeling by the USEPA at the website: http://www.epa.gov/scram/dispersion_related.htm

1.3 Model Comparison Demonstration

Section 3.2 of the proposed revisions to USEPA *Guideline* (USEPA, 2015a) describes the process associated with gaining approval to use an alternative modeling approach instead of a USEPA-approved model.

The Regional Administrator may approve the use of an alternative model if there is a demonstration that "(1) a preferred air quality model is not appropriate for the particular application; or (2) a more appropriate model or analytical procedure is available and applicable." The alternative model must be tested for both performance and in a theoretical sense before approval. The alternative model may be approved if it can be demonstrated that the "model produces concentration estimates equivalent to the estimates obtained using the preferred model." The alterative model may also be approved if it can be shown that the alternative model outperforms the accepted model in a statistical performance evaluation using air quality measurements. Lastly, the alternative model may be approved if it is shown that "the preferred model is less appropriate for the specific application, or if there is no preferred model."

The model justification demonstration presented in this report compares modeled concentrations from two alternative models, AERMOD and CALPUFF, to the approved model, OCD. All three dispersion models are driven by meteorological inputs from WRF output processed using MMIF. The demonstration will be conducted in two parts, using three modeling combinations:

- **WRF-MMIF-AERMOD**: AERMOD using meteorological data from WRF, processed through MMIF.
- **WRF-MMIF-OCD**: OCD using meteorological data from WRF, processed through MMIF, and re-formatted for OCD.
- **WRF-MMIF-CALPUFF**: CALPUFF using meteorological data from WRF, processed through MMIF.

The first part of this study compares dispersion modeling results to measurements from four offshore tracer studies, which are further described in Section 2. These tracer studies have been used previously to demonstrate the validity of OCD (Hanna et al., 1984), CALPUFF (Earth Tech, 2006), and AERCOARE (ENVIRON, 2010, 2012, Wong et al., 2016).

In the second part of this study, AERMOD, OCD, and CALPUFF will be used to model the dispersion of several synthetic OCS sources in the Gulf of Mexico Region (GOMR). Similar to the tracer studies in part 1, MMIF will be used to process WRF meteorological output fields and create meteorological inputs for each model. A "consequence" type of analysis will be performed as the model results are compared and contrasted.

2. TRACER STUDIES METHODOLOGY

2.1 Description of the Four Tracer Studies

The four historical tracer dispersion field studies selected for this study are as follows:

- **Cameron, LA**: July 1981 and February 1982 (Dabberdt, et al. 1982)
- **Carpinteria, CA**: September 1985 (Johnson and Spangler 1986)
- **Pismo Beach, CA**: December 1981 and June 1982 (Schacher, et al. 1982)
- **Ventura, CA**: September 1980 and January 1981 (Schacher, et al. 1982)

As mentioned above, these tracer studies have been used for benchmark testing and development of OCD, CALPUFF, and AERCOARE, and the USEPA is familiar with these tracer experiments. The meteorology and concentration data from the tracer studies were gathered from the OCS Model Evaluation Archive (Earth Tech, 2006). Concentrations of passive tracers (sulfur hexafluoride [SF6] at all sites, SF6 and Freon at Carpinteria) were measured at arrays of receptors located near the coast at each site. Each of these sites are coastal; Cameron, Pismo Beach, and Ventura sites have relatively flat terrain, while Carpinteria has complex terrain. During the tracer studies, the receptors were located near the coast at Cameron and Pismo Beach. At Ventura, the receptors were located 500 to 1000 m inland of the coast, and at Carpinteria, the receptors were positioned on tall bluffs along the shoreline.

A fifth tracer study that occurred between Denmark and Sweden (the "Øresund" study) has been considered by some (USEPA, 2015b, 2015c). However, the release points were not over water during the Øresund experiments and were often several km inland, in some cases on tall towers. The receptors were almost all placed several km inland as well, in many cases above considerable terrain. We therefore discarded the Øresund study as not being similar to both the releases expected in BOEM jurisdictions and the receptors (the shoreline or the state seaward boundary).

These four tracer studies are particularly useful for analyzing model performance under marine meteorology. WRF was used to provide the meteorology for each of the four tracer studies, and the configuration of the WRF modeling domains for each site is described below. Meteorological observations were collected during each tracer experiment and have been compared to modeled WRF output in USEPA (2015b).

WRF performance was assessed both quantitatively using statistics that compared the modeled and measured meteorology and qualitatively using the Meteorological Statistics (METSTAT) software (ENVIRON, 2014), which calculates a variety of model performance statistics using observations of wind speed and direction, temperature, and moisture. USEPA (2015b) reported satisfactory agreement between observed meteorology and WRF output fields, with the exception of air-sea temperature differences and PBL heights in some cases, although measurement techniques of both fields have improved since the time of the tracer studies (early-to-mid 1980s).

Air-sea temperature differences influence overwater stability and PBL heights; unstable conditions generally lead to higher PBL heights and more chemical dilution within the PBL. In this model justification study, we use the WRF modeling scenario from USEPA (2015b), which showed the best agreement to the meteorological measurements from each tracer study. The following sections describe the tracer study configurations and the WRF meteorological modeling domains.

2.1.1 Cameron

The Cameron experiment occurred during July 1981 and February 1982 and was designed to capture both summer and winter conditions in coastal Louisiana. During the experiment, tracer gas (SF6) was released from a height of 13 meters (m) on both a boat and an offshore platform. Receptors were located on flat terrain along the coast, roughly 4 to 10 km away from the release points. Figure 1 shows the spatial locations of the emission sources and the receptor array for the experiment. Figure 1–Figure 4 were developed from graphics files supplied by the USEPA from the OCS Model Evaluation Archive (Earth Tech, 2006).

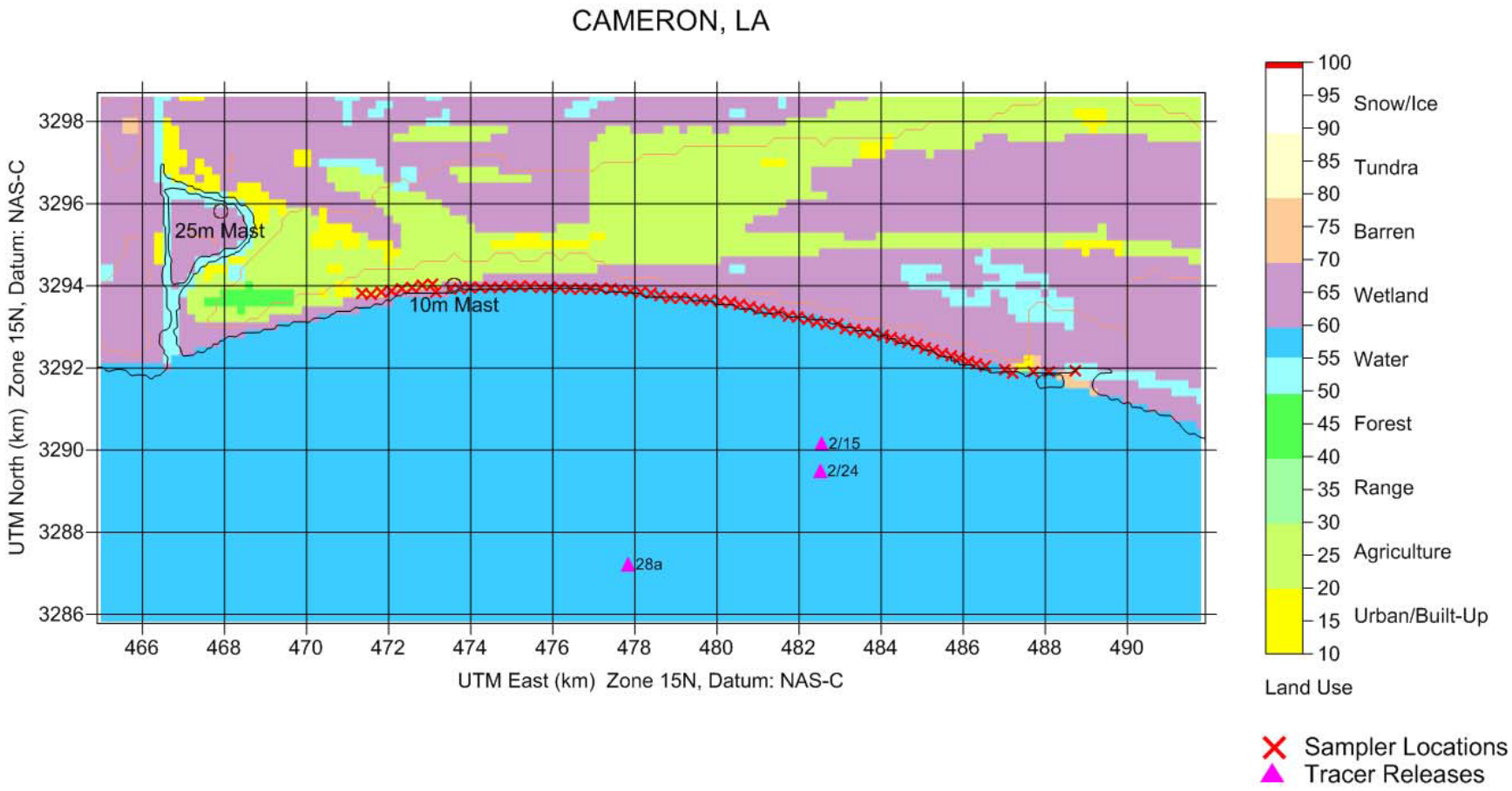

Figure 1. Cameron Experiment Configuration

2.1.2 Carpinteria

The Carpinteria tracer study was conducted between mid-September and early October 1985 in southern California to investigate the impact of OCS sources on coastal air quality in the presence of complex coastal terrain and shoreline fumigation. In this study, we focus only on the complex terrain dataset (September releases) because shoreline fumigation processes are not included in AERMOD. The receptor array was located on 20 to 30 m high bluffs roughly 800 to 1500 m from the coastal receptors. The experiment configuration is presented in Figure 2. Tracer gases (SF6 and Freon) were released at distances of 300 to 700 m from shore and at heights of 18 and 61 m. Over the course of the campaign, SF6 and Freon were generally released from two difference sources during different hours, but occasionally the two tracers were released from different sources during the same hour.

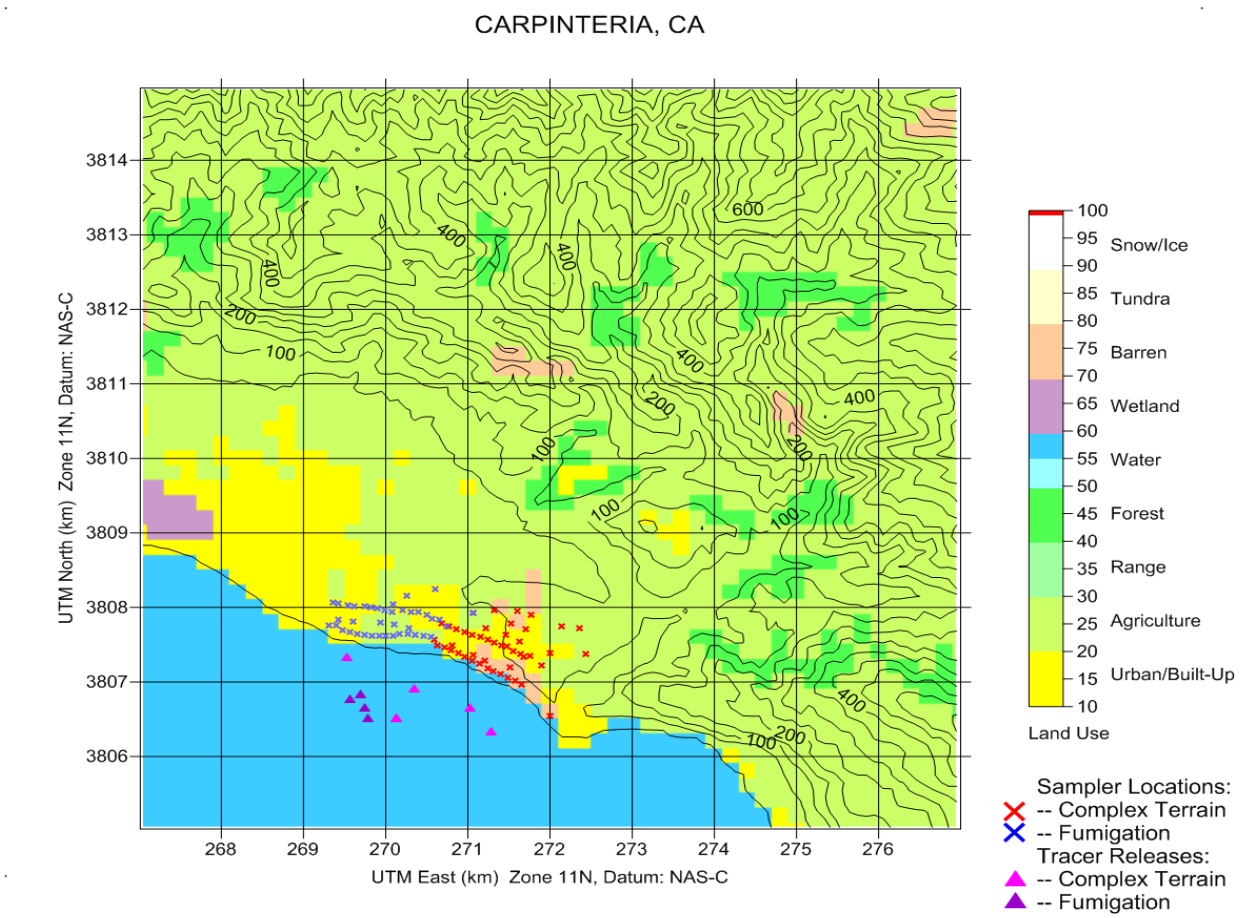

Figure 2. Carpinteria Experiment Configuration

2.1.3 Pismo Beach

The Pismo Beach tracer experiment was conducted in December 1981 and June 1982 in southern California during periods of onshore flow. Tracer gas was released at a height of 13 m from a boat located 5 to 7 km offshore. Downwash likely occurred during release from the boat, whose hull was approximately 7 m high and 20 m wide. Two arrays of receptors were placed onshore; one set in close proximity to the shoreline and other set located 7 to 8 km inland. The field campaign layout, including receptor arrays and tracer gas release points, are shown in Figure 3.

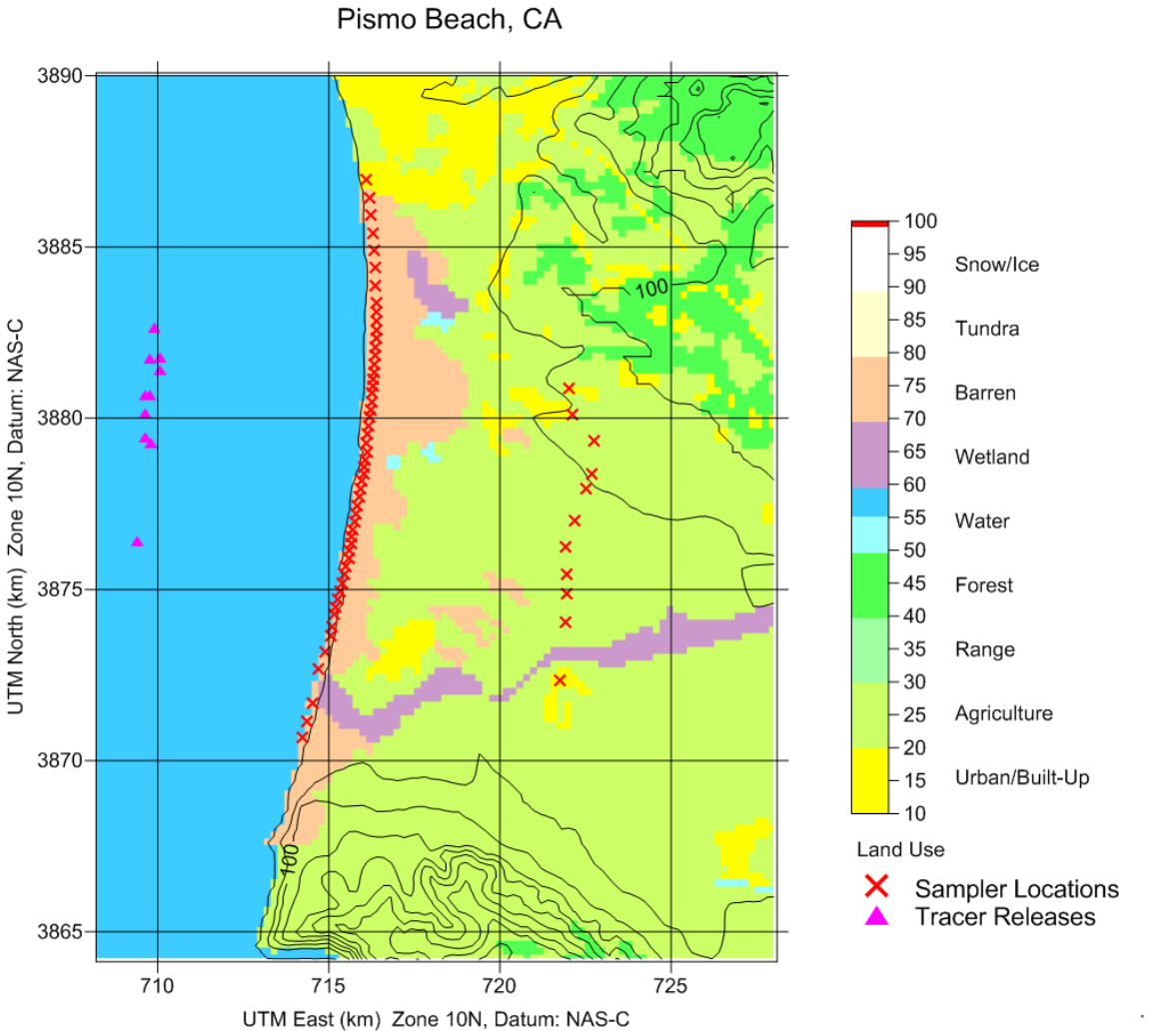

Figure 3. Pismo Beach Modeling Configuration

2.1.4 Ventura

The Ventura tracer experiment was conducted in September 1980 and January 1981 in southern California during onshore flow conditions. Non-buoyant, passive tracer was released at a height of 15 m from masts on boats roughly 7 m high and 20 m wide and likely experienced downwash. Two receptor arrays were placed onshore; one set between 0.5 and 1 km from the shoreline and another set between 7 and 9 km inland. The tracer release points and receptor arrays are shown in Figure 4.

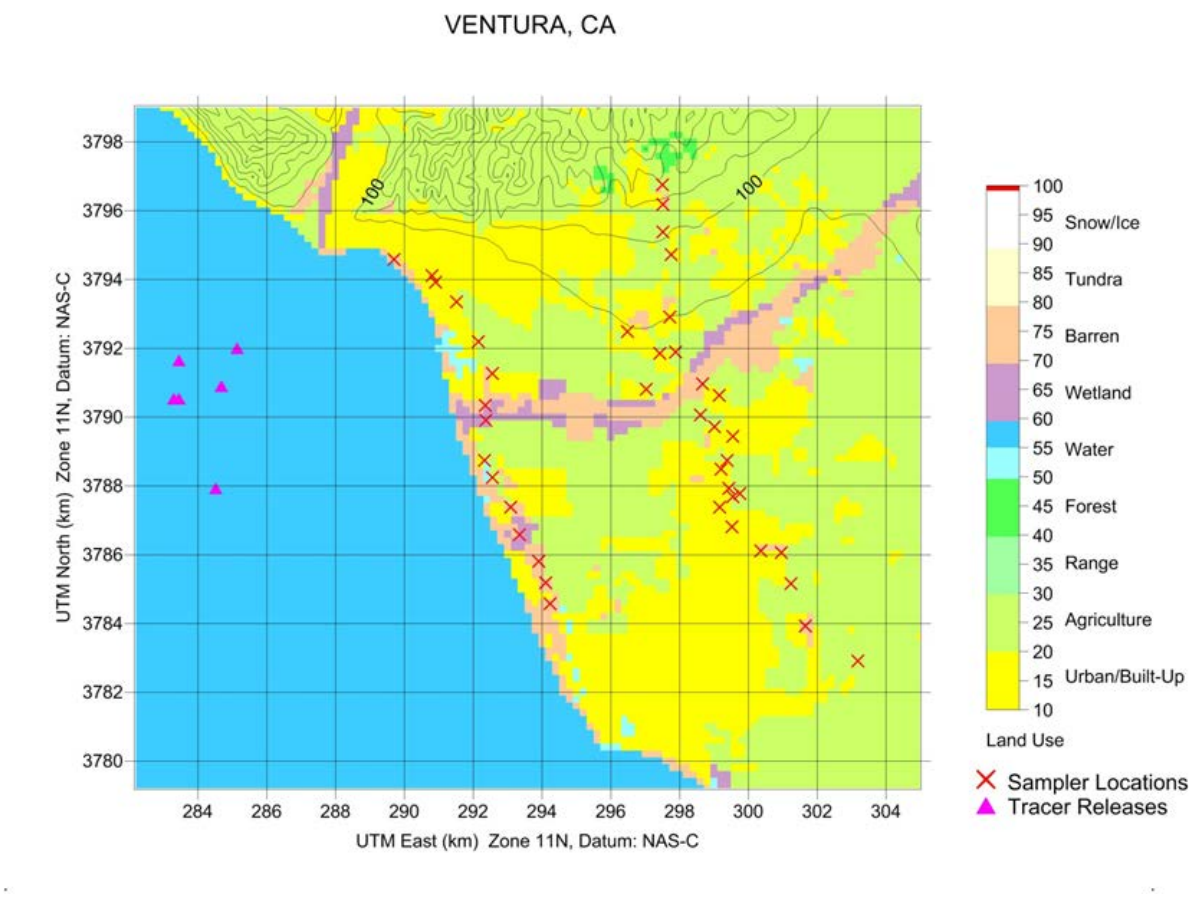

Figure 4. Ventura Modeling Configuration

2.2 WRF Modeling of the Four Tracer Studies

The mesoscale meteorological modeling simulations used in this study were developed using the National Center for Atmospheric Research's (NCAR's) community-developed WRF model (dynamical core version 3.4.1). WRF is a limited-area, non-hydrostatic, terrain-following "eta"-coordinate mesoscale model. WRF can use many different types of initialization datasets and contains numerous physics modules (Skamarock, et al. 2008), making it applicable to a wide range of air dispersion modeling scenarios. The sensitivity of WRF to various reanalysis datasets and PBL schemes was evaluated in USEPA (2015b). USEPA (2015b) found that the best agreement between measured and modeled meteorological fields in the WRF simulation that used the European Center for Medium-Range Weather Forecasts' (ECMWF) Reanalysis Project (ERA), ERA-Interim dataset reanalysis scheme, and the Yonsei University (YSU) (Hong, Noh, and Dudhia, 2006) PBL scheme. Therefore in this study, the WRF runs using the YSU PBL scheme and ECMWF ERA input data were used.

One serious drawback to the WRF modeling performed for these four tracer studies stems from the fact that about half the tracer study periods were before the first satellites with sensors capable of taking sea surface temperature (SST) measurements were placed into orbit. This means that the SST values in the input datasets were based on interpolation from rather sparse in-situ measurements (buoys, ships). Available SST datasets from this time period are also relatively coarse in resolution compared to modern SST datasets (~27 km compared to ~1 km today). In particular, the channel near the Ventura study is known to have strong SST gradients, but no such gradients exist in the input SST dataset because its resolution is simply too coarse. This negatively affects WRF performance, which in turn negatively affects dispersion model performance compared to observations.

PBL heights play an important role in the dispersion of offshore tracers. USEPA (2015b) found that AERMOD occasionally over-predicted the highest tracer concentrations when WRF-MMIF meteorology was used, possibly because PBL heights and Monin-Obukov lengths in WRF were too low. Given the importance of PBL height on tracer dispersion, sensitivity studies are performed in this analysis to investigate the impact of PBL height on modeled maximum tracer concentrations. In one set of dispersion model runs, the PBL heights from WRF are directly passed to AERMOD, OCD, and CALPUFF. In another set of dispersion model runs, MMIF calculates PBL heights using other parameters from WRF. The minimum PBL height and Monin-Obukov length in MMIF are set at 25 m and 5 m, respectively, which is consistent with the recommended values used in other offshore dispersion modeling studies (Richmond and Morris, 2012; USEPA, 2015b, 2015c; Wong et al., 2016).

The WRF modeling configuration included simulation periods ranging from 1.5 to 6.5 days for each tracer study, with at least 12 hours of model spin-up time before the first observed tracer release. The spin-up time allows the model to develop sub-grid scale processes, such as vorticity and moisture fields. Table 1 (taken from USEPA, 2015b) presents the dates associated with each tracer study and corresponding WRF initialization periods. See Table 8 in USEPA (2015b) for details about the physics parameterization schemes and nudging used in the WRF simulations.

Table 1. WRF Simulation Timeperiods for Tracer Studies

Location	Historical Field Study Date Ranges	WRF Initializations
Cameron, LA	Period 1: 08Z 07/20/1981 to 13Z 07/29/1981 Period 2: 08Z 02/15/1982 to 14Z 02/24/1982	Period 1: 12Z 07/19/1981 to 12Z 07/24/1981 Period 2: 12Z 02/14/1982 to 12Z 02/19/1982
Carpinteria, CA	Period 1: 09/19/1985 to 09/29/1985 (Complex Terrain Study only)	Period 1: 12Z 09/18/1985 to 12Z 09/24/1985
Pismo Beach, CA	Period 1: 12/08/1981 to 12/15/1981 Period 2: 06/21/1982 to 06/27/1982	Period 1: 12Z 12/06/1981 to 12Z 12/11/1981 Period 2: 12Z 06/19/1982 to 12Z 06/24/1982
Ventura, CA	Period 1: 09/27/1980 to 09/29/1980 Period 2: 01/06/1981 to 01/13/1981	Period 1: 12Z 09/23/1980 to 12Z 09/24/1980 Period 2: 12Z 01/05/1981 to 12Z 01/10/1981

WRF was run with 37 vertical atmospheric layers, with the lowest layer ranging from 12 to 25 m. See Table 10 in USEPA (2015b) for more information about the WRF vertical grid setup. The U.S. modeling domains for WRF are defined on the Lambert Conformal Conic (LCC) map projection identical to the National Regional Planning Organization (RPO) domains, with an outermost RPO domain (36 km) and telescoping 12 km–4 km–1.33 km nests to resolve the fine detail of coastlines and local topography. Each grid domain contains a "5-point" buffer zone to prevent boundary effects from the outer edge of each WRF domain from influencing dispersion modeling within the domain. The innermost WRF modeling domains (1.33 km) centered on each site are shown in Figure 5 through Figure 8, which are taken from USEPA (2015b).

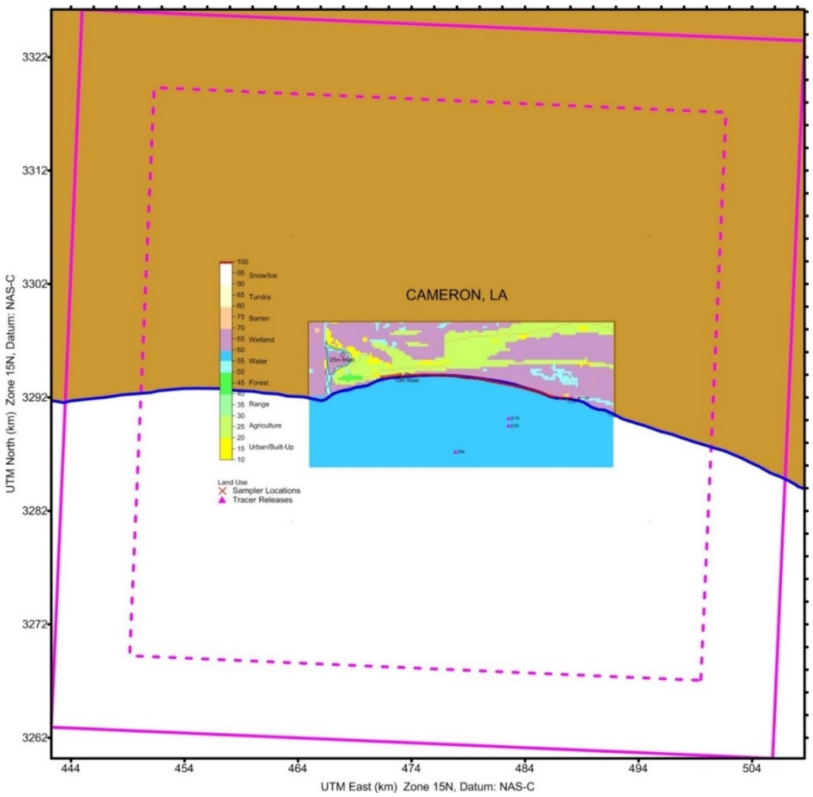

Figure 5. Cameron WRF 1.33-km Domain

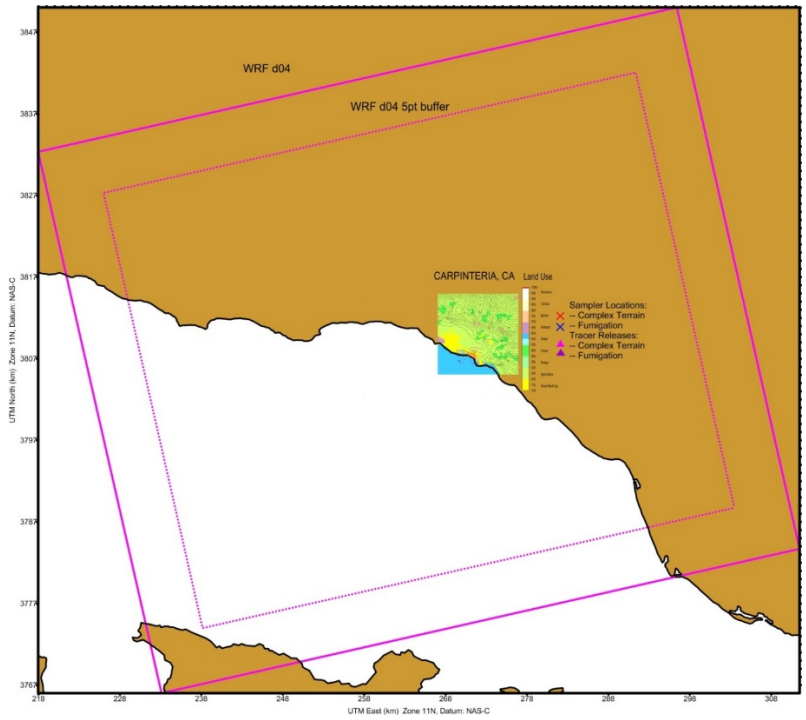

Figure 6. Carpinteria WRF 1.33-km Domain

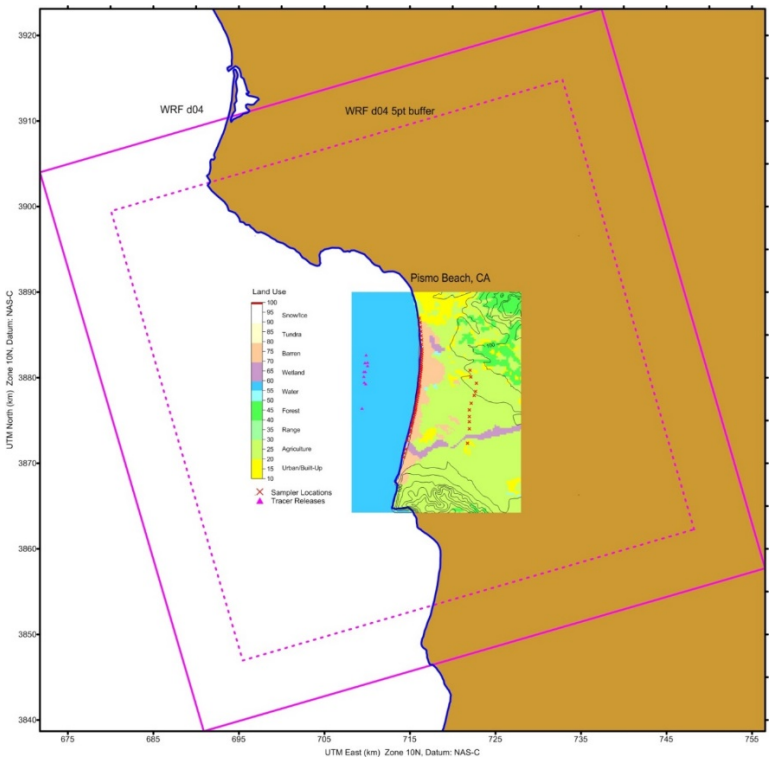

Figure 7. Pismo Beach WRF 1.33-km Domain

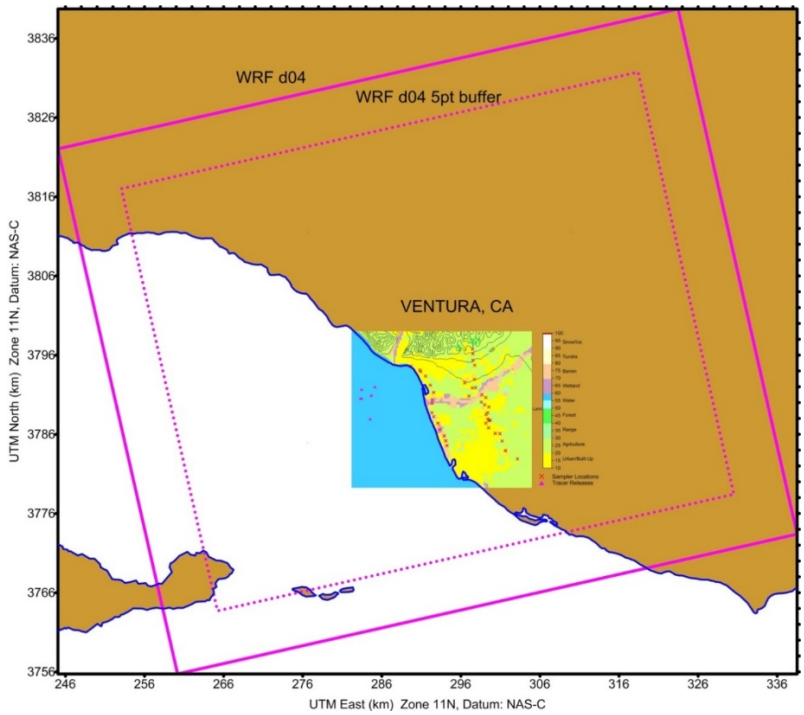

Figure 8. Ventura WRF 1.33-km Domain

2.3 Using MMIF to Provide Meteorological Inputs for OCD, AERMOD, and CALPUFF

For this model justification study, MMIF is used to supply AERMOD-, OCD-, and CALPUFF-ready meteorology directly from WRF. As mentioned above, MMIF maintains the horizontal map projection and grid resolution from WRF but can adjust the WRF vertical resolution as needed. According to an evaluation of the combined WRF/MMIF/AERCOARE/AERMOD overwater modeling approach for offshore emission sources (USEPA, 2015b, 2015c), there was no discernable advantage to using AERCOARE as an intermediary between MMIF and AERMOD. Building upon the results of USEPA (2015b, 2015c), MMIF output is directly incorporated into CALPUFF rather than using CALMET as an intermediary. MMIF does not produce files that can be directly fed into OCD but does produce an AERCOARE-formatted data file. Two simple utilities were created during this study to re-format MMIF-produced AERCOARE input files and AERMOD surface files into OCD overwater and overland input meteorology files, respectively.

Required meteorological variables that are not included in the WRF output fields, such as Monin-Obukov length (L) and convective scaling velocity (w_*), are calculated using MMIF and the Richardson-number methodology defined in Louis (1979). As mentioned above, PBL heights can also be calculated in MMIF using the bulk Richardson approach of Vogelezang and Holtslag (Vogelezang and Holtslag, 1996). The ability of MMIF to estimate PBL heights is useful because there are occasions in WRF where modeled PBL heights vary drastically over small spatial scales, likely because PBL heights in WRF are fixed to the nearest vertical grid cell center.

Many of the MMIF meteorological parameters used in AERMOD, OCD, and CALPUFF are similar (e.g., surface air temperature, wind speed, wind direction, relative humidity), although there are some notable differences, particularly in input file structure. AERMOD uses two meteorological input files associated with a specific on-land location; a surface meteorological file (SFC file) and an upper-air profile file (PFL file) that contain meteorological information at 11 atmospheric heights (2 m, 10 m, 30 m, 60 m, 120 m, 240 m, 480 m, 920 m, 1,600 m, 2,500 m, 3,500 m). These vertical layers were chosen to remain consistent with the USEPA-recommended vertical layers in CALPUFF, although Brashers, Sturtz, and Maranche (2016) recently showed that modeled SO_2 concentrations in AERMOD are not sensitive to the vertical layering scheme used. Both input files contain a time series of hourly-averaged meteorological parameters.

OCD requires hourly-averaged meteorology at two locations: one over land and another over water. The overwater meteorological inputs were derived from an AERCOARE file produced by MMIF, and the overland meteorology inputs were obtained from an AERMOD surface file also produced by MMIF. For the OCD overland meteorology data file, WRF output from an inland grid cell was used, and care was taken to ensure that none of the modeled hours were flagged as having calm winds. A notable difference between OCD and the other two dispersion models is that the air-sea temperature difference is a necessary OCD input parameter. The air-sea temperature difference is used to calculate surface layer energy fluxes.

Unlike OCD and AERMOD, which require meteorology at only one or two locations, CALPUFF requires 3-dimensional, gridded meteorology input files. In this study, CALPUFF hourly-averaged meteorology is provided at a horizontal resolution of 1.33 km and over 10 vertical layers (0–20 m, 20–40 m, 40–80 m, 80–160 m, 160–320 m, 320–640 m, 640–1,200 m, 1,200–2,000 m, 2,000–3,000 m, 3,000–4,000 m), which are vertical layers recommended by the USEPA. CALPUFF requires gridded fields of PG stability class. MMIF uses WRF output to calculate PG stability class using the Golder (1972) method, which uses a relationship between Monin-Obukhov lengths and surface roughness to determine stability.

Modeled wind directions from WRF were adjusted in all three dispersion models for all four tracer sites to ensure continuity between the observed and modeled receptor with the highest tracer concentration each hour. For every hour in each tracer study, the wind direction and distance between the source and the receptor with the highest tracer concentration is known (see Chapter 4 in DiCristofaro and Hannah [1989]). The wind directions are adjusted to point from the source to the receptor with the highest concentration in both AERMOD and OCD, following the approach used in DiCristofaro and Hannah (1989). For the complex terrain tracer study (Carpinteria), wind directions in AERMOD were adjusted in a similar fashion. For the tracer studies with flat terrain (Cameron, Pismo Beach, and Ventura), the wind directions in AERMOD were adjusted towards a single receptor located at the same downwind distance as the observed highest concentration receptor, assuming the observed maximum tracer concentration occurred at the plume centerline. A similar methodology was used for the AERMOD runs presented in USEPA (2015b). For CALPUFF, a special version of MMIF was developed that allowed the user to specify the wind direction at a specific point, for each hour. MMIF rotated the entire wind field to match that wind direction. By rotating the entire wind field, the (non-) divergence of the field was preserved. Because the source-receptor distances are relatively short, most of the wind field does not affect the result, only the part of the wind field between the source and receptor, which was forced to match the wind direction given AERMOD and OCD.

2.4 Dispersion Modeling Configuration

The current regulatory versions of AERMOD (version 15181), OCD (version 5), and CALPUFF (CALPUFF version 5.8.5; CALPOST version 6.221) are used in this study, with regulatory defaults applied except as noted. The tracer studies have been simulated in previous studies using OCD (DiCristofaro and Hanna, 1989), AERMOD (ENVIRON, 2012; USEPA, 2015b), and CALPUFF (Earth Tech, 2006). For consistency, we used the model input files from these previous studies as templates in this analysis. Similar to previous studies, AERMOD and OCD were run for each individual hour while CALPUFF was run for the entire multi-hour measurement period each day.

The OCD input files were developed based on the OCD input files used in Earth Tech (2006). There are two differences between the original input files and those used in this study. First, this study applied a minimum PBL height of 25 m, and second, the original meteorological files are replaced with the overland and overwater meteorological input files described in Section 2.3 of this appendix. OCD simulates a sloping thermal interface boundary layer near the coast (TIBL), while this option is turned off

in CALPUFF and not included in AERMOD. A notable difference between OCD and CALPUFF is that the regulatory default setting for minimum overwater lateral turbulence velocity (σ_v), a measure of horizontal plume dispersion, is 0.37 m/s in OCD compared to 0.5 m/s in CALPUFF.

The AERMOD input files used in this study are similar to those used to evaluate WRF/MMIF/AERCOARE/AERMOD overwater model performance for offshore emission sources (USEPA, 2015b), except that MMIF was used to directly supply AERMET-like surface and profile files, and the minimum boundary layer height was set to 25 m. For the simple terrain cases (Pismo, Ventura, Cameron), one receptor is modeled. For the complex terrain case (Carpinteria), a set of receptors along the coast was modeled that are identical to the receptors defined in CALPUFF and OCD.

The CALPUFF input files used in this tracer study analysis were adapted from the CALPUFF input files used in Earth Tech (2006). CALMET-like files from MMIF were specified in the CALPUFF input files. Because the meteorological files produced by MMIF are in LCC coordinates, the coordinates in the original CALPUFF input files were converted from Universal Transverse Mercator (UTM) to LCC. For all tracer study sites, the sets of receptors originally defined in the OCD tracer study model simulations were also used in CALPUFF. The minimum PBL height was set to 25 m in this study. Aside from the meteorology and grid domain modifications, most options remained the same between the CALPUFF and CALPUFF post-processor, CALPOST, versions originally used (CALPUFF version 5.75, CALPOST version 5.638), and the versions used in this study. In CALPUFF version 5.8.4., there is an additional option to diagnose the advective-decay turbulence timescale, and a different back-up method is used to compute dispersion when turbulence data is missing. All options comply with the regulatory defaults, except that wet deposition, dry deposition, and partial plume penetration of elevated inversion are not modeled and a probability density function is not used for dispersion under convective conditions. These settings deviate from the regulatory default settings in order to maintain consistency with the options used in the Earth Tech (2006) report.

3. STATISTICS USED TO EVALUATE MODEL PERFORMANCE

This section describes the methodology used to evaluate OCD, AERMOD, and CALPUFF results using two established statistical approaches. Following previous dispersion model evaluations (DiCristofaro and Hanna, 1989; Earth Tech, 2006; USEPA, 2015b), the maximum measured and modeled tracer concentrations each hour are used to construct the performance statistics described below. The first approach is a set of specific statistical measures, including Quantile-Quantile (Q-Q) plots, Robust Highest Concentration (*RHC*), fractional factor of two, and geometric correlation coefficient, mean, and variance. The second approach is known as Cox-Tikvart methodology (Cox and Tikvart, 1990). The specific statistical measures and the Cox-Tikvart methodology are described in more detail below.

3.1 Specific Statistical Metrics

The statistical measures and methods used in this analysis are similar to the techniques applied in the USEPA evaluation of other dispersion models (e.g., USEPA, 2003, 2015b; Wong et al., 2016). The statistical tools used in this analysis are described below:

- **Quantile-quantile (Q-Q) plots** show a series of ranked pairings of predicted and observed concentration, where any rank of the predicted concentration is plotted against the same ranking of the observed concentration. Q-Q plots are developed to evaluate a dispersion model's ability to represent the frequency distribution of the observed concentrations. Q-Q plots are useful for investigating whether predictions are biased high or low with respect to observed concentrations at the upper end of the frequency distribution.
- ***RHC*** is a comparison of modeled and observed concentrations at upper end of a frequency distribution and is calculated using E1, where n=5 for the tracer study analysis, and n=26 for the synthetic source analysis.

$$RHC = c_n + (\bar{c} - c_n) ln\left(\frac{3n-1}{2}\right) \quad (1)$$

  where c_n is the nth highest concentration and $\bar{c}$ is the average of the (n-1) highest concentrations.
- **Fractional factor of two (*FF2*)** is the ratio of the number of modeled concentrations within a factor of two of observed concentrations compared to the total number of modeled concentrations.
- **Geometric correlation coefficient (r_g)** is the standard correlation coefficient computed using the natural log of the modeled and measured concentrations, calculated in E2.

$$r_g = \frac{\sum\left(\ln(x) - \overline{\ln(x)}\right)\left(\ln(y) - \overline{\ln(y)}\right)}{\sqrt{\sum\left(\ln(x) - \overline{\ln(x)}\right)^2}\sqrt{\sum\left(\ln(y) - \overline{\ln(y)}\right)^2}} \quad (2)$$

- **Geometric mean (μ_g)** is the n[th] root of the product of n numbers, calculated in E3. The geometric mean is used to evaluate a general expected value with dampened outlier influence.

$$\mu_g = \left(\prod_{i=1}^{n} c_i\right)^{1/n} \quad (3)$$

- **Geometric mean variance (*VG*)** is a measure of the precision of the dataset. A perfect model would result in *VG* = 1. *VG* is calculated in E4, where c_o and c_p are the observed and predicted concentrations, respectively.

$$VG = e^{\left(\sqrt{\left(ln\left(\frac{c_o}{c_p}\right)\right)^2}\right)} \quad (4)$$

By comparing the maximum modeled and measured tracer concentration, we allow for a statistical comparison resolved in time rather than space. Although the modeled wind directions in the dispersion models are aligned between the emissions source and the receptor with the highest concentrations each

hour, the exact location of the receptor was not provided, and the receptors were often grouped closely together during the experiments.

In order to be independent of tracer emission rate, the tracer study simulations were performed with a unit emission rate of 1 gram per second (g/s), and the observed concentrations (microgram per cubic meter [$\mu g/m^3$]) were normalized by the tracer release rate (g/s), resulting in concentrations units of ($\mu g/m^3$) / (g/s) = $\mu s/m^3$.

3.2 Cox-Tikvart Methodology

3.2.1 General Cox-Tikvart Methodology

The Cox-Tikvart methodology was developed in 1990 as a statistically robust way to compare the performances of a variety of models against observations. Traditionally, this analysis has been performed on year-long datasets with hourly resolution. The Cox-Tikvart approach consists of two distinct pieces: a "scientific" component and an "operational" component.

The scientific piece assesses the 1-hr averages during six specific meteorological conditions. The meteorological conditions are unique combinations of unstable, neutral, or stable conditions and wind speeds above or below 4 m/s. For each meteorological condition, the *RHC* is calculated for both the observed and modeled dataset using E1 and the absolute fractional bias (*AFB*) between the modeled and measured *RHC* is calculated using E5.

$$AFB = \left| 2 \cdot \frac{(RHC_{measured} - RHC_{modeled})}{(RHC_{measured} + RHC_{modeled})} \right| \qquad (5)$$

The operational component evaluates the peak 3-hour and 24-hour averages independent of meteorology or spatial location. The absolute fractional bias between measured and modeled *RHC* is calculated in a similar manner, except that the data is grouped into 3-hour and 24-hour averages, respectively. A bootstrapping statistical technique is used to resample the observed and modeled data in 3-day blocks 1,000 separate times in order to estimate 5th and 95th percentile confidence intervals for the absolute fractional bias in both the scientific and operational components.

A composite performance metric (*CPM*) combines the 1-hr, 3-hr, and 24-hr absolute fractional biases in *RHC* for both the scientific and operational components, as shown in E6.

$$CPM = \frac{(\,average(AFB(i,j) + AFB(3) + AFB(24))}{3} \qquad (6)$$

where *AFB*(I,J) is the absolute fractional bias for each meteorological condition, *AFB*(3) is the absolute fractional bias for 3-hour averages, and *AFB*(24) is the absolute fractional bias for 24-hour averages.

The *CPM* is lowest when there is a good agreement between measured and modeled *RHC* values. Comparing the magnitudes of the *CPM* values from different models using the same observational data provides insight into the model performance of each dispersion model in a relative sense.

3.2.2 Adjustments to Cox-Tikvart Methodology for Tracer Studies

For the tracer study analysis, slight modifications to the standard Cox-Tikvart methodology were made because of the limited number of observations at each site. The data was grouped in several different ways and the absolute fractional biases are calculated for each different group of data:

- Each site using all hourly data
- All summer data (multiple sites combined)
- All winter data (multiple sites combined)
- All data (all sites combined)

Since tracer concentrations were observed for only several hours a day at each tracer study location, the *CPM* was not calculated for each individual site because the metric relies on 3- and 24-hour average *AFB* values. Instead, the hourly-averaged modeled and observed tracer concentrations at each site were used to calculate the absolute fractional bias for all three dispersion models. Given the limited data at each site, no data blocking was used to calculate the 5^{th} and 95^{th} percentile confidence intervals for the absolute fractional bias at each site.

To increase the amount of data used to calculate the *CPM,* all the summer data from all sites were combined. A similar approach was taken for the winter data, as well as an overall data set combined, regardless of site or season. For these calculations, 3-hour and 24-hour averages were used to calculate *AFB* by putting in blank (NaN) values for hours without tracer concentrations. Similar to the approach used for the individual sites, data was not blocked to calculate the confidence intervals associated with the *CPM*.

Additionally, since modeled meteorology is used exclusively in this study, the stability classes and wind speeds for each tracer study location were obtained from MMIF-produced, AERMET-like surface files based on WRF meteorological output fields.

4. MODEL COMPARISONS—TRACER STUDIES

This section presents Q-Q plots and tabular statistical results for each site using modeled concentrations from OCD, AERMOD, and CALPUFF. We also present tabular statistical results for various combinations of data from each site, including all summer data, all winter data, and all data. The observed tracer concentrations can be found in Appendix A of Earth Tech (2006) and modeled tracer concentrations along with model input files from this study are available upon request.

The figures and tables show results from cases where PBL heights from WRF were used (MIXHT-WRF), along with cases where MMIF was used to re-diagnose PBL heights (MIXHT-MMIF). In many cases, the modeled tracer concentrations are relatively insensitive to whether MMIF or WRF PBL heights are used. When there are differences, MMIF PBL heights are most often associated with higher concentrations. Modeled tracer concentration differences associated with the two PBL-height options are smaller

compared to differences between modeled tracer concentrations from the three dispersion models, suggesting that there are additional factors influencing tracer dispersion more than PBL heights.

Figure 9 through Figure 11 show Q-Q plots for Cameron using OCD, CALPUFF, and AERMOD for simulations using both WRF (MIXHT-WRF) and MMIF (MIXHT-MMIF) PBL heights. Figure 9 shows that OCD shares agreement with observed concentrations in the middle of the frequency distribution but overestimates the lowest concentrations and underestimates the highest concentrations. OCD concentrations show less variation compared to observations at Cameron. The highest concentrations are also underestimated in AERMOD and CALPUFF, but the lowest modeled concentrations are in better agreement with observed tracer concentrations. For AERMOD, the model-measurement agreement at lower concentrations is consistent with the results shown in Figure 5a in Wong et al. (2016) for Cameron.

Figure 12 through Figure 14 present Q-Q plots for Carpinteria using all three dispersion models. There is good model-measurement agreement when OCD is used, with the majority of modeled concentrations within a factor of two compared to observations. AERMOD slightly overestimates concentrations across the frequency domain, particularly in the middle range. CALPUFF under predicts the tracer concentrations, although highest tracer concentration is only slightly underestimated. CALPUFF is likely underestimating tracer concentrations because a minimum σ_v of 0.50 m/s is used (regulatory default), although Earth Tech (2006) used these tracer studies to show that CALPUFF underestimated tracer concentrations when σ_v was set to 0.50 m/s over water, rather than 0.37 m/s, which is the default in OCD. Additionally, the complex terrain surrounding Carpinteria may also lead to additional modeling challenges.

Figure 15 through Figure 17 show Q-Q plots at Pismo Beach for OCD, AERMOD, and CALPUFF. The modeled tracer concentrations from all three dispersion models show good agreement with observations. For OCD, the vast majority of modeled concentrations agree within a factor of two compared to observations and model-measurement agreement is very good at the low and high ends of the frequency domain. AERMOD slightly overestimates the highest concentrations and slightly underestimates concentrations in the low-to-mid end of the frequency distribution, which is generally consistent with the model-measurement comparison at Pismo shown in Figure 5C in Wong et al. (2016) for Pismo.

Figure 18 though Figure 20 present Q-Q plots for Ventura for all three models. OCD slightly overestimates tracer concentrations for Ventura, while AERMOD and CALPUFF overestimate to a greater degree. The receptors are located further inland at Ventura compared to the other tracer study locations, and thus are more affected by spatial gradients in PBL heights caused by stable conditions over water and unstable conditions over land. OCD is able to account for spatial gradients in stability classes and PBL heights through its shoreline fumigation algorithms and treatment of the TIBL. AERMOD does not treat shoreline fumigation, and, to be consistent with the CALPUFF tracer study presented in EarthTech (2006), the CALPUFF TIBL module was not used. In addition, Figure 72 in USEPA (2015b) shows that observed summertime air-sea temperature differences are generally negative (-2 to 0˚) at

Ventura during the tracer studies, suggesting instability in the region. Modeled air-sea temperature differences in WRF during the same time period range from -0.5 to 1, indicating that WRF is simulating a more stable environment compared to observations. In light of these differences, concentration overestimates in AERMOD and CALPUFF at Ventura are not unreasonable.

In general, the performance of OCD, AERMOD, and CALPUFF varies at each of these tracer study locations, which all have different terrain, geography, and source/receptor positioning. No dispersion model is a clear outperformer when the results from the four tracer studies are considered together.

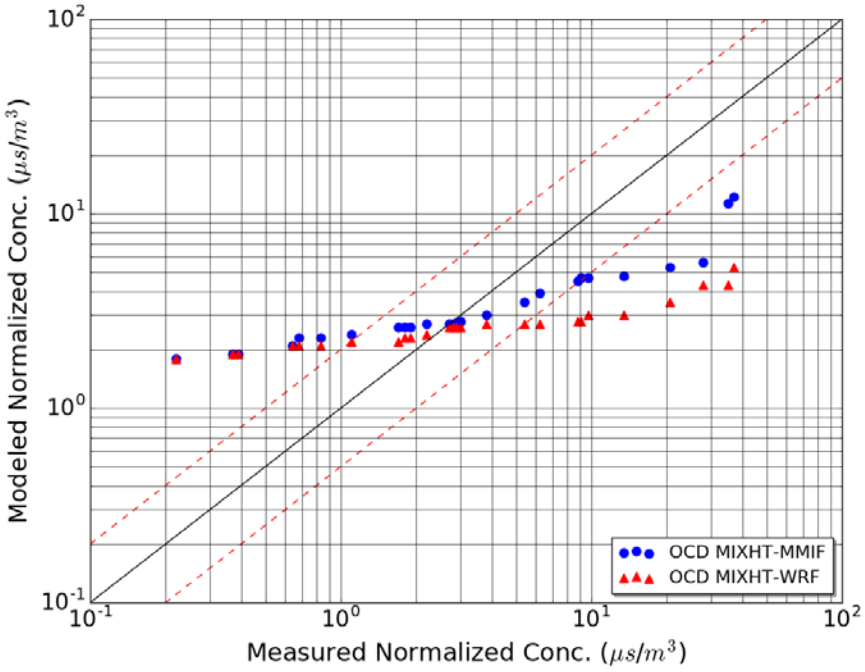

Figure 9. OCD Q-Q Plot of Tracer Concentration at Cameron

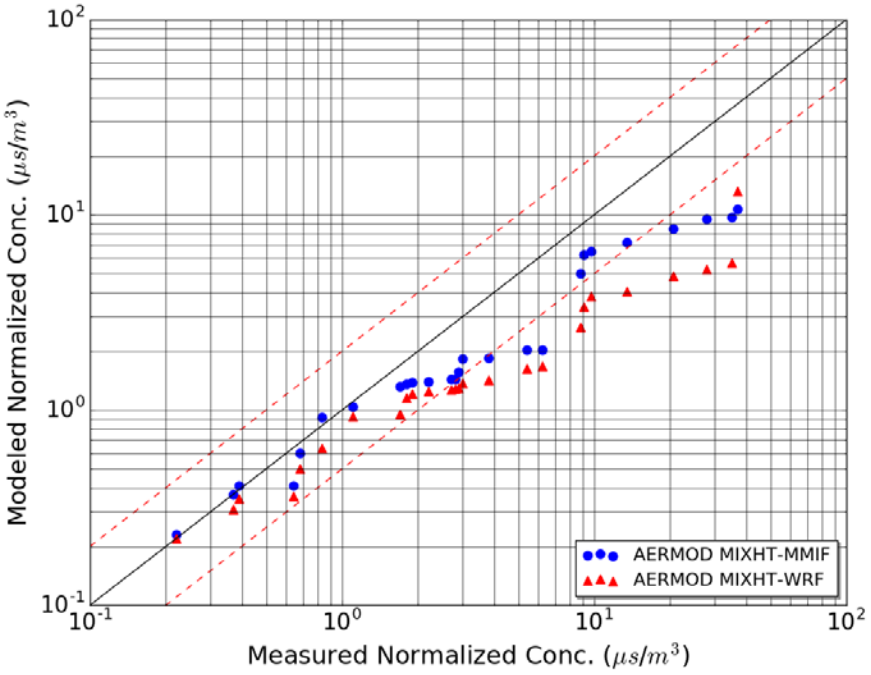

Figure 10. AERMOD Q-Q Plot of Tracer Concentration at Cameron

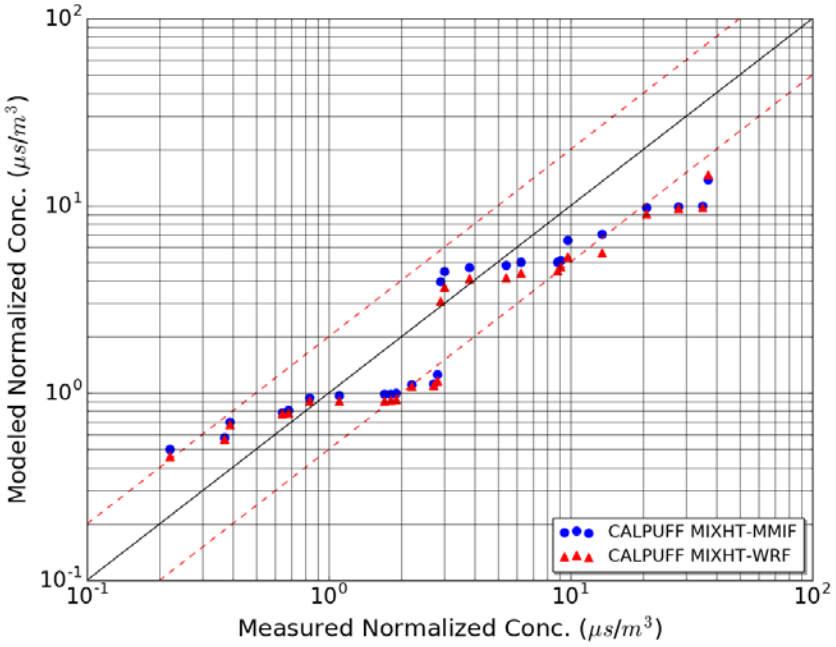

Figure 11. CALPUFF Q-Q Plot of Tracer Concentration at Cameron

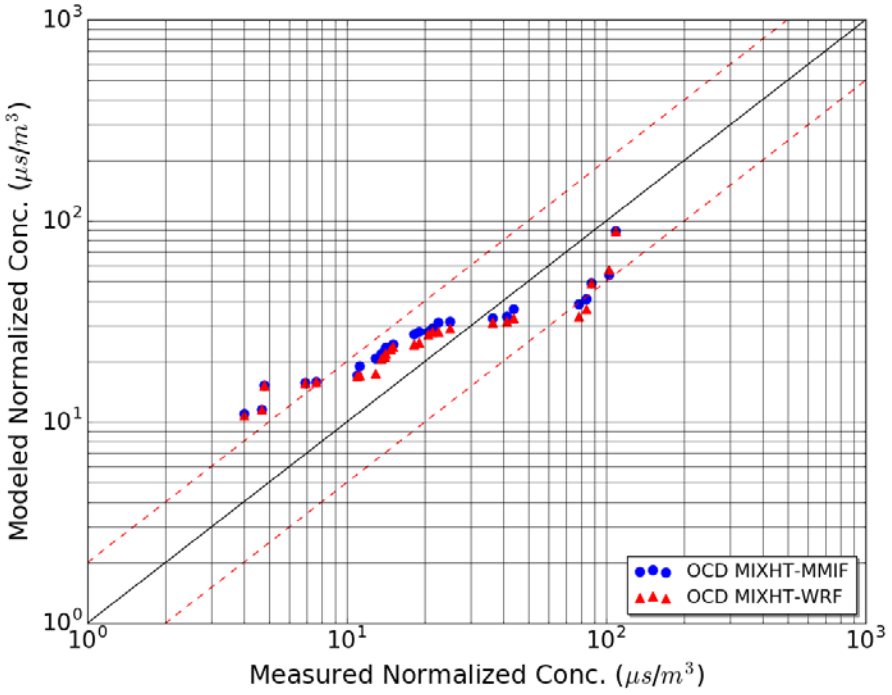

Figure 12. OCD Q-Q Plot of Tracer Concentrations at Carpinteria

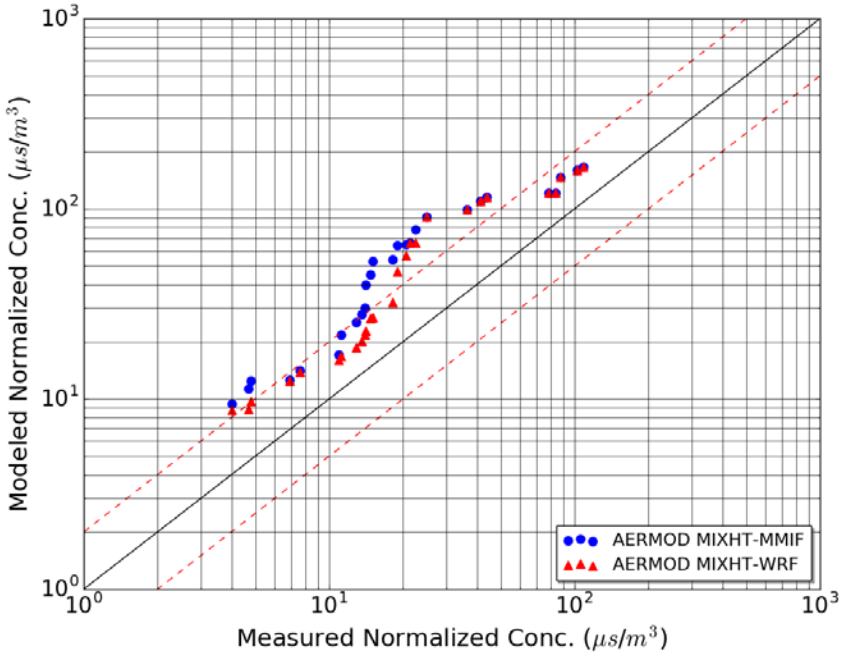

Figure 13. AERMOD Q-Q Plot of Tracer Concentrations at Carpinteria

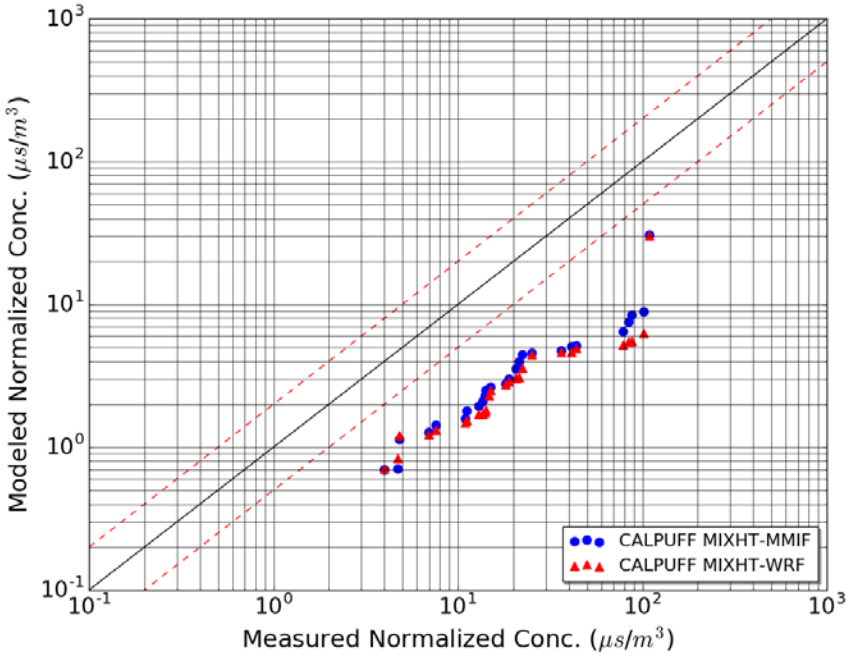

Figure 14. CALPUFF Q-Q Plot of Tracer Concentrations at Carpinteria

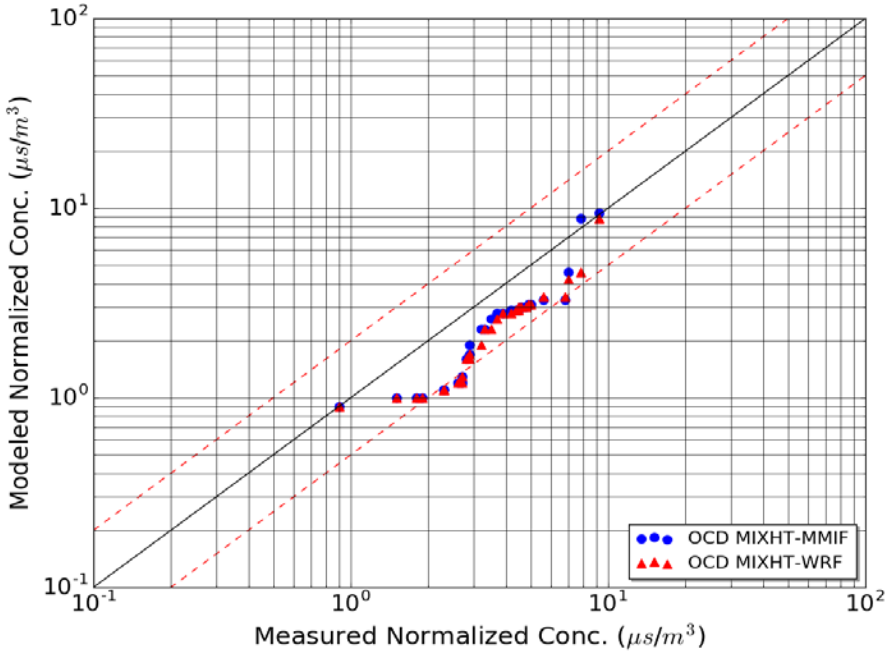

Figure 15. OCD Q-Q Plot of Tracer Concentrations at Pismo Beach

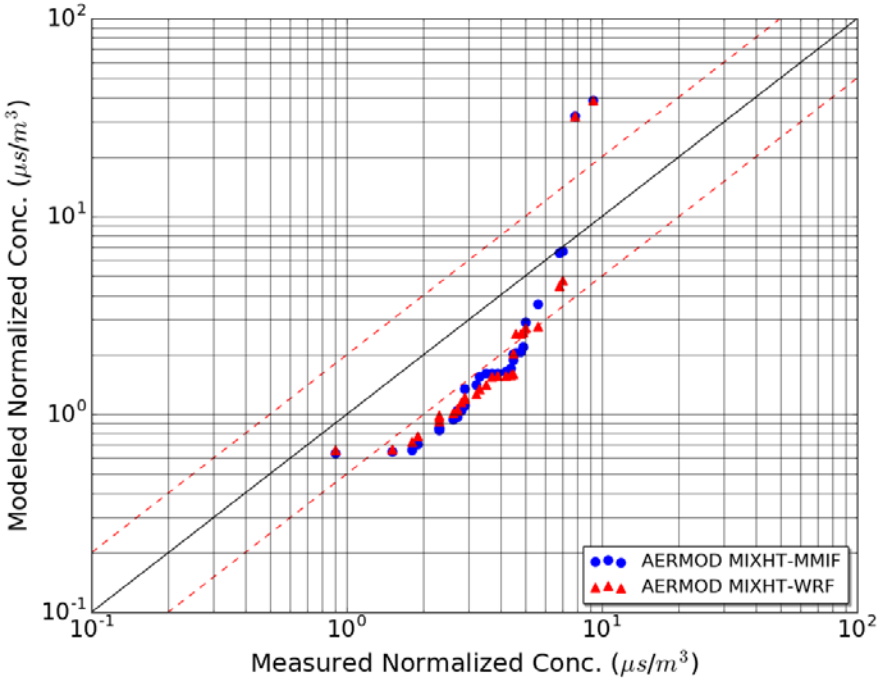

Figure 16. AERMOD Q-Q Plot of Tracer Concentrations at Pismo Beach

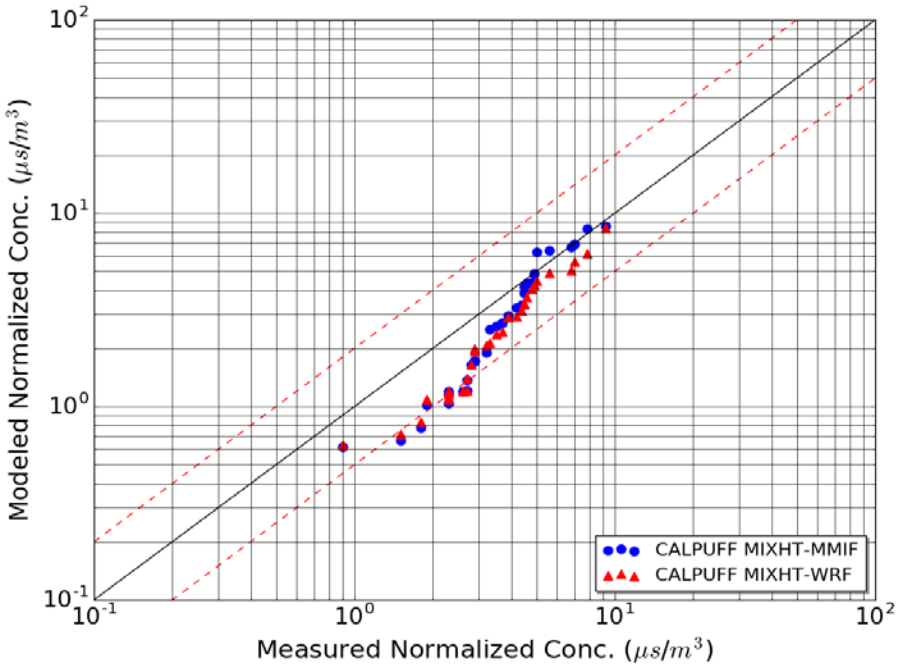

Figure 17. CALPUFF Q-Q Plot of Tracer Concentrations at Pismo Beach

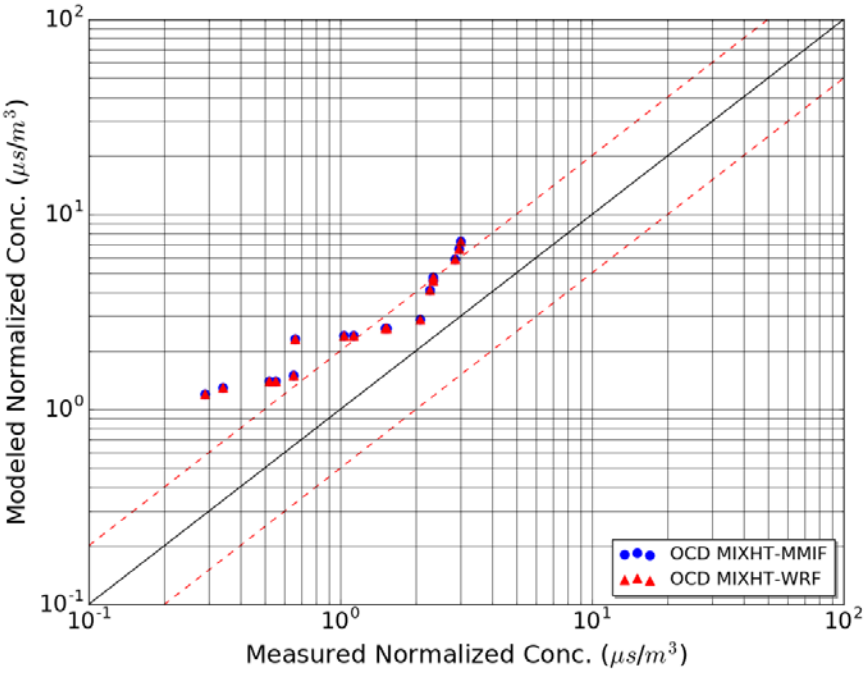

Figure 18. OCD Q-Q Plot of Tracer Concentrations at Ventura

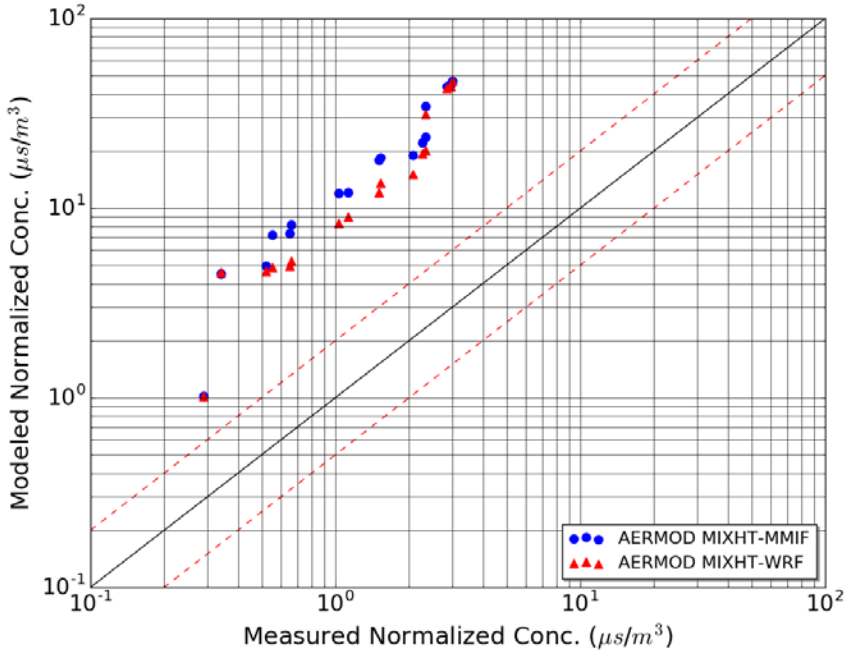

Figure 19. AERMOD Q-Q Plot of Tracer Concentrations at Ventura

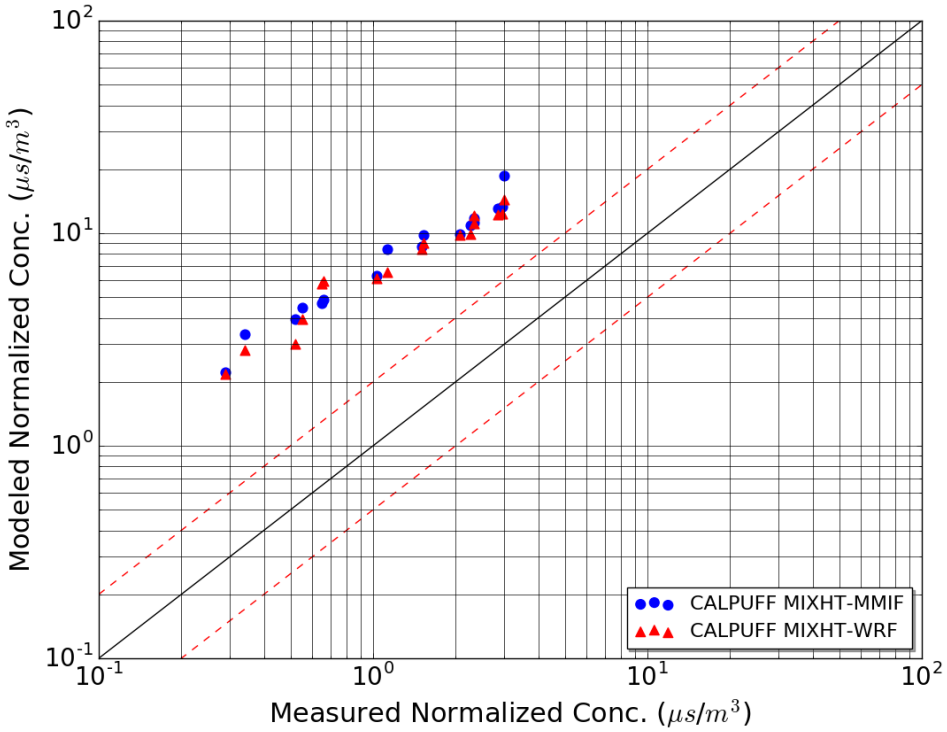

Figure 20. CALPUFF Q-Q Plot of Tracer Concentrations at Ventura

Table 2 through Table 5 show the statistical metrics used to compare modeled and measured tracer concentrations at each site. Table 2 presents statistical results for Cameron. The measured *RHC* values are three to eight times higher than modeled *RHC* values. Between 35 and 50% of modeled tracer concentrations are within a factor of two compared observed tracer concentrations. The geometric correlation coefficient (r_g) ranges from 0.82–0.84 for AERMOD, 0.75–0.76 for CALPUFF, and 0.62–0.80 for OCD, suggesting that AERMOD and CALPUFF concentrations are in better agreement with observations overall compared to OCD. The geometric mean (μ_g) from OCD is most closely aligned with the observed μ_g, which when combined with our interpretation of Figure 9, suggests that OCD does the best job reproducing concentrations in the middle of the frequency range, where outliers are excluded. Although it is best when modeled and observed concentrations are in agreement throughout the entire frequency distribution, for air quality regulatory purposes, it is most important that modeled and measurement concentrations are well aligned at the upper end of the frequency distribution. The precision of all three models is relatively high at Cameron compared to modeled variance (*VG*) at other sites.

Table 2. Measured-Modeled Statistical Metrics for Cameron

Metrics	Observed	PBL Height[1]	AERMOD	CALPUFF	OCD
RHC[2]	45.80	**MMIF**	11.84	14.52	12.19
		WRF	10.28	15.70	5.63
FF2	1	**MMIF**	0.50	0.46	0.42
		WRF	0.35	0.50	0.38
r_g	1	**MMIF**	0.82	0.75	0.62
		WRF	0.84	0.76	0.80
μ_g	3.17	**MMIF**	1.89	2.37	3.32
		WRF	1.44	2.19	2.63
VG	1	**MMIF**	2.50	2.62	3.95
		WRF	3.48	2.69	4.49

[1]Modeled PBL height from WRF or re-diagnosed using MMIF.
[2]*RHC* calculated using N=5.

Table 3 shows statistical results for Carpinteria. Compared to observed *RHC* values, AERMOD *RHC* values are 1.6 times higher, OCD *RHC* values are a factor of 1.3–1.5 times lower, and CALPUFF *RHC* values are 5-6 times lower. The *RHC* values indicate that AERMOD is overestimating concentrations while CALPUFF is underestimating concentrations, which is consistent with the Q-Q plots shown in Figure 13 and Figure 14. For AERMOD and OCD, between 41 and 56% of modeled tracer concentrations are within a factor of two agreement compared to observations and r_g ranges from 0.24 to 0.66; *FF2* and r_g are considerably lower for CALPUFF. AERMOD and OCD over predict the geometric mean by a factor of 2 to 2.3 and 1.2 to 1.3, respectively, and have relatively high precision compared to observations, while CALPUFF under predicts μ_g by a factor of up to 7.3 and has low precision (high *VG* values). AERMOD and OCD perform better than CALPUFF at this complex terrain site, although it is not clear which model performs best at this location. The difference between maximum modeled and observed concentrations is higher in AERMOD than OCD, but AERMOD has a considerably higher correlation coefficient, suggesting that it has better overall agreement with observations across the frequency domain.

Table 3. Measured-Modeled Statistical Metrics for Carpinteria

Metrics	Observed	PBL Height[1]	AERMOD	CALPUFF	OCD
RHC[2]	111.78	**MMIF**	174.43	21.01	77.03
		WRF	174.43	18.32	81.27
FF2	1	**MMIF**	0.41	0.19	0.44
		WRF	0.56	0.11	0.52
r_g	1	**MMIF**	0.66	0.12	0.24
		WRF	0.65	0.03	0.27
μ_g	20.12	**MMIF**	46.97	3.08	26.27
		WRF	39.33	2.72	24.89
VG	1	**MMIF**	3.61	129.79	2.58
		WRF	2.92	222.13	2.45

[1]Modeled PBL height from WRF or re-diagnosed using MMIF.
[2]*RHC* calculated using N=5.

Through comparison of dispersion model performance at Carpinteria and Cameron, it appears that AERMOD and OCD perform better overall at sites with simple, rather than complex, terrain, which is expected given the challenges associated with simulating complex coastal terrain. CALPUFF under predicts tracer concentrations at Carpinteria, which is at least partially due to using an overwater σ_v of 0.50 m/s compared to 0.37 m/s, which leads to enhanced lateral plume dispersion. In complex terrain, the extent of lateral plume spread may substantially impact dispersion.

Table 4 presents measured and modeled statistical metrics for Pismo Beach. The highest concentrations are well-predicted by CALPUFF and OCD, while AERMOD over predicts the top two highest concentrations. Similarly, there is a factor of two model-measurement agreement of 61–68% when CALPUFF and OCD are used, which are higher than *FF2* values at any other site. The *FF2* value is lower for AERMOD (0.39) because many of the modeled concentrations lie just beyond the lower *FF2* limit (see Figure 16). The geometric correlation coefficient is similar for AERMOD and CALPUFF (0.37–0.47) and much lower for OCD (0.05–0.08). Although r_g is lower at Pismo Beach compared to other sides, the high CALPUFF and OCD *FF2* values, along with AERMOD modeled concentrations just beyond the lower *FF2* limit, imply that all three dispersion models are performing well at Pismo Beach. All three models slightly underestimate the geometric mean and have relatively high precision (small *VG*) compared to the dispersion modeling results at the other tracer study locations.

Table 4. Measured-Modeled Statistical Metrics for Pismo Beach

Metrics	Observed	PBL Height[1]	AERMOD	CALPUFF	OCD
RHC[2]	9.69	**MMIF**	37.48	8.77	9.58
		WRF	36.33	7.63	7.00
FF2	1	**MMIF**	0.39	0.61	0.65
		WRF	0.39	0.61	0.68
r_g	1	**MMIF**	0.37	0.38	0.05
		WRF	0.39	0.47	0.08
μ_g	3.46	**MMIF**	1.81	2.44	2.18
		WRF	1.79	2.28	2.09
VG	1	**MMIF**	3.53	1.94	2.20
		WRF	3.26	1.74	2.14

[1]Modeled PBL height from WRF or re-diagnosed using MMIF.
[2]*RHC* calculated using N=5.

Table 5 shows statistical results for Ventura. All three models over predict the highest concentrations; *RHC* values are 2.4–19 times higher than the measured *RHC*, with AERMOD overpredicting the most. As Figure 18 through Figure 20 show, AERMOD and CALPUFF over predict concentrations across the entire frequency domain and OCD slightly over predicts at both the lower and upper end of the frequency domain. OCD has higher *FF2* values (0.35–0.47) compared to AERMOD (0.18) and CALPUFF (0.12). The r_g values are lower at Ventura compared to many of the other sites and even show anti-correlation in the case of OCD. All three models over predict μ_g, and the AERMOD model results exhibit particularly low precision compared to observations. As mentioned above, these model performance differences are likely at least somewhat due to differences in the treatment of spatial gradients in stability and PBL heights between the dispersion models. In addition, WRF simulates a more stable environment at Ventura compared to observed meteorology, further contributing to differences between observed and modeled tracer concentrations.

Table 5. Measured-Modeled Statistical Metrics for Ventura

Metrics	Observed	PBL Height[1]	AERMOD	CALPUFF	OCD
RHC[2]	3.22	**MMIF**	60.17	17.00	7.66
		WRF	61.14	14.34	7.66
FF2	1	**MMIF**	0.18	0.12	0.35
		WRF	0.18	0.12	0.47
r_g	1	**MMIF**	0.23	0.24	-0.04
		WRF	0.27	0.34	-0.06
μ_g	1.20	**MMIF**	13.44	7.41	2.76
		WRF	11.06	6.97	2.76
VG	1	**MMIF**	1,137.88	55.40	5.17
		WRF	452.78	40.63	5.26

[1]Modeled PBL height from WRF or re-diagnosed using MMIF.
[2]*RHC* calculated using N=5.

In general, Table 2 through Table 5 show that AERMOD and CALPUFF are able to simulate the short-range dispersion from offshore emission sources just as well as the regulatory default model, OCD. No model clearly outperforms the others at all tracer study locations, suggesting that the configurations specific to each tracer study (e.g., source-receptor distances, complex terrain) influence each model differently.

Table 6 shows the mean *AFB* along with the 5th and 95th percentile confidence intervals for each tracer study location, which compares the *RHC* values of the measured and modeled tracer concentrations. An absolute fractional bias of 0 indicates perfect agreement between the observed and modeled *RHC* values. Running OCD using MMIF PBL heights for Pismo Beach resulted in the lowest *AFB* (0.01), and running AERMOD with MMIF PBL heights for Ventura led to the highest *AFB* (1.80). Using CALPUFF at Pismo Beach, OCD at Carpinteria, and AERMOD at Carpinteria resulted in the second, third, and fourth lowest *AFB* values, respectively.

Table 6. Absolute Fractional Biases for Tracer Studies

Mean |Fractional Bias| (5^{th}-95^{th}) [2,3]				
Site	**PBL height[1]**	**AERMOD**	**CALPUFF**	**OCD**
Cameron	**MMIF**	1.18 (0.71–1.33)	1.04 (0.66–1.24)	1.16 (0.58–1.52)
	WRF	1.27 (0.82–1.56)	0.98 (0.67–1.25)	1.56 (1.39–1.66)
Carpinteria	**MMIF**	0.43 (0.07–0.65)	1.36 (0.90–1.76)	0.37 (0.09–0.85)
	WRF	0.43 (0.08–0.66)	1.44 (0.89–1.83)	0.32 (0.08–0.92)
Pismo	**MMIF**	1.18 (0.21–1.52)	0.10 (0.01–0.37)	0.01 (0.01–0.82)
	WRF	1.16 (0.50–1.52)	0.24 (0.02–0.55)	0.32 (0.03–0.85)
Ventura	**MMIF**	1.80 (1.67–1.82)	1.36 (1.18–1.52)	0.82 (0.54–1.0)
	WRF	1.80 (1.64–1.83)	1.27 (1.14–1.40)	0.82 (0.53–1.03)

[1]Modeled PBL height from WRF or re-diagnosed using MMIF.
[2]The 5^{th} and 95^{th} percentile confidence intervals are provided in parentheses.
[3]*RHC* calculated using N=5.

Table 6 shows that AERMOD and CALPUFF have lower mean *AFB*s compared to OCD at Cameron and that at least one of those models has lower *AFB* values in the 95^{th} percentile compared to OCD for all sites and PBL options except for Ventura. The results from Table 6 further suggests that model performance varies considerably at each site and that AERMOD and CALPUFF perform just as well as OCD for the majority of tracer studies simulations.

In addition to comparing model performance at each individual site, the data was grouped by season and combined together to elucidate AERMOD, OCD, and CALPUFF performance using a larger, more diverse sample set. Table 7 through Table 9 show statistical metrics for several different groupings of data: all data measured and modeled in the summer, all data measured and modeled in the winter, and all data from all tracer studies combined. Table 7 shows the statistical metrics for all summer data. CALPUFF and OCD underestimate the highest tracer concentrations by a factor of 5.9 and 1.9, respectively, while AERMOD slightly overestimates by a factor of 1.2. A moderate percentage (25–54%) of all modeled concentrations are within a factor of two compared to observations; *FF2* values from OCD are slightly higher compared to *FF2* values from AERMOD, and *FF2* values are lowest for CALPUFF. The geometric correlation coefficient ranges from 0.76 to 0.78 for OCD and is similar for AERMOD (0.72–0.73), while r_g is considerably lower in CALPUFF (0.13–0.17). CALPUFF underestimates μ_g and has the lowest precision, while AERMOD and OCD both overestimate μ_g with respect to observations and have better precision compared to CALPUFF. Table 7 suggests that AERMOD and OCD modeling results are comparable during the summer tracer study periods.

Table 7. Measured-Modeled Statistical Metrics for All Summer Tracer Study Data

Metrics	Observed	PBL Height[1]	AERMOD	CALPUFF	OCD
RHC[2]	144.30	**MMIF**	173.54	24.49	73.72
		WRF	173.54	24.33	74.76
FF2	1	**MMIF**	0.39	0.30	0.43
		WRF	0.43	0.25	0.54
r_g	1	**MMIF**	0.72	0.17	0.76
		WRF	0.73	0.13	0.78
μ_g	4.69	**MMIF**	7.52	2.49	7.09
		WRF	6.52	2.33	6.48
VG	1	**MMIF**	8.74	27.15	3.51
		WRF	6.73	31.05	3.01

[1]Modeled PBL height from WRF or re-diagnosed using MMIF.
[2]*RHC* calculated using N=6.

Table 8. Measured-Modeled Statistical Metrics for All Winter Tracer Study Data

Metrics	Observed	PBL Height[1]	AERMOD	CALPUFF	OCD
RHC[2]	45.80	**MMIF**	49.18	14.10	15.27
		WRF	48.87	15.14	8.95
FF2	1	**MMIF**	0.38	0.50	0.58
		WRF	0.33	0.55	0.50
r_g	1	**MMIF**	0.03	0.26	0.39
		WRF	-0.01	0.29	0.18
μ_g	4.30	**MMIF**	4.47	4.36	2.82
		WRF	3.78	3.90	2.59
VG	1	**MMIF**	8.37	2.99	2.54
		WRF	8.49	2.87	3.27

[1]Modeled PBL height from WRF or re-diagnosed using MMIF.
[2]*RHC* calculated using N=5.

Table 8 shows the statistical results using all winter data. Similar to Table 7, AERMOD slightly overestimates the highest concentrations, while CALPUFF and OCD underpredict. AERMOD over predicts by a factor of 1.1 compared to 3.0–5.1 for CALPUFF and OCD combined. Although the AERMOD *RHC* value is most similar to the observed *RHC* value, CALPUFF and OCD has higher *FF2* (0.50–0.58) compared to AERMOD (0.33–0.38). The r_g values are lowest for AERMOD (-0.01–0.03) and highest for OCD (0.18–0.39). AERMOD and CALPUFF predict a μ_g closer to the observed μ_g compared to OCD, although AERMOD has a higher VG compared to CALPUFF and OCD. The results shown in Table 8 suggest that while no model is fully able to reproduce the observed frequency distribution, no model is a clear underperformer.

Table 9 presents the statistics used to compare modeled tracer concentrations to observed concentrations using the combined data from all sites. AERMOD overestimates the highest concentrations by factors of 1.7 to 1.8, and OCD and CALPUFF underestimate the maximum concentrations by factors of 1.8 and 5.4–5.9, respectively. Between roughly 40 and 50% of modeled concentrations for all three dispersion models are within a factor of two compared to the observed concentrations. The r_g values range from roughly 0.6 for AERMOD, 0.65 for OCD, and 0.15 for CALPUFF, suggesting that AERMOD and OCD perform equally well across the frequency domain and that CALPUFF is model performance is not as strong. OCD has the best model-measurement agreement for μ_g and has the highest precision compared to AERMOD and CALPUFF.

Table 9. Measured-Modeled Statistical Metrics for All Tracer Study Data

Metrics	Observed	PBL Height[1]	AERMOD	CALPUFF	OCD
RHC[2]	124.26	**MMIF**	203.88	22.88	68.03
		WRF	222.61	21.22	68.28
FF2	1	**MMIF**	0.39	0.38	0.52
		WRF	0.39	0.37	0.49
r_g	1	**MMIF**	0.59	0.17	0.66
		WRF	0.60	0.15	0.65
μ_g	4.53	**MMIF**	6.12	3.11	4.92
		WRF	5.25	2.86	4.50
VG	1	**MMIF**	8.59	11.33	3.09
		WRF	7.38	12.09	3.11

[1]Modeled PBL height from WRF or re-diagnosed using MMIF.
[2]*RHC* calculated using N=10.

The tracer study data is grouped together (summer, winter, all) to increase the sample size in order to perform Cox-Tikvart analysis. The absolute fractional bias for each dataset is used to calculate a *CPM*. The *CPM* values and their associated standard deviations for each dispersion model are displayed visually in Figure 21 and shown in Table 10.

Figure 21 and Table 10 illustrate that OCD has the lowest *CPM* values and standard deviations of all the models for when all the data and just the summer data are considered. For all data and just summer data, the OCD *CPM* values are only slightly lower compared to AERMOD *CPM* values, indicating that AERMOD and OCD have similar overall model performance. In these cases, CALPUFF *CPM* values are higher than AERMOD and OCD *CPM* values, which suggests that CALPUFF does not perform quite as well for short-range, overwater dispersion of offshore emission sources. Interestingly, OCD and CALPUFF both have higher *CPM* values compared to AERMOD in the winter. Across all three data groupings, the AERMOD *CPM* is most consistent, suggesting that it performs equally well during all seasons.

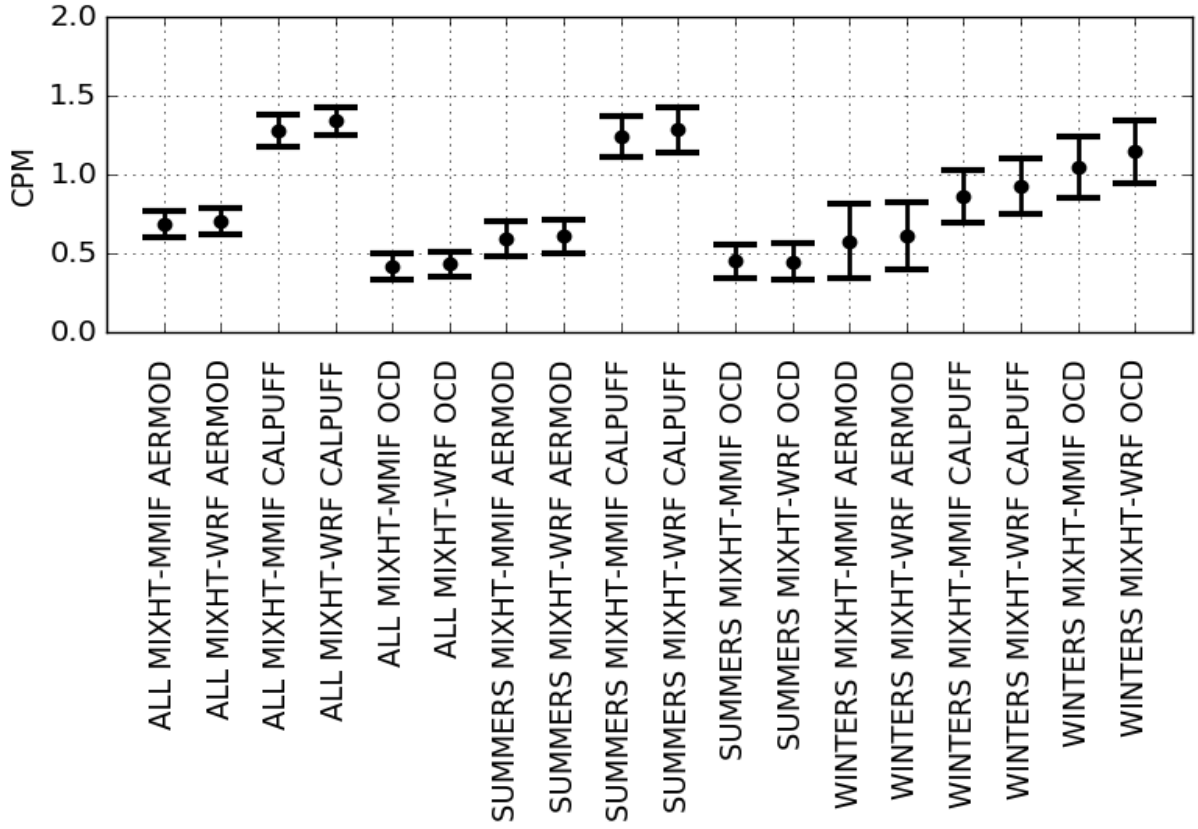

Figure 21. Composite Performance Metrics (CPM) for Tracer Studies

Table 10. Composite Performance Metrics (CPM) for Tracer Studies

Data	PBL height[1]	AERMOD		CALPUFF		OCD	
		CPM	Standard deviation	CPM	Standard deviation	CPM	Standard deviation
Summer	**MMIF**	0.59	0.11	1.24	0.13	0.45	0.11
	WRF	0.61	0.11	1.29	0.15	0.45	0.12
Winter	**MMIF**	0.58	0.23	0.86	0.17	1.05	0.20
	WRF	0.62	0.21	0.93	0.17	1.15	0.20
All	**MMIF**	0.69	0.08	1.28	0.10	0.42	0.08
	WRF	0.71	0.09	1.34	0.09	0.43	0.08

[1]Modeled PBL height from WRF or re-diagnosed using MMIF.

By using the same modeled meteorology to replicate established tracer studies using AERMOD, CALPUFF, and OCD, we gain insight into the model performance of these three dispersion models. The regulatory model currently preferred for near-field dispersion modeling of offshore emission sources is OCD. The results of this analysis have shown that AERMOD, OCD, and CALPUFF perform differently

at each individual tracer site, but that no model is an overall poor performer. When all the data is used and when the data is grouped by season, it becomes clear that AERMOD and OCD model performance are comparable and that AERMOD outperforms OCD in the winter, perhaps when the spatial gradients in stability and PBL heights are weakest. The results presented in this tracer study suggest AERMOD is comparable to, if not better than, the OCD model. The meteorological data used in these types of simulations must be chosen with care given the sensitivity of these dispersion models to various meteorological parameters. This study has shown that it is acceptable to use MMM output and the MMIF to develop meteorological inputs for atmospheric dispersions models.

5. SYNTHETIC SOURCE METHODOLOGY

In the second part of this report, several offshore synthetic sources in the GOMR are simulated using AERMOD, OCD, and CALPUFF using 5 years of recent mesoscale meteorology modeling data. For consistency, many of the methods used in the tracer study analysis are also used to simulate the emissions of synthetic sources in the GOMR. This assessment investigates the consequence of replacing OCD with AERMOD (or CALPUFF) by comparing model-to-model outcomes. There are no measurements of concentrations as in the tracer studies, but the 5-year modeling period provides much more statistical power than the tracer studies. The details of this modeling analysis are described below.

5.1 Description of the Offshore Synthetic Sources

The Central and Western GOM Planning Areas in the GOMR were modeled separately in this study. Figure 22 shows the modeling layout in the Central GOM Planning Area (CPA), Figure 23 shows the layout for the Western GOM Planning Area (WPA), and Table 11 provides source location information. The state seaward boundary (SSB) location was obtained through BOEM[1], and the shoreline position was obtained from a shoreline map provided with the latest version of CALMET. Four synthetic sources in the CPA are located 40 km from the coast, and four sources in the WPA were placed 20 km from the shore. These distances were taken following USEPA (2015b, 2015c) and represent a range of offshore drilling activity. The varied source placement allows us to compare AERMOD, CALPUFF, and OCD model performance for scenarios where sources are located both near and further from the coast. In each region, all four sources have the same coordinates. The same four synthetic offshore source types are used in the Central and Western GOM Planning Areas.

The four synthetic sources were also taken from USEPA (2015b, 2015c) and are representative of a range of typical emission points:

- an S4UI diesel engine (high stack temperature, tall stack height)
- an S2U3 burner (low stack temperature, short stack height)
- a support vessel represented as an area source
- a support vessel represented as a volume source

[1] http://www.boem.gov/GOMR-GIS-Data-and-Maps/

The two point sources are based upon hypothetical source parameters used in USEPA (2015c), with emission rates typical of OCS sources. The support vessel area source was developed using parameters and emission rates from the Shell Royal Discoverer drillship. The support vessel is also simulated as a volume source because OCD's treatment of area sources is somewhat similar to volume source treatment in AERMOD and CALPUFF. Table 12 provides the details of the four synthetic sources simulated in this study.

Figure 22 shows the approximate location of the synthetic sources and the receptors in the CPA. The location of the sources is shown as a pink triangle, and the receptors along the coast and SSB (thin black line) are red cross-hatches. Similarly, Figure 23 shows the approximate location of the synthetic sources and the receptors in the Western GOM Planning Area. In both the CPA and the WPA, receptors were placed along the SSB and along the coast with 500-m spacing.

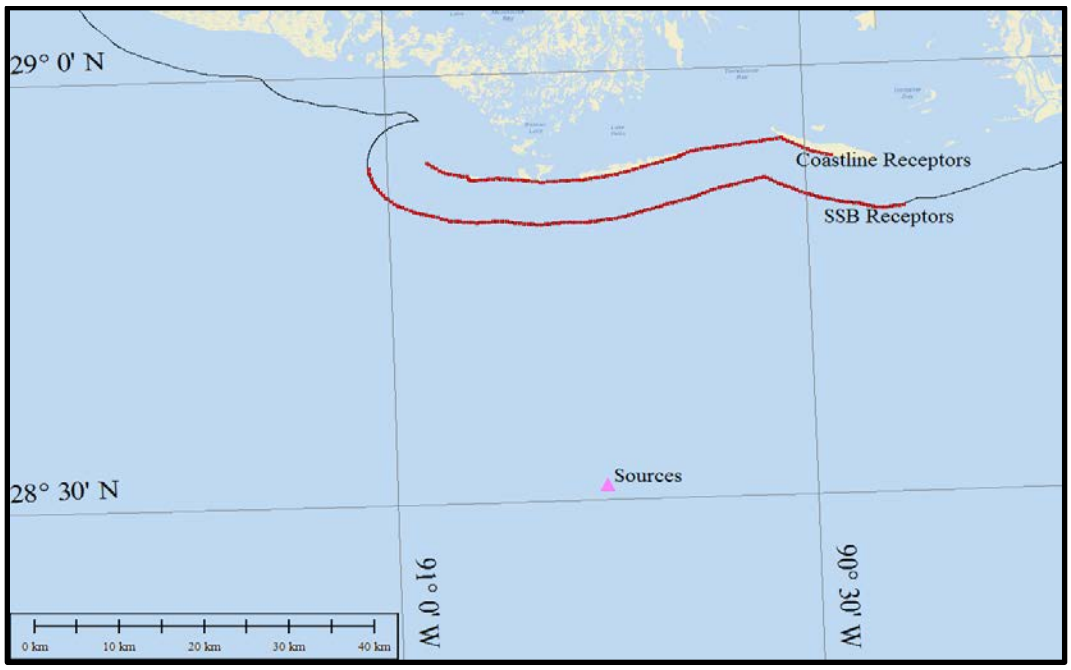

Figure 22. Central GOM Planning Area Modeling Configuration

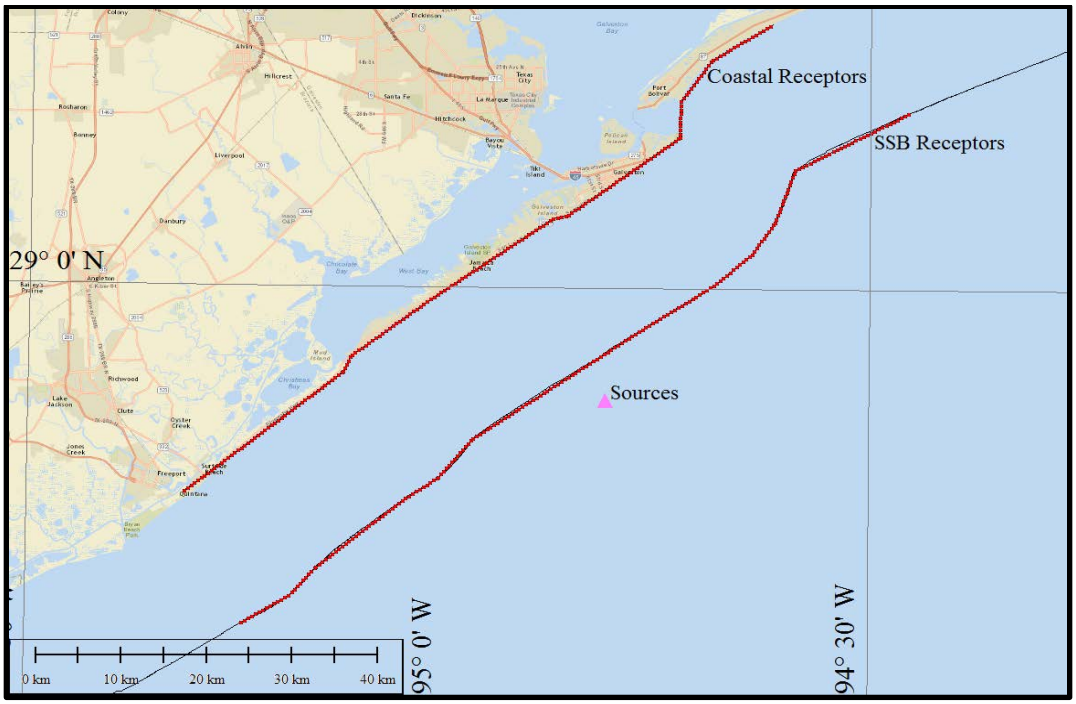

Figure 23. Western GOM Planning Area Modeling Configuration

Table 11. Location of Synthetic Sources

Region	Latitude (LCC X-coord, km)	Longitude (LCC Y-coord, km)	Distance from shore (km)	Shore to SSB (nautical miles)
Central	28.52˚ (616.710)	-90.75 ˚ (-1,254.749)	40	3
Western	28.88˚ (214.934)	-94.81˚ (-1,233.075)	20	9

Table 12. Description of Synthetic Sources

Source	Type	Height (m)	Area (km^2)[1]	Stack diam. (m)	Emiss. vel. (m/s)	Stack top temp. (K)	Tracer	Emiss. Rate (g/s)	σ_z Init (m)	σ_y Init (m)
Hot, tall	Diesel engine, S4U1	39	N/A	0.7	21	580	NO_x	12.6	N/A	N/A
Short, cold	Burner, S2U3	10	N/A	0.4	17	420	PM_{10}	4.0	N/A	N/A
Support area	Support vessel	10	4	N/A[2]	0[3]	295[4]	NO_x	63.0[5]	5[6]	N/A
Support volume[7]	Support vessel	10	4	N/A[2]	0	N/A	NO_x	63.0	5[6]	524.7[6]

1 In AERMOD and CALPUFF, area sources have square dimensions, while OCD requires area sources to be circular.
2 In OCD, the area source dimension is specified by setting the stack diameter equal to the area source diameter.
3 The emission velocity is set to $1.0x10^{-10}$ in OCD because non-zero emission velocity is forbidden.
4 Area source temperature is required in OCD. We define area source temperature as the median surface air temperature value from 5 years of WRF data.
5 Area source emission rate converted to $1.58x10^{-5}$ g m^2 s^{-1} in AERMOD and CALPUFF.
6 σ_y and σ_z only used in AERMOD and CALPUFF.
7 Support vessel simulated as volume source in AERMOD and CALPUFF only.

5.2 WRF Modeling of Synthetic Sources

Five years of recent WRF meteorological data (2010–2014) is used for this analysis. Because the tracer study results showed that tracer concentrations are relatively insensitive to whether PBL heights from WRF or re-diagnosed through MMIF are used, at least compared to other differences between the models, we choose to use MMIF-produced PBL heights for the synthetic source analysis. Using MMIF-recalculated PBL heights is a more conservative approach because the tracer study evaluation portion of this study revealed that MMIF-recalculated PBL heights were often associated with slightly higher tracer concentrations; therefore, using MMIF-recalculated PBL heights to simulate synthetic sources is a more conservative approach. All WRF settings are the same as in the tracer studies, except that the smallest

WRF grid cell domain is 4 km as opposed to 1.33 km in the tracer studies. Figure 24 shows the 4-km WRF modeling domain used in the GOMR. The full WRF domain is shown as a solid pink line, the usable WRF domain is a dashed pink line, and the domain subset used in CALPUFF is shown as the black line. For CALPUFF, a subset of this modeling domain was used for the CPA and WPA because of limitations in the CALPUFF modeling grid cell domain. Unlike the tracer studies, wind direction is not fixed in this analysis.

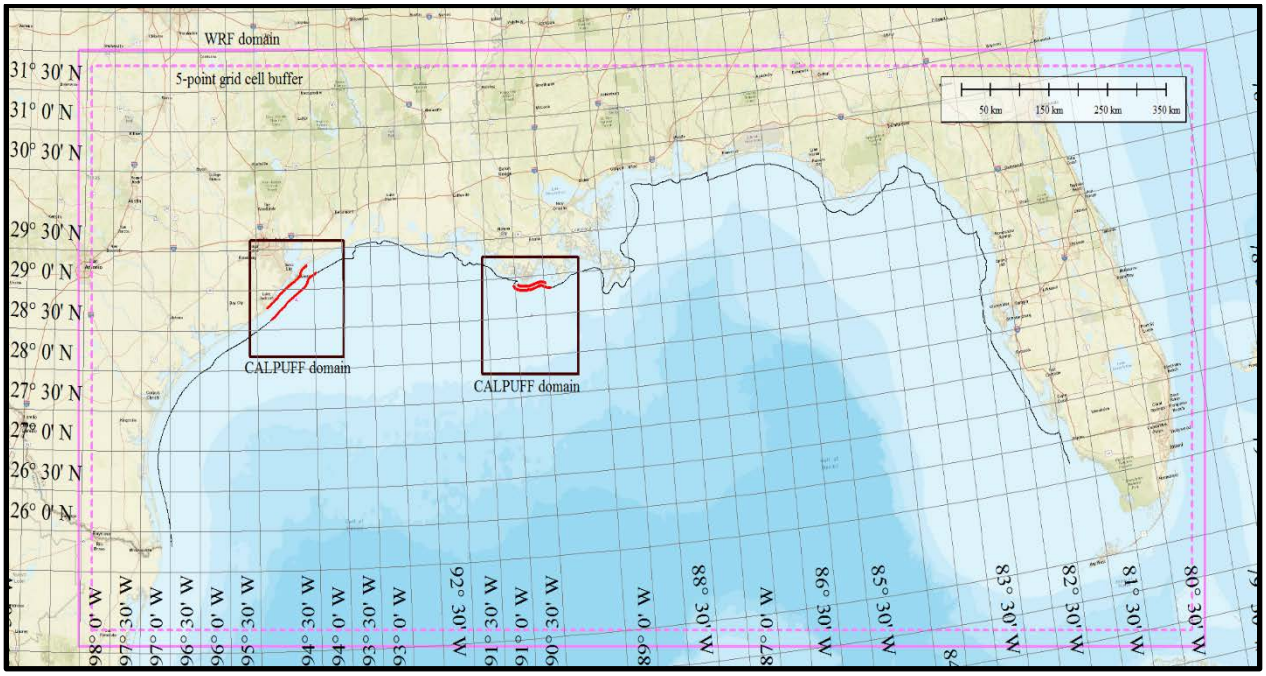

Figure 24. GOMR WRF 4-km Modeling Domain

5.3 Dispersion Modeling Configuration

AERMOD, CALPUFF, and OCD were run for a year at a time for 2010 through 2014. MMIF was used to produce the meteorological inputs in the same fashion as the tracer studies. The only difference is that the overwater AERMOD surface file produced through MMIF was used to create placeholder values for the OCD overland meteorological data—all receptors are located either over water (along the SSB) or directly at the coast, so overland meteorology is not actually used.

5.4 Statistical Evaluation Procedures for Synthetic Source Analysis

The same statistical metrics used in the tracer study analysis and described in Section 3 of this appendix—including Q-Q plots, *RHC*, fraction-factor-of-two (*FF2*), geometric correlation coefficient (r_g), geometric mean (μ_g), and geometric variance (*VG*)—are used to evaluate model performance with synthetic sources. In addition, the Cox-Tikvart methodology is also applied. One key difference is that observational data is not used in the synthetic source study. Instead, model output from OCD is used in place of observations, since OCD is the USEPA-preferred regulatory model for offshore, near-coast

sources. Since the lowest limit of non-zero data in OCD is 0.1, only data greater than or equal to 0.1 are used to calculate *RHC*, *FF2*, r_g, μ_g, and *VG* in all three models. Another difference is that these statistics are calculated using an entire year of data, which was not available from the tracer studies. Lastly, N=26 is used to calculate *RHC* values in the synthetic source analysis because the sample sizes are much larger compared to the tracer study analysis.

6. MODEL COMPARISONS—SYNTHETIC SOURCES

6.1 Q-Q Plot Analysis

Similar to the tracer study analysis, the spatial maximum of hourly concentrations across all receptors are used to compare the performance of AERMOD, CALPUFF, and OCD with synthetic offshore sources. Figure 25 through Figure 56 present Q-Q plots comparing AERMOD and CALPUFF concentrations to OCD concentrations for all sources and receptor locations in both the CPA and WPA. For a particular scenario, all years are grouped on one plot because year-to-year variations in concentrations for an individual case are small compared to differences in source type, receptor location, and region. These Q-Q plots use logarithmic axes, with red dashed lines to represent the region on the graph within a factor of two of the black "one-to-one" line. The factor of two lines are commonly shown in USEPA evaluations of AERMOD and other dispersion models. In the discussion that follows, we often refer to the "low end," "mid-range," and "high end" of the Q-Q plots. These correspond to roughly one third of the points each but are not a statistical quantity. Note also that USEPA places more value in the performance near the high end, because these are the values used to make decisions regarding ambient air quality standards and significant impact levels.

6.1.1 Central GOM Planning Area

6.1.1.1 Modeling a Tall, Hot Point Source

Figure 25 shows a Q-Q plot comparing OCD and AERMOD maximum hourly nitrogen oxide (NO_x) concentrations for the tall, hot point source at coastal receptors in the Central GOM Planning Area for 2010 through 2014, and Figure 26 shows the same comparison with receptors along the SSB. There is good overall agreement between OCD and AERMOD in both cases, although AERMOD concentrations are slightly lower in the middle of the frequency distribution. Figure 27 and Figure 28 compare OCD and CALPUFF concentrations for the same source and location. For both sets of receptors, CALPUFF concentrations are lower than OCD concentrations for all but the highest concentrations. Figure 25 through Figure 28 show that there are only minor differences in concentration between the SSB and coastal receptors in the CPA, which are separated by 3 nautical miles. As Figure 29 through Figure 40 show, the concentration differences between the two receptor sets are also small for the other three synthetic sources in the CPA.

6.1.1.2 Modeling a Short, Cold Point Source

Figure 29 and Figure 30 show Q-Q plots comparing OCD and AERMOD maximum hourly particulate matter with diameter less than 10 microns (PM_{10}) concentrations for the short, cold point source at coastal

and SSB CPA receptors for 2010 through 2014. There is excellent agreement between both models in the upper half of the frequency distribution, while AERMOD slightly underestimates at lower concentrations. Figure 31 and Figure 32 compare OCD and CALPUFF model results for the same scenarios and show that CALPUFF slightly underestimates compared to OCD at all concentrations. Overall, Figure 25 through Figure 32 suggests that AERMOD and CALPUFF exhibit slightly better agreement with OCD for the short, cold point source compared to the tall, hot point source (Figure 27 and Figure 28) in the CPA.

6.1.1.3 Modeling an Area Source

Figure 33 and Figure 34 show Q-Q plots for OCD and AERMOD maximum hourly area source NO_x concentrations at coastal and SSB CPA receptors for 2010 through 2014. Similar to the short, cold point source, AERMOD and OCD concentrations agree well at the upper end of the frequency distribution and AERMOD estimates lower concentrations elsewhere, although the disagreement at the low end of the range is more pronounced for the area source. Figure 35 and Figure 36 illustrate how CALPUFF and OCD compare under the same conditions. Compared to OCD, CALPUFF underestimates the highest concentrations and slightly overestimates the lowest concentrations. Overall, AERMOD outperforms CALPUFF for this scenario.

6.1.1.4 Modeling a Volume Source for AERMOD and CALPUFF, Area Source for OCD

Figure 37 shows a Q-Q plot comparing OCD and AERMOD maximum hourly NO_x concentrations for the volume source at coastal receptors in the CPA for 2010 through 2014 and Figure 38 shows the same comparison with receptors along the SSB. Volume sources in AERMOD and CALPUFF are compared to area sources in OCD because OCD's treatment of area sources resembles a volume source. The general shape of the distribution is similar to the area source Q-Q plots (Figure 33 and Figure 34) except that the agreement is significantly improved at the low end of the frequency distribution. This is likely because plume meander is accounted for in volume, but not area, sources in AERMOD. Plume meander algorithms redirect the portion of the plume that intercepts the ground and elevated terrain back into the plume. Figure 39 and Figure 40 show the corresponding Q-Q plots for CALPUFF and OCD. Figure 39 and Figure 40 are nearly identical to the area source Q-Q plots shown in Figure 35 and Figure 36, indicating that area and volume sources are treated similarly in CALPUFF.

6.1.2 Western GOM Planning Area

There are several noticeable differences between the modeling configurations in the CPA and WPA. The SSB and coastal receptors are 9 km apart in the WPA compared to 3 km in the CPA. Additionally, the SSB and coastal receptors are closer to the source in the WPA compared to the CPA. Since the source is closer to shore in the WPA, the relative source-to-receptor distances for SSB and coastal receptors differ more in the WPA compared to the CPA. These differences result in larger concentration differences between the SSB and coast receptors in the WPA compared to the CPA.

6.1.2.1 Modeling a Tall, Hot Point Source

Figure 41 and Figure 42 show Q-Q plots for OCD and AERMOD maximum hourly NO_x concentrations for the tall, hot point source at WPA coastal and SSB receptors for 2010 through 2014. The OCD-AERMOD agreement is weaker compared to the agreement for the tall, hot point source in the CPA. For the WPA, there is agreement at the upper end of the frequency domain and AERMOD estimates lower concentrations across the rest of the domain. In addition, there are larger concentration differences between the coastal and SSB receptors, likely because of the greater distance between the coastal and SSB receptors: 9 km in Texas compared to 3 km in Louisiana. Figure 43 and Figure 44 compare OCD and CALPUFF concentrations for the same source and location. Similar to AERMOD, CALPUFF and OCD agree within a factor of two for the highest concentrations and, CALPUFF concentrations are significantly lower compared to OCD throughout the rest of the distribution.

6.1.2.2 Modeling a Short, Cold Point Source

Figure 45 and Figure 46 show Q-Q plots comparing OCD and AERMOD maximum hourly PM_{10} concentrations for the short, cold point source at coastal and SSB WPA receptors for 2010 through 2014. Figure 47 and Figure 48 compare OCD and CALPUFF for the same scenario. For both AERMOD and CALPUFF, there is good agreement with OCD at higher concentrations and both models otherwise predict lower concentrations compared to OCD.

6.1.2.3 Modeling an Area Source

Figure 49 and Figure 50 show Q-Q plots for OCD and AERMOD maximum hourly area source NO_x concentrations at coastal and SSB WPA receptors for 2010 through 2014. Figure 51 and Figure 52 present a similar comparison for OCD and CALPUFF. For both AERMOD and CALPUFF, the agreement with OCD in the upper half of the frequency distribution is better for the receptors along the SSB compared to those along the coast. In the middle and in the low end of the distribution, AERMOD concentrations are lower than OCD concentrations, and the opposite is true for CALPUFF.

6.1.2.4 Modeling a Volume Source for AERMOD and CALPUFF, Area Source for OCD

Figure 53 shows a Q-Q plot comparing OCD and AERMOD maximum hourly NO_x concentrations for the volume source at coastal receptors in the CPA for 2010 through 2014, and Figure 54 shows the same comparison with receptors along the SSB. There is good agreement between AERMOD and OCD for all but the lowest concentrations at both the SSB and along the coast. Figure 55 and Figure 56 compare OCD and CALPUFF concentrations for the same source and location. The OCD-CALPUFF agreement along the SSB is excellent across much of the frequency distribution. Similar to the area source results (Figure 51 and Figure 52), the lowest concentrations are slightly higher in CALPUFF compared to OCD. The OCD-CALPUFF agreement is less favorable along the coast; CALPUFF concentrations are lower than OCD concentrations at the high end of the range and higher than OCD concentrations at the low end of the distribution. In general, OCD concentrations are more aligned with AERMOD and CALPUFF concentrations in the CPA compared to the WPA, despite the WPA source being located closer to the SSB and coast.

6.1.3 Summary of Q-Q Plot Analysis

This study has examined the performance of AERMOD, CALPUFF, and OCD in a variety of scenarios with different hypothetical source types, source and receptor positions, and locations within the Gulf of Mexico. Overall, there is better agreement between AERMOD and OCD concentrations than between CALPUFF and OCD, especially for the highest concentrations, which carry the most weight for regulatory purposes. From a model configuration perspective, this analysis has revealed that area sources in OCD agree more closely with volume sources in AERMOD compared to area sources in AERMOD. At the high end of the concentrations, AERMOD tends to agree well (not underpredict) compared to OCD. However, CALPUFF has a slight (for point sources) to larger (for area and volume sources) tendency to underpredict compared to OCD.

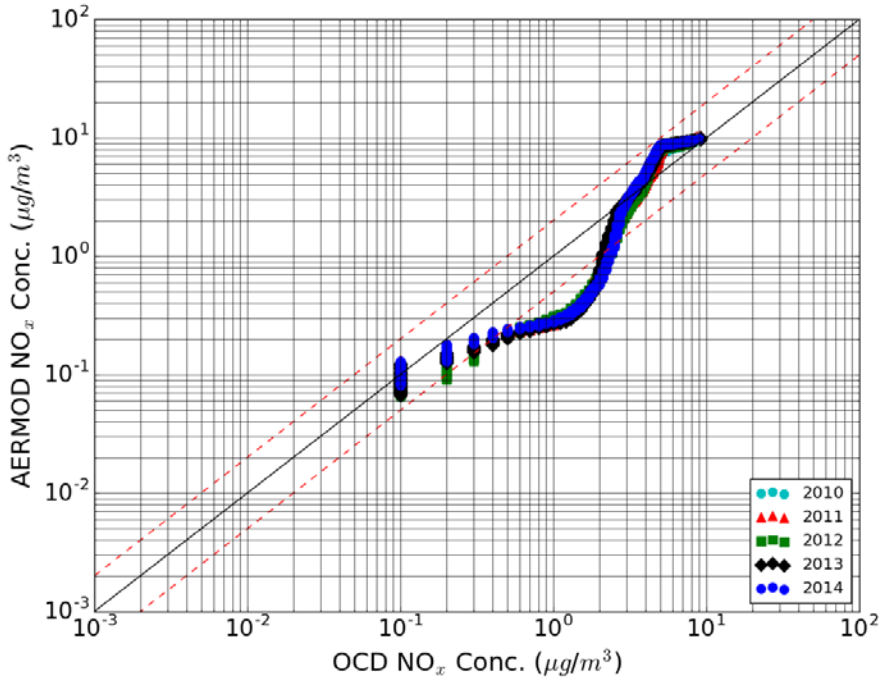

Figure 25. OCD vs. AERMOD Q-Q plot at CPA Coast for Tall, Hot Point Source

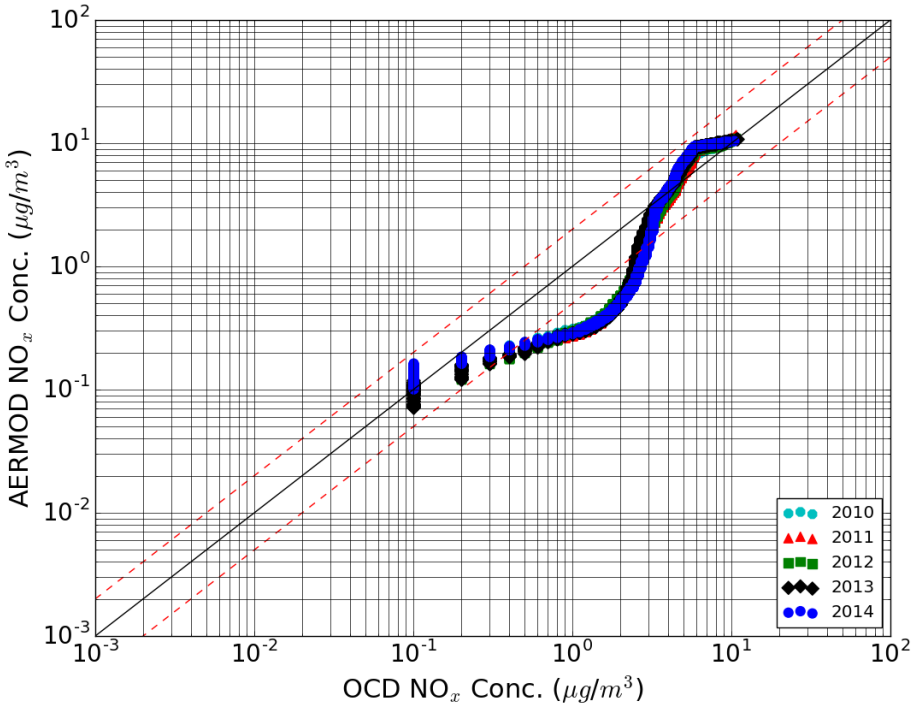

Figure 26. OCD vs. AERMOD Q-Q plot at CPA SSB for Tall, Hot Point Source

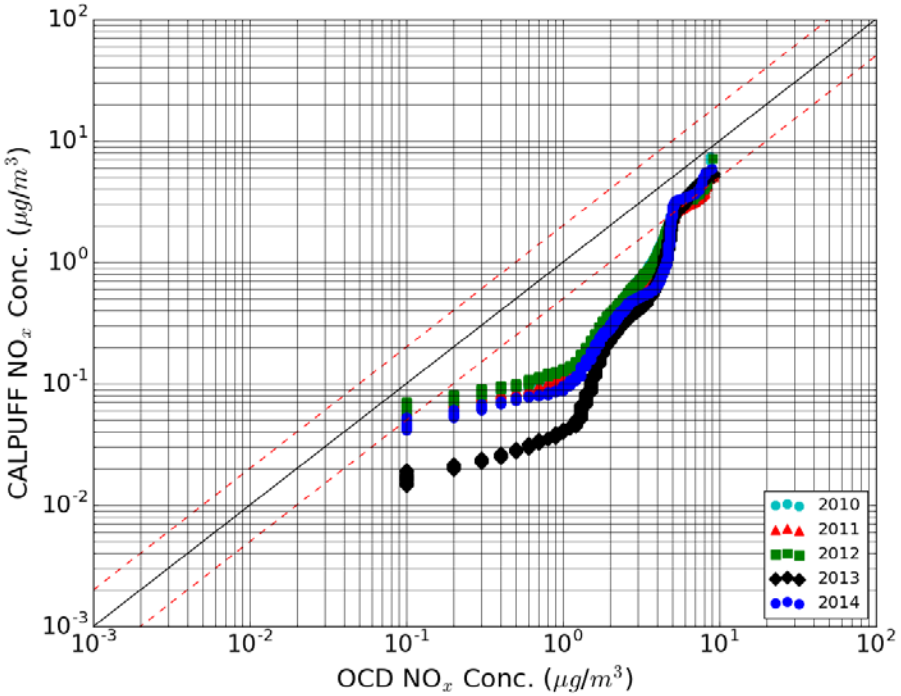

Figure 27. OCD vs. CALPUFF Q-Q plot at CPA Coast for Tall, Hot Point Source

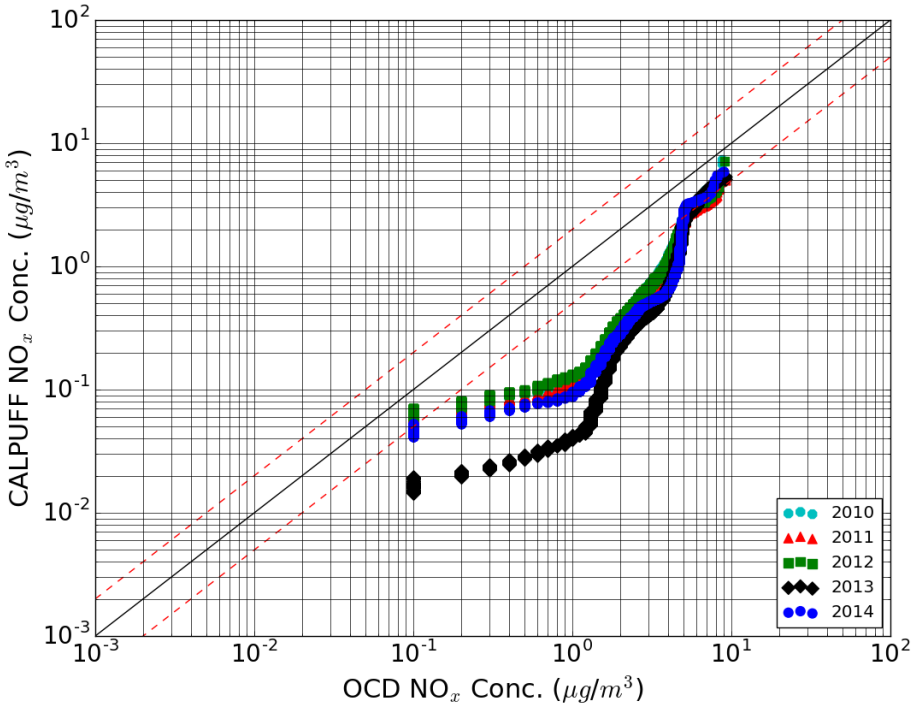

Figure 28. OCD vs. CALPUFF Q-Q plot at CPA SSB for Tall, Hot Point Source

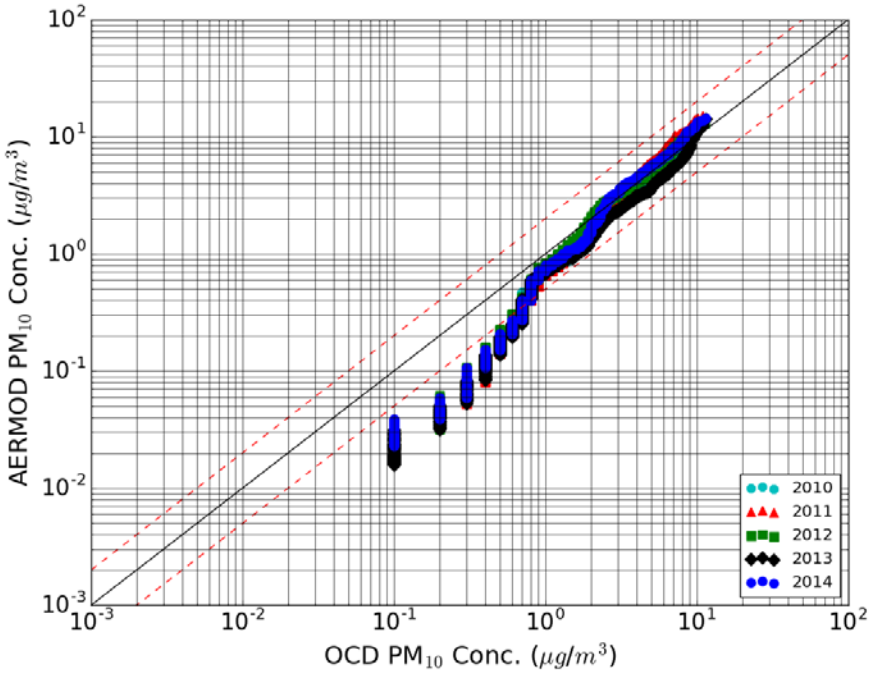

Figure 29. OCD vs. AERMOD Q-Q plot at CPA Coast for Short, Cold Point Source

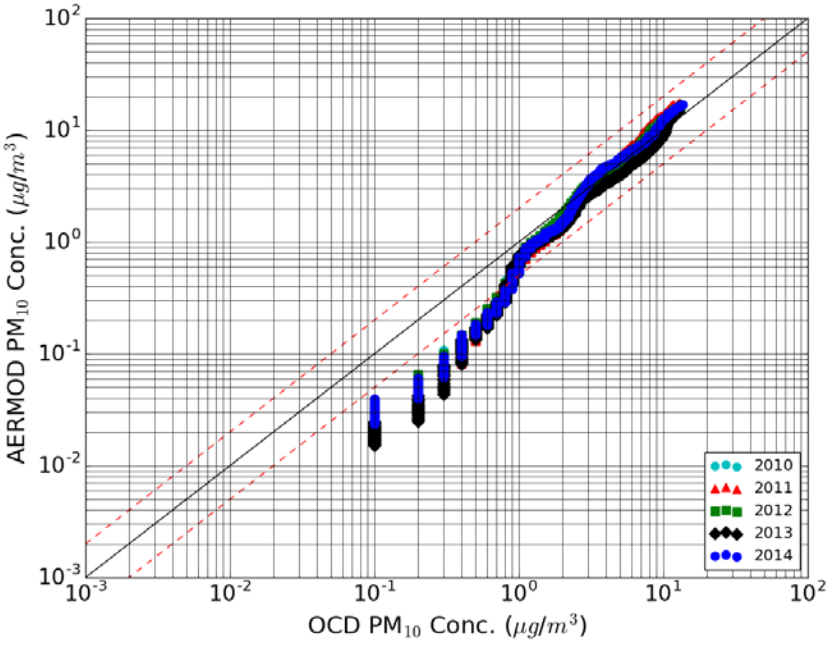

Figure 30. OCD vs. AERMOD Q-Q plot at CPA SSB for Short, Cold Point Source

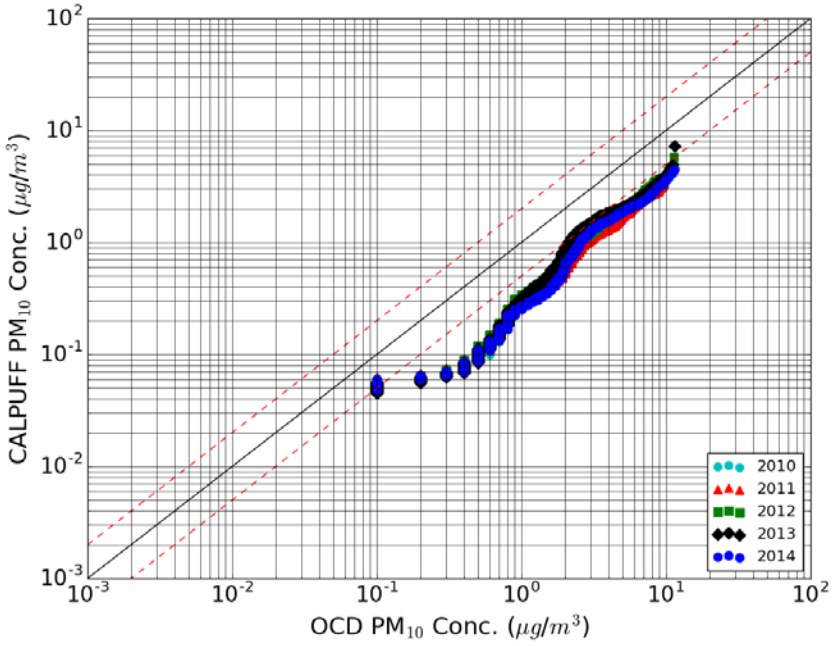

Figure 31. OCD vs. CALPUFF Q-Q plot at CPA Coast for Short, Cold Point Source

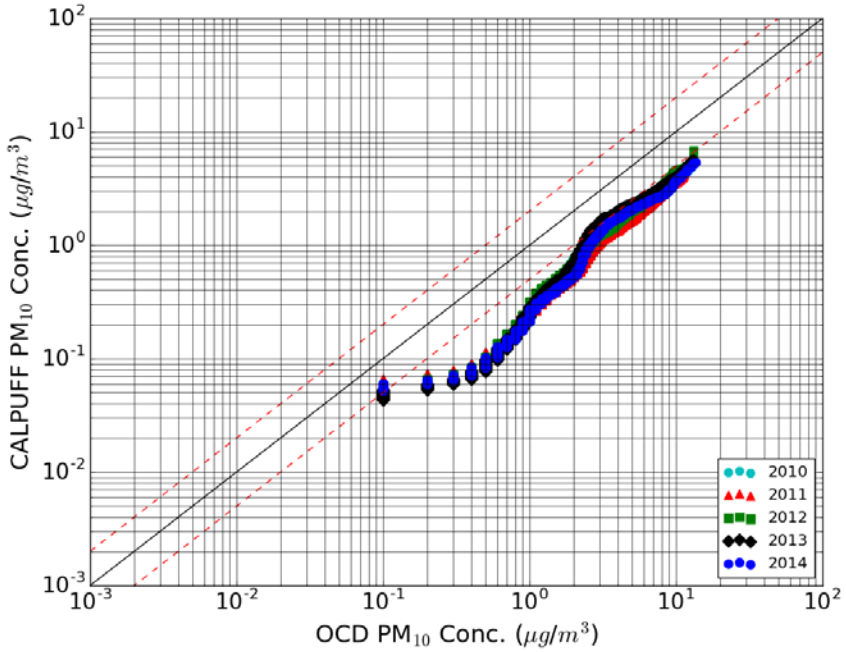

Figure 32. OCD vs. CALPUFF Q-Q plot at CPA SSB for Short, Cold Point Source

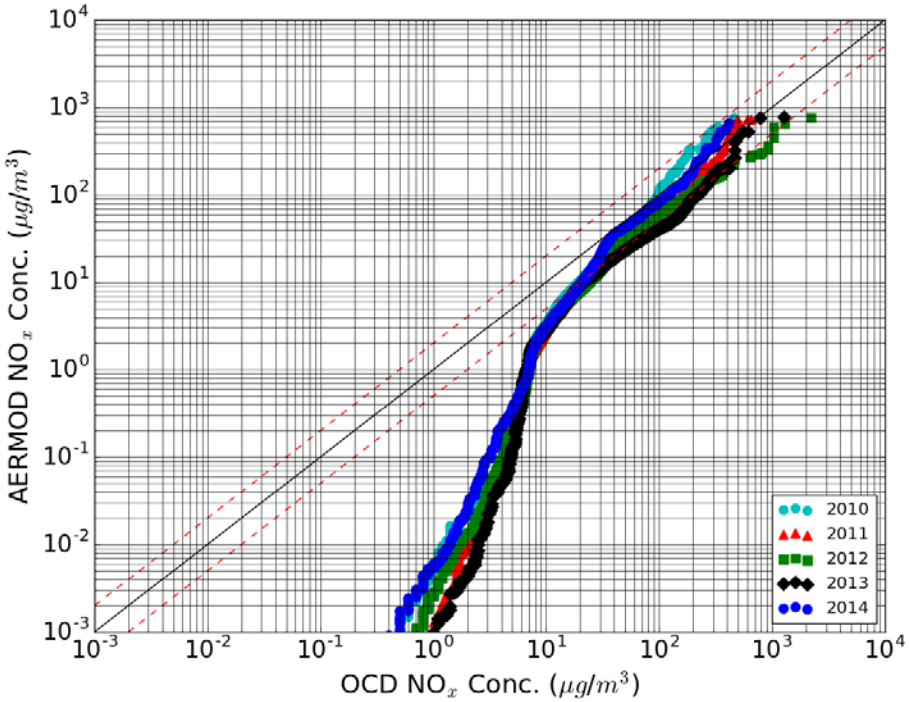

Figure 33. OCD vs. AERMOD Q-Q plot at CPA Coast for Area Source

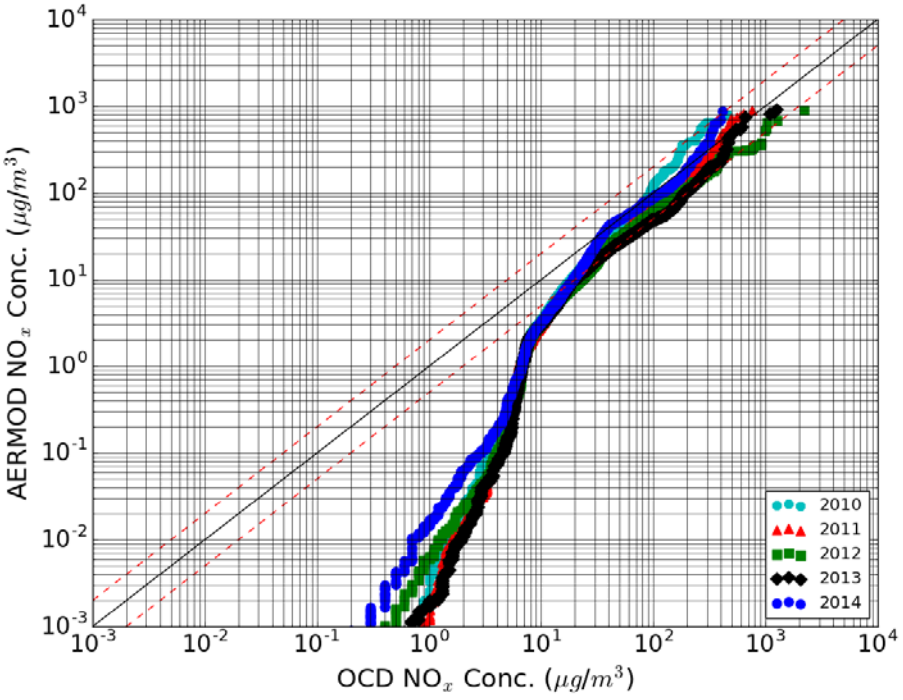

Figure 34. OCD vs. AERMOD Q-Q plot at CPA SSB for Area Source

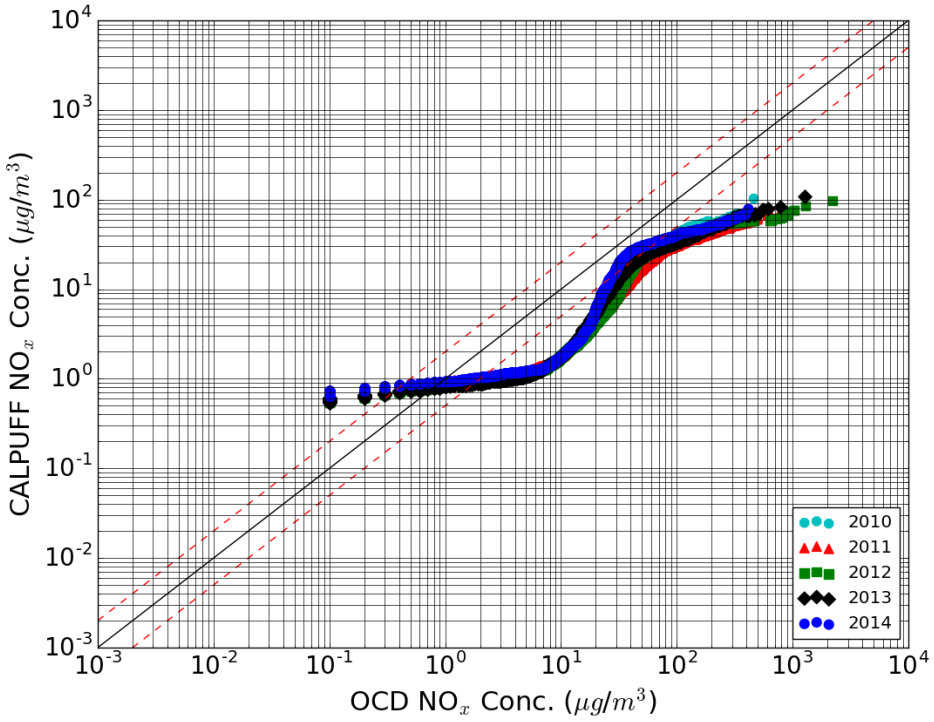

Figure 35. OCD vs. CALPUFF Q-Q plot at CPA Coast for Area Source

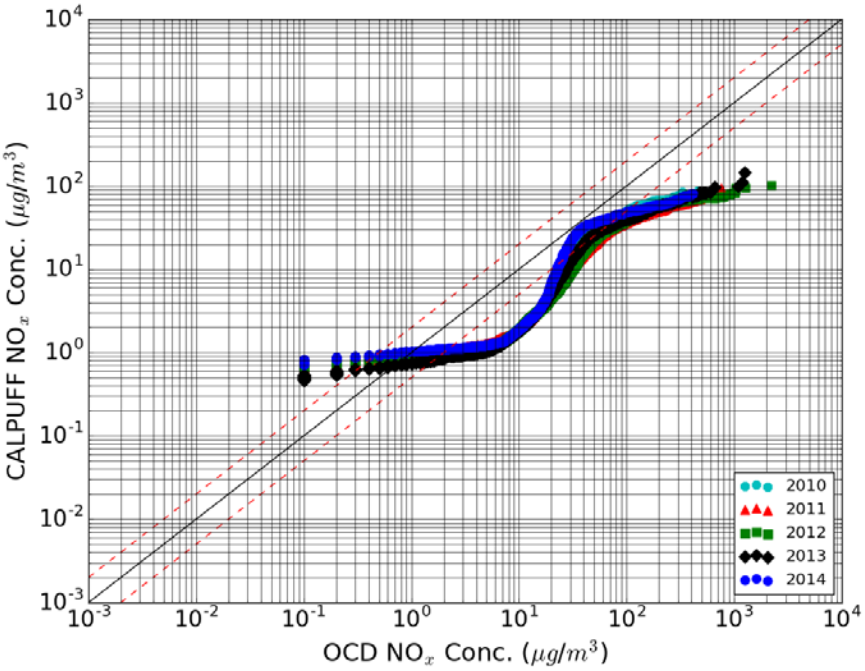

Figure 36. OCD vs. CALPUFF Q-Q plot at CPA SSB for Area Source

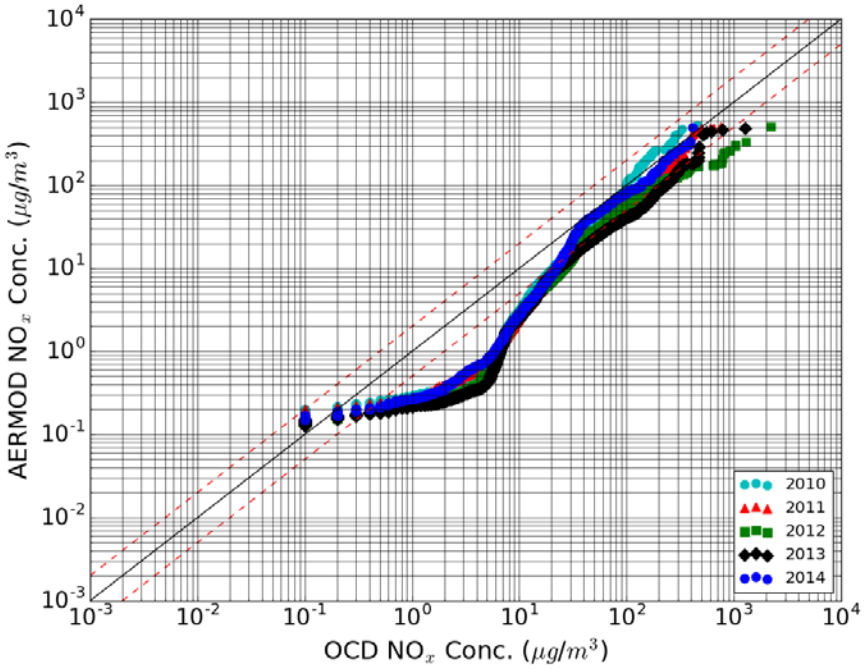

Figure 37. OCD vs. AERMOD Q-Q plot at CPA Coast for Volume Source

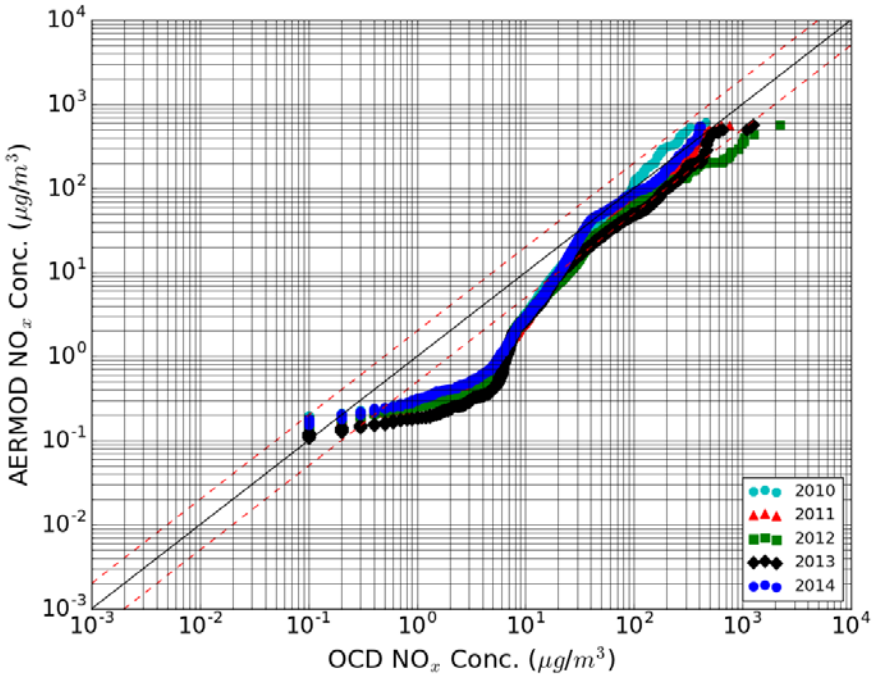

Figure 38. OCD vs. AERMOD Q-Q plot at CPA SSB for Volume Source

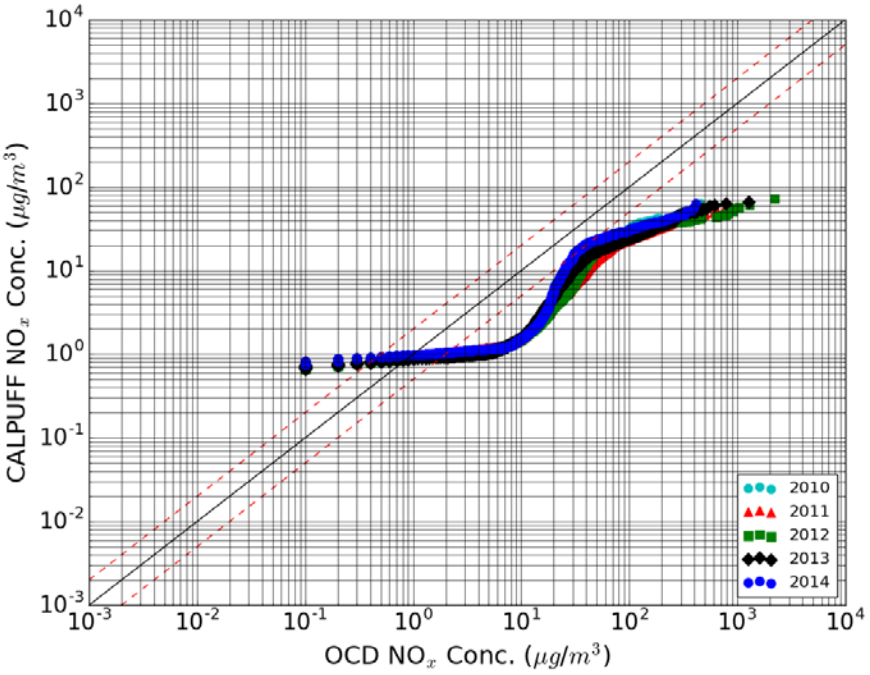

Figure 39. OCD vs. CALPUFF Q-Q plot at CPA Coast for Volume Source

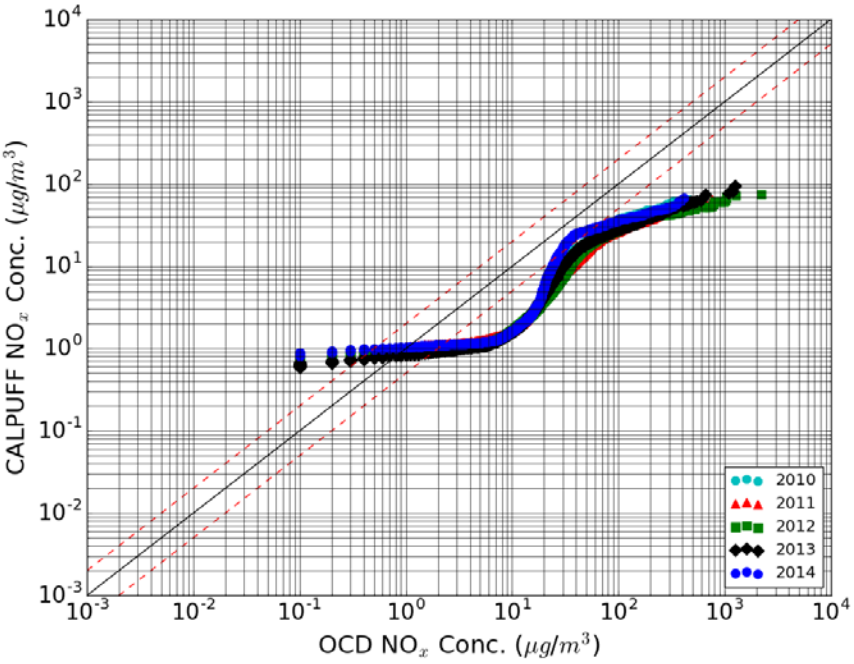

Figure 40. OCD vs. CALPUFF Q-Q plot at CPA SSB for Volume Source

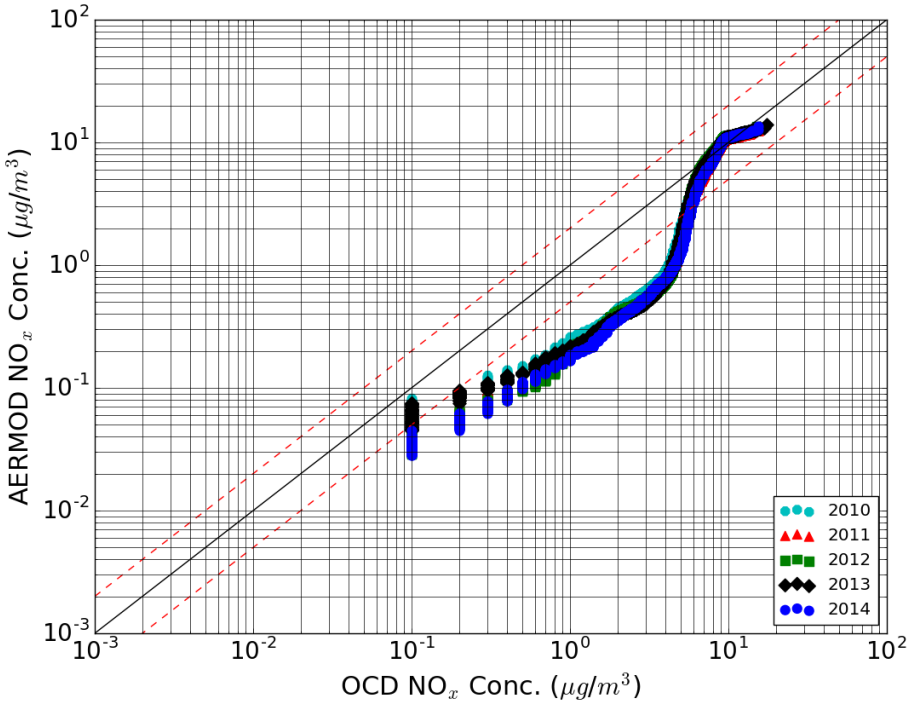

Figure 41. OCD vs. AERMOD Q-Q plot at WPA Coast for Tall, Hot Point Source

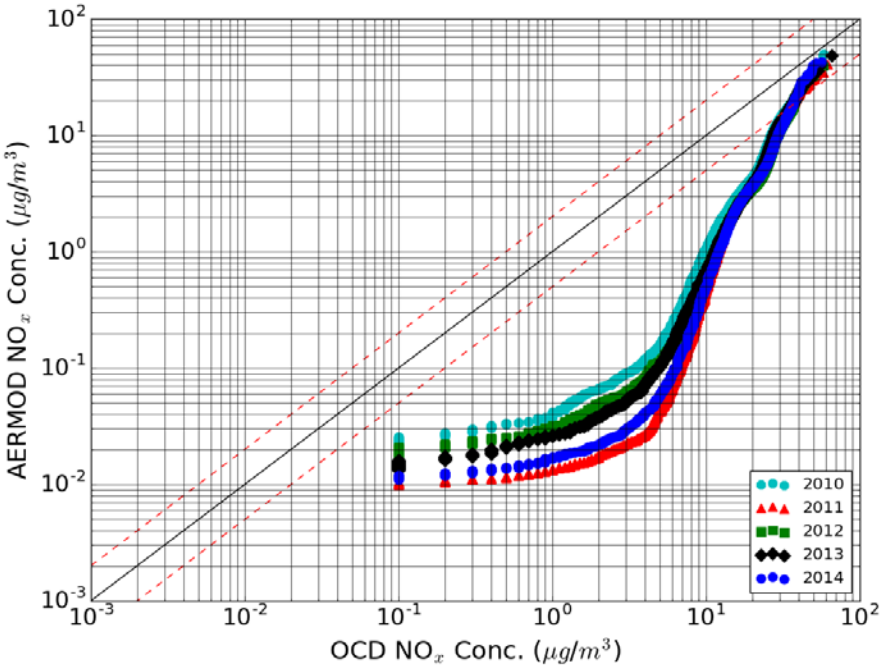

Figure 42. OCD vs. AERMOD Q-Q plot at WPA SSB for Tall, Hot Point Source

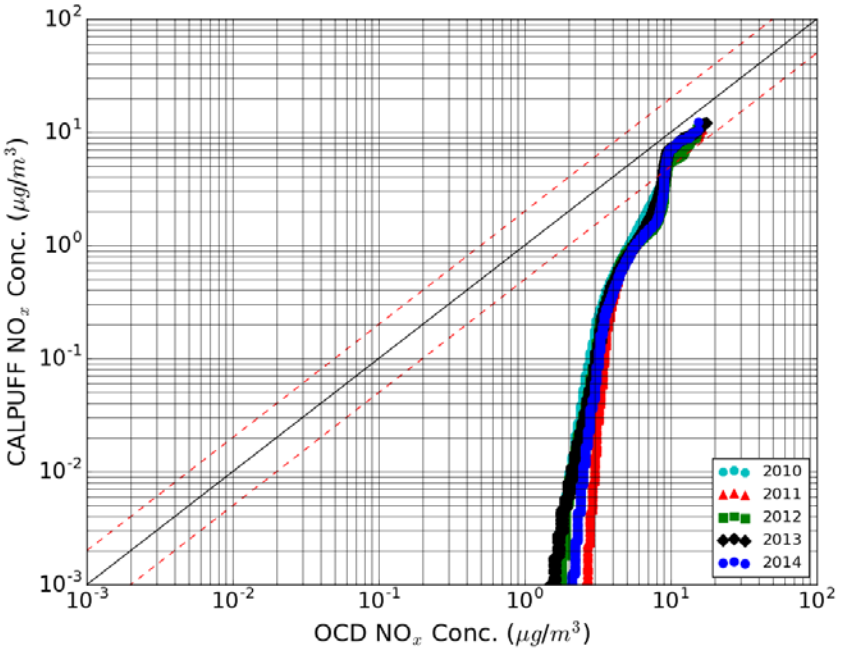

Figure 43. OCD vs. CALPUFF Q-Q plot at WPA coast for Tall, Hot Point Source

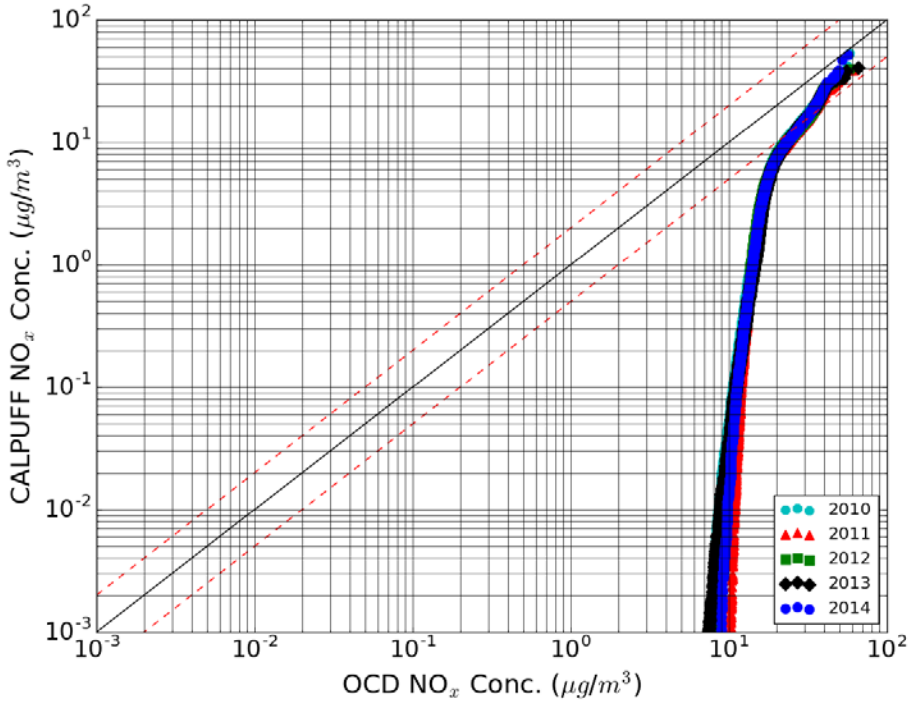

Figure 44. OCD vs. CALPUFF Q-Q plot at WPA SSB for Tall, Hot Point Source

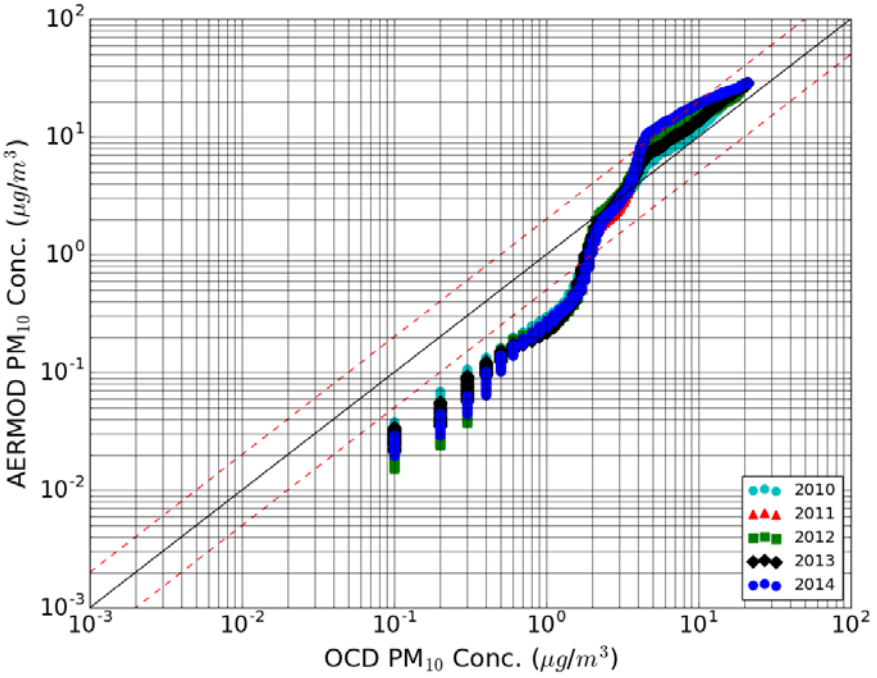

Figure 45. OCD vs. AERMOD Q-Q plot at WPA Coast for Short, Cold Point Source

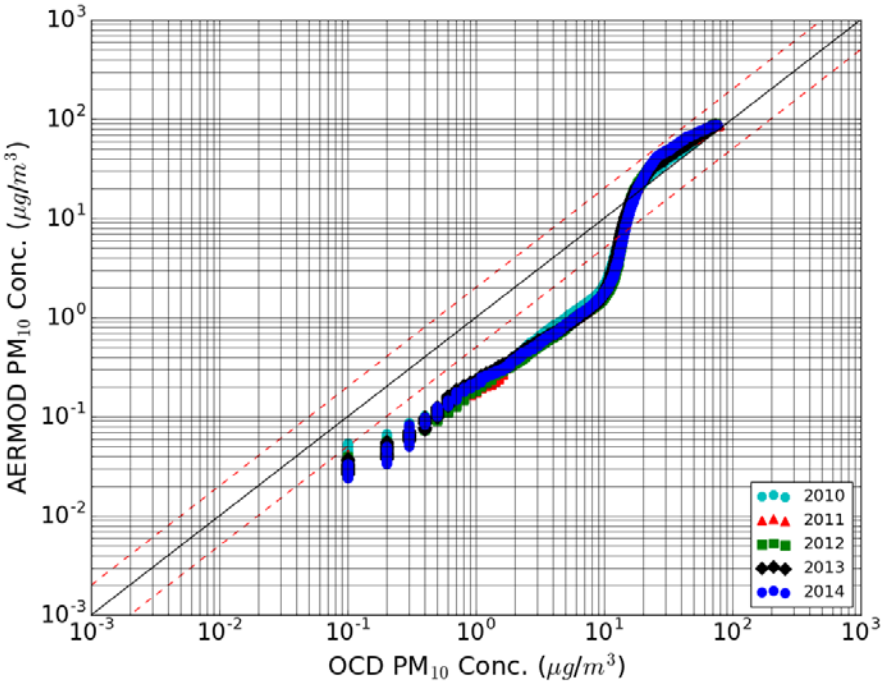

Figure 46. OCD vs. AERMOD Q-Q plot at WPA SSB for Short, Cold Point Source

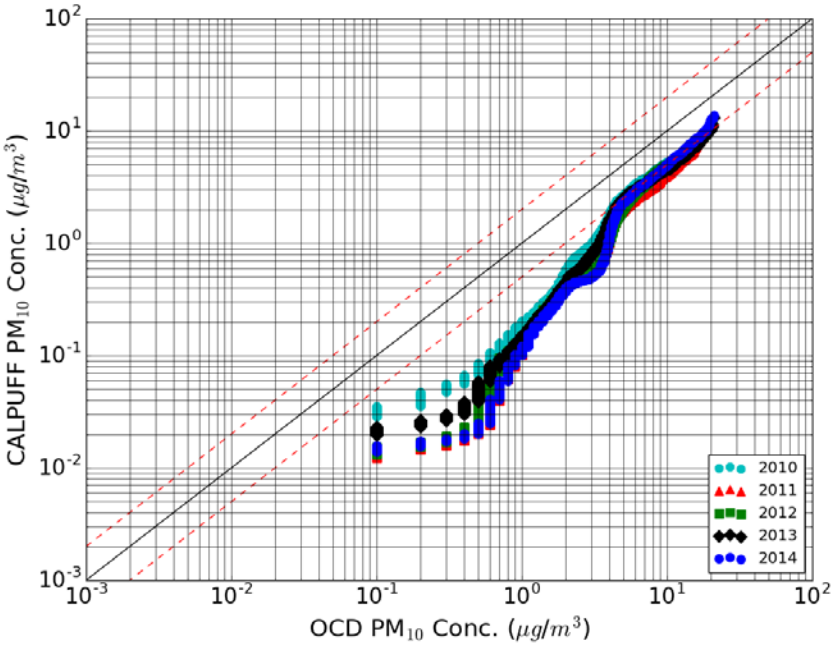

Figure 47. OCD vs. CALPUFF Q-Q plot at WPA Coast for Short, Cold Point Source

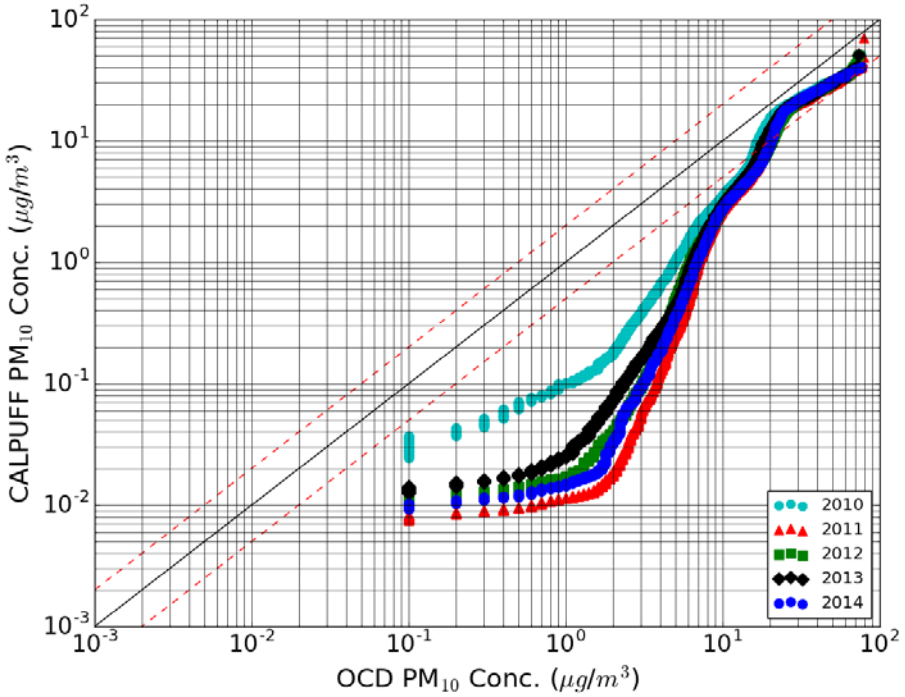

Figure 48. OCD vs. CALPUFF Q-Q plot at WPA SSB for Short, Cold Point Source

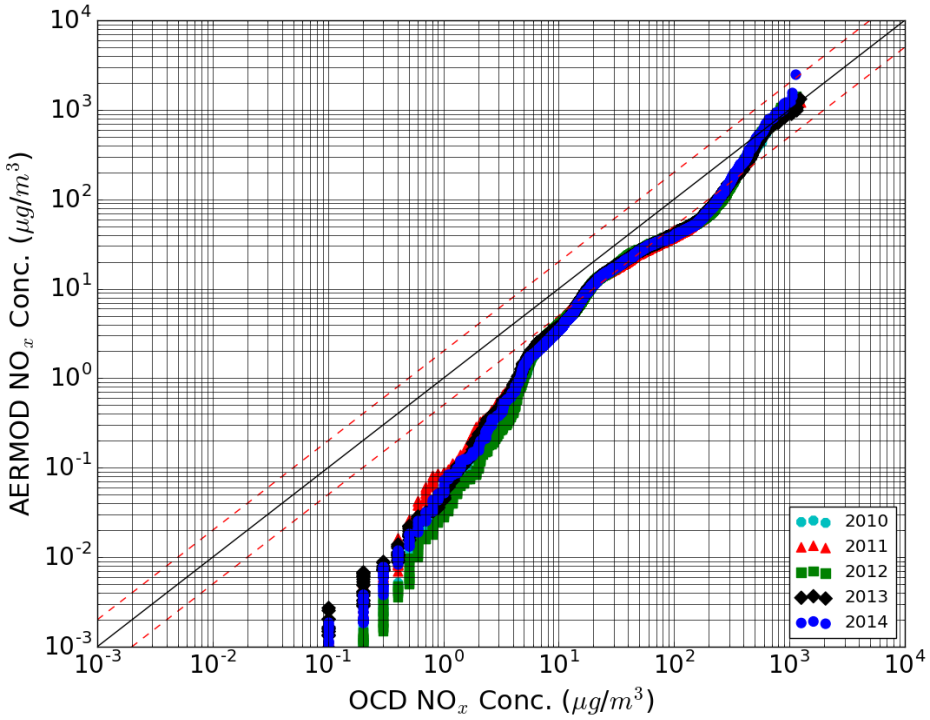

Figure 49. OCD vs. AERMOD Q-Q plot at WPA Coast for Area Source

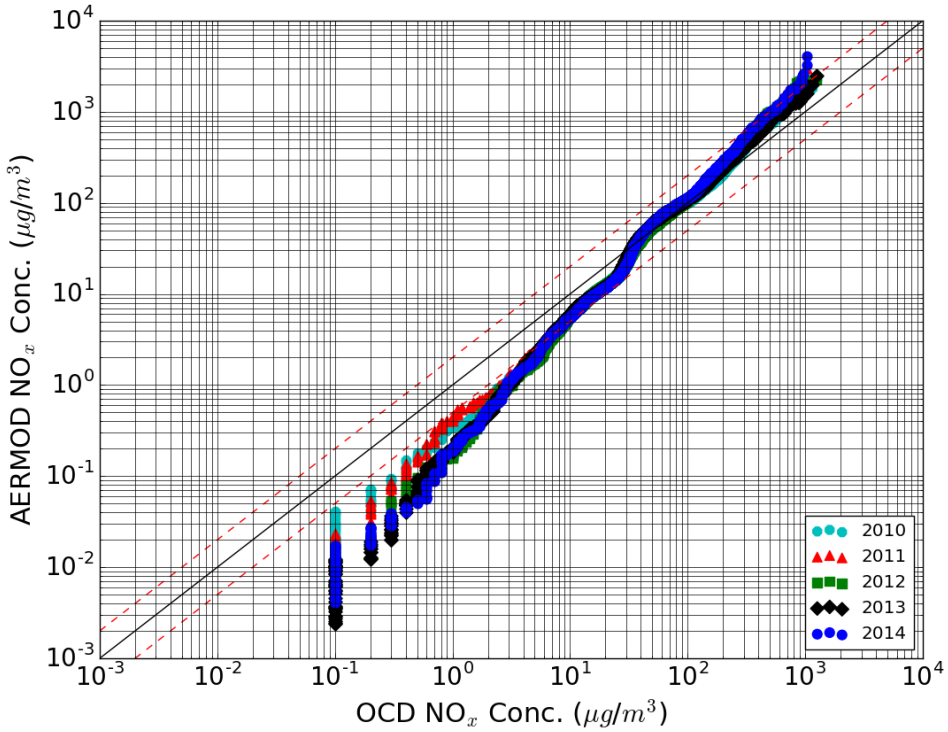

Figure 50. OCD vs. AERMOD Q-Q plot at WPA SSB for Area Source

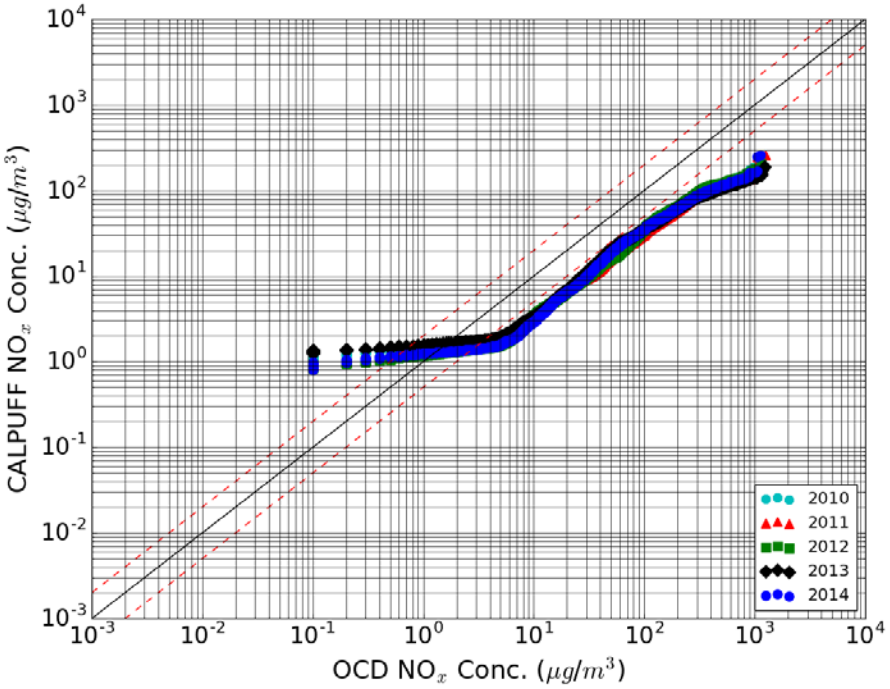

Figure 51. OCD vs. CALPUFF Q-Q plot at WPA Coast for Area Source

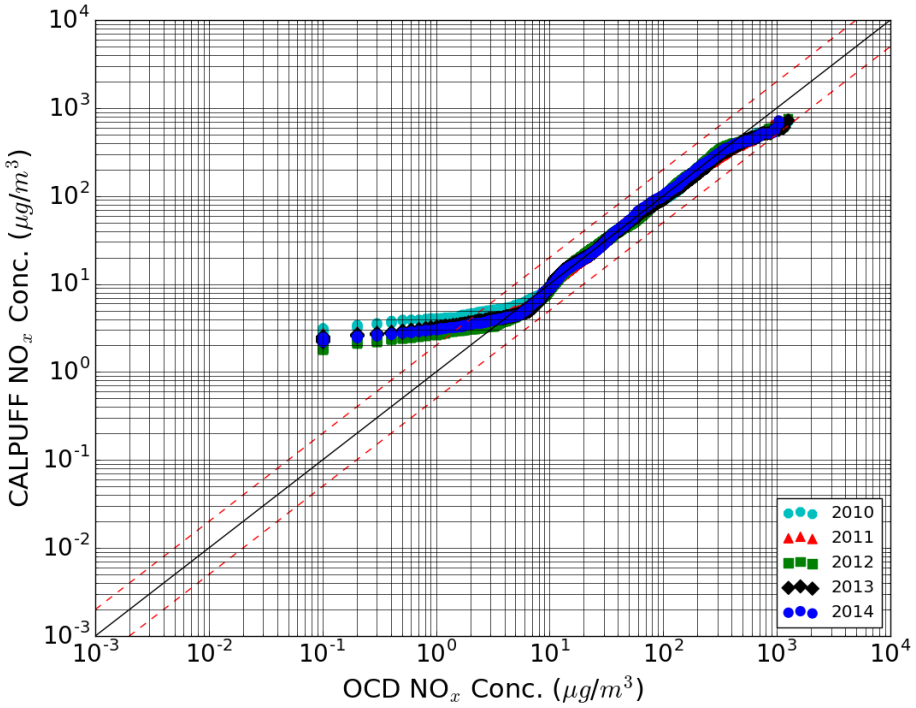

Figure 52. OCD vs. CALPUFF Q-Q plot at WPA SSB for Area Source

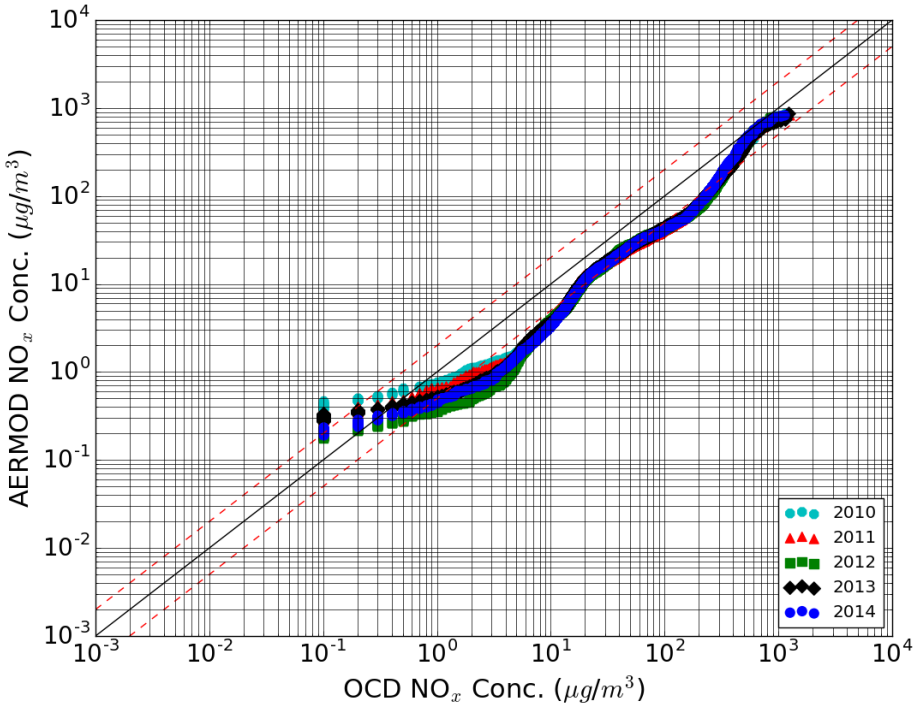

Figure 53. OCD vs. AERMOD Q-Q plot at WPA Coast for Volume Source

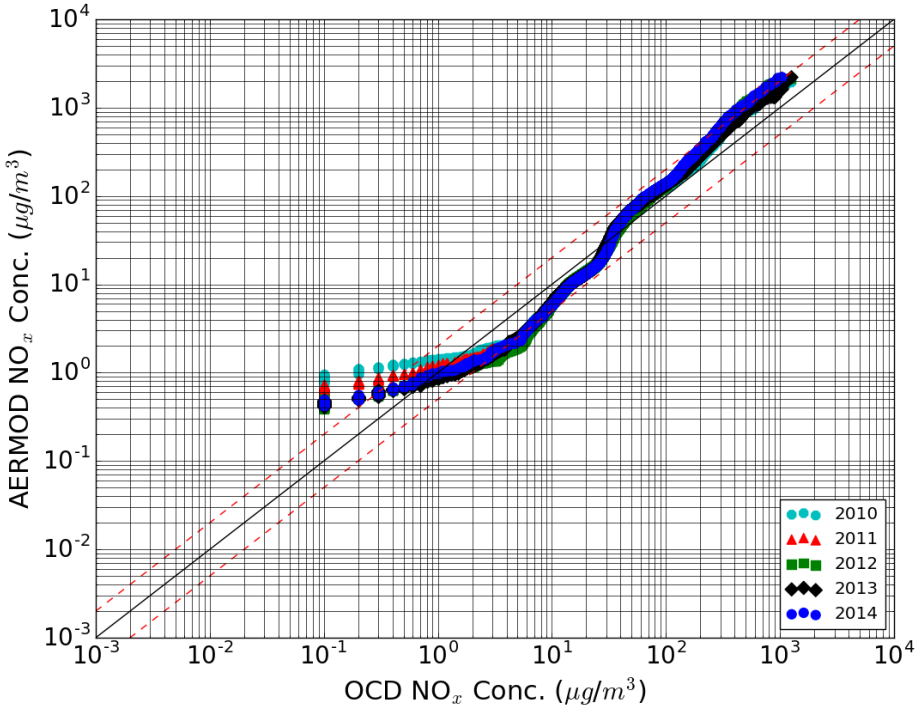

Figure 54. OCD vs. AERMOD Q-Q plot at WPA SSB for Volume Source

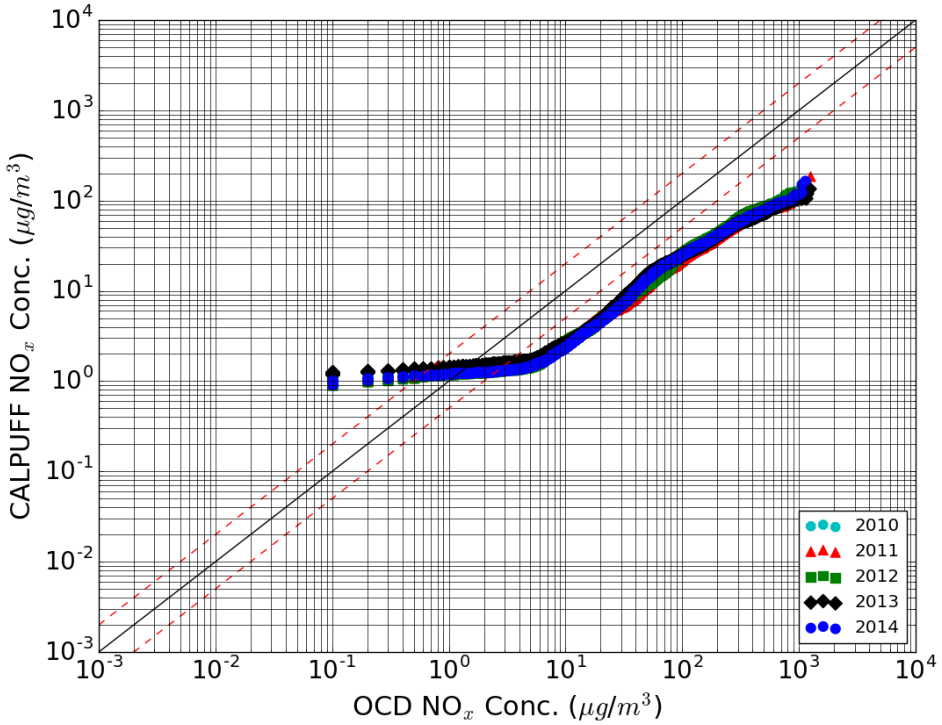

Figure 55. OCD vs. CALPUFF Q-Q plot at WPA coast for Volume Source

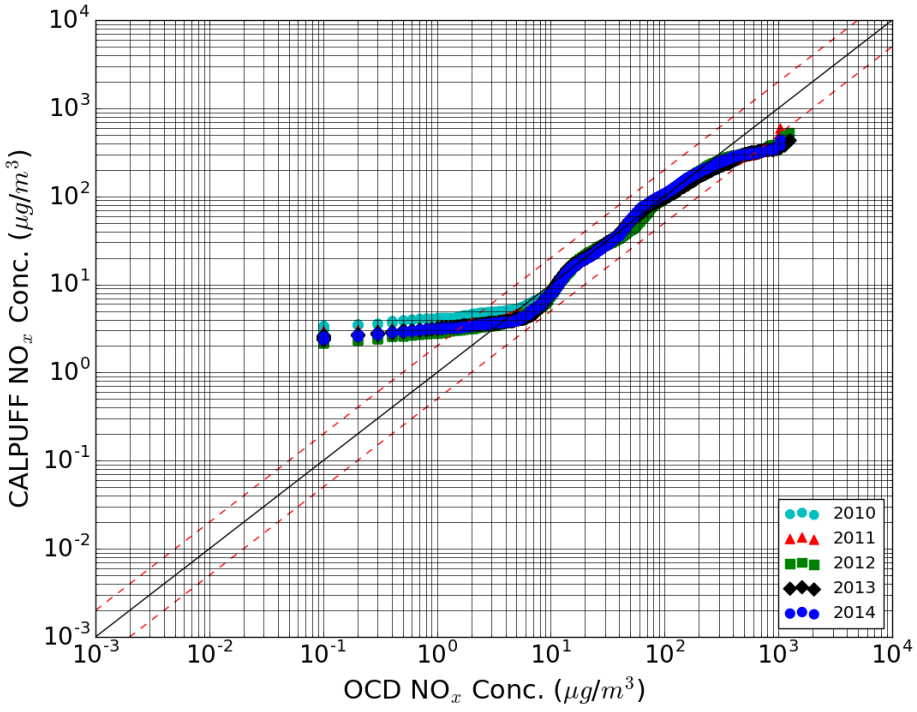

Figure 56. OCD vs. CALPUFF Q-Q plot at WPA SSB for Volume Source

6.2 Basic Statistics and Cox-Tikvart Analysis

Table 13 through Table 22 show the statistical metrics used to compare modeled concentrations at each site for all three air dispersion models. Similar to the observations column in Table 2 through Table 5 in the tracer study analysis, several statistical parameters (i.e., *FF2*, r_g, *VG*) are 1 for OCD because OCD model results are being treated as the "observations" in this part of the analysis.

Table 13 presents statistical results for AERMOD and CALPUFF model performance compared to OCD for the tall, hot point source in the CPA for 2010 through 2014. The *RHC* values for AERMOD are similar to OCD *RHC* values, with slight (~10%) yearly variations while CALPUFF *RHC* values are a factor of 1.5–1.9 times lower than OCD *RHC* values. Between 40 and 53% of AERMOD concentrations are within a factor of two compared to OCD concentrations, while only 13 to 20% of CALPUFF concentrations fall within that range. Similarly, the correlation coefficients for AERMOD are higher (0.45–0.53) compared to CALPUFF (0.14–0.30). AERMOD has geometric means more aligned with OCD values and also lower geometric variances compared to CALPUFF. These statistics suggests that AERMOD and OCD exhibit more similarity compared to CALPUFF for the tall, hot point source in the CPA.

Table 14 compares AERMOD, CALPUFF, and OCD model performance for the short, cold point source in the CPA for 2010 through 2014. Compared to OCD *RHC* values, AERMOD *RHC* values are 1.2 to 1.5 times higher and CALPUFF *RHC* values are 2.3 to 2.7 times lower. Similar to the tall, hot point source, AERMOD *FF2* values are higher than CALPUFF *FF2* values, ranging from 0.35–0.48 and 0.21–0.35, respectively. Additionally, CALPUFF has lower r_g and μ_g values and higher *VG* values compared to AERMOD, indicating that AERMOD outperforms CALPUFF for this source as well. The AERMOD correlation coefficients are higher (0.60–0.70) and the geometric variances are lower (2.08–2.62) than the AERMOD r_g and *VG* values for the tall, hot point source, suggesting that there is better agreement between AERMOD and OCD for the short, cold point source compared to the tall, hot point source.

Table 13. Statistical Metrics Comparing OCD Output to AERMOD and CALPUFF Output for the Tall, Hot Point Source in the CPA

Metrics	Year	OCD		AERMOD		CALPUFF	
		SSB	Coast	SSB	Coast	SSB	Coast
RHC	2010	11.60	9.97	11.06	9.94	7.47	6.04
	2011	11.17	9.51	11.60	10.69	6.34	5.10
	2012	10.93	9.72	10.98	10.30	6.92	5.29
	2013	10.94	9.23	10.89	9.87	7.53	5.64
	2014	11.06	9.84	10.61	9.91	7.38	5.71
FF2	2010	1.00	1.00	0.44	0.45	0.19	0.19
	2011	1.00	1.00	0.47	0.47	0.20	0.20
	2012	1.00	1.00	0.43	0.45	0.17	0.19
	2013	1.00	1.00	0.52	0.53	0.17	0.19
	2014	1.00	1.00	0.39	0.40	0.13	0.14
r_g	2010	1.00	1.00	0.48	0.45	0.22	0.18
	2011	1.00	1.00	0.51	0.48	0.30	0.27
	2012	1.00	1.00	0.50	0.52	0.19	0.14
	2013	1.00	1.00	0.53	0.53	0.22	0.16
	2014	1.00	1.00	0.48	0.47	0.19	0.19
μ_g	2010	2.32	1.96	1.26	1.18	0.65	0.58
	2011	2.43	2.15	1.39	1.31	0.69	0.60
	2012	2.26	1.90	1.17	1.06	0.59	0.54
	2013	2.48	2.13	1.55	1.45	0.59	0.53
	2014	2.23	1.90	1.10	1.02	0.51	0.44
VG	2010	1.00	1.00	2.99	2.77	10.29	10.30
	2011	1.00	1.00	3.11	2.95	9.51	9.58
	2012	1.00	1.00	3.20	2.79	11.17	9.53
	2013	1.00	1.00	2.92	2.79	14.03	13.64
	2014	1.00	1.00	3.63	3.36	13.36	12.96

Table 14. Statistical Metrics Comparing OCD Output to AERMOD and CALPUFF Output for the Short, Cold Point Source in the CPA

Metrics	Year	OCD		AERMOD		CALPUFF	
		SSB	Coast	SSB	Coast	SSB	Coast
RHC	2010	14.51	12.39	18.48	16.26	5.93	5.08
	2011	12.93	11.06	19.56	16.13	5.37	4.66
	2012	14.38	12.16	17.63	14.73	5.50	4.51
	2013	13.49	11.89	16.84	14.65	5.81	5.20
	2014	14.79	12.93	18.32	17.16	6.08	5.09
FF2	2010	1.00	1.00	0.48	0.48	0.28	0.30
	2011	1.00	1.00	0.39	0.39	0.23	0.23
	2012	1.00	1.00	0.43	0.45	0.25	0.28
	2013	1.00	1.00	0.40	0.35	0.32	0.35
	2014	1.00	1.00	0.35	0.35	0.21	0.23
r_g	2010	1.00	1.00	0.66	0.65	0.48	0.42
	2011	1.00	1.00	0.61	0.60	0.48	0.43
	2012	1.00	1.00	0.64	0.64	0.47	0.47
	2013	1.00	1.00	0.70	0.69	0.57	0.49
	2014	1.00	1.00	0.66	0.66	0.56	0.50
μ_g	2010	1.02	0.91	0.67	0.63	0.39	0.38
	2011	1.13	1.00	0.82	0.73	0.40	0.38
	2012	0.98	0.83	0.64	0.58	0.36	0.33
	2013	1.27	1.14	0.84	0.78	0.57	0.59
	2014	1.00	0.86	0.62	0.57	0.34	0.32
VG	2010	1.00	1.00	2.19	2.08	6.37	6.26
	2011	1.00	1.00	2.57	2.44	8.54	7.91
	2012	1.00	1.00	2.33	2.13	6.40	5.40
	2013	1.00	1.00	2.32	2.31	5.47	5.15
	2014	1.00	1.00	2.62	2.45	7.62	7.56

Table 15 compares AERMOD, CALPUFF, and OCD model performance for the area source in the CPA for 2010 through 2014. There is more disagreement between the highest concentrations in OCD, AERMOD, and CALPUFF for the area source compared to the point sources and also more year-to-year variation. AERMOD *RHC* values are 1.5–2.4 times higher in 2010, 2011, and 2014 and 1.1–2.3 times lower in 2012 and 2013. For CALPUFF, *RHC* values are 4.5 to 17.4 times lower compared to OCD *RHC* values, with the biggest disagreement in 2012. The correlation coefficients range from 0.19–0.27 for AERMOD and 0.12–0.18 for CALPUFF, which are lower than the r_g values associated with the two point sources. Similarly, the geometric variances for AERMOD and CALPUFF are higher compared for the area source compared to the point sources. AERMOD outperforms CALPUFF when compared to OCD concentrations, although both models perform better with respect to OCD for the area source compared to the point sources.

Table 16 compares the OCD area source to the AERMOD and CALPUFF volume sources in the CPA for 2010 to 2014. AERMOD *RHC* values are higher than OCD *RHC* values by up to a factor of 1.6 in 2010, 2011, and 2014 and lower than OCD *RHC* values by factors of 1.5–4 in 2012 and 2013. The CALPUFF *RHC* values are 6.1–22.4 times lower than OCD *RHC* values. For both AERMOD and CALPUFF, the *FF2*, $r_{g,}$ and μ_g values are similar to the area source results presented Table 15. The volume source geometric variances are generally higher than their area source counterparts for both models. Although the statistics for the area source (Table 15) are similar overall to the volume source statistics, these statistics were calculated by excluding all concentrations lower than 0.1. The area and volume source Q-Q plots for this site (Figure 49–Figure 50, Figure 53–Figure 54) show that the OCD-AERMOD agreement is significantly better at the low end of the frequency distribution for volume sources compared to area sources. For all source types, AERMOD performs more similarly to OCD compared to CALPUFF and has the best agreement for the short, cold point source. In general, the *RHC* values are higher in AERMOD compared to OCD, revealing that AERMOD is even more conservative in its prediction of the highest concentrations for all of the scenarios examined in this study.

Table 15. Statistical Metrics Comparing OCD Output to AERMOD and CALPUFF Output for the Area Source in the CPA

Metrics	Year	OCD		AERMOD		CALPUFF	
		SSB	Coast	SSB	Coast	SSB	Coast
RHC	2010	396.86	408.42	958.41	817.29	87.60	76.80
	2011	735.69	694.94	1,150.02	1,081.47	86.92	72.74
	2012	1,538.48	1,385.85	725.73	606.04	95.65	79.86
	2013	962.54	698.67	893.19	598.59	109.58	87.37
	2014	508.67	503.24	958.76	770.24	90.74	79.64
FF2	2010	1.00	1.00	0.27	0.25	0.16	0.15
	2011	1.00	1.00	0.23	0.22	0.13	0.12
	2012	1.00	1.00	0.24	0.23	0.17	0.16
	2013	1.00	1.00	0.23	0.22	0.18	0.18
	2014	1.00	1.00	0.20	0.19	0.14	0.13
r_g	2010	1.00	1.00	0.39	0.41	0.15	0.15
	2011	1.00	1.00	0.39	0.39	0.19	0.16
	2012	1.00	1.00	0.55	0.52	0.22	0.17
	2013	1.00	1.00	0.53	0.53	0.33	0.29
	2014	1.00	1.00	0.42	0.43	0.21	0.19
μ_g	2010	13.74	12.69	8.55	7.86	4.15	3.59
	2011	16.18	15.11	9.66	8.78	4.35	3.86
	2012	15.31	13.33	8.11	7.33	3.93	3.46
	2013	17.55	17.20	9.86	9.00	5.45	4.92
	2014	12.83	11.99	7.72	7.14	3.75	3.20
VG	2010	1.00	1.00	4.60	5.30	33.47	46.05
	2011	1.00	1.00	6.64	7.74	54.94	83.30
	2012	1.00	1.00	5.02	5.99	48.95	71.53
	2013	1.00	1.00	5.65	6.72	33.71	52.80
	2014	1.00	1.00	5.41	5.97	34.86	53.55

Table 16. Statistical Metrics Comparing OCD Output to AERMOD and CALPUFF Output for the Volume Source in the CPA

Metrics	Year	OCD[1]		AERMOD		CALPUFF	
		SSB	Coast	SSB	Coast	SSB	Coast
RHC	2010	396.86	408.42	633.01	563.40	64.78	54.51
	2011	735.69	694.94	739.74	765.60	67.99	55.21
	2012	1,538.48	1,385.85	446.78	348.11	79.24	61.91
	2013	962.54	698.67	638.89	447.73	79.27	64.78
	2014	508.67	503.24	579.50	416.87	68.06	59.94
FF2	2010	1.00	1.00	0.23	0.21	0.14	0.14
	2011	1.00	1.00	0.20	0.19	0.12	0.12
	2012	1.00	1.00	0.21	0.20	0.12	0.13
	2013	1.00	1.00	0.21	0.20	0.13	0.13
	2014	1.00	1.00	0.17	0.16	0.12	0.13
r_g	2010	1.00	1.00	0.39	0.39	0.15	0.15
	2011	1.00	1.00	0.40	0.39	0.20	0.17
	2012	1.00	1.00	0.52	0.49	0.23	0.19
	2013	1.00	1.00	0.52	0.53	0.35	0.31
	2014	1.00	1.00	0.41	0.41	0.20	0.19
μ_g	2010	13.74	12.69	7.64	7.05	3.31	2.93
	2011	16.18	15.11	8.76	7.71	3.48	3.04
	2012	15.31	13.33	7.31	6.46	3.25	2.78
	2013	17.55	17.20	9.06	8.09	4.22	3.96
	2014	12.83	11.99	6.95	6.34	3.06	2.65
VG	2010	1.00	1.00	5.86	6.81	49.91	67.70
	2011	1.00	1.00	8.03	10.66	84.45	150.99
	2012	1.00	1.00	6.62	8.37	72.60	113.45
	2013	1.00	1.00	7.04	8.83	53.21	74.78
	2014	1.00	1.00	6.90	7.96	53.26	78.05

[1] OCD area source results presented here for comparison with AERMOD and CALPUFF volume source results.

Table 17 presents statistical results for AERMOD and CALPUFF model performance compared to OCD for the tall, hot point source in the WPA for 2010 through 2014. AERMOD and CALPUFF *RHC* values are both lower than OCD *RHC* values by similar factors (1.2 to 1.7). The AERMOD-OCD agreement for this source is worse in the WPA compared to the CPA (Table 13). As seen in the Q-Q plots (Figure 41–Figure 42 and Figure 43–Figure 44), there are noticeable differences in concentration between the SSB and the coastal receptors, which is also evident in Table 17. For AERMOD, the *FF2* and r_g values are lower and the *VG* values are higher for the coastal receptors compared to the SSB receptors, indicating that there is better AERMOD-OCD agreement along the coast. For CALPUFF, the SSB receptors show better agreement with OCD concentrations.

Table 18 compares AERMOD, CALPUFF, and OCD model performance for the short, cold point source in the WPA for 2010 through 2014. Compared to OCD *RHC* values, AERMOD *RHC* values are 1.1 to 1.4 times higher, indicating similar levels of performance in both the CPA and WPA. The CALPUFF *RHC* values are 1.4 to 1.9 times lower than the OCD *RHC* values, suggesting better CALPUFF-OCD agreement at the upper end of the frequency distribution in the WPA compared to the CPA, where the same ratio is 2.3 to 2.7. Between 25 and 42% of AERMOD concentrations and 18 to 35% of CALPUFF concentrations are within a factor of two compared to OCD concentrations. The *FF2*, r_g, and *VG* differences are not as pronounced between the SSB and coastal receptors for this source compared to the tall, hot point source, although AERMOD still performs best along the coast and CALPUFF performs better overall along the SSB.

Table 17. Statistical Metrics Comparing OCD Output to AERMOD and CALPUFF Output for the Tall, Hot Point Source in the WPA

Metrics	Year	OCD		AERMOD		CALPUFF	
		SSB	Coast	SSB	Coast	SSB	Coast
RHC	2010	60.09	17.37	49.75	13.22	45.98	11.38
	2011	59.52	17.53	39.77	13.81	40.05	10.44
	2012	54.98	16.43	41.73	13.59	38.36	10.77
	2013	59.19	17.28	43.04	13.50	38.60	11.27
	2014	57.43	16.51	48.62	13.02	44.48	10.77
FF2	2010	1.00	1.00	0.22	0.45	0.44	0.21
	2011	1.00	1.00	0.17	0.38	0.40	0.16
	2012	1.00	1.00	0.14	0.36	0.37	0.12
	2013	1.00	1.00	0.16	0.39	0.36	0.15
	2014	1.00	1.00	0.15	0.37	0.38	0.14
r_g	2010	1.00	1.00	0.24	0.40	0.38	0.23
	2011	1.00	1.00	0.18	0.44	0.43	0.30
	2012	1.00	1.00	0.22	0.45	0.50	0.27
	2013	1.00	1.00	0.22	0.42	0.46	0.29
	2014	1.00	1.00	0.24	0.42	0.49	0.32
μ_g	2010	15.14	4.22	3.85	1.90	6.42	1.15
	2011	15.50	4.45	3.21	1.79	6.27	1.08
	2012	15.26	4.01	3.01	1.54	6.16	0.91
	2013	15.20	4.25	3.33	1.69	6.03	1.03
	2014	14.98	4.23	3.14	1.61	6.01	0.98
VG	2010	1.00	1.00	17.84	4.41	4.32	8.90
	2011	1.00	1.00	33.35	5.33	3.83	9.47
	2012	1.00	1.00	38.07	6.19	3.68	11.66
	2013	1.00	1.00	28.42	5.84	4.21	11.30
	2014	1.00	1.00	28.66	6.04	3.80	10.66

Table 18. Statistical Metrics Comparing OCD Output to AERMOD and CALPUFF Output for the Short, Cold Point Source in the WPA

Metrics	Year	OCD		AERMOD		CALPUFF	
		SSB	Coast	SSB	Coast	SSB	Coast
RHC	2010	79.22	21.09	93.28	29.83	44.76	12.34
	2011	83.72	21.45	92.00	30.68	45.03	13.00
	2012	78.00	20.84	99.15	29.29	54.84	12.16
	2013	75.15	21.81	92.17	29.89	44.80	12.00
	2014	77.99	21.02	91.49	29.75	43.76	13.71
FF2	2010	1.00	1.00	0.36	0.42	0.35	0.25
	2011	1.00	1.00	0.28	0.33	0.27	0.18
	2012	1.00	1.00	0.25	0.32	0.25	0.18
	2013	1.00	1.00	0.29	0.37	0.27	0.20
	2014	1.00	1.00	0.27	0.32	0.26	0.19
r_g	2010	1.00	1.00	0.48	0.60	0.48	0.52
	2011	1.00	1.00	0.49	0.61	0.51	0.57
	2012	1.00	1.00	0.51	0.62	0.56	0.56
	2013	1.00	1.00	0.48	0.62	0.52	0.56
	2014	1.00	1.00	0.47	0.60	0.55	0.58
μ_g	2010	8.92	1.92	3.58	1.15	3.91	0.65
	2011	9.42	2.03	3.41	1.21	3.46	0.56
	2012	8.86	1.78	2.96	0.99	3.29	0.50
	2013	8.93	1.92	3.20	1.09	3.39	0.56
	2014	8.64	1.87	3.08	1.13	3.15	0.52
VG	2010	1.00	1.00	7.64	3.15	3.92	6.49
	2011	1.00	1.00	10.94	3.91	4.78	8.57
	2012	1.00	1.00	12.58	4.21	4.37	8.66
	2013	1.00	1.00	10.76	3.85	4.63	8.25
	2014	1.00	1.00	11.34	4.21	4.46	8.40

Table 19. Statistical Metrics Comparing OCD Output to AERMOD and CALPUFF Output for the Area Source in the WPA

Metrics	Year	OCD		AERMOD		CALPUFF	
		SSB	Coast	SSB	Coast	SSB	Coast
RHC	2010	1,399.19	1,190.86	1,738.22	1,133.52	779.08	204.98
	2011	1,188.20	1,296.09	1,964.64	1,285.87	725.24	201.33
	2012	1,227.22	1,112.94	2,023.28	1,226.95	682.18	183.83
	2013	1,414.59	1,388.42	1,716.19	1,103.51	684.91	171.48
	2014	1,225.27	1,254.39	2,098.62	1,285.06	679.25	193.07
FF2	2010	1.00	1.00	0.76	0.45	0.77	0.23
	2011	1.00	1.00	0.73	0.44	0.78	0.20
	2012	1.00	1.00	0.70	0.42	0.77	0.21
	2013	1.00	1.00	0.72	0.44	0.77	0.23
	2014	1.00	1.00	0.68	0.40	0.78	0.18
r_g	2010	1.00	1.00	0.79	0.84	0.65	0.63
	2011	1.00	1.00	0.79	0.89	0.66	0.71
	2012	1.00	1.00	0.78	0.88	0.67	0.70
	2013	1.00	1.00	0.79	0.87	0.67	0.69
	2014	1.00	1.00	0.75	0.88	0.66	0.72
μ_g	2010	31.52	27.40	26.00	13.62	29.95	9.09
	2011	30.87	27.77	26.15	13.90	29.93	9.10
	2012	28.66	24.54	22.60	11.83	27.87	8.06
	2013	29.91	26.32	24.58	13.08	28.12	8.64
	2014	29.90	26.61	24.48	13.08	28.28	8.51
VG	2010	1.00	1.00	1.64	2.58	1.76	7.80
	2011	1.00	1.00	1.72	2.39	1.76	6.99
	2012	1.00	1.00	1.79	2.66	1.75	7.28
	2013	1.00	1.00	1.74	2.52	1.79	7.26
	2014	1.00	1.00	1.97	2.68	1.81	7.65

Table 20. Statistical Metrics Comparing OCD Output to AERMOD and CALPUFF Output for the Volume Source in the WPA

Metrics	Year	OCD[1]		AERMOD		CALPUFF	
		SSB	Coast	SSB	Coast	SSB	Coast
RHC	2010	1,399.19	1,190.86	2,013.64	939.64	431.90	147.52
	2011	1,188.20	1,296.09	2,028.52	963.51	431.50	144.04
	2012	1,227.22	1,112.94	2,096.50	901.46	466.59	149.85
	2013	1,414.59	1,388.42	1,844.46	904.36	394.28	129.18
	2014	1,225.27	1,254.39	2,074.15	955.45	386.02	134.89
FF2	2010	1.00	1.00	0.78	0.42	0.74	0.08
	2011	1.00	1.00	0.74	0.43	0.77	0.05
	2012	1.00	1.00	0.73	0.39	0.75	0.07
	2013	1.00	1.00	0.73	0.41	0.73	0.07
	2014	1.00	1.00	0.70	0.38	0.75	0.06
r_g	2010	1.00	1.00	0.78	0.84	0.63	0.64
	2011	1.00	1.00	0.79	0.88	0.66	0.73
	2012	1.00	1.00	0.79	0.87	0.67	0.73
	2013	1.00	1.00	0.79	0.87	0.66	0.72
	2014	1.00	1.00	0.75	0.88	0.65	0.74
μ_g	2010	31.52	27.40	29.03	13.33	28.68	6.72
	2011	30.87	27.77	29.34	13.72	29.39	6.71
	2012	28.66	24.54	25.28	11.52	26.03	5.98
	2013	29.91	26.32	27.46	12.78	26.89	6.37
	2014	29.90	26.61	27.57	12.87	26.79	6.28
VG	2010	1.00	1.00	1.70	2.69	1.80	15.60
	2011	1.00	1.00	1.76	2.47	1.77	14.11
	2012	1.00	1.00	1.79	2.85	1.76	14.20
	2013	1.00	1.00	1.77	2.63	1.83	14.10
	2014	1.00	1.00	2.00	2.78	1.86	15.61

[1] OCD area source results presented here for comparison with AERMOD and CALPUFF volume source results.

Table 19 compares AERMOD, CALPUFF, and OCD model performance for the area source in the WPA for 2010 through 2014. There are substantial differences in *RHC* values between the coastal and SSB receptors and also year-to-year variation in both AERMOD and CALPUFF, but overall, there is better *RHC* agreement between these models and OCD for the area source in the WPA compared to the CPA (Table 15). The *RHC* values for the AERMOD SSB receptors are 1.2 to 1.7 times higher than *RHC* values for OCD SSB receptors. The *RHC* values for AERMOD coastal receptors are 1.1 times higher in 2012 and up to 1.3 times lower for the rest of the years. For CALPUFF, the *RHC* values are 1.6–2.1 and 5.8–8.1 times lower compared to OCD *RHC* values for the SSB and coastal receptors, respectively. Interestingly, the correlation coefficient values for the SSB receptors in both AERMOD and CALPUFF are higher at this source and location compared to all scenarios previously discussed, ranging from 0.68–0.76 for AERMOD and 0.77–0.78 for CALPUFF. The geometric variances are also quite low for the SSB receptors in both models, suggesting that both AERMOD and CALPUFF concentrations are well aligned with OCD concentrations.

Table 20 compares the OCD area source to the AERMOD and CALPUFF volume sources in the WPA for 2010 to 2014. The volume and area source results are similar except that the volume source is associated with larger disagreements between CALPUFF and OCD concentrations at coastal receptors.

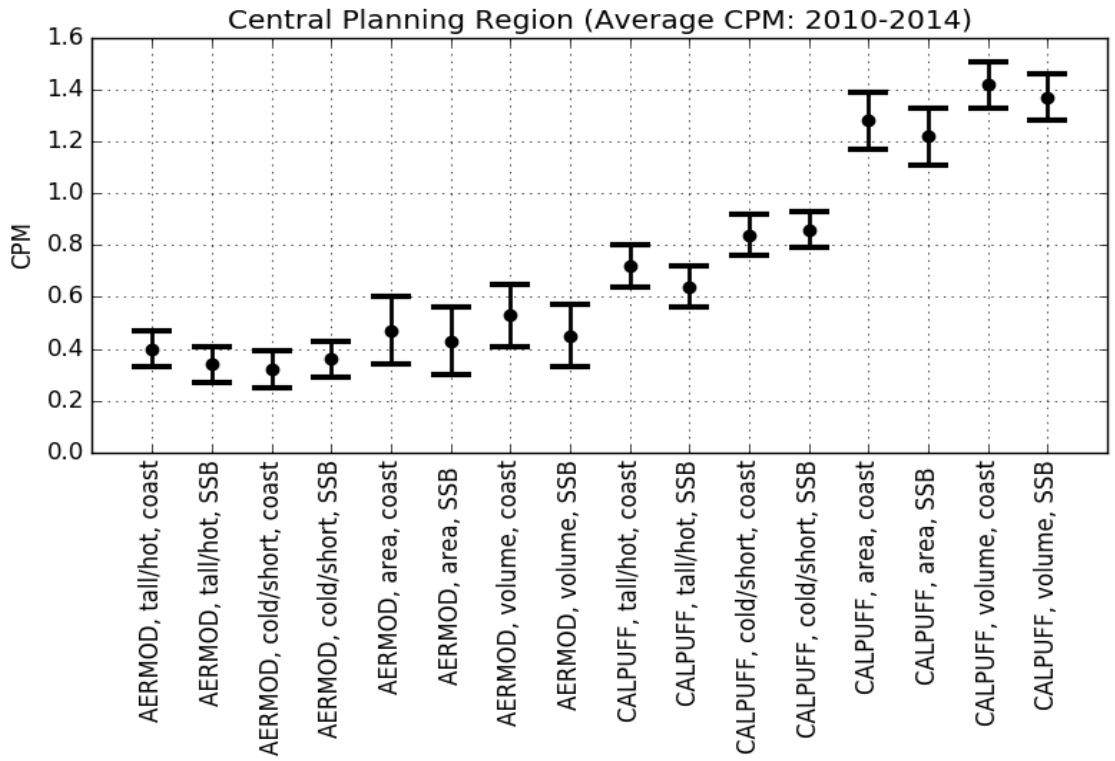

Figure 57. Composite Performance Metric for the CPA

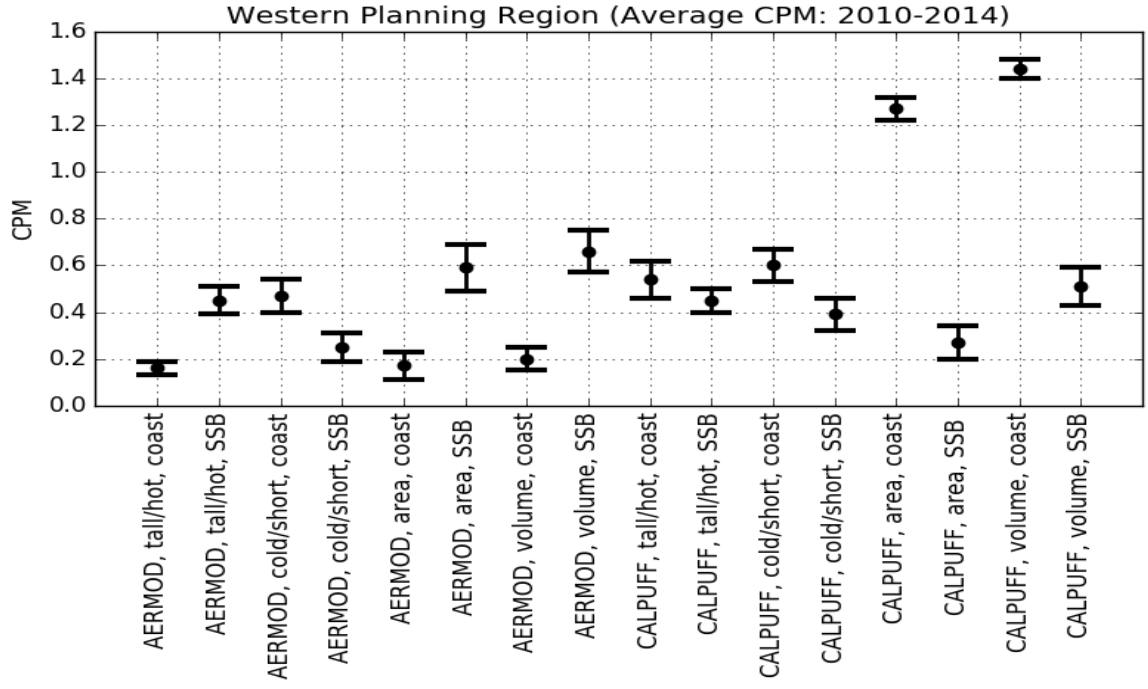

Figure 58. Composite Performance Metric for the WPA

Table 21. Composite Performance Metric (CPM) and CPM Standard Deviation for All Sources in the CPA

Source	Year	AERMOD				CALPUFF			
		CPM		Standard Deviation		CPM		Standard Deviation	
		SSB	Coast	SSB	Coast	SSB	Coast	SSB	Coast
Tall, hot point source	2010	0.33	0.40	0.07	0.08	0.61	0.64	0.08	0.08
	2011	0.31	0.34	0.08	0.08	0.65	0.78	0.06	0.05
	2012	0.32	0.36	0.06	0.07	0.72	0.80	0.08	0.09
	2013	0.34	0.40	0.05	0.05	0.60	0.67	0.09	0.10
	2014	0.42	0.48	0.05	0.06	0.61	0.69	0.09	0.09
Short, cold point source	2010	0.29	0.26	0.06	0.06	0.85	0.88	0.05	0.11
	2011	0.53	0.39	0.07	0.07	0.88	0.93	0.11	0.11
	2012	0.34	0.33	0.08	0.08	0.81	0.82	0.06	0.06
	2013	0.20	0.23	0.07	0.07	0.81	0.80	0.05	0.06
	2014	0.43	0.38	0.07	0.08	0.83	0.89	0.07	0.07
Area source	2010	0.46	0.37	0.12	0.11	0.89	1.01	0.11	0.12
	2011	0.29	0.35	0.10	0.09	1.23	1.33	0.09	0.08
	2012	0.65	0.79	0.18	0.18	1.39	1.43	0.09	0.10
	2013	0.38	0.51	0.07	0.05	1.32	1.36	0.10	0.08
	2014	0.40	0.35	0.15	0.20	1.25	1.26	0.14	0.19
Volume source	2010	0.32	0.33	0.10	0.11	1.09	1.21	0.09	0.09
	2011	0.23	0.31	0.13	0.11	1.37	1.43	0.07	0.06
	2012	0.83	0.95	0.17	0.18	1.53	1.55	0.06	0.08
	2013	0.50	0.67	0.09	0.06	1.47	1.51	0.09	0.07
	2014	0.34	0.41	0.12	0.15	1.39	1.38	0.11	0.16

Table 22. Composite Performance Metric (CPM) and CPM Standard Deviation for All Sources in the WPA

Source	Year	AERMOD				CALPUFF			
		CPM		Standard Deviation		CPM		Standard Deviation	
		SSB	Coast	SSB	Coast	SSB	Coast	SSB	Coast
Tall, hot point source	2010	0.41	0.18	0.08	0.03	0.43	0.51	0.05	0.10
	2011	0.45	0.18	0.06	0.03	0.46	0.51	0.07	0.05
	2012	0.44	0.14	0.06	0.04	0.46	0.68	0.05	0.12
	2013	0.48	0.13	0.06	0.04	0.42	0.52	0.04	0.08
	2014	0.46	0.15	0.06	0.03	0.48	0.49	0.06	0.06
Short, cold point source	2010	0.21	0.40	0.06	0.08	0.38	0.62	0.07	0.07
	2011	0.21	0.53	0.04	0.06	0.44	0.58	0.05	0.06
	2012	0.23	0.42	0.07	0.07	0.34	0.64	0.11	0.07
	2013	0.32	0.46	0.06	0.06	0.35	0.64	0.05	0.06
	2014	0.27	0.52	0.06	0.06	0.42	0.53	0.06	0.09
Area source	2010	0.50	0.14	0.11	0.06	0.29	1.23	0.09	0.05
	2011	0.63	0.19	0.13	0.05	0.25	1.29	0.10	0.04
	2012	0.64	0.19	0.11	0.08	0.26	1.21	0.06	0.06
	2013	0.46	0.18	0.09	0.06	0.25	1.34	0.07	0.04
	2014	0.73	0.17	0.07	0.06	0.29	1.29	0.05	0.04
Volume source	2010	0.58	0.22	0.09	0.05	0.52	1.40	0.07	0.03
	2011	0.71	0.18	0.12	0.04	0.51	1.46	0.10	0.03
	2012	0.71	0.19	0.09	0.06	0.45	1.38	0.07	0.05
	2013	0.57	0.27	0.09	0.06	0.59	1.48	0.09	0.03
	2014	0.75	0.14	0.06	0.04	0.46	1.46	0.06	0.03

Figure 57 and Table 21 above present *CPM* values for all scenarios in the CPA. In Figure 57, the average *CPM* from 2010 to 2014 is displayed. In this portion of the study, the lowest *CPM* value is associated with the scenario that has the best overall agreement with OCD concentrations. In the CPA, *CPM* values range from 0.26 to 1.55. The scenario with the lowest 5-year average *CPM* value is when AERMOD is used to estimate concentrations along the coast from the short, cold point source. The scenario with the highest average *CPM* value is when CALPUFF is used to estimate concentrations along the SSB from the volume source. All four AERMOD point source scenarios have similar *CPM* values, indicating good overall agreement with OCD. Figure 57 clearly demonstrates that *CPM* values are lower for AERMOD compared to CALPUFF, which is another indication that AERMOD and OCD perform more similarly in these scenarios compared to CALPUFF.

Figure 58 and Table 22 above show the *CPM* values for the WPA. The *CPM* values range from 0.13 to 1.48. The scenario with the lowest 5-year average *CPM* value is when AERMOD is used to estimate concentrations along the coast from a tall, hot point source. The *CPM* values are nearly as low for the other AERMOD simulations with coastal receptors, with the exception of the short, cold point source. Similar to the Central GOM Planning Area, the highest 5-year average *CPM* value is the CALPUFF volume source-coastal receptor modeling configuration. There is more variation in *CPM* values between the scenarios with coastal and SSB receptors in the WPA compared to the CPA (Figure 57), likely because the SSB-coast distance is greater in the WPA (9 km). The average of all AERMOD *CPM* values is 0.37 compared to 0.68 for CALPUFF, indicating that AERMOD and OCD have better agreement compared to CALPUFF and OCD in the WPA.

This portion of the report evaluates the model performance of AERMOD and CALPUFF against OCD for a wide range of scenarios in the GOM using a variety of statistical approaches. Overall, these results suggest that AERMOD and OCD perform similarly, although AERMOD has a tendency to estimate higher maximum concentrations, which is a more conservative approach. AERMOD outperforms CALPUFF in terms of agreement with OCD concentrations for the vast majority of source types, source/receptor locations, and regions within the GOMR considered in this study.

The possible interpretation of Figure 57 and Figure 58 (the *CPM* values) that CALPUFF performs worse than OCD and AERMOD is not necessarily supported by this work. CALPUFF performance for point sources is comparable. At short source-receptor distances, CALPUFF's area and volume sources are similar to OCD's area source. At longer source-receptor distances, CALPUFF area and volume sources differ from OCD's area source, but we cannot say which is more correct. None of the tracer studies' releases could be characterized by volume or area sources, so we have no way of comparing any of the model's performance to observations for these source types. Given that OCD's area source algorithm appears to be very similar to a "pseudo point source" (a point source with a large stack diameter and a small stack exit velocity), one might expect the volume sources to agree but have little expectation that the area source types would agree between models. The area source algorithms between the three models are just too different.

7. CONCLUSIONS

Through the mechanism of the Interagency Workgroup on Air Quality Modeling (IWAQM) Overwater Team, BOEM seeks to work cooperatively with the USEPA and other relevant States/Agencies to maintain good communication and ongoing consensus on methods and models to be used in overwater dispersion modeling.

The USEPA regulatory default dispersion model for overwater use is OCD. OCD has not been developed in the past few decades, both in terms of fundamental science and in terms of the ability to calculate results consistent with today's statistically based air quality standards. BOEM wishes to use the USEPA regulatory default dispersion model for over land (AERMOD) for source-receptor distances less than 50 km, in place of OCD.

The regulatory default meteorological preprocessor for AERMOD, named AERMET, contains certain assumptions and simplifications that are suitable for overland conditions but are not scientifically suitable for overwater conditions. AERMET's land-use preprocessor, named AERSURFACE, is also not scientifically suitable for overwater conditions. This led the USEPA to sponsor the development of an alternative meteorological preprocessing program for overwater conditions, named AERCOARE (Wong et al., 2016), based on a method developed by ENVIRON for a prevention of significant deterioration (PSD) project offshore.

The scientific methods implemented in AERCOARE are very similar to those contained in the Weather Research and Forecasting (WRF) prognostic MMM. The USEPA has sponsored the development the Mesoscale Model Interface Program (MMIF), which converts WRF output to the file format required by several other programs, including AERMOD, AERMET, AERCOARE, CALPUFF, and the Second-Order Closure Integrated Puff Model with Chemistry (SCICHEM). The USEPA has promulgated regulations (USEPA, 2017) stipulating that in locations where observed meteorology is not available, prognostic model output (WRF+MMIF) could be used instead. USEPA MMIF Guidance suggests that for overland locations, the meteorological preprocessor to AERMOD (i.e., AERMET) should be used, but for offshore situations, MMIF's AERMOD ("direct") mode can be used.

This model comparison study examined the use of WRF prognostic model output, processed through MMIF (in AERMOD mode) to drive the dispersion models AERMOD and CALPUFF. Two types of model assessments are presented herein: an assessment using four short-term overwater tracer studies performed in the 1980s, and a "consequence" type assessment using a long-term modern dataset.

For the tracer studies, predicted concentrations from the three models (OCD, AERMOD, and CALPUFF) were compared to observed concentrations, using the same meteorology for all three models. The "consequence" assessment investigated the consequence of replacing OCD with AERMOD (or CALPUFF) by comparing model-to-model outcomes; there are no measurements of concentrations as in

the tracer studies, but the 5-year modeling period provides much more statistical power than the relatively short tracer studies.

Using the Cox-Tikvart methodology (Cox and Tikvart, 1990), the Composite Performance Metrics (*CPM*) and *RHC* were used to assess model performance. Because the number of samples (hours) of the individual tracer studies was small, *CPM* and *RHC* results are not presented for individual experiments. Instead, three grouping across experiments were presented: all samples, summertime samples, and wintertime samples. The summertime tracer study analysis showed that AERMOD performs nearly as well as OCD, while CALPUFF performs notably worse at these relatively short source-receptor distances. For the tracer releases during winter, both AERMOD and CALPUFF performed better than OCD. The "consequence" assessment also used the Cox-Tikvart methodology and showed that AERMOD's performance (using a modern, 5-year prognostic meteorological dataset) was more similar to OCD's than CALPUFF's performance.

This analysis suggests that the WRF-MMIF-AERMOD method performs just as well as the regulatory default model OCD for offshore emission sources less than 50 km from a regulatory compliance point, such as a coastline or an SSB.

All of the tracer studies and the "consequence" assessment had source-receptor distances that were less than 50 km, the minimum applicable distance for CALPUFF, following USEPA Guidance (USEPA, 2008). Therefore no conclusions can be drawn from this report regarding the performance of CALPUFF in situations where the BOEM administrator has already approved its use (greater than 50 km, matching USEPA Guidance).

These results are similar to the conclusions presented in Wong et al. (2016), which suggest that an AERCOARE-AERMOD framework is a viable and practical alternative to OCD. The USEPA (2015b, 2015c) concluded that there was no advantage to using WRF-MMIF-AERCOARE-AERMOD over using WRF-MMIF-AERMOD. This is not surprising, considering the Monin-Obukhov parameterization in WRF is nearly identical to that in the COARE algorithm, which AERCOARE uses.

A key difference between this study and the work presented in Wong et al. (2016) is the source of the meteorological data used in the dispersion models. Wong et al. (2016) incorporated the observed meteorology from the tracer studies into AERCOARE to calculate the full suite of meteorological parameters needed in AERMOD, OCD, and CALPUFF. In this evaluation, only prognostic meteorological mesoscale model output (from WRF) is used to generate the necessary inputs for AERMOD, OCD, and CALPUFF, which is a useful approach for locations where reliable meteorological measurements are difficult to obtain. Although the meteorological configurations differ between these two studies, the general conclusion is the same: **WRF-MMIF-AERMOD can be used as an alternative to OCD when predicting concentration less than 50 km from offshore emissions sources**.

REFERENCES

Brashers, B., C. Emery. 2014. The Mesoscale Model Interface Program (MMIF) Draft User's Manual. Novato, CA: ENVIRON Int. Corp. Air Sciences Group. Prepared for U.S. EPA Air Quality Assessment Division.

Brashers, B., T. Sturtz, J. Maranche. 2016. Best Use of Numerical Weather Prediction Output for Nonattainment Modeling of SO2. Guideline on Air Quality Models: The New Path. April 13, 2016. Chapel Hill, NC.

Bridgers, G. 2011. Model Clearinghouse Review of AERMOD-COARE as an Alternative Model for Application in an Arctic Marine Ice Free Environment. Research Triangle Park, NC: U.S. EPA.

Cole, H.S., J.E. Summerhays. 1979. A Review of Techniques Available for Estimating Short-Term NO2 concentrations, Journal of the Air Pollution Control Association, 29:8, 812-817, DOI: 10.1080/00022470.1979.10470866.

Cox, W.M., J.A. Tikvart. 1990. A statistical procedure for determining the best performing air quality simulation model. Atmos. Environ., 24A, 9, 2387-2395.

Dabberdt, W., R. Brodzinsky, B. Cantrell, R. Ruff. 1982. Atmospheric Dispersion Over Water and in the Shoreline Transition Zone, Final Report Volume II: Data. Menlo Park, CA: Prepared for American Petroleum Institute by SRI International.

DiCristofaro, D.C., S.R. Hanna. 1989. OCD The Offshore and Coastal Dispersion Model, Version 4, Volume I: User's Guide. MMS Contract No. 14-12-001-30396, November 1989.

Earth Tech. 2006. Development of the Next Generation of Air Quality Models for the Outer Continental Shelf (OCS) Applications, Final Report: Volume 1. Herndon (VA): U.S. Department of the Interior, Minerals Management Service. MMS 2006-006.

ENVIRON Int. Corp. 2010. Evaluation of the COARE-AERMOD Alternative Modeling Approach Support for Simulation of Shell Exploratory Drilling Sources In the Beaufort and Chukchi Seas. Lynnwood, WA: ENVIRON.

ENVIRON Int. Corp. 2012. Evaluation of the Combined AERCOARE/AERMOD Modeling Approach for Offshore Sources. Novato, CA: ENVIRON Int. Corp.

ENVIRON Int. Corp. 2014. METSTAT. Retrieved from http://www.camx.com/download/support-software.aspx. Date accessed: May 22, 2017

Golder, D. 1972. Relations Among Stability Parameters in the Surface Layer. Boundary Layer Meteorology, 3(1):47-58.

Hanna, S., L. Schulman, R. Paine, J. Pleim. 1984. Users Guide to the Offshore and Coastal Dispersion (OCD) Model. Prepared for the Minerals Management Service of the U.S. Dept. of the Interior under Contract No. 14-08-0001-21138. Concord, MA: Environmental Research & Technology, Inc.

Hanrahan, P. 1999. The Plume Volume Molar Ratio Method for Determining NO2/NOx Ratios in Modeling – Part 1: Methodology. Journal of the Air and Waste Management Association, 49, 11, 1324-1331.

Hartmann, D. L. 1994. Global Physical Climatology. San Diego, CA: Academic Press, 105.

Hong, S.-Y., Y. Noh, J. Dudhia. 2006. A New Vertical Diffusion Package with an Explicit Treatment of Entrainment Processes. Mon. Weather Rev., 134, 2318-2341.

Johnson, V., T. Spangler. 1986. Tracer Study Conducted to Acquire Data for Evaluation of Air Quality Dispersion Models. San Diego, CA: WESTEC Services, Inc. for the American Petroleum Institute.

Louis, J.F. 1979. A parametric model of vertical eddy fluxes in the atmosphere. Boundary-Layer Meteorol. 17: 187. https://doi.org/10.1007/BF00117978. Date accessed: May 22, 2017.

Richmond, K., R. Morris. 2012. Evaluation of the Combined AERCOARE/AERMOD Modeling Approach for Offshore Sources. Seattle, WA: U.S. EPA Region 10. EPA-910-R-12-007.

Schacher, G., D. Spiel, C. Fairall, K. Davidson, C. Leonard, C. Reheis. (1982). California Coastal Offshore Transport and Diffusion Experiments: Meteorological Conditions and Data. Monterey, CA: Report NPS-61-82-007, Naval Postgraduate School.

Schulman, L.L., D.G. Strimaitis, J.S. Scire. 2000. Development and Evaluation of the PRIME Plume Rise and Building Downwash Model. Journal of the Air and Waste Management Association, 50, 378-390.

Scire, J.S., F.R. Robe, M.E. Fernau, R.J. Yamartino. 2000a. A User's Guide for the CALMET Meteorological Model (Version 5). Concord (MA): Earth Tech, Inc.

Scire, J.S., D.G. Strimaitis, R.J. Yamartino. 2000b. A User's Guide for the CALPUFF Dispersion Model (Version 5). Concord (MA): Earth Tech, Inc.

Skamarock, W.C., J.B. Klemp, J. Dudhia, D.O. Gill, D.M. Barker, M.G. Duda, X.-Y. Huang, W. Wang, J.G. Powers. 2008. A Description of the Advanced Research WRF version 3. NCAR Technical Note 475. http://www.mmm.ucar.edu/wrf/users/docs/arw_v3.pdf. Date accessed: May 25, 2017.

USEPA (U.S. Environmental Protection Agency). 1980. User's Guide for MPTER. Research Triangle Park, NC: U.S. EPA. EPA-600/8-80-016.

USEPA. 2003. AERMOD: Latest Features and Evaluation Results. Research Triangle Park, NC: U.S. EPA, OAQPS. EPA-454/R-03-003, 2003.

USEPA. 2004a. User's Guide for the AMS/EPA Regulatory Model – AERMOD. Research Triangle Park, NC: U.S. EPA, OAQPS. EPA-454/B-03-001.

USEPA. 2004b. User's Guide for the AERMOD Meteorological Preprocessor (AERMET). Research Triangle Park, NC: U.S. EPA, OAQPS. EPA-454/B-03-002.

USEPA. 2008. Clarification of Regulatory Status of CALPUFF for Near-field Applications. Research Triangle Park, NC: U.S. EPA. August 13, 2008.

USEPA. 2012. User's Manual AERCOARE Version 1.0, Seattle, WA: U.S. EPA Region 10. EPA-910-R-12-008.

USEPA. 2015a. Revision to the Guideline on Air Quality Models: Enhancements to the AERMOD Dispersion Modeling System and Incorporation of Approaches to Address Ozone and Fine Particulate Matter; Proposed Rule. Washington, D.C.: U.S. EPA. Federal Register, 40 CFR Part 51, 80, 145, EPA-HQ-OAR-2015-0210; FRL-9930-11-OAR.

USEPA. 2015b. Combined WRF/MMIF/AERCOARE/AERMOD Overwater Modeling Approach for Offshore Emission Sources, Volume 2: Evaluation of Weather Research and Forecasting Model Simulations for Five Tracer Gas Studies with AERMOD. Seattle, WA: U.S. EPA. EPA-910-R-15-001b.

USEPA. 2015c. Combined WRF/MMIF/AERCOARE/AERMOD Overwater Modeling Approach for Offshore Emission Sources, Volume 3: Analysis of AERMOD performance Using Weather Research and Forecasting Model Predicted Meteorology and Measured Meteorology in the Arctic. Seattle, WA: U.S. EPA. EPA-910-R-15-001c.

USEPA. 2017. Revisions to the Guideline on Air Quality Models: Enhancements to the AERMOD Dispersion Modeling System and Incorporation of Approaches To Address Ozone and Fine Particulate Matter. Washington, D.C.: U.S. EPA. Federal Register, 40 CFR 51 Part 51, Vol. 82 No 10, EPA-HQ-OAR-2015-0310; FRL-9956-23-OAR.

Vogelezang, D., A. Holtslag. 1996. Evaluation and Model Impacts of Alternative Boundary-Layer Height Formulations. Boundary Layer Meteor., 81, 245-269.

Wong, H. 2011. COARE Bulk Flux Algorithm to Generate Hourly Meteorological Data for Use With AERMOD. Seattle, WA: U.S. EPA Region 10.

Wong, H., R. Elleman, E. Wolvovsky, K. Richmond, J. Paumier. (2016) AERCOARE: An Overwater Meteorological Preprocessor for AERMOD. Journal of Air and Waste Management Association, 66:11, 1121-1140, doi:10.1080/10962247.2016.1202156.

Appendix E.2

Synthetic Source Scenario Equipment Summaries Used in Emission Exemption Threshold Evaluation

This appendix presents the equipment for each synthetic source by scenario as discussed in Section 5, Emission Exemption Threshold Evaluation, of this report. Tables E.2-1 through E.2-15 present the equipment type, count, activity level, and total hours of operation.

Table E.2-1. Equipment Included in Scenario 1 (Large)

Equipment Category	Equipment/Vessel Type	Activity	Activity Units	hr/yr
Drilling Rig	Drilling-Drillship	46,085	kW	8,760
Vessels	Support Vessel (crew)	46,085	kW	520
	Support Vessel (supply)	46,085	kW	1,248

Table E.2-2. Equipment Included in Scenario 1 (Medium)

Equipment Category	Equipment/Vessel Type	Activity	Activity Units	hr/yr
Drilling Rig	Drilling-Drillship	46,085	kW	2,736
Vessels	Support Vessel (crew)	1,865	kW	198
	Support Vessel (supply)	2,237	kW	392

Table E.2-3. Equipment included in Scenario 1 (Small)

Equipment Category	Equipment/Vessel Type	Activity	Activity Units	hr/yr
Prime Mover	Diesel Reciprocating Engine (> 600 hp)	16,975	hp	744
Vessels	Support Vessel (crew)	1,539	kW	24
	Support Vessel (supply)	1,539	kW	30
	Support Vessel (Tugs)	6,264	kW	24

Table E.2-4. Equipment Included in Scenario 2 (Large)

Operation	Equipment Category	Equipment/Vessel Type	Activity	Activity Units	Count	hr/yr
Drilling	Auxiliary Equipment	Diesel Reciprocating Engine (< 600 hp)	148,920	gal/yr	1	8,760
			221,555	gal/yr	1	8,760
			259,150	gal/yr	2	8,760
		Diesel Reciprocating Engine (> 600 hp)	148,920	gal/yr	1	8,760
			221,555	gal/yr	1	8,760
			259,150	gal/yr	2	8,760
			1,007,035	gal/yr	1	8,760
	Burner	Diesel Heater/Boiler/Burner (< 100 MMBtu/hr)	3	MMBtu/hr	2	8,760
	Prime Mover	Diesel Reciprocating Engine (> 600 hp)	669,775	gal/yr	1	8,760
			2,009,325	gal/yr	1	8,760
			2,734,920	gal/yr	1	5,136
			3,987,260	gal/yr	1	8,760
			4,664,700	gal/yr	1	8,760
	Vessels	Support Vessel (crew)	10,738	kW	1	1,176
			23,862	kW	1	7,008
			57,833	kW	1	8,760
		Support Vessel (supply)	33,557	kW	1	432
			59,059	kW	1	4,968

Table E.2-4. Equipment Included in Scenario 2 (Large) (Continued)

Operation	Equipment Category	Equipment/Vessel Type	Activity	Activity Units	Count	hr/yr
Production	NG Flares	Flare – Pilot	560	scf/hr	1	8,760
		Flare – Upsets	9,375,000	scf/hr	1	168
	Fugitives	Oil/Water/Gas	25,000	Count	1	8,760
	Glycol Dehydrator Vent	Glycol Dehydrator Vent	1	Count	1	432
	Reciprocating Engines	Diesel Reciprocating Engine (< 600 hp)	284	hp	1	21
			311	hp	1	3
			382	hp	1	240
		Diesel Reciprocating Engine (> 600 hp)	1,050	hp	1	2,920
			1,500	hp	1	4,272
			2,736	hp	1	24
			2,816	hp	1	192
			14,376	hp	1	3,000
	Turbine	Diesel Turbines	29,745	hp	4	480
		NG Turbines	29,745	hp	1	480
			29,745	hp	5	6,720
	Amine Gas Sweetening Unit	Amine Gas Sweetening Unit	1	Count	1	6,720
	Loading Operations	Loading Operations	1	Count	1	2,160
	Pneumatic Pumps	Pneumatic Pumps	20,505	SCF/hr	1	8,760
	Pressure Level Controller	Pressure Level Controller	196	SCF/hr	1	8,760

Table E.2-5. Equipment Included in Scenario 2 (Medium)

Operation	Equipment Category	Equipment/Vessel Type	Activity	Activity Units	Count	hr/yr
Drilling	Drilling Rig	Drilling-Drillship	1,353	kW	1	8,760
	Prime Mover	Diesel Reciprocating Engine (> 600 hp)	1,815	hp	1	2,920
			1,815	hp	1	4,380
Production	NG Flares	Flare – Pilot	1,000	scf/hr	1	8,760
		Flare – Upsets	8,000,000	scf/hr	1	48
	Fugitives	Light Oil (>20 API Gravity)	11,420	Count	1	8,760
	Heater/Boiler/Burner	NG Heater/Boiler/Burner (<100 MMBtu/hr)	35	MMBtu/hr	2	576
			35	MMBtu/hr	1	8,760
	Reciprocating Engines	Diesel Reciprocating Engine (< 600 hp)	500	hp	2	4,380
		Diesel Reciprocating Engine (> 600 hp)	1,065	hp	2	52
			1,435	hp	1	52
	Turbine	NG Turbines	4,300	hp	6	52
			4,300	hp	5	8,760
			16,172	hp	2	8,760
	Vessels	Support Vessel (crew)	2,327	kW	1	936
		Support Vessel (supply)	776	kW	1	312
			2,327	kW	1	936

Table E.2-6. Equipment Included in Scenario 2 (Small)

Operation	Equipment Category	Equipment/Vessel Type	Activity	Activity Units	Count	hr/yr
Drilling	Auxiliary Equipment	Diesel Reciprocating Engine (< 600 hp)	83	hp	2	122
			113	hp	1	122
			238	hp	1	122
			250	hp	1	2,684
	Prime Mover	Diesel Reciprocating Engine (> 600 hp)	1,250	hp	3	2,928
			1,400	hp	1	122
	Vessels	Support Vessel (Crew)	1,521	kW	1	122
		Support Vessel (Tugs)	12,826	kW	1	72
Production	NG flares	Flare – Upsets	4,000,000	scf/hr	1	48
	Fugitives	Light Oil (> 20 API Gravity)	11,420	Count	1	8,760
	Reciprocating Engines	Diesel Reciprocating Engine (< 600 hp)	83	hp	2	365
	Vessels	Support Vessel	1,521	kW	1	365

Table E.2-7. Equipment Included in Scenario 3 (Large)

Operation	Equipment Category	Equipment/Vessel Type	Activity	Activity Units	Count	hr/yr
Drilling	Prime Mover	Diesel Reciprocating Engine (> 600 hp)	61,800	hp	2	8,760
	Vessels	Support Vessel (Crew)	1,540	kW	1	1,248
		Support Vessel (Supply)	1,540	kW	1	624
Facility Installation	Vessels	Pipelaying	58,463	kW	1	1,080
		Support Vessel (Tugs)	8,054	kW	4	360
Pipeline Installation	Vessels	Pipelaying	33,557	kW	1	1,080
		Support Vessel (Tugs)	4,101	kW	1	1,080
Production	NG Flares	Flare – Pilot	860	scf/hr	1	6,600
		Flare – Upsets	11,000	scf/hr	1	550
	Fugitives	Light Oil (>20 API Gravity)	11,420	Count	1	6,600
	Turbine	NG Turbines NG 4-cycle Rich Engine	1,591	hp	1	6,600
			4,950	hp	1	6,600
			15,000	hp	1	2,400
	Reciprocating Engines	Diesel Reciprocating Engine (< 600 hp)	500	hp	1	948
		Diesel Reciprocating Engine (> 600 hp)	2,319	hp	1	6,600
	Vessels	Support Vessel	1,540	kW	1	632
	Amine Gas Sweetening Unit	Amine Gas Sweetening Unit	1	Count	1	6,600
	Mud Degassing	Water-Based	1	Count	1	8,760
Well Testing	Gas Flare	--	958	scf/hr	1	48

Table E.2-8. Equipment Included in Scenario 3 (Medium)

Operation	Equipment Category	Equipment/Vessel Type	Activity	Activity Units	Count	hr/yr
Drilling	Prime Mover	Diesel Reciprocating Engine (> 600 hp)	1,950	hp	3	3,624
	Vessels	Support Vessel (Crew)	746	kW	1	604
		Support Vessel (Supply)	1,540	kW	1	1,812
		Support Vessel (Tugs)	19,990	kW	1	4
Facility Installation	Vessels	Support Vessel (Supply tender)	3,132	kW	1	192
		Support Vessel	1,566	kW	1	192
		Support Vessel (Crew)	1119	kW	1	192
		Support Vessel (Supply)	1,566	kW	1	192
Pipeline Installation	Vessels	Pipelaying	1,566	kW	2	192
		Support Vessel	1,044	kW	1	80
			1,566	kW	1	192
Production	NG Flares	Flare – Pilot	860	scf/hr	1	3,672
		Flare – Upsets	11,000	scf/hr	1	10
	Fugitives	Light Oil (>20 API Gravity)	11,420	Count	1	3,672
	Heater/Boiler/Burner	NG Heater/Boiler/Burner (< 100 MMBtu/hr)	12	MMBtu/hr	1	3,672
	NG Reciprocating Engine	NG 4-cycle Rich Engine	1,680	hp	1	3,672
	Reciprocating Engines	Diesel Reciprocating Engine (< 600 hp)	525	hp	2	459
			572	hp	1	52
			572	hp	1	156
		Diesel Reciprocating Engine (> 600 hp)	1,019	hp	1	52
	Turbine	NG Turbines	1,591	hp	1	3,672
			4,950	hp	1	3,672
			15,000	hp	1	2,400
	Vessels	Support Vessel	1,119	kW	1	612
			2,983	kW	1	1,224
		Support Vessel (Tugs)	19,990	kW	1	612
Well Test	Gas Flare	--	958	scf/hr	1	48

Table E.2-9. Equipment Included in Scenario 3 (Small)

Operation	Equipment Category	Equipment/Vessel Type	Activity	Activity Units	Count	hr/yr
Drilling	Drilling Rig	Drilling-Drillship	2,360	kW	1	1,200
	Vessels	Vessel-Supply Tender	2,237	kW	1	648
		Support Vessel (Crew)	2,983	kW	1	360
		Support Vessel (Tugs)	20,059	kW	1	360
Facility Installation	Vessels	Vessel-Supply Tender	895	kW	1	504
		Support Vessel	416	kW	1	384
			694	kW	1	504
		Support Vessel (Tugs)	925	kW	1	384
Pipeline Installation	Vessels	Pipelaying	418	kW	1	504
			1,193	kW	1	336
		Support Vessel	694	kW	1	504
			925	kW	1	336
			925	kW	1	504
Production	Fugitives	Light Oil (>20 API Gravity)	11,420	Count	1	720
	Process Vent	Gas Venting	1	Count	1	720
	Reciprocating Engine	Diesel Reciprocating Engine (> 600 hp)	572	hp	1	720
	Turbine	NG Turbines	4,950	hp	1	720
	Vessels	Support Vessel	2,983	kW	1	180
Well Test	Gas Flare	--	958	scf/hr	1	144

Table E.2-10. Equipment Included in Scenario 4 (Large)

Operation	Equipment Category	Equipment/Vessel Type	Activity	Activity Units	Count	hr/yr
Production	Fugitives	Light Oil (>20 API Gravity)	11,420	Count	1	8,760
	Heater/Boiler/Burner	NG Heater/Boiler/Burner (<100 MMBtu/hr)	15	MMBtu/hr	1	12,410
	NG Reciprocating Engine	NG 4-cycle Rich Engine	818	hp	3	8,760
	Process Vent	Gas Venting	1	Count	1	8,760
	Reciprocating Engines	Diesel Reciprocating Engine (< 600 hp)	310	hp	1	4,380
		Diesel Reciprocating Engine (> 600 hp)	980	hp	1	52
			6,036	hp	1	1,825
			8,902	hp	1	1,825
	Turbine	NG Turbines	7,000	hp	2	8,760
			142,110	hp	1	8,760
	Vessels	Support Vessel	11,767	kW	1	2,190
	Pneumatic Pumps	Pneumatic Pumps	20,505	SCF/hr	1	8,760
	Pressure Level Controllers	Pressure Level Controllers	196	SCF/hr	1	8,760

Table E.2-11. Equipment Included in Scenario 4 (Medium)

Operation	Equipment Category	Equipment/Vessel Type	Activity	Activity Units	Count	hr/yr
Production	NG Flares	Flare - Pilot	1,100	scf/hr	1	48
	Fugitives	Light Oil (>20 API Gravity)	11,420	Count	1	8,760
	Heater/Boiler/Burner	NG Heater/Boiler/Burner (< 100 MMBtu/hr)	17	MMBtu/hr	1	8,760
	NG Reciprocating Engines	NG 4-cycle Lean Engine	3,300	hp	1	8,760
		NG 4-cycle Rich Engine	3,300	hp	1	8,760
	Reciprocating Engines	Diesel Reciprocating Engine (< 600 hp)	39	hp	2	52
			212	hp	1	52
			275	hp	1	4,380
			500	hp	1	4,380
		Diesel Reciprocating Engine (> 600 hp)	620	hp	1	52
			620	hp	1	416
	Turbine	NG Turbines	5,600	hp	2	8,760
	Vessels	Support Vessel	2,983	kW	1	1,248

Table E.2-12. Equipment Included in Scenario 4 (Small)

Operation	Equipment Category	Equipment/Vessel Type	Activity	Activity Units	Count	hr/yr
Production	NG Flares	Flare - Pilot	860	scf/hr	1	8,760
	Fugitives	Light Oil (> 20 API Gravity)	11,420	Count	1	8,760
	NG Reciprocating Engine	NG 4-cycle Lean Engine	265	hp	1	8,760
	Reciprocating Engines	Diesel Reciprocating Engine (< 600 hp)	350	hp	1	8,760
		Gasoline Reciprocating Engine (< 600 hp)	100	hp	1	104
			350	hp	1	8,760
	Vessels	Support Vessel	11,767	kW	1	2,190

Table E.2-13. Equipment Included in Scenario 5 (Large)

Operation	Equipment Category	Equipment/Vessel Type	Activity	Activity Units	Count	hr/yr
FPSO	NG Flares	Flare - Pilot	860	scf/hr	1	8,760
		Flare - Upsets	11,000	scf/hr	1	120
	FPSO/FSO propulsion	Vessel-FPSO	14,701	kW	1	8,760
	Fugitives	Light Oil (> 20 API Gravity)	11,420	Count	1	8,760
	Heater/Boiler/Burner	NG Heater/Boiler/Burner (<100 MMBtu/hr)	22	MMBtu/hr	1	8,760
			32	MMBtu/hr	1	1,248
	Turbine	NG Turbines	22,167	hp	1	12,410
	Vessels	Pipelaying	15,850	kW	1	288
		Support Vessel (Crew)	3,072	kW	2	1,716
		Support Vessel (Shuttle)	2,434	kW	1	1,248
			8,519	kW	1	480
		Support Vessel (Workboat)	9,247	kW	3	2,080
		Support Vessel (Tugs)	4,313	kW	1	8,760

Table E.2-14. Equipment Included in Scenario 5 (Medium)

Operation	Equipment Category	Equipment/Vessel Type	Activity	Activity Units	Count	hr/yr
FPSO	NG Flares	Flare - Pilot	1,000	scf/hr	1	8,760
		Flare - Upsets	410,000	scf/hr	1	120
	FPSO/FSO propulsion	Vessel-FPSO	14,701	kW	1	8,760
	Fugitives	Light Oil (> 20 API Gravity)	11,420	Count	1	8,760
	Glycol Dehydrator Vent	Glycol Dehydrator Vent	1	Count	1	8,592
	Heater/Boiler/Burner	NG Heater/Boiler/Burner (< 100 MMBtu/hr)	26	MMBtu/hr	1	8,760
	Process Vent	Gas Venting	1	Count	1	8,760
	Reciprocating Engines	Diesel Reciprocating Engine (< 600 hp)	110	hp	1	365
			572	hp	2	52
			572	hp	3	1,825
		Diesel Reciprocating Engine (> 600 hp)	670	hp	2	52
	Tank	Tank Vapors	1	Count	1	8,760
	Turbine	NG Turbines	5,500	hp	1	4,380
			5,500	hp	3	8,760
			14,500	hp	1	8,760
	Vessels	Support Vessel	776	kW	1	6,570
			5,537	kW	1	1,320

Table E.2-15. Equipment Included in Scenario 5 (Small)

Operation	Equipment Category	Equipment/Vessel Type	Activity	Activity Units	Count	hr/yr
FPSO	NG Flares	Flare - Pilot	860	scf/hr	1	3,744
		Flare - Upsets	11,000	scf/hr	1	120
	FPSO/FSO propulsion	Vessel-FPSO	14,701	kW	1	3,744
	Fugitives	Light Oil (> 20 API Gravity)	11,420	Count	1	3,744
	Heater/Boiler/Burner	NG Heater/Boiler/Burner (< 100 MMBtu/hr)	22	MMBtu/hr	1	3,744
			32	MMBtu/hr	1	1,248
	Reciprocating Engines	Diesel Reciprocating Engine (< 600 hp)	572	gal/yr	1	52
	Turbine	NG Turbines	5,500	hp	1	5,304
	Vessels	Support Vessel (Crew)	3,072	kW	1	1,716
		Support Vessel (Shuttle)	776	kW	1	1,248
		Support Vessel (Workboat)	5,537	kW	1	2,080

Appendix E.3

Emission Exemption Threshold Evaluation Vessel Characterization Testing Summary

E.3.1 Introduction

Eastern Research Group, Inc. (ERG) and Alpine Geophysics, LLC (Alpine) conducted dispersion modeling and photochemical modeling to assess whether the Bureau of Ocean Energy Management's (BOEM's) current emission exemption threshold (EET) amounts (E) used in 30 CFR 550.303 need to be revised based on newer National Ambient Air Quality Standards (NAAQS); if necessary, ERG will provide BOEM with options to consider for new EETs. As part of this task, ERG conducted a modeling sensitivity to determine what affect oil and gas support vessel characterization (i.e., as point, volume, or line sources) has on the concentration impacts seen onshore. This appendix summarizes the results of the sensitivity analysis.

The characterization of vessels has the potential to affect modeling results. Current air quality procedures in the Gulf of Mexico Region (GOMR) allow operators to treat vessels as point sources, volume sources, or line sources. When characterized as point sources, each vessel is a single identifiable source of pollutant emissions, typically placed at the platform. Point sources are defined by stack parameters, including temperature, and allow for buoyant plume rise. When characterized as volume sources, vessels are modeled as a three-dimensional source, basically a box, that releases diffuse emissions. When treated as line sources, the emissions are released along a line that stretches from the platform to port. The characterization of vessels as line sources is problematic when implementing the emission exemption threshold equations, because the effective distance to shore becomes zero as the line representing vessel emissions reaches shore. Because of this complication to the emission exemption threshold evaluation, treating the vessels as line sources was not considered in the study or this sensitivity. The goal of this sensitivity is to compare the difference in impacts of treating vessels as point and volume sources on the shoreline.

E.3.2 Model Set Up

ERG first conducted a modeling sensitivity to determine the optimal receptor spacing to provide a common set of receptors for modeling submitted to BOEM. The receptors were placed 100 m apart along the shoreline. The shoreline receptors follow a generalized coastline definition (1:20,000,000 resolution) (U.S. Census Bureau, 2014a), rather than a strict shoreline definition that would follow every coastal feature (1:500,000 resolution) (U.S. Census Bureau, 2014b). This simplifies the receptor placement by not strictly following large coastal features such as bays, lagoons, and mouths of rivers. Figure E.3-1 provides an example of this generalization along the shoreline. The receptors, shown with 100-m spacing receptors, cut across the mouth of a bay and take a straight-line path instead of strictly following the coast. A generalized shoreline was also used to generate receptors along the Louisiana delta coast. Elevation for all receptors was set at sea level.

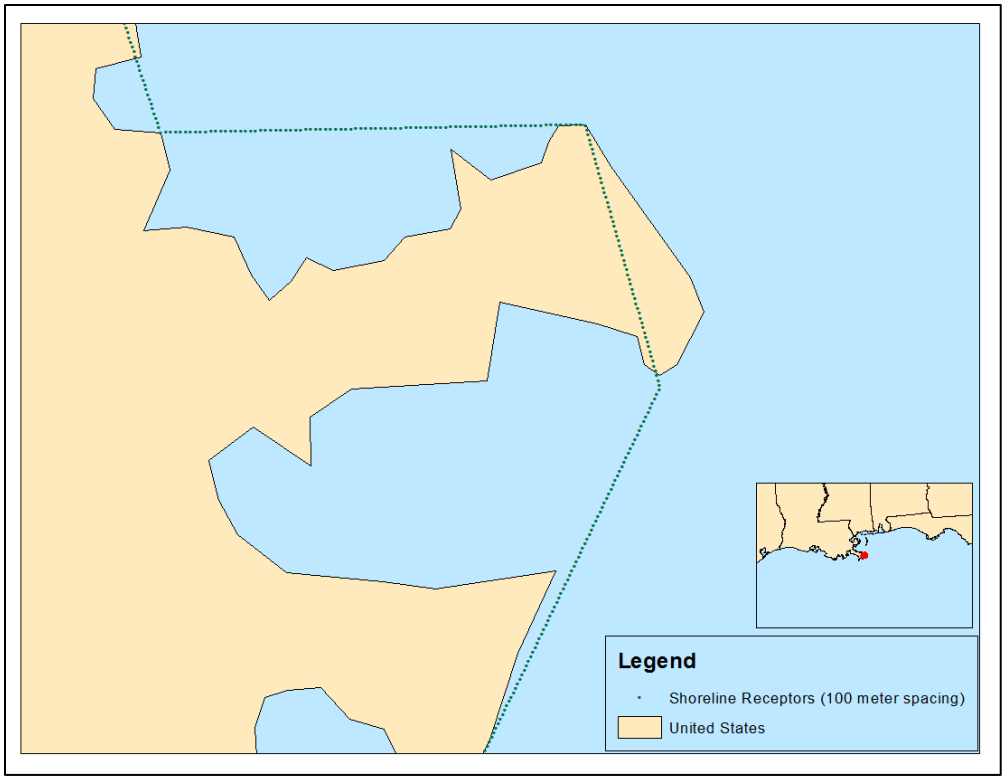

Figure E.3-1. Example of Shoreline 100-m Spaced Receptors Following a Generalized Coastline

To evaluate the impacts of characterizing vessels as point or volume sources, ERG chose 16 locations along the Gulf Coast for the sensitivity modeling (Figure E.3-2). Table E.3-1 lists the distance to shore for each of these locations. Locations were selected to reflect several distances to shore, as well as locations with different shoreline orientations (i.e., north-south or east-west), to consider the effects of location on the impacts.

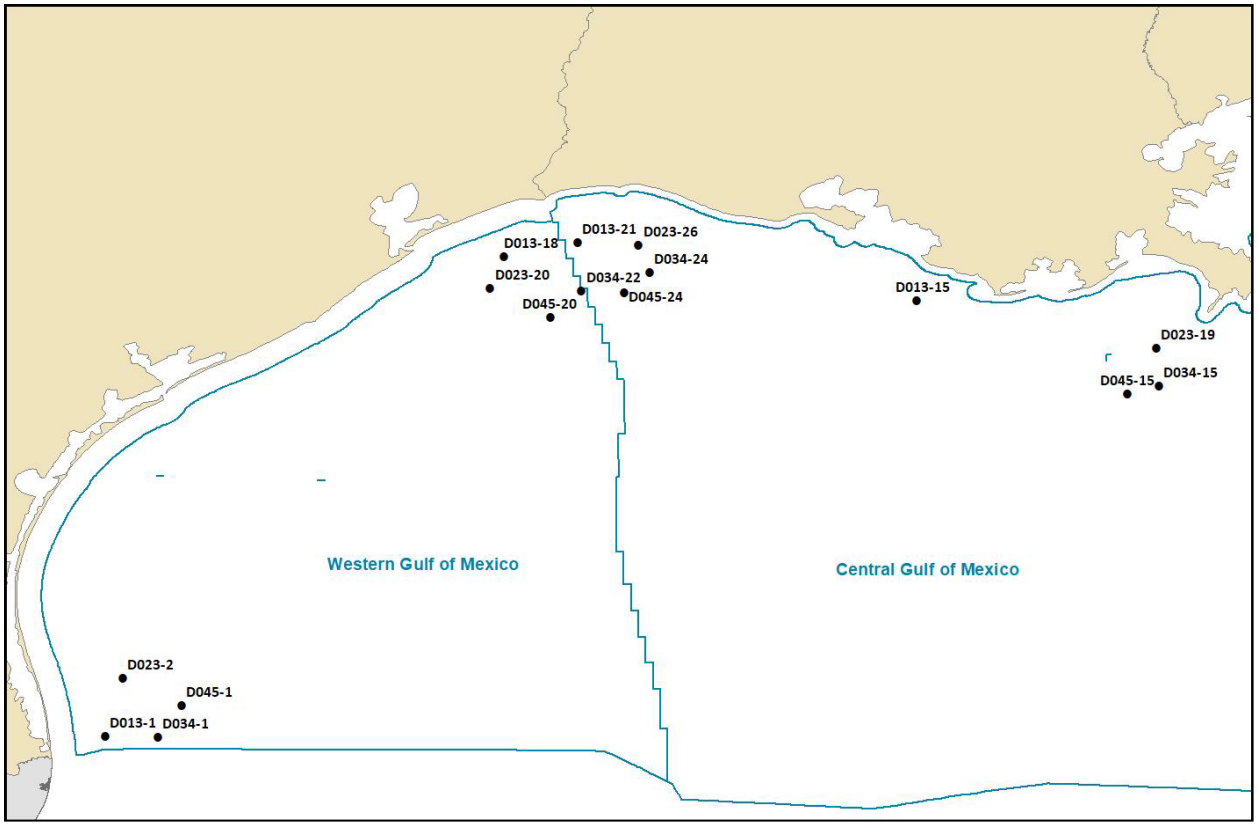

Figure E.3-2. Source Locations for Vessel Testing

Table E.3-1. Modeled Locations

Location	Distance to Shore (statute miles)
D013-1	23.24
D013-15	17.83
D013-18	22.65
D013-21	24.56
D023-19	24.78
D023-2	34.95
D023-20	33.86
D023-26	27.21
D034-1	45.09
D034-15	37.37
D034-22	45.32
D034-24	37.43
D045-1	56.69
D045-15	47.92
D045-20	54.44
D045-24	49.55

Point and volume sources were modeled for six scenarios: 1L, 1M, 1S, 5L, 5M, and 5S. Two different single source scenarios were also modeled: a single vessel as point source (1X) and vessel as volume source (1V). Both single source scenarios were modeled with a unit emissions rate (i.e., 1 g/s).

Table E-3.2 provides the total NO_x emissions for each scenario and brief description of the equipment included. All emissions listed as platform sources were modeled as point sources. A full list of the individual equipment and activity levels is provided in Appendix E.2. Equipment and activity data were derived from publicly available plans for existing platforms to represent typical platform operations. The 1L, 1M, and 1S scenarios represent exploration drilling operations, which is comprised primarily of vessel emissions. The 5L, 5M, and 5S scenarios represent the production operations with an floating production storage and offloading (FPSO). Modeling of the 1X scenario in addition to the 1V scenario allowed a comparison of stack parameters effect on impacts.

Table E.3-2. NO_X Emissions Scenario Summary

Scenario	Emission Rate (g/s)		Equipment
	Platform (Point) Sources	Vessel Sources	
1L	--	582.34	Drillship, prime mover, diesel engine, crew, supply, and tug support vessel
1M	--	203.54	
1S	51.33	0.02	
5L	9.91	335.71	Support vessel, diesel engine, flare or vent, fugitives (default of 11,420 components with light oil stream type), and one FPSO vessel/prime mover
5M	22.63	88.51	
5S	3.19	101.45	
1X	--	1.00	Single vessel as point
1V	--	1.00	Single vessel as volume

Equipment-specific stack parameters for the theoretical sources were determined from average stack parameters from the 2011 Gulfwide inventory (Wilson et al., 2014). To be consistent with the future modeling scenario for the cumulative air quality impacts analysis, separate averages were calculated for equipment on shallow water (depth less than 200 ft) and deep water (depth greater than or equal to 200 ft) platforms. Table E.3-3 lists the equipment-specific stack parameters used in the modeling. Not all equipment types are present under each scenario.

Stack parameters for the vessels are presented in Table E.3-4 and are the same as those used in the USEPA modeling studies (Mason et al., 2008), which were based on several inventory sources.

All selected source locations were in the near-field environment and tested with AERMOD version 16216r using U.S. Environmental Protection Agency (USEPA) standard regulatory default settings. Five years of 4-km grid resolution Weather Research and Forecasting Mesoscale Model (WRF) simulations, representing 2010 through 2014, were used as the meteorological inputs for the sensitivity modeling (described in Section 2 of this report). These hind-cast WRF runs provided a complete meteorological dataset for each year, including upper-air values. Mesoscale model interface (MMIF) version 3.2 was used to output the meteorological data from the WRF modeling output for dispersion modeling locations.

Table E.3-3. Point Source Average Equipment and Vessel Stack Parameters by Water Depth

Equipment Type	Water Depth	Stack Parameter				
		Height (ft)	Diameter (ft)	Temperature (°F)	Flow Rate (ft^3/s)	Velocity (ft/sec)
Boiler/heater/burner (BOI)	Deep	95.85	1.90	471.03	145.45	51.53
	Shallow	82.93	1.19	406.93	34.99	31.48
Diesel or gasoline engine (DIE)	Deep	101.08	0.86	824.48	90.36	153.93
	Shallow	73.81	0.61	836.01	34.23	118.15
Drilling rig (DRI)	Deep	10.00	0.50	70.00	3.93	20.00
	Shallow					
Combustion flare (FLA)	Deep	220.40	1.17	1744.18	36.41	34.00
	Shallow	192.76	1.02	1743.58	47.42	57.97
Fugitives (FUG)	Deep	87.47	0.003	72.00	0	0.0003
	Shallow	62.88				
Glycol dehydrator unit (GLY)	Deep	61.60	0.37	188.10	0.77	7.27
	Shallow	77.35	0.51	202.19	1.82	8.94
Natural gas, diesel, and dual-fuel turbine (NGT)	Deep	119.30	3.32	880.01	2347.29	271.94
	Shallow	74.71	1.98	945.21	566.16	183.28
Storage tank (STO)	Deep	65.60	0.45	76.40	6.45	40.55
	Shallow	67.30	0.49	81.86	2.16	11.21
Cold vent (VEN)	Deep	154.58	0.80	77.46	10.67	21.25
	Shallow	84.88	0.71	73.06	3.40	8.68
Vessels (VES)	Deep	65.6	2.6	539.6	434.6	82.0
	Shallow					
Vessel (1X)	Deep	19.92	0.79	555	-	25
	Shallow					
FPSO	Deep	65.6	2.6	539.6	434.6	82.0
	Shallow					

Table E.3-4. Volume Source Vessel Parameters

Vessel Type	Stack Parameter		
	Height (ft)	Sigma Y(ft)	Sigma Z (ft)
Single Volume Source (1V)	5.00	100.00	5.00
Crew	3.27	25.70	1.52
Drillship	5.87	53.42	2.73
FPSO	5.63	46.89	2.62
Pipelaying	4.23	40.90	1.97
Shuttle	3.27	25.70	1.52
Supply	2.10	14.56	0.98
Support	3.27	25.70	1.52
Tug	2.31	8.18	1.08
Workboat	3.27	25.70	1.52

E.3.3 Results

AERMOD results report the highest value for the averaging time for each receptor. The maximum of the first highest (H1H) value is typically what is compared to the Significant Impact Level (SIL) for a pollutant during a modeling analysis. For this analysis, ERG examined the H1H modeling results for 1-hour, 3-hour, 8-hour, 24-hour averages, which correspond to the averaging periods for the various short-term NAAQS.

In general, the 1-hr average modeling results show a substantial difference in modeling the vessels as volume sources compared to point sources. As shown in Figure E.3-3 for scenario 5L (with support vessel, diesel engine, flare or vent, fugitive, and one FPSO vessel/prime mover emissions), volume sources yield a much higher impact, over 95% greater impact than when vessels were modeled as point sources. Although the overall impact decreases with distance to shore, there is no impact on the percent difference in H1H results between the modeled point and volume sources (i.e., the ratio of point to volume impacts). The volume source impacts are much larger because the emissions are distributed over a larger area than for point sources.

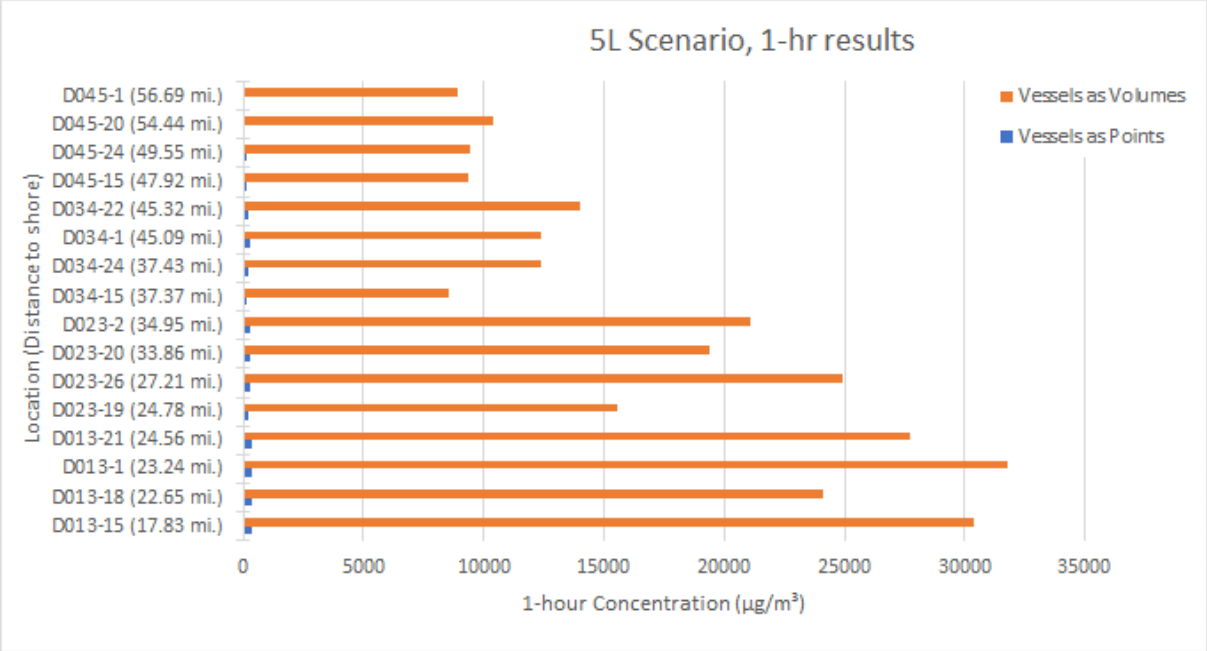

Figure E.3-3. Highest Average 1-hr Concentration Results for the 5L Scenario with Vessels Modeled as Volume and Point Sources

Unlike the other scenarios, the 1S scenario (with drillship/prime mover, crew, supply, and tug support vessel emissions shown in Figure E.3-4) shows the point and volume source concentrations are very close for all locations. This is because the vessel emissions used in this scenario were much lower than the platform emissions due to very low vessel utilization.

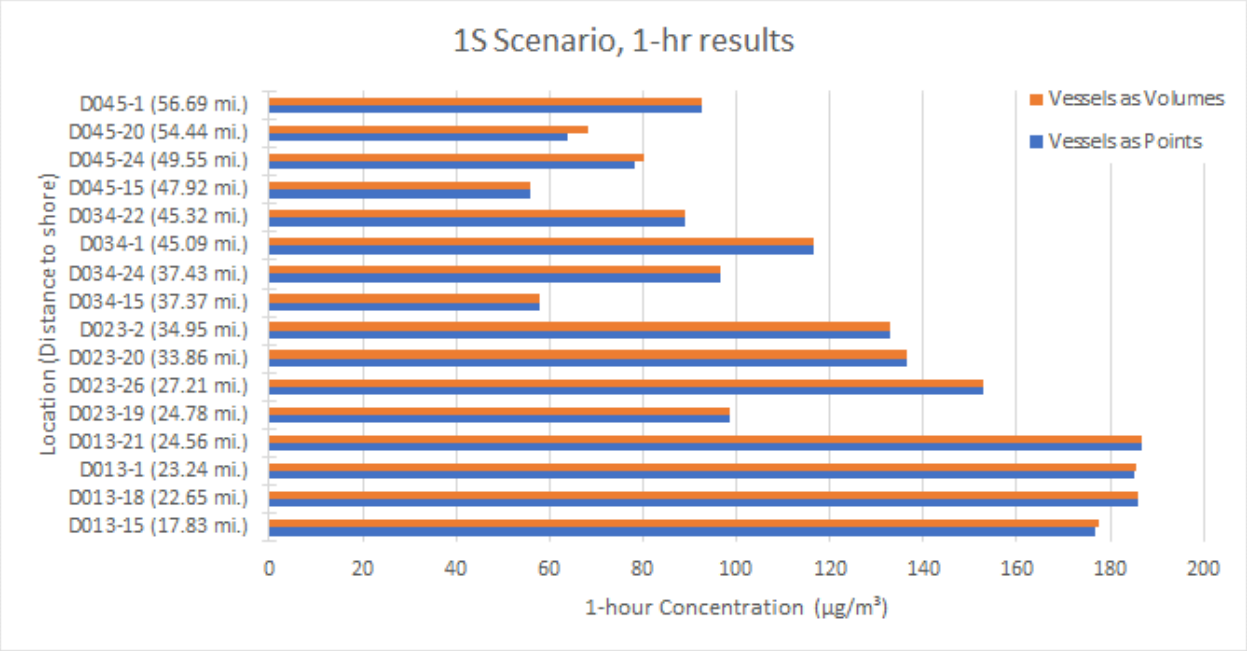

Figure E.3-4. Highest Average 1-hr Concentration Results for the 1S Scenario with Vessels Modeled as Volume and Point Sources

Looking at the single source vessel run comparisons (Figure E.3-5), volume source modeling results in a higher modeled impact even with the same emission rate.

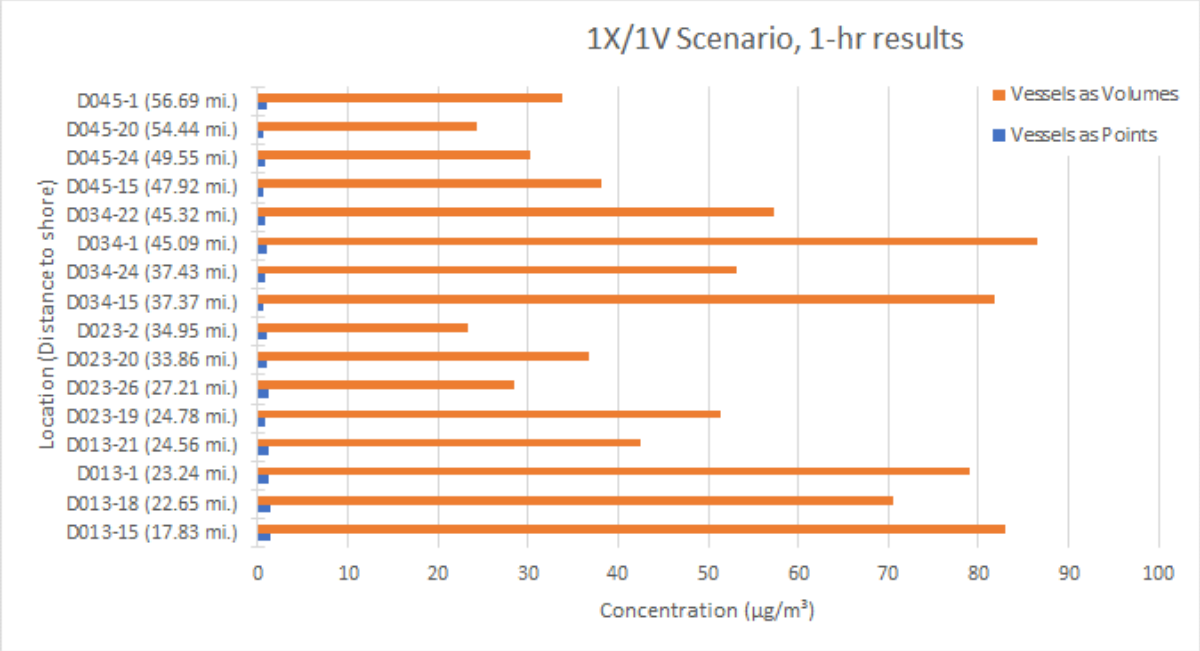

Figure E.3-5. Highest Average 1-hr Point and Volume Concentration Results for 1X/1V Scenarios

Further review of the tabular results for other emission scenarios and for other averaging times shows similar trends, where results for vessels characterized as volumes are greater than the results when they

are modeled as point sources. The difference between the vessel characterizations does decrease with longer averaging times; however, modeling vessels as volume sources still has a notable higher impact than the point source modeling.

E.3.4 Conclusions

AERMOD was used to test the sensitivity of the modeled impact to vessel characterization. Vessels were modeled as point sources or volume sources in several locations spread across the GOMR for eight different emissions levels.

Overall, the characterization of the source had a substantial impact of the modeled impacts. Generally, modeling vessels as volume sources will yield higher impacts than when modeled as point sources. However, when vessels are a small fraction of a complex emissions scenario, like the 1S scenario, the difference in characterization on the overall impact can be minimal. If vessels are a large portion of the emissions, however, or the only source of emissions, the difference is substantial.

For the emission exemption threshold evaluation study, the vessels were characterized as volume sources to provide conservatively high estimates of impacts. Additional study, particularly a field study of vessel emissions, would help to determine the best characterization to use for vessels in GOMR modeling to support BOEM policy decisions.

E.3.5 References

Mason, R., P. Dolwick, P. Carey, E. Kinnee, M. Wilson. 2008. Emissions processing and sensitivity air quality modeling of category 3 commercial marine vessel emissions. In: Proceedings from 17th Annual International Emission Inventory Conference, Portland, OR, 2008 June 04. 14 p.

U.S. Census Bureau. 2014a. Cartographic boundary shapefiles [cb_2014_us_state_500k]. Washington, D.C.: Bureau of the Census, 2014. Available at: https://www.census.gov/geo/maps-data/data/cbf/cbf_state.html

U.S. Census Bureau. 2014b. Cartographic boundary shapefiles [cb_2014_us_state_20m]. Washington, D.C.: Bureau of the Census, 2014. Available at: https://www.census.gov/geo/maps-data/data/cbf/cbf_state.html

Wilson, D., R. Billings, R. Chang, H. Perez, J. Sellers. 2014. Year 2011 Gulfwide Emissions Inventory Study. OCS Study BOEM 2014-666., New Orleans, LA: U.S. Department of Interior, Bureau of Ocean Energy Management, Gulf of Mexico OCS Region.

Appendix E.4

Air Quality Modeling in the Gulf of Mexico Region Study—Emission Exemption Threshold Receptor Testing Summary

Air Quality Modeling in the Gulf of Mexico Region Study—Emission Exemption Threshold Receptor Testing Summary

Prepared by:

Eastern Research Group, Inc.
1600 Perimeter Park Drive, Suite 200
Morrisville, NC 27560

Prepared for:

U.S Department of Interior
Bureau of Ocean Energy Management
45600 Woodland Road
Sterling, VA 20166

Contract Number M14PC00007

March 19, 2019

Contents

Figures

Tables

E.4.1 Introduction

The Bureau of Ocean Energy Management (BOEM) is required under the Outer Continental Shelf Lands Act (OCSLA) 1334(a)(8) to comply with the National Ambient Air Quality Standards (NAAQS) to the extent that offshore oil and gas exploration, development, and production sources on the Outer Continental Shelf (OCS) do not significantly affect the air quality of any state. The BOEM Gulf of Mexico Region (GOMR) office manages the responsible development of oil and gas and mineral resources for the 430 million acres in the Central, Western, and Eastern GOM OCS Planning Areas that constitute the GOMR (Figure E.4-1). Part of this management includes the review of modeling included with Exploration Plans (EPs) and Development Operations Coordination Documents (DOCDs).

On August 26, 2014, BOEM contracted with Eastern Research Group, Inc. (ERG) and team members Ramboll Environ, Inc. (Environ) and Alpine Geophysics, LLC (Alpine) to complete an air quality modeling study in the GOMR. As part of BOEM Contract Number M14PC00007, BOEM requested ERG conduct a modeling sensitivity to determine the optimal receptor spacing to provide a common set of receptors for modeling submitted to BOEM. This would ensure consistency across modeling submitted in support of EPs and DOCDs. This white paper summarizes the preliminary results of the sensitivity analysis.

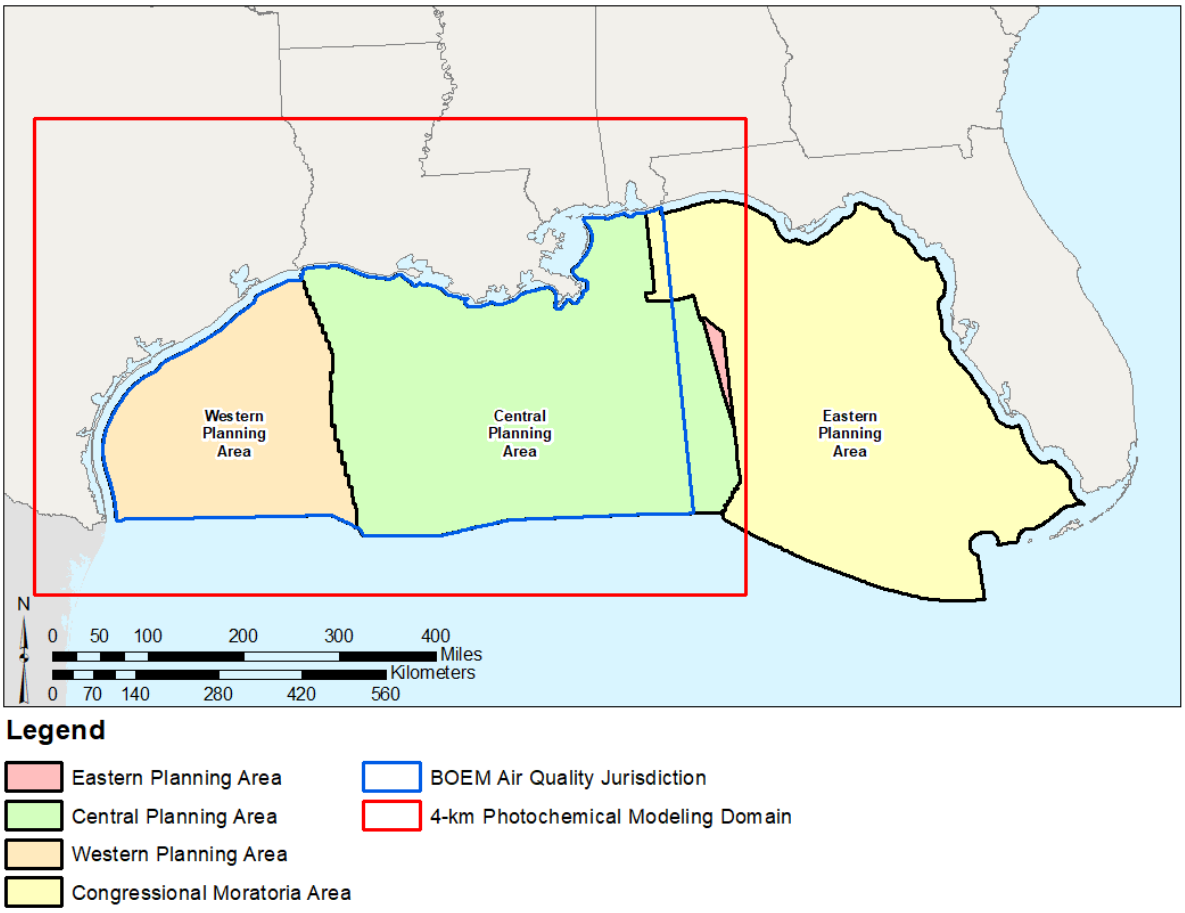

Figure E.4-1. GOMR Planning Areas and Modeling Study Domain (red box)

At issue is that receptor spacing has the potential to affect modeling results, as a receptor must be positioned within the center of the plume to capture peak concentrations. Finer receptor spacing, that is, smaller distance between receptors, typically will have a receptor hit the center of the plume but at the cost of longer model run times. Figure E.4-2 attempts to visually depict this issue. In Figure E.4-2, the coarser receptor spacing (the filled circles) do not have a point within the peak contour of the plume (depicted as the red outline). Instead, the course spacing only picks up on the light green outer edge of the plume. The finer receptor spacing (open circles) does have a receptor within the innermost contour and will report a higher impact.

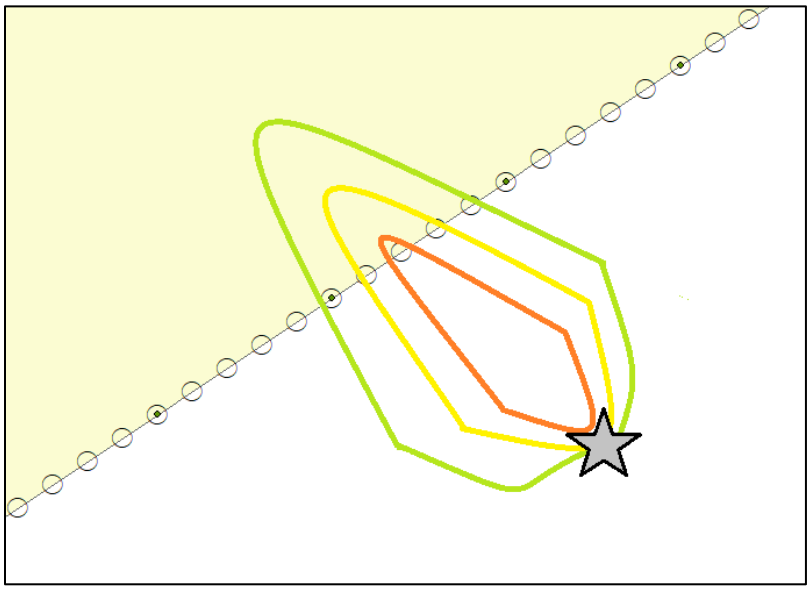

Figure E.4-2. Schematic Demonstrating Coarser Receptors (filled circles) Missing the Peak Plume (red contour)

The goal is to see if there is a receptor spacing that maximizes the impact captured and minimizes the number of receptors used in modeling.

Current BOEM guidance (USDOI, BOEM, 2018) states that a higher number of receptors should be placed along the shoreline where there are the highest concentrations and possible NAAQS exceedances. For U.S. Environmental Protection Agency (USEPA) Region 4 OCS permits in the Eastern GOM Planning Area, the agency has previously requested discrete receptors be placed 25 nautical miles out to sea from the seaward boundaries of Gulf Coast states at 1,000-m intervals (Trinity Consultants, 2013). ERG tested the impact differences for these receptor spacings and more refined receptor spacings to determine if there was an optimal spacing for the GOMR.

E.4.2 Model Set up

ERG started with the initial receptor placement used for the emission exemption threshold evaluation modeling. The receptors were placed 100 m apart along the shoreline. The shoreline receptors follow a generalized coastline definition (1:20,000,000 resolution) (U.S. Census Bureau, 2014a), rather than a strict shoreline definition that would follow every coastal feature (1:500,000 resolution) (U.S. Census Bureau, 2014b). This simplifies the receptor placement by not strictly following large coastal features, such as bays, lagoons, and mouths of rivers. Figure E.4-3 provides an example of this generalization along the shoreline. The receptors, shown with 100-m spacing, cut across the mouth of a bay and take a straight-line path instead of strictly following the coast. A generalized shoreline was also used to generate receptors along the Louisiana delta coast. The receptors 100-meter spacing were then subset to provide receptors with 200-, 250-, 300-, 350-, 400-, 450-, 500-, 1,000-, and 5,000-meter spacing for testing. Elevation for all receptors was set at sea level.

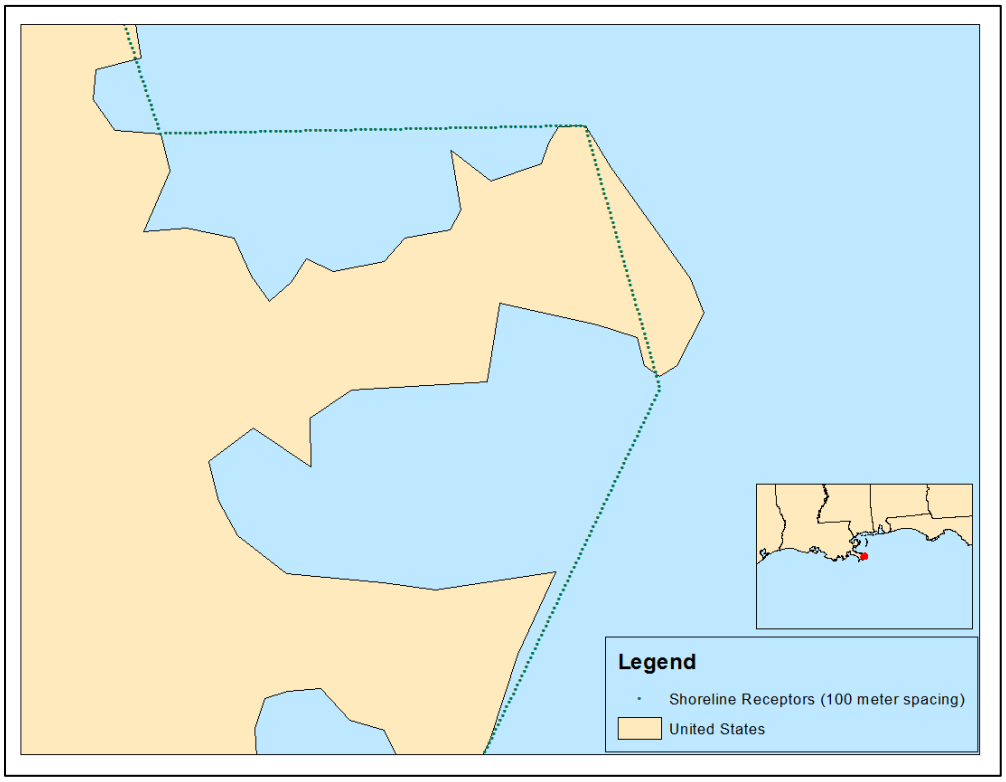

Figure E.4-3. Example of Shoreline 100-m Spaced Receptors Following a Generalized Coastline

ERG modeled three different sources: a cold short stack (1C), a hot tall stack (1P), and a volume source (1V) to replicate a vessel source. This allowed the testing of the generalization of the types of equipment seen on platforms, and how receptor spacing might affect the estimation of impact of each. Tables E.4-1 and E.4-2 contain the source parameters that are used to characterize the emission sources in the modeling. The 1C (for a short vent) and the 1P source parameters match the natural gas engine parameters used in study's modeling inventory.

For the 1V source parameters (Table E.4-2), vessel dimensions needed to define volume sources were obtained from the PortVision Automatic Identification System (AIS) database (described in

BOEM's Year 2014 Gulfwide Emissions Inventory study report [Wilson et al., 2017]) based on vessels known to operate in the GOMR. These dimensions were used to determine the average dimension for each vessel type. These average vessels were then merged to produce an average vessel for modeling.

Table E.4-1. Source Parameters for 1C and 1P Scenarios

Scenario	Height (m)	Diameter (m)	Exit Velocity (m/s)	Exit Temperature (degree K)
1C	12	0.73	10.5	0
1P	28.75	0.44	42.7	832

Table E.4-2. Source Parameters for 1V Scenario

Scenario	Height (m)	Sigma Y	Sigma Z
1V	5	100	5

All sources were modeled with the same emissions rate (i.e., emissions equal to 1 g/s, which is equivalent to 7.9 lb/hr) to remove impact variance due to emission rate.

ERG chose three locations at random for the sensitivity modeling (D013-6, D023-26, and D034-26). Figure E.4-4 shows these locations in the Western and Central GOM Planning Areas, and the difference in the curvature of the shoreline associated with the nearest onshore area. The distances from shore varied with each location and with the features of the coastline (Table E.4-3).

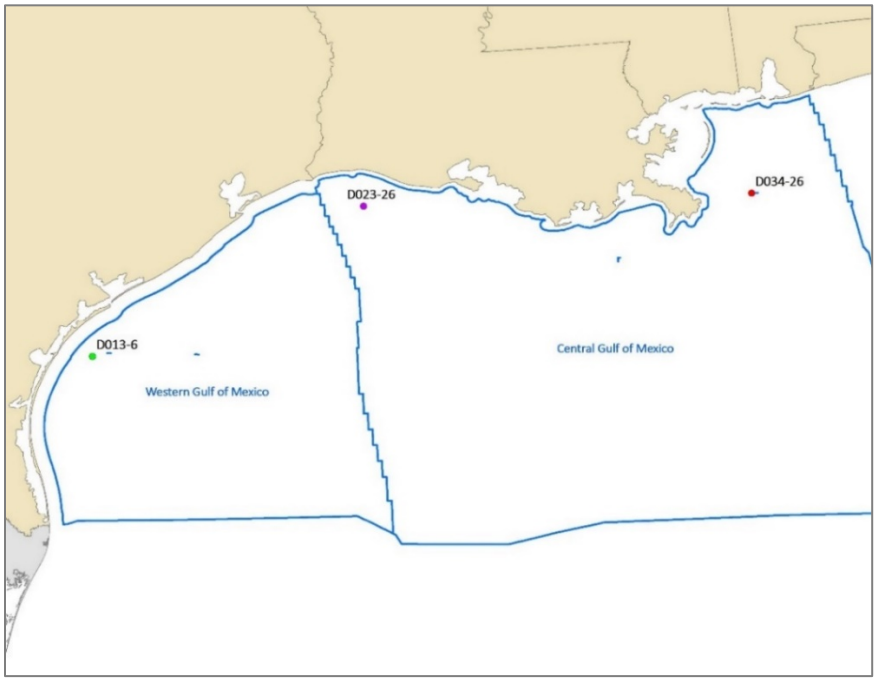

Figure E.4-4. Source Locations for Receptor Testing

Table E.4-3. Modeled Locations

Location	Distance to Shore (miles)
D013-6	22.91
D023-26	27.21
D034-26	38.18

All source locations selected were in the near-field environment and modeled with AERMOD version 16216r using the USEPA standard regulatory default settings.

Consistent with near-field modeling conducted for this study, 5 years of 4-km grid resolution WRF simulations, representing 2010 through 2014, were used for the sensitivity modeling. These hind-cast WRF runs provided a complete meteorological dataset for each year and included upper-air values. MMIF version 3.2 was used to output the needed meteorological data from the WRF modeling output for dispersion modeling for the proposed synthetic locations.

E.4.3 Results

AERMOD results report the highest value for the averaging time for each receptor. The maximum of these first highest receptors impact (H1H) is the value that is compared to the significant impact level (SIL) for a pollutant during a modeling analysis. For this analysis, ERG examined the H1H modeling results for 1-hour, 3-hour, 8-hour, and 24-hour averages, which correspond to the averaging periods for the various short-term NAAQS. In the absence of observed data, ERG used the 100-m spacing results as a baseline for comparison, as the refined spacing should capture the peak of the plume.

In general, the 1-hour average modeling results (Figure E.4-5) for each receptor spacing show little variability for each location-emission scenario combination. The coarser receptor spacing generally yields equal or lower impacts than the 100-m spacing. The 5,000-m spacing can have significantly lower impacts than the other tested spacings.

With each scenario, the impact diminishes as the source location moves further away from shore. The further from shore the emissions occur, the lower the impact onshore. This is expected, as the plume has more time to disperse due to the resulting concentration becoming diluted over a larger area.

Figures E.4-6, E.4-7, and E.4-8 offer a closer look at the single source runs 1V (vessel as volume), 1C (cold short stack), and 1P (hot tall stack) scenarios. From these figures, it is easier to see the variability in results due to receptor spacing for each location. For each emissions scenario, the variability decreases the further from shore the location is. For example, differences between the 100-m run and the other receptor spacing for the 1C D013-6 runs varies from 0.00–9.67 micrograms per cubic meter ($\mu g/m^3$). For the 1C D034-26 runs, the difference ranges from 0.00–3.33 $\mu g/m^3$.

Further review of the tabular results (Tables E.4-4 through E.4-6 and Figures E.4-9 through E.4-11) for other averaging times shows similar trends, and results for emission sources further from shore have less variability in H1H impact for the receptor spacing tested. Furthermore, the longer NAAQS averaging periods (i.e., 8-hour and 24-hour) also show less sensitivity to receptor spacing.

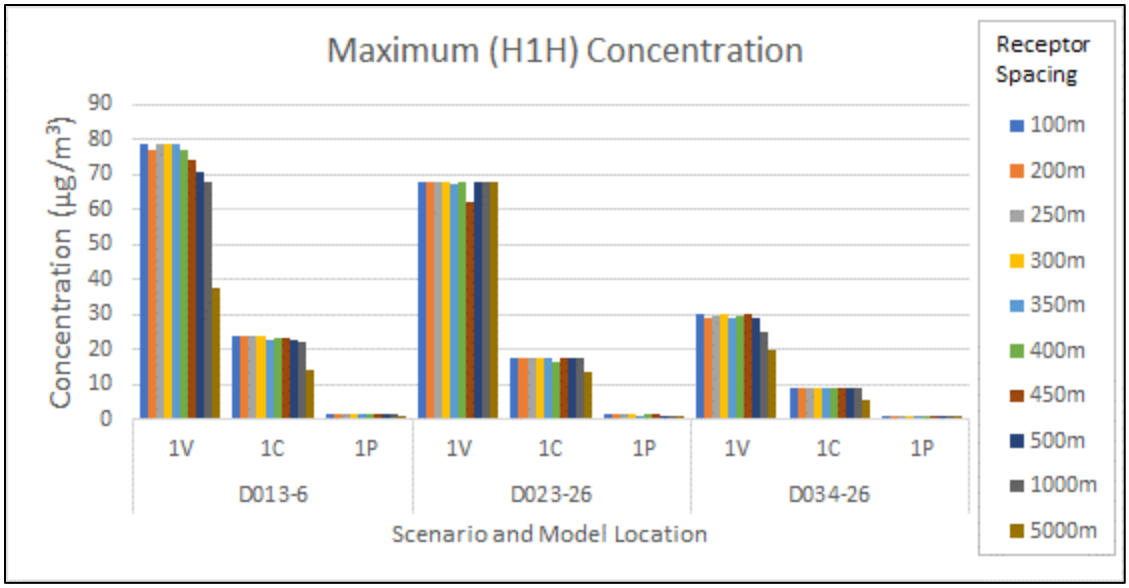

Figure E.4-5. Highest Average 1-hr Concentration Results

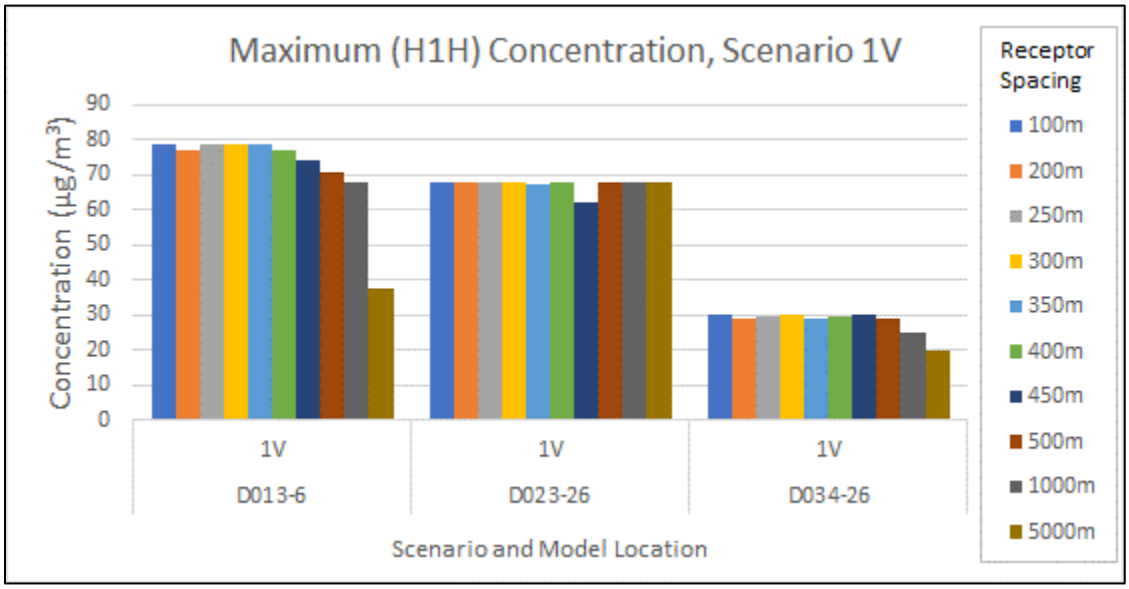

Figure E.4-6. Highest Average 1-hr Concentration Results for 1V Results
Sensitivity results for a single vessel source, modeled as a volume at 1 gram per second emission rate.

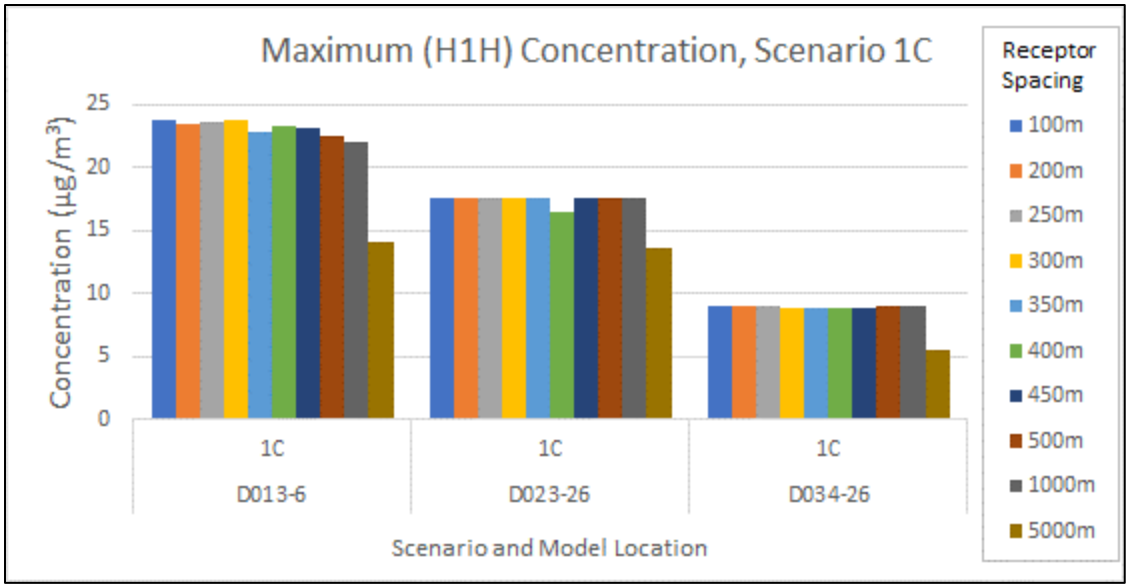

Figure E.4-7. Highest Average 1-hr Concentration Results for 1C Results
Sensitivity results for a single short cold stack, modeled at 1 gram per second emission rate.

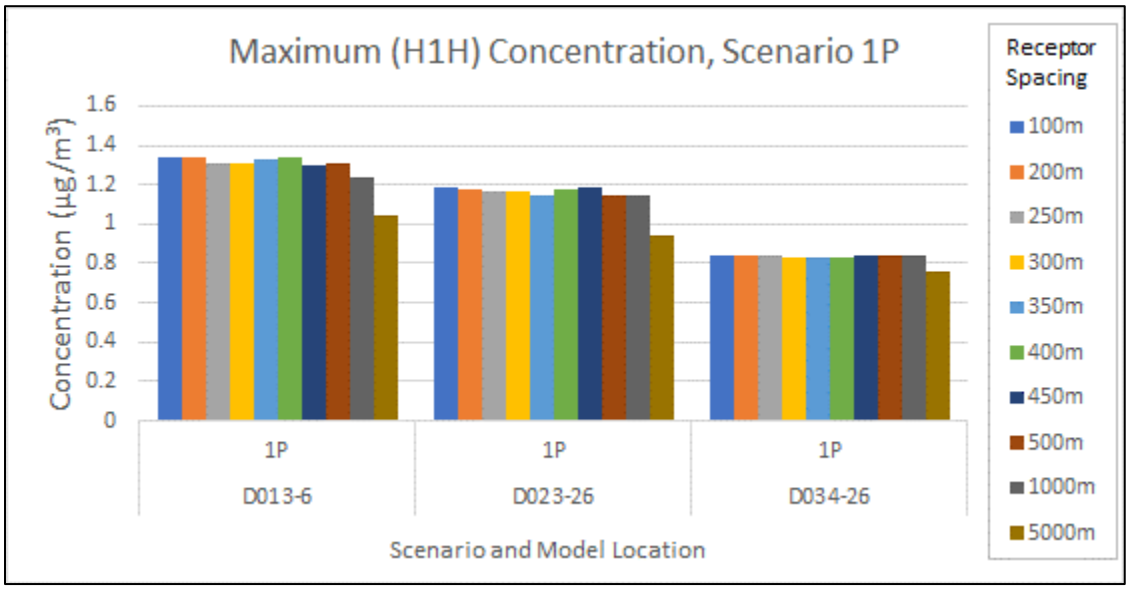

Figure E.4-8. Highest Average 1-hr Concentration Results for 1P Results
Sensitivity results for a single tall hot stack, modeled at 1 gram per second emission rate.

Table E.4-4. 1C Scenario Results

Scenario	Location	Spacing (m)	1-Hour [µg/m³]	3-Hour [µg/m³]	8-Hour [µg/m³]	24-Hour [µg/m³]
1C	D013-6	100	23.79	7.94	4.42	1.48
1C	D013-6	200	23.51	7.85	4.42	1.48
1C	D013-6	250	23.66	7.90	4.41	1.47
1C	D013-6	300	23.79	7.94	4.41	1.47
1C	D013-6	350	22.88	7.64	4.41	1.47
1C	D013-6	400	23.35	7.79	4.29	1.43
1C	D013-6	450	23.11	7.71	4.41	1.47
1C	D013-6	500	22.54	7.52	4.41	1.47
1C	D013-6	1,000	22.03	7.35	3.55	1.20
1C	D013-6	5,000	14.12	4.73	2.47	0.83
1C	D023-26	100	17.57	7.46	2.80	0.93
1C	D023-26	200	17.57	7.46	2.80	0.93
1C	D023-26	250	17.57	7.44	2.79	0.93
1C	D023-26	300	17.57	7.46	2.80	0.93
1C	D023-26	350	17.52	7.44	2.79	0.93
1C	D023-26	400	16.46	7.40	2.77	0.92
1C	D023-26	450	17.57	7.34	2.75	0.92
1C	D023-26	500	17.57	7.40	2.77	0.92
1C	D023-26	1,000	17.57	7.40	2.77	0.92
1C	D023-26	5,000	13.54	4.52	1.70	0.58
1C	D034-26	100	8.99	3.00	1.13	0.38
1C	D034-26	200	8.94	2.98	1.12	0.38
1C	D034-26	250	8.94	2.98	1.12	0.38
1C	D034-26	300	8.85	2.95	1.11	0.37
1C	D034-26	350	8.84	2.95	1.11	0.37
1C	D034-26	400	8.85	2.95	1.11	0.37
1C	D034-26	450	8.85	2.95	1.11	0.37
1C	D034-26	500	8.94	2.98	1.12	0.38
1C	D034-26	1,000	8.94	2.98	1.12	0.04
1C	D034-26	5,000	5.52	2.04	0.76	0.34

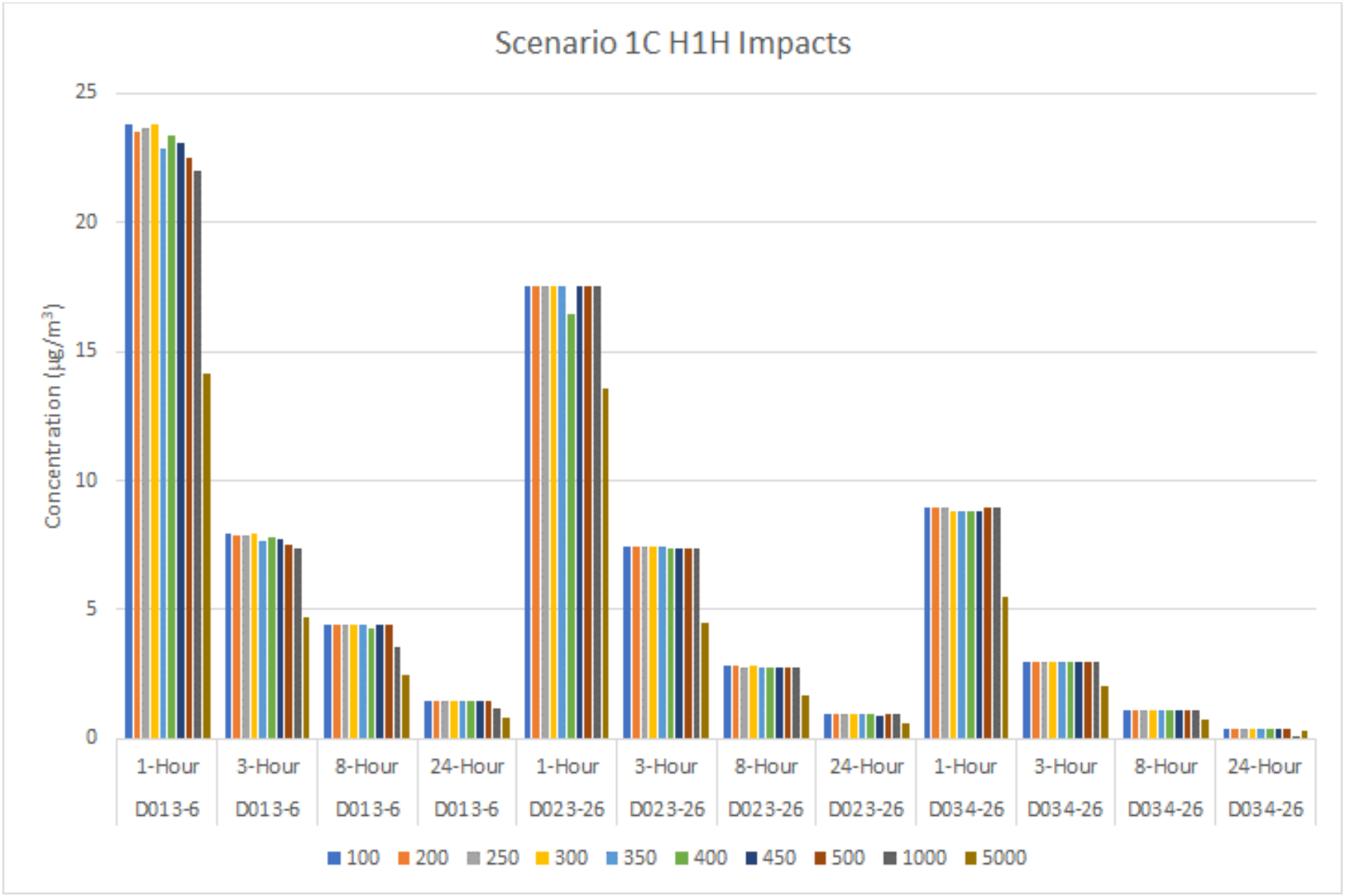

Figure E.4-9 Scenario 1C Modeled Impacts by Location and Averaging Time

Table E.4-5. 1P Scenario Spacing Results

Scenario	Location	Spacing (m)	1-Hour [µg/m³]	3-Hour [µg/m³]	8-Hour [µg/m³]	24-Hour [µg/m³]
1P	D013-6	100	1.34	0.76	0.56	0.24
1P	D013-6	200	1.34	0.75	0.56	0.24
1P	D013-6	250	1.31	0.76	0.56	0.24
1P	D013-6	300	1.31	0.76	0.56	0.24
1P	D013-6	350	1.33	0.74	0.55	0.24
1P	D013-6	400	1.34	0.75	0.56	0.23
1P	D013-6	450	1.30	0.72	0.56	0.23
1P	D013-6	500	1.31	0.76	0.55	0.24
1P	D013-6	1,000	1.24	0.66	0.55	0.24
1P	D013-6	5,000	1.05	0.57	0.44	0.17
1P	D023-26	100	1.18	0.59	0.39	0.18
1P	D023-26	200	1.17	0.59	0.39	0.18
1P	D023-26	250	1.17	0.59	0.39	0.18
1P	D023-26	300	1.17	0.59	0.39	0.18
1P	D023-26	350	1.15	0.59	0.39	0.18
1P	D023-26	400	1.17	0.59	0.38	0.18
1P	D023-26	450	1.18	0.59	0.39	0.18
1P	D023-26	500	1.15	0.59	0.38	0.18
1P	D023-26	1,000	1.15	0.59	0.38	0.18
1P	D023-26	5,000	0.95	0.50	0.28	0.14
1P	D034-26	100	0.84	0.46	0.17	0.08
1P	D034-26	200	0.84	0.46	0.17	0.08
1P	D034-26	250	0.84	0.46	0.17	0.08
1P	D034-26	300	0.83	0.45	0.17	0.08
1P	D034-26	350	0.83	0.46	0.17	0.08
1P	D034-26	400	0.84	0.45	0.17	0.08
1P	D034-26	450	0.84	0.45	0.17	0.08
1P	D034-26	500	0.84	0.45	0.17	0.08
1P	D034-26	1,000	0.84	0.45	0.17	0.08
1P	D034-26	5,000	0.75	0.27	0.11	0.05

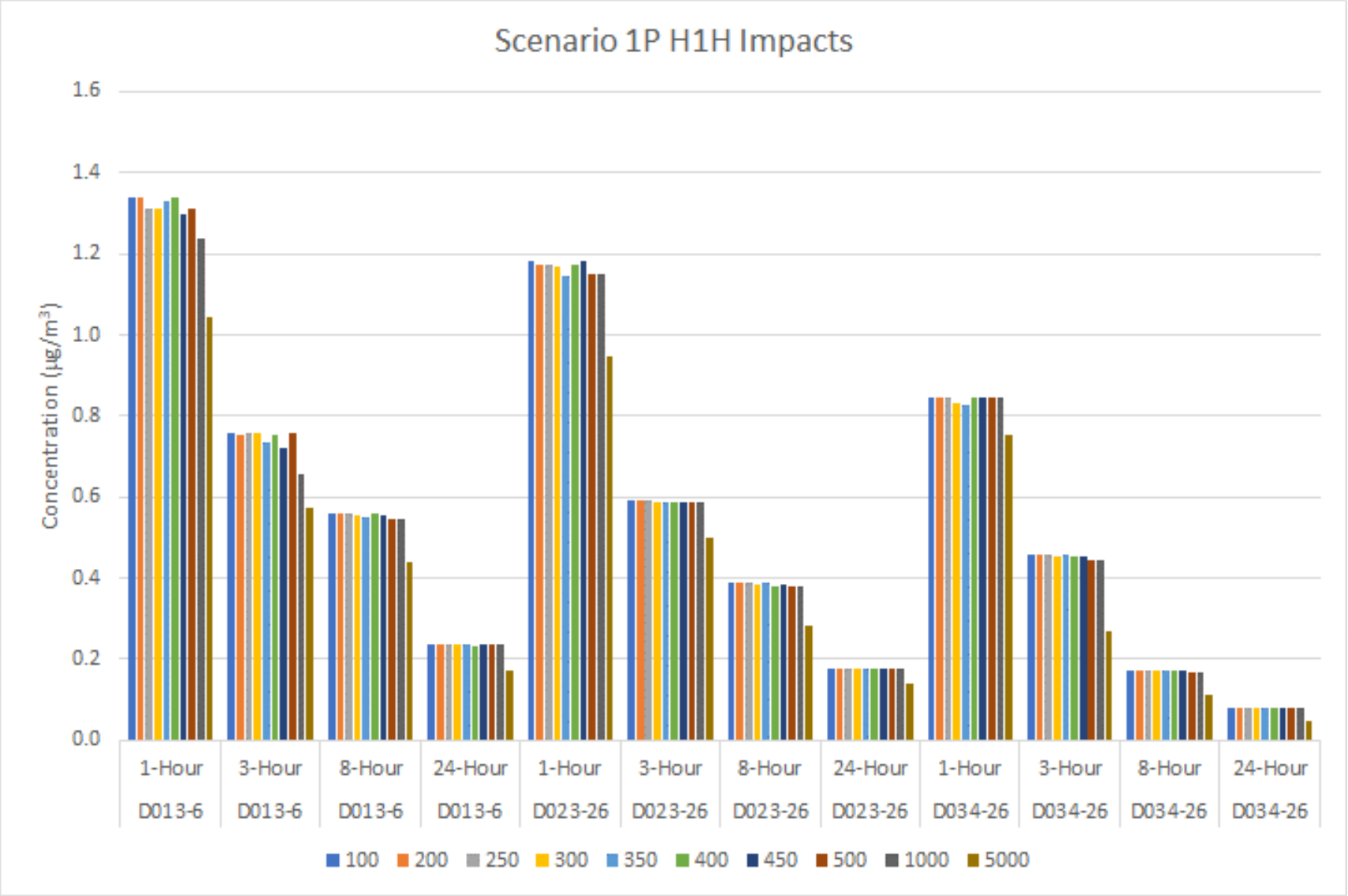

Figure E.4-10 Scenario 1P Modeled Impacts by Location and Averaging Time

Table E.4-6. 1V Scenario Results

Scenario	Location	Spacing (m)	1-Hour [µg/m³]	3-Hour [µg/m³]	8-Hour [µg/m³]	24-Hour [µg/m³]
1V	D013-6	100	79.03	29.97	12.88	3.92
1V	D013-6	200	77.01	29.88	12.84	3.91
1V	D013-6	250	78.55	29.88	12.84	3.91
1V	D013-6	300	79.03	29.33	12.60	3.84
1V	D013-6	350	78.55	29.88	12.84	3.91
1V	D013-6	400	77.01	29.33	12.60	3.84
1V	D013-6	450	74.49	29.33	12.60	3.84
1V	D013-6	500	70.76	29.88	12.84	3.91
1V	D013-6	1,000	67.66	29.88	12.84	3.91
1V	D013-6	5,000	37.30	14.25	5.34	1.80
1V	D023-26	100	68.16	22.72	12.76	4.26
1V	D023-26	200	68.16	22.72	12.58	4.20
1V	D023-26	250	68.16	22.72	12.58	4.20
1V	D023-26	300	68.16	22.72	12.58	4.20
1V	D023-26	350	67.24	22.42	12.27	4.09
1V	D023-26	400	68.16	22.72	12.58	4.20
1V	D023-26	450	62.43	20.82	11.43	3.81
1V	D023-26	500	68.16	22.72	12.58	4.20
1V	D023-26	1,000	68.16	22.72	12.58	4.20
1V	D023-26	5,000	68.16	22.72	12.58	4.20
1V	D034-26	100	29.82	9.94	3.73	1.30
1V	D034-26	200	28.69	9.57	3.59	1.27
1V	D034-26	250	29.46	9.82	3.68	1.28
1V	D034-26	300	29.82	9.94	3.73	1.27
1V	D034-26	350	28.69	9.57	3.59	1.28
1V	D034-26	400	29.76	9.92	3.72	1.26
1V	D034-26	450	29.82	9.94	3.73	1.27
1V	D034-26	500	28.69	9.57	3.59	1.27
1V	D034-26	1,000	24.83	8.28	3.11	1.09
1V	D034-26	5,000	19.66	6.55	2.81	0.86

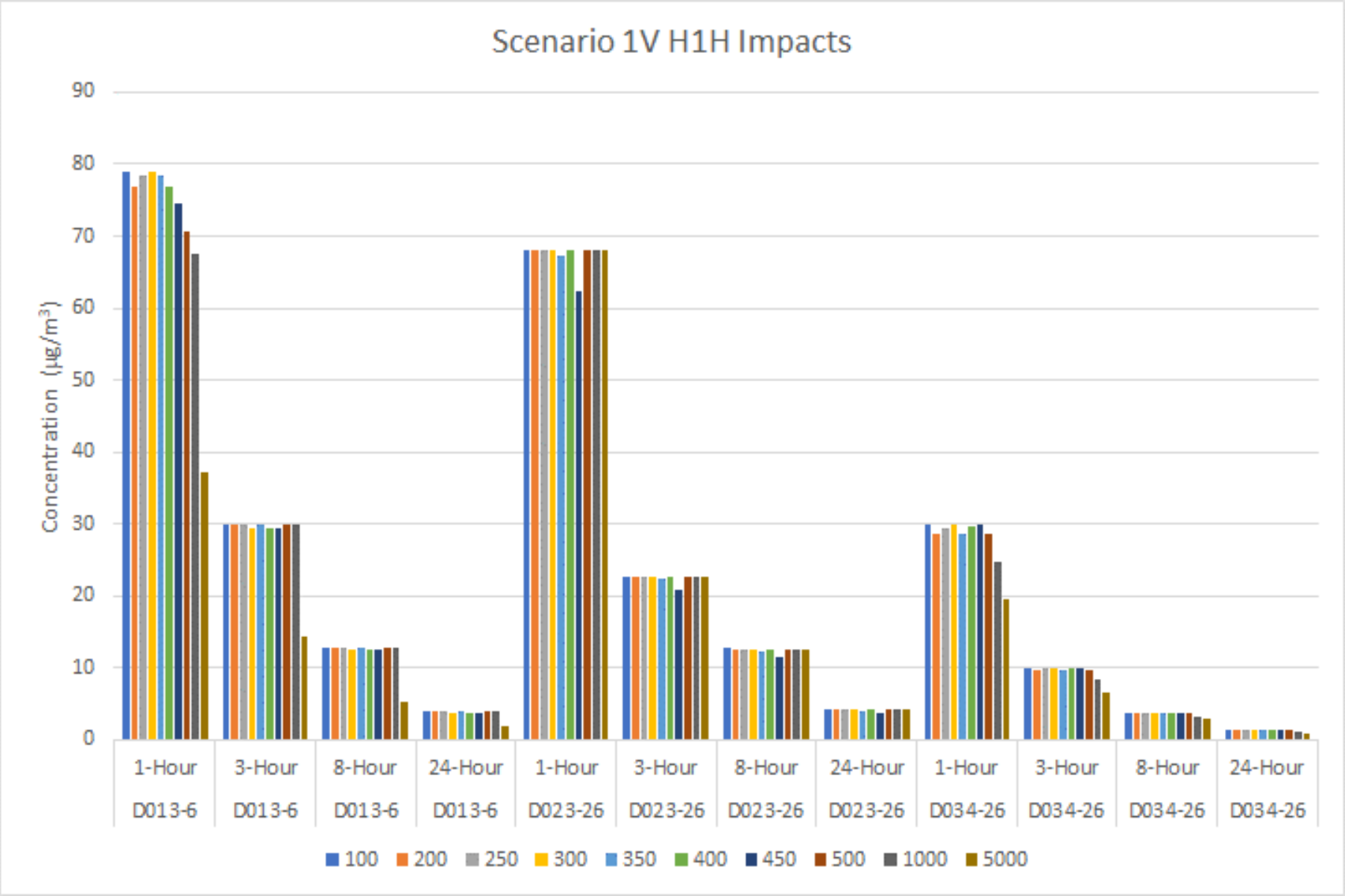

Figure E.4-11 Scenario 1V Modeled Impacts by Location and Averaging Time

E.4.4 Conclusions

AERMOD was used to test sensitivity of receptors at 100-, 200-, 250-, 300-, 350-, 400-, 450- and 500-m spacing for a cold short stack (1C), hot tall stack (1P), and volume source (1V) scenarios at three distances from shore along the Gulf Coast. ERG used the 100-m receptor spacing as the "truth" of the peak concentration in the plume to compare all other receptor spacings. The receptor spacing is most important close to shore, where the highest average concentration value captured by the 100-m receptors can be much larger than coarser receptor spacing, especially at shorter averaging times. As distance from shore increases, the difference between highest value of concentration of the receptor spacings decreases.

The type of source modeled (that is, point versus volume) also affects the ability of the coarser resolutions to capture the peak plume concentration. Volume sources had more variability in the peak impact captured, even for sources further away from the receptors. This is likely due to the initial characterization of volume sources, as the initial plume starts as a broader plume than point sources. Therefore, the resultant impact field would be broader and likely more varied in concentration, especially at shorter averaging times. Longer averaging times would smear the peaks—that is, hourly peaks would average out into broader areas as the location of peaks changes with hourly changes in wind direction.

To standardize the receptor placement for BOEM modeling efforts, BOEM revised their modeling guidance in 2018 to recommend the use of a higher number of receptors placed in areas along the shoreline where the highest concentrations, and possible NAAQS exceedances, are possible. BOEM will continue to assess receptor spacing and will provide future guidance, as necessary. The receptors used in this study have been provided to BOEM, should they elect to release them, as a common set of receptors as a starting point for operators/lessees.

BOEM may consider revisiting this analysis after any new tracer studies are conducted for the GOMR. A tracer study would provide the opportunity to compare modeled results directly with observed values to determine if the peak plumes are being captured.

E.4.5 References

U.S. Census Bureau. 2014a. Cartographic Boundary Shapefiles [cb_2014_us_state_500k]. Washington, D.C.: Bureau of the Census, 2014. Internet address: https://www.census.gov/geo/maps-data/data/cbf/cbf_state.html

U.S. Census Bureau. 2014b. Cartographic Boundary Shapefiles [cb_2014_us_state_20m]. Washington, D.C.: Bureau of the Census, 2014. Internet address: https://www.census.gov/geo/maps-data/data/cbf/cbf_state.html

USDOI, BOEM (U.S. Department of the Interior, Bureau of Ocean Energy Management). 2018. BOEM's GOMR Dispersion Modeling Guidelines. January 2018. Internet address: https://www.boem.gov/Dispersion-Modeling-Guidelines/ (accessed March 19, 2019).

Trinity Consultants. 2013. Air Quality Dispersion Modeling Protocol Anadarko Petroleum Corporation. EGOM Completion and Maintenance Project. May 2013. Submitted as part of EPA docketEPA-R04-OAR-2014-0487-0010. Internet address: https://www.regulations.gov/docket?D=EPA-R04-OAR-2014-0487 (accessed October 27, 2017).

Wilson, D., R. Billings, R. Chang, S. Enoch, B. Do, H. Perez, and J. Sellers. 2017. Year 2014 Gulfwide Emissions Inventory Study. U.S. Dept. of the Interior, Bureau of Ocean Energy Management, Gulf of Mexico OCS Region, New Orleans, LA. OCS Study BOEM 2017-044.

Appendix E.5

Emission Exemption Threshold Evaluation Results

This appendix presents scatter plots for all pollutants. The scatter plots show all distance and emissions combinations modeled. These points are color coded based on the error type seen, with the black line indicating the current emission exemption threshold (EET) formula (33.3*D for all pollutants except carbon monoxide (CO) and $3400\times(D)^{(2/3)}$ for CO).

Figures E.5-1 through E.5-5 show three outcomes with respect to the EET analysis:

- **Pass (a correct evaluation):** Emissions from the scenario were above the EET threshold, which indicated modeling was needed and the modeling impacts were above the significant impact level (SIL), or emissions from the scenario were below the EET threshold, which indicated modeling was not needed and the modeled impacts were below the SIL.
- **False positive (Type I error):** Emissions from the scenario were above the EET threshold, which indicated modeling was needed; however, the modeled impact was below the SIL.
- **False negative (Type II error):** Emissions from the scenario were below the EET threshold, which indicated modeling was not necessary; however, the modeled impact was above the SIL.

Most of the false negative Type II errors occur closer to shore, which makes sense as the near shore location would not have a lot of time to disperse could have higher impact. Most of the false positive Type I errors occur at further distances to shore, with lower emissions rates.

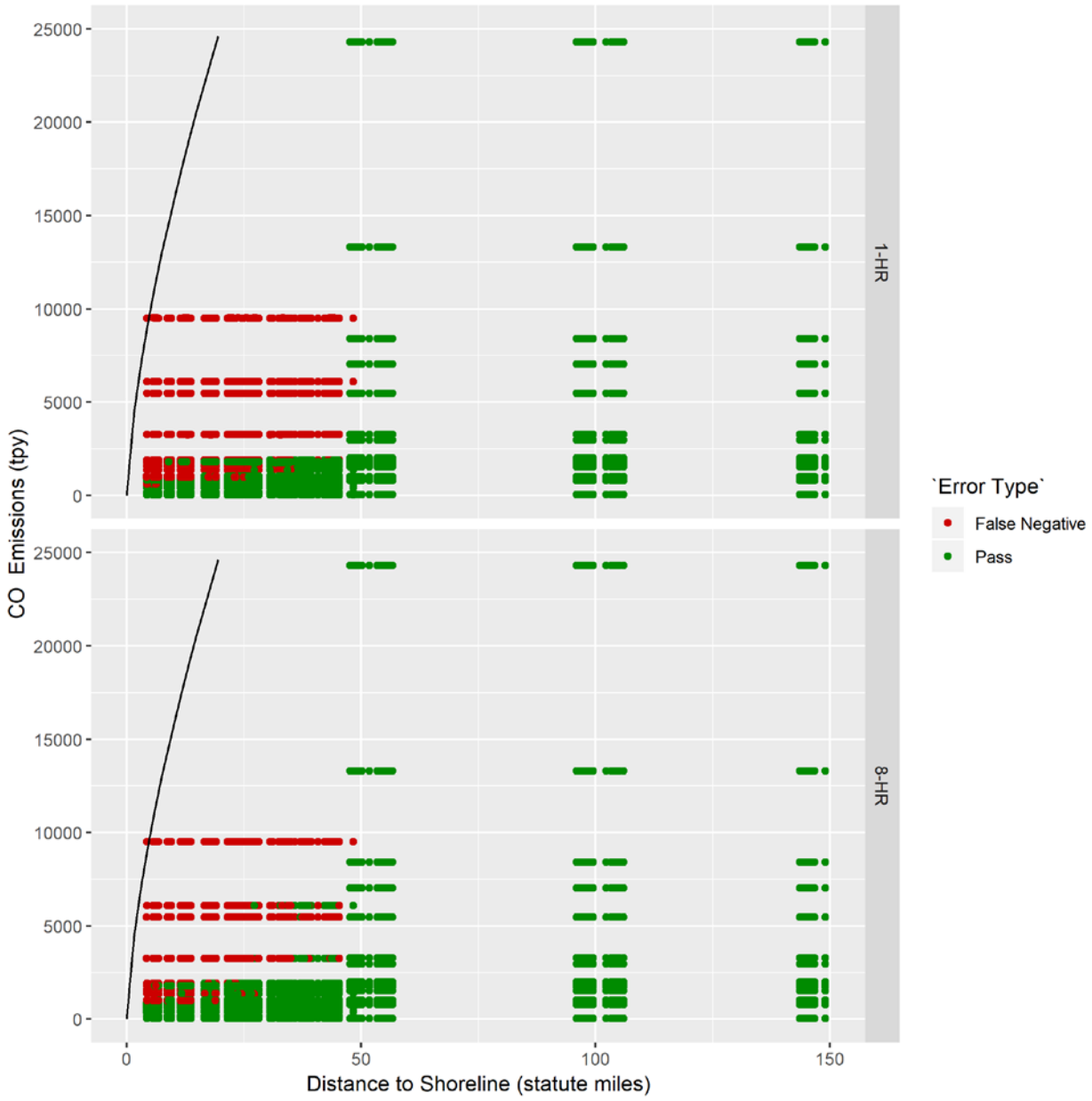

Figure E.5-1. Scatter Plot of CO 1-hour (top) and 8-hour (bottom) Modeling Results at the Shoreline

Black line indicates the current formulation of the EET.

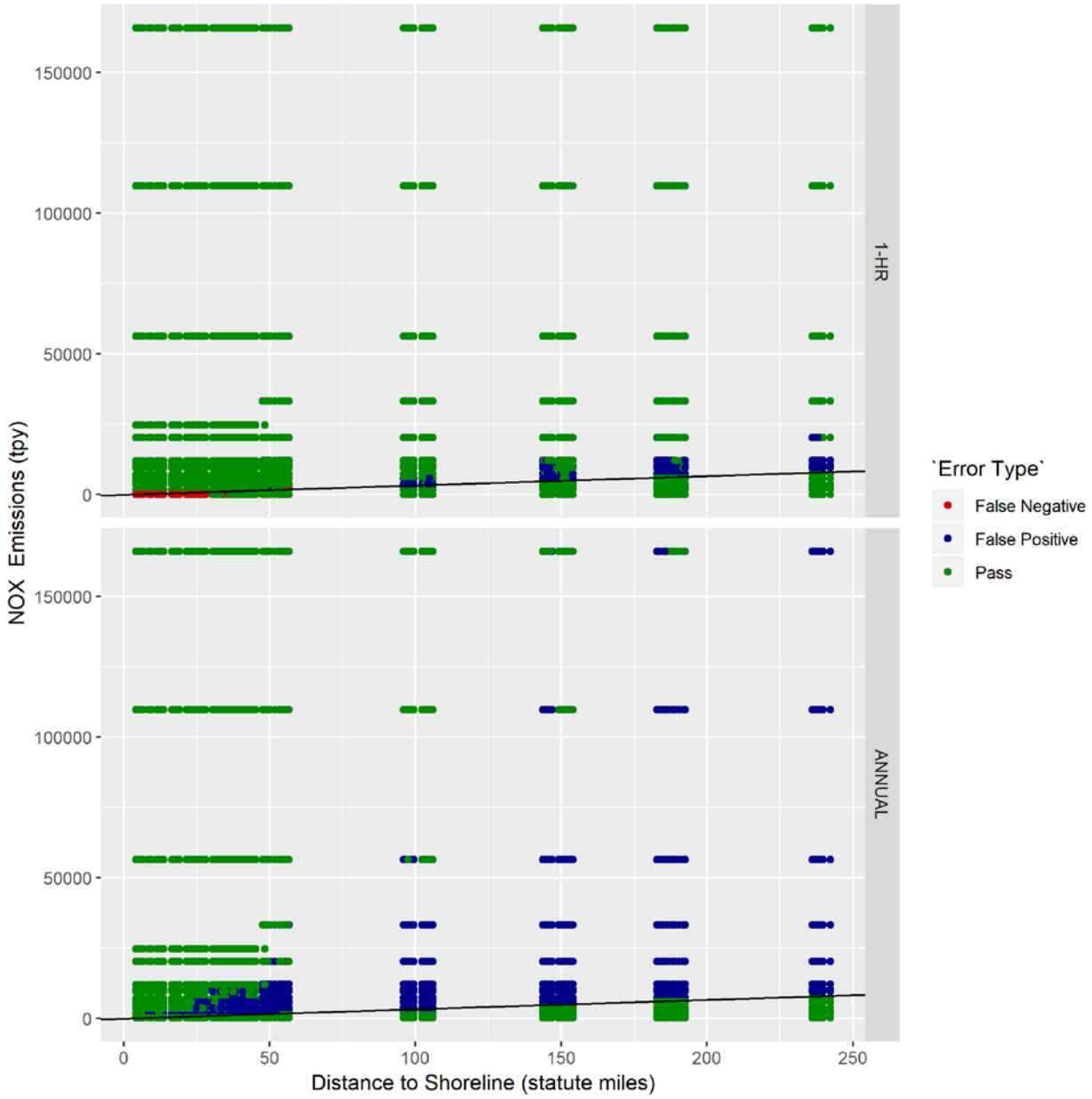

Figure E.5-2. Scatter Plot of NO_x 1-hour (top) and Annual (bottom) Modeling Results at the Shoreline

Black line indicates the current formulation of the EET.

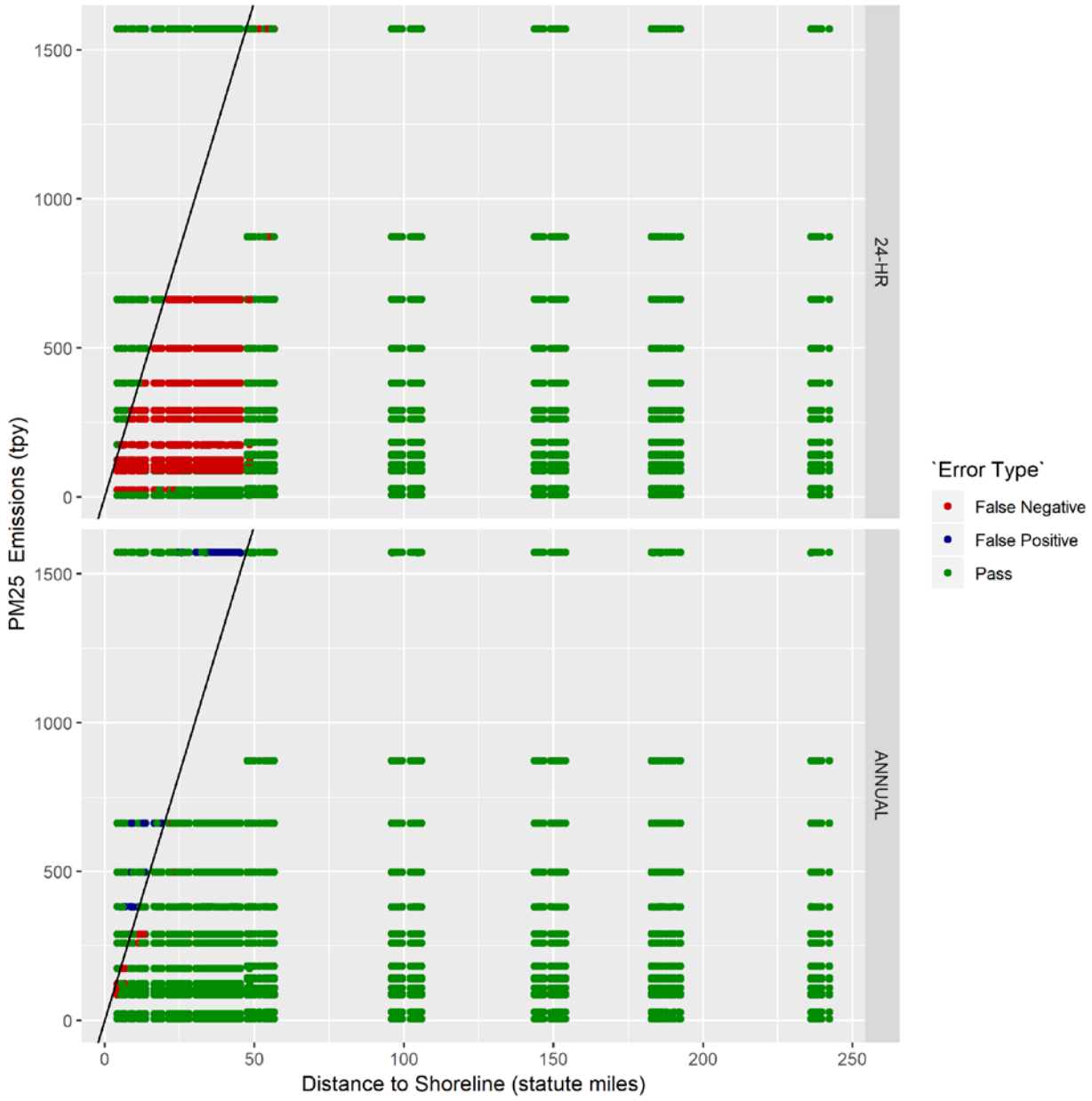

Figure E.5-3. Scatter Plot of $PM_{2.5}$ 24-hour (top) and Annual (bottom) Modeling Results at the Shoreline

Black line indicates the current formulation of the EET.

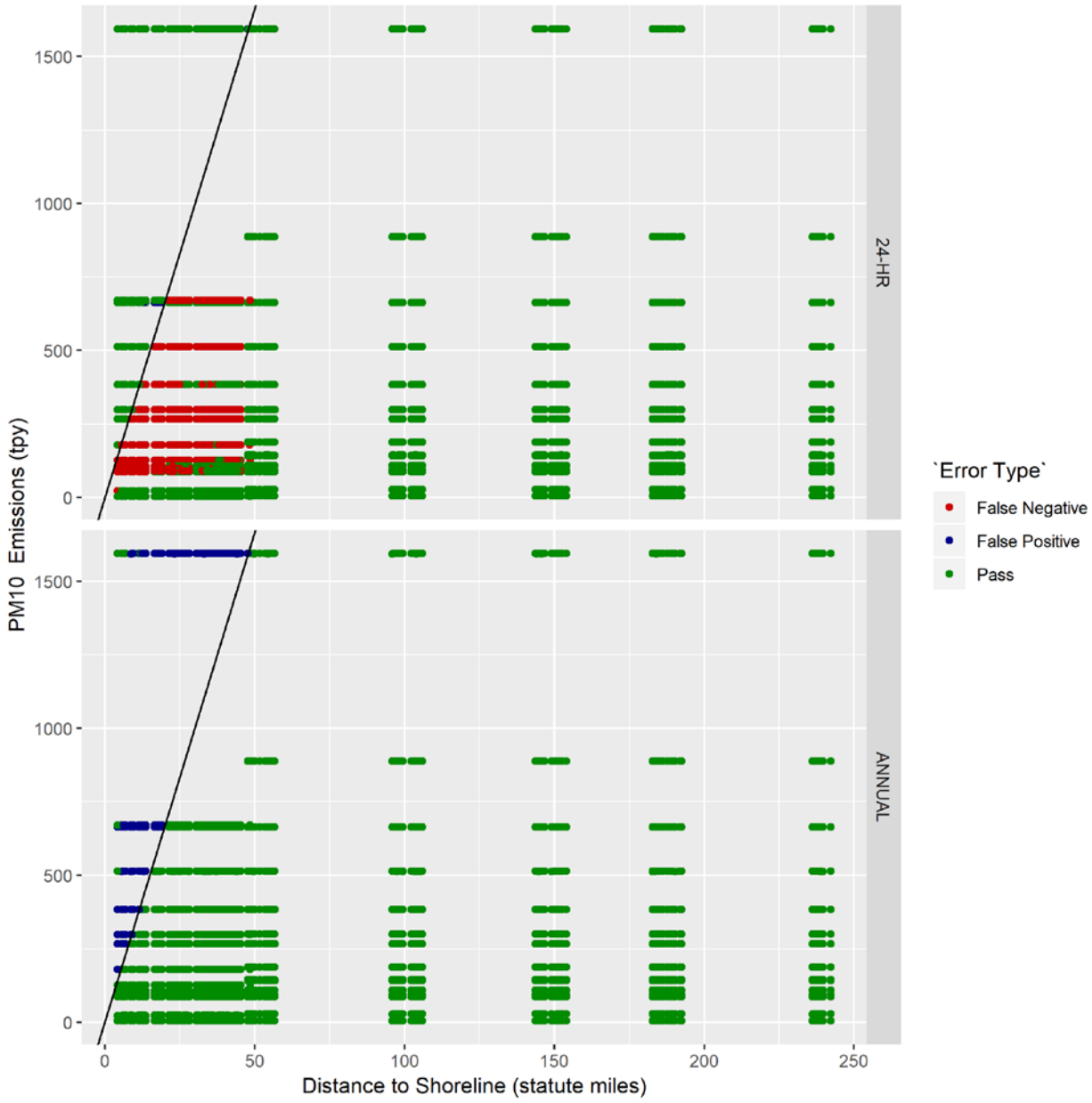

Figure E.5-4. Scatter Plot of PM_{10} 24-hour (top) and Annual (bottom) Modeling Results at the Shoreline

Black line indicates the current formulation of the EET.

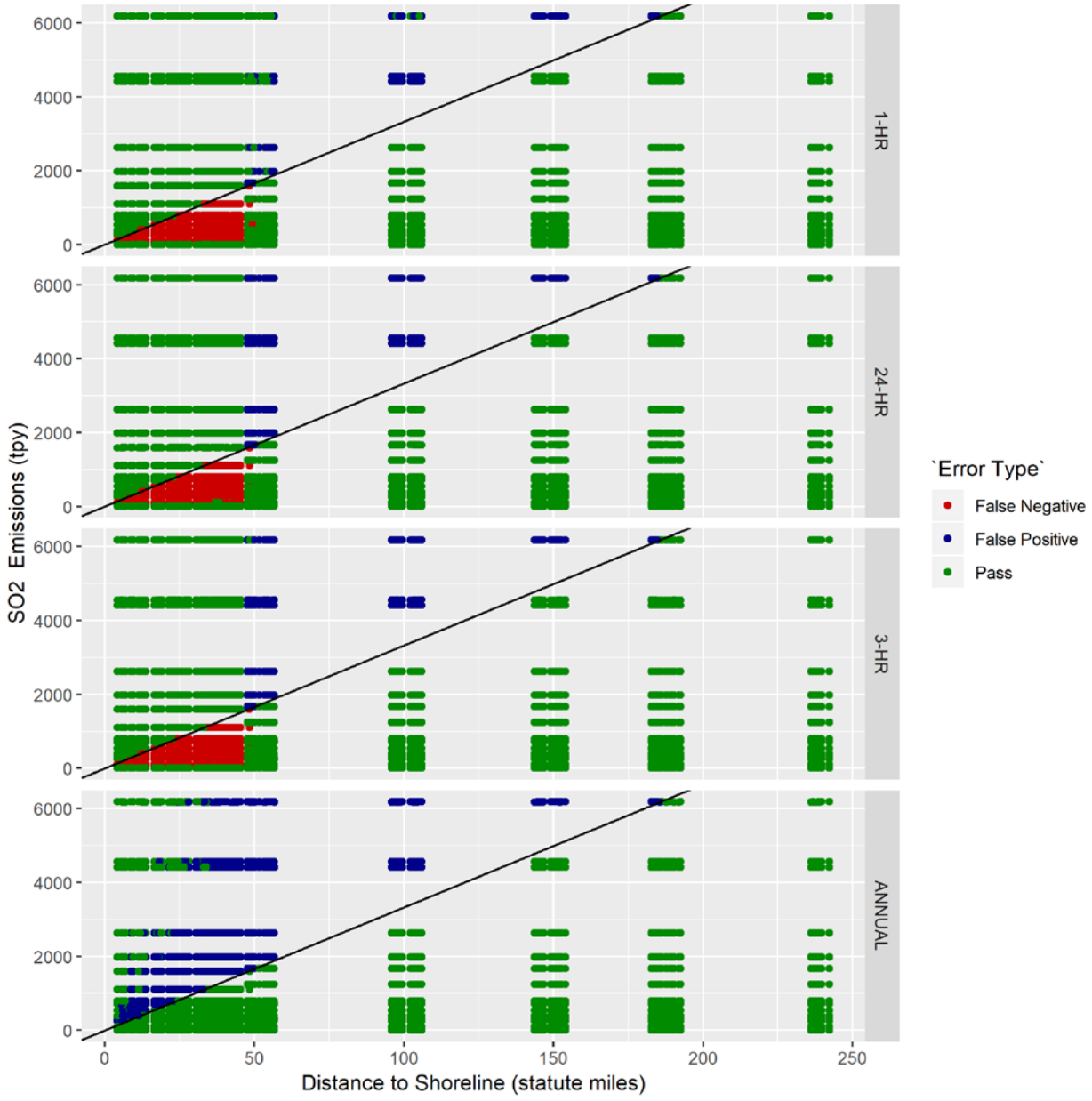

Figure E.5-5. Scatter Plot of SO_2 1-hour (top), 24-hour, 3-hour, and Annual (bottom) Modeling Results at the Shoreline

Black line indicates the current formulation of the EET.

Appendix E.6

Emission Exemption Threshold Evaluation Results for State Seaward Boundary

Modeling was performed for a set of receptors that followed the state seaward boundary and the shoreline as part of an exploratory analysis to quantify how results changed with the shift in point of impact. This appendix provides a summary of the results at the state seaward boundary as supplemental information to the shoreline runs.

The CALPUFF modeling runs for the seaward boundary are slightly different, as the vessel emission sources were run as point sources as opposed to volume sources. Early sensitivity work has shown that characterizing vessels as point sources produces lower impacts due to the difference in plume characteristics for the different source types. The CALPUFF state seaward boundary results were run prior to making this change.

Overall results at the seaward boundary were similar to the shoreline in that the highest impacts occurred for sources closest to shore (Figure E.6-1). For the emission exemption threshold (EET) comparisons, the intent of the distance in the EET formulas is to represent the distance to the point of impact. As such, Eastern Research Group, Inc. (ERG) adjusted the EET calculations for the state seaward boundary to use the distance to the seaward boundary as opposed to the distance to shore. With this change, there was a high level of agreement between the modeling and EET estimated significance (Table E.6-1 and Figure E.6-2). There is a slight increase in the miss rate for each carbon monoxide (CO) averaging time with the move to the state seaward boundary. The lower impacts from the CALPUFF modeling lead to a decrease in the Type II errors across the remaining National Ambient Air Quality Standards (NAAQS). Despite this, the overall performance of the current EET formulas is similar at the seaward boundary and at the shoreline boundary.

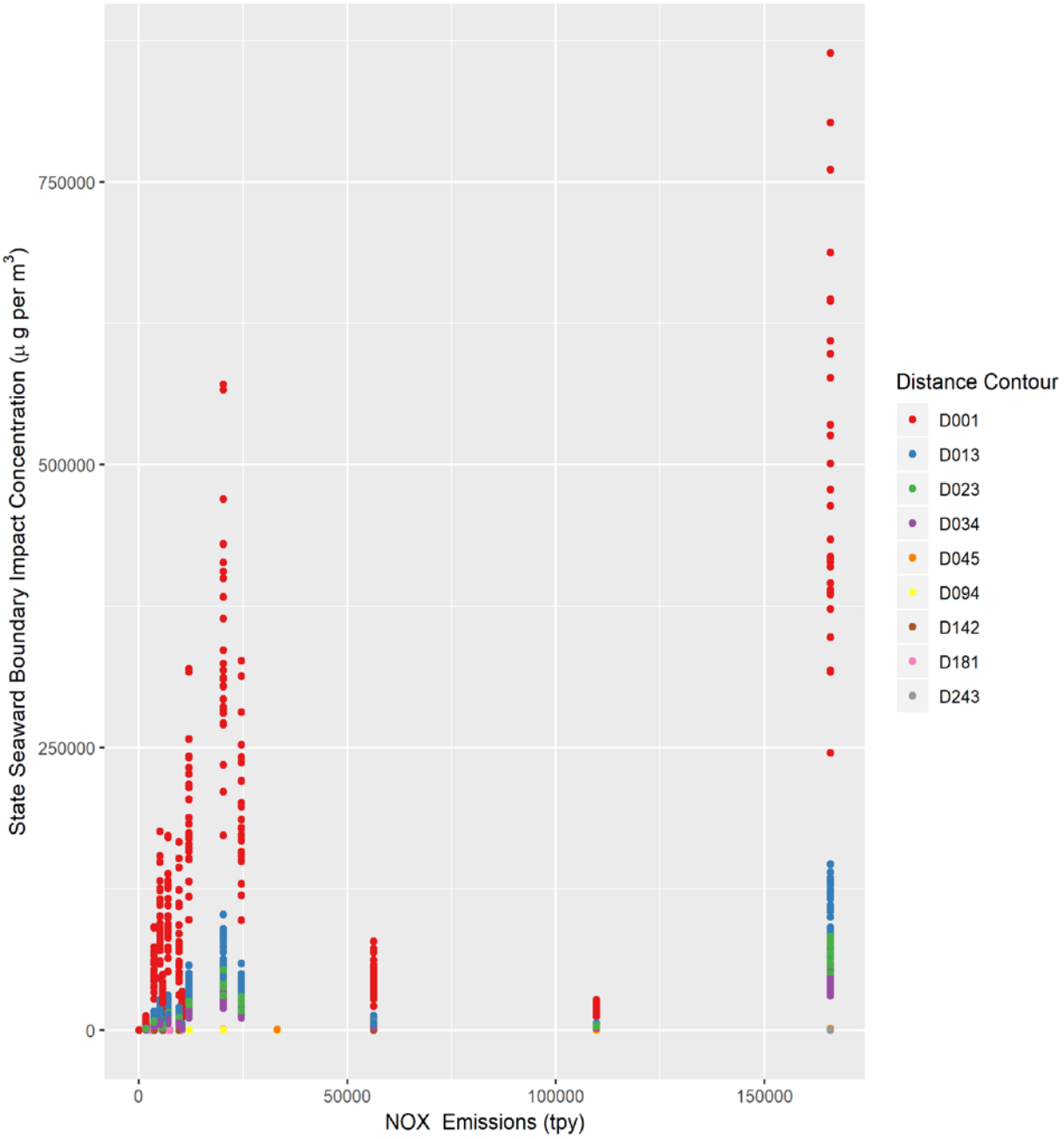

Figure E.6-1. Scatter Plot of NO_2 1-hour Impact at the State Seaward Boundary

Table E.6-1. Short-Term NAAQS Outcomes at the State Seaward Boundary[a]

Pollutant	Averaging Time	Evaluation Outcome (percentage of total)		
		Pass	False Positive (Type I)	False Negative (Type II)
CO	1-hour	74%	0%	26%
	8-hour	80%	0%	20%
NO_2	1-hour	91%	7%	2%
$PM_{2.5}$	24-hour	70%	0%	29%
PM_{10}	24-hour	76%	1%	23%
SO_2	1-hour	77%	7%	15%
	3-hour	76%	9%	15%
	24-hour	76%	9%	15%

[a] Based on 3,300 modeling runs.

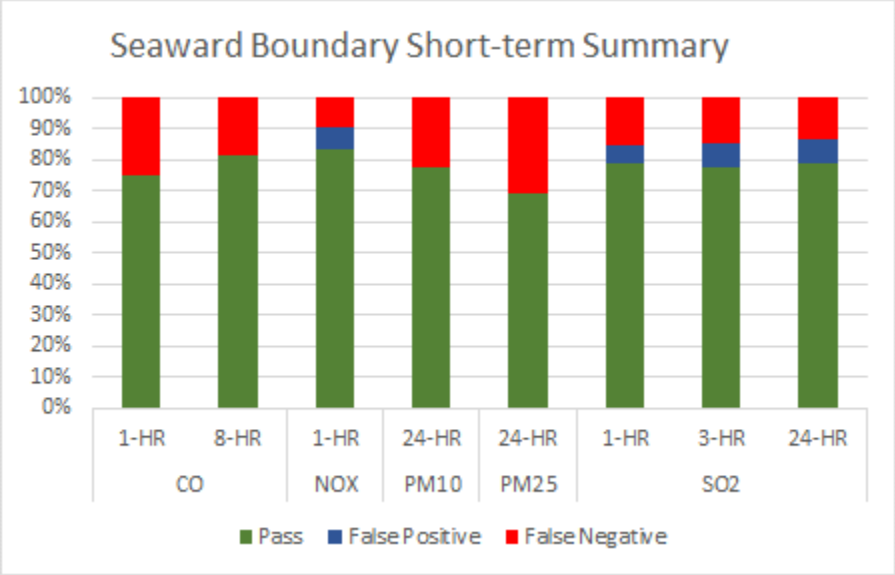

Figure E.6-2. State Seaward Boundary Short-Term Standard Results

The results at the state seaward boundary were similar to the results at the shoreline. The highest impacts were again seen at locations closest to the receptors and with the highest emissions rates (Figure E.6-3). The outcomes of the modeling to EET formula comparison were similar (Table E.6-2 and Figure E.6-4), with most pollutants showing a high pass rate, or comparable pass and false positive rates. The false positives were typically seen at the farthest distances to the seaward boundary. Overall, the existing EET formulas perform similarly at the state seaward boundary as at the shoreline.

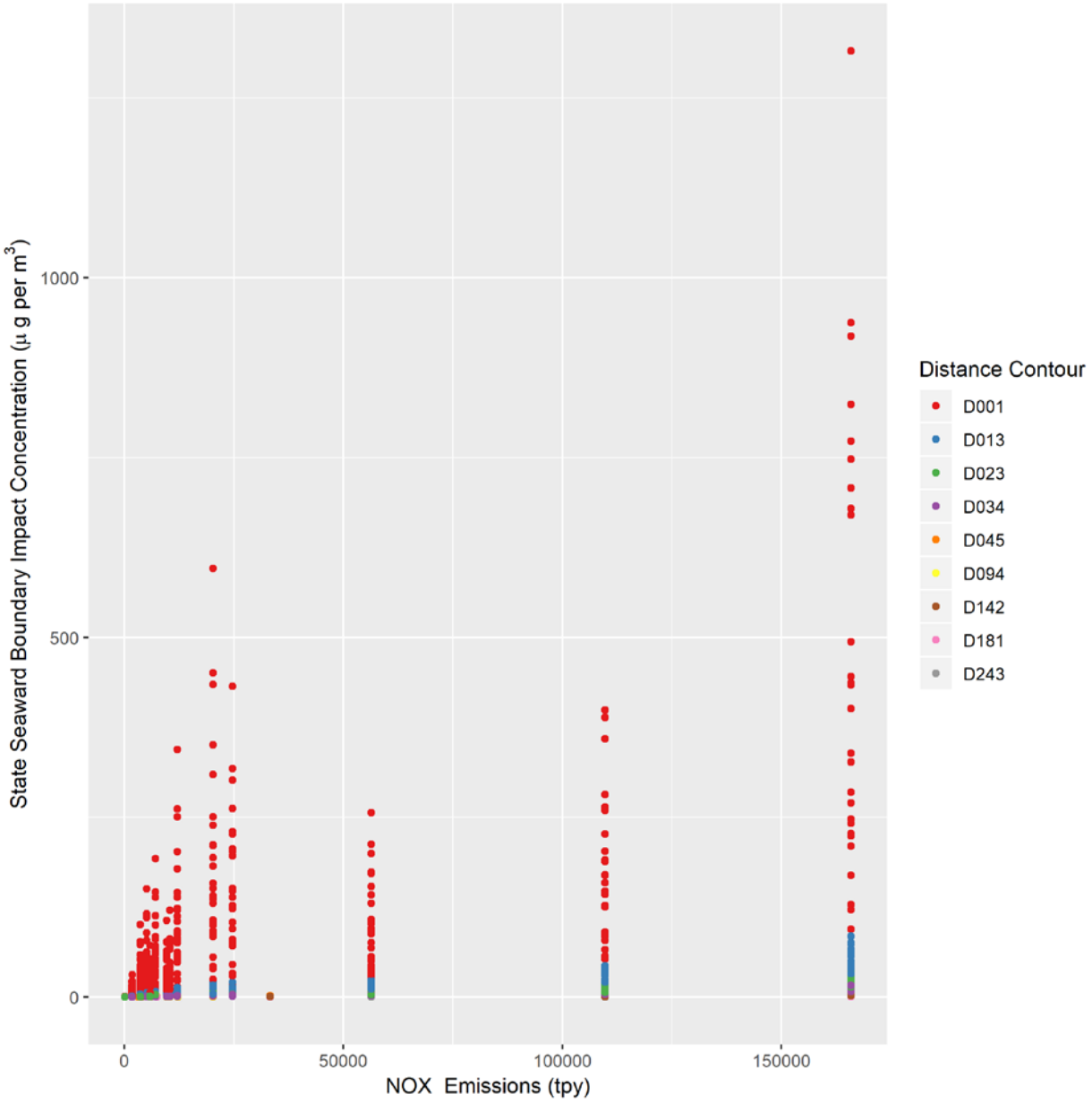

Figure E.6-3. Scatter Plot of NO_2 Annual Results at the Shoreline

Table E.6-2. Long-term NAAQS Outcomes at the State Seaward Boundary[a]

Pollutant[b]	Evaluation Outcome (percentage of total)		
	Pass	False Positive (Type I)	False Negative (Type II)
NO_2	63%	37%	0%
$PM_{2.5}$	96%	3%	1%
PM_{10}	90%	10%	0%
SO_2	76%	24%	0%

[a] Based on 3,300 modeling runs.
[b] There is no long-term NAAQS for CO.

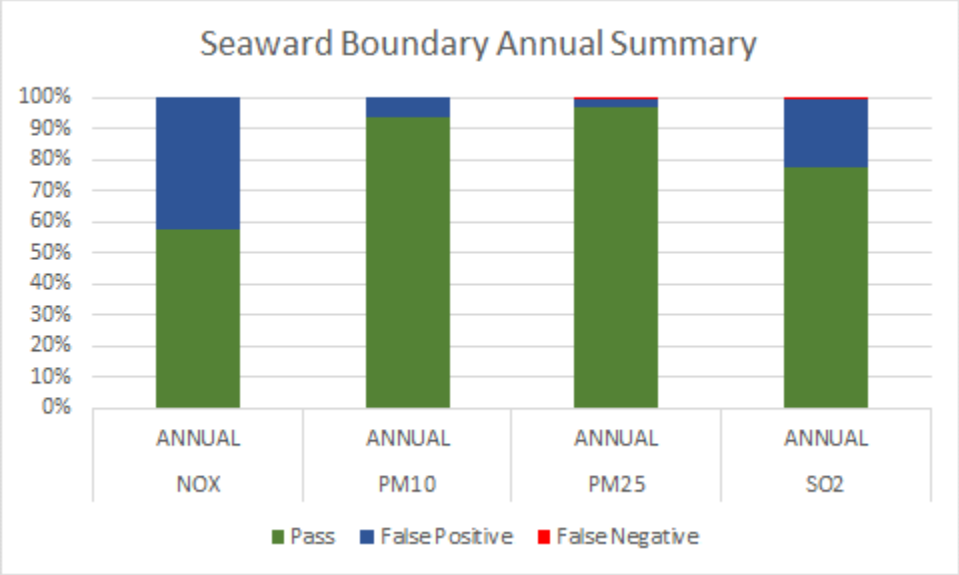

Figure E.6-4. State Seaward Boundary Annual Standard Results Summary

Scatter plots for all pollutants are in the remaining sections. The scatter plots show all of the distance and emission combinations modeled. These points are color coded based on the error type seen, with the black line indicating the current EET formula (33.3*D for all pollutants other than CO; $3400\times(D)^{(2/3)}$ for CO).

Figures E.6-5 through E.6-9 show three outcomes with respect to the EET analysis:

- **Pass (a correct evaluation):** Emissions from the scenario were above the EET threshold, which indicated modeling was needed and the modeling impacts were above the significant impact level (SIL), or emissions from the scenario were below the EET threshold, which indicated modeling was not needed and the modeled impacts were below the SIL.
- **False positive (Type I error):** Emissions from the scenario were above the EET threshold, which indicated modeling was needed; however, the modeled impact was below the SIL.

- **False negative (Type II error):** Emissions from the scenario were below the EET threshold, which indicated modeling was not necessary; however, the modeled impact was above the SIL.

Most of the false negative Type II errors occur closer to shore, which makes sense as the near shore location would not have a lot of time to disperse could have higher impact. Most of the false positive Type I errors occur at further distances to shore, with lower emissions rates.

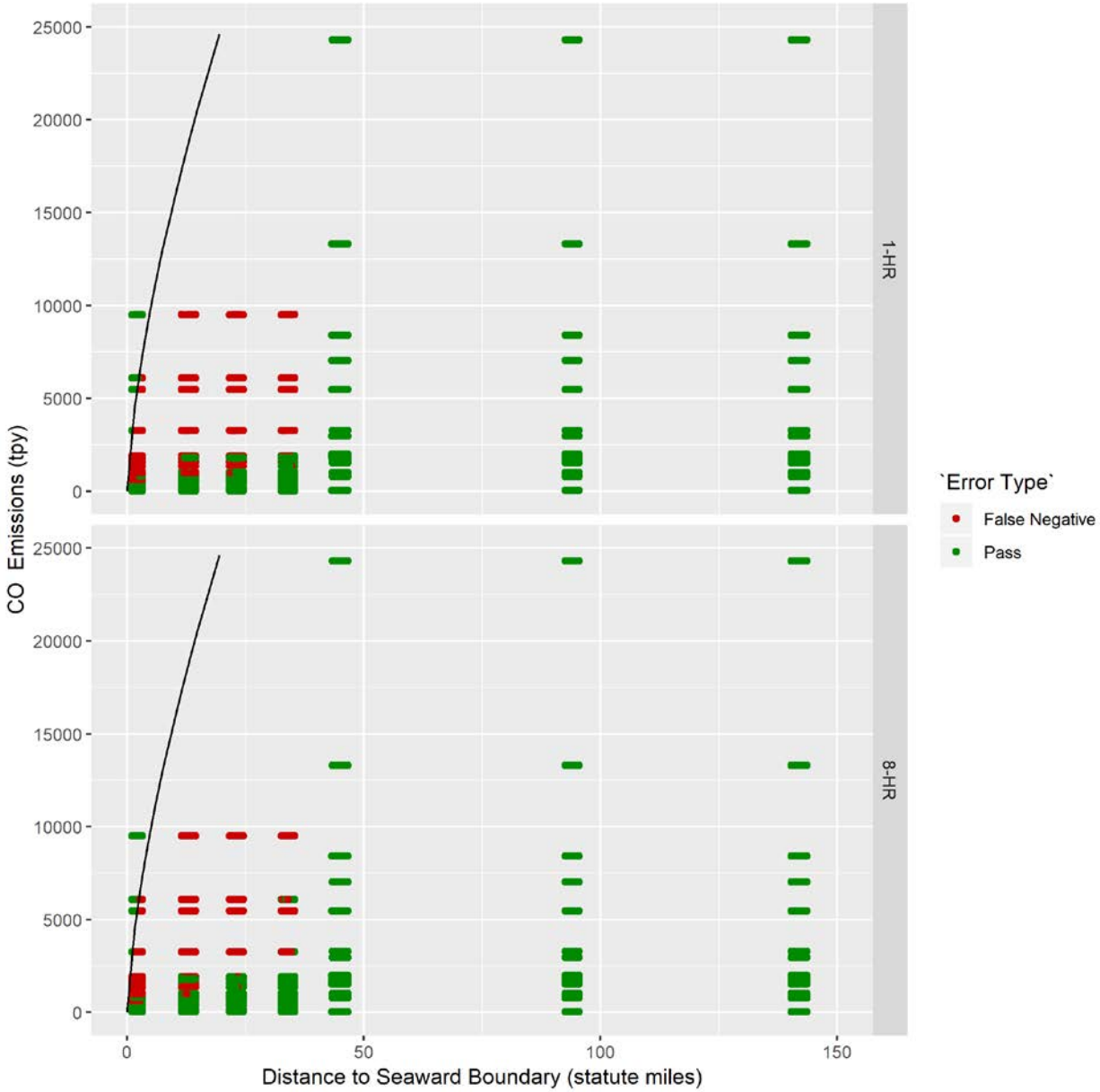

Figure E.6-5. Scatter Plot of CO 1-hour (top) and 8-hour (bottom) Modeling Results at the Seaward Boundary

Black line indicates the current formulation of the EET.

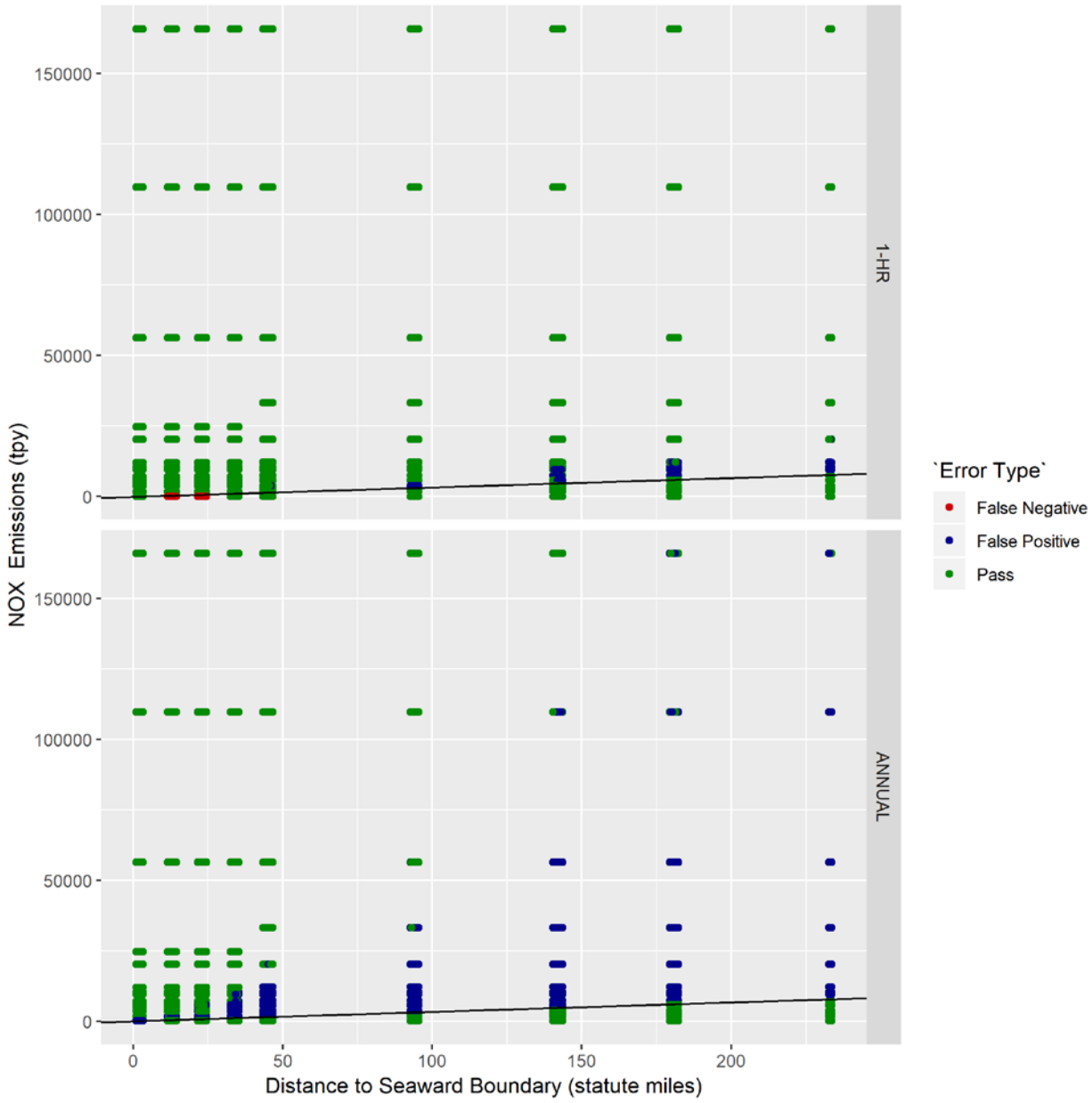

Figure E.6-6. Scatter Plot of NO_x 1-hour (top) and Annual (bottom) Modeling Results at the Seaward Boundary

Black line indicates the current formulation of the EET.

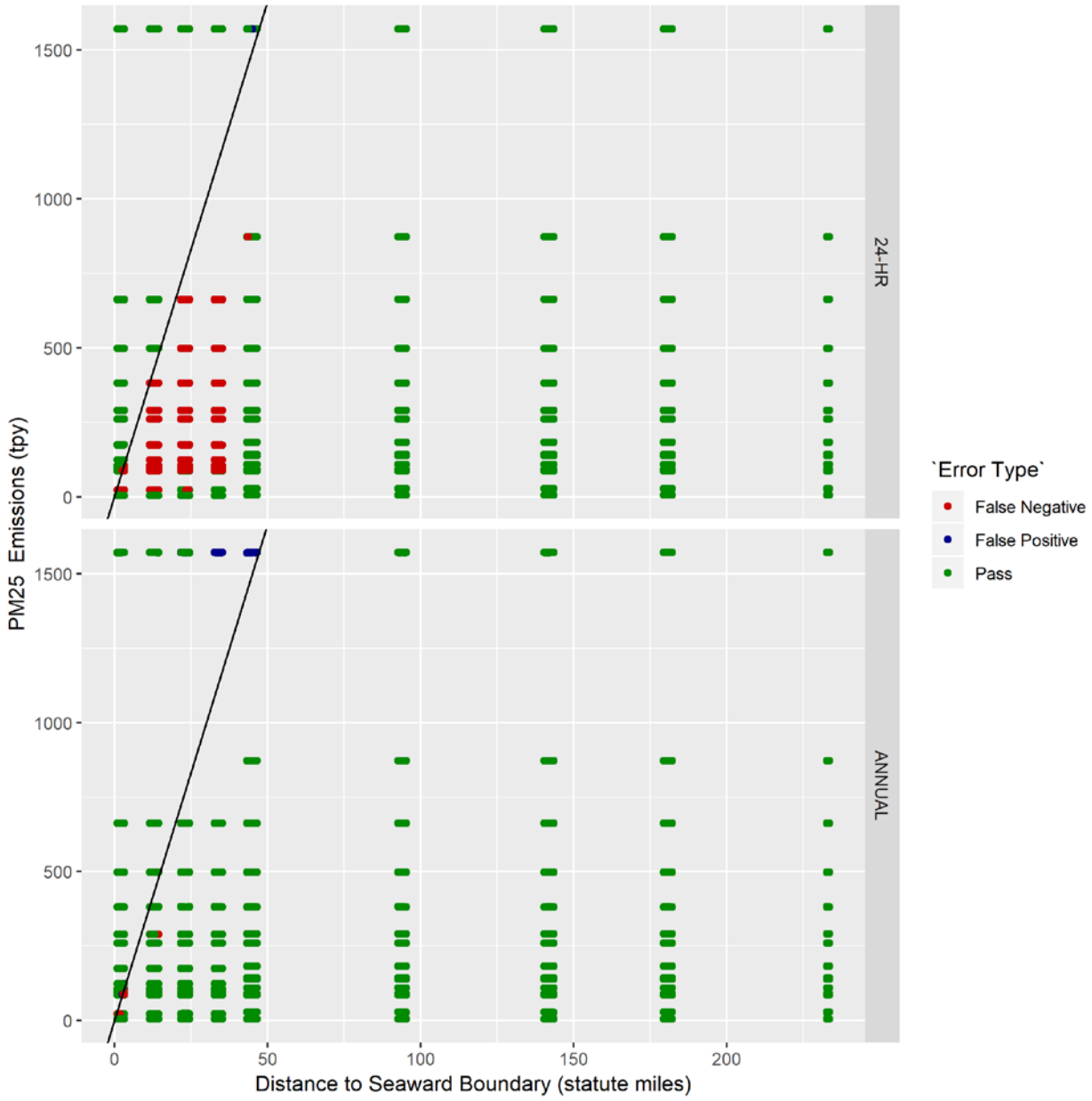

Figure E.6-7. Scatter plot of $PM_{2.5}$ 24-hour (top) and Annual (bottom) Modeling Results at the Seaward Boundary

Black line indicates the current formulation of the EET.

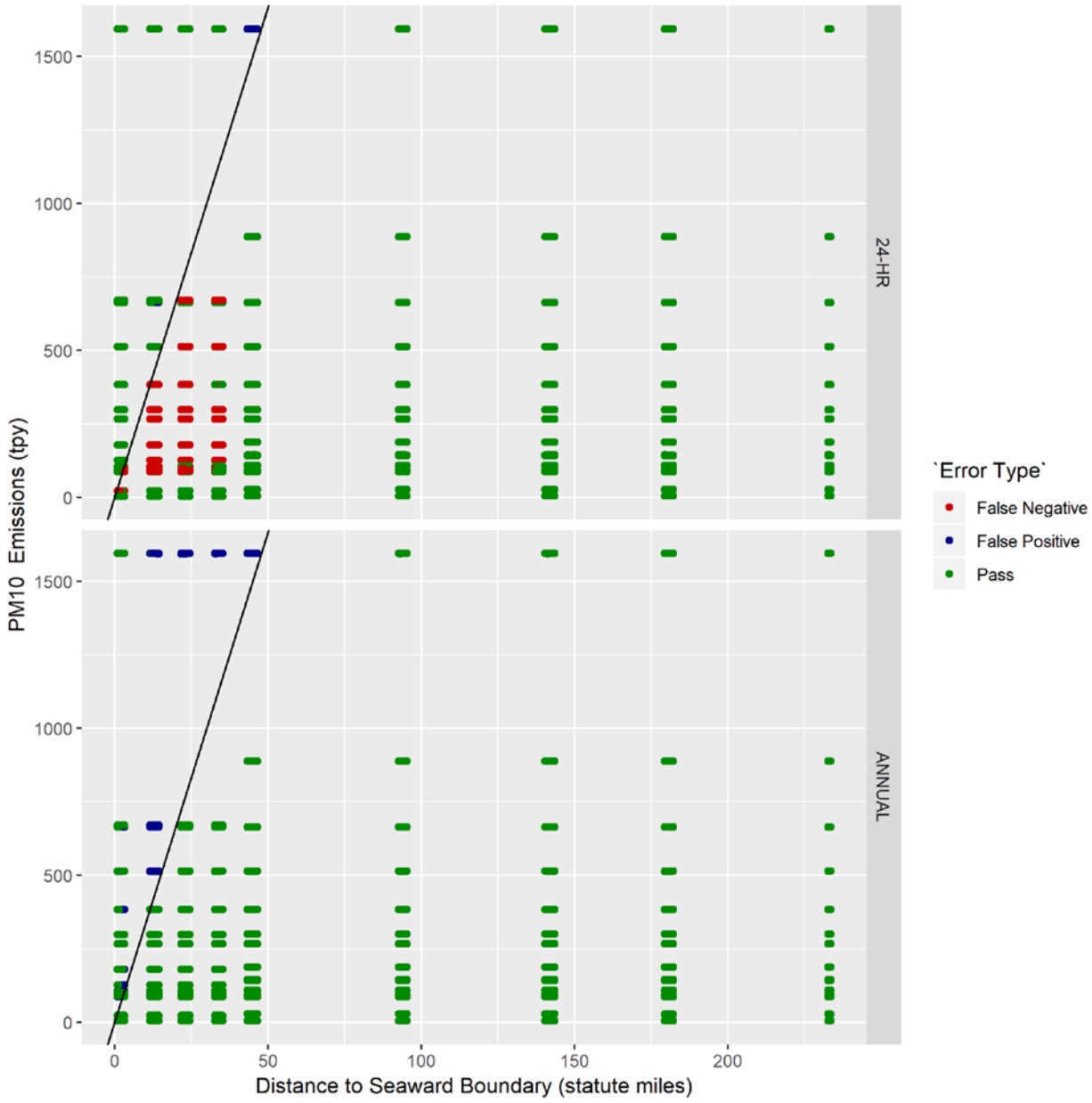

Figure E.6-8. Scatter Plot of PM_{10} 24-hour (top) and Annual (bottom) Modeling Results at the Seaward Boundary

Black line indicates the current formulation of the EET.

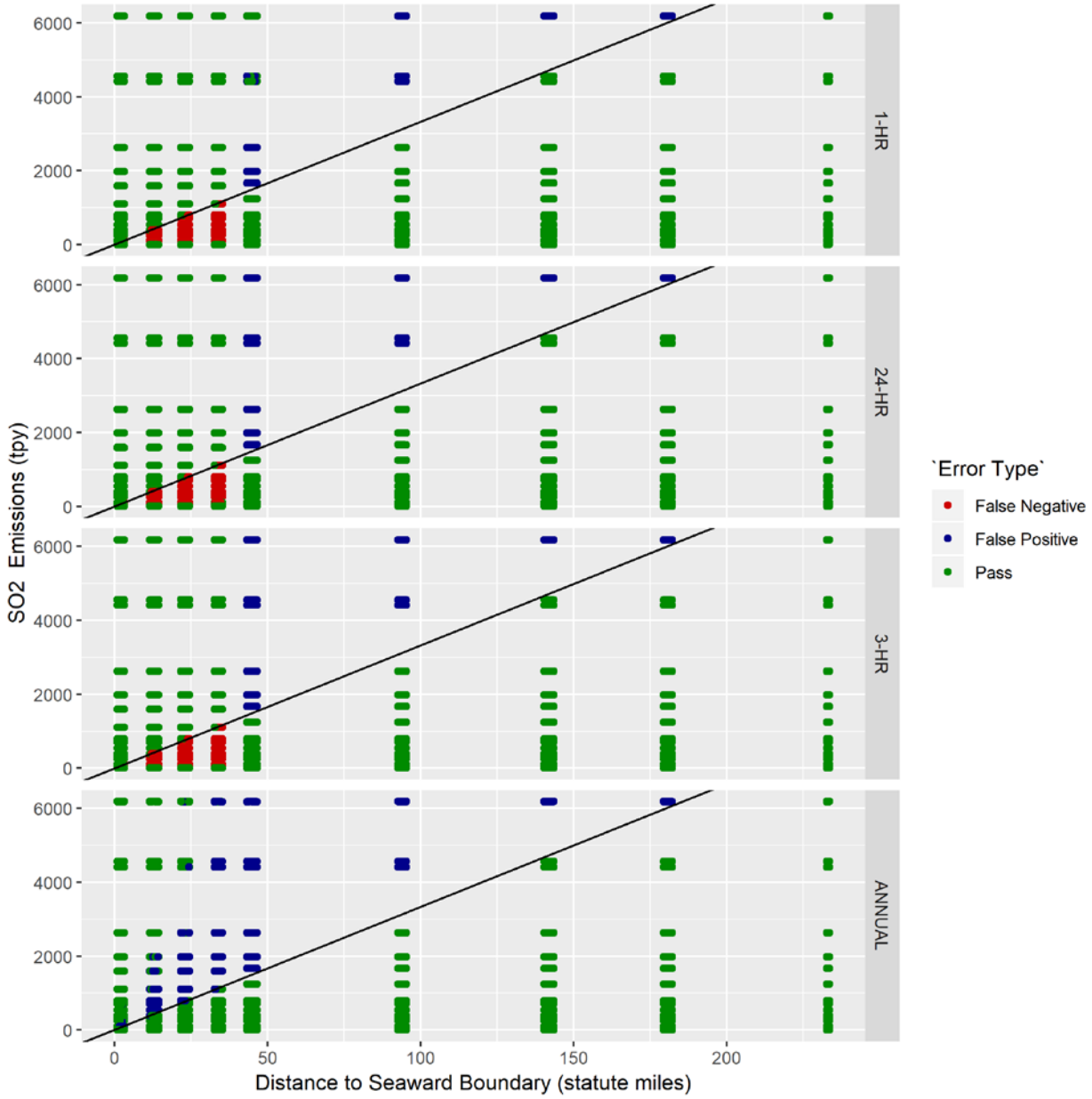

Figure E.6-9. Scatter plot of SO_2 1-hour (top), 24-hour, 3-hour, and Annual (bottom) Modeling Results at the Shoreline

Black line indicates the current formulation of the EET.

Appendix E.7

Emission Exemption Threshold Evaluation Results for Lead

Lead (Pb) was also included in the modeling runs to determine the impact of emissions from offshore platforms. The goal was to establish the potential range of onshore impacts of lead from offshore sources. The emissions of lead from any offshore structure falls below the Significant Emissions Rate (SER) of 0.6 tons per year for any of the synthetic source scenarios used in the study (Table E.7-1).

The complicating factor to the analysis is that the current lead National Ambient Air Quality Standard (NAAQS) (0.15 μgm^{-3}) has no Significant Impact Level (SIL) associated with it. Because most Significant Impact Levels (SILs) range between 1–5% of their NAAQS, a 0.0075 μgm^{-3} (5% of the NAAQS) was used to generate comparisons comparable to other criteria pollutants.

Like most pollutants, higher emission rates yielded higher impacts (Figure E.7-1), but all impact were well below 5% of the NAAQS (Figure E.7-2).

Table E.7-1. Lead Emissions From Hypothetical Platforms

Scenario	Description[a]	Size	Lead Emissions	
			Tons per year	lb per hour
1	DRI EP with support vessels, well testing	L	0.013	0.003
		M	0.005	0.001
		S	0.001	0.0002
2	PROD & DRI DOCD with support vessels	L	0.09	0.021
		M	0.001	0.0002
		S	0.002	0.0004
3	PROD & DRI DOCD with support vessels, pipeline emissions, facility installation, and well testing	L	0.013	0.003
		M	0.006	0.0013
		S	0.004	0.001
4	PROD-only DOCD with support vessels	L	0.001	0.0003
		M	0.0003	0.0001
		S	0.0	0
5	FPSO	L	0.008	0.002
		M	0.002	0.001
		S	0.002	0.001

[a] DRI: drilling rig
EP: Exploration Plan
PROD: Production
DOCD: Development Operations Coordination Document
FPSO: floating production storage and offloading

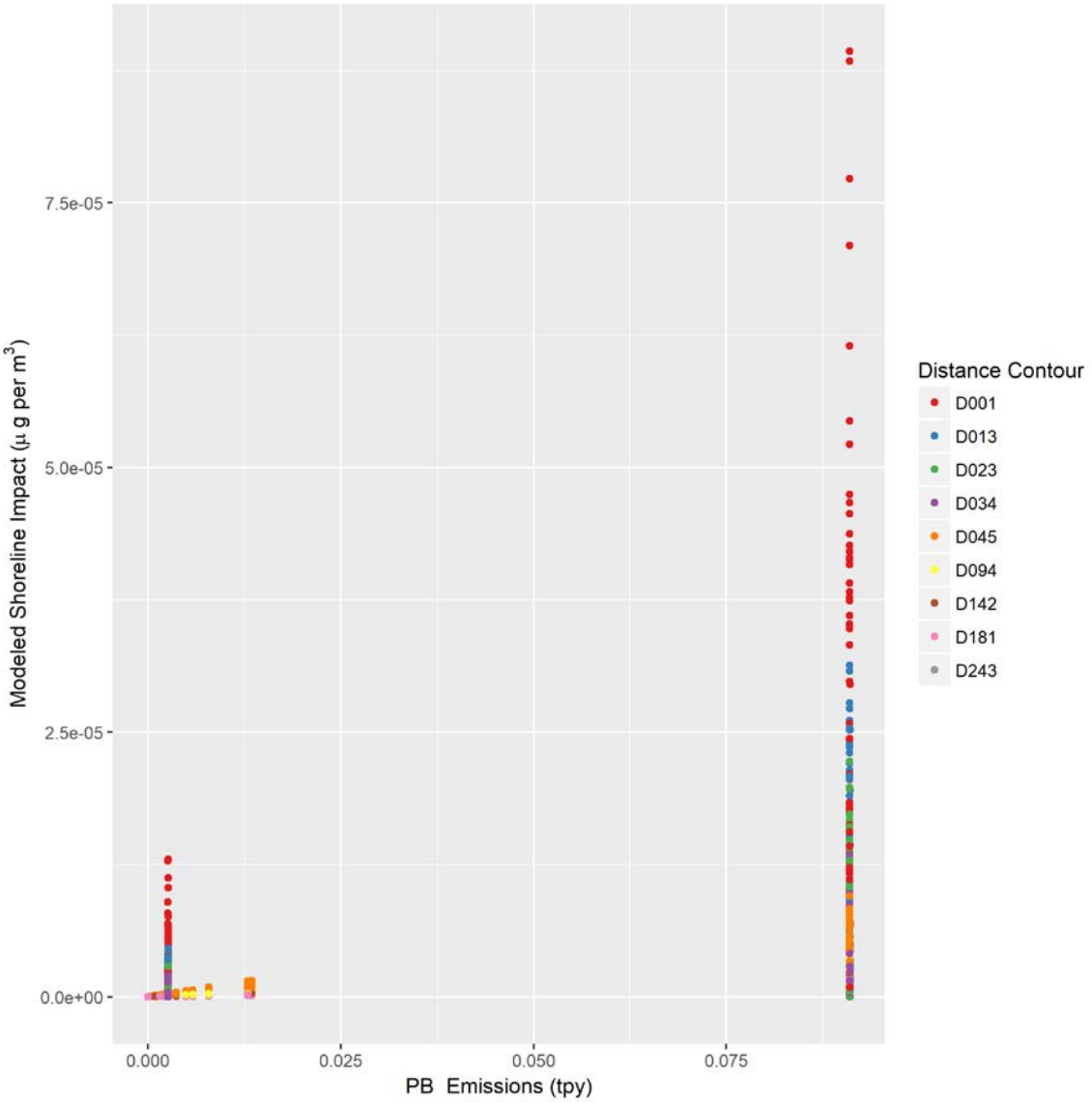

Figure E.7-1. Scatter Plot of Pb 3-Month Modeling Results at the Shoreline

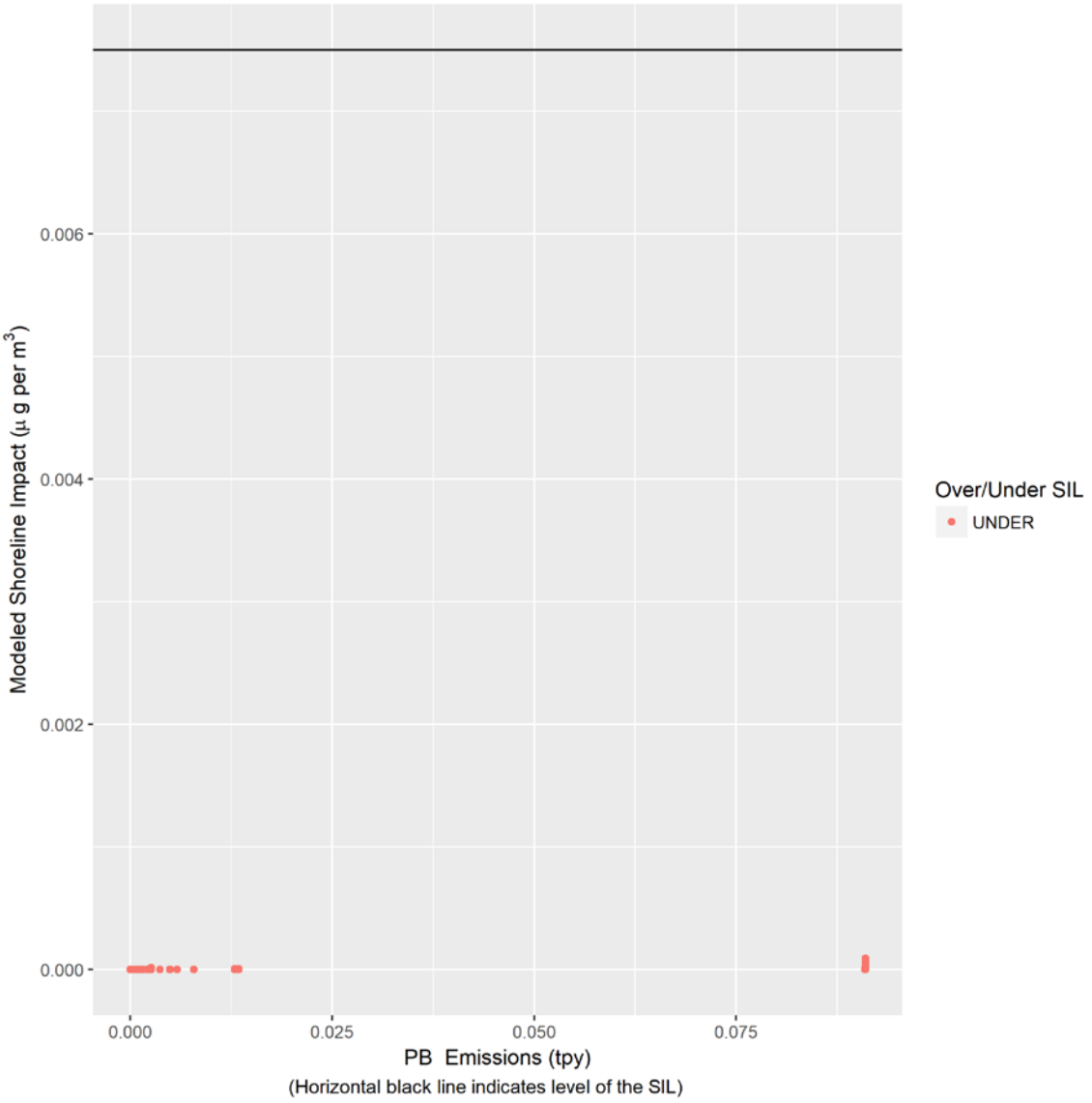

Figure E.7-2. Scatter Plot of Pb 3-month Modeling Results at the Shoreline
Black line indicates 5% of the NAAQS.

Appendix E.8

Emission Exemption Threshold Evaluation CART Analyses

Contents

List of Figures

List of Tables

E.8.1 Introduction

This study's photochemical modeling and dispersion modeling results were used by Eastern Research Group, Inc. (ERG) and Alpine Geophysics, LLC (Alpine) to assess whether the Bureau of Ocean Energy Management's (BOEM's) emission exemption threshold (EET) formulas used in 30 CFR 550.303 need to be revised based on newer National Ambient Air Quality Standards (NAAQS) and whether BOEM may choose to propose new EET formulas to protect the current NAAQS, if necessary.

In general, the study found that the EET formulas were overly conservative for the long-term, or annual, NAAQS. That is, the existing EET formulas for annual NAAQS only had false positive (Type I) errors, which called for modeling when an impact larger than the significant impact level (SIL) was not seen. The short-term NAAQS (i.e., NAAQS with averaging times of 24-hours or less) EET formula results were mixed, in that most pollutants saw both false positive (Type I) and false negative (Type II) errors. The false negative error rates (i.e., the impact was over the SIL, but the formula determined that modeling not necessary) were higher than the false positive rates and ranged from 2% for the NO_2 1-hour NAAQS to 34% for $PM_{2.5}$ 1-hour NAAQS. A more detailed summary of the modeling results and assessment of the EET formulas are available in Section 5 of this report.

Section 5 also offers several different options for EET formula revisions for BOEM's consideration. After deliberation, BOEM chose to proceed with a classification and regression tree (CART) analysis that would produce decision trees for each NAAQS. The CART analysis captures the low emission sources near shore as under the SIL, unlike the other options presented in the Section 5. The CART analysis also performed very well, with a higher pass rate (92 percent) than any of the regression models tested for the $PM_{2.5}$ 24-hour NAAQS. Additionally, the error rate was evenly split between false positive and false negative results, which suggests the CART solution was well balanced (not overly conservative or lenient). The if-then decisions can be also be easily coded in the Exploration Plan (EP) and Development and Operations Coordination Document (DOCD) worksheets using "if statements" to arrive at each bin, with the decision tree flow chart providing a transparent decision mechanism for operators.

E.8.2 Summary of Approach

ERG conducted a CART analysis to develop a classification decision tree for each NAAQS. A classification decision tree predicts whether a new source will produce a significant impact based on air quality modeling results and is composed of if-then conditions that lead to a classification prediction. The conditions are determined via a recursive portioning method, based on specified predictor variables. Put simply, CART recursively bins the data based on binary (true/false) decisions, like a flow chart, until additional decisions no longer add to the value of the model.

For the EET analysis, both the distance to shore and total annual emissions in tons per year were used as predictors of whether the source would model above the SIL for the NAAQS. These predictive parameters (distance to shore [in statute miles] and total annual emissions [in tons per year]) are the same as the existing EET formulas. These are parameters operators actively know about in their operations and already provide to BOEM in their plans and therefore do not represent an additional burden for the operators.

For the short-term NAAQS, it may prove beneficial for BOEM to move to using the maximum hourly rate, as opposed to the total annual emissions, because the modeled rate for these standards is based on the

maximum hourly rate. This analysis was not conducted at this time; however, the data is available for BOEM to investigate this change in input in the future.

ERG used the *R* statistical software to develop the CART decision trees. The code primarily uses the standard regression functions and the *caret* (Classification And REgression Training) package[15] and the *rpart* (Recursive Partitioning and Regression Trees) package[16]. Each tree was run with a five-fold cross-validation process. In this process, the dataset is evenly divided into five subsets. The code estimates the statistical model with four of the five subsets and then tests the model with the withheld subset to quantify model accuracy. This is repeated for each subset, so each subset is used only once in validation to ensure the developed exemption threshold models appropriately screen the different platform scenarios.

E.8.3 Data Set

The data used to develop the decision trees started with the 15 emission scenarios noted in the Section 5 of the report and here in Table E.8-1.

Table E.8-1. Modeled Emission Levels for Synthetic Sources in Grams Per Second

Scenario	Description[a]	Size	Maximum Hourly Emissions (grams/second)					
			PM_{10}	$PM_{2.5}$	SO_2	NO_x	CO	Pb
1	DRI EP with support vessels, well testing	L	15	14	131	582	157	3.87×10^{-4}
		M	5.28	5.12	47	208	56	1.42×10^{-4}
		S	2.5	2.47	8.89	91	17	1.27×10^{-5}
2	PROD & DRI DOCD with support vessels	L	46	45	178	4,772	481	2.62×10^{-3}
		M	19	19	7.34	3,157	195	2.53×10^{-5}
		S	11	11	16	1,621	101	4.44×10^{-5}
3	PROD & DRI DOCD with support vessels, pipeline emissions, facility installation, and well testing	L	22	22	127	830	208	3.72×10^{-4}
		M	7.67	7.48	57	298	65	1.20×10^{-4}
		S	3.86	3.75	34	154	41	1.06×10^{-4}
4	PROD-only DOCD with support vessels	L	3.11	3.07	11	168	52	3.38×10^{-5}
		M	0.73	0.72	3.08	50	24	9.40×10^{-6}
		S	0.13	0.13	0.12	3.61	0.87	0
5	FPSO	L	8.59	8.34	76	348	94	2.26×10^{-4}
		M	3.49	3.42	21	277	33	6.04×10^{-5}
		S	2.63	2.56	23	107	29	7.06×10^{-5}

[a] DRI: drilling rig
PROD: .production
FPSO: floating production storage and offloading

[15] The *caret* package is available at https://CRAN.R-project.org/package=caret.
[16] The *rpart* package is available at https://CRAN.R-project.org/package=rpart.

After the initial EET evaluation, additional single source runs at a unit emission rate (i.e., 1 g/s) were executed to better define the transition between categories in the nearshore environment. These single source runs included a cold stack (1C), a hot stack (1P), a vessel modeled as a point source (1X), and a single vessel as a volume source (1V). The 1C source parameters for a short vent are based on select permits with low-level cold vents. The 1P source parameters match the natural gas engine parameters used in study's modeling inventory developed for the cumulative air quality impacts analysis. The 1X source use stack parameters based on those used in the USEPA modeling studies (Mason et al., 2008), which were based on several inventory sources. Table E.8-2 summarizes the stack parameters for the point sources.

For the 1V source parameters, vessel dimensions (needed to define volume sources) were obtained from the PortVision Automatic Identification System (AIS) database (developed in BOEM's Year 2014 Gulfwide Emissions Inventory Study) based on vessels known to operate in the GOMR. These dimensions were used to determine the average dimension for each vessel type. The average by vessel type was then merged to produce an average vessel for modeling. Table E.8-3 lists the volume source parameterization. Runs were conducted at all the synthetic source locations along in the near shore environment (i.e., first five contours of Figure E.8-1).

The dataset was further supplemented with modeling runs from modeling sensitivity analysis and other reruns. For example, a batch of runs was conducted at a slightly higher emission rate from the original 15 scenarios due to a duplication of a piece of equipment in the input file (1D, 2A, 2B, 2C, 3A, 3B, 3E, 5B). A second batch of reruns was due to an inconsistency with a source parameter, such as stack height, (1G, 2E, 2F, 2G, 3F). These runs are included in the data set as they help to inform any reformulation of the EET formulas. The emissions level for each of these scenarios is presented tin Table E.8-4. The CART analysis should not be extrapolated for emission values beyond what are presented in Tables E.8-1 and E.8-4. That is, the maximum values presented in the emissions tables should be considered the upper limit of the decision trees. If an operator were to present a plan that exceeds these values, modeling would be warranted to quantify the significance of the impact to onshore air quality.

A second version of this dataset was developed to omit vessel emissions from the analysis. The dataset took advantage of the fact that the AERMOD model is a linear steady-state plume model. This means that changes in impact are linearly proportional to changes in emissions level. Sensitivity runs confirmed that the CALPUFF set up used in the study was effectively a linear model due to the isolated nature of the sources (i.e., the synthetic source was the only source included and impact were essentially linear with emissions level). The emissions level for each scenario, omitting the vessel emissions, is presented tin Table E.8-5.

Table E.8-2. Single Source Scenario Point Source Parameters

Scenario	Stack Parameter			
	Height (ft)	Diameter (ft)	Temperature (F)	Velocity (ft/sec)
Cold stack (1C)	39.3	2.4	– [a]	34.4
Hot stack (1P)	94.3	1.4	1,037.8	140.2
Vessel as points (1X)	65.5	2.6	539.6	82.0

[a] Modeled at ambient temperature based on meteorological inputs.

Table E.8-3. Single Source Scenario Volume Source Parameters

Scenario	Stack Parameter		
	Height (ft)	Sigma Y(ft)	Sigma Z (ft)
Single volume source (1V)	16.4	328.1	16.4

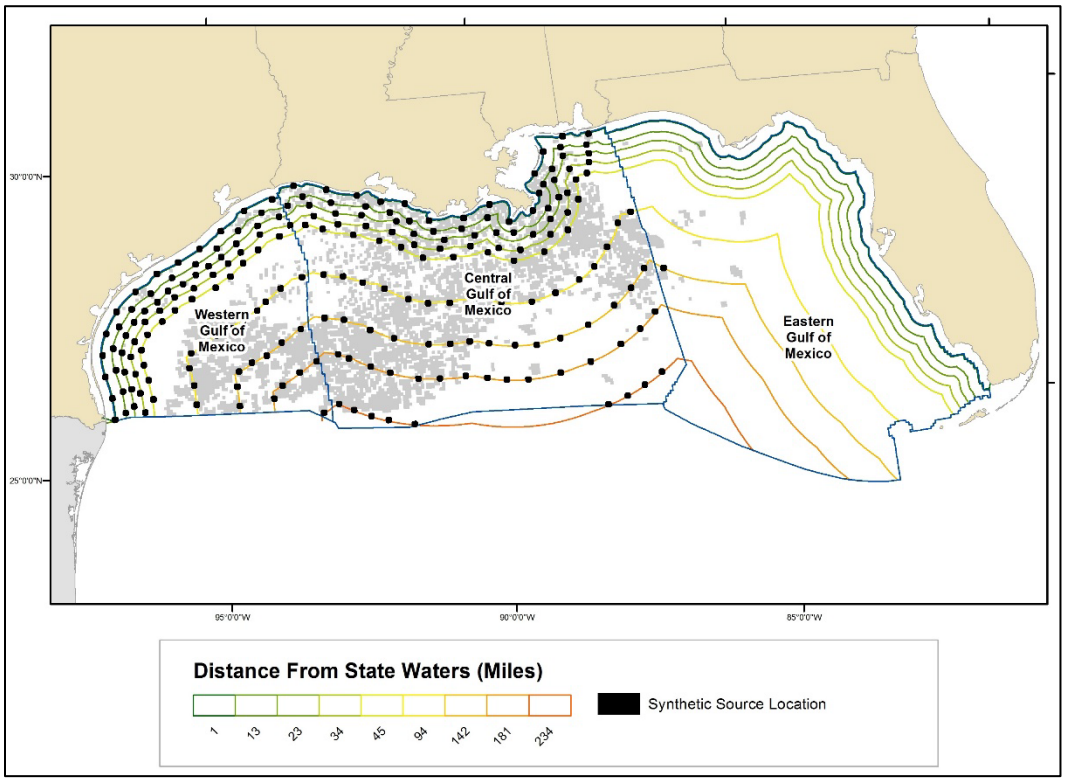

Figure E.8-1. Locations of Dispersion Modeling Runs Table E.8-4. Additional Modeled Emission Levels for Synthetic Sources

Scenario	Size	Maximum Hourly Emissions (grams/second)				Scenario Variation
		NO_X	PM_{10}	PM_{25}	SO_2	
1	D	51	1.5	1.5	0.03	1S, with adjusted emissions
1	G	--	2.5	--	8.89	1S, with adjusted heights
2	A	1,158	25	24	--	2L, with adjusted emissions
2	B	68	1.49	1.46	--	2M, with adjusted emissions
2	C	21	0.62	0.61	1.56	2S, with adjusted emissions
2	E	1,621	46	11	--	2L, with adjusted heights
2	F	3,157	19	19	--	2M, with adjusted heights
2	G	4,772	11	45	16	2S, with adjusted heights
3	A	--	--	--	72	3L, with adjusted emissions
3	B	147	3.7	3.62	25	3M, with adjusted emissions
3	E	--	--	--	127	3L, with adjusted heights
3	F	--	7.67	--	57	3M, with adjusted heights
5	B	111	--	--	--	5M, with adjusted emissions

Table E.8-5. Modeled Emission Levels for Synthetic Sources (without vessel emissions)

Scenario	Description[a]	Size	Maximum Hourly Emissions (grams/second)					
			PM_{10}	$PM_{2.5}$	SO_2	NO_x	CO	Pb
1	DRI EP with support vessels, well testing	L	0.00	0.00	0.00	0.00	0.00	0.00
		M	0.00	0.00	0.00	0.00	0.00	0.00
		S	1.50	1.50	0.03	51.33	11.76	0.00
2	PROD & DRI DOCD with support vessels	L	26.07	26.01	1.97	3992.47	269.75	2.1×10^{-3}
		M	18.37	18.37	0.60	3128.73	187.63	6.31×10^{-6}
		S	9.33	9.33	0.54	1554.20	91.23	0.00
3	PROD & DRI DOCD with support vessels, pipeline emissions, facility installation, and well testing	L	11.32	11.32	0.88	396.11	90.45	0.00
		M	1.32	1.32	0.60	47.89	16.27	7.18×10^{-7}
		S	0.06	0.06	0.00	3.90	0.93	0.00
4	PROD-only DOCD with support vessels	L	1.85	1.85	0.22	117.97	38.73	8.95×10^{-7}
		M	0.41	0.41	0.25	37.46	20.58	1.02×10^{-6}
		S	0.14	0.14	0.12	3.61	0.87	0.00
5	FPSO	L	0.08	0.08	0.02	11.96	3.11	3.2×10^{-6}
		M	1.24	1.24	0.66	188.37	9.52	1.56×10^{-6}
		S	0.05	0.07	0.03	5.65	1.47	3.2×10^{-6}

[a] DRI: drilling rig
PROD: production
FPSO: floating production storage and offloading

E.8.4 Classification and Regression Tree Analysis Output

ERG developed a decision tree based on the distance to shore and total annual emissions. The *R* code was written to generate images and tables to show the decision trees and accuracy statistics. For each NAAQS, a figure showing the decision region and boundary for the decision tree was developed. Figure E.8-2 shows the decision region and boundary for the $PM_{2.5}$ 24-hour NAAQS. The *R* code then uses *rpart* to develop the decision tree, which presents as a flow chart for with a series if-then/yes-no decisions that result in final classification bins for the bins. Figure E.8-3 presents the decision tree for the $PM_{2.5}$ 24-hour NAAQS. For each NAAQS, the *R* code is also designed to calculate the accuracy statistics for comparison to the existing EET. These are provided for each NAAQS in tables similar to Table E.8-4. These images and caveats for the decision trees for each NAAQS are presented in Section E.8.5 for the shoreline receptors. Section E.8.6 presents CART decision trees that exclude the contribution of vessel emissions.

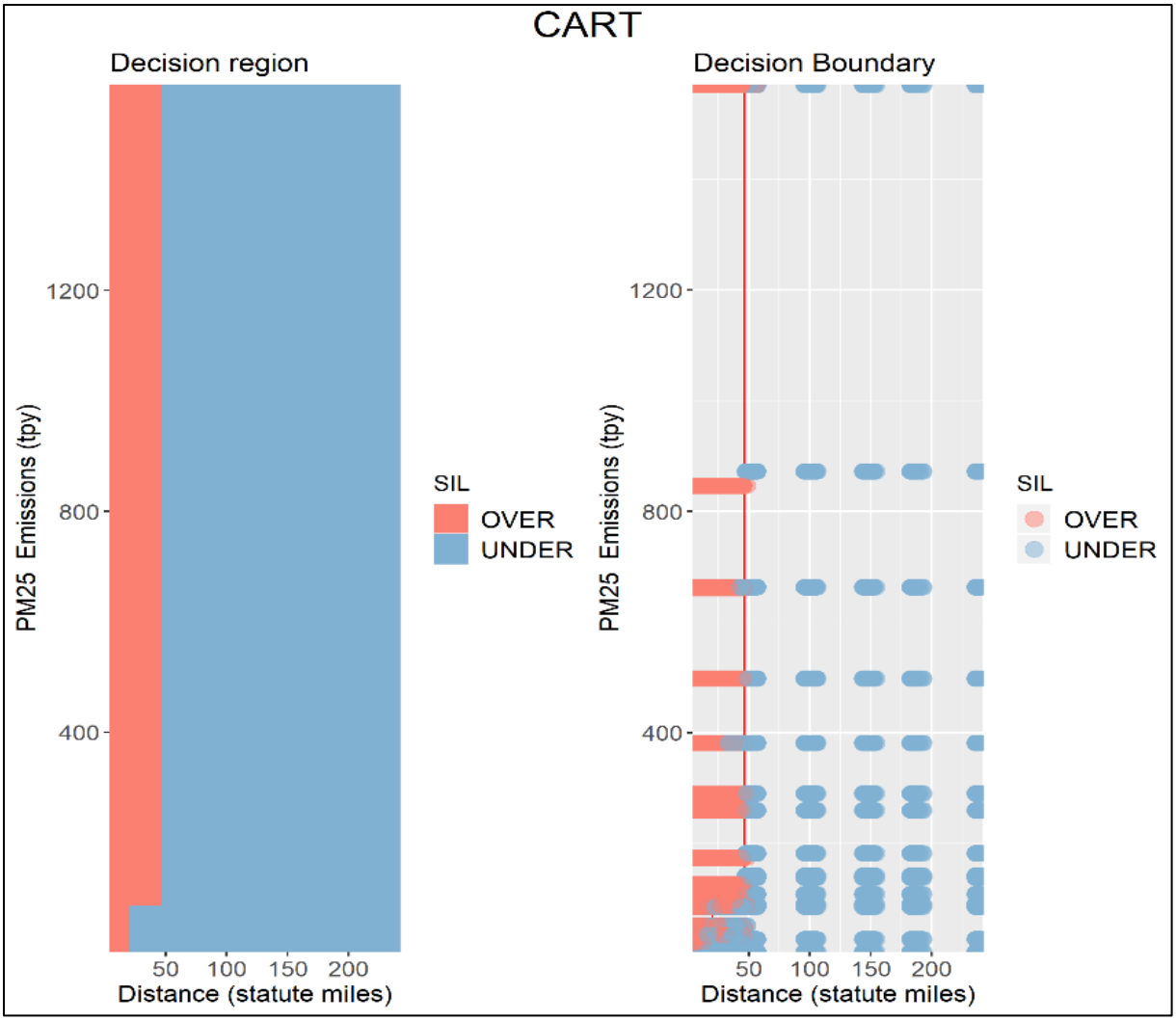

Figure E.8-2. CART Analysis for the $PM_{2.5}$ 24-Hour Modeling Results
The plot on the left shows the determine-decision regions, with red shading indicating results above the SIL and blue shading below. The plot on the right shows the decision boundary (red line) overlaid on the original data.

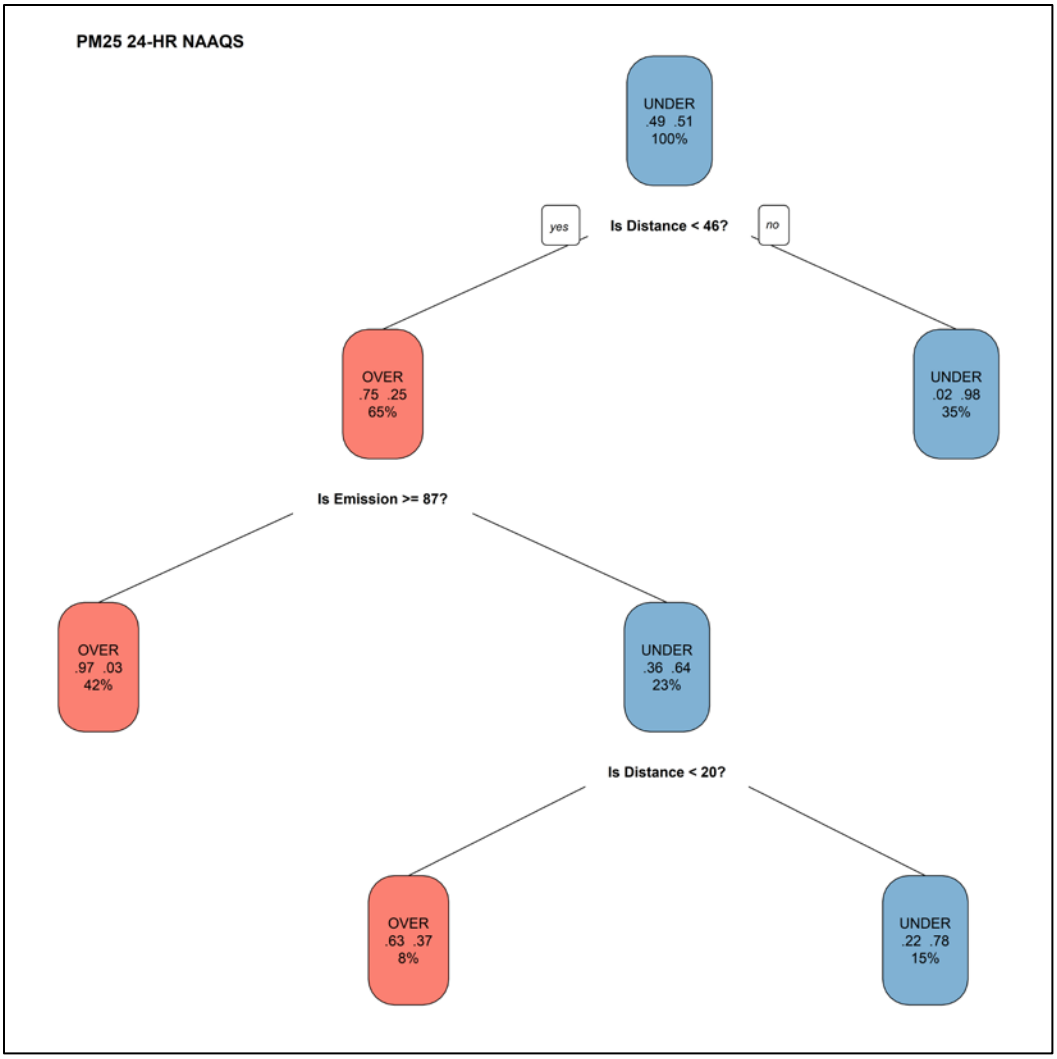

Figure E.8-3. CART Decision Tree for the $PM_{2.5}$ 24-Hour Modeling Results

At each decision point, the branch to the right indicates a response of "no." The boxes at each decision point indicate the probability that the source is over (middle row, left) or under (middle row, right) the SIL and the percentage of the total values in the bin (bottom).

Table E.8-6. Comparison of CART Outcomes to the Original EET for the $PM_{2.5}$ 24-Hour NAAQS

Formula ID	False Positive	False Negative	Pass	Formula
Original	0.00%	36.27%	63.73%	33.3*D
CART	4.27%	3.93%	91.80%	– [a]

[a] The CART tool is a decision tree coded as a series of nested "if statements" to calculate false positive, false negative, and pass rates.

E.8.5 CART Results, Shoreline with Vessels

E.8.5.1 Carbon Monoxide

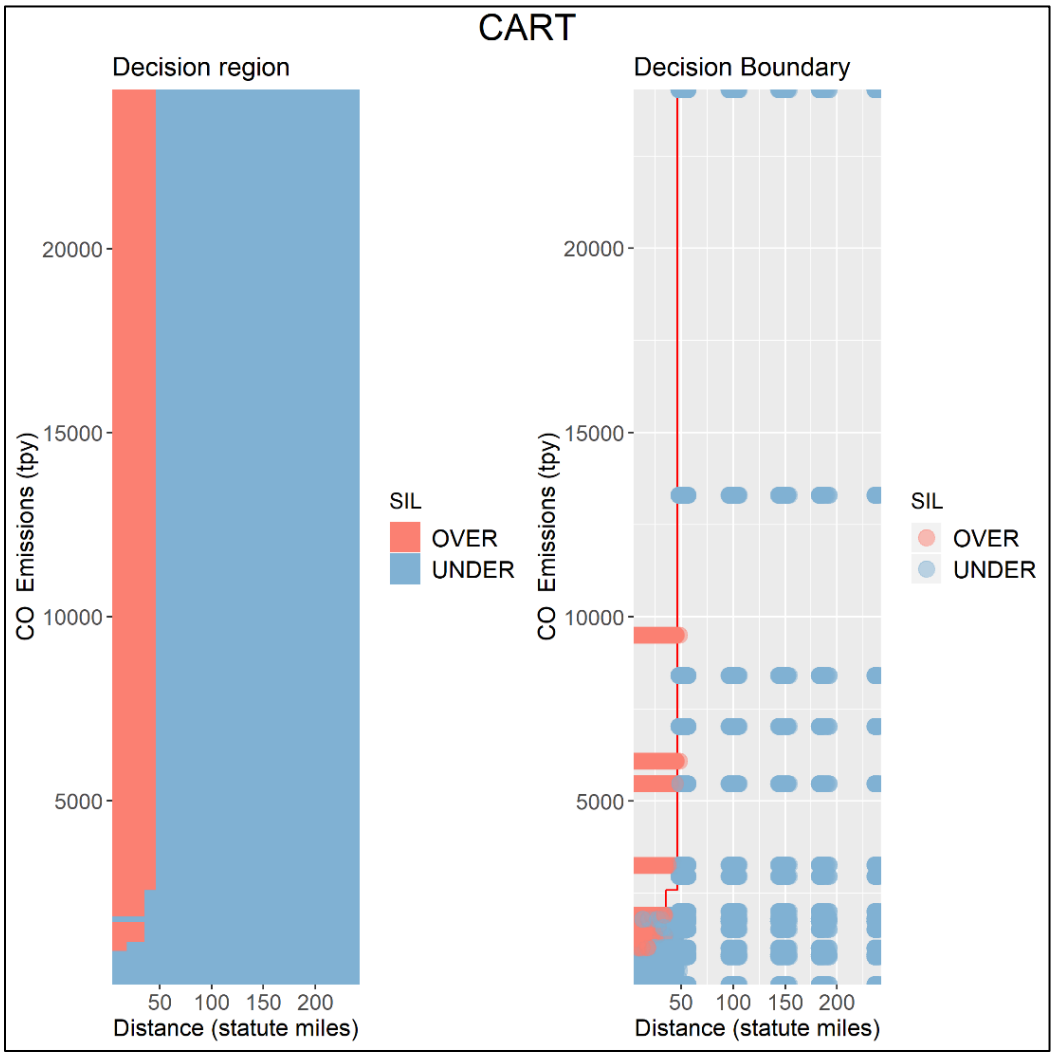

Figure E.8-4. CART Analysis for the CO 1-Hour Modeling Results
The plot on the left shows the determine-decision regions, with red shading indicating results above the SIL and blue shading below. The plot on the right shows the decision boundary (red line) overlaid on the original data.

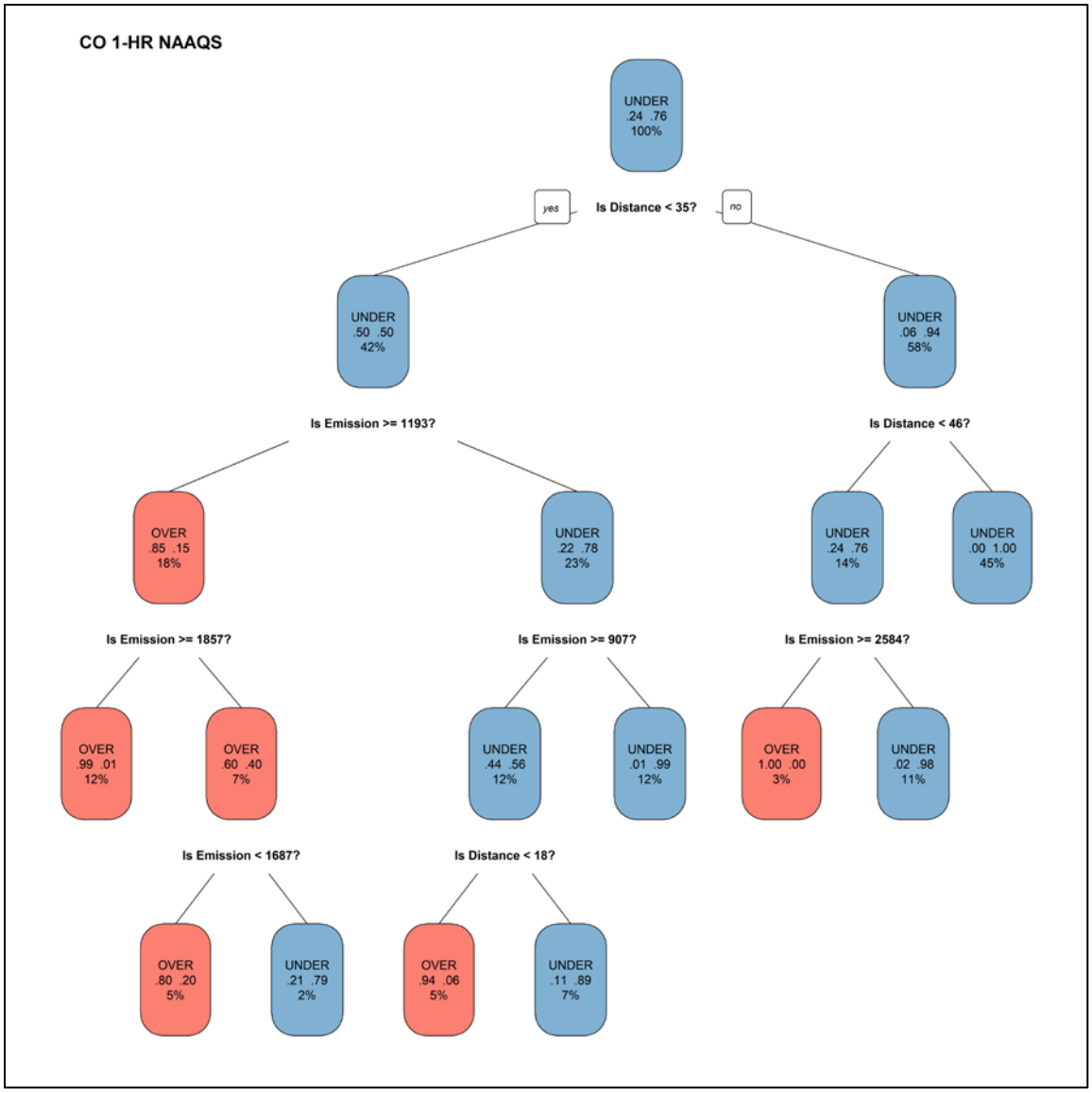

Figure E.8-5. CART Decision Tree for the CO 1-Hour Modeling Results

At each decision point, the branch to the right indicates a response of "no." The boxes at each decision point indicate the probability that the source is over (middle row, left) or under (middle row, right) the SIL and the percentage of the total values in the bin (bottom).

Table E.8-7. Comparison of CART Outcomes to the Original EET for the CO 1-Hour NAAQS

Formula ID	False Positive	False Negative	Pass	Formula
Original	0.00%	23.42%	76.58%	$3400\times(D)^{(2/3)}$
CART	1.32%	1.68%	97.00%	– [a]

[a] The CART tool is a decision tree coded as a series of nested "if statements" to calculate false positive, false negative, and pass rates.

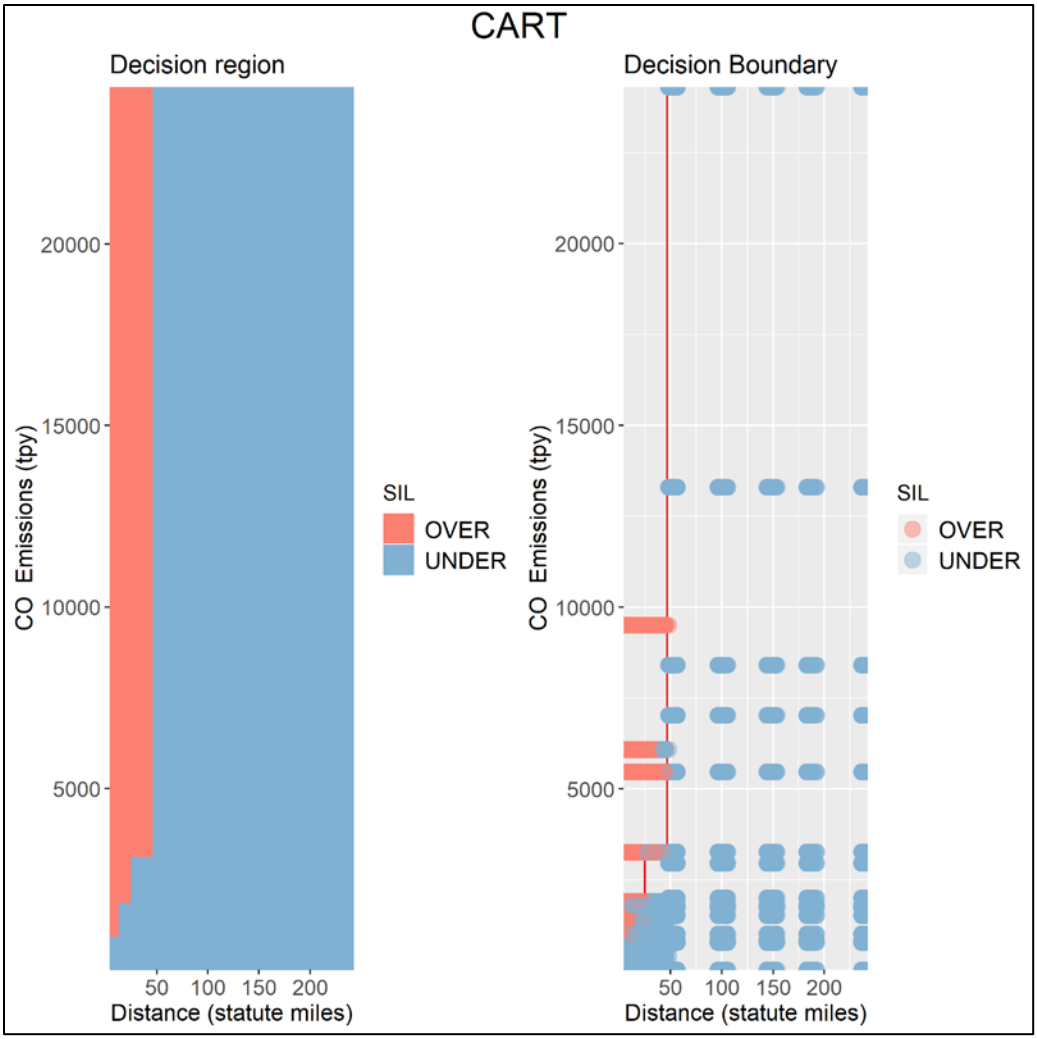

Figure E.8-6. CART Analysis for the CO 8-Hour Modeling Results
The plot on the left shows the determine-decision regions, with red shading indicating results above the SIL and blue shading below. The plot on the right shows the decision boundary (red line) overlaid on the original data.

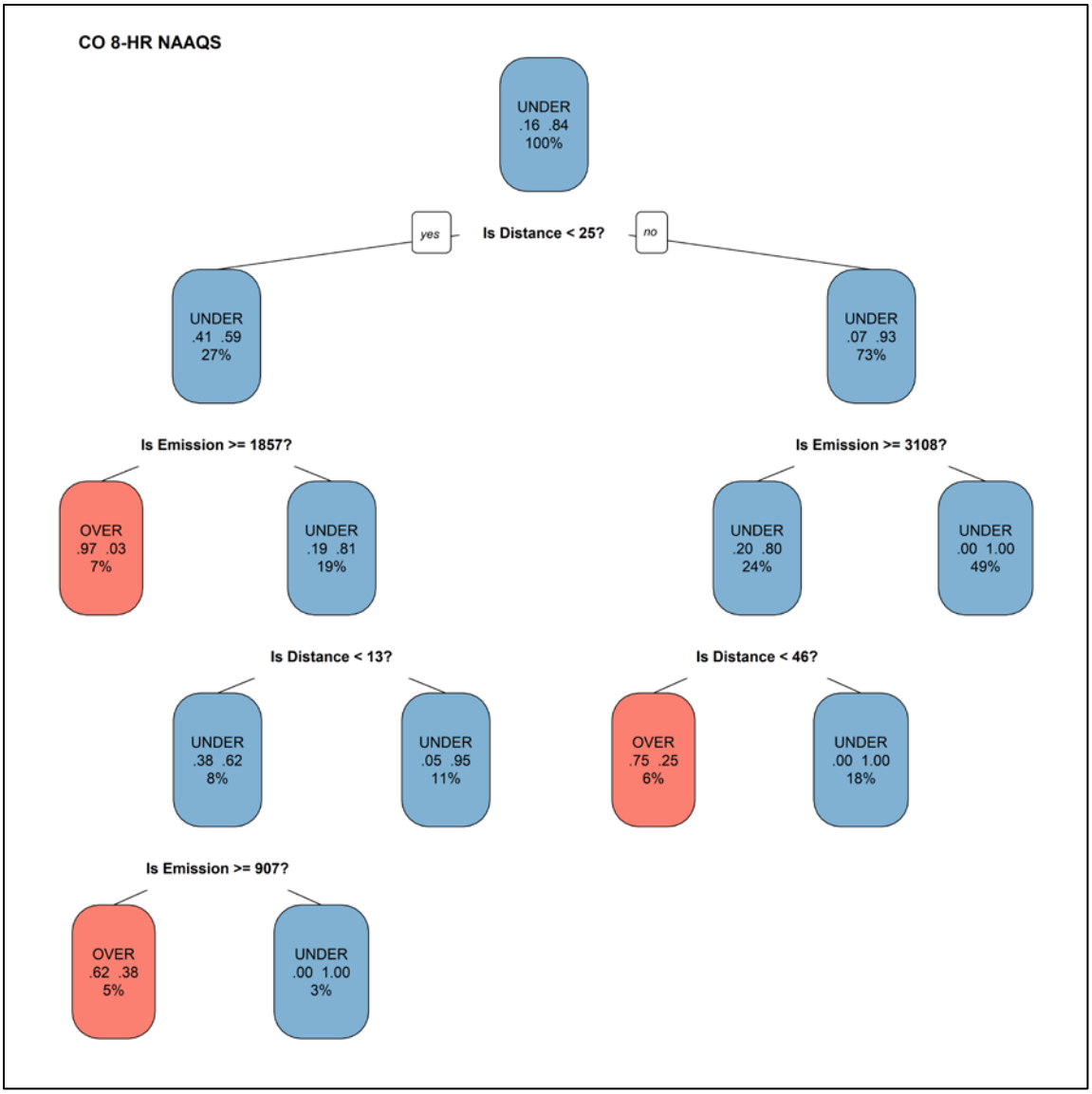

Figure E.8-7. CART Decision Tree for the CO 8-Hour Modeling Results

At each decision point, the branch to the right indicates a response of "no." The boxes at each decision point indicate the probability that the source is over (middle row, left) or under (middle row, right) the SIL and the percentage of the total values in the bin (bottom).

Table E.8-8. Comparison of CART Outcomes to the Original EET for the CO 8-Hour NAAQS

Formula ID	False Positive	False Negative	Pass	Formula
Original	0.00%	16.30%	83.70%	$3400\times(D)^{(2/3)}$
CART	3.74%	0.66%	95.60%	– [a]

[a] The CART tool is a decision tree coded as a series of nested "if statements" to calculate false positive, false negative, and pass rates.

E.8.5.2 PM_{10}

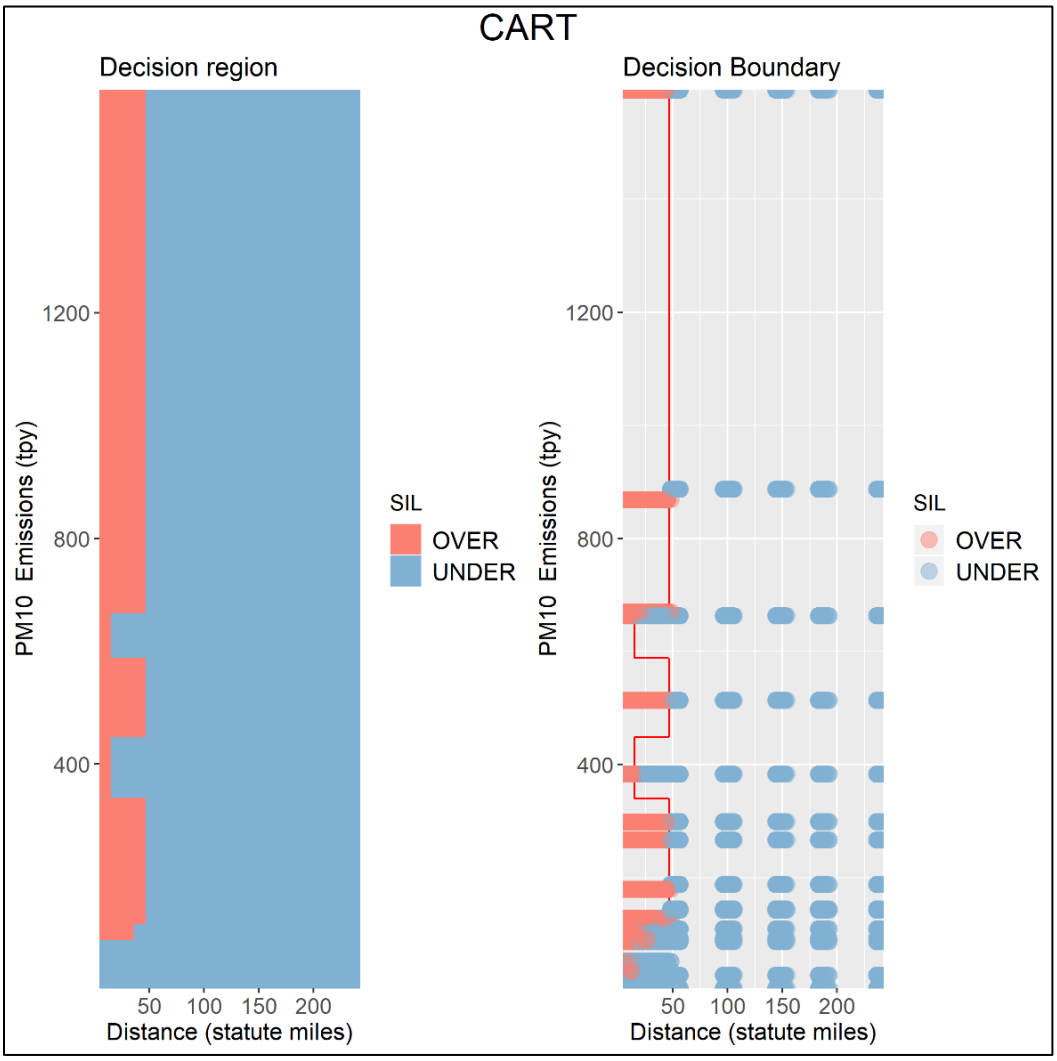

Figure E.8-8. CART Analysis for the PM_{10} 24-Hour Modeling Results
The plot on the left shows the determine-decision regions, with red shading indicating results above the SIL and blue shading below. The plot on the right shows the decision boundary (red line) overlaid on the original data.

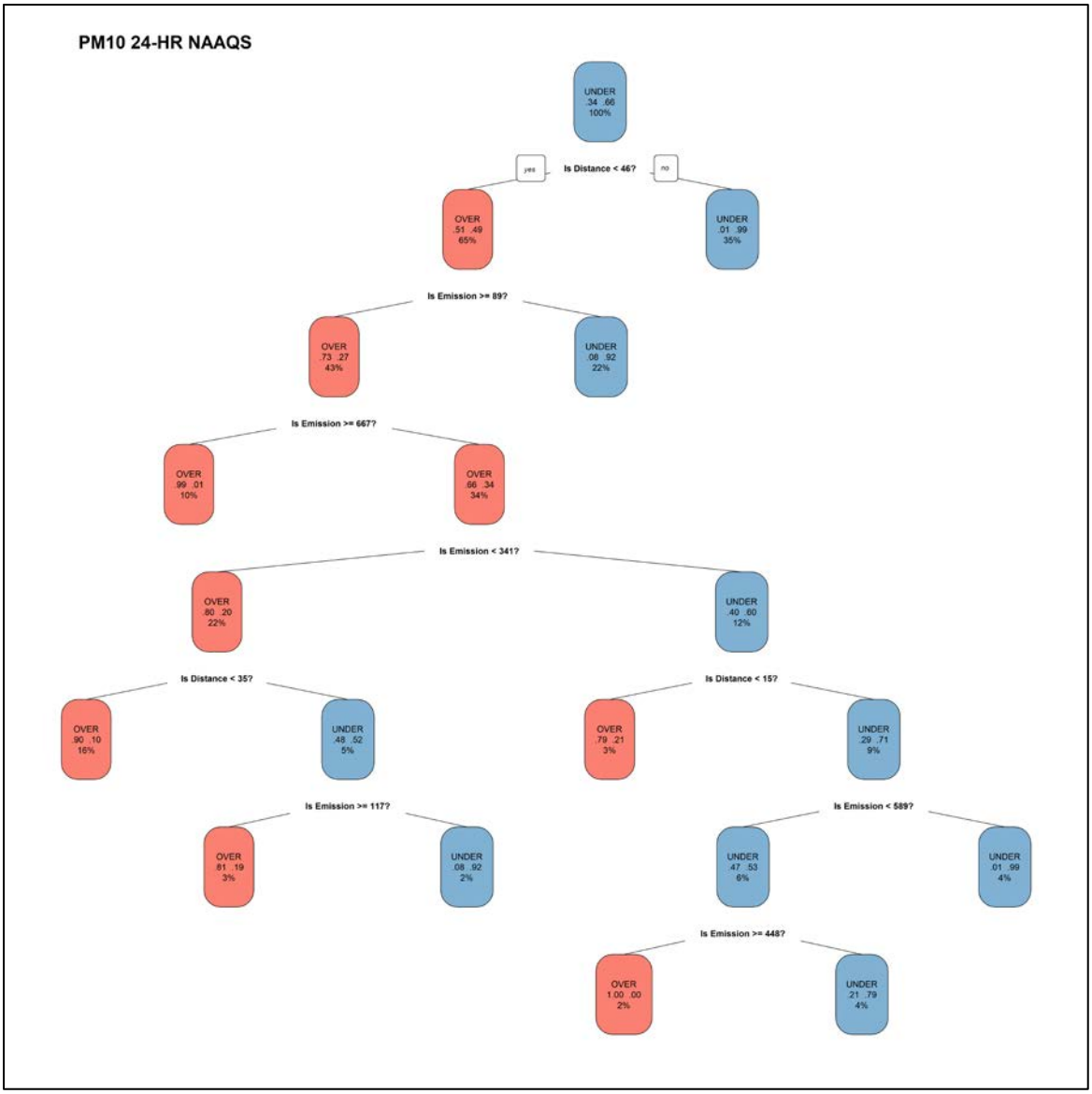

Figure E.8-9. CART Decision Tree for the PM_{10} 24-Hour Modeling Results

At each decision point, the branch to the right indicates a response of "no." The boxes at each decision point indicate the probability that the source is over (middle row, left) or under (middle row, right) the SIL and the percentage of the total values in the bin (bottom).

Table E.8-9. Comparison of CART Outcomes to the Original EET for the PM_{10} 24-Hour NAAQS

Formula ID	False Positive	False Negative	Pass	Formula
Original	0.48%	26.12%	73.39%	33.3*D
CART	2.92%	2.94%	94.14%	– [a]

[a] The CART tool is a decision tree coded as a series of nested "if statements" to calculate false positive, false negative, and pass rates.

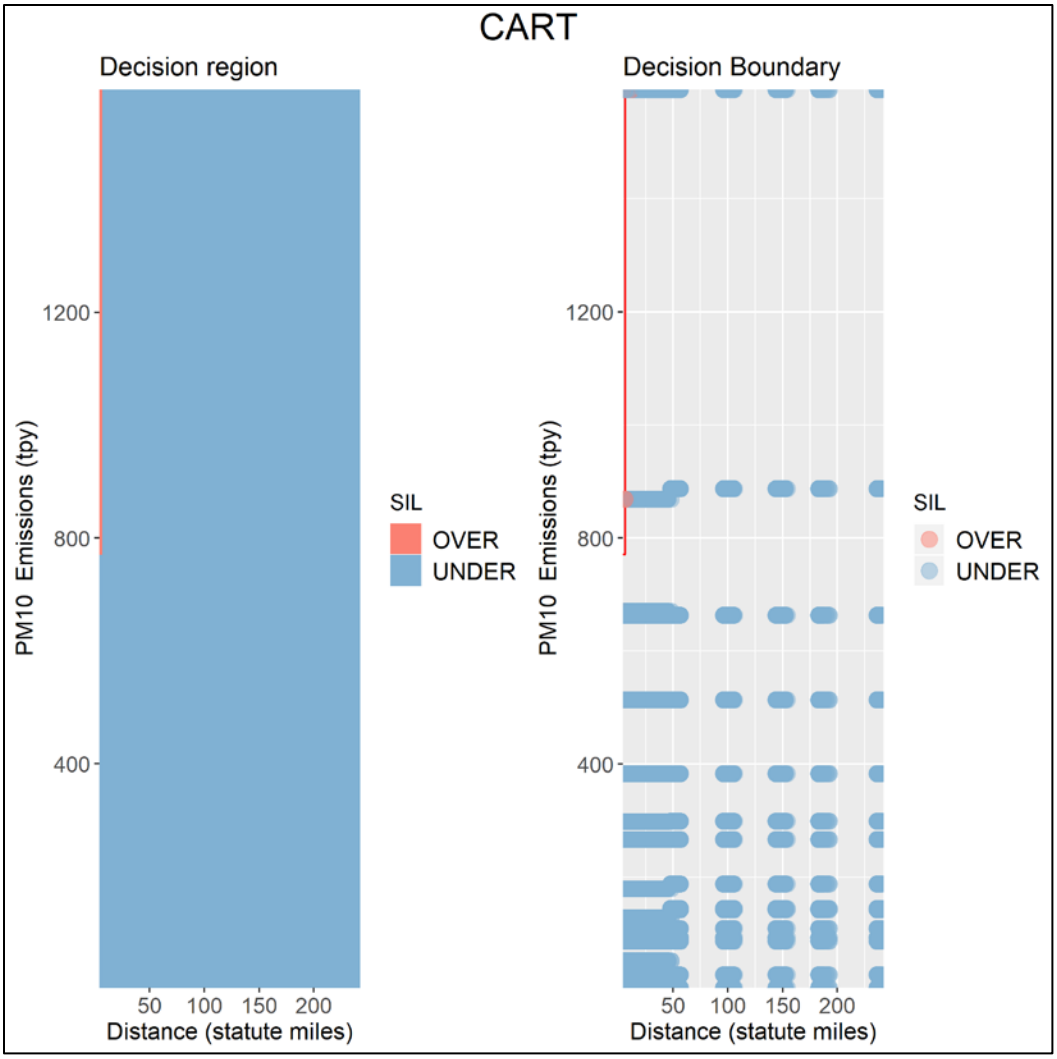

Figure E.8-10. CART Analysis for the PM_{10} Annual Modeling Results[17]
The plot on the left shows the determine-decision regions, with red shading indicating results above the SIL and blue shading below. The plot on the right shows the decision boundary (red line) overlaid on the original data.

[17] Although the PM_{10} annual standard has been revoked by the USEPA, it is included in the analysis to assess the impact on maintenance areas.

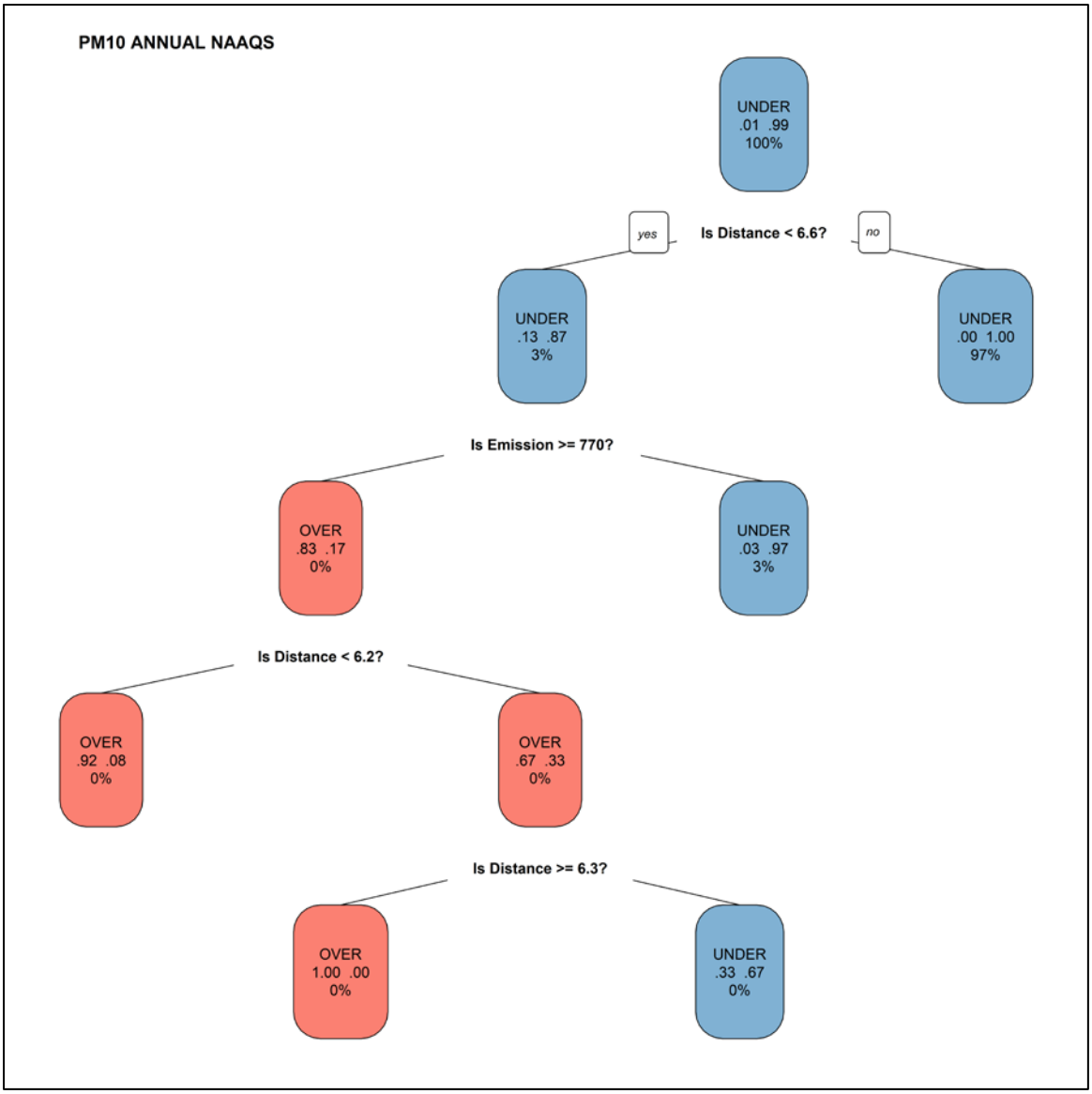

Figure E.8-11. CART Decision Tree for the PM_{10} Annual Modeling Results[18]
At each decision point, the branch to the right indicates a response of "no." The boxes at each decision point indicate the probability that the source is over (middle row, left) or under (middle row, right) the SIL and the percentage of the total values in the bin (bottom).

Table E.8-10. Comparison of CART Outcomes to the Original EET for the PM_{10} Annual NAAQS

Formula ID	False Positive	False Negative	Pass	Formula
Original	6.97%	0.00%	93.03%	33.3*D
CART	0.02%	0.23%	99.75%	– [a]

[a] The CART tool is a decision tree coded as a series of nested "if statements" to calculate false positive, false negative, and pass rates.

[18] Although the PM_{10} annual standard has been revoked by USEPA, it is included in the analysis to assess the impact on maintenance areas.

E.8.5.3 $PM_{2.5}$

The CART analysis does not include contributions due to the secondary formation of $PM_{2.5}$ through chemical transformation of NO_x and SO_2 in the atmosphere. The photochemical modeling analysis conducted as part of the EET evaluation found that source would have to emit approximately 2,500,000 tons of NO_x or 454,000 tons of SO_2 to produce enough secondary $PM_{2.5}$ show a significant impact onshore. Based on current platform emission estimates, this would be an exceptional operation. If a proposed source were to ever approach these values, photochemical modeling would be warranted. Additionally, as NAAQS are refined by EPA, these estimates should be revisited and reconsidered within the context of the decision trees.

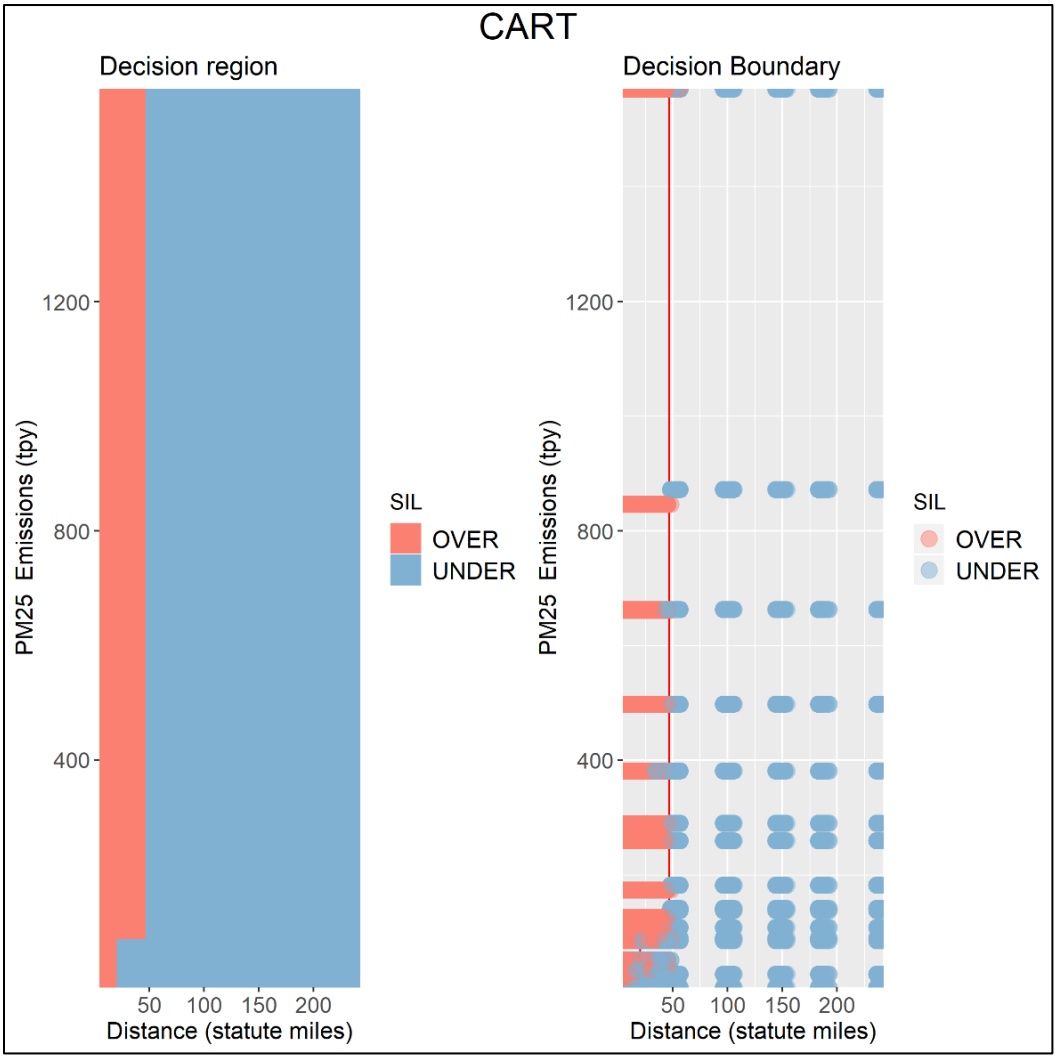

Figure E.8-12. CART Analysis for the $PM_{2.5}$ 24-Hour Modeling Results
The plot on the left shows the determine-decision regions, with red shading indicating results above the SIL and blue shading below. The plot on the right shows the decision boundary (red line) overlaid on the original data.

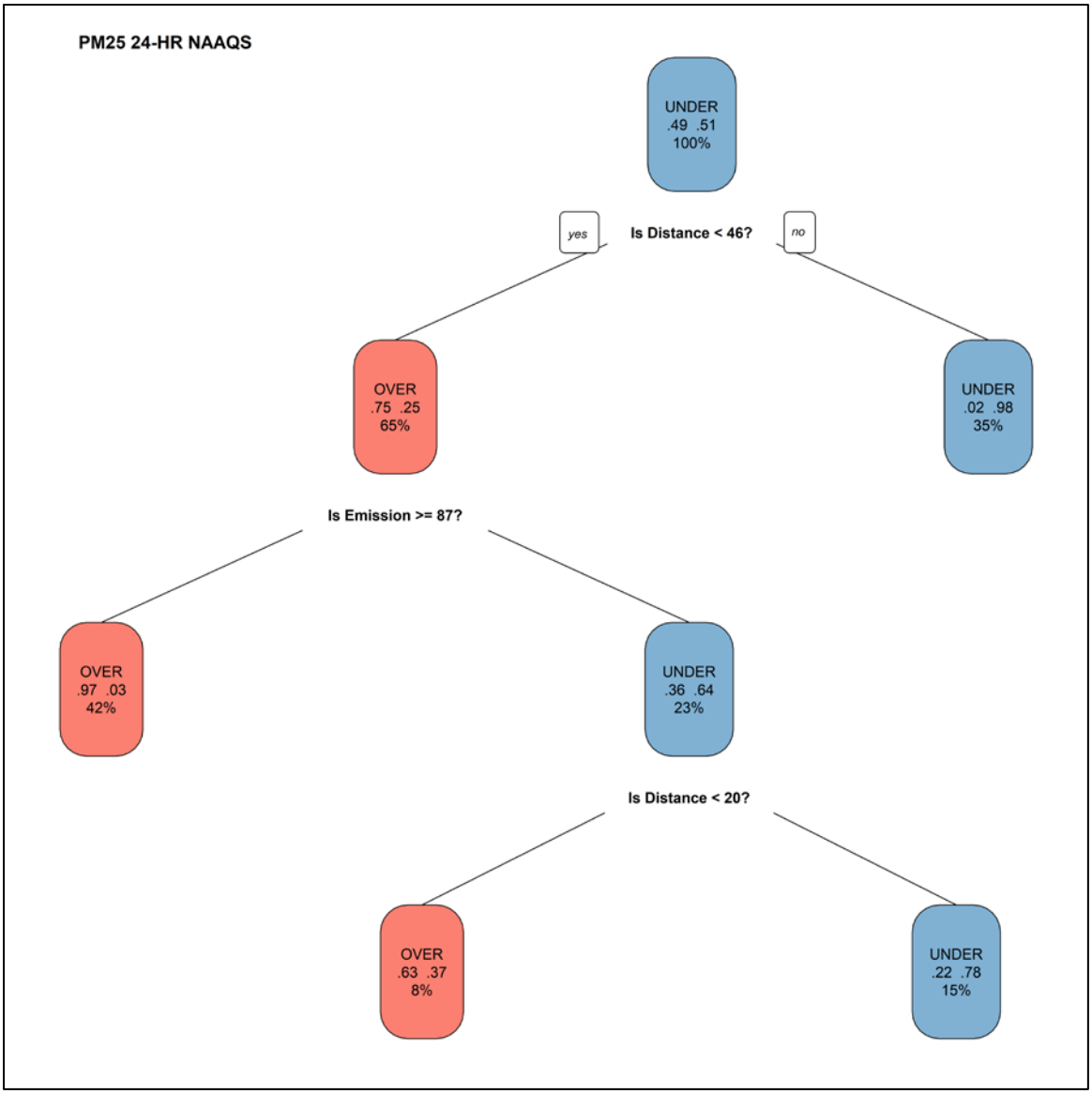

Figure E.8-13. CART Decision Tree for the $PM_{2.5}$ 24-Hour Modeling Results

At each decision point, the branch to the right indicates a response of "no." The boxes at each decision point indicate the probability that the source is over (middle row, left) or under (middle row, right) the SIL and the percentage of the total values in the bin (bottom).

Table E.8-11. Comparison of CART Outcomes to the Original EET for the $PM_{2.5}$ 24-Hour NAAQS

Formula ID	False Positive	False Negative	Pass	Formula
Original	0.00%	36.27%	63.73%	33.3*D
CART	4.27%	3.93%	91.80%	– [a]

[a] The CART tool is a decision tree coded as a series of nested "if statements" to calculate false positive, false negative, and pass rates.

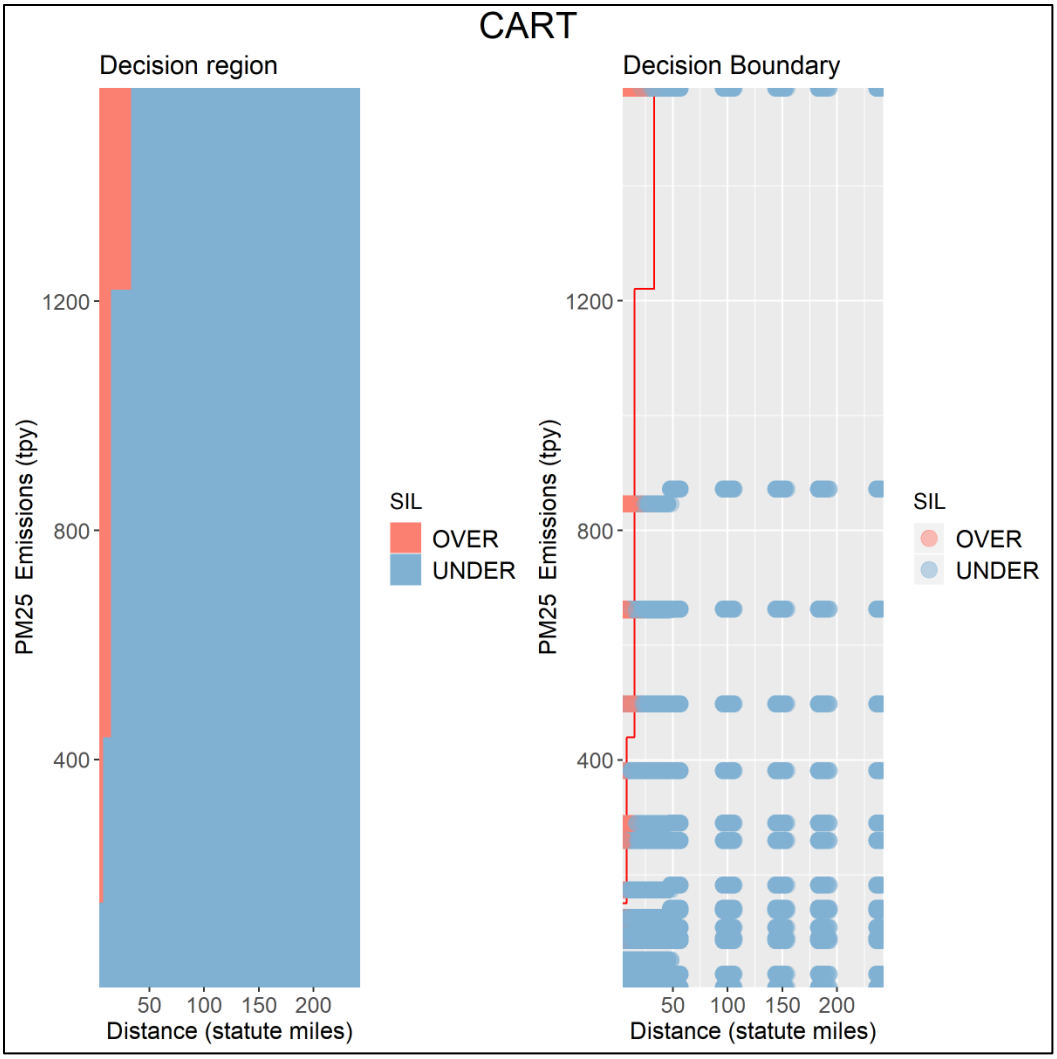

Figure E.8-14. CART Analysis for the $PM_{2.5}$ Annual Modeling Results
The plot on the left shows the determine-decision regions, with red shading indicating results above the SIL and blue shading below. The plot on the right shows the decision boundary (red line) overlaid on the original data.

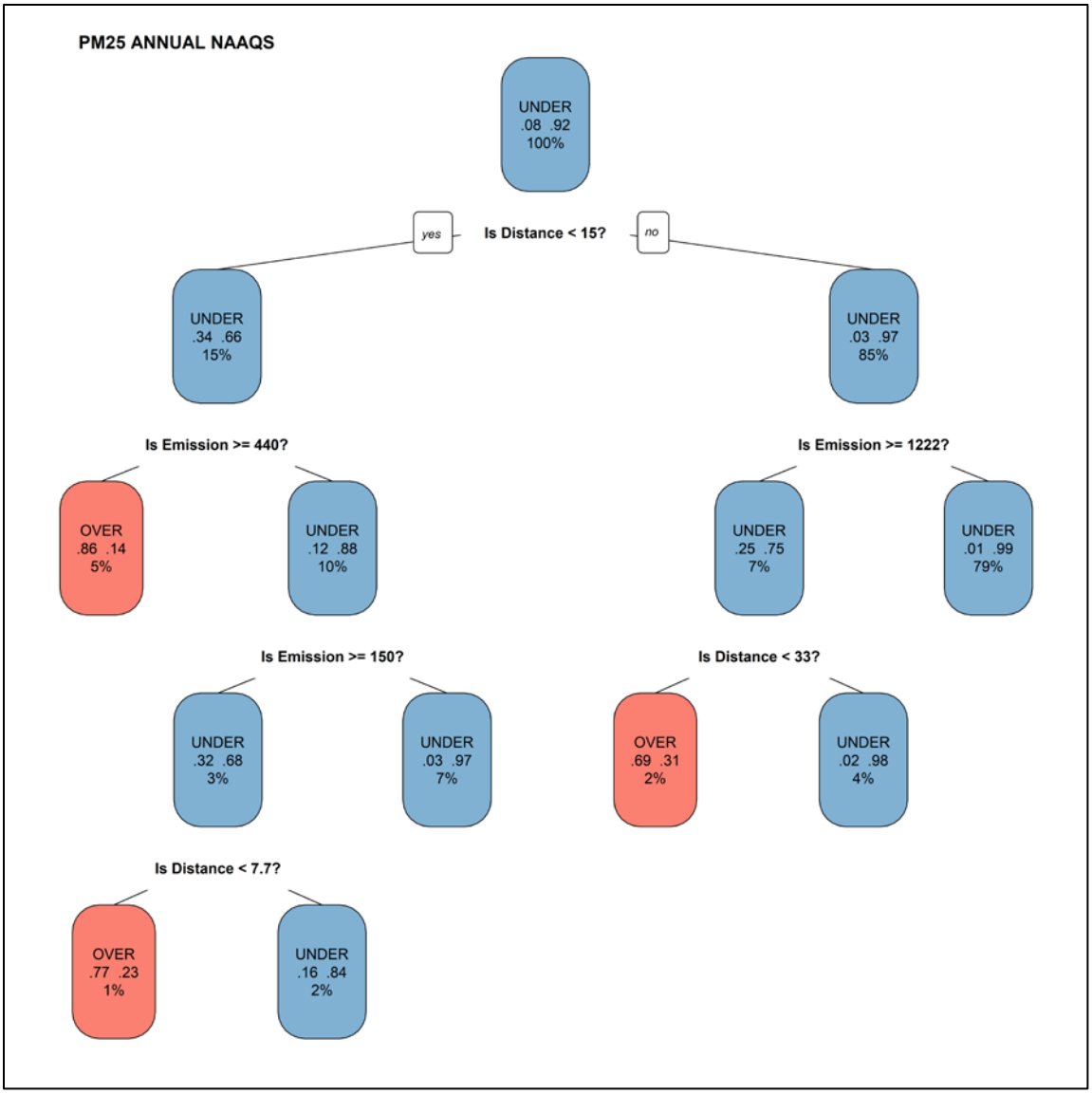

Figure E.8-15. CART Decision Tree for the $PM_{2.5}$ Annual Modeling Results

At each decision point, the branch to the right indicates a response of "no." The boxes at each decision point indicate the probability that the source is over (middle row, left) or under (middle row, right) the SIL and the percentage of the total values in the bin (bottom).

Table E.8-12. Comparison of CART Outcomes to the Original EET for the $PM_{2.5}$ Annual NAAQS

Formula ID	False Positive	False Negative	Pass	Formula
Original	2.85%	1.18%	95.97%	33.3*D
CART	1.51%	1.54%	96.95%	– [a]

[a] The CART tool is a decision tree coded as a series of nested "if statements" to calculate false positive, false negative, and pass rates.

E.8.5.4 Nitrogen Oxides

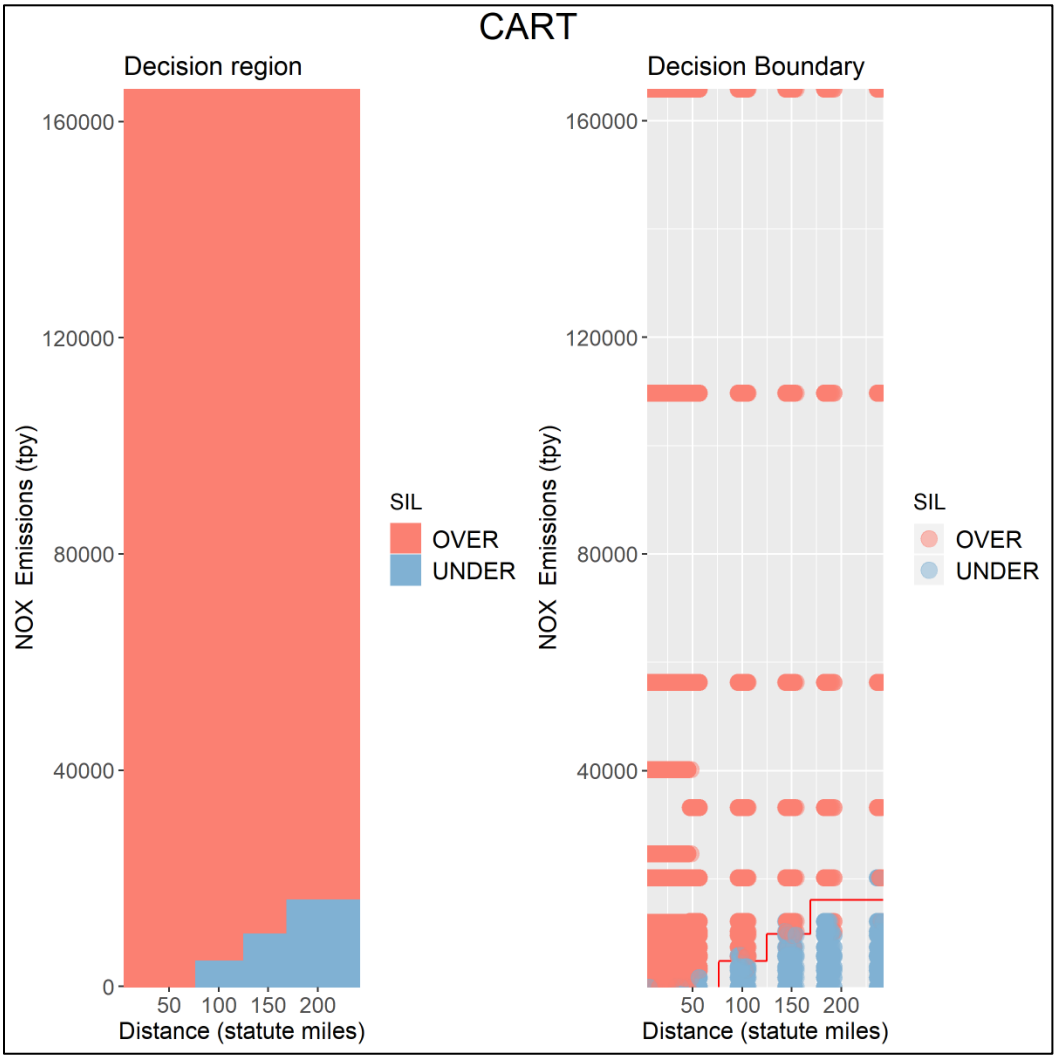

Figure E.8-16. CART Analysis for the NO_x 1-Hour Modeling Results
The plot on the left shows the determine-decision regions, with red shading indicating results above the SIL and blue shading below. The plot on the right shows the decision boundary (red line) overlaid on the original data.

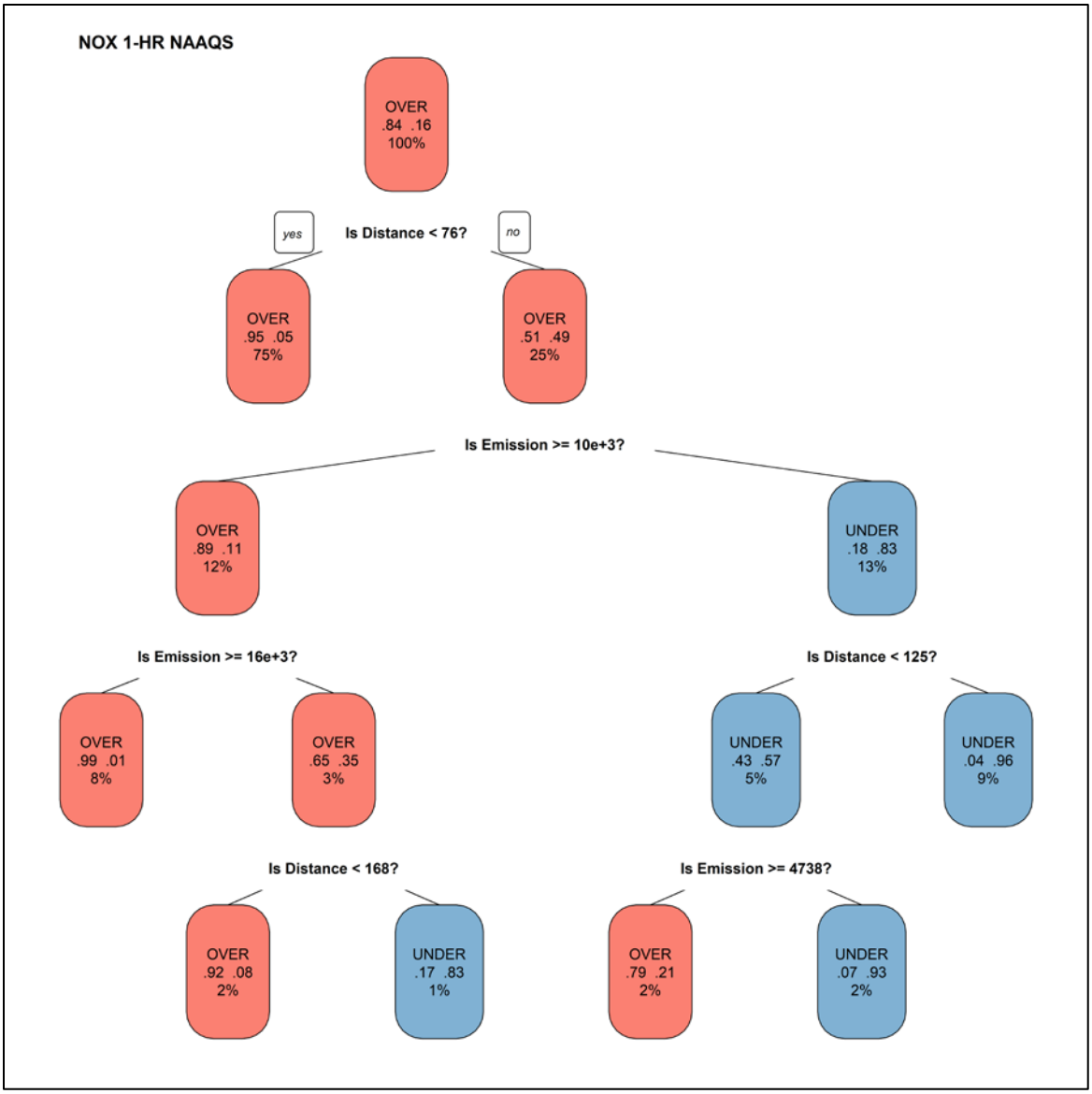

Figure E.8-17. CART Decision Tree for the NO_x 1-Hour Modeling Results

At each decision point, the branch to the right indicates a response of "no." The boxes at each decision point indicate the probability that the source is over (middle row, left) or under (middle row, right) the SIL and the percentage of the total values in the bin (bottom).

Table E.8-13. Comparison of CART Outcomes to the Original EET for the NO_x 1-Hour NAAQS

Formula ID	False Positive	False Negative	Pass	Formula
Original	6.85%	2.33%	90.82%	33.3*D
CART	4.81%	0.68%	94.51%	– [a]

[a] The CART tool is a decision tree coded as a series of nested "if statements" to calculate false positive, false negative, and pass rates.

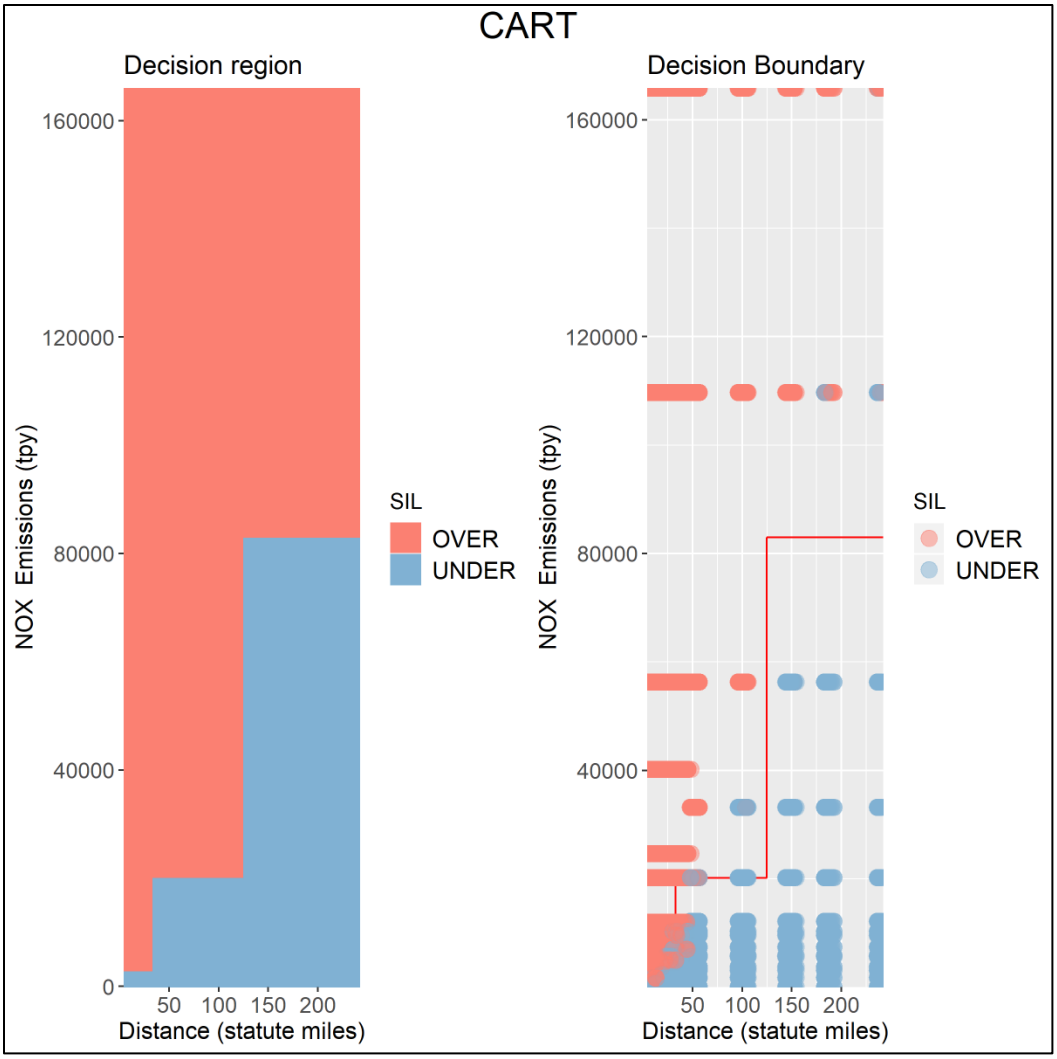

Figure E.8-18. CART Analysis for the NO_x Annual Modeling Results
The plot on the left shows the determine-decision regions, with red shading indicating results above the SIL and blue shading below. The plot on the right shows the decision boundary (red line) overlaid on the original data.

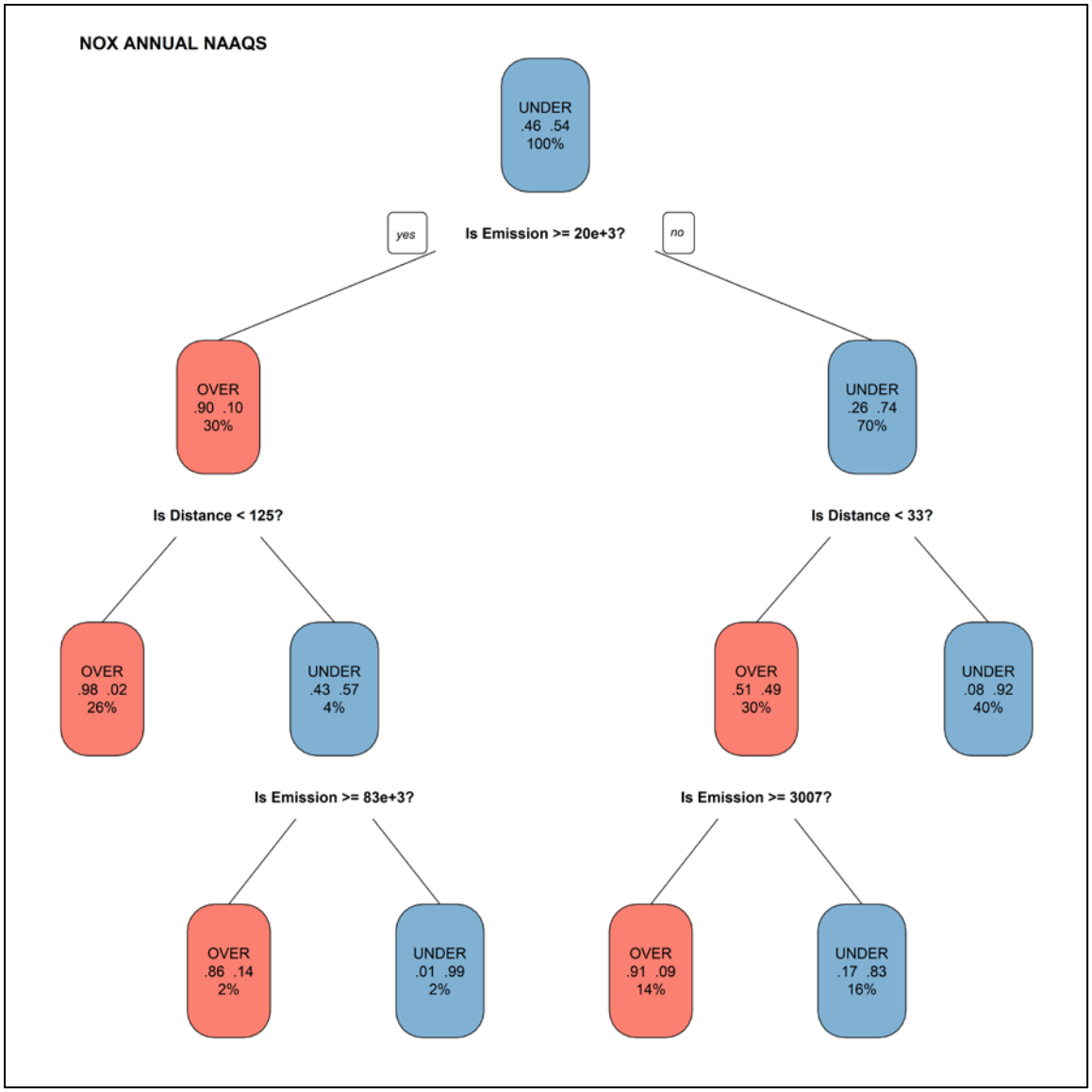

Figure E.8-19. CART Decision Tree for the NO_x Annual Modeling Results

At each decision point, the branch to the right indicates a response of "no." The boxes at each decision point indicate the probability that the source is over (middle row, left) or under (middle row, right) the SIL and the percentage of the total values in the bin (bottom).

Table E.8-14. Comparison of CART Outcomes to the Original EET for the NO_x Annual NAAQS

Formula ID	False Positive	False Negative	Pass	Formula
Original	40.58%	0.00%	59.42%	33.3*D
CART	2.16%	5.90%	91.94%	– [a]

[a] The CART tool is a decision tree coded as a series of nested "if statements" to calculate false positive, false negative, and pass rates.

E.8.5.5 Ozone

The CART analysis does not include decision trees for ozone. Ozone is formed through chemical transformation of NO_x and VOC in the atmosphere. The photochemical modeling analysis conducted as part of the EET evaluation found that source would have to emit approximately 104,000 tons of NO_x or 200,000 tons of VOC to produce enough ozone show a significant impact onshore. Based on current platform emission estimates, this would be an exceptionally large operation. If a proposed source were to ever approach these values, photochemical modeling would be warranted. Additionally, as NAAQS are refined by EPA, these estimates should be revisited and reconsidered within the context of the decision trees.

E.8.5.6 Sulfur Dioxide

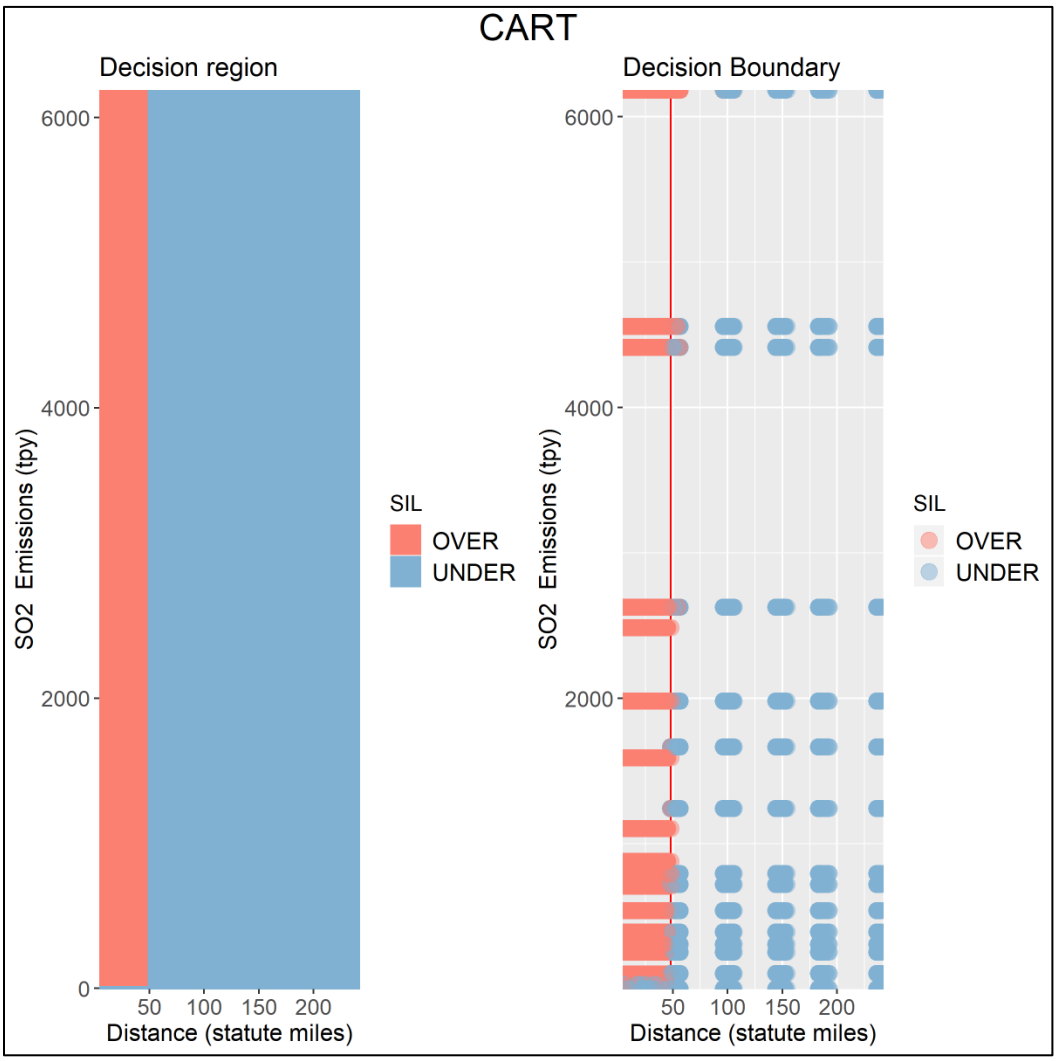

Figure E.8-20. CART Analysis for the SO_2 1-Hour Modeling Results
The plot on the left shows the determine-decision regions, with red shading indicating results above the SIL and blue shading below. The plot on the right shows the decision boundary (red line) overlaid on the original data.

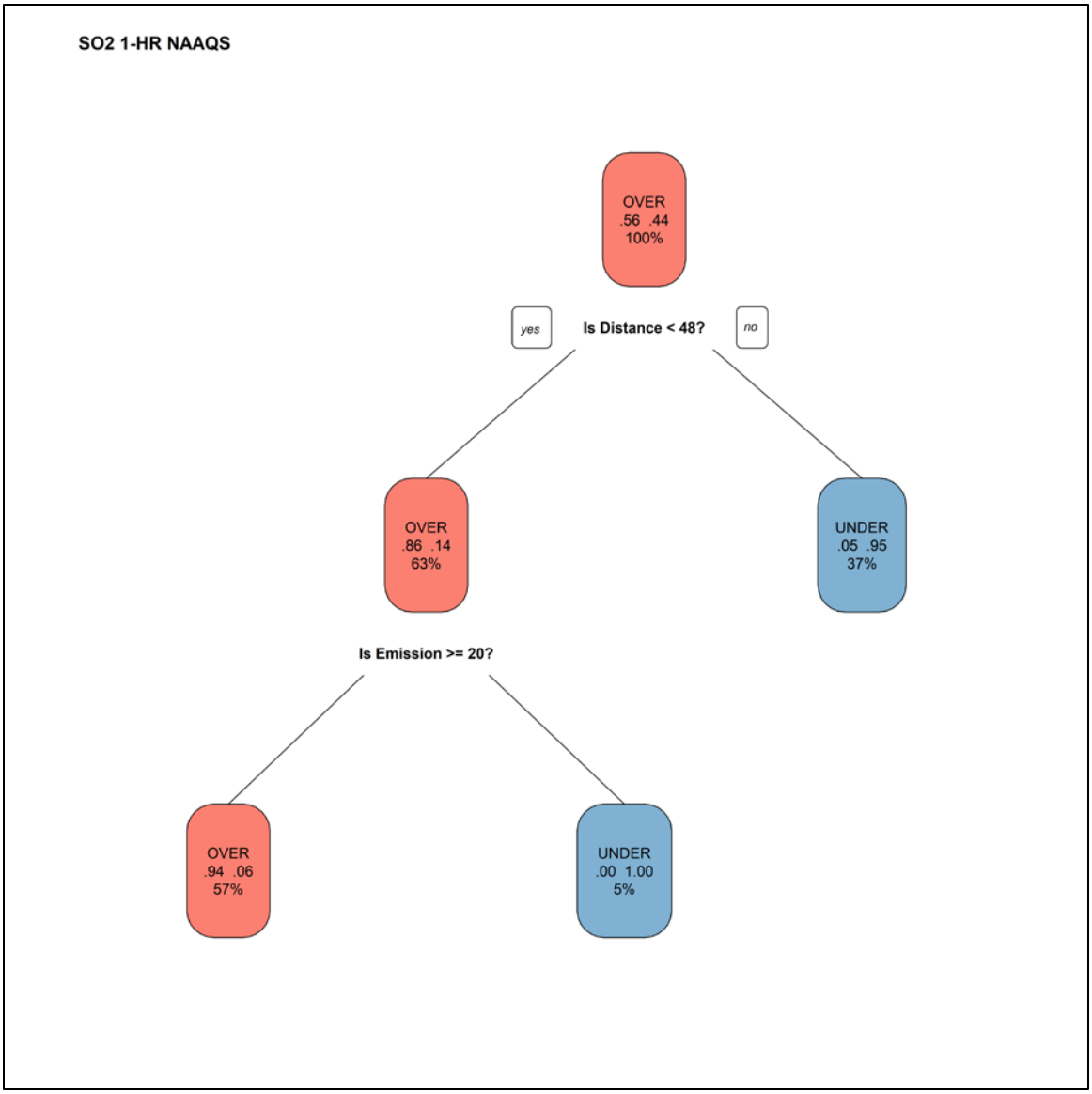

Figure E.8-21. CART Decision Tree for the SO_2 1-Hour Modeling Results

At each decision point, the branch to the right indicates a response of "no." The boxes at each decision point indicate the probability that the source is over (middle row, left) or under (middle row, right) the SIL and the percentage of the total values in the bin (bottom).

Table E.8-15. Comparison of CART Outcomes to the Original EET for the SO_2 1-Hour NAAQS

Formula ID	False Positive	False Negative	Pass	Formula
Original	5.61%	20.91%	73.48%	33.3*D
CART	5.88%	1.45%	92.67%	– [a]

[a] The CART tool is a decision tree coded as a series of nested "if statements" to calculate false positive, false negative, and pass rates.

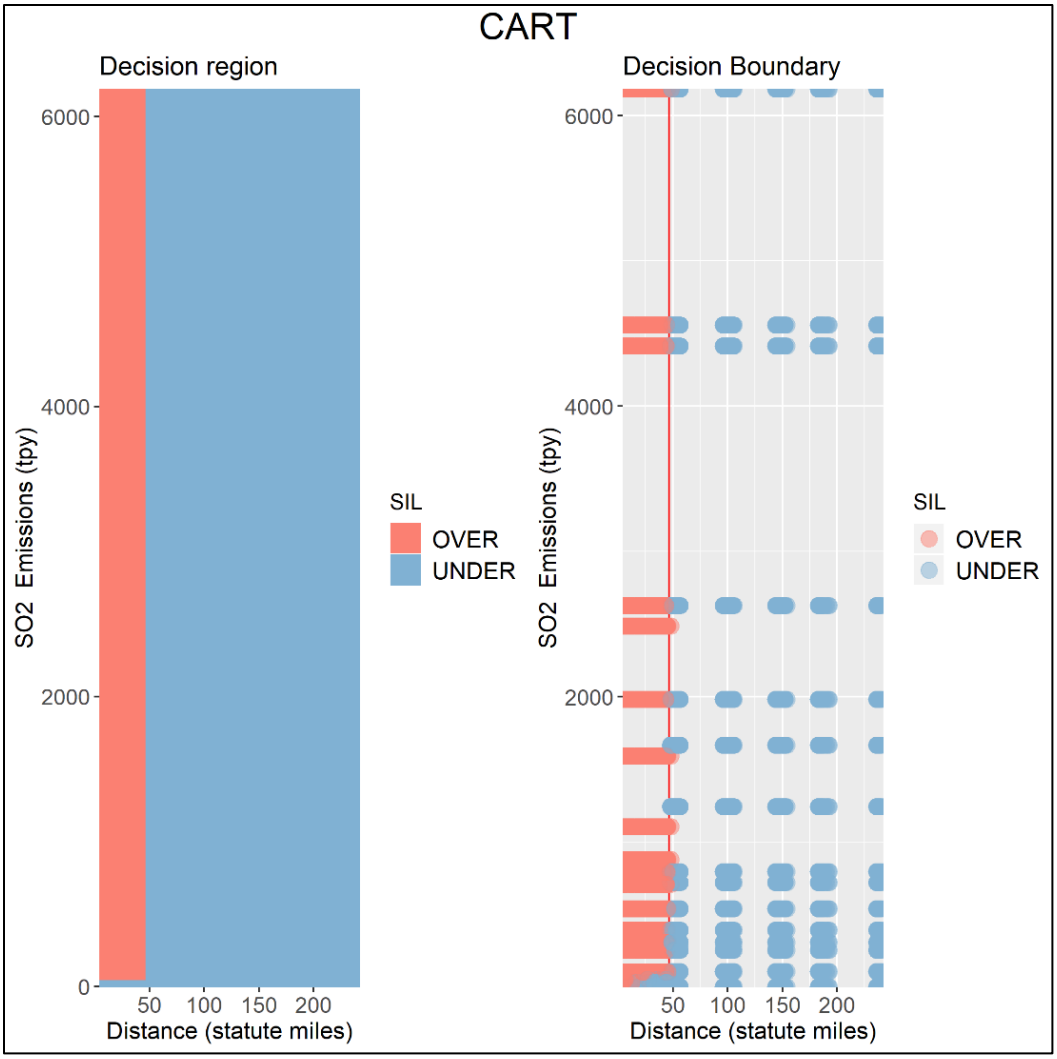

Figure E.8-22. CART Analysis for the SO_2 3-Hour Modeling Results

The plot on the left shows the determine-decision regions, with red shading indicating results above the SIL and blue shading below. The plot on the right shows the decision boundary (red line) overlaid on the original data.

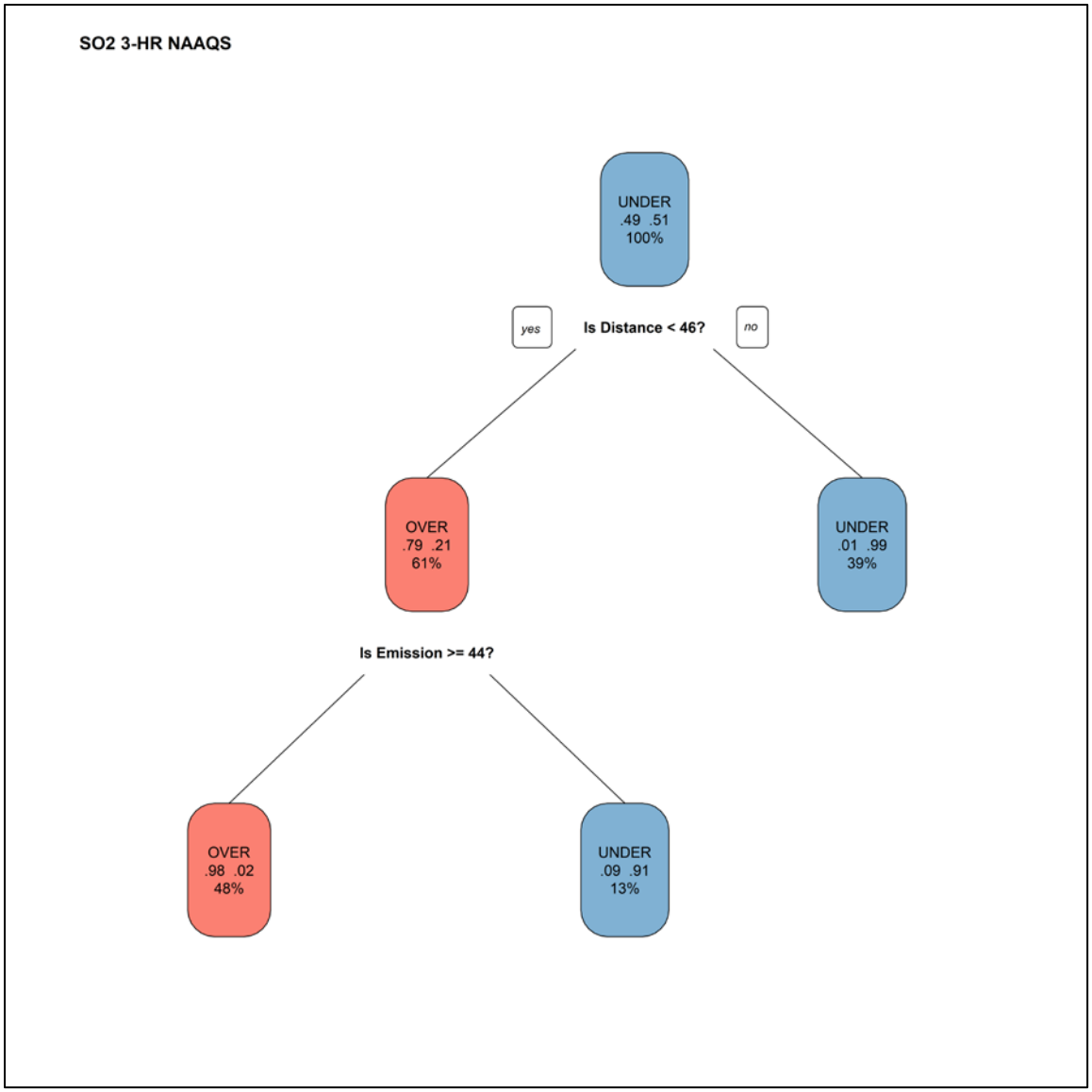

Figure E.8-23. CART Decision Tree for the SO_2 3-Hour Modeling Results

At each decision point, the branch to the right indicates a response of "no." The boxes at each decision point indicate the probability that the source is over (middle row, left) or under (middle row, right) the SIL and the percentage of the total values in the bin (bottom).

Table E.8-16. Comparison of CART Outcomes to the Original EET for the SO_2 3-Hour NAAQS

Formula ID	False Positive	False Negative	Pass	Formula
Original	7.97%	20.76%	71.27%	33.3*D
CART	0.36%	1.83%	97.81%	– [a]

[a] The CART tool is a decision tree coded as a series of nested "if statements" to calculate false positive, false negative, and pass rates.

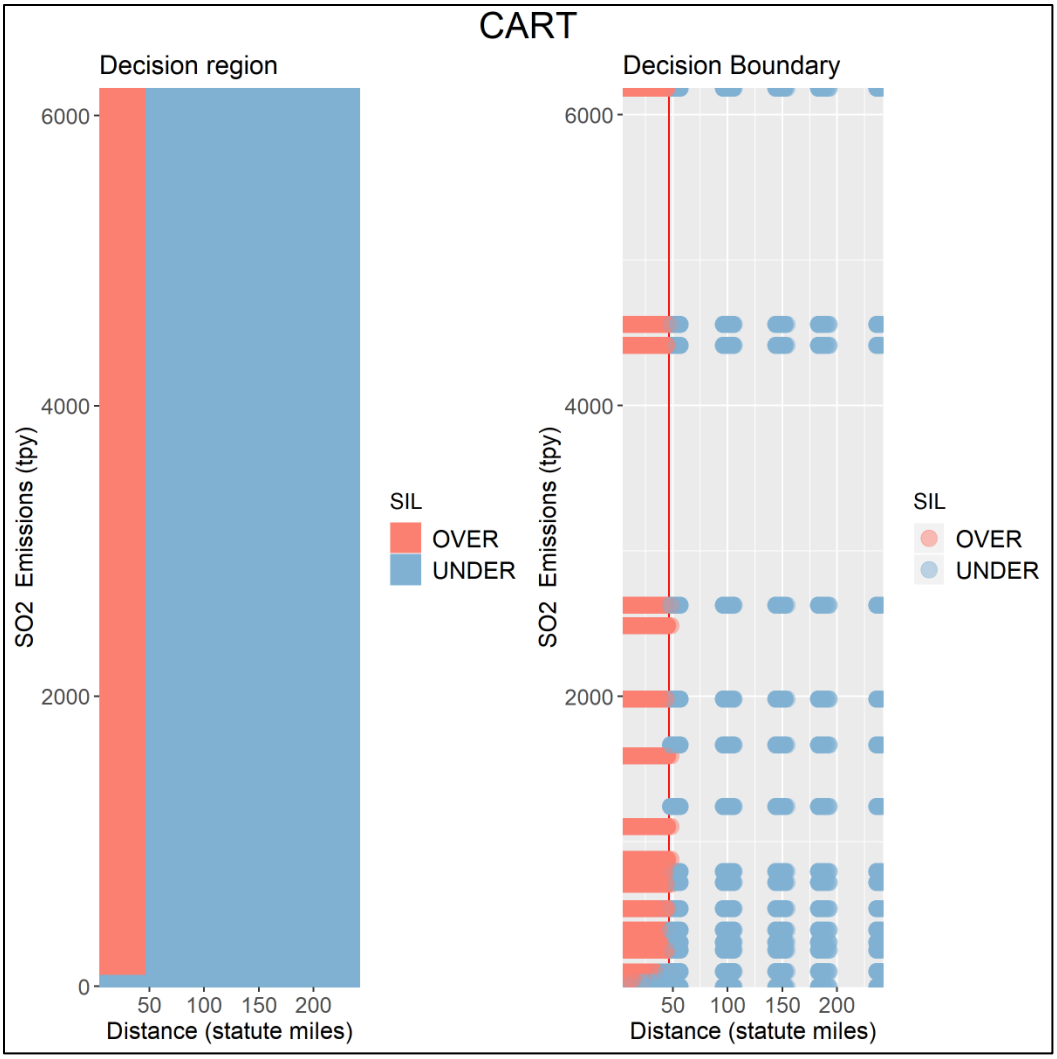

Figure E.8-24. CART Analysis for the SO_2 24-Hour Modeling Results
The plot on the left shows the determine-decision regions, with red shading indicating results above the SIL and blue shading below. The plot on the right shows the decision boundary (red line) overlaid on the original data.[19]

[19] Although the SO_2 24-hour standard has been revoked by USEPA, it is included in the analysis to assess the impact on maintenance areas.

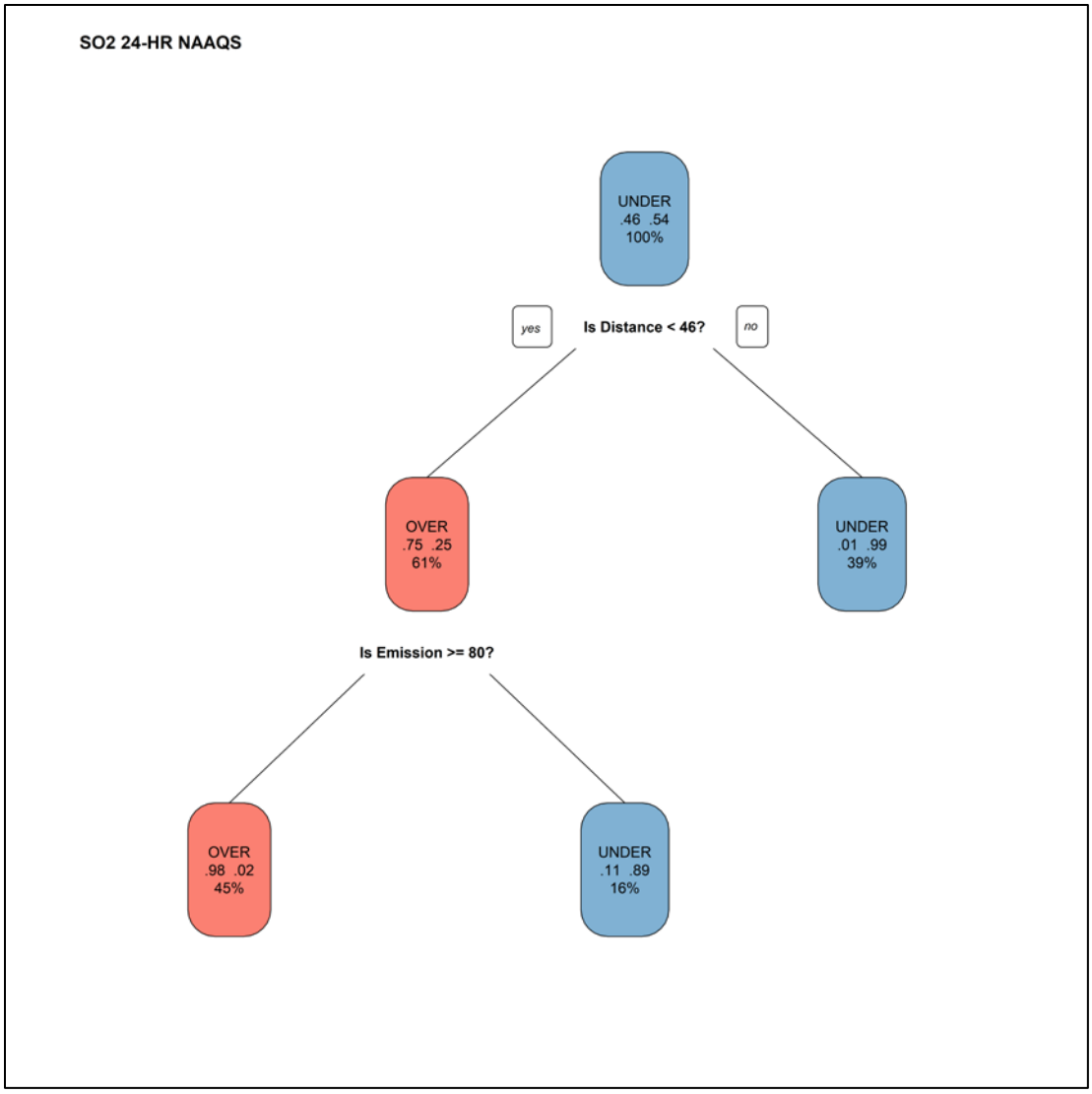

Figure E.8-25. CART Decision Tree for the SO_2 24-Hour Modeling Results[20]
At each decision point, the branch to the right indicates a response of "no." The boxes at each decision point indicate the probability that the source is over (middle row, left) or under (middle row, right) the SIL and the percentage of the total values in the bin (bottom).

Table E.8-17. Comparison of CART Outcomes to the Original EET for the SO_2 24-Hour NAAQS

Formula ID	False Positive	False Negative	Pass	Formula
Original	8.00%	20.06%	71.94%	33.3*D
CART	0.21%	0.78%	99.00%	– [a]

[a] The CART tool is a decision tree coded as a series of nested "if statements" to calculate false positive, false negative, and pass rates.

[20] Although the SO_2 24-hour standard has been revoked by USEPA, it is included in the analysis to assess the impact on maintenance areas.

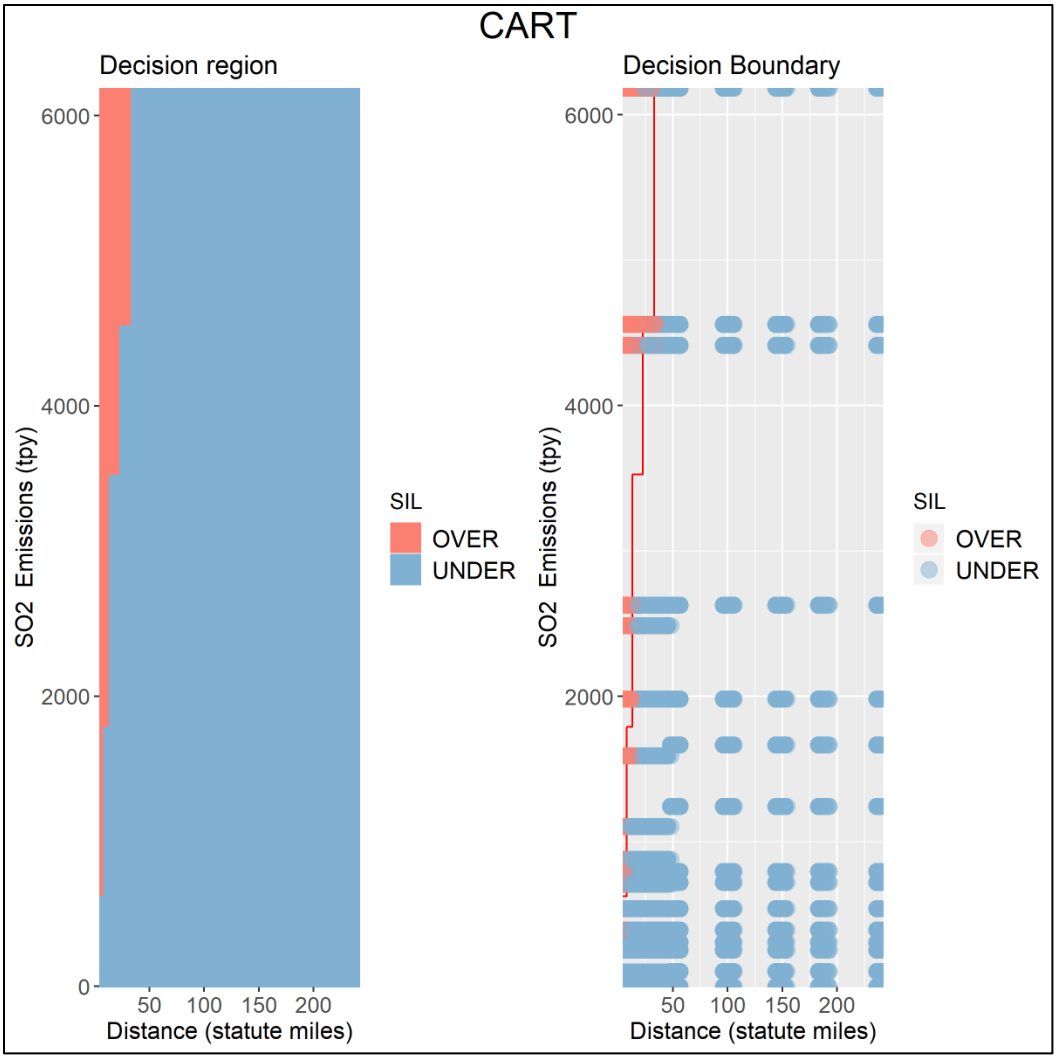

Figure E.8-26. CART Analysis for the SO_2 Annual Modeling Results[21]
The plot on the left shows the determine-decision regions, with red shading indicating results above the SIL and blue shading below. The plot on the right shows the decision boundary (red line) overlaid on the original data.

[21] Although the SO_2 annual standard has been revoked by USEPA, it is included in the analysis to assess the impact on maintenance areas.

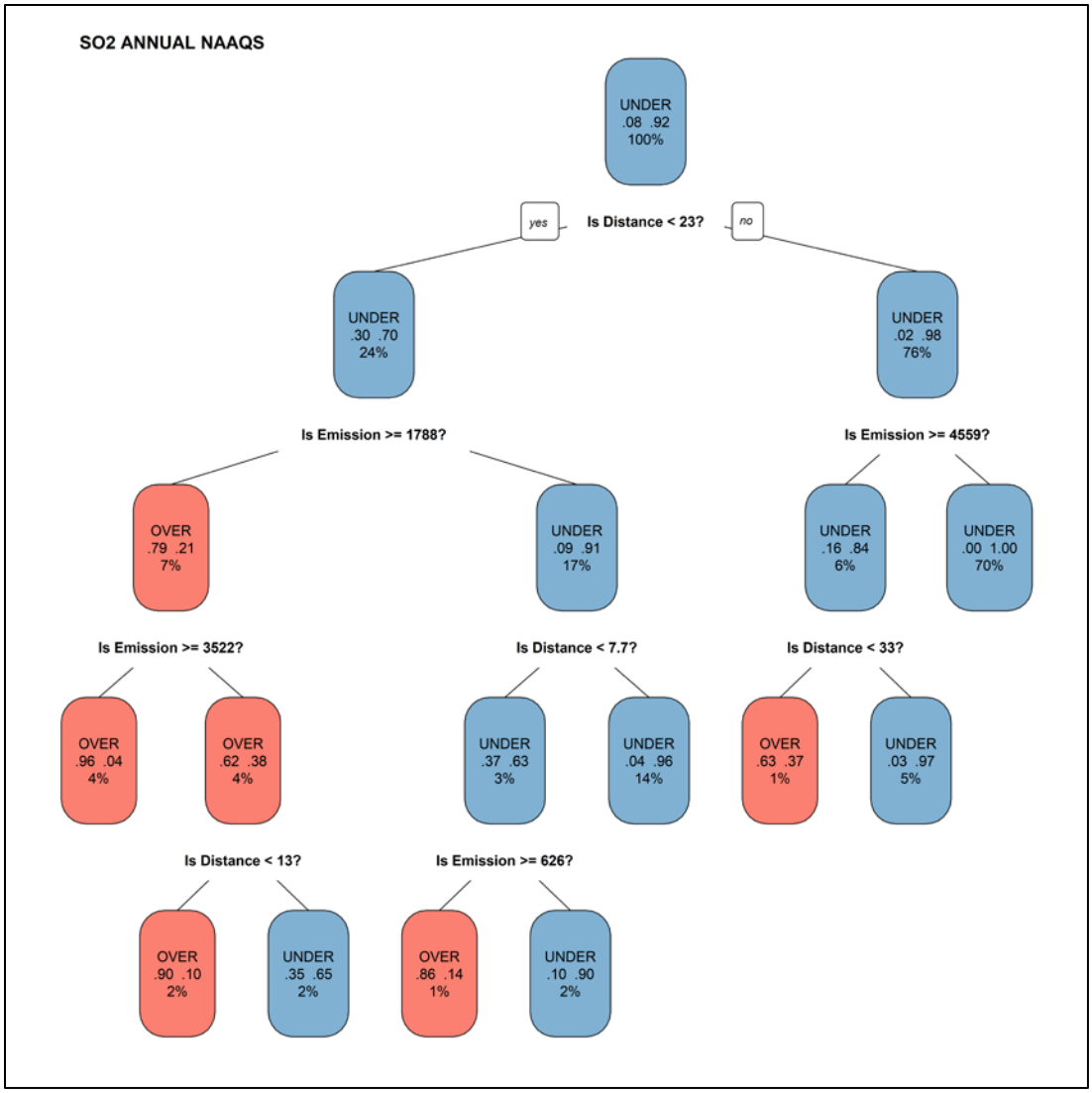

Figure E.8-27. CART Decision Tree for the SO_2 Annual Modeling Results[22]
At each decision point, the branch to the right indicates a response of "no." The boxes at each decision point indicate the probability that the source is over (middle row, left) or under (middle row, right) the SIL and the percentage of the total values in the bin (bottom).

Table E.8-18. Comparison of CART Outcomes to the Original EET for the SO_2 Annual NAAQS

Formula ID	False Positive	False Negative	Pass	Formula
Original	26.61%	0.00%	73.39%	33.3*D
CART	0.03%	0.03%	99.95%	– [a]

[a] The CART tool is a decision tree coded as a series of nested "if statements" to calculate false positive, false negative, and pass rates.

[22] Although the SO_2 annual standard has been revoked by USEPA, it is included in the analysis to assess the impact on maintenance areas.

E.8.6 CART Results, Shoreline Without Vessels

E.8.6.1 Carbon Monoxide

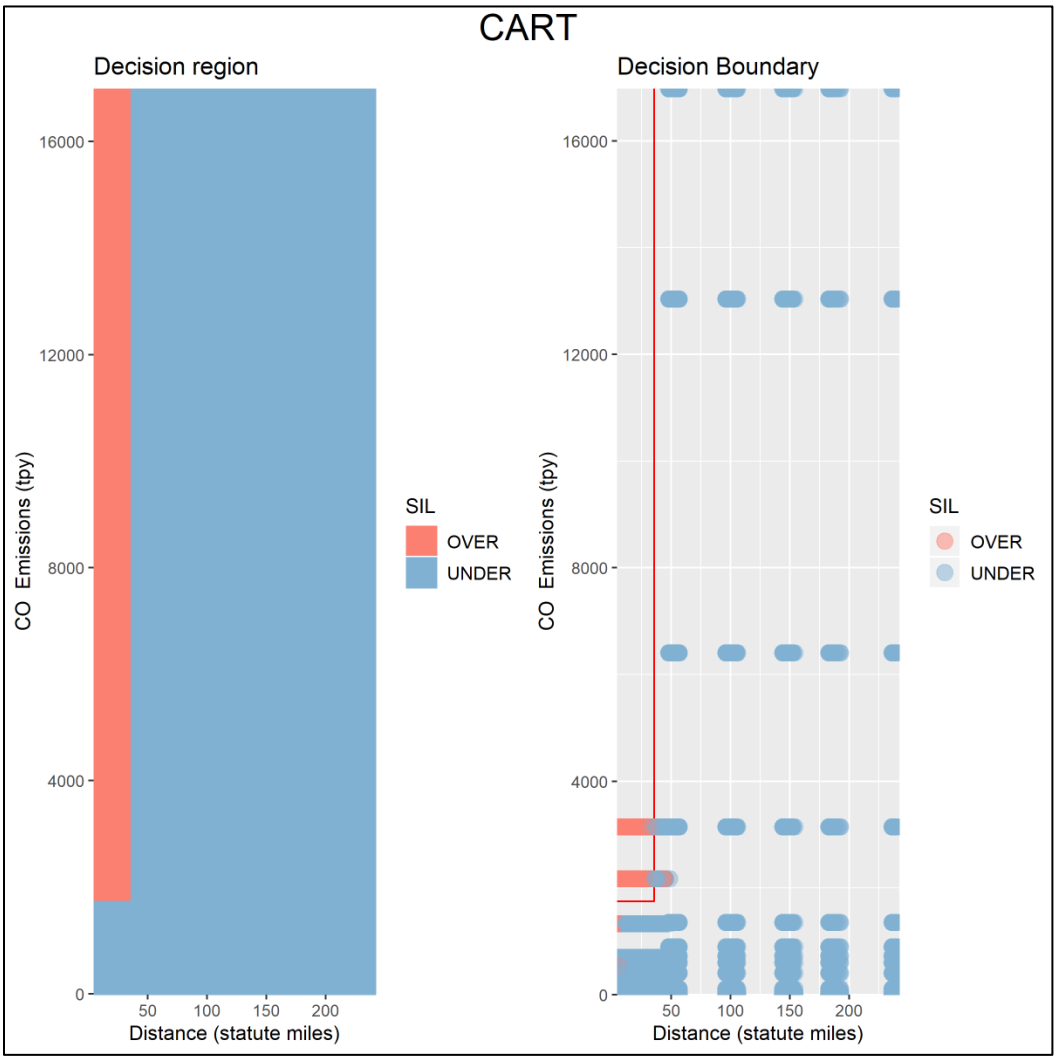

Figure E.8-28. CART Analysis for the CO 1-Hour Modeling Results (Without Vessel Emissions)

The plot on the left shows the determine-decision regions, with red shading indicating results above the SIL and blue shading below. The plot on the right shows the decision boundary (red line) overlaid on the original data.

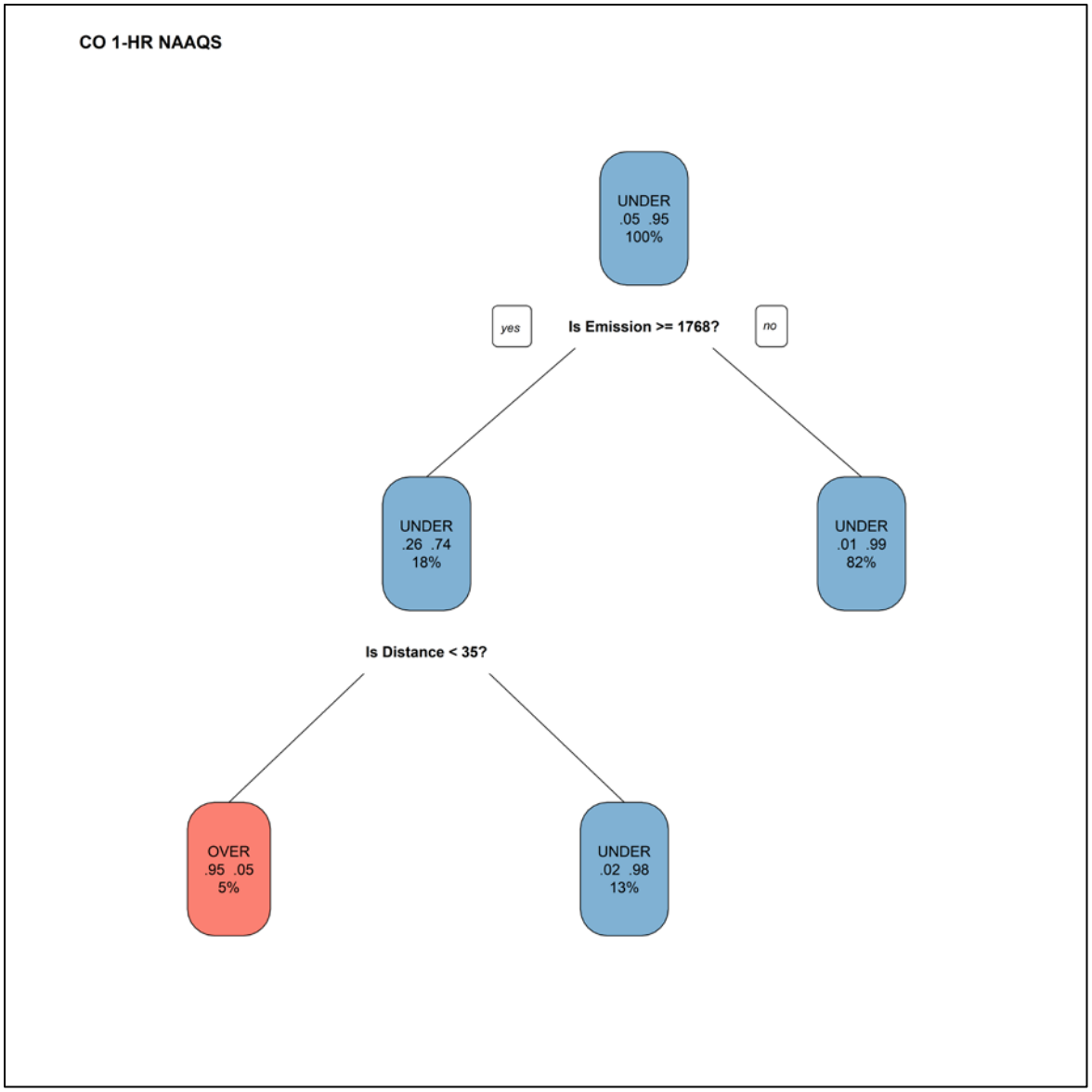

Figure E.8-29. CART Decision Tree for the CO 1-Hour Modeling Results (Without Vessel Emissions)

At each decision point, the branch to the right indicates a response of "no." The boxes at each decision point indicate the probability that the source is over (middle row, left) or under (middle row, right) the SIL and the percentage of the total values in the bin (bottom).

Table E.8-19. CART Outcomes for the CO 1-Hour NAAQS (Without Vessel Emissions)

Formula ID	False Positive	False Negative	Pass	Formula
CART	0.22%	0.66%	99.12%	– [a]

[a] The CART tool is a decision tree coded as a series of nested "if statements" to calculate false positive, false negative, and pass rates.

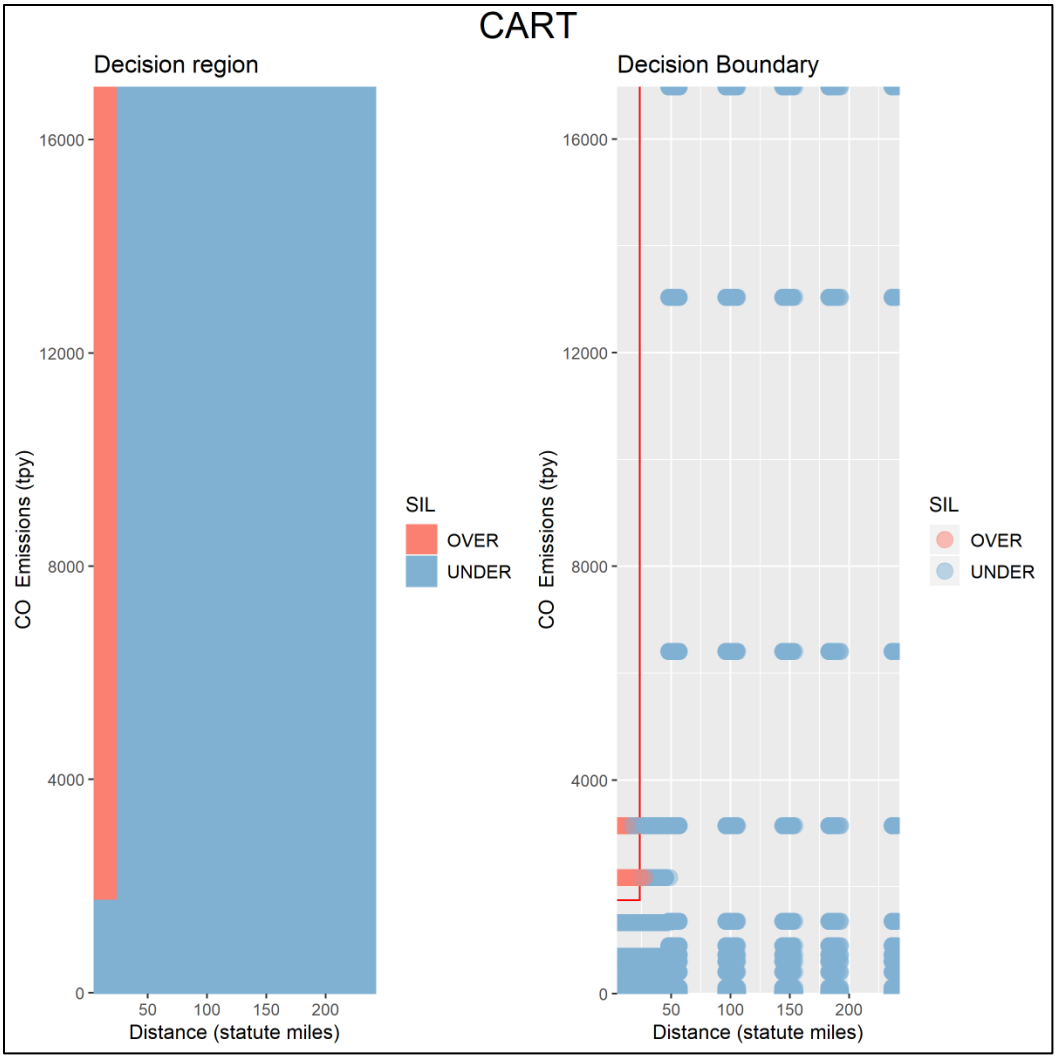

Figure E.8-30. CART Analysis for the CO 8-Hour Modeling Results (Without Vessel Emissions)

The plot on the left shows the determine-decision regions, with red shading indicating results above the SIL and blue shading below. The plot on the right shows the decision boundary (red line) overlaid on the original data.

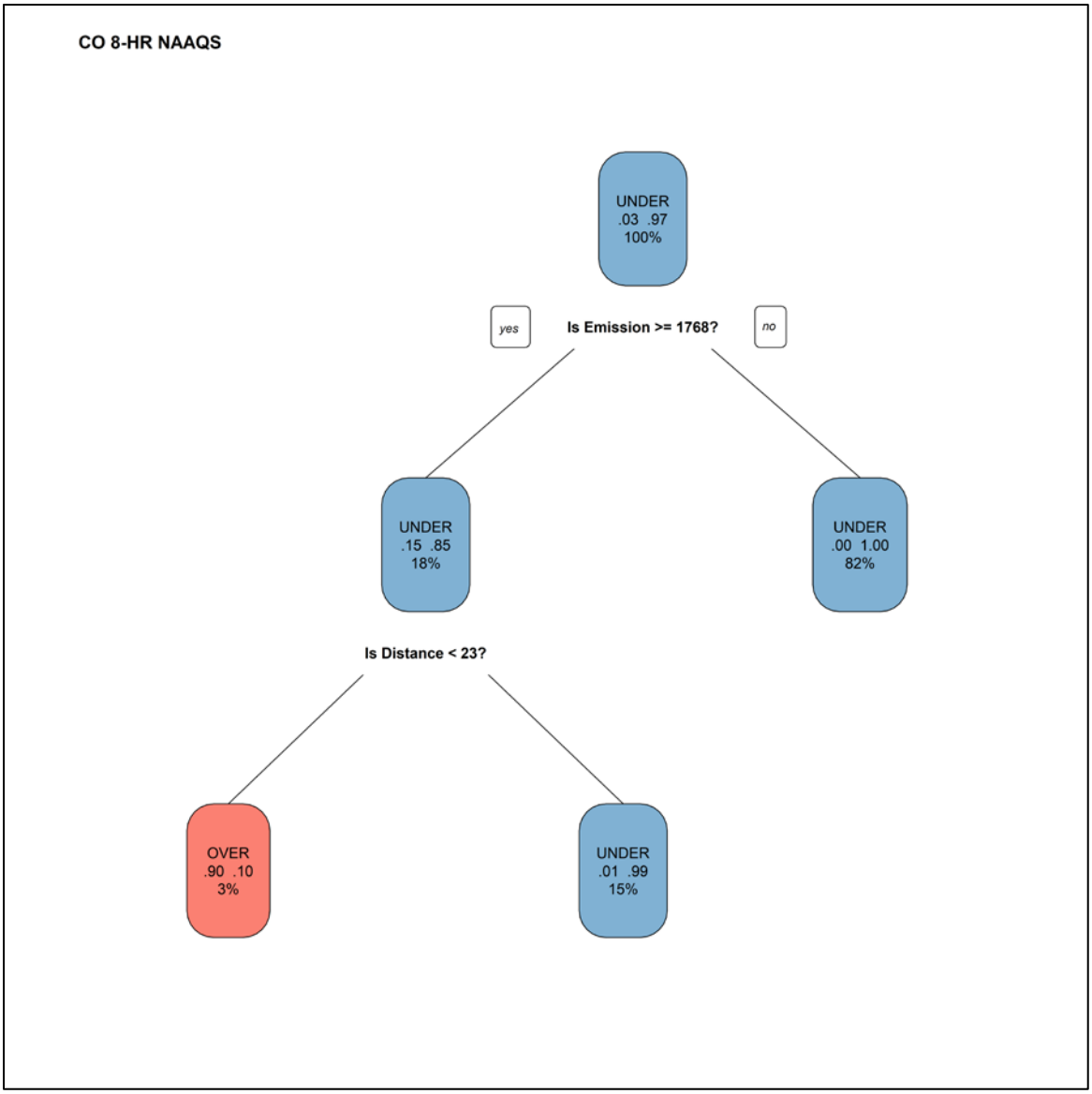

Figure E.8-31. CART Decision Tree for the CO 8-Hour Modeling Results (Without Vessel Emissions)

At each decision point, the branch to the right indicates a response of "no." The boxes at each decision point indicate the probability that the source is over (middle row, left) or under (middle row, right) the SIL and the percentage of the total values in the bin (bottom).

Table E.8-20. CART Outcomes for the CO 8-Hour NAAQS (Without Vessel Emissions)

Formula ID	False Positive	False Negative	Pass	Formula
CART	0.27%	0.27%	99.45%	– [a]

[a] The CART tool is a decision tree coded as a series of nested "if statements" to calculate false positive, false negative, and pass rates.

E.8.6.2 PM_{10}

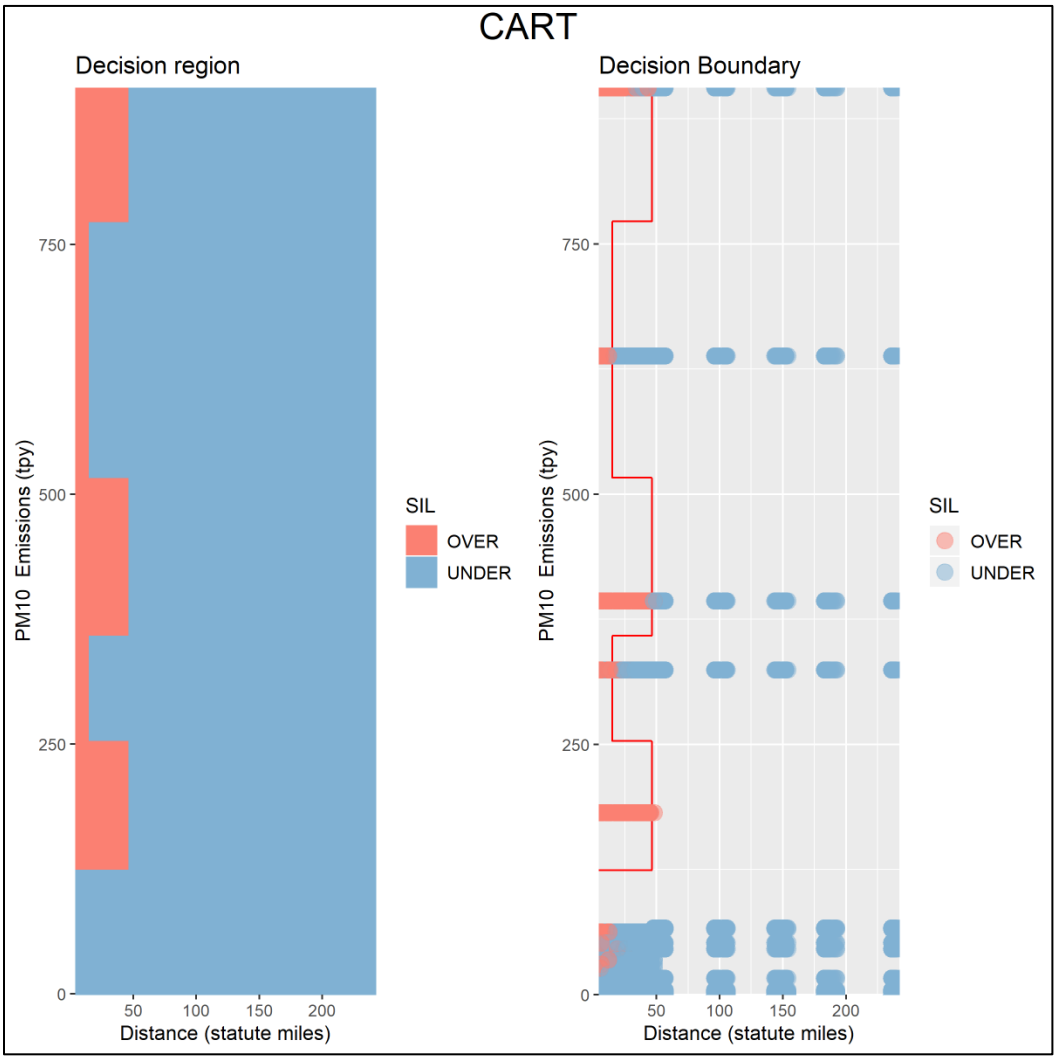

Figure E.8-32. CART Analysis for the PM_{10} 24-Hour Modeling Results (Without Vessel Emissions)

The plot on the left shows the determine-decision regions, with red shading indicating results above the SIL and blue shading below. The plot on the right shows the decision boundary (red line) overlaid on the original data.

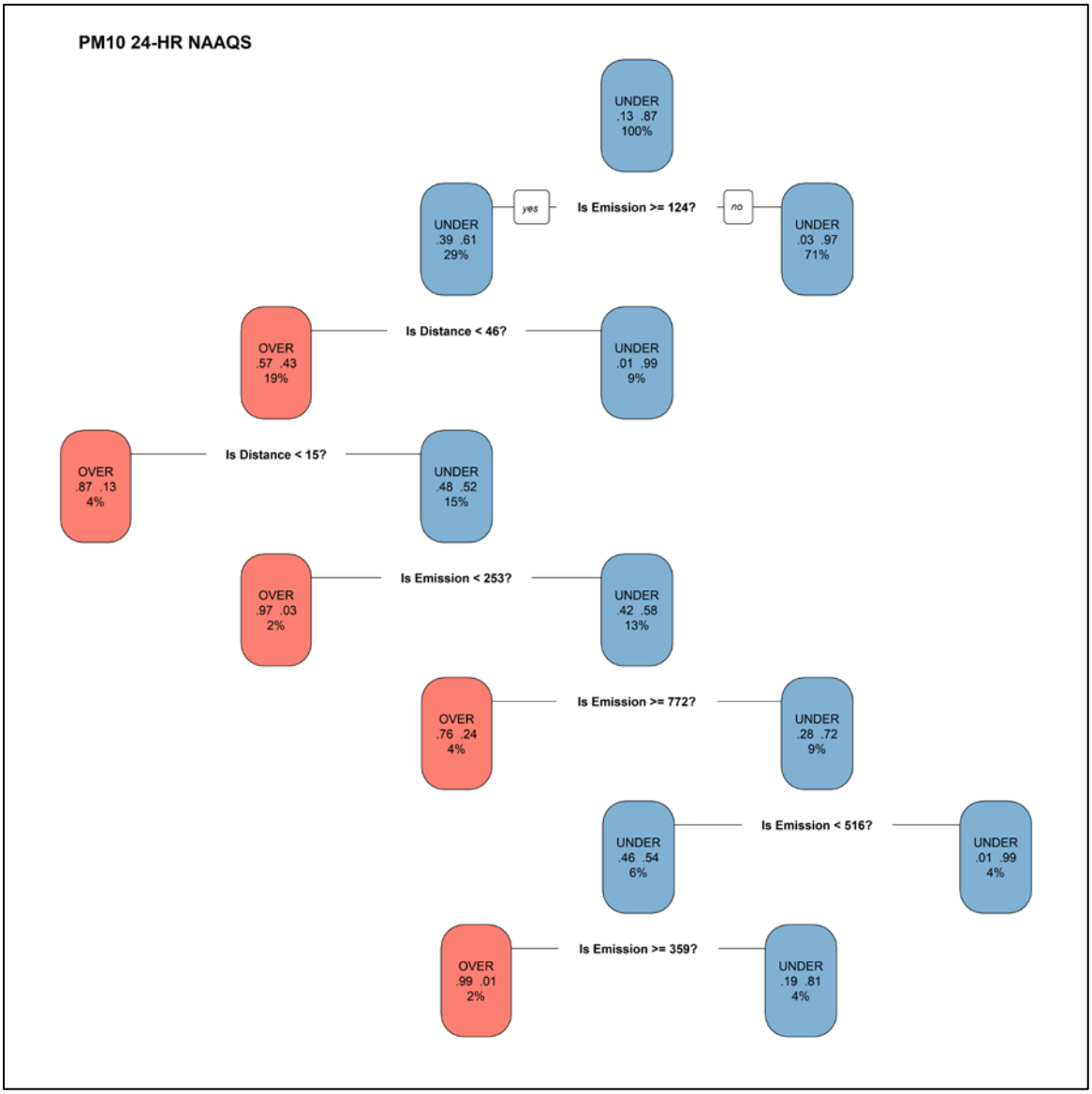

Figure E.8-33. CART Decision Tree for the PM_{10} 24-Hour Modeling Results (Without Vessel Emissions)

At each decision point, the branch to the right indicates a response of "no." The boxes at each decision point indicate the probability that the source is over (middle row, left) or under (middle row, right) the SIL and the percentage of the total values in the bin (bottom).

Table E.8-21. CART Outcomes for the PM_{10} 24-Hour NAAQS (Without Vessel Emissions)

Formula ID	False Positive	False Negative	Pass	Formula
CART	1.55%	2.90%	95.55%	– [a]

[a] The CART tool is a decision tree coded as a series of nested "if statements" to calculate false positive, false negative, and pass rates.

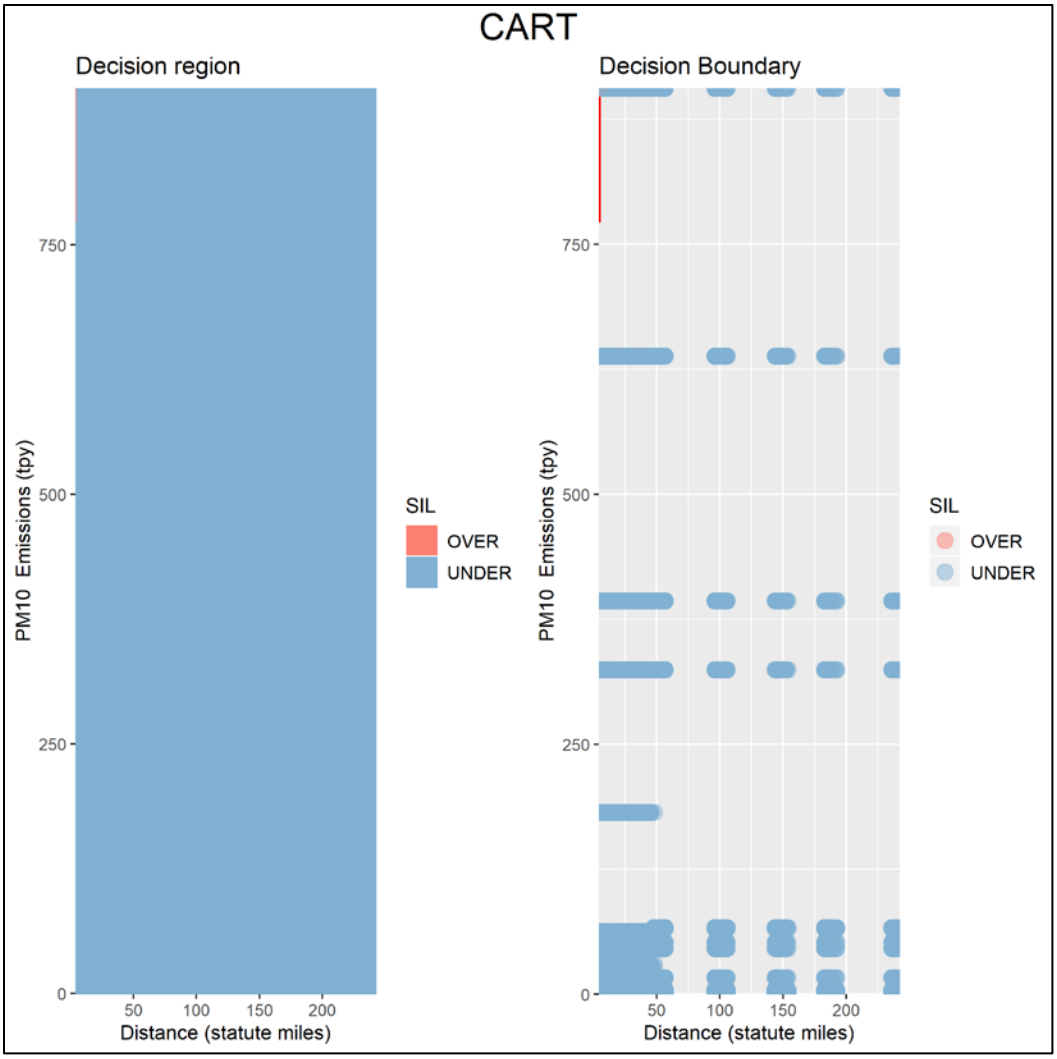

Figure E.8-34. CART Analysis for the PM_{10} Annual Modeling Results (Without Vessel Emissions)

The plot on the left shows the determine-decision regions, with red shading indicating results above the SIL and blue shading below. The plot on the right shows the decision boundary (red line) overlaid on the original data.

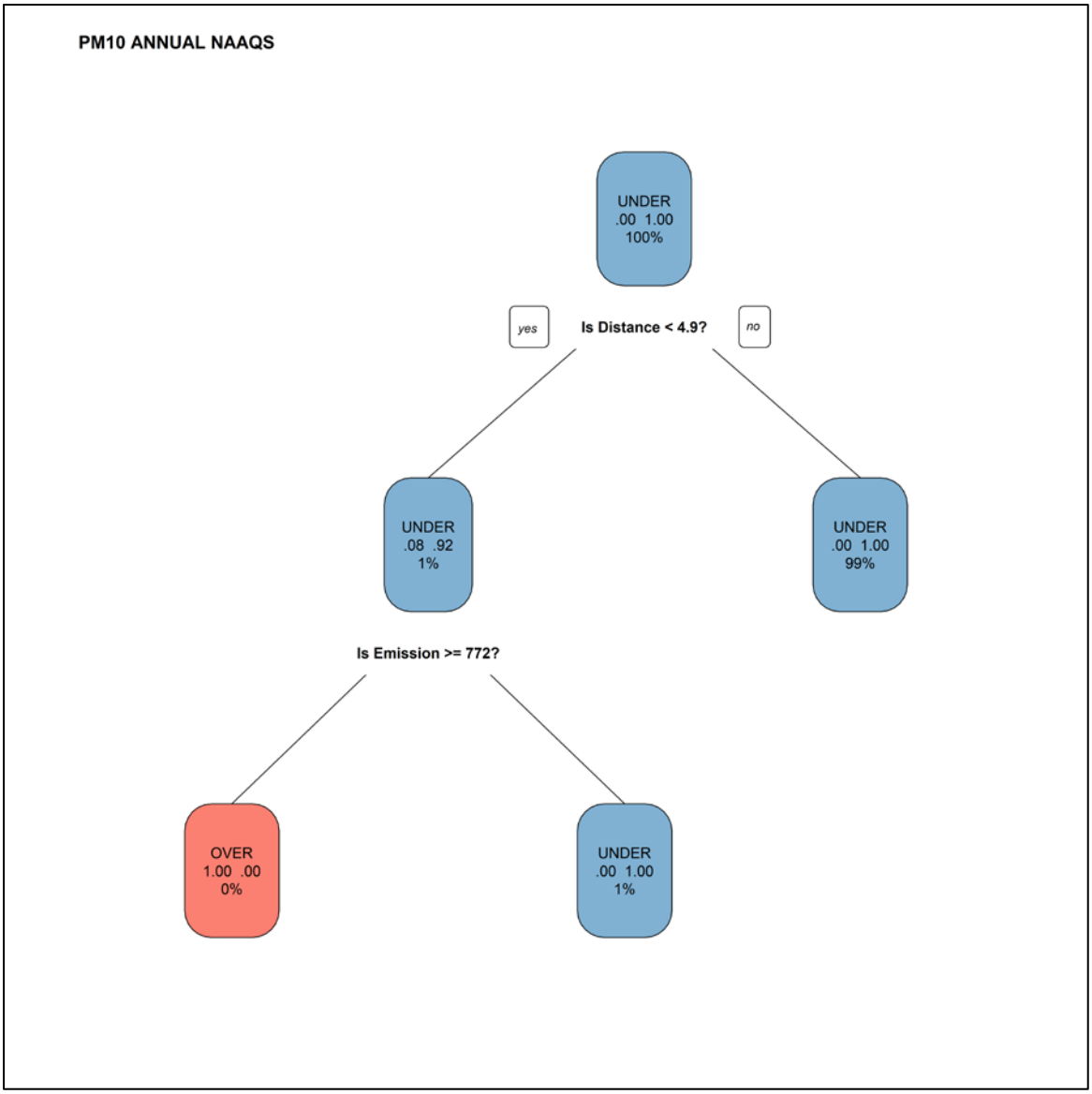

Figure E.8-35. CART Decision Tree for the PM_{10} Annual Modeling Results (Without Vessel Emissions)

At each decision point, the branch to the right indicates a response of "no." The boxes at each decision point indicate the probability that the source is over (middle row, left) or under (middle row, right) the SIL and the percentage of the total values in the bin (bottom).

Table E.8-22. CART Outcomes for the PM_{10} Annual NAAQS (Without Vessel Emissions)

Formula ID	False Positive	False Negative	Pass	Formula
CART	0.00%	0.02%	99.98%	– [a]

[a] The CART tool is a decision tree coded as a series of nested "if statements" to calculate false positive, false negative, and pass rates.

E.8.6.3 $PM_{2.5}$

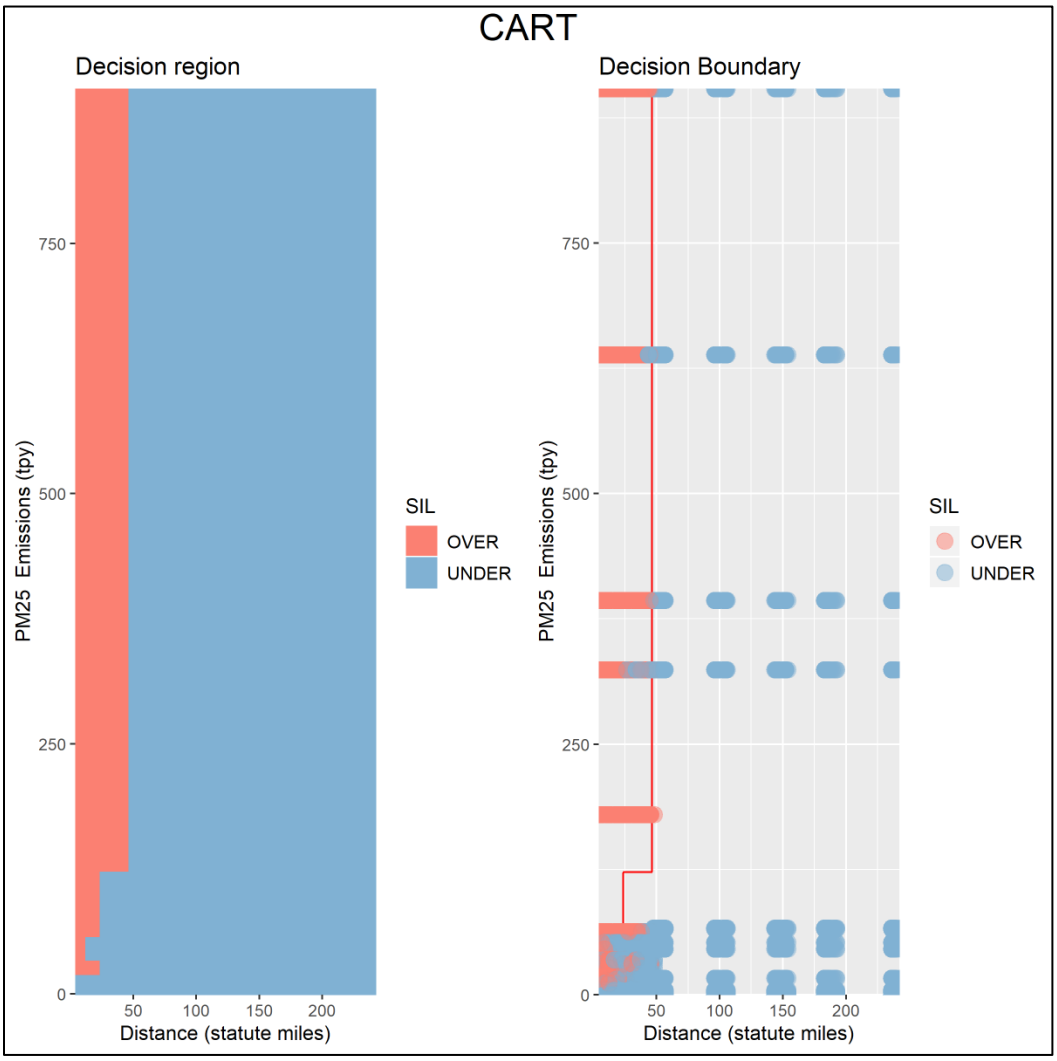

Figure E.8-36. CART Analysis for the $PM_{2.5}$ 24-Hour Modeling Results (Without Vessel Emissions)

The plot on the left shows the determine-decision regions, with red shading indicating results above the SIL and blue shading below. The plot on the right shows the decision boundary (red line) overlaid on the original data.

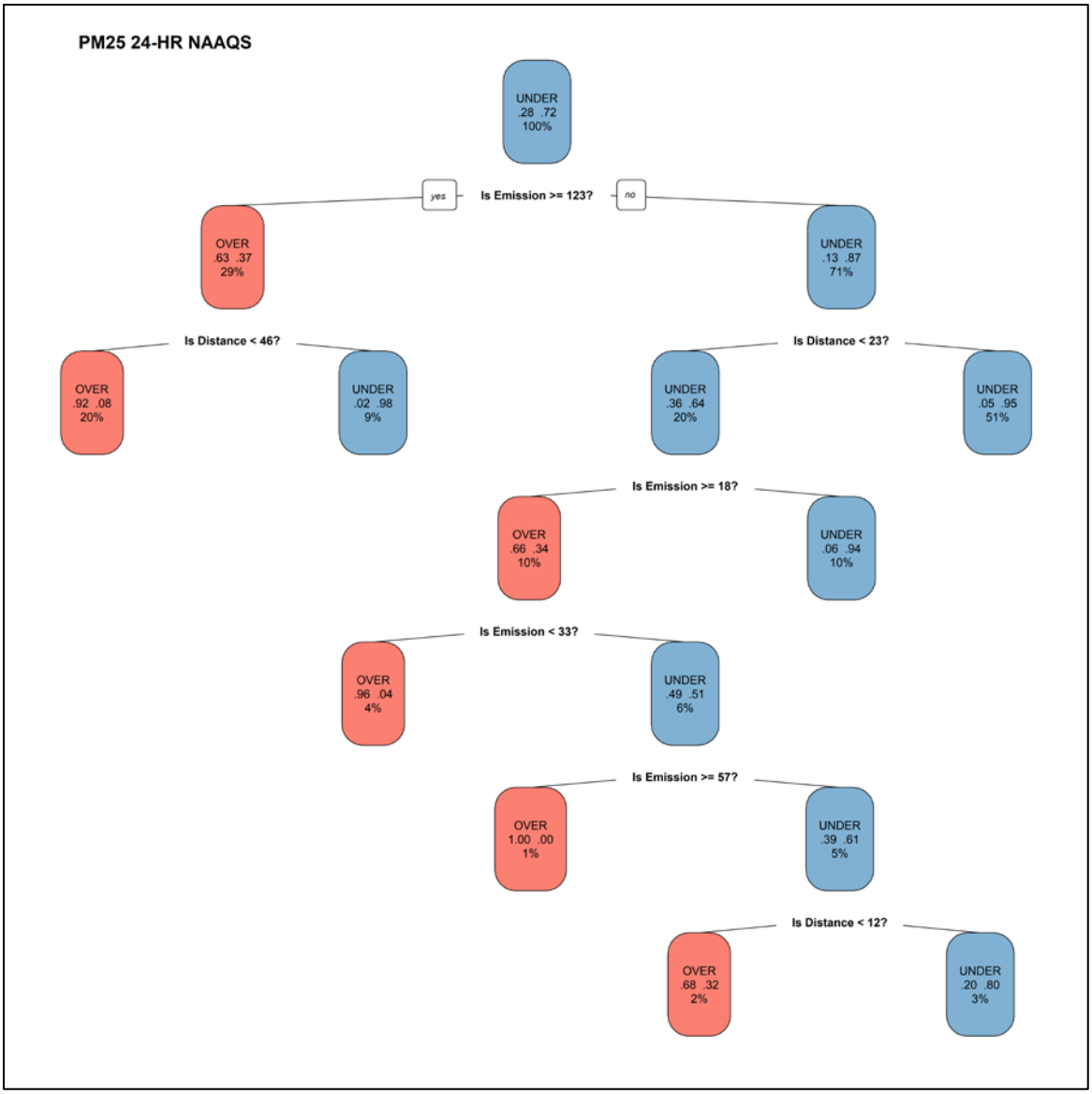

Figure E.8-37. CART Decision Tree for the $PM_{2.5}$ 24-Hour Modeling Results (Without Vessel Emissions)

At each decision point, the branch to the right indicates a response of "no." The boxes at each decision point indicate the probability that the source is over (middle row, left) or under (middle row, right) the SIL and the percentage of the total values in the bin (bottom).

Table E.8-23. CART Outcomes for the $PM_{2.5}$ 24-Hour NAAQS (Without Vessel Emissions)

Formula ID	False Positive	False Negative	Pass	Formula
CART	2.35%	3.77%	93.87%	– [a]

[a] The CART tool is a decision tree coded as a series of nested "if statements" to calculate false positive, false negative, and pass rates.

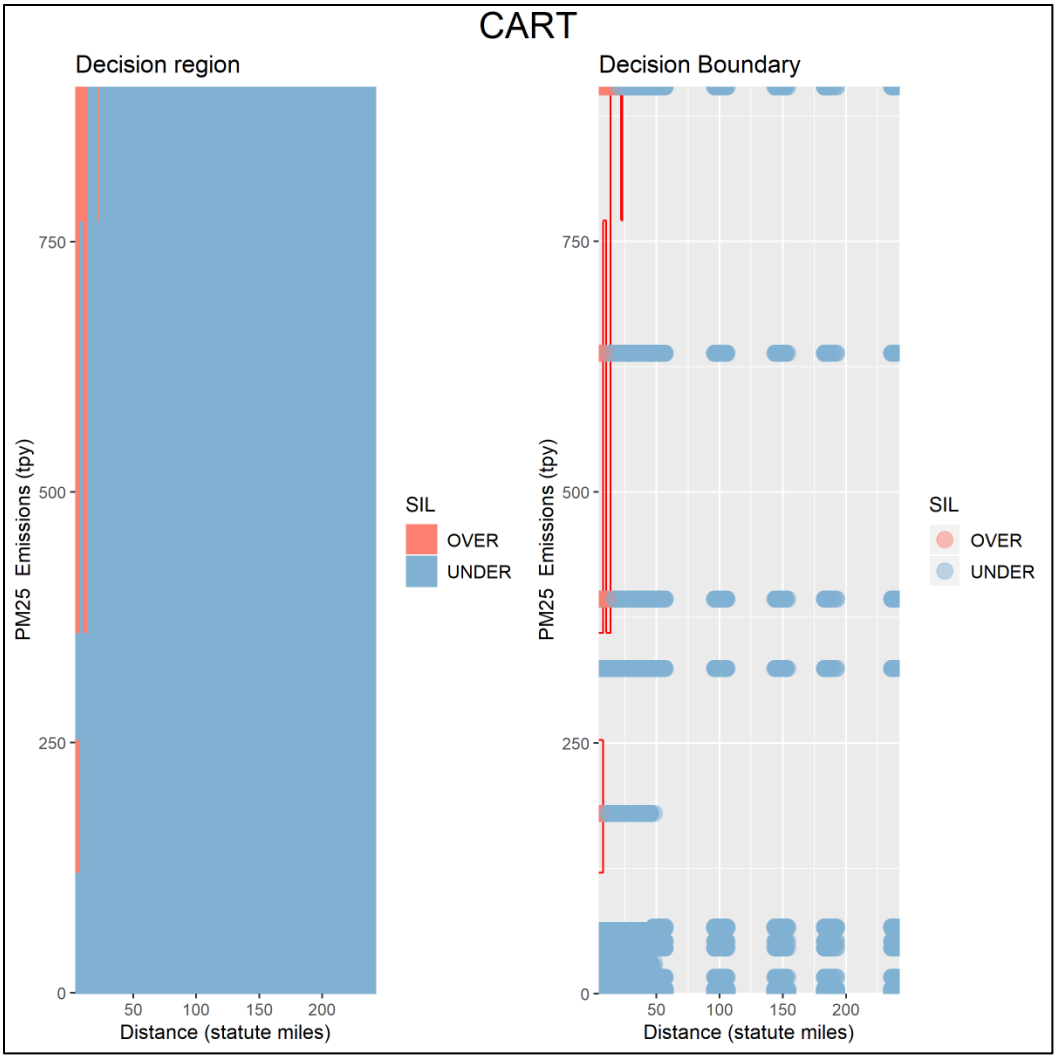

Figure E.8-38. CART Analysis for the $PM_{2.5}$ Annual Modeling Results (Without Vessel Emissions)

The plot on the left shows the determine-decision regions, with red shading indicating results above the SIL and blue shading below. The plot on the right shows the decision boundary (red line) overlaid on the original data.

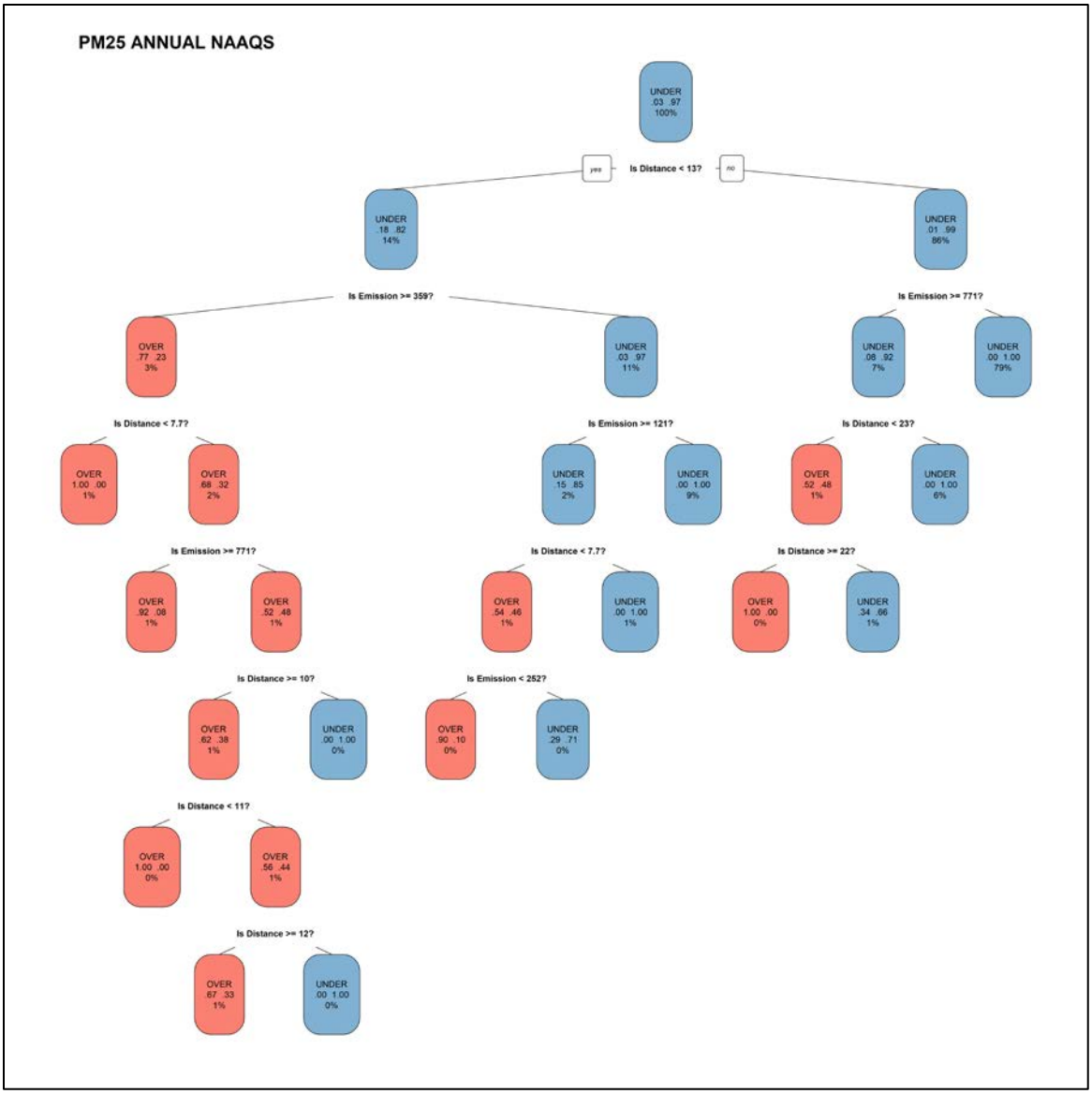

Figure E.8-39. CART Decision Tree for the $PM_{2.5}$ Annual Modeling Results (Without Vessel Emissions)

At each decision point, the branch to the right indicates a response of "no." The boxes at each decision point indicate the probability that the source is over (middle row, left) or under (middle row, right) the SIL and the percentage of the total values in the bin (bottom).

Table E.8-24. CART Outcomes for the $PM_{2.5}$ Annual NAAQS (Without Vessel Emissions)

Formula ID	False Positive	False Negative	Pass	Formula
CART	0.35%	0.37%	99.28%	– [a]

[a] The CART tool is a decision tree coded as a series of nested "if statements" to calculate false positive, false negative, and pass rates.

E.8.6.4 Nitrogen Oxides

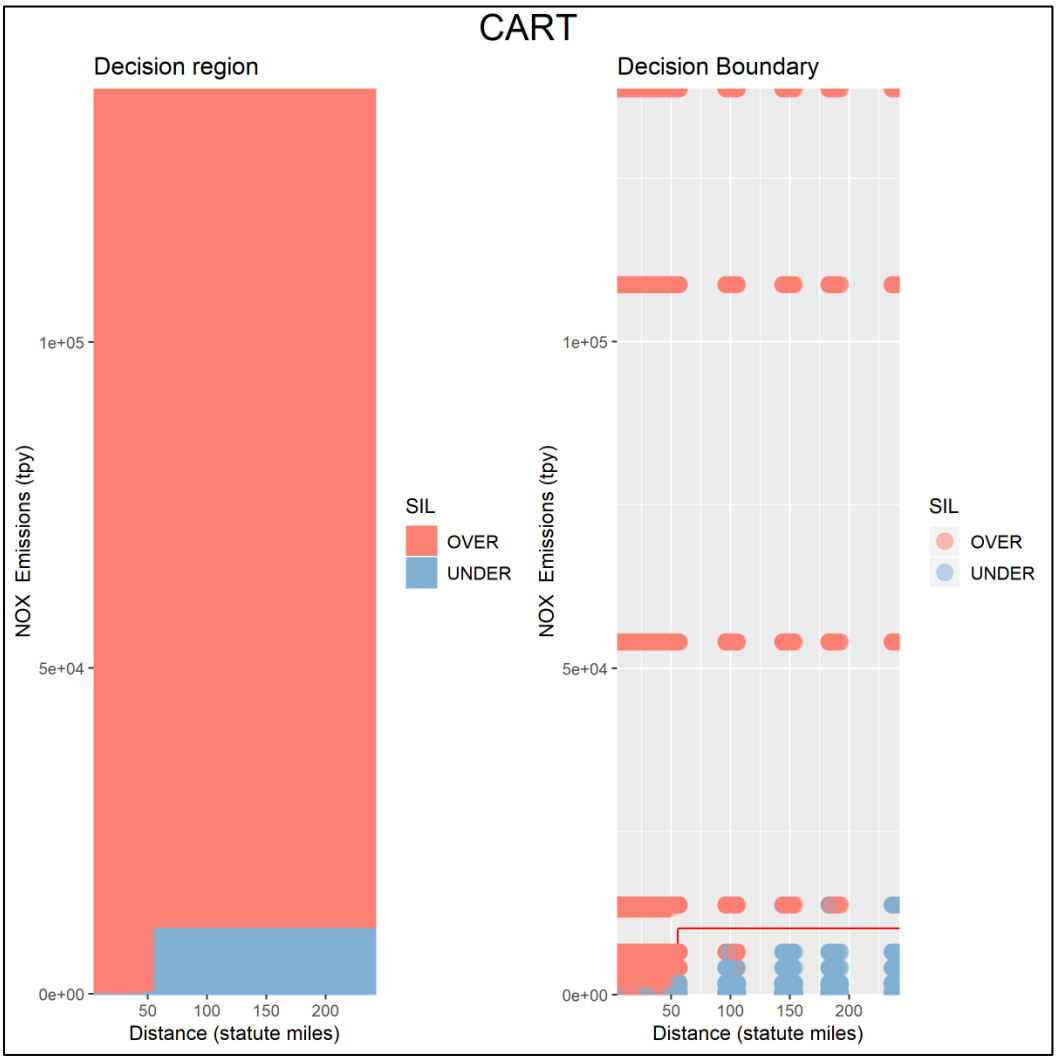

Figure E.8-40. CART Analysis for the NO_x 1-Hour Modeling Results (Without Vessel Emissions)

The plot on the left shows the determine-decision regions, with red shading indicating results above the SIL and blue shading below. The plot on the right shows the decision boundary (red line) overlaid on the original data.

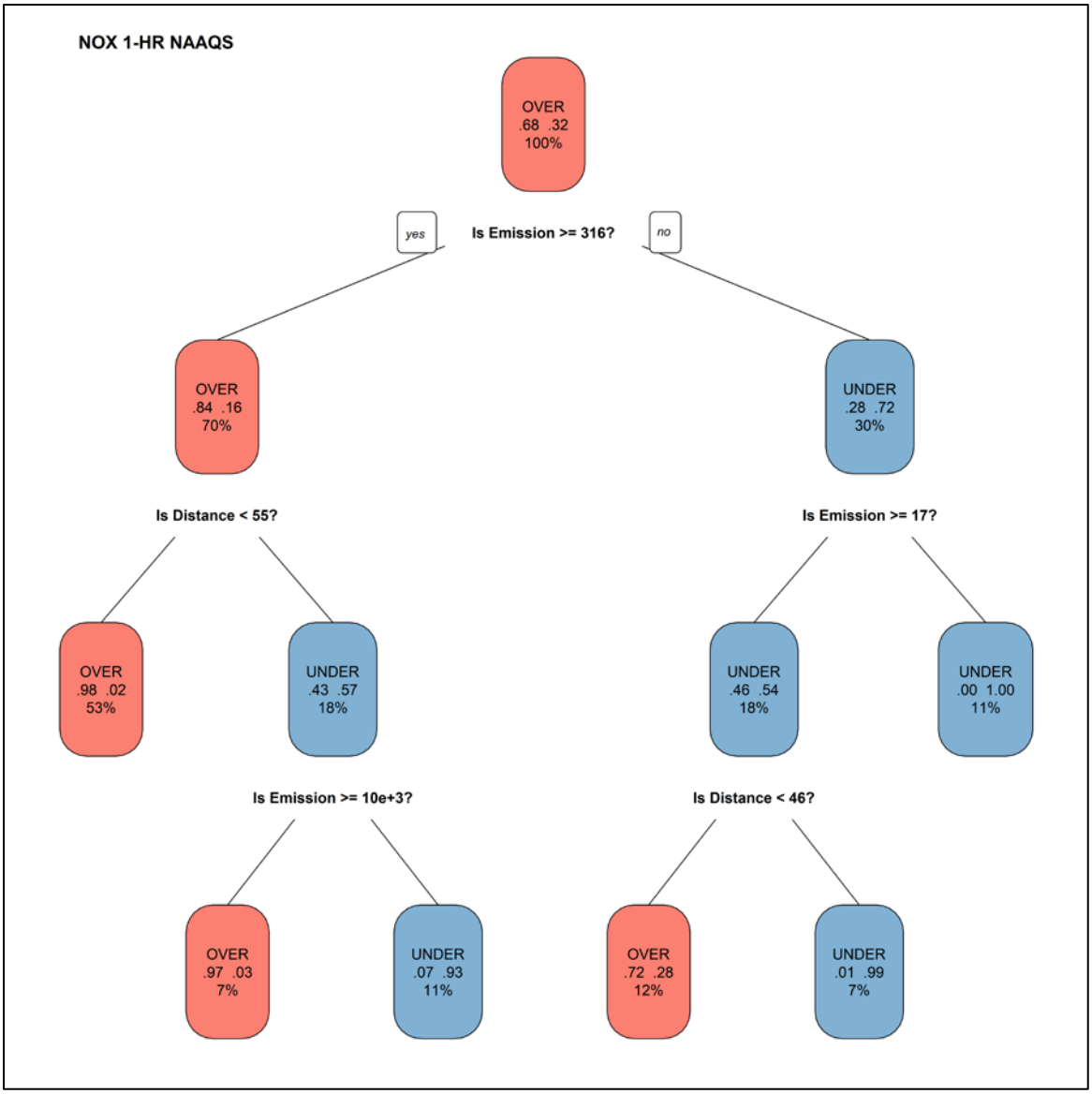

Figure E.8-41. CART Decision Tree for the NO_x 1-Hour Modeling Results (Without Vessel Emissions)

At each decision point, the branch to the right indicates a response of "no." The boxes at each decision point indicate the probability that the source is over (middle row, left) or under (middle row, right) the SIL and the percentage of the total values in the bin (bottom).

Table E.8-25. CART Outcomes for the NO_x 1-Hour NAAQS (Without Vessel Emissions)

Formula ID	False Positive	False Negative	Pass	Formula
CART	4.51%	0.76%	94.73%	– [a]

[a] The CART tool is a decision tree coded as a series of nested "if statements" to calculate false positive, false negative, and pass rates.

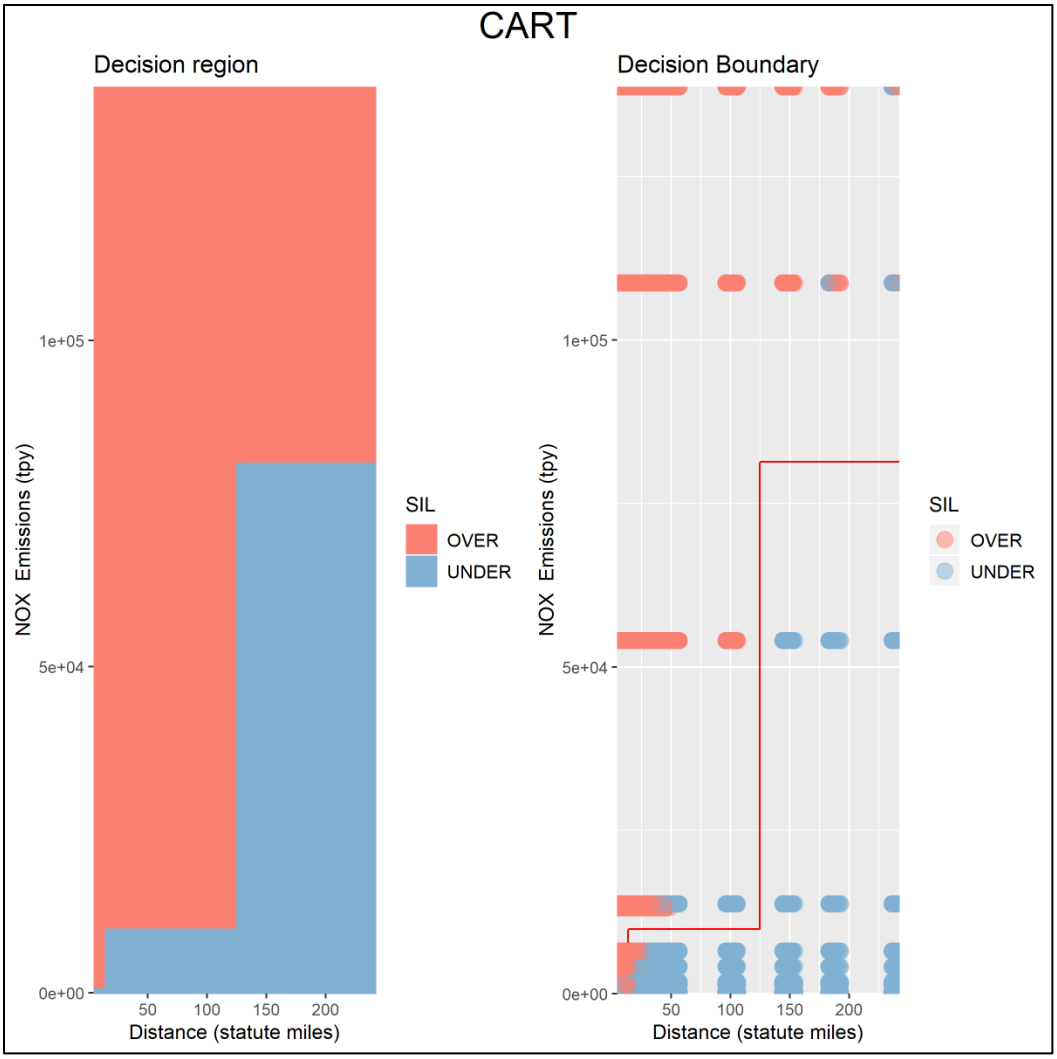

Figure E.8-42. CART Analysis for the NO_x Annual Modeling Results (Without Vessel Emissions)

The plot on the left shows the determine-decision regions, with red shading indicating results above the SIL and blue shading below. The plot on the right shows the decision boundary (red line) overlaid on the original data.

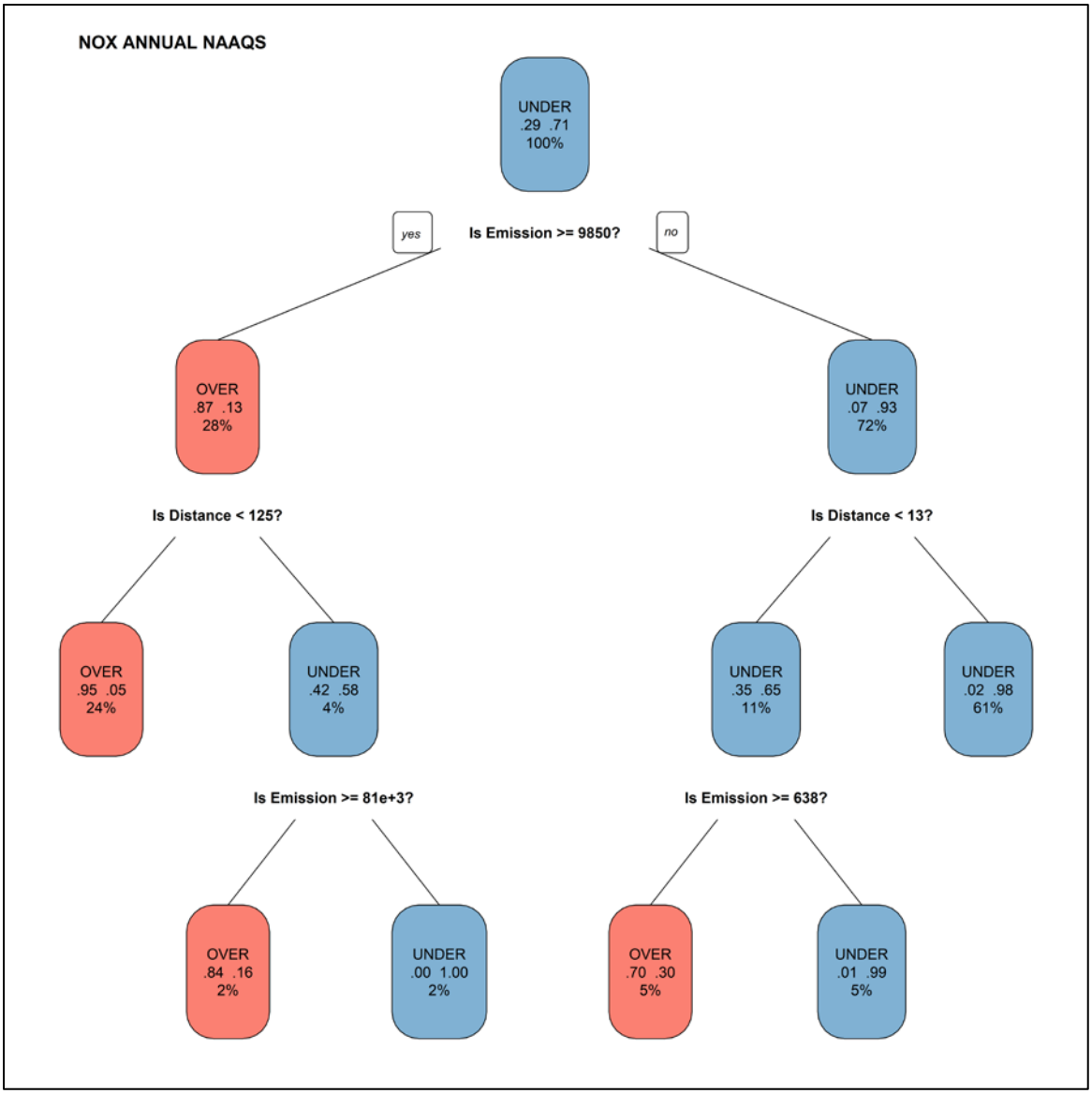

Figure E.8-43. CART Decision Tree for the NO_x Annual Modeling Results (Without Vessel Emissions)

At each decision point, the branch to the right indicates a response of "no." The boxes at each decision point indicate the probability that the source is over (middle row, left) or under (middle row, right) the SIL and the percentage of the total values in the bin (bottom).

Table E.8-26. CART Outcomes for the NO_x Annual NAAQS (Without Vessel Emissions)

Formula ID	False Positive	False Negative	Pass	Formula
CART	3.19%	1.34%	95.47%	– [a]

[a] The CART tool is a decision tree coded as a series of nested "if statements" to calculate false positive, false negative, and pass rates.

E.8.6.5 Sulfur Dioxide

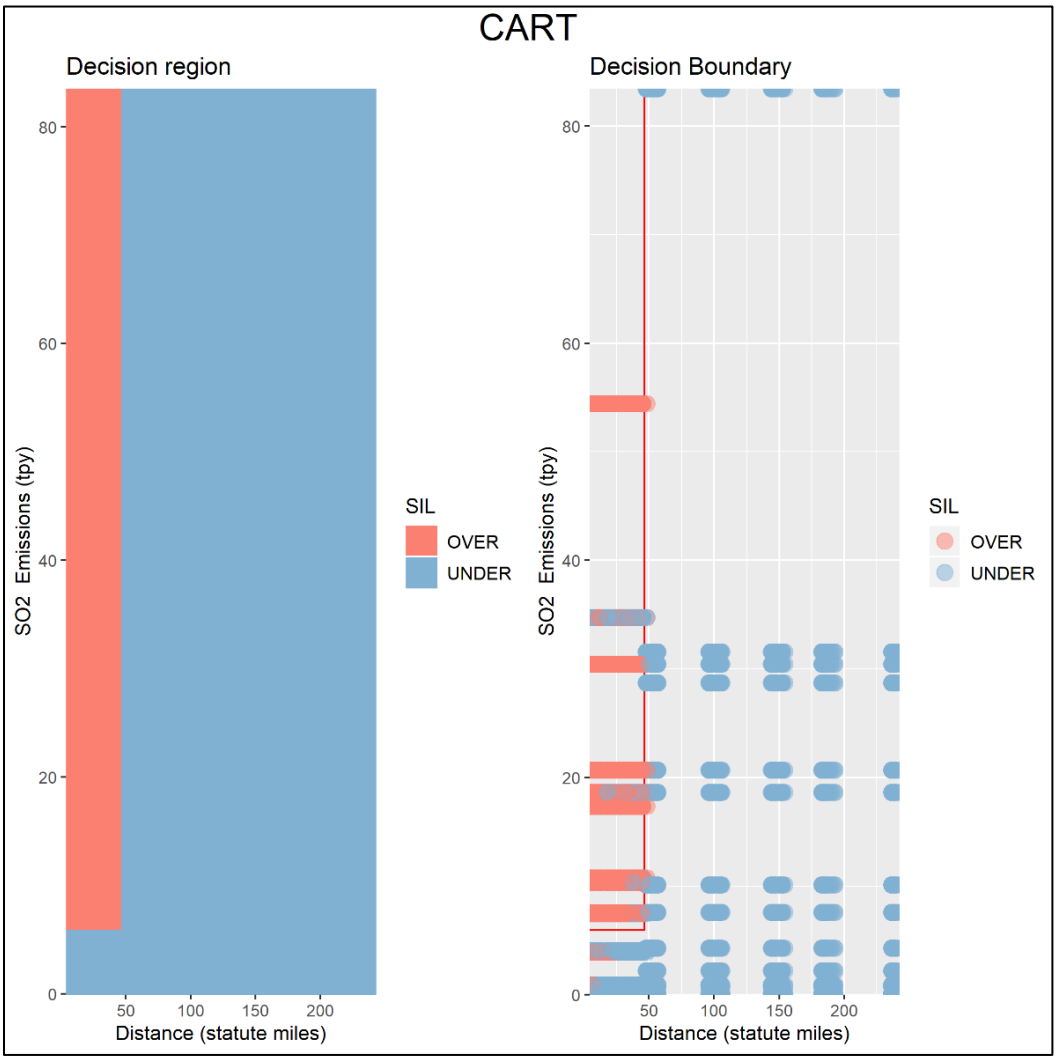

Figure E.8-44. CART Analysis for the SO_2 1-Hour Modeling Results (Without Vessel Emissions)

The plot on the left shows the determine-decision regions, with red shading indicating results above the SIL and blue shading below. The plot on the right shows the decision boundary (red line) overlaid on the original data.

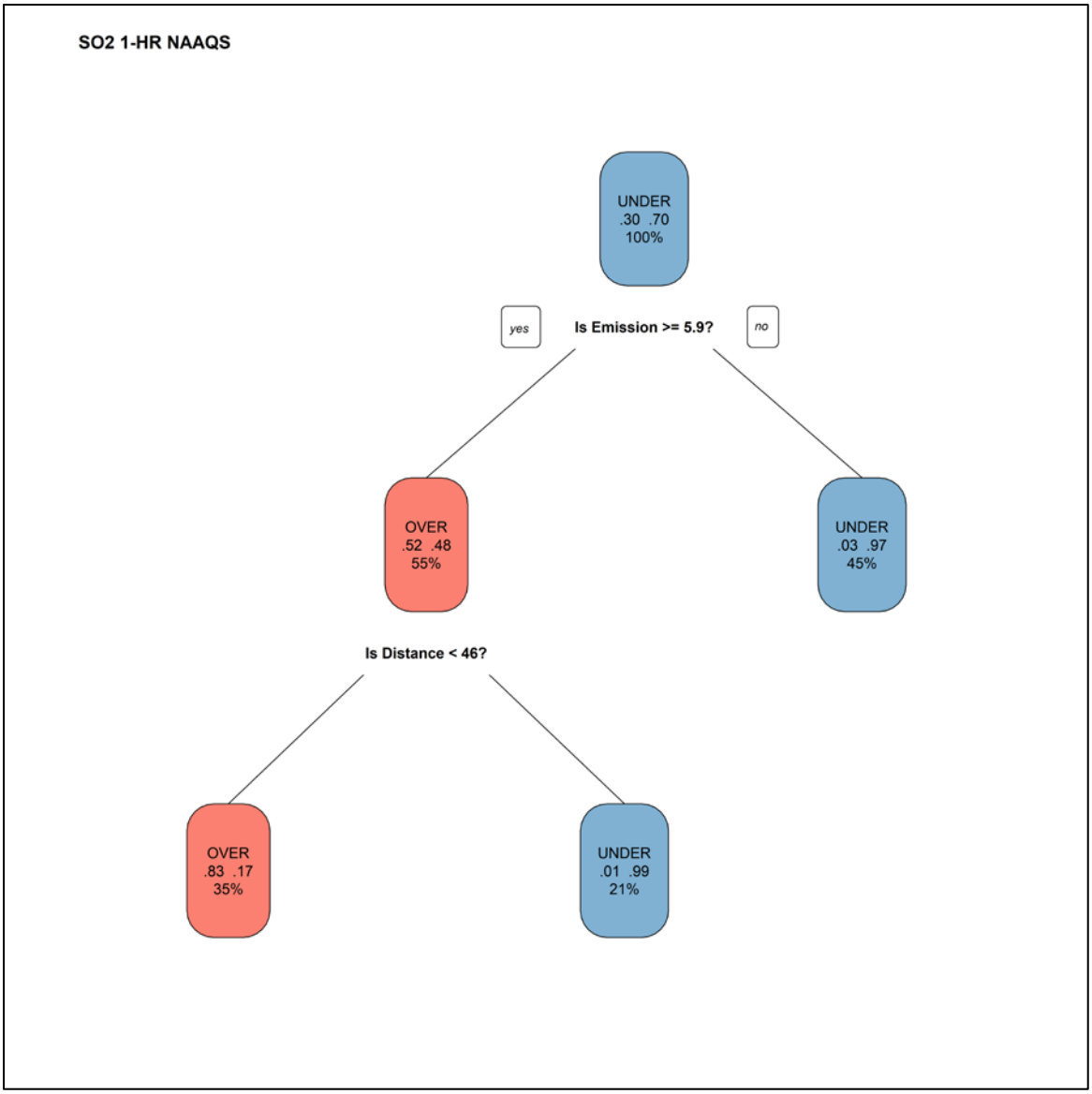

Figure E.8-45. CART Decision Tree for the SO_2 1-Hour Modeling Results (Without Vessel Emissions)

At each decision point, the branch to the right indicates a response of "no." The boxes at each decision point indicate the probability that the source is over (middle row, left) or under (middle row, right) the SIL, and the percentage of the total values in the bin (bottom).

Table E.8-27. CART Outcomes for the SO_2 1-Hour NAAQS (Without Vessel Emissions)

Formula ID	False Positive	False Negative	Pass	Formula
CART	5.88%	1.45%	92.67%	– [a]

[a] The CART tool is a decision tree coded as a series of nested "if statements" to calculate false positive, false negative, and pass rates.

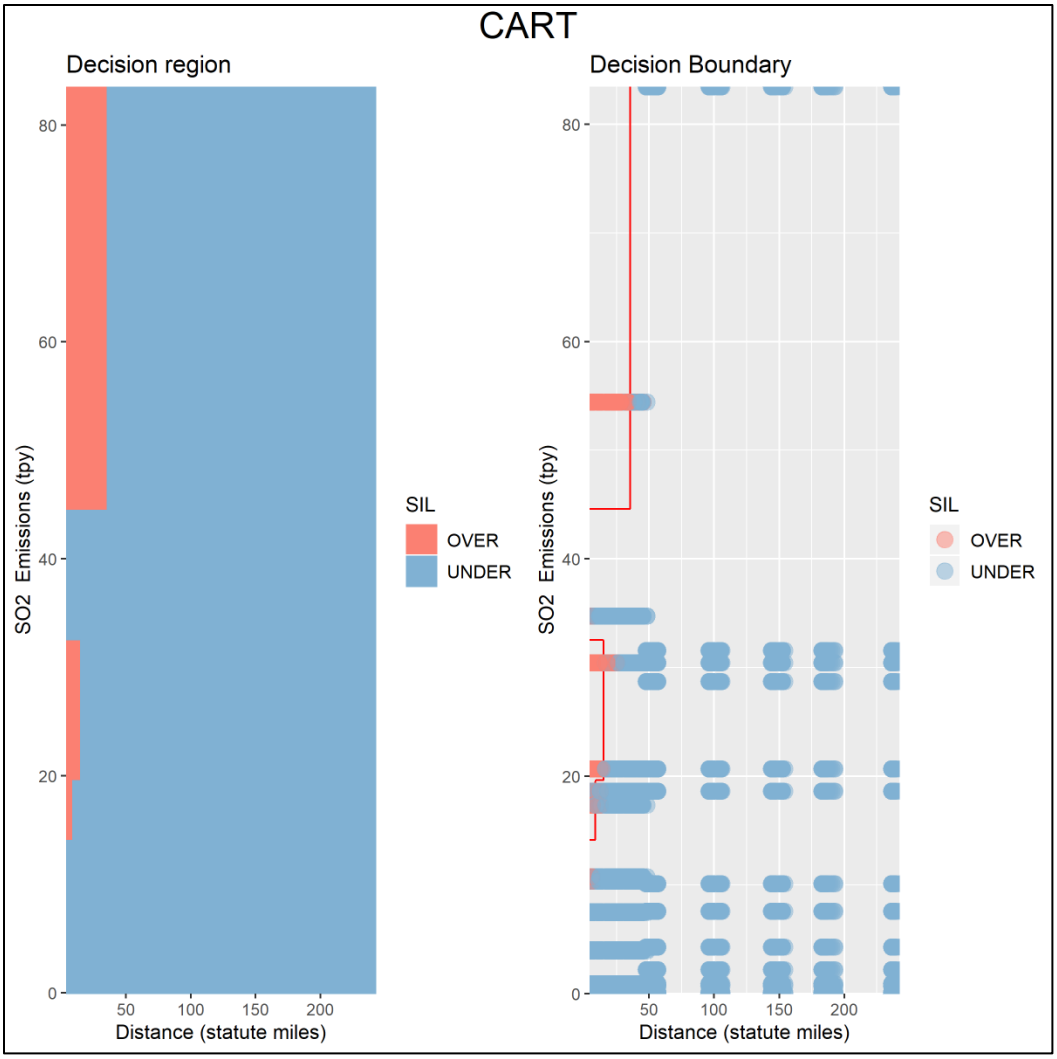

Figure E.8-46. CART Analysis for the SO_2 3-Hour Modeling Results (Without Vessel Emissions)

The plot on the left shows the determine-decision regions, with red shading indicating results above the SIL and blue shading below. The plot on the right shows the decision boundary (red line) overlaid on the original data.

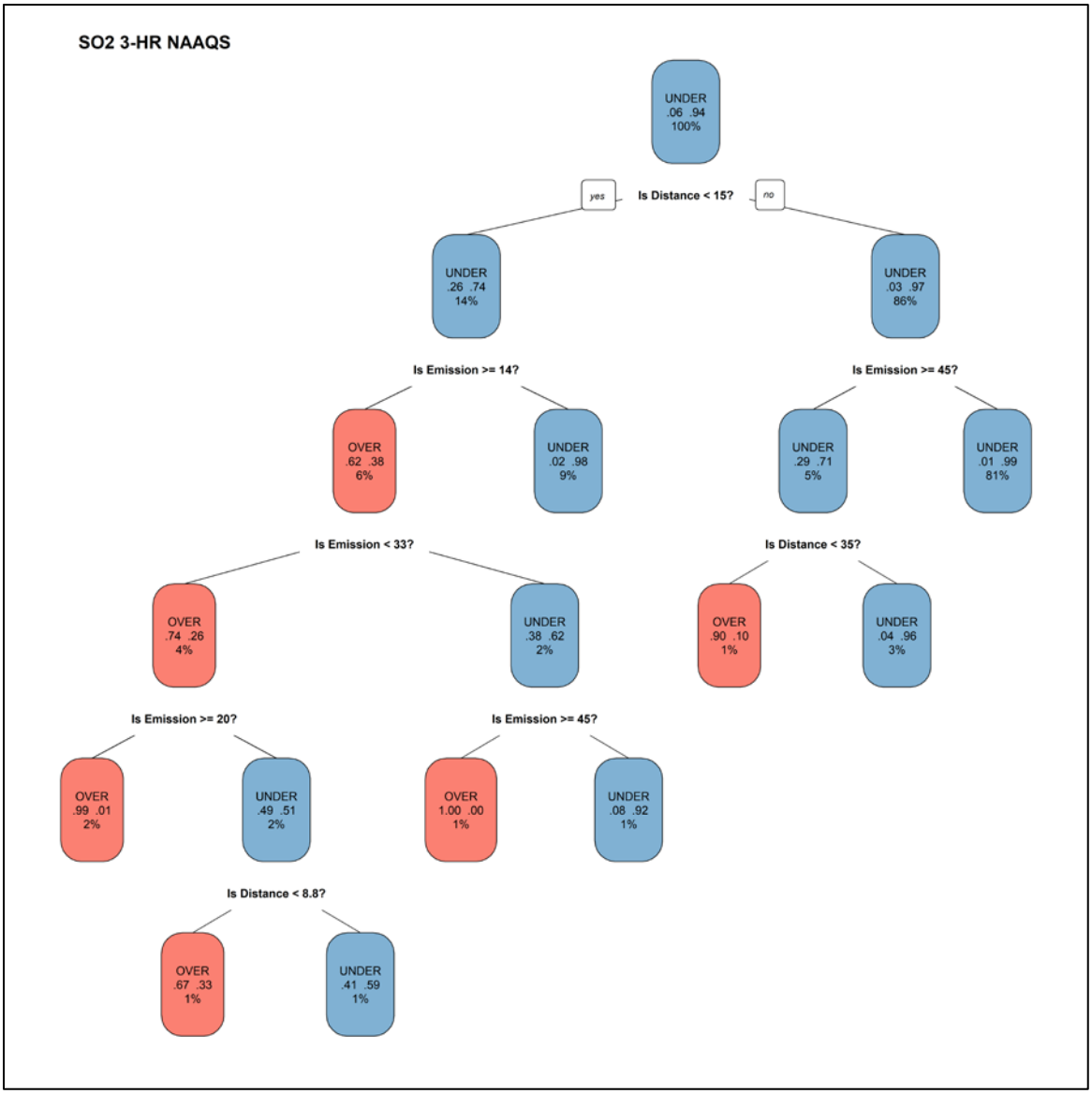

Figure E.8-47. CART Decision Tree for the SO_2 3-Hour Modeling Results (Without Vessel Emissions)

At each decision point, the branch to the right indicates a response of "no." The boxes at each decision point indicate the probability that the source is over (middle row, left) or under (middle row, right) the SIL and the percentage of the total values in the bin (bottom).

Table E.8-28. CART Outcomes for the SO_2 3-Hour NAAQS (Without Vessel Emissions)

Formula ID	False Positive	False Negative	Pass	Formula
CART	0.36%	1.83%	97.81%	– [a]

[a] The CART tool is a decision tree coded as a series of nested "if statements" to calculate false positive, false negative, and pass rates.

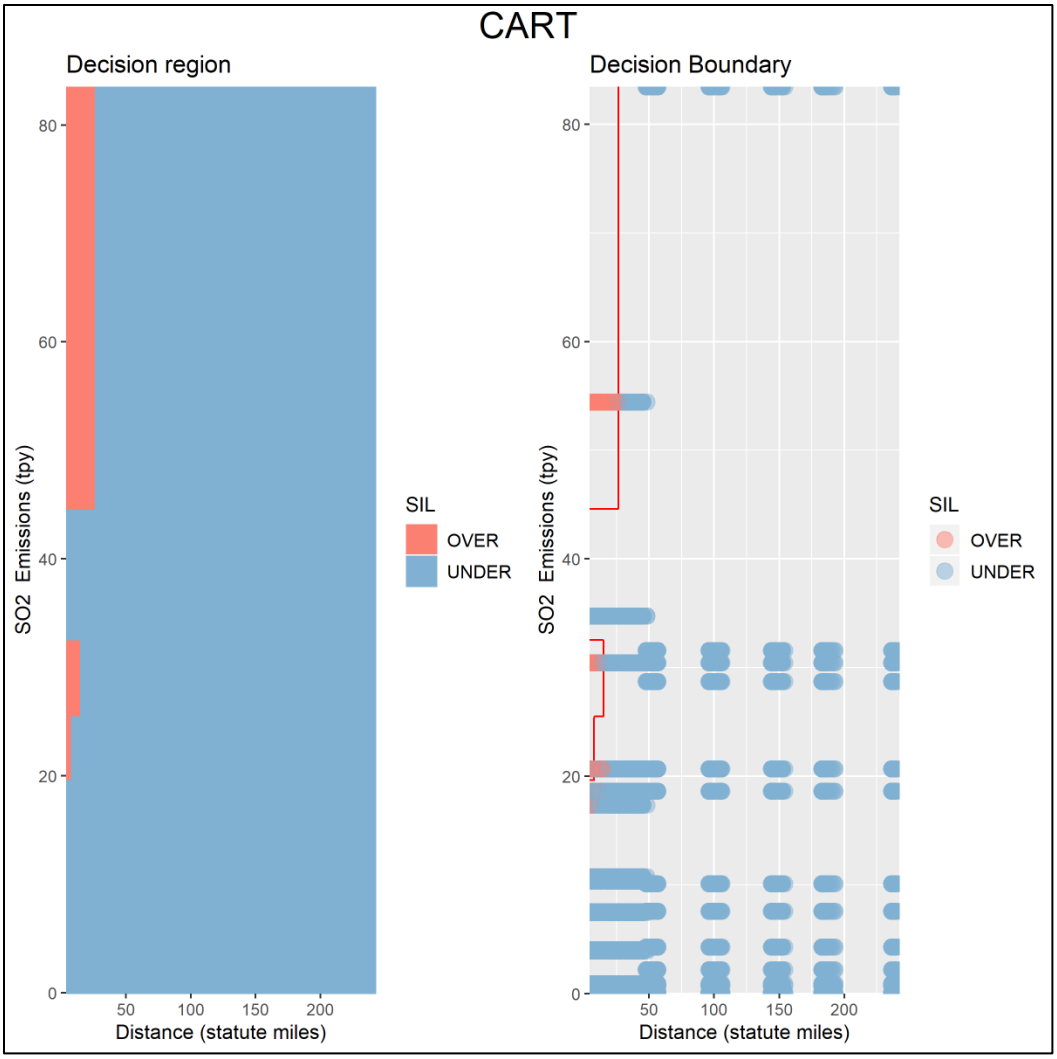

Figure E.8-48. CART Analysis for the SO_2 24-Hour Modeling Results (Without Vessel Emissions)

The plot on the left shows the determine-decision regions, with red shading indicating results above the SIL and blue shading below. The plot on the right shows the decision boundary (red line) overlaid on the original data.

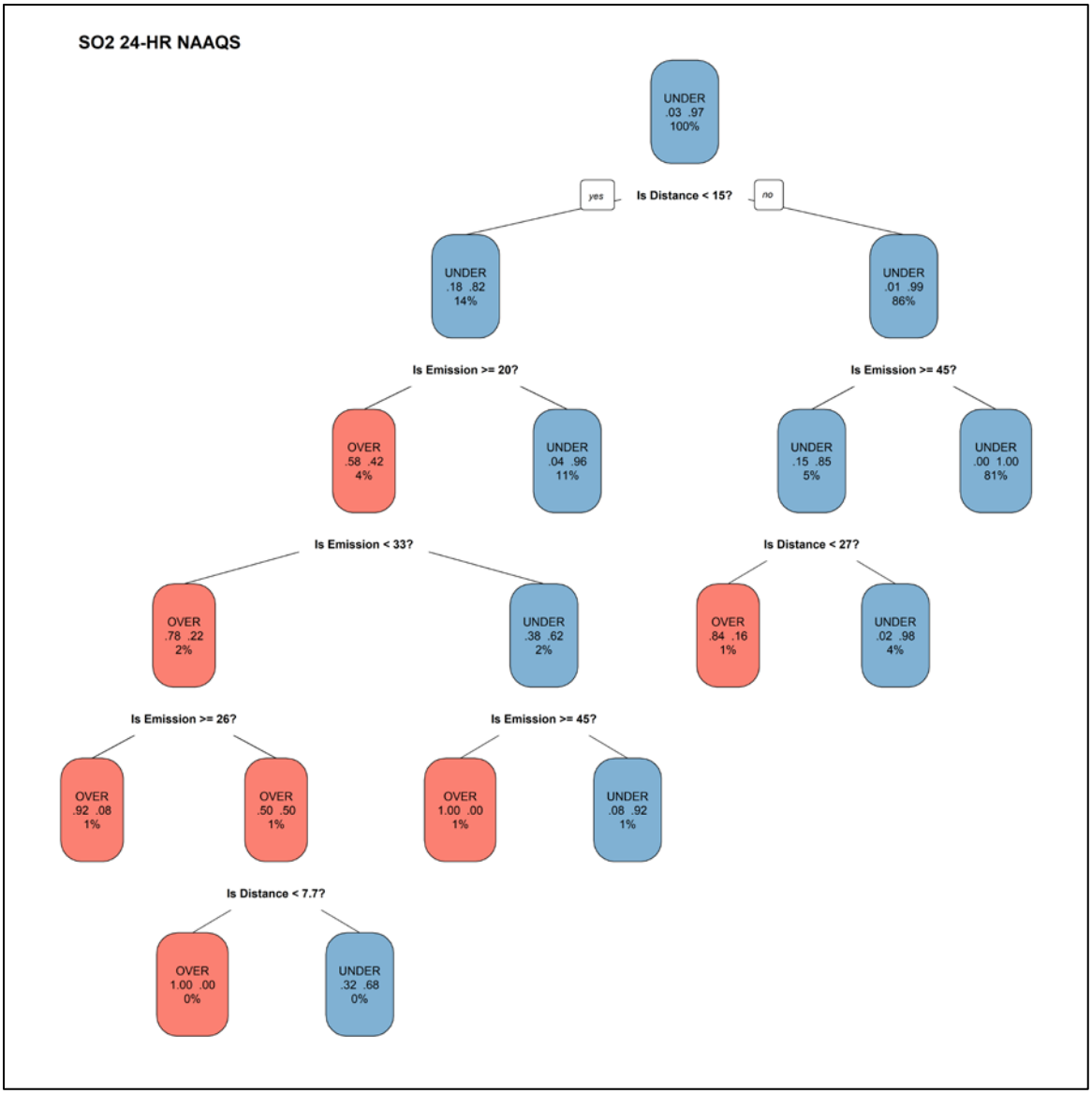

Figure E.8-49. CART Decision Tree for the SO_2 24-Hour Modeling Results (Without Vessel Emissions)

At each decision point, the branch to the right indicates a response of "no." The boxes at each decision point indicate the probability that the source is over (middle row, left) or under (middle row, right) the SIL and the percentage of the total values in the bin (bottom).

Table E.8-29. CART Outcomes for the SO_2 24-Hour NAAQS (Without Vessel Emissions)

Formula ID	False Positive	False Negative	Pass	Formula
CART	0.21%	0.78%	99.00%	– [a]

[a] The CART tool is a decision tree coded as a series of nested "if statements" to calculate false positive, false negative, and pass rates

For the Annual SO_2 NAAQS, once the data set is scaled to remove vessel emissions, all modeled scenarios fall under the SIL. That is, no scenario showed modeling was necessary. That is not to say there is no level of SO_2 emissions that would warrant modeling for the annual NAAQS. This data set only included emission scenarios up to 1.97 grams per second, or 68.54 tons per year. Sources that emit more than this would need to prove modeling is not necessary or submit modeling to supplement this database.

Table E.8-30. CART Outcomes for the SO_2 Annual NAAQS (Without Vessel Emissions)

Formula ID	False Positive	False Negative	Pass	Formula
CART	0.00%	0.00%	100.00%	– [a]

[a] The CART tool is a decision tree coded as a series of nested "if statements" to calculate false positive, false negative, and pass rates.

E.8.7 References

Mason, R., P. Dolwick, P. Carey, E. Kinnee, M. Wilson. 2008. Emissions processing and sensitivity air quality modeling of category 3 commercial marine vessel emissions. In: Proceedings from 17th Annual International Emission Inventory Conference, Portland, OR, 2008 June 04. 14 p.

Department of the Interior (DOI)

The Department of the Interior protects and manages the Nation's natural resources and cultural heritage; provides scientific and other information about those resources; and honors the Nation’s trust responsibilities or special commitments to American Indians, Alaska Natives, and affiliated island communities.

Bureau of Ocean Energy Management (BOEM)

The mission of the Bureau of Ocean Energy Management is to manage development of U.S. Outer Continental Shelf energy and mineral resources in an environmentally and economically responsible way.

BOEM Environmental Studies Program

The mission of the Environmental Studies Program is to provide the information needed to predict, assess, and manage impacts from offshore energy and marine mineral exploration, development, and production activities on human, marine, and coastal environments. The proposal, selection, research, review, collaboration, production, and dissemination of each of BOEM’s Environmental Studies follows the DOI Code of Scientific and Scholarly Conduct, in support of a culture of scientific and professional integrity, as set out in the DOI Departmental Manual (305 DM 3).